ALTERNATIVES TO COMBAT BACTERIAL INFECTIONS

EDITED BY: Rodolfo García-Contreras, Mariano Martinez-Vazquez, Thomas Keith Wood, Bertha González-Pedrajo and Israel Castillo-Juárez

PUBLISHED IN: Frontiers in Microbiology

frontiers Research Topics

frontiers

ISSN 1664-8714
ISBN 978-2-88976-242-2
DOI 10.3389/978-2-88976-242-2

About Frontiers

Frontiers is more than just an open-access publisher of scholarly articles: it is a pioneering approach to the world of academia, radically improving the way scholarly research is managed. The grand vision of Frontiers is a world where all people have an equal opportunity to seek, share and generate knowledge. Frontiers provides immediate and permanent online open access to all its publications, but this alone is not enough to realize our grand goals.

Frontiers Journal Series

The Frontiers Journal Series is a multi-tier and interdisciplinary set of open-access, online journals, promising a paradigm shift from the current review, selection and dissemination processes in academic publishing. All Frontiers journals are driven by researchers for researchers; therefore, they constitute a service to the scholarly community. At the same time, the Frontiers Journal Series operates on a revolutionary invention, the tiered publishing system, initially addressing specific communities of scholars, and gradually climbing up to broader public understanding, thus serving the interests of the lay society, too.

Dedication to Quality

Each Frontiers article is a landmark of the highest quality, thanks to genuinely collaborative interactions between authors and review editors, who include some of the world's best academicians. Research must be certified by peers before entering a stream of knowledge that may eventually reach the public - and shape society; therefore, Frontiers only applies the most rigorous and unbiased reviews.
Frontiers revolutionizes research publishing by freely delivering the most outstanding research, evaluated with no bias from both the academic and social point of view. By applying the most advanced information technologies, Frontiers is catapulting scholarly publishing into a new generation.

What are Frontiers Research Topics?

Frontiers Research Topics are very popular trademarks of the Frontiers Journals Series: they are collections of at least ten articles, all centered on a particular subject. With their unique mix of varied contributions from Original Research to Review Articles, Frontiers Research Topics unify the most influential researchers, the latest key findings and historical advances in a hot research area! Find out more on how to host your own Frontiers Research Topic or contribute to one as an author by contacting the Frontiers Editorial Office: frontiersin.org/about/contact

ALTERNATIVES TO COMBAT BACTERIAL INFECTIONS

Topic Editors:
Rodolfo García-Contreras, National Autonomous University of Mexico, Mexico
Mariano Martinez-Vazquez, Universidad Nacional Autónoma de México, Mexico
Thomas Keith Wood, The Pennsylvania State University (PSU), United States
Bertha González-Pedrajo, National Autonomous University of Mexico, Mexico
Israel Castillo-Juárez, Colegio de Postgraduados (COLPOS), Mexico

Citation: García-Contreras, R., Martinez-Vazquez, M., Wood, T. K., González-Pedrajo, B., Castillo-Juárez, I., eds. (2022). Alternatives to Combat Bacterial Infections. Lausanne: Frontiers Media SA.
doi: 10.3389/978-2-88976-242-2

Table of Contents

frontiers | Frontiers in Microbiology

EDITORIAL
published: 04 May 2022
doi: 10.3389/fmicb.2022.909866

Editorial: Alternatives to Combat Bacterial Infections

Rodolfo García-Contreras[1], Mariano Martínez-Vázquez[2]*, Bertha González-Pedrajo[3]* and Israel Castillo-Juárez[4]**

[1] Departamento de Microbiología y Parasitología, Facultad de Medicina, Universidad Nacional Autónoma de México, Ciudad de México, Mexico, [2] Departamento de Productos Naturales, Instituto de Química, Universidad Nacional Autónoma de México, Ciudad de México, Mexico, [3] Departamento de Genética Molecular, Instituto de Fisiología Celular, Universidad Nacional Autónoma de México, Ciudad de México, Mexico, [4] Laboratorio de Fitoquímica, Posgrado de Botánica, Colegio de Postgraduados, Texcoco, Mexico

Keywords: bacteriophage, drug repurposing, nanoparticles, antimicrobial peptides, quorum quenching, biofilms, probiotics

Editorial on the Research Topic

Alternatives to Combat Bacterial Infections

OPEN ACCESS

Edited and reviewed by:
Rustam Aminov,
University of Aberdeen,
United Kingdom

****Correspondence:***
Rodolfo García-Contreras
rgarc@bq.unam.mx
Mariano Martínez-Vázquez
marvaz@unam.mx
Bertha González-Pedrajo
bpedrajo@ifc.unam.mx
Israel Castillo-Juárez
israel.castillo@colpos.mx

Specialty section:
This article was submitted to Antimicrobials, Resistance and Chemotherapy, a section of the journal Frontiers in Microbiology

Received: *31 March 2022*
Accepted: *06 April 2022*
Published: *04 May 2022*

Citation:
García-Contreras R, Martínez-Vázquez M, González-Pedrajo B and Castillo-Juárez I (2022) Editorial: Alternatives to Combat Bacterial Infections. Front. Microbiol. 13:909866. doi: 10.3389/fmicb.2022.909866

In 2019, infections due to multidrug resistant (MDR) bacteria caused 1.27 million deaths (Collaborators, 2022), and the projections indicate that if the current prevalence of antibiotic resistance continues increasing and if no new effective therapies are implemented, in the year 2050, there will be around 10 million deaths worldwide because of these infections (de Kraker et al., 2016). Hence, the World Health Organization has urged for the development of new antibiotics or other alternatives to combat MDR bacteria. Of particular importance are those bacteria belonging to the ESKAPE group since they are responsible for difficult or impossible to treat nosocomial infections related to multidrug and pan drug resistance. Many other bacteria such as members of the *Mycobacterium* genus or the Enterobacteriaceae family are also a serious threat to global health. In this Research Topic, 30 excellent articles dealing with different proposals of alternatives to combat bacterial infections are included.

BACTERIOPHAGES AND PHAGE COMPONENTS

Bacteriophages are viruses that replicate and kill bacteria and although they have been used in some eastern European countries, their use in western medicine remains underutilized due the availability and efficacy of antibiotics. However, currently there is renewed enthusiasm, and several researchers and clinical doctors are working in their utilization to treat recalcitrant infections.

In the research of Manohar et al. the effect of bacterial coinfections during pulmonary viral disease was studied, with an emphasis on COVID patients. Viral respiratory infections increase the susceptibility for bacterial infections, which cause epithelial damage and mucociliary clearance impairment. Around 50% of the deaths of infected SARS-COV-2 patients are caused by secondary MDR bacterial infections; hence bacteriophages or phage components like endolysins could reduce the mortality of coinfected patients, since phages are specific, self-replicating, nontoxic to hosts, and can have synergy with antibiotics.

In the review by Kumar et al. an overview of resistance and the role of anthropogenic sources and commercial livestock as generators of resistance on a global scale are discussed. Also, they uncovered some of the main unconventional and novel strategies currently being investigated that have the potential to reduce infections and to prevent the increase in resistance. Some of them are the identification of stem cell-derived antimicrobial peptides, CRISPR-Cas based

therapies, nanoantibiotics, fecal transplantation, immunotherapies, microbial therapies (probiotics, postbiotics, and synbiotics), and phages, as well as the inhibition of quorum sensing (QS).

DRUG REPURPOSING AND COMBINATION THERAPIES

Repurposing drugs for their utilization as antimicrobials could significantly accelerate the implementation of novel antimicrobial therapies that otherwise may take decades to be launched. Gallium nitrate, previously used for hypercalcemia in malignity, was repurposed as an antibacterial agent for treating infections in humans (Goss et al., 2018). Gallium is a non-REDOX mimetic form of Iron 3^+, which is incorporated into iron-containing enzymes rendering them unable to perform their functions. Gallium also sequesters pyoverdine, the main siderophore of *P. aeruginosa*, decreasing iron uptake. Zemke et al. demonstrated that combining gallium treatment with nitric oxide (NO) had synergistic effects against *P. aeruginosa*, since nitrosative stress induces damage to iron metalloproteins both in aerobic and anaerobic conditions. Furthermore, *P. aeruginosa hitA* mutants resistant to gallium (García-Contreras et al., 2013) were also sensitized by nitrite.

An example that suggests that the combination of drugs prevents resistance to enterococci is the research carried out by Jiang et al. In their study, they analyzed five clinical isolates of *Enterococcus*, identifying that resistance to linezolid was due to mutations in ribosomal proteins, while resistance to fosfomycin in some isolates was due to mutations in *murA*. In these strains, two synergistic combinations of linezolid and fosfomycin were able to suppress the selection of resistant mutants. These results prove that a correct combination of linezolid with fosfomycin favors synergy and reduces resistance induction.

Li et al. used high-throughput screening and drug repurposing to develop combined therapy of a tetracyline antibiotic and an AMP to combat *P. aeruginosa*. They showed that this combination had a significant synergistic effect on antibacterial activity as compared to monotherapies. Also, the effectiveness of the combined approach was verified *in vivo* in a cutaneous murine model of infection, in which both the abscess size and inflammation of the skin abscess caused by this pathogen were considerably reduced with the treatment. These data illustrate the relevance of improving the effects of existing antibiotics as an encouraging method to enhance the efficacy of antibacterial treatments.

NANOPARTICLES AND BACTERICIDAL COMPOUNDS

Nanoparticles containing metals such as silver and copper have been shown to be effective antibacterial compounds, in addition they can be used as carriers of bactericidal compounds and their synthesis using extracts from plants is simple and scalable. Cheng et al. synthesized silver nanoparticles using *Canna indica* L, Cosmo bipinnata Cav., and Lantana camara flower aqueous extracts and tested them against the phytopathogen Ralstonia solanaceum. The functionalized silver nanoparticles were characterized by UV-visible spectroscopy, FTIR, and XRD. The results showed that *L. camara* silver nanoparticles had the smallest particle size and the highest effect on bacterial growth, biofilm formation, swimming motility, efflux of nucleic acid, cell death, cell membrane damage, and ROS generation. The silver nanoparticles synthesized with the *L. camara*, *C. bipinnata,* and *C. indica* flower aqueous extracts could be used as an efficient and environmentally friendly antibacterial agent against *R. solanaceum*.

The bactericidal actions of Azadirachta indica are well known (Herrera-Calderon et al., 2019). As a new proposal to fight bacterial infections, a hydrogel constituted by silver particles synthesized from an aqueous extract of *A. indica* loaded on PF127, a biocompatible-biodegradable polymer, was used. *A. indica* silver nanoparticles (AI-AgNPs) are effective antibacterial compounds, showing higher antioxidant effects than leaf extracts alone. Additionally, the AI-AgNPs did not show toxicity on *Drosophila melanogaster*. The application of the AI-AgNPs-PF127 hydrogel improved the wound contraction rate in mice. The synergistic interactions between the Ag^+ ions and phytochemicals in the extract formed stable bioactive AI-AgNP molecules that displayed better antibacterial efficacy than the AI extract (Chinnasamy et al.).

Enterococci, normal microbiota in the gastrointestinal tract of humans, can infect wounds, the bloodstream, and urinary tract. *Enterococcus faecalis* are the cause of most infections which are difficult to treat due to resistance against antibiotics. Xiong et al. evaluated the antibacterial properties of telithromycin, a semi-synthetic derivative of erythromycin, against a panel of 280 *E. faecalis* and 122 *E. faecium* isolates, finding good antibacterial activity. Moreover, telithromycin also showed antibiofilm activity at growth sub inhibitory doses, and at higher doses, combined with ampicillin, it was able to kill biofilm cells and reduce established biofilms. This is a promising alternative for the successful treatment of enterococci infections.

ANTIMICROBIAL PEPTIDES AND COMPOUNDS

One of the most promising alternatives for combating MDR bacterial infections are antimicrobial peptides (AMPs), which are part of the innate immune response of mammals and other animals. AMPs disrupt the membrane of pathogens and have immunomodulatory effects, hence, their utilization in antibacterial activities is very attractive.

Staphylococcus aureus is a Gram-positive bacterium of the ESKAPE group. In their work, Zhang X et al. evaluated the mechanism of the novel antimicrobial agent isopropoxy benzene guanidine (IBG) against *S. aureus*. IBG has a low MIC against several *S. aureus* strains, including MRSA. The IBG mechanism of action involves membrane disruption and lysis. Remarkably, the rate of resistance selection against this compound was very low, compared to the resistance selection against ciprofloxacin.

Moreover, IBG increased the survival of mice with septicemia approximately 4-fold relative to untreated mice.

AMPs are less prone than regular antibiotics to induce resistance; however, resistance mechanisms against them exist. In their review work, Assoni et al. discuss the known mechanisms of AMP resistance in Gram-positive bacteria. These include modifications of the membrane and cell wall, reduction of the negative charge of the bacterial surface, decrease in peptide affinity, efflux pumps that expel the peptides, variation in the capsule polysaccharide, and, in some cases, AMP sequestration and cleavage by proteases.

The implementation of AMPs in the clinic is challenging because of their high development and production costs, cytotoxicity, reduced activity in clinically relevant environments, and bacterial resistance. Furthermore, AMPs acting on membranes are not entirely selective for microbes. Several strategies have been designed to overcome these challenges, such as the preparation of ultra-short/truncated AMPs, delivery systems, chemical modifications, and the careful selection of a counter-ion in the last step of AMP synthesis. Nonetheless, several AMPs in clinical trials have failed. The following practical strategies should be considered in future clinical testing: defining optimal doses and administration of regimens to reduce cytotoxicity, including bacterial resistance development as a primary outcome parameter in the trials, the bioavailability and efficacy of AMPs can be improved using delivery systems, and combining AMPs with antibiotics or other compounds might improve antimicrobial effects (Dijksteel et al.).

Bacillus produce several polypeptide antibiotics. Some of them like bacitracin, gramicidin S, polymyxin, and tyrotricidin are used in the clinic (Yilmaz et al., 2006). In the paper of Lin et al., three *Bacillus* strains with excellent antimicrobial properties named JFL21, LQG17, and LQG36, were isolated and identified to be related to *B. amyloliquefaciens, B. subtilis,* and *B. halotolerans,* respectively. The antimicrobial substances produced by *B. amyloliquefaciens* JFL21 had low toxicity to most probiotics but exhibited strong and extensive antimicrobial activities against MDR foodborne pathogens. The FITR, HPLC, and MALDI-TOF MS analysis revealed that the partially purified anti-JFL21 substance comprises multiple lipopeptides of the surfactin, fengycin, and iturin families. Fengycins were also highly stable against a variety of enzymes, chemical reagents, and extreme conditions.

Another work on the topic of dealing with AMPs was that of Mazumdar et al., in which two peptides derived from a bacteriocin of *Lactobacillus casei* were designed, synthesized, and characterized. Remarkably, both peptides showed low MICs (10 to 30 μg/ml) against *E. coli* and several Gram-positive pathogenic bacteria, including methicillin and vancomycin-resistant *S. aureus* (MRSA and VSRA) and *Enterococcus faecalis* resistant to vancomycin. The peptides caused damage to the bacterial cell wall leading to leakage of intracellular content and bacterial death, and were also effective against clinical strains isolated from wounds. In contrast, they presented low toxicity against mammary glands and epithelial cells and were effective at promoting bacterial clearance *in vivo* and recovery of mice infected with VRSA, making them very promising for the eventual treatment of animal or human infections.

PROBIOTICS

Probiotics are beneficial microorganisms that promote intestinal health when consumed, due to their regulatory effects in the microbiota and metabolism. In their work, Zeng et al. isolated *Bacillus* proteolyticus (Z1 and Z2), *Bacillus amyloliquefaciens* (J), and *Bacillus subtilis* (K), from yak intestinal micro-ecosystems. Their probiotic potential was evaluated. Antioxidant activity examinations indicated that Z1 had the most elevated DPPH and hydroxyl radical scavenging activities, whereas Z2 had higher reducing power and inhibited lipid peroxidation. All strains were antagonistic to three indicator pathogens, *E. coli*, *S. aureus*, and *S. enteritidis*. These isolates also had a higher hydrophobicity, auto-aggregation, and acid and bile tolerance, all of which permitted survival and kept dangerous bacteria out of the host intestine. Importantly, all strains could be considered safe because of their antibiotic susceptibility and lack of hemolysis. This is the first study to show that *B. proteolyticus* and *B. amyloliquefaciens* isolated from yaks have a probiotic potential.

INHIBITION OF QUORUM SENSING AND BIOFILM FORMATION

Biofilms are the preferred lifestyle of bacteria and are involved in approximately 60% of infections; they shield bacteria from several stressors, including antibiotics, increasing their tolerance up to 1,000-fold. Part of the maturation of biofilms is mediated by QS that allows bacteria to sense their population density and change gene expression accordingly. In their review, Zhou et al. described the regulatory circuits of QS in Gram-positive bacteria, and the approaches to interfere with them that led to biofilm inhibition, degradation of signal molecules, receptor blocking, and inhibition of QS cascades. They identified several approaches for the discovery of more QS-interfering agents and discussed the application of QS inhibitors in the clinic, food industry, and water treatment strategies.

Sethupathy et al. reported the activity of 51 indole derivatives on the inhibition of QS and biofilm formation in *Serratia marcescens*, of which 6-fluoroindole and 7-methylindole stood out for their ability to reduce virulence, QS, and biofilms.

Valliammai et al. identified a strong anti-virulence activity of thymol on methicillin-resistant *Staphylococcus aureus*. Also, thymol exhibited SarA-dependent anti-biofilm activity reducing its ability to adhere to glass and metal surfaces. Similarly, it improved the bactericidal, biofilm, and persistent cell eradication efficacy of rifampicin.

An et al. reviewed biological and computational methods for designing mechanism-informed anti-biofilm agents. They postulated the use of omics analyses to provide a biological approach to the complex processes of biofilm formation, uncovering many potential protein targets and pathways required for biofilm formation in a variety of species. To find modulators for these targets, they completed a virtual screening

of large databases of molecules before experimental validation. Another approach to identify novel anti-biofilm agents is through machine learning, where a computational model is trained using a collection of known antibiofilm and non-antibiofilm molecules and then is used to find potential previously unknown antibiofilm compounds. Finally, these new agents must be evaluated in biologically accurate biofilm models including *in vitro*, *in vivo,* and organoid-on-a-chip models.

A. baumannii has a QS system (*abaI*/*abaR*) mediated by acyl-homoserine-lactones (AHLs) and several quorum quenching (QQ) enzymes. Nevertheless, the roles of this complex network in the control of the expression of surface-associated motility and biofilms are not evident. Therefore, the effect of the mutation of the AHL synthase *abaI* and the exogenous addition of the QQ enzyme Aii20J on surface-associated motility and biofilm formation in *A. baumannii* ATCCR 17978TM was studied. The results showed that extracellular DNA is a main component of the extracellular matrix in *A. baumannii* biofilms since the QQ enzyme Aii20J and DNases reduced biofilm formation in all tested strains. These findings revealed that QQ strategies combined with other enzymes such as DNase can prevent *A. baumannii* colonization and survival on surfaces (Mayer et al.).

Another important health problem affecting millions of people are dental caries, caused by the bacterial metabolism of species such as *Streptococcus mutans*, which catabolize carbohydrates producing acid. The expression of acid resistance mechanisms is fundamental for the survival of these bacteria, among them, F0F1-ATPase expels protons from the cytosol. Zhang M et al. evaluated bedaquiline, an inhibitor of this enzyme used for MDR tuberculosis, against *S. mutants* and related bacteria. They found that bedaquiline had bacteriostatic activity and an antibiofilm effect at acidic pH. It also showed low cytotoxicity, selectively attacking caries promoting bacteria in acidic environments.

Sateriale et al. evaluated the effect of hydroethanolic extracts (rich in polyphenols) of myrtle leaf and dry pomegranate fruit peel, alone and in combination, on biofilm formation of *S. mutans*, *S. oralis*, *S. mitis,* and *Rhotia dentocariosa* oral isolates, finding effective concentrations in the range of 10 to 40 mg/ml. Moreover, at higher concentrations the extracts eradicated preformed single and multispecies biofilms. Although oral biofilm such as dental plaque is complex, this study encourages further investigation into the implementation of polyphenolic extracts for the inhibition of dental plaque.

PHOTODYNAMIC THERAPY

One novel approach to combat MDR bacterial infections is the utilization of photosensitizer compounds that react with light-producing reactive oxygen species, killing bacteria. In their work, Maldonado-Carmona et al. encapsulated a porphyrin derivate into acetylated lignin nanoparticles, and characterized the physicochemical characteristics of the particles. They showed that the particles were stable in a wide pH range (4–10) and retained their activity after 2 months. The encapsulated compound generated an oxygen singlet and was effective for killing both Gram-negative and positive bacteria including *P. aeruginosa* and *S. aureus*, when exposed to white light, targeting the cell wall. The utilization of these kinds of antimicrobials in topical infections could be effective to treat MDR bacteria.

In addition to the use of exogenous photosensitizers, violet and blue light directly excite endogenous molecules present in bacteria allowing the production of reactive oxygen species upon contact with O_2. Based on this phenomenon, Hoenes et al. evaluated the effect of this radiation in ESKAPE bacteria. Light irradiation decreased the colony-forming units of all tested bacteria in a dose response manner; interestingly the most sensitive bacteria were *Acinetobacter*, the number one critical bacteria for which it is urgent to develop new antimicrobials.

Another work dealing with the application of photodynamic therapy for the treatment of bacterial infections was done by Zhao et al. They used protoporphyrin IX-methyl ethylenediamine (PPIX-MED) as a photosensitizer which produced an oxygen singlet, and was first tested *in vitro* against clinical isolates of *E. coli*, *P. aeruginosa,* and MRSA *S. aureus*. The compound had MIC100 and bactericidal concentrations in the micromolar range. Later, its effect alone and in combination with ceftriaxone for treating mixed infections in burned rats was tested. The treatment, including the antibiotic plus PPIX-MED and light, promoted faster healing of the wounds than treatments with PPIX-MED or ceftriaxone alone, resulting in a decrease in bacterial counts in the wounds and blood, neovascularization, and wound.

Beyond their applications for human and animal infections, photosensitizers can also be used to treat plant diseases, such as citrus canker, produced by *Xanthomonas citri subsp. Citri* (Xcc) which damages citrus plants and economically affects the citrus industry. Jiang et al. used photodynamic therapy to kill this bacterial pathogen. They developed a stable photosensitizer complex (PSC) which, when activated by sunlight, produces reactive oxygen species that kill bacteria. This antibacterial agent was shown to be much more potent than the copper salts currently used to control it. It also showed low toxicity on citrus leaves when using a solar simulator. Therefore, treatment with this PSC is an effective method to eradicate *Xcc* and a promising strategy to control citrus canker.

Beyond small molecules, enzymes, and bacteriophages, the utilization of certain host cells is also a robust alternative to combat MDR infections. In their review work, Russell et al. explain that mesenchymal stromal cells (MSCs) have several direct and indirect mechanisms that make them suitable for this purpose. Among the direct mechanisms, these cells are producers of AMPs, indoleamine 2,3-dioxygenase, and nitric oxide, and result in phagocytosis. Indirect mechanisms include recruitment of immune cells, macrophage stimulation, and phenotype modulation. Then they discuss what is known about the interaction of MSCs with antimicrobials, and provide current evidence supporting their beneficial effects in veterinary medicine.

The elucidation of the resistance mechanisms against antibiotics in MDR bacteria helped to identify therapeutic targets for the development of antibacterials. In this regard, Yang et al. evaluated the role of the cytosolic glucosaminidase

NagZ in the overexpression of the chromosomally encoded β-lactamase AmpC in *Enterobacter cloacae*, using clinical isolates. The findings revealed a higher expression of *nagZ* and *ampC* in isolates resistant to one 3rd or 4th generation cephalosporin, relative to sensitive ones, correlating with higher β-lactamase activity. Moreover, deletion of *nagZ* in a resistant isolate decreased its β-lactam resistance, while ectopic expression of *nagZ* in a sensitive isolate, rendered it resistant. Their work indicates that the mechanism of the NagZ-mediated *ampC* overexpression is due the production of 1,6-anhydromuropeptides by NagZ, which activates AmpR).

In addition to finding new drugs for the treatment of MDR bacterial infections, it is also important to optimize the administration schemes of currently used antibiotics. Song et al. compared the traditional administration of vancomycin [intermittent i.v. infusion (ITII)] with a newly designed two-step infusion method (OTSI), using pharmacokinetic and pharmacodynamic modeling. Their analysis indicated that the new method outperformed the traditional one for the treatments of several infections including pericarditis, mastitis, bacteremia, and pleura infections, and could be effective to treat infections caused by isolates of bacteria such *E. faecalis*, *S. aureus*, *S. epidermidis*, and S. *bovis* with high MICs against vancomycin.

NOVEL ANTIBACTERIAL MECHANISMS

Classical antibiotics disrupt processes such as cell wall synthesis, protein synthesis, DNA replication, and membrane integrity, nevertheless many other processes and targets are also essential for bacterial replication or viability and hence could be exploited as novel antibacterial targets. In an interesting work, Chen et al. investigated the details of the antibacterial agent cryptotanshinone (CT), which is a quinone isolated from the plant *Salvia miltiorrhiza*, which has a wide antibacterial effect against Gram-positive bacteria. They demonstrated that it has bacteriostatic activity and that it targets the membrane-causing dissipation of membrane potential. Further experiments showed that CT is a respiratory chain inhibitor, specifically targeting type II NADH:quinone dehydrogenase, a fact that would provide specificity due to the lack of this enzyme in mammalian mitochondria. Another attractive property of CT is that it has synergistic effects with respiratory inhibitors that have different targets, and hence a possible combinatory therapy may be formulated to combat MDR Gram-positive infections.

EFFLUX PUMPS

Efflux pumps simultaneously confer resistance against several antibiotic classes. In their opinion work, Nazarov et al. discuss the main efflux pump in *Escherichia coli*, the AcrAB-TolC system, and its role in resistance against the novel antimicrobial agent SkQ1, which interferes with bacterial bioenergetics. SkQ1 is effective against Gram-positive bacteria—it is *E. coli*-resistant—since AcrAB-TolC effluxes SkQ1. Regarding other Gram-negative bacteria that have the AcrAB-TolC pump, some of them like *Klebsiella pneumoniae* that have an identity of 91.5% with the pump of *E. coli* are also resistant, while others which have lower identities are sensitive, indicating their AcrAB-TolC pump is unable to efflux SkQ1. Hence, although being phylogenetical homologs, they are not homologous in function and should be considered paralogs.

AUTHOR CONTRIBUTIONS

All authors listed have made a substantial, direct, and intellectual contribution to the work and approved it for publication.

FUNDING

RG-C research is funded by CONACYT grant CB 2017–2018 number A1-S-8530 and by DGAPA-UNAM grant no. IN214218. BG-P research is funded by DGAPA-UNAM grant no. IN212420 and by CONACYT grant no. 284081. IC-J research is funded by Cátedras-CONACyT program.

REFERENCES

Collaborators, A. R. (2022). Analysis, Global burden of bacterial antimicrobial resistance in 2019: a systematic. *Lancet* 399, 629–655. doi: 10.1016/S0140-6736(21)02724-0

de Kraker, M. E. A., Stewardson, A. J., and Harbarth, S. (2016). Will 10 million people die a year due to antimicrobial resistance by 2050? *PLoS Med.* 13, e1002184. doi: 10.1371/journal.pmed.1002184

García-Contreras, R., Lira-Silva, E., Jasso-Chávez, R., Hernández-González, I. L., Maeda, T., Hashimoto, T., et al. (2013). Isolation and characterization of gallium resistant *Pseudomonas aeruginosa* mutants. *Int. J. Med. Microbiol.* 303, 574–582. doi: 10.1016/j.ijmm.2013.07.009

Goss, C. H., Kaneko, Y., Khuu, L., Anderson, G. D., Ravishankar, S., Aitken, M. L., et al. (2018). Gallium disrupts bacterial iron metabolism and has therapeutic effects in mice and humans with lung infections. *Sci. Transl. Med.* 10, eaat7520. doi: 10.1126/scitranslmed.aat7520

Herrera-Calderon, O., Ejaz, K., Wajid, M., Shehzad, M., Tinco-Jayo, J. A., Enciso-Roca, E., et al. (2019). Azadirachta indica: antibacterial activity of neem against different strains of bacteria and their active constituents as preventive in various diseases. *Pharmacogn. J.* 11, 1597–1604. doi: 10.5530/PJ.2019.11.244

Yilmaz, M., Soran, H., and Beyatli, Y. (2006). Antimicrobial activities of some *Bacillus* spp. strains isolated from the soil. *Microbiol. Res.* 161, 127–131. doi: 10.1016/j.micres.2005.07.001

Conflict of Interest: The authors declare that the research was conducted in the absence of any commercial or financial relationships that could be construed as a potential conflict of interest.

Publisher's Note: All claims expressed in this article are solely those of the authors and do not necessarily represent those of their affiliated organizations, or those of the publisher, the editors and the reviewers. Any product that may be evaluated in this article, or claim that may be made by its manufacturer, is not guaranteed or endorsed by the publisher.

frontiers in Microbiology

REVIEW
published: 26 June 2020
doi: 10.3389/fmicb.2020.01434

Secondary Bacterial Infections During Pulmonary Viral Disease: Phage Therapeutics as Alternatives to Antibiotics?

*Prasanth Manohar[1,2†], Belinda Loh[1†], Sudarsanan Athira[3], Ramesh Nachimuthu[3], Xiaoting Hua[4,5], Susan C. Welburn[1,6] and Sebastian Leptihn[1,4,6]**

[1] Zhejiang University-University of Edinburgh Institute, Zhejiang University, Haining, China, [2] The Second Affiliated Hospital, School of Medicine, Zhejiang University, Hangzhou, China, [3] Antibiotic Resistance and Phage Therapy Laboratory, School of Biosciences and Technology, Vellore Institute of Technology, Vellore, India, [4] Department of Infectious Diseases, Sir Run Run Shaw Hospital, School of Medicine, Zhejiang University, Hangzhou, China, [5] Key Laboratory of Microbial Technology and Bioinformatics of Zhejiang Province, Hangzhou, China, [6] Infection Medicine, Biomedical Sciences, Edinburgh Medical School, College of Medicine and Veterinary Medicine, The University of Edinburgh, Edinburgh, United Kingdom

OPEN ACCESS

Edited by:
Rodolfo García-Contreras, National Autonomous University of Mexico, Mexico

Reviewed by:
Jingmin Gu, Jilin University, China
Zhimin Guo, The First Hospital of Jilin University, China

***Correspondence:**
Sebastian Leptihn
Leptihn@intl.zju.edu.cn

[†]These authors have contributed equally to this work

Specialty section:
This article was submitted to Antimicrobials, Resistance and Chemotherapy, a section of the journal Frontiers in Microbiology

Received: 11 May 2020
Accepted: 03 June 2020
Published: 26 June 2020

Citation:
Manohar P, Loh B, Athira S, Nachimuthu R, Hua X, Welburn SC and Leptihn S (2020) Secondary Bacterial Infections During Pulmonary Viral Disease: Phage Therapeutics as Alternatives to Antibiotics? Front. Microbiol. 11:1434. doi: 10.3389/fmicb.2020.01434

Secondary bacterial infections manifest during or after a viral infection(s) and can lead to negative outcomes and sometimes fatal clinical complications. Research and development of clinical interventions is largely focused on the primary pathogen, with research on any secondary infection(s) being neglected. Here we highlight the impact of secondary bacterial infections and in particular those caused by antibiotic-resistant strains, on disease outcomes. We describe possible non-antibiotic treatment options, when small molecule drugs have no effect on the bacterial pathogen and explore the potential of phage therapy and phage-derived therapeutic proteins and strategies in treating secondary bacterial infections, including their application in combination with chemical antibiotics.

Keywords: secondary bacterial infection, pulmonary viruses, SARS-CoV-2, COVID-19, phage therapy, phage endolysins

INTRODUCTION

The past two decades have seen the emergence of four severe viral outbreaks including the 2002 Severe Acute Respiratory Syndrome (SARS) Coronavirus (CoV) epidemic, the 2009 influenza A H1N1 pandemic, 2012 Middle East Respiratory Syndrome (MERS) outbreak, and most recently the COVID-19 pandemic. Emergence of novel lethal CoV strains in human populations are becoming more frequent and are of increasing global concern; SARS-CoV-2, a novel CoV that caused a first major outbreak in China in 2019 has now infected almost 8 million people globally and resulted in 434,000 deaths (as of June 15, 2020), a far greater disease burden than SARS and MERS (Guarner, 2020; Kannan et al., 2020). The spectrum of clinical presentations of COVID-19 is highly variable; infections range from being asymptomatic to severe viral pneumonia with respiratory failure, often leading to death (Li et al., 2020). During an epidemic, or pandemic, early development and roll-out of antiviral treatments that can reduce morbidity and mortality is critical. However, even with many potential repurposed and new anti-viral drug candidates able to inhibit replication or attachment of the virus, a major consequence of

disease progression in patients at later stages of infection, are secondary bacterial infections. At least one in seven COVID-19 patients was found to be additionally infected with a secondary bacterial infection with 50% of the fatalities during the SARS-CoV-2 epidemic caused by untreated or untreatable secondary bacterial infections, in most cases in the lung (Zhou et al., 2020). While antibiotics do not have impact on the virus itself, almost all seriously ill patients are treated with antibiotics to attempt to prevent the occurrence of secondary bacterial infections. Any surge in antibiotic use during the COVID-19 pandemic will have a detrimental effect on antibiotic resistance rates for nosocomial bacterial pathogens, fueling global growth of antibiotic resistant bacterial pathogens (Reardon, 2020).

Secondary Bacterial Infections

Secondary bacterial infections develop in patients during or after initial infection with an infective pathogen, often a virus (Morris et al., 2017; Wang et al., 2018) and are associated with high morbidity and mortality rates (**Figure 1**) (Mallia et al., 2012). Co-infections, secondary infections, or "superinfections" occur during viral epidemics; around 50 million deaths were ascribed to bacterial co-infections during the 1918–1919 Spanish Flu pandemic; although clinical records often do now record such infection complications (Kash and Taubenberger, 2015; MacIntyre et al., 2018). While secondary infections occur in succession to the primary infection, co-infections are caused by multiple pathogens of viral, bacterial, or fungal origin and occur simultaneously at the same time. There tends to be a strong focus on a single pathogen rather than a combination of pathogens, especially for the viral–bacterial infections most commonly observed in patients (Jamieson et al., 2010). *Staphylococcus aureus*, *Streptococcus pneumoniae*, *Neisseria meningitides*, *Haemophilus influenzae*, *Klebsiella pneumoniae*, and members of the genus *Proteus*, *Enterobacter*, and *Citrobacter* spp., are some of the most commonly isolated bacteria during secondary infections (Handel et al., 2009). Hospitals are a common source of the pathogens that cause secondary infections, these so-called nosocomial pathogen infections are acquired from an environment in which antibiotics are commonplace, and as such; many have acquired resistance to a broad range of antibiotics. Decades of misuse and, over-prescribing of antibiotics has resulted in selection of pathogens that show multi-drug resistance (MDR). MDR is a global health challenge as in many cases no (chemical) antibiotics exist to treat such infections, including secondary infections. Secondary bacterial infections are facilitated by the exposure to a pathogen together with an immune system that is inapt to appropriately react to both pathogen types, as a consequence of the primary viral infection. For such patients, the only option is to support their immune system and prevent progression of the infection that could lead to the death of the patient such as septic shock. Antibiotics therapies deployed as a "last resort" or the use of exceptionally high doses of antibiotics often have negative consequences. Many key human pathogens are showing resistance to antibiotics including Methicillin-resistant *S. aureus* (MRSA), multidrug-resistant *Streptococcus*, Vancomycin-resistant *Enterococci* (VRE), resistant *Mycobacterium*, Carbapenem-resistant *Enterobacteriaceae* (CRE), Colistin-resistant *Klebsiella*, Carbapenem-resistant *Pseudomonas aeruginosa*, and Carbapenem-resistant *Acinetobacter baumannii* (Kumar and Chordia, 2017). The problem is exacerbated by the discontinuation by big pharma of chemical antibiotics discovery programs in the search for chemical antibiotics (Loh and Leptihn, 2020). Other options to treat MDR infections would be beneficial.

Molecular Basis of Manifestation of Secondary Bacterial Infections

There are several hypotheses why secondary infections quickly establish in patients with a pulmonary viral infection, including immunological host changes, mechanical damage and diffusion, and removal of mucus within the lungs. Much of how secondary infections manifest themselves and what role the immune response to a virus influences the defense against a prokaryotic pathogen, is poorly understood. The prevalence of secondary bacterial infections during a primary virus disease is due to the altered immune response to one pathogen (here: the virus) that often changes the response of the system to the other infectious agent (here: the bacterium), resulting in increased morbidity (Hendaus et al., 2015). Severe viral infections initiate changes in the immune response of the host that persist for a prolonged period of time. These immune alterations termed "trained immunity," "innate imprinting," or "immune paralysis," change the inflammatory response of immune cells (Williams et al., 2004; Bordon, 2014; Cheng et al., 2014; Roquilly et al., 2017; Morgan et al., 2018). In addition, viral infections of the respiratory system can lead to immune responses that alter the microbiome of the host. This change in the microbiome has been suggested to possibly modulate immune cell priming against secondary bacterial challenge (Hanada et al., 2018).

In most cases, epithelial cells are damaged during the primary viral infection, impeding mucociliary clearance that leads to an accumulation of mucus (Perry et al., 2005). Bacteria are able to diffuse into the mucus but thickened dense mucus impedes penetration of host immune cells. Secondary bacterial infections are also facilitated by the immune response of the host to a viral attack. One of the more important factors seems to be the immunosuppression of the host innate immune response initiated by the viral infection which facilitates opportunistic bacteria, like *Streptococcus* to infect the host (Kim et al., 2011). Cells of a host suffering from a viral infection are more susceptible to bacterial attachment and colonization (Pittet et al., 2010; Nyangacha et al., 2017). Many viruses, including influenza virus, rhinovirus, and respiratory syncytial virus (RSV), have detrimental effects on the mucosal layer facilitating bacterial adherence of, e.g., *S. pneumoniae*, *P. aeruginosa*, and *H. influenzae*, as well as biofilm formation on the linings of the lungs (Morris, 2007). For some pulmonary viruses such as influenza, Toll-like receptor (TLR) pathways are altered, possibly from sustained de-sensitization, which results in an increase of attachment of bacteria to epithelial cells (Kurt-Jones et al., 2000; Haynes et al., 2001). TLR and RIG-I-like receptor activation results in the production of Type I Interferon, changing the inflammatory response to TLR ligands,

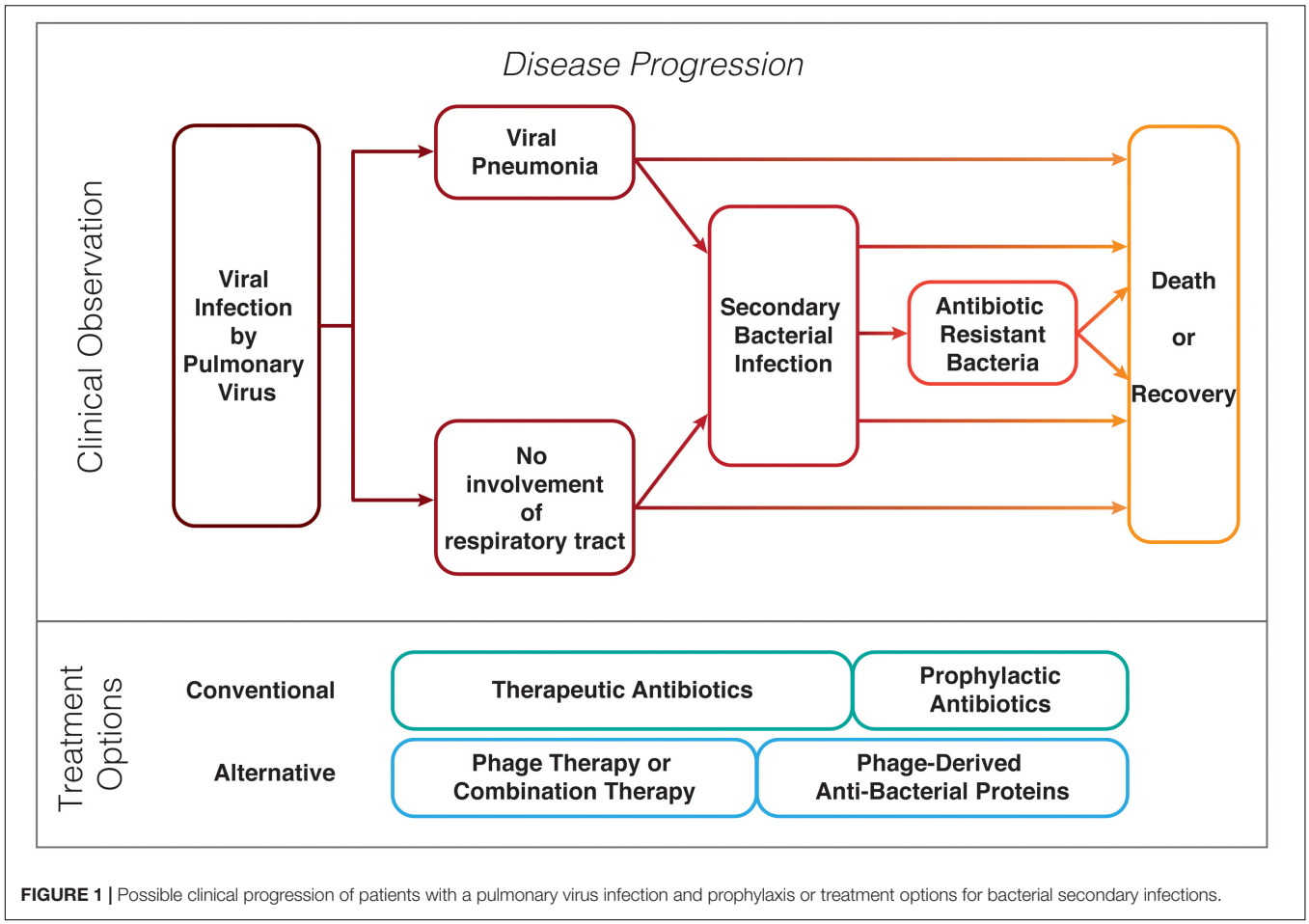

FIGURE 1 | Possible clinical progression of patients with a pulmonary virus infection and prophylaxis or treatment options for bacterial secondary infections.

e.g., bacterial lipopolysaccharide (Doughty et al., 2001; Nansen and Thomsen, 2001). Polymicrobial, viral–bacterial co-infections can develop as a result of an altered immune response combined with accessible routes of entry for the bacterial pathogen(s).

For patients with viral–bacterial infections, the availability of therapeutic options for both infectious agents is crucial. Antivirals are deployed to combat the virus, which have no effect on the bacterial pathogens (McCullers, 2011), and bacterial infections are treated with antibiotics, or such small-molecule compounds to try and prevent secondary infections. Broad-spectrum antibiotic may result in undesirable inflammatory responses in the afflicted person (Brook, 1995, 2002; Mahar et al., 2014). To prevent complications caused by secondary bacterial infections and to eliminate bacterial pathogens, alternative antibacterial therapies are needed.

Coronavirus, Pneumonia, Antibiotics, and Antibiotic Resistance

Some of the most significant outbreaks, epidemics, and global pandemics, with high morbidities and mortality are from viral respiratory infections caused by influenza virus or CoV species; for which treatment is compromised by secondary bacterial infections (Yang et al., 2020; Zhou et al., 2020). While a viral infection alone can be detrimental to a patient, the pathogen that exasperates disease progression is most commonly of bacterial origin (Yang et al., 2020). During the 2009 H1N1 influenza pandemic, between 29 and 55% of fatal cases were caused by secondary bacterial infections (Center for Disease Control and Prevention, 2012). During the ongoing COVID-19 pandemic, around 15% of hospital cases have been associated with secondary bacterial pathogens, and 50% of patients died (Zhou et al., 2020). Clinical cases of COVID-19 have developed high rates of up to 50% of secondary bacterial infections leading to secondary bacterial pneumonia. Half of COVID-19 fatalities experienced some form of secondary infection (pulmonary or other) that may have contributed to their death. During severe COVID-19 disease with pneumonia, the air sacs of the lungs fill with pus and fluids, nutritious substrates for pathogens including *P. aeruginosa* and *S. aureus*. Tissues are breached by the cytolytic activity of the virus and bacteria invade deeper into the tissue, continuing to secrete toxins that further destroying surrounding cells. The frequency (30–40%) of complications due to bacterial involvement was significantly higher in fatal COVID-19 patients than for COVID-19 survivors (Zhou et al., 2020). In fatal COVID-19 cases, death is most frequently a result of respiratory failure from severe pneumonia, caused either by SARS-CoV-2 itself or as a result of a secondary bacterial infection (Tetro, 2020).

Patients suffering of a pulmonary virus infection, including COVID-19, are often administered prophylactic antibiotics, including azithromycin, moxifloxacin, ceftriaxone, vancomycin, or cefepime, to reduce the risk of secondary infections; often in addition to another antibiotic that is deployed once the infection is identified (Holshue et al., 2020; Wang et al., 2020). As the numbers of antibiotic-resistant bacterial strains continue to grow, there is increased the risk of superinfection in severely ill patients, especially in intensive care units (ICUs). During the COVID-19 pandemic, many clinical case studies of COVID-19 patients have been reported, but mainly these focus on the viral infection itself. There are few reports detailing secondary bacterial infections and even less describing AMR. Until a vaccine is deployed globally, bacterial secondary infections will continue to be important in COVID-19 clinical care. New antibiotics or alternative treatments targeted against secondary bacterial infections need to be developed for COVID-19 and subsequent pandemics.

Antibacterial Therapy in Patients With Non-bacterial Primary Infections

To reduce the risk of superinfections, cases of pneumonia caused by respiratory viruses including SARS-CoV-2 are often prophylactically treated with antibiotics that target a broad-spectrum of bacteria. The alternative, i.e., no prophylactic treatment, often results in bacterial infections, in principle, demonstrating the effectiveness of this strategy. Prophylactic use of antibiotics, however, contributes to the AMR crisis and is ineffective when patients acquire antibiotic-resistant strains—nosocomial hospital-acquired infections are commonly observed for ICU patients infected with a respiratory virus (Zhou et al., 2020). Nosocomial infections are becoming more common due to the rise of resistant bacterial pathogens. Alternative antibacterial therapeutic strategies are needed; such as phage therapy or phage-derived therapeutic proteins.

Phage Therapy and Phage-Based Strategies During Viral Epidemics

An alternative approach to treating secondary bacterial infections, especially AMR pathogens, is the application of phage therapy; using microbial viruses to kill their host, ideally clearing the bacterial infection (Altamirano and Barr, 2019). Bacteriophages are naturally occurring viruses that use bacteria as hosts after employing the host machinery for propagation, including genome replication, protein synthesis, and phage assembly (**Figure 2**). Lysogenic bacteriophages undergo a "dormant" state as non-replicative, genome-integrated phages (Monteiro et al., 2019; Hampton et al., 2020). Some filamentous phages allow the host to continue to grow and divide while the phages are being produced (Loh et al., 2017, 2019; Kuhn and Leptihn, 2019). Phage therapy was discovered before antibiotics but the opportunities from the "dawn of the antibiotic era" delayed pursuit of commercial therapeutic phage strategies (Pirisi, 2000; Housby and Mann, 2009; Manohar et al., 2019c). With increasing AMR, and depletion of antibiotic resources, phage therapy has once more piqued the interest of the scientific community and pharmaceutical industry (Seguin et al., 2006; Nyangacha et al., 2017; Manohar et al., 2019c; Loh and Leptihn, 2020). Phages and phage-derived therapeutic proteins have advantages and disadvantages as compared with antibiotic therapies (**Figure 3**).

A major advantage of phages is that they exhibit bacterial host specificity (Seguin et al., 2006) and selectively target pathogenic bacteria without adverse effects on the normal microflora (Brüssow, 2005). Phages may be genus- or species-specific, and even strain-specific, infecting and killing their target bacterium. As most secondary bacterial infections are caused by one bacterial genus, species or strain, phage therapy offers a promising treatment option. Clinical studies using phages have demonstrated success at eliminating resistant bacterial strains (Capparelli et al., 2007; Kutter et al., 2010; Chan et al., 2013). Intact phage particles do not adversely interact with human cells and are not able to cause infections in humans (Barr, 2019; Van Belleghem et al., 2019). The self-replicating nature of phages enables them to function as "active and self-replicating" drugs once administered to the patient so dosage is less important to reach therapeutic levels; however—in practice—a large quantity of phages are being deployed (Barr, 2019). Phages show low toxicity; being mainly composed of protein and DNA and eventually undergo degradation inside a patient's body. Degradation of phage particles does not result in the production of toxic molecules, unlike antibiotics that could apply strain on the liver and might result in organ failure. Since most secondary bacterial infections occur in immunocompromised or immunodeficient patients, it is necessary to study the efficacy of phage therapy under such conditions. Previous studies on cancer patients and renal allograft patients showed that phage therapy can be effective in treating secondary bacterial infections and co-infections (Weber-Dabrowska et al., 2001; Międzybrodzki et al., 2012). Phages often do not cause an immune response, in contrast to human-pathogenic viruses (Manohar et al., 2019a). The levels to which administered phages can induce immune responses have been well studied and no adverse side effects have been observed (Borysowski and Górski, 2008; Ahmadi et al., 2016; Jault et al., 2019; Voelker, 2019). While there is a lack of evidence showing the efficacy of phage therapy during viral infections, bacteriophages have been shown to be effective prophylactic agents (Ahmadi et al., 2016).

Synergistic Effects of Phages and Antibiotics

A number of factors can result in phage resistance in bacteria, such as the alteration in phage receptors on the bacterial cell surface; degradation of phage DNA by restriction endonuclease produced by the host bacteria; emergence of mechanisms inhibiting the penetration of phage DNA into the bacterial host, among others (Jo et al., 2016b; Valério et al., 2017). Under certain conditions, such as low phage to bacterium ratios, or when using a single phage to treat an infection, phage-resistant bacteria can emerge. This selection of resistant mutants is a shortcoming of phage therapy. Clinical applications often make

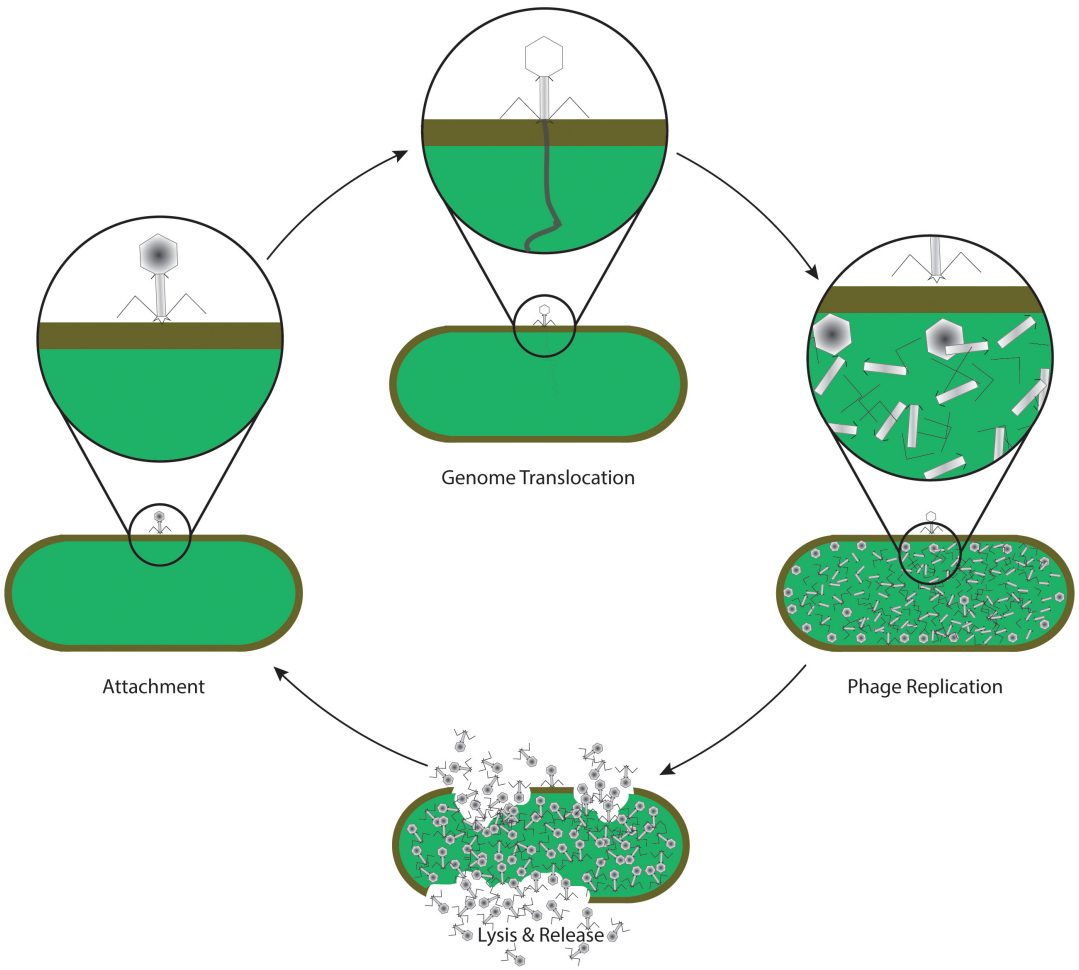

FIGURE 2 | Life cycle of a lytic phage, commonly used in phage therapy. After specific recognition and attachment to the host cell (attachment), phage proteins insert into the envelope of the cell, forming a channel through which the viral genome is translocated into the cytoplasm of the bacterium (genome translocation). The host machinery replicates the genomic information, and synthesizes phage proteins which self-assemble to form the virus structure (phage replication). Later in the life cycle, specific phage proteins such as holins and endolysins are synthesized. Enzymatic activity of endolysins leads to a disintegration of the host envelope, resulting in host cell lysis and release of phage progeny (lysis and release). The new phages are now able to attach and infect new host cells again, continuing the life cycle.

use of multiple phages, making the occurrence of multiple resistance mechanisms unlikely (Summers, 2001; Lin et al., 2017).

Another solution to overcome such limitations is to conduct combination therapy. The combined use of phages and antibiotics is expected to provide stronger suppression of bacterial growth and is expected to help reduce bacterial resistance against phages and antibiotics (different targets are used by the two agents). Recent *in vitro* and *in vivo* studies have shown improved efficacy in controlling the growth of bacterial pathogens such as *Pseudomonas fluorescens*, *Pseudomonas aeruginosa*, *Escherichia coli*, and *S. aureus* using combinations of phages and antibiotics (Torres-Barceló et al., 2016; Chaudhry et al., 2017). Phage-antibiotic therapy is reported to have higher success rates in preventing the emergence of bacterial resistance as bacteria that become non-susceptible to one agent can still be killed by the other and *vice versa*. Phage-antibiotic therapy can prevent the emergence of double resistant bacterial mutants, as a bacterium is unlikely to acquire phage and antibiotic resistance simultaneously. For the success of combination therapies, it is essential to carefully choose the dosage as well as the point of administration of each antibacterial agent. Administration of antibiotics prior to the phage resulted in the decreased evolution of phage resistance due to antibiotic stress (Torres-Barceló, 2018; Tagliaferri et al., 2019). Phage-antibiotic combinations that have different bacterial targets can assist in enhanced bacterial inactivation.

The use of sub-lethal concentrations (concentration of antibiotics lower than minimal inhibitory concentrations) of antibiotics can enhance phage productivity mediating phage induced bacterial decline (Tagliaferri et al., 2019), known as phage-antibiotic synergy. One factor proposed responsible for phage-antibiotic synergy is bacterial elongation or filamentation induced by sub-lethal concentrations of antibiotics (Kim et al., 2018). While different antibiotics exhibit different inhibitory

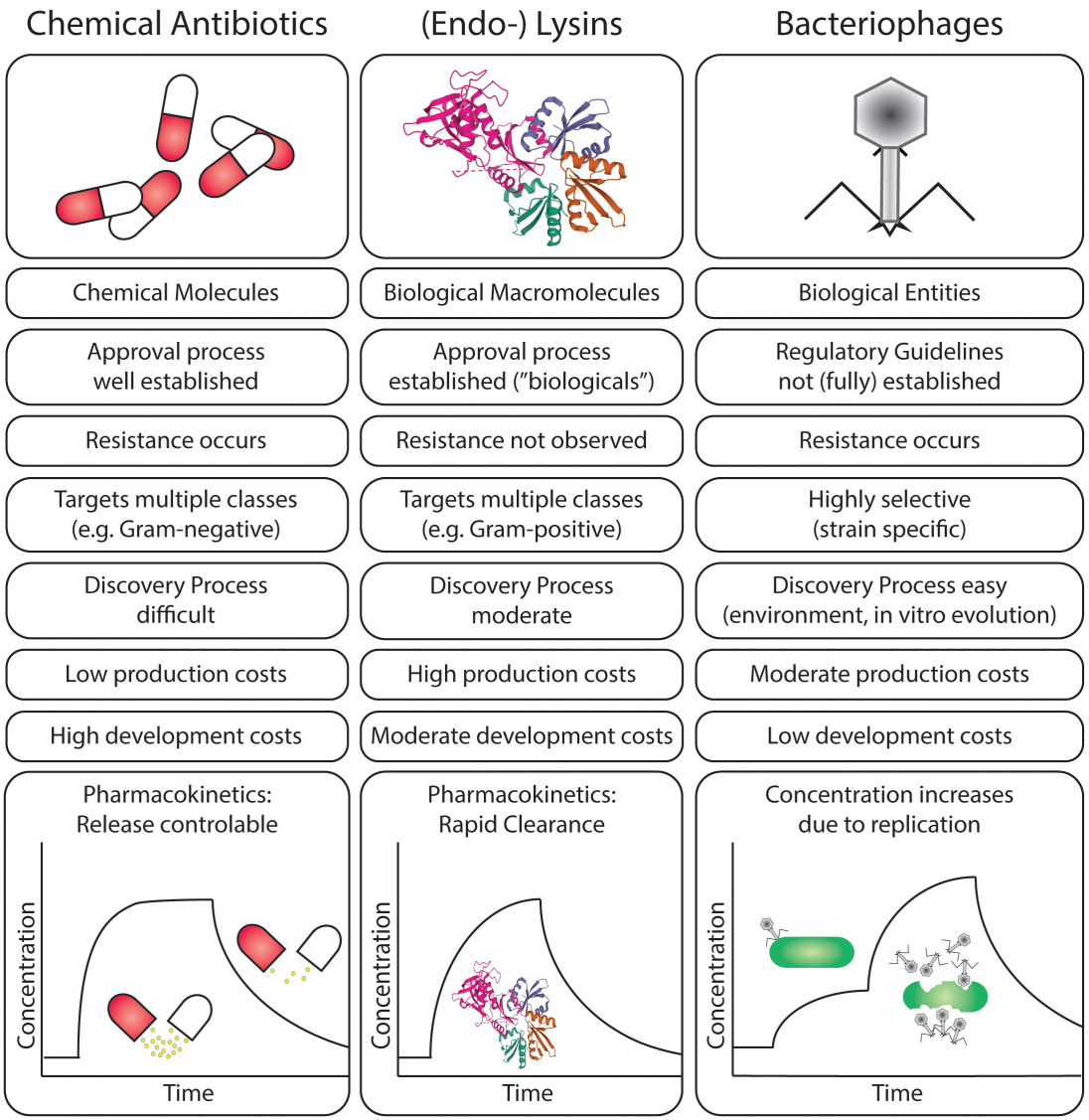

FIGURE 3 | Comparison of scientific, clinical, and pharmaceutical characteristics of chemical antibiotics, endolysins, and bacteriophages in the treatment of bacterial infections.

mechanisms, they often result in the blocking of bacterial cell division causing elongation of the bacterial cell, as a large bacterial surface area is available for phage attachment, bacterial cells are vulnerable toward phage infection, increasing the efficacy of phage lytic activity (Comeau et al., 2007; Kim et al., 2018). Antibiotic-induced morphological changes in the host bacterium can permit faster phage assembly due to altered or abundant precursors required for phage maturation, which ultimately can result in an acceleration of cell lysis (Nouraldin et al., 2016). Beta-lactam antibiotics and quinolones can stimulate virulent phage production, together with the changes induced in bacterial membrane proteins by antibiotics and may enhance the lytic activity of phages and increase phage burst size observed in phage-antibiotic studies (Jo et al., 2016a). A further advantage of using sub-inhibitory concentrations of antibiotics is avoidance of side effects from administration of otherwise necessary higher doses of the antibiotic (Knezevic et al., 2013).

Infections caused by biofilm-forming bacteria, especially nosocomial infections, are difficult to treat using antibiotics (Pires et al., 2017). The emergence of ventilator-associated secondary pneumonia is often due to biofilm forming bacteria such as *Pseudomonas* and *Staphylococcus* (Zhou et al., 2020). Phage-antibiotic therapy has shown promise for biofilms and in embedded bacteria; phages can enzymatically penetrate the microenvironment created by biofilm-forming cells to infect and kill target bacteria (Pires et al., 2017). Phages, when administered in combination with an antibiotic, can increase the susceptibility of bacteria and reduce plasmid-borne bacterial resistance by targeting plasmid bearing bacteria in the biofilm (Łusiak-Szelachowska et al., 2020). Combined phage and

antibiotic therapy with a sequential approach of administering the antibiotic after phage treatment of the biofilm has shown success; initial treatment of the biofilm with phages caused biofilm disintegration, while later administration of the antibiotic prevented biofilm regrowth as well as the emergence of phage-resistant mutants. Phages can enable antibiotics to penetrate biofilm layers by degrading the biofilm matrix; phages penetrate into deeper layers of the biofilm, replicating in the lower layers and facilitating the destruction of the biofilm (Łusiak-Szelachowska et al., 2020). Antibiotics administered following biofilm treatment by phages enhance bacterial reduction Akturk et al., 2019.

Phage Endolysins as Antibacterial Agents

Phage proteins can be extracted and also engineered for deployment as an alternative to whole phage therapeutic applications. Endolysins are phage-encoded enzymes produced at the end of the bacteriophage lytic lifecycle that facilitate release of phage progeny into the environment, degrading the peptidoglycan layer of the host bacterial cell wall (Imanishi et al., 2019). The ability of endolysins to digest the bacterial cell wall when applied exogenously offers the opportunity for their deployment as potential antibacterial agents, to target and kill pathogenic bacteria, potentially without harming the normal microflora due to specificity of enzyme activity (Haddad Kashani et al., 2017). The chances of bacteria developing resistance toward endolysins are low since endolysins target cell wall molecules essential for bacterial viability (Łusiak-Szelachowska et al., 2020). Phage-derived endolysins are promising candidates for treating secondary bacterial infections or multi-drug resistant infections (Imanishi et al., 2019; Kim et al., 2020). There are five main classes of endolysins based on their enzymatic specificity (**Figure 4**) (Schmelcher et al., 2012). Several applications for endolysins have been reported, including use in biocontrol agents against bacterial

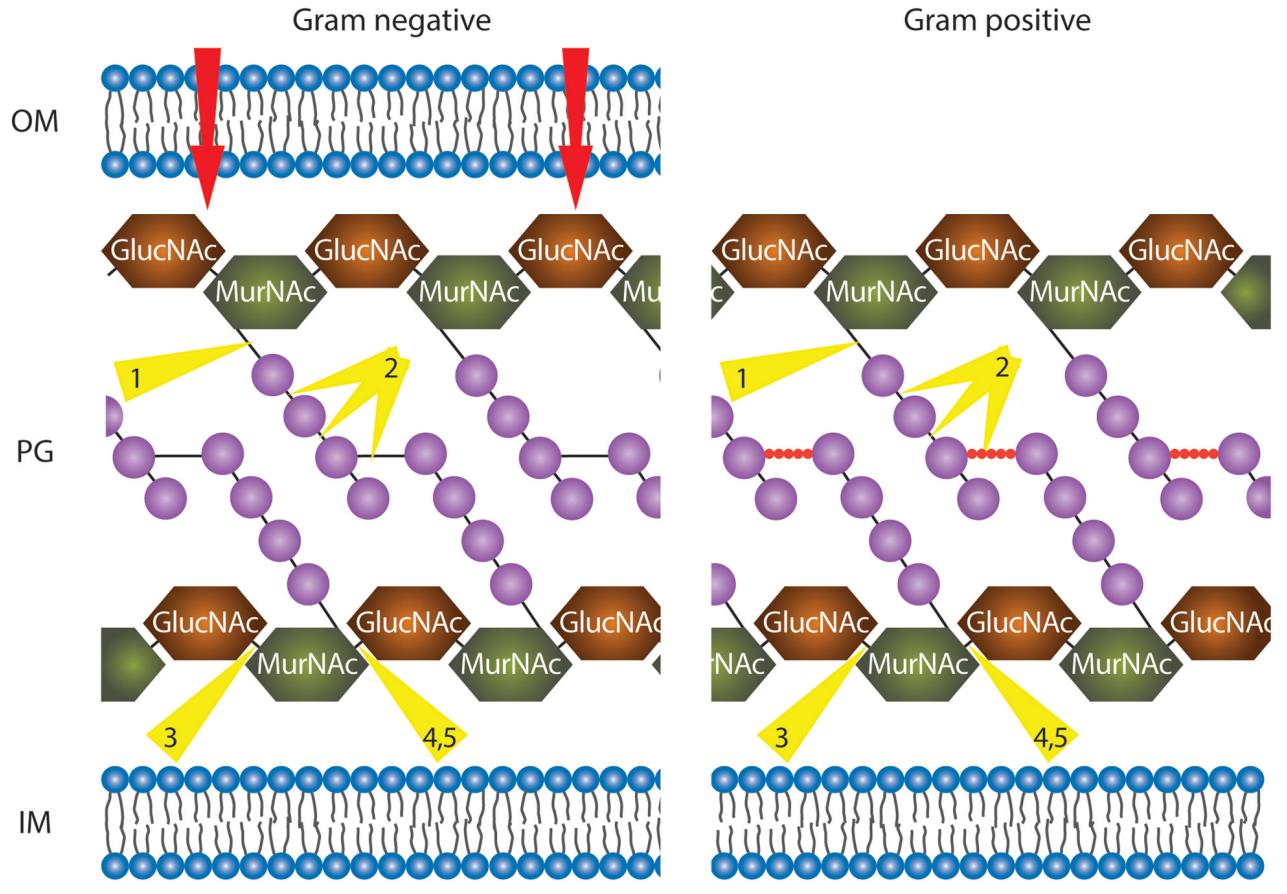

FIGURE 4 | Illustration of phage endolysins classified by their enzymatic activity. In order to reach the peptidoglycan (PG) layer, in the case of Gram-negative bacteria, the outer membrane (OM) has to be traversed (red arrows, details in text).The PG layer is represented with alternate repeating sugar units, *N*-acetylglucosamine (GlucNAc), and *N*-acetylmuramic acid (MurNAc). In Gram-negative bacteria, tetrapeptide chains (purple spheres) extend from each MurNAc of the long sugar chains and are directly cross-linked by short interpeptide bridges (black solid line) via the third residue to D-Ala of another peptide chain. In Gram-positive bacteria, the tetrapeptide chains (purples spheres) are linked via pentapeptide bridges (red spheres). All residues are purple spheres. IM, inner membrane. Depending on the organism, residues at position 3 are either L603 Lysine (mainly Gram-positive bacteria) or meso-diaminopimelic acid (Gram-negative bacteria and Gram-positive bacilli). Endolysin cleavage sites are indicated by yellow triangles: 1, *N*-acetylmuramoyl-L-alanine amidases; 2, endopeptidases; 3, endo-*N*-acetyl606 glucosaminidases; 4, *N*-acetyl muramidases; 5, lytic transglycosylases.

pathogens in food and agricultural industries (Matamp and Bhat, 2019) and as strong antibacterial agents for human pathogens in animal models (Guo et al., 2017; Haddad Kashani et al., 2017; de Wit et al., 2019). Most naturally occurring endolysins have limited effect on Gram-negative bacteria as the outer membrane (OM) protects the peptidoglycan layer from being attacked by the enzyme. However, efficient endolysin-mediated inactivation of Gram-negative pathogens can be achieved by either chemical/physical permeabilization of the OM (such as pressure or chelation of divalent ions), or by creating endolysin-peptide-fusions that have the ability to permeabilize the OM (Briers and Lavigne, 2015).

The application of bacteriophages in therapy has been successful in treating: (i) MDR *A. baumannii* infections (Schooley et al., 2017); (ii) against Mycobacterial infections (Dedrick et al., 2019); (iii) burn-wound infections caused by *P. aeruginosa* (Jault et al., 2019); (iv) infections caused by *S. aureus* (Fabijan et al., 2020); (v) Enterococcal infections (Khalifa et al., 2016); and (vi) against MDR *E. coli* infections (Sarker et al., 2016; Kakasis and Panitsa, 2019). Preparations of phage cocktails, phage banks, phage powders, and phage-derived endolysins as part of phage therapeutic approaches are possible and bring strategies closer to clinical applications (Manohar et al., 2019b,c).

Hurdles for Deployment of Phages

With the looming crisis of increasing numbers of MDR bacterial infections, alternatives to chemical antibiotics are urgently needed. To prevent secondary bacterial infections, prophylactic use of phages could be applied similar to small-molecule broadband antibiotics. This would require a "phage cocktail" that targets a broad range of pathogenic species likely to cause bacterial pneumonia. Since phages are highly specific, a phage cocktail would need to contain a variety of phages. Regulatory guidelines for the medical application of phages are not (fully) established in most countries; each component of a therapeutic requires to be approved, making deployment of phages as prophylactics in patients infected with pulmonary viruses, complex. Phage-derived therapeutic proteins such as endolysins would be advantageous as they would have a lower specificity toward bacteria and be able to inactivate a broader range of bacterial pathogens.

Phages can also be used as therapeutic agents for an established bacterial infection. Due to the high specificity of phages, phage therapy can be considered a personalized medicine (Loh and Leptihn, 2020). However, a phage to which the causative pathogen is susceptible would need to be rapidly identified. To treat multi-drug resistant pathogens, and to be prepared for the next pandemic where such infections, especially nosocomial ones, have a major impact on patient survival, phage libraries, and rapid on-site (hospital) screening platforms should be made available for use.

While phage therapy is unlikely to replace chemical antibiotics in clinical practice, it offers a potential solution to be used in combination with antibiotics or alone. Limitations of phage therapy in treating secondary bacterial infections include: the preparation of therapeutic cGMP (Good Manufacturing Practice) phages; a lack of proper clinical trials or guidelines to treat patients in different clinical conditions; a lack of regulatory guidelines to prepare and administer phages; patient acceptance, and possibly, adverse immune responses leading to primary treatment failure.

CONCLUSION

Secondary bacterial infections play a critical role in the morbidity and mortality rates of patients initially falling ill with pulmonary viral diseases. Evidence from the current SARS-CoV-2 pandemic shows that the antibiotic-resistant bacterial infections are a significant threat to hospitalized COVID-19 patients. Nosocomial infections including ventilator-associated infections are often unavoidable and especially so during a pandemic, and the use of broad-spectrum antibiotics is often a routine preventative measure. Phage therapy is one of the most promising options for treating secondary bacterial infections. Phage therapy either as a stand-alone treatment or in combination with antibiotics may offer a valuable alternative for treating secondary bacterial infections. Clinical studies should evaluate the efficacy of phage therapy in virus infected patients.

The potential for application of phage products, such as endolysins, should be investigated. Pulmonary CoVs will likely be a clinical challenge for many years to come. Viral pandemics from CoVs and emerging pathogens are inevitable in our globalized world with interconnected societies, travel, and commerce. We require to be well prepared for long-term management of COVID-19 and for the next pandemic, exploring and establishing new avenues to treat bacterial pathogens commonly observed in secondary infections. To avert an emerging healthcare crisis due from COVID-1 and antibiotic-resistance of secondary infections; medical interventions employing phage products or phage therapy itself might be our most promising options.

AUTHOR CONTRIBUTIONS

PM contributed to the initial idea. PM, BL, SW, and SL contributed to the concept and writing. BL and SL prepared the figures. SA, RN, and XH contributed to the review and comments.

FUNDING

We thank the Global Challenges Research Fund (The University of Edinburgh), and acknowledge the support by the Zhejiang University Special Scientific Research Fund for COVID-19 prevention and control (2020XGZX037) and the NSFC (32011530116).

REFERENCES

Ahmadi, M., Karimi Torshizi, M. A., Rahimi, S., and Dennehy, J. J. (2016). Prophylactic bacteriophage administration more effective than post-infection administration in reducing *Salmonella enterica* serovar Enteritidis shedding in quail. *Front. Microbiol.* 7:1253. doi: 10.3389/fmicb.2016.01253

Akturk, E., Oliveira, H., Santos, S. B., Costa, S., Kuyumcu, S., Melo, L. D., et al. (2019). Synergistic action of phage and antibiotics: parameters to enhance the killing efficacy against mono and dual-species biofilms. *Antibiotics* 8:103. doi: 10.3390/antibiotics8030103

Altamirano, F. L., and Barr, J. J. (2019). Phage therapy in the postantibiotic era. *Clin. Microbiol. Rev.* 32:e00066-18.

Barr, J. J. (2019). Missing a phage: unraveling tripartite symbioses within the human gut. *mSystems* 4:e00105-19.

Bordon, Y. (2014). Macrophages: innate memory training. *Nat. Rev. Immunol.* 14:713. doi: 10.1038/nri3759

Borysowski, J., and Górski, A. (2008). Is phage therapy acceptable in the immunocompromised host? *Int. J. Infect. Dis.* 12, 466–471. doi: 10.1016/j.ijid.2008.01.006

Briers, Y., and Lavigne, R. (2015). Breaking barriers: expansion of the use of endolysins as novel antibacterials against Gram-negative bacteria. *Future Microbiol.* 10, 377–390. doi: 10.2217/fmb.15.8

Brook, I. (1995). Microbiology of secondary bacterial infection in scabies lesions. *J. Clin. Microbiol.* 33, 2139–2140. doi: 10.1128/jcm.33.8.2139-2140.1995

Brook, I. (2002). Secondary bacterial infections complicating skin lesions. *J. Med. Microbiol.* 51, 808–812. doi: 10.1099/0022-1317-51-10-808

Brüssow, H. (2005). Phage therapy: the *Escherichia coli* experience. *Microbiol* 151, 2133–2140. doi: 10.1099/mic.0.27849-0

Capparelli, R., Parlato, M., Borriello, G., Salvatore, P., and Iannelli, D. (2007). Experimental phage therapy against *Staphylococcus aureus* in mice. *Antimicrob. Agents Chemother.* 51, 2765–2773. doi: 10.1128/aac.01513-06

Center for Disease Control and Prevention (2012). Available online at: https://www.cdc.gov/flu/spotlights/pandemic-global-estimates.htm (accessed June 15, 2020).

Chan, B. K., and Abedon, S. T. (2012). Phage therapy pharmacology: phage cocktails. *Adv. Appl. Microbiol.* 78, 1–23.

Chan, B. K., Abedon, S. T., and Loc-Carrillo, C. (2013). Phage cocktails and the future of phage therapy. *Future Microbiol.* 8, 769–783. doi: 10.2217/fmb.13.47

Chaudhry, W. N., Concepcion-Acevedo, J., Park, T., Andleeb, S., Bull, J. J., and Levin, B. R. (2017). Synergy and order effects of antibiotics and phages in killing *Pseudomonas aeruginosa* biofilms. *PLoS One* 12:e0168615. doi: 10.1371/journal.pone.0168615

Cheng, S. C., Quintin, J., Cramer, R. A., Shepardson, K. M., Saeed, S., Kumar, V., et al. (2014). mTOR-and HIF-1α–mediated aerobic glycolysis as metabolic basis for trained immunity. *Science* 345:1250684. doi: 10.1126/science.1250684

Comeau, A. M., Tétart, F., Trojet, S. N., Prere, M. F., and Krisch, H. M. (2007). Phage-antibiotic synergy (PAS): β-lactam and quinolone antibiotics stimulate virulent phage growth. *PLoS One* 2:e799. doi: 10.1371/journal.pone.0000799

de Wit, J., Totté, J. E., van Mierlo, M. M., van Veldhuizen, J., van Doorn, M. B., Schuren, F. H., et al. (2019). Endolysin treatment against *Staphylococcus aureus* in adults with atopic dermatitis: a randomized controlled trial. *J. Allergy Clin. Immunol.* 144, 860–863. doi: 10.1016/j.jaci.2019.05.020

Dedrick, R. M., Guerrero-Bustamante, C. A., Garlena, R. A., Russell, D. A., Ford, K., Harris, K., et al. (2019). Engineered bacteriophages for treatment of a patient with a disseminated drug-resistant *Mycobacterium abscessus*. *Nat. Med.* 25, 730–733. doi: 10.1038/s41591-019-0437-z

Doughty, L. A., Nguyen, K. B., Durbin, J. E., and Biron, C. A. (2001). A role for IFN-αβ in virus infection-induced sensitization to endotoxin. *J. Immunol.* 166, 2658–2664. doi: 10.4049/jimmunol.166.4.2658

Fabijan, A. P., Lin, R. C., Ho, J., Maddocks, S., Zakour, N. L., and Iredell, J. R. (2020). Safety of bacteriophage therapy in severe *Staphylococcus aureus* infection. *Nat. Microbiol.* 5, 465–472. doi: 10.1038/s41564-019-0634-z

Guarner, J. (2020). Three emerging coronaviruses in two decades. *Am. J. Clin. Pathol.* 153, 420–421. doi: 10.1093/ajcp/aqaa029

Guo, M., Feng, C., Ren, J., Zhuang, X., Zhang, Y., Zhu, Y., et al. (2017). A novel antimicrobial endolysin, LysPA26, against *Pseudomonas aeruginosa*. *Front. Microbiol.* 8:293. doi: 10.3389/fmicb.2017.00293

Haddad Kashani, H., Fahimi, H., Dasteh Goli, Y., and Moniri, R. (2017). A novel chimeric endolysin with antibacterial activity against methicillin-resistant *Staphylococcus aureus*. *Front. Cell. Infect. Microbiol.* 7:290. doi: 10.3389/fcimb.2017.00290

Hampton, H. G., Watson, B. N., and Fineran, P. C. (2020). The arms race between bacteria and their phage foes. *Nature* 577, 327–336. doi: 10.1038/s41586-019-1894-8

Hanada, S., Pirzadeh, M., Carver, K. Y., and Deng, J. C. (2018). Respiratory viral infection-induced Microbiome alterations and secondary bacterial pneumonia. *Front. Immunol.* 9:2640. doi: 10.3389/fimmu.2018.02640

Handel, A., Longini, I. M., and Antia, R. (2009). Intervention strategies for an influenza pandemic taking into account secondary bacterial infections. *Epidem* 1, 185–195. doi: 10.1016/j.epidem.2009.09.001

Haynes, L. M., Moore, D. D., Kurt-Jones, E. A., Finberg, R. W., Anderson, L. J., and Tripp, R. A. (2001). Involvement of toll-like receptor 4 in innate immunity to respiratory syncytial virus. *J. Virol.* 75, 10730–10737. doi: 10.1128/jvi.75.22.10730-10737.2001

Hendaus, M. A., Jomha, F. A., and Alhammadi, A. H. (2015). Virus-induced secondary bacterial infection: a concise review. *Ther. Clin. Risk Manag.* 11, 1265–1271.

Holshue, M. L., DeBolt, C., Lindquist, S., Lofy, K. H., Wiesman, J., Bruce, H., et al. (2020). First case of 2019 novel coronavirus in the United States. *N. Engl. J. Med.* 382, 929–936.

Housby, J. N., and Mann, N. H. (2009). Phage therapy. *Drug Discov. Today* 14, 536–540.

Imanishi, I., Uchiyama, J., Tsukui, T., Hisatsune, J., Ide, K., Matsuzaki, S., et al. (2019). Therapeutic potential of an endolysin derived from kayvirus S25-3 for staphylococcal impetigo. *Viruses* 11:769. doi: 10.3390/v11090769

Jamieson, A. M., Yu, S., Annicelli, C. H., and Medzhitov, R. (2010). Article influenza virus-induced glucocorticoids compromise innate host defense against a secondary bacterial infection. *Cell Host Microbe* 7, 103–114. doi: 10.1016/j.chom.2010.01.010

Jault, P., Leclerc, T., Jennes, S., Pirnay, J. P., Que, Y. A., Resch, G., et al. (2019). Efficacy and tolerability of a cocktail of bacteriophages to treat burn wounds infected by *Pseudomonas aeruginosa* (PhagoBurn): a randomised, controlled, double-blind phase 1/2 trial. *Lancet Infect. Dis.* 19, 35–45. doi: 10.1016/s1473-3099(18)30482-1

Jo, A., Ding, T., and Ahn, J. (2016a). Synergistic antimicrobial activity of bacteriophages and antibiotics against *Staphylococcus aureus*. *Food Sci. Biotechnol.* 25, 935–940. doi: 10.1007/s10068-016-0153-0

Jo, A., Kim, J., Ding, T., and Ahn, J. (2016b). Role of phage-antibiotic combination in reducing antibiotic resistance in *Staphylococcus aureus*. *Food Sci Biotechnol.* 25, 1211–1215. doi: 10.1007/s10068-016-0192-6

Kakasis, A., and Panitsa, G. (2019). Bacteriophage therapy as an alternative treatment for human infections. A comprehensive review. *Int. J. Antimicrob. Agents* 53, 16–21. doi: 10.1016/j.ijantimicag.2018.09.004

Kannan, S., Shaik Syed Ali, P., Sheeza, A., and Hemalatha, K. (2020). COVID-19 (Novel Coronavirus 2019) - recent trends. *Eur. Rev. Med. Pharmacol. Sci.* 24, 2006–2011.

Kash, J. C., and Taubenberger, J. K. (2015). Infectious disease theme issue the role of viral, host, and secondary bacterial factors in influenza pathogenesis. *Am. J. Pathol.* 185, 1528–1536. doi: 10.1016/j.ajpath.2014.08.030

Khalifa, L., Shlezinger, M., Beyth, S., Houri-Haddad, Y., Coppenhagen-Glazer, S., Beyth, N., et al. (2016). Phage therapy against *Enterococcus faecalis* in dental root canals. *J. Oral Microbiol.* 8:32157.

Kim, M., Jo, Y., Hwang, Y. J., Hong, H. W., Hong, S. S., Park, K., et al. (2018). Phage-antibiotic synergy via delayed lysis. *Appl. Environ. Microbiol.* 84: e02085-18.

Kim, S., Lee, D. W., Jin, J. S., and Kim, J. (2020). Antimicrobial activity of LysSS, a novel phage endolysin, against *Acinetobacter baumannii* and *Pseudomonas aeruginosa*. *J. Glob. Antimicrob. Res.* doi: 10.1016/j.jgar.2020.01.005 [Epub ahead of print].

Kim, Y. G., Park, J. H., Reimer, T., Baker, D. P., Kawai, T., Kumar, H., et al. (2011). Viral infection augments Nod1/2 signaling to potentiate lethality associated with secondary bacterial infections. *Cell Host Microbe* 9, 496–507. doi: 10.1016/j.chom.2011.05.006

Knezevic, P., Curcin, S., Aleksic, V., Petrusic, M., and Vlaski, L. (2013). Phage-antibiotic synergism : a possible approach to combatting *Pseudomonas aeruginosa*. *Res. Microbiol.* 164, 55–60. doi: 10.1016/j.resmic.2012.08.008

Kuhn, A., and Leptihn, S. (2019). "Helical and filamentous phages," in *Reference Module in Life Sciences* ed. M. G. Feiss (Amsterdam: Elsevier). doi: 10.1016/B978-0-12-809633-8.20986-2

Kumar, A., and Chordia, N. (2017). "Bacterial resistance against antibiotics," in *Drug Resistance in Bacteria, Fungi, Malaria, and Cancer*, eds G. Arora, A. Sajid, and V. Kalia (Cham: Springer), 171–192. doi: 10.1007/978-3-319-48683-3_7

Kurt-Jones, E. A., Popova, L., Kwinn, L., Haynes, L. M., Jones, L. P., Tripp, R. A., et al. (2000). Pattern recognition receptors T*LR*4 and CD14 mediate response to respiratory syncytial virus. *Nat. Immunol.* 1, 398–401. doi: 10.1038/80833

Kutter, E., De Vos, D., Gvasalia, G., Alavidze, Z., Gogokhia, L., Kuhl, S., et al. (2010). Phage therapy in clinical practice: treatment of human infections. *Curr. Pharm. Biotechnol.* 11, 69–86. doi: 10.2174/138920110790725401

Li, X., Geng, M., Peng, Y., Meng, L., and Lu, S. (2020). Molecular immune pathogenesis and diagnosis of COVID-19. *J. Pharm. Anal.* 10, 102–108. doi: 10.1016/j.jpha.2020.03.001

Lin, D. M., Koskella, B., and Lin, H. C. (2017). Phage therapy: an alternative to antibiotics in the age of multi-drug resistance. *World J. Gastrointest. Pharmacol. Ther.* 8, 162–173.

Loh, B., Haase, M., Mueller, L., Kuhn, A., and Leptihn, S. (2017). The transmembrane morphogenesis protein gp1 of filamentous phages contains walker A and walker B motifs essential for phage assembly. *Viruses* 9:73. doi: 10.3390/v9040073

Loh, B., Kuhn, A., and Leptihn, S. (2019). The fascinating biology behind phage display: filamentous phage assembly. *Mol. Microbiol.* 111, 1132–1138. doi: 10.1111/mmi.14187

Loh, B., and Leptihn, S. (2020). A call for a multidisciplinary future of phage therapy to combat multi-drug resistant bacterial infections. *Infect. Microbes Dis.* 2, 1–2. doi: 10.1097/im9.0000000000000018

Łusiak-Szelachowska, M., Weber-Dąbrowska, B., and Górski, A. (2020). Bacteriophages and lysins in biofilm control. *Virol. Sin.* 35, 125–133. doi: 10.1007/s12250-019-00192-3

MacIntyre, C. R., Chughtai, A. A., Barnes, M., Ridda, I., Seale, H., Toms, R., et al. (2018). The role of pneumonia and secondary bacterial infection in fatal and serious outcomes of pandemic influenza a (H1N1) pdm09. *BMC Infect. Dis.* 18:637. doi: 10.1186/s12879-018-3548-0

Mahar, P. D., Wasiak, J., Cleland, H., Paul, E., Gin, D., Watters, D. A., et al. (2014). Secondary bacterial infection and empirical antibiotic use in toxic epidermal necrolysis patients. *J. Burn Care Res.* 35, 518–524. doi: 10.1097/bcr.0000000000000062

Mallia, P., Footitt, J., Sotero, R., Jepson, A., Contoli, M., Trujillo-Torralbo, M. B., et al. (2012). Rhinovirus infection induces degradation of antimicrobial peptides and secondary bacterial infection in chronic obstructive pulmonary disease. *Am. J. Respir. Crit. Care Med.* 186, 1117–1124. doi: 10.1164/rccm.201205-0806oc

Manohar, P., Tamhankar, A. J., Leptihn, S., and Ramesh, N. (2019a). Pharmacological and immunological aspects of phage therapy. *Infect. Microbes Dis.* 1, 34–42. doi: 10.1097/im9.0000000000000013

Manohar, P., Tamhankar, A. J., Leptihn, S., and Ramesh, N. (2019b). Improved lyophilization conditions for long-term storage of bacteriophages. *Sci. Rep.* 9:15242.

Manohar, P., Tamhankar, A. J., Lundborg, C. S, and Nachimuthu, R. (2019c). Therapeutic characterization and efficacy of bacteriophage cocktails infecting *Escherichia coli*, *Klebsiella pneumoniae* and *Enterobacter* species. *Front. Microbiol.* 10:574. doi: 10.3389/fmicb.2019.00574

Matamp, N., and Bhat, S. G. (2019). Phage endolysins as potential antimicrobials against multidrug resistant *Vibrio alginolyticus* and *Vibrio parahaemolyticus*: current status of research and challenges ahead. *Microorganisms* 7:84. doi: 10.3390/microorganisms7030084

McCullers, J. A. (2011). Preventing and treating secondary bacterial infections with antiviral agents. *Antivir. Ther.* 16, 123–135. doi: 10.3851/imp1730

Międzybrodzki, R., Borysowski, J., Weber-Dąbrowska, B., Fortuna, W., Letkiewicz, S., Szufnarowski, K., et al. (2012). Clinical aspects of phage therapy. *Adv. Virus Res.* 83, 73–121.

Monteiro, R., Pires, D. P., Costa, A. R., and Azeredo, J. (2019). Phage therapy: going temperate? *Trends Microbiol.* 27, 368–378. doi: 10.1016/j.tim.2018.10.008

Morgan, D. J., Casulli, J., Chew, C., Connolly, E., Lui, S., Brand, O. J., et al. (2018). Innate immune cell suppression and the link with secondary lung bacterial pneumonia. *Front. Immunol.* 9:2943. doi: 10.3389/fimmu.2018.02943

Morris, D. E., Cleary, D. W., and Clarke, S. C. (2017). Secondary bacterial infections associated with influenza pandemics. *Front. Microbiol.* 8:1041. doi: 10.3389/fmicb.2017.01041

Morris, D. P. (2007). Bacterial biofilm in upper respiratory tract infections. *Curr. Infect. Dis. Rep.* 9, 186–192. doi: 10.1007/s11908-007-0030-3

Nansen, A., and Thomsen, A. R. (2001). Viral infection causes rapid sensitization to lipopolysaccharide: central role of IFN-αβ. *J. Immunol.* 166, 982–988. doi: 10.4049/jimmunol.166.2.982

Nouraldin, A. A., Baddour, M. M., Harfoush, R. A., and Essa, S. A. (2016). Bacteriophage-antibiotic synergism to control planktonic and biofilm producing clinical isolates of *Pseudomonas aeruginosa*. *Alexandria J. Med.* 52, 99–105. doi: 10.1016/j.ajme.2015.05.002

Nyangacha, R. M., Odongo, D., Oyieke, F., Ochwoto, M., Korir, R., Ngetich, R. K., et al. (2017). Secondary bacterial infections and antibiotic resistance among tungiasis patients in Western, Kenya. *PLoS Negl. Trop. Dis.* 11, e0005901. doi: 10.1371/journal.pntd.0005901

Perry, A. K., Gang, C. H., Zheng, D., Hong, T. A., and Cheng, G. (2005). The host type I interferon response to viral and bacterial infections. *Cell Res.* 15, 407–422. doi: 10.1038/sj.cr.7290309

Pires, D. P., Melo, L. D., Boas, D. V., Sillankorva, S., and Azeredo, J. (2017). Phage therapy as an alternative or complementary strategy to prevent and control biofilm-related infections. *Curr. Opin. Microbiol.* 39, 48–56. doi: 10.1016/j.mib.2017.09.004

Pirisi, A. (2000). Phage therapy-advantages over antibiotics? *Lancet* 356:1418. doi: 10.1016/s0140-6736(05)74059-9

Pittet, L. A., Hall-Stoodley, L., Rutkowski, M. R., and Harmsen, A. G. (2010). Influenza virus infection decreases tracheal mucociliary velocity and clearance of Streptococcus pneumoniae. *Am. J. Respir. Cell Mol.* 42, 450–460. doi: 10.1165/rcmb.2007-0417oc

Reardon, S. (2020). *Antibiotic Treatment for COVID-19 Complications Could Fuel Resistant Bacteria*. Available online at: https://www.sciencemag.org/news/2020/04/antibiotic-treatment-covid-19-complications-could-fuel-resistant-bacteria (accessed June 15, 2020).

Roquilly, A., McWilliam, H. E., Jacqueline, C., Tian, Z., Cinotti, R., Rimbert, M., et al. (2017). Local modulation of antigen-presenting cell development after resolution of pneumonia induces long-term susceptibility to secondary infections. *Immunity* 47, 135–147.

Sarker, S. A., Sultana, S., Reuteler, G., Moine, D., Descombes, P., Charton, F., et al. (2016). Oral phage therapy of acute bacterial diarrhea with two coliphage preparations: a randomized trial in children from Bangladesh. *EBioMedicine* 4, 124–137. doi: 10.1016/j.ebiom.2015.12.023

Schmelcher, M., Donovan, D. M., and Loessner, M. J. (2012). Bacteriophage endolysins as novel antimicrobials. *Future Microbiol.* 7, 1147–1171. doi: 10.2217/fmb.12.97

Schooley, R. T., Biswas, B., Gill, J. J., Hernandez-Morales, A., Lancaster, J., Lessor, L., et al. (2017). Development and use of personalized bacteriophage-based therapeutic cocktails to treat a patient with a disseminated resistant *Acinetobacter baumannii* infection. *Antimicrob. Agents Chemother.* 61: e00954-17.

Seguin, P., Laviolle, B., Chanavaz, C., Donnio, P. Y., Gautier-Lerestif, A. L., Campion, J. P., et al. (2006). Factors associated with multidrug-resistant bacteria in secondary peritonitis: impact on antibiotic therapy. *Clin. Microbiol. Infect.* 12, 980–985. doi: 10.1111/j.1469-0691.2006.01507.x

Summers, W. C. (2001). Bacteriophage therapy. *Annu. Rev. Microbiol.* 55, 437–451.

Tagliaferri, T. L., Jansen, M., and Horz, H. P. (2019). Fighting pathogenic bacteria on two fronts: phages and antibiotics as combined strategy. *Front. Cell. Infect. Microbiol.* 9:22. doi: 10.3389/fcimb.2019.00022

Tetro, J. A. (2020). Is COVID-19 receiving ADE from other coronaviruses? *Microb. Infect.* 22, 72–73. doi: 10.1016/j.micinf.2020.02.006

Torres-Barceló, C. (2018). The disparate effects of bacteriophages on antibiotic-resistant bacteria. *Emerg. Microbes Infect.* 7, 1–2.

Torres-Barceló, C., Franzon, B., Vasse, M., and Hochberg, M. E. (2016). Long-term effects of single and combined introductions of antibiotics and bacteriophages

on populations of *Pseudomonas aeruginosa*. *Evol. Appl.* 9, 583–595. doi: 10.1111/eva.12364

Valério, N., Oliveira, C., Jesus, V., Branco, T., Pereira, C., Moreirinha, C., et al. (2017). Effects of single and combined use of bacteriophages and antibiotics to inactivate *Escherichia coli*. *Virus Res.* 240, 8–17. doi: 10.1016/j.virusres.2017.07.015

Van Belleghem, J. D., Dąbrowska, K., Vaneechoutte, M., and Barr, J. J. (2019). "Phage interaction with the mammalian immune system," in *Phage Therapy: A Practical Approach*, eds (Cham: Springer), 91–122. doi: 10.1007/978-3-030-26736-0_4

Voelker, R. (2019). FDA approves bacteriophage trial. *JAMA* 321, 638–638.

Wang, D., Hu, B., Hu, C., Zhu, F., Liu, X., Zhang, J., et al. (2020). Clinical characteristics of 138 hospitalized patients with 2019 novel coronavirus–infected pneumonia in Wuhan, China. *JAMA* 323, 1061–1069.

Wang, H., Anthony, D., Selemidis, S., Vlahos, R., and Bozinovski, S. (2018). Resolving viral-induced secondary bacterial infection in COPD: A concise review. *Front. Immunol.* 9:2345. doi: 10.3389/fimmu.2018.02345

Weber-Dabrowska, B., Mulczyk, M., and Górski, A. (2001). Bacteriophage therapy for infections in cancer patients. *Clin. Appl. Immunol. Rev.* 1, 131–134. doi: 10.1016/s1529-1049(01)00015-0

Williams, A. E., Edwards, L., Humphreys, I. R., Snelgrove, R., Rae, A., Rappuoli, R., et al. (2004). Innate imprinting by the modified heat-labile toxin of *Escherichia coli* (LTK63) provides generic protection against lung infectious disease. *J. Immunol.* 173, 7435–7443. doi: 10.4049/jimmunol.173.12.7435

Yang, X., Yu, Y., Xu, J., Shu, H., Liu, H., Wu, Y., et al. (2020). Clinical course and outcomes of critically ill patients with SARS-CoV-2 pneumonia in Wuhan, China: a single-centered, retrospective, observational study. *Lancet Respir. Med.* 8, 475–481. doi: 10.1016/s2213-2600(20)30079-5

Zhou, F., Yu, T., Du, R., Fan, G., Liu, Y., Liu, Z., et al. (2020). Clinical course and risk factors for mortality of adult inpatients with COVID-19 in Wuhan, China: a retrospective cohort study. *Lancet* 395, 1054–1062. doi: 10.1016/s0140-6736(20)30566-3

Conflict of Interest: The authors declare that the research was conducted in the absence of any commercial or financial relationships that could be construed as a potential conflict of interest.

frontiers in Microbiology

ORIGINAL RESEARCH
published: 31 July 2020
doi: 10.3389/fmicb.2020.01744

sarA-Dependent Antibiofilm Activity of Thymol Enhances the Antibacterial Efficacy of Rifampicin Against *Staphylococcus aureus*

*Alaguvel Valliammai[1], Anthonymuthu Selvaraj[1], Udayakumar Yuvashree[1], Chairmandurai Aravindraja[1,2] and Shunmugiah Karutha Pandian[1]**

[1] Department of Biotechnology, Alagappa University, Karaikudi, India, [2] Department of Periodontology, College of Dentistry, University of Florida, Gainesville, FL, United States

Methicillin-resistant *Staphylococcus aureus* (MRSA) is a serious human pathogen which has been listed as a high-priority multi-drug resistance pathogen by the World Health Organization (WHO). Persistent MRSA infections are often associated with biofilm formation and resistance to conventional antimicrobial therapy. Inhibiting the surface adherence and the virulence of the bacterium is the current alternative approach without affecting growth to reduce the possibility of resistance development. Although numerous antibiofilm agents have been identified, their mode of action remains unclear. Combining two drugs with different modes of action will improve the efficiency of the treatment strategy against MRSA. The present study was aimed to decipher the molecular mechanism underlying the antibiofilm activity of thymol against MRSA and assess the ability of thymol to improve the antibacterial activity of rifampicin. Thymol significantly inhibited 88% of MRSA biofilm formation at 100 μg/ml and reduced the surface adherence of MRSA on glass, stainless steel, and titanium surface coated with human plasma as evidenced by microscopic analyses. qPCR analysis of global virulence regulatory genes and biofilm assay with *S. aureus* wild type, Δ*sarA*, and Δ*agr* strains revealed the *sarA*-mediated antibiofilm activity of thymol and inhibition of *sarA*-controlled virulence factors. Congo red assay and erythrocyte lysis assay further confirmed the reduction in polysaccharide intracellular adhesin and hemolysin. Importantly, thymol enhanced the antibacterial and the biofilm eradication efficiency of rifampicin against MRSA and also reduced the formation of persisters. Thus, the present study reveals the *sarA*-dependent antibiofilm efficacy of MRSA and suggests thymol as the promising combinatorial candidate in potentiating the antibacterial activity of rifampicin against persistent MRSA infections.

Keywords: MRSA, thymol, rifampicin, *sarA*, biofilm inhibition, biofilm eradication

OPEN ACCESS

Edited by:
Israel Castillo-Juárez, Colegio de Postgraduados (COLPOS), Mexico

Reviewed by:
Adline Princy Solomon, SASTRA University, India
Ayaz Ahmed, University of Karachi, Pakistan
Yan Q. Xiong, David Geffen School of Medicine at UCLA, United States

****Correspondence:***
Shunmugiah Karutha Pandian
sk_pandian@rediffmail.com

Specialty section:
This article was submitted to Antimicrobials, Resistance and Chemotherapy, a section of the journal Frontiers in Microbiology

Received: *08 April 2020*
Accepted: *03 July 2020*
Published: *31 July 2020*

Citation:
Valliammai A, Selvaraj A, Yuvashree U, Aravindraja C and Karutha Pandian S (2020) sarA-Dependent Antibiofilm Activity of Thymol Enhances the Antibacterial Efficacy of Rifampicin Against Staphylococcus aureus. Front. Microbiol. 11:1744. doi: 10.3389/fmicb.2020.01744

Abbreviations: *agr*, accessory gene regulator; BIC, biofilm inhibitory concentration; CFCS, cell-free culture supernatant; CFU, colony forming unit; CLSM, confocal laser scanning microscope; CRA, congo red agar; EPS, extracellular polysaccharide; MRSA, methicillin-resistant *Staphylococcus aureus;* MTP, microtiter plate; PIA, polysaccharide intracellular adhesion; *sarA*, staphylococcal accessory regulator A; SEM, scanning electron microscopy; TSBS, tryptone soya broth supplemented with 1% sucrose; WHO, World Health Organization.

INTRODUCTION

Staphylococcus aureus, a Gram-positive human commensal bacterium of the nasal epithelium turns virulent when the individual is immune-compromised. *S. aureus* not alone causes simple skin infections but also causes lethal infections such as pulmonary infections, invasive endocarditis, septic arthritis, osteomyelitis, and peri-implantitis (Taylor and Unakal, 2020). The treatment of these lethal conditions is a challenging task due to evolving multi-drug-resistant strains such as methicillin-resistant *S. aureus* (MRSA). MRSA is majorly involved in community-associated, hospital-associated as well as livestock-associated infections (Palavecino, 2014). Numerous virulence traits of MRSA make it stubborn against the conventional antibiotic therapy. Biofilm formation is one such trait which enables the bacterium to survive against various physiological stresses. Bacterial cells adhered to a surface with the help of slimy polymeric substances called biofilm, and this biofilm provides multicellular behavior to the unicellular bacterial cells. The rate of gene transfer inside the biofilm is higher than that between planktonic cells (Kumar et al., 2019). Bacterial cells especially living in biofilm mode are having a peculiar behavior of synchronized virulence gene expression, and many enzymes present in biofilm matrix are reported to cleave the antibiotics. In addition, the biofilm blocks the penetration of antibiotics as it is slimy and mucus in nature. Altogether the bacterial cells residing in biofilm are much more resistant to antibiotics than their planktonic counterparts (Olsen, 2015; Hall and Mah, 2017).

Bacterium has an intricate regulatory network to coordinate the synthesis of virulence factors. Although various global regulatory systems have been identified in *S. aureus*, the accessory gene regulatory (*agr*) system and the staphylococcal accessory regulatory system (*sarA*) are prototypes in nature. More specifically, both systems are well known to regulate biofilm formation and virulence factor production in a reciprocal way (Jenul and Horswill, 2018). That is, the active *agr* system negatively regulates the adhesion genes responsible for biofilm formation and leads to biofilm dispersal, whereas the active *sarA* system enhances the biofilm formation. Hence, *agr* and *sarA* systems act as molecular switches in regulating biofilm formation in *S. aureus* (Vasudevan, 2019).

As biofilm plays a critical role in the development of antibiotic resistance, targeting biofilm formation has become an alternative strategy to antibiotics (Buommino et al., 2014). Notably, antibiofilm agents are reported to potentiate the efficacy of antibiotics against bacterial biofilm when combined with antibiotics. Plenty of compounds with antibiofilm activity have been identified from various natural resources so far (Abraham et al., 2012; Sethupathy et al., 2016, 2017; Selvaraj et al., 2019; Valliammai et al., 2019). Thymol is a major constituent in the essential oil of thyme plant (*Thymus vulgaris*), and it is known to have various biological properties such as antibacterial, antifungal, antioxidant, and cognitive-enhancing activities (Braga, 2005; Tohidpour et al., 2010; Azizi et al., 2012). Few reports are available on the antibiofilm activity of thymol against *S. aureus*, but the molecular mechanism underlying the biofilm inhibitory potential of thymol remains unclear (Nostro et al., 2007; García-Salinas et al., 2018). Henceforth, the goal of the present study is to unravel the molecular mechanism of the antibiofilm efficacy of thymol and to find out the ability of thymol to improve the efficacy of rifampicin.

MATERIALS AND METHODS

Bacterial Strains and Growth Conditions

The *S. aureus* strains used in the present study are listed in **Table 1**. The reference MRSA strain used throughout the study was obtained from the American Type Culture Collection (ATCC). The clinical isolates were collected from pharingitis patients at the Rajaji Government Hospital, Madurai, Tamil Nadu for our earlier work (Gowrishankar et al., 2012). Newman wild-type and mutant strains of *S. aureus* were gifted by Dr. Christiane Wolz, a professor at the Institute for Medical Microbiology and Hygiene, University of Tubingen, Germany. For the biofilm assays, all the bacterial strains were cultured in tryptone soya broth (TSB) supplemented with 1% sucrose (TSBS) and kept at 37°C in the shaking incubator for 24 h. For maintenance, the bacterial cultures were grown in TSB and stored as glycerol stocks at −80°C.

Stock Solution

Thymol was purchased from Sigma-Aldrich, India. Ten milligrams of thymol dissolved in 1 ml of methanol was used as stock solution (10 mg/ml). Methanol alone was used as vehicle control in all the assays.

Determination of Biofilm Inhibitory Concentration

A 24-well polystyrene microtiter plate (MTP) containing 1 ml of TSBS with various concentrations of thymol (20–200 μg/ml) was inoculated with 1% of 6-h cultures of *S. aureus* strains (1×10^8 cells) and incubated at 37°C for 24 h. Methanol was used as vehicle control. For biofilm quantification, planktonic cells were carefully removed and biofilm cells were washed with sterile saline solution to remove unbound cells, and the plate was air-dried. Then, the

TABLE 1 | *Staphylococcus aureus* strains used in the present study.

Strain name	Details
MRSA	ATCC 33591
MSSA 46	Clinical isolate (Genebank ID: JN315153)
MSSA 51	Clinical isolate (Genebank ID: JN315154)
MRSA 44	Clinical isolate (Genebank ID: JN315148)
S. aureus	Newman wild-type strain
Δ*sarA*	ALC 637-Newman Δ*sarA:Tn917LTV1*
Δ*agr*	ALC 355-Newman Δ*agr:tetM*

biofilm cells were stained with 0.4% crystal violet solution for 20 min, washed to remove the excess stain, and air-dried. For quantification, the biofilm cells were destained with 30% glacial acetic acid solution, and absorbance was read at 570 nm using a multi-label reader (Spectramax M3, United States). The percentage of biofilm inhibition was calculated using the formula:

$$\%\ \text{of inhibition} = [(\text{control OD}_{570\ \text{nm}} - \text{treated OD}_{570\ \text{nm}}) / \text{control OD}_{570\ \text{nm}}] \times 100.$$

The lowest concentration of thymol which exhibited maximum biofilm inhibition was set as the biofilm inhibitory concentration (BIC) (Valliammai et al., 2019).

Colony-Forming Unit and Alamar Blue Assay

Two milliliters of MRSA cultures grown in the absence and the presence of thymol (25, 50, and 100 μg/ml) for 24 h was measured for absorbance at 600 nm. The control and the treated cultures were serially diluted and spread on a plate for colony-forming unit (CFU) counting. Then, the control and the treated cells were pelletized by centrifugation and dispersed in 2 ml of phosphate-buffered saline (PBS). A total of 900 μl of this suspension was aliquoted into wells of a 24-well MTP and 100 μl of Alamar blue solution (6.5 mg/ml) was added to each well. This plate was kept in the dark for 4 h, and fluorescence was measured at 530 and 590 nm for excitation and emission, respectively (Sarker et al., 2007).

Light and Confocal Laser Scanning Microscopic Analyses

For microscopic analysis, biofilm was allowed to form on glass/stainless steel slides (1 cm × 1 cm) immersed in TSBS in the absence and the presence of thymol (25, 50, and 100 μg/ml) for 24 h at 37°C. After 24 h, the glass slides were taken out and washed with sterile saline solution. For the light microscopic analysis, the glass slides were stained with 0.4% crystal violet for 20 min and washed. After drying, the glass slides were observed under a light microscope (Nikon Eclipse 80i, United States) at ×400 magnification. For confocal laser scanning microscopic analysis, stainless steel slides were stained with 0.1% acridine orange in the dark for 20 min and washed. After drying, the stainless steel slides were observed under CLSM (LSM 710, Carl Zeiss, Germany) at ×200 magnification (Valliammai et al., 2019).

Plasma Coating on Titanium Surface and Scanning Electron Microscopy Analysis

Plasma extracted from healthy human blood was diluted to 20% concentration using 50 mM sodium bicarbonate solution. Titanium slides (1 cm × 1 cm) placed in a 24-well MTP were covered with 1 ml of the prepared plasma solution and incubated at 4°C overnight. After the incubation period, the plasma solution was removed and the titanium slides were washed with sterile distilled water. Then, biofilm was allowed to form on the titanium surface in the absence and the presence of thymol (25, 50, and 100 μg/ml) as mentioned earlier. After 24 h of biofilm formation, the titanium slides were taken out and washed. For SEM analysis, the titanium slides were fixed with 2% glutaraldehyde at 4°C overnight and dehydrated with increasing concentrations of ethanol (20, 40, 60, 80, and 100%). After drying, the titanium slides were subjected to gold sputtering and observed under SEM (VEGA 3 TESCAN, Czech Republic) (Walker and Horswill, 2012).

qPCR Analysis

Total RNA from 24-h control and thymol (100 μg/ml)-treated MRSA cultures was extracted using the TRIzol method of RNA extraction and converted to cDNA using High Capacity cDNA Reverse Transcription Kit (Applied Biosystems, United States). The quantification of gene expression in the control and the thymol-treated samples was performed in triplicate on a thermal cycler (7500 Sequence Detection System, Applied Biosystems Inc., Foster, CA, United States) using a PCR mix (SYBR Green Kit, Applied Biosystems, United States) at a predefined ratio. The fold change in gene expression was calculated by the $2^{-\Delta\Delta Ct}$ method with gyrB as the housekeeping gene (Livak and Schmittgen, 2001). The details of the primer sequences of the genes (*agrA*, *agrC*, *sarA*, *icaA*, *icaD*, *fnbA*, *fnbB*, and *hla*) used in this study are given in **Table 2**.

Biofilm Assay With Mutant Strains

As stated earlier, a 24-well MTP assay was performed with the *S. aureus* wild-type strain and isogenic Δ*sarA* and Δ*agr* strains. All these strains were treated with increasing concentrations of thymol (20–100 μg/ml) for 24 h at 37°C and observed for biofilm inhibition using crystal violet as mentioned.

Congo Red Agar Assay

Tryptone soya broth supplemented with 1% sucrose containing 2% bacteriological agar and 0.08% Congo red was prepared and sterilized. After sterilization, thymol (25, 50, and 100 μg/ml) or methanol was mixed with the media and poured into Petri plates. The MRSA culture was streaked on the agar plates with and without thymol and incubated at 37°C for 24 h. After 24 h of incubation, the plates were photographed (Knobloch et al., 2002).

Extracellular Polysaccharide Quantification

Biofilm formation assay was done in the absence and the presence of thymol (25, 50, and 100 μg/ml) as stated earlier. After 24 h of biofilm formation, planktonic cells were discarded and the biofilm matrix was scraped and collected using sterile PBS. To the collected biofilm, an equal volume of 5% phenol and five volumes of concentrated sulfuric acid containing 0.2% hydrazine sulfate were added and mixed well. This mixture was incubated in the dark at room temperature for 1 h. Then, the samples were centrifuged at 10,000 rpm for 10 min to collect the supernatants, and absorbance was measured at 490 nm (Dubois et al., 1951).

TABLE 2 | List of primers used for qPCR analysis.

Genes	Forward primer	Reverse primer
agrA	5′-TGATAATCCTTATGAGGTGCTT-3′	5′-CACTGTGACTCGTAACGAAAA-3′
agrC	5′-CATTCGCGTTGCATTTATTG-3′	5′-CCTAAACCACGACCTTCACC-3′
sarA	5′-CAAACAACCACAAGTTGTTAAAGC-3′	5′-TGTTTGCTTCAGTGATTCGTTT-3′
fnbA	5′-ATCAGCAGATGTAGCGGAAG-3′	5′-TTTAGTACCGCTCGTTGTCC-3′
fnbB	5′-AAGAAGCACCGAAAACTGTG-3′	5′-TCTCTGCAACTGCTGTAACG-3′
icaA	5′-ACACTTGCTGGCGCAGTCAA-3′	5′-TCTGGAACCAACATCCAACA-3′
icaD	5′-ATGGTCAAGCCCAGACAGAG-3′	5′-AGTATTTTCAATGTTTAAAGCA-3′
hla	5′-CAACTGATAAAAAAGTAGGCTGGAAAGTGAT-3′	5′-CTGGTGAAAACCCTGAAGATAATAGAG-3′
gyrB	5′-GGTGCTGGGCAAATACAAGT-3′	5′-TCCCACACTAAATGGTGCAA-3′

Erythrocyte Lysis Assay

The 48-h MRSA cultures grown in the absence and the presence of thymol (25, 50, and 100 μg/ml) were centrifuged to collect cell-free culture supernatant (CFCS). Then, 100 μl of CFCS was mixed with 900 μl of 2% human red blood cell suspension prepared in PBS. This mixture was incubated at 37°C for 1 h and centrifuged at 10,000 rpm for 10 min. The collected supernatant was read for absorbance at 540 nm (Bernheimer, 1988).

Determination of Minimum Inhibitory Concentration and Combinatorial Growth Inhibition Assay

Test tubes containing 2 ml of TSB with 1% MRSA cells (1×10^8 cells) were treated with either thymol (0–200 μg/ml) or rifampicin (0–1 μg/ml) for 24 h at 37°C. After incubation, growth optical density (OD) at 600 nm was measured to determine the BIC. For the combinatorial assay, MRSA cells were treated with rifampicin (0.015, 0.03, and 0.06 μg/ml) in the presence and the absence of thymol (100 μg/ml) and incubated at 37°C for 24 h. After incubation along with growth OD at 600 nm, metabolic viability was also measured using Alamar blue assay as mentioned previously (Sarker et al., 2007).

Disc Diffusion Assay

Methicillin-resistant *Staphylococcus aureus* cells (5×10^8 cells) were spread on the surface of tryptic soya agar (TSA) plates without and with thymol (100 μg/ml) using sterile cotton swabs. The sterile discs were placed in the center of the agar surface and loaded with increasing concentrations of rifampicin (0.015, 0.03, and 0.06 μg/ml). The agar plates were incubated at 37°C for 24 h and photographed.

Time Killing Assay

Methicillin-resistant *Staphylococcus aureus* cultures (1×10^8 cells) were treated with rifampicin (0.06 μg/ml) and/or thymol (100 μg/ml), and 5 μl of the control and the treated cultures was spotted on the TSA plates every 1 h. In addition, 100 μl of the control and the treated cultures was spread on TSA plates every 2 h after serial dilution for CFU counting. The agar plates were incubated for 24 h at 37°C and photographed (Poonacha et al., 2017).

Persister Formation Assay

An overnight culture of MRSA was diluted to 1:1,000 ratio using TSB and incubated at 37°C in the shaking incubator at 250 rpm to reach an exponential phase (0.8 OD at 600 nm). Then, the exponential-phase MRSA cultures were challenged with ×100 concentration of rifampicin (6 μg/ml) in the absence and the presence of thymol (25, 50, and 100 μg/ml) and incubated at 37°C in the shaking incubator at 250 rpm for 3 h. After incubation, 100 μl of the culture was spread on TSA, and persister cell survival was determined by counting the number of colonies formed on TSA after incubation for 24 h at 37°C (Lee et al., 2016).

Biofilm Eradication Assay

Methicillin-resistant *Staphylococcus aureus* cells were allowed to form a biofilm in a 24-well MTP for 24 h without any treatment. The preformed biofilm was then treated with rifampicin (0.06 μg/ml) and/or thymol (100 μg/ml) for 12 h. After treatment, the planktonic cells were discarded and the biofilm cells were scraped out using sterile PBS and assessed for viability using Alamar blue as mentioned earlier. Additionally, the biofilm cells were serially diluted and plated for CFU counting.

Statistics

All the experiments were carried out in three biological replicates with at least two experimental replicates, and the results were expressed as mean ± standard deviation. Statistical analysis was performed using SPSS 17.0 software package (SPSS Inc., Chicago, IL, United States), and one-way ANOVA followed by Duncan's *post hoc* test was used to assess the significance. A p-value ≤ 0.05 was set as statistically significant.

RESULTS

Thymol Inhibits MRSA Biofilm Formation Without Affecting Growth

The crystal violet quantification of biofilm formed in the absence and the presence of various concentrations of thymol (20–200 μg/ml) exhibited a dose-dependent antibiofilm activity with maximum biofilm inhibition of 88% at 100 μg/ml without affecting growth. Beyond this concentration, thymol started to affect the growth of MRSA and biofilm inhibition was not much increased. Hence, 100 μg/ml of thymol was considered

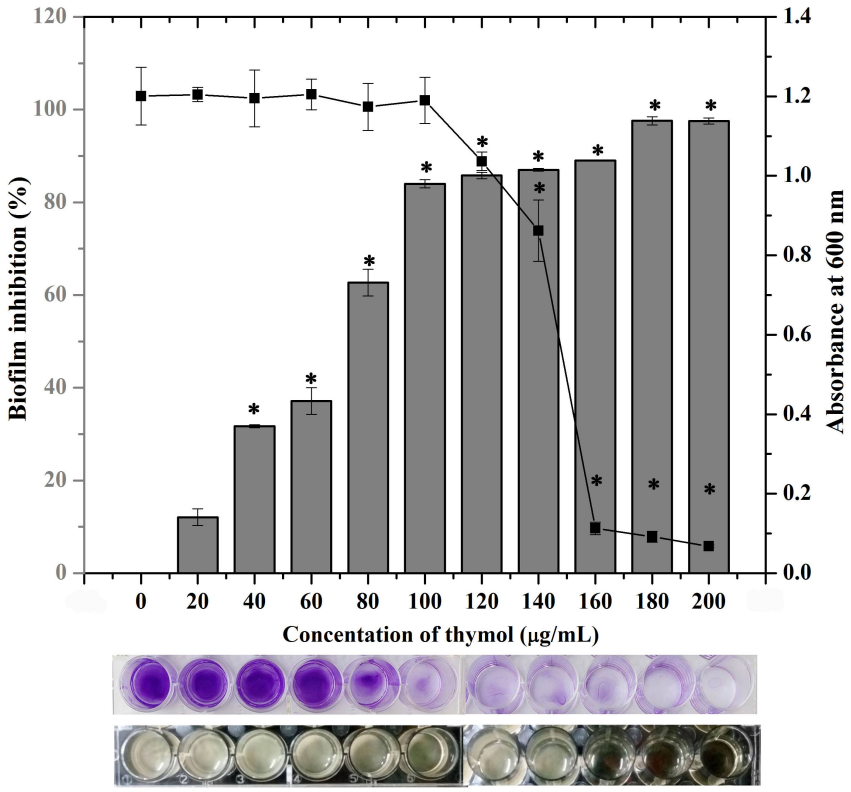

FIGURE 1 | Effect of thymol on the biofilm formation of methicillin-resistant *Staphylococcus aureus* (MRSA) as assessed by crystal violet staining. The bar graph indicates the percentage of biofilm inhibition and the line graph indicates the growth at $OD_{600\ nm}$. The bottom images show the corresponding crystal violet-stained biofilm and the growth of MRSA in microtitre plate. The error bars indicate standard deviations. The asterisks represent statistical significance ($p < 0.05$).

as the BIC and taken for further assays (**Figure 1**). The same concentration of thymol was also found to inhibit the biofilm formation of clinical isolates, namely, MSSA-51, MSSA-46, and MRSA-44 (**Supplementary Figure S1**). CFU analysis and growth OD demonstrated the non-antibacterial activity of thymol at 25, 50, and 100 μg/ml (**Supplementary Figure S2A**). In the Alamar blue assay, the metabolic viability of thymol-treated MRSA cells was comparable to that of the control cells, confirming that thymol did not affect the metabolic viability of MRSA (**Supplementary Figure S2B**).

Thymol Impedes the Adherence of MRSA on Glass, Stainless Steel Slides, and Titanium Slide Coated With Human Plasma

After confirming the non-antibacterial nature of thymol, the antibiofilm efficacy of thymol was further assessed by microscopic analysis. Light micrographs showed the gradual reduction in surface coverage with increasing concentrations of thymol. Furthermore, CLSM micrographs confirmed the ability of thymol to inhibit the surface adherence of MRSA, and notably, the thickness of the biofilm was also reduced upon increasing concentrations of thymol treatment (**Figure 2**). The human-plasma-coated titanium slides were subjected to MRSA biofilm formation in the absence and the presence of thymol and observed under SEM. The control titanium surface was observed to be completely covered by three-dimensional MRSA biofilm, whereas a monolayer of dispersed MRSA cells was observed in the thymol-treated titanium surface (**Figure 3**).

sarA-Dependent Antibiofilm Activity of Thymol

The expression of important regulatory genes involved in biofilm formation in the presence of thymol was examined by qPCR analysis. The expression of *sarA* was found to be decreased by twofold, whereas the expression of *agrA* and *agrC* was found to be unaltered by thymol treatment (**Figure 4**). Furthermore, the decreased expression of *sarA*-regulated virulence genes such as *fnbA*, *fnbB*, *icaA*, *icaD*, and *hla* was observed. The expression of *fnbA* and *fnbB* was slightly reduced by 0.02- and 0.11-fold, respectively, and nearly onefold down-regulation was observed in the expression of other virulence genes [*icaA* (1.08), *icaD* (0.89), and *hla* (1.23), respectively]. In order to identify the molecular-level target, the effect of thymol on biofilm formation of *S. aureus* wild type and Δ*sarA* and Δ*agr* strains was examined by crystal violet quantification assay as mentioned earlier. Biofilm quantification using $OD_{570\ nm}$ revealed that thymol was able to inhibit the biofilm formation of *S. aureus* wild type and Δ*agr*

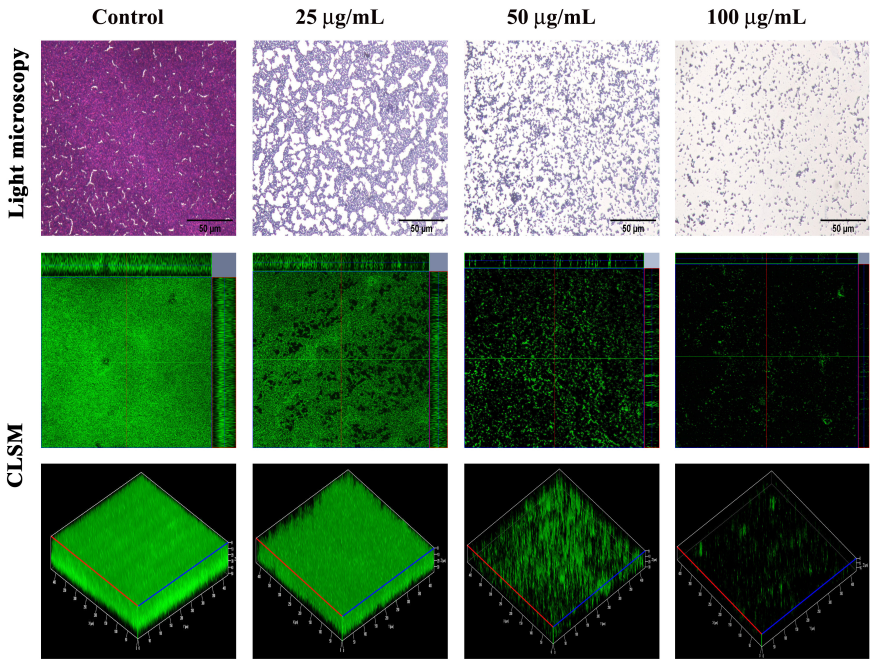

FIGURE 2 | Light microscopic images (400×) and ortho- and three-dimensional confocal laser scanning microscopy images (200×) depicting the dose-dependent antibiofilm potential of thymol against methicillin-resistant *Staphylococcus aureus*. Scale bar = 50 μm in the light micrographs.

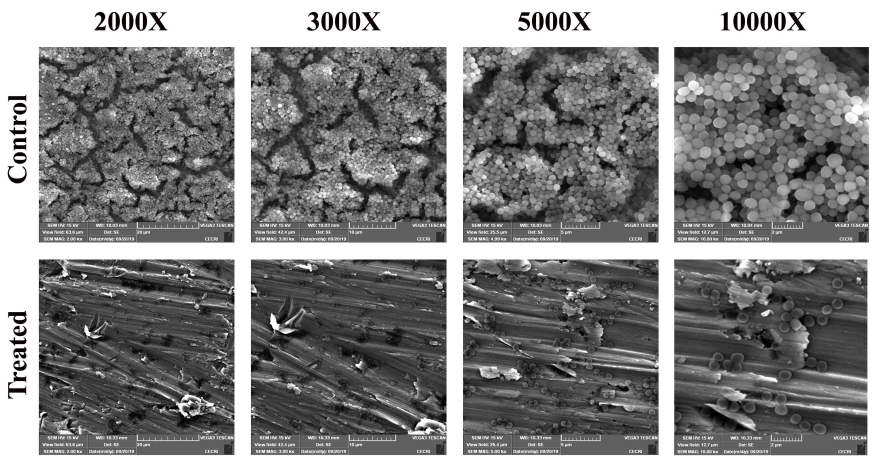

FIGURE 3 | SEM images showing the reduction in adherence of methicillin-resistant *Staphylococcus aureus* on plasma-coated titanium surface upon thymol treatment (100 μg/ml) at different magnifications.

strains at 100 μg/ml. However, the biofilm formation by Δ*sarA* was found to be unaffected by thymol treatment (**Figures 5A,B**).

Thymol Hampers *sarA*-Controlled Virulence in MRSA

In the congo red agar (CRA) assay, the MRSA colonies appeared black in the absence of thymol; thymol treatment gradually inhibited the black coloration, and at 100 μg/ml, the MRSA cells appeared white, with complete inhibition of polysaccharide intracellular adhesion (PIA) (**Figure 6A**). Extracellular polysaccharide (EPS) present in MRSA biofilm was quantified by phenol-sulfuric acid method of carbohydrate quantification, and a significant reduction in EPS was observed at $OD_{490\ nm}$ in the thymol-treated samples when compared to the control sample (**Figure 6B**). In the erythrocyte lysis assay, the production of hemolysin was assessed by mixing CFCS of the control and the thymol-treated MRSA with human erythrocytes. The thymol treatment resulted in the complete inhibition of erythrocyte lysis when compared to the red-colored erythrocyte lysis in the control sample (**Figure 6C**). On the whole, thymol significantly reduced the virulence factors under

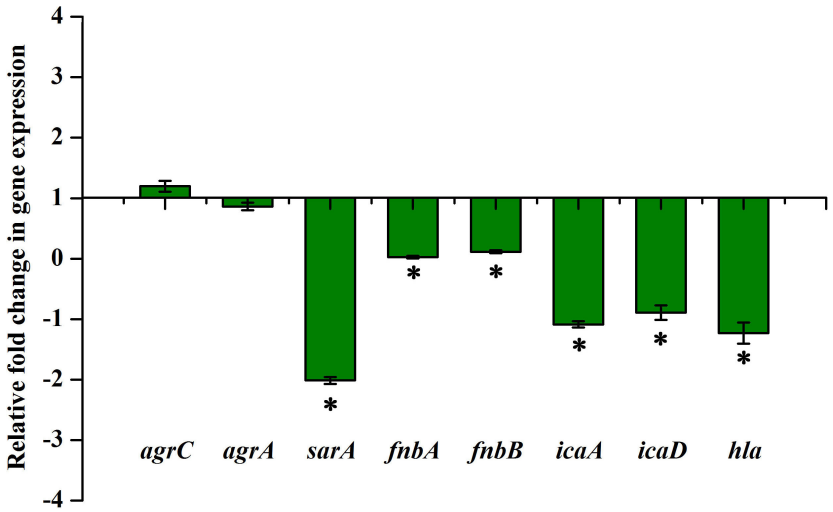

FIGURE 4 | qPCR analysis of the expression of biofilm and virulence-associated genes after 24 h of thymol treatment. The error bars indicate standard deviations. The asterisks represent statistical significance ($p < 0.05$).

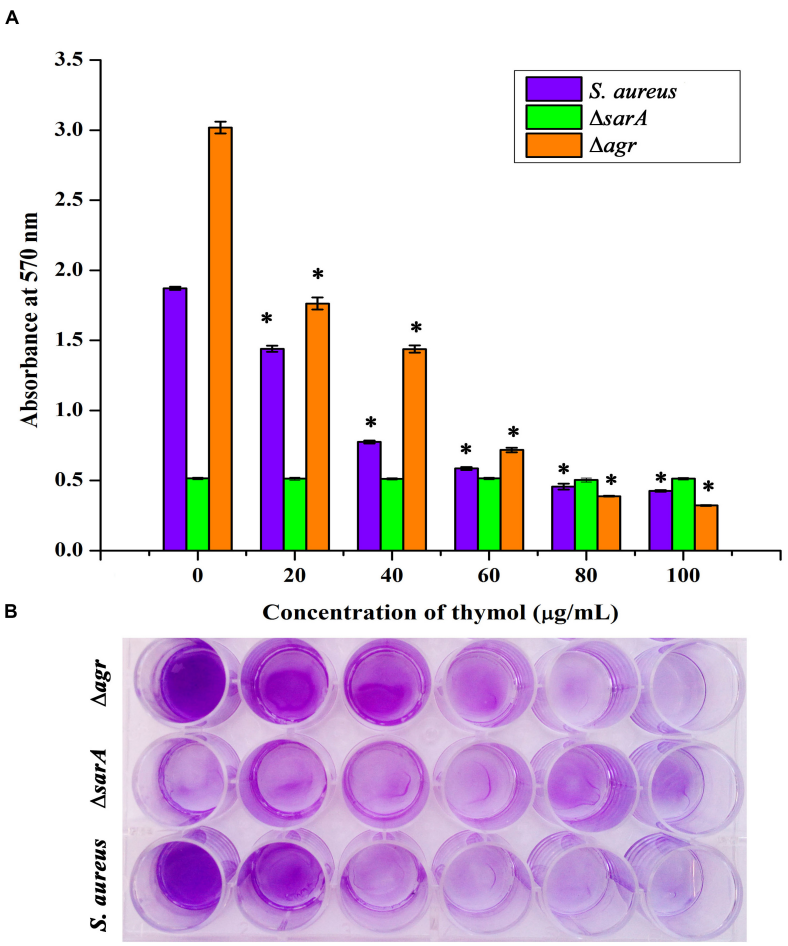

FIGURE 5 | (A) Antibiofilm efficacy of thymol on wild-type *Staphylococcus aureus* and Δ*agr* (affected) and on Δ*sarA* (not affected) as depicted by crystal violet quantification of biofilm. **(B)** The 24-well microtiter plate assay depicting the effect of thymol on the biofilm formation of wild-type *S. aureus,* Δ*agr*, and Δ*sarA*. The error bars indicate standard deviations. The asterisks represent statistical significance ($p < 0.05$).

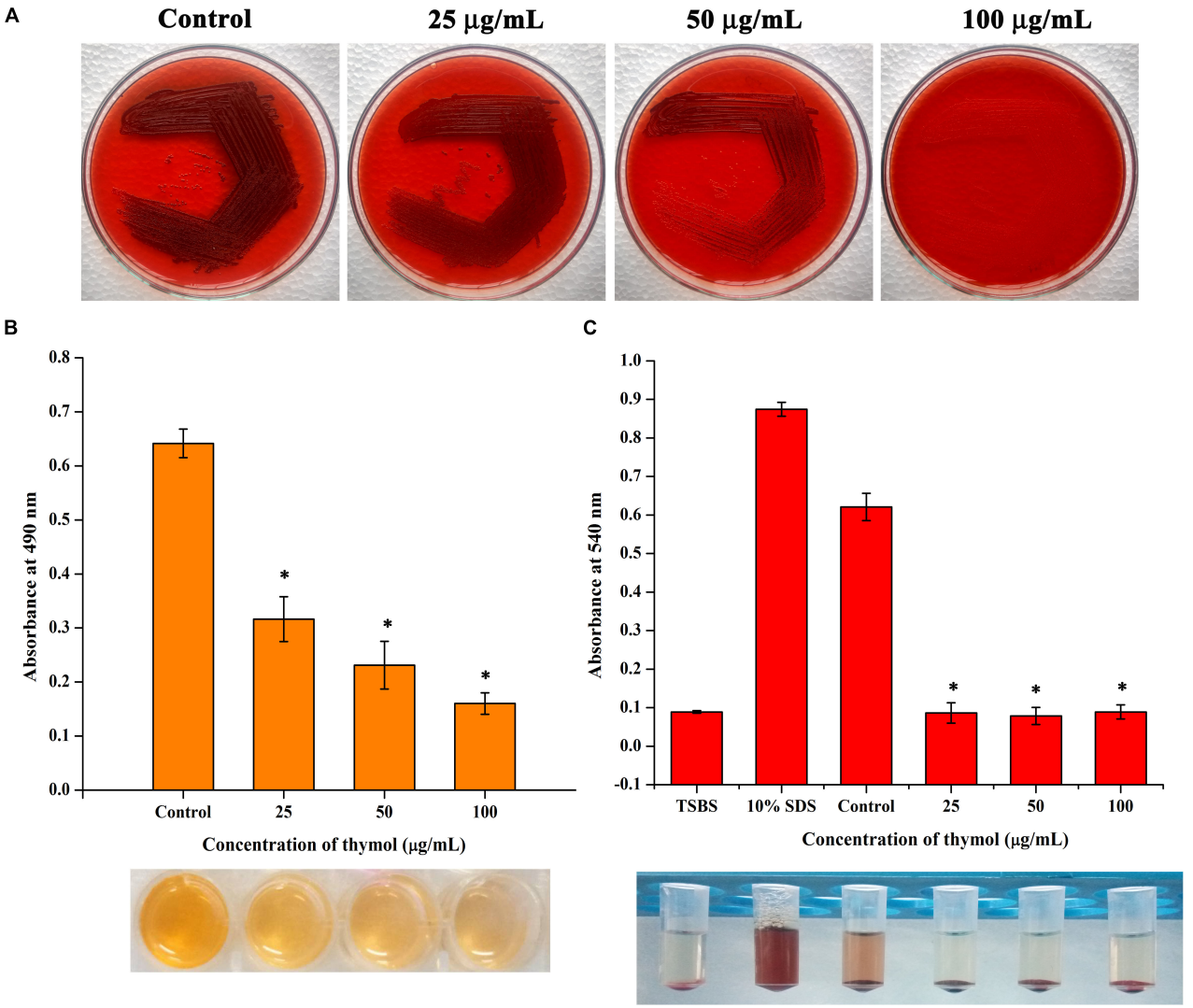

FIGURE 6 | (A) Congo red assay representing the reduction in polysaccharide intracellular adhesion synthesis upon thymol treatment. **(B)** Thymol inhibits extracellular polysaccharide synthesis as revealed by phenol sulfuric acid quantification. **(C)** Thymol greatly inhibits the production of hemolysin as exhibited by erythrocyte lysis assay. The bottom image shows the corresponding assay tubes. The error bars indicate standard deviations. The asterisks represent statistical significance ($p < 0.05$).

the control of *sarA* which is clearly depicted in the schematic representation (**Figure 7**).

Thymol Improves the Antibacterial Activity of Rifampicin Against Planktonic Cells, Mature Biofilm, and Persister Formation of MRSA

Antibacterial Activity of Rifampicin on Planktonic Cells

The minimum inhibitory concentration (MIC) of thymol and rifampicin was determined as 160 and 0.06 µg/ml, respectively (**Supplementary Figures S3, S4**), as maximum growth was inhibited at the minimum concentrations. Hence, for the combinatorial assay, the BIC of thymol (100 µg/ml) was selected as it does not affect the growth of MRSA. The antibacterial activity of rifampicin at MIC (0.06 µg/ml) and at sub-MIC (0.015 and 0.03 µg/ml) concentrations in the presence of thymol was examined by growth OD measurement (**Figure 8A**) and Alamar blue-based viability assay (**Figure 8B**). The results demonstrated the enhanced reduction in growth as well as viability upon combinatorial treatment with rifampicin and thymol than treatment with rifampicin alone. In addition, images of disc diffusion assay (**Figure 8C**) clearly displayed the increased zone of clearance at all the tested concentrations of rifampicin in the presence of thymol. The zone of clearance (mm) of each plate was measured and presented as bar graph (**Figure 8D**). Interestingly, the MRSA cells appeared white in color in the TSA plates containing thymol because of staphyloxanthin inhibition, in contrast to the yellow-colored cells on the control TSA plates.

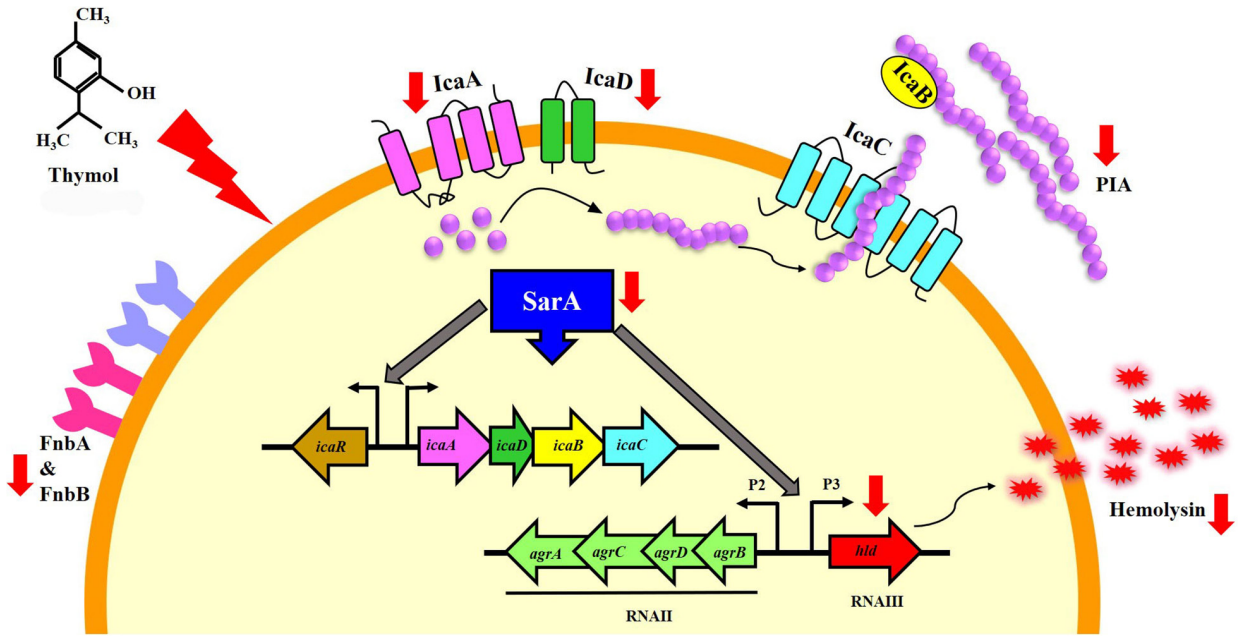

FIGURE 7 | Schematic representation of the molecular mechanism of thymol mediated by *sarA*. The red arrows indicate the down-regulation of *sarA*-regulated virulence genes by thymol.

Time Killing Kinetics and Persister Formation of Rifampicin

The killing efficacy of rifampicin in the absence and the presence of thymol on overnight-grown MRSA culture was measured for 12 h by spot assay and CFU counting (**Figures 9A,B**). From the results, it is clear that although rifampicin reduced the number of surviving cells for first 6 h, a certain subpopulation of cells remained viable for 12 h. In the case of the combinatorial treatment with rifampicin and thymol, the entire population was killed within 6 h. Furthermore, a concentration-dependent reduction of persister formation was observed upon combinatorial treatment when compared to the persisters formed upon treatment with ×100 concentration of rifampicin alone (**Figure 9C**). The 100-μg/ml concentration of thymol especially completely inhibited the persister formation by rifampicin.

Antibacterial Activity of Rifampicin on Mature Biofilm

The effect of thymol on the antibacterial activity of rifampicin against the mature biofilm of MRSA was assessed. The viability of 24-h mature biofilm cells after a 12-h treatment with rifampicin and thymol alone and in combination was examined by CFU and Alamar blue assay (**Figure 9D**). The results of both assays unveiled that thymol treatment enhanced the antibacterial activity of rifampicin on preformed MRSA biofilm.

DISCUSSION

Thymol drastically inhibited the *in vitro* biofilm formation of *S. aureus* strains (MRSA ATCC strain and clinical isolates) at 100 μg/ml without affecting the growth and the metabolic viability. This is more advantageous in excluding the possibility of drug resistance as thymol did not apply any selection pressure on MRSA. Surface adherence in the form of biofilm provides a protective stay to MRSA from adverse conditions. Light and CLSM microscopic analyses further confirmed the ability of thymol to interfere with surface adherence of MRSA on glass and stainless steel slides. MRSA was reported to be the predominant human pathogen involved in infections associated with various implantable medical devices (Pinto et al., 2019). The adhesion of host matrix proteins on implant surfaces serves as an initiative factor for biofilm formation. MRSA produces specialized adhesive proteins that are named as microbial surface components recognizing adhesive matrix molecules, which could interact with host proteins (Foster and Höök, 1998). Thus, titanium surface coated with human plasma was taken for biofilm assays to mimic this natural phenomenon. As evidenced by SEM micrographs, a multilayered biofilm, with three-dimensional microcolonies, was observed in the control surface coated with plasma, whereas thymol treatment efficiently inhibited the adherence of MRSA even on plasma-coated titanium surface. The antibiofilm efficacy observed on various surfaces such as polystyrene, glass, stainless steel, and titanium irrespective of the nature of the surface makes thymol a better antibiofilm therapeutic candidate.

In order to find out the molecular mechanism of thymol at the transcriptional level, the expression of important biofilm regulatory genes such as *sarA*, *agrA*, and *agrC* was examined in the presence of thymol. SarA is basically a DNA binding protein which regulates the expression of genes involved in pathogenesis and stands as the global regulator of virulence in *S. aureus* (Bayer et al., 1996). On the other hand, *agr* is a two-component

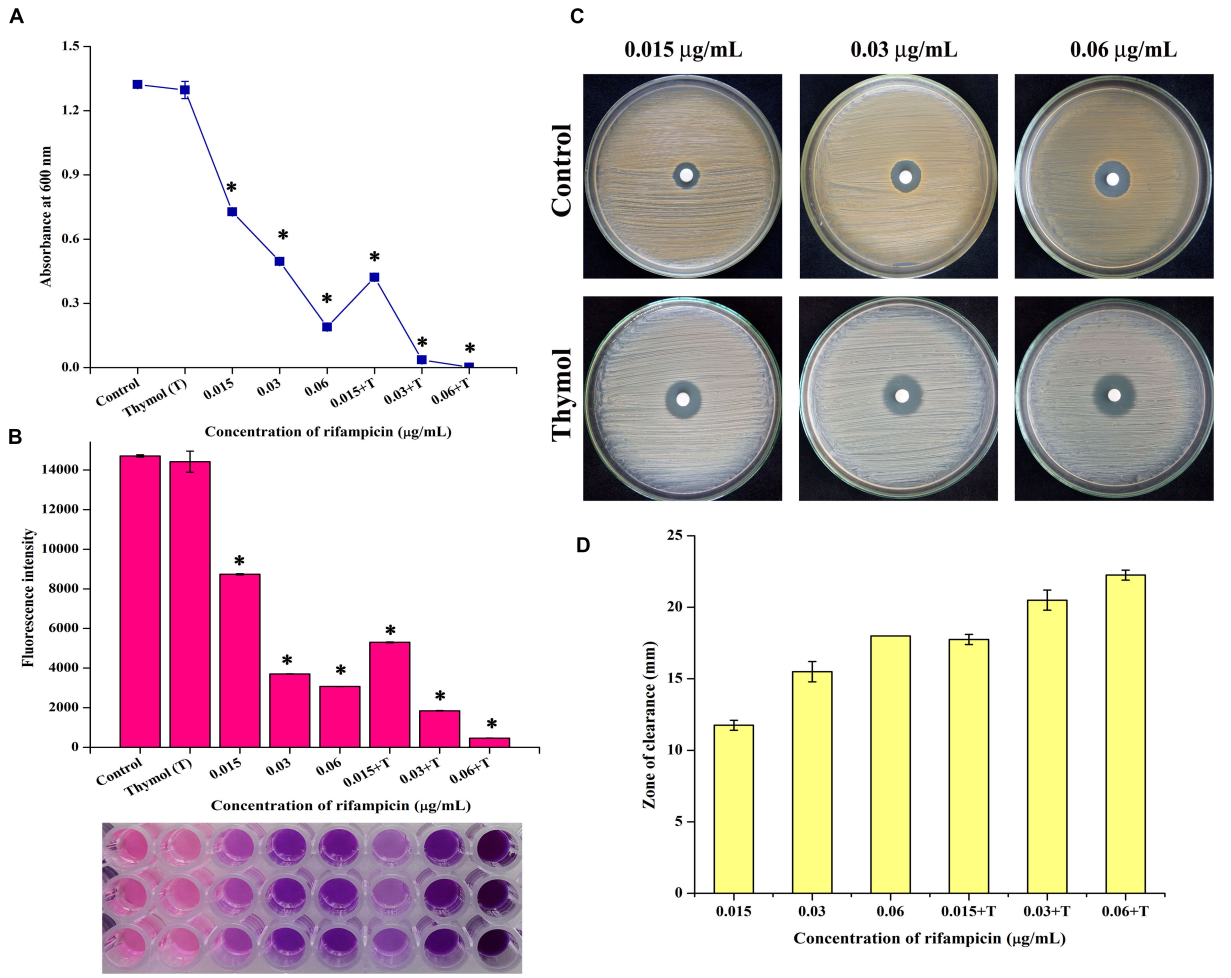

FIGURE 8 | Thymol enhances the antibacterial activity of rifampicin as shown by growth optical density measurement **(A)**, Alamar blue assay **(B)**, disc diffusion assay **(C)**, and its zone of clearance **(D)**. The error bars indicate standard deviations. The asterisks represent statistical significance ($p < 0.05$).

regulatory system which regulates toxin production and adhesion according to the quorum of bacteria present in a particular environment. An active *agr* system turns on the toxin gene expression and suppresses the adhesion gene expression (Boles and Horswill, 2008). Previous research on DNA binding sites of SarA revealed that SarA binds to the intergenic region between P2 and P3 promoters of the *agr* system and activates the expression of hemolysin *via* the RNAIII transcript. Apart from this, SarA binds to the upstream promoter regions of several target genes encoding fibronectin binding proteins (FnbA & FnbB), protein A (Spa), enterotoxin C, and PIA synthesis proteins (Chan and Foster, 1998; Chien et al., 1999). It is well known that *sarA* regulates the virulence of MRSA in both *agr*-dependent and *agr*-independent manner and serves as the therapeutic target to attenuate the virulence. Notably, previous studies have shown the *sarA* based repression of biofilm formation by various drugs in MRSA (Arya and Princy, 2013; Arya et al., 2015; Balamurugan et al., 2015, 2017). In the present study, thymol reduced the expression of *sarA* but did not alter the expression of *agrA* and *agrC*. This result leads to the hypothesis that the antibiofilm activity of thymol could be *sarA*-mediated. To verify this hypothesis, the antibiofilm activity of thymol was assessed on Δ*sarA* and Δ*agr* strains. It was already reported that *sarA* mutation reduces the ability of *S. aureus* to form a biofilm, whereas *agr* mutation induces biofilm formation. In the present study also, Δ*sarA* formed less biofilm than that of the wild-type strain. As predicted, thymol was found to be ineffective on Δ*sarA*, and interestingly, thymol effectively inhibited the biofilm formation by Δ*agr*. The inefficacy of thymol on Δ*sarA* validated the *sarA*-dependent antibiofilm activity of thymol.

To further prove this mechanism, the effect of thymol on the transcription of *sarA*-controlled virulence genes was investigated. The result revealed the down-regulation of *sarA*-controlled virulence genes such as *icaA*, *icaD*, *fnbA*, *fnbB*, and *hla*. PIA produced by *ica* operon plays a vital role in MRSA biofilm formation. It is well reported that the expression of the *ica* locus is positively regulated by *sarA* in *S. aureus* (Cerca et al., 2008). The PIA polymer is synthesized in the cytoplasm and transported outside the cell, which then mediates the intracellular adhesion and thereby provides the structural stability to biofilm

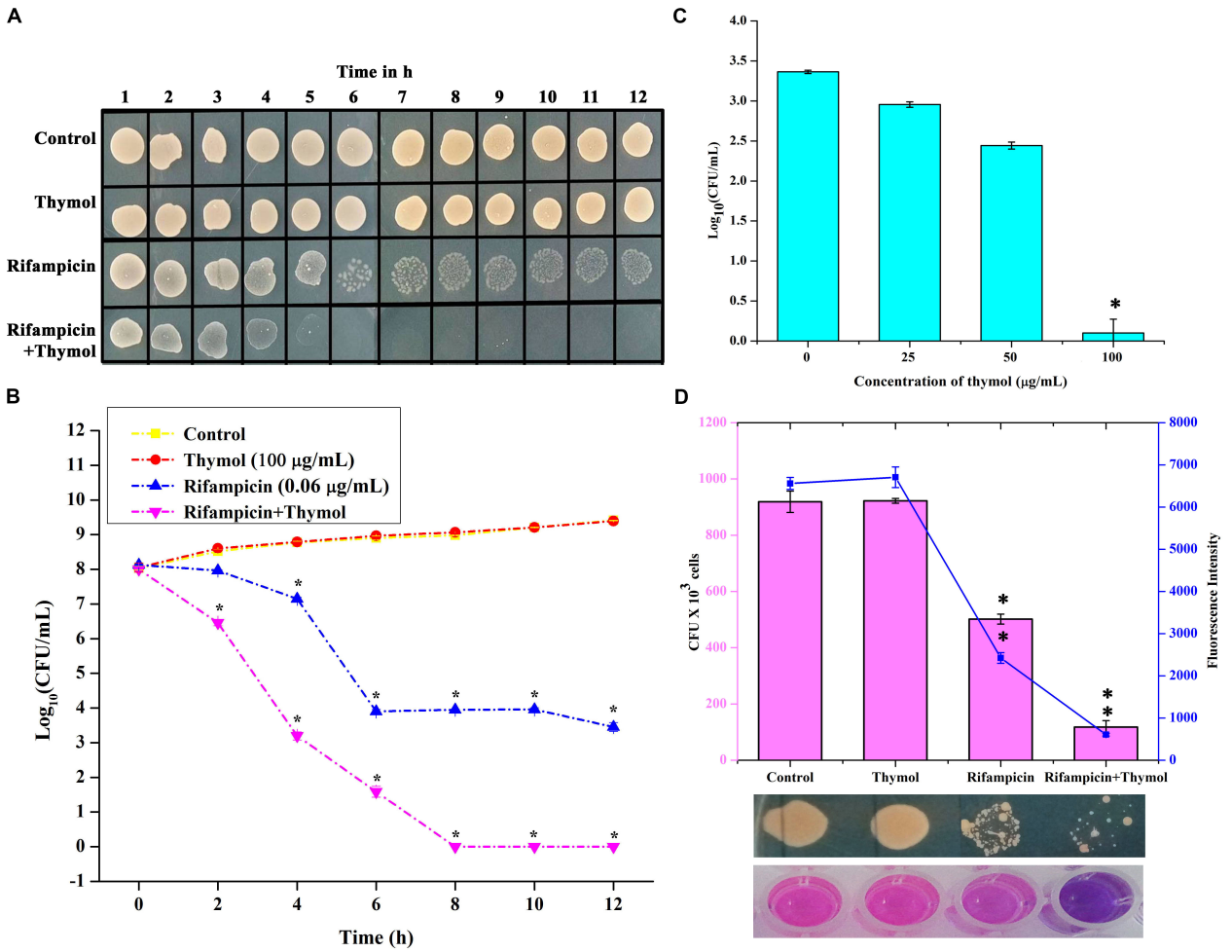

FIGURE 9 | Thymol potentiates the killing efficacy of rifampicin as shown by time killing kinetics studied by spot assay **(A)** and colony-forming unit (CFU) counting **(B)** and reduces persister formation **(C)**. Thymol improves the biofilm eradication ability of rifampicin as shown by CFU analysis and Alamar blue assay **(D)**. The error bars indicate standard deviations. The asterisks represent statistical significance ($p < 0.05$).

(O'Gara, 2007). The reduction in the expression of *icaA* and *icaD* was further confirmed by CRA assay as it is an important method to identify the PIA production and *ica*-positive *S. aureus* by means of black coloration. The results of the CRA assay revealed that, as a downstream impact of *sarA* inhibition by thymol, the treated cells appeared white in color due to the complete inhibition of PIA synthesis. Phenol-sulfuric acid quantification of EPS also evidenced that thymol inhibited the EPS present in the biofilm matrix. Hemolysin is an important pore-forming virulence factor produced by *S. aureus* and plays a crucial role in invasive staphylococcal infections. The synthesis of hemolysin was affected by *sarA* inhibitors in previous studies (Arya et al., 2015; Balamurugan et al., 2017). In the present study also, the inhibition of *sarA* expression by thymol ultimately reduced the production of hemolysin, as exhibited by the erythrocyte lysis assay. The *in vitro* assays confirmed that the reduction in *sarA* expression could be the central mechanism involved in the antibiofilm activity of thymol, and a schematic representation of the molecular mechanism of thymol is depicted in **Figure 7**. Rifampicin, also known as rifampin, is the broad-spectrum antibiotic used to treat several microbial infections and commonly used to treat skin infections, prosthetic joint infections, and biofilm-associated infections caused by *S. aureus* (Lebeaux et al., 2014). Mostly, rifampicin is included in the combinatorial treatment strategy because of its ability to easily penetrate cells, and the development of resistance against rifampicin can also be minimized (Chang et al., 2020). Thus, the present study evaluated the efficacy of thymol to enhance the antibacterial efficacy of rifampicin against MRSA and found a great reduction in the growth and the viability of MRSA upon combinatorial treatment. The increased zone of clearance in the disc diffusion assay and the enhanced killing efficacy with less time span (6 h) confirmed the potential of the combinatorial treatment. Persisters are antibiotic-tolerant bacterial cells but different from antibiotic-resistant mutants since the antibiotic tolerance of persisters is not inheritable and reversible. Persisters play a critical role in the recurrence of a bacterial infection after the course of an antibiotic treatment, and this condition is

clinically challenging (Lechner et al., 2012). Interestingly, thymol was found to be effective in reducing persister formation upon rifampicin treatment, and it would be of great advantage in the clinical settings. The eradication of preformed biofilm on medical devices is another hard task which could not be done with the available antibiotics, and possibly the combinatorial treatment of antibiotics and antibiofilm agents could solve this critical issue (Roy et al., 2013). Thus, the effect of combinatorial treatment on mature biofilm was evaluated in the present study. The number of viable bacteria in the mature biofilm after treatment with the rifampicin and thymol combination was greatly reduced than the rifampicin-alone-treated sample as revealed by CFU analysis and Alamar blue viability assay. Thus, all these results strongly suggest that thymol has the ability to boost the antibacterial activity of rifampicin in the form of combinatorial treatment against planktonic, biofilm, and persister cells of MRSA, and this property of thymol is highly appreciable in terms of clinical applications.

CONCLUSION

The present study unveiled the *sarA*-dependent antibiofilm activity and inhibition of other virulence factors such as PIA and hemolysin synthesis by thymol. The inhibition of MRSA adherence on various surfaces such as polystyrene, glass, stainless steel, and plasma-coated titanium advocates the potential of thymol as a surface-independent antibiofilm candidate in clinical context. The possibility of resistance development is also meager as thymol exerts non-antibacterial antibiofilm activity at 100 μg/ml. Thymol potentiated the antibacterial activity of rifampicin on planktonic as well as biofilm cells and reduced the persister formation. The ability of thymol to enhance the antibacterial and the biofilm eradication efficiency of rifampicin makes it a promising therapeutic candidate for combinatorial treatment strategy.

DATA AVAILABILITY STATEMENT

All datasets generated for this study are included in the article/**Supplementary Material**.

ETHICS STATEMENT

The studies involving human participants were reviewed and approved by Institutional Ethical Committee, Alagappa University, Karaikudi (IEC Ref No: IEC/AU/2016/1/4). The patients/participants provided their written informed consent to participate in this study.

AUTHOR CONTRIBUTIONS

AV and SK designed the study. AV, AS, and UY performed the experiments. AV analyzed the data, prepared the figures and tables, and wrote the manuscript. AS performed the statistical analysis. SK and CA revised the manuscript. All authors have read and approved the final version of the manuscript.

ACKNOWLEDGMENTS

The authors sincerely acknowledge the computational and bioinformatics facility provided by the Alagappa University Bioinformatics Infrastructure Facility (funded by DBT, GOI; File No. BT/BI/25/012/2012, BIF). The authors also acknowledge DST-FIST [Grant No. SR/FST/LSI-639/2015(C)], UGC-SAP [Grant No. F.5-1/2018/DRS-II(SAP-II)], and DST-PURSE [Grant No. SR/PURSE Phase 2/38(G)] for providing instrumentation facilities. The authors thank RUSA 2.0 [F.24-51/2014-U, Policy (TN Multi-Gen), Dept. of Edn, GoI]. SK is thankful to UGC for Mid-Career Award [F.19-225/2018(BSR)]. AV is thankful to RUSA 2.0 for financial assistance rendered in the form of RUSA Ph.D. Fellowship. The authors are grateful to Dr. Prof. Christiane Wolz, Institute for Medical Microbiology and Hygiene, University of Tubingen, Germany, for providing the *S. aureus* wild type, Δ*agr* and Δ*sarA* strains.

SUPPLEMENTARY MATERIAL

The Supplementary Material for this article can be found online at: https://www.frontiersin.org/articles/10.3389/fmicb.2020.01744/full#supplementary-material

REFERENCES

Abraham, K. P., Srieenivas, J., Venkateswarulu, T. C., Indira, M., Babu, D. J., Diwakar, T., et al. (2012). Investigation of the potential anti biofilm activities of plant extracts. *Int. J. Pharm. Pharm. Sci.* 4, 282–285.

Arya, R., and Princy, S. A. (2013). Computational approach to design small molecule inhibitors and identify *SarA*as a potential therapeutic candidate. *Med. Chem. Res.* 22, 1856–1865. doi: 10.1007/s00044-012-0185-9

Arya, R., Ravikumar, R., Santhosh, R. S., and Princy, S. A. (2015). *Sar*Abased novel therapeutic candidate against *Staphylococcus aureus*associated with vascular graft infections. *Front. Microbiol.* 6:416. doi: 10.3389/fmicb.2015.00416

Azizi, Z., Ebrahimi, S., Saadatfar, E., Kamalinejad, M., and Majlessi, N. (2012). Cognitive-enhancing activity of thymol and carvacrol in two rat models of dementia. *Behav. Pharmacol.* 23, 241–249. doi: 10.1097/FBP.0b013e3283534301

Balamurugan, P., Hema, M., Kaur, G., Sridharan, V., Prabu, P. C., Sumana, M. N., et al. (2015). Development of a biofilm inhibitor molecule against multidrug resistant *Staphylococcus aureus*associated with gestational urinary tract infections. *Front. Microbiol.* 6:832. doi: 10.3389/fmicb.2015.00832

Balamurugan, P., Praveen Krishna, V., Bharath, D., Lavanya, R., Vairaprakash, P., and Adline Princy, S. (2017). *Staphylococcus aureus*Quorum regulator *sarA*targeted compound, 2-[(Methylamino) methyl] phenol inhibits biofilm and down-regulates virulence genes. *Front. Microbiol.* 8:1290. doi: 10.3389/fmicb.2017.01290

Bayer, M. G., Heinrichs, J. H., and Cheung, A. L. (1996). The molecular architecture of the sar locus in *Staphylococcus aureus*. *J. Bacteriol.* 178, 4563–4570. doi: 10.1128/jb.178.15.4563-4570.1996

Bernheimer, A. W. (1988). Assay of hemolytic toxins. *Methods Enzymol.* 165, 213–217. doi: 10.1016/s0076-6879(88)65033-6

Boles, B. R., and Horswill, A. R. (2008). Agr-mediated dispersal of *Staphylococcus aureus*biofilms. *PLoS Pathog.* 4:e1000052. doi: 10.1371/journal.ppat.1000052

Braga, P. C. (2005). Thymol: antibacterial, antifungal and antioxidant activities. *G. Ital. Ostet. Ginecol.* 27, 267–272.

Buommino, E., Scognamiglio, M., Donnarumma, G., Fiorentino, A., and D'Abrosca, B. (2014). Recent advances in natural product-based anti-biofilm approaches to control infections. *Mini Rev. Med. Chem.* 14, 1169–1182. doi: 10.2174/1389557515666150101095853

Cerca, N., Brooks, J. L., and Jefferson, K. K. (2008). Regulation of the intercellular adhesin locus regulator (*icaR*) by SarA, σB, and IcaR in *Staphylococcus aureus*. *J. Bacteriol.* 190, 6530–6533. doi: 10.1128/JB.00482-08

Chan, P. F., and Foster, S. J. (1998). Role of SarA in virulence determinant production and environmental signal transduction in *Staphylococcus aureus*. *J. Bacteriol.* 180, 6232–6241. doi: 10.1128/.180.23.6232-6241.1998

Chang, A. T., Cosimi, R. A., and Bochan, M. R. (2020). Treatment of Staphylococcal Device infections: synergistic daptomycin with ceftaroline versus rifampin-adjunct therapy. *Open Forum Infect. Dis.* 7:ofaa072. doi: 10.1093/ofid/ofaa072

Chien, Y., Manna, A. C., Projan, S. J., and Cheung, A. L. (1999). SarA, a global regulator of virulence determinants in *Staphylococcus aureus*, binds to a conserved motif essential for sar-dependent gene regulation. *J. Biol. Chem.* 274, 37169–37176. doi: 10.1074/jbc.274.52.37169

Dubois, M., Gilles, K., Hamilton, J. K., Rebers, P. A., and Smith, F. (1951). A colorimetric method for the determination of sugars. *Nature* 168:167. doi: 10.1038/168167a0

Foster, T. J., and Höök, M. (1998). Surface protein adhesins of *Staphylococcus aureus*. *Trends Microbiol.* 6, 484–488. doi: 10.1016/s0966-842x(98)01400-0

García-Salinas, S., Elizondo-Castillo, H., Arruebo, M., Mendoza, G., and Irusta, S. (2018). Evaluation of the antimicrobial activity and cytotoxicity of different components of natural origin present in essential oils. *Molecules* 23:1399. doi: 10.3390/molecules23061399

Gowrishankar, S., Duncun Mosioma, N., and Karutha Pandian, S. (2012). Coral-associated bacteria as a promising antibiofilm agent against methicillin-resistant and-susceptible *Staphylococcus aureus*biofilms. *Evid. Based Complementary Altern.* 2012:862374. doi: 10.1155/2012/862374

Hall, C. W., and Mah, T.-F. (2017). Molecular mechanisms of biofilm-based antibiotic resistance and tolerance in pathogenic bacteria. *FEMS Microbiol. Rev.* 41, 276–301. doi: 10.1093/femsre/fux010

Jenul, C., and Horswill, A. R. (2018). Regulation of *Staphylococcus aureus*virulence. *Microbiol. Spectr.* 6:1. doi: 10.1128/microbiolspec.GPP3-0031-2018

Knobloch, J. K.-M., Horstkotte, M. A., Rohde, H., and Mack, D. (2002). Evaluation of different detection methods of biofilm formation in *Staphylococcus aureus*. *Med. Microbiol. Immunol.* 191, 101–106. doi: 10.1007/s00430-002-0124-3

Kumar, S., Chandra, N., Singh, L., Hashmi, M. Z., and Varma, A. (2019). *Biofilms in Human Diseases: Treatment and Control*. Cham: Springer.

Lebeaux, D., Ghigo, J.-M., and Beloin, C. (2014). Biofilm-related infections: bridging the gap between clinical management and fundamental aspects of recalcitrance toward antibiotics. *Microbiol. Mol. Biol. Rev.* 78, 510–543. doi: 10.1128/MMBR.00013-14

Lechner, S., Lewis, K., and Bertram, R. (2012). *Staphylococcus aureus*persisters tolerant to bactericidal antibiotics. *J. Mol. Microbiol. Biotechnol.* 22, 235–244. doi: 10.1159/000342449

Lee, J.-H., Kim, Y.-G., Gwon, G., Wood, T. K., and Lee, J. (2016). Halogenated indoles eradicate bacterial persister cells and biofilms. *AMB Express* 6:123. doi: 10.1186/s13568-016-0297-6

Livak, K. J., and Schmittgen, T. D. (2001). Analysis of relative gene expression data using real-time quantitative PCR and the 2(-Delta Delta C(T)) method. *Methods* 25, 402–408. doi: 10.1006/meth.2001.1262

Nostro, A., Sudano Roccaro, A., Bisignano, G., Marino, A., Cannatelli, M. A., Pizzimenti, F. C., et al. (2007). Effects of oregano, carvacrol and thymol on *Staphylococcus aureus*and *Staphylococcus epidermidis*biofilms. *J. Med. Microbiol.* 56, 519–523. doi: 10.1099/jmm.0.46804-0

O'Gara, J. P. (2007). ica and beyond: biofilm mechanisms and regulation in *Staphylococcus epidermidis* and *Staphylococcus aureus*. *FEMS Microbiol. Lett.* 270, 179–188. doi: 10.1111/j.1574-6968.2007.00688.x

Olsen, I. (2015). Biofilm-specific antibiotic tolerance and resistance. *Eur. J. Clin. Microbiol. Infect. Dis. Off. Publ. Eur. Soc. Clin. Microbiol.* 34, 877–886. doi: 10.1007/s10096-015-2323-z

Palavecino, E. L. (2014). Clinical, epidemiologic, and laboratory aspects of methicillin-resistant *Staphylococcus aureus*infections. *Methods Mol. Biol.* 1085, 1–24. doi: 10.1007/978-1-62703-664-1_1

Pinto, R. M., Lopes-de-Campos, D., Martins, M. C. L., Van Dijck, P., Nunes, C., and Reis, S. (2019). Impact of nanosystems in *Staphylococcus aureus*biofilms treatment. *FEMS Microbiol. Rev.* 43, 622–641. doi: 10.1093/femsre/fuz021

Poonacha, N., Nair, S., Desai, S., Tuppad, D., Hiremath, D., Mohan, T., et al. (2017). Efficient killing of planktonic and biofilm-embedded coagulase-negative Staphylococci by bactericidal protein P128. *Antimicrob. Agents Chemother.* 61:e00457-17. doi: 10.1128/AAC.00457-17

Roy, V., Meyer, M. T., Smith, J. A. I., Gamby, S., Sintim, H. O., Ghodssi, R., et al. (2013). AI-2 analogs and antibiotics: a synergistic approach to reduce bacterial biofilms. *Appl. Microbiol. Biotechnol.* 97, 2627–2638. doi: 10.1007/s00253-012-4404-6

Sarker, S. D., Nahar, L., and Kumarasamy, Y. (2007). Microtitre plate-based antibacterial assay incorporating resazurin as an indicator of cell growth, and its application in the *in vitro*antibacterial screening of phytochemicals. *Methods* 42, 321–324. doi: 10.1016/j.ymeth.2007.01.006

Selvaraj, A., Jayasree, T., Valliammai, A., and Pandian, S. K. (2019). Myrtenol attenuates MRSA biofilm and virulence by suppressing *sarA e*xpression dynamism. *Front. Microbiol.* 10:2027. doi: 10.3389/fmicb.2019.02027

Sethupathy, S., Ananthi, S., Selvaraj, A., Shanmuganathan, B., Vigneshwari, L., Balamurugan, K., et al. (2017). Vanillic acid from *Actinidia deliciosa*impedes virulence in *Serratia marcescens*by affecting S-layer, flagellin and fatty acid biosynthesis proteins. *Sci. Rep.* 7:16328. doi: 10.1038/s41598-017-16507-x

Sethupathy, S., Prasath, K. G., Ananthi, S., Mahalingam, S., Balan, S. Y., and Pandian, S. K. (2016). Proteomic analysis reveals modulation of iron homeostasis and oxidative stress response in *Pseudomonas aeruginosa*PAO1 by curcumin inhibiting quorum sensing regulated virulence factors and biofilm production. *J. Proteomics* 145, 112–126. doi: 10.1016/j.jprot.2016.04.019

Taylor, T. A., and Unakal, C. G. (2020). *Staphylococcus Aureus*. Treasure Island, FL: StatPearls Publishing.

Tohidpour, A., Sattari, M., Omidbaigi, R., Yadegar, A., and Nazemi, J. (2010). Antibacterial effect of essential oils from two medicinal plants against Methicillin-resistant *Staphylococcus aureus*(MRSA). *Phytomedicine* 17, 142–145. doi: 10.1016/j.phymed.2009.05.007

Valliammai, A., Sethupathy, S., Priya, A., Selvaraj, A., Bhaskar, J. P., Krishnan, V., et al. (2019). 5-Dodecanolide interferes with biofilm formation and reduces the virulence of Methicillin-resistant *Staphylococcus aureus*(MRSA) through up regulation of agr system. *Sci. Rep.* 9:13744. doi: 10.1038/s41598-019-50207-y

Vasudevan, R. (2019). Agr/sarA: molecular switches of biofilm regulation in *Staphylococcus aureus*.J. *Microbiol. Exp.* 7, 17–18. doi: 10.15406/jmen.2019.07.00233

Walker, J., and Horswill, A. (2012). A coverslip-based technique for evaluating *Staphylococcus aureus*biofilm formation on human plasma. *Front. Cell. Infect. Microbiol.* 2:39. doi: 10.3389/fcimb.2012.00039

Conflict of Interest: The authors declare that the research was conducted in the absence of any commercial or financial relationships that could be construed as a potential conflict of interest.

frontiers in Microbiology

ORIGINAL RESEARCH
published: 25 August 2020
doi: 10.3389/fmicb.2020.01963

Characterization and *in vitro* Analysis of Probiotic-Derived Peptides Against Multi Drug Resistance Bacterial Infections

Aninda Mazumdar[1,2], Yazan Haddad[1,2], Vishma Pratap Sur[1,2], Vedran Milosavljevic[1,2], Sukanya Bhowmick[1,2], Hana Michalkova[1], Roman Guran[1,2], Radek Vesely[3] and Amitava Moulick[1,2]**

[1] Department of Chemistry and Biochemistry, Faculty of AgriSciences, Mendel University in Brno, Brno, Czechia, [2] Central European Institute of Technology, Brno University of Technology, Brno, Czechia, [3] Department of Traumatology at the Medical Faculty, Masaryk University and Trauma Hospital of Brno, Brno, Czechia

OPEN ACCESS

Edited by:
Thomas Keith Wood,
Pennsylvania State University,
United States

Reviewed by:
Ratchaneewan Aunpad,
Thammasat University, Thailand
Rosa Del Campo,
Ramón y Cajal Institute for Health Research, Spain

***Correspondence:**
Aninda Mazumdar
anindamazumdar@gmail.com;
xmazumda@mendelu.cz
Amitava Moulick
amitavamoulick@gmail.com;
amitava.moulick@mendelu.cz

Specialty section:
This article was submitted to Antimicrobials, Resistance and Chemotherapy, a section of the journal Frontiers in Microbiology

Received: 06 May 2020
Accepted: 24 July 2020
Published: 25 August 2020

Citation:
Mazumdar A, Haddad Y, Sur VP, Milosavljevic V, Bhowmick S, Michalkova H, Guran R, Vesely R and Moulick A (2020) Characterization and in vitro Analysis of Probiotic-Derived Peptides Against Multi Drug Resistance Bacterial Infections. Front. Microbiol. 11:1963. doi: 10.3389/fmicb.2020.01963

An inexorable switch from antibiotics has become a major desideratum to overcome antibiotic resistance. Bacteriocin from *Lactobacillus casei*, a cardinal probiotic was used to design novel antibacterial peptides named as Probiotic Bacteriocin Derived and Modified (PBDM) peptides (PBDM1: YKWFAHLIKGLC and PBDM2: YKWFRHLIKKLC). The loop-shaped 3D structure of peptides was characterized *in silico* via molecular dynamics simulation as well as biophysically via spectroscopic methods. Thereafter, *in vitro* results against multidrug resistant bacterial strains and hospital samples demonstrated the strong antimicrobial activity of PBDM peptides. Further, *in vivo* studies with PBDM peptides showed downright recovery of balb/c mice from Vancomycin Resistant *Staphylococcus aureus* (VRSA) infection to its healthy condition. Thereafter, *in vitro* study with human epithelial cells showed no significant cytotoxic effects with high biocompatibility and good hemocompatibility. In conclusion, PBDM peptides displayed significant antibacterial activity against certain drug resistant bacteria which cause infections in human beings. Future analysis are required to unveil its mechanism of action in order to execute it as an alternative to antibiotics.

Keywords: antibacterial peptides, antibiotics, multidrug resistance, bacteria, infections

INTRODUCTION

Antibiotic resistant bacterial infections are a global health problem due to considerable threat to morbidity and mortality (Tacconelli et al., 2018; Bhowmick et al., 2020). The clinical need for the generation of new antibiotics is constantly putting pressure on pharmaceutical research and development. Whereas, antibiotic resistance is increasing due to incomplete course of antibiotic dose and its misuse (McNeece et al., 2014), exposure to constant stress, horizontal gene transfer and changes in genomic level (Ventola, 2015). The rapid increase in the number of resistant bacteria have forcefully reduced the use of antibiotics and an urge to introduce the development

of new alternatives (Rincón et al., 2014). The World Health Organization (WHO) listed a report on Antibiotic Resistance in 2017, which classify resistance bacteria into three main categories depending on the priority of threat levels of bacterial pathogenicity like high, critical and medium (Tacconelli et al., 2018).

The *Staphylococcus aureus* and many of its relative taxonomic class are opportunistic pathogens of significant threat level being a common cause for hospital infections ranging from soft tissue infections to life threatening infections with some assistance in chronic infections (McGuinness et al., 2017). In the Intensive Care Unit (ICU) of many hospital, resistant bacterial strains like *Klebsiella pneumoniae* (9.7%), *Staphylococcus aureus* (10.7%), Enterococcus spp. (10.6%), *Stenotrophomonas maltophilia* (11.5%), *Pseudomonas aeruginosa* (15.6%), and *Acinetobacter baumannii* (19.5%) can be acquired which are responsible behind deadly infections that are difficult to treat (Tan et al., 2014). In burn patients cases, *S. aureus* can cause sepsis which leads to death (Thomer et al., 2016). The Vancomycin-resistant *Staphylococcus aureus* (VRSA) is even a greater threat due its ability to prevent vancomycin penetration into the cells, alterations in gene transcription and altered autolysis (Alexander et al., 2014). Thus, resistance toward vancomycin being the last resort against Gram-positive bacterial infections and other antibiotics have made VRSA a serious problem; also prioritized as the high threat level by WHO with high clinical global burden (Cui et al., 2006; Davies and Davies, 2010).

Antimicrobial peptides have started gaining interest due to their natural occurrence, permeating ability, providing defense against invading pathogens, acting as an element for innate immunity, amphipathic nature, disruption of cell wall and high effectivity (Zhu et al., 2006; Groh et al., 2015; Wang et al., 2017). They have limited bacterial resistance compared to the antibiotics. Currently, major limitations to the use of peptides include the expensive cost of production, and few information about their specificity (Brunetti et al., 2016). In order to address these limitations, we introduce our peptides of interest PBDM1 and PBDM2, derived from *Lactobacillus* sp. well-known probiotic bacteria. It had been reported *Lactobacillus* sp. when cultivated together with *S. aureus* showed inhibitory effects on *S. aureus* (Mohammedsaeed et al., 2014). PBDM1 and PBDM2 are short 12 amino acid sequence peptides derived from a bacteriocin present in *Lactobacillus casei*. The peptides are shorter version from m2163 and m2386 peptides reported previously (Tsai et al., 2015). Multiple sequence alignment of the four peptides is shown in **Supplementary File Section 1** (**Supplementary Figure S1**). PBDM peptides are amphipathic peptides with positive net charge which was further studied to analyze its antibacterial activity (Lorenzón et al., 2012; Vicente et al., 2013).

Our main focus during the present study was to design, synthesize and characterize the PBDM peptides and examine their antimicrobial activity against multidrug resistant pathogenic strains. The results were promising against the antibiotic resistant bacteria with no toxicity and prominent hemocompatibility *in vitro* and high biocompatibility *in vivo*. Thus, PBDM peptides can be used for a better treatment strategy as a potent replacement for antibiotics with negligible toxicity and medicinal values.

MATERIALS AND METHODS

Designing of PBDM Peptides

The peptide PBDM1 and PBDM2 were designed from a previously reported bacteriocin like peptide m2163 (KRKCPKTPFDNTPGAWFAHLILGC) present in *Lactobacillus casei* ATCC 334 (Tsai et al., 2015). Both the peptides were 12 amino acids long selected from the C-terminal sequence with the startup sequence as WFAHLILGC with no net charge. PDBM1 with the sequence YKWFAHLIKGLC was designed by adding Tyr and two Lys to increase the presence of aromatic amino acid, net positive charge of two and improved solubility. Whereas, in case of PDBM2 with sequence YKWFRHLIKKLC had similar modifications like PDBM1 with two additional replacements of an Ala to Arg and Gly to Lys, that increased the net positive charge to four, improves water solubility and stabilize the peptide backbone (Haug et al., 2016). It was previously reported that the Arg and Trp complement each other to increase antimicrobial activity (Chan et al., 2006). Finally, the choice of the C-terminus for cystination was to avoid too many modifications at both ends of peptide. Cys residue provides thiol (–SH) group which is capable of forming chemical bonds with other molecules (e.g., gold nanoparticles).

Molecular Dynamics Simulation

GPU-accelerated Molecular Dynamics (MD) simulation was performed in isothermal-isobaric NPT ensemble (constant number, pressure, and temperature) using Gromacs v2018 on GeForce GTX 1080Ti card (Nvidia, Santa Clara, CA, United States). Peptide sequence of PBDM1 and PBDM2 (YKWFAHLIKGLC and YKWFRHLIKKLC) was used to build alpha helix structure in UCSF Chimera v1.10.2 (Backbone dihedrals $\Phi = -57°$ and $\Psi = -47°$; Side-chains via Dunbrack rotamer library). Positive charges were assumed for lysines and arginine while histidine protonation was assigned on Nε atom. The peptides were put in rhombic dodecahedron periodic box and solvated with 1920 and 1911 explicit SPC water molecules then neutralized with two and four Cl- ions in Amber99SB force field, respectively. Total number of atoms were 5976 and 5980 atoms. Box vector dimensions were 44.036 Å and 44.047 Å. Trajectories were calculated via leap-frog integrator every 2 fs. Neighbor searching was done via Verlet scheme while the Cut-off method was used for Van der Waals interactions at 12Å. For electrostatics calculations, the Particle Mesh Ewald (PME) was used with 12Å cutoff. The peptide was minimized via steepest descent (Convergence after 263 and 312 steps at maximum force < 1000 kJ/mol/nm, respectively). NVT ensembles (constant number, volume, and temperature) equilibration was done for duration of 1 ns using LINCS constraints for modified Berendsen thermostat coupling (300 K) in two groups (protein and non-protein), and H-bonds. Next, NPT ensemble equilibration for a duration of 1 ns with LINCS constraints for modified Berendsen thermostat coupling (300 K), H-bonds and isotropic Berendsen

pressure coupling (1 bar). MD Production was performed in NPT ensemble for 1 microsecond using LINCS constraints for Parrinello-Rahman isotropic pressure coupling (1 bar), modified Berendsen thermostat coupling (300 K) and H-bonds. The total number of trajectory frames was 100,000 for which trajectories and energies were saved every 10 ps. Post MD analysis was done by putting the protein in the center of the box, followed by fitting of backbone and removal of all water molecules from the system. Standard DSSP method was used to perform time evolution of secondary structure. UCSF Chimera was used for visualization and further analysis. The most stable confirmations (largest clusters) was identified by clustering analysis of minimal backbone in steps of 50 frames. The representative 3D structures were superposed using Needleman-Wunsch alignment algorithm and BLOSUM-62 blocks substitution matrix. Root mean square deviations (RMSD) for all heavy atoms were calculated with reference to the representative frame of top cluster and to the first frame (α-helix).

Chemicals, Synthesis and Characterization of the PBDM Peptides

All the chemicals for peptide synthesis, different assays and other chemicals were purchased from Sigma-Aldrich (St. Louis, MO, United States) in ACS purity, unless noted otherwise and to perform experiments and obtain the best results, sterile conditions were maintained.

PBDM1 (sequence – YKWFAHLIKGLC, with amidated C-terminus) and PBDM2 (sequence – YKWFRHLIKKLC, with amidated C-terminus) were synthesized using standard Fmoc solid phase synthesis on Liberty Blue peptide synthesizer (CEM, Matthews, NC, United States). Deblocking of Fmoc protecting group was performed with 20% piperidine v/v in *N,N*-dimethylformamide (DMF). Coupling was achieved using *N,N,N′,N′*-tetramethyl-O-(1H-benzotriazol-1-yl)uroniumhexafluorophosphate (HBTU), *N,N*-diisopropylethylamine (DIEA) and DMF. Cleavage of side chain protecting groups was performed by treating the peptides resin with 95% trifluoroacetic acid (TFA) *v/v*, 2.5% H_2O *v/v* and 2.5% triisopropylpropylsilane v/v for 30 min at 38°C under microwave irradiation. Isolation of NVC was performed by multiple centrifugation (6000 rpm, 3 min) under cold diethyl ether then re-suspended in ACS water and lyophilized. Further, the formation of PBDM1–5(6)–Carboxyfluorescein and PBDM2–5(6)–Carboxyfluorescein conjugates were obtained using PBDM peptides and 5(6)–Carboxyfluorescein N–hydroxysuccinimide ester in the ratio of 10:1, kept in rotator Multi Bio RS–24 (Biosan, Riga, Latvia) for 24 h under constant rotation with time interval vibration. Thereafter, the HPLC (ESA Inc., Chelmsford, MA, United States) system consisted of two pumps ESA Model 584 and an autosampler ESA Model 542 (ESA Inc., Chelmsford, MA, United States) along with the column Kinetex EVO C18 (150 × 4.6 mm, 5 μm) was used to perform purification of the peptides and their conjugates. The wavelength was set to 214 nm and the injected sample volume was 20 μL. Mobile phase A and B consisted of water with 0.1% formic acid and methanol with 0.1% formic acid. Flow rate was 0.5 mL/min. Prior analyses the samples were diluted 100× with water containing 0.1% formic acid. The molecular weight of the peptide and its conjugate was verified by a MALDI-TOF mass spectrometer Bruker UltrafleXtreme (Bruker Daltonik GmbH, Germany). As a matrix 2,5-dihydroxybenzoic acid (DHB) prepared in 30% acetonitrile and 0.1% trifluoroacetic acid at concentration 20 mg/mL was used. The final spectrum was averaged from 5000 mass spectra per sample spot. Reflector positive mode was used. Laser power was set 5–10% above the threshold.

Finally, the ATR FT-IR spectra were collected using a Nicolet iS10 FT-IR spectrometer with a diamond attenuated total reflectance (ATR) attachment (Thermo Electron Inc., San Jose, CA, United States). Initially, to the diamond crystal of the ATR cell, the sample was added drop-wise (5 μL) and then the film was measured after spontaneous evaporation of the solvent. At a resolution of 4 cm^{-1}, the IR spectra were recorded from 4000 to 650 cm^{-1} at 22°C. Each spectrum was acquired by adding together 64 interferograms. Lastly, the fluorescence emission and absorbance spectra of PBDM peptides and their conjugates were obtained using a multifunctional micro-titration plate reader, Tecan infinite M200 PRO (Tecan group Ltd., Mannedorf, Switzerland) (Moulick et al., 2018). The absorbance spectrum was measured within the range from 230 to 850 nm with the 2 nm step. For the fluorescence spectra measurement, 230 nm was used as excitation wavelengths and the fluorescence scan was measured within the range from 260 to 650 nm with the 2 nm step. The fractions were placed in UV-transparent 96 well microplate with flat bottom by Costar® (Corning Inc., Corning, NY, United States).

Cultivation of Bacterial Strains

Bacterial strains (*Staphylococcus aureus* NCTC 8511, Methicillin-Resistant *Staphylococcus aureus* (MRSA) ST239: SCCmecIIIA CCM 7111, Vancomycin-Resistant *Staphylococcus aureus* (VRSA) CCM 1767, Vancomycin-Resistant *Enterococcus faecalis* (VRE) ATCC 51299, *Escherichia coli* ATCC BAA 2340, *Enterococcus faecalis* ATCC 11700) were obtained from the National Collection of Type Cultures, England; American Type Culture Collection (ATCC), United States and the Czech Collection of Microorganisms, Faculty of Science, Masaryk University, Brno, Czechia. To the Mueller Hinton (MH) media of 15 mL in Erlenmeyer flask bacteria was inoculated and kept at 37°C, 130 rpm for 24 h. Further, the cultures were diluted using the Mueller Hinton (MH) broth to 0.1 Absorbance [0.5 MacFarland (McF) standards] at OD_{600nm} and used for successive experiments (Jelinkova et al., 2018a).

Antibacterial Assays

Growth Curves, Minimum Inhibitory Concentration (MIC) Determination and Viability Percentage

To determine the susceptibility of bacterial cultures the standard broth micro-dilution method (European Committee on Antimicrobial Susceptibility Testing) was used and detection was done by an unaided eye. The PBDM peptides were incubated with bacterial cultures (OD_{600nm} = 0.5 McF

and final dilution 1:100 with MH medium) in different concentrations (50, 25, 20, 10, and 5 μg/mL) at 37°C for 24 h. The lowest inhibiting concentration of the antimicrobial agent against each bacterium is the MIC of the antimicrobial agent with respect to that bacterium (Mazumdar et al., 2020).

The antibacterial activity of the PBDM peptides were determined using the Multiskan EX (Thermo Fisher Scientific, Waltham, MA, United States) by measuring the absorbance to obtain the growth curves. Different concentrations (50, 25, 20, 10, and 5 μg/mL) of the peptides were used to check the antibacterial activities. The control was without the peptides. Microplates with the volume of 300 μL were used to measure the absorbance. The solutions with different concentration of antimicrobial agent were added to the microplate wells and mixed with the bacterial cultures (0.5 MacFarland with final dilution 1:100 using MH medium). Later the plate was used in Multiskan EX for 24 h and results were evaluated the next day after 24 h to obtain the growth curves (Jelinkova et al., 2018a; Mazumdar et al., 2020; Sur et al., 2020a).

Further, the viability percentage was also calculated by using Multiskan EX, the final absorbance value at OD_{600nm} after 24 h of treatment of bacteria using the different concentrations (50, 25, 20, 10, and 5 μg/mL) of peptides in comparison with the positive control (Jelinkova et al., 2018b; Mazumdar et al., 2020).

Colony Forming Unit (CFU) Assay

The bacterial strains were grown in MH medium for overnight at 37°C in a shaking incubator at 140 rpm. The very next day the culture was diluted to OD_{600nm} = 0.1, in fresh MH medium overnight in the same condition until the OD_{600nm} = 0.3–0.5 was obtained. The culture was then diluted to OD_{600nm} = 0.1 and further diluted by 1:100 dilution factor which was followed by adding the peptides at their pre–determined Minimum Inhibitory Concentrations (MIC) (as mentioned in **Table 2**). Thereafter, the samples were drawn and results were obtained after 24 h incubation. Dilutions were made and the culture was spread on MH agar plates, which was incubated at 37°C incubator overnight and CFUs were determined the next day. Bacterial culture without PBDM peptides treatment wasere used as negative control and positive control was spread of untreated bacterial culture on agar plates prepared with tetracycline (10 μg/mL) and cefoxitin (32 μg/mL)kanamyicin (Zhou et al., 2012; Haque et al., 2017; Sur et al., 2019).

Application of Peptide on Bacterial Samples From Hospital Patients

The collection of swabs from infected wounds of three patients with the proper signed information and consent of the volunteer and subsequent bacteria cultivation was carried out according to Hegerova et al. (2017). Patient's enrollment into the clinical study was approved by the Ethics Committee of Trauma hospital in Brno, Czechia in accordance to act no. 378/2007 coll. For the bacteria identification, bacterial DNA was extracted using the Nucleo Spin Microbial DNA kit (Macherey-Nagel, Duren, Germany). The samples were obtained from the three different hospital patients and named accordingly (P1, P2, and P3). To amplify the 16S rRNA gene fragments, primers 27F-CC and 1492R were employed (Frank et al., 2008). Amplified products were purified analyzed using Sanger sequencing platform and obtained sequences were queried against the standard non-redundant nucleotide database (nr/nt) using Basic Local Alignment Search Tool for nucleotides (BLAST, blastn suite[1]). Multiple sequence alignment was performed using Clustal omega (Link[2]) to obtain the phylogenetic tree as shown in **Supplementary Section 3**. Later, the isolated samples were inoculated in MH broth and kept overnight at 37°C. They were diluted to obtain 0.1 Absorbance or 0.5 MacFarland with final dilution of 1:100 to study the growth curve in presence of different concentrations (50, 25, 20, 15, and 10 μg/mL) of PBDM peptides. Control was the sample bacteria without any treatment.

Microscopy

Microscopy of PBDM Against Bacteria in Ambient Light and Live/Dead Cell Assay and Detection of VRSA Using PBDM Peptides Conjugate

Initially the samples were incubated with bacteria culture and PBDM peptides (respective MIC) at 37°C for 4 h in shaking incubator. To study the antibacterial activity of the peptides against *S. aureus*, MRSA, VRSA, *E. faecalis*, VRE, and *E. coli* using respective MIC values of PBDM peptides (as mentioned in **Table 2**), the optical Olympus BX51 fluorescence microscope equipped with a 40X phase contrast lens was used. The number of cells visualized per samples was observed from 10 randomized microscopic grid fields.

Thereafter, an inverted Olympus IX 71S8F-3 fluorescence microscope (Olympus Corporation, Tokyo, Japan) equipped with Olympus UIS2 series objective LUCPlanFLN 40 × (N.A. 0.6, WD 2.7–4 mm, F.N. 22), a mercury arc lamp X-cite 12 (120 W; Lumen Dynamics, Mississauga, ON, Canada), and, a Camera Olympus DP73 was used for live/dead cell imaging and bright field microscopy. The images were processed using the Stream Basic 1.7 Software. The bacterial samples were incubated with respective MIC values of PBDM peptides for 4 h at 37°C in a shaking incubator. The two fluorescent dyes, SYTO9 stain cells by permeating both damaged and intact cell membranes and propidium iodide (PI) to stain the cells with damaged cell membranes (Jelinkova et al., 2018a). The optical bright field microscopic (Boulos et al., 1999) image analysis was also performed for both peptides with respective MIC values of PBDM peptides against *S. aureus*, MRSA, VRSA, *E. faecalis*, VRE, and *E. coli*, with number of cells visualized per samples was observed from 10 randomized microscopic grid fields. Furthermore, VRSA samples were incubated with PBDM peptide conjugates for 4 h at 37°C in a shaking incubator and observed under microscope (Milosavljevic et al., 2016; Hussain et al., 2018; Mazumdar et al., 2020). The number of cells visualized per samples was observed from 10 randomized microscopic grid fields.

[1]blast.ncbi.nlm.nih.gov/Blast.cgi

[2]https://www.ebi.ac.uk/Tools/msa/clustalo/

Detection of VRSA by PBDM–5(6)–Carboxyfluorescein and Cryo-SEM (Scanning Electron Microscope) Image Analysis to Understand the Mechanism

The VRSA cells were incubated with PBDM–5(6)–Carboxyfluorescein conjugates (15 and 10 μg/mL for PBDM1–5(6)–Carboxyfluorescein and PBDM2–5(6)–Carboxyfluorescein, respectively) for 30 min in dark and visualized under an inverted Olympus IX 71S8F-3 fluorescence microscope as discussed in the previous section. The images were processed using Stream Basic 1.7 Software (Milosavljevic et al., 2016).

Whereas, for Cryo-SEM the VRSA incubated for 4 h with PBDM peptides (15 and 10 μg/mL for PBDM1 and PBDM2, respectively) at 37°C in a shaking incubator and the control was VRSA without any treatment. Then the Cryo-SEM experiment method of plunge freezing was used. For plunging and storing of samples liquid nitrogen was used. Cryo-SEM visualization of samples was performed with FEI Versa3D equipped with a Quorum Cryo stage and transfer station (FEI Company) (Wu et al., 2014).

Testing of the Cytotoxicity (MTT Assay) and Estimation of Hemocompatibility Against Eukaryotic Cells

The HBL 100 (mammary gland epithelial cells) and MDA MB 468 (mammary gland adenocarcinoma cells) human cell lines were cultured by immortalization of cells in RPMI-1640 medium with 10% fetal bovine serum, supplemented with penicillin (100 U/mL) and streptomycin (0.1 mg/mL). The treatment with different concentrations of PBDM peptides (125, 62.5, 31.25, 15.63, 7.81, 3.9, 1.95, 0.98, 0.49, 0.24, and 0.12 μg/mL) was initiated after the cells reached ∼60 – 80% confluence. They were used to study the viability using MTT [3-(4,5-dimethylthiazol-2-yl)-2,5-diphenyltetrazolium bromide] assay. Briefly, the suspension of 5000 cells in 50 μL medium was added to each well of microplates, followed by incubation for 24 h at 37°C with 5% CO_2. After 24 h treatment using PBDM peptides, 10 μL of MTT [5 mg/mL in phosphate buffered saline (PBS)] was added to the cells and incubated for 4 h at 37°C. After that, MTT-containing medium was replaced by 100 μL of 99.9% dimethyl sulfoxide (DMSO) for 5 min incubation, absorbance of the samples was determined at 570 nm using Infinite m200 PRO (Tecan, Männedorf, Switzerland) (Heger et al., 2016). Further, the IC_{50} value of the PBDM peptides were calculated (**Supplementary Section S10**).

For hemocompatibility, Red blood cells (RBCs) were diluted with PBS (pH 7.4) and subsequently PBDM were added to RBCs solution in different concentration separately (40, 20, and 10 μg/mL) incubate at 37°C for 1 h. The positive and the negative control was 0.1% Triton X-100 and PBS, respectively. Thereafter, the samples were centrifuged at 3000 × *g* for 10 min and the absorbance of the samples was measured at 540 nm (Jelinkova et al., 2018a; Mazumdar et al., 2020). The formula is provided in the **Supplementary Section 5**.

In vivo Study of VRSA on BALB/C and the Treatment Using PBDM Peptides

The preparation of *in vivo* model infection and treatment was performed using the 7–8 weeks old, 18 to 19.5 g weight female Balb/c mice. Mice were divided into 4 sets each contains 3 balb/c mice (**Table 1**). They were anesthetized using an intramuscular injection of a mixture of xylazine (Rometar,® Spofaa.s., Prague, Czechia) at 10 mg/kg and ketamine (Narkamon,® Spofaa.s., Prague, Czechia) at 100 mg/kg with an 1 mL insulin syringe (BD Veo™ insulin syringes with BD Ultra-Fine™ 6 mm × 31G needle) (Welberg et al., 2006; Gargiulo et al., 2012; Spunda et al., 2018; Sur et al., 2020b). The fur was removed from mice using Nair® hair removal solution (Church & Dwight Co., Inc., Princeton, NJ, United States) and electric trimmer, 1 day prior to the experiment (Malachowa et al., 2013). The experimental condition throughout were maintained at 22 ± 1°C, light administration (12 h L and 12 h D) with maximum illumination of 200 lux and 60% humidity. The negative control was balb/c mice with no treatment and the positive control were balb/c mice infected with VRSA without any treatment. The experiments were approved by the Ethics Commission at the Faculty of AgriSciences, Mendel University in Brno, Czechia in accordance with Act No. 246/1992 Coll. to protect the animal from cruelty.

Introducing the Skin Infection

An overnight VRSA culture was cultivated at 37°C before the administration of the infection. The absorbance at 600 nm was used to make the culture 0.1 absorbance. Skin infection was introduced by subcutaneous injection with 0.05 mL of inoculum of VRSA (concentration 10^7 CFU/mL) using 1 mL insulin syringe (Malachowa et al., 2013; Hussain et al., 2018; Sur et al., 2020b).

Treatment With PBDM Peptides and Monitoring the Mice

The treatment of the VRSA infected mice was done two times a day with PBDM1 and PBDM2 peptides, respectively, by subcutaneous injection at the site of infection and topical administration of the peptides on the surface of the exposed infected area until the mice recovered. During the treatment the final concentration of PBDM1 and PBDM2 peptides final concentration was 15 and 10 μg/mL, respectively. The images were taken using digital camera (Nikon digital camera (D40), NIKON Corp., Japan) to keep the record of the changes that underwent before and after the treatment (Koch, 2006; O'Toole

TABLE 1 | Preparation of animal sets.

Animal Set	*Purpose of use*
One	Uninfected control
Two	Infected control without treatment
Three	Infected mice treated with PBDM1
Four	Infected mice treated with PBDM2

et al., 2012; Sevgi et al., 2013; Sykes et al., 2014; Sur et al., 2020b). The images of the control set were also take using the same camera.

RESULTS AND DISCUSSION

The design, synthesis and characterization of the PBDM peptides were done using different computational, biophysical and biochemical technique. Thereafter, antibacterial activity of the peptides, against *S. aureus*, VRSA, MRSA, VRE, *E. coli*, *E. faecalis* and hospital samples from live patients were studied. Followed by the understanding of the mechanism of action using Cryo-SEM. Further, the *in vitro* and *in vivo* studies helped to obtain the information about peptide toxicity, biocompatibility and medicinal value. Since, VRSA has a high resistance toward almost all antibiotics effective against gram positive bacteria, thus it proves to be an ideal test model for a novel antimicrobial agent (Jelinkova et al., 2018a). Thus, VRSA infection was introduced in balb/c to which PBDM peptides were applied and change in infection was studied.

Molecular Dynamics Simulation Analysis

One microsecond MD simulation was used to study the structure of the peptides at room temperature condition. For PBDM1 and PBDM2 peptides, the average total energy of simulation was −6.59e + 04 kJ/mol (−8.09e + 04 kJ/mol potential energy and 1.50e + 04 kJ/mol kinetic energy) and −6.69e + 04 kJ/mol (−8.20e + 04 kJ/mol potential energy and 1.50e + 04 kJ/mol kinetic energy), respectively. Average temperature was 3.00e + 02 K for both the peptide and average pressure was 1.79 bar and 1.45 bar. Cluster analysis of trajectories every 500 ps showed three stable and highly similar clusters (**Figures 1A,B**) but in case of PBDM2 every 500 ps showed the top three major clusters covering 23.4% of simulation time (**Figure 2A**), which is indicative of the random conformations throughout the simulation. The PBDM1 The PBDM1 peptide forms a U-shaped backbone with highly stable termini for periods of ∼200 ns (**Figures 1A,B**). Upon detachment of the B-bridge between K2 and L11 residues, the peptide switches to random coil secondary structure for ∼200 ns as well (**Figure 1C**). Average secondary structure compositions were Coil (55%), Bend (24%), B-bridge (9%), and Turn (9%) (**Figure 1D**). RMSD analysis showed similarity in the three major clusters as compared to the random coil conformation (**Figure 1E**). The whole peptide RMSD against first frame (alpha-helix) was in the range of 6–8 Å. Whole peptide RMSD against the representative frame of the major cluster was in the range 4 Å or lower. The terminal pairs YK (N-terminus) and LC (C-terminus) have very stable conformations and very low deviation below 2 Å.

Whereas in case of PBDM2 peptide, most of the conformational similarity between the three top clusters was in the HLIK loop (sixth to ninth residues) (**Figure 2B**). A B-Bridge between K2 and L11 residues was formed within the first 100 ns of simulation, however, it was not stable due to possible positive charge repulsion between K2 and K9/K10 residues (**Figure 2C**). Average secondary structure compositions were Coil (67%), Bend (16%), Turn (8%), and 3-Helix (6%) (**Figure 2D**). RMSD analysis shows deviations in the range of 5–9 Å. The top cluster showed RMSD values below 4 Å (**Figure 2E**). Despite the peptide sequence of alternating residues (two charged and two hydrophobic), no alpha helix was observed. On the other hand, the stability of a U-shaped conformation was destabilized by the repulsion between the positively charged lysines.

Molecular dynamics simulation showed the PBDM1 peptide to alternate between stable U-shaped backbone and random coil in 200 ns intervals. One explanation for the stability of the U-shaped conformation is the stability of the terminal pairs YK (N-terminus) and LC (C-terminus). Also the proximity of aromatic side-chain of F4 residue to aliphatic side-chain of L11 and the carbon chain of K2 can play role via hydrophobic interactions. But in case of PBDM2 peptides the structure was mainly random coil and U-shaped conformation was destabilized due to the presence of positively charged lysines and the repulsion between them.

Characterization of PBDM

The PBDM peptides and their conjugates were purified using HPLC-UV. The chromatogram for PBDM1 contains two peaks showing at two different retention time. The peak 1 denotes PBDM1 and peak 2 is the PBDM1–5(6)–Carboxyfluorescein conjugate as shown in **Supplementary Figure S11A**. Whereas in case of PBDM2 similar results were seen but the retention time were different as shown in **Supplementary Figure S11B**. The eluates obtained from the HPLC-UV at respective time intervals were used to perform MALDI-TOF mass spectrometry.

The MALDI-TOF MS for each samples were performed and two different peaks were obtained which represents PBDM peptides and their related PBDM–5(6)–Carboxyfluorescein conjugates as shown in **Supplementary Figure S11D and S11F**. The peak of PBDM1 and PBDM2 peptides were obtained at 1477.605 Da and 1633.797 Da whereas, their conjugates produced peaks at 1835.632 Da and 1991.803 Da, respectively. The mass difference of 358.03 and 358.01 were seen due to the displacement of N–hydroxysuccinimide (115.09 Da) after formation of the PBDM–5(6)–Carboxyfluorescein. Thus, the formation of conjugates was confirmed.

The absorbance spectra were obtained for PBDM–5(6)–Carboxyfluorescein conjugates, with each showing similar pattern in spectrum (305 to 1000 nm) with absorbance maxima at 485 and 470 nm, respectively but PBDM peptides showed no prominent absorbance. Thus the formation of conjugate showed visible change in absorbance spectra as shown in **Supplementary Figure S11C**. The reported λ_{em} (emission) of Carboxyfluorescein N-hydroxysuccinimide ester is at 518 nm (Keller et al., 2002). Similarly, the emission spectra (380 to 600 nm) for the PBDM1 and PBDM2 conjugates showed the λ_{max} (emission maxima) peak at 540 and 542 nm with high fluorescence intensity but no emission was observed for PBDM peptide (**Supplementary Figure S11E**). Thus, the conjugates can be used for detection of bacteria using fluorescence microscope in the red fluorescence region.

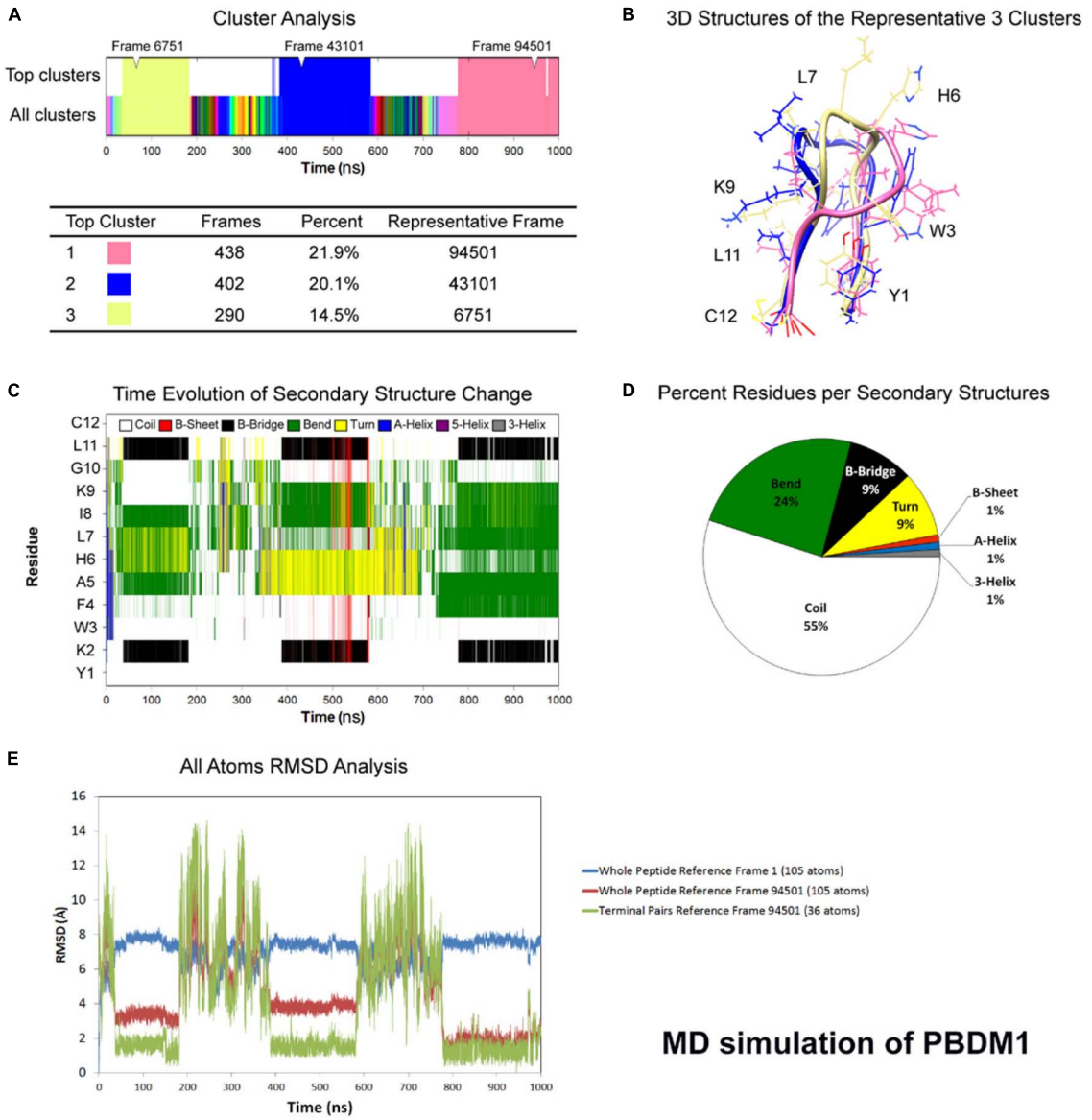

FIGURE 1 | Atomistic molecular dynamics of PBDM1 in explicit water in NPT ensemble for 1000 ns at 300 K temperature. **(A)** Cluster analysis showing three major clusters covering 56.5% of simulation time (∼565 ns). **(B)** 3D structures of the representative frames of the three major clusters. The terminal pairs YK (N-terminus) and LC (C-terminus) have very stable conformations and very low deviation below 2Å. **(C)** Time evolution graph of secondary structure change with clear formation of B-Bridge between K2 and L11 (black color). The bends and turns are clear in the center of the peptide (green and yellow colors, respectively). **(D)** Secondary structures described by percent residues per assignment, and calculated by averaging the counts of residues for each secondary structure assignment in each frame. Coils, Bends, B-bridges and turns are predominant. **(E)** Root mean square deviations (RMSD) analysis. In the timeframe of the three major clusters, whole peptide RMSD against first frame (alpha-helix) was in the range of 6–8 Å. Whole peptide RMSD against the major cluster was in the range 4 Å or lower.

ATR-FT-IR analysis (**Supplementary Figure S11G**) of the amide I band correlated with MD simulation results. The amide I (peak at 1650 cm^{-1}) corresponds to the C = O stretching and it is clear indication of vibrations that are connected with alpha helix and random coil. Furthermore, the peak indicates absence of beta-sheet, a signature of short range interaction between backbones seen in peptide aggregations (Adochitei and Drochioiu, 2011). The amide II band (peak at 1539 cm^{-1}) and amide III band (double peak at 1200–1210 cm^{-1}) correspond to N-H bending and C-N stretching. The broad bands in 2500–3500 cm^{-1} correspond to O-H (peak at 3290–3305 cm^{-1}) and C-H (double peak at 2945–2965 cm^{-1}) stretching (Coates, 2006).

Finally, after the characterization of the PBDM peptides, they were used to study its antibacterial efficacy using different microbiological assays. Whereas the PBDM–5(6)–Carboxyfluorescein conjugates were used for the detection of the interaction of bacteria with the peptides using fluorescence microscope.

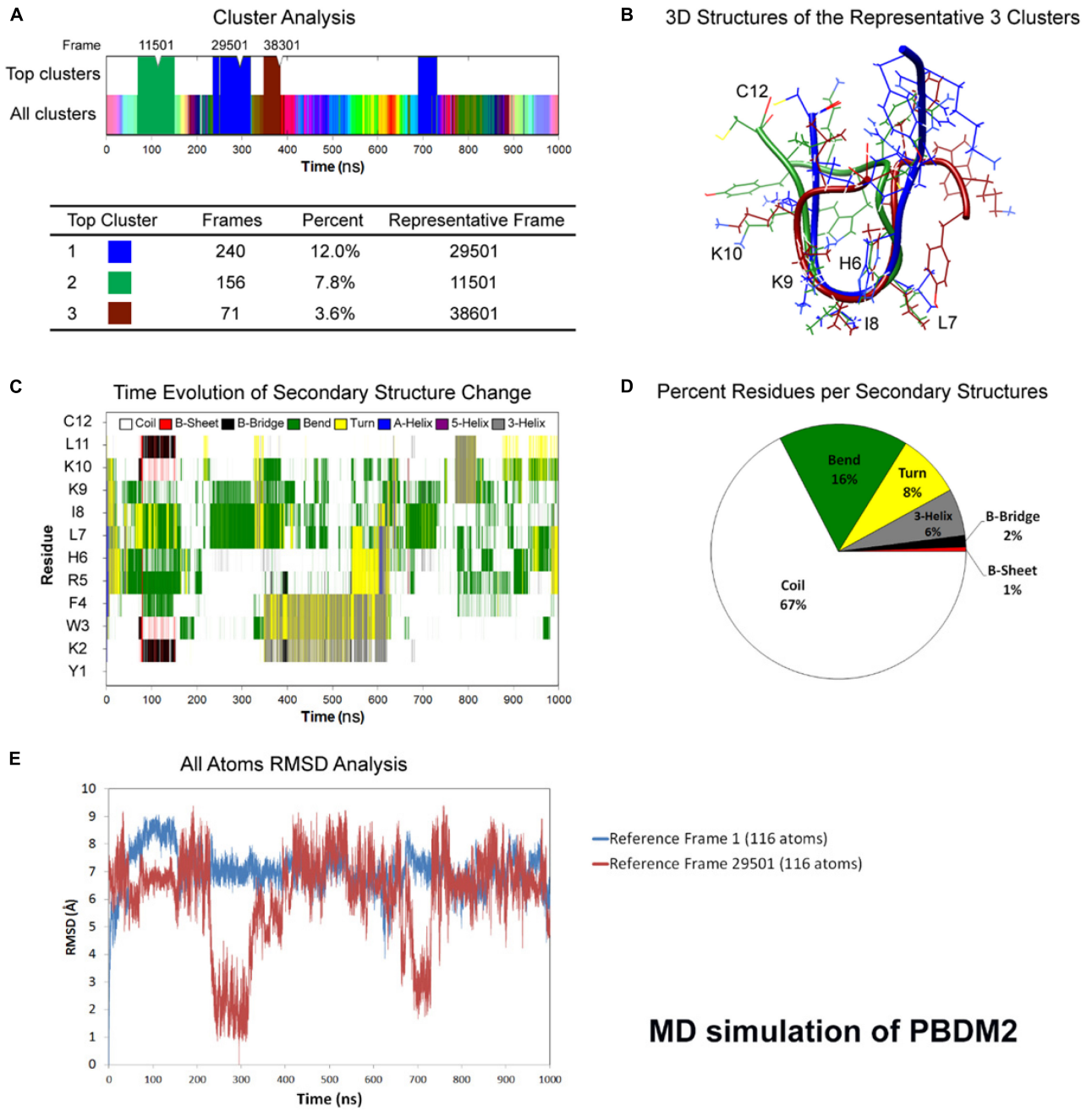

FIGURE 2 | Atomistic molecular dynamics of PBDM2 in explicit water in NPT ensemble for 1000 ns at 300 K temperature. **(A)** Cluster analysis showing top three major clusters covering 23.4% of simulation time (~234 ns). **(B)** 3D structures of the representative frames of the three major clusters. The most similar conformation is in the center of the peptide between sixth and ninth residues. **(C)** Time evolution graph of secondary structure change. **(D)** Secondary structures described by percent residues per assignment, and calculated by averaging the counts of residues for each secondary structure assignment in each frame. Coils were the most predominant. **(E)** Root mean square deviations (RMSD) analysis shows deviations in the range of 5–9 Å. The top cluster showed RMSD values below 4 Å.

PBDM Activity Against Different Bacterial Strains

The initiation to understand the antibacterial efficacy of PBDM peptides was done by determining their MIC (shown in **Table 2**) against *S. aureus*, MRSA, VRSA, *E. faecalis*, VRE and *E. coli* using broth microdilution method. The MIC value of PBDM1 was found to be as 10 μg/mL against *S. aureus*, MRSA, and *E. coli*. Whereas, in case of *E. faecalis*, VRSA and VRE the MIC was found to be 30, 15, and 20 μg/mL. But, the MIC value for PBDM2 was 10 μg/mL when tested against *S. aureus*, MRSA, VRSA, VRE, and *E. coli*. Whereas, in case of *E. faecalis* the MIC was found to be 20 μg/mL. The concentration

TABLE 2 | Minimum Inhibitory Concentrations (MICs) of PBDM1 and PBDM2 by broth micro–dilution method.

Bacterial Strains	PBDM1 (μg/mL)	PBDM2 (μg/mL)
S. aureus	10	10
MRSA	10	10
VRSA	15	10
E. faecalis	30	20
VRE	20	10
E. coli	10	10

below the MIC value showed turbid solution which concludes the presence of bacteria with less or no antibacterial activity (Mazumdar et al., 2020).

Thereafter, the growth curve analysis was performed with *S. aureus*, MRSA, VRSA, *E. faecalis*, VRE, and *E. coli* in the presence of PDBM peptides to study the growth pattern of each bacterium over 24 h time duration. The PBDM1 treated *S. aureus* showed high inhibition of 94.3% at 50 μg/mL and lower in concentration of 20 and 10 μg/mL also showed inhibitions of more than 94% but further lower concentration of 5 μg/mL showed no inhibition (**Figure 3A**). In case of PBDM2 treated *S. aureus* steady 93% inhibition at 50 μg/mL and similar effects for 20 and 10 μg/mL were observed but increase in growth was seen at 5 μg/mL (**Figure 4A**). Similar results were obtained when PBDM1 treated MRSA was analyzed (**Figure 3C**). However, MRSA treated PBDM2 also showed similar effects as *S. aureus* till 10 μg/mL (98.2%) (**Figure 4C**). Further, PBDM1 treated VRSA showed almost 99% inhibition till 15 μg/mL concentration but lower concentrations showed increase in growth (**Figure 3E**). In case of VRSA treated with PBDM2 (**Figure 4E**) showed more than 94% inhibition till 10 μg/mL but concentration below showed no inhibition. Whereas, PBDM1 treated *E. faecalis* growth curve showed good inhibitions of 95% at 50 μg/mL but decrease in concentrations with time showed increase in growth and inhibition of more than 55% until 10 μg/mL but lower concentration of 5 μg/mL showed no inhibition as shown in **Figure 3G**. PBDM2 treated *E. faecalis* (**Figure 4G**) showed 90% inhibitions for 50, 20, and 10 μg/mL until 15 h but after that the gradual increase in growth was observed whereas, 5 μg/mL treatment showed a steady growth. For PBDM1 treated VRE, almost all of the concentrations showed inhibition of more than 52% but 50 μg/mL concentration treatment showed significant inhibition of 93% as shown in **Figure 3I**. Similarly, for PBDM2 treated VRE (**Figure 4I**) inhibition of 89% at 50 μg/mL but lower concentration until 10 μg/mL showed more 50% inhibition but 5 μg/mL showed less than 40% inhibition. Finally, for PBDM1 treated *E. coli* growth showed steady inhibition till 10 μg/mL with 96% inhibition but below this concentration no prominent inhibition was obtained (**Figure 3K**). Similarly, PBDM2 treated *E. coli* showed more than 92% inhibition until 10 μg/mL but concentration below had no prominent inhibition (**Figure 4K**). Thus, PBDM1 showed good antibacterial effects against all the tested bacteria whereas PBDM2 had similar effects toward the tested bacterial strains except in case of *E. faecalis* the antibacterial effect was moderate (50%).

Henceforth, to further validate the antibacterial activity the viability percentage assay was performed. The viability percentage of PBDM1 treated *S. aureus* was very low when treated with 50 μg/mL (5.72%) until 10 μg/mL (2.72%) but concentration below showed viability of 95% (**Figure 3B**). Whereas, PBDM2 treated *S. aureus* showed very low viability from 50 μg/mL (7.4%) until 10 μg/mL (2.8%) showing significant inhibitory effects, but lower concentrations showed increase in viability to 43.5% at 5 μg/mL (**Figure 4B**). For PBDM1 treated MRSA similar results as seen for *S. aureus* was obtained (viability less than 2.6% until 10 μg/mL) but lower concentration showed rapid increase in viability (**Figure 3D**). Similarly, PBDM2 treated MRSA showed no inhibition at 5 μg/mLbut concentration of 10 μg/mL and higher showed low viability around 1.8% (**Figure 4D**). In case of PBDM1 treated VRSA the viability was very low until 15 μg/mL (0.61%) but the concentration below (10 and 5 μg/mL) showed no prominent inhibition (**Figure 3F**). Whereas, PBDM2 treated VRSA showed low viability till 10 μg/mL (0.97%) but lower concentration showed prominent increase in viability up to 80% (**Figure 4F**). The viability of VRE and *E. faecalis* was not low in comparison to *S. aureus* and it resistant strains at lower concentrations 15and 20 μg/mL. But the viability was less than 4.6% for *E. faecalis* when treated with 50 μg/mL of PBDM1 and lower concentrations like 15 μg/mL (41.7%) and 20 μg/mL (39.5%) showed some inhibitory effects but concentration below showed no inhibition (**Figure 3H**). Whereas, PBDM2 treated *E. faecalis* (**Figure 4H**) showed overall viability less than 50% viability until 20 μg/mL but the lower concentration of 10 μg/mL showed an inhibition of less than 35.6% and concentration below showed increase in viability (63.3%). For PBDM1 treated VRE (**Figures 3J**, **4J**) showed inhibitory effects for all the concentrations with viability below 48% and lowest viability was 6.6% at 50 μg/mL. Similarly, PBDM2 treated VRE showed viability of 10.5% at 50 μg/mL and further lower in concentration like 20 μg/mL (51.7%) to 5 μg/mL (63.9%) showed increase in viability (**Figure 4J**). Finally, *E. coli* (gram negative bacteria) treated with PBDM1 showed very low viability at 50 μg/mL (5.6%) and 20 μg/mL (2.9%). PBDM2 treated *E. coli* showed constant inhibition from 50 μg/mL (8.1%) to 20 μg/mL (3%). Whereas, both the PBDM peptides showed lowest viability at 10 μg/mL for PBDM1(3.5%) and PBDM2 (2.8%) but concentration below showed no prominent inhibitory effects as shown in **Figures 3L**, **4L**, respectively. The control of the experiment was bacterial cultures without any treatment showing normal stable viability of 100%. Further, the colony forming assay was performed to confirm the antibacterial effects of PBDM peptides against *S. aureus*, MRSA, VRSA, *E. faecalis*, VRE, and *E. coli*. PBDM1 treated bacterial strains with respective MICs showed no colonies for any bacterial strains except four colonies visible for *E. faecalis* after 24 h. Similarly, in case of PBDM2 treated bacterial strains showed identical results except in case of *E. faecalis* few more number of colonies were obtained. Whereas, the negative control showed significant bacterial growth but in case of positive control (tetracycline and cefoxitin) no bacterial growth was observed (**Supplementary Figure S10**).

Thus, the above tests confirmed the significant antibacterial activity of PBDM peptides against *S. aureus*, MRSA, VRSA, and

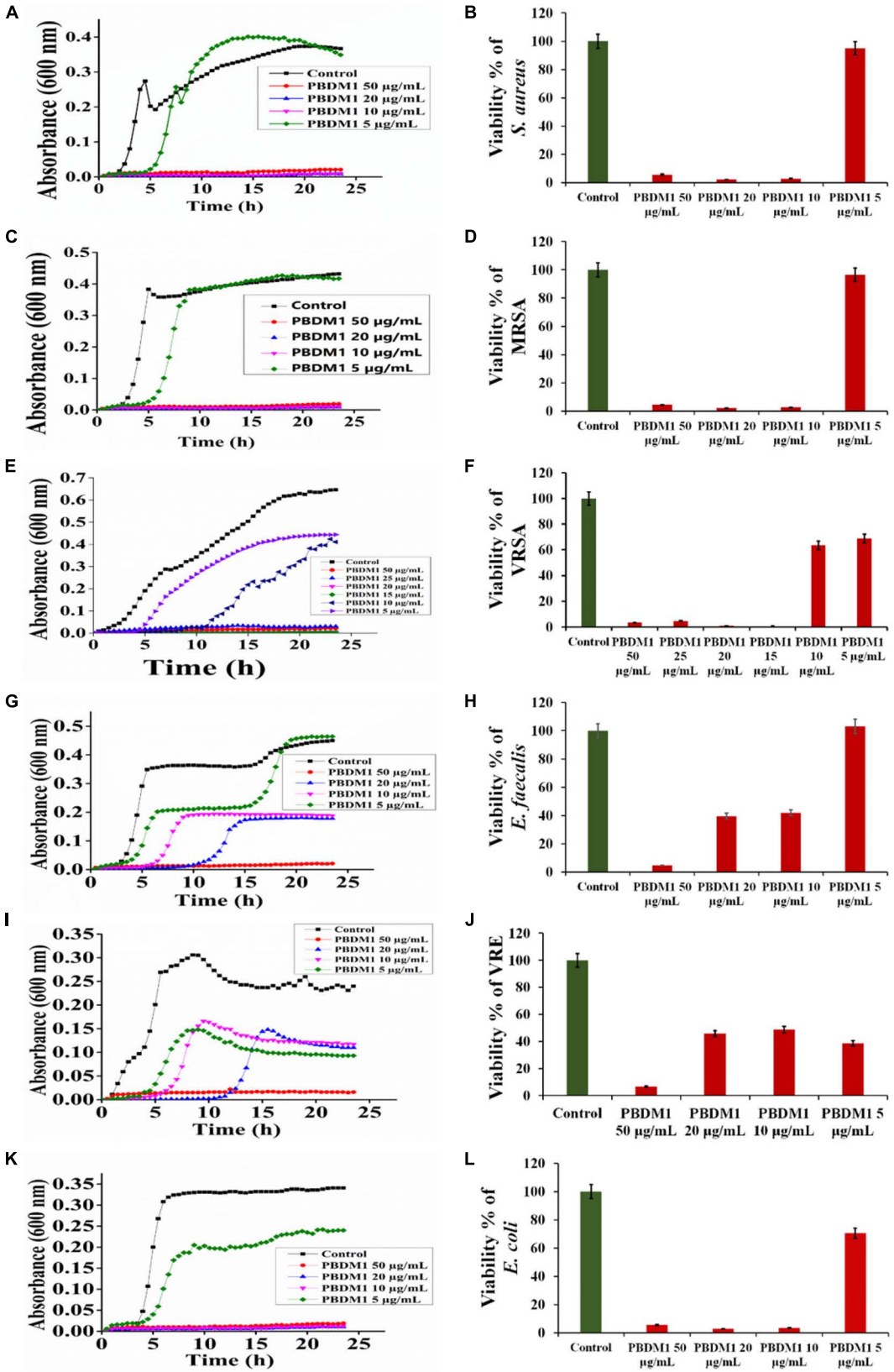

FIGURE 3 | The Growth curve and Viability percentage of *S. aureus* **(A,B)**, MRSA **(C,D)**, VRSA **(E,F)**, *E. faecalis* **(G,H)**, VRE **(I,J)** and *E. coli* **(K,L)** in presence of PBDM1. Data represent the mean ± SD, $n = 3$.

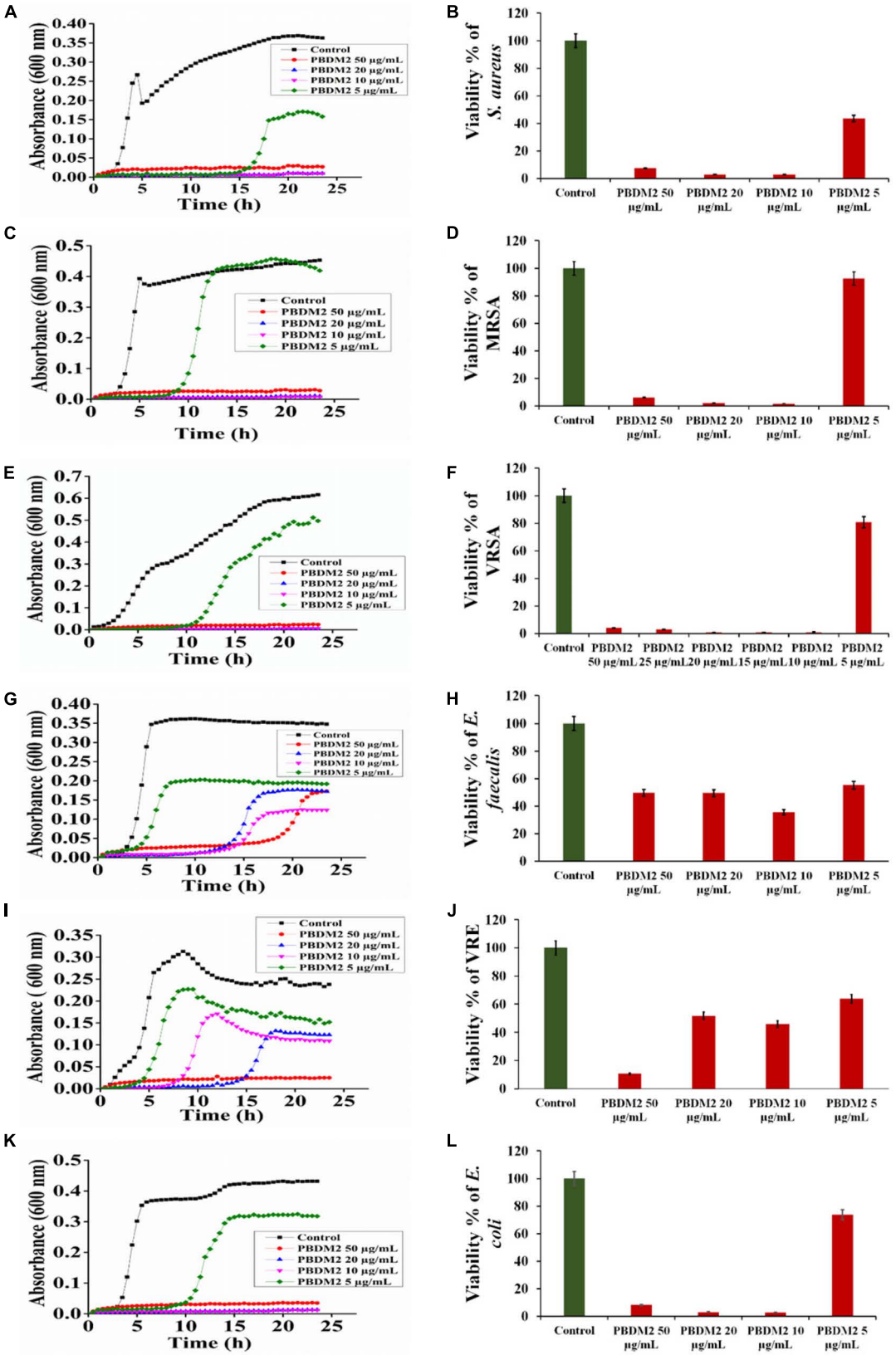

FIGURE 4 | The Growth curve and Viability percentage of *S. aureus* **(A,B)**, MRSA **(C,D)**, VRSA **(E,F)**, *E. faecalis* **(G,H)**, VRE **(I,J)** and *E. coli* **(K,L)** in presence of PBDM2. Data represent the mean ± SD, $n = 3$.

E. coli. But in case of *E. faecalis* and VRE the concentration of the peptide showing high antibacterial activity was higher in comparison to other bacterial strains. The *E. faecalis* strain used in our study was a wild type strain. We do not know if resistance to peptide could arise through plasmids, therefore we can only postulate. We have preliminary LC-MS data (unpublished) for peptide-treated VRSA protein extracts showing high levels of proteases expressed, and to our knowledge that is the only mechanism that can explain resistance in *E. faecalis*. Further studies are required to explain possible peptide resistance mechanisms. However, to further validate the antibacterial activity of PBDM peptides microscopic analysis were performed.

Microscopic Analysis of Treated Bacterial Cells Under Phase Contrast Condition and Live/Dead Cell Imaging

The phase contrast condition was used to further visually confirm the antibacterial efficacy of PBDM peptides against *S. aureus*, MRSA, VRSA, VRE, *E. faecalis*, and *E. coli*. The number of viable bacterial cells decreased after the treatment with the PBDM peptides for all the bacterial strains. The loss of cell integrity and morphological changes were observed. Further, cell wall rupture caused the cytoplasmic leakage and presence of cell debris was visualized for all the treated bacterial strains (**Figure 5A**). Whereas, the control bacterial cells showed high number of viable cells with no cell debris, sign of change in morphology and cellular integrity. Thus, the PBDM peptides showed prominent antibacterial effects against the bacterial samples tested.

Further, the viability of the bacterial strains in the presence of PBDM peptides were observed by the live/dead cell assay using the inverted fluorescence microscopy (**Figure 5B**). The bacterial samples treated with the PBDM peptides showed a visible increase in the red fluorescent dots. Thus, its clearly indicates the decrease in the viability of the bacteria (negligible green fluorescent) and increase in number of dead cells with high red fluorescent dot as compared to control samples. Due to the inhibitory effects of the PBDM peptides the number of bacterial cells were less compared to the control. Conversely, the bacterial samples without treatments were used for control, showing high numbers of live green fluorescence bacterial cells with negligible dead red fluorescence cells.

Thereafter, the ambient light illumination by optical bright field microscopy also confirmed the antibacterial effect of the PBDM peptides against *S. aureus*, MRSA, VRSA, VRE, *E. faecalis*, and *E. coli*. Decrease in the viable bacterial cell numbers and disruption of cells with loss of integrity and presence of cell debris were seen in almost all the bacterial samples in comparison to the control groups (**Supplementary Figure S6**). These results were in good agreement with the phase contrast analysis. Thus, the results for all the different treated bacterial samples showed prominent reduction in the viability establishing their high antibacterial potential (Stiefel et al., 2015). So, the probable mechanism of action for PBDM peptides were assumed to be via the cell wall disruption of bacterial cells. Moreover, as a lot of studies are well known for both VRE and MRSA till date. Whereas few studies are published with VRSA which was the main focus for their study. Also when we performed a thorough search in the Web of Science portal with parameter as "VRSA infection," "*in vivo*," "Vancomycin resistant Staphylococcus aureus" and "antibacterial activity" showed only 5 articles. However, it has been already well proven that VRSA has acquired resistance from VRE against Vancomycin. Furthermore, VRSA is also one of the pathogenic bacteria prioritized by WHO (World Health Organization) which too needs immediate check. Thus, we wanted to study the potential of the peptides against a vancomycin resistant strain. Therefore, further studies were carried out by the representative pathogenic bacterial strain, VRSA for consecutive analysis (Jelinkova et al., 2018a; Sur et al., 2020b).

Detection of VRSA Using PBDM–5(6)–Carboxyfluorescein and Cryo-SEM Microscopic Investigation of Vancomycin Resistant Staphylococcus Aureus

To understand the way PBDM peptides interacts with the VRSA cells, PBDM peptides conjugates were formed, which were used for detection under fluorescence microscope. The conditions of controls were VRSA cells with and without PBDM peptides, both the control conditions showed no red fluorescence as shown in **Supplementary Figure S7**. Whereas the VRSA cells incubated with the conjugates showed red fluorescence emitting from the VRSA cells proving that PBDM–5(6)–Carboxyfluorescein conjugates emits a red fluorescence after interacting with the VRSA cells under fluorescence microscope. The interaction of PBDM1–5(6)–Carboxyfluorescein and PBDM2–5(6)–Carboxyfluorescein with the VRSA cells provide evidence that the cells are present in the same field showed by red fluorescence which were in identical position when observed under bright field microscope (**Figure 6**). Thus, it can be used to understand the interaction of peptides with the help of its conjugates emitting red fluorescence.

The analysis of VRSA with and without PBDM peptides were done using the Cryo SEM. The sample preparation by plunging method using liquid nitrogen results in the production of many layer of artifact. The best field was searched and selected for further analysis (Wu et al., 2014). The VRSA cells treated with PBDM1 showed distorted cell wall and rupture in the cell surface. These cells also showed the property to agglomerate and change in cell integrity, which is due to the after effects of cell damage by PBDM1.

Whereas in case of VRSA without any treatment showed round spherical cell surface with intact cell membrane (**Figure 8**). In case of PBDM2 treated VRSA cells showed deformed globular cell surface with change in morphology but no visible rupture. Thus, the damage to VRSA cells was clearly observed due to the presence of PBDM peptides, however, the interaction was different. It can be concluded that PBDM behave like a cell penetrating peptide by destroying VRSA cell wall but in case of PBDM1 the mechanism can be the cell wall damage followed by damaged cell aggregations (**Figure 7**) whereas the mechanism for PBDM2 was observed to damage the VRSA cell

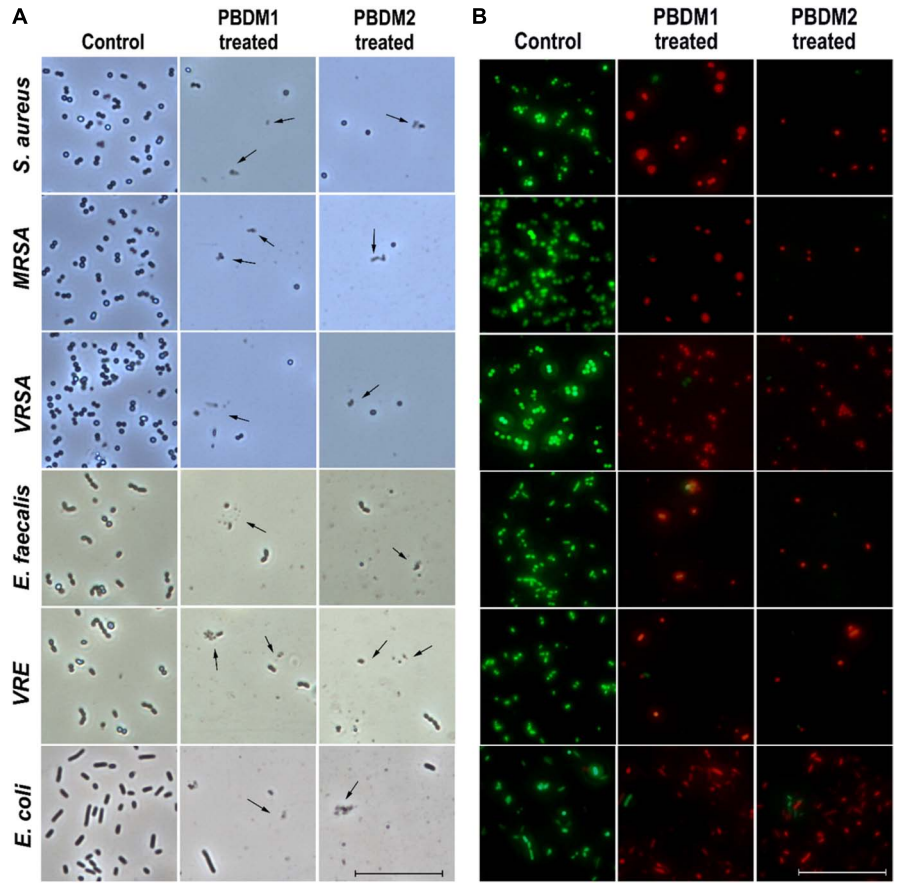

FIGURE 5 | (A) The phase contrast microscopic image of *S. aureus*, MRSA, VRSA, *E. faecalis*, VRE, and *E. coli* after treatment with PBDM peptides, black arrows showing cell rupture with cellular debris but cells in comparison to the control. Scale is 5 μm. **(B)** The live/dead cell image of *S. aureus*, MRSA, VRSA, *E. faecalis*, VRE, and *E. coli* after treatment with PBDM peptides showing green fluorescence for live cells and red fluorescence for dead cells. Scale is 10 μm.

walls forming small bubble shaped leading to change in integrity of cells and their morphology but no aggregations were observed (**Figure 7**). It is also likely that these bubble-shaped formations are attributed to the crystalized peptides during the Cryo-SEM procedure. Thereafter, the PBDM peptides were used to study its antibacterial effects against hospital patient bacterial samples.

Hospital Patient Bacterial Samples in the Presence of PBDM

Probiotic Bacteriocin Derived and Modified peptides were tested on samples obtained from wounds of three different hospital patients, designated P1, P2, and P3 The samples P1A1, P1B1, and P1B2 were identified as strains of *Staphylococcus aureus*. When the samples were tested by growth curve analysis using PBDM1 showed inhibition (**Supplementary Figure S2**) of more than 99% for all the concentrations (50, 25, and 10 μg/mL) tested except for P1A1 (71% viability) which showed no prominent inhibition at 10 μg/mL. Whereas, PBDM2 showed inhibitory effects of 99% for all the concentrations (50, 25, and 10 μg/mL) tested. Similar, results were obtained for both the peptides when the viability percentage was performed which confirmed the significant antibacterial activity of PBDM peptides against P1 patient samples (**Supplementary Figure S2A**).

For samples from patient P2 were identified as *Staphylococcus epidermidis* (P2A1) and *Klebsiella pneumoniae* (P2B1, P2C1, and P2C2). The growth curve and viability percentage showed significant inhibitions of more than 98% for all the concentrations (50, 25, and 10 μg/mL) (**Supplementary Figure S3A**) except for sample P2A1 (72%) at 10 μg/mL (**Supplementary Figure S3B**). Whereas the P2 samples when tested with PBDM2 showed significant inhibition and almost negligible viability for all the concentrations tested (**Supplementary Figure S3**).

Lastly, the samples from patient P3 were identified as *Staphylococcus aureus* (P3A1), and *Enterobacter cloacae* (P3B1 and P3C1). PBDM1 tested against P3A1 showed prominent inhibition of 99% till 25 μg/mL (**Supplementary Figure S4A**) but 30% inhibition at 10 μg/mL. Whereas, PBDM1 tested against P3C1 (*Enterobacter cloacae*) was effective and caused an 98.7% inhibition till 15 μg/mL but lower concentration of 10 μg/mL showed viability of 72% (**Supplementary Figures S4E,F**). Growth curves in presence of PBDM1 supports the results obtained through viability

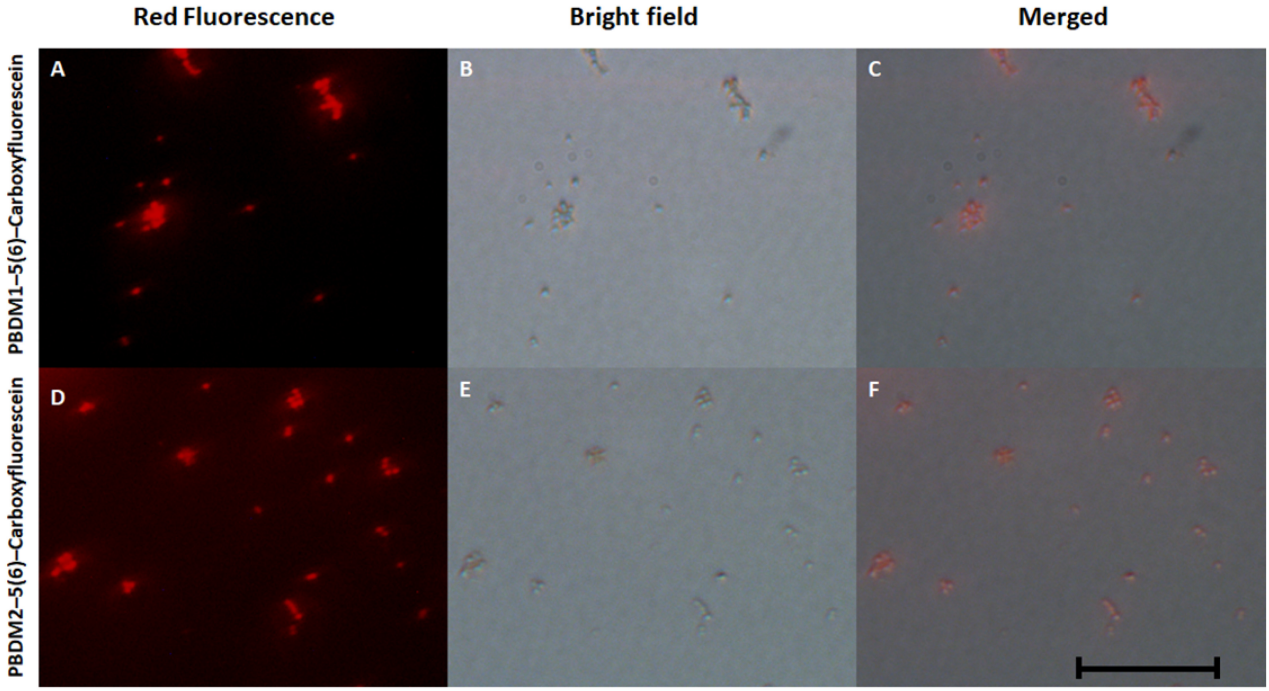

FIGURE 6 | (A,D) showing he fluorescence microscopic image of PBDM1–5(6)–Carboxyfluorescein and PBDM–5(6)–Carboxyfluorescein interacts with the VRSA cells, respectively; **(B,C)** showing bright field image of PBDM1–5(6)–Carboxyfluorescein and PBDM2–5(6)–Carboxyfluorescein interacts with the VRSA cells; **(C,F)** showing the merged image of **(A)** with **(B)** and **(D)** with **(E)**. Scale is 20 μm.

percentage assay. Whereas, in case of PBDM2, all the sample from P3 patients showed significant inhibition of more than 98% for both growth curve and viability percentage assay (**Supplementary Figure S4**).

Thus, PBDM2 peptide showed better antibacterial activity in comparison to PBDM1 peptide even at 10 μg/mL against, P1A1, P2A1, P3A1, and P3C1 (**Supplementary Table S1**). So both the peptides can be used with some medicinal value against hospital associated pathogenic bacteria. PBDM peptides showed high antibacterial activity against gram positive bacteria as seen in nisin peptides but in case of VRE and *E. faecalis* the activity of PBDM peptides needed higher concentrations for prominent antibacterial efficacy. However, PBDM not only showed activity against gram positive bacteria but also was effective against gram negative bacteria which were not seen in case of nisin peptides without any modification (Jozala et al., 2015; Shin et al., 2016; Vukomanović et al., 2017; Fernández-Pérez et al., 2018). So, further *in vitro* studies using human cell lines to study toxicity and *in vivo* studies were performed to check the antibacterial activity and biocompatibility against infected balb/c mice.

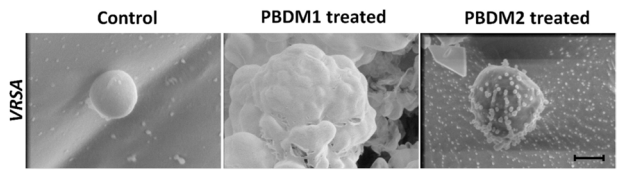

FIGURE 7 | Cryo-SEM microscopic analysis of VRSA cells treated with PBDM1 and PBDM2 peptides, respectively. Control is untreated VRSA. Scale is 500 nm.

Influence and Toxicity Test of PBDM on Eukaryotic Cells

The efficiency of any novel antimicrobial agent is enhanced if the molecule is effective and non-toxic toward normal mammalian cells. Thus, cytotoxicity of PBDM peptides were evaluated using MDA MB 468 and HBL 100 cell lines by MTT assay. The HBL 100 cells showed no sign of toxicity until 31.25 μg/mL of PBDM1. However, 19% inhibition around 62.5 μg/mL with viability more than 80% was observed but higher concentrations reduces the viability (50%). Therefore, PBDM1 was found to be non-toxic at its effective MIC against HBL 100 cells but toxicity increases with concentrations higher than 62.5 μg/mL. Similarly, PBDM2 showed no toxicity until 31.25 μg/mL (MIC range) but higher concentrations showed reduction in viability (58.6 to 40%). Whereas, the MDA MB 468 adenocarcinoma cells in presence of PBDM peptides showed viability below 25% at 31.25 μg/mL and higher concentrations showed even further reduction of viability for both the peptides. At 15 μg/mL showed 79.9% viability for PBDM2 but no reduction of viability was seen for PBDM1 concentrations below showed no toxicity. The IC_{50} values of PBDM1 and PBDM2 peptides were 115.02 and

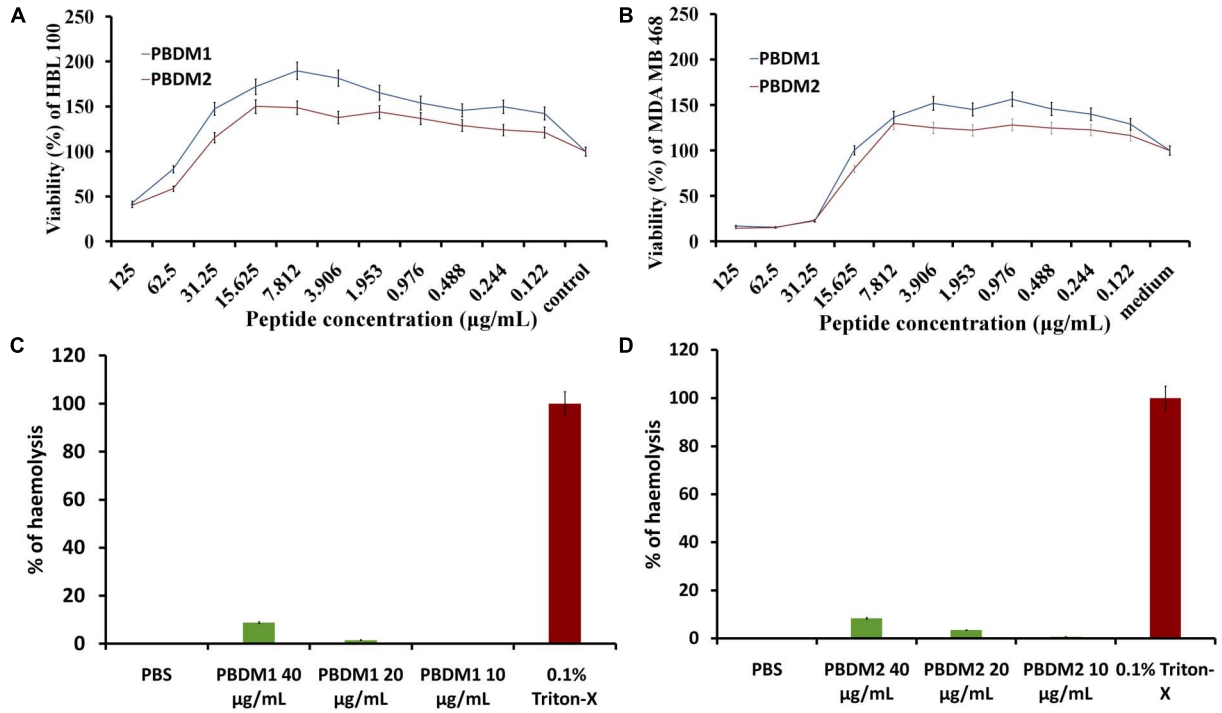

FIGURE 8 | (A,B) are MTT assay of PBDM1 and PBDM2 against HBL100 and MDA MB 468; **(C,D)** are hemolytic assay of PBDM1 and PBDM2, where Positive control is 0.1% Triton-X and negative control PBS.

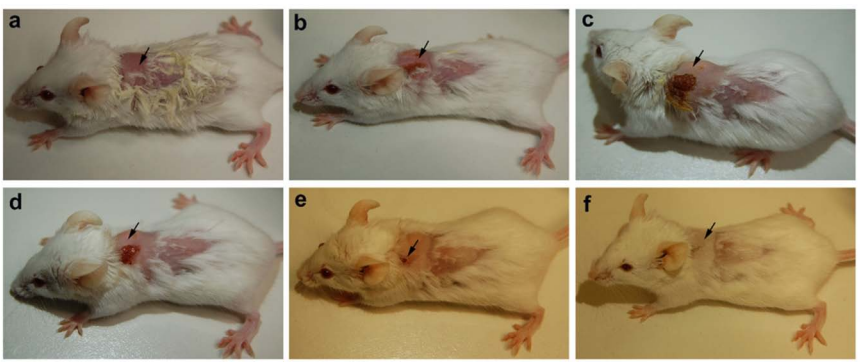

FIGURE 9 | Balb/c mice infected with VRSA and treated with PBDM1. **(A)** is Day 1, **(B)** is Day 5, **(C)** is Day 11, **(D)** is Day 12, **(E)** is Day 17, and **(F)** is Day 19.

103.8 µg/mL for HBL 100 and 67.55, and 61.52 µg/mL for MDA MB 468, respectively (**Supplementary Table S2**). However, the MIC value of the peptides were much lower than the IC_{50} values of the peptides obtained. Thus, PBDM peptides were effective against the cancer cells and pathogenic bacterial cells but showed no prominent toxicity against normal human epithelial cells at the MICs range as shown in **Figures 8A,B**.

Finally, the hemolytic effects of the PBDM peptides showed negligible hemolysis that is less than 9% at 40 µg/mL and lower concentration showed less than 4% in case of PBDM2 (20 µg/mL) and less than 1.5% for PBDM1 (20 µg/mL) which is very close to negative control (PBS) as shown in **Figures 8C,D**. But peptides like nisin have hemolysis at 1000-fold higher than its antimicrobial activity concentration (Jozala et al., 2015). Usually peptides have higher percentage of hemolysis even in low concentration which makes them complicated for the actual application of medicine (Sanches et al., 2015). Thus, the results showed that the PBDM peptides without any modification has a strong antimicrobial effects with no prominent toxicity and with good hemocompatibility toward mammalian cells, *in vitro* (Jelinkova et al., 2018a). Further, *in vivo* analysis of the PBDM peptides using balb/c mice were performed.

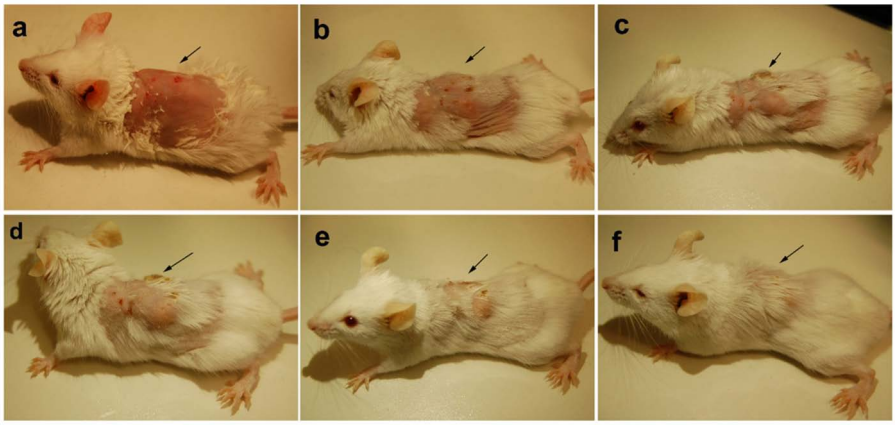

FIGURE 10 | Balb/c mice infected with VRSA and treated with PBDM2. **(A)** is Day 1, **(B)** is Day 4, **(C)** is Day 10, **(D)** is Day 14, **(E)** is Day 17, and **(F)** is Day 23.

In vivo Analysis of Infected Balb/c Treated With PBDM Peptides

The animals were infected with VRSA by subcutaneous injection. After the initiation of the infection and its spreading in the near neck dermal region of the mouse, it led to wound and swells formation. Henceforth, after the wound and swelling was prominent as shown in **Figures 9**, **10**, the treatment with the PBDM peptides was started. With the initiation of treatment day by day the healing of the wound and reduction in infection showed the recovery of the mice from the severe infection state to normal healthy state as shown in **Figures 9**, **10**, respectively. The PBDM1 treated infected animals showed faster recovery from the infection when compared to PBDM2 treated infected animals. Thus, with the commence of VRSA infection in mice and the start of treatment with the concentration of 10 μg/mL of PBDM1 and 15 μg/mL of PBDM2 peptides, showed complete cure of the mice from infection. One of the prime findings was the complete cure of the infection in mice by combination of topical administration and subcutaneously injecting the PBDM peptides.

The infected untreated control (Set two) was prepared by the introduction of VRSA infection and was monitored (**Supplementary Figure S8**). The infected untreated control set of animals were monitored and under experimental condition showed the morbidity were 100% within 14 days, wherein internal infection growth along with the dermal infection growth was observed. The untreated infected mice underwent dermal infection alongside internal growing infection causing fever and whole body twitching (**Supplementary Figure S9**). Whereas, the uninfected control animal group was maintained and monitored throughout the experiment and showed no changes in its condition (**Supplementary Figure S8**).

Thereafter the mice treated with PBDM peptides were being further monitored and kept under observation for one more week after recovery and they were alive, normal and healthy with no unusual behavior. Finally, PBDM1 and PBDM2 peptides were able to treat VRSA infection showing no negligible toxicity toward the balb/c mice and they were biocompatible showing full recovery after treatment. Another major finding was PBDM1 was more effective in short number of days compared to PBDM2 but the concentration needed for PBDM1 was higher than PBDM2. Overall, MTT assays have showed that PBDM2 was more toxic than PBDM1, likely due to the presence of two extra positively charged amino acids (Arg5 and Lys10). From peptide structure point of view, both peptides form a U-shape 3D structure, however, PBDM1 forms a more stable structure due to beta bridge between Lys2 and Leu11 residues. We hypothesize that the rigidity of PBDM1 structure may also contribute to poor toxicity as compared to PBDM2 structure which has less rigid U-shape 3D structure (due to repulsion between positively charged lysines). Increased positive charge has been previously reported in antimicrobial peptides (reference). We can also hypothesize that the bioavailability of the peptides was highly influenced by the concentration used, and hence the effect on recovery time. Electron microscopy images have shown different effects for peptides on bacterial cell morphology. PBDM1 treatment showed cellular shrinkage caused by rupture of the cell walls and leakage of cytoplasm. On the other hand, PBDM2 treatment resulted in bubble shaped debris on the bacterial cell wall. Thus, PBDM peptide can further be used for clinical studies to develop theranostics against bacterial infection as an alternative to antibiotics.

CONCLUSION

The outcome of the whole experiment helped us to ensue new antibacterial peptides to overcome the limitation of antibiotics to treat the multidrug resistant pathogenic bacterial infections. The designing and synthesis of PBDM–5(6)–Carboxyfluorescein conjugates (purification by HPLC-UV) allowed real-time follow-up of peptide effect. The *in silico* structural analysis of the PBDM peptides correlated with biophysical and spectroscopic characterization that was performed by MALD-TOF MS, ATR-FTIR, absorbance and fluorescence emission spectra. The PBDM peptides were used against *S. aureus*, MRSA, VRSA, VRE, *E. faecalis*, and *E. coli* to study the MICs, growth curves, viability and CFUs of the bacteria in their presence, which proves that

they have a significant antibacterial effects against the pathogenic bacterial strains studied. Further, the activity of the PBDM was proven by testing it against the pathogenic live hospital samples (variants of *Staphylococcus aureus*, *Enterobacter cloacae*, *Klebsiella pneumonia*e, and *Staphylococcus epidermidis*). Further, to confirm the antibacterial activity visually, the phase contrast and bright field microscopic images analysis were performed, which revealed that PBDM peptides are effective against bacterial cells causing loss of cell integrity, change in morphology and cell disruption leading to cell leakage and presence cell debris. The live/dead cell imaging of PBDM treated bacterial strains supported the antibacterial activity. Thereafter, Cryo-SEM imaging revealed the mechanism of the PBDM1 as it was found to damage the cell wall causing aggregations of other VRSA cells and PBDM2 interacts with the cell wall causing bubble like structure (suspected to be crystalized peptides) and change in cell integrity and morphology but no cell wall damage was observed.

Finally, the *in vitro* toxicity test was done for PBDM using human blood cells, mammary gland epithelial cells (HBL 100) and mammary gland adenocarcinoma cells (MDA MB 468)proving it has some effects on cancer cells but negligible toxicity against normal mammary gland epithelial cells at similar concentrations with negligible hemolysis. IC_{50} values in comparison to the MIC value shows the effective concentration for antibacterial activity was lower than the IC_{50} values. Lastly, the *in vivo* analysis of the VRSA infected balb/c mice treated with PBDM1 and PBDM2 showed the recovery from severe to healthy condition showing with negligible toxicity and high biocompatibility. PBDM1 was more effective in less number of days than PBDM2. Thus, PBDM peptides can be considered a great replacement to antibiotics as it helps to overcome the limitations exhibited by most of the antibiotics.

DATA AVAILABILITY STATEMENT

The original contributions presented in the study are publicly available. This data can be found in GenBank, under accession numbers MT792519–MT792528.

ETHICS STATEMENT

The studies involving human participants were reviewed and approved by the Ethics Committee of Trauma Hospital in Brno, Czechia in accordance to Act No. 378/2007 coll. The patients/participants provided their written informed consent to participate in this study. The animal study was reviewed and approved by the Ethics Commission at the Faculty of AgriSciences, Mendel University in Brno, Czechia in accordance with Act No. 246/1992 Coll.

AUTHOR CONTRIBUTIONS

All the authors contributed researched data, wrote their respective sections in the manuscript, reviewed and edited the article substantially. AMa performed most of the experiments including designing peptide, spectrophotometry, microbiological tests, microscopy, some part of animal experiment, and wrote the most part of the manuscript. YH helped in the MD simulation and development of the mechanism of action. VS helped in animal experiment. VM helped in the synthesis of the peptide and the characterization of the peptide. SB helped in microbiological test. HM and RG helped with different experiments. RV provided the hospital samples. AMo supervised the whole experiment.

FUNDING

This work was financially supported by CEITEC 2020 (LQ1601) and by EFRR project "Multidisciplinary research to increase application potential of nanomaterials in agricultural practice" (No. CZ.02.1.01/0.0/0.0/16_025/0007314).

SUPPLEMENTARY MATERIAL

The Supplementary Material for this article can be found online at: https://www.frontiersin.org/articles/10.3389/fmicb.2020.01963/full#supplementary-material

FIGURE S1 | Multiple Sequence alignment of the four peptides.

FIGURE S2 | Growth curve and viability percentage of bacterial samples from P1.

FIGURE S3 | Growth curve and viability percentage of bacterial samples from P2.

FIGURE S4 | Growth curve and viability percentage of bacterial samples from P3.

FIGURE S5 | The phylogenetic tree of the hospital sample from P1, P2, and P3 patients.

FIGURE S6 | The bright field microscopic images.

FIGURE S7 | The bright field and fluorescence microscopic image of control VRSA cells with and without peptide and no presence of dye.

FIGURE S8 | The uninfected control balb/c without treatment and infection.

FIGURE S9 | The Infected untreated control with infection by VRSA and no treatment.

FIGURE S10 | The Colony Forming Unit assay.

FIGURE S11 | Characterization of peptides.

TABLE S1 | Overview of the antibacterial activity of PBDM peptide against Hospital samples from P1, P2, and P3.

REFERENCES

Adochitei, A., and Drochioiu, G. (2011). Rapid characterization of peptide secondary structure By Ft-Ir spectroscopy. *Revue Roumaine De Chimie* 56, 783–791.

Alexander, E. L., Gardete, S., Bar, H. Y., Wells, M. T., Tomasz, A., and Rhee, K. Y. (2014). Intermediate-type vancomycin resistance (VISA) in genetically-distinct *Staphylococcus aureus* isolates is linked to specific, reversible metabolic alterations. *PLoS One* 9:e97137. doi: 10.1371/journal.pone.0097137

Bhowmick, S., Mazumdar, A., Moulick, A., and Adam, V. (2020). Algal metabolites: An inevitable substitute for antibiotics. *Biotechnol. Adv.* 43:107571. doi: 10.1016/j.biotechadv.2020.107571

Boulos, L., Prévost, M., Barbeau, B., Coallier, J., and Desjardins, R. (1999). LIVE/DEAD® BacLight™: application of a new rapid staining method for direct enumeration of viable and total bacteria in drinking water. *J. Microbiol. Methods* 37, 77–86. doi: 10.1016/S0167-7012(99)00048-42

Brunetti, J., Falciani, C., Roscia, G., Pollini, S., Bindi, S., Scali, S., et al. (2016). In vitro and in vivo efficacy, toxicity, bio-distribution and resistance selection of a novel antibacterial drug candidate. *Sci. Rep.* 6:26077. doi: 10.1038/srep26077

Chan, D. I., Prenner, E. J., and Vogel, H. J. (2006). Tryptophan- and arginine-rich antimicrobial peptides: Structures and mechanisms of action. *Biochim. Biophys. Acta Biomembr.* 1758, 1184–1202. doi: 10.1016/j.bbamem.2006.04.006

Coates, J. (2006). "Interpretation of infrared spectra, a practical approach," in Encyclopedia of Analytical Chemistry, eds R. A. Meyers and M. L. McKelvy. doi: 10.1002/9780470027318.a5606

Cui, L., Iwamoto, A., Lian, J.-Q., Neoh, H.-M., Maruyama, T., Horikawa, Y., et al. (2006). Novel mechanism of antibiotic resistance originating in vancomycin-intermediate *Staphylococcus aureus*. *Antimicrob. Agents Chemother.* 50, 428–438. doi: 10.1128/aac.50.2.428-438.2006

Davies, J., and Davies, D. (2010). Origins and evolution of antibiotic resistance. *Microbiol. Mol. Biol. Rev.* 74, 417–433. doi: 10.1128/mmbr.00016-10

Fernández-Pérez, R., Sáenz, Y., Rojo-Bezares, B., Zarazaga, M., Rodríguez, J. M., Torres, C., et al. (2018). Production and antimicrobial activity of nisin under enological conditions. *Fron. Microbiol.* 9:1918. doi: 10.3389/fmicb.2018.01918

Frank, J. A., Reich, C. I., Sharma, S., Weisbaum, J. S., Wilson, B. A., and Olsen, G. J. (2008). Critical evaluation of two primers commonly used for amplification of bacterial 16S rRNA genes. *Appl. Environ. Microbiol.* 74, 2461–2470. doi: 10.1128/aem.02272-2277

Gargiulo, S., Greco, A., Gramanzini, M., Esposito, S., Affuso, A., Brunetti, A., et al. (2012). Mice anesthesia, analgesia, and care, Part I: anesthetic considerations in preclinical research. *ILAR J.* 53, E55-E69.

Groh, T., Hrabeta, J., Khalil, M. A., Doktorova, H., Eckschlager, T., and Stiborova, M. (2015). The synergistic effects of DNA-damaging drugs cisplatin and etoposide with a histone deacetylase inhibitor valproate in high-risk neuroblastoma cells. *Int. J. Oncol.* 47, 343–352. doi: 10.3892/ijo.2015.2996

Haque, M. A., Imamura, R., Brown, G. A., Krishnamurthi, V. R., Niyonshuti, I. I., Marcelle, T., et al. (2017). An experiment-based model quantifying antimicrobial activity of silver nanoparticles on *Escherichia coli*. *RSC Adv.* 7, 56173–56182. doi: 10.1039/C7RA10495B

Haug, B. E., Camilio, K. A., Eliassen, L. T., Stensen, W., Svendsen, J. S., Berg, K., et al. (2016). Discovery of a 9-mer cationic peptide (LTX-315) as a potential first in class oncolytic peptide. *J. Med. Chem.* 59, 2918–2927. doi: 10.1021/acs.jmedchem.5b02025

Heger, Z., Merlos Rodrigo, M. A., Michalek, P., Polanska, H., Masarik, M., Vit, V., et al. (2016). Sarcosine Up-regulates expression of genes involved in cell cycle progression of metastatic models of prostate cancer. *PLoS One* 11:e0165830. doi: 10.1371/journal.pone.0165830

Hegerova, D., Vesely, R., Cihalova, K., Kopel, P., Milosavljevic, V., Heger, Z., et al. (2017). Antimicrobial agent based on selenium nanoparticles and carboxymethyl cellulose for the treatment of bacterial infections. *J. Biomed. Nanotechnol.* 13, 767–777. doi: 10.1166/jbn.2017.2384

Hussain, S., Joo, J., Kang, J., Kim, B., Braun, G. B., She, Z. -G., et al. (2018). Antibiotic-loaded nanoparticles targeted to the site of infection enhance antibacterial efficacy. *Nat. Biomed. Eng.* 2, 95–103. doi: 10.1038/s41551-017-0187-185

Jelinkova, P., Splichal, Z., Jimenez, A. M. J., Haddad, Y., Mazumdar, A., Sur, V. P., et al. (2018a). Novel vancomycin-peptide conjugate as potent antibacterial agent against vancomycin-resistant Staphylococcus aureus. *Infect. Drug Resist.* 11, 1807–1817. doi: 10.2147/idr.s160975

Jelinkova, P., Vesely, R., Cihalova, K., Hegerova, D., Ananbeh, H. A. A., Richtera, L., et al. (2018b). Effect of arsenic (III and V) on oxidative stress parameters in resistant and susceptible *Staphylococcus aureus*. *Environ. Res.* 166, 394–401. doi: 10.1016/j.envres.2018.06.024

Jozala, A. F., de Lencastre Novaes, L. C., and Junior, A. P. (2015). *Concepts, Compounds and the Alternatives of Antibacterials*. London: IntechOpen

Keller, R., Winde, G., Terpe, H. J., Foerster, E. C., and Domschke, W. (2002). Fluorescence endoscopy using a fluorescein-labeled monoclonal antibody against carcinoembryonic antigen in patients with colorectal carcinoma and adenoma. *Endoscopy* 34, 801–807. doi: 10.1055/s-2002-34254

Koch, M. A. (2006). "Chapter 18 experimental modeling and research methodology," in *The Laboratory Rat*, eds M. A. Suckow, S. H. Weisbroth, and C. L. Franklin (Burlington, NJ: Academic Press) 587–625 doi: 10.1016/b978-012074903-4/50021-2

Lorenzón, E. N., Cespedes, G. F., Vicente, E. F., Nogueira, L. G., Bauab, T. M., Castro, M. S., et al. (2012). Effects of dimerization on the structure and biological activity of antimicrobial peptide Ctx-Ha. *Antimicrob. Agents Chemother.* 56, 3004–3010. doi: 10.1128/aac.06262-6211

Malachowa, N., Kobayashi, S.D., Braughton, K.R., and DeLeo, F.R. (2013). "Mouse model of staphylococcus aureus skin infection," in *Mouse Models of Innate Immunity: Methods and Protocols*, ed. I.C. Allen. (Totowa, NJ: Humana Press), 109–116 doi: 10.1007/978-1-62703-481-4_14

Mazumdar, A., Haddad, Y., Milosavljevic, V., Michalkova, H., Guran, R., Bhowmick, S., et al. (2020). Peptide-carbon quantum dots conjugate, derived from human retinoic acid receptor responder protein 2, against antibiotic-resistant gram positive and gram negative pathogenic bacteria. 10:325. doi: 10.3390/nano10020325

McGuinness, W. A., Malachowa, N., and DeLeo, F. R. (2017). Vancomycin resistance in *Staphylococcus aureus*. *Yale J. Biol. Med.* 90, 269–281

McNeece, G., Naughton, V., Woodward, M. J., Dooley, J. S. G., and Naughton, P. J. (2014). Array based detection of antibiotic resistance genes in Gram negative bacteria isolated from retail poultry meat in the UK and Ireland. *Int. J. Food Microbiol.* 179, 24–32. doi: 10.1016/j.ijfoodmicro.2014.03.019

Milosavljevic, V., Haddad, Y., Merlos Rodrigo, M. A., Moulick, A., Polanska, H., Hynek, D., et al. (2016). The zinc-schiff base-novicidin complex as a potential prostate cancer therapy. *PLoS One* 11:e0163983. doi: 10.1371/journal.pone.0163983

Mohammedsaeed, W., McBain, A. J., Cruickshank, S. M., and O'Neill, C. A. (2014). *Lactobacillus rhamnosus* GG inhibits the toxic effects of *Staphylococcus aureus* on epidermal keratinocytes. *Appl. Environ. Microbiol.* 80, 5773–5781. doi: 10.1128/AEM.00861-814

Moulick, A., Heger, Z., Milosavljevic, V., Richtera, L., Barroso-Flores, J., Merlos Rodrigo, M. A., et al. (2018). Real-time visualization of cell membrane damage using gadolinium–schiff base complex-doped quantum dots. *ACS Appl. Mater. Interfac.* 10, 35859–35868. doi: 10.1021/acsami.8b15868

O'Toole, M. G., Henderson, R. M., Soucy, P. A., Fasciotto, B. H., Hoblitzell, P. J., Keynton, R. S., et al. (2012). Curcumin Encapsulation in submicrometer spray-dried Chitosan/Tween 20 particles. *Biomacromolecules* 13, 2309–2314. doi: 10.1021/bm300564v

Rincón, S., Panesso, D., Díaz, L., Carvajal, L. P., Reyes, J., Munita, J. M., et al. (2014). Resistencia a antibióticos de última línea en cocos gram positivos: la era posterior a la vancomicina. *Biomedica* 34, 191–208. doi: 10.1590/s0120-41572014000500022

Sanches, P. R. S., Carneiro, B. M., Batista, M. N., Braga, A. C. S., Lorenzón, E. N., Rahal, P., et al. (2015). A conjugate of the lytic peptide Hecate and gallic acid: structure, activity against cervical cancer, and toxicity. *Amino Acids* 47, 1433–1443. doi: 10.1007/s00726-015-1980-1987

Sevgi, M., Toklu, A., Vecchio, D., and Hamblin, M. R. (2013). Topical antimicrobials for burn infections - an update. *Recent Patents Antiinfect. Drug Discov.* 8, 161–197. doi: 10.2174/1574891x08666131112143447

Shin, J. M., Gwak, J. W., Kamarajan, P., Fenno, J. C., Rickard, A. H., and Kapila, Y. L. (2016). Biomedical applications of nisin. *J. Appl. Microbiol.* 120, 1449–1465. doi: 10.1111/jam.13033

Spunda, R., Hruby, J., Mericka, P., Mlcek, M., Pecha, O., Splith, K., et al. (2018). Immunosuppressive protocols with tacrolimus after cryopreserved aortal allotransplantation in rats. *PLoS One* 13:e0201984. doi: 10.1371/journal.pone.0201984

Stiefel, P., Schmidt-Emrich, S., Maniura-Weber, K., and Ren, Q. (2015). Critical aspects of using bacterial cell viability assays with the fluorophores SYTO9 and propidium iodide. *BMC Microbiol.* 15:36. doi: 10.1186/s12866-015-0376-x

Sur, V. P., Kominkova, M., Buchtova, Z., Dolezelikova, K., Zitka, O., and Moulick, A. (2019). CdSe QD biosynthesis in yeast using tryptone-enriched media and their conjugation with a peptide hecate for bacterial detection and killing. *Nanomaterials* 9:1463. doi: 10.3390/nano9101463

Sur, V. P., Mazumdar, A., Ashrafi, A., Mukherjee, A., Milosavljevic, V., Michalkova, H., et al. (2020a). A novel biocompatible titanium–gadolinium quantum dot as a bacterial detecting agent with high antibacterial activity. *Nanomaterials* 10:778 doi: 10.3390/nano10040778

Sur, V. P., Mazumdar, A., Kopel, P., Mukherjee, S., Vítek, P., Michalkova, H., et al. (2020b). A novel ruthenium based coordination compound against pathogenic bacteria. *Int. J. Mol. Sci.* 21:2656 doi: 10.3390/ijms21072656

Sykes, E. A., Dai, Q., Tsoi, K. M., Hwang, D. M., and Chan, W. C. W. (2014). Nanoparticle exposure in animals can be visualized in the skin and analysed via skin biopsy. *Nat. Commun.* 5, 3796–3796. doi: 10.1038/ncomms 4796

Tacconelli, E., Carrara, E., Savoldi, A., Harbarth, S., Mendelson, M., Monnet, D. L., et al. (2018). Discovery, research, and development of new antibiotics: the WHO priority list of antibiotic-resistant bacteria and tuberculosis. *Lancet Infect. Dis.* 18, 318–327. doi: 10.1016/S1473-3099(17)30753-30753

Tan, R., Liu, J., Li, M., Huang, J., Sun, J., and Qu, H. (2014). Epidemiology and antimicrobial resistance among commonly encountered bacteria associated with infections and colonization in intensive care units in a university-affiliated hospital in Shanghai. *J. Microbiol. Immunol. Infect.* 47, 87–94. doi: 10.1016/j.jmii.2012.11.006

Thomer, L., Schneewind, O., and Missiakas, D. (2016). Pathogenesis of *Staphylococcus aureus* bloodstream infections. *Annu. Rev. Pathol.* 11, 343–364. doi: 10.1146/annurev-pathol-012615-044351

Tsai, T.-L., Li, A.-C., Chen, Y.-C., Liao, Y. -S., and Lin, T.-H. (2015). Antimicrobial peptide m2163 or m2386 identified from *Lactobacillus* casei ATCC 334 can trigger apoptosis in the human colorectal cancer cell line SW480. *Tumor Biol.* 36, 3775–3789. doi: 10.1007/s13277-014-3018-3012

Ventola, C. L. (2015). The antibiotic resistance crisis: part 1: causes and threats. *P & T* 40, 277–283.

Vicente, E. F., Basso, L. G. M., Cespedes, G. F., Lorenzón, E. N., Castro, M. S., Mendes-Giannini, M. J. S., et al. (2013). Dynamics and conformational studies of TOAC spin labeled analogues of Ctx(Ile21)-Ha peptide from hypsiboas albopunctatus. *PLoS One* 8:e60818. doi: 10.1371/journal.pone.0060818

Vukomanović, M., Žuniè, V., Kunej, Š., Janèar, B., Jeverica, S., and Suvorov, D. J. S. R. (2017). Nano-engineering the antimicrobial spectrum of lantibiotics: activity of nisin against gram negative bacteria. *Sci. Rep.* 7: 4324.

Wang, S., Wang, Q., Zeng, X., Ye, Q., Huang, S., Yu, H., et al. (2017). Use of the antimicrobial peptide sublancin with combined antibacterial and immunomodulatory activities to protect against methicillin-resistant staphylococcus aureus infection in mice. *J. Agric. Food Chem.* 65, 8595–8605. doi: 10.1021/acs.jafc.7b02592

Welberg, L. A., Kinkead, B., Thrivikraman, K., Huerkamp, M. J., Nemeroff, C. B., and Plotsky, P. M. (2006). Ketamine–xylazine–acepromazine anesthesia and postoperative recovery in rats. *J. Am. Assoc. Lab. Anim. Sci.* 45, 13–20

Wu, Y., Liang, J., Rensing, K., Chou, T., and Libera, M. (2014). *Extracellular Matrix Reorganization during Cryo Preparation for Scanning Electron Microscope Imaging of Staphylococcus aureus Biofilms*. Cambridge: Cambridge University Press.

Zhou, Y., Kong, Y., Kundu, S., Cirillo, J. D., and Liang, H. (2012). Antibacterial activities of gold and silver nanoparticles against Escherichia coli and bacillus Calmette-Guérin. *J. Nanobiotechnol.* 10:19. doi: 10.1186/1477-3155-10-19

Zhu, W. L., Lan, H., Park, I. -S., Kim, J. I., Jin, H. Z., Hahm, K.-S., et al. (2006). Design and mechanism of action of a novel bacteria-selective antimicrobial peptide from the cell-penetrating peptide Pep-1. *Biochem. Biophys. Res. Commun.* 349, 769–774. doi: 10.1016/j.bbrc.2006.08.094

Conflict of Interest: The authors declare that the research was conducted in the absence of any commercial or financial relationships that could be construed as a potential conflict of interest.

frontiers in Microbiology

ORIGINAL RESEARCH
published: 31 August 2020
doi: 10.3389/fmicb.2020.02113

Antimicrobial Synergism Toward *Pseudomonas aeruginosa* by Gallium(III) and Inorganic Nitrite

Anna C. Zemke[1,2], Cody J. Madison[2], Naomi Kasturiarachi[1], Linda L. Pearce[2] and James Peterson[2]*

[1] Division of Pulmonary, Allergy and Critical Care Medicine, Department of Medicine, University of Pittsburgh, Pittsburgh, PA, United States, [2] Environmental and Occupational Health, Graduate School of Public Health, University of Pittsburgh, Pittsburgh, PA, United States

The ubiquitous involvement of key iron-containing metalloenzymes in metabolism is reflected in the dependence of virtually all bacteria on iron for growth and, thereby, potentially provides multiple biomolecular targets for antimicrobial killing. We hypothesized that nitrosative stress, which induces damage to iron metalloproteins, would sensitize bacteria to the ferric iron mimic gallium(III) (Ga^{3+}), potentially providing a novel therapeutic combination. Using both laboratory and clinical isolates of *Pseudomonas aeruginosa*, we herein demonstrate that Ga^{3+} and sodium nitrite synergistically inhibit bacterial growth under both aerobic and anaerobic conditions. Nitric oxide also potentiated the antimicrobial effect of Ga^{3+}. Because many chronic pulmonary infections are found as biofilms and biofilms have very high antibiotic tolerance, we then tested the combination against biofilms grown on plastic surfaces, as well as the apical surface of airway epithelial cells. Ga^{3+} and sodium nitrite had synergistic antimicrobial activity against both biofilms grown on plastic and on airway epithelial cell. Both Ga^{3+} and various NO donors are (independently) in clinical development as potential antimicrobials, however, we now propose the combination to have some particular advantages, while anticipating it should ultimately prove similarly safe for translation to treatment of human disease.

Keywords: biofilm, Ga^{3+}, gallium(III), nitrite, nitric oxide, *Pseudomonas aeruginosa*

OPEN ACCESS

Edited by:
Rodolfo García-Contreras, National Autonomous University of Mexico, Mexico

Reviewed by:
Lawrence Richard Bernstein, Gallixa LLC, United States
Andrea Cochis, University of Eastern Piedmont, Italy

****Correspondence:***
Anna C. Zemke
zemkea@upmc.edu

Specialty section:
This article was submitted to Antimicrobials, Resistance and Chemotherapy, a section of the journal Frontiers in Microbiology

Received: *07 April 2020*
Accepted: *11 August 2020*
Published: *31 August 2020*

Citation:
Zemke AC, Madison CJ, Kasturiarachi N, Pearce LL and Peterson J (2020) Antimicrobial Synergism Toward Pseudomonas aeruginosa by Gallium(III) and Inorganic Nitrite. Front. Microbiol. 11:2113. doi: 10.3389/fmicb.2020.02113

INTRODUCTION

Antibiotic resistance, especially in relation to the management of nosocomial infections, continues to be a growing problem worldwide. This matter is of some particular concern in the treatment of chronic suppurative lung diseases such as cystic fibrosis (CF). *Pseudomonas aeruginosa* is the most common Gram-negative pathogen in adults with CF, and decades of antibiotic exposure leads to acquired antibiotic resistance in addition to the high innate antibiotic resistance of the organism (Patient Registry, 2011). Beyond its prominence in CF, *P. aeruginosa* is one of the *ESKAPE* pathogens, causing a variety of respiratory infections and chronic wound infections, including those at surgical sites, that can be recalcitrant to treatment (Rice, 2010; Mulani et al., 2019). Thus, there is clearly an ongoing need for the development of new antimicrobial approaches toward *P. aeruginosa*.

Iron is a required nutrient for growth of nearly all bacteria, certainly including pathogens like *P. aeruginosa*. Moreover, iron is a main growth limiting nutrient in sputum (Goss et al., 2018). There is intense competition for iron in the airway, with the bacterium producing siderophores to scavenge iron and the host attempting to sequester available iron (reviewed in Palmer and Skaar, 2016). Once imported by the bacterium, iron becomes incorporated into a wide variety of metalloenzymes, including those of the bioenergetic pathways and core carbon metabolism such as NADH dehydrogenase (complex I), aconitase and various other dehydrogenases, dehydratases and reductases. Because of the critical requirement of iron for *P. aeruginosa* growth, blocking iron uptake or metabolism has been discussed as a possible treatment approach (Banin et al., 2006). The Ga^{3+} and Fe^{3+} ions have similar radii and other chemical properties, allowing Ga^{3+} to be an iron mimetic in biologic systems (Chitambar, 2016). Ga^{3+} is imported via a subset of *P. aeruginosa* iron uptake systems, and incorporated into metalloproteins in the place of iron (García-Contreras et al., 2013). As Ga^{3+} is unable to be reduced to Ga^{2+} under physiologic conditions, Ga^{+3} incorporation leads to catalytically inactive holoproteins. The full physiologic effects of Ga^{3+} on bacterial metabolism are still being determined, however, it is known that in *P. aeruginosa,* Ga^{3+} is bound by the siderophore pyoverdine and, as the Ga^{3+} cannot be reduced, it traps pyoverdine preventing its recycling (Kaneko et al., 2007; Yeterian et al., 2010). Additionally, growth in Ga^{3+} leads to decreased catalase activity (or potentially decreased expression), with a consequent increase in susceptibility to oxidative stress and decrease in ribonucleotide reductase activity (Goss et al., 2018). Ga^{3+} is currently in drug development for treatment of *P. aeruginosa* infections in CF (nebulized Ga^{3+} citrate, Aridis Pharmaceuticals). The recently published IGNITE study, which used a molar equivalent solution of gallium nitrate and sodium citrate dihydrate, provides proof of concept for the therapeutic approach (Goss et al., 2018).

One approach being studied to increase the biologic activity of Ga^{3+} is by complexing Ga^{3+} with protoporphyrin and starving the bacterium of iron with the addition of the iron chelator deferiprone (Richter et al., 2017). Alternatively, increasing turnover of iron metalloproteins might increase susceptibility to Ga^{3+}. Nitrosative stress, specifically peroxynitrite derived from nitric oxide, causes damage to Fe-S clusters. Nitric oxide and acidified (pH 6.5) nitrite, which is metabolized to nitric oxide, are both being tested as antimicrobial approaches for chronic airway infections in CF (clinicaltrials.gov locators NCT02694393 and Howlin et al., 2017). Note that pH 6.5 is being used in our studies to mimic airway mucus conditions in CF (Yoon et al., 2006), but NO is readily generated from the nitrite anion at pH 7.4 *in vivo* (Cambal et al., 2011, 2013).

Given the common broad target of iron biochemistry, we hypothesized that sodium nitrite and Ga^{3+} salts may have synergistic antimicrobial activity. Nitric oxide, produced from nitrite, should cause widespread damage to iron-containing proteins resulting in, for example, increased turnover of iron-sulfur (Fe-S) proteins. If Ga^{3+} were available, it would be incorporated in the place of Fe^{3+} during this state of increased turnover, leading to dysfunctional metalloproteins and consequent widespread bacterial metabolic arrest. Thus, nitrite-derived nitric oxide should potentiate the antibacterial effects of Ga^{3+}.

MATERIALS AND METHODS

Reagents

Reagents were purchased from Sigma Aldrich except for PAPA-NONOate (Caymen Chemicals) and Bacto Agar (BD). Solutions were made fresh immediately prior to the experiment and were not used if precipitation was present. The pH of media was confirmed to be 6.5 under all conditions tested.

Strains and Growth Conditions

Strains were cultured in Lysogeny Broth (LB) overnight on a roller drum at 37°C prior to experimentation. The laboratory strains PAO1 and PA14 were used (obtained from George O'Toole, Dartmouth). The *P. aeruginosa* clinical isolate panel was described in Zemke et al. (2014). The PA14-*hitA:*IS strain was obtained from the PA14 non-redundant transposon library (Liberati et al., 2006). Clinical Isolates were obtained from the Cystic Fibrosis Isolate Core at Seattle Children's Hospital.

Checkerboard Synergy Testing

Studies were done using M-9 minimal media with glucose as a carbon source and 4μM $FeCl_3$. For aerobic studies, checkerboard agar dilution plates were made with 0–1,600 μg/ml $Ga(NO_3)_3$ and 0–30 mM $NaNO_2$. Overnight cultures were diluted to 5×10^5 CFU/ml and spotted on plates. Plates were grown for 48 h at 37°C and scored for growth. In some cases, liquid MIC assays were done with a similar protocol using 96-well plates and optical density as the endpoint, with positive growth scored as an optical density above the sterility well. Anaerobic studies were done using M9-glucose plates with 1% KNO_3 to support anaerobic respiration. For anaerobic studies, strains PAO1 and PA14 were diluted, spotted on plates, and the plates were incubated in GasPak jars for 4 days prior to scoring. Plates were scanned at high resolution on an HP Scanner in groups of 8 and images were scored based on if growth was visible on the image. Images were stored so that they could be reviewed by a second scorer if needed. The Fractional Inhibitory Concentration (FIC) was used to define synergy. FIC was calculated with the following formula: $FIC = (MIC_{Acombo}/MIC_A + MIC_{Bcombo}/MIC_B)$, where A represents $Ga(NO_3)_3$ and B represents $NaNO_2$. Synergy was defined as $FIC \leq 0.5$; no interaction is defined as $FIC > 0.5$ to = 4 (Petersen et al., 2006).

Abiotic Biofilm Prevention Assay

Abiotic biofilms were grown on plastic microtiter plates as described in Zhang and Mah (2008). Overnight cultures were rinsed with M-9 media twice prior to dilution to remove residual LB broth. Biofilms were grown in pH 6.5 M-9 media with glucose as a carbon source and 4μM $FeCl_3$ for 24 h, then stained with crystal violet and visually examined for growth. $Ga(NO_3)_3$ and $NaNO_2$ were added at the beginning of the experiment. Data were analyzed by two methods. First, the wells were photographed

TABLE 1 | Checkerboard assay for nitrite-Ga(III) interaction for *P. aeruginosa* grown aerobically on M9 media with glucose as a carbon source.

Strain	Ga MIC (μM)	NIT MIC (mM)	Ga MIC (μM) (3.25 mM NIT)	FIC
PAO1	12	15	3	0.47
PA14	24	15	6	0.47
Strain 31-1	12	15	3	0.47
Strain 31-2	24	15	24	1.22
Strain 33-2	24	15	12	0.72
Strain 36-2	24	15	12	0.72
Strain 36-3	12	15	3	0.47
Strain 41-2	24	15	6	0.47
Strain 47-2	24	15	6	0.47
Strain 47-3	96	15	24	0.47
Strain 60-2	48	15	12	0.47
Strain 60-3	24	15	6	0.47
Strain 66-1	24	15	24	1.22
Strain 66-2	48	15	12	0.47
Strain 71-1	24	15	6	0.47
Strain 71-2	24	15	6	0.47
Strain 74-1	12	15	6	0.72
Strain 74-2	6	15	1.5	0.47

and scored for visible growth. In the second method, the crystal violet was dissolved in acetic acid and the optical density was determined at 570 nm. The background was subtracted and wells were scored based on an 80–90% reduction in OD as compared to the control well. For a well to be considered the MIC, next two adjacent wells were required to be scored negative for growth. Seven total replicates were done.

Biotic Biofilm Assays

The biotic biofilm dispersal protocol was modified from Moreau-Marquis et al. (2008). The strain PAO1 was used for these experiments. The human airway epithelial cell line CFBE41o- was grown at air-liquid interface on Transwell filters. Epithelial cells were grown submerged for 48 h after seeding, and then grown at air-liquid interface for an additional 5–12 days. Cells were fed through the basolateral compartment. The day of the experiment, filters were rinsed three times on both apical and basolateral compartments to remove any residual antibiotics present from the growth medium. Detailed descriptions of this assay are found in Moreau-Marquis et al. (2010). Filters were inoculated at a Multiplicity of Infection of 25:1. After 6 h of growth, the apical and basolateral compartments were rinsed twice with phosphate buffered saline (PBS), pH 6.5 to remove residual free amino acids present in the cell culture media. Biotic biofilms were treated with 50 mM $NaNO_2$ and $Ga(NO_3)_3$ for 60 min. Bacteria were counted by serial dilution, and the limit of detection was 100 CFU/ml. Five replicates were done. We confirmed epithelial barrier function integrity through the measurement of trans-epithelial electrical resistance with an EVOM device as described in Zemke et al. (2014). Filters were allowed to equilibrate with PBS on both sides for 60 min, then nitrite and/or gallium(III) was applied to the apical surface and the resistence was measured after 60 min. At least three replicates were done for each condition.

Statistical Analysis

At least three replicates were done of all experiments. Statistical analysis was done using PRISM 8.0 software (GraphPad, San Diego California). Data are displayed as mean ± standard deviation. CFU counts were log transformed, and then one-way ANOVA was used.

RESULTS

Nitrite and Ga^{3+} Have Synergistic Antimicrobial Activity

If nitrite and Ga^{3+} are targeting iron metalloprotein-dependent metabolism through complementary mechanisms, we would predict that the two compounds would display antimicrobial

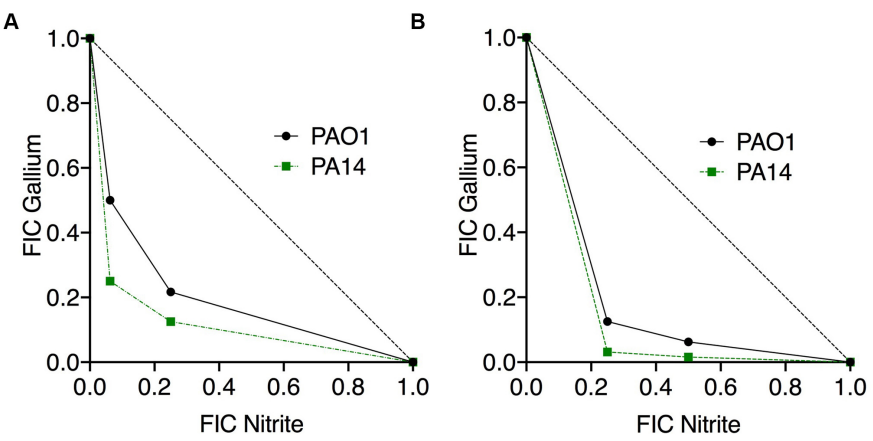

FIGURE 1 | Nitrite and Ga^{3+} have synergistic antibacterial activity. Isobolograms show the results of checkerboard assays using PAO1 and PA14 presented showing the fractional inhibitory concentration (FICs) of the two compounds in combination under aerobic **(A)** and anaerobic **(B)** conditions. Six aerobic replicates done, three anaerobic replicates done, representative isobologram shown.

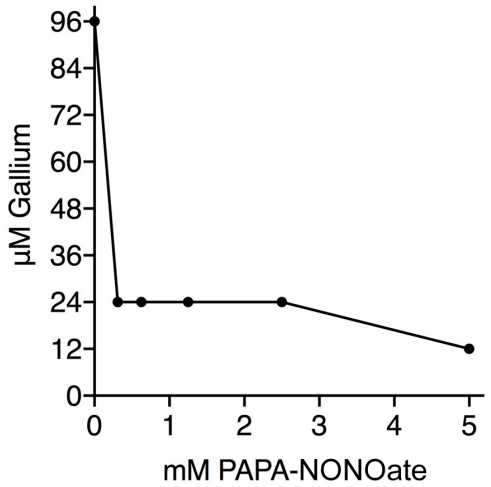

FIGURE 2 | Nitric Oxide and Ga^{3+} have synergistic antibacterial activity. Isobologram shows the results of aerobic checkerboard assays using PA14. The MIC for PAPA-NONOate was >5 mM. Three replicates done.

synergy. Therefore, we performed checkerboard testing to determine the Fractional Inhibitor Concentration (FIC) of Ga^{3+} and nitrite for both laboratory strains and CF clinical isolates of *P. aeruginosa*. Minimum Inhibitory Concentrations (MICs) and FIC values for the laboratory strains PAO1 and PA14 grown aerobically on glucose are shown in **Table 1**. The concavity of isobolograms showing the relationship between the nitrite and Ga^{3+} FICs for PAO1 and PA14 are visually indicative of synergy (**Figure 1A**), and the Ga^{3+}-nitrite FIC for both strains was < 0.5, meeting the definition of antimicrobial synergy (Petersen et al., 2006). We determined the Ga^{3+}-nitrite FICs for a panel of CF *P. aeruginosa* isolates. The Ga^{3+} MICs ranged from 6 to 96 µM, while the MIC for nitrite was 15 mM for all isolates (**Table 1**). In the isolate panel, 11/16 strains displayed synergy. Anaerobic growth, such as that found in the CF lung, causes increased antimicrobial tolerance as well as reliance on alternative metabolic pathways which may have different sensitives to inhibition by Ga^{3+} and nitrite (Alvarez-Ortega and Harwood, 2007; Arai, 2011; Schaible et al., 2012). Under anaerobic conditions, the Ga^{3+} MIC increased to 100–200 µM for PAO1 and 800–1,600 µM for PA14. The anaerobic nitrite MIC was 5 mM for both strains and, again, synergy was seen for both strains (**Figure 1B**). While the MICs for Ga^{3+} and nitrite varied with oxygen availability, the compounds were clearly synergistic under both aerobic and anaerobic conditions.

Nitric Oxide Is the Agent Responsible for the Observed Synergism With Ga^{3+}

The nitrite anion is reduced to NO within minutes upon administration (ip or iv) to mammals (Cambal et al., 2011, 2013). *P. aeruginosa* also reduces nitrite to nitric oxide, including in CF airway surface liquid (Yoon et al., 2006). Consequently, our working hypothesis is that NO is the active antimicrobial agent. Therefore, it was important to show that similar results were achievable with an alternative NO donor to nitrite. Addition of PAPA-NONOate to 312 µM dropped the MIC for Ga^{+3} from 96 µM to 24 µM (**Figure 2**) demonstrating the observed synergy to be qualitatively independent of the particular NO donor species. The half-life of PAPA-NON-oate is 15 min at 37°C min and that of nitrite *in vivo* is just a few min (Cambal et al., 2011, 2013). Thus, a comparatively brief exposure to NO is responsible for potentiating the antimicrobial activity of Ga^{3+} against *P. aeruginosa*. The synergistic consequences, however,

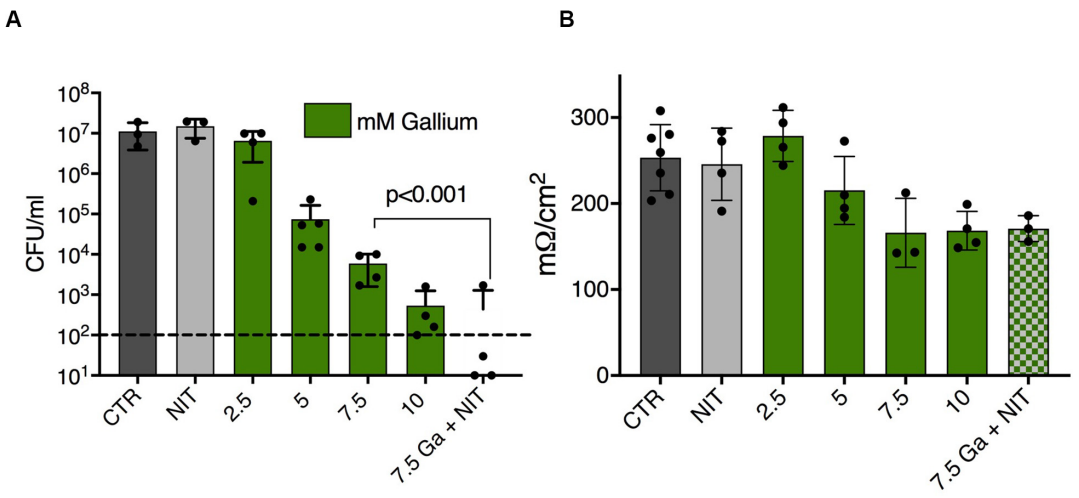

FIGURE 3 | Ga^{3+} and nitrite have synergistic antibiofilm activity. **(A)** Biofilm growth prevention assays done with PAO1 grown in PVC microtiter disks and stained with crystal violet. Asterisks indicated well scored with no growth. Four replicates done. **(B)** Representative results of a biofilm prevention assay in which final optical density of the crystal violet was measured spectrophotometrically. Highlighted cells show growth as defined as <20% reduction in OD compared to the control well. Three replicates were done.

A

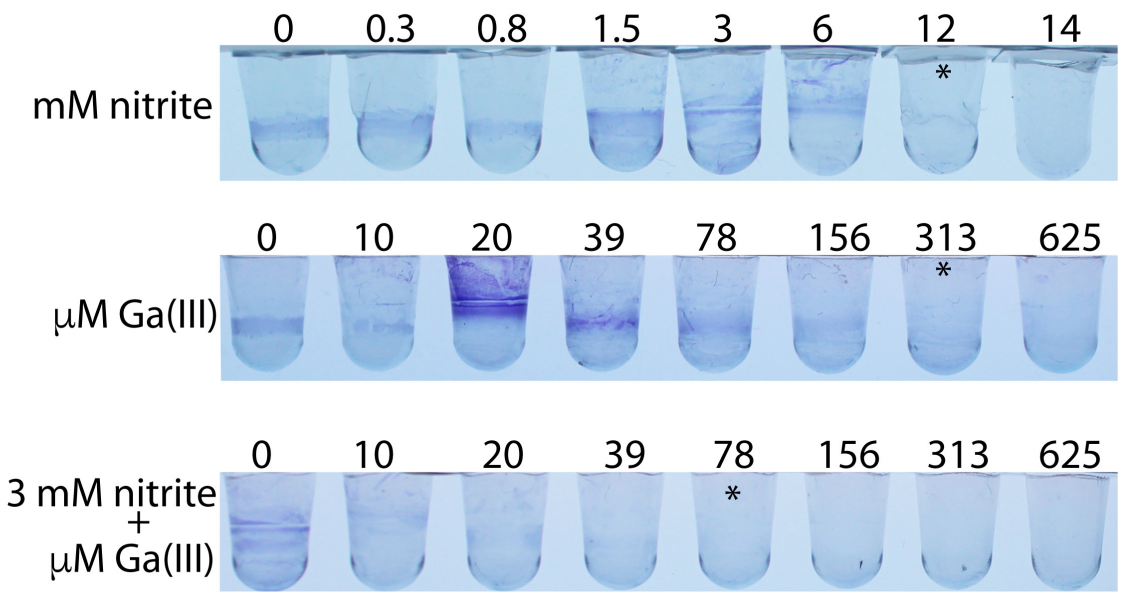

B

μM Ga	mM Nitrite 0	2	4	6	8	10	12
0	0.351	0.252	0.314	0.140	0.106	0.012	0.005
0.65	0.430	0.305	0.082	0.075	0.006	0.012	
1.3	0.373	0.129	0.069	0.036	-0.010		
2.6	0.369	0.152	0.102	0.030			
5.25	0.093	0.152	0.028	0.010			
10.5	0.037	0.059	0.014				
21	0.068	0.022					
42	0.073	0.029					
84	0.034						
167	0.007						

FIGURE 4 | (A) PAO1 biofilms grown on CF airway epithelial cells were treated for 90 min with Ga or NIT for 90 min and live CFUs were plated. Ga^{3+} shows dose dependent bacterial killing that is increased with the addition of nitrite. Dashed line is assay detection limit. **(B)** Tran-epithelial electrical resistance of airway cells treated with the indicated combinations for 60 min. $p < 0.001$ by one-way ANOVA followed by *post hoc* test. Replicates done: 3–4/condition tested. *Indicates visual MIC value.

are evident during the subsequent 24 hr of bacterial growth in the assays.

Nitrite and Ga^{3+} Have Anti-biofilm Activity

Growth conditions have wide ranging effects on bacterial physiology, and biofilms specifically have high antimicrobial tolerance in many settings, including growth in the human airway. We therefore tested the interaction between nitrite and Ga^{3+} against *P. aeruginosa* biofilms grown on polyvinyl chloride. In this assay, 14 mM nitrite prevented PAO1 biofilm growth, as did 313 μM Ga^{3+} (asterisks, **Figure 3A**). In the presence of 3 mM nitrite, 37 μM Ga^{3+} prevented biofilm growth, giving an FIC < 0.5. Using OD_{570} as a quantitative endpoint, we determined the concentration required to decrease biofilm formation by at least 80% (**Figure 3B**). A representative checkerboard result is shown, where the MIC for nitrite was 10 mM, the MIC for gallium(III) was 84 μM, which dropped to 5.25 μM in the presence of 4 mM nitrite. Biofilm growth in the presence of airway epithelial cells can be associated with even higher antimicrobial tolerance, thus we tested the combination in a model where *P. aeruginosa* biofilms are grown on the apical surface of the human airway epithelial cell line CFBE41o- (Moreau-Marquis et al., 2009). Biofilms were grown for 6 h and then treated for 90 min with 75 mM sodium nitrite or Ga^{3+}. We observed a dose dependent reduction in CFU with increasing concentrations of Ga^{3+}. No decrease in CFU was seen with nitrite, consistent with prior observations that nitrite

is bacteriostatic under these conditions. The addition of nitrite to 7.5 mM Ga^{3+} reduced CFU to below the limit of detection. Trans-epithelial electrical resistance of the did not drop until 7.5 mM Ga^{+3} and the addition of nitrite did not potentiate the drop in resistance (**Figure 4B**). In summary, we saw additional antibiofilm activity with addition of nitrite to Ga^{3+} in biofilms grown on plastic, as well as those grown on airway epithelial cells.

Nitrite Also Sensitizes Otherwise Ga^{3+} Resistant Isolates

The main route for bacterial uptake of Ga^{3+} is the iron transporter HitAB, and two independent studies have demonstrated that loss of HitAB function is the predominant route for development of Ga^{3+} resistance (García-Contreras et al., 2013; Goss et al., 2018). Insertional disruption of *hitA* increased the Ga^{3+} MIC to 150 μM (compared with 24–48μM for the parental strain). The nitrite MIC was 12 mM for PA14 *hitA*:IS, and the addition of 3 mM nitrite dropped the Ga^{3+} MIC to 37μM (**Figure 5**). These results are consistent with those of the more Ga^{3+} resistant clinical isolates, where nitrite also lowered the Ga^{3+} MIC (**Table 1**).

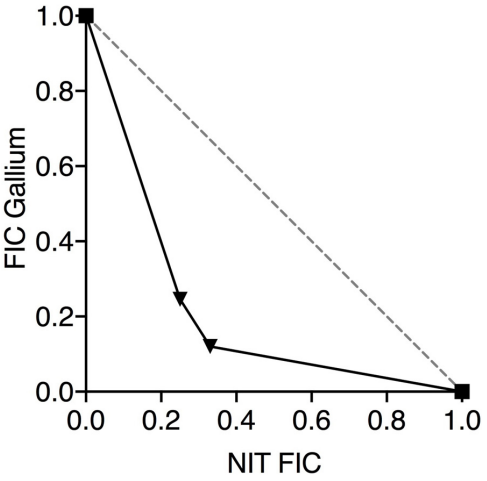

FIGURE 5 | Decreased Ga intake raises MIC but synergy is preserved. Isobolograms show the results of checkerboard assays using PA14 *hitA*:IS under aerobic conditions. Three replicates done.

DISCUSSION

Ga^{3+}, nitric oxide and sodium nitrite are all independently in early development as antimicrobial approaches for cystic fibrosis. NO is a gas with an inconveniently short half-life making delivery problematic, although approaches such as nocturnal delivery and NO release polymers are being investigated (Reighard and Schoenfisch, 2015; Howlin et al., 2017). Sodium nitrite has the potential advantage that it can be dosed less frequently via nebulization (Simon et al., 2016). While there has not been convincing efficacy data from these compounds to date, the existing safety data is reassuring (Miller et al., 2012; Simon et al., 2016). Ga^{3+} has broad antimicrobial activity, including growth inhibition of *P. aeruginosa, Rhodococcus equii* (Harrington et al., 2006)*, Mycobacterium tuberculosis* (Olakanmi et al., 2000) *Acinetobacter baumannii* (de Léséleuc et al., 2014), and *Staphylococcus aureus* (Baldoni et al., 2010). Subcutaneous administration of Ga^{3+} maltolate rescued thermally injured mice from infection with *P. aeruginosa* (DeLeon et al., 2009). Proof-of-concept studies in patients were completed using a well-tolerated intravenous formulation of Ga^{3+} as an antimicrobial in cystic fibrosis (Goss et al., 2018). No decrease in sputum bacterial density was seen, however, lung function improved with the treatment. An inhaled formulation of Ga^{3+}citrate is currently being tested in individuals with cystic fibrosis (ClinicalTrials.gov identifier NCT03669614). Given the existing sets of safety data, further translational studies are feasible.

Bacterial replication is essential for most bacterial pathogenesis, and core metabolic pathways such as oxidative phosphorylation, DNA synthesis, denitrification and the Krebs cycle are rich in iron-metalloproteins, particularly those containing Fe-S clusters. These cofactors seem to be more stable in mammalian enzymes than their bacterial counterparts, and consequently, agents causing widespread Fe-S cluster damage may prove useful antimicrobials (Pearce et al., 2005, 2009). Both nitrite and Ga^{3+} have been proposed separately as antimicrobial agents targeting core bacterial metabolism, but the idea of using them together in a combination therapy seems to be a new development. Almost certainly, peroxynitrite generated secondary to the NO-donor activity of nitrite will be the agent primarily responsible for any widespread damage to iron-containing proteins. It is anticipated that, in many instances, the more rapid reproduction of the pathogen compared to host cells will further ensure that the bacterial metabolism is more significantly affected by the treatment than that of the host. Consistent with this proposition, we have shown that Ga^{3+} and nitrite-derived nitrosative stress have synergistic antimicrobial activity against *P. aeruginosa* under aerobic and anaerobic conditions (**Figures 1**, **2**). More encouragingly still, nitrite and Ga^{3+} are also synergistic in preventing biofilm growth on plastic (**Figure 4**), and the addition of nitrite to Ga^{3+} increases the disruption of biofilms grown on human airway epithelial cells (**Figure 3**).

The specific bacterial protein targets of combined nitrite and Ga^{3+} exposure are presently not identified but are almost certainly multiple and will likely vary between species (Peterson et al., in preparation). Media carbon source influences *P. aeruginosa* susceptibility to Ga^{3+}, probably due to reliance on metabolic pathways differing with carbon source (Rzhepishevska et al., 2011). The net effect of nitrite plus Ga^{3+} under varying conditions will likely reflect a combination of individual enzymes susceptibilities to nitrosative damage, their comparative efficiencies of regeneration and the essentiality of any single enzyme under the particular conditions. Additionally, our results do not exclude a model where nitrosative stress creates a state of iron deprivation exacerbated by Ga^{3+} quenching the principal siderophore pyoverdine (Kaneko et al., 2007; Yeterian et al., 2010). Resistance to Ga^{3+} occurs through loss of *hitAB,* which is the principal uptake transporter, as well as through increased

expression of pyocyanin (García-Contreras et al., 2013). While inactivation of *hitAB* led to Ga^{3+} resistance, the MIC for nitrite was unchanged, and nitrite lowered the MIC to Ga^{3+} comparably to the parental strain; suggesting that this multi-targeting, synergistic approach may render the development of resistance less problematic. The effects of Ga + 3 and nitrite on the development of resistance remain to be experimentally determined.

In summary, we have demonstrated that inorganic nitrite and Ga^{3+} have synergistic antibacterial activity against *P. aeruginosa* under a range of test conditions and in biofilms. These findings appear to be novel in that they use a double attack on multiple targets within core bacterial metabolism with inexpensive and stable compounds that could feasibly be moved into human testing. The choices of particular nitrite compound(s) to be employed and the specific gallium(III) salt(s) serving as a source of Ga^{3+} could be dependent upon pharmacodynamic and pharmacokinetic considerations not addressed here. The compounds will also require *in vivo* toxicity testing in combination. The most direct application of these finding might be the combination of systemic gallium, which is already FDA approved, with topical or inhaled nitrite formations that are capable of safely achieving high local concentrations of nitrite. Another attractive alternative is the combination of inhaled nitrite or gaseous NO with gallium maltolate, which can be administered orally. Ultimately, though, new syntheses should not be required, since there are probably enough pre-existing compounds available for combining into suitable formulations.

DATA AVAILABILITY STATEMENT

The raw data supporting the conclusions of this article will be made available by the authors, without undue reservation, to any qualified researcher.

AUTHOR CONTRIBUTIONS

AZ conducted the experiments, wrote the first draft of manuscript, and analyzed the data. CM, NK, and LP conducted the experiments. JP conceived the concept, supervised experimental conduct and data analysis, and revised the manuscript. All authors contributed to the article and approved the submitted version.

FUNDING

CF Isolate Core at Seattle Children's as the source of the isolates, funded by the NIDDK 5P30DK089507. Cystic Fibrosis Foundation Grant: ZEMKEQ160 and NHLBI award K23HL131930.

ACKNOWLEDGMENTS

We thank Matt DuPont and Emily D'Amico for technical assistance.

REFERENCES

Alvarez-Ortega, C., and Harwood, C. S. (2007). Responses of *Pseudomonas aeruginosa* to low oxygen indicate that growth in the cystic fibrosis lung is by aerobic respiration. *Mol. Microbiol.* 65, 153–165. doi: 10.1111/j.1365-2958.2007.05772.x

Arai, H. (2011). Regulation and function of versatile aerobic and anaerobic respiratory metabolism in *Pseudomonas aeruginosa*. *Front. Microbiol.* 2:103. doi: 10.3389/fmicb.2011.00103

Baldoni, D., Steinhuber, A., Zimmerli, W., and Trampuz, A. (2010). *In vitro* activity of gallium maltolate against staphylococci in logarithmic, stationary, and biofilm growth phases: comparison of conventional and calorimetric susceptibility testing methods. *Antimicrob. Agents Chemother.* 54, 157–163. doi: 10.1128/aac.00700-09

Banin, E., Brady, K. M., and Greenberg, E. P. (2006). Chelator-induced dispersal and killing of *Pseudomonas aeruginosa* cells in a biofilm. *Appl. Environ. Microbiol.* 72, 2064–2069. doi: 10.1128/aem.72.3.2064-2069.2006

Cambal, L. K., Swanson, M. R., Yuan, Q., Weitz, A. C., Li, H. H., Pitt, B. R., et al. (2011). Acute, sublethal cyanide poisoning in mice is ameliorated by nitrite alone: complications arising from concomitant administration of nitrite and thiosulfate as an antidotal combination. *Chem. Res. Toxicol.* 24, 1104–1112. doi: 10.1021/tx2001042

Cambal, L. K., Weitz, A. C., Li, H. H., Zhang, Y., Zheng, X., Pearce, L. L., et al. (2013). Comparison of the relative propensities of isoamyl nitrite and sodium nitrite to ameliorate acute cyanide poisoning in mice and a novel antidotal effect arising from anesthetics. *Chem. Res. Toxicol.* 26, 828–836. doi: 10.1021/tx400103k

Chitambar, C. R. (2016). Gallium and its competing roles with iron in biological systems. *Biochim. Biophys. Acta Mol. Cell. Res.* 1863, 2044–2053. doi: 10.1016/j.bbamcr.2016.04.027

de Léséleuc, L., Harris, G., KuoLee, R., Xu, H. H., and Chen, W. (2014). Serum resistance, gallium nitrate tolerance and extrapulmonary dissemination are linked to heme consumption in a bacteremic strain of *Acinetobacter baumannii*. *Int. J. Med. Microbiol.* 304, 360–369. doi: 10.1016/j.ijmm.2013.12.002

DeLeon, K., Balldin, F., Watters, C., Hamood, A., Griswold, J., Sreedharan, S., et al. (2009). Gallium maltolate treatment eradicates *Pseudomonas aeruginosa* infection in thermally injured mice. *Antimicrob. Agents Chemother.* 53, 1331–1337. doi: 10.1128/aac.01330-08

García-Contreras, R., Lira-Silva, E., Jasso-Chávez, R., Hernández-González, I. L., Maeda, T., Hashimoto, T., et al. (2013). Isolation and characterization of gallium resistant *Pseudomonas aeruginosa* mutants. *Int. J. Med. Microbiol.* 303, 574–582. doi: 10.1016/j.ijmm.2013.07.009

Goss, C. H., Kaneko, Y., Khuu, L., Anderson, G. D., Ravishankar, S., Aitken, M. L., et al. (2018). Gallium disrupts bacterial iron metabolism and has therapeutic effects in mice and humans with lung infections. *Sci. Transl. Med.* 10:eaat7520. doi: 10.1126/scitranslmed.aat7520

Harrington, J. R., Martens, R. J., Cohen, N. D., and Bernstein, L. R. (2006). Antimicrobial activity of gallium against virulent *Rhodococcus equiin* vitro and *in vivo*. *J. Vet. Pharmacol. Ther.* 29, 121–127. doi: 10.1111/j.1365-2885.2006.00723.x

Howlin, R. P., Cathie, K., Hall-Stoodley, L., Cornelius, V., Duignan, C., Allan, R. N., et al. (2017). Low-dose nitric oxide as targeted anti-biofilm adjunctive therapy to treat chronic *Pseudomonas aeruginosa* infection in cystic fibrosis. *Mol. Ther.* 25, 2104–2116. doi: 10.1016/j.ymthe.2017.06.021

Kaneko, Y., Thoendel, M., Olakanmi, O., Britigan, B. E., and Singh, P. K. (2007). The transition metal gallium disrupts *Pseudomonas aeruginosa* iron metabolism and has antimicrobial and antibiofilm activity. *J. Clin. Invest.* 117, 877–888. doi: 10.1172/jci30783

Liberati, N. T., Urbach, J. M., Miyata, S., Lee, D. G., Drenkard, E., Wu, G., et al. (2006). An ordered, nonredundant library of *Pseudomonas aeruginosa*

strain PA14 transposon insertion mutants. *Proc. Natl. Acad. Sci. U.S.A.* 103, 2833–2838. doi: 10.1073/pnas.0511100103

Miller, C., Miller, M., McMullin, B., Regev, G., Serghides, L., Kain, K., et al. (2012). A phase I clinical study of inhaled nitric oxide in healthy adults. *J. Cyst, Fibros* 11, 324–331. doi: 10.1016/j.jcf.2012.01.003

Moreau-Marquis, S., Bomberger, J. M., Anderson, G. G., Swiatecka-Urban, A., Ye, S., O'Toole, G. A., et al. (2008). The DeltaF508-CFTR mutation results in increased biofilm formation by *Pseudomonas aeruginosa* by increasing iron availability. *Am. J. Physiol. Lung Cell. Mol. Physiol.* 295, L25–L37.

Moreau-Marquis, S., O'Toole, G. A., and Stanton, B. A. (2009). Tobramycin and FDA-approved iron chelators eliminate *Pseudomonas aeruginosa* biofilms on cystic fibrosis cells. *Am. J. Respir. Cell. Mol. Biol.* 41, 305–313. doi: 10.1165/rcmb.2008-0299oc

Moreau-Marquis, S., Redelman, C. V., Stanton, B. A., and Anderson, G. G. (2010). Co-culture models of *Pseudomonas aeruginosa* biofilms grown on live human airway cells. *J. Vis. Exp.* 6:2186.

Mulani, M. S., Kamble, E. E., Kumkar, S. N., Tawre, M. S., and Pardesi, K. R. (2019). Emerging strategies to combat ESKAPE pathogens in the era of antimicrobial resistance: a review. *Front. Microbiol.* 10:539. doi: 10.3389/fmicb.2019.00539

Olakanmi, O., Britigan, B. E., and Schlesinger, L. S. (2000). Gallium disrupts iron metabolism of mycobacteria residing within human macrophages. *Infect. Immun.* 68, 5619–5627. doi: 10.1128/iai.68.10.5619-5627.2000

Palmer, L. D., and Skaar, E. P. (2016). Transition metals and virulence in bacteria. *Annu. Rev. Genet.* 50, 67–91. doi: 10.1146/annurev-genet-120215-035146

Patient Registry (2011). *Annual Data Report 2011*. Available online at: http://www.cff.org/UploadedFiles/research/ClinicalResearch/2011-Patient-Registry.pdf (accessed April 1, 2020).

Pearce, L. L., Kanai, A. J., Epperly, M. W., and Peterson, J. (2005). Nitrosative stress results in irreversible inhibition of purified mitochondrial complexes I and III without modification of cofactors. *Nitric Oxide Biol. Chem.* 13, 254–263. doi: 10.1016/j.niox.2005.07.010

Pearce, L. L., Martinez-Bosch, S., Manzano, E. L., Winnica, D. E., Epperly, M. W., and Peterson, J. (2009). The resistance of electron-transport chain Fe-S clusters to oxidative damage during the reaction of peroxynitrite with mitochondrial complex II and rat-heart pericardium. *Nitric Oxide Biol. Chem.* 20, 135–142. doi: 10.1016/j.niox.2008.12.001

Petersen, P. J., Labthavikul, P., Jones, C. H., and Bradford, P. A. (2006). In vitro antibacterial activities of tigecycline in combination with other antimicrobial agents determined by chequerboard and time-kill kinetic analysis. *J. Antimicrob. Chemother.* 57, 573–576. doi: 10.1093/jac/dki477

Reighard, K. P., and Schoenfisch, M. H. (2015). Antibacterial action of nitric oxide-releasing chitosan oligosaccharides against *Pseudomonas aeruginosa* under aerobic and anaerobic conditions. *Antimicrob. Agents Chemother.* 59, 6506–6513. doi: 10.1128/aac.01208-15

Rice, L. B. (2010). Progress and challenges in implementing the research on ESKAPE pathogens. *Infect. Control. Hosp. Epidemiol.* 31(Suppl. 1), S7–S10.

Richter, K., Thomas, N., Claeys, J., McGuane, J., Prestidge, C. A., Coenye, T., et al. (2017). A topical hydrogel with deferiprone and gallium-protoporphyrin targets bacterial iron metabolism and has antibiofilm activity. *Antimicrob. Agents Chemother.* 61:e00481-17.

Rzhepishevska, O., Ekstrand-Hammarstrom, B., Popp, M., Bjorn, E., Bucht, A., Sjostedt, A., et al. (2011). The antibacterial activity of Ga3+ is influenced by ligand complexation as well as the bacterial carbon source. *Antimicrob. Agents Chemother.* 55, 5568–5580. doi: 10.1128/aac.00386-11

Schaible, B., Taylor, C. T., and Schaffer, K. (2012). Hypoxia increases antibiotic resistance in *Pseudomonas aeruginosa* through altering the composition of multidrug efflux pumps. *Antimicrob. Agents Chemother.* 56, 2114–2118. doi: 10.1128/aac.05574-11

Simon, M. A., Vanderpool, R. R., Nouraie, M., Bachman, T. N., White, P. M., Sugahara, M., et al. (2016). Acute hemodynamic effects of inhaled sodium nitrite in pulmonary hypertension associated with heart failure with preserved ejection fraction. *JCI Insight* 1:e89620.

Yeterian, E., Martin, L. W., Lamont, I. L., and Schalk, I. J. (2010). An efflux pump is required for siderophore recycling by *Pseudomonas aeruginosa*. *Environ. Microbiol. Rep.* 2, 412–418. doi: 10.1111/j.1758-2229.2009.00115.x

Yoon, S. S., Coakley, R., Lau, G. W., Lymar, S. V., Gaston, B., Karabulut, A. C., et al. (2006). Anaerobic killing of mucoid *Pseudomonas aeruginosa* by acidified nitrite derivatives under cystic fibrosis airway conditions. *J. Clin. Invest.* 116, 436–446. doi: 10.1172/jci24684

Zemke, A. C., Shiva, S., Burns, J. L., Moskowitz, S. M., Pilewski, J. M., Gladwin, M. T., et al. (2014). Nitrite modulates bacterial antibiotic susceptibility and biofilm formation in association with airway epithelial cells. *Free Radic. Biol. Med.* 77, 307–316. doi: 10.1016/j.freeradbiomed.2014.08.011

Zhang, L., and Mah, T.-F. (2008). Involvement of a novel efflux system in biofilm-specific resistance to antibiotics. *J. Bacteriol.* 190, 4447–4452. doi: 10.1128/jb.01655-07

Conflict of Interest: The authors declare that the research was conducted in the absence of any commercial or financial relationships that could be construed as a potential conflict of interest.

frontiers in Microbiology

ORIGINAL RESEARCH
published: 15 September 2020
doi: 10.3389/fmicb.2020.02110

Phytofabrication of Silver Nanoparticles Using Three Flower Extracts and Their Antibacterial Activities Against Pathogen *Ralstonia solanacearum* Strain YY06 of Bacterial Wilt

*Hai-Jun Cheng, Hui Wang and Jing-Ze Zhang**

Institute of Biotechnology, College of Agriculture and Biotechnology, Zhejiang University, Hangzhou, China

OPEN ACCESS

Edited by:
Mariano Martinez-Vazquez, National Autonomous University of Mexico, Mexico

Reviewed by:
Palanivel Velmurugan, Alagappa University, India
Murugan Kasi, Manonmaniam Sundaranar University, India

***Correspondence:**
Jing-Ze Zhang
jzzhang@zju.edu.cn

Specialty section:
This article was submitted to Antimicrobials, Resistance and Chemotherapy, a section of the journal Frontiers in Microbiology

Received: *08 May 2020*
Accepted: *11 August 2020*
Published: *15 September 2020*

Citation:
Cheng H-J, Wang H and Zhang J-Z (2020) Phytofabrication of Silver Nanoparticles Using Three Flower Extracts and Their Antibacterial Activities Against Pathogen Ralstonia solanacearum Strain YY06 of Bacterial Wilt. Front. Microbiol. 11:2110. doi: 10.3389/fmicb.2020.02110

Bacterial wilt caused by the phytopathogen *Ralstonia solanacearum* (*R. solanacearum*) is a devastating plant disease worldwide. The use of bactericides and antibiotics for controlling bacterial wilt has shown low efficiency and posed environmental risks. This study was to phytofabricate silver nanoparticles (AgNPs) mediated by canna lily flower (*Canna indica* L.), Cosmos flower (*Cosmos bipinnata* Cav.), and Lantana flower (*Lantana camara* L.). The biosynthesized AgNPs were confirmed and characterized by UV-visible spectroscopy, Fourier transform infrared spectroscopy (FTIR), X-ray diffraction (XRD), transmission electron microscope (TEM), and scanning electron microscopy (SEM). UV-visible spectra showed absorption peak bands at 448, 440, and 428 nm of AgNPs synthesized by *C. indica* L., *C. bipinnata* Cav., and *L. camara* L. flowers, respectively. FTIR spectra confirmed that biofunctional groups of flower extract were involved in the synthesis of AgNPs as capping and stabilizing agents. The spherical AgNPs synthesized by *C. indica* L., *C. bipinnata* Cav., and *L. camara* L. flowers had average diameters of 43.1, 36.1, and 24.5 nm, respectively. The AgNPs (10.0 μg/ml) synthesized by *L. camara* L. flower had a maximum suppression zone of 18 mm against *R. solanacearum* strain YY06 compared with AgNPs synthesized by *C. indica* L. and *C. bipinnata* Cav. flowers. Bacterial growth, biofilm formation, swimming motility, efflux of nucleic acid, cell death, cell membrane damage, and reactive oxygen species (ROS) generation of *R. solanacearum* were also negatively affected by AgNPs with high concentration and small size. In summary, the biosynthesized AgNPs can be used as an efficient and environmentally friendly antibacterial agent to reasonably inhibit *R. solanacearum*.

Keywords: *Ralstonia solanacearum*, silver nanoparticles, *Canna indica* L. flower, *Cosmos bipinnata* Cav. flower, *Lantana camara* L. flower, characterization, antibacterial activity, antibacterial mechanism

INTRODUCTION

Bacterial wilt caused by the phytopathogen *Ralstonia solanacearum* is a devastating plant disease worldwide, which can affect more than 200 plant species in over 50 families such as eggplants, tomatoes, olives, groundnuts, potatoes, and bananas (Hayward, 1964; Schell, 2000). The use of bactericides and antibiotics for controlling bacterial wilt has shown low efficiency due to resistant mutation of bacteria (Levy, 2001). Hence, the development of an effective and broad-spectrum antimicrobial agent is urgently required against the pathogens.

Nanotechnology is one of the evolving and most fascinating sciences, which have broad application prospects thanks to many superior properties of nanomaterials. Among the all noble metal nanoparticles, silver nanoparticles (AgNPs) occupy a prominent position due to its unique characteristics such as antibacterial, antifungal, antiviral, and anti-inflammatory properties, which can be applied to food science and anti-cancer medicine (Oves et al., 2018), especially agriculture (Oves et al., 2013).

The synthesis of AgNPs includes chemical (Sotiriou and Pratsinis, 2010; Sotiriou et al., 2011; Zhang et al., 2011; Roldán et al., 2013), physical (Tien et al., 2008; El-Nour et al., 2010; Asanithi et al., 2012), and biological (Husen and Siddiqi, 2014a; Siddiqi and Husen, 2016) routes. However, compared to biological synthesis of nanoparticle, physiochemical methods have difficulty applying on a large scale owing to the production of high temperature and harmful chemicals (Ahmed et al., 2016).

Biological stuff such as plants, bacteria, and fungi were used for green synthesis of AgNPs (Castro-Longoria et al., 2011; Husen and Siddiqi, 2014b), especially plants are more advantageous because of less contamination threat and easy availability. Recent studies have reported that AgNPs can be synthesized by using various plants parts such as leaves extract of *Nigella sativa* (Amooaghaie et al., 2015), roots extract of red ginseng (Singh et al., 2015b), seeds extract of *Pistacia atlantica* (Sadeghi et al., 2015), flowers extract of *Nyctanthes arbortristis* (Gogoi et al., 2015), fruits extract of orange and pineapple (Hyllested et al., 2015), etc. *Canna indica* L. have been reported to use as diaphoretic and diuretic in fevers and dropsy, as a demulcent to stimulate menstruation, treat suppuration, and rheumatism (Duke and Ayensu, 1984). *Cosmos bipinnata* Cav. is used traditionally as a hepatoprotective agent and for the management of leukemia, headache, jaundice, splenomegaly, stomach aches, flatulence, and intermittent malarial fever (Jo et al., 2012; Olajuyigbe and Ashafa, 2014). *Lantana camara* L. is used in medicine against influenza, measles, stomachache, chicken pox, fever, rheumatisms, asthma, and hypertension (Kumar et al., 2015). In addition, the major functional molecules of three plants extract include alkaloids, carbohydrates, proteins, flavonoids, terpenoids, steroids, saponins, and tannins (Ghisalberti, 2000; Wang et al., 2007; Saleem et al., 2019) as capping and stabilizing agents play a significant role for the synthesis of nanoparticles (Duan et al., 2015).

At the same time, we have limited knowledge about antibacterial mechanisms of nano-silver against *R. solanacearum* and need to continue to investigate it. Therefore, the work of this research was mainly to green synthesize AgNPs mediated by Canna lily flower (*C. indica* L.), Cosmos flower (*C. bipinnata* Cav.), and Lantana flower (*L. camara* L.) and demonstrate the antibacterial activities and mechanisms against the pathogen *R. solanacearum* of bacterial wilt. To the best of our knowledge, this is the first report to synthesize AgNPs using flower extract of *C. indica* L. and *C. bipinnata* Cav.

MATERIALS AND METHODS

Materials

Three plants namely Canna lily flower (*C. indica* L.), Cosmos flower (*C. bipinnata* Cav.), and Lantana flower (*L. camara* L.), were collected from Zijingang campus, Zhejiang University, Hangzhou, China. The analytical grade silver nitrate ($AgNO_3$) was purchased from Sinopharm Chemical Reagent Co., Ltd. company (Shanghai, China). The bacterial wilt pathogen *R. solanacearum* strain YY06 (a highly aggressive strain from eggplant) was provided from the Institute of Biotechnology, Zhejiang University, Hangzhou, China. The bacteria were routinely cultured in nutrient agar (NA) medium composed of beef extract 3 g, NaCl 5 g, peptone 10 g, ddH_2O 1,000 ml, without/with agar 15 g, pH 7.2–7.4 at 37°C.

Preparation of Flower Extracts

Flower extracts of *C. indica* L., *C. bipinnata* Cav., and *L. camara* L. were prepared following the procedure of Moteriya and Chanda (2017) with small adjustments. Briefly, the flowers were carefully rinsed with ddH_2O and then crushed into small pieces. Two gram air-dried flowers were stirred with a blender in 200 ml ddH_2O to acquire 1% (w/v) flower broth. The resulting extracts were filtered with a muslin cloth, centrifuged for 10 min at 14,000 rpm, and retained at 4°C.

Synthesis of AgNPs Using Different Flower Extracts

According to Gogoi et al. (2015) with minor modifications, 20 ml aqueous flower extract was mixed with 100 ml $AgNO_3$ solution (4 mM) in an Erlenmeyer flask, which was then kept under the dark condition at rotating 180 rpm at 55°C. $AgNO_3$ solution was mixed with ddH_2O instead of flower extracts, which was used a control. When the color of the solution became dark brown, it indicated that the silver ions had been reduced to AgNPs. The produced AgNPs solution was centrifuged (JEOL, JEM-200EX; Tokyo, Japan) at 14,000 rpm for 10 min and removed the supernatant. The collected pellets were carefully washed with ddH_2O and freeze-dried according to Alpha1-2 LDplus (GmbH, Germany) instruction and then saved at −4°C for further use.

Confirmation and Characterization of Synthesized AgNPs

The collected pellets were measured under the wavelength range of 300–700 nm at 1 nm resolution in a spectrophotometer (Shimadzu Corporation, Kyoto, Japan). The infrared spectra

of the dried AgNPs was recorded at room temperature by a Fourier transform infrared spectroscopy (FTIR) machine (Vector 22, Bruker, Germany) scanned at a resolution of 4 cm^{-1} and range between 450 and 4,000 cm^{-1}. The X-ray diffraction (XRD) value of nanoparticles was obtained by using a diffractometer (Siemens D5000, Germany) at 2Θ range of 20–90°. Scanning electron microscopy (SEM; SU8010, Hitachi, Japan) and transmission electron microscope (TEM; JEM-1230, JEOL, Akishima, Japan) were used to document the size and shape of AgNPs according to the operating instruction.

Inhibition Zone Assay

The effect of AgNPs on the *R. solanacearum* strain YY06 was investigated by plate assay as depicted by Singh et al. (2015a) with few amendments. Four hundred microliter bacterial suspension (1×10^8 CFU/ml) cultured overnight in NA broth at 37°C was mixed with 10 ml unsolidified NA in a Petri dish plate. Forty microliter AgNPs suspension (2.5, 5.0, and 10.0 μg/ml) was, respectively, dropped in holes of the air-dried NA plate and incubated at 37°C for 24 h. The same quantity of the filter-sterilized flower extract was used as control. The antagonistic activity was estimated by averaging the diameter of the cleared zones. The experiment was performed three times with three replications.

Minimum Inhibitory Concentration of AgNPs

A broth dilution procedure was used to assess the minimum inhibitory concentration (MIC) of AgNPs in a 96-well microplate (Corning-Costar Corp, Corning, NY, United States). According to Mohanta et al. (2017) with slight modifications, 100 μl overnight bacterial broth (approximately 1×10^8 CFU/ml) was mixed with 100 μl AgNPs suspension of 2-fold serial dilutions (2.5, 5.0, and 10.0 μg/ml) followed by culturing at 37°C for 24 h, bacterial broth culture without AgNPs was used as control. A microplate spectrophotometer (Thermo Fisher Scientific Inc., Waltham, MA) was used to measure the optical density of the mixed solution at 600 nm. There were three replicates for each treatment and three repeats for each experiment.

Biofilm Inhibition Assay

The effect of AgNPs on bacterial biofilm formation was determined on the 96-well microplate (Corning-Costar Corp., Corning, NY). According to Ibrahim et al. (2019) with slight adjustments, *R. solanacearum* strain YY06 suspension adjusted to OD600 = 0.3 (100 μl) was transferred into each well of the 96-well microplate with 100 μl of suspension without or with AgNPs. The microplate was placed without shaking at 37°C for 3 days. After bacterial adhesion, the suspension was discarded followed by a gentle wash with ddH_2O three times to remove the free cells. As soon as air was dry, an aqueous solution of 1% crystal violet (100 μl) was transferred into each well and the 96-well microplate placed for half an hour to stain the attached bacteria. The dye was discarded and wells of the microplate were subsequently washed gently with ddH_2O. A 33% acetic acid (100 μl) was then added to dissolve the dye, and the intensity of the reaction mixture was measured using a spectrophotometer at 570 nm.

Swimming Motility Assay

The impact of AgNPs on swimming motility of *R. solanacearum* strain YY06 was tested on semi-solid NA [0.4% (w/v)]. AgNPs were mixed into the soft agar medium to obtain a final concentration of 2.5, 5.0, and 10.0 μg/ml. Three microliter *R. solanacearum* strain YY06 suspension at a concentration of 10^8 CFU/ml was dropped in the center of the semi-solid NA plates containing AgNPs or no AgNPs, which were incubated at 37°C for 48 h. The migration diameter of *R. solanacearum* strain YY06 was measured to assess the swimming ability due to the exposure to AgNPs. There were three replicates for each treatment and three repeats for each experiment.

Efflux of the Cytoplasmic Materials

Upon damage to the cell membrane, substances (DNA and RNA) were released out of the cell, which was documented the optical density of the solution at 260 nm. As described by Cai et al. (2018) with slight modifications, the 1,000 μl overnight bacterial suspension with AgNPs (2.5, 5.0, and 10.0 μg/ml) was cultured at 37°C for 12 h. The samples were then centrifuged at 5,000 *g* for 4 min to remove the bacteria and AgNPs. OD value of the solution was noted at 260 nm ultraviolet light using a spectrophotometer.

Live/Dead Assay

BacLight bacterial viability kit (Invitrogen), a mixture of red propidium iodide fluorescent nucleic acid dye and green SYTO 9 fluorescent nucleic acid dye, was applied to detect live/dead bacterial cells. One thousand microliter overnight bacterial suspension (1×10^8 CFU/ml) was mixed with 1 ml solution of AgNPs to acquire a concentration of 10.0 μg/ml and was subsequently incubated in a shaker at 180 rpm, 37°C. Fluorescence emission of bacteria was recorded by using a laser scanning confocal microscope (LSM780) as mentioned before (Cui et al., 2014).

Flow Cytometry Observation

Propidium iodide (PI) is a type of fluorochrome that can just penetrate the compromised cell and embed in double-stranded nucleic acid. Therefore PI can be applied to assess the damage of the cell membrane upon exposure to nanoparticles (Kumar et al., 2011). The *R. solanacearum* strain YY06 suspension treated with AgNPs (10.0 μg/ml) was incubated in a rotary shaker with 180 rpm at 37°C for 36 h and subsequently dyed with propidium iodide (PI) in the dark for half an hour. The staining cells can be monitored using flow cytometry (BD FACSVerse).

Electron Microscopy Analysis

The cellular adsorption assay was conducted using the method described in the preceding studies (Cai et al., 2018; Abdallah et al., 2019). One thousand microliter *R. solanacearum* strain YY06 suspension (1×10^8 CFU/ml) was mixed with

10 μg/ml AgNPs mediated by *L. camara* L. The bacterial suspensions treated with or without the AgNPs were put in a shaker with 180 rpm at 37°C for 12 h. After centrifugated at 5,000 *g* for 4 min, the bacterial cells were washed three times with 0.1 mol/l phosphate buffered saline (PBS) followed by fixing with 2.5% (v/v) glutaraldehyde in 0.1 M PBS. The samples were then post-fixed with 1% (w/v) osmium tetroxide in 0.1 M PBS for 1 h followed by washing three times with 0.1 M PBS buffer. The samples were dehydrated with a range of ethanol solutions (50, 70, 80, 90, 95, and 100%). TEM (JEM-1230, JEOL, Akishima, Japan) and SEM (SU8010, Hitachi, Japan) were used to document the changes of bacteria according to the operating instruction. The energy dispersive X-ray spectroscopy (EDS; Hitachi, Japan) was used to detect the elements of the cell surface.

Determination of the Reactive Oxygen Species

DCFH-DA is a non-polar dye that can be converted to polar derivative DCFH by cellular esterase; non-fluorescent DCFH reacts further with ROS to form the DCF which can fluoresce at a wavelength of 488 nm (Applerot et al., 2012). To detect the intracellular ROS, 1,000 μl *R. solanacearum* strain YY06 suspension (1×10^8 CFU/ml) was mixed with 10 μg/ml AgNPs mediated by *L. camara* L. and cultured in a rotary shaker with 180 rpm at 37°C for 12 h. The bacterial suspension not treated with AgNPs was used as the experimental control. Subsequently, the treated samples were gently rinsed three times with sterilized water and inoculated with 10 mM DCFH-DA at 37°C for 30 min in the dark. The fluorescence was detected by using the laser scanning confocal microscope (LSM780) as described previously (Prasad et al., 2019). The experiment was repeated three times.

Statistical Analysis

The ANOVA test was analyzed by the software SPSS21 (America), mean values of treatments were done using the least significant difference (LSD) method at $p < 0.05$.

RESULTS AND DISCUSSION

Biosynthesis and Characterization of AgNPs

The synthesis of AgNPs through the aqueous flower extracts of *C. indica* L., *C. bipinnata* Cav., and *L. camara* L. was as a result of the reduction of silver ions (Ag^+) to Ag^0 in $AgNO_3$ (4 mM) solution at the optimum temperature (**Figure 1**). The change of the solution color to dark brown indicated that the silver ions have been reduced to AgNPs (Nayak et al., 2016). The UV-visible spectra of nanoparticles mediated by *C. indica* L., *C. bipinnata* Cav., and *L. camara* L. flowers showed absorption peak bands at 448, 440, and 428 nm, respectively (**Supplementary Figure S1**). Similar results of wavelength were obtained for *Iresine herbstii* leaf and *Erigeron annuus* flower aqueous extracts mediated synthesis of AgNPs (Dipankar and Murugan, 2012; Velmurugan et al., 2014).

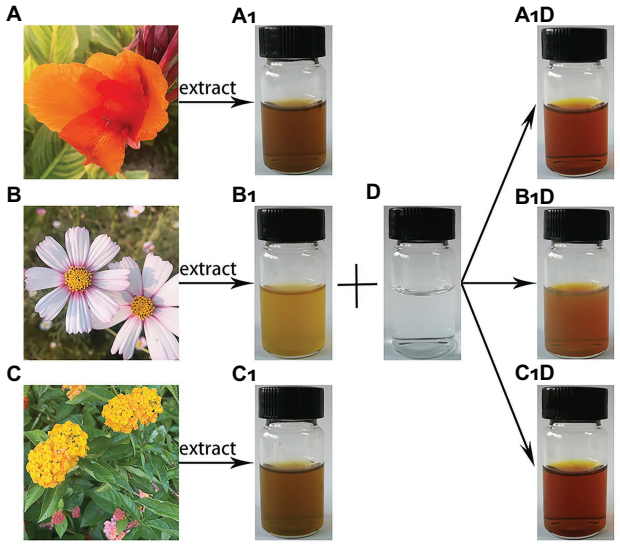

FIGURE 1 | Schematic presentation of silver nanoparticles (AgNPs) synthesis. **(A)** *Canna indica* L. flower; **(B)** *Cosmos bipinnata* Cav. flower; **(C)** *Lantana camara* L. flower; **(A_1)** filtered *C. indica* L. flower aqueous extract; **(B_1)** filtered *C. bipinnata* Cav. flower aqueous extract; **(C_1)** filtered *L. camara* L. flower aqueous extract; **(D)** silver nitrate solution; **(A_1D)** solution AgNPs synthesized by *C. indica* L. flower; **(B_1D)** solution AgNPs synthesized by *C. bipinnata* Cav. flower; and **(C_1D)** solution AgNPs synthesized by *L. camara* L. flower.

The FTIR spectra of AgNPs derived from *C. indica* L., *C. bipinnata* Cav., and *L. camara* L. flowers are illustrated in **Supplementary Figure S2**. The main band intensity was as follows: 3,421, 3,419, and 3,416 cm^{-1} corresponded to N−H and O−H stretching vibrations of amine groups. Bands at 2,919, 2,918, and 2,920 cm^{-1} appeared due to stretching vibration of C−H, and the bands at 1,598, 1,636, and 1,649 cm^{-1} were assigned to C═O amide groups. The bands at 1,309, 1,384, and 1,384 cm^{-1} represented COO− anions and the spectra bands at 1,070, 1,072, and 1,048 cm^{-1} appeared due to the C−N stretching vibration. The infrared spectra of AgNPs revealed that the flower extracts performed a dual role in the solution mixture, i.e., as a reducing agent of Ag^+ and stabilizing agent of Ag with the biological functional groups. Carboxylic acids, ketones, aldehydes, and amine linked to the silver ions reduction, which stabilize nanoparticles due to the oxidation of hydroxyl radical (Aziz et al., 2019).

The XRD image of three synthesized AgNPs was shown in **Supplementary Figure S3**. The synthesized AgNPs from *C. indica* L. flower had diffraction peaks at 38.137, 44.274, 64.504, and 77.370, while the AgNPs derived from *C. bipinnata* Cav. flower showed diffractions peaks at 38.076, 44.171, 64.442, and 77.472. On the other hand, the AgNPs synthesized by *L. camara* L. flower emitted diffraction peaks at 38.158, 44.274, 64.504, and 77.431, corresponding to the silver crystal planes (111), (200), (220), and (311), which revealed that AgNPs had varied face-centered cubic (fcc) planes in agreement with earlier reports (Ma et al., 2012; Velmurugan et al., 2015).

Herein, electron micrographs of AgNPs synthesized by the flowers were shown in **Figure 2**, the TEM micrographs indicated

that AgNPs were mono-dispersed in irregularly spherical particle-like shapes, which conformed to the pictures of the SEM. The TEM images showed that AgNPs had average diameters of 43.1, 36.1, and 24.5 nm synthesized by *C. indica* L., *C.bipinnata* Cav., and *L. camara* L. flowers, respectively. The SEM images showed that the diameters ranged from 28.7 to 45.5 nm for AgNPs synthesized by *C. indica* L. flower, 33.5 to 44.4 nm for AgNPs synthesized by *C. bipinnata* Cav. flower, and 21.1 to 30.2 nm for AgNPs synthesized by *L. camara* L. flower. In the study, we observed the AgNPs clusters that may cause the difference of particle size, which were reported by previous studies (Rasheed et al., 2017).

Antibacterial Activities

The antagonistic activity of AgNPs against *R. solanacearum* strain YY06 was determined by measuring the bacterial growth inhibition zone formation in solid agar media. The result showed that the diameter of the bacteriostatic zone enlarged with the increase in concentration of AgNPs having its maximum antibacterial effect at 10.0 μg/ml. The AgNPs synthesized by *L. camara* L. flower had the highest bacteriostatic zone of 18 mm against *R. solanacearum* strain YY06 compared with AgNPs synthesized by *C. indica* L. and *C. bipinnata* Cav. flowers (**Figure 3**), while the control flower aqueous extract had no inhibition zone (data not shown). We also tested the inhibitory activity of AgNPs against *Xanthomonas oryzae* pv. oryzae (Xoo) strain GZ 0003, which had a good bacteriostatic effect (**Supplementary Figure S4**). Silver nanoparticle as a bacteriostatic agent was reported previously on *Escherichia coli*, *Pseudomonas aeruginosa*, *Bacillus subtilis*, and *Staphylococcus aureus* (Ahmed et al., 2016).

The MIC of AgNPs on *R. solanacearum* strain YY06 was tested on a 96-well microplate. As shown in **Figure 4**, the bacterial number reduced by 3.93, 3.33, and 23.64% at 2.5 μg/ml, and 5.62, 15.88, and 81.89% at 5.0 μg/ml owing to exposure of AgNPs synthesized by *C. indica* L., *C. bipinnata* Cav., and *L. camara* L., respectively. On the other hand, AgNPs synthesized by *L. camara* L. at 10.0 μg/ml had the highest reduction of OD600 by 96.40% compared to the other synthesized AgNPs. The nano-size particles with high surface area, strong adsorption, and positive charge enable them to effectively inhibit bacterial growth (Wang et al., 2017). Furthermore, the result revealed that the higher concentration and smaller size of nanoparticles, the greater impact on bacterial growth as described previously (Kim et al., 2007).

The biofilm formation played an important role in the virulence of plant pathogen by increasing the survivability of bacteria in harsh conditions, resisting to bacteriostatic substances derived from plants and motivating colonization in the host plants (Dang and Lovell, 2016). In this study, it was evaluated whether the synthesized AgNPs (2.5, 5.0, and 10.0 μg/ml) could inhibit the biofilm formation of *R. solanacearum* strain YY06 by staining with crystal violet in 96-well plates. As shown in

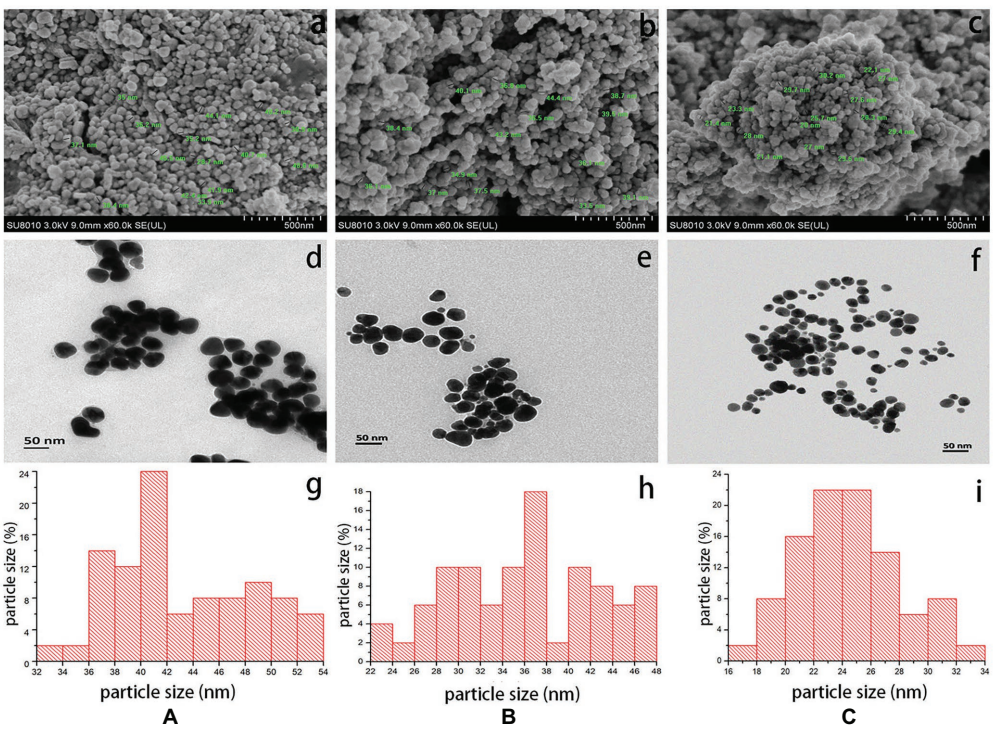

FIGURE 2 | Scanning electron micrographs of AgNPs synthesized by **(a)** *C. indica* L. flower; **(b)** *C. bipinnata* Cav. flower; and **(c)** *L. camara* L. flower; scale bar = 500 nm. Transmission electron micrographs of AgNPs synthesized by **(d)** *C. indica* L. flower; **(e)** *C. bipinnata* Cav. flower; and **(f)** *L. camara* L. flower; scale bar = 50 nm. The size distribution of particles in transmission electron micrographs of AgNPs synthesized by **(g)** *C. indica* L. flower; **(h)** *C. bipinnata* Cav. flower; and **(i)** *L. camara* L. flower.

Figure 5, with the increase of AgNPs concentration, the color of solution in wells gradually lightened, which indicated that the biomass of biofilm decreased. The AgNPs synthesized by *C. indica* L., *Cosmos bipinnata* Cav., and *L. camara* L. flowers decreased the biofilm formation of *R. solanacearum* strain YY06 by 49.85, 58.78, and 61.55% at 10.0 μg/ml, compared to the control OD570 value 0.39 of *R. solanacearum* strain YY06 without AgNPs.

Swimming motility of bacteria is directly involved in its growth and pathogenesis, crucial for surface adherence, structural disassembly, and discharge from the matrix of biofilm (Klausen et al., 2003). To assess the effect of AgNPs on bacterial movement, the diameter of the vicinity covered by *R. solanacearum* strain YY06 was measured on soft NA medium supplied with AgNPs (2.5, 5.0, and 10.0 μg/ml) after 24 h of incubation. The result showed that compared with the control, 10.0 μg/ml AgNPs synthesized by *C. indica* L., *C. bipinnata* Cav., and *L. camara* L. led to a significant reduction in the halo diameter by 67.08, 73.91, and 86.65%, respectively (**Figure 6A**). Although the AgNPs at 2.5 and 5.0 μg/ml inhibited the bacterial movement

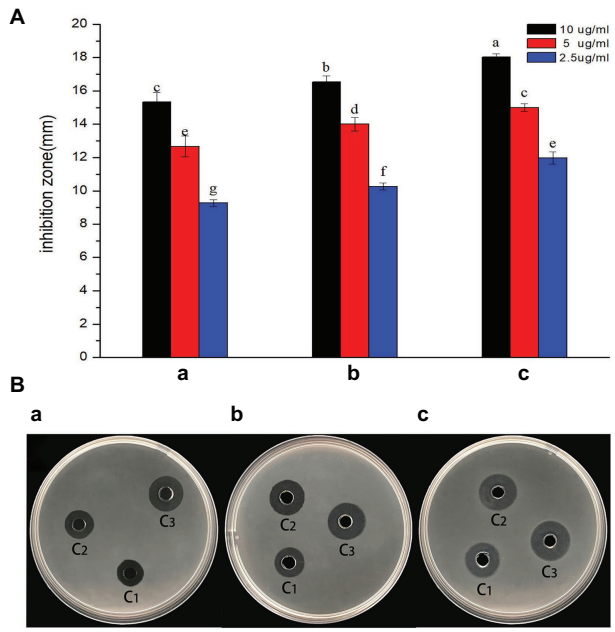

FIGURE 3 | *In vitro* inhibitory effect of AgNPs synthesized by flower extract against *R. solanacearum* strain YY06. **(a)** Diameter of bacterial growth inhibition (mm) caused by AgNPs; **(b)** bacterial growth inhibition zone caused by AgNPs, which were synthesized by (A) *C. indica* L. flower; (B) *C. bipinnata* Cav. flower; and (C) *L. camara* L. flower; C1 = 2.5 μg/ml, C2 = 5 μg/ml, and C3 = 10 μg/ml. Vertical bars represent standard errors of the means (n = 3). Bars followed by the same letter(s) are not significantly different in least significant difference (LSD) test ($p \leq 0.05$).

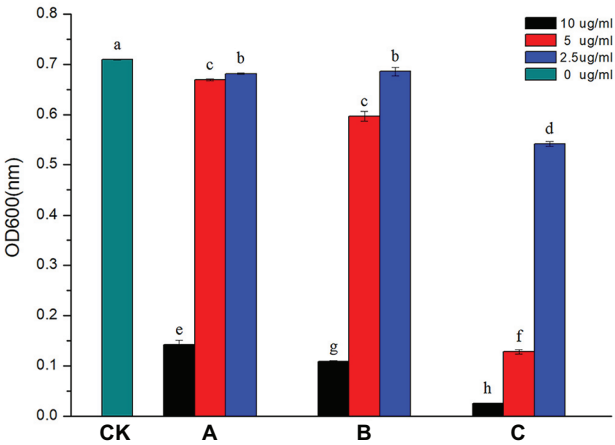

FIGURE 4 | Effect of AgNPs on the growth of *R. solanacearum* strain YY06. AgNPs mediated by (A) *C. indica* L. flower; (B) *C. bipinnata* Cav. flower; and (C) *L. camara* L. flower. Vertical bars represent standard errors of the means (n = 3). Bars followed by the same letter(s) are not significantly different in LSD test ($p \leq 0.05$).

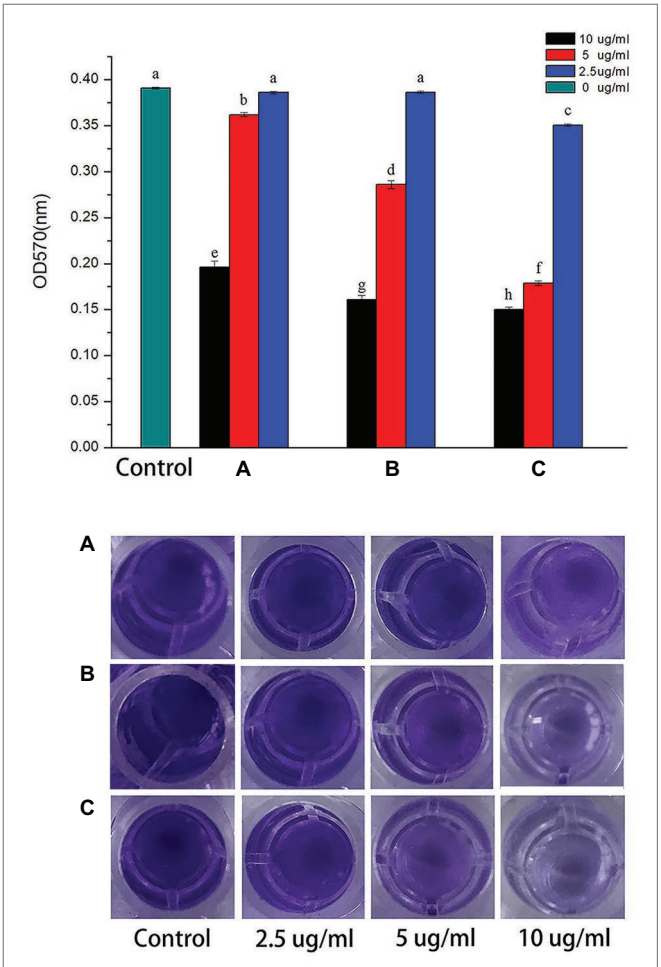

FIGURE 5 | Effect of AgNPs on biofilm formation of *R. solanacearum* strain YY06. AgNPs synthesized by **(A)** *C. indica* L. flower; **(B)** *C. bipinnata* Cav. flower; and **(C)** *L. camara* L. flower. Vertical bars represent standard errors of the means (n = 3). Bars followed by the same letter(s) are not significantly different in LSD test ($p \leq 0.05$).

somewhat but statistically less than the swimming inhibition for AgNPs at 10 μg/ml.

When the cell membranes ruptured, DNA and RNA were released out of the cell, which could be documented at an optical density of 260 nm (Chen et al., 2013). The value of nucleic acid efflux of *R. solanacearum* strain YY06 after inoculated AgNPs for 12 h at 30°C was shown in **Figure 6B**. Compared to the OD260 value of control treatment of 0.05, AgNPs mediated by *C. indica* L., *C. bipinnata* Cav., and *L. camara* L. at 10.0 μg/ml had an OD260 value of 0.28, 0.31, and 0.32 nm, respectively, which indicated that the cell membrane was seriously damaged.

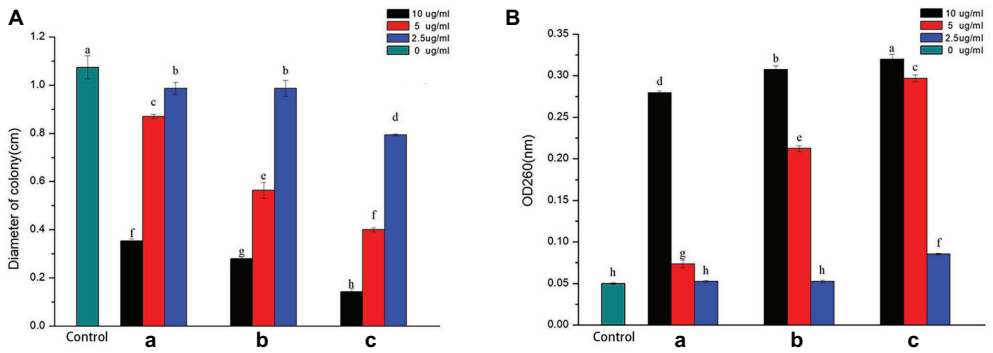

FIGURE 6 | (a) Effect of AgNPs on the swimming motility of *R. solanacearum* strain YY06. **(b)** Effect of AgNPs on the efflux of cytoplasmic materials of *R. solanacearum* strain YY06. AgNPs synthesized by (A) *C. indica* L. flower; (B) *C. bipinnata* Cav. flower; and (C) *L. camara* L. flower. Vertical bars represent standard errors of the means (n = 3). Bars followed by the same letter(s) are not significantly different in LSD test ($p \leq 0.05$).

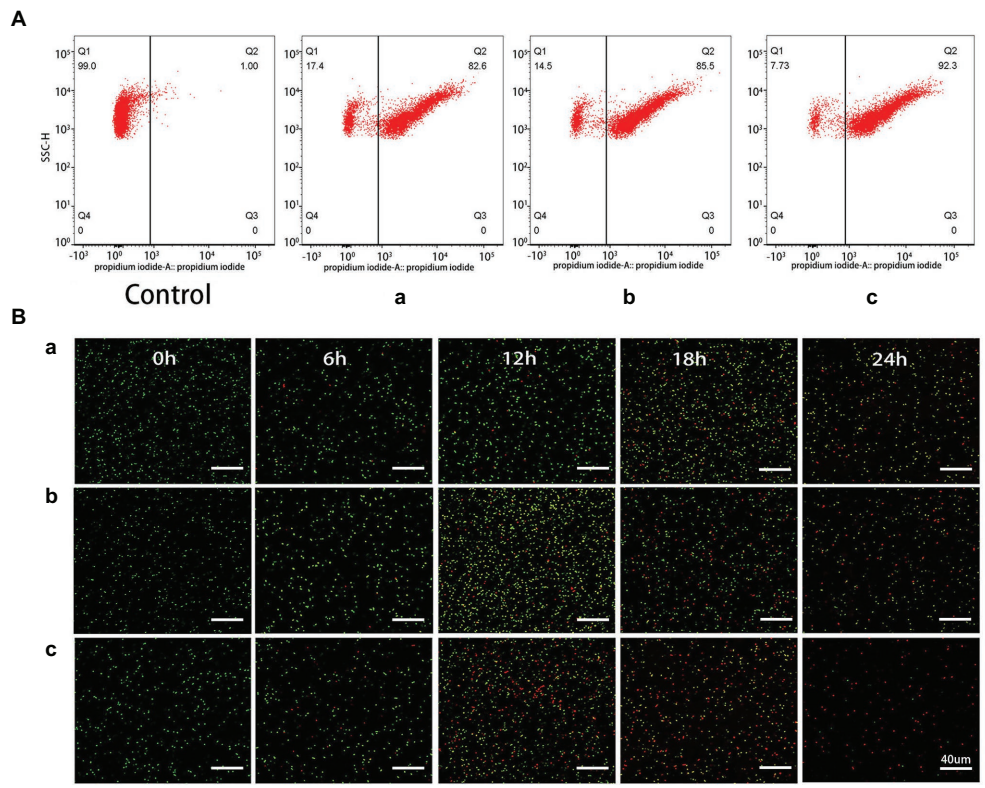

FIGURE 7 | (a) Flow cytometry images of *R. solanacearum* strain YY06 cells after 36 h incubation without (CK) and with AgNPs synthesized by (A) *C. indica* L. flower; (B) *C. bipinnata* Cav. flower; and (C) *L. camara* L. flower. **(b)** Confocal fluorescence microscopic images of *R. solanacearum* strain YY06 cells at different times (0, 6, 12, 18, and 24 h) treated with AgNPs synthesized by (A) *C. indica* L. flower; (B) *C. bipinnata* Cav. flower; and (C) *L. camara* L. flower. Cells with green fluorescence represent live bacteria, whereas red cells are representative of dead bacteria, scale bar = 40 μm.

Bacterial Death Measurement

After a short period of staining with the live/dead viability kit, dead or dying cells with damaged membranes could be stained red, while alive cells with intact membranes could be stained green. **Figure 7B** showed the fluorescence pictures of bacterial cells when exposed to AgNPs (10.0 μg/ml) for 0, 6, 12, 18, and 24 h. At the beginning of adding AgNPs, almost all of the cells remained alive which can be deduced from the green fluorescence. As the incubation time increased, the images showed increasing red fluorescence. The AgNPs (10.0 μg/ml) synthesized *L. camara* L. resulted in the largest decrease in the number of living bacteria and total bacteria at 24 h compared with AgNPs synthesized by *C. indica* L. and *C. bipinnata* Cav.

Flow cytometry test was conducted for the rapid detection of the living and dead cells (Berney et al., 2007). Here, the bacterial death caused by AgNPs was examined based on the flow cytometric analysis in combination with PI. As shown in **Figure 7A**, the death rate of *R. solanacearum* strain YY06 increased by 82.5, 85.5, and 92.3% in comparison with the control (1%) after treated for 36 h with 10 μg/ml AgNPs synthesized by *C. indica* L., *C. bipinnata* Cav., and *L. camara* L., respectively. The result showed that the AgNPs improved the permeability of the *R. solanacearum* strain YY06 cell membrane resulting in injury and ultimately cell death, which was also observed in the live/dead cell staining test.

The Mechanism of Silver Nanoparticles Against *R. solanacearum*

TEM can be applied to explore the ultrastructural changes of cell, and SEM is usually used to observe surface of the external cell (Sun et al., 2017). In this study, the images of SEM and TEM revealed the changes of *R. solanacearum* strain YY06 cells after incubating in the nutrient broth with 10 μg/ml AgNPs mediated by *L. camara* L. The integrity of cells grown without AgNPs remained intact with dense cytoplasm filled in the bacteria (**Figure 8A**). In contrast, the bacterial cells exposed to the AgNPs were severely disrupted and twisted while cytoplasm was shrunk (**Figure 8B**). In addition, we hypothesized that AgNPs powders adhered to the walls of the bacterial cells and obtained the expected results. According to EDS analysis (**Figures 8C,D**), there was a peak of the Ag element on the surface of the bacteria exposed to AgNPs, whereas the control cell remained without any Ag element (data not shown).

As far as we know, *R. solanacearum* is a kind of negatively charged Gram-negative bacteria that has an electrostatic attraction to positively charged nanoparticles (Leung et al., 2014). Furthermore, compared to chemically synthesized nanoparticles, green nanoparticles can adhere to the membrane of bacteria more fastly and firmly (Sudhasree et al., 2014; Happy et al., 2018).

ROS such as superoxide (O_2^-), hydroxyl (OH), peroxy (RCOO), and hydrogen peroxide (H_2O_2; Gülçin et al., 2011) can destroy cell structures including lipid peroxidation, DNA oxidative damage, protein denaturation, and enzyme inactivation (Birben et al., 2012), leading to bacterial decomposition and death (Mendis et al., 2005; Madl et al., 2014). The fluorescence intensity of *R. solanacearum* strain YY06 increased significantly after treated with 10 μg/ml AgNPs for 12 h in comparison with control (without AgNPs) in **Figures 8E–H**. Cells exposed to AgNPs synthesized by *L. camara* L. flower had higher intensity of fluorescence significantly more than AgNPs synthesized by *C. indica* L. and *C. bipinnata* Cav. flowers.

Most bacteria are divided into Gram-positive and Gram-negative on the basis of the cell wall structure. Gram-positive

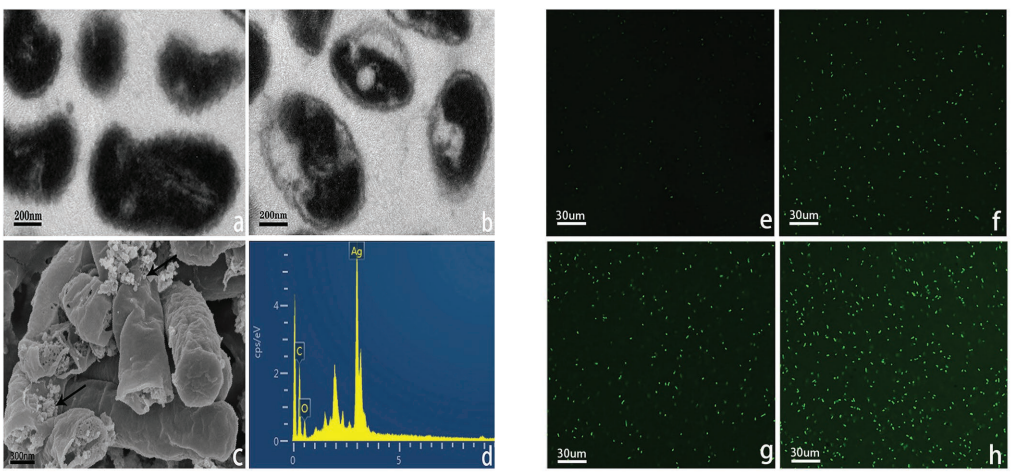

FIGURE 8 | Transmission electron microscope (TEM) images of *R. solanacearum* strain YY06 treated without **(a)** and **(b)** 10 μg/ml of AgNPs synthesized by *L. camara* L. flower, scale bar = 200 nm. Scanning electron microscopy (SEM) images of *R. solanacearum* strain YY06 **(c)** treated with 10 μg/ml AgNPs synthesized by *L. camara* L. flower, arrows point to AgNPs; with **(d)** energy dispersive X-ray spectroscopic (EDS) analysis of particles on the surface of the cells, scale bar = 300 nm. Formation of reactive oxygen species (ROS) in *R. solanacearum* strain YY06 cells after a 12 h incubation period without **(e)** and with 10.0 μg/ml AgNPs synthesized by **(f)** *C. indica* L. flower; **(g)** *C. bipinnata* Cav. flower; and **(h)** *L. camara* L. flower, scale bar = 30 μm.

bacteria contain a thick peptidoglycan layer of the cell wall, while the peptidoglycan layer of Gram-negative bacteria wall is thin. Many studies have found that Gram-positive bacteria are more resistant to nanoparticle than Gram-negative bacteria (Velmurugan et al., 2017). The thick peptidoglycan layer of Gram-positive bacteria may act as a protective function when exposing to nanoparticles. Another reason is that the negatively charged Gram-negative bacteria have a higher affinity for the positive ions released by nanoparticles, resulting in accumulation and absorption of ions, which cause intracellular damage (Feng et al., 2000; Kim et al., 2012; Mukha et al., 2013; Cavassin et al., 2015; Dorobantu et al., 2015).

Secondary metabolites such as alkaloids, carbohydrates, proteins, flavonoids, terpenoids, steroids, saponins, and tannins from plants acted as capping and stabilizing agents responsible for the synthesis of AgNPs and control of the particle size (Duan et al., 2015). However, due to complex structure and variety of functional molecules, what reason causes the different sizes of AgNPs mediated by three plants requires further research. AgNPs as an antibacterial agent can prevent the growth of plant pathogens but at the same time may kill beneficial microorganisms. In recent years, the impact of AgNPs on environmental safety and human health have led to public concerns (Lansdown, 2006). Current reports on AgNPs are mainly *in vitro* studies, and *in vivo* studies are still not sufficiently documented due to lack of safe environmental protocol. In our research, AgNPs showed low cytotoxicity to mammalian cells (**Supplementary Figure S5**). In previous studies, Mirzajani et al. (2013) revealed that AgNPs could not penetrate the root cells of rice when the concentration of AgNP was less than 30 μg/ml, while AgNPs above 30 μg/ml can damage the cell membrane and produce side effect that had an impact on root growth. Therefore, more in-depth research will be needed in the interaction of the plant-microbe-nano system to grasp clear agricultural consequences of AgNPs.

CONCLUSION

In this work, AgNPs were successfully phytofabricated using extracts of Canna lily flower (*C. indica* L.), Cosmos flower (*C. bipinnata* Cav.), and Lantana flower (*L. camara* L.). The biosynthesized AgNPs were confirmed and characterized by UV-visible spectroscopy, FTIR, XRD, and electron microscopy (TEM and SEM). The results of antagonistic experiments showed that AgNPs synthesized by *L. camara* L. flower had the highest impact on the bacterial growth, biofilm formation, swimming motility, efflux of nucleic acid, cell death, cell membrane damage, and ROS generation of *R. solanacearum*, which were ascribed to the particle size of 24.5 nm smaller than other AgNPs. Therefore, our study concluded that the particle size of AgNPs played a very important role in their antibacterial activities. To sum up, the biosynthesized AgNPs can be used as an efficient and environmentally friendly antibacterial agent to reasonably inhibit *R. solanacearum*.

DATA AVAILABILITY STATEMENT

The raw data supporting the conclusions of this article will be made available by the authors, without undue reservation.

AUTHOR CONTRIBUTIONS

H-JC and J-ZZ designed the experiment. H-JC and HW carried out the experiment. H-JC wrote the manuscript. J-ZZ improved the manuscript. All authors contributed to the article and approved the submitted version.

FUNDING

The research was funded by the Key Science and Technology Project of Zhejiang Province (no. 2015C02023).

SUPPLEMENTARY MATERIAL

The Supplementary Material for this article can be found online at: https://www.frontiersin.org/article/10.3389/fmicb.2020.02110/full#supplementary-material

REFERENCES

Abdallah, Y., Ogunyemi, S. O., Abdelazez, A., Zhang, M., Hong, X., Ibrahim, E., et al. (2019). The green synthesis of MgO nano-flowers using *Rosmarinus officinalis* L. (rosemary) and the antibacterial activities against *Xanthomonas oryzae* pv. oryzae. *Biomed. Res. Int.* 2019:5620989. doi: 10.1155/2019/5620989

Ahmed, S., Ahmad, M., Swami, B. L., and Ikram, S. (2016). A review on plants extract mediated synthesis of silver nanoparticles for antimicrobial applications: a green expertise. *J. Adv. Res.* 7, 17–28. doi: 10.1016/j.jare.2015.02.007

Amooaghaie, R., Saeri, M. R., and Azizi, M. (2015). Synthesis, characterization and biocompatibility of silver nanoparticles synthesized from *Nigella sativa* leaf extract in comparison with chemical silver nanoparticles. *Ecotoxicol. Environ. Saf.* 120, 400–408. doi: 10.1016/j.ecoenv.2015.06.025

Applerot, G., Lellouche, J., Lipovsky, A., Nitzan, Y., Lubart, R., Gedanken, A., et al. (2012). Understanding the antibacterial mechanism of CuO nanoparticles: revealing the route of induced oxidative stress. *Small* 8, 3326–3337. doi: 10.1002/smll.201200772

Asanithi, P., Chaiyakun, S., and Limsuwan, P. (2012). Growth of silver nanoparticles by DC magnetron sputtering. *J. Nanomater.* 2012:79. doi: 10.1155/2012/963609

Aziz, N., Faraz, M., Sherwani, M., Fatma, T., and Prasad, R. (2019). Illuminating the anticancerous efficacy of a new fungal chassis for silver nanoparticle synthesis. *Front. Chem.* 7:65. doi: 10.3389/fchem.2019.00065

Berney, M., Hammes, F., Bosshard, F., Weilenmann, H. U., and Egli, T. (2007). Assessment and interpretation of bacterial viability by using the LIVE/DEAD BacLight Kit in combination with flow cytometry. *Appl. Environ. Microbiol.* 73, 3283–3290. doi: 10.1128/AEM.02750-06

Birben, E., Sahiner, U. M., Sackesen, C., Erzurum, S., and Kalayci, O. (2012). Oxidative stress and antioxidant defense. *World Allergy Organ.* 5, 9–19. doi: 10.1097/WOX.0b013e3182439613

Cai, L., Chen, J., Liu, Z., Wang, H., Yang, H., and Ding, W. (2018). Magnesium oxide nanoparticles: effective agricultural antibacterial agent against *Ralstonia solanacearum*. *Front. Microbiol.* 9:790. doi: 10.3389/fmicb.2018.00790

Castro-Longoria, E., Vilchis-Nestor, A. R., and Avalos-Borja, M. (2011). Biosynthesis of silver, gold and bimetallic nanoparticles using the filamentous fungus *Neurospora crassa*. *Colloids Surf. B Biointerfaces* 83, 42–48. doi: 10.1016/j.colsurfb.2010.10.035

Cavassin, E. D., Figueiredo, L. F. P. D., Otoch, J. P., Seckler, M. M., Oliveira, R. A. D., Franco, F. F., et al. (2015). Comparison of methods to detect the in vitro activity of silver nanoparticles (AgNPs) against multidrug resistant bacteria. *J. Nanobiotechnol.* 13:64. doi: 10.1186/S12951-015-0120-6

Chen, J., Wang, X., and Han, H. (2013). A new function of graphene oxide emerges: inactivating phytopathogenic bacterium *Xanthomonas oryzae* pv. Oryzae. *J. Nanopart. Res.* 15:1658. doi: 10.1007/S11051-013-1658-6

Cui, Z., Ibrahim, M., Yang, C., Fang, Y., Annam, H., Li, B., et al. (2014). Susceptibility of opportunistic *Burkholderia glumae* to copper surfaces following wet or dry surface contact. *Molecules* 19, 9975–9985. doi: 10.3390/molecules19079975

Dang, H. Y., and Lovell, C. R. (2016). Microbial surface colonization and biofilm development in marine environments. *Microbiol. Mol. Biol. Rev.* 80, 91–138. doi: 10.1128/mmbr.00037-15

Dipankar, C., and Murugan, S. (2012). The green synthesis, characterization and evaluation of the biological activities of silver nanoparticles synthesized from *Iresine herbstii* leaf aqueous extracts. *Colloids Surf. B Biointerfaces* 98, 112–119. doi: 10.1016/j.colsurfb.2012.04.006

Dorobantu, L. S., Fallone, C., Noble, A. J., Veinot, J., Ma, G., Goss, G. G., et al. (2015). Toxicity of silver nanoparticles against bacteria, yeast, and algae. *J. Nanopart. Res.* 17:172. doi: 10.1007/S11051-015-2984-7

Duan, H., Wang, D., and Li, Y. (2015). Green chemistry for nanoparticle synthesis. *Chem. Soc. Rev.* 44, 5778–5792. doi: 10.1039/C4CS00363B

Duke, J. A., and Ayensu, E. S. (1984). *Medicinal plants of China*. Algonac: Reference Publications.

El-Nour, K. M. M. A., Eftaiha, A. A., Al-Warthan, A., and Ammar, R. A. A. (2010). Synthesis and applications of silver nanoparticles. *Arab. J. Chem.* 3, 135–140. doi: 10.1016/j.arabjc.2010.04.008

Feng, Q. L., Wu, J., Chen, G. Q., Cui, F. Z., Kim, T. N., and Kim, J. O. (2000). A mechanistic study of the antibacterial effect of silver ions on *Escherichia coli* and *Staphylococcus aureus*. *J. Biomed. Mater. Res.* 52, 662–668. doi: 10.1002/1097-4636(20001215)52:4<662::AID-JBM10>3.0.CO;2-3

Ghisalberti, E. (2000). *Lantana camara* L. (Verbenaceae). *Fitoterapia* 71, 467–486. doi: 10.1016/S0367-326X(00)00202-1

Gogoi, N., Babu, P. J., Mahanta, C., and Bora, U. (2015). Green synthesis and characterization of silver nanoparticles using alcoholic flower extract of *Nyctanthes arbortristis* and in vitro investigation of their antibacterial and cytotoxic activities. *Mater. Sci. Eng. C Mater. Biol. Appl.* 46, 463–469. doi: 10.1016/j.msec.2014.10.069

Gülçin, İ., Topal, F., Çakmakçı, R., Bilsel, M., Gören, A. C., and Erdogan, U. (2011). Pomological features, nutritional quality, polyphenol content analysis, and antioxidant properties of domesticated and 3 wild ecotype forms of raspberries (*Rubus idaeus* L.). *J. Food Sci.* 76, C585–C593. doi: 10.1111/j.1750-3841.2011.02142.x

Happy, A., Soumya, M., Venkat Kumar, S., and Rajeshkumar, S. (2018). Mechanistic study on antibacterial action of zinc oxide nanoparticles synthesized using green route. *Chem. Biol. Interact.* 286, 60–70. doi: 10.1016/j.cbi.2018.03.008

Hayward, A. C. (1964). Characteristics of *Pseudomonas solanacearum*. *J. Appl. Microbiol.* 27, 265–277. doi: 10.1111/J.1365-2672.1964.TB04912.X

Husen, A., and Siddiqi, K. S. (2014a). Phytosynthesis of nanoparticles: concept, controversy and application. *Nanoscale Res. Lett.* 9:229. doi: 10.1186/1556-276X-9-229

Husen, A., and Siddiqi, K. S. (2014b). Plants and microbes assisted selenium nanoparticles: characterization and application. *J. Nanobiotechnol.* 12:28. doi: 10.1186/S12951-014-0028-6

Hyllested, J. Æ., Palanco, M. E., Hagen, N., Mogensen, K. B., and Kneipp, K. (2015). Green preparation and spectroscopic characterization of plasmonic silver nanoparticles using fruits as reducing agents. *Beilstein J. Nanotechnol.* 6, 293–299. doi: 10.3762/BJNANO.6.27

Ibrahim, E., Fouad, H., Zhang, M., Zhang, Y., Qiu, W., Yan, C., et al. (2019). Biosynthesis of silver nanoparticles using endophytic bacteria and their role in inhibition of rice pathogenic bacteria and plant growth promotion. *RSC Adv.* 9, 29293–29299. doi: 10.1039/C9RA04246F

Jo, Y. -H., Seo, G. -U., Yuk, H. -G., and Lee, S. -C. (2012). Antioxidant and tyrosinase inhibitory activities of methanol extracts from *Magnolia denudata* and *Magnolia denudata* var. purpurascens flowers. *Food Res. Int.* 47, 197–200. doi: 10.1016/j.foodres.2011.05.032

Kim, T. -H., Kim, M., Park, H. -S., Shin, U. S., Gong, M. -S., and Kim, H. -W. (2012). Size-dependent cellular toxicity of silver nanoparticles. *J. Biomed. Mater. Res. A* 100, 1033–1043. doi: 10.1002/jbm.a.34053

Kim, J. S., Kuk, E., Yu, K. N., Kim, J. -H., Park, S. J., Lee, H. J., et al. (2007). Antimicrobial effects of silver nanoparticles. *Nanomed. Nanotechnol. Biol. Med.* 3, 95–101. doi: 10.1016/j.nano.2006.12.001

Klausen, M., Heydorn, A., Ragas, P. C., Lambertsen, L. M., Aaes-Jorgensen, A., Molin, S., et al. (2003). Biofilm formation by *Pseudomonas aeruginosa* wild type, flagella and type IV pili mutants. *Mol. Microbiol.* 48, 1511–1524. doi: 10.1046/j.1365-2958.2003.03525.x

Kumar, B., Kumari, S., Cumbal, L., and Debut, A. (2015). *Lantana camara* berry for the synthesis of silver nanoparticles. *Asian Pac. J. Trop. Biomed.* 5, 192–195. doi: 10.1016/S2221-1691(15)30005-8

Kumar, A., Pandey, A. K., Singh, S. S., Shanker, R., and Dhawan, A. (2011). A flow cytometric method to assess nanoparticle uptake in bacteria. *Cytometry A* 79, 707–712. doi: 10.1002/cyto.a.21085

Lansdown, A. B. G. (2006). Silver in health care: antimicrobial effects and safety in use. *Curr. Probl. Dermatol.* 33, 17–34. doi: 10.1159/000093928

Leung, Y., Ng, A. M. C., Xu, X., Shen, Z., Gethings, L., Wong, M. T., et al. (2014). Mechanisms of antibacterial activity of MgO: non-ROS mediated toxicity of MgO nanoparticles towards *Escherichia coli*. *Small* 10, 1171–1183. doi: 10.1002/smll.201302434

Levy, S. B. (2001). Antibiotic resistance: consequences of inaction. *Clin. Infect. Dis.* 33, S124–S129. doi: 10.1086/321837

Ma, R., Levard, C., Marinakos, S. M., Cheng, Y. W., Liu, J., Michel, F. M., et al. (2012). Size-controlled dissolution of organic-coated silver nanoparticles. *Environ. Sci. Technol.* 46, 752–759. doi: 10.1021/es201686j

Madl, A. K., Plummer, L. E., Carosino, C., and Pinkerton, K. E. (2014). Nanoparticles, lung injury, and the role of oxidant stress. *Annu. Rev. Physiol.* 76, 447–465. doi: 10.1146/annurev-physiol-030212-183735

Mendis, E., Rajapakse, N., Byun, H. -G., and Kim, S. -K. (2005). Investigation of jumbo squid (*Dosidicus gigas*) skin gelatin peptides for their in vitro antioxidant effects. *Life Sci.* 77, 2166–2178. doi: 10.1016/j.lfs.2005.03.016

Mirzajani, F., Askari, H., Hamzelou, S., Farzaneh, M., and Ghassempour, A. (2013). Effect of silver nanoparticles on *Oryza sativa* L. and its rhizosphere bacteria. *Ecotoxicol. Environ. Saf.* 88, 48–54. doi: 10.1016/j.ecoenv.2012.10.018

Mohanta, Y. K., Panda, S. K., Bastia, A. K., and Mohanta, T. K. (2017). Biosynthesis of silver nanoparticles from *Protium serratum* and investigation of their potential impacts on food safety and control. *Front. Microbiol.* 8:626. doi: 10.3389/fmicb.2017.00626

Moteriya, P., and Chanda, S. (2017). Synthesis and characterization of silver nanoparticles using *Caesalpinia pulcherrima* flower extract and assessment of their in vitro antimicrobial, antioxidant, cytotoxic, and genotoxic activities. *Artif. Cells Nanomed. Biotechnol.* 45, 1556–1567. doi: 10.1080/21691401.2016.1261871

Mukha, I. P., Eremenko, A. M., Smirnova, N. P., Mikhienkova, A. I., Korchak, G. I., Gorchev, V. F., et al. (2013). Antimicrobial activity of stable silver nanoparticles of a certain size. *Appl. Biochem. Microbiol.* 49, 199–206. doi: 10.1134/S0003683813020117

Nayak, D., Ashe, S., Rauta, P. R., Kumari, M., and Nayak, B. (2016). Bark extract mediated green synthesis of silver nanoparticles: evaluation of antimicrobial activity and antiproliferative response against osteosarcoma. *Mater. Sci. Eng. C Mater. Biol. Appl.* 58, 44–52. doi: 10.1016/j.msec.2015.08.022

Olajuyigbe, O., and Ashafa, A. (2014). Chemical composition and antibacterial activity of essential oil of *Cosmos bipinnatus* Cav. leaves from South Africa. *Iran. J. Pharm. Res.* 13, 1417–1423.

Oves, M., Aslam, M., Rauf, M. A., Qayyum, S., Qari, H. A., Khan, M. S., et al. (2018). Antimicrobial and anticancer activities of silver nanoparticles synthesized from the root hair extract of *Phoenix dactylifera*. *Mater. Sci. Eng. C Mater. Biol. Appl.* 89, 429–443. doi: 10.1016/j.msec.2018.03.035

Oves, M., Khan, M. S., Zaidi, A., Ahmed, A. S., Ahmed, F., Ahmad, E., et al. (2013). Antibacterial and cytotoxic efficacy of extracellular silver nanoparticles biofabricated from chromium reducing novel OS4 strain of *Stenotrophomonas maltophilia*. *PLoS One* 8:e59140. doi: 10.1371/journal.pone.0059140

Prasad, A., Pospisil, P., and Tada, M. (2019). Editorial: reactive oxygen species (ROS) detection methods in biological system. *Front. Physiol.* 10:1316. doi: 10.3389/fphys.2019.01316

Rasheed, T., Bilal, M., Iqbal, H. M. N., and Li, C. L. (2017). Green biosynthesis of silver nanoparticles using leaves extract of *Artemisia vulgaris* and their potential biomedical applications. *Colloids Surf. B Biointerfaces* 158, 408–415. doi: 10.1016/j.colsurfb.2017.07.020

Roldán, M. V., Pellegri, N., and Sanctis, O. D. (2013). Electrochemical method for Ag-PEG nanoparticles synthesis. *J. Nanopart. Res.* 2013, 1–7. doi: 10.1155/2013/524150

Sadeghi, B., Rostami, A., and Momeni, S. S. (2015). Facile green synthesis of silver nanoparticles using seed aqueous extract of *Pistacia atlantica* and its antibacterial activity. *Spectrochim. Acta A* 134, 326–332. doi: 10.1016/J.SAA.2014.05.078

Saleem, M., Ali, H. A., Akhtar, M. F., Saleem, U., Saleem, A., and Irshad, I. (2019). Chemical characterisation and hepatoprotective potential of *Cosmos sulphureus* Cav. and *Cosmos bipinnatus* Cav. *Nat. Prod. Res.* 33, 897–900. doi: 10.1080/14786419.2017.1413557

Schell, M. A. (2000). Control of virulence and pathogenicity genes of *Ralstonia Solanacearum* by an elaborate sensory network. *Annu. Rev. Phytopathol.* 38, 263–292. doi: 10.1146/annurev.phyto.38.1.263

Siddiqi, K. S., and Husen, A. (2016). Fabrication of metal nanoparticles from fungi and metal salts: scope and application. *Nanoscale Res. Lett.* 11:98. doi: 10.1186/S11671-016-1311-2

Singh, P., Kim, Y. J., Singh, H., Wang, C., Hwang, K. H., Farh, M. E. -A., et al. (2015a). Biosynthesis, characterization, and antimicrobial applications of silver nanoparticles. *Int. J. Nanomedicine* 10, 2567–2577. doi: 10.2147/IJN.S72313

Singh, P., Kim, Y. J., Wang, C., Mathiyalagan, R., Farh, M. E. -A., and Yang, D. C. (2015b). Biogenic silver and gold nanoparticles synthesized using red ginseng root extract, and their applications. *Artif. Cells Nanomed. Biotechnol.* 44, 811–816. doi: 10.3109/21691401.2015.1008514

Sotiriou, G. A., and Pratsinis, S. E. (2010). Antibacterial activity of nanosilver ions and particles. *Environ. Sci. Technol.* 44, 5649–5654. doi: 10.1021/es101072s

Sotiriou, G. A., Teleki, A., Camenzind, A., Krumeich, F., Meyer, A., Panke, S., et al. (2011). Nanosilver on nanostructured silica: antibacterial activity and Ag surface area. *Chem. Eng. J.* 170, 547–554. doi: 10.1016/j.cej.2011.01.099

Sudhasree, S., Banu, A. S., Brindha, P., and Kurian, G. A. (2014). Synthesis of nickel nanoparticles by chemical and green route and their comparison in respect to biological effect and toxicity. *Toxicol. Environ. Chem.* 96, 743–754. doi: 10.1080/02772248.2014.923148

Sun, D., Zhang, W., Mou, Z., Chen, Y., Guo, F., Yang, E., et al. (2017). Transcriptome analysis reveals silver nanoparticle-decorated quercetin antibacterial molecular mechanism. *ACS Appl. Mater. Interfaces* 9, 10047–10060. doi: 10.1021/acsami.7b02380

Tien, D. -C., Tseng, K. -H., Liao, C. -Y., Huang, J. -C., and Tsung, T. -T. (2008). Discovery of ionic silver in silver nanoparticle suspension fabricated by arc discharge method. *J. Alloys Compd.* 463, 408–411. doi: 10.1016/J.JALLCOM.2007.09.048

Velmurugan, P., Cho, M., Lee, S. -M., Park, J. -H., Bae, S., and Oh, B. -T. (2014). Antimicrobial fabrication of cotton fabric and leather using green-synthesized nanosilver. *Carbohydr. Polym.* 106, 319–325. doi: 10.1016/j.carbpol.2014.02.021

Velmurugan, P., Cho, M., Lim, S. -S., Seo, S. -K., Myung, H., Bang, K. -S., et al. (2015). Phytosynthesis of silver nanoparticles by *Prunus yedoensis* leaf extract and their antimicrobial activity. *Mater. Lett.* 138, 272–275. doi: 10.1016/j.matlet.2014.09.136

Velmurugan, P., Kim, J. -I., Kim, K., Park, J. -H., Lee, K. -J., Chang, W. -S., et al. (2017). Extraction of natural colorant from purple sweet potato and dyeing of fabrics with silver nanoparticles for augmented antibacterial activity against skin pathogens. *J. Photochem. Photobiol. B* 173, 571–579. doi: 10.1016/J.JPHOTOBIOL.2017.07.001

Wang, L., Hu, C., and Shao, L. (2017). The antimicrobial activity of nanoparticles: present situation and prospects for the future. *Int. J. Nanomedicine* 12, 1227–1249. doi: 10.2147/ijn.S121956

Wang, H. Y., Li, Y. F., and Huang, C. Z. (2007). Detection of ferulic acid based on the plasmon resonance light scattering of silver nanoparticles. *Talanta* 72, 1698–1703. doi: 10.1016/j.talanta.2007.02.028

Zhang, Q., Li, N., Goebl, J., Lu, Z., and Yin, Y. (2011). A systematic study of the synthesis of silver nanoplates: is citrate a "magic" reagent? *J. Am. Chem. Soc.* 133, 18931–18939. doi: 10.1021/ja2080345

Conflict of Interest: The authors declare that the research was conducted in the absence of any commercial or financial relationships that could be construed as a potential conflict of interest.

frontiers in Microbiology

ORIGINAL RESEARCH
published: 30 September 2020
doi: 10.3389/fmicb.2020.565548

Quorum Sensing as a Target for Controlling Surface Associated Motility and Biofilm Formation in *Acinetobacter baumannii* ATCC® 17978™

Celia Mayer[1,2†], Andrea Muras[1†], Ana Parga[1], Manuel Romero[2], Soraya Rumbo-Feal[3], Margarita Poza[3], José Ramos-Vivas[4] and Ana Otero[1]*

[1] Departamento de Microbioloxía e Parasitoloxía, Facultade de Bioloxía, Edificio CIBUS, Universidade de Santiago de Compostela, Santiago de Compostela, Spain, [2] National Biofilms Innovation Centre, Biodiscovery Institute and School of Life Sciences, University of Nottingham, Nottingham, United Kingdom, [3] Microbioloxía, Instituto de Investigación Biomédica da Coruña, Centro de Investigacións Científicas Avanzadas da Coruña, Universidade da Coruña, A Coruña, Spain, [4] Servicio de Microbiología, Hospital Universitario Marqués de Valdecilla–Instituto de Investigación Valdecilla, Santander, Spain

OPEN ACCESS

Edited by:
Mariano Martinez-Vazquez, National Autonomous University of Mexico, Mexico

Reviewed by:
Phil Rather, Emory University, United States
Joseph Boll, University of Texas at Arlington, United States
Jintae Lee, Yeungnam University, South Korea

***Correspondence:**
Ana Otero
anamaria.otero@usc.es

† These authors have contributed equally to this work

Specialty section:
This article was submitted to Antimicrobials, Resistance and Chemotherapy, a section of the journal Frontiers in Microbiology

Received: *25 May 2020*
Accepted: *10 September 2020*
Published: *30 September 2020*

Citation:
Mayer C, Muras A, Parga A, Romero M, Rumbo-Feal S, Poza M, Ramos-Vivas J and Otero A (2020) Quorum Sensing as a Target for Controlling Surface Associated Motility and Biofilm Formation in Acinetobacter baumannii ATCC® 17978™. Front. Microbiol. 11:565548. doi: 10.3389/fmicb.2020.565548

The important nosocomial pathogen *Acinetobacter baumannii* presents a quorum sensing (QS) system (*abaI*/*abaR*) mediated by acyl-homoserine-lactones (AHLs) and several quorum quenching (QQ) enzymes. However, the roles of this complex network in the control of the expression of important virulence-related phenotypes such as surface-associated motility and biofilm formation is not clear. Therefore, the effect of the mutation of the AHL synthase AbaI, and the exogenous addition of the QQ enzyme Aii20J on surface-associated motility and biofilm formation by *A. baumannii* ATCC® 17978™ was studied in detail. The effect of the enzyme on biofilm formation by several multidrug-resistant *A. baumannii* clinical isolates differing in their motility pattern was also tested. We provide evidence that a functional QS system is required for surface-associated motility and robust biofilm formation in *A. baumannii* ATCC® 17978™. Important differences were found with the well-studied strain *A. nosocomialis* M2 regarding the relevance of the QS system depending on environmental conditions The *in vitro* biofilm-formation capacity of *A. baumannii* clinical strains was highly variable and was not related to the antibiotic resistance or surface-associated motility profiles. A high variability was also found in the sensitivity of the clinical strains to the action of the QQ enzyme, revealing important differences in virulence regulation between *A. baumannii* isolates and confirming that studies restricted to a single strain are not representative for the development of novel antimicrobial strategies. Extracellular DNA emerges as a key component of the extracellular matrix in *A. baumannii* biofilms since the combined action of the QQ enzyme Aii20J and DNase reduced biofilm formation in all tested strains. Results demonstrate that QQ strategies in combination with other enzymatic treatments such as DNase could represent an alternative approach for the prevention of *A. baumannii* colonization and survival on surfaces and the prevention and treatment of infections caused by this pathogen.

Keywords: *Acinetobacter baumannii*, quorum sensing, surface-associated motility, biofilm, quorum quenching, extracellular DNA

INTRODUCTION

The genus *Acinetobacter* comprises Gram-negative, strictly aerobic coccobacilli that are widely present in the environment but also includes a variety of species that cause opportunistic nosocomial infections like septicemia, pneumonia, endocarditis, meningitis, skin, wound, and urinary tract infections (Towner, 2009). *Acinetobacter baumannii*, the most relevant pathogenic species in the genus, has emerged as one of the most troublesome hospital-acquired pathogens because the increase in the prevalence of multidrug-resistant (MDR) strains has reduced the treatment options for this pathogen (Peleg et al., 2008; Roca et al., 2012; Lee et al., 2017; Moubareck and Halat, 2020). Therefore, a better understanding of the mechanisms controlling the expression of virulence traits and propagation in *Acinetobacter* spp. has become critical for the discovery and development of new therapeutic strategies.

In *Acinetobacter* spp. a complex network of sensors controls the expression of virulence factors integrating intra- and extracellular signals (Harding et al., 2018; Wood et al., 2018a; De Silva and Kumar, 2019). Among these, quorum sensing (QS), a mechanism of control of gene expression dependent on bacterial cell density, seems to play a central role, constituting an interesting target for the development on antimicrobial strategies. *Acinetobacter* spp. present a QS system homologous to the canonical LuxI/LuxR system of Gram-negatives that produces and sense QS signals belonging to the family of the acyl-homoserine-lactones (AHLs) that is known as AbaI/AbaR (Niu et al., 2008; Bhargava et al., 2010; Mayer et al., 2018). The system was first identified in *A. nosocomialis* M2, formerly classified as *A. baumannii* (Carruthers et al., 2013) and later found in *A. baumannii* (Smith et al., 2007; Niu et al., 2008; Mayer et al., 2018) and other species of the genus of both human or environmental origin (Kang and Park, 2010; Bitrian et al., 2012; How et al., 2015; Oh and Choi, 2015). *N*-hydroxydodecanoyl-L-homoserine lactone (OHC12-HSL) is the main QS signal produced by the clinically relevant species belonging to the *A. calcoaceticus–A. baumannii* complex, including the well-studied strains *A. nosocomialis* M2 and *A. baumannii* ATCC® 17978™, although other AHLs are also produced in smaller amounts (Niu et al., 2008; Chan et al., 2011, 2014; Clemmer et al., 2011; How et al., 2015; Mayer et al., 2018). *In vitro*, these signals are produced only in static cultures (Mayer et al., 2018), indicating a strong correlation between QS and biofilm formation and/or surface attachment. Besides producing QS signals, the capacity to enzymatically degrade these molecules, a process known as Quorum Quenching (QQ), has been described in several *Acinetobacter* spp. of environmental and clinical origin (Kang et al., 2004; Chan et al., 2011; Kim et al., 2014; Ochiai et al., 2014; Arivett et al., 2015; López et al., 2017; Mayer et al., 2018). Up to 8 putative QQ enzymes have been found in the genome of *A. baumannii* ATCC® 17978™ and, in this strain, QQ activity correlates with the disappearance of the AHLs from the culture media, indicating that AHL production may be self-regulated (Mayer et al., 2018).

QS controls many different functions in *Acinetobacter* spp., including some key virulence factors such as motility, biofilm formation and other stress responses (Gaddy and Actis, 2009; Roca et al., 2012; Eze et al., 2018; Harding et al., 2018; Mayer et al., 2020; Shin et al., 2020), although most work was done with *A. nosocomialis* M2 (Niu et al., 2008; Clemmer et al., 2011; Stacy et al., 2012; Oh and Choi, 2015). Surface-associated motility is related to virulence since it has been identified as a common trait in clinical isolates of *A. baumannii* (Eijkelkamp et al., 2011) and increased motility has been related to increased adherence and lethality in *Caenorhabditis elegans* assays (Eijkelkamp et al., 2013). Several regulatory proteins have been described as involved in the control of surface-associated motility in *Acinetobacter* spp. (Mayer et al., 2018; Moubareck and Halat, 2020). The AHL-mediated QS system seems to be central in this regulatory network since an impairment in surface motility was recorded for QS defective mutants in *A. nosocomialis*, a phenotype that could be restored by the addition of OHC12-HSL (Clemmer et al., 2011; Oh and Choi, 2015). The role of QS on motility in *A. baumannii* is less studied, but recently, important differences in motility characteristics have been reported for clinical isolates of *A. baumannii* differing in their antibiotic resistance (López et al., 2017). In *A. baumannii* ATCC® 17978™ (Mayer et al., 2018) and in some but not all the clinical strains studied (López et al., 2017), the addition of the AHL-degrading enzyme Aii20J reduced or even blocked motility completely, supporting a role of AHL-mediated QS on this phenotype in *A. baumannii*, as previously described for *A. nosocomialis*. However, the effect of the mutation of the QS genes on motility in *A. baumannii* and its correlation with biofilm formation has not been studied so far.

Acinetobacter baumannii has a strong ability to form biofilms, a capacity that has been linked to this species resistance to desiccation, nutrient starvation, and antimicrobial treatments (Gaddy and Actis, 2009). Potential virulence genes, including those involved in antibiotic resistance, seem to be overexpressed in *A. baumannii* biofilms (Marti et al., 2011; Rumbo-Feal et al., 2017) and a positive correlation was found between biofilm formation and multiple drug resistance in *A. baumannii* clinical isolates (Yang et al., 2019; Zeighami et al., 2019). The infective capacity and the development of chronic infections are related to the capacity to form biofilms (Eze et al., 2018) since genes required for biofilm formation are widespread in *A. baumannii* clinical strains but are partially or completely missing in environmental isolates (Yakkala et al., 2019). Numerous evidence correlates surface-associated motility and biofilm formation in several species and strains of the genus *Acinetobacter* (Stacy et al., 2012; Tucker et al., 2014; Giles et al., 2015; Chen et al., 2017), indirectly indicating that both traits are controlled by QS (Niu et al., 2008; Gaddy and Actis, 2009; Bhargava et al., 2010; Anbazhagan et al., 2012; Stacy et al., 2012; Chen et al., 2017; Rumbo-Feal et al., 2017). A hyper-motile variant of *A. baumannii* ATCC® 17978™ lost its motility and produced less pellicle when two genes of the QS genomic region were mutated (Giles et al., 2015). The reduction of biofilm formation by QQ lactonases has been already demonstrated in clinical isolates of *A. baumannii* (Chow et al., 2014; Zhang et al., 2017) although the effect of these enzymes on biofilm formation was low in comparison with a QS null mutant (Chow et al., 2014). The exogenous

addition of the AHL-lactonase Aii20J strongly inhibited biofilm formation in *A. baumannii* ATCC® 17978™ despite the presence of endogenous QQ activity (Mayer et al., 2018), indicating that the endogenous enzymes might be involved in the fine-tuning of the QS system and/or be active during specific periods or conditions. On the contrary, a previous study showed that the AHL-lactonase MomL showed little or no-activity activity on *A. nosocomialis* M2 and several clinical isolates and lost its antibiofilm activity when a QQ-sensitive *A. baumannii* strain was co-cultured with *Pseudomonas aeruginosa* PAO1 (Zhang et al., 2017). It should be noted that most biofilm assays are performed in microtiter plates in which the formation of biofilm by this strictly aerobic species is weak and highly variable. Therefore, to assess the potential use of QQ enzymes for the control of these important virulence traits in *A. baumannii*, it is necessary to assess the effect of the inactivation of *abaI* and the addition of QQ enzymes in conditions that drive to robust biofilm formation and to evaluate the response of different clinical isolates in comparison with *A. baumannii* ATCC® 17978™. Moreover, extracellular DNA (eDNA) is present in *A. baumannii* biofilms and a reduction of biofilm formation by DNase I has been already reported, even in preformed biofilms (Tetz et al., 2009; Sahu et al., 2012) and therefore, the impact of combining QQ strategies with eDNA digestion deserves further exploration.

The key role of QS in the control of virulence factors, including surface-associated motility and biofilm formation in different species/strains of *Acinetobacter* points to the use of QQ enzymes as a possible antimicrobial strategy in these species. Nevertheless, previous studies revealed important differences between species and strains (Vijayakumar et al., 2016; López et al., 2017; Zhang et al., 2017). Therefore, a more detailed study of the role of QS in surface-associated and biofilm formation in *A. baumannii* ATCC® 17978™ and a comparison with clinical strains is required. In order to better understand the influence of QS regulatory mechanisms on these virulence-associated traits in the reference strain *A. baumannii* ATCC® 17978™, in this work, we used a QS defective mutant and QQ strategies. Data presented here reveal that QS regulates both traits in *A. baumannii* ATCC® 17978™ and its behavior differs from *A. nosocomialis* M2. The study of biofilm formation capacity of different multidrug-resistant *A. baumannii* strains and their susceptibility to the QQ enzyme Aii20J and other biofilm-disrupting enzymes revealed a great variability among clinical isolates, indicating that studies targeting the development of novel antimicrobial strategies should be based on multiple strains of different origin and characteristics. Extracellular DNA emerges as a key component of extracellular matrix in *Acinetobacter* biofilms, since the combined action of the QQ enzyme Aii20J and a DNase reduced biofilm formation in all the tested strains.

MATERIALS AND METHODS

Bacterial Strains, Culture Conditions, and Genetic Methods

Bacterial strains and primers used in this study are listed in **Table 1**. Luria-Bertani (LB) broth and LB agar were used to grow and maintain *Acinetobacter* spp. routinely at 37°C. LB broth was prepared in our laboratory with 1% Bacto-tryptone (Life Technologies Corporation, Thermo Fisher Scientific), 0.5% yeast extract (BD Biosciences) and 1% NaCl (Panreac AppliChem).

Construction of Isogenic Deletion Derivatives

Plasmid pMo130, a suicide vector containing the genes *xylE*, *sacB* and a kanamycin resistance marker, was used as described by Hamad et al. (2009). Briefly, 900–1000 bp upstream and downstream regions flanking the genes selected for deletion in *A. baumannii* ATCC® 17978™ were PCR-amplified and cloned into the pMo130 vector using primers listed in **Table 1**. The resulting plasmid (pMo130-0109) and (pMo130-1750) were transformed into ATCC® 17978™ cells by electroporation (Rumbo-Feal et al., 2013). Recombinant colonies representing the first crossover event were selected by resistance to kanamycin and visual detection of XylE activity following the catechol-based method (Hamad et al., 2009). Bright yellow kanamycin-resistant colonies were then grown overnight in LB supplemented with 15% sucrose and then plated on LB agar without antibiotics. Second crossover event leading to gene deletion was then confirmed by PCR using primers listed in **Table 1**. The Δ*0109* isogenic deletion and derivative of ATCC® 17978™ was constructed by deleting a region encompassing the *A1S_0109* gene, without affecting the upstream and downstream surrounding genes as described previously (Hamad et al., 2009).

Motility Assays

Surface-associated motility assays were performed as described by Mayer et al. (2018). Petri dishes were prepared with LB or low-nutrients low-salt LB (0.5% NaCl, 0.2% tryptone, and 0.1% yeast extract; LNLS-LB) media supplemented with 0.25% Difco (Bacto™ Agar) or Eiken agar (Eiken Chemical, Co. Ltd., Japan). Plates with a reduced concentration of NaCl (0.5%), tryptone (0.2%), or yeast extract (0.1%) or media with different concentrations of NaCl (0.1–0.4M) or sucrose (5–20%) were also prepared to determinate the impact of culture media or osmolarity effect on motility, respectively. *N*-Hydroxydodecanoyl-L-homoserine lactone (OHC12-HSL from Sigma, 10 μM), or the AHL-lactonase Aii20J (20 μg/mL) obtained from the marine bacterium *Tenacibaculum* sp. 20J (Mayer et al., 2015) were mixed with the inoculum or with the culture media. One microliter from agitated overnight cultures at 0.3 optical density (OD_{600} nm) was inoculated in the center of the plates. Plates were incubated at 37°C in the dark, and surface-associated motility was inspected after 14 h. Three plates were prepared for each condition, and experiments were repeated at least twice.

Assessment of Biofilm Formation by *Acinetobacter* spp.

Biofilms were grown in a modification of the *Amsterdam Active Attachment model* (AAA-model) (Exterkate et al., 2010; Muras et al., 2020) assembled with glass coverslips (18 mm × 18 mm). In

TABLE 1 | Bacterial strains, and primers used in this study.

Strains	Description	Source or reference
Acinetobacter baumannii		
ATCC® 17978™		ATCC[a]
Δ*abaI* (ATCC® 17978™)	Δ*0109 knock out* (KO) mutant without synthase AHLs gene *abaI* (*A1S_0109*)	This study
Ab1 (ROC013)	*A. baumannii* clinical isolate (respiratory). TM: ST2	López et al., 2017
Ab4 (VAL001)	*A. baumannii* clinical isolate (respiratory). TM: ST169	López et al., 2017
Ab5 (DOM009)	*A. baumannii* clinical isolate (respiratory). TM: ST80	López et al., 2017
Ab7 (HUI001)	*A. baumannii* clinical isolate (respiratory). TM: ST79	López et al., 2017
MAR002	*A. baumannii* biofilm hyper-producing clinical isolate (wound sample) TM: ST271	Álvarez-Fraga et al., 2016
Δ*11085*	MAR002 mutant defective in biofilm formation and cell attachment	Álvarez-Fraga et al., 2016
Acinetobacter nosocomialis		
M2		Niu et al., 2008
abaI:Km (M2)	*abaI* mutant *(abaI:Km),* Km^r	Niu et al., 2008
Escherichia coli		
BL21(DE3)plysS pET28c(+)-*aii20J*	*E. coli* containing a cloning vector (pET28c(+), Km^r) and *aii20J* gene from *Tenacibaculum* sp. 20J	Mayer et al., 2015
BL21(DE3)plysS pET28c(+)	*E. coli* containing a cloning vector without the *aii20J* gene	Mayer et al., 2015
Plasmids	**Reference**	**Use in this work**
pMo130	GenBank: EU862243	Construction of knockout strains
Primers	**Sequence (5′–3′)**	**Use in this work**
0109UpFPstI	CCCCTGCAGGGGACTGGTGTCGTTATTACC	Construction of knockout strain Δ*0109*
0109UpREcoRI	GGGGAATTCCCCCTTGGAGTAGAACGTTTATTA	Construction of knockout strain Δ*0109*
0109DownFEcoRI	CCCGAATTCGGGACATAGGCTGTATCGACTT	Construction of knockout strain Δ*0109*
0109DownRBamHI	GGGGGATCCCCCACTGTAGAAATCCCTATACTT	Construction of knockout strain Δ*0109*
0109extF	TGTTCCCGATTATGTATG	Confirmation of Δ*0109*
0109extR	GCAACTTCACAAACTCCA	Confirmation of Δ*0109*
pMo130site2F	ATTCATGACCGTGCTGAC	Checking of pMo130
pMo130site2R	CTTGTCTGTAAGCGGATG	Checking of pMo130

[a]*American type culture collection.*

short, coverslips were vertically submerged in 3 mL of LB or LS-LB (0.5% NaCl, 1% tryptone, and 0.5% yeast extract) inoculated with 24 h-cultures of *A. baumannii* strains at an optical density of 0.05 (OD_{600} nm) in 12-well culture plates. Biofilms were grown at 37°C for 12, 24, or 48 h. The QQ enzyme Aii20J (Mayer et al., 2015) at a final concentration of 20 μg/mL, DNase at 2 U/mL, α-amylase (10 U/mL) were added to the cultures alone or in combination. Wells with only culture medium were incubated in the same conditions as negative growth controls. Three replicates for each strain or treatment were performed. For biofilm biomass quantification, after incubation, the coverslips were removed, deposited in a clean 12-wells culture plate, and allowed to dry in a clean bench. Once dried, wells were filled with Crystal Violet solution (0.04%, Gram-Hucker, Panreac), and after 20 min, the excess of dye was removed, and coverslips washed several times with distilled water. Bound crystal violet was released by adding 33% acetic acid. The absorbance was measured at 600 nm (Muras et al., 2020).

Transmission Electron Microscopy

Biofilms and planktonic cells of *A. baumannii* ATCC® 17978™, its isogenic mutant Δ*abaI,* and *A. baumannii* ATCC® 17978™ supplemented with 20 μg/mL Aii20J enzyme, were examined by transmission electron microscopy (TEM) to confirm the presence of surface appendages. Coverslips were incubated for 24 h in LS-LB as explained above. Biofilms and planktonic cells obtained by centrifugation (1 mL) were fixed with ice-cold 3.5% paraformaldehyde for 20 min at 4°C. Bacteria were applied to Formvar-coated grids and were air-dried. At least two different formvar coated grids prepared from two different experiments. The cells were then negatively stained with 1% phosphotungstic acid in distilled water for 5 s and were examined with a JEM-1011 transmission electron microscope (JEOL) operating at 80 kV and equipped with an Orius SC1000 charge-coupled device (CCD) camera (Gatan).

Statistical Methods

Mann–Whitney test ($p < 0.05$) was applied for all statistical analyses using GraphPad Prisma 8.3.0.

RESULTS

QS and Surface-Associated Motility in *A. baumannii* ATCC® 17978™

The deletion of gene *A1S_0109*, encoding a putative AHL synthase in *A. baumannii* ATCC® 17978™, showing an amino acid sequence identity of 93.4% with the AbaI

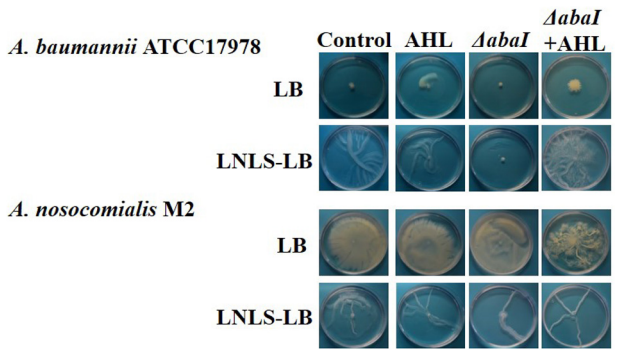

FIGURE 1 | Effect of the mutation of the *abaI* gene on surface-associated motility of *A. baumannii* ATCC® 17978™, and *A. nosocomialis* M2. The capacity of OHC12-HSL (10 μM) to restore the phenotype in the mutants was tested. Plates were prepared in LB or low-nutrient low-salt LB (LNLS-LB) with 0.25% Eiken agar and were incubated at 37°C for 14 h. Images are representative of three independent experiments carried out with three replicates per condition.

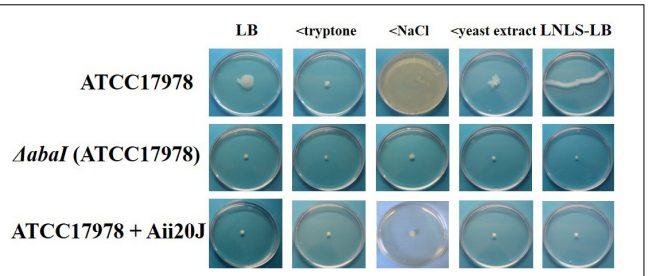

FIGURE 2 | Effect of the components of LB culture medium on surface-associated motility of *A. baumannii* ATCC® 17978™ and its isogenic mutant Δ*abaI*, on different media plates with 0.25% Eiken agar. The effect of the QQ enzyme Aii20J (20 μg/mL) on *A. baumannii* ATCC® 17978™ was also evaluated. Plates were incubated at 37°C for 14 h and images are representative of three independent experiments carried out carried out with three replicates per condition (< tryptone: LB with reduced tryptone concentration, < NaCl: LB with reduced NaCl concentration, < yeast extract: LB with reduced yeast extract concentration, and LNLS-LB: low-nutrient low-salt LB).

synthase of *A. nosocomialis* M2 (Carruthers et al., 2013), caused the disappearance of AHLs from the culture media under the conditions that promoted the production of these signals in the wild-type (Mayer et al., 2018). No differences in growth were observed between the Δ*abaI* mutant and the parental strain in shaken liquid cultures (data not shown).

LB medium completely hindered surface-associated migration in *A. baumannii* ATCC® 17978™ (**Figure 1**), while a "tentacle-like," branched motility pattern was observed in LNLS-LB for this species at 37°C. This phenotype was not affected by the type of agar used (**Supplementary Figure 1**). On the contrary, *A. nosocomialis* M2 maintained the motility in both LB and LNLS-LB (**Figure 1**) but only on plates prepared with Eiken agar (**Supplementary Figure 1**). Deletion of the *abaI* gene completely abolished motility under permissive conditions in *A. baumannii* ATCC® 17978™ while almost no effect could be observed in the *A. nosocomialis* M2 *abaI:Km* mutant at 37°C (**Figure 1**). The exogenous addition of OHC12-HSL, the major AHL signal found in the supernatants of *A. baumannii* ATCC® 17978™ and *A. nosocomialis* M2 cultures (Niu et al., 2008; Mayer et al., 2018) was able to restore this phenotype in the Δ*abaI* mutant of ATCC® 17978™ under permissive conditions, confirming that AHL-mediated QS is crucial for surface-associated motility in this species, while no significant effect was observed when added to the wild type (**Figure 1**).

A systematic study of plate motility was performed by reducing the concentrations of each LB medium component to that of LNLS-LB to define better the LB-medium component responsible for abrogating surface-associated motility in *A. baumannii* ATCC17978 and its effect on the role of the QS system. The experiments were performed in Eiken agar, that was shown to be more motile-permissive for *A. nosocomialis* M2 strain (**Supplementary Figure 1**). Results showed that a reduction in salt concentration from 1 to 0.5% while keeping other LB constituent concentrations, promotes a hyper-motile phenotype in ATCC® 17978™ (**Figure 2**) similar to that observed in M2 in LB medium (**Figure 1** and **Supplementary Figure 2**). Lowering tryptone or yeast extract concentrations did not change the non-motile phenotype observed in LB (**Figure 2**), indicating that NaCl concentrations higher than 0.5% are responsible for the inhibition of motility observed in LB medium for ATCC® 17978™. Additional experiments carried out by substituting NaCl by sucrose indicated that high osmolarity conditions, and not simply ionic strength, are responsible for the abrogation of motility in this strain (**Supplementary Figure 3**). In the case of *A. nosocomialis* M2, the reduction of tryptone, the main source of C and N in LB medium, was responsible for the change in the motility pattern observed in LNLS-LB (**Figure 1**), with no effect of NaCl concentration (**Supplementary Figure 2**). The loss of surface-associated motility capacity in the Δ*abaI* mutant of ATCC® 17978™ was confirmed in all the tested media (**Figure 2**). The exogenous addition of the QQ enzyme Aii20J, mixed with the inoculum, had a similar effect that the mutation of the synthase, completely blocking motility (**Figure 2**) in LNLS-LB plates. On the contrary and in accordance with the higher production of AHLs that has been reported in low-salt LB liquid cultures in comparison with LNLS-LB (Mayer et al., 2018), in the case of the low-salt LB-plates, mixing the enzyme with the inoculum was not enough to block the motility, and it was necessary to mix the enzyme with all the culture media in order to fully abrogate this phenotype. At 37°C the *abaI*:*Km* mutant of *A. nosocomialis* M2 presented the same spreading phenotype as the parental strain in all culture media (**Supplementary Figure 2**).

Biofilm Formation Is Under the Control of QS in *A. baumannii* ATCC® 17978™

A preliminary experiment was performed in order to assess if low salinity promoted biofilm formation in *A. baumannii* ATCC® 17978™, as observed for surface-associated motility. Results

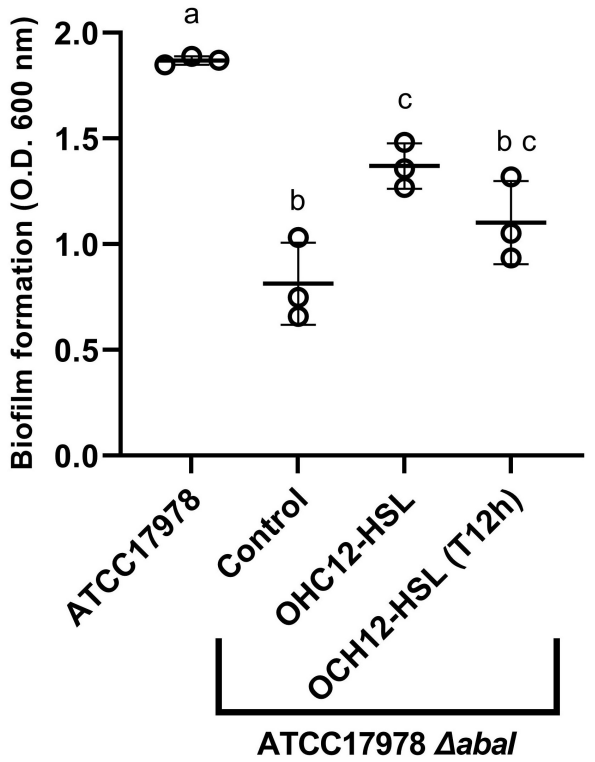

FIGURE 3 | Biofilm formation by *A. baumannii* ATCC® 17978™ and its Δ*abal* mutant as measured with crystal violet staining. The capacity of OHC12-HSL (10 μM) to restore the phenotype in the mutant was also tested. The addition of OHC12-HSL was performed at the beginning of the experiment and after 12 h of incubation (T12h). Biofilms (n = 3) were inoculated in LS-LB, incubated at 37°C for 24 h and stained with crystal violet staining. Different letters indicate statistically significant differences (Mann–Whitney test, $p < 0.05$).

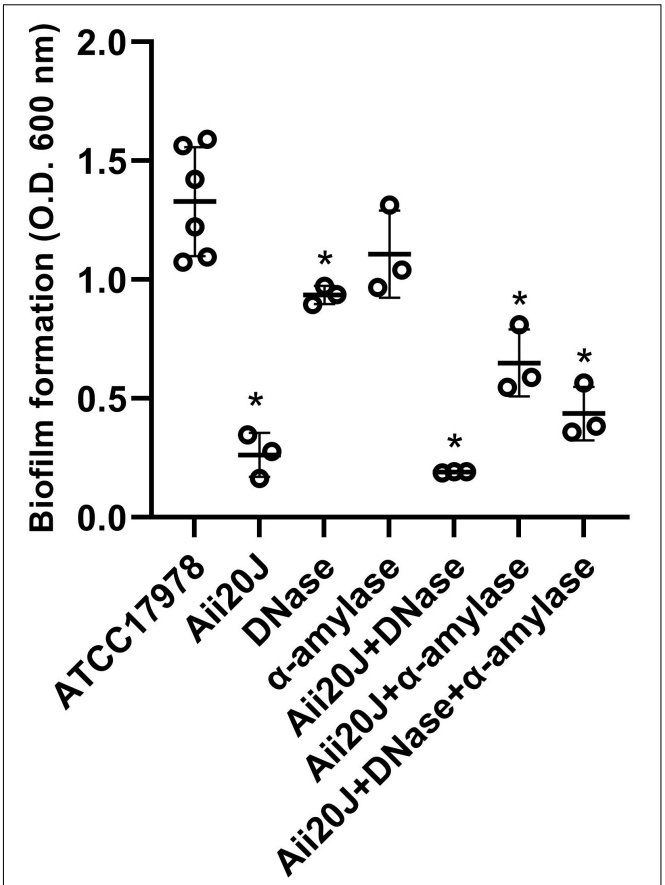

FIGURE 4 | Effect of different enzymes on biofilm formation by *A. baumannii* ATCC® 17978™. The QQ enzyme Aii20J (20 μg/mL), DNase (2 U/mL), and α-amylase (10 U/mL) were added alone or in combination. Biofilms were produced in LS-LB in glass coverslips, incubated for 24 h at 37°C and stained with the crystal violet assay. The cultures were inoculated with cells from an agitated culture. Values are averages ± SD (n = 3). Asterisks indicate statistically significant differences in comparison with the untreated control (Mann–Whitney test, $p < 0.05$).

clearly show a significantly higher biofilm formation (Mann–Whitney test, $p < 0.05$) in ATCC® 17978™ in the LS-LB medium in the first 12 h, while no differences were observed thereafter with the crystal violet assay quantification (**Supplementary Figure 4**). The mutation of *abaI* gene caused a strong reduction in biofilm formation in *A. baumannii* ATCC® 17978™ in both culture media (**Supplementary Figure 4**). In an experiment performed in LS-LB, the addition of the QS signal OHC12-HSL to the mutant partially restored the phenotype, causing an increase of the biofilm biomass, that was statistically significant (Mann–Whitney test, $p < 0.05$, **Figure 3**). The addition of the AHL to a preformed-biofilm (T12h) of the mutant also produced an increase in biofilm biomass, although this difference was not statistically significant (Mann–Whitney test, $p > 0.05$).

Effect of the QQ Enzyme Aii20J and Other Biofilm Inhibitory Enzymes on Biofilm Formation by *A. baumannii* ATCC® 17978™

The purified QQ enzyme Aii20J reduced biofilm formation in *A. baumannii* ATCC® 17978™ by 80% after 24 h when grown on glass coverslips at 37°C (**Figure 4**). The enzyme also affected biofilm formation in *A. nosocomialis* M2 in the same system, although the reduction was lower (38.54%). The clinical strain MAR002 and an isogenic mutant impaired in biofilm formation and eukaryotic-cell attachment capacity were equally affected by the enzyme, suffering a reduction of biofilm formation of around 45% (**Supplementary Figure 5**). Biofilm formation in MAR002 and its mutant was similar to that observed for ATCC® 17978™, even though MAR002 has been described as a biofilm hyper-forming strain (Álvarez-Fraga et al., 2016).

The effect of the purified QQ enzyme Aii20J was compared with the effect of two enzymes with potential biofilm inhibitory effect: a DNase and an α-amylase. The α-amylase did not affect biofilm formation by ATCC® 17978™ (Mann–Whitney test, $p = 0.16$, **Figure 4**). On the contrary, DNase significantly reduced biofilm formation by 20% (Mann–Whitney test, $p < 0.05$, **Figure 4**). In ATCC® 17978™ the simultaneous addition of the QQ enzyme Aii20J and DNase did not improve significantly

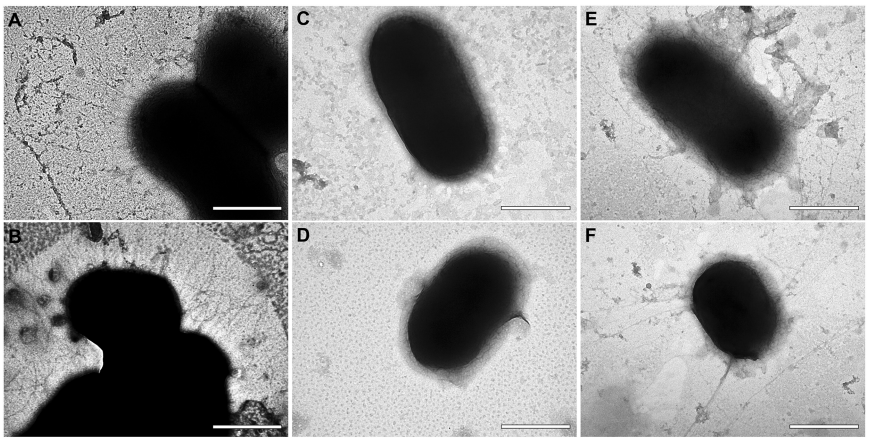

FIGURE 5 | TEM microphotographs of *A. baumannii* ATCC® 17978™ **(A,B)**, its isogenic mutant Δ*abaI* **(C,D)** and *A. baumannii* ATCC® 17978™ treated with the QQ enzyme Aii20J (20 μg/mL) **(E,F)**. Original magnification: 80.000×. Scale bars: 500 nm.

the results obtained with the QQ enzyme (Mann–Whitney test, $p = 0.35$, **Figure 4**).

In order to observe the effect of Aii20J on cell appendages, biofilm and planktonic cells were observed with TEM. Important differences could be observed among wild type, the Δ*abaI* mutant and the cells treated with the pure Aii20J enzyme (**Figure 5**). *A. baumannii* ATCC® 17978™ cells showed many short appendages (**Figures 5A,B**). On the contrary, cells of the Δ*abaI* mutant and Aii20J-treated cells were almost completely devoid of these short appendages (**Figures 5C–F**). Cells surrounded by long, thin individual filaments were observed in the cultures in the presence of the Aii20J enzyme (**Figures 5E,F**). The same morphology was observed in attached and unattached cells (data not shown).

Effect of the QQ Enzyme Aii20J and DNase on Biofilm Formation by Multidrug-Resistant Clinical Isolates of *A. baumannii*

Several clinical isolates that had been previously characterized regarding antibiotic-resistance profile, AHL production and surface-associated motility (López et al., 2017; Mayer et al., 2018) were selected and tested regarding its capacity to form biofilm on glass coverslips and their sensitivity to the enzymes Aii20J and DNase. Large differences in biofilm formation were found in all strains depending on the incubation conditions of the inoculum, with much higher biofilm formation being observed when the inoculum was maintained under static conditions (**Figure 6B**). Moreover, important differences among the tested strains were observed. *A. baumannii* ATCC® 17978™ formed much more biofilm than any of the clinical MDR strains, independently of the culture conditions of the inoculum (**Figures 6A,B**). Among these, the biofilm formation capacity was not related to the antibiotic resistance or surface-associated motility profiles. Strains with high motility profile (Ab1, Ab5, Ab7) showed low or intermediate biofilm formation capacity *in vitro*. The effect of the enzymes was also variable among the strains (**Figures 6A,B**). However, no significant effect on bacterial growth, measured as optical density in the supernatant of the cultures was observed, except for ATCC17978 in which OD in the supernatants in the presence of the enzymes was significantly higher than in the control culture (data not shown). Strains ATCC® 17978™ and Ab7, showing a very similar surface-associated motility pattern and response to the QQ enzyme (López et al., 2017) showed a very different response regarding biofilm formation. Best inhibitory results were obtained with the combination of the QQ enzyme and DNase in all cases (**Figures 6A,B**).

DISCUSSION

The study of the factors controlling the expression of virulence factors is crucial for the development of novel antimicrobial strategies in antibiotic-resistant pathogens like *A. baumannii*. Multiple transcriptional regulatory systems are involved in the persistence and pathogenesis of this species (Wood et al., 2018a; De Silva and Kumar, 2019). Among these regulatory circuits, QS has emerged as an interesting target for the control of virulence factors (Zhang et al., 2017; Mayer et al., 2018). Most studies regarding the role of the AHL-mediated QS system in the expression of virulence-related traits have been carried out with *A. nosocomialis* strain M2 (formerly *A. baumannii* M2) (Niu et al., 2008; Bhargava et al., 2010; Clemmer et al., 2011; Stacy et al., 2012, 2013; Saroj and Rather, 2013; Oh and Choi, 2015). The role of the QS system in this intricate signaling system seems to be crucial, since the mutation of the AbaI synthase significantly reduces virulence in *in vivo* models (Peleg et al., 2009; Fernández-García et al., 2018). Nevertheless, in the view that some important features, such as motility, behave differently between *A. nosocomialis* M2 and *A. baumannii* ATCC® 17978™ (Clemmer et al., 2011), it is important to fully characterize the role of QS system in the latter and to study the variations among clinical strains of *A. baumannii*. As previously reported for other

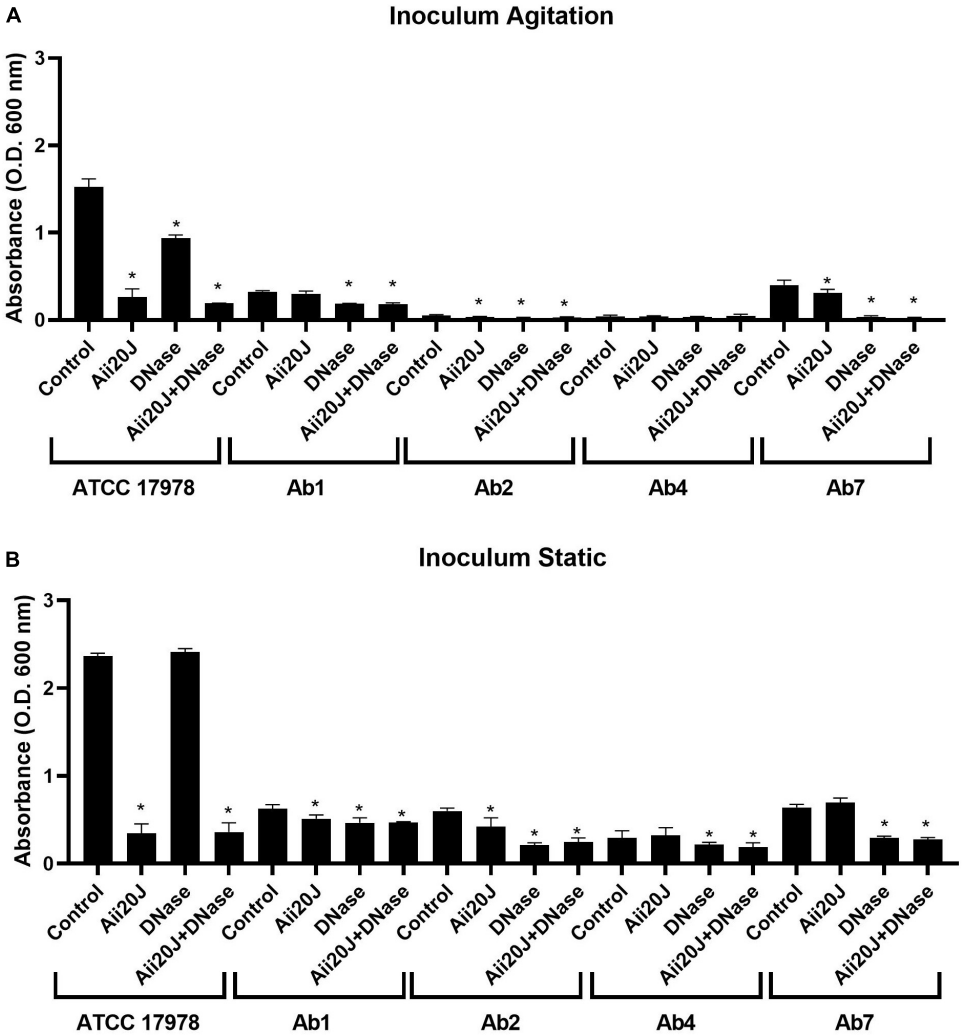

FIGURE 6 | Effect of the QQ enzyme Aii20J (20 μg/mL), DNase (2 U/mL) or both on biofilm formation by *A. baumannii* ATCC® 17978™ and different multidrug-resistant clinical strains presenting different motility patterns (López et al., 2017). Biofilms were cultivated on 18 mm × 18 mm glass coverslips in LS-LB during 24 h at 37°C and stained with crystal violet ($n = 3$). The cultures were inoculated with cells from an agitated **(A)** or a static **(B)** culture. Asterisks indicate statistically significant differences in comparison with the untreated control (Mann–Whitney test, $p < 0.05$).

species of the genus (Niu et al., 2008; Bitrian et al., 2012; How et al., 2015), the mutation of the *abaI* gene (A1S_0109) fully abolished AHL production in *A. baumannii* ATCC® 17978™, indicating that this gene probably codifies the only synthase responsible for AHL-mediated QS in this species.

Both, motility (**Figures 1**, 2) and biofilm formation (**Figure 3**) were impaired in the Δ*abaI* mutant in *A. baumannii* ATCC® 17978™, corroborating previous reports on the control of these two important traits related to virulence by the AHL-mediated QS system in other *Acinetobacter* spp. (Niu et al., 2008; Kang and Park, 2010; Anbazhagan et al., 2012; Bhargava et al., 2012; Kim and Park, 2013; Chow et al., 2014; Oh and Choi, 2015; Mayer et al., 2018). The exogenous addition of OHC12-HSL, the main AHL found in *Acinetobacter* spp., restored the motility of the Δ*abaI* mutant under motile-permissive, low-salt conditions (**Figure 1**) and partially restored biofilm forming capacity (**Figure 3**). Consistent with these outcomes, in ATCC® 17978™ the wide-spectrum AHL-lactonase Aii20J blocked motility even in highly inductive conditions (**Figure 2**). Moreover, it drastically reduced biofilm formation (**Figures 4**, **6** and **Supplementary Figure 5**), confirming a key role of QS in the regulation of these two traits in this strain and further supporting the potential of QQ strategies for virulence control in *Acinetobacter* (Stacy et al., 2013; Chow et al., 2014; Mayer et al., 2015, 2018, 2020; López et al., 2017; Zhang et al., 2017). Nevertheless, a wide variability in surface-associated motility and response to QQ strategies has been previously described in *A. baumannii* clinical isolates presenting different antibiotic resistance profiles (López et al., 2017). Also, the well-studied strain *A. nosocomialis* M2 presented very different behavior in response to culture conditions and QQ strategies in comparison with ATCC® 17978™, maintaining a strong motility phenotype

in conditions in which *A. baumannii* ATCC® 17978™ motility was completely blocked (**Supplementary Figure 2**). Unlike what was observed for the QS-impaired mutant of ATCC® 17978™, the *A. nosocomialis* M2 *abaI:Km* mutant maintained the motility pattern at 37°C in contrast with the impairment of motility reported at 30°C (Clemmer et al., 2011) and confirmed in our laboratory (data not shown), indicating a strong effect of temperature in this type of *in vitro* assays. Our results demonstrate that surface-associated motility in M2 is not so strongly dependent on QS regulatory pathways, at least in motile-permissive conditions, revealing important differences in the role of QS on this phenotype among species and isolates of the genus *Acinetobacter*.

High salinity negatively affected both surface-associated motility and initial biofilm formation in ATCC® 17978™ (**Figure 2** and **Supplementary Figure 4**). Salinity lost its influence during biofilm maturation under the conditions tested (**Figure 2**), indicating that the factors that favor motility at low salinities are important for the initial steps of biofilm formation, and linking the mechanisms responsible for surface-associated motility with the surface-attachment phase of biofilm formation. Indeed, AHL production is higher in low-salinity liquid cultures (Mayer et al., 2018), which also correlates QS with these two physiological processes. In low-salt solid cultures it was necessary to increase the concentration of the QQ enzyme Aii20J in order to reduce motility, indicating a higher production of QS signals also in semi-solid LS-LB. High osmolarity was shown to repress motility but to activate biofilm formation in *Vibrio cholerae* (Shikuma and Yildiz, 2009), suggesting that medium osmolarity is an important environmental signal regulating lifestyle in biofilm-forming pathogens.

The electron microscope analysis of cells obtained during early biofilm formation shows a clear decrease in surface short pili in the Δ*abaI* mutant (**Figure 5**), which could be the result of lower expression of the *csu* operon. The chaperone/usher pili-associated *csu* operon, responsible for the assembly and extension of type I pilus (Tomaras et al., 2003, 2008), important for biofilm formation in *A. nosocomialis* M2 and *A. baumannii* ATCC® 19606™ (Tomaras et al., 2008; Gaddy and Actis, 2009; Clemmer et al., 2011; Luo et al., 2015), has been previously described to be overexpressed in biofilms in comparison with planktonic cultures of *A. baumannii* ATCC® 17978™ (Rumbo-Feal et al., 2013). The *csu* operon has also been related to surface-associated motility in *A. baumannii* ATCC® 17978™ since the conditions that promote motility and AHL signal production also generate an increase in the expression of *csuD* (Mayer et al., 2018). The mutation of A1S_2811, a CheA/Y-like hybrid, a two-component regulator in *A. baumannii* ATCC® 17978™, resulted in a decrease in surface motility and biofilm formation at the gas-liquid interface and the transcription of *abaI* and the *csu* operon. The reduction of biofilm and motility in the mutant was accompanied by a decrease in pilus-like structures and exopolymeric substances on the cell surface (Chen et al., 2017). Moreover, Luo et al. (2015) showed that addition of AHL signals to *A. baumannii* ATCC19606™ cultures induces the expression of bacterial pili structural genes, including *csuD*, and an increase of pili-like structures around the bacteria. Our results further support a role of the *csu* operon in surface-associated motility and biofilm formation, both being under the control of the QS signals in ATCC® 17978™. Consistent with a control of *csu* expression by the QS system, short pili were also absent in cells treated with the QQ enzyme Aii20J; instead, long filaments were found around the cells treated with the enzyme, that were absent in the wild type and in the Δ*abaI* mutant (**Figure 5**), indicating that the QQ enzyme could not block the production of a different type appendages. These filaments could be attributed, among others, to type IV pili (TFP), involved in several bacterial processes such as natural transformation or adherence to biotic and abiotic surfaces and twitching motility (Clemmer et al., 2011; Harding et al., 2013; Eijkelkamp et al., 2014). However, the involvement of TFP in surface-associated motility and its regulation by the QS system is controversial (reviewed by Harding et al., 2018). A novel photo-regulated type I chaperone/usher pilus assembly system, encoded by the *prpABCD* operon, involved in surface-associated motility, biofilm formation and virulence to *Galleria mellonella* (Wood et al., 2018b) could be also responsible for the observed phenotype in the Aii20J-treated cells. Additionally, the synthesis of 1,3-diaminopropane (DAP), lipid oligosaccharides, other external envelope components or extracellular DNA, important for motility and biofilm formation in this species (McQueary et al., 2012; Harding et al., 2018; Geisinger et al., 2019) may also be under the control of the QS system, contributing to the observed effect of the mutation of the *aba*I gene and Aii20J lactonase on both, surface-associated motility and biofilm formation.

The status of the inoculum strongly influenced the formation of biofilm in the *Amsterdam Active* Attachment model (**Figure 6**). More biofilm was formed when the inoculum was maintained in static conditions, a phenomenon already reported for pellicle formation in the liquid-air interface and motility in *A. baumannii* ATCC® 17978™ (Chen et al., 2017). This fact also links biofilm formation with the QS system, since AHLs are only produced in significant amounts in static cultures (Mayer et al., 2018). Therefore, the cells maintained in such conditions should display a set of physiological activities that favor or accelerate the initiation of biofilm formation when transferred to fresh medium.

As previously reported for surface-associated motility (López et al., 2017), strong variations in biofilm formation were found among the different strains tested, and no clear correlation was found between strain origin, antibiotic resistance profile and *in vitro* biofilm formation ability (**Figure 6**). A large number of works have analyzed the correlation between biofilm formation and antibiotic resistance in *A. baumannii* (reviewed by Eze et al., 2018; Mayer et al., 2020). Biofilm formation has been found to be correlated with MDR among clinical isolates (Babapour et al., 2016; Yang et al., 2019; Zeighami et al., 2019). Higher incidence of antibiotic resistance has also been associated with the presence of *abaI* and *csuE* genes in clinical *A. baumannii* strains (Liu et al., 2016). On the contrary, another study could not find any relationship between isolation site, multidrug resistance, pulsed-field type and biofilm production among *A. baumannii* clinical and environmental strains isolated from a hospital (de Campos et al., 2016). Finally, it was reported that isolates with a higher level of resistance tended to form weaker biofilms (Qi et al., 2016) driving to the hypothesis that biofilm-forming

bacterial strains do not depend on antibiotic resistance and colonization characteristics as do non-biofilm formers for their survival in hospital settings (Hall and Mah, 2017). In our case, the low-antibiotic resistant strain ATCC® 17978™, isolated from a case of infant meningitis, shows a much higher biofilm-forming capacity than the MDR strains (**Figure 6**).

The QQ lactonase Aii20J strongly reduced biofilm formation in *A. baumannii* ATCC® 17978™. This fact indicates that the many existing QQ enzymes present in this strain may be active only under particular conditions or during specific periods, probably related to the self-control of AHL production during stationary phase (Mayer et al., 2018). The lactonase was also capable of reducing biofilm formation in *A. nosocomialis* M2 and in MAR002, that was previously reported as a biofilm hyper-forming strain, even though in our cultivation system the amount of biofilm formed was similar to that observed in *A. baumannii* ATCC® 17978™ (**Supplementary Figure 5**). This difference is probably the result of the different cultivation methodology and culture medium used, since in tubes, these strains form biofilm only in the interphase liquid:air (Tomaras et al., 2003). The lactonase Aii20J also reduced biofilm formation significantly in two of the four MDR clinical strains tested (**Figure 6**). Sensitivity to the enzymes in the clinical MDR strains was not dependent of MDR profile or biofilm-forming capacity. However, it could be somehow related to the amount of AHLs produced since strains Ab5 and Ab7 produced a negligible amount of AHLs in LB medium at 37°C (Mayer et al., 2018) and demonstrated no-sensitivity to the action of the QQ enzyme (**Figure 6**). A recombinant lactonase successfully disrupted the biofilm formation of clinical isolates of *A. baumannii* (Chow et al., 2014). However, MomL was ineffective in treating mixed species and wound-associated biofilm models containing *A. baumannii* (Zhang et al., 2017). The differences observed in biofilm formation when the inoculum was maintained in static or shaken conditions indicate that the published results regarding biofilm formation may be strongly influenced by cultivation conditions and should be interpreted carefully. Temperatures lower than 30°C seem to favor biofilm formation (Eze and El Zowalaty, 2019), and QS regulated genes that are relevant for biofilm formation are upregulated at lower temperatures (De Silva and Kumar, 2019). Current biofilm experiments were carried out at 37°C, and therefore the effect of the QQ lactonase Aii20J may be higher at lower temperatures. Also, the weak biofilm formation by this species in the microtiter-plate method generally used to cultivate the biofilms, and the low sensitivity of the crystal-violet-staining method used for the assessment of biofilm biomass in most studies should be taken into account when evaluating anti-biofilm activity (Muras et al., 2018).

Despite the variability in response to the QQ lactonase Aii20J and DNase, the simultaneous addition of both enzymes reduced biofilm formation in the five strains tested, and therefore constitutes a promising strategy for controlling biofilm formation in this species. The presence of eDNA in *A. baumannii* biofilms has been reported before in a clinical isolate and a reduction of biofilm formation by DNase I has been already reported, even in preformed biofilms (Tetz et al., 2009; Sahu et al., 2012). Since the sequence of eDNA is similar to genomic DNA, the production of eDNA may also constitute a way of transferring antibiotic resistance in this species (Li et al., 2008). eDNA has been reported in numerous Gram-positive and Gram-negative bacterial pathogens, and the efficacy of the use of DNase has been demonstrated in many of them, increasing the efficacy of antibiotics (Tetz et al., 2009; Okshevsky et al., 2015). In our case, the efficacy of DNase to reduce biofilm formation in *A. baumannii* ATCC® 17978™ and different clinical isolates was highly strain-dependent (**Figure 6**). In the view of the obtained results, the pathway of eDNA secretion in *A. baumannii* deserves further investigation since it constitutes a promising target for developing combined antibiofilm strategies.

Based on the study of the Δ*abaI* mutant and the action of the QQ enzyme Aii20J, results confirm a central role of the QS in the control of biofilm formation and surface-associated motility in *A. baumannii* ATCC® 17978™. This role seems to be strain-specific and strongly dependent on the cultivation conditions. Results demonstrate that QQ strategies, in combination with other enzymatic treatments such as DNase, could represent an alternative approach for the prevention of *A. baumannii* colonization and survival of surfaces and the prevention and treatment of infections caused by this pathogen. The wide variability observed in surface-associated motility, biofilm forming capacity and sensitivity to the QQ enzyme among the tested *A. baumannii* isolates indicate that the development of any novel antimicrobial strategy targeting virulence traits should be carefully evaluated on a large number of strains.

DATA AVAILABILITY STATEMENT

All datasets generated for this study are included in the article/**Supplementary Material**.

AUTHOR CONTRIBUTIONS

CM, AM, and AP conducted the experiments and contributed to the writing of the manuscript. SR-F constructed the mutant. JR-V performed the TEM analysis and contributed to the writing of the manuscript. MR and MP contributed to the writing of the manuscript. AO designed the experiments and wrote the manuscript. All authors contributed to the article and approved the submitted version.

FUNDING

AM was supported by a predoctoral fellowship from Xunta de Galicia (ED481A-2015/311). CM was supported by a postdoctoral fellowship from Xunta de Galicia (IN606B-2019/010). MR was supported by the Biotechnology and Biological Sciences Research Council (BB/R012415/1). AP was supported by a predoctoral fellowship from Xunta de Galicia (ED481A-2019/194).

ACKNOWLEDGMENTS

We thank Prof. Philip N. Rather from the Emory University School of Medicine of Atlanta (United States) for kindly providing us with the *abaI:Km* mutant strain of *A. nosocomialis* M2. The clinical strains of *A. baumannii* were provided by Dr. María Tomás Carmona (CHUAC-INIBIC, A Coruña, Spain) on behalf of the GEIH-GEMARA (SEIMC).

SUPPLEMENTARY MATERIAL

The Supplementary Material for this article can be found online at: https://www.frontiersin.org/articles/10.3389/fmicb.2020.565548/full#supplementary-material

Supplementary Figure 1 | Effect of culture media composition and type of agar on surface-associated motility of *A. baumannii* ATCC17978, *A. nosocomialis* M2 and their respective mutants of the AbaI AHL-synthase. LB and Low Salt-Low Nutrient LB (LSLN-LB 0.5% NaCl, 0.2% tryptone, and 0.1% yeast extract) were tested. Eiken or Difco agar were added at 0.25%. Plates were incubated at 37°C for 14 h, and they are representative of three independent experiments carried out with three replicates per condition.

Supplementary Figure 2 | Effect of the components of LB culture medium on the motility of *A. nosocomialis* M2 and its *abaI:Km* mutant. 0.25% Eiken agar plates were incubated at 37°C for 14 h. Images are representative of three independent experiments carried out with three replicates per condition.

Supplementary Figure 3 | Effect of osmolarity on surface-associated motility in *A. baumannii* ATCC® 17978™ **(A)** and *A. nosocomialis* M2 **(B)**. Cells were inoculated on LB plates with different NaCl (0.1–0.4M) or sucrose (5–20%) concentrations. Plates were incubated at 37°C for 14 h. Images are representative of three independent experiments carried out carried out with three replicates per condition. NaCl concentration in standard LB medium is 0.17M.

Supplementary Figure 4 | Biofilm formation by *A. baumannii* ATCC® 17978™ and its isogenic mutant Δ*abaI* in LB (gray bars) and low-salt LB (LS-LB, NaCl 0.5%, white bars) culture media. Biofilms were formed on 18 mm × 18 mm glass coverslips using a modification of the *Active Attachment* model (Exterkate et al., 2010), incubated for 24 h at 37°C and quantified using the crystal violet assay. Values are shown as average ± SD ($n = 3$). The asterisk shows statistically significant differences (Mann–Whitney test, $p < 0.05$) between LB and LS-LB.

Supplementary Figure 5 | Effect of the QQ lactonase Aii20J (20 μg/mL) on biofilm formation by *A. baumannii* ATCC® 17978™, the *A. baumannii* clinical strain MAR002, which was reported to be a biofilm hyper-former, its isogenic mutant Δ11085, which was reported to be defective in biofilm formation and eukaryotic cell attachment in comparison with the parental strain (Álvarez-Fraga et al., 2016) and *A. nosocomialis* M2. **(A)** Biofilm quantification using the Crystal Violet staining method. Values are averages ± SD ($n = 3$). The asterisks show statistically significant differences (Mann–Whitney test, $p < 0.05$) between treated and untreated biofilms for the same strain. **(B)** Pictures showing the aspect of the untreated (left) and treated (right) biofilms stained with crystal violet. Biofilms were produced on 18 mm × 18 mm glass coverslips using a modification of the *Amsterdam Active Attachment* model (Exterkate et al., 2010) in LS-LB, incubated for 24 h at 37°C.

REFERENCES

Álvarez-Fraga, L., Pérez, A., Rumbo-Feal, S., Merino, M., Vallejo, J. Á, Ohneck, E. J., et al. (2016). Analysis of the role of the LH92_11085 gene of a biofilm hyper-producing *Acinetobacter baumannii* strain on biofilm formation and attachment to eukaryotic cells. *Virulence* 7, 443–445. doi: 10.1080/21505594.2016.1145335

Anbazhagan, D., Mansor, M., Yan, G. O., Md Yusof, M. Y., Hassan, H., and Sekaran, S. D. (2012). Detection of quorum sensing signal molecules and identification of an autoinducer synthase gene among biofilm forming clinical isolates of *Acinetobacter* spp. *PLoS One* 7:e36696. doi: 10.1371/journal.pone.0036696

Arivett, B. A., Fiester, S. E., Ream, D. C., Centrón, D., Ramírez, M. S., Tolmasky, M. E., et al. (2015). Draft Genome of the multidrug-resistant *Acinetobacter baumannii* strain A155 clinical isolate. *Genome Announc.* 3, e212–e215. doi: 10.1128/genomeA.00212-15

Babapour, E., Haddadi, A., Mirnejad, R., Angaji, S.-A., and Amirmozafari, N. (2016). Biofilm formation in clinical isolates of nosocomial *Acinetobacter baumannii* and its relationship with multidrug resistance. *Asian Pac. J. Trop. Biomed.* 6, 528–533. doi: 10.1016/j.apjtb.2016.04.006

Bhargava, N., Sharma, P., and Capalash, N. (2010). Quorum sensing in *Acinetobacter*: an emerging pathogen. *Crit. Rev. Microbiol.* 36, 349–360. doi: 10.3109/1040841X.2010.512269

Bhargava, N., Sharma, P., and Capalash, N. (2012). N-acyl homoserine lactone mediated interspecies interactions between *A. baumannii* and *P. aeruginosa*. *Biofouling* 28, 813–822. doi: 10.1080/08927014.2012.714372

Bitrian, M., Solari, C. M., González, R. H., and Nudel, C. B. (2012). Identification of virulence markers in clinically relevant strains of *Acinetobacter* genospecies. *Int. Microbiol.* 15, 79–88.

Carruthers, M. D., Harding, C. M., Baker, B. D., Bonomo, R. A., Hujer, K. M., Rather, P. N., et al. (2013). Draft genome sequence of the clinical isolate *Acinetobacter nosocomialis* strain M2. *Genome Announc.* 1, e906–e913. doi: 10.1128/genomeA.00906-13

Chan, K. G., Atkinson, S., Mathee, K., Sam, C. K., Chhabra, S. R., Cámara, M., et al. (2011). Characterization of N-acylhomoserine lactone-degrading bacteria associated with the *Zingiber officinale* (ginger) rhizosphere: co-existence of quorum quenching and quorum sensing in *Acinetobacter* and *Burkholderia*. *BMC Microbiol.* 11:51. doi: 10.1186/1471-2180-11-51

Chan, K. G., Cheng, H. J., Chen, J. W., Yin, W. F., and Ngeow, Y. F. (2014). Tandem mass spectrometry detection of quorum sensing activity in multidrug resistant clinical isolate *Acinetobacter baumannii*. *Scientific WorldJournal* 2014:891041. doi: 10.1155/2014/891041

Chen, R., Lv, R., Xiao, L., Wang, M., Du, Z., Tan, Y., et al. (2017). A1S_2811, a CheA/Y-like hybrid two-component regulator from *Acinetobacter baumannii* ATCC17978, is involved in surface motility and biofilm formation in this bacterium. *Microbiologyopen* 6:e00510. doi: 10.1002/mbo3.510

Chow, J. Y., Yang, Y., Tay, S. B., Chua, K. L., and Yew, W. S. (2014). Disruption of biofilm formation by the human pathogen *Acinetobacter baumannii* using engineered quorum-quenching lactonase. *Antimicrob. Agent Chemother.* 58, 1802–1805. doi: 10.1128/AAC.02410-13

Clemmer, K. M., Bonomo, R. A., and Rather, P. N. (2011). Genetic analysis of surface motility in *Acinetobacter baumannii*. *Microbiology* 157, 2534–2544. doi: 10.1099/mic.0.049791-0

de Campos, P. A., Royer, S., da Fonseca Batistão, D. W., Araújo, B. F., Queiroz, L. L., de Brito, C. S., et al. (2016). Multidrug resistance related to biofilm formation in *Acinetobacter baumannii* and *Klebsiella pneumonia* clinical strains from different pulsotype. *Curr. Microbiol.* 72, 617–627. doi: 10.1007/s00284-016-0996-x

De Silva, P. M., and Kumar, A. (2019). Signal transduction proteins in *Acinetobacter baumannii*: role in antibiotic resistance, virulence, and potential as drug targets. *Front. Microbiol.* 10:49. doi: 10.3389/fmicb.2019.00049

Eijkelkamp, B. A., Stroeher, U. H., Hassan, K. A., Elbourne, L. D., Paulsen, I. T., and Brown, M. H. (2013). H-NS plays a role in expression of *Acinetobacter baumannii* virulence features. *Infect. Immun.* 81, 2574–2783. doi: 10.1128/IAI.00065-13

Eijkelkamp, B. A., Stroeher, U. H., Hassan, K. A., Papadimitrious, M. S., Paulsen, I. T., and Brown, M. H. (2011). Adherence and motility characteristics of clinical *Acinetobacter baumannii* isolates. *FEMS Microbiol. Lett.* 323, 44–51. doi: 10.1111/j.1574-6968.2011.02362.x

Eijkelkamp, B. A., Stroeher, U. H., Hassan, K. A., Paulsen, I. T., and Brown, M. H. (2014). Comparative analysis of surface-exposed virulence factors of

Acinetobacter baumannii. *BMC Genomics* 15:1020. doi: 10.1186/1471-2164-15-1020

Exterkate, R. A., Crielaard, W., and Ten Cate, J. M. (2010). Different response to amine fluoride by *Streptococcus mutans* and polymicrobial biofilms in a novel high-throughput active attachment model. *Caries Res.* 44, 372–379. doi: 10.1159/000316541

Eze, E. C., Chenia, H. Y., and El Zowalaty, M. E. (2018). *Acinetobacter* biofilms: effects of physicochemical factors, virulence, antibiotic resistance determinants, gene regulation, and future antimicrobial treatments. *Infect. Drug Resist.* 11, 2277–2299. doi: 10.2147/IDR.S169894

Eze, E. C., and El Zowalaty, M. E. (2019). Combined effect of low incubation temperature, minimal growth medium, and low hydrodynamics optimize *Acinetobacter baumannii* biofilm formation. *Infect. Drug Resist.* 12, 3523–3536. doi: 10.2147/IDR.S203919

Fernández-García, L., Ambroa, A., Blasco, L., Bleriot, I., López, M., Alvarez-Marin, R., et al. (2018). Relationship between the quorum network (sensing/quenching) and clinical features of pneumonia and bacteraemia caused by *A. baumannii*. *Front. Microbiol.* 9:3105. doi: 10.3389/fmicb.2018.03105

Gaddy, J. A., and Actis, L. A. (2009). Regulation of *Acinetobacter baumannii* biofilm formation. *Future Microbiol.* 4, 273–278. doi: 10.2217/fmb.09.5

Geisinger, E., Huo, W., Hernandez-Bird, J., and Isberg, R. R. (2019). *Acinetobacter baumannii*: envelope determinants that control drug resistance, virulence, and surface variability. *Annu. Rev. Microbiol.* 73, 481–506. doi: 10.1146/annurev-micro-020518-115714

Giles, S. K., Stroeher, U. H., Eijkelkamp, B. A., and Brown, M. H. (2015). Identification of genes essential for pellicle formation in *Acinetobacter baumannii*. *BMC Microbiol.* 15:116. doi: 10.1186/s12866-015-0440-6

Hall, C. W., and Mah, T. F. (2017). Molecular mechanisms of biofilm-based antibiotic resistance and tolerance in pathogenic bacteria. *FEMS Microbiol. Lett. Rev.* 41, 276–301. doi: 10.1093/femsre/fux010

Hamad, M. A., Zajdowicz, S. L., Holmes, R. K., and Voskuil, M. I. (2009). An allelic exchange system for compliant genetic manipulation of the select agents *Burkholderia pseudomallei* and *Burkholderia mallei*. *Gene* 430, 123–131.

Harding, C. M., Hennon, S. W., and Feldman, M. F. (2018). Uncovering the mechanisms of *Acinetobacter baumannii* virulence. *Nat. Rev. Microbiol.* 16, 91–102. doi: 10.1038/nrmicro.2017.148

Harding, C. M., Tracy, E. N., Carruthers, M. D., Rather, P. N., Actis, L. A., and Munson, R. S. Jr. (2013). *Acinetobacter baumannii* strain M2 produces type IV pili which play a role in natural transformation and twitching motility but not surface-associated motility. *mBio* 4:e00360-13. doi: 10.1128/mBio.00360-13

How, K. Y., Hong, K. W., Sam, C. K., Koh, C. L., Yin, W. F., and Chan, K. G. (2015). Unravelling the genome of long chain N-acylhomoserine lactone-producing *Acinetobacter* sp. strain GG2 and identification of its quorum sensing synthase gene. *Front. Microbiol.* 6:240. doi: 10.3389/fmicb.2015.00240

Kang, B. R., Lee, J. H., Ko, S. J., Lee, Y. H., Cha, J. S., Cho, B. H., et al. (2004). Degradation of acyl-homoserine lactone molecules by *Acinetobacter* sp. strain C1010. *Can. J. Microbiol.* 50, 935–941.

Kang, Y. S., and Park, W. (2010). Contribution of quorum-sensing system to hexadecane degradation and biofilm formation in *Acinetobacter* sp. strain DR1. *J. Appl. Microbiol.* 109, 1650–1659. doi: 10.1111/j.1365-2672.2010.04793.x

Kim, A. L., Park, S. Y., Lee, C. H., Lee, C. H., and Lee, J. K. (2014). Quorum quenching bacteria isolated from sludge of a wastewater treatment plant and their application for controlling biofilm formation. *J. Microbiol. Biotechnol.* 24, 1574–1582.

Kim, J., and Park, W. (2013). Identification and characterization of genes regulated by AqsR, a LuxR-type regulator in *Acinetobacter oleivorans* DR1. *Appl. Microbiol. Biotechnol.* 97, 6967–6978. doi: 10.1007/s00253-013-5006-5007

Lee, C. R., Lee, J. H., Park, M., Park, K. S., Bae, I. K., Kim, Y. B., et al. (2017). Biology of *Acinetobacter baumannii*: pathogenesis, antibiotic resistance mechanisms, and prospective treatment options. *Front. Cell. Infect. Microbiol.* 7:55. doi: 10.3389/fcimb.2017.00055

Li, L., Xia, Z., Hu, Z., Zhou, Z., and Li, H. (2008). Expression of class I integrase gene in *Acinetobacter baumannii* and drug-resistance. *Zhong Nan Da Xue Xue Bao Yi Xue Ban* 33, 952–957.

Liu, H., Wu, Y. Q., Chen, L. P., Gao, X., Huang, H. N., Qiu, F. L., et al. (2016). Biofilm-related genes: analyses in multi-antibiotic resistant *Acinetobacter baumannii* isolates from mainland China. *Med. Sci. Monit.* 22:1801.

López, M., Mayer, C., Fernández-García, L., Blasco, L., Muras, A., Ruiz, F. M., et al. (2017). Quorum sensing network in clinical strains of *A. baumannii*: AidA is a new quorum quenching enzyme. *PLoS One* 12:e0174454. doi: 10.1371/journal.pone.0174454

Luo, L. M., Wu, L. J., Xiao, Y. L., Zhao, D., Chen, Z. X., Kang, M., et al. (2015). Enhancing pili assembly and biofilm formation in *Acinetobacter baumannii* ATCC19606 using non-native acyl-homoserine lactones. *BMC Microbiol.* 15:62. doi: 10.1186/s12866-015-0397-395

Marti, S., Nait Chabane, Y., Alexandre, S., Coquet, L., Vila, J., Jouenne, T., et al. (2011). Growth of *Acinetobacter baumannii* in pellicle enhanced the expression of potential virulence. *PLoS One* 6:e26030. doi: 10.1371/journal.pone.0026030

Mayer, C., Muras, A., Romero, M., López, M., Tomás, M., and Otero, A. (2018). Multiple quorum quenching enzymes are active in the nosocomial pathogen *Acinetobacter baumannii* ATCC17978. *Front. Cell. Infect. Microbiol.* 8:310. doi: 10.3389/fcimb.2018.00310

Mayer, C., Romero, M., López, M., Muras, A., and Otero, A. (2020). *Quorum Sensing in Acinetobacter Virulence*. Washington, DC: ACS Books.

Mayer, C., Romero, M., Muras, A., and Otero, A. (2015). Aii20J, a wide-spectrum termostable *N*-acylhomoserine lactonase from the marine bacterium *Tenacibaculum* sp. 20J, can quench AHL-mediated acid resistance in *Escherichia coli*. *Appl. Microbiol. Biotechnol.* 99, 9523–9539. doi: 10.1007/s00253-015-6741-8

McQueary, C. N., Kirkup, B. C., Si, Y., Barlow, M., Actis, L. A., Craft, D. W., et al. (2012). Extracellular stress and lipopolysaccharide modulate *Acinetobacter* surface-associated motility. *J. Microbiol.* 50, 434–443. doi: 10.1007/s12275-012-1555-1

Moubareck, C. A., and Halat, D. H. (2020). Insights into *Acinetobacter baumannii*: a review of microbiological, virulence, and resistance traits in a threatening nosocomial pathogen. *Antibiotics* 9:119. doi: 10.3390/antibiotics9030119

Muras, A., Mayer, C., Romero, M., Camino, T., Ferrer, M. D., Mira, A., et al. (2018). Inhibition of *Streptococcus mutans* biofilm formation by extracts of *Tenacibaculum* sp. 20J, a bacterium with wide-spectrum quorum quenching activity. *J. Oral Microbiol.* 10:1429788. doi: 10.1080/20002297.2018.1429788

Muras, A., Otero-Casal, P., Blanc, V., and Otero, A. (2020). Acyl homoserine lactone-mediated quorum sensing in the oral cavity: a paradigm revisited. *Sci. Rep.* 10:9800. doi: 10.1038/s41598-020-66704-4

Niu, C., Clemmer, K. M., Bonomo, R. A., and Rather, P. N. (2008). Isolation and characterization of an autoinducer synthase from *Acinetobacter baumannii*. *J. Bacteriol.* 190, 3386–3392. doi: 10.1128/JB.01929-07

Ochiai, S., Yasumoto, S., Morohoshi, T., and Ikeda, T. (2014). AmiE, a novel *N*-acylhomoserine lactone acylase belonging to the amidase family, from the activated-sludge isolate *Acinetobacter* sp. strain Ooi24. *Appl. Environ. Microbiol.* 80, 6919–6925. doi: 10.1128/AEM.02190-14

Oh, M. H., and Choi, C. H. (2015). Role of LuxIR homologue AnoIR in *Acinetobacter nosocomialis* and the effect of virstatin on the expression of *anoR* gene. *J. Microbiol. Biotechnol.* 25, 1390–1400. doi: 10.4014/jmb.1504.04069

Okshevsky, M., Regina, V. R., and Meyer, R. L. (2015). Extracellular DNA as a target for biofilm control. *Curr. Opin. Biotechnol.* 33, 73–80. doi: 10.1016/j.copbio.2014.12.002

Peleg, A. Y., Jara, S., Monga, D., Eliopoulos, G. M., Moellering, R. C. Jr., and Mylonakis, E. (2009). *Galleria mellonella* as a model system to study *Acinetobacter baumannii* pathogenesis and therapeutics. *Antimicrob. Agents Chemother.* 53, 2605–2609. doi: 10.1128/AAC.01533-08

Peleg, A. Y., Seifert, H., and Paterson, D. L. (2008). *Acinetobacter baumannii*: emergence of a successful pathogen. *Clin. Microbiol. Rev.* 21, 538–582. doi: 10.1128/CMR.00058-07

Qi, L., Li, H., Zhang, C., Liang, B., Li, J., Wang, L., et al. (2016). Relationship between antibiotic resistance,biofilm formation, and biofilm-specific resistance in *Acinetobacter baumannii*. *Front. Microbiol.* 7:483. doi: 10.3389/fmicb.2016.00483

Roca, I., Espinal, P., Vila-Farrés, X., and Vila, J. (2012). The *Acinetobacter baumannii* oxymoron: commensal hospital dweller turned pan-drug-resistant menace. *Front. Microbiol.* 3:148. doi: 10.3389/fmicb.2012.00148

Rumbo-Feal, S., Gómez, M. J., Gayoso, C., Álvarez-Fraga, L., Cabral, M. P., Aransay, A. M., et al. (2013). Whole transcriptome analysis of *Acinetobacter*

baumannii assessed by RNA-sequencing reveals different mRNA expression profiles in biofilm compared to planktonic cells. *PLoS One* 8:e72968. doi: 10.1371/journal.pone.0072968

Rumbo-Feal, S., Pérez, A., Ramelot, T. A., Álvarez-Fraga, L., Vallejo, J. A., Beceiro, A., et al. (2017). Contribution of the *A. baumannii* A1S_0114 gene to the interaction with eukaryotic cells and virulence. *Front. Cell. Infect. Microbiol.* 7:108. doi: 10.3389/fcimb.2017.00108

Sahu, P. K., Iyer, P. S., Oak, A. M., Pardesi, K. R., and Chopade, B. A. (2012). Characterization of eDNA from the clinical strain *Acinetobacter baumannii* AIIMS 7 and its role in biofilm formation. *ScientificWorldJournal* 2012:973436. doi: 10.1100/2012/973436

Saroj, S. D., and Rather, P. N. (2013). Streptomycin inhibits quorum sensing in *Acinetobacter baumannii*. *Antimicrob. Agents Chemother.* 57, 1926–1929. doi: 10.1128/AAC.02161-12

Shikuma, N. J., and Yildiz, F. H. (2009). Identification and characterization of OscR, a transcriptional regulator involved in osmolarity adaptation in *Vibrio cholerae*. *J. Bacteriol.* 191, 4082–4096. doi: 10.1128/JB.01540-08

Shin, B., Park, C., and Park, W. (2020). Stress responses linked to antimicrobial resistance in *Acinetobacter* species. *Appl. Microbiol. Biotechnol.* 104, 1423–1435. doi: 10.1007/s00253-019-10317-z

Smith, M. G., Gianoulis, T. A., Pukatzki, S., Mekalanos, J. J., Ornston, L. N., Gerstein, M., et al. (2007). New insights into *Acinetobacter baumannii* pathogenesis revealed by high-density pyrosequencing and transposon mutagenesis. *Genes Dev.* 21, 601–614.

Stacy, D. M., Le Quement, S. T., Hansen, C. L., Clausen, J. W., Toker-Nielsen, T., Brummond, J. W., et al. (2013). Synthesis and biological evaluation of triazole-containing *N*-acyl homoserine lactones as quorum sensing modulators. *Org. Biomol. Chem.* 11, 938–954. doi: 10.1039/c2ob27155a

Stacy, D. M., Welsh, M. A., Rather, P. N., and Blackwell, H. E. (2012). Attenuation of quorum sensing in the pathogen *Acinetobacter baumannii* using non-native *N*-acyl homoserine lactones. *ACS Chem. Biol.* 7, 1719–1728. doi: 10.1021/cb300351x

Tetz, G. V., Artemenko, N. K., and Tetz, V. V. (2009). Effect of DNase and antibiotics on biofilm characteristics. *Antimicrob. Agents Chemother.* 53, 1204–1209. doi: 10.1128/AAC.00471-08

Tomaras, A. P., Dorsey, C. W., Edelmann, R. E., and Actis, L. A. (2003). Attachment to and biofilm formation on abiotic surfaces by *Acinetobacter baumannii*: involvement of a novel chaperone-usher pili assembly system. *Microbiology* 149, 3473–3484. doi: 10.1099/mic.0.26541-0

Tomaras, A. P., Flagler, M. J., Dorsey, C. W., Gaddy, J. A., and Actis, L. A. (2008). Characterization of a two-component regulatory system from *Acinetobacter baumannii* that controls biofilm formation and cellular morphology. *Microbiology* 154, 3398–3409. doi: 10.1099/mic.0.2008/019471-0

Towner, K. J. (2009). *Acinetobacter*: an old friend, but a new enemy. *J. Hosp. Infect.* 73, 355–363. doi: 10.1016/j.jhin.2009.03.032

Tucker, A. T., Nowicki, E. M., Boll, J. M., Knauf, G. A., Burdis, N. C., Trent, M. S., et al. (2014). Defining gene-phenotype relationships in *Acinetobacter baumannii* through one-step chromosomal gene inactivation. *mBio* 5:e01313-14. doi: 10.1128/mBio.01313-14

Vijayakumar, S., Rajenderan, S., Laishram, S., Anandan, S., Balaji, V., and Biswas, I. (2016). Biofilm formation and motility depend on the nature of the *Acinetobacter baumannii* clinical isolates. *Front. Public Health* 4:105. doi: 10.3389/fpubh.2016.00105

Wood, C. R., Mack, L. E., and Actis, L. A. (2018a). An update on the *Acinetobacter baumannii* regulatory circuitry. *Trends Microbiol.* 26, 560–562. doi: 10.1016/j.tim.2018.05.005

Wood, C. R., Ohneck, E. J., Edelmann, R. E., and Actis, L. A. (2018b). A light-regulated type I pilus contributes to *Acinetobacter baumannii* biofilm, motility, and virulence functions. *Infect Immun.* 86:e00442-18. doi: 10.1128/IAI.00442-18

Yakkala, H., Samantarrai, D., and Gribskov, M. (2019). Comparative genome analysis reveals niche-specific genome expansion in *Acinetobacter baumannii* strains. *PLoS One* 14:e0218204. doi: 10.1371/journal.pone.0218204

Yang, C. H., Su, P. W., Moi, S. H., and Chuang, L. Y. (2019). Biofilm formation in *Acinetobacter baumannii*: genotype-phenotype correlation. *Molecules* 24:1849. doi: 10.3390/molecules24101849

Zeighami, H., Valadkhani, F., Shapouri, R., Samadi, E., and Haghi, F. (2019). Virulence characteristics of multidrug resistant biofilm forming *Acinetobacter baumannii* isolated from intensive care unit patients. *BMC Infect. Dis.* 19:629. doi: 10.1186/s12879-019-4272-0

Zhang, Y., Brackman, G., and Coenye, T. (2017). Pitfalls associated with evaluating enzymatic quorum quenching activity: the case of MomL and its effect on *Pseudomonas aeruginosa* and *Acinetobacter*. *PeerJ* 5:e3251. doi: 10.7717/peerj.3251

Conflict of Interest: The enzyme Aii20J, used in some experiments described in this work, is protected by the following patent: AO, MR, and CM (2016). Peptide with quorum-sensing inhibitory activity, polynucleotide that encodes said peptide, and the uses thereof. PCT/ES2014/070569.

The remaining authors declare that the research was conducted in the absence of any commercial or financial relationships that could be construed as a potential conflict of interest.

frontiers in Microbiology

REVIEW
published: 15 October 2020
doi: 10.3389/fmicb.2020.589640

Regulatory Mechanisms and Promising Applications of Quorum Sensing-Inhibiting Agents in Control of Bacterial Biofilm Formation

*Lantian Zhou, Yue Zhang, Yongze Ge, Xuan Zhu and Jianyi Pan**

Zhejiang Provincial Key Laboratory of Silkworm Bioreactor and Biomedicine, College of Life Sciences and Medicine, Zhejiang Sci-Tech University, Hangzhou, China

A biofilm is an assemblage of microbial cells attached to a surface and encapsulated in an extracellular polymeric substance (EPS) matrix. The formation of a biofilm is one of the important mechanisms of bacterial resistance, which not only leads to hard-to-control bacterial infections in humans and animals but also enables bacteria to be a major problem in various fields, such as food processing, wastewater treatment and metalworking. Quorum sensing (QS) is a bacterial cell-to-cell communication process that depends on the bacterial population density and is mediated by small diffusible signaling molecules called autoinducers (AIs). Bacteria use QS to regulate diverse arrays of functions, including virulence and biofilm formation. Therefore, the interference with QS by using QS inhibiting agents, including QS inhibitors (QSIs) and quorum quenching (QQ) enzymes, to reduce or even completely repress the biofilm formation of pathogenic bacteria appears to be a promising approach to control bacterial infections. In this review, we summarize the mechanisms of QS-regulating biofilm formation and QS-inhibiting agents that control bacterial biofilm formation, strategies for the discovery of new QS inhibiting agents, and the current applications of QS-inhibiting agents in several fields to provide insight into the development of effective drugs to control pathogenic bacteria.

Keywords: biofilm formation, quorum sensing, QS inhibitors, quorum quenching, bacteria

OPEN ACCESS

Edited by:
Rodolfo García-Contreras, National Autonomous University of Mexico, Mexico

Reviewed by:
Kibaek Lee, Chonnam National University, South Korea
Fohad Mabood Husain, King Saud University, Saudi Arabia
Fazlurrahman Khan, Sharda University, India

****Correspondence:***
Jianyi Pan
jianyi.pan@zstu.edu.cn

Specialty section:
This article was submitted to Antimicrobials, Resistance and Chemotherapy, a section of the journal Frontiers in Microbiology

Received: *31 July 2020*
Accepted: *23 September 2020*
Published: *15 October 2020*

Citation:
Zhou L, Zhang Y, Ge Y, Zhu X and Pan J (2020) Regulatory Mechanisms and Promising Applications of Quorum Sensing-Inhibiting Agents in Control of Bacterial Biofilm Formation. Front. Microbiol. 11:589640. doi: 10.3389/fmicb.2020.589640

INTRODUCTION

A biofilm is a large number of bacterial cell aggregates coated in an extracellular mucous comprised of a polysaccharide matrix, lipids, and proteins, which they secrete (Sutherland, 2001; Branda et al., 2005). Bacteria tend to form biofilms when exposed to external environmental pressure, such as extreme nutrient deficiency or excess, high osmotic pressure, low pH, oxidative stress, antibiotics and antimicrobial agents (Costerton et al., 1994). It is a state of self-protection formed when bacteria grow on the surfaces of objects under natural conditions. Any bacteria in nature can form a biofilm under mature conditions, and more than 90% of bacteria live and grow primarily in the form of biofilms (Donlan, 2002).

Biofilms may irreversibly form on a wide variety of surfaces, including living tissues, industrial or potable water system piping, indwelling medical devices, and natural aquatic systems, and once

it is formed, it cannot be removed by gentle rinsing (Donlan, 2002). More than 60% of all bacterial infections are caused by biofilm formation, according to a public announcement from the National Institutes of Health (NIH) (Lewis, 2001). The formation of biofilms leads to not only common bacterial infections, such as infections of the urinary tract, catheters, children's middle-ear, common dental plaque formation, and gingivitis, but also to hard-to-treat or relapsing infections and severe infections that cause serious morbidity and mortality (Lewis, 2001).

Currently, the use of antibiotics is still the major treatment for bacterial infectious diseases. However, biofilms, being a barrier that exists around bacterial cells, reduces the susceptibility of bacteria to antibiotics and causes persistent infections (Stewart, 2002). It has been shown that bacteria in a biofilm increase their resistance against antibiotics by about 1000-fold (Hoiby et al., 2010). Thus, it is hard to control bacterial infections with conventional antibiotics due to the presence of biofilms. Therefore, it is urgent to find a strategy to inhibit the formation of biofilms to control these increasingly serious infections.

At present, it is well known that bacteria forming a biofilm is under the control of the quorum sensing system (QS) (Ding et al., 2011). The QS involves cell-to-cell communication among bacteria using small diffusible chemical signaling molecules called autoinducers (AIs) (Waters and Bassler, 2005). The signaling molecules accumulate in the surrounding environment with an increase of bacterial density. When the concentration of signaling molecules reaches a minimal threshold, they bind to receptor proteins, thereby activating the expression of genes associated with biofilm formation (Williams, 2007). QS inhibiting agents, including QS inhibitors (QSIs) and quorum quenching (QQ) enzymes, can cut off QS cell communication via a variety of mechanisms, consequently inhibiting the formation of biofilms (Augustine et al., 2010; Chatterjee et al., 2017). In addition, QS inhibiting agents can also increase bacterial sensitivity to antibiotics (Ozcan et al., 2019). Therefore, the use of QS inhibiting agents would be a promising approach to control bacterial infections.

In this review, we summarize the mechanisms by which QS inhibiting agents regulate biofilm formation, some strategies for the discovery of new QS inhibiting agents, and the current applications of QS inhibiting agents in medical and industrial fields. We aim to provide a new perspective for exploring more effective antibiotic drugs through the use of QS inhibiting agents.

MECHANISMS OF BIOFILM FORMATION REGULATED BY QS

Quorum sensing regulatory networks are not only very complicated but also vary among bacterial species (Solano et al., 2014). Therefore, the regulatory mechanisms of QS on biofilm formation cannot be described in general. However, based on the types of employed AIs, QS systems can be divided into several categories, namely, AHL system, AIP system (these two system known as AI-1 system previously), AI-2 system and AI-3 system.

The AHL system exists in Gram-negative bacteria and the signaling molecules employed in this system are *N*-acyl homoserine lactones (AHLs) (Slock et al., 1990; Stevens et al., 1994). While, autoinducing peptides (AIPs) are employed in the AIP system and this system is found only in Gram-positive bacteria (Kleerebezem et al., 1997; Irie and Parsek, 2008). Presently, there are a large number of studies on these two systems.

However, there are only a few reports about AI-2 and AI-3 systems, although these two systems have been found to be present in both Gram-positive and Gram-negative bacterial species and to participate in interspecies signal exchange (Surette and Bassler, 1998). AI-2 signaling molecules are a class of furanosyl borate diesters whose precursors are 4,5-dihydroxy-2,3-glutara dione (DPD) (Bassler et al., 1997). The AI-3 signaling molecules have recently been identified as pyrethroids (Sperandio et al., 2003; Kim et al., 2020). The mechanism of how the QS system regulates biofilm formation is described in detail below for Gram-negative and positive bacteria separately.

QS Regulation of Biofilm Formation in Gram-Negative Bacteria

The signaling molecule of the AHL system in Gram-negative bacteria is AHL. The AHL-mediated QS system was first found in *Vibrio fischeri* (Nealson and Hastings, 1979). In this bacterium, the AHL signal, *N*-(3-oxohexanoyl)-L-homoserine lactone (OHHL), is biosynthesized by AI synthase LuxI, and the resulting OHHL diffuses out of the bacterial cell. When the concentration of OHHL reaches a critical threshold with the increase of cell density, OHHL binds to LuxR, which is not only an OHHL receptor, but also a DNA-binding transcriptional activator, thereby activating the expression of genes associated with biofilm formation (Engebrecht et al., 1983; Engebrecht and Silverman, 1984). Presently, it is well known that this regulatory process is a typical model for the regulation of biofilm formation by AHL systems in most Gram-negative bacteria.

Take *Pseudomonas aeruginosa* for instance, which has two AI synthase genes, *lasI* and *rhlI*, which both share significant sequence homologies to *luxI* of *V. fischeri* (Lee and Zhang, 2015). Their signals, *N*-(3-oxo-dodecanoyl)-l-homoserine lactone (OdDHL) and *N*-butyryl-l-homoserine lactone (BHL), are separately synthesized by LasI and RhlI. When they reach the concentration threshold, these two AHL signaling molecules bind to their receptors, LasR and RhlR, respectively, to activate the expression of regulatory genes related to biofilm formation and virulence (Wade et al., 2005). Among these two AHL systems, the *rhl* system is involved in regulating swarming motility that participates in the early stage of biofilm establishment (Khan et al., 2020c), and the biosynthesis of virulence factors, such as rhamnolipid and pyocyanine (Winzer et al., 2000; Daniels et al., 2004; Dusane et al., 2010). The *las* system controls genes encoding elastase, alkaline protease, endotoxin A and other genes related to biofilm formation (Wilder et al., 2011).

In addition, in *P. aeruginosa*, there are also two other types of AHLs-mediated systems, the *pqs* system and the *iqs* system. These two systems work in a way similar to the *rhl* and *las* systems, though their AIs, PQS (2-heptyl3-hydroxy-4-quinolone) and IQS

(2-(2-hydroxyphenyl)-thiazole-4-carbaldehyde), are chemically different from AHLs (Lee and Zhang, 2015). Additionally, the *pqs* system has been reported to be related to the synthesis of bacterial extracellular DNA, which is important for the formation of biofilms (Allesen-Holm et al., 2006). In brief, the four AHL systems, *las*, *rhl*, *iqs* and *pqs*, cross-interact to form a complicated QS network that co-regulates biofilm formation by *P. aeruginosa*.

The AHL system is also involved in the regulation of biofilm formation in *Escherichia coli* (Walters and Sperandio, 2006). However, different from the AHL system in *P. aeruginosa*, only the receptor gene *sdiA* homologous to *luxR* is found and the AHL synthase gene homologous to *luxI* is absent (Walters and Sperandio, 2006). Hence, it is speculated that the receptor SdiA may respond to the AHLs produced by other bacterial species to regulate biofilm-related gene expression. The finding that in the presence of exogenous AHLs, there is an increase of EPS production in *E. coli* and the attachment of bacterial cells (Aswathanarayan and Vittal, 2016) confirms that bacteria can utilize the signaling molecules of other bacterial species for biofilm formation.

Currently, AI-2 systems have been found to affect biofilm formation in several Gram-negative species, such as *Helicobacter pylori*, *E. coli, V. parahemolyticus*, *P. aeruginosa* and *V. cholerae* (Hammer and Bassler, 2003; Li et al., 2007; Anderson et al., 2015; Li et al., 2015; Guo et al., 2018). However, at present, only the regulatory mechanisms of the AI-2 systems in *E. coli* and *V. cholerae* have been clarified. In *E. coli*, the AI-2 signaling molecule is transported into the cell by an ABC transporter protein when the extracellular concentration of the AI-2 signaling molecule reaches its threshold (Li et al., 2007). The resulting signaling molecule is then phosphorylated by LsrK kinase followed by binding to the transcriptional regulator LsrR, thereby activating gene expression (Li et al., 2007). In *V. cholerae*, the AI-2 signaling molecule is detected by the receptor complex LuxPQ. When the signaling molecule concentration reaches its threshold, the kinase activity of LuxQ is converted to phosphatase, which dephosphorylates downstream regulatory protein LuxO, resulting in the production of transcriptional regulatory protein HapR, thereby inhibiting the transcription of genes related to biofilm formation (Hammer and Bassler, 2003, 2007).

AI-3 signaling molecules are currently known to be related to the formation of flagellum and adhesin in *E. coli* (Sperandio et al., 2002), but their regulatory mechanisms for biofilm formation remain unclear.

QS Regulation of Biofilm Formation in Gram-Positive Bacteria

In Gram-positive bacteria, the AIs of the AIP system are AIPs, and the regulation of biofilm formation by the AIPs-mediated QS system is also a typical pattern. Bacteria produce a small oligopeptide in their cells, and the oligopeptide is processed into a mature AIP through modification and then it is transported outside of the cells (Sturme et al., 2002). When the concentration of AIP reaches its threshold, it binds to the extracellular segment of histidine kinase, a transmembrane receptor localized on the cell membrane, which leads to the activation of the kinase, followed by phosphorylation of downstream response regulatory factors, resulting in regulation of the expression of genes related to biofilm formation (Sturme et al., 2002).

For example, in *Staphylococcus aureus*, five genes, *agrA*, *agrB*, *agrC*, *agrD* and *hld* in the *agr* operon constitute the *agr* AIP system (Painter et al., 2014). The signaling AIP is converted from its precursor peptide AgrD, and AgrB, a transmembrane protein, is responsible for the conversion of AgrD to mature AIP and transportation of the resulting AIP outside of the cell. When the extracellular AIP concentration reaches its threshold, the AIP binds to an extracellular part of AgrC, an integral transmembrane protein functioning as a histidine kinase, resulting in the activation of the kinase. The activated AgrC in turn phosphorylates the downstream response regulator AgrA. Phosphorylated AgrA binds to the intergenic DNA between promoters P2 and P3, and thus activates promoter transcription. The *agr* system has been shown to play a major role in the dispersion phase, which is the last stage of biofilm formation (Yarwood et al., 2004). *Agr* mutants formed a thicker biofilm comparing with the wild type, but this increased biofilm thickness has been attributed to the inability of cells to detach from the mature biofilm, not to cell growth or death (Vuong et al., 2000, 2004).

Presently, there are several reports about the regulation of biofilm formation by the AI-2 system in Gram-positive bacteria. For example, a study has shown that the lack of *luxS*, which encodes AI-2 synthase, promotes the transcription of *rbf*, a positive regulatory factor for biofilm formation, and results in an increase of biofilm formation and higher levels of production of polysaccharide intercellular adhesion (PIA) in *S. aureus* (Ma et al., 2017). However, the opposite finding, that the absence of *luxS* decreases biofilm formation, was also found in *Enterococcus faecalis* (Wang et al., 2011; Yang et al., 2018) and *Streptococcus suis* (Wang et al., 2011; Yang et al., 2018). Nevertheless, the AI-2 system is involved in the regulation of biofilm formation in Gram-positive bacteria, but its regulatory mechanism has not yet been fully characterized.

In addition, there is still no report about the AI-3 system in regard to the control of biofilm formation in Gram-positive bacteria.

THE MECHANISMS OF QS INHIBITING AGENTS SUPPRESSING BIOFILM FORMATION

In the past two decades, a number of effective QS inhibiting agents have been developed and successfully used to control the formation of bacterial biofilms. These QS inhibiting agents are mainly QS inhibitors (QSIs) and quorum quenching (QQ) enzymes. Although different types of QSIs or QQ enzymes interfere with different parts of the QS signaling pathway, the inhibitory mechanism can be divided into three categories based on their functional targets, i.e., targeted to AI signaling molecules, receptors and downstream signaling cascades (**Figure 1**). These three mechanisms are described in detail with examples as follows.

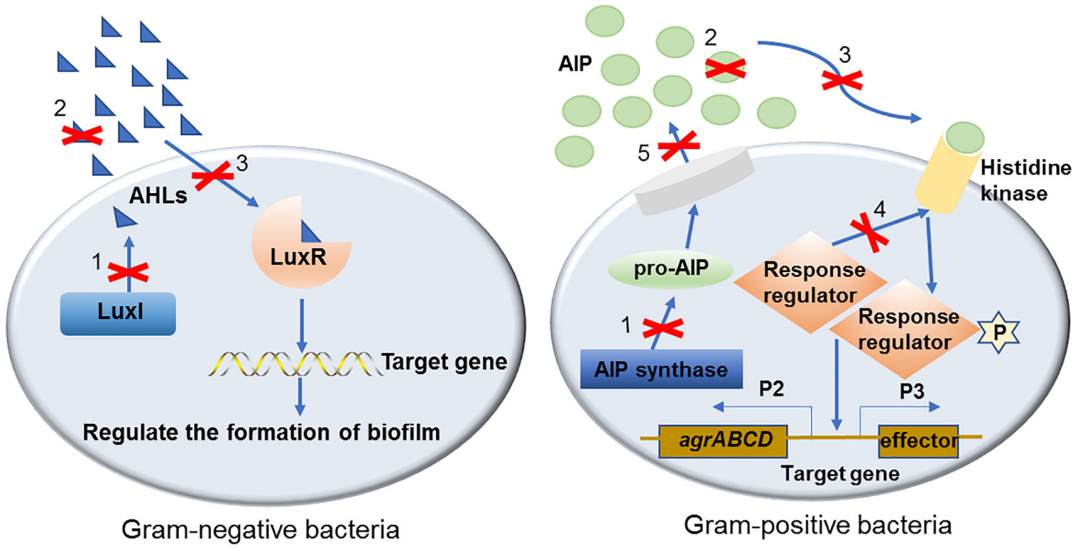

FIGURE 1 | The mechanisms of QS inhibiting agents in controlling bacterial biofilm formation. Mechanisms of QS inhibiting agents in controlling bacterial biofilm formation are marked with numbers on the diagram: (1). Inhibit AIs synthesis; (2). Degrade or inactivate AIs by AHL-lactonases, oxidoreductases, antibodies, etc.; (3). Interfere with the signal receptors using AI antagonists; (4). Interfere with the response regulators thus disturbing signaling cascade; (5). Reduce the extracellular AIs accumulation by inhibiting AIs efflux hence inhibited cell-to-cell signaling.

Target Signal Molecule

The QS inhibiting agents that target the AI signaling molecules are mainly AHL-lactonases, oxidoreductases, antibodies, and some other molecular compounds (**Table 1**). These agents inhibit the QS system by inactivation of signaling molecule synthases, neutralization of AIPs with antibodies, modification or degradation of the signaling molecules, etc.

Degradation or neutralization of QS signaling molecules by QQ enzymes are a direct and effective way to inhibit the QS system. In Gram-negative bacteria, AHLs can be degraded by two types of hydrolases, AHL-lactonase and AHL-acylase. An AHL-lactonase, encoded by *aiiA* of *Bacillus spp* and belonging to the metallo-β-lactamase superfamily, has been determined to effectively inhibit biofilm formation and attenuate virulence factors in several bacterial species (Augustine et al., 2010; dos Reis Ponce et al., 2012; Anandan and Vittal, 2019). Another QQ enzyme, AHL-acylase, is not widespread in Gram-negative bacteria. However, the enzyme has been found to be present at least in *P. aeruginosa*, and it has been shown to degrade AHLs with side chains and hence enable the bacteria to modulate the QS system (Sio et al., 2006). Currently, there are few reports on the degradation of AIPs by QQ enzymes in Gram-positive bacteria. However, AIPs can be neutralized by antibodies and cause interruption of QS signaling. For example, an anti-AI monoclonal antibody can efficiently inhibit QS via neutralization of an AI peptide (AIP-4) that is produced by *S. aureus* (Park et al., 2007).

N-acyl homoserine lactones oxidoreductase, another class of QQ enzyme, has also been reported in Gram-negative bacteria, it modifies the AIs and thereby attenuates the specific binding of the AIs to the corresponding receptors, resulting in a decrease of biofilm formation. BpiB09 is a metagenome-derived NADP-dependent reductase and it has been found to be involved in inactivation of the QS signaling molecule OdDHL. Although the AHLs of *P. aeruginosa* are probably not the native substrate of BpiB09, the expression of the enzyme in *P. aeruginosa* results in poor biofilm formation, significantly reduced pyocyanin production and decreased motility (Bijtenhoorn et al., 2011). Another AHL oxidoreductase, Hod, a 2,4-dioxygenase, is capable of catalyzing the conversion of PQS to *N*-octanoylanthranilic acid and carbon monoxide. Exogenous supplementation of Hod protein into *P. aeruginosa* cultures reduces expression of the PQS biosynthetic enzyme PqsA and the PQS-regulated virulence factors (Pustelny et al., 2009). In short, these QQ enzymes can effectively inhibit bacterial biofilm formation.

Inhibiting the biosynthesis of QS signaling molecules may be a more direct way to interrupt the QS system and inhibit biofilm formation. Some QS inhibitors have been found to inhibit the synthetic activities of AIs synthases. TofI is an AHL synthase identified in the Gram-negative bacterium *Burkholderia gluma*. The binding site of TofI can be occupied by an AHL analog and therefore disturb AHL synthesis (Chung et al., 2011). Another example is diketopiperazines that target CepI, an AHL synthase of *B. cenocepacia*, can interfere with the activity of signaling molecule synthases, rendering the bacteria unable to produce biofilms (Buroni et al., 2018).

Targeting the Signaling Molecule Receptors

The second mechanism of QS inhibiting agents is by targeting the receptors of the QS signaling molecules, thereby inactivating the receptor or competing for the receptor. In most cases, the ligand binding domains of receptors with the native AIs are highly conserved (Khan et al., 2019), which can be competitively or non-competitively bound by most AIs (**Table 2**). Two classes of

TABLE 1 | Studies on controlling biofilm by targeting QS signaling molecule.

Source	QS-inhibiting agents	Chemical structure	Target bacteria	Effects	References
Bacillus cereus VT96	AHL-lactonase AiiA	NA	*P. aeruginosa* *V. cholerae* *E. cloacae*	Degraded AHLs, prevent the biofilm formation and production of virulence factors	Augustine et al., 2010; dos Reis Ponce et al., 2012; Anandan and Vittal, 2019
Synthesis	Molecularly imprinted polymers (MIPs)	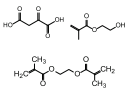	*P. aeruginosa*	Captured OdDHL, therefor interrupted QS, and subsequently inhibit biofilm formation	Ma et al., 2018
Arthrobacter nitroguajacolicus strain Rü61a	3-Hydroxy-2-methyl-4(1H)-quinolone 2,4-dioxygenase Hod	NA	*P. aeruginosa*	Catalyzed the conversion of PQS to N-octanoylanthranilic acid and carbon monoxide, reduced the expression of the PQS-regulated virulence	Pustelny et al., 2009
Derivative	Boronic acid derivate SM23	NA	*P. aeruginosa*	Decreased 3-oxo-C12-HSL and C4-HSL and reduced biofilm formation	Peppoloni et al., 2020
Synthesis	Acyl-HSL analog J8-C8	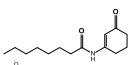	*B. gluma*	Bound to TofI, disturbed C8-HSL synthesis, affected biofilm formation	Chung et al., 2011
Synthesis	Diketopiperazines	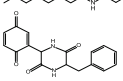	*B. cenocepacia*	Interfered with the activity of signal molecule synthase CepI and rendered the bacteria unable to produce biofilm	Buroni et al., 2018
Synthesis	Anti-autoinducer monoclonal antibody AP4-24H11	NA	*S. aureus* RN4850	Sequestrated the autoinducing peptide (AIP)-4, inhibited QS and biofilm formation	Park et al., 2007
Gene from a soil metagenome	NADP-dependent reductase BpiB09	NA	*P. aeruginosa* PAO1	Reduced pyocyanin production, decreased motility, poor biofilm formation	Bijtenhoorn et al., 2011
Synthesis	3-(dibromomethylene) isobenzofuran-1(3H)-one derivatives		*F. nucleatum* *P.gingivalis* *T. forsythia*	Inhibited biofilm formation through the inhibition of AI- 2 activity	Park et al., 2017

NA, not available.

QS inhibiting agents, flavonoids and furanones, have been found that can bind to receptors of a variety of pathogenic bacteria (Paczkowski et al., 2017; Proctor et al., 2020). A plant flavonoid, naringenin, competes with the physiological signaling molecule OdDHL by directly binding to the receptor LasR, resulting in inhibition of the production of the QS-regulated virulence factors, pyocyanin and elastase, etc., in *P. aeruginosa* (Hernando-Amado et al., 2020). Also in *P. aeruginosa*, the receptor LasR can interact with sitagliptin, a drug used for the treatment of diabetes mellitus type 2, and a minor inhibitory concentration of sitagliptin significantly inhibits biofilm formation (Abbas et al., 2020). In addition, flavonoids can non-competitively bind to the LasR LBD and prevent the protein from binding to DNA, causing repression of certain QS behaviors (Paczkowski et al., 2017). Moreover, some QS inhibiting agents can bind to different receptors at the same time. For example, 3-benzene lactic acid (PLA), a QS inhibiting agent produced by Lactobacillus, antagonistically binds to the receptors RhlR and PqsR with a higher affinity than its cognate ligands BHL and PQS in *P. aeruginosa* (Chatterjee et al., 2017).

As another class of QS inhibiting agents, furanones, can compete with the native AIs to bind to, and subsequently block, the AHL receptors. They have been demonstrated to significantly decrease virulence factor production and biofilm formation in a range of bacterial species (Proctor et al., 2020). In addition to competing with signaling molecules for receptors, some QS inhibiting agents, such as meta-bromo-thiolactone, can also directly inactivate the receptors to prevent virulence factors expression and biofilm formation (Sully et al., 2014).

Blocking the Signaling Cascade

The third mechanism of inactivation of QS systems is blocking the signaling cascade by deactivating the downstream response regulators or other regulatory factors. For example, in the AIP system of *S. aureus*, downstream response regulator AgrA is phosphorylated and thereby activated, which is triggered by upstream signaling, and it binds to DNA sequences associated with promoters and upregulates the expression of relevant genes as described above. Inhibiting the response regulators can block the signaling cascade and prevent the formation of a bacterial biofilm (**Table 3**). Savarin, for example, is a small molecule identified as an *S. aureus* virulence inhibitor, which can specially target AgrA to disrupt *agr* operon-mediated QS, and hence inhibit biofilm formation (Sully et al., 2014).

TABLE 2 | Studies on controlling biofilm by targeting QS signaling receptors.

Source	QS-inhibiting agents	Chemical structure	Target bacteria	Effects	References
Lactobacillus	3-Phenyllactic acid (PLA)		*P. aeruginosa*	Bound to QS receptors RhlR and PqsR with high affinity, thus inhibited the expression of virulence factors such as protease, pyocyanin and rhamnolipids that are involved in the biofilm formation	Chatterjee et al., 2017
Synthesis	Sitagliptin	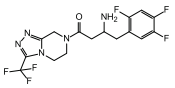	*P. aeruginosa*	Interacted with LasR receptors, and significantly inhibited the biofilm formation	Abbas et al., 2020
Plant	Naringenin	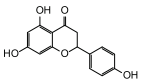	*P. aeruginosa*	Competed with OdDHL by directly binding the QS regulator LasR, inhibited the production of the QS-regulated virulence factors, pyocyanin and elastase	Hernando-Amado et al., 2020
Plant	Fructose-furoic acid	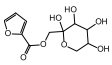	Uropathogenic *E. coli*	Competed with the SdiA native ligand C8HSL to down regulate its target specific expression and biofilm phenotypic characters	Vinothkannan et al., 2018
Synthesis	Furanones	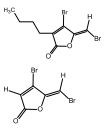	*P. aeruginosa*	Competed with the native autoinducers to bind to the AHL receptors, and significantly decreased virulence factor production and biofilm formation	Proctor et al., 2020
Synthesis	Meta-bromo-thiolactone	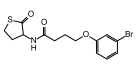	*P. aeruginosa*	Inhibited receptors LasR and RhlR, prevented virulence factor expression and biofilm formation	O'Loughlin et al., 2013
Synthesis	N-phenyl-4-(3-phenylthioureido) benzenesulfonamide	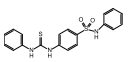	*E. coli*(EAEC) O104:H4	allosterically modified AI-3 receptor QseC,impeded virulence expression and decreased biofilm formation	Curtis et al., 2014

TABLE 3 | Studies on controlling biofilm by blocking the signaling cascade.

Source	QS-inhibiting agents	Chemical structure	Target bacteria	Effects	Reference
Synthesis	Savirin	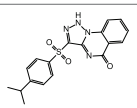	*S. aureus*	Targeted AgrA to disrupt *agr* operon-mediated QS	Sully et al., 2014
Synthesis	Virstatin	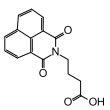	*A. nosocomialis*	Repressed the expression of AnoR, leading to decreased synthesis of OH-dDHL, thus adversely affecting the signal transduction cascade, reducing biofilm formation and motility	Oh and Choi, 2015
Synthesis	Curcumin	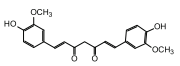	*P. aeruginosa* PAO1	Inhibited QS controlled protease and biofilm formation	Sethupathy et al., 2016
Synthesis	Efflux pumps inhibitor PAβN	NA	*P. aeruginosa* clinical isolate	Reduced the extracellular accumulation of QS signals and significantly diminished the relative expression of QS cascade (*pqsA, pqsR, lasI, lasR, rhlI* and *rhlR*)	El-Shaer et al., 2016

NA, not available.

In addition to acting on the response regulator, the QS inhibiting agents can also act on other regulatory factors to block signaling cascades. For example, virstatin, a small molecule that acts to prevent the expression of cholerae virulence factors, can repress the expression of AnoR, which is a positive regulator of the LuxI-like synthase AnoI in *Acinetobacter nosocomialis*, leading to decreased synthesis of *N*-(3-hydroxy-dodecanoyl)-L-homoserine lactone (OH-dDHL), thus affecting the signaling cascade, and reducing biofilm formation and motility (Oh and Choi, 2015). Moreover, efflux pumps inhibitor PAβN reduces the extracellular accumulation of QS signaling molecules and significantly decreases the relative expression of the QS cascade (*pqsA*, *pqsR*, *lasI*, *lasR*, *rhlI* and *rhlR*) in *P. aeruginosa* clinical isolates, and this is followed by a reduction of bacterial virulence (El-Shaer et al., 2016).

STRATEGIES OF EXPLOITING NEW QS INHIBITING AGENTS

In the past two decades, researchers have discovered plenty of QS inhibiting agents that can effectively inhibit biofilm formation in bacteria. The development of new QS inhibiting agents that can effectively replace antibiotics has been a hot topic in the antibacterial research field. With the increasing degree of bacterial resistance to antibiotics, it has become more urgent to develop new QS inhibiting agents that can effectively inhibit biofilm formation. Here, we will introduce four strategies for exploiting new QS inhibitors.

Synthesis of Derivatives of Known QSIs

Some QS inhibitors are usually structural analogs of AIs, which cause the inactivation of QS by competitively binding to the receptor. Therefore, the synthesis of derivatives of known QSIs that do not alter the core structure may be an effective strategy. Actually, researchers have used natural and chemically synthesized halogenated furanones to successfully synthesize furanone analogs bearing alkyl chains, vinyl bromide keys or aromatic rings, and these analogs can also inhibit biofilm formation (Chang et al., 2019). In addition, C-5 aromatic substituted furanones have been designed and synthesized based on 5-hydroxyl-3,4-halogenated-5H-furan-2-ones, and this compound shows remarkable inhibition of biofilm formation as well as inhibition of virulence factor production in *P. aeruginosa* (Chang et al., 2019). Moreover, a new class of brominated furanones that contained a bicyclic structure were designed and synthesized, and this class of molecules exhibited reduction in the toxicity to mammalian cells, but retained the inhibitory activity toward biofilm formation of bacteria (Yang et al., 2014).

Modification of Existing QQ Enzymes

The use of quenching enzymes to interfere with QS is an attractive strategy to fight bacterial infections. Intentional modification of QQ enzymes by using protein engineering methods may obtain greater efficiency and stability of quenching enzymes. Thus, this could be an effective strategy for developing new QQ enzymes. MomL is a marine lactonase that can degrade various AHLs. Two MomL mutants, $MomL^{I144V}$ and $MomL^{V149A}$, exhibit higher activities to block the production of virulence factors of *Pectobacterium carotovorum subsp. carotovorum* (Pcc) (Wang et al., 2019). PvdQ is an acylase with effective QQ activity in *P. aeruginosa*, but it hardly hydrolyses short-chain AHLs. However, its variant $PvdQ^{L\alpha\ 146W,F\beta\ 24Y}$ has an altered substrate specificity, and it exhibits high hydrolysis activity toward shorter-chain AHLs such as C8-HSL (Koch et al., 2014).

Search for QS Inhibiting Agents in Natural Products

There are abundant biochemical resources in plants and microorganisms in nature. In recent years, a number of natural products have been found to have potential abilities of inhibition of QS signaling and biofilm formation with the extensive use of computer-aided programs like structure-based virtual screening (SB-VS) and molecular docking bioassays (Ahmed et al., 2019; Borges and Simoes, 2019). Natural plant-derived compounds trans-cinnamaldehyde (CA) and salicylic acid (SA) can significantly inhibit the expression of QS-regulated genes involved in virulence, rhamnolipid and reduced biofilm formation in *P. aeruginosa* (Ahmed et al., 2019). Recently, a novel AHL acylase, MacQ, has been identified from a multidrug-resistant bacterium, *Acidovorax sp.* strain MR-S7, and it was able to degrade a wide variety of AHLs, ranging from C6 to C14 side chains with or without 3-oxo substitutions, thus interfering with the QS system in the bacterial pathogen (Kusada et al., 2017).

Identify Approved Drugs as QS Inhibiting Agents

The search for QS inhibiting agents from the library of drugs approved for clinical applications may be a promising way to shorten the period of development of an anti-QS drug from discovery to clinical use, since long-term clinical trials are needed to ensure QS inhibiting agents are safe and reliable before they can be used to treat infectious diseases. A typical example of a new therapeutic use of an old drug is niclosamide, which is an FDA approved anti-helminthic drug. Niclosamide has been identified to strongly inhibit the QS response by targeting the *las* QS system, thereby reducing the expression of *las* regulon-controlled virulence factors and biofilm formation in *P. aeruginosa* (Imperi et al., 2013). Another FDA approved drug that is used for the treatment of upper respiratory tract infections and for tracheobronchial infections caused by Gram-positive pathogens, clofoctol, has also been found to significantly reduce biofilm formation through inhibiting the *pqs* QS system in *P. aeruginosa* (D'Angelo et al., 2018). In addition, albendazole, also an FDA approved clinical drug, has been found to have great potential to act as a QS inhibitor. It quenches the QS by interacting with the hydrophobic amino acid residues of the hydrophobic pocket of CviR and LasR receptors in *P. aeruginosa* (Singh and Bhatia, 2018). Antibiotics have also shown great potential as QS inhibiting agents. For exsample, aminoglycosides, a commonly used class of antibiotics, exhibit biofilm inhibition by targeting the QS

regulatory protein LasR in *P. aeruginosa* (Khan et al., 2020a; Khan et al., 2020b).

APPLICATIONS OF QS-INHIBITING AGENTS IN CONTROLLING BACTERIAL BIOFILM FORMATION

As a new type of antimicrobial agent, QS inhibiting agents have been applied in several fields, such as in medical treatments, food processing and water treatment.

Currently, QS inhibiting agents are widely used in health-related fields. *P. aeruginosa* is a major cause of nosocomial infections, especially in the pulmonary infections associated with cystic fibrosis. This organism shows a remarkable capacity to resist antibiotics. Alternative drugs have proven useful against this multiresistant strain. The acylase PvdQ has been identified as an QS inhibiting agent that can irreversibly hydrolyze AHL signaling molecules and has great therapeutic efficacy against pulmonary infections in a mouse model (Utari et al., 2018).

In addition, owing to biofilms being one of the important virulence factors of pathogenic bacteria, infections resulting from the formation of biofilms on medical devices remains a significant clinical problem (Ozcelik et al., 2017). Therefore, a poly(ethylene glycol) (PEG) based multifunctional coating that allows for the covalent incorporation of the synthetic QS inhibitor 5-methylene-1-(prop-2-enoyl)-4-(2-fluorophenyl)-dihydropyrrol-2-one (DHP) in a surface can reduce biofilm formation, and the use of this coating can reduce bacterial colonization (Ozcelik et al., 2017). Obviously, this provides a useful way to prevent device-related infections. Moreover, QS inhibiting agents can also be used as antibiotic accelerants for treating bacterial infections. Two cinnamic acid derivatives, 4-dimethylaminocinnamic acid (DCA) and 4-methoxycinnamic acid (MCA) as AHL inhibitors, were both found to not only markedly inhibit biofilm formation, but also to enhance the susceptibility of biofilms to tobramycin (Cheng et al., 2020).

In addition to great application prospects in the health-related fields, QS inhibiting agents can also be used in the food industry. Food safety has always been a major concern in the food industry. The formation of biofilms enhances the attachment of bacterial pathogen to the surface of food packaging bags or processing equipment, which increases post-processing contamination and risks to public health due to their persistence and resistance to cleaning and disinfection procedures (Shi and Zhu, 2009). Thus, the extraction of QS inhibiting agents from foodborne materials to solve food contamination problems is a relatively effective approach. The essential oils that were extracted from *Murraya koenigii* were found to have strong QS inhibitory and anti-biofilm activities that can reduce cell attachment, metabolic activity and EPS production, and in addition, they could delay the decomposition of refrigerated milk caused by *psychrophila* PSPF19 (Bai and Vittal, 2014). Additional applications of QS inhibiting agents in the food industry are still being explored.

At present, the application of quenching QS in water treatment has also been reported, and it shows great potential and commercial prospects. In wastewater treatment, membrane bioreactor (MBR) is an important technique that combines the activated sludge and membrane filtration processes (Yeon et al., 2009a,b; Lee et al., 2018; Oh and Lee, 2018). However, biofouling, which is mainly caused by the generation of a thickened biofilm layer resulting from bacterial gathering, is a primary problem during the use of MBR (Kose-Mutlu et al., 2019), which seriously affects the efficiency of wastewater treatment. QQ enzymes can be employed to prevent biofouling in MBR. For instance, Kim et al. (2011) immobilized a QQ enzyme (acylase) onto a nano-filtration membrane, and found the acylase-immobilized membrane prohibits the formation of the mushroom-shaped mature biofilm and prevents more than 90% of the initial flux after 38 h operation, while the un-immobilized raw membrane dropped to 60% accompanied by severe biofouling.

There are studies showing that the use of QS inhibiting agents may also be an effective strategy to eradicate biofilm contamination in metalworking fluids (MWFs). Biofilm contamination is a critical problem in MWFs, which not only affects product quality, but also shortens the lifetime of MWFs. Two QS inhibiting agents, patulin and furanone C-30, both reduced biofilm formation in MWF when compared to untreated controls (Ozcan et al., 2019).

CONCLUSION AND FUTURE RESEARCH

Biofilms can promote bacteria survival in harsh environments. Conventional antibiotics and bactericides cannot penetrate the extracellular matrix of biofilms, resulting in decreased bacterial sensitivity, and therefore, biofilm-related pollution poses serious problems in many fields, including the environment, food, and human diseases. The formation of a biofilm is regulated by the QS system, and thus the use of QS inhibiting agents is a promising strategy to control biofilm formation, and it has been successfully applied in a number of fields.

QS inhibiting agents control biofilm formation generally by targeting QS signaling molecules or their receptors, or downstream regulatory factors. They do not kill bacteria or inhibit the growth of bacteria, and instead they interfere with the expression of virulence factors and inhibit biofilm formation, which puts less pressure on bacterial survival and reduces their drug resistance. This is completely different from the mechanism of antibiotics killing bacteria.

In recent years, many natural or synthetic QS inhibiting agents that effectively reduce biofilm formation have been exploited. However, there are still several problems to be overcome: (1) the mechanisms of some QS inhibiting agents in controlling biofilms are still unclear; (2) some known QS inhibiting agents are cytotoxic or unstable; (3) the anti-biofilm effect is not broad enough, only being effective against one or two bacterial species; (4) what are the best conditions for QS inhibiting agents in controlling biofilms? (5) whether QS inhibiting agents have an impact on beneficial bacteria in the environment. These problems all need to be overcome to develop more efficient, less toxic QS inhibiting agents that will provide great value in the future for biofilm prevention and treatment.

AUTHOR CONTRIBUTIONS

JP and LZ provided the general concept and designed the manuscript and revised and approved the manuscript. LZ, YG, YZ, and XZ wrote the manuscript. LZ contributed to create the figure. All authors contributed to the article and approved the submitted version.

FUNDING

This work was supported by grants from the National Natural Science Foundation of China (31701572), the National Natural Science Foundation of China (31770141), and the 521 Talent Program of Zhejiang Sci-Tech University, China, to JP.

REFERENCES

Abbas, H. A., Shaldam, M. A., and Eldamasi, D. (2020). Curtailing quorum sensing in *Pseudomonas aeruginosa* by Sitagliptin. *Curr. Microbiol.* 77, 1051–1060. doi: 10.1007/s00284-020-01909-1904

Ahmed, S., Rudden, M., Smyth, T. J., Dooley, J. S. G., Marchant, R., and Banat, I. M. (2019). Natural quorum sensing inhibitors effectively downregulate gene expression of *Pseudomonas aeruginosa* virulence factors. *Appl. Microbiol. Biotechnol.* 103, 3521–3535. doi: 10.1007/s00253-019-09618-9610

Allesen-Holm, M., Barken, K. B., Yang, L., Klausen, M., Webb, J. S., Kjelleberg, S., et al. (2006). A characterization of DNA release in *Pseudomonas aeruginosa* cultures and biofilms. *Mol. Microbiol.* 59, 1114–1128. doi: 10.1111/j.1365-2958.2005.05008.x

Anandan, K., and Vittal, R. R. (2019). Quorum quenching activity of AiiA lactonase KMMI17 from endophytic Bacillus thuringiensis KMCL07 on AHL- mediated pathogenic phenotype in *Pseudomonas aeruginosa*. *Microb. Pathog.* 132, 230–242. doi: 10.1016/j.micpath.2019.05.015

Anderson, J. K., Huang, J. Y., Wreden, C., Sweeney, E. G., Goers, J., Remington, S. J., et al. (2015). Chemorepulsion from the Quorum Signal Autoinducer-2 Promotes *Helicobacter* pylori Biofilm Dispersal. *mBio* 6:e00379-15. doi: 10.1128/mBio.00379-315

Aswathanarayan, J. B., and Vittal, R. R. (2016). Effect of small chain N acyl homoserine lactone quorum sensing signals on biofilms of food-borne pathogens. *J. Food Sci. Technol.* 53, 3609–3614. doi: 10.1007/s13197-016-2346-2341

Augustine, N., Kumar, P., and Thomas, S. (2010). Inhibition of *Vibrio cholerae* biofilm by AiiA enzyme produced from *Bacillus* spp. *Arch. Microbiol.* 192, 1019–1022. doi: 10.1007/s00203-010-0633-631

Bai, A. J., and Vittal, R. R. (2014). Quorum sensing inhibitory and anti-biofilm activity of essential oils and their in vivo efficacy in food systems. *Food Biotechnol.* 28, 269–292. doi: 10.1080/08905436.2014.932287

Bassler, B. L., Greenberg, E. P., and Stevens, A. M. (1997). Cross-species induction of luminescence in the quorum-sensing bacterium *Vibrio harveyi*. *J. Bacteriol.* 179, 4043–4045. doi: 10.1128/jb.179.12.4043-4045.1997

Bijtenhoorn, P., Mayerhofer, H., Muller-Dieckmann, J., Utpatel, C., Schipper, C., Hornung, C., et al. (2011). A novel metagenomic short-chain dehydrogenase/reductase attenuates *Pseudomonas aeruginosa* biofilm formation and virulence on *Caenorhabditis elegans*. *PLoS One* 6:e26278. doi: 10.1371/journal.pone.0026278

Borges, A., and Simoes, M. (2019). Quorum sensing inhibition by marine bacteria. *Mar. Drugs* 17:427. doi: 10.3390/md17070427

Branda, S. S., Vik, S., Friedman, L., and Kolter, R. (2005). Biofilms: the matrix revisited. *Trends Microbiol.* 13, 20–26. doi: 10.1016/j.tim.2004.11.006

Buroni, S., Scoffone, V. C., Fumagalli, M., Makarov, V., Cagnone, M., Trespidi, G., et al. (2018). Investigating the mechanism of action of diketopiperazines inhibitors of the *Burkholderia cenocepacia* quorum sensing synthase cepi: a site-directed mutagenesis study. *Front. Pharmacol.* 9:836. doi: 10.3389/fphar.2018.00836

Chang, Y. Q., Wang, P. C., Ma, H. M., Chen, S. Y., Fu, Y. H., Liu, Y. Y., et al. (2019). Design, synthesis and evaluation of halogenated furanone derivatives as quorum sensing inhibitors in *Pseudomonas aeruginosa*. *Eur. J. Pharm. Sci.* 140:105058. doi: 10.1016/j.ejps.2019.105058

Chatterjee, M., D'Morris, S., Paul, V., Warrier, S., Vasudevan, A. K., Vanuopadath, M., et al. (2017). Mechanistic understanding of Phenyllactic acid mediated inhibition of quorum sensing and biofilm development in *Pseudomonas aeruginosa*. *Appl. Microbiol. Biotechnol.* 101, 8223–8236. doi: 10.1007/s00253-017-8546-8544

Cheng, W. J., Zhou, J. W., Zhang, P. P., Luo, H. Z., Tang, S., Li, J. J., et al. (2020). Quorum sensing inhibition and tobramycin acceleration in Chromobacterium violaceum by two natural cinnamic acid derivatives. *Appl. Microbiol. Biotechnol.* 104, 5025–5037. doi: 10.1007/s00253-020-10593-10590

Chung, J., Goo, E., Yu, S., Choi, O., Lee, J., Kim, J., et al. (2011). Small-molecule inhibitor binding to an N-acyl-homoserine lactone synthase. *Proc. Natl. Acad. Sci. U.S.A.* 108, 12089–12094. doi: 10.1073/pnas.1103165108

Costerton, J. W., Lewandowski, Z., DeBeer, D., Caldwell, D., Korber, D., and James, G. (1994). Biofilms, the customized microniche. *J. Bacteriol.* 176, 2137–2142. doi: 10.1128/jb.176.8.2137-2142.1994

Curtis, M. M., Russell, R., Moreira, C. G., Adebesin, A. M., Wang, C. G., Williams, N. S., et al. (2014). QseC inhibitors as an antivirulence approach for gram-negative pathogens. *mBio* 5:e2165-14. doi: 10.1128/mBio.02165-2114

D'Angelo, F., Baldelli, V., Halliday, N., Pantalone, P., Polticelli, F., Fiscarelli, E., et al. (2018). Identification of FDA-Approved Drugs as Antivirulence Agents Targeting the pqs Quorum-Sensing System of *Pseudomonas aeruginosa*. *Antimicrob. Agents Chemother.* 62:e01296-18.

Daniels, R., Vanderleyden, J., and Michiels, J. (2004). Quorum sensing and swarming migration in bacteria. *FEMS Microbiol. Rev.* 28, 261–289. doi: 10.1016/j.femsre.2003.09.004

Ding, X., Yin, B., Qian, L., Zeng, Z., Yang, Z., Li, H., et al. (2011). Screening for novel quorum-sensing inhibitors to interfere with the formation of *Pseudomonas aeruginosa* biofilm. *J. Med. Microbiol.* 60(Pt 12), 1827–1834. doi: 10.1099/jmm.0.024166-24160

Donlan, R. M. (2002). Biofilms: microbial life on surfaces. *Emerg. Infect. Dis.* 8, 881–890. doi: 10.3201/eid0809.020063

dos Reis Ponce, A., Martins, M. L., de Araujo, E. F., Mantovani, H. C., and Vanetti, M. C. (2012). AiiA quorum-sensing quenching controls proteolytic activity and biofilm formation by *Enterobacter cloacae*. *Curr. Microbiol.* 65, 758–763. doi: 10.1007/s00284-012-0226-220

Dusane, D. H., Zinjarde, S. S., Venugopalan, V. P., McLean, R. J., Weber, M. M., and Rahman, P. K. (2010). Quorum sensing: implications on rhamnolipid biosurfactant production. *Biotechnol. Genet. Eng. Rev.* 27, 159–184. doi: 10.1080/02648725.2010.10648149

El-Shaer, S., Shaaban, M., Barwa, R., and Hassan, R. (2016). Control of quorum sensing and virulence factors of *Pseudomonas aeruginosa* using phenylalanine arginyl beta-naphthylamide. *J. Med. Microbiol.* 65, 1194–1204. doi: 10.1099/jmm.0.000327

Engebrecht, J., Nealson, K., and Silverman, M. (1983). Bacterial bioluminescence: isolation and genetic analysis of functions from *Vibrio fischeri*. *Cell* 32, 773–781. doi: 10.1016/0092-8674(83)90063-90066

Engebrecht, J., and Silverman, M. (1984). Identification of genes and gene products necessary for bacterial bioluminescence. *Proc. Natl. Acad. Sci. U.S.A.* 81, 4154–4158. doi: 10.1073/pnas.81.13.4154

Guo, M., Fang, Z., Sun, L., Sun, D., Wang, Y., Li, C., et al. (2018). Regulation of thermostable direct hemolysin and biofilm formation of *Vibrio parahaemolyticus* by Quorum-Sensing Genes luxM and luxS. *Curr. Microbiol.* 75, 1190–1197. doi: 10.1007/s00284-018-1508-y

Hammer, B. K., and Bassler, B. L. (2003). Quorum sensing controls biofilm formation in *Vibrio cholerae*. *Mol. Microbiol.* 50, 101–104. doi: 10.1046/j.1365-2958.2003.03688.x

Hammer, B. K., and Bassler, B. L. (2007). Regulatory small RNAs circumvent the conventional quorum sensing pathway in pandemic *Vibrio cholerae*. *Proc. Natl. Acad. Sci. U.S.A.* 104, 11145–11149. doi: 10.1073/pnas.0703860104

Hernando-Amado, S., Alcalde-Rico, M., Gil-Gil, T., Valverde, J. R., and Martinez, J. L. (2020). Naringenin Inhibition of the *Pseudomonas aeruginosa* Quorum

Sensing Response Is Based on Its Time-Dependent Competition With N-(3-Oxo-dodecanoyl)-L-homoserine Lactone for LasR Binding. *Front. Mol. Biosci.* 7:25. doi: 10.3389/fmolb.2020.00025

Hoiby, N., Bjarnsholt, T., Givskov, M., Molin, S., and Ciofu, O. (2010). Antibiotic resistance of bacterial biofilms. *Int. J. Antimicrob. Agents* 35, 322–332. doi: 10.1016/j.ijantimicag.2009.12.011

Imperi, F., Massai, F., Ramachandran Pillai, C., Longo, F., Zennaro, E., Rampioni, G., et al. (2013). New life for an old drug: the anthelmintic drug niclosamide inhibits *Pseudomonas aeruginosa* quorum sensing. *Antimicrob. Agents Chemother.* 57, 996–1005. doi: 10.1128/AAC.01952-1912

Irie, Y., and Parsek, M. R. (2008). Quorum sensing and microbial biofilms. *Curr. Top. Microbiol. Immunol.* 322, 67–84. doi: 10.1007/978-3-540-75418-3_4

Khan, F., Javaid, A., and Kim, Y. M. (2019). Functional diversity of quorum sensing receptors in pathogenic bacteria: interspecies, intraspecies and interkingdom level. *Curr. Drug Targets* 20, 655–667. doi: 10.2174/1389450120666181123123333

Khan, F., Lee, J. W., Javaid, A., Park, S. K., and Kim, Y. M. (2020a). Inhibition of biofilm and virulence properties of *Pseudomonas aeruginosa* by sub-inhibitory concentrations of aminoglycosides. *Microb. Pathog.* 146:104249. doi: 10.1016/j.micpath.2020.104249

Khan, F., Pham, D. T. N., and Kim, Y. M. (2020b). Alternative strategies for the application of aminoglycoside antibiotics against the biofilm-forming human pathogenic bacteria. *Appl. Microbiol. Biotechnol.* 104, 1955–1976. doi: 10.1007/s00253-020-10360-10361

Khan, F., Pham, D. T. N., Oloketuyi, S. F., and Kim, Y. M. (2020c). Regulation and controlling the motility properties of *Pseudomonas aeruginosa*. *Appl. Microbiol. Biotechnol.* 104, 33–49. doi: 10.1007/s00253-019-10201-w

Kim, C. S., Gatsios, A., Cuesta, S., Lam, Y. C., Wei, Z., Chen, H., et al. (2020). Characterization of autoinducer-3 structure and biosynthesis in *E. coli*. *ACS Cent. Sci.* 6, 197–206. doi: 10.1021/acscentsci.9b01076

Kim, J. H., Choi, D. C., Yeon, K. M., Kim, S. R., and Lee, C. H. (2011). Enzyme-immobilized nanofiltration membrane to mitigate biofouling based on quorum quenching. *Environ. Sci. Technol.* 45, 1601–1607. doi: 10.1021/es103483j

Kleerebezem, M., Quadri, L. E., Kuipers, O. P., and de Vos, W. M. (1997). Quorum sensing by peptide pheromones and two-component signal-transduction systems in Gram-positive bacteria. *Mol. Microbiol.* 24, 895–904. doi: 10.1046/j.1365-2958.1997.4251782.x

Koch, G., Nadal-Jimenez, P., Reis, C. R., Muntendam, R., Bokhove, M., Melillo, E., et al. (2014). Reducing virulence of the human pathogen *Burkholderia* by altering the substrate specificity of the quorum-quenching acylase PvdQ. *Proc. Natl. Acad. Sci. U.S.A.* 111, 1568–1573. doi: 10.1073/pnas.1311263111

Kose-Mutlu, B., Ergon-Can, T., Koyuncu, I., and Lee, C. H. (2019). Quorum quenching for effective control of biofouling in membrane bioreactor: a comprehensive review of approaches, applications, and challenges. *Environ. Eng. Res.* 24, 543–558. doi: 10.4491/eer.2018.380

Kusada, H., Tamaki, H., Kamagata, Y., Hanada, S., and Kimura, N. (2017). A Novel Quorum-Quenching N-Acylhomoserine lactone acylase from *Acidovorax* sp. Strain MR-S7 Mediates Antibiotic Resistance. *Appl. Environ. Microbiol.* 83:e00080-17. doi: 10.1128/AEM.00080-17

Lee, J., and Zhang, L. (2015). The hierarchy quorum sensing network in *Pseudomonas aeruginosa*. *Protein Cell* 6, 26–41. doi: 10.1007/s13238-014-0100-x

Lee, K., Yu, H. R., Zhang, X. L., and Choo, K. H. (2018). Quorum sensing and quenching in membrane bioreactors: opportunities and challenges for biofouling control. *Bioresour. Technol.* 270, 656–668. doi: 10.1016/j.biortech.2018.09.019

Lewis, K. (2001). Riddle of biofilm resistance. *Antimicrob. Agents Chemother.* 45, 999–1007. doi: 10.1128/AAC.45.4.999-1007.2001

Li, H., Li, X., Wang, Z., Fu, Y., Ai, Q., Dong, Y., et al. (2015). Autoinducer-2 regulates *Pseudomonas aeruginosa* PAO1 biofilm formation and virulence production in a dose-dependent manner. *BMC Microbiol.* 15:192. doi: 10.1186/s12866-015-0529-y

Li, J., Attila, C., Wang, L., Wood, T. K., Valdes, J. J., and Bentley, W. E. (2007). Quorum sensing in *Escherichia coli* is signaled by AI-2/LsrR: effects on small RNA and Biofilm architecture. *J. Bacteriol.* 189, 6011–6020. doi: 10.1128/Jb.00014-17

Ma, L., Feng, S., Fuente-Nunez, C., Hancock, R. E. W., and Lu, X. (2018). Development of molecularly imprinted polymers to block quorum sensing and inhibit bacterial biofilm formation. *ACS Appl. Mater. Interfaces* 10, 18450–18457. doi: 10.1021/acsami.8b01584

Ma, R., Qiu, S., Jiang, Q., Sun, H., Xue, T., Cai, G., et al. (2017). AI-2 quorum sensing negatively regulates rbf expression and biofilm formation in *Staphylococcus aureus*. *Int. J. Med. Microbiol.* 307, 257–267. doi: 10.1016/j.ijmm.2017.03.003

Nealson, K. H., and Hastings, J. W. (1979). Bacterial bioluminescence: its control and ecological significance. *Microbiol. Rev.* 43, 496–518. doi: 10.1128/mmbr.43.4.496-518.1979

Oh, H. S., and Lee, C. H. (2018). Origin and evolution of quorum quenching technology for biofouling control in MBRs for wastewater treatment. *J. Membr. Sci.* 554, 331–345. doi: 10.1016/j.memsci.2018.03.019

Oh, M. H., and Choi, C. H. (2015). Role of LuxIR Homologue AnoIR in *Acinetobacter nosocomialis* and the effect of virstatin on the expression of anoR Gene. *J. Microbiol. Biotechnol.* 25, 1390–1400. doi: 10.4014/jmb.1504.04069

O'Loughlin, C. T., Miller, L. C., Siryaporn, A., Drescher, K., Semmelhack, M. F., and Bassler, B. L. (2013). A quorum-sensing inhibitor blocks *Pseudomonas aeruginosa* virulence and biofilm formation. *Proc. Natl. Acad. Sci. U.S.A.* 110, 17981–17986. doi: 10.1073/pnas.1316981110

Ozcan, S. S., Dieser, M., Parker, A. E., Balasubramanian, N., and Foreman, C. M. (2019). Quorum sensing inhibition as a promising method to control biofilm growth in metalworking fluids. *J. Indus. Microbiol. Biotechnol.* 46, 1103–1111. doi: 10.1007/s10295-019-02181-7

Ozcelik, B., Ho, K. K. K., Glattauer, V., Willcox, M., Kumar, N., and Thissen, H. (2017). Poly(ethylene glycol)-Based Coatings Combining Low-Biofouling and Quorum-Sensing Inhibiting Properties to Reduce Bacterial Colonization. *ACS Biomater. Sci. Eng.* 3, 78–87. doi: 10.1021/acsbiomaterials.6b00579

Paczkowski, J. E., Mukherjee, S., McCready, A. R., Cong, J. P., Aquino, C. J., Kim, H., et al. (2017). Flavonoids suppress *Pseudomonas aeruginosa* virulence through allosteric inhibition of quorum-sensing receptors. *J. Biol. Chem.* 292, 4064–4076.

Painter, K. L., Krishna, A., Wigneshweraraj, S., and Edwards, A. M. (2014). What role does the quorum-sensing accessory gene regulator system play during *Staphylococcus aureus* bacteremia? *Trends Microbiol.* 22, 676–685. doi: 10.1016/j.tim.2014.09.002

Park, J., Jagasia, R., Kaufmann, G. F., Mathison, J. C., Ruiz, D. I., Moss, J. A., et al. (2007). Infection control by antibody disruption of bacterial quorum sensing signaling. *Chem. Biol.* 14, 1119–1127. doi: 10.1016/j.chembiol.2007.08.013

Park, J. S., Ryu, E. J., Li, L. Z., Choi, B. K., and Kim, B. M. (2017). New bicyclic brominated furanones as potent autoinducer-2 quorum-sensing inhibitors against bacterial biofilm formation. *Eur. J. Med. Chem.* 137, 76–87. doi: 10.1016/j.ejmech.2017.05.037

Peppoloni, S., Pericolini, E., Colombari, B., Pinetti, D., Cermelli, C., Fini, F., et al. (2020). The beta-lactamase inhibitor boronic acid derivative SM23 as a new anti-*Pseudomonas aeruginosa* Biofilm. *Front. Microbiol.* 11:35. doi: 10.3389/fmicb.2020.00035

Proctor, C. R., McCarron, P. A., and Ternan, N. G. (2020). Furanone quorum-sensing inhibitors with potential as novel therapeutics against *Pseudomonas aeruginosa*. *J. Med. Microbiol.* 69, 195–206. doi: 10.1099/jmm.0.001144

Pustelny, C., Albers, A., Buldt-Karentzopoulos, K., Parschat, K., Chhabra, S. R., Camara, M., et al. (2009). Dioxygenase-mediated quenching of quinolone-dependent quorum sensing in *Pseudomonas aeruginosa*. *Chem. Biol.* 16, 1259–1267. doi: 10.1016/j.chembiol.2009.11.013

Sethupathy, S., Prasath, K. G., Ananthi, S., Mahalingam, S., Balan, S. Y., and Pandian, S. K. (2016). Proteomic analysis reveals modulation of iron homeostasis and oxidative stress response in *Pseudomonas aeruginosa* PAO1 by curcumin inhibiting quorum sensing regulated virulence factors and biofilm production. *J. Proteomics* 145, 112–126. doi: 10.1016/j.jprot.2016.04.019

Shi, X. M., and Zhu, X. N. (2009). Biofilm formation and food safety in food industries. *Trends Food Sci. Technol.* 20, 407–413. doi: 10.1016/j.tifs.2009.01.054

Singh, S., and Bhatia, S. (2018). In silico identification of albendazole as a quorum sensing inhibitor and its in vitro verification using CviR and LasB receptors based assay systems. *Bioimpacts* 8, 201–209. doi: 10.15171/bi.2018.23

Sio, C. F., Otten, L. G., Cool, R. H., Diggle, S. P., Braun, P. G., Bos, R., et al. (2006). Quorum quenching by an N-acyl-homoserine lactone acylase from *Pseudomonas aeruginosa* PAO1. *Infect. Immun.* 74, 1673–1682. doi: 10.1128/IAI.74.3.1673-1682.2006

Slock, J., VanRiet, D., Kolibachuk, D., and Greenberg, E. P. (1990). Critical regions of the Vibrio fischeri luxR protein defined by mutational analysis. *J. Bacteriol.* 172, 3974–3979. doi: 10.1128/jb.172.7.3974-3979.1990

Solano, C., Echeverz, M., and Lasa, I. (2014). Biofilm dispersion and quorum sensing. *Curr. Opin. Microbiol.* 18, 96–104. doi: 10.1016/j.mib.2014.02.008

Sperandio, V., Torres, A. G., Jarvis, B., Nataro, J. P., and Kaper, J. B. (2003). Bacteria-host communication: the language of hormones. *Proc. Natl. Acad. Sci. U.S.A.* 100, 8951–8956. doi: 10.1073/pnas.1537100100

Sperandio, V., Torres, A. G., and Kaper, J. B. (2002). Quorum sensing *Escherichia coli* regulators B and C (QseBC): a novel two-component regulatory system involved in the regulation of flagella and motility by quorum sensing in *E. coli*. *Mol. Microbiol.* 43, 809–821. doi: 10.1046/j.1365-2958.2002.02803.x

Stevens, A. M., Dolan, K. M., and Greenberg, E. P. (1994). Synergistic binding of the *Vibrio fischeri* LuxR transcriptional activator domain and RNA polymerase to the lux promoter region. *Proc. Natl. Acad. Sci. U.S.A.* 91, 12619–12623. doi: 10.1073/pnas.91.26.12619

Stewart, P. S. (2002). Mechanisms of antibiotic resistance in bacterial biofilms. *Int. J. Med. Microbiol.* 292, 107–113. doi: 10.1078/1438-4221-4196

Sturme, M. H., Kleerebezem, M., Nakayama, J., Akkermans, A. D., Vaugha, E. E., and de Vos, W. M. (2002). Cell to cell communication by autoinducing peptides in gram-positive bacteria. *Antonie Van Leeuwenhoek* 81, 233–243. doi: 10.1023/a:1020522919555

Sully, E. K., Malachowa, N., Elmore, B. O., Alexander, S. M., Femling, J. K., Gray, B. M., et al. (2014). Selective chemical inhibition of agr quorum sensing in Staphylococcus aureus promotes host defense with minimal impact on resistance. *PLoS Pathog.* 10:e1004174. doi: 10.1371/journal.ppat.1004174

Surette, M. G., and Bassler, B. L. (1998). Quorum sensing in *Escherichia coli* and *Salmonella typhimurium*. *Proc. Natl. Acad. Sci. U.S.A.* 95, 7046–7050. doi: 10.1073/pnas.95.12.7046

Sutherland, I. W. (2001). The biofilm matrix–an immobilized but dynamic microbial environment. *Trends Microbiol.* 9, 222–227. doi: 10.1016/s0966-842x(01)02012-2011

Utari, P. D., Setroikromo, R., Melgert, B. N., and Quax, W. J. (2018). PvdQ quorum quenching acylase attenuates *Pseudomonas aeruginosa* virulence in a mouse model of pulmonary infection. *Front. Cell Infect. Microbiol.* 8:119. doi: 10.3389/fcimb.2018.00119

Vinothkannan, R., Tamizh, M. M., Raj, C. D., and Princy, S. A. (2018). Fructose furoic acid ester: an effective quorum sensing inhibitor against uropathogenic *Escherichia coli*. *Bioorganic Chem.* 79, 310–318. doi: 10.1016/j.bioorg.2018.05.009

Vuong, C., Durr, M., Carmody, A. B., Peschel, A., Klebanoff, S. J., and Otto, M. (2004). Regulated expression of pathogen-associated molecular pattern molecules in Staphylococcus epidermidis: quorum-sensing determines pro-inflammatory capacity and production of phenol-soluble modulins. *Cell Microbiol.* 6, 753–759. doi: 10.1111/j.1462-5822.2004.00401.x

Vuong, C., Saenz, H. L., Gotz, F., and Otto, M. (2000). Impact of the agr quorum-sensing system on adherence to polystyrene in *Staphylococcus aureus*. *J. Infect. Dis.* 182, 1688–1693. doi: 10.1086/317606

Wade, D. S., Calfee, M. W., Rocha, E. R., Ling, E. A., Engstrom, E., Coleman, J. P., et al. (2005). Regulation of *Pseudomonas quinolone* signal synthesis in *Pseudomonas aeruginosa*. *J. Bacteriol.* 187, 4372–4380. doi: 10.1128/JB.187.13.4372-4380.2005

Walters, M., and Sperandio, V. (2006). Quorum sensing in *Escherichia coli* and *Salmonella*. *Int. J. Med. Microbiol.* 296, 125–131. doi: 10.1016/j.ijmm.2006.01.041

Wang, J., Lin, J., Zhang, Y., Zhang, J., Feng, T., Li, H., et al. (2019). Activity improvement and vital amino acid identification on the marine-derived quorum quenching enzyme momL by protein engineering. *Mar. Drugs* 17:300. doi: 10.3390/md17050300

Wang, Y., Zhang, W., Wu, Z. F., Zhu, X. L., and Lu, C. P. (2011). Functional analysis of luxS in *Streptococcus suis* reveals a key role in biofilm formation and virulence. *Vet. Microbiol.* 152, 151–160. doi: 10.1016/j.vetmic.2011.04.029

Waters, C. M., and Bassler, B. L. (2005). Quorum sensing: cell-to-cell communication in bacteria. *Annu. Rev. Cell Dev. Biol.* 21, 319–346. doi: 10.1146/annurev.cellbio.21.012704.131001

Wilder, C. N., Diggle, S. P., and Schuster, M. (2011). Cooperation and cheating in *Pseudomonas aeruginosa*: the roles of the las, rhl and pqs quorum-sensing systems. *ISME J.* 5, 1332–1343. doi: 10.1038/ismej.2011.13

Williams, P. (2007). Quorum sensing, communication and cross-kingdom signalling in the bacterial world. *Microbiology* 153(Pt 12), 3923–3938. doi: 10.1099/mic.0.2007/012856-12850

Winzer, K., Falconer, C., Garber, N. C., Diggle, S. P., Camara, M., and Williams, P. (2000). The *Pseudomonas aeruginosa* lectins PA-IL and PA-IIL are controlled by quorum sensing and by RpoS. *J. Bacteriol.* 182, 6401–6411. doi: 10.1128/jb.182.22.6401-6411.2000

Yang, S. J., Abdel-Razek, O. A., Cheng, F., Bandyopadhyay, D., Shetye, G. S., Wang, G. R., et al. (2014). Bicyclic brominated furanones: a new class of quorum sensing modulators that inhibit bacterial biofilm formation. *Bioorgan. Med. Chem.* 22, 1313–1317. doi: 10.1016/j.bmc.2014.01.004

Yang, Y., Li, W., Hou, B., and Zhang, C. (2018). Quorum sensing LuxS/autoinducer-2 inhibits Enterococcus faecalis biofilm formation ability. *J. Appl. Oral. Sci.* 26:e20170566. doi: 10.1590/1678-7757-2017-2566

Yarwood, J. M., Bartels, D. J., Volper, E. M., and Greenberg, E. P. (2004). Quorum sensing in *Staphylococcus aureus* biofilms. *J. Bacteriol.* 186, 1838–1850. doi: 10.1128/jb.186.6.1838-1850.2004

Yeon, K. M., Cheong, W. S., Oh, H. S., Lee, W. N., Hwang, B. K., Lee, C. H., et al. (2009a). Quorum sensing: a new biofouling control paradigm in a membrane bioreactor for advanced wastewater treatment. *Environ. Sci. Technol.* 43, 380–385. doi: 10.1021/es8019275

Yeon, K. M., Lee, C. H., and Kim, J. (2009b). Magnetic enzyme carrier for effective biofouling control in the membrane bioreactor based on enzymatic quorum quenching. *Environ. Sci. Technol.* 43, 7403–7409. doi: 10.1021/es901323k

Conflict of Interest: The authors declare that the research was conducted in the absence of any commercial or financial relationships that could be construed as a potential conflict of interest.

frontiers in Microbiology

REVIEW
published: 21 October 2020
doi: 10.3389/fmicb.2020.593215

Resistance Mechanisms to Antimicrobial Peptides in Gram-Positive Bacteria

*Lucas Assoni, Barbara Milani, Marianna Ribeiro Carvalho, Lucas Natanael Nepomuceno, Natalha Tedeschi Waz, Maria Eduarda Souza Guerra, Thiago Rojas Converso and Michelle Darrieux**

Laboratório de Biologia Molecular de Microrganismos, Universidade São Francisco, Bragança Paulista, Brazil

With the alarming increase of infections caused by pathogenic multidrug-resistant bacteria over the last decades, antimicrobial peptides (AMPs) have been investigated as a potential treatment for those infections, directly through their lytic effect or indirectly, due to their ability to modulate the immune system. There are still concerns regarding the use of such molecules in the treatment of infections, such as cell toxicity and host factors that lead to peptide inhibition. To overcome these limitations, different approaches like peptide modification to reduce toxicity and peptide combinations to improve therapeutic efficacy are being tested. Human defense peptides consist of an important part of the innate immune system, against a myriad of potential aggressors, which have in turn developed different ways to overcome the AMPs microbicidal activities. Since the antimicrobial activity of AMPs vary between Gram-positive and Gram-negative species, so do the bacterial resistance arsenal. This review discusses the mechanisms exploited by Gram-positive bacteria to circumvent killing by antimicrobial peptides. Specifically, the most clinically relevant genera, *Streptococcus spp.*, *Staphylococcus spp.*, *Enterococcus spp.* and Gram-positive bacilli, have been explored.

Keywords: antimicrobial peptides, gram-positive, AMP, resistance, streptococci

OPEN ACCESS

Edited by:
Rodolfo García-Contreras, National Autonomous University of Mexico, Mexico

Reviewed by:
Cesar de la Fuente-Nunez, University of Pennsylvania, United States
Lucinda Janete Bessa, LAQV Network of Chemistry and Technology, Portugal

****Correspondence:***
Michelle Darrieux
sampaiomichelle@uol.com.br

Specialty section:
This article was submitted to Antimicrobials, Resistance and Chemotherapy, a section of the journal Frontiers in Microbiology

Received: *10 August 2020*
Accepted: *03 September 2020*
Published: *21 October 2020*

Citation:
Assoni L, Milani B, Carvalho MR, Nepomuceno LN, Waz NT, Guerra MES, Converso TR and Darrieux M (2020) Resistance Mechanisms to Antimicrobial Peptides in Gram-Positive Bacteria. Front. Microbiol. 11:593215. doi: 10.3389/fmicb.2020.593215

INTRODUCTION

Antimicrobial peptides, also known as host defense peptides (HDPs), are found in most life forms, being part of the innate immune system against pathogenic bacteria, fungi, parasites and viruses (Zasloff, 2002; Torrent et al., 2012). Due to the alarming increase in antimicrobial resistance to the commonly used drugs around the world and the lack in discovery of new drugs and alternative treatments, there is a growing concern among the scientific community that in a near future, the current clinical approaches might not be able to deal effectively with microbial infections. Therefore, AMPs have been suggested as an alternative therapeutic strategy, in combination or as a replacement for traditional antibiotics.

The development of antimicrobial resistance against AMPs is not as prevalent when compared to antibiotics, since AMPs targets are diverse and changes can interfere with the functionality of the cell, especially since the cell membrane is the main point of attack (Mahlapuu et al., 2016). However, bacteria can evolve quickly and grow resistant against AMPs *in vitro* (Andersson et al., 2016). Another approach in the use of AMPs is combination with traditional antibiotics, since both have shown to synergize, reducing microbial resistance (Moravej et al., 2018). A few AMPs

have been translated into the clinic; polymyxins B, bacitracin, gramicidin S, daptomycin and vancomycin have been used for treatment of several types of bacteria. However, a number of questions are yet to be answered, such as the toxicity and stability *in vivo* of many peptides, as thoroughly reviewed (Jenssen et al., 2006; Vaara, 2009; Yount and Yeaman, 2012). The contact with human cells, such as erythrocytes, was shown to inhibit the activity of AMPs (Starr et al., 2016). Furthermore, physiological conditions of the host can interfere with the effectiveness of these molecules, along with the peptide's pharmacokinetics (Jenssen et al., 2006). Though these are significant challenges, AMPs remain an interesting strategy and still expanding field, as many studies have tried molecular engineering as an approach to solve the concerns cited above. One such example is the production of synthetic D-enantiomeric peptides to avoid proteolytic degradation (de la Fuente-Nunez et al., 2015). So far, over three thousand different peptides have been identified, distributed among six different kingdoms (animalia, archaea, bacteria, fungi, plantae, protist), according to the Antimicrobial Peptide Database (APD) (aps.unmc.edu/AP/) (Wang et al., 2016). In humans, over 130 peptides have been described, and while the vast majority has been tested as potential antimicrobial drugs, AMPs have a larger impact than just direct antimicrobial effects, actively engaging with the host immune system, modulating its activity, promoting chemotaxis and cell recruitment, meddling with the inflammatory and wound healing pathways, among many different functions (Hancock et al., 2016; Mahlapuu et al., 2016; Haney et al., 2017). AMPs were also shown to have an anticarcinogenic effect, as extensively reviewed (Wang, 2014; Hancock et al., 2016; Haney et al., 2017; Yavari et al., 2018; Wang et al., 2019; Kunda, 2020).

An important group of antimicrobial peptides is the cathelicidins. The human representant of this group is LL-37, a cationic, amphipathic peptide, composed by 37 amino acid residues. Its precursor, hCAP18, was first isolated in neutrophils (Cowland et al., 1995; Sørensen et al., 1997) but can also be found in other cells, such as keratinocytes and mast cells (Frohm et al., 1997; Di Nardo et al., 2003). After its cleavage by neutrophil proteases, the peptide acquires its functional form (Sørensen et al., 2001). LL-37 effects have been extensively investigated, and include direct antimicrobial activity and immune modulation (Fabisiak et al., 2016; Mahlapuu et al., 2016; Xhindoli et al., 2016; Haney et al., 2017; Chen et al., 2018; Moravej et al., 2018). Cathelicidins are also found in many vertebrates, including farm animals, birds, reptiles and fish (Kościuczuk et al., 2012). Indolicidin, a 13 amino acid peptide expressed in bovine neutrophils, has antimicrobial activity against Gram-positive and Gram-negative bacteria (van Harten et al., 2018).

Another class of cationic and amphipathic antimicrobial peptides is the defensins, which can be divided in three main groups: α-defensins, β-defensins and θ-defensins. In humans, only α- and β-defensins can be found, while θ-defensins are present exclusively in Old World primates (Nguyen et al., 2003). Among human α-defensins, there are six peptides expressed: Human Neutrophil Peptide (HNP) 1 through 4 and Human Defensins (HD) 5 and 6. α-defensins can be found in many different tissues such as the gastrointestinal and respiratory epithelia, female reproductive tract and blood cells (Hancock et al., 2016). These peptides display direct antimicrobial activities and immunomodulatory effects, including chemotaxis (Wang, 2014; Moravej et al., 2018; Xu and Lu, 2020). β-defensins are expressed mainly in epithelial cells but also in monocytes, macrophages and dendritic cells (Hancock et al., 2016) and have an important role regulating the host microbiome (Meade and O'Farrelly, 2018; Xu and Lu, 2020).

Human Lactoferrin (hLF) is an 80 kDa bilobal glycoprotein, present in bodily fluids and neutrophils, which acts in the transport of metal ions, especially ferric iron (Fe^{3+}) (Vogel, 2012). hLF displays a bacteriostatic effect through iron chelation, decreasing the extracellular concentration of this ion available to the microorganism. Furthermore, the iron-free molecule, Apolactoferrin (ApoLF), is able to interact with microbial cellular membranes, undergoing subsequent proteolysis which results in release of smaller and more potent cationic peptides, especially those found in the N-terminal lobe: Lactoferricin (LFcin), Lactoferrampin (LFampin) and LF1-11 (Sinha et al., 2013).

Human lysozyme, also named N-acetylmuramide glycanhydrolase, is often cited as the first antimicrobial protein discovered and is extensively used in industry (Ercan and Demirci, 2016; Wu T. et al., 2019). Lysozyme is a 14 kDa enzyme that binds to cell wall peptidoglycans, cleaving the links between different sugars, thus inducing cell rupture (Nawrocki et al., 2014; Wang, 2014). Similarly, to lactoferrin, peptides derived from the cleavage of lysozyme exhibit antimicrobial activity against Gram-positive and Gram-negative bacteria (Ibrahim et al., 2001, 2011; Mine et al., 2004; Hunter et al., 2005; Carrillo et al., 2018).

With an array of antimicrobial peptides being produced by different human cells, bacteria have developed a number of strategies to prevent AMP binding, to avoid their lytic effects or to degrade the peptides, in order to thrive in the human host. In the next sections, the different mechanisms employed by Gram-positive bacteria to circumvent AMP action will be explored. **Table 1** and **Figure 1** summarize the resistance mechanisms employed by these bacteria.

AMP RESISTANCE MECHANISMS IN PATHOGENIC GRAM-POSITIVE BACTERIA

Gram-Positive Bacilli

Gram-positive bacilli include some pathogenic, anaerobic spore-forming species, such as *Clostridium spp.*, *Listeria monocytogenes*, *Bacillus anthracis*, and *Bacillus cereus* (Chukwu et al., 2016; Schlech, 2019).

The genus *Clostridium* is composed of about 15 pathogenic species, of which the most common are *Clostridium difficile, Clostridium perfringens, Clostridium tetani*, and *Clostridium botulinum*. Although these species are similar, the pathologies caused by them are diverse (Fisher et al., 2005). *C. tetani* produces the tetanus neurotoxin (TeNT) that causes neurological disease (tetanus), characterized by muscle spasms and spastic

TABLE 1 | AMP resistance mechanisms in Gram-positive bacteria.

Resistance mechanisms	Species						References
Modifications in membrane/cell wall structure	**Gram-positive bacilli**	***Staphylococcus***	***Enterococcus***	**GAS**	**GBS**	**Pneumococci**	
D-alanylation of the membrane	X	X	X	X		X	Peschel et al., 1999; Poyart et al., 2001, 2003; Abachin et al., 2002; Frick et al., 2003; Cao and Helmann, 2004; Kristian et al., 2005; May et al., 2005; Fabretti et al., 2006; Fisher et al., 2006; Kovacs et al., 2006; Palumbo et al., 2006; Walter et al., 2007; Beiter et al., 2008; Abi Khattar et al., 2009; Cox et al., 2009; Jann et al., 2009; McBride and Sonenshein, 2011a; Saar-Dover et al., 2012; Simanski et al., 2013; Carvalho et al., 2015; Wydau-Dematteis et al., 2015; Kamar et al., 2017; Hirt et al., 2018
Lysinylation of the membrane	X	X	X				Oku et al., 2004; Staubitz et al., 2004; Kraus and Peschel, 2006; Thedieck et al., 2006; Ernst et al., 2009; Samant et al., 2009; Bao et al., 2012; Shireen et al., 2013; Kumariya et al., 2015; Nasser et al., 2019
O-acetylation of the peptidoglycan	X					X	Crisostomo et al., 2006; Pfeffer et al., 2006; Hebert et al., 2007; Aubry et al., 2011; Laaberki et al., 2011; Rae et al., 2011
N-deacetylation of the peptidoglycan	X					X	Vollmer and Tomasz, 2000; Psylinakis et al., 2005; Boneca et al., 2007
Glycosylation of the wall teichoic acids	X						Meireles et al., 2020
Deacetylation of the N-acetylmuramic acid	X		X				Fukushima et al., 2005; Popowska et al., 2009; Benachour et al., 2012; Kobayashi et al., 2012; Grifoll-Romero et al., 2019
Alterations in the membrane composition	X	X	X				Ming and Daeschel, 1993; Maisnier-Patin and Richard, 1996; Mazzotta and Montville, 1997; Verheul et al., 1997; Crandall and Montville, 1998; Dhawan et al., 1998; Bayer et al., 2000; Tsuda et al., 2002; Xue et al., 2005; Cremniter et al., 2006; Naghmouchi et al., 2006, 2007; Hachmann et al., 2011; Mishra et al., 2011, 2012; Kandaswamy et al., 2013
Alterations in the transmembrane pH and potential	X						Bonnet et al., 2006
Alterations in capsular polysaccharides						X	Beiter et al., 2008; Llobet et al., 2008; van der Windt et al., 2012; Geno et al., 2015; Kietzman et al., 2016; Bruce et al., 2018
Transport systems and efflux pumps							
Transport systems	X		X	X	X	X	Manson et al., 2004; Matos et al., 2009; Majchrzykiewicz et al., 2010; McBride and Sonenshein, 2011b; Suárez et al., 2013; Martinez et al., 2019; Rafei et al., 2020
AMP sequestration/ inactivation							
AMP sequestration		X			X		Braff et al., 2007; Maisey et al., 2008
Inactivation		X				X	Jin et al., 2004; Ren et al., 2004; Braff et al., 2007; Mukerji et al., 2012
Proteases and other proteins							
Inactivation/degradation		X	X	X			Schmidtchen et al., 2002; Sieprawska-Lupa et al., 2004; Sedgley et al., 2009; Nesuta et al., 2017; Hirt et al., 2018
Inhibitory molecules					X		Porta et al., 2019

(Continued)

TABLE 1 | continued

Resistance mechanisms	Species						References
Modifications in membrane/cell wall structure	**Gram-positive bacilli**	***Staphylococcus***	***Enterococcus***	**GAS**	**GBS**	**Pneumococci**	
AMP induced gene expression/repression							
Sigma factors	X		X				Robichon et al., 1997; Dalet et al., 2000; Palmer et al., 2009; Le Jeune et al., 2010; Guariglia-Oropeza and Helmann, 2011; Ho et al., 2011
Regulators	X	X	X		X	X	Dunman et al., 2001; Mascher et al., 2004; Mandin et al., 2005; Hyyryläinen et al., 2007; Meehl et al., 2007; Neoh et al., 2008; Dawid et al., 2009; Hachmann et al., 2009; Pietiäinen et al., 2009; Arias et al., 2011; Ho and Ellermeier, 2011; Boone and Tyrrell, 2012; Monniot et al., 2012; Yang et al., 2012, 2013, 2018; Bergholz et al., 2013; Khosa et al., 2013, 2016; Shaaly et al., 2013; Patel and Golemi-Kotra, 2015; Reyes et al., 2015; Wang et al., 2017; Xu and Lu, 2020
Transcriptome/proteome alterations	X					X	Majchrzykiewicz et al., 2010; McQuade et al., 2012; Mucke et al., 2020
Mannose phosphotransferase (Man-PTS) pathway	X		X				Ramnath et al., 2000; Héchard et al., 2001; Gravesen et al., 2002a,b; Vadyvaloo et al., 2004a,b; Diep et al., 2007; Tessema et al., 2009; Opsata et al., 2010; Kjos et al., 2011; Geldart and Kaznessis, 2017; Wu X. et al., 2019; Zasloff, 2002
Cell sensors		X			X	X	Hamilton et al., 2006; Jones et al., 2007; Li et al., 2007a,b; Yung and Murphy, 2012; Tran et al., 2013; Joo and Otto, 2015; Khan et al., 2019; Martínez-García et al., 2019

paralysis of the limb muscles (Chapeton-Montes et al., 2019). *C. botulinum* produces the potent botulinum neurotoxin that causes a serious and fatal neuro-paralytic disease in humans and animals (botulism) (Brunt et al., 2018). *C. difficile* is the main causative agent of nosocomial diarrhea and gastroenteritis, which can lead to the development of asymptomatic or symptomatic diseases. Infection by *C. difficile* (ICD) has been increasingly reported in the United States (Lessa et al., 2015; Crobach et al., 2020). *C. perfringens* can also cause acute diarrhea, with an estimated death toll of 200,000 each year in Nigeria according to The World Health Organization (WHO) (Fisher et al., 2005; Chukwu et al., 2016).

Listeria monocytogenes is a foodborne pathogen that causes gastroenteritis in immunocompromised individuals, children, pregnant women and the elderly (Schlech, 2019). *L. monocytogenes* outbreaks in South Africa have reported around 1000 confirmed cases and 200 deaths in 2017–2018; in the United States, the bacterium was the causative agent in 147 confirmed cases and 33 deaths, making it the third most expensive foodborne pathogen in 2010, after *C. botulinum* (de Noordhout et al., 2014; Desai et al., 2019).

B. anthracis is the causative agent of anthrax and can manifest in four ways, namely: cutaneous, inhalation, gastrointestinal or injectable (Hagan et al., 2018; Chen et al., 2020). *B. cereus* causes foodborne diseases, such as gastrointestinal, diarrhea and emesis (Yu et al., 2019; Huang et al., 2020). In 2016, the European Union (EU) reported about 413 food-borne outbreaks caused by *Bacillus* toxins that affected 6657 people, ranking it the second most common cause of food-borne outbreaks in that year (Fiedler et al., 2019).

Mechanisms of AMP Resistance in Gram-Positive Bacilli

Modifications in membrane/cell wall structure

Since one of the most important mechanisms of AMP-based killing is the interaction with the negatively charged membrane, changing the membrane composition is a strategy used by many bacteria to survive AMPs action. Among those changes, the insertion of D-alanine in the lipoteichoic acids, a process named D-alanylation, is used to reduce the negative membrane charge, thus inhibiting interaction with AMPs. This resistance mechanism is regulated by the *dlt* operon, and it has been described in several *Bacillus* species, such as *B. cereus* (Abi Khattar et al., 2009), *B. anthracis* (Fisher et al., 2006), *B. thuringiensis* (Kamar et al., 2017) and *B. subtilis* (Cao and Helmann, 2004; May et al., 2005), *L. monocytogenes* (Abachin et al., 2002; Carvalho et al., 2015), *C. difficile* (McBride and Sonenshein, 2011a), *C. butyricum* (Wydau-Dematteis et al., 2015), *Lactobacillus plantarum* (Palumbo et al., 2006), and *Lactobacillus reuteri* (Walter et al., 2007).

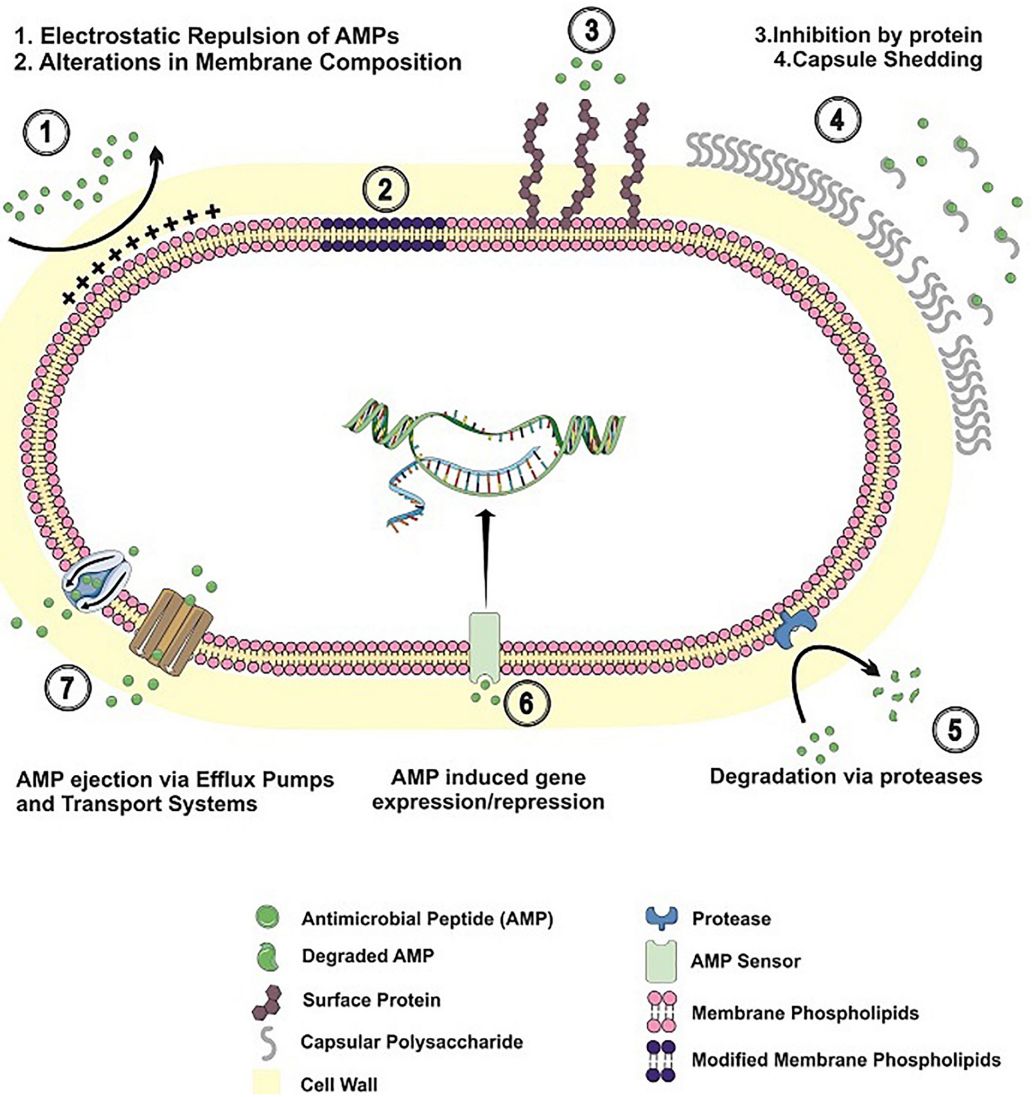

FIGURE 1 | Resistance mechanisms to antimicrobial peptides in Gram-positive bacteria. AMP resistance mechanisms employed by Gram-positive bacteria are shown, including alterations in cell envelope charge/composition; AMP inhibition by binding to surface proteins/released capsular polysaccharide; AMP degradation by bacterial proteases; bacterial adaptation to AMP challenge; AMP extrusion by efflux pumps and transport systems.

Another mechanism of envelope modification is called lysinylation of the membrane; it consists of addition of L-lysine to the phosphatidylglycerol. A protein called MprF is essential for membrane lysinylation. In *B. anthracis*, a strain deficient in MprF was more susceptible to LL-37 and HNP-1 when compared with the wild type strain (Samant et al., 2009). In *L. monocytogenes*, MprF was shown to be essential in protection against gallidermin, HNP-1 and HNP-2 (Thedieck et al., 2006).

Bacteria can modify cell wall components, such as the peptidoglycan. O-acetylation of the peptidoglycan is able to reduce killing by lysozyme in *L. monocytogenes* and *B. anthracis* (Aubry et al., 2011; Laaberki et al., 2011; Rae et al., 2011). Modifications on cell wall constituents also include the N-deacetylation of the peptidoglycan and the glycosylation of the wall teichoic acids, which in *L. monocytogenes* and *B. cereus* (Psylinakis et al., 2005) is crucial to protect against lysozyme (Boneca et al., 2007), LL-37 and CRAMP, a cathelicidins found in mice (Meireles et al., 2020).

In *B. subtilis*, deacetylation of the N-acetylmuramic acid by the protein PdaC confers resistance against lysozyme attack (Fukushima et al., 2005; Kobayashi et al., 2012; Grifoll-Romero et al., 2019). Another protein, PdgA described in *L. monocytogenes* is responsible for a similar resistance mechanism inducing N-acetylation of the peptidoglycan; a study by Popowska et al. (2009) showed that a *L. monocytogenes* strain lacking PdgA was more susceptible to lysozyme and mutanolysin.

Changes in lipid composition are able to interfere with AMPs action, as shown for *L. monocytogenes*, where different proportions of lipids are found in bacteriocin resistant strains (Ming and Daeschel, 1993; Mazzotta and Montville, 1997;

Verheul et al., 1997; Crandall and Montville, 1998; Naghmouchi et al., 2006, 2007). In *Listeria innocua*, changes in the proton motive force, via FoF1 ATPase, which altered the membrane potential were related with resistance to nisin (Maisnier-Patin and Richard, 1996; Bonnet et al., 2006).

A *B. subtilis* mutant resistant to daptomycin presents an irregular and more cationic membrane than the wild type, due to mutations in *pgsA* gene. The PgsA protein is responsible for the addition of phosphatidylglycerol to the membrane; in that sense, the diminished phosphatidylglycerol synthase function in the mutant strain was responsible for the increased resistance to daptomycin (Hachmann et al., 2011).

Transport systems and efflux pumps

A strategy employed by many bacterial species to evade antimicrobial host defense is by expelling the molecules using efflux pumps or ABC transporters. The same mechanism has been implicated in AMP expulsion (Bernard et al., 2007; Collins et al., 2010; McBride and Sonenshein, 2011b).

Subtilin is an antibiotic produced by *B. subtilis*; to avoid self-destruction, the bacterium possess an ABC transporter called SpaIFEG, this transporter ejects the subtilin to the extracellular environment (Stein et al., 2005). *B. licheniformis* is capable of producing bacitracin, an antibacterial peptide also produced by other *Bacilli*; similarly, to *B. subtilis*, the bacterium is immune to the antimicrobial due to the action of the BcrABC transporter, which ejects the AMP before it affects the producer cell (Podlesek et al., 1995; Ohki et al., 2003b).

In *C. difficile*, the *cpr* operon is responsible for the extracellular transport of peptides (McBride and Sonenshein, 2011b; Suárez et al., 2013). A similar ABC transporter, AnrAB, is also found in *L. monocytogenes*, able to export AMPs and antimicrobials, hence hindering their efficiency (Collins et al., 2010). *B. subtilis* also has similar detoxification systems, BceAB-RS, PsdRS-AB (also named Yvc-PQ-RS) and YxdJK-LM. These transporters are important for resistance and cell wall stress signaling against AMPs and antimicrobial drugs, such as bacitracin and lantibiotics (Mascher et al., 2003; Ohki et al., 2003a; Bernard et al., 2007; Rietkotter et al., 2008; Dintner et al., 2011; Staron et al., 2011; Kallenberg et al., 2013). The YtsCD ABC transporter, independently or in association with YwoA, is responsible for bacitracin resistance in *B. subtilis* (Bernard et al., 2003).

AMP induced gene expression/repression

Cell wall signaling can trigger the expression of many resistance-related genes such as sigma (σ) factors and global regulators in bacteria. In *L. monocytogenes*, sigma factors σ^B and σ^L and regulators such as VirR and LiaR regulate the expression of many virulence genes, such as the *dlt* operon, MprF – a protein responsible for adding L-lysine to membrane phospholipids– and ABC transporters, contributing to antimicrobial resistance (Mandin et al., 2005; Palmer et al., 2009; Samant et al., 2009; Bergholz et al., 2013). Lia-related regulators are also present in *B. subtilis*; in the presence of peptides that target the cell envelope, the stress sensor is activated and induces the expression of resistance genes such as LiaRS and other membrane modification genes (Mascher et al., 2004; Jordan et al., 2006; Hyyryläinen et al., 2007; Hachmann et al., 2009).

Clostridium difficile gene expression is also altered in the presence of AMPs. LL-37 induces overexpression of genes related to crucial functions; including those involved with cell wall and envelope homeostasis, ABC transporters and lysine metabolism (McQuade et al., 2012); similarly, bacitracin and lysozyme can alter the expression of extracellular σ factors (Ho and Ellermeier, 2011).

The mannose phosphotransferase (Man-PTS) pathway is an important resistance mechanism against bacteriocins. In *L. monocytogenes,* the activation of the Man-PTS pathway led to changes in metabolism, alteration of the membrane charge and addition of alanine in teichoic acids in strains resistant to class IIa bacteriocin (Ramnath et al., 2000; Gravesen et al., 2002a,b; Vadyvaloo et al., 2004a,b; Tessema et al., 2009; Wu X. et al., 2019). Although the Man-PTS pathway is a target for bacteriocins, in *Lactococcus lactis* and *Lactococcus garvieae,* it was shown to participate in resistance mechanisms, specifically in combination with LciA (Diep et al., 2007; Kjos et al., 2011; Daba et al., 2018; Tymoszewska et al., 2018). This pathway is also involved in bacteriocin resistance in *L. plantarum*, *Leuconostoc mesenteroides*, *Lactobacillus salivarius*, and *Lactobacillus acidophilus,* in combination with PedB, a protein that provides protection against the bacteriocin pediocin PA-1, in a complex, being able to avoid cell lysis by this AMP (Zhou et al., 2016). Similarly, in *Listeria innocua*, overexpression of *pedB* generated a more resistant phenotype (Monniot et al., 2012). In *L. innocua*, Man-PTS is regulated by a transcriptional activator (*lin0142*); inactivation of *lin0142* is related to resistance to pediocin (Xue et al., 2005).

The *B. subtilis* sigma factor ^{V} (*sigV*) is activated in presence of Lysozyme, regulating important resistance genes such as *oatA*, *dltABCD*, and *pbpX*, promoting protection by virtue of membrane alterations (Guariglia-Oropeza and Helmann, 2011; Ho et al., 2011). The alternative sigma factor 54 (*rpoN*) is relevant in mesentericin Y105 resistance in *Listeria monocytogenes*; strains lacking the monocistronic unit of *rpoN* showed a higher susceptibility to this AMP - a phenotype reverted after complementation - indicating that the resistance genes are under regulation of *rpoN* (Robichon et al., 1997).

Staphylococci

The genus *Staphylococcus* is responsible for various infections in humans like impetigo, scalded skin syndrome, toxic shock syndrome, pneumonia, endocarditis, urinary tract infections, and many others. The most clinically relevant members of this genus are *Staphylococcus aureus*, *Staphylococcus epidermidis*, and *Staphylococcus saprophyticus*. They are grape-shaped, catalase producing Gram-positive spherical cocci. *S. aureus* are classified as coagulase positive, while *S. epidermidis* and *S. saprophyticus* do not show coagulase activity. Another trait shared by many staphylococci species is the presence of a carotenoid pigment called staphyloxanthin, which gives the colonies a golden color and has an inhibitory role against microbicide molecules and reactive oxygen species (ROS). Among their antigenic structures are the protein A, which binds to Fc region of immunoglobulin G (IgG) and prevents complement activation; the teichoic acids, which modulate mucosal adhesion and induce toxic shock through release of interleukin 1 (IL-1) and tumor necrosis factor

(TNF); and polysaccharide capsule, with 11 different serotypes. Defense against AMPs in *Staphylococcus spp*.

Mechanisms of AMP Resistance in Staphylococci

Modifications in membrane/cell wall structure

Staphylococcus aureus is able to prevent AMP-mediated killing through modifications of the phosphatidylglycerol in the bacterial membrane by the multiple peptide resistance factor protein (MprF). The protein promotes the reaction of phosphatidylglycerol with lysin, generating lysylphosphatidylglycerol (Lys-PG), which is then translocated to the outer leaflet of the membrane (Oku et al., 2004; Staubitz et al., 2004; Ernst et al., 2009; Nasser et al., 2019). This results in a shift in membrane charge, and a subsequent repulsion of cationic AMPs.

The enhanced synthesis of the cationic phospholipid Lys-PG promotes changes in membrane fluidity also associated with increased resistance against different classes of AMPs in staphylococci. A study investigating the development of bacterial resistance to antimicrobial peptides demonstrated that exposure of *S. aureus* cultures to sub-lethal concentrations of magainin 2 and gramicidin D over several passages *in vitro* promoted resistance to these AMPs. The bacterial membrane adaptations induced by AMP exposure included an increase in net charge and altered membrane rigidity (Shireen et al., 2013).

Similarly, resistance to platelet microbicidal proteins (PMPs) in *S. aureus* has been linked with adaptations affecting membrane fluidity. A study investigating the mechanisms underlying *S. aureus* susceptibility to thrombin-induced PMP (tPMP-1) demonstrated that mutant strains with increased resistance to this AMP (either naturally occurring or artificially generated) displayed a high content of unsaturated lipids with longer chains (Bayer et al., 2000), which led to an enhanced membrane fluidity. Interestingly, tPMP resistance in *S. aureus* correlated with an increased virulence in both human and experimental endocarditis (Dhawan et al., 1998), highlighting the importance of this AMP in controlling *S. aureus* infection.

Resistance to cationic AMPs has also been associated with modifications in the cell wall teichoic acid by esterification with D-alanine, through the *dlt* operon, which reduces the net negative charge of the molecule. In *S. aureus* and *S. xylosus,* deletions of parts of the *dlt* operon induced a higher sensitivity to a variety of AMPs when compared to wild type strains. Interestingly, the increased susceptibility of the mutant strains were limited to cationic peptides, suggesting that electrostatic repulsion may be involved in resistance to cAMPs in *S. aureus* (Peschel et al., 1999; Jann et al., 2009; Simanski et al., 2013).

The presence of carotenoid pigments is another described mechanism of AMP resistance in staphylococci. These molecules are depicted as virulence factors, for their protective role against oxidative host defense mechanisms (Clauditz et al., 2006). Evidence suggests staphylococcal carotenoids can also provide protection against different antimicrobial peptides, through their effect on cell membrane stability (Mishra et al., 2011). In that work, a mutant strain with a defect in staphyloxanthin synthesis was compared with its supplemented counterpart in terms of susceptibility to a range of antimicrobial agents, including human HNP-1, PMPs, and polymyxin B. The supplemented strain showed a reduced susceptibility to the AMPs, which in this case was linked to a higher rigidity in the cell membrane. This apparent contrast with previous work showing a positive correlation between membrane fluidity and AMP resistance (Bayer et al., 2000) evidences the intricate balance driving peptide-cell membrane interactions. In that sense, extremes in rigidity or fluidity may hinder AMP insertion in the bacterial membrane.

AMP sequestration/ inactivation

Another mechanism of *S. aureus* evasion from AMPs is trapping them by surface or secreted proteins and polysaccharides. *S. aureus* secrets a plasminogen activating protein, staphylokinase (SK), which converts it into plasmin. High concentrations of plasmin on the bacterial surface promote fibrinolysis, favoring tissue invasion and dissemination (Braff et al., 2007). It has been shown that SK can bind to and inactivate mCRAMPs (cathelicidin murine antimicrobial peptides) and α-defensins secreted by neutrophils, including HNP 1-3 (Jin et al., 2004; Braff et al., 2007) reducing the activity of AMPs in 80%. In an *in vivo* trial with mice, *S. aureus* strains expressing SK were more resistant to α-defensin. Similarly, addition of purified SK was able to increase survival of strains that did not produce this protein in presence of α-defensin, *in vitro* (Jin et al., 2004).

Staphylococcus epidermidis synthesizes the exopolysaccharide intercellular adhesin (PIA), a positively charged polymer of the extracellular matrix in biofilms, which can promote hemagglutination. Studies using mutant strains lacking this polysaccharide have shown a role for PIA in resistance to LL-37 and β-defensin (HBD-3) (Vuong et al., 2004a,b; Kocianova et al., 2005). The mechanism responsible for PIA-mediated protection against AMPs seems to involve electrostatic repulsion, since the lytic activities of these antimicrobial peptides are dependent on the salt concentrations (Vuong et al., 2004b). Besides the protective effect against AMPs produced in the skin, PIA can also limit destruction of *Staphylococcus* by neutrophils, by forming a mechanical barrier that prevents bacterial uptake by phagocytes (Vuong et al., 2004b).

Additionally, *S. aureus* is able to sequester iron from the heme site of hemoglobin through the Iron-regulated surface determinant (Isd), which is then released into the cytoplasm for metabolization (Foster et al., 2014). This ability is responsible for the bacterial resistance to the bacteriostatic effects of lactoferrin and other iron-binding peptides. Furthermore, resistance to the bactericidal action of lactoferricin can be induced in *S. aureus* by growing the bacterium in increasing peptide concentrations–which also promoted cross-resistance to other antimicrobials, like indolicidin and penicillin G (Samuelsen et al., 2005).

Proteases and other proteins

Antimicrobial peptides are relatively resistant to bacterial surface or secreted proteases, yet some proteases can cleave a broad spectrum of AMPs; one such example is aureolysin, which inactivates LL-37 by cleaving peptide bonds in its C-terminus, between residues Arg_{19}-Ile_{20}, Arg_{23}-Ile_{24}, and Leu_{31}-Val_{32} (Sieprawska-Lupa et al., 2004). Thus, Aureolysin

expression allows a higher survival in environments with high concentrations of LL-37 such as the phagolysosomes in macrophages and neutrophils.

AMP induced gene expression/repression

Staphylococcus aureus displays a phenotype known as small colony variant (SCV), which has been associated with persistent skin infections (Glaser et al., 2014). This phenotypic change allows *S. aureus* strains to evade innate immune responses, one of those being AMPs, since in SCVs, a higher MIC was observed (von Eiff et al., 2006; Garcia et al., 2013).

Analysis of four different AMPs found on the skin (beta-defensin – hBD-2 and -3, RNase 7, and LL-37) showed that SCV were more resistant to AMPs when compared with the wild type strains (Glaser et al., 2014). Similarly, a mutant strain with a hemin biosynthesis gene deletion, *hemB,* displaying a SCV phenotype, was less susceptible to three of the four AMPs tested, when compared with its complemented mutant exhibiting normal phenotype (Glaser et al., 2014). These results suggest that phase variation may be a mechanism of bacterial resistance to AMPs. This effect could be attributed to differences in membrane charge in the SCV strains, as suggested by Sadowska et al. (2002), however, in that work, SCVs showed an increased resistance to only a fraction of the AMPs tested.

Staphylococcus aureus expresses an AMP recognition system named Antimicrobial Peptide Sensor; this system comprises a sensor histidine kinase (ApsS), a DNA-binding response regulator (ApsR) and ApsX, responsible for interacting with the AMP. The ApsRSX regulators are responsible for the regulation of important genes related to AMP resistance, such as *mprF*, *vraFG* and the *dlt* operon (Li et al., 2007a,b; Martínez-García et al., 2019). Aps from *S. epidermidis* has shown the ability to interact with a broad variety of AMPs; in contrast to *S. aureus* in which Aps are active over a more limited spectrum of peptides (Joo and Otto, 2015). The ApsS is a transmembrane protein with an extracellular group sensitive to AMPs, composed by nine amino acids with a negative charge, which binds to AMPs and rapidly inactivates them (Li et al., 2007b).

The GraRS regulators induce the expression of *mprF* and *dltABCD*, when activated together with *vraFG*, as a response to AMPs and glycopeptides, whereas mutant strains negative for *graRS* or *vraFG* were more susceptible to the peptides as the surface alterations generated as protection mechanisms were reduced (Meehl et al., 2007; Neoh et al., 2008; Yang et al., 2012).

The *agr* global transcriptional regulator induced a super expression of *dltD*, a member of the *dlt* operon (Dunman et al., 2001). Another regulator is the LytSR, a transmembrane electrical potential sensor (Patel and Golemi-Kotra, 2015). AMP cell wall damage is partially due to changes in membrane polarization; therefore, deletion of LytSR increased susceptibility to HNP-1 and tPMPs, Interestingly, no conformational changes were found in mutant cells membrane, indicating an alternative resistance pathway (Yang et al., 2013).

The VraTSR is a bacterial sensor which responds to stress; it is involved in *S. aureus* resistance do methicillin (MRSA) and other antimicrobials that target the cell wall (Boyle-Vavra et al., 2013; Lee et al., 2019). Exposure to AMPs activates operons VraSR e VraDE, leading to a change in the transcriptional profile with the repression of virulence and metabolism genes, and an induction of genes that regulate envelope homeostasis (Pietiäinen et al., 2009).

Enterococcus

Enterococci are a group of Gram-positive cocci comprising more than 30 species, of which *E. faecalis* and *Enterococcus faecium* are the most clinically relevant (*Fiore* et al., *2019*). They can be found in several environments such as water, soil and food, and are able to colonize the gastrointestinal tract of different animals. Enterococci are a leading cause of nosocomial infections – including endocarditis, urinary tract infections and bacteremia–being responsible for 14% of hospital infections in the United States (Weiner et al., 2016). The problem is aggravated by the increased intrinsic resistance and tolerance exhibited by these bacteria against several commercial antimicrobial agents, including β–lactams such as cephalosporins, and vancomycin (Kristich et al., 2014). In addition, enterococci rapidly acquire resistance to many classes of antibiotics upon treatment, thus posing a great public health threat.

Mechanisms of AMP Resistance in Enterococci

Modifications in membrane/cell wall structure

Similarly, to many other species previously cited, enterococci reshape their cell envelope composition in response to AMPs (Cremniter et al., 2006; Mehla and Sood, 2011; Mishra et al., 2012; Kandaswamy et al., 2013), with lysinated phosphatidylglycerol (Kraus and Peschel, 2006; Bao et al., 2012; Kumariya et al., 2015), addition of D-alanine to teichoic acids via *dlt* (Fabretti et al., 2006; Hirt et al., 2018) or MprF (Bao et al., 2012), also, the *N*-acetylglucosamine deacetylase PdgA (EF1843) contributes to lysozyme resistance in *E. faecalis*, by promoting peptidoglycan deacetylation (Benachour et al., 2012).

Many Enterococci species are able to perform O-acetylation of the cell wall peptidoglycan (Pfeffer et al., 2006) a mechanism related with resistance to lysozyme (Hebert et al., 2007).

Proteases and other proteins

Proteases and inhibitors are found in *E. faecalis*, either degrading or binding to the peptide, preventing their lytic effects. Among the proteases, GelE and SerE, a gelatinase and a serine protease, respectively, are able to degrade LL-37, HYL-20 – an α-helical amphipathic analog of a natural AMP present in bees – and GL13K, a peptide found in human saliva (Schmidtchen et al., 2002; Sieprawska-Lupa et al., 2004; Sedgley et al., 2009; Nesuta et al., 2017; Hirt et al., 2018). In addition, extracellular dermatan sulfate – a product released from proteoglycans after the activity of extracellular proteinases – was able to inhibit the activity of HNP-1 on *E. faecalis* (Schmidtchen et al., 2001), representing an important virulence mechanism for this bacterium.

Transport systems and efflux pumps

The Bcr transporter family is related to bacitracin resistance and is found in many enterococci species (Matos et al., 2009). In *E. faecalis*, BcrABD is an ABC transporter expressed in the presence of bacitracin. It is regulated by BcrR, which is responsible for the extracellular pumping of the polypeptide

(Manson et al., 2004). However, the BcrAB is not the only mechanism of bacitracin resistance in *E. faecalis*; other two-component regulatory systems and ABC transporters were also described (Gebhard et al., 2014). In *S. aureus,* LtnIFE is responsible for protection against lacticin. *E. faecium* possess homologs with similar function (Draper et al., 2009).

AMP induced gene expression/repression

In *E. faecalis* and *E. faecium*, the Man-PTS pathway is also related to resistance against bacteriocins, however, there are several implications in metabolic pathways which could hinder the host colonization (Héchard et al., 2001; Opsata et al., 2010; Geldart and Kaznessis, 2017). Undecaprenyl pyrophosphate phosphatase (UppP) is also related to bacitracin resistance in *E. faecium* by reducing the amount of substrate for bacitracin-mediated cell death (Shaaly et al., 2013). Another regulator crucial for successful host colonization is the sigma factor SigV, which is involved in resistance to lysozyme, but not to nisin (Le Jeune et al., 2010). *rpoN* is responsible for encoding the sigma factor 54 in *E. faecalis*, an important factor for bacteriocin resistance. Interestingly, sensibility to other AMPs did not change in absence of this sigma factor (Dalet et al., 2000).

Both *E. faecalis* and *E. faecium* share the LiaFSR stress-induced regulatory pathway. LiaFS is the homolog of VraTS from *S. aureus*. Strains lacking *liaR* showed higher sensitivity against daptomycin, and LL-37, HBD-3, nisin, gallidermin–a type A lantibiotic, the synthetic antimicrobial peptide RP-1, mersacidin–a type B lantibiotic and friulimicin, a cationic lipopeptide in *E. faecalis* (Reyes et al., 2015; Wang et al., 2017). The deletion of *liaF*, along with *gdpD*, promoted a similar increase in resistance against daptomycin (Arias et al., 2011). The *liaFSR* and related genes, such as *liaX*, a sensor that inhibits LiaFSR, are directly related to the cell envelope alterations in response to antimicrobials (Tran et al., 2013; Khan et al., 2019).

Group A Streptococci

Group A Streptococci (GAS) includes bacterial species such as *Streptococcus pyogenes* and *Streptococcus mutans* (Gold et al., 1973; Bessen et al., 1996). These bacteria are beta-hemolytic cocci and known to cause several diseases in humans, including mild conditions like scarlet fever, impetigo, strep throat, caries and cellulitis, and more severe illnesses like necrotizing fasciitis (flesh eating disease) and toxic shock syndrome (TSS) (Kristian et al., 2005).

Streptococcus pyogenes

Streptococcus pyogenes comprises the considerable majority of Group A Streptococci (GAS); it is a pathogen responsible for several human diseases such as pharyngitis, scarlet fever, toxic shock syndrome, pneumonia and others (Lauth et al., 2009). Recent studies have shown that GAS was able to resist the action of several human antimicrobial peptides such as cathelicidin, LL-37 and the α-defensin (HNP-1) (Kristian et al., 2005; Lauth et al., 2009; Rafei et al., 2020). The surface exposed M-protein is used to classify the bacterium into different serotypes (Bessen et al., 1996; Lauth et al., 2009). Lauth et al. (2009) have shown that the N-terminal portion of M-protein can interact with LL-37, preventing its action on the bacterium membrane.

Streptococcus mutans

Streptococcus mutans is an important pathogen that colonizes the human oral cavity being the most important caries agent (Gold et al., 1973). Interestingly, several *S. mutans* strains have been described as resistant to salivary AMPs and bacitracin (Tsuda et al., 2002; Kitagawa et al., 2011; Tian et al., 2018).

A study by Phattarataratip et al. (2011) compared *S. mutans* strains isolated from 60 children divided into two groups (caries-free and caries-active) and they found that strains isolated from the caries-active group were significantly more resistant to salivary AMPs such as LL-37, α-defensins and β-defensins, in comparison to caries-free strains. Their analysis also correlates this resistance to an ecological advantage over the less resistant strains, which reinforces the importance of AMPs in controlling *S. mutans* colonization (Phattarataratip et al., 2011).

Mechanisms of AMP Resistance in Group A Streptococci

Modifications in membrane/cell wall structure

Since most AMPs present cationic nature, the negative charge of the bacterial surface is important for the bactericidal activity of these molecules. Kristian et al. (2005) showed that the D-alanylation (regulated by the *operon dlt* (DltABCD)) of *S. pyogenes* lipoteichoic acid is related with resistance to cationic AMPs, lysozyme and low pH, and it was also associated with an increased survival against neutrophil killing; this phenomenon is due to the increase of positive surface charge caused by the D-alanylation on the cell membrane. In another study, (Cox et al., 2009) using a knockout strain for the dltABCD operon found that the DltA mutant displayed a drastic reduction in the expression of M protein and SIC (Serum Inhibitor of Complement) (Frick et al., 2003), showing that the *operon dlt* (DltABCD), specifically the *dltA* gene regulates the expression of genes involved in AMP resistance.

A study published by Tsuda et al. (2002) investigated the mechanisms that allow *S. mutans* to resist bacitracin; they found that mutant strains lacking the *rgp* locus (a six gene operon) presented up to five times more sensibility to bacitracin than the wild type counterpart. A possible mechanism to explain this sensitiveness is the fact that the *rgp* locus is involved in the synthesis of rhamnose-glucose polysaccharide (RGP), a cell wall component; mutations affecting this process render the bacterium more sensitive to bacitracin (Yamashita et al., 1998).

Proteases and other proteins

Streptococcus pyogenes is able to limit LL-37 action through degradation by the cysteine proteinase, SpeB. In presence of the inhibitor E64 (which inhibited the cysteine proteinase) the bacterium's ability to degrade LL-37 was hampered, making it more susceptible to this CAMP. This effect highlights the importance of proteinase SpeB in LL-37 degradation (Schmidtchen et al., 2002).

Similarly, to previously described for *Enterococci*, *S. pyogenes* secretes proteases that are able to cleave proteoglycans containing

dermatan sulfate, releasing it to the extracellular space. The extracellular dermatan sulfate was able to neutralize neutrophil-derived alpha-defensin, protecting the bacteria from its bactericidal activity (Schmidtchen et al., 2002).

M-protein is the most studied protein in *S. pyogenes*; variations in M-protein sequence are used to classify the bacterium into different serotypes (Lauth et al., 2009). A study by Lauth et al. (2009), showed that the M protein type 1 protects the bacterium from killing by cathelicidins LL-37 (human) and mCRAMP (mouse). The proposed mechanism involves M1 binding to and trapping the cathelicidin before it can reach the cell wall. They also showed that this protection is type specific once M protein type 49 did not protects the bacterium the same extension of M1, moreover, they found that strains isolated from invasive diseases patients were more resistant to LL-37 action than the strains isolated from asymptomatic patients (Lauth et al., 2009).

Another strategy employed by *S. pyogenes* to resist AMP attack is the Serum Inhibitor of Complement (SIC). This protein was initially identified as a virulence factor protecting the bacterium against killing by the complement system membrane attack complex (Akesson et al., 1996). Further studies from the same group showed that SIC is important for bacterium full virulence, once it is able to bind to defensins and LL-37, protecting the bacterium against these molecules (Frick et al., 2003).

Transport systems and efflux pumps

Streptococcus mutans express the ABC transporter, *mbr*, an operon composed by 4 genes. Mutant strains that do not express the full transporter were 100 to 120-fold more sensitive to bacitracin than the wild type strain (Tsuda et al., 2002). A more recent study from the same group, analyzed the transcriptome of the bacterium after exposure to bacitracin. They found 8 genes (SMU.302, SMU.862, SMU.863, SMU.864, *mbrA, mbrB*, SMU.1479, SMU.1856c) that were upregulated upon AMP challenge; of those, the MbrC protein acts as a transcriptional regulator for MbrA and MbrB–which are part of the ABC transporter and are required for bacitracin resistance–and it also controls the expression of SMU.863 and SMU.864, also described as ABC transporters involved in bacitracin resistance by *S. mutans* (Kitagawa et al., 2011).

The *S. mutans bceABRS* operon encodes an ABC transporter (BceAB) and a two-component system BceRS. The entire four-component system was shown to be important for protection against bacitracin, defensins (α and β), LL-37 and histatin (Tian et al., 2018). In contrast with wild type *S. mutans*, mutant strains lacking each *bceABRS* gene failed to form biofilms in response to a sub-inhibitory concentration of β-defensin. This data suggest that BceABRS also acts as a sensor, promoting a switch to an AMP resistant phenotype upon challenge (Tian et al., 2018).

Group B Streptococci

Streptococcus agalactiae, also referred to as Group B Streptococci (GBS), is an opportunistic pathogen that colonizes the gastrointestinal, genitourinary tracts and, in women, the vaginal mucosa. The biggest concern regarding infections with GBS is in pregnant women, because it can be transmitted vertically and results in serious neonatal consequences, causing several diseases to the newborn, such as meningitis, sepsis and pneumonia (Shabayek and Spellerberg, 2017).

The incidence of infections by *S. agalactiae* is twice as high in pregnant women when compared to non-pregnant women. Most GBS infections occur during labor, but there is also a chance of infection after delivery. In the United States, GBS infection rates range from 0.1 to 0.8 per 1,000 childbirths. Worldwide, the rates in pregnant women are 0.38 per 1,000 childbirths, with 0.2 in 1000 mortality rate (Raabe and Shane, 2019). GBS infection is also associated with an increased chance of premature delivery. Around the world, premature birth is an important contribution to the death of newborns; approximately 10% of deaths in neonates are caused by GBS infection (Vornhagen et al., 2017).

Mechanisms of AMP Resistance in Group B Streptococci

Modifications in membrane/cell wall structure

In *S. agalactiae*, the *dlt* operon is essential for resistance against AMPs. Deletion of *dltA* hinders bacterial survival ability *in vivo* and reduces the resistance to AMPs, possibly due to an increased interaction with the peptide. Interestingly, the D-alanylation of the membrane seems to induce resistance by enhancing cell envelope strength rather than the interference with the ionic charge of the membrane (Poyart et al., 2001, 2003; Saar-Dover et al., 2012).

Proteases and other proteins

Streptococcus agalactiae is intrinsically resistant to nisin via NSR or SaNSR, a nisin-specific enzyme that cleaves and hinders the activity of the peptide. It is expressed by the *nsr* operon with other lantibiotic resistance genes, such as nsrFP and nsrRK (Khosa et al., 2013, 2015, 2016). However, modified nisin molecules were able to maintain activity against strains possessing SaNSR (Hayes et al., 2019; Zaschke-Kriesche et al., 2019). Another mode of escaping the degrading activity of AMPs is via inhibitory molecules capable of binding to the nisin site of SaNSR (Porta et al., 2019). A phosphoglycerate kinase of GBS was also identified to participate in AMP resistance. Though the mechanism is unknown, it is supposed to include direct binding of the peptides (Boone and Tyrrell, 2012).

Transport systems and efflux pumps

NsrFP is an ABC transporter which exports nisin to the extracellular medium. The transporter binds to the N-terminal portion of the peptide and releases it, preventing cell death, even in absence of the two-component regulator NsrRK (Reiners et al., 2017).

In *S. sanguinis*, a study involving multiple gene screening reported a role for sag1003 in AMP resistance against nisin and bacitracin. The gene is predicted to be an efflux pump against AMPs and a transposon-induced mutagenesis caused a higher sensitivity against both AMPs in a plate-based minimum inhibitory concentration (MIC) assay (Boone and Tyrrell, 2012).

AMP sequestration and inactivation

Streptococcus agalactiae pili are important against host defense mechanisms, such as AMPs. The sequestration of AMPs by pili prevents the interaction with the membrane targets. Strains

lacking *pilB*, one of the pilus subunit proteins, were more sensitive to AMPs and less virulent overall, supposedly by virtue of resistance against LL-37, mCRAMP and polymyxin B. Heterologous overexpression of PilB from *S. agalactiae* in *L. lactis* showed similar results (Maisey et al., 2008).

AMP induced gene expression/repression

The *bceRSAB* is a detoxification system in GBS, regulating the gene expression against AMPs, such as *dltA*, promoting resistance. Strains lacking the regulator BceR showed an increased susceptibility against bacitracin and LL-37 and reduced overall virulence (Yang et al., 2019).

The insertion of an inactivation transposon in *sag1003* induced a reduction of phosphoglycerate kinase in the cell wall (Boone and Tyrrell, 2012).

The two-component regulator NsrRK is responsible for the transcriptional control of the NSR pathway (*nsr* and *nsrFP*) in *L. lactis* strains capable of synthesizing nisin. In GBS, a very similar *nsr* operon was described, indicating the possibility of an analogous system (Khosa et al., 2013, 2016).

Hamilton et al. (2006) identified a surface-associated penicillin-binding protein called PBP1a, which is encoded by the *ponA* gene. A mutant Δ*ponA* strain was more susceptible to AMPs from cathelicidin and defensin families, but the exact mechanism involved in this protection is still unknown (Hamilton et al., 2006; Jones et al., 2007).

Streptococcus pneumoniae

Streptococcus pneumoniae (pneumococcus) is responsible for around 1 million deaths worldwide every year, and an increasing drug resistance case reporting (Tramper-Stranders, 2018). It is the main causative agent in community acquired bacterial pneumonia, and it can also cause otitis media, conjunctivitis, sinusitis and more severe diseases like meningitis and bacteremia.

Pneumococci are frequent colonizers of the upper respiratory tract, and a single person may be colonized with multiple strains concomitantly for months. Asymptomatic carriers are also the main source of pneumococcal transmission (Khan and Pichichero, 2014). In this highly colonized niche, AMP resistance confers an important competitive advantage both inter and intra species. Pneumococci display a vast number of adaptations that promote increased AMP resistance, from envelope modifications to AMP sequestration, as described next.

Mechanisms of AMP Resistance in *S. pneumoniae*

Envelope modifications

A vast majority of clinically relevant pneumococcal isolates are covered by a thick polysaccharide capsule with variable structure, which protects the bacterium from host immune defenses. Based on their high immunogenicity and protective efficacy, capsular polysaccharides comprise the basis of the current pneumococcal vaccines, alone or in fusion with carrier proteins (Darrieux et al., 2015; Geno et al., 2015; Converso et al., 2020).

Variations in capsule polysaccharide () locus determine the classification of pneumococci in over 95 different serotypes. These include mainly negative structures, with a few being neutral or positive. Negatively charged free capsular polysaccharides (but not neutral or positive ones) have displayed a role in preventing AMP attack. These purified anionic CPS were able to increase the resistance of non-encapsulated mutant pneumococci to HNP-1 and polymyxin B, an effect that was abrogated when the CPSs lost their negative charge through reaction with polycations. One proposed mechanism is that exposure to antimicrobial peptides triggers CPS release, which trap the AMPs and shield the bacterium (Llobet et al., 2008). This capsule shedding has been demonstrated to occur *in vivo*, thus comprising a potential strategy to prevent AMP-mediated killing. Capsule shedding can be triggered by autolysin (LytA) activity, promoting bacterial resistance to LL-37 and favoring colonization (Kietzman et al., 2016).

Surface-attached capsular polysaccharides, on the other hand, have shown the opposite effect, rendering the bacteria more susceptible to AMP action, in comparison with non-encapsulated isogenic mutants (Beiter et al., 2008). This effect was observed with different capsular types, including CPS 2, 4, 9V and 19F, and the zwitterionic serotype 1. As shown for other Gram-positive bacteria, D-alanylation of teichoic acids in non-encapsulated pneumococci results in increased resistance against killing by neutrophil extracellular trap (NET)-derived components (Beiter et al., 2008). This effect is aided by surface proteins, like the choline binding protein LytA and PgdE, which contribute to reduce the surface negative charge (discussed further). In that sense, the presence of capsule could mask the underlying protective mechanisms against AMPs. This apparent detrimental effect of capsule production over pneumococcal sensitivity to AMPs is possibly overcome by the capsule shedding as previously discussed, and also by its ability to protect the bacterium against mucus and phagocytic cell repulsion (Geno et al., 2015). Furthermore, the effect may not be applicable to all capsular serotypes; great variations in carriage, invasiveness and prevalence exist among capsule types, which have been associated with variations in surface net charge (Li et al., 2013). In that sense, the investigation of AMP resistance in a higher number of pneumococcal serotypes may provide new insights into the role of surface CPS on AMP resistance. For instance, type 4 TIGR4 and its isogenic capsule-negative mutant have shown increased sensibility to CXCL10, LL-37, and nisin, when compared with the type 2 strain, D39 (Bruce et al., 2018).

Another study has shown that non-encapsulated pneumococci are more resistant to neutrophil proteases, elastase and cathepsin G–a feature that also contributes to the ability to colonize the nasopharynx (van der Windt et al., 2012).

Cell wall modifications by the *dlt* operon have also been shown to promote resistance against nisin and gallidermin in pneumococci, an effect that was consistent with an increased release of D-alanine upon hydrolysis in wild type versus *dltA*-negative mutant stains (Kovacs et al., 2006).

Pneumococci express two enzymes, PgdA and Adr, that modify peptidoglycans on the bacterial cell wall. PgdA is a N-acetylglucosamine deacetylase (Vollmer and Tomasz, 2000), while Adr is an O-acetyl transferase that acetylates muramic acid residues on the peptidoglycan backbone (Crisostomo et al., 2006). Double mutant strains unable to perform these modifications displayed lower ability to colonize lysozyme-sufficient mice, but

behaved similarly, to wild type pneumococci in mice lacking lysozyme production. In contrast, mutants in only one of the molecules colonized mice more efficiently than the wild type strain, in both Lys-producing and Lys-deficient mice (Davis et al., 2008). Taken together, these results indicate that the ability to limit lysozyme attack by modifying the cell wall contributes to successful colonization of the host.

AMP sequestration/inactivation

Studies from our group and others have reported a role for pneumococcal surface protein A (PspA) in bacterial resistance to AMPs. PspA is an exposed virulence factor with structural and serological variability (Goulart et al., 2013; Converso et al., 2017b) that has been successfully evaluated as a vaccine candidate in different infection models (Darrieux et al., 2007; Goulart et al., 2013; Converso et al., 2017a, 2020). It prevents complement activation/deposition on the pneumococcal surface, limiting bacterial uptake by phagocytes (Ren et al., 2004; Mukerji et al., 2012).

Pneumococcal surface protein A can bind to and prevent the lytic action of lactoferrin (Hakansson et al., 2001; Shaper et al., 2004). Furthermore, anti-PspA antibodies induced by vaccination were able to enhance the bactericidal effect of apolactoferrin (the iron-free form of the molecule) by blocking PspA interaction with that protein (Shaper et al., 2004; Andre et al., 2015). This protective effect of PspA over pneumococci was diminished when lactoferrin was combined with lysozyme (Andre et al., 2015). This set of data suggests PspA is able to prevent the lytic action of cationic peptides against pneumococci, possibly by binding to these molecules through their active sites. This interaction has been demonstrated for lactoferrin (Senkovich et al., 2007).

Pneumococcal surface protein A has also been shown to interfere with the bactericidal activity of NETs (Martinez et al., 2019). Mutants lacking PspA were more susceptible to trapping by NETs, an effect that was dependent on PspA type. In addition, incubation with anti-PspA antibodies promoted NET formation (Martinez et al., 2019). Taken together, the data indicates that PspA is able to directly prevent killing by AMPs, and also to limit the bactericidal mechanisms of neutrophils.

Efflux pumps and transport systems

Pneumococci express and efflux pump, MefE/Mel, which confers resistance to macrolides. *mfE* expression is induced upon bacterial incubation in presence of LL-37. In consequence, pneumococci develop resistance to LL-37 and erythromycin *in vitro* (Zahner et al., 2010).

A second, MacAB-like efflux pump described in *S. pneumoniae*, comprised by the spr0693-spr0694-spr0695 operon, is also involved in resistance against antimicrobial peptides and antibiotics, like LL-37, nisin and bacitracin (Majchrzykiewicz et al., 2010; Yang et al., 2018).

The oligopeptide import ABC transport system Opp (AmiACDEF) has been implicated in resistance against CXCL10, a chemokine with antimicrobial activity against several pathogens (Yung and Murphy, 2012). In that work, mutant strains lacking the permease were less susceptible to CXCL10 and nisin, when compared with the parent D39 strain. Although the precise mechanism responsible for this effect is not fully understood, it is known that AmiA-F has additional pleiotropic roles in pneumococcal physiology, quorum sensing, and virulence (Bruce et al., 2018).

AMP induced gene expression/repression

Cell wall modifications in pneumococci can be triggered by AMPs. Treatment with lysozyme leads to upregulation of the *dlt* locus through the CiaRH sensoring system, resulting in lipoteichoic acid (LTA) modifications and increased inflammatory responses, which in that case contributed to bacterial shedding and transmission (Zafar et al., 2019). Thus, D-alanylation of the cell wall – a mechanism of AMP resistance shared among different Gram-positive microbes–can be induced, in pneumococci, by treatment with antimicrobial proteins that target the bacterial cell wall.

Incubation with LL-37 can also trigger an adaptive response in pneumococci. The transcriptome analysis of pneumococci treated with LL-37 revealed a profound effect on the bacterial genome, with 10% of the genes displaying an altered expression upon challenge (Majchrzykiewicz et al., 2010). The up-regulated genes included those involved in cell wall biosynthesis (dlt), bacteriocin production, virulence (such as the proteases HtrA e PrtA) and bacteriocin production, as well as transcriptional regulators and putative ABC transporters. Interestingly, the serino-protease HtrA is also involved in resistance against other environmental stressors, like high temperature and oxidative stress (Dawid et al., 2009). The choline binding protein PspA and LysM protein (SP 0107)–predicted to be involved in cell wall metabolism–were down regulated in presence of LL-37. Interestingly, LL-37 had a much more dramatic effect on pneumococcal gene expression patterns, when compared with bacterial-derived AMPs that act on the same bacterial targets (nisin and bacitracin). Furthermore, mutant strains lacking these genes revealed an increased susceptibility to treatment with LL-37, confirming the employment of multiple defense strategies against AMPs in pneumococci (Majchrzykiewicz et al., 2010). A more recent study evaluating the proteome of pneumococci treated with LL-37 has also reported a large number of proteins with altered abundance, including transporters, proteins involved in gene regulation and cell wall modification, virulence factors (such as Pht family) and the protease HtrA (Mucke et al., 2020). This result suggests that multiple mechanisms cooperate in pneumococcal response to AMPs.

AMP resistance as a competitive advantage

A study investigating the susceptibility of multiple pneumococcal isolates – both clinical and from carriage–to LL-37 and HNP-1 found great variations in AMP resistance, with no correlation with AMP or capsule type, although clinical isolates were, in general, more susceptible than were carriage isolates (Habets et al., 2012). Furthermore, the study reported that AMP challenge could affect bacterial fitness in competitive assays. This result suggests a role for AMPs in driving intraspecific competition among pneumococci in the nasopharynx, contributing the bacterial genetic diversity in this niche.

DISCUSSION

Antimicrobial peptides are central players in the innate immune defense against pathogenic bacteria. Unsurprisingly, microbes have developed several strategies to overcome AMP activity, which allow them to efficiently colonize/invade the host. The present review summarizes the strategies adopted by Gram-positive pathogenic bacteria to resist AMP action. Some of these mechanisms, like cell wall modifications, are shared by several pathogens, highlighting their pivotal contribution to bacterial survival within the host. Other factors such as surface proteins and virulence factors are microbe-specific, revealing a myriad of adaptations that comprise the bacterial arsenal against AMPs.

The alarming increase in antibiotic resistance has prompted the search for alternative treatment options. In this scenario, AMPs emerge as a promising strategy to control bacterial infections. This rationale is reinforced by the demonstration that antibiotic resistance in bacteria usually correlates with a collateral sensitivity to AMPs (Lazar et al., 2018).

Several approaches employing AMPs have been tested with encouraging results. The use of AMP combinations is of particular interest, since these molecules can potentiate each other's action, and also improve the therapeutic efficacy of conventional antibiotics, through synergistic interactions (Reffuveille et al., 2014), This represents an excellent strategy to slow down or minimize bacterial resistance development. In that sense, a better comprehension of the mechanisms employed by bacteria to resist AMP action is pivotal for the development of more effective therapeutic strategies. Furthermore, since many bacterial molecules involved in AMP resistance are important virulence factors, the present review presents numerous potential targets for vaccine development, and also contributes to elucidate the mechanisms driving intra-and interspecies competition within the host.

AUTHOR CONTRIBUTIONS

LA, TC, BM, MC, NW, LN, MG, and MD drafted the manuscript. LA, TC, and MD revised the manuscript. LA and MC drafted the table. LA, MC, and MD produced the Figure. All authors read and approved the final manuscript. None of the authors have any competing interests.

REFERENCES

Abachin, E., Poyart, C., Pellegrini, E., Milohanic, E., Fiedler, F., Berche, P., et al. (2002). Formation of D-alanyl-lipoteichoic acid is required foradhesion and virulence of Listeria monocytogenes. *Mol. Microbiol* 43, 1–14. doi: 10.1046/j.1365-2958.2002.02723.x

Abi Khattar, Z., Rejasse, A., Destoumieux-Garzón, D., Escoubas, J. M., Sanchis, V., Lereclus, D., et al. (2009). The dlt operon of *Bacillus cereus* is required for resistance to cationic antimicrobial peptides and for virulence in insects. *J. Bacteriol.* 191, 7063–7073. doi: 10.1128/jb.00892-09

Akesson, P., Sjoholm, A. G., and Bjorck, L. (1996). Protein SIC, a novel extracellular protein of Streptococcus pyogenes interfering with complement function. *J. Biol. Chem.* 271, 1081–1088. doi: 10.1074/jbc.271.2.1081

Andersson, D. I., Hughes, D., and Kubicek-Sutherland, J. Z. (2016). Mechanisms and consequences of bacterial resistance to antimicrobial peptides. *Drug Resist. Updat.* 26, 43–57. doi: 10.1016/j.drup.2016.04.002

Andre, G. O., Politano, W. R., Mirza, S., Converso, T. R., Ferraz, L. F., Leite, L. C., et al. (2015). Combined effects of lactoferrin and lysozyme on Streptococcus pneumoniae killing. *Microb. Pathog.* 89, 7–17. doi: 10.1016/j.micpath.2015.08.008

Arias, C. A., Panesso, D., McGrath, D. M., Qin, X., Mojica, M. F., Miller, C., et al. (2011). Genetic basis for in vivo daptomycin resistance in enterococci. *N. Engl. J. Med.* 365, 892–900. doi: 10.1056/NEJMoa1011138

Aubry, C., Goulard, C., Nahori, M. A., Cayet, N., Decalf, J., Sachse, M., et al. (2011). OatA, a peptidoglycan O-acetyltransferase involved in Listeria monocytogenes immune escape, is critical for virulence. *J. Infect. Dis.* 204, 731–740. doi: 10.1093/infdis/jir396

Bao, Y., Sakinc, T., Laverde, D., Wobser, D., Benachour, A., Theilacker, C., et al. (2012). Role of mprF1 and mprF2 in the pathogenicity of *Enterococcus faecalis*. *PLoS One* 7:e38458. doi: 10.1371/journal.pone.0038458

Bayer, A. S., Prasad, R., Chandra, J., Koul, A., Smriti, M., Varma, A., et al. (2000). In vitro resistance of Staphylococcus aureus to thrombin-induced platelet microbicidal protein is associated with alterations in cytoplasmic membrane fluidity. *Infect. Immun.* 68, 3548–3553. doi: 10.1128/iai.68.6.3548-3553.2000

Beiter, K., Wartha, F., Hurwitz, R., Normark, S., Zychlinsky, A., and Henriques-Normark, B. (2008). The capsule sensitizes *Streptococcus pneumoniae* to alpha-defensins human neutrophil proteins 1 to 3. *Infect. Immun.* 76, 3710–3716. doi: 10.1128/IAI.01748-07

Benachour, A., Ladjouzi, R., Le Jeune, A., Hebert, L., Thorpe, S., Courtin, P., et al. (2012). The lysozyme-induced peptidoglycan N-acetylglucosamine deacetylase PgdA (EF1843) is required for Enterococcus faecalis virulence. *J. Bacteriol.* 194, 6066–6073. doi: 10.1128/JB.00981-12

Bergholz, T. M., Tang, S., Wiedmann, M., and Boor, K. J. (2013). Nisin Resistance of *Listeria monocytogenes* is increased by exposure to salt stress and is mediated via LiaR. *Appl. Environ. Microbiol.* 79, 5682–5688. doi: 10.1128/aem.01797-13

Bernard, R., Guiseppi, A., Chippaux, M., Foglino, M., and Denizot, F. (2007). Resistance to bacitracin in *Bacillus subtilis*: unexpected requirement of the BceAB ABC transporter in the control of expression of its own structural genes. *J. Bacteriol.* 189, 8636–8642. doi: 10.1128/JB.01132-07

Bernard, R., Joseph, P., Guiseppi, A., Chippaux, M., and Denizot, F. (2003). YtsCD and YwoA, two independent systems that confer bacitracin resistance to *Bacillus subtilis*. *FEMS Microbiol. Lett.* 228, 93–97. doi: 10.1016/S0378-1097100300738-00739

Bessen, D. E., Sotir, C. M., Readdy, T. L., and Hollingshead, S. K. (1996). Genetic correlates of throat and skin isolates of group A streptococci. *J. Infect. Dis.* 173, 896–900. doi: 10.1093/infdis/173.4.896

Boneca, I. G., Dussurget, O., Cabanes, D., Nahori, M. A., Sousa, S., Lecuit, M., et al. (2007). A critical role for peptidoglycan N-deacetylation in Listeria evasion from the host innate immune system. *Proc. Natl. Acad. Sci. U.S.A.* 104, 997–1002. doi: 10.1073/pnas.0609672104

Bonnet, M., Rafi, M. M., Chikindas, M. L., and Montville, T. J. (2006). Bioenergetic mechanism for nisin resistance, induced by the acid tolerance response of *Listeria monocytogenes*. *Appl. Environ. Microbiol.* 72, 2556–2563. doi: 10.1128/AEM.72.4.2556-2563.2006

Boone, T. J., and Tyrrell, G. J. (2012). Identification of genes affecting expression of phosphoglycerate kinase on the surface of group B streptococcus. *Can. J. Microbiol.* 58, 433–441. doi: 10.1139/w2012-015

Boyle-Vavra, S., Yin, S., Jo, D. S., Montgomery, C. P., and Daum, R. S. (2013). VraT/YvqF is required for methicillin resistance and activation of the VraSR regulon in *Staphylococcus aureus*. *Antimicrob. Agents Chemother.* 57, 83–95. doi: 10.1128/AAC.01651-01612

Braff, M. H., Jones, A. L., Skerrett, S. J., and Rubens, C. E. (2007). *Staphylococcus aureus* exploits cathelicidin antimicrobial peptides produced during early pneumonia to promote staphylokinase-dependent fibrinolysis. *J. Infect. Dis.* 195, 1365–1372. doi: 10.1086/513277

Bruce, K. E., Rued, B. E., Tsui, H. T., and Winkler, M. E. (2018). The Opp (AmiACDEF) oligopeptide transporter mediates resistance of Serotype 2

Streptococcus pneumoniae D39 to killing by chemokine CXCL10 and other antimicrobial peptides. *J. Bacteriol.* 200:e00745-17. doi: 10.1128/JB.00745-17

Brunt, J., Carter, A. T., Pye, H. V., and Peck, M. W. (2018). The orphan germinant receptor protein GerXAO (but not GerX3b) is essential for L-alanine induced germination in *Clostridium botulinum* Group II. *Sci. Rep.* 8:7060. doi: 10.1038/s41598-018-25411-x

Cao, M., and Helmann, J. D. (2004). The Bacillus subtilis extracytoplasmic-function sigmaX factor regulates modification of the cell envelope and resistance to cationic antimicrobial peptides. *J. Bacteriol.* 186, 1136–1146. doi: 10.1128/jb.186.4.1136-1146.2004

Carrillo, W., Lucio, A., Gaibor, J., Morales, D., and Vasquez, G. (2018). Isolation of antibacterial hydrolysates from hen egg white lysozyme and identification of antibacterial peptides. *J. Med. Food* 21, 808–818. doi: 10.1089/jmf.2017.0134

Carvalho, F., Atilano, M. L., Pombinho, R., Covas, G., Gallo, R. L., Filipe, S. R., et al. (2015). L-rhamnosylation of *Listeria monocytogenes* wall teichoic acids promotes resistance to antimicrobial peptides by delaying interaction with the membrane. *PLoS Pathog.* 11:e1004919. doi: 10.1371/journal.ppat.1004919

Chapeton-Montes, D., Plourde, L., Bouchier, C., Ma, L., Diancourt, L., Criscuolo, A., et al. (2019). The population structure of *Clostridium tetani* deduced from its pan-genome. *Sci. Rep.* 9:11220. doi: 10.1038/s41598-019-47551-4

Chen, M., Lyu, Y., Feng, E., Zhu, L., Pan, C., Wang, D., et al. (2020). SpoVG is necessary for sporulation in *Bacillus anthracis*. *Microorganisms* 8:548. doi: 10.3390/microorganisms8040548

Chen, X., Zou, X., Qi, G., Tang, Y., Guo, Y., Si, J., et al. (2018). Roles and mechanisms of human cathelicidin LL-37 in cancer. *Cell Physiol. Biochem.* 47, 1060–1073. doi: 10.1159/000490183

Chukwu, E. E., Nwaokorie, F. O., Coker, A. O., Avila-Campos, M. J., Solis, R. L., Llanco, L. A., et al. (2016). Detection of toxigenic *Clostridium perfringens* and *Clostridium botulinum* from food sold in Lagos, Nigeria. *Anaerobe* 42, 176–181. doi: 10.1016/j.anaerobe.2016.10.009

Clauditz, A., Resch, A., Wieland, K. P., Peschel, A., and Gotz, F. (2006). Staphyloxanthin plays a role in the fitness of *Staphylococcus aureus* and its ability to cope with oxidative stress. *Infect. Immun.* 74, 4950–4953. doi: 10.1128/IAI.00204-06

Collins, B., Curtis, N., Cotter, P. D., Hill, C., and Ross, R. P. (2010). The ABC transporter AnrAB contributes to the innate resistance of Listeria monocytogenes to nisin, bacitracin, and various beta-lactam antibiotics. *Antimicrob. Agents Chemother.* 54, 4416–4423. doi: 10.1128/AAC.00503-10

Converso, T. R., Assoni, L., Andre, G. O., Darrieux, M., and Leite, L. C. C. (2020). The long search for a serotype independent pneumococcal vaccine. *Expert. Rev. Vaccines* 19, 57–70. doi: 10.1080/14760584.2020.1711055

Converso, T. R., Goulart, C., Darrieux, M., and Leite, L. C. C. (2017a). A protein chimera including PspA in fusion with PotD is protective against invasive pneumococcal infection and reduces nasopharyngeal colonization in mice. *Vaccine* 35, 5140–5147. doi: 10.1016/j.vaccine.2017.08.010

Converso, T. R., Goulart, C., Rodriguez, D., Darrieux, M., and Leite, L. C. C. (2017b). Rational selection of broadly cross-reactive family 2 PspA molecules for inclusion in chimeric pneumococcal vaccines. *Microb. Pathog.* 109, 233–238. doi: 10.1016/j.micpath.2017.06.004

Cowland, J. B., Johnsen, A. H., and Borregaard, N. (1995). hCAP-18, a cathelin-pro-bactenecin-like protein of human neutrophil specific granules. *FEBS Lett.* 368, 173–176. doi: 10.1016/0014-5793(95)00634-l

Cox, K. H., Ruiz-Bustos, E., Courtney, H. S., Dale, J. B., Pence, M. A., Nizet, V., et al. (2009). Inactivation of DltA modulates virulence factor expression in Streptococcus pyogenes. *PLoS One* 4:e5366. doi: 10.1371/journal.pone.0005366

Crandall, A. D., and Montville, T. J. (1998). Nisin resistance in *Listeria monocytogenes* ATCC 700302 is a complex phenotype. *Appl. Environ. Microbiol.* 64, 231–237. doi: 10.1128/aem.64.1.231-237.1998

Cremniter, J., Mainardi, J. L., Josseaume, N., Quincampoix, J. C., Dubost, L., Hugonnet, J. E., et al. (2006). Novel mechanism of resistance to glycopeptide antibiotics in *Enterococcus faecium*. *J. Biol. Chem.* 281, 32254–32262. doi: 10.1074/jbc.M606920200

Crisostomo, M. I., Vollmer, W., Kharat, A. S., Inhulsen, S., Gehre, F., Buckenmaier, S., et al. (2006). Attenuation of penicillin resistance in a peptidoglycan O-acetyl transferase mutant of *Streptococcus pneumoniae*. *Mol. Microbiol.* 61, 1497–1509. doi: 10.1111/j.1365-2958.2006.05340.x

Crobach, M. J. T., Ducarmon, Q. R., Terveer, E. M., Harmanus, C., Sanders, I., Verduin, K. M., et al. (2020). The bacterial gut microbiota of adult patients infected, colonized or noncolonized by *Clostridioides difficile*. *Microorganisms* 8:677. doi: 10.3390/microorganisms8050677

Daba, G. M., Ishibashi, N., Gong, X., Taki, H., Yamashiro, K., Lim, Y. Y., et al. (2018). Characterisation of the action mechanism of a Lactococcus-specific bacteriocin, lactococcin Z. *J. Biosci. Bioeng.* 126, 603–610. doi: 10.1016/j.jbiosc.2018.05.018

Dalet, K., Briand, C., Cenatiempo, Y., and Hechard, Y. (2000). The rpoN gene of *Enterococcus faecalis* directs sensitivity to subclass IIa bacteriocins. *Curr. Microbiol.* 41, 441–443. doi: 10.1007/s002840010164

Darrieux, M., Goulart, C., Briles, D., and Leite, L. C. (2015). Current status and perspectives on protein-based pneumococcal vaccines. *Crit. Rev. Microbiol.* 41, 190–200. doi: 10.3109/1040841X.2013.813902

Darrieux, M., Miyaji, E. N., Ferreira, D. M., Lopes, L. M., Lopes, A. P., Ren, B., et al. (2007). Fusion proteins containing family 1 and family 2 PspA fragments elicit protection against *Streptococcus pneumoniae* that correlates with antibody-mediated enhancement of complement deposition. *Infect. Immun.* 75, 5930–5938. doi: 10.1128/IAI.00940-07

Davis, K. M., Akinbi, H. T., Standish, A. J., and Weiser, J. N. (2008). Resistance to mucosal lysozyme compensates for the fitness deficit of peptidoglycan modifications by *Streptococcus pneumoniae*. *PLoS Pathog.* 4:e1000241. doi: 10.1371/journal.ppat.1000241

Dawid, S., Sebert, M. E., and Weiser, J. N. (2009). Bacteriocin activity of *Streptococcus pneumoniae* is controlled by the serine protease HtrA via posttranscriptional regulation. *J. Bacteriol.* 191, 1509–1518. doi: 10.1128/JB.01213-08

de la Fuente-Nunez, C., Reffuveille, F., Mansour, S. C., Reckseidler-Zenteno, S. L., Hernandez, D., Brackman, G., et al. (2015). D-enantiomeric peptides that eradicate wild-type and multidrug-resistant biofilms and protect against lethal *Pseudomonas aeruginosa* infections. *Chem. Biol.* 22, 196–205. doi: 10.1016/j.chembiol.2015.01.002

de Noordhout, C. M., Devleesschauwer, B., Angulo, F. J., Verbeke, G., Haagsma, J., Kirk, M., et al. (2014). The global burden of listeriosis: a systematic review and meta-analysis. *Lancet Infect. Dis.* 14, 1073–1082. doi: 10.1016/S1473-3099(14)70870-9

Desai, A. N., Anyoha, A., Madoff, L. C., and Lassmann, B. (2019). Changing epidemiology of Listeria monocytogenes outbreaks, sporadic cases, and recalls globally: a review of ProMED reports from 1996 to 2018. *Int. J. Infect. Dis.* 84, 48–53. doi: 10.1016/j.ijid.2019.04.021

Dhawan, V. K., Bayer, A. S., and Yeaman, M. R. (1998). In vitro resistance to thrombin-induced platelet microbicidal protein is associated with enhanced progression and hematogenous dissemination in experimental Staphylococcus aureus infective endocarditis. *Infect. Immun.* 66, 3476–3479. doi: 10.1128/iai.66.7.3476-3479.1998

Di Nardo, A., Vitiello, A., and Gallo, R. L. (2003). Cutting edge: mast cell antimicrobial activity is mediated by expression of cathelicidin antimicrobial peptide. *J. Immunol.* 170, 2274–2278. doi: 10.4049/jimmunol.170.5.2274

Diep, D. B., Skaugen, M., Salehian, Z., Holo, H., and Nes, I. F. (2007). Common mechanisms of target cell recognition and immunity for class II bacteriocins. *Proc. Natl. Acad. Sci. U.S.A.* 104, 2384–2389. doi: 10.1073/pnas.0608775104

Dintner, S., Staron, A., Berchtold, E., Petri, T., Mascher, T., and Gebhard, S. (2011). Coevolution of ABC transporters and two-component regulatory systems as resistance modules against antimicrobial peptides in Firmicutes Bacteria. *J. Bacteriol.* 193, 3851–3862. doi: 10.1128/JB.05175-11

Draper, L. A., Grainger, K., Deegan, L. H., Cotter, P. D., Hill, C., and Ross, R. P. (2009). Cross-immunity and immune mimicry as mechanisms of resistance to the lantibiotic lacticin 3147. *Mol. Microbiol.* 71, 1043–1054. doi: 10.1111/j.1365-2958.2008.06590.x

Dunman, P. M., Murphy, E., Haney, S., Palacios, D., Tucker-Kellogg, G., Wu, S., et al. (2001). Transcription profiling-based identification of *Staphylococcus aureus* genes regulated by the agr and/or sarA loci. *J. Bacteriol.* 183, 7341–7353. doi: 10.1128/jb.183.24.7341-7353.2001

Ercan, D., and Demirci, A. (2016). Recent advances for the production and recovery methods of lysozyme. *Crit. Rev. Biotechnol.* 36, 1078–1088. doi: 10.3109/07388551.2015.1084263

Ernst, C. M., Staubitz, P., Mishra, N. N., Yang, S. J., Hornig, G., Kalbacher, H., et al. (2009). The bacterial defensin resistance protein MprF consists of

separable domains for lipid lysinylation and antimicrobial peptide repulsion. *PLoS Pathog.* 5:e1000660. doi: 10.1371/journal.ppat.1000660

Fabisiak, A., Murawska, N., and Fichna, J. (2016). LL-37: cathelicidin-related antimicrobial peptide with pleiotropic activity. *Pharmacol. Rep.* 68, 802–808. doi: 10.1016/j.pharep.2016.03.015

Fabretti, F., Theilacker, C., Baldassarri, L., Kaczynski, Z., Kropec, A., Holst, O., et al. (2006). Alanine esters of enterococcal lipoteichoic acid play a role in biofilm formation and resistance to antimicrobial peptides. *Infect. Immun.* 74, 4164–4171. doi: 10.1128/IAI.00111-06

Fiedler, G., Schneider, C., Igbinosa, E. O., Kabisch, J., Brinks, E., Becker, B., et al. (2019). Antibiotics resistance and toxin profiles of *Bacillus cereus*-group isolates from fresh vegetables from German retail markets. *BMC Microbiol.* 19:250. doi: 10.1186/s12866-019-1632-2

Fiore, E., Van Tyne, D., and Gilmore, M. S. (2019). Pathogenicity of enterococci. *Microbiol. Spectr.* 7, 1–23. doi: 10.1128/microbiolspec.GPP3-0053-2018

Fisher, D. J., Miyamoto, K., Harrison, B., Akimoto, S., Sarker, M. R., and McClane, B. A. (2005). Association of beta2 toxin production with *Clostridium perfringens* type A human gastrointestinal disease isolates carrying a plasmid enterotoxin gene. *Mol. Microbiol.* 56, 747–762. doi: 10.1111/j.1365-2958.2005.04573.x

Fisher, N., Shetron-Rama, L., Herring-Palmer, A., Heffernan, B., Bergman, N., and Hanna, P. (2006). The dltABCD operon of *Bacillus anthracis* sterne is required for virulence and resistance to peptide, enzymatic, and cellular mediators of innate immunity. *J. Bacteriol.* 188, 1301–1309. doi: 10.1128/jb.188.4.1301-1309.2006

Foster, T. J., Geoghegan, J. A., Ganesh, V. K., and Hook, M. (2014). Adhesion, invasion and evasion: the many functions of the surface proteins of *Staphylococcus aureus*. *Nat. Rev. Microbiol.* 12, 49–62. doi: 10.1038/nrmicro3161

Frick, I. M., Akesson, P., Rasmussen, M., Schmidtchen, A., and Bjorck, L. (2003). SIC, a secreted protein of *Streptococcus pyogenes* that inactivates antibacterial peptides. *J. Biol. Chem.* 278, 16561–16566. doi: 10.1074/jbc.M301995200

Frohm, M., Agerberth, B., Ahangari, G., Stâhle-Bäckdahl, M., Lidén, S., Wigzell, H., et al. (1997). The expression of the gene coding for the antibacterial peptide LL-37 is induced in human keratinocytes during inflammatory disorders. *J. Biol. Chem.* 272, 15258–15263. doi: 10.1074/jbc.272.24.15258

Fukushima, T., Kitajima, T., and Sekiguchi, J. (2005). A polysaccharide deacetylase homologue, PdaA, in *Bacillus subtilis* acts as an N-acetylmuramic acid deacetylase in vitro. *J. Bacteriol.* 187, 1287–1292. doi: 10.1128/jb.187.4.1287-1292.2005

Garcia, L. G., Lemaire, S., Kahl, B. C., Becker, K., Proctor, R. A., Denis, O., et al. (2013). Antibiotic activity against small-colony variants of *Staphylococcus aureus*: review of in vitro, animal and clinical data. *J. Antimicrob. Chemother.* 68, 1455–1464. doi: 10.1093/jac/dkt072

Gebhard, S., Fang, C., Shaaly, A., Leslie, D. J., Weimar, M. R., Kalamorz, F., et al. (2014). Identification and characterization of a bacitracin resistance network in *Enterococcus faecalis*. *Antimicrob. Agents Chemother.* 58, 1425–1433. doi: 10.1128/AAC.02111-13

Geldart, K., and Kaznessis, Y. N. (2017). Characterization of class IIa bacteriocin resistance in *Enterococcus faecium*. *Antimicrob. Agents Chemother.* 61:e02033-16. doi: 10.1128/AAC.02033-16

Geno, K. A., Gilbert, G. L., Song, J. Y., Skovsted, I. C., Klugman, K. P., Jones, C., et al. (2015). Pneumococcal capsules and their types: past, present, and future. *Clin. Microbiol. Rev.* 28, 871–899. doi: 10.1128/CMR.00024-15

Glaser, R., Becker, K., von Eiff, C., Meyer-Hoffert, U., and Harder, J. (2014). Decreased susceptibility of Staphylococcus aureus small-colony variants toward human antimicrobial peptides. *J. Invest. Dermatol.* 134, 2347–2350. doi: 10.1038/jid.2014.176

Gold, O. G., Jordan, H. V., and Van Houte, J. (1973). A selective medium for *Streptococcus mutans*. *Arch. Oral Biol.* 18, 1357–1364. doi: 10.1016/0003-9969(73)90109-x

Goulart, C., da Silva, T. R., Rodriguez, D., Politano, W. R., Leite, L. C., and Darrieux, M. (2013). Characterization of protective immune responses induced by pneumococcal surface protein A in fusion with pneumolysin derivatives. *PLoS One* 8:e59605. doi: 10.1371/journal.pone.0059605

Gravesen, A., Jydegaard Axelsen, A. M., Mendes da Silva, J., Hansen, T. B., and Knochel, S. (2002a). Frequency of bacteriocin resistance development and associated fitness costs in *Listeria monocytogenes*. *Appl. Environ. Microbiol.* 68, 756–764. doi: 10.1128/aem.68.2.756-764.2002

Gravesen, A., Ramnath, M., Rechinger, K. B., Andersen, N., Jänsch, L., Héchard, Y., et al. (2002b). High-level resistance to class IIa bacteriocins is associated with one general mechanism in Listeria monocytogenes. *Microbiology* 148(Pt 8), 2361–2369. doi: 10.1099/00221287-148-8-2361

Grifoll-Romero, L., Sainz-Polo, M. A., Albesa-Jove, D., Guerin, M. E., Biarnes, X., and Planas, A. (2019). Structure-function relationships underlying the dual N-acetylmuramic and N-acetylglucosamine specificities of the bacterial peptidoglycan deacetylase PdaC. *J. Biol. Chem.* 294, 19066–19080. doi: 10.1074/jbc.RA119.009510

Guariglia-Oropeza, V., and Helmann, J. D. (2011). *Bacillus subtilis* sigma(V) confers lysozyme resistance by activation of two cell wall modification pathways, peptidoglycan O-acetylation and D-alanylation of teichoic acids. *J. Bacteriol.* 193, 6223–6232. doi: 10.1128/JB.06023-11

Habets, M. G., Rozen, D. E., and Brockhurst, M. A. (2012). Variation in *Streptococcus pneumoniae* susceptibility to human antimicrobial peptides may mediate intraspecific competition. *Proc. Biol. Sci.* 279, 3803–3811. doi: 10.1098/rspb.2012.1118

Hachmann, A. B., Angert, E. R., and Helmann, J. D. (2009). Genetic analysis of factors affecting susceptibility of Bacillus subtilis to daptomycin. *Antimicrob. Agents Chemother.* 53, 1598–1609. doi: 10.1128/AAC.01329-08

Hachmann, A. B., Sevim, E., Gaballa, A., Popham, D. L., Antelmann, H., and Helmann, J. D. (2011). Reduction in membrane phosphatidylglycerol content leads to daptomycin resistance in *Bacillus subtilis*. *Antimicrob. Agents Chemother.* 55, 4326–4337. doi: 10.1128/AAC.01819-10

Hagan, A. K., Plotnick, Y. M., Dingle, R. E., Mendel, Z. I, Cendrowski, S. R., Sherman, D. H., et al. (2018). Petrobactin protects against oxidative stress and enhances sporulation efficiency in *Bacillus anthracis* sterne. *mBio* 9:e02079-18. doi: 10.1128/mBio.02079-18

Hakansson, A., Roche, H., Mirza, S., McDaniel, L. S., Brooks-Walter, A., and Briles, D. E. (2001). Characterization of binding of human lactoferrin to pneumococcal surface protein A. *Infect. Immun.* 69, 3372–3381. doi: 10.1128/IAI.69.5.3372-3381.2001

Hamilton, A., Popham, D. L., Carl, D. J., Lauth, X., Nizet, V., and Jones, A. L. (2006). Penicillin-binding protein 1a promotes resistance of group B streptococcus to antimicrobial peptides. *Infect. Immun.* 74, 6179–6187. doi: 10.1128/IAI.00895-06

Hancock, R. E., Haney, E. F., and Gill, E. E. (2016). The immunology of host defence peptides: beyond antimicrobial activity. *Nat. Rev. Immunol.* 16, 321–334. doi: 10.1038/nri.2016.29

Haney, E. F., Mansour, S. C., and Hancock, R. E. (2017). Antimicrobial peptides: an introduction. *Methods Mol. Biol.* 1548, 3–22. doi: 10.1007/978-1-4939-6737-7_1

Hayes, K., Field, D., Hill, C., O'Halloran, F., and Cotter, L. (2019). A novel bioengineered derivative of nisin displays enhanced antimicrobial activity against clinical *Streptococcus agalactiae* isolates. *J. Glob. Antimicrob. Resist.* 19, 14–21. doi: 10.1016/j.jgar.2019.04.010

Hebert, L., Courtin, P., Torelli, R., Sanguinetti, M., Chapot-Chartier, M. P., Auffray, Y., et al. (2007). *Enterococcus faecalis* constitutes an unusual bacterial model in lysozyme resistance. *Infect. Immun.* 75, 5390–5398. doi: 10.1128/IAI.00571-07

Héchard, Y., Pelletier, C., Cenatiempo, Y., and Frère, J. (2001). Analysis of sigma(54)-dependent genes in *Enterococcus faecalis*: a mannose PTS permease (EII(Man)) is involved in sensitivity to a bacteriocin, mesentericin Y105. *Microbiology.* 147(Pt 6), 1575–1580. doi: 10.1099/00221287-147-6-1575

Hirt, H., Hall, J. W., Larson, E., and Gorr, S. U. (2018). A D-enantiomer of the antimicrobial peptide GL13K evades antimicrobial resistance in the Gram positive bacteria *Enterococcus faecalis* and *Streptococcus gordonii*. *PLoS One* 13:e0194900. doi: 10.1371/journal.pone.0194900

Ho, T. D., and Ellermeier, C. D. (2011). PrsW is required for colonization, resistance to antimicrobial peptides, and expression of extracytoplasmic function sigma factors in *Clostridium difficile*. *Infect. Immun.* 79, 3229–3238. doi: 10.1128/IAI.00019-11

Ho, T. D., Hastie, J. L., Intile, P. J., and Ellermeier, C. D. (2011). The Bacillus subtilis extracytoplasmic function σ factor σ(V) is induced by lysozyme and provides resistance to lysozyme. *J. Bacteriol.* 193, 6215–6222. doi: 10.1128/jb.05467-11

Huang, Y., Flint, S. H., and Palmer, J. S. (2020). Bacillus cereus spores and toxins – The potential role of biofilms. *Food Microbiol.* 90:103493. doi: 10.1016/j.fm.2020.103493

Hunter, H. N., Jing, W., Schibli, D. J., Trinh, T., Park, I. Y., Kim, S. C., et al. (2005). The interactions of antimicrobial peptides derived from lysozyme with model membrane systems. *Biochim. Biophys. Acta* 1668, 175–189. doi: 10.1016/j.bbamem.2004.12.004

Hyyryläinen, H. L., Pietiäinen, M., Lundén, T., Ekman, A., Gardemeister, M., Murtomäki-Repo, S., et al. (2007). The density of negative charge in the cell wall influences two-component signal transduction in *Bacillus subtilis*. *Microbiology* 153(Pt 7), 2126–2136. doi: 10.1099/mic.0.2007/008680-0

Ibrahim, H. R., Imazato, K., and Ono, H. (2011). Human lysozyme possesses novel antimicrobial peptides within its N-terminal domain that target bacterial respiration. *J. Agric. Food Chem.* 59, 10336–10345. doi: 10.1021/jf2020396

Ibrahim, H. R., Thomas, U., and Pellegrini, A. (2001). A helix-loop-helix peptide at the upper lip of the active site cleft of lysozyme confers potent antimicrobial activity with membrane permeabilization action. *J. Biol. Chem.* 276, 43767–43774. doi: 10.1074/jbc.M106317200

Jann, N. J., Schmaler, M., Kristian, S. A., Radek, K. A., Gallo, R. L., Nizet, V., et al. (2009). Neutrophil antimicrobial defense against *Staphylococcus aureus* is mediated by phagolysosomal but not extracellular trap-associated cathelicidin. *J. Leukoc. Biol.* 86, 1159–1169. doi: 10.1189/jlb.0209053

Jenssen, H., Hamill, P., and Hancock, R. E. (2006). Peptide antimicrobial agents. *Clin. Microbiol. Rev.* 19, 491–511. doi: 10.1128/CMR.00056-05

Jin, T., Bokarewa, M., Foster, T., Mitchell, J., Higgins, J., and Tarkowski, A. (2004). *Staphylococcus aureus* resists human defensins by production of staphylokinase, a novel bacterial evasion mechanism. *J. Immunol.* 172, 1169–1176. doi: 10.4049/jimmunol.172.2.1169

Jones, A. L., Mertz, R. H., Carl, D. J., and Rubens, C. E. (2007). A streptococcal penicillin-binding protein is critical for resisting innate airway defenses in the neonatal lung. *J. Immunol.* 179, 3196–3202. doi: 10.4049/jimmunol.179.5.3196

Joo, H. S., and Otto, M. (2015). Mechanisms of resistance to antimicrobial peptides in staphylococci. *Biochim. Biophys. Acta* 1848(Pt B), 3055–3061. doi: 10.1016/j.bbamem.2015.02.009

Jordan, S., Junker, A., Helmann, J. D., and Mascher, T. (2006). Regulation of LiaRS-dependent gene expression in bacillus subtilis: identification of inhibitor proteins, regulator binding sites, and target genes of a conserved cell envelope stress-sensing two-component system. *J. Bacteriol.* 188, 5153–5166. doi: 10.1128/JB.00310-06

Kallenberg, F., Dintner, S., Schmitz, R., and Gebhard, S. (2013). Identification of regions important for resistance and signalling within the antimicrobial peptide transporter BceAB of Bacillus subtilis. *J. Bacteriol.* 195, 3287–3297. doi: 10.1128/JB.00419-13

Kamar, R., Rejasse, A., Jehanno, I., Attieh, Z., Courtin, P., Chapot-Chartier, M. P., et al. (2017). DltX of *Bacillus thuringiensis* is essential for D-alanylation of teichoic acids and resistance to antimicrobial response in insects. *Front. Microbiol.* 8:1437. doi: 10.3389/fmicb.2017.01437

Kandaswamy, K., Liew, T. H., Wang, C. Y., Huston-Warren, E., Meyer-Hoffert, U., Hultenby, K., et al. (2013). Focal targeting by human beta-defensin 2 disrupts localized virulence factor assembly sites in *Enterococcus faecalis*. *Proc. Natl. Acad. Sci. U.S.A.* 110, 20230–20235. doi: 10.1073/pnas.1319066110

Khan, A., Davlieva, M., Panesso, D., Rincon, S., Miller, W. R., Diaz, L., et al. (2019). Antimicrobial sensing coupled with cell membrane remodeling mediates antibiotic resistance and virulence in *Enterococcus faecalis*. *Proc. Natl. Acad. Sci. U.S.A.* 116, 26925–26932. doi: 10.1073/pnas.1916037116

Khan, M. N., and Pichichero, M. E. (2014). The host immune dynamics of pneumococcal colonization: implications for novel vaccine development. *Hum. Vaccin. Immunother.* 10, 3688–3699. doi: 10.4161/21645515.2014.979631

Khosa, S., AlKhatib, Z., and Smits, S. H. (2013). NSR from *Streptococcus agalactiae* confers resistance against nisin and is encoded by a conserved nsr operon. *Biol. Chem.* 394, 1543–1549. doi: 10.1515/hsz-2013-0167

Khosa, S., Hoeppner, A., Kleinschrodt, D., and Smits, S. H. (2015). Overexpression, purification, crystallization and preliminary X-ray diffraction of the nisin resistance protein from Streptococcus agalactiae. *Acta Crystallogr. F Struct. Biol. Commun.* 71(Pt 6), 671–675. doi: 10.1107/S2053230X15006226

Khosa, S., Lagedroste, M., and Smits, S. H. (2016). Protein defense systems against the lantibiotic nisin: function of the immunity protein NisI and the resistance protein NSR. *Front. Microbiol.* 7:504. doi: 10.3389/fmicb.2016.00504

Kietzman, C. C., Gao, G., Mann, B., Myers, L., and Tuomanen, E. I. (2016). Dynamic capsule restructuring by the main pneumococcal autolysin LytA in response to the epithelium. *Nat. Commun.* 7:10859. doi: 10.1038/ncomms10859

Kitagawa, N., Shiota, S., Shibata, Y., Takeshita, T., and Yamashita, Y. (2011). Characterization of MbrC involved in bacitracin resistance in Streptococcus mutans. *FEMS Microbiol. Lett.* 318, 61–67. doi: 10.1111/j.1574-6968.2011.02238.x

Kjos, M., Nes, I. F., and Diep, D. B. (2011). Mechanisms of resistance to bacteriocins targeting the mannose phosphotransferase system. *Appl. Environ. Microbiol.* 77, 3335–3342. doi: 10.1128/AEM.02602-10

Kobayashi, K., Sudiarta, I. P., Kodama, T., Fukushima, T., Ara, K., Ozaki, K., et al. (2012). Identification and characterization of a novel polysaccharide deacetylase C (PdaC) from *Bacillus subtilis*. *J. Biol. Chem.* 287, 9765–9776. doi: 10.1074/jbc.M111.329490

Kocianova, S., Vuong, C., Yao, Y., Voyich, J. M., Fischer, E. R., DeLeo, F. R., et al. (2005). Key role of poly-gamma-DL-glutamic acid in immune evasion and virulence of Staphylococcus epidermidis. *J. Clin. Invest.* 115, 688–694. doi: 10.1172/JCI23523

Kościuczuk, E. M., Lisowski, P., Jarczak, J., Strzałkowska, N., Jóźwik, A., Horbańczuk, J., et al. (2012). Cathelicidins: family of antimicrobial peptides: a review. *Mol. Biol. Rep.* 39, 10957–10970.

Kovacs, M., Halfmann, A., Fedtke, I., Heintz, M., Peschel, A., Vollmer, W., et al. (2006). A functional dlt operon, encoding proteins required for incorporation of d-alanine in teichoic acids in gram-positive bacteria, confers resistance to cationic antimicrobial peptides in *Streptococcus pneumoniae*. *J. Bacteriol.* 188, 5797–5805. doi: 10.1128/JB.00336-06

Kraus, D., and Peschel, A. (2006). Molecular mechanisms of bacterial resistance to antimicrobial peptides. *Curr. Top. Microbiol. Immunol.* 306, 231–250. doi: 10.1007/3-540-29916-5_9

Kristian, S. A., Datta, V., Weidenmaier, C., Kansal, R., Fedtke, I., Peschel, A., et al. (2005). D-alanylation of teichoic acids promotes group a streptococcus antimicrobial peptide resistance, neutrophil survival, and epithelial cell invasion. *J. Bacteriol.* 187, 6719–6725. doi: 10.1128/JB.187.19.6719-6725.2005

Kristich, C. J., Rice, L. B., and Arias, C. A. (2014). "Enterococcal infection—treatment and antibiotic resistance," in *Enterococci: From Commensals to Leading Causes of Drug Resistant Infection*, eds M. S. Gilmore, D. B. Clewell, Y. Ike, and N. Shankar (Boston, MA: Massachusetts Eye and Ear Infirmary).

Kumariya, R., Sood, S. K., Rajput, Y. S., Saini, N., and Garsa, A. K. (2015). Increased membrane surface positive charge and altered membrane fluidity leads to cationic antimicrobial peptide resistance in Enterococcus faecalis. *Biochim. Biophys. Acta* 1848, 1367–1375. doi: 10.1016/j.bbamem.2015.03.007

Kunda, N. K. (2020). Antimicrobial peptides as novel therapeutics for non-small cell lung cancer. *Drug Discov. Today* 25, 238–247. doi: 10.1016/j.drudis.2019.11.012

Laaberki, M. H., Pfeffer, J., Clarke, A. J., and Dworkin, J. (2011). O-Acetylation of peptidoglycan is required for proper cell separation and S-layer anchoring in *Bacillus anthracis*. *J. Biol. Chem.* 286, 5278–5288. doi: 10.1074/jbc.M110.183236

Lauth, X., von Kockritz-Blickwede, M., McNamara, C. W., Myskowski, S., Zinkernagel, A. S., Beall, B., et al. (2009). M1 protein allows Group A streptococcal survival in phagocyte extracellular traps through cathelicidin inhibition. *J. Innate Immun.* 1, 202–214. doi: 10.1159/000203645

Lazar, V., Martins, A., Spohn, R., Daruka, L., Grezal, G., Fekete, G., et al. (2018). Antibiotic-resistant bacteria show widespread collateral sensitivity to antimicrobial peptides. *Nat. Microbiol.* 3, 718–731. doi: 10.1038/s41564-018-0164-0

Le Jeune, A., Torelli, R., Sanguinetti, M., Giard, J. C., Hartke, A., Auffray, Y., et al. (2010). The extracytoplasmic function sigma factor SigV plays a key role in the original model of lysozyme resistance and virulence of Enterococcus faecalis. *PLoS One* 5:e9658. doi: 10.1371/journal.pone.0009658

Lee, H., Boyle-Vavra, S., Ren, J., Jarusiewicz, J. A., Sharma, L. K., Hoagland, D. T., et al. (2019). Identification of small molecules exhibiting oxacillin synergy through a novel assay for inhibition of vraTSR expression in methicillin-resistant *Staphylococcus aureus*. *Antimicrob. Agents Chemother.* 63:e02593-18.

Lessa, F. C., Mu, Y., Bamberg, W. M., Beldavs, Z. G., Dumyati, G. K., Dunn, J. R., et al. (2015). Burden of *Clostridium difficile* infection in the United States. *N. Engl. J. Med.* 372, 825–834. doi: 10.1056/NEJMoa1408913

Li, M., Cha, D. J., Lai, Y., Villaruz, A. E., Sturdevant, D. E., and Otto, M. (2007a). The antimicrobial peptide-sensing system aps of *Staphylococcus aureus*. *Mol. Microbiol.* 66, 1136–1147. doi: 10.1111/j.1365-2958.2007.05986.x

Li, M., Lai, Y., Villaruz, A. E., Cha, D. J., Sturdevant, D. E., and Otto, M. (2007b). Gram-positive three-component antimicrobial peptide-sensing system. *Proc. Natl. Acad. Sci. U.S.A.* 104, 9469–9474. doi: 10.1073/pnas.0702159104

Li, Y., Weinberger, D. M., Thompson, C. M., Trzcinski, K., and Lipsitch, M. (2013). Surface charge of Streptococcus pneumoniae predicts serotype distribution. *Infect. Immun.* 81, 4519–4524. doi: 10.1128/IAI.00724-13

Llobet, E., Tomas, J. M., and Bengoechea, J. A. (2008). Capsule polysaccharide is a bacterial decoy for antimicrobial peptides. *Microbiology (Reading)* 154(Pt 12), 3877–3886. doi: 10.1099/mic.0.2008/022301-0

Mahlapuu, M., Hakansson, J., Ringstad, L., and Bjorn, C. (2016). Antimicrobial peptides: an emerging category of therapeutic agents. *Front. Cell Infect. Microbiol.* 6:194. doi: 10.3389/fcimb.2016.00194

Maisey, H. C., Quach, D., Hensler, M. E., Liu, G. Y., Gallo, R. L., Nizet, V., et al. (2008). A group B streptococcal pilus protein promotes phagocyte resistance and systemic virulence. *FASEB J.* 22, 1715–1724. doi: 10.1096/fj.07-093963

Maisnier-Patin, S., and Richard, J. (1996). Cell wall changes in nisin-resistant variants of Listeria innocua grown in the presence of high nisin concentrations. *FEMS Microbiol. Lett.* 140, 29–35. doi: 10.1111/j.1574-6968.1996.tb08310.x

Majchrzykiewicz, J. A., Kuipers, O. P., and Bijlsma, J. J. (2010). Generic and specific adaptive responses of Streptococcus pneumoniae to challenge with three distinct antimicrobial peptides, bacitracin, LL-37, and nisin. *Antimicrob. Agents Chemother.* 54, 440–451. doi: 10.1128/AAC.00769-09

Mandin, P., Fsihi, H., Dussurget, O., Vergassola, M., Milohanic, E., Toledo-Arana, A., et al. (2005). VirR, a response regulator critical for *Listeria monocytogenes* virulence. *Mol. Microbiol.* 57, 1367–1380. doi: 10.1111/j.1365-2958.2005.04776.x

Manson, J. M., Keis, S., Smith, J. M., and Cook, G. M. (2004). Acquired bacitracin resistance in *Enterococcus faecalis* is mediated by an ABC transporter and a novel regulatory protein, BcrR. *Antimicrob. Agents Chemother.* 48, 3743–3748. doi: 10.1128/AAC.48.10.3743-3748.2004

Martinez, P. J., Farhan, A., Mustafa, M., Javaid, N., Darkoh, C., Garrido-Sanabria, E., et al. (2019). PspA facilitates evasion of pneumococci from bactericidal activity of neutrophil extracellular traps (NETs). *Microb. Pathog.* 136:103653. doi: 10.1016/j.micpath.2019.103653

Martínez-García, S., Chávez-Cabrera, C., Quintana, E. T., Marsch-Moreno, R., Ibáñez-Hernández, M. A., Zenteno, J. C., et al. (2019). Differential expression of the apsXRS system by antimicrobial peptide LL-37 in commensal and clinical *Staphylococcus epidermidis* isolates. *Indian J. Microbiol.* 59, 295–303. doi: 10.1007/s12088-019-00800-6

Mascher, T., Margulis, N. G., Wang, T., Ye, R. W., and Helmann, J. D. (2003). Cell wall stress responses in *Bacillus subtilis*: the regulatory network of the bacitracin stimulon. *Mol. Microbiol.* 50, 1591–1604. doi: 10.1046/j.1365-2958.2003.03786.x

Mascher, T., Zimmer, S. L., Smith, T. A., and Helmann, J. D. (2004). Antibiotic-inducible promoter regulated by the cell envelope stress-sensing two-component system LiaRS of *Bacillus subtilis*. *Antimicrob. Agents Chemother.* 48, 2888–2896. doi: 10.1128/AAC.48.8.2888-2896.2004

Matos, R., Pinto, V. V., Ruivo, M., and Lopes Mde, F. (2009). Study on the dissemination of the bcrABDR cluster in Enterococcus spp. reveals that the BcrAB transporter is sufficient to confer high-level bacitracin resistance. *Int. J. Antimicrob. Agents* 34, 142–147. doi: 10.1016/j.ijantimicag.2009.02.008

May, J. J., Finking, R., Wiegeshoff, F., Weber, T. T., Bandur, N., Koert, U., et al. (2005). Inhibition of the D-alanine:D-alanyl carrier protein ligase from *Bacillus subtilis* increases the bacterium's susceptibility to antibiotics that target the cell wall. *FEBS J.* 272, 2993–3003. doi: 10.1111/j.1742-4658.2005.04700.x

Mazzotta, A. S., and Montville, T. J. (1997). Nisin induces changes in membrane fatty acid composition of Listeria monocytogenes nisin-resistant strains at 10 degrees C and 30 degrees C. *J. Appl. Microbiol.* 82, 32–38. doi: 10.1111/j.1365-2672.1997.tb03294.x

McBride, S. M., and Sonenshein, A. L. (2011a). The dlt operon confers resistance to cationic antimicrobial peptides in *Clostridium difficile*. *Microbiology* 157(Pt 5), 1457–1465. doi: 10.1099/mic.0.045997-0

McBride, S. M., and Sonenshein, A. L. (2011b). Identification of a genetic locus responsible for antimicrobial peptide resistance in *Clostridium difficile*. *Infect. Immun.* 79, 167–176. doi: 10.1128/IAI.00731-10

McQuade, R., Roxas, B., Viswanathan, V. K., and Vedantam, G. (2012). *Clostridium difficile* clinical isolates exhibit variable susceptibility and proteome alterations upon exposure to mammalian cationic antimicrobial peptides. *Anaerobe* 18, 614–620. doi: 10.1016/j.anaerobe.2012.09.004

Meade, K. G., and O'Farrelly, C. (2018). beta-defensins: farming the microbiome for homeostasis and health. *Front. Immunol.* 9:3072. doi: 10.3389/fimmu.2018.03072

Meehl, M., Herbert, S., Gotz, F., and Cheung, A. (2007). Interaction of the GraRS two-component system with the VraFG ABC transporter to support vancomycin-intermediate resistance in *Staphylococcus aureus*. *Antimicrob. Agents Chemother.* 51, 2679–2689. doi: 10.1128/AAC.00209-07

Mehla, J., and Sood, S. K. (2011). Substantiation in *Enterococcus faecalis* of dose-dependent resistance and cross-resistance to pore-forming antimicrobial peptides by use of a polydiacetylene-based colorimetric assay. *Appl. Environ. Microbiol.* 77, 786–793. doi: 10.1128/AEM.01496-10

Meireles, D., Pombinho, R., Carvalho, F., Sousa, S., and Cabanes, D. (2020). *Listeria monocytogenes* wall teichoic acid glycosylation promotes surface anchoring of virulence factors, resistance to antimicrobial peptides, and decreased susceptibility to antibiotics. *Pathogens* 9:290. doi: 10.3390/pathogens9040290

Mine, Y., Ma, F., and Lauriau, S. (2004). Antimicrobial peptides released by enzymatic hydrolysis of hen egg white lysozyme. *J. Agric. Food Chem.* 52, 1088–1094. doi: 10.1021/jf0345752

Ming, X., and Daeschel, M. A. (1993). Nisin resistance of foodborne bacteria and the specific resistance responses of *Listeria monocytogenes* scott A. *J. Food Protoc.* 56, 944–948. doi: 10.4315/0362-028X-56.11.944

Mishra, N. N., Bayer, A. S., Tran, T. T., Shamoo, Y., Mileykovskaya, E., Dowhan, W., et al. (2012). Daptomycin resistance in enterococci is associated with distinct alterations of cell membrane phospholipid content. *PLoS One* 7:e43958. doi: 10.1371/journal.pone.0043958

Mishra, N. N., Liu, G. Y., Yeaman, M. R., Nast, C. C., Proctor, R. A., McKinnell, J., et al. (2011). Carotenoid-related alteration of cell membrane fluidity impacts *Staphylococcus aureus* susceptibility to host defense peptides. *Antimicrob. Agents Chemother.* 55, 526–531. doi: 10.1128/AAC.00680-10

Monniot, C., Zebre, A. C., Ake, F. M., Deutscher, J., and Milohanic, E. (2012). Novel listerial glycerol dehydrogenase- and phosphoenolpyruvate-dependent dihydroxyacetone kinase system connected to the pentose phosphate pathway. *J. Bacteriol.* 194, 4972–4982. doi: 10.1128/JB.00801-12

Moravej, H., Moravej, Z., Yazdanparast, M., Heiat, M., Mirhosseini, A., Moosazadeh Moghaddam, M., et al. (2018). Antimicrobial peptides: features, action, and their resistance mechanisms in bacteria. *Microb. Drug Resist.* 24, 747–767. doi: 10.1089/mdr.2017.0392

Mucke, P. A., Maass, S., Kohler, T. P., Hammerschmidt, S., and Becher, D. (2020). Proteomic adaptation of *Streptococcus pneumoniae* to the human antimicrobial peptide LL-37. *Microorganisms* 8:413. doi: 10.3390/microorganisms8030413

Mukerji, R., Mirza, S., Roche, A. M., Widener, R. W., Croney, C. M., Rhee, D. K., et al. (2012). Pneumococcal surface protein A inhibits complement deposition on the pneumococcal surface by competing with the binding of C-reactive protein to cell-surface phosphocholine. *J. Immunol.* 189, 5327–5335. doi: 10.4049/jimmunol.1201967

Naghmouchi, K., Drider, D., Kheadr, E., Lacroix, C., Prevost, H., and Fliss, I. (2006). Multiple characterizations of Listeria monocytogenes sensitive and insensitive variants to divergicin M35, a new pediocin-like bacteriocin. *J. Appl. Microbiol.* 100, 29–39. doi: 10.1111/j.1365-2672.2005.02771.x

Naghmouchi, K., Kheadr, E., Lacroix, C., and Fliss, I. (2007). Class I/Class IIa bacteriocin cross-resistance phenomenon in Listeria monocytogenes. *Food Microbiol.* 24, 718–727. doi: 10.1016/j.fm.2007.03.012

Nasser, A., Moradi, M., Jazireian, P., Safari, H., Alizadeh-Sani, M., Pourmand, M. R., et al. (2019). *Staphylococcus aureus* versus neutrophil: scrutiny of ancient combat. *Microb Pathog* 131, 259–269. doi: 10.1016/j.micpath.2019.04.026

Nawrocki, K. L., Crispell, E. K., and McBride, S. M. (2014). Antimicrobial peptide resistance mechanisms of gram-positive bacteria. *Antibiotics (Basel)* 3, 461–492. doi: 10.3390/antibiotics3040461

Neoh, H. M., Cui, L., Yuzawa, H., Takeuchi, F., Matsuo, M., and Hiramatsu, K. (2008). Mutated response regulator graR is responsible for phenotypic conversion of *Staphylococcus aureus* from heterogeneous vancomycin-intermediate resistance to vancomycin-intermediate resistance. *Antimicrob. Agents Chemother.* 52, 45–53. doi: 10.1128/AAC.00534-00507

Nesuta, O., Budesinsky, M., Hadravova, R., Monincova, L., Humpolickova, J., and Cerovsky, V. (2017). How proteases from *Enterococcus faecalis* contribute to its resistance to short alpha-helical antimicrobial peptides. *Pathog. Dis.* 75:ftx091. doi: 10.1093/femspd/ftx091

Nguyen, T. X., Cole, A. M., and Lehrer, R. I. (2003). Evolution of primate theta-defensins: a serpentine path to a sweet tooth. *Peptides* 24, 1647–1654. doi: 10.1016/j.peptides.2003.07.023

Ohki, R., Giyanto, Tateno, K., Masuyama, W., Moriya, S., Kobayashi, K., et al. (2003a). The BceRS two-component regulatory system induces expression of the bacitracin transporter, BceAB, in *Bacillus subtilis*. *Mol. Microbiol.* 49, 1135–1144. doi: 10.1046/j.1365-2958.2003.03653.x

Ohki, R., Tateno, K., Okada, Y., Okajima, H., Asai, K., Sadaie, Y., et al. (2003b). A bacitracin-resistant *Bacillus subtilis* gene encodes a homologue of the membrane-spanning subunit of the Bacillus licheniformis ABC transporter. *J. Bacteriol.* 185, 51–59. doi: 10.1128/jb.185.1.51-59.2003

Oku, Y., Kurokawa, K., Ichihashi, N., and Sekimizu, K. (2004). Characterization of the *Staphylococcus aureus* mprF gene, involved in lysinylation of phosphatidylglycerol. *Microbiology (Reading)* 150(Pt 1), 45–51. doi: 10.1099/mic.0.26706-0

Opsata, M., Nes, I. F., and Holo, H. (2010). Class IIa bacteriocin resistance in *Enterococcus faecalis* V583: the mannose PTS operon mediates global transcriptional responses. *BMC Microbiol.* 10:224. doi: 10.1186/1471-2180-10-224

Palmer, M. E., Wiedmann, M., and Boor, K. J. (2009). sigma(B) and sigma(L) contribute to Listeria monocytogenes 10403S response to the antimicrobial peptides SdpC and nisin. *Foodborne Pathog. Dis.* 6, 1057–1065. doi: 10.1089/fpd.2009.0292

Palumbo, E., Deghorain, M., Cocconcelli, P. S., Kleerebezem, M., Geyer, A., Hartung, T., et al. (2006). D-alanyl ester depletion of teichoic acids in Lactobacillus plantarum results in a major modification of lipoteichoic acid composition and cell wall perforations at the septum mediated by the Acm2 autolysin. *J. Bacteriol.* 188, 3709–3715. doi: 10.1128/jb.188.10.3709-3715.2006

Patel, K., and Golemi-Kotra, D. (2015). Signaling mechanism by the Staphylococcus aureus two-component system LytSR: role of acetyl phosphate in bypassing the cell membrane electrical potential sensor LytS. *F1000Res.* 4:79. doi: 10.12688/f1000research.6213.2

Peschel, A., Otto, M., Jack, R. W., Kalbacher, H., Jung, G., and Gotz, F. (1999). Inactivation of the dlt operon in Staphylococcus aureus confers sensitivity to defensins, protegrins, and other antimicrobial peptides. *J. Biol. Chem.* 274, 8405–8410. doi: 10.1074/jbc.274.13.8405

Pfeffer, J. M., Strating, H., Weadge, J. T., and Clarke, A. J. (2006). Peptidoglycan O acetylation and autolysin profile of Enterococcus faecalis in the viable but nonculturable state. *J. Bacteriol.* 188, 902–908. doi: 10.1128/JB.188.3.902-908.2006

Phattarataratip, E., Olson, B., Broffitt, B., Qian, F., Brogden, K. A., Drake, D. R., et al. (2011). Streptococcus mutans strains recovered from caries-active or caries-free individuals differ in sensitivity to host antimicrobial peptides. *Mol. Oral Microbiol.* 26, 187–199. doi: 10.1111/j.2041-1014.2011.00607.x

Pietiäinen, M., François, P., Hyyryläinen, H. L., Tangomo, M., Sass, V., Sahl, H. G., et al. (2009). Transcriptome analysis of the responses of *Staphylococcus aureus* to antimicrobial peptides and characterization of the roles of vraDE and vraSR in antimicrobial resistance. *BMC Genomics* 10:1471–2164. doi: 10.1186/1471-2164-10-429

Podlesek, Z., Comino, A., Herzog-Velikonja, B., Zgur-Bertok, D., Komel, R., and Grabnar, M. (1995). *Bacillus licheniformis* bacitracin-resistance ABC transporter: relationship to mammalian multidrug resistance. *Mol. Microbiol.* 16, 969–976. doi: 10.1111/j.1365-2958.1995.tb02322.x

Popowska, M., Kusio, M., Szymanska, P., and Markiewicz, Z. (2009). Inactivation of the wall-associated de-N-acetylase (PgdA) of *Listeria monocytogenes* results in greater susceptibility of the cells to induced autolysis. *J. Microbiol. Biotechnol.* 19, 932–945. doi: 10.4014/jmb.0810.557

Porta, N., Zaschke-Kriesche, J., Frieg, B., Gopalswamy, M., Zivkovic, A., Etzkorn, M., et al. (2019). Small-molecule inhibitors of nisin resistance protein NSR from the human pathogen *Streptococcus agalactiae*. *Bioorg. Med. Chem.* 27:115079. doi: 10.1016/j.bmc.2019.115079

Poyart, C., Lamy, M. C., Boumaila, C., Fiedler, F., and Trieu-Cuot, P. (2001). Regulation of D-alanyl-lipoteichoic acid biosynthesis in *Streptococcus agalactiae* involves a novel two-component regulatory system. *J. Bacteriol.* 183, 6324–6334. doi: 10.1128/JB.183.21.6324-6334.2001

Poyart, C., Pellegrini, E., Marceau, M., Baptista, M., Jaubert, F., Lamy, M. C., et al. (2003). Attenuated virulence of Streptococcus agalactiae deficient in D-alanyl-lipoteichoic acid is due to an increased susceptibility to defensins and phagocytic cells. *Mol. Microbiol.* 49, 1615–1625. doi: 10.1046/j.1365-2958.2003.03655.x

Psylinakis, E., Boneca, I. G., Mavromatis, K., Deli, A., Hayhurst, E., Foster, S. J., et al. (2005). Peptidoglycan N-acetylglucosamine deacetylases from *Bacillus cereus*, highly conserved proteins in *Bacillus anthracis*. *J. Biol. Chem.* 280, 30856–30863. doi: 10.1074/jbc.M407426200

Raabe, V. N., and Shane, A. L. (2019). Group B Streptococcus (*Streptococcus agalactiae*). *Microbiol. Spectr.* 7, 1–13. doi: 10.1128/microbiolspec.GPP3-0007-2018

Rae, C. S., Geissler, A., Adamson, P. C., and Portnoy, D. A. (2011). Mutations of the Listeria monocytogenes peptidoglycan N-deacetylase and O-acetylase result in enhanced lysozyme sensitivity, bacteriolysis, and hyperinduction of innate immune pathways. *Infect. Immun.* 79, 3596–3606. doi: 10.1128/IAI.00077-11

Rafei, R., Hawli, M., Osman, M., Dabboussi, F., and Hamze, M. (2020). Distribution of emm types and macrolide resistance determinants among group A streptococci in the Middle East and North Africa region. *J. Glob. Antimicrob. Resist.* 22, 334–348. doi: 10.1016/j.jgar.2020.02.005

Ramnath, M., Beukes, M., Tamura, K., and Hastings, J. W. (2000). Absence of a putative mannose-specific phosphotransferase system enzyme IIAB component in a leucocin A-resistant strain of Listeria monocytogenes, as shown by two-dimensional sodium dodecyl sulfate-polyacrylamide gel electrophoresis. *Appl. Environ. Microbiol.* 66, 3098–3101. doi: 10.1128/aem.66.7.3098-3101.2000

Reffuveille, F., de la Fuente-Nunez, C., Mansour, S., and Hancock, R. E. (2014). A broad-spectrum antibiofilm peptide enhances antibiotic action against bacterial biofilms. *Antimicrob. Agents Chemother.* 58, 5363–5371. doi: 10.1128/AAC.03163-14

Reiners, J., Lagedroste, M., Ehlen, K., Leusch, S., Zaschke-Kriesche, J., and Smits, S. H. J. (2017). The N-terminal region of nisin is important for the BceAB-Type ABC transporter NsrFP from *Streptococcus agalactiae* COH1. *Front. Microbiol.* 8:1643. doi: 10.3389/fmicb.2017.01643

Ren, B., McCrory, M. A., Pass, C., Bullard, D. C., Ballantyne, C. M., Xu, Y., et al. (2004). The virulence function of *Streptococcus pneumoniae* surface protein A involves inhibition of complement activation and impairment of complement receptor-mediated protection. *J. Immunol.* 173, 7506–7512. doi: 10.4049/jimmunol.173.12.7506

Reyes, J., Panesso, D., Tran, T. T., Mishra, N. N., Cruz, M. R., Munita, J. M., et al. (2015). A liaR deletion restores susceptibility to daptomycin and antimicrobial peptides in multidrug-resistant Enterococcus faecalis. *J. Infect. Dis.* 211, 1317–1325. doi: 10.1093/infdis/jiu602

Rietkotter, E., Hoyer, D., and Mascher, T. (2008). Bacitracin sensing in *Bacillus subtilis*. *Mol. Microbiol.* 68, 768–785. doi: 10.1111/j.1365-2958.2008.06194.x

Robichon, D., Gouin, E., Débarbouillé, M., Cossart, P., Cenatiempo, Y., and Héchard, Y. (1997). The rpoN (sigma54) gene from Listeria monocytogenes is involved in resistance to mesentericin Y105, an antibacterial peptide from Leuconostoc mesenteroides. *J. Bacteriol.* 179, 7591–7594. doi: 10.1128/jb.179.23.7591-7594.1997

Saar-Dover, R., Bitler, A., Nezer, R., Shmuel-Galia, L., Firon, A., Shimoni, E., et al. (2012). D-alanylation of lipoteichoic acids confers resistance to cationic peptides in group B streptococcus by increasing the cell wall density. *PLoS Pathog* 8:e1002891. doi: 10.1371/journal.ppat.1002891

Sadowska, B., Bonar, A., von Eiff, C., Proctor, R. A., Chmiela, M., Rudnicka, W., et al. (2002). Characteristics of *Staphylococcus aureus*, isolated from airways of cystic fibrosis patients, and their small colony variants. *FEMS Immunol. Med. Microbiol.* 32, 191–197. doi: 10.1111/j.1574-695x.2002.tb00553.x

Samant, S., Hsu, F. F., Neyfakh, A. A., and Lee, H. (2009). The *Bacillus anthracis* protein MprF is required for synthesis of lysylphosphatidylglycerols and for resistance to cationic antimicrobial peptides. *J. Bacteriol.* 191, 1311–1319. doi: 10.1128/jb.01345-08

Samuelsen, O., Haukland, H. H., Jenssen, H., Kramer, M., Sandvik, K., Ulvatne, H., et al. (2005). Induced resistance to the antimicrobial peptide lactoferricin B in *Staphylococcus aureus*. *FEBS Lett.* 579, 3421–3426. doi: 10.1016/j.febslet.2005.05.017

Schlech, W. F. (2019). Epidemiology and clinical manifestations of *Listeria monocytogenes* infection. *Microbiol. Spectr.* 7, 1–12. doi: 10.1128/microbiolspec.GPP3-0014-2018

Schmidtchen, A., Frick, I. M., Andersson, E., Tapper, H., and Bjorck, L. (2002). Proteinases of common pathogenic bacteria degrade and inactivate the antibacterial peptide LL-37. *Mol. Microbiol.* 46, 157–168. doi: 10.1046/j.1365-2958.2002.03146.x

Schmidtchen, A., Frick, I. M., and Björck, L. (2001). Dermatan sulphate is released by proteinases of common pathogenic bacteria and inactivates antibacterial alpha-defensin. *Mol. Microbiol.* 39, 708–713. doi: 10.1046/j.1365-2958.2001.02251.x

Sedgley, C. M., Clewell, D. B., and Flannagan, S. E. (2009). Plasmid pAMS1-encoded, bacteriocin-related "Siblicide" in *Enterococcus faecalis*. *J. Bacteriol.* 191, 3183–3188. doi: 10.1128/JB.00147-09

Senkovich, O., Cook, W. J., Mirza, S., Hollingshead, S. K., Protasevich, I. I., Briles, D. E., et al. (2007). Structure of a complex of human lactoferrin N-lobe with pneumococcal surface protein a provides insight into microbial defense mechanism. *J. Mol. Biol.* 370, 701–713. doi: 10.1016/j.jmb.2007.04.075

Shaaly, A., Kalamorz, F., Gebhard, S., and Cook, G. M. (2013). Undecaprenyl pyrophosphate phosphatase confers low-level resistance to bacitracin in *Enterococcus faecalis*. *J. Antimicrob. Chemother.* 68, 1583–1593. doi: 10.1093/jac/dkt048

Shabayek, S., and Spellerberg, B. (2017). Acid stress response mechanisms of group B Streptococci. *Front. Cell Infect. Microbiol.* 7:395. doi: 10.3389/fcimb.2017.00395

Shaper, M., Hollingshead, S. K., Benjamin, W. H. Jr., and Briles, D. E. (2004). PspA protects *Streptococcus pneumoniae* from killing by apolactoferrin, and antibody to PspA enhances killing of pneumococci by apolactoferrin [corrected]. *Infect. Immun.* 72, 5031–5040. doi: 10.1128/IAI.72.9.5031-5040.2004

Shireen, T., Singh, M., Das, T., and Mukhopadhyay, K. (2013). Differential adaptive responses of Staphylococcus aureus to in vitro selection with different antimicrobial peptides. *Antimicrob. Agents Chemother.* 57, 5134–5137. doi: 10.1128/AAC.00780-13

Sieprawska-Lupa, M., Mydel, P., Krawczyk, K., Wojcik, K., Puklo, M., Lupa, B., et al. (2004). Degradation of human antimicrobial peptide LL-37 by *Staphylococcus aureus*-derived proteinases. *Antimicrob. Agents Chemother.* 48, 4673–4679. doi: 10.1128/AAC.48.12.4673-4679.2004

Simanski, M., Glaser, R., Koten, B., Meyer-Hoffert, U., Wanner, S., Weidenmaier, C., et al. (2013). *Staphylococcus aureus* subverts cutaneous defense by D-alanylation of teichoic acids. *Exp. Dermatol.* 22, 294–296. doi: 10.1111/exd.12114

Sinha, M., Kaushik, S., Kaur, P., Sharma, S., and Singh, T. P. (2013). Antimicrobial lactoferrin peptides: the hidden players in the protective function of a multifunctional protein. *Int. J. Pept.* 2013:390230. doi: 10.1155/2013/390230

Sørensen, O., Arnljots, K., Cowland, J. B., Bainton, D. F., and Borregaard, N. (1997). The human antibacterial cathelicidin, hCAP-18, is synthesized in myelocytes and metamyelocytes and localized to specific granules in neutrophils. *Blood* 90, 2796–2803. doi: 10.1182/blood.v90.7.2796.2796_2796_2803

Sørensen, O. E., Follin, P., Johnsen, A. H., Calafat, J., Tjabringa, G. S., Hiemstra, P. S., et al. (2001). Human cathelicidin, hCAP-18, is processed to the antimicrobial peptide LL-37 by extracellular cleavage with proteinase 3. *Blood* 97, 3951–3959. doi: 10.1182/blood.v97.12.3951

Staron, A., Finkeisen, D. E., and Mascher, T. (2011). Peptide antibiotic sensing and detoxification modules of *Bacillus subtilis*. *Antimicrob. Agents Chemother.* 55, 515–525. doi: 10.1128/AAC.00352-10

Starr, C. G., He, J., and Wimley, W. C. (2016). Host cell interactions are a significant barrier to the clinical utility of peptide antibiotics. *ACS Chem. Biol.* 11, 3391–3399. doi: 10.1021/acschembio.6b00843

Staubitz, P., Neumann, H., Schneider, T., Wiedemann, I., and Peschel, A. (2004). MprF-mediated biosynthesis of lysylphosphatidylglycerol, an important determinant in staphylococcal defensin resistance. *FEMS Microbiol. Lett.* 231, 67–71. doi: 10.1016/S0378-1097(03)00921-2

Stein, T., Heinzmann, S., Dusterhus, S., Borchert, S., and Entian, K. D. (2005). Expression and functional analysis of the subtilin immunity genes spaIFEG in the subtilin-sensitive host Bacillus subtilis MO1099. *J. Bacteriol.* 187, 822–828. doi: 10.1128/JB.187.3.822-828.2005

Suárez, J. M., Edwards, A. N., and McBride, S. M. (2013). The *Clostridium difficile* cpr Locus is regulated by a noncontiguous two-component system in response to type A and B. *J. Bacteriol.* 195, 2621–2631. doi: 10.1128/jb.00166-13

Tessema, G. T., Moretro, T., Kohler, A., Axelsson, L., and Naterstad, K. (2009). Complex phenotypic and genotypic responses of Listeria monocytogenes strains exposed to the class IIa bacteriocin sakacin P. *Appl. Environ. Microbiol.* 75, 6973–6980. doi: 10.1128/AEM.00608-09

Thedieck, K., Hain, T., Mohamed, W., Tindall, B. J., Nimtz, M., Chakraborty, T., et al. (2006). The MprF protein is required for lysinylation of phospholipids in listerial membranes and confers resistance to cationic antimicrobial peptides (CAMPs) on Listeria monocytogenes. *Mol. Microbiol.* 62, 1325–1339. doi: 10.1111/j.1365-2958.2006.05452.x

Tian, X. L., Salim, H., Dong, G., Parcells, M., and Li, Y. H. (2018). The BceABRS four-component system that is essential for cell envelope stress response is involved in sensing and response to host defence peptides and is required for the biofilm formation and fitness of Streptococcus mutans. *J. Med. Microbiol.* 67, 874–883. doi: 10.1099/jmm.0.000733

Torrent, M., Pulido, D., Rivas, L., and Andreu, D. (2012). Antimicrobial peptide action on parasites. *Curr. Drug Targets* 13, 1138–1147. doi: 10.2174/138945012802002393

Tramper-Stranders, G. A. (2018). Childhood community-acquired pneumonia: a review of etiology- and antimicrobial treatment studies. *Paediatr. Respir. Rev.* 26, 41–48. doi: 10.1016/j.prrv.2017.06.013

Tran, T. T., Panesso, D., Mishra, N. N., Mileykovskaya, E., Guan, Z., Munita, J. M., et al. (2013). Daptomycin-resistant *Enterococcus faecalis* diverts the antibiotic molecule from the division septum and remodels cell membrane phospholipids. *mBio* 4:e00281-13. doi: 10.1128/mBio.00281-13

Tsuda, H., Yamashita, Y., Shibata, Y., Nakano, Y., and Koga, T. (2002). Genes involved in bacitracin resistance in Streptococcus mutans. *Antimicrob. Agents Chemother.* 46, 3756–3764. doi: 10.1128/aac.46.12.3756-3764.2002

Tymoszewska, A., Diep, D. B., and Aleksandrzak-Piekarczyk, T. (2018). The extracellular loop of Man-PTS subunit IID is responsible for the sensitivity of *Lactococcus garvieae* to garvicins A, B and C. *Sci. Rep.* 8:15790.

Vaara, M. (2009). New approaches in peptide antibiotics. *Curr. Opin. Pharmacol.* 9, 571–576. doi: 10.1016/j.coph.2009.08.002

Vadyvaloo, V., Arous, S., Gravesen, A., Hechard, Y., Chauhan-Haubrock, R., Hastings, J. W., et al. (2004a). Cell-surface alterations in class IIa bacteriocin-resistant *Listeria monocytogenes* strains. *Microbiology* 150(Pt 9), 3025–3033. doi: 10.1099/mic.0.27059-0

Vadyvaloo, V., Snoep, J. L., Hastings, J. W., and Rautenbach, M. (2004b). Physiological implications of class IIa bacteriocin resistance in Listeria monocytogenes strains. *Microbiology* 150(Pt 2), 335–340. doi: 10.1099/mic.0.26731-0

van der Windt, D., Bootsma, H. J., Burghout, P., van der Gaast-de Jongh, C. E., Hermans, P. W., and van der Flier, M. (2012). Nonencapsulated *Streptococcus pneumoniae* resists extracellular human neutrophil elastase- and cathepsin G-mediated killing. *FEMS Immunol. Med. Microbiol.* 66, 445–448. doi: 10.1111/j.1574-695X.2012.01028.x

van Harten, R. M., van Woudenbergh, E., van Dijk, A., and Haagsman, H. P. (2018). Cathelicidins: immunomodulatory antimicrobials. *Vaccines (Basel)* 6:63. doi: 10.3390/vaccines6030063

Verheul, A., Russell, N. J., Van, T. H. R., Rombouts, F. M., and Abee, T. (1997). Modifications of membrane phospholipid composition in nisin-resistant *Listeria monocytogenes* Scott A. *Appl. Environ. Microbiol.* 63, 3451–3457. doi: 10.1128/AEM.63.9.3451-3457.1997

Vogel, H. J. (2012). Lactoferrin, a bird's eye view. *Biochem. Cell Biol.* 90, 233–244. doi: 10.1139/o2012-016

Vollmer, W., and Tomasz, A. (2000). The pgdA gene encodes for a peptidoglycan N-acetylglucosamine deacetylase in *Streptococcus pneumoniae*. *J. Biol. Chem.* 275, 20496–20501. doi: 10.1074/jbc.M910189199

von Eiff, C., Peters, G., and Becker, K. (2006). The small colony variant (SCV) concept – the role of staphylococcal SCVs in persistent infections. *Injury* 37(Suppl. 2), S26–S33. doi: 10.1016/j.injury.2006.04.006

Vornhagen, J., Adams Waldorf, K. M., and Rajagopal, L. (2017). Perinatal group B streptococcal infections: virulence factors, immunity, and prevention strategies. *Trends Microbiol.* 25, 919–931. doi: 10.1016/j.tim.2017.05.013

Vuong, C., Kocianova, S., Voyich, J. M., Yao, Y., Fischer, E. R., DeLeo, F. R., et al. (2004a). A crucial role for exopolysaccharide modification in bacterial biofilm formation, immune evasion, and virulence. *J. Biol. Chem.* 279, 54881–54886. doi: 10.1074/jbc.M411374200

Vuong, C., Voyich, J. M., Fischer, E. R., Braughton, K. R., Whitney, A. R., DeLeo, F. R., et al. (2004b). Polysaccharide intercellular adhesin (PIA) protects

Staphylococcus epidermidis against major components of the human innate immune system. *Cell Microbiol.* 6, 269–275. doi: 10.1046/j.1462-5822.2004.00367.x

Walter, J., Loach, D. M., Alqumber, M., Rockel, C., Hermann, C., Pfitzenmaier, M., et al. (2007). D-alanyl ester depletion of teichoic acids in *Lactobacillus reuteri* 100-23 results in impaired colonization of the mouse gastrointestinal tract. *Environ. Microbiol.* 9, 1750–1760. doi: 10.1111/j.1462-2920.2007.01292.x

Wang, G. (2014). Human antimicrobial peptides and proteins. *Pharmaceuticals (Basel)* 7, 545–594. doi: 10.3390/ph7050545

Wang, G., Li, X., and Wang, Z. (2016). APD3: the antimicrobial peptide database as a tool for research and education. *Nucleic Acids Res.* 44, D1087–D1093. doi: 10.1093/nar/gkv1278

Wang, J., Dou, X., Song, J., Lyu, Y., Zhu, X., Xu, L., et al. (2019). Antimicrobial peptides: promising alternatives in the post feeding antibiotic era. *Med. Res. Rev.* 39, 831–859. doi: 10.1002/med.21542

Wang, X., Davlieva, M., Reyes, J., Panesso, D., Arias, C. A., and Shamoo, Y. (2017). A novel phosphodiesterase of the GdpP family modulates cyclic di-AMP levels in response to cell membrane stress in daptomycin-resistant enterococci. *Antimicrob. Agents Chemother.* 61:e01422-16. doi: 10.1128/AAC.01422-16

Weiner, L. M., Webb, A. K., Limbago, B., Dudeck, M. A., Patel, J., Kallen, A. J., et al. (2016). Antimicrobial-resistant pathogens associated with healthcare-associated infections: summary of data reported to the national healthcare safety network at the centers for disease control and prevention, 2011-2014. *Infect. Control Hosp. Epidemiol.* 37, 1288–1301. doi: 10.1017/ice.2016.174

Wu, T., Jiang, Q., Wu, D., Hu, Y., Chen, S., Ding, T., et al. (2019). What is new in lysozyme research and its application in food industry? A review. *Food Chem.* 274, 698–709. doi: 10.1016/j.foodchem.2018.09.017

Wu, X., Ju, X., Du, L., Wang, L., He, R., and Chen, Z. (2019). The Man-PTS subunit IIC is responsible for the sensitivity of *Listeria monocytogenes* to durancin GL. *Food Sci. Nutr.* 8, 150–161. doi: 10.1002/fsn3.1285

Wydau-Dematteis, S., Louis, M., Zahr, N., Lai-Kuen, R., Saubamea, B., Butel, M. J., et al. (2015). The functional dlt operon of Clostridium butyricum controls the D-alanylation of cell wall components and influences cell septation and vancomycin-induced lysis. *Anaerobe* 35(Pt B), 105–114. doi: 10.1016/j.anaerobe.2015.09.001

Xhindoli, D., Pacor, S., Benincasa, M., Scocchi, M., Gennaro, R., and Tossi, A. (2016). The human cathelicidin LL-37 — A pore-forming antibacterial peptide and host-cell modulator. *Biochim. Biophys. Acta* 1858, 546–566. doi: 10.1016/j.bbamem.2015.11.003

Xu, D., and Lu, W. (2020). Defensins: a double-edged sword in host immunity. *Front. Immunol.* 11:764. doi: 10.3389/fimmu.2020.00764

Xue, J., Hunter, I., Steinmetz, T., Peters, A., Ray, B., and Miller, K. W. (2005). Novel activator of mannose-specific phosphotransferase system permease expression in Listeria innocua, identified by screening for pediocin AcH resistance. *Appl. Environ. Microbiol.* 71, 1283–1290. doi: 10.1128/AEM.71.3.1283-1290.2005

Yamashita, Y., Tsukioka, Y., Tomihisa, K., Nakano, Y., and Koga, T. (1998). Genes involved in cell wall localization and side chain formation of rhamnose-glucose polysaccharide in *Streptococcus mutans*. *J. Bacteriol.* 180, 5803–5807. doi: 10.1128/JB.180.21.5803-5807.1998

Yang, H. B., Hou, W. T., Cheng, M. T., Jiang, Y. L., Chen, Y., and Zhou, C. Z. (2018). Structure of a MacAB-like efflux pump from *Streptococcus pneumoniae*. *Nat. Commun.* 9:196. doi: 10.1038/s41467-017-02741-4

Yang, S. J., Bayer, A. S., Mishra, N. N., Meehl, M., Ledala, N., Yeaman, M. R., et al. (2012). The *Staphylococcus aureus* two-component regulatory system, GraRS, senses and confers resistance to selected cationic antimicrobial peptides. *Infect. Immun.* 80, 74–81. doi: 10.1128/IAI.05669-11

Yang, S. J., Xiong, Y. Q., Yeaman, M. R., Bayles, K. W., Abdelhady, W., and Bayer, A. S. (2013). Role of the LytSR two-component regulatory system in adaptation to cationic antimicrobial peptides in Staphylococcus aureus. *Antimicrob. Agents Chemother.* 57, 3875–3882. doi: 10.1128/AAC.00412-13

Yang, Y., Luo, M., Zhou, H., Li, C., Luk, A., Zhao, G., et al. (2019). Role of two-component system response regulator bceR in the antimicrobial resistance, virulence, biofilm formation, and stress response of group B *Streptococcus*. *Front. Microbiol.* 10:10. doi: 10.3389/fmicb.2019.00010

Yavari, B., Mahjub, R., Saidijam, M., Raigani, M., and Soleimani, M. (2018). The potential use of peptides in cancer treatment. *Curr Protein Pept. Sci.* 19, 759–770. doi: 10.2174/1389203719666180111150008

Yount, N. Y., and Yeaman, M. R. (2012). Emerging themes and therapeutic prospects for anti-infective peptides. *Annu. Rev. Pharmacol. Toxicol.* 52, 337–360. doi: 10.1146/annurev-pharmtox-010611-134535

Yu, S., Yu, P., Wang, J., Li, C., Guo, H., Liu, C., et al. (2019). A study on prevalence and characterization of *Bacillus cereus* in ready-to-eat foods in China. *Front. Microbiol.* 10:3043. doi: 10.3389/fmicb.2019.03043

Yung, S. C., and Murphy, P. M. (2012). Antimicrobial chemokines. *Front. Immunol.* 3:276. doi: 10.3389/fimmu.2012.00276

Zafar, M. A., Hammond, A. J., Hamaguchi, S., Wu, W., Kono, M., Zhao, L., et al. (2019). Identification of pneumococcal factors affecting pneumococcal shedding shows that the dlt locus promotes inflammation and transmission. *mBio* 10:e01032-19. doi: 10.1128/mBio.01032-19

Zahner, D., Zhou, X., Chancey, S. T., Pohl, J., Shafer, W. M., and Stephens, D. S. (2010). Human antimicrobial peptide LL-37 induces MefE/Mel-mediated macrolide resistance in *Streptococcus pneumoniae*. *Antimicrob. Agents Chemother.* 54, 3516–3519. doi: 10.1128/AAC.01756-09

Zaschke-Kriesche, J., Behrmann, L. V., Reiners, J., Lagedroste, M., Groner, Y., Kalscheuer, R., et al. (2019). Bypassing lantibiotic resistance by an effective nisin derivative. *Bioorg. Med. Chem.* 27, 3454–3462. doi: 10.1016/j.bmc.2019.06.031

Zasloff, M. (2002). Antimicrobial peptides of multicellular organisms. *Nature* 415, 389–395. doi: 10.1038/415389a

Zhou, W., Wang, G., Wang, C., Ren, F., and Hao, Y. (2016). Both IIC and IID components of mannose phosphotransferase system are involved in the specific recognition between immunity protein PedB and bacteriocin-receptor complex. *PLoS One* 11:e0164973. doi: 10.1371/journal.pone.0164973

Conflict of Interest: The authors declare that the research was conducted in the absence of any commercial or financial relationships that could be construed as a potential conflict of interest.

frontiers in Microbiology

ORIGINAL RESEARCH
published: 30 October 2020
doi: 10.3389/fmicb.2020.584812

Antibiofilm and Antivirulence Properties of Indoles Against *Serratia marcescens*

Sivasamy Sethupathy†, Ezhaveni Sathiyamoorthi†, Yong-Guy Kim, Jin-Hyung Lee and Jintae Lee**

School of Chemical Engineering, Yeungnam University, Gyeongsan, South Korea

OPEN ACCESS

Edited by:
Thomas Keith Wood, Pennsylvania State University (PSU), United States

Reviewed by:
Robert J. C. McLean, Texas State University, United States
Mikael Elias, University of Minnesota Twin Cities, United States

***Correspondence:**
Jin-Hyung Lee
jinhlee@ynu.ac.kr
Jintae Lee
jtlee@ynu.ac.kr

† These authors have contributed equally to this work

Specialty section:
This article was submitted to Antimicrobials, Resistance and Chemotherapy, a section of the journal Frontiers in Microbiology

Received: *18 July 2020*
Accepted: *30 September 2020*
Published: *30 October 2020*

Citation:
Sethupathy S, Sathiyamoorthi E, Kim Y-G, Lee J-H and Lee J (2020) Antibiofilm and Antivirulence Properties of Indoles Against Serratia marcescens. Front. Microbiol. 11:584812. doi: 10.3389/fmicb.2020.584812

Indole and its derivatives have been shown to interfere with the quorum sensing (QS) systems of a wide range of bacterial pathogens. While indole has been previously shown to inhibit QS in *Serratia marcescens*, the effects of various indole derivatives on QS, biofilm formation, and virulence of *S. marcescens* remain unexplored. Hence, in the present study, we investigated the effects of 51 indole derivatives on *S. marcescens* biofilm formation, QS, and virulence factor production. The results obtained revealed that several indole derivatives (3-indoleacetonitrile, 5-fluoroindole, 6-fluoroindole, 7-fluoroindole, 7-methylindole, 7-nitroindole, 5-iodoindole, 5-fluoro-2-methylindole, 2-methylindole-3-carboxaldehyde, and 5-methylindole) dose-dependently interfered with quorum sensing (QS) and suppressed prodigiosin production, biofilm formation, swimming motility, and swarming motility. Further assays showed 6-fluoroindole and 7-methylindole suppressed fimbria-mediated yeast agglutination, extracellular polymeric substance production, and secretions of virulence factors (e.g., proteases and lipases). QS assays on *Chromobacterium violaceum* CV026 confirmed that indole derivatives interfered with QS. The current results demonstrate the antibiofilm and antivirulence properties of indole derivatives and their potentials in applications targeting *S. marcescens* virulence.

Keywords: biofilm, indoles, motility, protease, prodigiosin, quorum sensing, *S. marcescens*

INTRODUCTION

Serratia marcescens is a Gram-negative, rod-shaped bacterium that belongs to the *Enterobacteriaceae* family and well-known for its ability to produce prodigiosin a red pigment (Williamson et al., 2006). The bacterium is often isolated from clinical samples and is ubiquitous in nature. During the past four decades, *S. marcescens* has been increasingly recognized as an important opportunistic pathogen that has developed resistance to many antibiotics and is frequently associated with nosocomial infections in pediatric, adult, aged, and immunocompromised patients. *S. marcescens* causes surgical site, eye, respiratory tract, bloodstream, urinary tract, urinary catheter-associated, and gastrointestinal tract infections and endocarditis, meningitis, and other diseases (Cristina et al., 2019). It has been estimated that 6.5% of Gram-negative bacterial pathogenic infections

are caused by *Serratia* spp. in the United States and Europe (Sader et al., 2014). *Serratia* spp. is also known to be the 7th and 10th most common cause of pneumonia and bloodstream infections, respectively, in United States and Europe (Acar and Goldstein, 1997; Jones, 2010). *S. marcescens* isolates of clinical origin have been shown to produce extended-spectrum-β-lactamase (Yang et al., 2012), and to acquire multiple drug resistance via horizontal gene transfer from other members of the *Enterobacteriaceae* family (Ivanova et al., 2008). The bacterium is known to utilize a broad array of nutrients and to grow in the presence of antiseptics, detergents, and disinfectants (Cooney et al., 2014).

Quorum sensing (QS) in *S. marcescens* plays important roles in antibiotic resistance, biofilm formation, synchronizing the productions of proteases, lipases, prodigiosin, and butanediol, and swimming and swarming motilities (Van Houdt et al., 2007). *S. marcescens* strains produce a wide range of *N*-acylhomoserine lactones (AHLs) (e.g., C4-AHL, C6-AHL, 3-oxo-C6-AHL, C7-AHL, and C8-AHL), which it uses as QS signal molecules (Eberl et al., 1996; Horng et al., 2002; Coulthurst et al., 2006). Furthermore, biofilms formed by *S. marcescens* clinical isolates are resistant to commonly used antibiotics (Ray et al., 2017), and biofilm formation by clinically important bacterial pathogens is primarily responsible for device-associated chronic infections. QS defective mutants have been reported to be less virulent and incapable of forming robust biofilms, and thus, QS inhibition is a strategy used to control the virulence of *S. marcescens* (LaSarre and Federle, 2013). Several bioactive compounds, including alpha-bisabolol and vanillic acid, have been successfully used to inhibit virulence factor production and biofilm formation by *S. marcescens* (Sethupathy et al., 2016b, 2017).

In biofilms, bacterial cells are surrounded by a self-secreted polymeric matrix comprised of macromolecules such as proteins, lipids, carbohydrates, and extracellular DNA, which protect the bacterium from environmental stress factors, disinfectants, host immune system, and antibiotics (Stewart and Costerton, 2001; Høiby et al., 2010). Bacterial cells in biofilms are metabolically less active and grow more slowly and this characteristic facilitates their acquisition of antibiotic resistance (Stewart, 2002). Hence, it appears suitable combinations of biofilm/QS inhibitors and conventional antibiotics might usefully enhance the antibiotic susceptibilities of bacterial cells in biofilms (Brackman et al., 2011).

It has been reported that more than 85 species of Gram-positive and Gram-negative bacteria can synthesize indole (Lee and Lee, 2010). Indole is an important bacterial signal molecule that regulates several important biological processes such as genetic stability, metabolism, biofilm formation, pathogenesis, antibiotic resistance, and oxidative stress responses and also acts as an interspecies and interkingdom signal to regulate diverse functions (Lee et al., 2015b). Several studies have described the antibiofilm and antivirulence activities of indole derivatives (e.g., 7-hydroxyindole, 3-indoleacetonitrile, 7-fluoroindole, 7-benzyloxyindole, and methylindoles) against clinically important pathogens, such as enterohemorrhagic *Escherichia coli* (Lee et al., 2007), *Pseudomonas aeruginosa* (Lee et al., 2009, 2011, 2012), *Staphylococcus aureus* (Lee et al., 2013), and *Candida albicans* (Lee et al., 2018; Manoharan et al., 2018). In addition, indole and 3-indolylacetonitrile have been shown to inhibit the maturation of *Paenibacillus alvei* endospores (Kim Y.-G.et al., 2011), and halogenated indoles have been reported to have nematicidal and insecticidal potentials (Rajasekharan et al., 2019, 2020). Although the QS inhibitory activity of indole in *S. marcescens* has been clearly reported in previous work (Hidalgo-Romano et al., 2014), the effects of indole derivatives on the biofilm and virulence of indole-negative *S. marcescens* have yet to be evaluated, and thus in the present study, we investigated the antibiofilm and antivirulence potentials of several indole derivatives against *S. marcescens*.

MATERIALS AND METHODS

Indole Compounds

Indole and 50 indole derivatives (**Supplementary Figure 1**) were purchased from Sigma-Aldrich (St. Louis, MO, United States) and Combi-Blocks, Inc. (San Diego, CA, United States), dissolved in dimethyl sulfoxide (DMSO) to produce 1 M stock solutions, and stored at −20°C. DMSO (0.1% v/v) was used as the negative control and at the concentrations present (<0.1%) did not affect bacterial growth or biofilm formation.

Bacterial Culture Conditions

S. marcescens ATCC 14756 was streaked on Luria-Bertani (LB) agar and incubated at 30°C for 24 h. Plates were stored at 4°C until required. For biofilm and other assays, a single colony of *S. marcescens* was inoculated in LB broth and cultured at 30°C for 12 h at 160 rpm. Two percentage of the overnight culture (adjusted to 0.5 McFarland containing $\sim 1 \times 10^8$ CFU mL^{-1}) was used as an inoculum for biofilm and other virulence assays.

Prodigiosin Assay

S. marcescens was grown in the absence or presence of indole or indole derivatives at 30°C for 20 h and centrifuged at 12,000 rpm for 10 min. Acidified ethanol (1 mL of 4% 1 M HCl in ethanol) was added to the cell pellets obtained and vortexed vigorously to extract prodigiosin. After centrifugation, supernatant absorbances were measured at 534 nm as previously reported (Slater et al., 2003).

Biofilm Inhibition Assay

S. marcescens cells were inoculated in 2 mL LB and incubated at 30°C for 20 h. To assess biofilm inhibitory activity, cells were re-inoculated into LB (dilution ratio 1:50) and cultured overnight in 96-well plates in the absence or presence of indole or indole derivatives under static conditions at 30°C for 20 h. After incubation, planktonic cell densities were measured at 620 nm and culture supernatant were discarded. Residual planktonic cells were removed by washing plates three times with water. Biofilms that formed on the plates were stained with crystal violet (0.1%) for 20 min, excess dye was removed by washing three times, and bound crystal violet was solubilized in 95% ethanol. Absorbances were measured at 570 nm using a Multiskan EX

microplate photometer (Thermo Fisher Scientific, Waltham, MA, United States) (Lee et al., 2011).

Growth Curve Analysis and Determination of Minimum Inhibitory Concentrations (MICs)

S. marcescens was grown in the absence or presence of indole or selected indole derivatives, as described above, and planktonic cell growth was monitored periodically at 600 nm for 24 h using an Optizen 2120UV spectrophotometer (Mecasys Co., Ltd., Daejeon, Korea). MIC was defined as the lowest concentration that inhibited planktonic cell growth by 80% and also confirmed by colony counting. MICs were determined for 3-indoleacetonitrile, 5-fluoro-2-methylindole, 5-fluoroindole, 6-fluoroindole, 5-methylindole, 7-methylindole, and indole as previously described (Lee et al., 2013).

Microscopic Observation of Biofilms

S. marcescens cells were inoculated in 2 mL of LB and incubated at 30°C for 20 h. Cells were then re-inoculated in LB at a dilution ratio of 1:50, cultured overnight in 96-well plates with indole, 6-fluoroindole, or 7-methylindole at 1 mM, and then incubated at 30°C for 24 h without shaking. For confocal laser scanning microscope (CLSM) analysis, cells were stained with 100 μL of pre-warmed PBS containing carboxyfluorescein diacetate succinimidyl ester for 20 min at 30°C (final concentration, 5 μM) and then washed with PBS (Lee et al., 2011). Cells were visualized by a CLSM (Nikon Eclipse Ti, Tokyo, Japan) using a 20× objective and an Ar laser (excitation wavelength 488 nm, emission wavelength range 500–550 nm). In each experiment, at least 10 random positions in three independent cultures were chosen for microscopic analysis.

Swarming and Swimming Assay

Swimming agar (1% peptone, 0.5% NaCl, and 0.3% agar) and swarming agar plates (1% peptone, 0.5% NaCl, and 0.6% agar) were prepared with or without indole (0.5 or 1 mM) or selected indole derivatives. Plates were spotted with 5 μL overnight culture of *S. marcescens*, incubated in an upright position at 30°C for 16 h, and then swimming and swarming motility inhibitions were assessed as previously described (Pearson, 2019).

Protease Assay

Extracellular casein degrading protease activities of supernatants from *S. marcescens* grown in the absence or presence of indole or indole derivatives were measured using 2% w/v of azocasein. Briefly, equal volumes of azocasein and culture supernatants were reacted at 37°C for 30 min and then 600 μL of 10% trichloroacetic acid was added to stop the proteolysis. Reaction tubes were kept for 30 min at −20°C to precipitate unreacted azocasein and centrifuged. An equal volume of 1 M NaOH was added to supernatants (700 μL), and absorbances were read at 440 nm as previously described (Coulthurst et al., 2006).

Lipase Assay

The effects of indole and indole derivatives on extracellular lipase production were evaluated by incubating 1 volume of supernatant from a *S. marcescens* control with 9 volumes of substrate buffer [1 volume of buffer A containing 3 mg/mL of *p*-nitrophenyl palmitate in isopropyl alcohol, 9 volumes of buffer B containing 1 mg/mL of gummi arabicum and 2 mg/mL sodium deoxycholate in 50 mM Na_2PO_4 buffer (pH-8.0)] for 30 min in the dark at room temperature. After incubation, reaction tubes were centrifuged at 12,000 rpm for 10 min and lipase activity was terminated by adding 1 volume of 1 M Na_2CO_3. Absorbances was measured at 405 nm as previously described (Patel et al., 2018).

Fimbria Activity Assay

Effects of indole and indole derivatives on *S. marcescens* fimbria activity were accessed using *Saccharomyces cerevisiae* (Sigma, product no. YSC2), as previously described (Shanks et al., 2007). Yeast agglutination was measured spectrophotometrically by adding 1.5 mL of PBS containing 0.5 mL of *S. cerevisiae* (2% w/v in PBS) and 0.4 mL of *S. marcescens* cells in PBS (OD_{600}, 0.5). To achieve a uniform mixture of *Saccharomyces cerevisiae* and *Serratia marcescens* cell suspension, the reaction tubes were gently vortexed for 5 s and the initial OD_{600} was measured. After 10 min of incubation at room temperature, 100 μL of upper phase was transferred to a 96 well plate and OD_{600} was measured. During 10 min incubation, fimbria present on the *S. marcescens* cell binds with *S. cerevisiae* and agglutinates *S. cerevisiae*. Formation of agglutination indicates the presence of fimbria on *S. marcescens* cells and a decrease in the fimbria results in the reduction of aggregate formation. Presence of visible aggregates of agglutinated cells affected the OD_{600} measurement and hence vigorous vortexing for 30 s was done to disturb the agglutinated cells before the reading of the second OD_{600} values. Percentage agglutination was calculated using 100 × (1-OD_{600} before vortexing/OD_{600} after vortexing).

H_2O_2 Sensitivity Assay

Disk diffusion assays were performed by spreading control and treated cells on LB agar plates, placing 6-mm sterile paper disks on the agar, loading disks with 10 μL of 30% H_2O_2, and then incubating plates for 24 h at 30°C. Zones of inhibition were measured as previously described (Shanks et al., 2007).

Extracellular Polymeric Substance (EPS) Extraction and FTIR

Extracellular polymeric substance (EPS) extraction was carried as previously described (Badireddy et al., 2008). Briefly, 100 mL of *S. marcescens* control and 6-fluoroindole or 7-methylindole (1 mM) treated cultures for 24 h were centrifuged at 7,000 rpm for 15 min at 4°C to collect cells. Cell-free culture supernatants were stored at −20°C for cell-free EPS extraction. Collected cell pellets were washed with wash buffer (10 mM Tris/HCl pH 8.0, 10 mM EDTA), resuspended in 100 mL of isotonic extraction buffer (10 mM Tris/HCl pH 8.0, 10 mM EDTA, 2.5 mM NaCl), incubated at 4°C for 12 h, vortexed for 5 min, and centrifuged at 5,000 rpm for 15 min to collect supernatants containing cell bound

EPS. Cell-free culture supernatants containing cell free EPS and isotonic buffer containing cell bound EPS were pooled, mixed with 3 volumes of ice-cold ethanol, and kept at −20°C for 18 h to precipitate EPS. Precipitated EPS was collected by centrifugation at 10,000 rpm for 10 min at 4°C, vacuum dried, and analyzed by FTIR spectrometry (Spectrum Two^{TM} FTIR, PerkinElmer, Massachusetts, United States) at 400–4,000 cm^{-1}.

RNA Isolation and Transcriptomic Studies

For transcriptomic analyses, 25 mL of *S. marcescens* at an initial turbidity of 0.05 at OD_{600} was inoculated into LB broth in 250 mL Erlenmeyer flasks and incubated for 6 h at 30°C with agitation at 250 rpm in the presence or absence of 6-fluoroindole (0.5 mM). To prevent RNA degradation, RNase inhibitor (RNAlater, Ambion, TX, United States) was added to cells immediately after incubation. Total RNA was isolated using a hot acidic phenol method (Amin-ul Mannan et al., 2009), and RNA was purified using a Qiagen RNeasy mini Kit (Valencia, CA, United States).

Quantitative reverse transcriptase PCR (qRT-PCR) was used to determine the expressions of 10 QS-related genes list all *bmsA* (biofilm), *carA* (prodigiosin production), *fimA* (type 1 fimbriae), *flhD* (motility), *luxS* (quorum sensing), *pigA* (prodigiosin production), *pigC* (prodigiosin production), *Sma*I/*R* (LuxIR-type quorum sensing system), and *rpoS* (motility and biofilm). The specific primers and housekeeping gene (*16S rRNA*) used for qRT-PCR are listed in **Supplementary Table 1**. The expression of *16S rRNA* was not affected by 6-fluoroindole. The qRT-PCR method used was as described by Kim Y.-G.et al. (2016), and was performed using SYBR Green master mix (Applied Biosystems, Foster City, United States) and an ABI StepOne Real-Time PCR System (Applied Biosystems). At least two independent cultures with four repetitions were used.

Quorum Sensing Inhibition Assay

Quorum sensing (QS) inhibition was assayed as previously described (Kim Y.-G.et al., 2015). *Chromobacterium violaceum* CV026 is deficient in QS signal production, and thus, cannot produce the purple pigment violacein. However, pigment production can be restored by the exogenous addition of AHLs [*N*-butanoyl-L-homoserine lactone (BHL) or *N*-hexanoyl homoserine lactone (HHL) at 500 μM]. An overnight culture of CV026 was diluted with fresh LB broth (1:20), aliquoted (300 μL) into 96-well polystyrene microtiter plate, and treated with indoles. Mixtures were incubated at 30°C for 2 days.

Statistical Analysis

Most assays were conducted with two independent cultures with six repetitions while motility, EPS quantification, and qRT-PCR assays were performed with two independent cultures with four repetitions. Results are expressed as means ± standard deviations. The student's *t*-test was used to determine the significances of intergroup differences, and statistical significance was accepted for $P < 0.05$.

RESULTS

Effects of Indole Derivatives on Prodigiosin Production, Biofilm Formation, and Swarming and Swimming Motilities

The quorum sensing inhibitory activities of the 51 indole derivatives were assessed by measuring their abilities to inhibit prodigiosin production by *S. marcescens*. Among the indole derivatives tested, 2-oxindole, 5-fluoroxindole, 3-indoleacetonitrile, 5-fluoroindole, 6-fluoroindole, 7-fluoroindole, 5-fluoroindole-2,3-dione, 7-methylindole, 7-nitroindole, 7-azaindole, 5-iodoindole, 5-fluoro-2-methylindole, 5-chloro-2-methylindole, 5-indoindolin-2-one, indole-3-acetamide, and 5-methylindole at 1 mM reduced prodigiosin production by 50–80% (**Supplementary Figure 1**). Additional assays with 3-indoleacetonotrile, 5-fluoro-2-methylindole, 5-fluoroindole, 6-fluoroindole, 5-methylindole, and 7-methylindoles demonstrated concentration-dependent reductions in prodigiosin production (**Figures 1A,D,G** and **Supplementary Figure 2**). These inhibitions suggested the above mentioned indole derivatives interfere with the QS system in *S. marcescens*.

In our previous studies, we demonstrated the antibiofilm activities of indole derivatives, such as 7-hydroxyindole (Lee et al., 2009), 3-indoleacetonitrile, indole-3-carboxyaldehyde (Lee et al., 2011), 7-fluoroindole (Lee et al., 2012), 5-iodoindole (Lee et al., 2016), and methylindoles (Lee et al., 2018). In the current study, indole derivatives such as 5-fluoroxindole, 3-indoleacetonitrile, 5-fluoroindole, 6-fluoroindole, 7-methylindole, 7-nitroindole, 5-chloro-2-methylindole, 7-methylindole-3-carboxaldehyde, 5-methylindole, indole-3-acetamide, indole-3-propionic acid, 4-benzyloxyindole and 5-benzyloxyindole inhibited biofilm formation by *S. marcescens* by 40–75% (**Figures 1B,E,H** and **Supplementary Figure 3**). Particularly, 3-indoleacetonitrile, 5-fluoro-2-methylindole, 5-fluoroindole, 6-fluoroindole, 5-methylindole, 7-methylindole, 5-iodoindole, and indole dose-dependently reduced both biofilm formation and prodigiosin production (**Figure 1** and **Supplementary Figures 1–4**). CLSM analysis confirmed the biofilm inhibitory activities of these two indole derivatives and indole as evidenced by obvious reductions in surface coverage and biomass in biofilms (**Figure 1J**).

Growth curve analysis was used to evaluate the effects of these six derivatives and indole on the growth of *S. marcescens*. The obtained results revealed 6-fluoroindole and 7-methylindole had slight bacteriostatic activity but not in the presence of indole up to 1 mM (**Figures 1C,F,I**). Growth curve analysis results for *S. marcescens* grown in the presence or absence of 3-indoleacetonitrile, 5-fluoro-2-methylindole, 5-fluoroindole, or 5-methylindole are presented in **Supplementary Figure 5**. We also found the MICs of 6-fluoroindole (**Figure 3A**), 7-methylindole (**Figure 3B**), indole (**Figure 3C**), 3-indoleacetonitrile, 5-fluoro-2-methylindole, 5-fluoroindole, and 5-methylindole (**Supplementary Figure 6**) were ranged from 2.5 to 5 mM. These results indicate indoles

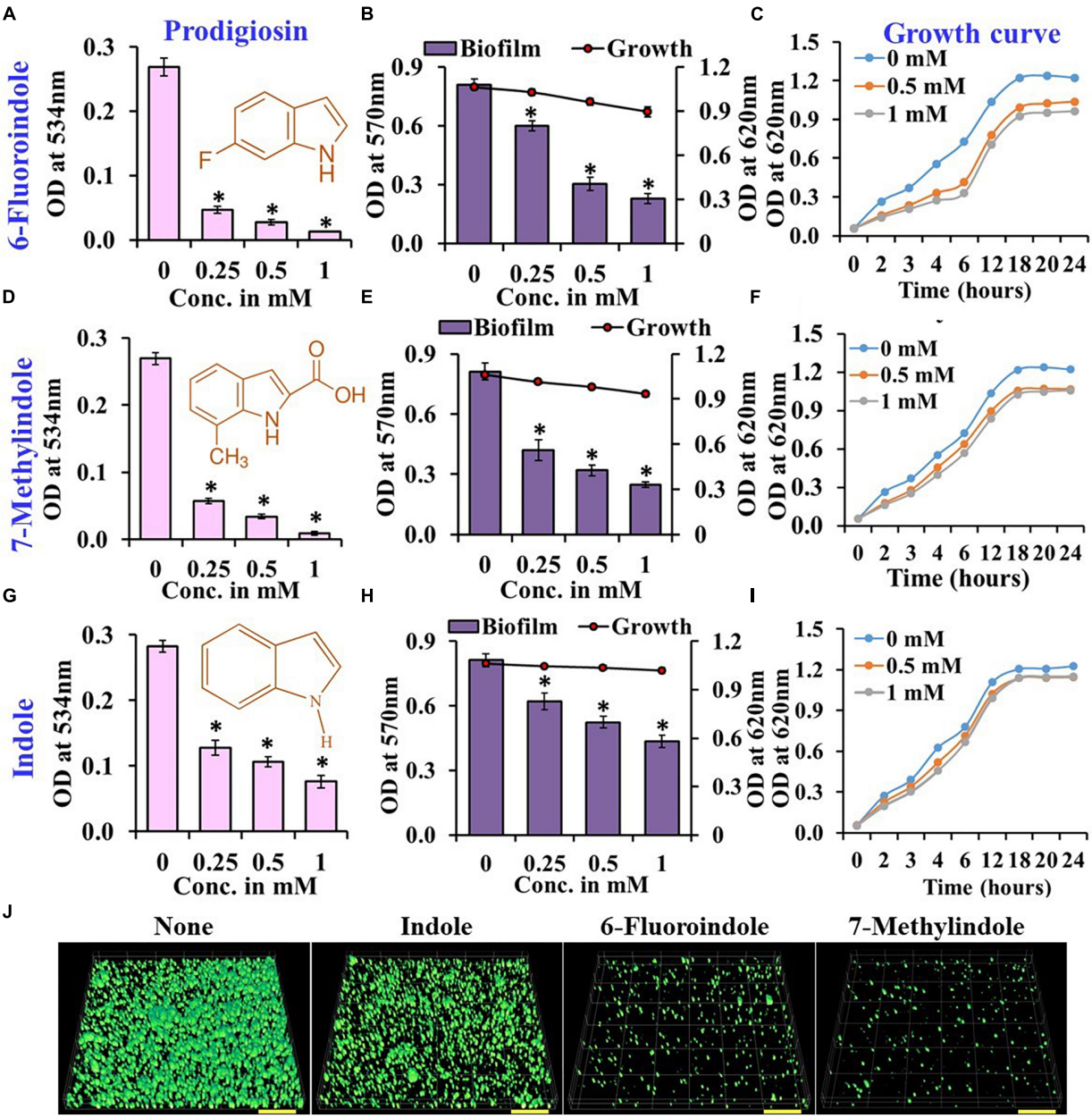

FIGURE 1 | Effects of indole, 6-fluoroindole, or 7-methylindole on prodigiosin production **(A,D,G)**, biofilm formation and planktonic cell growth **(B,E,H)**, and the planktonic cell growth **(C,F,I)** of *S. marcescens*. Error bars represent standard deviations. CLSM images of *S. marcescens* biofilms formed in the presence or absence of 1 mM indole, 6-fluoroindole, and 7-methylindole **(J)**. Scale bars represent 100 μM. Error bars and asterisks (*) represent standard deviations and statistically significant differences ($p < 0.05$), respectively, vs. non-treated controls.

effectively suppress prodigiosin synthesis and biofilm formation by *S. marcescens* by inhibiting QS activity rather than by exhibiting antimicrobial activity, which suggests indoles may be less prone to the development of drug resistance than conventional antibiotics.

In *S. marcescens*, AHL mediated QS controls swarming and swimming motilities (Horng et al., 2002; Coulthurst et al., 2006). Our results on the swarming and swimming inhibitory activities of indole and the six indole derivatives are presented in **Figure 2** and **Supplementary Figure 7**. Of the indole derivatives tested, 3-indoleacetonitrile, 5-fluoroindole, 6-fluoroindole, 5-methylindole, and 7-methylindole markedly inhibited the swarming motility of *S. marcescens*, whereas indole had a moderate inhibitory effect (**Figure 2** and **Supplementary Figure 7**). As regards the inhibition of swimming motility, 5-fluoroindole, 6-fluoroindole, 5-methylindole, and 7-methylindole were found to be most effective (**Figure 2** and **Supplementary Figure 7**).

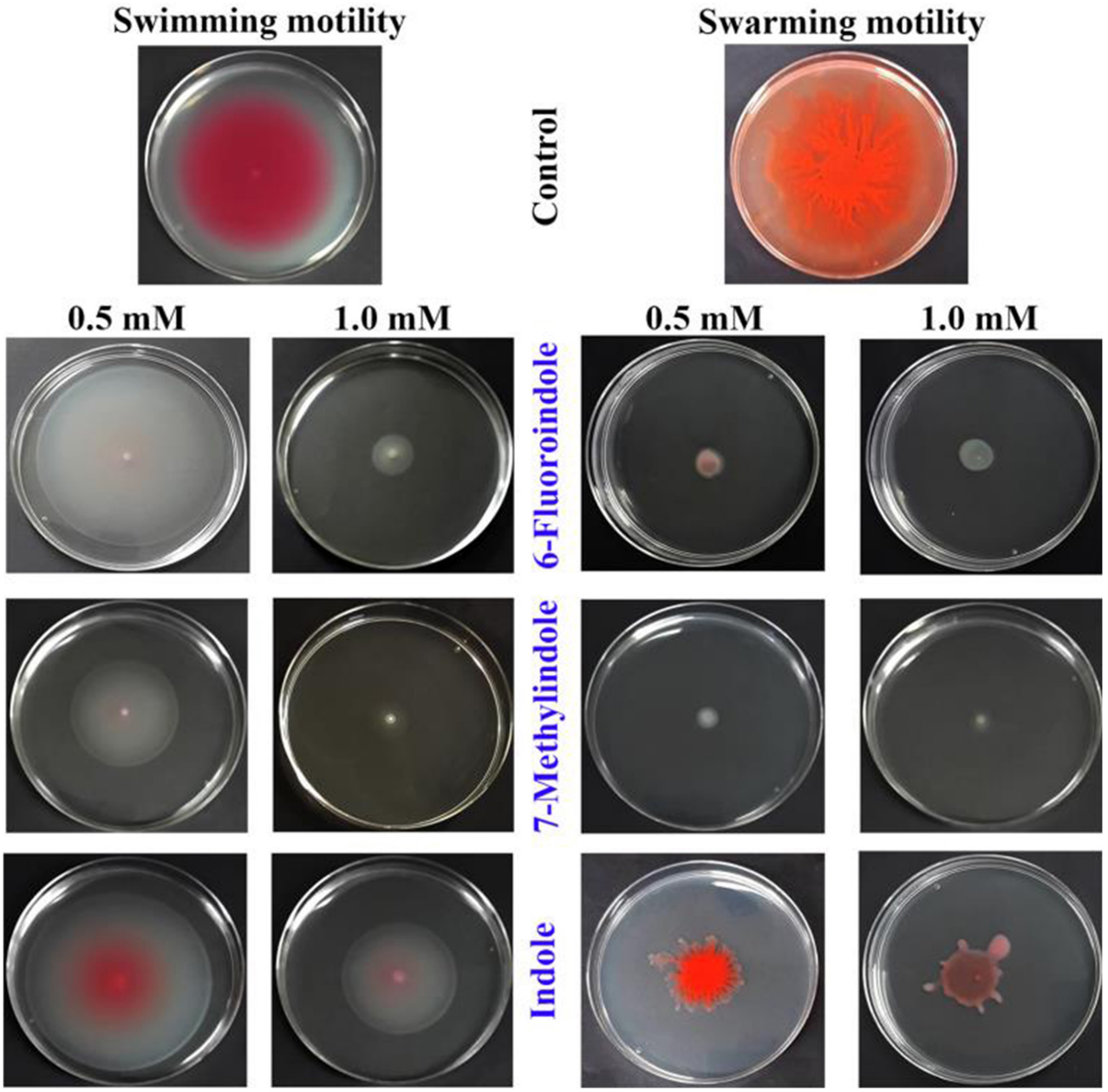

FIGURE 2 | Effects of indole and indole derivatives on the swimming and swarming motilities of *S. marcescens*.

Effects of Indole Derivatives on Protease and Lipase Productions

Proteases secreted by bacterial pathogens play important roles in the establishment of infections and in systemic dissemination by degrading host defense proteins (Saint-Criq et al., 2018). Indole and 3-indoleacetonitrile, 5-fluoroindole, 6-fluoroindole, 5-methylindole, and 7-methylindole at 1 mM were found to inhibit extracellular protease production effectively and dose-dependently by 25–60% (**Figures 3D–F** and **Supplementary Figure 8**). Among the six indole derivatives tested, 3-indoleacetonitrile, 5-fluoroindole, 6-fluoroindole, 5-fluoro-2-methylindole, and 7-methylindole at a concentration of 1 mM were found to inhibit lipase production by 60–80% (**Figures 3G–I** and **Supplementary Figure 9**).

Effects of Indole Derivatives on Fimbria-Mediated Yeast Agglutination and on Sensitivity to H_2O_2

In *S. marcescens*, the transcriptional regulator OxyR is required for the regulation of oxidative stress response and the initial stages of biofilm formation via the modulation of the expression

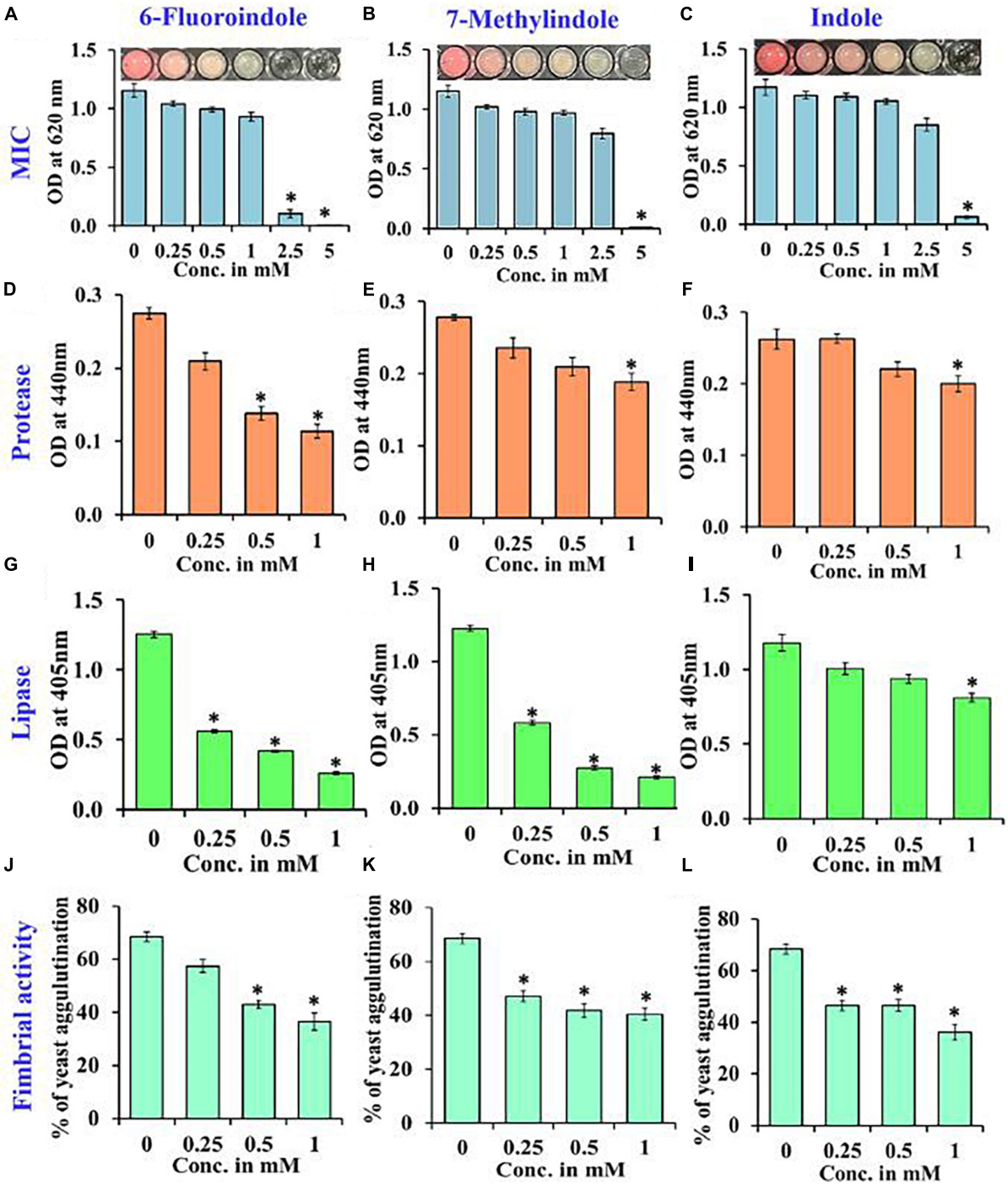

FIGURE 3 | Determination of the MICs of 6-fluoroindole **(A)**, 7-methylindole **(B)**, and indole **(C)** against *S. marcescens*. Effects of 6-fluoroindole, 7-methylindole, and indole on protease **(D–F)**, lipase **(G–I)** levels and on fimbria-mediated yeast agglutination **(J–L)** of *S. marcescens*. Error bars and asterisks (*) represent standard deviations and significant differences ($p < 0.05$), respectively, vs. non-treated controls.

of type I fimbria (Shanks et al., 2007). Furthermore, QS inhibitors such as phenol, 2,4-bis(1,1-dimethylethyl) (Padmavathi et al., 2014), and phytol (Srinivasan et al., 2016) have been shown to inhibit fimbrial expression in *S. marcescens*, and hence, we evaluated the effect of selected indole derivatives on fimbria-mediated yeast agglutination and sensitivity to H_2O_2. We found *S. marcescens* cells in the presence of 5-fluoroindole, 6-fluoroindole, 5-fluoro-2-methylindole, 5-methylindole, 7-methylindole, or indole at 1 mM *S. cerevisiae* agglutination by 36–68% (**Figures 3J–L** and **Supplementary Figure 10**). Also,

we found the sensitivities of 6-fluoroindole, 7-methylindole, or indole treated *S. marcescens* cells to H_2O_2 were greater than that of non-treated controls (**Figure 4A**).

Effects of 6-Fluoroindole and 7-Methylindole on EPS Production

Bacterial cells constitute 10–20% of wound biofilms, whereas EPS accounts for 80–90% of total biofilm mass (Percival et al., 2014). We observed EPS production was inhibited in 6-fluoroindole or 7-methylindole treated *S. marcescens* (**Figure 4B**). Extracted EPS was subjected to FTIR, which showed the presence of polysaccharides (1,200–900 cm^{-1}), amide I proteins (peaks corresponding to C=O and C-N stretching vibrations at 1,600 and 1,700 cm^{-1}), amide II proteins (peaks corresponding to N-H bending and C-N and C-C stretching vibrations at 1,510 and 1,580 cm^{-1}), and lipids (signature peaks at 2,850–3,020 cm^{-1}) (Naumann, 2001; Badireddy et al., 2008; **Figure 4C**). Reductions in saccharide, protein, and lipid absorptions showed 6-fluoroindole and 7-methylindole reduced EPS production by *S. marcescens*. In addition, EPS extracted from 6-fluoroindole, and 7-methylindole treated *S. marcescens* showed less hydration than the non-treated control (**Figure 4C**).

Differential Expressions of Genes by 6-Fluoroindole in *S. marcescens*

qRT-PCR was used to investigate the effects of 6-fluoroindole on the expressions of 10 QS-related genes associated with inhibitions of QS and biofilm formation. Notably, six key biofilm-, prodigiosin- and QS-genes, that is, *bmsA* (-3.1 ± 0.2), *fimA* (-3.0 ± 0.1), *pigA* (-3.2 ± 0.1), *pigC* (-3.0 ± 0.2), *Sma*I (-1.4 ± 0.2), and *rpoS* (-1.8 ± 0.1), were significantly repressed by 6-fluoroindole at 0.5 mM (**Figure 5**). These transcriptomic data partially support the inhibition of prodigiosin production and biofilm formation (**Figure 1**) and swarming inhibition (**Figure 2**). Interestingly, *Sma*I was more significantly inhibited than that of *SmaR* and *luxS* by 6-fluoroindole.

QS Inhibition by Indoles

Reporter strain *C. violaceum* CV026 is widely used as a biosensor strain for the screening of QS inhibitors that lack AHL synthase (CviI), and exogenous AHL supplementation restores QS-mediated violacein pigment production (McClean et al., 1997). We assessed violacein production using CV026 in the presence of exogenous AHL and indole or six indole derivatives (3-indoleacetonitrile, 5-fluoroindole, 6-fluoroindole, 5-fluoro-2-methylindole, 5-methylindole, and 7-methylindole). We found that at 0.25 mM indole and the six indole derivatives markedly inhibited violacein pigment production (**Figure 6A**), and thus, QS activity. For example, two active 6-fluoroindole and 7-methylindole at 0.25 mM decreased cell growth by only 9 and 24% while QS activity was decreased by 71 and 77% (**Supplementary Table 2**).

Additionally, the addition of AHLs (BHL or HHL) partially complemented QS inhibition by indoles. For example, BHL

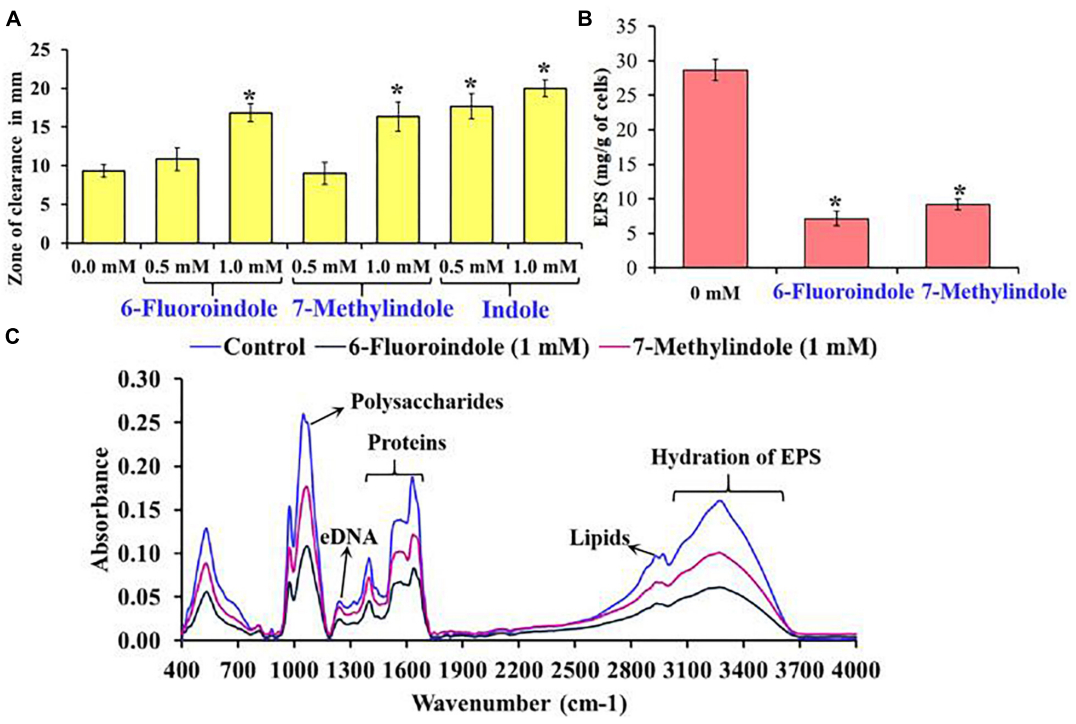

FIGURE 4 | Effects of 6-fluoroindole, 7-methylindole, and indole on the sensitivity of *S. marcescens* to H_2O_2 **(A)**. Effects of 6-fluoroindole and 7-methylindole at 1 mM on EPS production by *S. marcescens* **(B)**. Error bars and asterisks (*) represent standard deviation and significant differences ($p < 0.05$), respectively, vs. non-treated controls. FTIR analysis of EPS extracted from control, 6-fluoroindole, and 7-methylindole treated *S. marcescens* **(C)**.

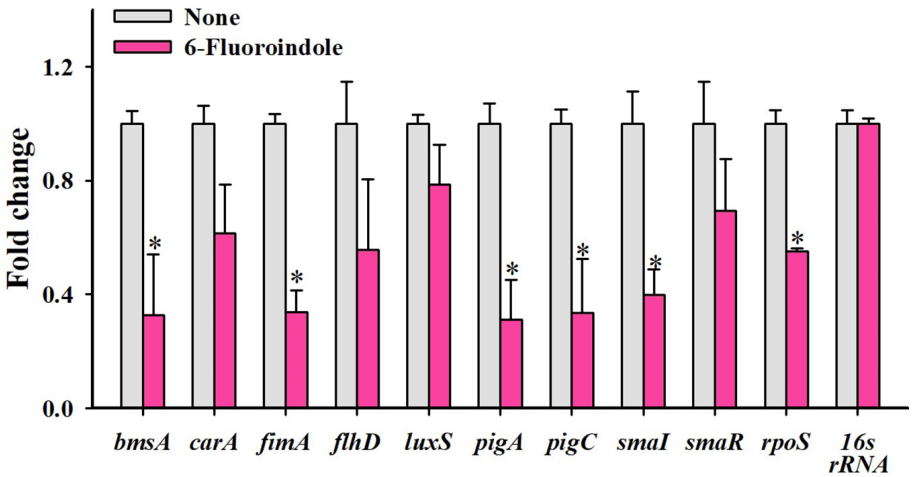

FIGURE 5 | Relative transcriptional profiles of *S. marcescens* cells treated with or without 6-fluoroindole. *S. marcescens* was incubated with or without 6-fluoroindole at 0.5 mM for 6 h with shaking at 250 rpm. Transcriptional profiles were obtained by qRT-PCR. Fold changes represent changes in the transcriptions of treated vs. untreated *S. marcescens*. *16s rRNA* was a housekeeping gene. *$P < 0.05$ vs. non-treated controls (None).

or HHL mostly restored QS activity in the presence of 6-fluoroindole (6FI) and 7-methylindole (7MI) at 0.25 mM while two AHLs could not complement the presence of the higher amount of two indoles at 0.5 mM (**Figure 6B**). This result also supports the previous finding that violacein inhibition by indole could be counteracted by the exogenous C10-AHL (Hidalgo-Romano et al., 2014).

DISCUSSION

Several phenolics are known to inhibit prodigiosin synthesis by *S. marcescens* (Kalia, 2013). Indole and its derivatives are synthesized by various microbes as signaling molecules that control various aspects of bacterial and eukaryotic physiology (Lee and Lee, 2010; Lee et al., 2015b). These interspecies and interkingdom signaling molecules inhibit QS, biofilm formation, and the expressions of virulence factors in non-indole producing bacteria (Kalia, 2013; Lee et al., 2015b). The current study shows that indoles have diverse antivirulence roles in *S. marcescens*. Like indoles, furocoumarins (Girennavar et al., 2008), coumarins (Gutiérrez-Barranquero et al., 2015; D'Almeida et al., 2017), 6,7-dihydroxycoumarin, and 7-hydroxycoumarin (Ta and Arnason, 2016) inhibit AHL-mediated QS and biofilm formation.

The *pig*-gene cluster encodes for a group of enzymes responsible for the biosynthesis of prodigiosin in *S. marcescens*, and the majority of these genes are involved in the conversion of 2-octenal to monopyrrole MAP (2-methyl-3-amylpyrrole) and the bipyrrole moiety MBC (4-methoxy-2-2′-bipyrrole-5-carbaldehyde). *pigC* encodes for an enzyme that condenses MBC and MAP to produce prodigiosin (Pan et al., 2020). A significant reduction in prodigiosin levels was observed after exposing with the QS inhibitor hordenine, which down-regulated the expressions of *pig*-genes (Zhou et al., 2019). The expression of the *pig*-gene cluster is also affected by various transcriptional factors (Pan et al., 2020), and is a potential target of indole derivatives.

Indole and its derivatives are viewed as potential antivirulence compounds against antibiotic-resistant pathogens because of their ability to inhibit quorum sensing and virulence factor production (Lee et al., 2015b). Interestingly these indoles affect bacterial physiology in different ways. For example, indoles activate efflux pump systems in *Escherichia* sp. (Kawamura-Sato et al., 1999; Lee et al., 2010), *Vibrio* sp. (Howard et al., 2019), *Pseudomonas* sp. (Lee et al., 2009, 2012; Molina-Santiago et al., 2014), *Agrobacterium* sp. (Lee et al., 2015a), *Cylindrotheca* sp. (Yang et al., 2014), and *Salmonella* sp. (Nikaido et al., 2008, 2012; Blair et al., 2013) and inhibit QS systems in *Pseudomonas* sp. (Lee et al., 2009, 2011, 2012; Tashiro et al., 2010; Chu et al., 2012; Frei et al., 2012; Biswas et al., 2015), *Acinetobacter* sp. (Kim and Park, 2013), and *Chromobacterium* sp. and *Serratia* sp. (Hidalgo-Romano et al., 2014). Although the exact mechanisms responsible for the effects of indoles have not been determined (Kim and Park, 2015; Lee et al., 2015b; Zarkan et al., 2020), the abundance of indole derivatives presents an opportunity to identify indoles active against super bacteria.

Bacterial swarming involves the well-coordinated migration of cells driven by flagella and plays an important role in nutrient sensing, surface colonization, biofilm formation, virulence, and host-pathogen interactions (Kearns, 2010). In addition, swarming motility is associated with the resistance to antimicrobial agents displayed by several clinically important pathogens (Kearns, 2010). Thus, compounds that diminish swarming motility are likely to affect biofilm formation and virulence factor production (Corral et al., 2020; Rütschlin and Böttcher, 2020). Similarly, swimming motility is also involved in the initial phase of the infection process (Kumar et al., 2018;

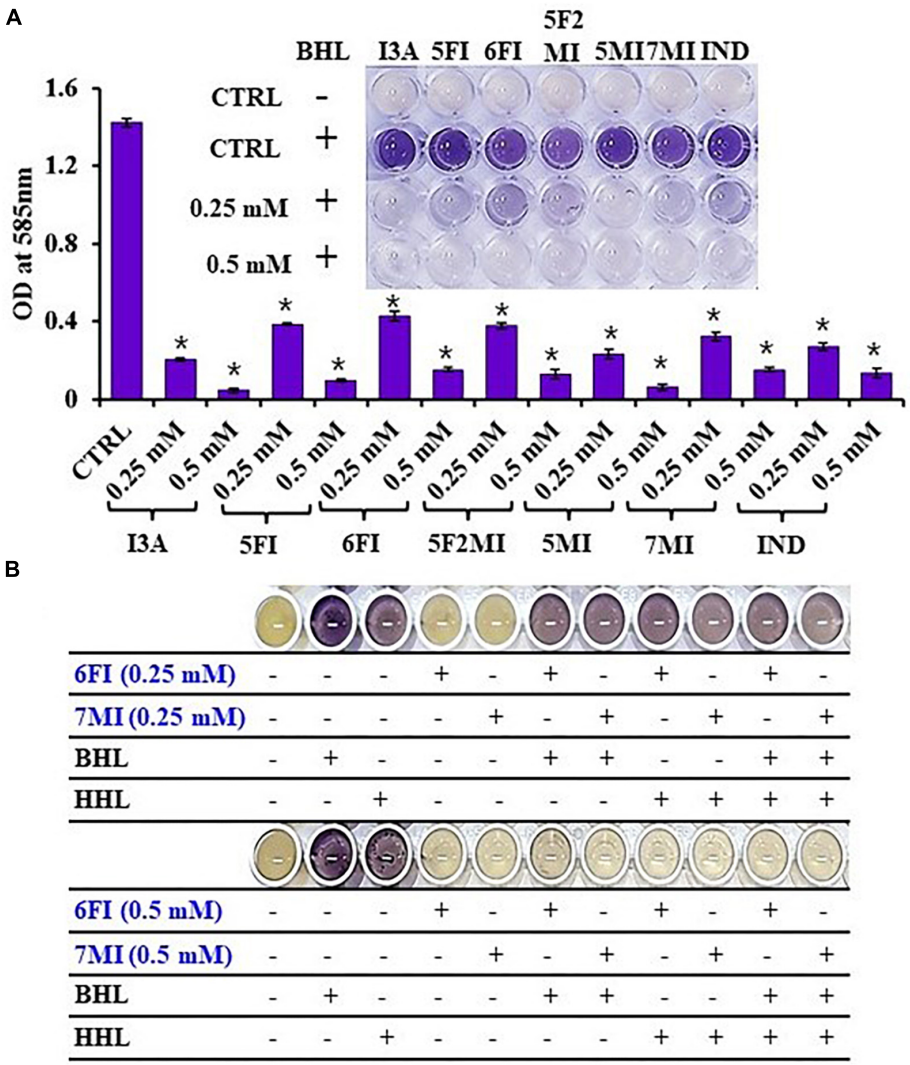

FIGURE 6 | Indole (IND) and selected indole derivatives [3-indoleacetonitrile (I3A), 5-fluoroindole (5FI), 6-fluoroindole (6FI), 5-fluoro-2-methylindole (5F2MI), 5-methylindole (5MI), and 7-methylindole (7MI)] inhibited QS controlled violacein pigment production in *Chromobacterium violaceum* CV026. The inset shows the inhibition of violacein pigment production by indole and selected indole derivatives. Error bars and asterisks (*) represent standard deviations and significant differences ($p < 0.05$), respectively, vs. non-treated controls (CTRL) **(A)**. *N*-butanoyl homoserine lactone (BHL) or *N*-hexanoyl homoserine lactone (HHL) at 500 μM was used for complementing violacein production in the presence of 6-fluoroindole (6FI) and 7-methylindole (7MI) **(B)**.

Corral et al., 2020). In this study, several indoles significantly inhibit swarming and swimming motilities (**Figure 2** and **Supplementary Figure 7**).

Therapeutic agents that reduce the virulence of pathogens are topics of active research in the pharmaceutical industry and in academia. Protease defective strains of *P. aeruginosa* (Breidenstein et al., 2012) and *Vibrio cholera* (Rogers et al., 2016) reduce motility, biofilm formation, and virulence, and bioactive compounds like N-mercaptoacetyl-Phe-Tyr-amide (Cathcart et al., 2011), curcumin (Rudrappa and Bais, 2008; Sethupathy et al., 2016a), and hydroxamic acid (Kany et al., 2018) have been reported to reduce the virulence and biofilm formation by *P. aeruginosa* by targeting protease. Lipases are important secreted virulence factors that support bacterial and fungal pathogens during the early infection stage by damaging the phospholipid layers of host cells and disrupting innate defenses (Chen and Alonzo, 2019). Bioactive compounds such as alpha-bisabolol (Sethupathy et al., 2016b), vanillic acid (Sethupathy et al., 2017), and phytol (Srinivasan et al., 2016) have been shown to affect protease and lipase production in *S. marcescens* by interfering with QS. The protease and lipase inhibitory activities of indole derivatives against *S. marcescens* (**Figure 3** and **Supplementary Figures 8**, **9**) warrant further investigation as potential therapeutic agents, and the results of our H_2O_2 sensitivity assay also suggest the disruption of oxidative stress response in *S. marcescens*, which is one of the prerequisites of biofilm formation under challenging conditions *in vivo*.

Our findings indicate that both 6-fluoroindole and 7-methylindole reduce yeast agglutination and increase sensitivity to H_2O_2 probably through the differential regulation of OxyR in *S. marcescens*.

Previously, the addition of exogenous C10-AHL could restore the production of QS activity (Hidalgo-Romano et al., 2014) and the current studies also showed that the additions of other AHLs (BHL or HHL) mostly restored QS activity in the presence of indole derivatives (**Figure 6B**). Similarly, 6-gingerol (Kim H.-S.et al., 2015) and quercetin (Gopu et al., 2015) were reported to inhibit violacein production in the presence of AHL by blocking AHL-transcriptional receptor protein complex, which is essential for the violacein biosynthesis. In the majority of Gram-negative pathogens, AHL-transcriptional receptor protein complex formation is essentially required for the activation of QS controlled phenotypes and virulence gene expression (Miller and Bassler, 2001; Mukherjee and Bassler, 2019) and unlike antimicrobial agents, inhibiting AHL-transcriptional receptor protein complex formation by indoles is expected to reduce pressure favoring the development of drug resistance.

While indole and most of the indole derivatives did not have significant antimicrobial activity in *S. marcescens* (**Figure 1** and **Supplementary Figure 3**), a few indoles such as 5-fluoroindole, 5-iodoindole and 5-methylindole showed significant antimicrobial activity (**Supplementary Figure 4**). Also, in the *C. violaceum* strain, most indoles at 0.25 and 0.5 mM markedly affect planktonic cell growth (**Supplementary Table 2**). Furthermore, it was reported that 5-iodoindole showed strong bactericidal activity against *Escherichia coli* strains and *Staphylococcus aureus* (Lee et al., 2016) and could rapidly kill *Acinetobacter baumannii* (Raorane et al., 2020). Therefore, it is important to carefully assess the toxicity of indoles on bacteria and animals.

The present study demonstrates the abilities of indole derivatives to inhibit QS in *S. marcescens,* and thus, to inhibit prodigiosin pigment production, biofilm formation, swimming motility, swarming motility, and fimbrial activity. Of the indole derivatives tested, 6-fluoroindole and 7-methylindole potently inhibited lipase, protease, and EPS production in *S. marcescens*. AHL supplementation assay using *C. violaceum* CV026 confirmed the disruption of QS by indole derivatives. Based on the results obtained, we suggest that indole and indole derivatives interfere with QS in *S. marcescens* and *C. violaceum* possibly by preventing AHL molecules binding to their cognate receptors. Based on our observation that indole derivatives differentially inhibit the virulence of and biofilm formation by *S. marcescens*, we suggest further studies be undertaken to determine the molecular mechanism involved.

DATA AVAILABILITY STATEMENT

All datasets generated for this study are included in the article/**Supplementary Materials**, further inquiries can be directed to the corresponding authors.

AUTHOR CONTRIBUTIONS

SS, J-HL, and JL: conceptualization. SS, ES, Y-GK, and JL: methodology. SS, ES, J-HL, Y-GK, and JL: writing of the original manuscript. J-HL and JL: project administration and funding acquisition. All authors contributed to the article and approved the submitted version.

FUNDING

This work was supported by the National Research Foundation of Korea (NRF) funded by the Ministry of Education (2018R1D1A3B07040699 to J-HL) and by the Priority Research Centers Program through the NRF funded by the Ministry of Education (2014R1A6A1031189).

SUPPLEMENTARY MATERIAL

The Supplementary Material for this article can be found online at: https://www.frontiersin.org/articles/10.3389/fmicb.2020.584812/full#supplementary-material

Supplementary Figure 1 | Screening of indole derivatives for the QS controlled inhibition of prodigiosin production in *S. marcescens* [Indole-3-carboxaldehyde (1), indole-3-butyric acid (2), indole-3-carbinol (3), indole-3-acetic acid (4), indole-3-carboxylic acid (5), 2-oxindole (6), 7-methoxyindole (7), 5-fluoroxindole (8), 7-fluoroindole-2,3-dione (9), 3-indoleacetonitrile (10), 5-fluoroindole (11), 6-fluoroindole (12), 7-fluoroindole (13), 5-fluoroindole-2,3-dione (14), 3,3'-methylenebis-indole (15), methyl-indole-7-carboxylate (16), 2,5-dimethylindole (17), 7-methylindole (18), 7-methyl-1H-indole-2,3-dione (19), 4-formyl indole (20), 5-formyl indole (21), 6-formyl indole (22), 7-formyl indole (23), 7-nitroindole (24), 7-azaindole (25), 6-(trifluoromethyl)indole (26), 1H-indole-2-carboxaldehyde (27), 5-iodoindole (28), 2-methylindole-3-acetic acid (29), 5-amino-2-methylindole (30), 5-indoindolin-2-one (31), 5-fluoro-2-methylindole (32), 5-chloro-2-methylindole (33), 7-fluoro-5-iodoindole (34), indole-3-acetamide (35), indole-3-propionic acid (36), indole-7-carboxylic acid (37), 1-methylindole-3-carboxaldehyde (38), 7-methylindole-3-carboxaldehyde (39), 2-methylindole-3-carboxaldehyde (40), 5-benzyloxyindole (41), 1,2-dimethylindole (42), 5-methylindole (43), 4-benzyloxyindole (44), 6-benzyloxyindole (45), 7-benzyloxyindole (46), 7-fluoro-5-iodoindole-3-carboxaldehyde (47), 1-BOC-5-iodoindole (48), 3-(2-hydroxyethyl)indole (49), 4-fluoroindole (50), 7-fluoroindoline-2, 3-dione (51), and indole (52)]. Error bars and asterisks represent standard deviation and the statistically significant difference ($p < 0.05$), respectively.

Supplementary Figure 2 | Concentration-dependent inhibition of prodigiosin production by selected indole derivatives in *S. marcescens*. Error bars and asterisks represent standard deviation and the statistically significant difference ($p < 0.05$), respectively.

Supplementary Figure 3 | Screening of indole and indole derivatives for *S. marcescens* antibiofilm activity. Error bars and asterisks represent standard deviation and the statistically significant difference ($p < 0.05$), respectively. Tested indole derivatives names are indicated in **Supplementary Figure 1**. Biofilm formation Planktonic cell growth.

Supplementary Figure 4 | Concentration-dependent antibiofilm activities of selected indole derivatives against *S. marcescens*. Error bars and asterisks represent standard deviation and the statistically significant difference ($p < 0.05$), respectively. Biofilm formation Planktonic cell growth

Supplementary Figure 5 | Effects of indole derivatives on the planktonic cell growth of *S. marcescens*.

Supplementary Figure 6 | Determination of the MICs of 3-indoleacetonitrile, 5-fluoroindole, 7-methylindole, and 5-fluoro-2-methylindole against *S. marcescens*. Error bars and asterisks represent standard deviation and the statistically significant difference ($p < 0.05$), respectively.

Supplementary Figure 7 | Inhibitory effects of indole derivatives on the swimming and swarming motilities of *S. marcescens*.

Supplementary Figure 8 | Effects of indole derivatives on protease production by *S. marcescens*. Error bars and asterisks represent standard deviation and the statistically significant difference ($p < 0.05$), respectively.

Supplementary Figure 9 | Effects of indole derivatives on lipase production in *S. marcescens*. Error bars and asterisks represent standard deviation and the statistically significant difference ($p < 0.05$), respectively.

Supplementary Figure 10 | Effects of indole derivatives on the fimbria-mediated yeast agglutination by *S. marcescens*. Error bars and asterisks represent standard deviation and the statistically significant difference ($p < 0.05$), respectively.

Supplementary Table 1 | Primer sequences for qRT-PCR.

Supplementary Table 2 | Comparison of QS inhibition and growth inhibition by indoles in *C. violaceum* CV026. This table supports the **Figure 6** of QS inhibition assay.

REFERENCES

Acar, J. F., and Goldstein, F. W. (1997). Trends in bacterial resistance to fluoroquinolones. *Clin. Infect. Dis.* 24, S67–S73. doi: 10.1093/clinids/24.Supplement_1.S67

Amin-ul Mannan, M., Sharma, S., and Ganesan, K. (2009). Total RNA isolation from recalcitrant yeast cells. *Anal. Biochem.* 389, 77–79. doi: 10.1016/j.ab.2009.03.014

Badireddy, A. R., Korpol, B. R., Chellam, S., Gassman, P. L., Engelhard, M. H., Lea, A. S., et al. (2008). Spectroscopic characterization of extracellular polymeric substances from *Escherichia coli* and *Serratia marcescens*: suppression using sub-inhibitory concentrations of bismuth thiols. *Biomacromolecules* 9, 3079–3089. doi: 10.1021/bm800600p

Biswas, N. N., Kutty, S. K., Barraud, N., Iskander, G. M., Griffith, R., Rice, S. A., et al. (2015). Indole-based novel small molecules for the modulation of bacterial signalling pathways. *Org. Biomol. Chem.* 13, 925–937. doi: 10.1039/C4OB02096K

Blair, J. M. A., Cloeckaert, A., Nishino, K., and Piddock, L. J. V. (2013). Alternative explanation for indole-induced antibiotic tolerance in *Salmonella*. *Proc. Natl. Acad. Sci. U.S.A.* 110, E4569–E4569. doi: 10.1073/pnas.1318318110

Brackman, G., Cos, P., Maes, L., Nelis, H. J., and Coenye, T. (2011). Quorum sensing inhibitors increase the susceptibility of bacterial biofilms to antibiotics. *Antimicrob. Agents Chemother.* 55, 2655–2661. doi: 10.1128/AAC.00045-11

Breidenstein, E. B., Janot, L., Strehmel, J., Fernandez, L., Taylor, P. K., Kukavica-Ibrulj, I., et al. (2012). The Lon protease is essential for full virulence in *Pseudomonas aeruginosa*. *PLoS One* 7:e49123. doi: 10.1371/journal.pone.0049123

Cathcart, G. R. A., Quinn, D., Greer, B., Harriott, P., Lynas, J. F., Gilmore, B. F., et al. (2011). Novel inhibitors of the *Pseudomonas aeruginosa* virulence factor LasB: a potential therapeutic approach for the attenuation of virulence mechanisms in pseudomonal infection. *Antimicrob. Agents Chemother.* 55, 2670–2678. doi: 10.1128/AAC.00776-10

Chen, X., and Alonzo, F. (2019). Bacterial lipolysis of immune-activating ligands promotes evasion of innate defenses. *Proc. Natl. Acad. Sci. U.S.A.* 116, 3764–3773. doi: 10.1073/pnas.1817248116

Chu, W., Zere, T. R., Weber, M. M., Wood, T. K., Whiteley, M., Hidalgo-Romano, B., et al. (2012). Indole production promotes *Escherichia coli* mixed-culture growth with *Pseudomonas aeruginosa* by inhibiting quorum signaling. *Appl. Environ. Microbiol.* 78, 411–419. doi: 10.1128/AEM.06396-11

Cooney, S., O'brien, S., Iversen, C., and Fanning, S. (2014). Bacteria: other pathogenic *Enterobacteriaceae–Enterobacter* and other genera. *Encycl. Food Saf.* 1, 433–441. doi: 10.1016/B978-0-12-378612-8.00104-9

Corral, J., Sebastià, P., Coll, N. S., Barbé, J., Aranda, J., and Valls, M. (2020). Twitching and swimming motility play a role in *Ralstonia solanacearum* pathogenicity. *Msphere* 5:e00740-19. doi: 10.1128/mSphere.00740-19

Coulthurst, S. J., Williamson, N. R., Harris, A. K. P., Spring, D. R., and Salmond, G. P. C. (2006). Metabolic and regulatory engineering of *Serratia marcescens*: mimicking phage-mediated horizontal acquisition of antibiotic biosynthesis and quorum-sensing capacities. *Microbiology* 152, 1899–1911. doi: 10.1099/mic.0.28803-0

Cristina, M. L., Sartini, M., and Spagnolo, A. M. (2019). *Serratia marcescens* infections in neonatal intensive care units (NICUs). *Int. J. Environ. Res. Public Health.* 16:610. doi: 10.3390/ijerph16040610

D'Almeida, R. E., Molina, R. D. I., Viola, C. M., Luciardi, M. C., Nieto Peñalver, C., Bardón, A., et al. (2017). Comparison of seven structurally related coumarins on the inhibition of quorum sensing of *Pseudomonas aeruginosa* and *Chromobacterium violaceum*. *Bioorg. Chem.* 73, 37–42. doi: 10.1016/j.bioorg.2017.05.011

Eberl, L., Winson, M. K., Sternberg, C., Stewart, G. S., Christiansen, G., Chhabra, S. R., et al. (1996). Involvement of *N*-acyl-$_L$-homoserine lactone autoinducers in controlling the multicellular behaviour of *Serratia liquefaciens*. *Mol. Microbiol.* 20, 127–136. doi: 10.1111/j.1365-2958.1996.tb02495.x

Frei, R., Breitbach, A. S., and Blackwell, H. E. (2012). 2-Aminobenzimidazole derivatives strongly inhibit and disperse *Pseudomonas aeruginosa* biofilms. *Angew. Chem.* 124, 5316–5319. doi: 10.1002/ange.201109258

Girennavar, B., Cepeda, M. L., Soni, K. A., Vikram, A., Jesudhasan, P., Jayaprakasha, G. K., et al. (2008). Grapefruit juice and its furocoumarins inhibits autoinducer signaling and biofilm formation in bacteria. *Int. J. Food Microbiol.* 125, 204–208. doi: 10.1016/j.ijfoodmicro.2008.03.028

Gopu, V., Meena, C. K., and Shetty, P. H. (2015). Quercetin influences quorum sensing in food borne bacteria: *in-vitro* and *in-silico* evidence. *PLoS One* 10:e0134684. doi: 10.1371/journal.pone.0134684

Gutiérrez-Barranquero, J. A., Reen, F. J., Mccarthy, R. R., and O'gara, F. (2015). Deciphering the role of coumarin as a novel quorum sensing inhibitor suppressing virulence phenotypes in bacterial pathogens. *Appl. Microbiol. Biotechnol.* 99, 3303–3316. doi: 10.1007/s00253-015-6436-1

Hidalgo-Romano, B., Gollihar, J., Brown, S. A., Whiteley, M., Valenzuela, E., Kaplan, H. B., et al. (2014). Indole inhibition of *N*-acylated homoserine lactone-mediated quorum signalling is widespread in Gram-negative bacteria. *Microbiology* 160, 2464–2473. doi: 10.1099/mic.0.081729-0

Høiby, N., Bjarnsholt, T., Givskov, M., Molin, S., and Ciofu, O. (2010). Antibiotic resistance of bacterial biofilms. *Int. J. Antimicrob. Agents* 35, 322–332. doi: 10.1016/j.ijantimicag.2009.12.011

Horng, Y.-T., Deng, S.-C., Daykin, M., Soo, P.-C., Wei, J.-R., Luh, K.-T., et al. (2002). The LuxR family protein SpnR functions as a negative regulator of *N*-acylhomoserine lactone-dependent quorum sensing in *Serratia marcescens*. *Mol. Microbiol.* 45, 1655–1671. doi: 10.1046/j.1365-2958.2002.03117.x

Howard, M. F., Bina, X. R., and Bina, J. E. (2019). Indole inhibits ToxR regulon expression in *Vibrio cholerae*. *Infect. Immun.* 87:e00776-18. doi: 10.1128/IAI.00776-18

Ivanova, D., Markovska, R., Hadjieva, N., Schneider, I., Mitov, I., and Bauernfeind, A. (2008). Extended-spectrum β-lactamase-producing *Serratia marcescens* outbreak in a Bulgarian hospital. *J. Hosp. Infect.* 70, 60–65. doi: 10.1016/j.jhin.2008.04.033

Jones, R. N. (2010). Microbial etiologies of hospital-acquired bacterial pneumonia and ventilator-associated bacterial pneumonia. *Clin. Infect. Dis.* 51, S81–S87. doi: 10.1086/653053

Kalia, V. C. (2013). Quorum sensing inhibitors: an overview. *Biotechnol. Adv.* 31, 224–245. doi: 10.1016/j.biotechadv.2012.10.004

Kany, A. M., Sikandar, A., Yahiaoui, S., Haupenthal, J., Walter, I., Empting, M., et al. (2018). Tackling *Pseudomonas aeruginosa* virulence by a hydroxamic acid-based LasB inhibitor. *ACS Chem. Biol.* 13, 2449–2455. doi: 10.1021/acschembio.8b00257

Kawamura-Sato, K., Shibayama, K., Horii, T., Iimuma, Y., Arakawa, Y., and Ohta, M. (1999). Role of multiple efflux pumps in *Escherichia coli* in indole expulsion. *FEMS Microbiol. Lett.* 179, 345–352. doi: 10.1111/j.1574-6968.1999.tb08748.x

Kearns, D. B. (2010). A field guide to bacterial swarming motility. *Nat. Rev. Microbiol.* 8, 634–644. doi: 10.1038/nrmicro2405

Kim, H.-S., Lee, S.-H., Byun, Y., and Park, H.-D. (2015). 6-Gingerol reduces *Pseudomonas aeruginosa* biofilm formation and virulence via quorum sensing inhibition. *Sci. Rep.* 5:8656. doi: 10.1038/srep08656

Kim, J., and Park, W. (2013). Indole inhibits bacterial quorum sensing signal transmission by interfering with quorum sensing regulator folding. *Microbiology* 159, 2616–2625. doi: 10.1099/mic.0.070615-0

Kim, J., and Park, W. (2015). Indole: a signaling molecule or a mere metabolic byproduct that alters bacterial physiology at a high concentration? *Res. J. Microbiol.* 53, 421–428. doi: 10.1007/s12275-015-5273-3

Kim, Y.-G., Lee, J.-H., Cho, M. H., and Lee, J. (2011). Indole and 3-indolylacetonitrile inhibit spore maturation in *Paenibacillus alvei*. *BMC Microbiol.* 11:119. doi: 10.1186/1471-2180-11-119

Kim, Y.-G., Lee, J.-H., Gupta, V. K., Manoharan, R. K., and Lee, J. (2015). Cinnamon bark oil and its components inhibit biofilm formation and toxin production. *Int. J. Food Microbiol.* 195, 30–39. doi: 10.1016/j.ijfoodmicro.2014.11.028

Kim, Y.-G., Lee, J.-H., Gwon, G., Kim, S.-I., Park, J. G., and Lee, J. (2016). Essential oils and eugenols inhibit biofilm formation and the virulence of *Escherichia coli* O157:H7. *Sci. Rep.* 6:36377. doi: 10.1038/srep36377

Kumar, B., Sorensen, J. L., and Cardona, S. T. (2018). A c-di-GMP-modulating protein regulates swimming motility of *Burkholderia cenocepacia* in response to arginine and glutamate. *Front. Cell. Infect. Microbiol.* 8:56. doi: 10.3389/fcimb.2018.00056

LaSarre, B., and Federle, M. J. (2013). Exploiting quorum sensing to confuse bacterial pathogens. *Microbiol. Mol. Biol. Rev.* 77, 73–111. doi: 10.1128/MMBR.00046-12

Lee, H. H., Molla, M. N., Cantor, C. R., and Collins, J. J. (2010). Bacterial charity work leads to population-wide resistance. *Nature* 467, 82–85. doi: 10.1038/nature09354

Lee, J., Attila, C., Cirillo, S. L. G., Cirillo, J. D., and Wood, T. K. (2009). Indole and 7-hydroxyindole diminish *Pseudomonas aeruginosa* virulence. *Microb. Biotechnol.* 2, 75–90. doi: 10.1111/j.1751-7915.2008.00061.x

Lee, J., Bansal, T., Jayaraman, A., Bentley, W. E., and Wood, T. K. (2007). Enterohemorrhagic *Escherichia coli* biofilms are inhibited by 7-hydroxyindole and stimulated by Isatin. *Appl. Environ. Microbiol.* 73, 4100–4109. doi: 10.1128/AEM.00360-07

Lee, J.-H., Cho, H. S., Kim, Y., Kim, J.-A., Banskota, S., Cho, M. H., et al. (2013). Indole and 7-benzyloxyindole attenuate the virulence of *Staphylococcus aureus*. *Appl. Microbiol. Biotechnol.* 97, 4543–4552. doi: 10.1007/s00253-012-4674-z

Lee, J.-H., Cho, M. H., and Lee, J. (2011). 3-Indolylacetonitrile decreases *Escherichia coli* O157:H7 biofilm formation and *Pseudomonas aeruginosa* virulence. *Environ. Microbiol.* 13, 62–73. doi: 10.1111/j.1462-2920.2010.02308.x

Lee, J.-H., Kim, Y.-G., Baek, K.-H., Cho, M. H., and Lee, J. (2015a). The multifaceted roles of the interspecies signalling molecule indole in *Agrobacterium tumefaciens*. *Environ. Microbiol.* 17, 1234–1244. doi: 10.1111/1462-2920.12560

Lee, J.-H., Kim, Y.-G., Cho, M. H., Kim, J.-A., and Lee, J. (2012). 7-fluoroindole as an antivirulence compound against *Pseudomonas aeruginosa*. *FEMS Microbiol. Lett.* 329, 36–44. doi: 10.1111/j.1574-6968.2012.02500.x

Lee, J.-H., Kim, Y.-G., Gupta, V. K., Manoharan, R. K., and Lee, J. (2018). Suppression of fluconazole resistant *Candida albicans* biofilm formation and filamentation by methylindole derivatives. *Front. Microbiol.* 9:2641. doi: 10.3389/fmicb.2018.02641

Lee, J.-H., Kim, Y.-G., Gwon, G., Wood, T. K., and Lee, J. (2016). Halogenated indoles eradicate bacterial persister cells and biofilms. *AMB Express* 6:123. doi: 10.1186/s13568-016-0297-6

Lee, J.-H., and Lee, J. (2010). Indole as an intercellular signal in microbial communities. *FEMS Microbiol. Rev.* 34, 426–444. doi: 10.1111/j.1574-6976.2009.00204.x

Lee, J.-H., Wood, T. K., and Lee, J. (2015b). Roles of indole as an interspecies and interkingdom signaling molecule. *Trends Microbiol.* 23, 707–718. doi: 10.1016/j.tim.2015.08.001

Manoharan, R. K., Lee, J.-H., and Lee, J. (2018). Efficacy of 7-benzyloxyindole and other halogenated indoles to inhibit *Candida albicans* biofilm and hyphal formation. *Microb. Biotechnol.* 11, 1060–1069. doi: 10.1111/1751-7915.13268

McClean, K. H., Winson, M. K., Fish, L., Taylor, A., Chhabra, S. R., Camara, M., et al. (1997). Quorum sensing and *Chromobacterium violaceum*: exploitation of violacein production and inhibition for the detection of *N*-acylhomoserine lactones. *Microbiology* 143, 3703–3711. doi: 10.1099/00221287-143-12-3703

Miller, M. B., and Bassler, B. L. (2001). Quorum sensing in bacteria. *Annu. Rev. Microbiol.* 55, 165–199. doi: 10.1146/annurev.micro.55.1.165

Molina-Santiago, C., Daddaoua, A., Fillet, S., Duque, E., and Ramos, J.-L. (2014). Interspecies signalling: *Pseudomonas putida* efflux pump TtgGHI is activated by indole to increase antibiotic resistance. *Environ. Microbiol.* 16, 1267–1281. doi: 10.1111/1462-2920.12368

Mukherjee, S., and Bassler, B. L. (2019). Bacterial quorum sensing in complex and dynamically changing environments. *Nat. Rev. Microbiol.* 17, 371–382. doi: 10.1038/s41579-019-0186-5

Naumann, D. (2001). FT-Infrared and FT-Raman spectroscopy in biomedical research. *Appl. Spectrosc. Rev.* 36, 239–298. doi: 10.1081/ASR-100106157

Nikaido, E., Giraud, E., Baucheron, S., Yamasaki, S., Wiedemann, A., Okamoto, K., et al. (2012). Effects of indole on drug resistance and virulence of *Salmonella enterica* serovar Typhimurium revealed by genome-wide analyses. *Gut Pathog.* 4:5. doi: 10.1186/1757-4749-4-5

Nikaido, E., Yamaguchi, A., and Nishino, K. (2008). AcrAB multidrug efflux pump regulation in *Salmonella enterica* serovar Typhimurium by RamA in response to environmental signals. *J. Biol. Chem.* 283, 24245–24253. doi: 10.1074/jbc.M804544200

Padmavathi, A. R., Abinaya, B., and Pandian, S. K. (2014). Phenol, 2,4-bis(1,1-dimethylethyl) of marine bacterial origin inhibits quorum sensing mediated biofilm formation in the uropathogen *Serratia marcescens*. *Biofouling* 30, 1111–1122. doi: 10.1080/08927014.2014.972386

Pan, X., Sun, C., Tang, M., You, J., Osire, T., Zhao, Y., et al. (2020). LysR-type transcriptional regulator MetR controls prodigiosin production, methionine biosynthesis, cell motility, tolerance, heat tolerance, and exopolysaccharide synthesis in *Serratia marcescens*. *Appl. Environ. Microbiol.* 86:e02241-19. doi: 10.1128/AEM.02241-19

Patel, U., Chandpura, J., Chauhan, K., and Gupte, S. (2018). Screening and isolation of an organic solvent tolerant lipase producing bacteria from various oil contaminated sites. *Indian J. Microbiol.* 21, 22–36. doi: 10.46798/ijam.2018.v21i01.004

Pearson, M. M. (2019). "Methods for studying swarming and swimming motility," in *Proteus Mirabilis, Methods in Molecular Biology*, Vol. 2021, ed. M. Pearson (New York, NY: Humana), 15–25. doi: 10.1007/978-1-4939-9601-8_3

Percival, S. L., Vuotto, C., Donelli, G., and Lipsky, B. A. (2014). Biofilms and wounds: an identification algorithm and potential treatment options. *Adv. Wound Care* 4, 389–397. doi: 10.1089/wound.2014.0574

Rajasekharan, S. K., Kim, S., Kim, J.-C., and Lee, J. (2020). Nematicidal activity of 5-iodoindole against root-knot nematodes. *Pestic. Biochem. Phys.* 163, 76–83. doi: 10.1016/j.pestbp.2019.10.012

Rajasekharan, S. K., Lee, J.-H., Ravichandran, V., Kim, J.-C., Park, J. G., and Lee, J. (2019). Nematicidal and insecticidal activities of halogenated indoles. *Sci. Rep.* 9:2010. doi: 10.1038/s41598-019-38561-3

Raorane, C. J., Lee, J.-H., and Lee, J. (2020). Rapid killing and biofilm inhibition of multidrug-resistant *Acinetobacter baumannii* strains and other microbes by iodoindoles. *Biomolecules* 10:1186. doi: 10.3390/biom10081186

Ray, C., Shenoy, A. T., Orihuela, C. J., and González-Juarbe, N. (2017). Killing of *Serratia marcescens* biofilms with chloramphenicol. *Ann. Clin. Microbiol. Antimicrob.* 16:19. doi: 10.1186/s12941-017-0192-2

Rogers, A., Townsley, L., Gallego-Hernandez, A. L., Beyhan, S., Kwuan, L., and Yildiz, F. H. (2016). The LonA protease regulates biofilm formation, motility, virulence, and the type VI secretion system in *Vibrio cholerae*. *J. Bacteriol.* 198, 973–985. doi: 10.1128/JB.00741-15

Rudrappa, T., and Bais, H. P. (2008). Curcumin, a known phenolic from curcuma longa, attenuates the virulence of *Pseudomonas aeruginosa* PAO1 in whole plant and animal pathogenicity models. *J. Agric. Food Chem.* 56, 1955–1962. doi: 10.1021/jf072591j

Rütschlin, S., and Böttcher, T. (2020). Inhibitors of bacterial swarming behavior. *Chem. Eur.J.* 26, 964–979. doi: 10.1002/chem.201901961

Sader, H. S., Farrell, D. J., Flamm, R. K., and Jones, R. N. (2014). Antimicrobial susceptibility of Gram-negative organisms isolated from patients hospitalized in intensive care units in United States and European hospitals (2009–2011).

Diagn. Microbiol. Infect. Dis. 78, 443–448. doi: 10.1016/j.diagmicrobio.2013.11.025

Saint-Criq, V., Villeret, B., Bastaert, F., Kheir, S., Hatton, A., Cazes, A., et al. (2018). *Pseudomonas aeruginosa* LasB protease impairs innate immunity in mice and humans by targeting a lung epithelial cystic fibrosis transmembrane regulator–IL-6–antimicrobial–repair pathway. *Thorax* 73, 49–61. doi: 10.1136/thoraxjnl-2017-210298

Sethupathy, S., Ananthi, S., Selvaraj, A., Shanmuganathan, B., Vigneshwari, L., Balamurugan, K., et al. (2017). Vanillic acid from *Actinidia deliciosa* impedes virulence in *Serratia marcescens* by affecting S-layer, flagellin and fatty acid biosynthesis proteins. *Sci. Rep.* 7:16328. doi: 10.1038/s41598-017-16507-x

Sethupathy, S., Prasath, K. G., Ananthi, S., Mahalingam, S., Balan, S. Y., and Pandian, S. K. (2016a). Proteomic analysis reveals modulation of iron homeostasis and oxidative stress response in *Pseudomonas aeruginosa* PAO1 by curcumin inhibiting quorum sensing regulated virulence factors and biofilm production. *J. Proteom.* 145, 112–126. doi: 10.1016/j.jprot.2016.04.019

Sethupathy, S., Shanmuganathan, B., Kasi, P. D., and Karutha Pandian, S. (2016b). Alpha-bisabolol from brown macroalga *Padina gymnospora* mitigates biofilm formation and quorum sensing controlled virulence factor production in *Serratia marcescens*. *J. Appl. Phycol.* 28, 1987–1996. doi: 10.1007/s10811-015-0717-z

Shanks, R. M. Q., Stella, N. A., Kalivoda, E. J., Doe, M. R., O'dee, D. M., Lathrop, K. L., et al. (2007). A *Serratia marcescens* OxyR homolog mediates surface attachment and biofilm formation. *J. Bacteriol.* 189, 7262–7272. doi: 10.1128/JB.00859-07

Slater, H., Crow, M., Everson, L., and Salmond, G. P. C. (2003). Phosphate availability regulates biosynthesis of two antibiotics, prodigiosin and carbapenem, in *Serratia via* both quorum-sensing-dependent and -independent pathways. *Mol. Microbiol.* 47, 303–320. doi: 10.1046/j.1365-2958.2003.03295.x

Srinivasan, R., Devi, K. R., Kannappan, A., Pandian, S. K., and Ravi, A. V. (2016). Piper betle and its bioactive metabolite phytol mitigates quorum sensing mediated virulence factors and biofilm of nosocomial pathogen *Serratia marcescens in vitro*. *J. Ethnopharmacol.* 193, 592–603. doi: 10.1016/j.jep.2016.10.017

Stewart, P. S. (2002). Mechanisms of antibiotic resistance in bacterial biofilms. *Int. J. Med. Microbiol.* 292, 107–113. doi: 10.1078/1438-4221-00196

Stewart, P. S., and Costerton, J. W. (2001). Antibiotic resistance of bacteria in biofilms. *Lancet* 358, 135–138. doi: 10.1016/S0140-6736(01)05321-1

Ta, C. A. K., and Arnason, J. T. (2016). Mini review of phytochemicals and plant taxa with activity as microbial biofilm and quorum sensing inhibitors. *Molecules* 21:29. doi: 10.3390/molecules21010029

Tashiro, Y., Toyofuku, M., Nakajima-Kambe, T., Uchiyama, H., and Nomura, N. (2010). Bicyclic compounds repress membrane vesicle production and *Pseudomonas* quinolone signal synthesis in *Pseudomonas aeruginosa*. *FEMS Microbiol. Lett.* 304, 123–130. doi: 10.1111/j.1574-6968.2010.01897.x

Van Houdt, R., Givskov, M., and Michiels, C. W. (2007). Quorum sensing in *Serratia*. *FEMS Microbiol. Rev.* 31, 407–424. doi: 10.1111/j.1574-6976.2007.00071.x

Williamson, N. R., Fineran, P. C., Leeper, F. J., and Salmond, G. P. C. (2006). The biosynthesis and regulation of bacterial prodiginines. *Nat. Rev. Microbiol.* 4, 887–899. doi: 10.1038/nrmicro1531

Yang, C., Yu, Y., Sun, W., and Xia, C. (2014). Indole derivatives inhibited the formation of bacterial biofilm and modulated Ca^{2+} efflux in diatom. *Mar. Pollut. Bull.* 88, 62–69. doi: 10.1016/j.marpolbul.2014.09.027

Yang, H.-F., Cheng, J., Hu, L.-F., Ye, Y., and Li, J.-B. (2012). Plasmid-mediated quinolone resistance in extended-spectrum-β-lactamase- and AmpC β-lactamase-producing *Serratia marcescens* in China. *Antimicrob. Agents Chemother.* 56, 4529–4531. doi: 10.1128/AAC.00493-12

Zarkan, A., Liu, J., Matuszewska, M., Gaimster, H., and Summers, D. K. (2020). Local and universal action: the paradoxes of indole signalling in bacteria. *Trends Microbiol.* 28, 566–577. doi: 10.1016/j.tim.2020.02.007

Zhou, J.-W., Ruan, L.-Y., Chen, H.-J., Luo, H.-Z., Jiang, H., Wang, J.-S., et al. (2019). Inhibition of quorum sensing and virulence in *Serratia marcescens* by Hordenine. *J. Agr. Food Chem.* 67, 784–795. doi: 10.1021/acs.jafc.8b05922

Conflict of Interest: The authors declare that the research was conducted in the absence of any commercial or financial relationships that could be construed as a potential conflict of interest.

frontiers in Microbiology

ORIGINAL RESEARCH
published: 04 November 2020
doi: 10.3389/fmicb.2020.586729

Elevating NagZ Improves Resistance to β-Lactam Antibiotics via Promoting AmpC β-Lactamase in *Enterobacter cloacae*

Xianggui Yang[1]†, Jun Zeng[2]†, Qin Zhou[1]†, Xuejing Yu[3], Yuanxiu Zhong[4], Fuying Wang[3], Hongfei Du[1], Fang Nie[1], Xueli Pang[1], Dan Wang[1], Yingzi Fan[1], Tingting Bai[1] and Ying Xu[1]**

[1] Department of Laboratory Medicine, Clinical Medical College and The First Affiliated Hospital of Chengdu Medical College, Chengdu, China, [2] Division of Pulmonary and Critical Care Medicine, Clinical Medical College and The First Affiliated Hospital of Chengdu Medical College, Chengdu, China, [3] Department of Cardiothoracic Surgery, University of Utah, Salt Lake City, UT, United States, [4] Department of Biotechnology, Chengdu Medical College, Chengdu, China

Enterobacter cloacae complex (ECC), one of the most common opportunistic pathogens causing multiple infections in human, is resistant to β-lactam antibiotics mainly due to its highly expressed chromosomal AmpC β-lactamase. It seems that regulation of chromosomal AmpC β-lactamase is associated with peptidoglycan recycling. However, underlying mechanisms are still poorly understood. In this study, we confirmed that NagZ, a glycoside hydrolase participating in peptidoglycan recycling in Gram-negative bacteria, plays a crucial role in developing resistance of *E. cloacae* (EC) to β-lactam antibiotics by promoting expression of chromosomal AmpC β-lactamase. Our data shows that NagZ was significantly up-regulated in resistant EC (resistant to at least one type of the third or fourth generation cephalosporins) compared to susceptible EC (susceptible to all types of the third and fourth generation cephalosporins). Similarly, the expression and β-lactamase activity of *ampC* were markedly enhanced in resistant EC. Moreover, ectopic expression of *nagZ* enhanced *ampC* expression and resistance to β-lactam antibiotics in susceptible EC. To further understand functions of NagZ in β-lactam resistance, *nagZ*-knockout EC model (Δ*nagZ* EC) was constructed by homologous recombination. Conversely, *ampC* mRNA and protein levels were down-regulated, and resistance to β-lactam antibiotics was attenuated in Δ*nagZ* EC, while specific complementation of *nagZ* was able to rescue *ampC* expression and resistance in Δ*nagZ* EC. More interestingly, NagZ and its hydrolyzates 1,6-anhydromuropeptides (anhMurNAc) could induce the expression of other target genes of AmpR (a global transcriptional factor), which suggested that the promotion of AmpC by NagZ is mediated AmpR activated by anhMurNAc in EC. In conclusion, these findings provide new elements for a better understanding of resistance in EC, which is crucial for the identification of novel potential drug targets.

Keywords: ***nagZ*, β-lactam antibiotics, resistance, AmpC, *Enterobacter cloacae***

OPEN ACCESS

Edited by:
Rodolfo García-Contreras, National Autonomous University of Mexico, Mexico

Reviewed by:
Piotr Majewski, Medical University of Bialystok, Poland
Christophe Isnard, Université de Caen Normandie, France
Caleb Perez, National Autonomous University of Mexico, Mexico

***Correspondence:**
Xianggui Yang
yxg204@163.com
Ying Xu
yingxu@cmc.edu.cn

† These authors have contributed equally to this work and share first authorship

Specialty section:
This article was submitted to Antimicrobials, Resistance and Chemotherapy, a section of the journal Frontiers in Microbiology

Received: *23 July 2020*
Accepted: *02 October 2020*
Published: *04 November 2020*

Citation:
Yang X, Zeng J, Zhou Q, Yu X, Zhong Y, Wang F, Du H, Nie F, Pang X, Wang D, Fan Y, Bai T and Xu Y (2020) Elevating NagZ Improves Resistance to β-Lactam Antibiotics via Promoting AmpC β-Lactamase in Enterobacter cloacae. Front. Microbiol. 11:586729. doi: 10.3389/fmicb.2020.586729

INTRODUCTION

Enterobacter cloacae complex (ECC), including *E. cloacae* (EC), *Enterobacter asburiae*, *Enterobacter hormaechei*, *Enterobacter kobei*, *Enterobacter ludwigii,* and *Enterobacter nimipressuralis* (Guerin et al., 2015), are widely distributed in nature. They are parts of commensal microbiota in human gastrointestinal tract as well. Over past few decades, ECC has emerged as troublesome pathogens for nosocomial infection worldwide, with an infection rate ranging from 5 to 10% in intensive care unit (ICU) (Mezzatesta et al., 2012; Annavajhala et al., 2019). Among ECC species, *E. cloacae* (EC) is the most significant and frequently isolated in clinical practice, accounting for a high proportion of infections, including 5% of hospital-acquired sepsis, 5% of hospital-acquired pneumonia, 4% of hospital-acquired urinary tract infection, and 10% of postoperative peritonitis (Nicolas et al., 1987; da Silva et al., 2018). The clinical significance of EC has been widely reported especially in the recent 15 years since it has a strong ability to acquire antibiotic resistance, making it the most worrisome microorganism in current era of antibiotics (Mezzatesta et al., 2012).

It is well known that EC has an intrinsic ability to be resistant to ampicillin, amoxicillin/clavulanate, the first and second generation cephalosporins due to its low expression of chromosomal *ampC* gene which encodes AmpC β-lactamase under a basal condition (Jacoby, 2009; Ito et al., 2019). AmpC β-lactamase is the first-discovered bacterial β-lactamase to hydrolyze penicillin in *Escherichia coli* in 1940, but it is not named until 1965 (Eriksson-Grennberg et al., 1965; Eriksson-Grennberg, 1968; Abraham and Chain, 1988). The sequence of AmpC β-lactamase is quite different from penicillin-typed β-lactamase (such as TEM-1), but it has a same amino acid of serine at its active site (Pimenta et al., 2014). For classification, AmpC β-lactamase is classified to be class C based on Ambler method, while it is assigned to be group 1 according to Bush functional classification (Silveira et al., 2018; Mack et al., 2019). The chromosomal AmpC β-lactamase is highly inducible in presence of some β-lactams, such as imipenem, cefoxitin, and clavulanate (Jacoby, 2009; Gomez-Simmonds et al., 2018), but it is still not clear about underlying genetic regulation in AmpC β-lactamase associated with peptidoglycan recycling in *E. cloacae* clinical isolates.

NagZ, a cytosolic glucosaminidase involved in peptidoglycan recycling, has an ability to hydrolyze *N*-acetylglucosaminyl-1,6-anhydromuropeptides (peptidoglycan monomers) to be *N*-acetylglucosaminyl (GlcNAc) and 1,6-anhydromuropeptides (anhMurNAc). anhMurNAc acts as an activated ligand for AmpR in *Pseudomonas aeruginosa* (Stubbs et al., 2008; Huang et al., 2015b). It has been reported that inactivation of NagZ can prevent and revert β-lactam resistance in *P. aeruginosa* (Asgarali et al., 2009; Zamorano et al., 2010b; Acebron et al., 2017), *Y. enterocolitica* (Liu et al., 2017), and *Stenotrophomonas maltophilia* (Huang et al., 2012, 2015a). In addition, NagZ has a moonlighting activity to modulate biofilm accumulation in *Neisseria gonorrhoeae* (Bhoopalan et al., 2016). Despite those promising findings, precise regulation of NagZ to resistance remains largely unknown in EC.

The aims of this study were to determine roles of NagZ in EC resistance development and in chromosomal AmpC β-lactamase regulation. Our study showed that NagZ was overexpressed in resistant EC (resistant to at least one type of the third or fourth generation cephalosporins) compared with susceptible EC (susceptible to all types of the third and fourth generation cephalosporins), complementation of NagZ enhanced EC resistance by up-regulating expression of AmpC. Moreover, NagZ hydrolyzates 1,6-anhydromuropeptides (anhMurNAc) induce the expression of target genes of AmpR. Our findings demonstrated NagZ plays an indispensable role in developing resistance in EC and provided a novel insight into understanding of molecular mechanisms of resistance to β-lactam antibiotics.

MATERIALS AND METHODS

Bacterial Strains, Plasmids, Primers

Detailed information of bacterial strains (**Supplementary Table 2**), plasmids (**Supplementary Table 3**), and primers (**Supplementary Table 4**) used in this study are listed in **Supplementary Material**.

Ethics Approval and Consent to Participate

The microorganism research and animal subject research (for preparation of anti-NagZ antibody) were approved by the Ethics Committee of the Clinical Medical College and the First Affiliated Hospital of Chengdu Medical College. After clearly explaining the nature and purposes of this scientific research to all participants, sufficient time was provided for questions and answers, written consents were acquired from all participants.

Antibiotic Susceptibility Test

Antibiotic susceptibility test was performed by using broth microdilution and Kirby-Bauer method according to protocols recommended by Clinical Laboratory Standard Institute (CLSI, 2018). *E. cloacae* subsp. *cloacae* ATCC 13047 and *E. coli* ATCC 25922 were used for quality control. All antibiotics and culture medium used in antibiotic susceptibility test were purchased from Wenzhou Kangtai company (Bio-kont Co., Ltd., Wenzhou, China). Each assay was performed independently at least three times.

Generation of Anti-NagZ Antibody

Anti-NagZ antibody was generated through rabbit immunization by an "antigen intersection" strategy immunization and purification (Arora et al., 2014; Zhou et al., 2016). Briefly, *nagZ* coding sequence (CDS) from EC was obtained by polymerase chain reaction (PCR), cloned into a pET28a vector with a 6His-label. Then, pET28a-*nagZ*-6His vector was transformed into *E. coli B21* for expression of NagZ recombinant protein, which was purified by Ni-NAT and identified by electrophoresis. Next, purified NagZ-6His recombinant protein was used to immunize rabbit. Enzyme linked immunosorbent assay (ELISA)

was applied to evaluate titer of antiserum (over 1:8000) after immunization of NagZ-6His. Finally, antiserum was purified by affinity of antibody to NagZ-6His-coupled antigen. Western blot showed an excellent specificity of the antibody (**Supplementary Figure 1**). Reagents and materials used in generation of anti-NagZ antibody were purchased Shenggong Biological Company (Sangon Biotech Co., Ltd., Shanghai, China), primers for obtaining *nagZ* CDS are listed in **Supplementary Table 4**.

AmpC β-Lactamase Activity Assay

AmpC β-lactamase activity was determined by a nitrocefin hydrolysis assay as previously described (Cavallari et al., 2013; Guerin et al., 2015). EC isolates were inoculated into LB medium and incubated at 37°C with 250 rpm overnight. It was sub-cultured in LB medium with a concentration of 1:100. When absorbance of OD600 reached 0.8, bacteria were collected and washed once with 1 ml of phosphate buffer (pH 7.0), and resuspended in 1 ml of protein lysate (Sangon Biotech Co., Ltd., Shanghai, China). Samples were placed on ice and lysed by sonication with a microprobe by using a 10-s pulse three times with a 10-s interval during each pulse. The samples were centrifuged at 10,000*g* for 10 min and supernatant was collected. The concentration of protein in supernatant was determined by a protein quantitative kit (Beyotime, Biotechnology, Shanghai, China). The nitrocefin hydrolysis assay was performed in 250 μl of phosphate buffer (pH 7.0) containing 5 μg of total protein and 50 μg/ml nitrocefin (Sigma-Aldrich; Merck KGaA, St. Louis, MO, United States). The hydrolysis rate of nitrocefin was determined at 486 nm at room temperature every 5 min. AmpC β-lactamase activity was calculated by extinction coefficient of nitrocefin 20, 500 M^{-1} cm^{-1}, each assay was performed independently at least three times.

RNA Extraction

The total RNA was extracted from cellular lysates by using RNA extraction kit (Sangon Biotech Co., Ltd., Shanghai, China) according to the manufacturer's instructions. Briefly, genus (EC isolates) were inoculated into LB medium and incubated at 37°C with 250 rpm overnight. It was sub-cultured in LB medium with a concentration of 1:100. When absorbance of OD600 reached 0.8, bacteria were collected by centrifuge at 12,000*g* for 2 min and the supernatant was discarded, the precipitate was washed once with 1 ml of phosphate buffer (pH 7.0), bacterial pellet was resuspended in 100 μl of TE buffer containing 400 μg/ml lysozyme, and incubated for 5 min at room temperature. Next, 900 μl of lysis solution was added and mixed at room temperature for 3 min, 200 μl of chloroform (Sangon Biotech Co., Ltd., Shanghai, China) was added, mixed, and centrifuged at 12,000*g* at 4°C for 5 min. Consequently, 600 μl of supernatant (aqueous liquid) was acquired and 200 μl anhydrous ethanol was added, the mixture was incubated at room temperature for 3 min, centrifuged at 12,000*g* at 4°C for 5 min. The supernatant was discarded, and precipitate was washed with 70% ethanol twice, dried naturally, dissolved in ddH_2O, the concentration of RNA was determined by NanoDrop^{TM}8000 spectro-photometer (Thermo Fisher Scientific, Waltham, MA, United States) and stored at −70°C. For detecting the expression of AmpR target genes, LB medium containing 5 mg/L 1,6-anhydromuropeptides (anhMurNAc, Medicilon, Co., Ltd., Shanghai, China) was used at the stage of sub-culture.

RT-qPCR Assays

cDNA was synthesized from 500 ng of total RNA with a FastKing gDNA Dispelling RT SuperMix kit (Tiangen Biotech Co., Ltd., Beijing, China) according to the manufacturer's instructions. Real-time fluorescence quantitative PCR (qPCR) was performed with a SuperReal PreMix Color (SYBR Green) kit (Tiangen Biotech Co., Ltd., Beijing, China) according to the manufacturer's instructions (volume: 20 μL. PCR program: pre-denaturation: 95°C/10 min. Denaturation: 95°C/30 s, Annealing:58°C/30 s, Elongation:72°C/30 s, and 30 cycles), with 16S as an internal control. Sequences of primers used in RT-qPCR assays are listed in the **Supplementary Table 4**. Each assay was performed independently at least three times.

Protein Extraction and Western Blot Analysis

Total protein was extracted from EC by a bacterial protein extraction kit (Sangon Biotech Co., Ltd., Shanghai, China) according to the manufacturer's instructions. Briefly, strains were inoculated into LB medium and incubated at 37°C with 250 rpm overnight. It was sub-cultured in LB medium with a dilution concentration of 1:100 and continue incubated at 37°C with 250 rpm. When absorbance of OD600 reached 0.8, bacteria were collected by centrifuge at 12,000*g* for 2 min and the supernatant was discarded, the precipitate was washed once with 1 ml of phosphate buffer (pH 7.0), bacterial pellet was resuspended 1 ml of protein lysate (Sangon Biotech Co., Ltd., Shanghai, China). Samples were placed on ice and lysed by sonication with a microprobe by using a 10-s pulse three times with a 10-s interval during each pulse. The samples were centrifuged at 10,000*g* for 10 min and supernatant was collected. The concentration of protein in supernatant was determined by a protein quantitative kit (Beyotime, Biotechnology, Shanghai, China), and 30 μg total protein was used to western blot assay. Western blot analysis was performed with a standard method as previously described (Yang et al., 2017). Information of antibodies used are as followings: rabbit anti-AmpC (Abnova Taipei, Taiwan, China), mouse anti-DnaK (Abcam, Cambridge, MA, United States), rabbit anti-NagZ (preparation by ourselves), goat anti-rabbit IgG-HRP (Santa Cruz Biotechnology, Inc., Santa Cruz, CA, United States), goat anti-mouse IgG-HRP (Santa Cruz Biotechnology, Inc., Santa Cruz, CA, United States). Images were taken with a SPOT-CCD camera. For quantitative analysis of western blot, intensities of protein bands were quantified by application of ImageJ, and DnaK was applied as an internal control. Each assay was performed independently at least three times.

Construction of *nagZ*-Knockout EC Model

nagZ-knockout EC was obtained by homologous recombination method with application of a suicide vector (Luo et al., 2015).

Briefly, two homologous arms of DNA fragments (A: 522 bp-upstream fragment of initiator codon, and B: 544 bp-downstream fragment of termination codon) of *nagZ* gene were obtained by PCR. The fusion DNA fragment (AB fragment: 1066 bp) was obtained by the fusion PCR. The fused DNA fragment of AB was cloned into the suicide plasmid pLP12 and verified by PCR and sequencing. The recombinant plasmid was transformed into *E. coli*β2163. Finally, *nagZ*-knockout *EC* strain was obtained by co-culture *E. coli*β2163 with DNA fragment AB and wild-type *E, cloacae*. The strains and reagents used in this experiment were purchased from Nuojing Biological Company (Knogen Biotech Co., Ltd., Guangzhou, China).

Preparation of EC Models of NagZ Complementation

The CDS of *nagZ* was obtained by PCR, then cloned into a plasmid of pBAD33cm-rp4 (Knogen Biotech Co., Ltd., Guangzhou, China), and verified by sequencing. The recombinant plasmid (pBAD33-*nagZ*) was transformed into competent *E. coli*β2163 (Knogen Biotech Co., Ltd., Guangzhou, China). Finally, the recombinant plasmid from *E. coli* β2163 was transformed into *E. cloacae* by a conjugation assay, 0.05% L-Arabinose (Sangon Biotech Co., Ltd., Shanghai, China) was used to induce gene expressions of the recombinant plasmids. For antibiotic susceptibility test, L-Arabinose was added at the initial stage of antibiotic susceptibility test. For western blot, RNA Extraction and AmpC β-lactamase Activity Assay, L-Arabinose was added at the stage of sub-culture. Primers for obtaining CDS of *nagZ* are listed in the **Supplementary Table 4**.

Statistical Analysis

All data were presented as mean ± standard deviation. Two-tailed *t*-test was used to determine the significant difference between two groups by GraphPad Prism 5. $^{*}P < 0.05$ and $^{**}P < 0.01$ were applied to be statistically significant and statistically highly significant, respectively. All experiments were performed independently at least three times.

RESULTS

Enhanced NagZ and AmpC Expression in the Resistant EC Clinical Isolates

To clarify mechanism of developing resistance in EC, 12 clinically isolated EC were randomly collected. Minimum inhibitory concentrations (MICs) of piperacillin (PIP), piperacillin-tazobactam (TZP), aztreonam (ATM), ceftriaxone (CRO), cefotaxime (CTX), cefoperazone (CFP), ceftazidime (CAZ), cefepime (FEP), imipenem (IMP), meropenem (MEM), levofloxacin (LVX), ciprofloxacin (CIP), amikacin (AMK) and gentamicin (GEN) against the 12 clinically isolated EC were determined according to protocols recommended by Clinical Laboratory Standard Institute (**Supplementary Table 1**; CLSI, 2018). Based on the MICs, 12 clinical isolates were divided into two groups (six susceptible and six resistant isolates, abbreviated as S1, S2, S3, S4, S5, S6, and R1, R2, R3, R4, R5, R6, respectively. Susceptible isolate: susceptible to all types of the third and fourth generation cephalosporins; resistant isolate: resistant to at least one type of the third or fourth generation cephalosporins). To determine whether NagZ was involved in developing resistance in EC, *nagZ* mRNA expression was examined by reverse transcription-quantitative polymerase chain reaction (RT-qPCR), as indicated in **Figure 1A**. *nagZ* mRNA expression was significantly enhanced in the resistant isolates compared with susceptible ones. To further detect the different protein expressions of *nagZ* between susceptible and resistant strains, we prepared anti-NagZ antibody for the first time, and its specificity was verified by *nagZ*-knockout EC model (**Supplementary Figure 1**). *nagZ* protein expressions were detected by western blot in six resistant and six susceptible strains, as indicated in **Figures 1B,C**, protein expressions of *nagZ* were dramatically up-regulated in six resistant EC isolates compared to susceptible ones.

NagZ is a cytosolic glucosaminidase and acts a crucial role in peptidoglycan recycling pathway, some publications reported there also exists a correlation between peptidoglycan recycling and *ampC* expression in *P. aeruginosa* (Reith and Mayer, 2011; Mayer, 2019). Therefore, mRNA expression level of *ampC* in 12 clinically isolated EC was determined by RT-qPCR (**Figure 1D**), the results indicated *ampC* mRNA expression was up-regulated in the resistant EC compared to the susceptible ones. Furthermore, protein expressions of *ampC* were enhanced in resistant EC isolates, which is shown in **Figures 1E,F**. Additionally, to investigate whether a highly expressed AmpC β-lactamase was associated with a higher β-lactamase activity, nitrocefin hydrolysis assay was used to determine the β-lactamase activity of AmpC. Our results confirmed that increasing protein level of AmpC had an excellent ability to hydrolyze nitrocefin (**Figure 1G**). All these data confirmed that expression of NagZ and β-lactamase activity of AmpC were enhanced in resistant EC isolates.

NagZ Enhances Resistance to β-Lactam Antibiotics and Promotes AmpC Expression in Susceptible EC Isolates

As indicated in **Figure 1**, our results demonstrated that *nagZ* expression was up-regulated in resistant EC isolates. It was further determined whether increased NagZ was significantly functional in developing resistance in EC. *nagZ* CDS was cloned into the pBAD33cm-rp4 vector (pBAD33-*nagZ*), and then pBAD33-*nagZ* (NagZ complementation vector) and a pBAD33cm-rp4 vector (pBAD33, control vector) were transformed into S1 and S2, respectively. RT-qPCR and western blot were used to detect whether pBAD33-*nagZ* vector was effective (**Figures 2A,B**), the results indicated that mRNA and protein expressions of *nagZ* were significantly increased complemented with the pBAD33-*nagZ* vector compared with pBAD33 vector. To further identify the role of NagZ in developing resistance, inhibition zones and MICs of PIP, TZP, ATM, CRO, cefoperazone-sulbactam (SCF), CAZ against S1 and S2 complemented with or without pBAD33-*nagZ* vector were determined by Kirby-Bauer method

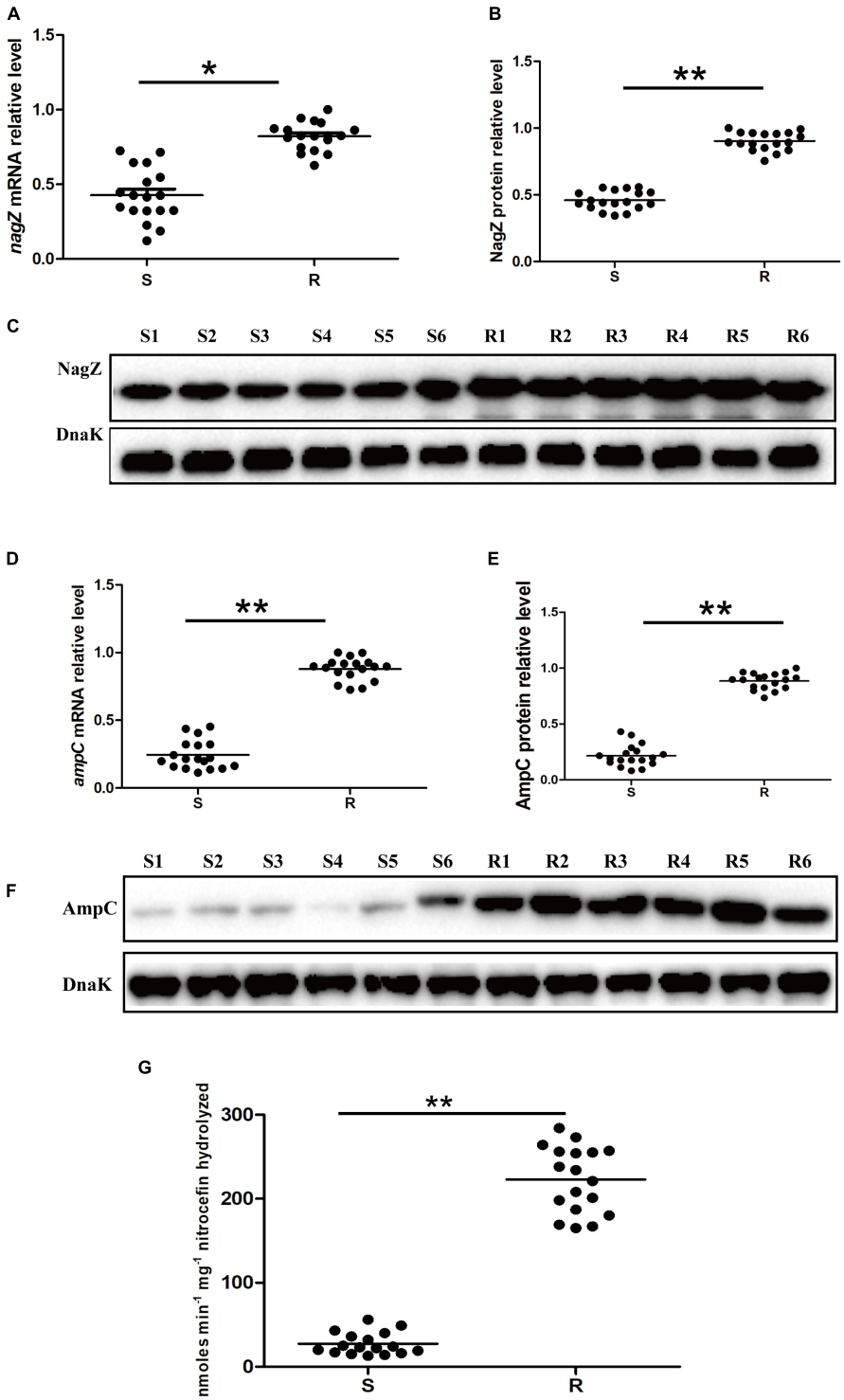

FIGURE 1 | The expression levels of *nagZ* and *ampC* in *Enterobacter cloacae* (EC) isolated from clinical samples. **(A)** Quantification by reverse transcription-quantitative polymerase chain reaction (RT-qPCR) analysis of *nagZ* in susceptible and resistant EC isolates. **(B)** Quantitative analysis of the results of western blot **(C)**, DnaK was used as an internal control. **(C)** Western blot analysis of *nagZ* protein expression in the susceptible and resistant EC. **(D)** RT-qPCR analysis of *ampC* at mRNA level in susceptible and resistant EC strains. **(E)** Quantitative analysis of the results of western blot **(F)**, DnaK was used as an internal control. **(F)** Western blot analysis of *ampC* at protein level in susceptible and resistant isolates of EC. **(G)** AmpC β-lactamase activity (measured in nanomoles per minute per milligram nitrocefin hydrolyzed) were measured by nitrocefin hydrolysis assay. S, susceptible EC isolated from the clinical sample; R, resistant EC isolated from the clinical sample; S1, susceptible *EC* isolates number 1; R1, resistant *EC* isolates number 1, and so on. $^{*}P < 0.05$ and $^{**}P < 0.01$ indicate statistically significant and statistically highly significant, respectively.

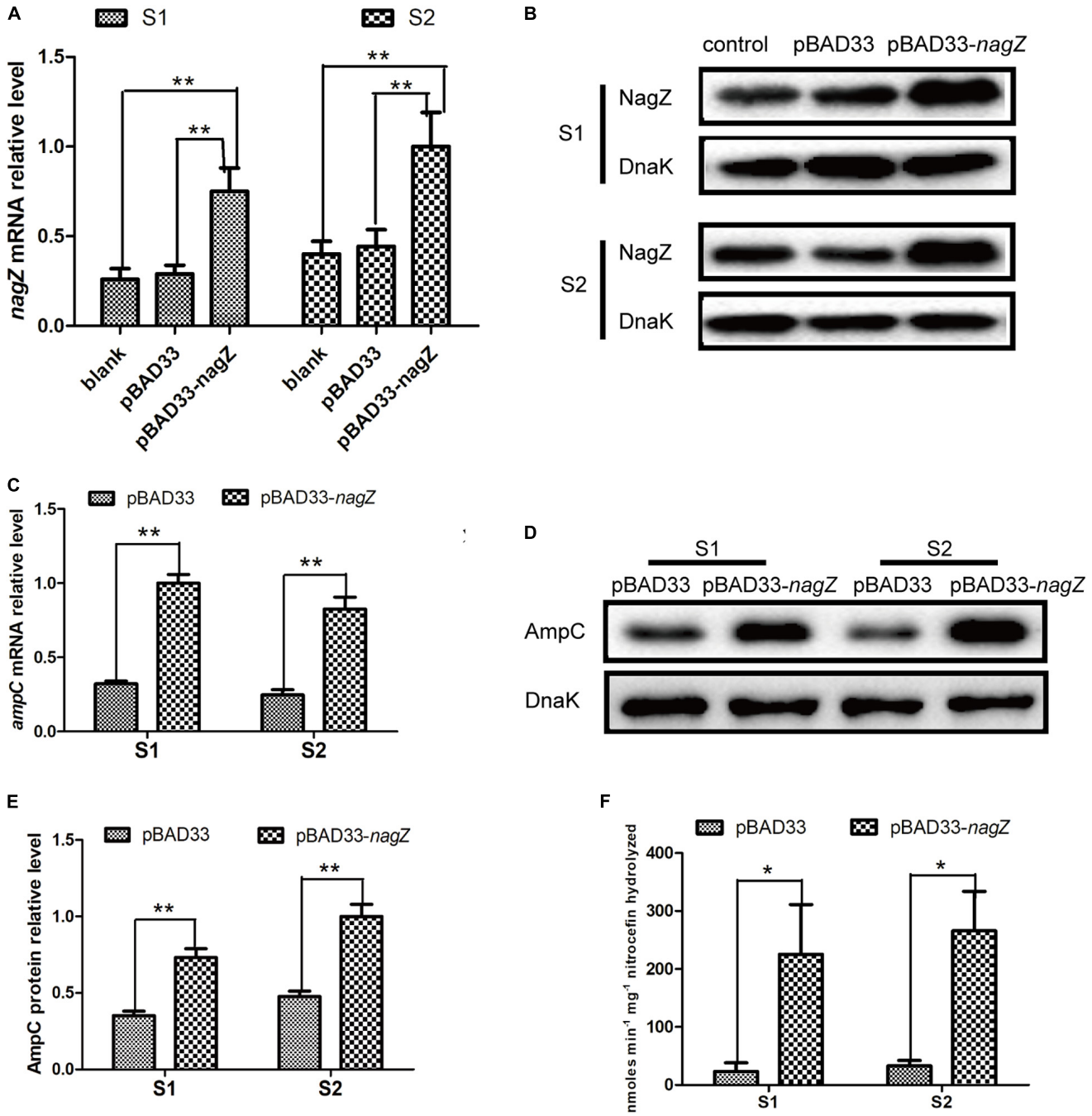

FIGURE 2 | The effects of NagZ on expression of *ampC* in susceptible EC isolates. RT-qPCR **(A)** and western blot **(B)** confirmed that NagZ complementation vector (pBAD33-*nagZ*) was successful constructed. **(C)** Effects of NagZ complementation on mRNA expression of *ampC* in S1 and S2 isolates. **(D)** Western blot indicated effects of NagZ on AmpC β-lactamase in S1 and S2 isolates. **(E)** Quantitative analysis of western blot **(D)**, DnaK was used as an internal control. **(F)** Nitrocefin hydrolysis assay was used to evaluate role of NagZ in AmpC β-lactamase activity. pBAD33-*nagZ* and pBAD33 were used as the experiment group and control, respectively. $^{*}P < 0.05$ and $^{**}P < 0.01$ indicate statistically significant and statistically highly significant, respectively.

and broth microdilution according to Clinical Laboratory Standard Institute guideline (CLSI, 2018). As shown in **Supplementary Figure 2A**, inhibition zones of S1 and S2 complemented with pBAD33-*nagZ* were severely reduced compared with pBAD33. Furthermore, MICs of PIP, TZP, ATM, CRO, SCF, and CAZ were significantly increased in the EC complemented with pBAD33-*nagZ* compared to EC complemented with pBAD33 (**Table 1**). These results indicated

TABLE 1 | The effect of NagZ on resistance in EC.

Strain	MICs (μg/ml)					
	TZP	ATM	PIP	CRO	CAZ	SCF
S1+pBAD33	2	1	2	0.125	0.25	0.5
S1+pBAD33-*nagZ*	8	128	16	128	256	8
S2+pBAD33	2	4	4	0.5	0.125	0.5
S2+pBAD33-*nagZ*	32	>512	64	256	512	2
S3+pBAD33	2	2	8	0.25	1	0.5
S3+pBAD33-*nagZ*	16	128	128	64	256	4
S4+pBAD33	4	1	8	0.5	0.5	0.5
S4+pBAD33-*nagZ*	32	64	64	64	256	8
S5+pBAD33	1	0.5	1	0.5	2	1
S5+pBAD33-*nagZ*	32	64	32	32	512	8
S6+pBAD33	0.25	1	0.5	1	0.25	1
S6+pBAD33-*nagZ*	16	256	32	128	64	8
R1	2	64	2	128	128	4
R-Δ*nagZ*	0.5	0.125	0.5	0.125	0.25	0.25
R1-Δ*nagZ*+pBAD33	0.5	0.125	0.5	0.25	0.5	0.25
R1-Δ*nagZ*+pBAD33-*nagZ*	8	64	8	64	64	8

EC, Enterobacter cloacae; MIC, minimum inhibitory concentration; PIP, piperacillin; TZP, piperacillin-tazobactam; ATM, aztreonam; CRO, ceftriaxone; CAZ, ceftazidime; SCF, cefoperazone-sulbactam; S, susceptible EC isolated from the clinical sample; S1, susceptible EC isolates number 1, and so on; R1, resistant Enterobacter cloacae clinical isolates number 1; R1-ΔnagZ, nagZ knockout R1; pBAD33, control vector; pBAD33-nagZ, NagZ complementation vector; R1-ΔnagZ+pBAD33, R1-ΔnagZ complemented with pBAD33; R1-ΔnagZ+pBAD33-nagZ, R1-ΔnagZ complemented with pBAD33-nagZ.

that increased expression of NagZ enhanced resistance of EC to β-lactam antibiotics.

Next, we aimed to investigate whether expression of *ampC* is regulated by NagZ in EC isolates. pBAD33-*nagZ* and pBAD33 were transformed into S1 and S2, respectively. RT-qPCR and western blot were adopted to detect the effect of NagZ on AmpC expression. It is shown in **Figures 2C–E**, NagZ promoted mRNA (**Figure 2C**) and protein (**Figures 2D,E**) expressions of *ampC*. Nitrocefin hydrolysis assay was used to determine the β-lactamase activity of AmpC, results showed that AmpC hydrolysis activity was significantly improved in EC complemented with pBAD33-*nagZ* compared with pBAD33 (**Figure 2F**). Therefore, NagZ enhanced AmpC expression and increased AmpC β-lactamase activity in susceptible EC isolates.

Knockout of *nagZ* Attenuated *ampC* Expression and Resistance to β-Lactam Antibiotics in EC Isolate

To investigate the regulating role of NagZ in resistance and AmpC β-lactamase expression, we constructed a R1 *nagZ*-knockout model (R1-Δ*nagZ*) by homologous recombination. RT-qPCR (**Figure 3A**) and western blot (**Figure 3B**) confirmed that *nagZ* gene was successfully knocked out in clinical isolate of R1. Firstly, mRNA and protein levels of AmpC were detected by RT-qPCR and western blot, which suggested loss of NagZ reduced expression of *ampC* (**Figures 3C–E**). Secondly, nitrocefin hydrolysis assay indicated that β-lactamase activity of R1-Δ*nagZ* was significantly decreased compared with wild-type R1 (**Figure 3F**). Finally, the effect of NagZ on resistance of R1 was evaluated by broth microdilution and Kirby-Bauer method. The results suggested deletion of NagZ increased inhibition zones of CRO, CAZ, ATM, SCF, PIP, and TZP in R1 (**Supplementary Figure 2B**), while MICs of CRO, CAZ, ATM, SCF, PIP, and TZP against R1-Δ*nagZ* were at least fourfold lower than wild-type R1 (**Table 1**).

To further explore whether complementation of NagZ could rescue *ampC* expression and resistance in R1-Δ*nagZ* model, pBAD33 and pBAD33-*nagZ* were transformed into R1-Δ*nagZ* strain, respectively. RT-qPCR analyses confirmed that mRNA level of *ampC* was significantly increased by complementation of NagZ (**Figure 3C**). Moreover, the protein expression of *ampC* was rescued by NagZ complementation (**Figures 3D,E**). Furthermore, decreased β- lactamase activity induced by deletion of *nagZ* was rescued by complementation of NagZ (**Figure 3F**). In addition, inhibition zones and MICs of CRO, CAZ, ATM, SCF, PIP, and TZP against R1-Δ*nagZ* complemented with pBAD33 or pBAD33-*nagZ* vector were measured, and the results showed that increased inhibition zones induced by knockout of *nagZ* were reversed by complementation of NagZ (**Supplementary Figure 2C**). Consistently, knockout of *nagZ* significantly reduced MICs, which was rescued by complementation of NagZ as well (**Table 1**). In summary, NagZ promoted expression of *ampC* and β-lactamase activity, and enhanced resistance in strain of R1-Δ*nagZ*.

NagZ Activates AmpR Through anhMurNAc

In *P. aeruginosa,* overproduction of the chromosomally encoded AmpC β-lactamase is the major mechanism of β-lactam resistance (Lodge et al., 1990; Kong et al., 2005). During normal physiological growth, *N*-acetylglucosaminyl-1,6-anhydromuropeptides (GlcNAc-1,6-anhydroMurNAc) are been transport into the cytoplasm by permease AmpG (Park and Uehara, 2008), where the glucosaminidase NagZ removes the GlcNAc moiety and form 1,6-anhydromuropeptides (anhMurNAc) (Park and Uehara, 2008; Ho et al., 2018). It has been proposed that anhMurNAc induces a conformational change of AmpR and maintains AmpR in an active conformation that promote the expression of *ampC* in *P. aeruginosa* (Caille et al., 2014), AmpR is a global transcriptional factor that regulates expression of hundreds of genes (such as *rsmA*, *oxyR*, *rpoS*, *grpE*, and *phoP*) (Kong et al., 2005; Caille et al., 2014). To explore the detail mechanism of NagZ promoting AmpC expression in *E. cloacae*, NagZ and AmpR Sequence homology were analyzed between *P. aeruginosa* and *E. cloacae*, the results revealed that *E. cloacae* NagZ (66.9%) and AmpR (100%) bears a high degree of homology to its counterpart *P. aeruginosa* (**Figures 4A,B**). A high degree of homology is also seen in the upstream region (transcriptional factor binding zone) of *ampC* between *P. aeruginosa* and *E. cloacae* (**Figure 4C**). Here, to further verify whether the regulation of NagZ on AmpC is mediated by the activation of AmpR by anhMurNAc, we examined the effect of NagZ on the expression of target genes of AmpR. The results indicate that NagZ can promote the expression of AmpR target genes such as *rsmA*, *oxyR*, *rpoS*,

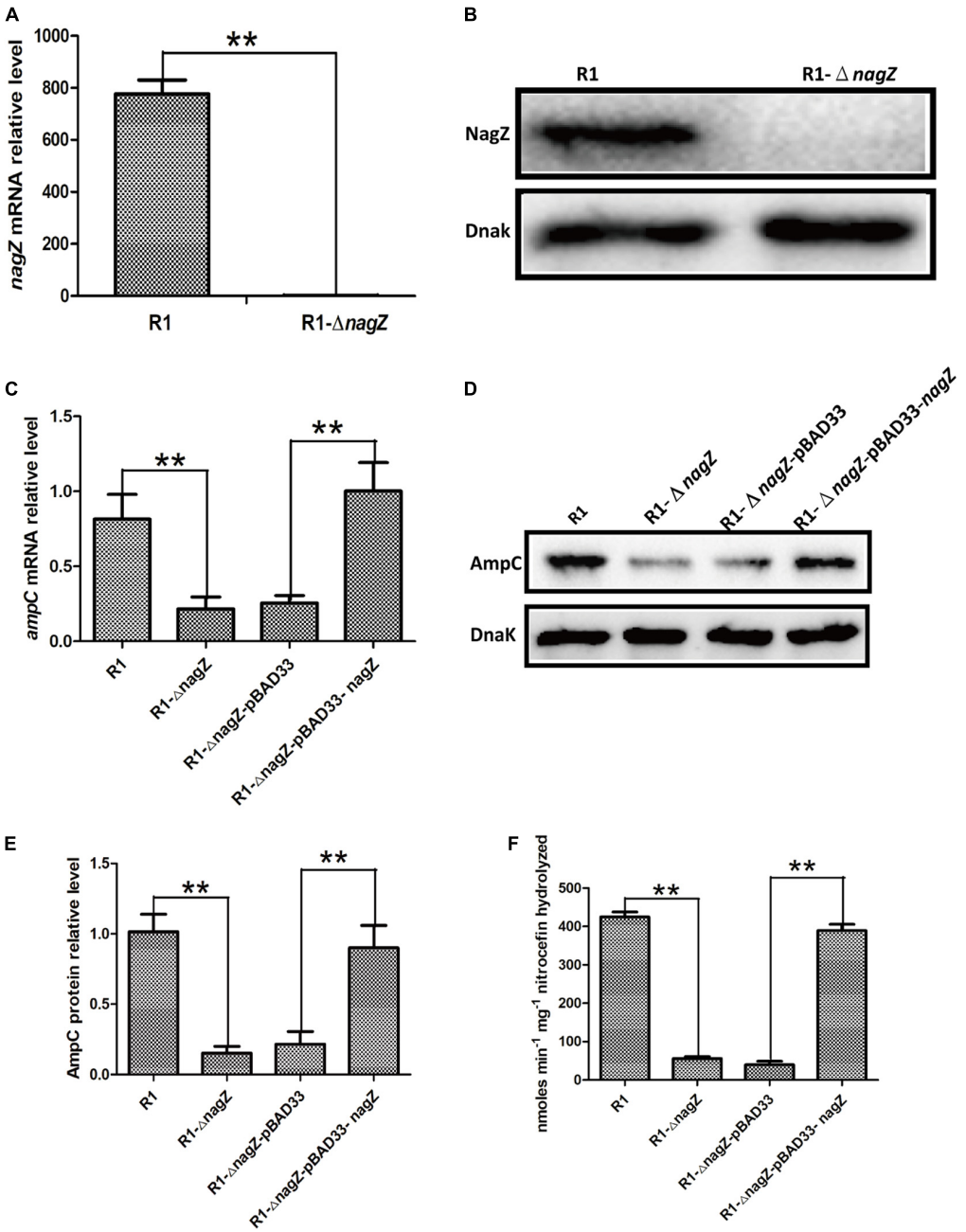

FIGURE 3 | The effects of *nagZ* knockout and complementation on *ampC* expression. RT-qPCR **(A)** and western blot **(B)** confirmed that R1 *nagZ*-knockout model (R1-Δ*nagZ*) was successful prepared. **(C)** mRNA expressions of *ampC* were detected by RT-qPCR in strains of R1, R1-Δ*nagZ*, R1-Δ*nagZ*-pBAD33 (complemented with pBAD33 vector), and R1-Δ*nagZ*-pBAD33-*nagZ* (complemented with NagZ complementation vector). **(D)** Western blot was used to determine *ampC* protein expressions in R1, R1-Δ*nagZ*, R1-Δ*nagZ*-pBAD33, and R1-Δ*nagZ*-pBAD33-*nagZ*. **(E)** Quantitative analysis of the results of western blot **(D)**, DnaK was used as an internal control. **(F)** AmpC β-lactamase activity was analyzed by nitrocefin hydrolysis assay in R1, R1-Δ*nagZ*, R1-Δ*nagZ*-pBAD33, and R1-Δ*nagZ*-pBAD33-*nagZ*. $^{**}P < 0.01$ indicate statistically highly significant.

grpE, *phoP*, etc. (**Figure 5**). To further verify that the activation of AmpR is initiated by the NagZ hydrolyzate anhMurNAc, the effect of anhMurNAc on expression of AmpR target genes were examined. The results showed, consistent with NagZ, anhMurNAc could enhance the expression of *rsmA*, *oxyR*, *rpoS*, *grpE*, and *phoP* genes (**Figure 5**).

DISCUSSION

Enterobacter cloacae is ubiquitous in nature, existing in both terrestrial and aquatic environments. It is a well-known nosocomial pathogen that can cause multiple infections, such as lower respiratory tract infection, bacteremia, endocarditis,

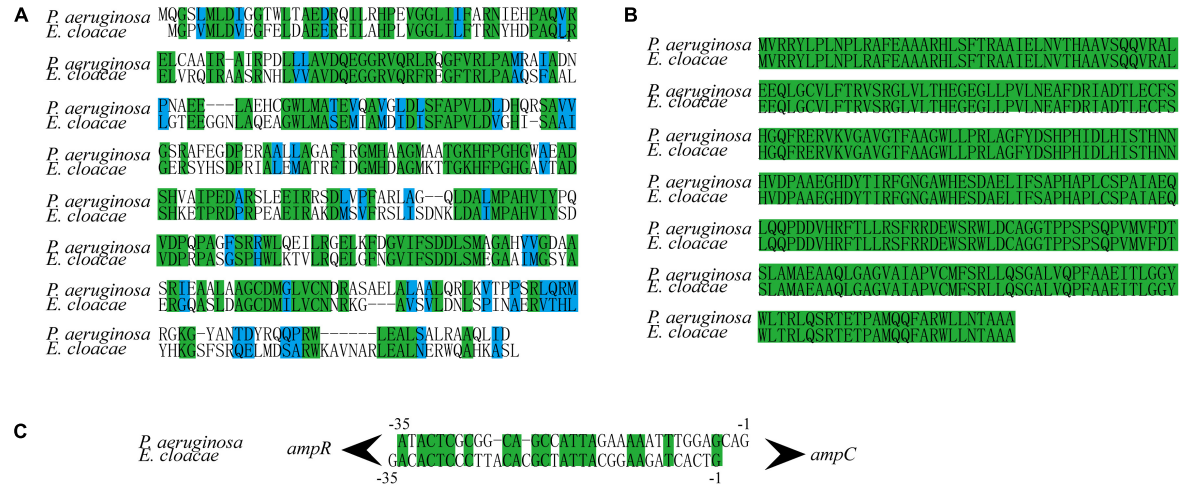

FIGURE 4 | NagZ and AmpR sequence homology analysis between *Pseudomonas aeruginosa* and *Enterobacter cloacae*. **(A)** NagZ amino acid sequence alignment. **(B)** AmpR amino acid sequence alignment. **(C)** Upstream nucleotide sequence alignment of AmpC (about –35 bp). The identical sequences are marked by green, and those in blue belong to the same class of amino acids in terms of structure or function.

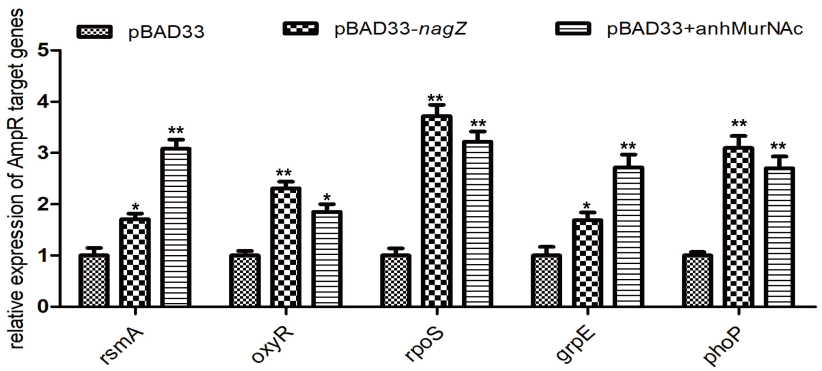

FIGURE 5 | Effects of NagZ and anhMurNAc on expressions of AmpR target genes. *rsmA*, *oxyR*, *rpoS*, *grpE*, and *phoP* are target genes of AmpR. pBAD33, control vector; pBAD33-*nagZ*, NagZ complementation vector; anhMurNAc, the hydrolyzate of NagZ. $^{*}P < 0.05$ and $^{**}P < 0.01$ indicate statistically significant and statistically highly significant, respectively.

osteomyelitis, and etc. (Mezzatesta et al., 2012; Guerin et al., 2015). EC has an inherent resistance to ampicillin, amoxicillin, the first and second generation cephalosporins, and cefoxitin due to production of chromosomal AmpC β-lactamase (Pechere, 1991; Ito et al., 2018). Current literatures indicate overexpression of *ampC*, destruction of membrane permeability, and acquisition of plasmid-encoded carbapenemase genes are main mechanisms of carbapenem-resistant strain of EC (Cao et al., 2017; Rees et al., 2018; Wu et al., 2018). Despite those prominent studies, specific molecular mechanisms of chromosome-encoded AmpC β-lactamase in EC remain largely unknown. Our study provided three novel findings implicating NagZ could enhance the resistance of EC to β-lactam antibiotics. Firstly, there existed a strong positive correlation between the expression of *nagZ* and the resistance to β-lactam antibiotics, the expression of *nagZ* was increased in resistant EC isolates, and ectopic expression of *nagZ* enhanced resistance to β-lactam antibiotics in susceptible EC. Secondly, expression of NagZ is positively correlated with expression of AmpC, in resistant EC isolates, *nagZ* and *ampC* expression levels were significantly elevated, and AmpC β-lactamase activity was remarkably enhanced, specific complementation of NagZ could promote expression of *ampC* and enhance resistance of EC to β-lactam antibiotics. Our third novel finding is that NagZ hydrolyzate anhMurNAc promote the expression of target genes of AmpR, which indicates that NagZ regulates the expression of AmpC through the activation of AmpR by anhMurNAc.

Cell-wall remodeling, known as peptidoglycan recycling, is tightly regulated to guarantee bacterial survival (Gisin et al., 2013; Borisova et al., 2016). Cell-wall fragments produced during remodeling are recycled and act as signaling messengers for bacterial communication (Reith and Mayer, 2011). Emerging evidence indicates that peptidoglycan recycling pathway is strongly associated with the development of resistance, especially to β-lactams (Borisova et al., 2016; Gil-Marques et al., 2018; Torrens et al., 2019). Several enzymes or metabolites produced in

peptidoglycan recycling can regulate expressions of antibiotics-resistant genes (Gomez-Simmonds et al., 2018). GlcNAc-1,6-anhydromuropeptide, a product generated during degradation of peptidoglycan, is transported into cytoplasm through AmpG (a transmembrane protein with a permease activity that transports meuropeptide from periplasm to cytoplasm) and then is hydrolyzed to form 1,6-anhydromuropeptides, which promotes the expression of β-lactamase in *P. aeruginosa* (Zamorano et al., 2010a; Yang et al., 2014; Huang et al., 2015a). Besides, stem peptides of GlcNAc-1,6-anhydromuropeptide and 1,6-anhydromuropeptides can be removed by AmpD (N-acetylmuramyl-L-alanine amidase) and eventually recycled to yield UDP-MurNAc pentapeptide, which inhibits β-lactamase expression (Juan et al., 2006; Balasubramanian et al., 2015; Liu et al., 2016). Moreover, penicillin-binding proteins (PBPs) play a vital role in regulation of β-lactamase (Pfeifle et al., 2000). In *P. aeruginosa*, PBP4, PBP5, and PBP7 are involved in AmpC β-lactamase regulation, and PBP4 is the main inhibitor of expression of AmpC β-lactamase (Moya et al., 2009; Ropy et al., 2015).

In this study, we proved that resistance to β-lactam in clinically isolated EC was closely relevant to the expression of *nagZ*. NagZ, encoded by gene *nagZ*, is a glucosaminidase present in Gram-negative bacteria, and acts a critical role in peptidoglycan recycling pathway by removing N-acetyl-glucosamine (GlcNAc) from degraded peptidoglycan. Here, we found that *nagZ* expression was increased at RNA and protein levels in clinically isolated resistant EC compared to susceptible ones. To test whether resistance of EC was caused by increasing expression of NagZ, NagZ complementation vector was constructed and transformed into susceptible EC. Our results indicated that complementation and knockout of *nagZ* could increase and decrease resistance to β-lactams in EC, respectively. These findings highlighted that NagZ plays a dispensable role in developing resistance of EC.

Another novel finding in this study was that expression of NagZ was discovered to be positively correlated with expression of AmpC and the activity of β-lactamase, in the resistant strains of EC, *nagZ* and *ampC* expression levels were significantly elevated, and AmpC β-lactamase activity was enhanced.

ampC is usually found in the chromosomes of *Enterobacteriaceae* (such as *Enterobacteria*) and non-fermenting bacteria (such as *P. aeruginosa*) (Jacoby, 2009). Overexpression of *ampC* makes bacteria resistant to penicillin, cephalosporins, monobactams, and carbapenems (especially with deficiency of membrane porin) (Quale et al., 2006; Majewski et al., 2016). In *P. aeruginosa*, overexpression of chromosomal AmpC β-lactamase is the major mechanism related with cephalosporin resistance, and occurs during exposure to β-lactam antibiotics which leads to inactivation of *ampD* and *dacB* (gene regulating *ampC* expression) (Zamorano et al., 2010a; Perez-Gallego et al., 2016). Constitutive overexpression of chromosomal AmpC β-lactamase in Gram-negative bacteria can develop antibiotic resistance and lead to a limited choice of antibiotics, since excessive AmpC causes development of resistance to multiple β-lactam antibiotics, including the third and fourth generation cephalosporins and carbapenem (Quale et al., 2006; Majewski et al., 2016). However, underlying molecular mechanisms are still poorly understood regarding to AmpC β-lactamase, especially its relation to peptidoglycan recycling.

To investigate whether resistance was relevant with the expression of *ampC* in EC, expression of *ampC* and activity of β-lactamase were determined in resistant strains of EC. In consistent with our hypothesis, expression of *ampC* and activity of β-lactamase were significantly up-regulated compared with the susceptible strains. Furthermore, expression of *ampC* and ability to hydrolyze β-lactams were also enhanced with overexpression of *nagZ* in susceptible strains of EC. To further study the interaction between NagZ and AmpC, *nagZ*-knockout EC was constructed. It was found that loss of NagZ resulted downregulation of *ampC* and weakened ability to hydrolyze β-lactam antibiotics in EC.

In addition, we evaluated the effects of NagZ and anhMurNAc on the expression of AmpR target genes except AmpC, the results show that NagZ and anhMurNAc could promote the expression of many AmpR target genes, which confirmed that NagZ regulate AmpC through activating transcription factor AmpR by anhMurNAc.

In conclusion, in present study, antibody against NagZ was prepared for the first time, and *nagZ*-knockout and complementation models in EC were successfully constructed. This is the first study that we have read about the mechanism of NagZ regulating AmpC in *E. cloacae*. We confirmed that NagZ promotes AmpC β-lactamase expression through activating AmpR, and enhances resistance to β-lactam antibiotics in *E. cloacae*, which is essential for the identification of novel potential drug targets.

DATA AVAILABILITY STATEMENT

The datasets presented in this study can be found in online repositories. The names of the repository/repositories and accession number(s) can be found in the article/**Supplementary Material**.

ETHICS STATEMENT

The animal study was reviewed and approved by the Ethics Committee of the Clinical Medical College and the First Affiliated Hospital of Chengdu Medical College.

AUTHOR CONTRIBUTIONS

XGY and YX conceived this study and wrote the manuscript. XY and JZ contributed to searching literatures and writing manuscript. YZ, FW, HD, JZ, and FN performed the experiments. XP, DW, and YF contributed to designing experiments and analyzing the data. QZ and TB were responsible for reading

and reviewing manuscript. XGY was the responsible person funded in this project. All authors have read and approved the final manuscript.

FUNDING

This work was supported by the National Natural Science Foundation of China program (81802072), the First Affiliated Hospital of Chengdu Medical College program (CYFY2018YB03), and Chengdu Medical College program (CYZ16-17).

ACKNOWLEDGMENTS

We are very grateful for technical guidance provided by ChinaPeptides Co., Ltd. (Shanghai, China) in antibody preparation and technical guidance provided by Knogen Biotech Co., Ltd. (Guangzhou, China) in genetic modification.

SUPPLEMENTARY MATERIAL

The Supplementary Material for this article can be found online at: https://www.frontiersin.org/articles/10.3389/fmicb.2020.586729/full#supplementary-material

Supplementary Figure 1 | Western blot was used to evaluate specificity of anti-NagZ antibody, the result demonstrated that the antibody had a specific binding site (41 kD) to the total protein of *Enterobacter cloacae*. R1, resistant strain of *Enterobacter cloacae* of number 1; R1-Δ*nagZ*, *nagZ*-knockout R1.

Supplementary Figure 2 | Antibiotic susceptibility test (Kirby-Bauer method) was used to identify impacts of NagZ on resistance in clinical isolates. **(A)** The effects of NagZ complementation on resistance were determined in S1 and S2 isolates. **(B)** The roles of *nagZ* knockout in resistance were determined in R1 isolate. **(C)** The effects of NagZ complementation on resistance were determined in R1-Δ*nagZ*.

REFERENCES

Abraham, E. P., and Chain, E. (1988). An enzyme from bacteria able to destroy penicillin. 1940. *Rev. Infect. Dis.* 10, 677–678.

Acebron, I., Mahasenan, K. V., De Benedetti, S., Lee, M., Artola-Recolons, C., Hesek, D., et al. (2017). Catalytic cycle of the N-acetylglucosaminidase NagZ from *Pseudomonas aeruginosa*. *J. Am. Chem. Soc.* 139, 6795–6798. doi: 10.1021/jacs.7b01626

Annavajhala, M. K., Gomez-Simmonds, A., and Uhlemann, A. C. (2019). Multidrug-resistant *Enterobacter cloacae* complex emerging as a global, diversifying threat. *Front. Microbiol.* 10:44. doi: 10.3389/fmicb.2019.00044

Arora, S., Ayyar, B. V., and O'kennedy, R. (2014). Affinity chromatography for antibody purification. *Methods Mol. Biol.* 1129, 497–516. doi: 10.1007/978-1-62703-977-2_35

Asgarali, A., Stubbs, K. A., Oliver, A., Vocadlo, D. J., and Mark, B. L. (2009). Inactivation of the glycoside hydrolase NagZ attenuates antipseudomonal beta-lactam resistance in *Pseudomonas aeruginosa*. *Antimicrob. Agents Chemother.* 53, 2274–2282. doi: 10.1128/AAC.01617-08

Balasubramanian, D., Kumari, H., and Mathee, K. (2015). *Pseudomonas aeruginosa* AmpR: an acute-chronic switch regulator. *Pathog. Dis.* 73, 1–14. doi: 10.1111/2049-632X.12208

Bhoopalan, S. V., Piekarowicz, A., Lenz, J. D., Dillard, J. P., and Stein, D. C. (2016). nagZ triggers gonococcal biofilm disassembly. *Sci. Rep.* 6:22372. doi: 10.1038/srep22372

Borisova, M., Gaupp, R., Duckworth, A., Schneider, A., Dalugge, D., Muhleck, M., et al. (2016). Peptidoglycan recycling in gram-positive bacteria is crucial for survival in stationary phase. *mBio* 7:e00923-16. doi: 10.1128/mBio.00923-16

Caille, O., Zincke, D., Merighi, M., Balasubramanian, D., Kumari, H., Kong, K. F., et al. (2014). Structural and functional characterization of *Pseudomonas aeruginosa* global regulator AmpR. *J. Bacteriol.* 196, 3890–3902. doi: 10.1128/JB.01997-14

Cao, X. L., Cheng, L., Zhang, Z. F., Ning, M. Z., Zhou, W. Q., Zhang, K., et al. (2017). Survey of clinical extended-spectrum beta-lactamase-producing *Enterobacter cloacae* isolates in a chinese tertiary hospital, 2012-2014. *Microb. Drug Resist.* 23, 83–89. doi: 10.1089/mdr.2015.0128

Cavallari, J. F., Lamers, R. P., Scheurwater, E. M., Matos, A. L., and Burrows, L. L. (2013). Changes to its peptidoglycan-remodeling enzyme repertoire modulate beta-lactam resistance in *Pseudomonas aeruginosa*. *Antimicrob. Agents Chemother.* 57, 3078–3084. doi: 10.1128/AAC.00268-13

CLSI (2018). *2018CLSI.Performance Standards for Antimicrobial Susceptibility Testing: CLSI Supplement M100*, 28th Edn. Wayne, PA: CLSI.

da Silva, A. E. B., Martins, A. F., Nodari, C. S., Magagnin, C. M., and Barth, A. L. (2018). Carbapenem-heteroresistance among isolates of the *Enterobacter cloacae* complex: is it a real concern? *Eur. J. Clin. Microbiol. Infect. Dis.* 37, 185–186. doi: 10.1007/s10096-017-3138-x

Eriksson-Grennberg, K. G. (1968). Resistance of *Escherichia coli* to penicillins. II. An improved mapping of the ampA gene. *Genet. Res.* 12, 147–156. doi: 10.1017/S0016672300011769

Eriksson-Grennberg, K. G., Boman, H. G., Jansson, J. A., and Thoren, S. (1965). Resistance of *Escherichia coli* to Penicillins I. Genetic study of some ampicillin-resistant mutants. *J. Bacteriol.* 90, 54–62. doi: 10.1128/JB.90.1.54-62.1965

Gil-Marques, M. L., Moreno-Martinez, P., Costas, C., Pachon, J., Blazquez, J., and Mcconnell, M. J. (2018). Peptidoglycan recycling contributes to intrinsic resistance to fosfomycin in *Acinetobacter baumannii*. *J. Antimicrob. Chemother.* 73, 2960–2968. doi: 10.1093/jac/dky289

Gisin, J., Schneider, A., Nagele, B., Borisova, M., and Mayer, C. (2013). A cell wall recycling shortcut that bypasses peptidoglycan de novo biosynthesis. *Nat. Chem. Biol.* 9, 491–493. doi: 10.1038/nchembio.1289

Gomez-Simmonds, A., Annavajhala, M. K., Wang, Z., Macesic, N., Hu, Y., Giddins, M. J., et al. (2018). Genomic and geographic context for the evolution of high-risk carbapenem-resistant *Enterobacter cloacae* complex clones ST171 and ST78. *mBio* 9:e00542-18. doi: 10.1128/mBio.00542-18

Guerin, F., Isnard, C., Cattoir, V., and Giard, J. C. (2015). Complex regulation pathways of AmpC-mediated beta-lactam resistance in *Enterobacter cloacae* complex. *Antimicrob. Agents Chemother.* 59, 7753–7761. doi: 10.1128/AAC.01729-15

Ho, L. A., Winogrodzki, J. L., Debowski, A. W., Madden, Z., Vocadlo, D. J., Mark, B. L., et al. (2018). A mechanism-based GlcNAc-inspired cyclophellitol inactivator of the peptidoglycan recycling enzyme NagZ reverses resistance to beta-lactams in *Pseudomonas aeruginosa*. *Chem. Commun.* 54, 10630–10633. doi: 10.1039/C8CC05281F

Huang, Y. W., Hu, R. M., Lin, C. W., Chung, T. C., and Yang, T. C. (2012). NagZ-dependent and NagZ-independent mechanisms for beta-lactamase expression in *Stenotrophomonas* maltophilia. *Antimicrob. Agents Chemother.* 56, 1936–1941. doi: 10.1128/AAC.05645-11

Huang, Y. W., Hu, R. M., Lin, C. W., Chung, T. C., and Yang, T. C. (2015a). Correction for Huang et al., NagZ-dependent and NagZ-independent mechanisms for beta-lactamase expression in *Stenotrophomonas* maltophilia. *Antimicrob. Agents Chemother.* 59:5094. doi: 10.1128/AAC.01322-15

Huang, Y. W., Wu, C. J., Hu, R. M., Lin, Y. T., and Yang, T. C. (2015b). Interplay among membrane-bound lytic transglycosylase D1, the CreBC two-component regulatory system, the AmpNG-AmpDI-NagZ-AmpR regulatory circuit, and L1/L2 beta-lactamase expression in *Stenotrophomonas* maltophilia. *Antimicrob. Agents Chemother.* 59, 6866–6872. doi: 10.1128/AAC.05179-14

Ito, A., Nishikawa, T., Ota, M., Ito-Horiyama, T., Ishibashi, N., Sato, T., et al. (2018). Stability and low induction propensity of cefiderocol against chromosomal AmpC beta-lactamases of *Pseudomonas aeruginosa* and *Enterobacter cloacae*. *J. Antimicrob. Chemother.* 73, 3049–3052. doi: 10.1093/jac/dky317

Ito, A., Nishikawa, T., Ota, M., Ito-Horiyama, T., Ishibashi, N., Sato, T., et al. (2019). Stability and low induction propensity of cefiderocol against chromosomal AmpC beta-lactamases of *Pseudomonas aeruginosa* and *Enterobacter cloacae*. *J. Antimicrob. Chemother.* 74:539. doi: 10.1093/jac/dky482

Jacoby, G. A. (2009). AmpC beta-lactamases. *Clin. Microbiol. Rev.* 22, 161–182. doi: 10.1128/CMR.00036-08

Juan, C., Moya, B., Perez, J. L., and Oliver, A. (2006). Stepwise upregulation of the *Pseudomonas aeruginosa* chromosomal cephalosporinase conferring high-level beta-lactam resistance involves three AmpD homologues. *Antimicrob. Agents Chemother.* 50, 1780–1787. doi: 10.1128/AAC.50.5.1780-1787.2006

Kong, K.-F., Jayawardena, S. R., Indulkar, S. D., Del Puerto, A., Koh, C.-L., Hoiby, N., et al. (2005). *Pseudomonas aeruginosa* AmpR is a global transcriptional factor that regulates expression of AmpC and PoxB ?-lactamases, proteases, quorum sensing, and other virulence factors. *Antimicrob. Agents Chemother.* 49, 4567–4575. doi: 10.1128/AAC.49.11.4567-4575.2005

Liu, C., Li, C., Chen, Y., Hao, H., Liang, J., Duan, R., et al. (2017). Role of low-molecular-mass penicillin-binding proteins, NagZ and AmpR in AmpC beta-lactamase regulation of *Yersinia enterocolitica*. *Front. Cell. Infect. Microbiol.* 7:425. doi: 10.3389/fcimb.2017.00425

Liu, C., Wang, X., Chen, Y., Hao, H., Li, X., Liang, J., et al. (2016). Three *Yersinia enterocolitica* AmpD homologs participate in the multi-step regulation of chromosomal cephalosporinase AmpC. *Front. Microbiol.* 7:1282. doi: 10.3389/fmicb.2016.01282

Lodge, J. M., Minchin, S. D., Piddock, L. J. V., and Busby, S. J. W. (1990). Cloning, sequencing and analysis of the structural gene and regulatory region of the *Pseudomonas aeruginosa* chromosomal ampC β-lactamase. *Biochem. J.* 272:627. doi: 10.1042/bj2720627

Luo, P., He, X., Liu, Q., and Hu, C. (2015). Developing universal genetic tools for rapid and efficient deletion mutation in vibrio species based on suicide T-vectors carrying a novel counterselectable marker, vmi480. *PLoS One* 10:e0144465. doi: 10.1371/journal.pone.0144465

Mack, A. R., Barnes, M. D., Taracila, M. A., Hujer, A. M., Hujer, K. M., Cabot, G., et al. (2019). A standard numbering scheme for class C beta-lactamases. *Antimicrob. Agents Chemother.* 64:e01841-19. doi: 10.1128/AAC.01841-19

Majewski, P., Wieczorek, P., Ojdana, D., Sienko, A., Kowalczuk, O., Sacha, P., et al. (2016). Altered outer membrane transcriptome balance with AmpC overexpression in carbapenem-resistant *Enterobacter cloacae*. *Front. Microbiol.* 7:2054. doi: 10.3389/fmicb.2016.02054

Mayer, C. (2019). Peptidoglycan recycling, a promising target for antibiotic adjuvants in antipseudomonal therapy. *J. Infect. Dis.* 220, 1713–1715. doi: 10.1093/infdis/jiz378

Mezzatesta, M. L., Gona, F., and Stefani, S. (2012). *Enterobacter cloacae* complex: clinical impact and emerging antibiotic resistance. *Future Microbiol.* 7, 887–902. doi: 10.2217/fmb.12.61

Moya, B., Dotsch, A., Juan, C., Blazquez, J., Zamorano, L., Haussler, S., et al. (2009). Beta-lactam resistance response triggered by inactivation of a nonessential penicillin-binding protein. *PLoS Pathog.* 5:e1000353. doi: 10.1371/journal.ppat.1000353

Nicolas, M. H., Honore, N., Jarlier, V., Philippon, A., and Cole, S. T. (1987). Molecular genetic analysis of cephalosporinase production and its role in beta-lactam resistance in clinical isolates of *Enterobacter cloacae*. *Antimicrob. Agents Chemother.* 31, 295–299. doi: 10.1128/AAC.31.2.295

Park, J. T., and Uehara, T. (2008). How bacteria consume their own exoskeletons (turnover and recycling of cell wall peptidoglycan). *Microbiol. Mol. Biol. Rev.* 72, 211–227. doi: 10.1128/MMBR.00027-07

Pechere, J. C. (1991). Why are carbapenems active against *Enterobacter cloacae* resistant to third generation cephalosporins? *Scand. J. Infect. Dis. Suppl.* 78, 17–21.

Perez-Gallego, M., Torrens, G., Castillo-Vera, J., Moya, B., Zamorano, L., Cabot, G., et al. (2016). Impact of AmpC derepression on fitness and virulence: the mechanism or the pathway? *mBio* 7:e01783-16. doi: 10.1128/mBio.01783-16

Pfeifle, D., Janas, E., and Wiedemann, B. (2000). Role of penicillin-binding proteins in the initiation of the AmpC beta-lactamase expression in *Enterobacter cloacae*. *Antimicrob. Agents Chemother.* 44, 169–172. doi: 10.1128/AAC.44.1.169-172.2000

Pimenta, A. C., Fernandes, R., and Moreira, I. S. (2014). Evolution of drug resistance: insight on TEM beta-lactamases structure and activity and beta-lactam antibiotics. *Mini Rev. Med. Chem.* 14, 111–122. doi: 10.2174/1389557514666140123145809

Quale, J., Bratu, S., Gupta, J., and Landman, D. (2006). Interplay of efflux system, ampC, and oprD expression in carbapenem resistance of *Pseudomonas aeruginosa* clinical isolates. *Antimicrob. Agents Chemother.* 50, 1633–1641. doi: 10.1128/AAC.50.5.1633-1641.2006

Rees, C. A., Nasir, M., Smolinska, A., Lewis, A. E., Kane, K. R., Kossmann, S. E., et al. (2018). Detection of high-risk carbapenem-resistant *Klebsiella pneumoniae* and *Enterobacter cloacae* isolates using volatile molecular profiles. *Sci. Rep.* 8:13297. doi: 10.1038/s41598-018-31543-x

Reith, J., and Mayer, C. (2011). Peptidoglycan turnover and recycling in Gram-positive bacteria. *Appl. Microbiol. Biotechnol.* 92, 1–11. doi: 10.1007/s00253-011-3486-x

Ropy, A., Cabot, G., Sanchez-Diener, I., Aguilera, C., Moya, B., Ayala, J. A., et al. (2015). Role of *Pseudomonas aeruginosa* low-molecular-mass penicillin-binding proteins in AmpC expression, beta-lactam resistance, and peptidoglycan structure. *Antimicrob. Agents Chemother.* 59, 3925–3934. doi: 10.1128/AAC.05150-14

Silveira, M. C., Catanho, M., and Miranda, A. B. (2018). Genomic analysis of bifunctional Class C-Class D beta-lactamases in environmental bacteria. *Mem. Inst. Oswaldo Cruz* 113:e180098. doi: 10.1590/0074-02760180098

Stubbs, K. A., Scaffidi, A., Debowski, A. W., Mark, B. L., Stick, R. V., and Vocadlo, D. J. (2008). Synthesis and use of mechanism-based protein-profiling probes for retaining beta-D-glucosaminidases facilitate identification of *Pseudomonas aeruginosa* NagZ. *J. Am. Chem. Soc.* 130, 327–335. doi: 10.1021/ja0763605

Torrens, G., Sanchez-Diener, I., Jordana-Lluch, E., Barcelo, I. M., Zamorano, L., Juan, C., et al. (2019). In Vivo validation of peptidoglycan recycling as a target to disable AmpC-mediated resistance and reduce virulence enhancing the cell-wall-targeting immunity. *J. Infect. Dis.* 220, 1729–1737. doi: 10.1093/infdis/jiz377

Wu, C., Lin, C., Zhu, X., Liu, H., Zhou, W., Lu, J., et al. (2018). The beta-lactamase gene profile and a plasmid-carrying multiple heavy metal resistance genes of *Enterobacter cloacae*. *Int. J. Genomics* 2018:4989602. doi: 10.1155/2018/4989602

Yang, T. C., Chen, T. F., Tsai, J. J., and Hu, R. M. (2014). NagZ is required for beta-lactamase expression and full pathogenicity in *Xanthomonas campestris* pv. campestris str. 17. *Res. Microbiol.* 165, 612–619. doi: 10.1016/j.resmic.2014.08.008

Yang, X., Wu, D., Du, H., Nie, F., Pang, X., and Xu, Y. (2017). MicroRNA-135a is involved in podocyte injury in a transient receptor potential channel 1-dependent manner. *Int. J. Mol. Med.* 40, 1511–1519. doi: 10.3892/ijmm.2017.3152

Zamorano, L., Moya, B., Juan, C., and Oliver, A. (2010a). Differential beta-lactam resistance response driven by ampD or dacB (PBP4) inactivation in genetically diverse *Pseudomonas aeruginosa* strains. *J. Antimicrob. Chemother.* 65, 1540–1542. doi: 10.1093/jac/dkq142

Zamorano, L., Reeve, T. M., Deng, L., Juan, C., Moya, B., Cabot, G., et al. (2010b). NagZ inactivation prevents and reverts beta-lactam resistance, driven by AmpD and PBP 4 mutations, in *Pseudomonas aeruginosa*. *Antimicrob. Agents Chemother.* 54, 3557–3563. doi: 10.1128/AAC.00385-10

Zhou, Y., He, Q., Chen, J., Liu, Y., Mao, Z., Lyu, Z., et al. (2016). The expression patterns of Tetratricopeptide repeat domain 36 (Ttc36). *Gene Expr. Patterns* 22, 37–45. doi: 10.1016/j.gep.2016.11.001

Conflict of Interest: The authors declare that the research was conducted in the absence of any commercial or financial relationships that could be construed as a potential conflict of interest.

frontiers in Microbiology

ORIGINAL RESEARCH
published: 05 November 2020
doi: 10.3389/fmicb.2020.592265

Phytocompounds vs. Dental Plaque Bacteria: *In vitro* Effects of Myrtle and Pomegranate Polyphenolic Extracts Against Single-Species and Multispecies Oral Biofilms

*Daniela Sateriale[1], Roberta Imperatore[1], Roberta Colicchio[2], Chiara Pagliuca[2], Ettore Varricchio[1], Maria Grazia Volpe[3], Paola Salvatore[2,4], Marina Paolucci[1] and Caterina Pagliarulo[1]**

[1] Department of Science and Technology, University of Sannio, Benevento, Italy, [2] Department of Molecular Medicine and Medical Biotechnology, Federico II University, Naples, Italy, [3] Institute of Food Science-National Research Council, Avellino, Italy, [4] CEINGE, Advanced Biotechnologies s.c.ar.l., Naples, Italy

OPEN ACCESS

Edited by:
Rodolfo García-Contreras, National Autonomous University of Mexico, Mexico

Reviewed by:
Zhejun Wang, University of British Columbia, Canada
Biao Ren, Sichuan University, China

***Correspondence:**
Caterina Pagliarulo
caterina.pagliarulo@unisannio.it

Specialty section:
This article was submitted to Antimicrobials, Resistance and Chemotherapy, a section of the journal Frontiers in Microbiology

Received: 06 August 2020
Accepted: 09 October 2020
Published: 05 November 2020

Citation:
Sateriale D, Imperatore R, Colicchio R, Pagliuca C, Varricchio E, Volpe MG, Salvatore P, Paolucci M and Pagliarulo C (2020) Phytocompounds vs. Dental Plaque Bacteria: In vitro Effects of Myrtle and Pomegranate Polyphenolic Extracts Against Single-Species and Multispecies Oral Biofilms. Front. Microbiol. 11:592265. doi: 10.3389/fmicb.2020.592265

In the last decades, resistant microbial infection rate has dramatically increased, especially infections due to biofilm-producing strains that require increasingly complex treatments and are responsible for the increased mortality percentages compared with other infectious diseases. Considering that biofilms represent a key factor for a wide range of chronic infections with high drug tolerance, the treatment of biofilm-causing bacterial infections represents a great challenge for the future. Among new alternative strategies to conventional antimicrobial agents, the scientific interest has shifted to the study of biologically active compounds from plant-related extracts with known antimicrobial properties, in order to also evaluate their antibiofilm activity. In this regard, the aim of this study has been to assess the antibiofilm activity of polyphenolic extracts from myrtle leaf and pomegranate peel against oral pathogens of dental plaque, an excellent polymicrobial biofilm model. In particular, the *in vitro* antibiofilm properties of myrtle and pomegranate extracts, also in binary combination, were highlighted. In addition to inhibiting the biofilm formation, the tested polyphenolic extracts have been proven to destroy both preformed single-species and multispecies biofilms formed by *Streptococcus mutans*, *Streptococcus oralis*, *Streptococcus mitis*, and *Rothia dentocariosa* oral isolates, suggesting that the new natural sources are rich in promising compounds able to counteract biofilm-related infections.

Keywords: *in vitro* antibiofilm agents, polyphenolic extracts, dental plaque bacteria, *Streptococcus mutans*, *Streptococcus oralis*, *Streptococcus mitis*, *Rothia dentocariosa*

INTRODUCTION

Biofilms are complex microbial aggregations encapsulated in a hydrated polymeric matrix of their own synthesis (Aparna and Yadav, 2008). This bacterial complex limits the penetration of antimicrobial drugs, thus protecting the microbial cells entrapped. Furthermore, the biofilm microenvironment is favorable to microbial proliferation and exchange of genetic material,

including the transmission of resistance genes (Chambless et al., 2006). About 80% of human bacterial infections were shown to be caused by biofilm-associated microorganisms (Wenzel, 2007), and more than half of infectious diseases related to biofilm formation involves bacterial species that are commensal or common in the human body environment (WHO, 2014). Oral bacteria are an example of human opportunistic species that can cause biofilm-related infections. Epithelial cells, dental surfaces, and orthodontic prosthesis are some of the numerous surfaces prone to the establishment of multispecies biofilms in the oral cavity (Marsh, 2004). They can cause several infectious diseases, including gingivitis, periodontitis, and dental caries, that still represent some of the most common chronic diseases, in both children and adults (Nishikawara et al., 2007). In addition, some oral bacterial species can also be responsible for critical infections outside the oral environment, such as bacteremia (Yang et al., 2009), endocarditis (Keng et al., 2012), and peritonitis (Khan et al., 2014). The oral microbiota can act as a reservoir for respiratory pathogens. Therefore, there is a close association between oral bacterial species and several forms of lung diseases, such as pneumonia (Raghavendran et al., 2007). *Streptococcus mutans* is considered the most cariogenic of all oral streptococci but is also implicated in subacute bacterial endocarditis and other extraoral pathologies, like nephropathy and atherosclerosis (Lemos et al., 2019). *Streptococcus oralis* belongs to the human oral microbiota but is also capable of opportunistic infections. It has been related to periodontal diseases and also to bacterial endocarditis (Byers et al., 2000), otitis media, septicemia, and pneumonia in children, in association with *Streptococcus pneumoniae* (Whalan et al., 2006). *Streptococcus mitis* and *Rothia dentocariosa* are commensal bacteria of the human mouth and the upper respiratory tract. These usually represent the etiologic agents in odontogenic infections and may contribute to dental caries. In addition, outside their niche, they can cause a wide range of infectious complications, such as endocarditis and septicemia (Mitchell, 2011).

It has been reported that bacteria living within biofilm, also in oral ones, are more tolerant to antibiotics as they are insensitive to the host's immune response (Caraher et al., 2007). Therefore, biofilm-related infections can persist for a long time, thus progressing from acute infections to chronic infections (Leid et al., 2002). The increasing critical role of biofilms in pathogenesis and antimicrobial resistance led scientists to consider this complex structure as a drug target to tackle resistant infections. Unconventional antibiofilm agents with demonstrated antimicrobial activity could represent important alternatives for drug development to counteract infections due to major biofilm-forming pathogens.

In the last decades, the natural compounds have attracted the attention of scientists (Cowan, 1999). Since plant extracts have been used for the treatment of various infectious diseases for hundreds of years, they have sparked considerable interest in this context (Ahmad and Beg, 2001). Technological advances in modern science have accelerated the discovery of new phytocompounds of plant origin with therapeutic activity and without side effects (Ahmad and Aqil, 2009). The role of several phytocompounds, like polyphenols, as anti-infective agents is well-established today (Gibbons, 2005; Savoia, 2012). Among constituents of plants, polyphenols have received great scientific interest due to their numerous biological functions, such as promising activity against bacterial and fungal infections (Slobodníková et al., 2016). However, research regarding the antimicrobial effects of active plant-derived constituents against resistant biofilms appears still incomplete, compared to the demonstrated effects against their planktonic counterparts (Costerton et al., 2003).

Among the extensively studied natural sources rich in phytocompounds, especially polyphenols, *Myrtus communis* L. and *Punica granatum* L. could represent safe and economical alternatives to antibiotics, in the struggle against resistant infections caused by biofilm-related microorganisms. The antibacterial and antifungal effects of myrtle extracts (*M. communis* L.) were the object of recent scientific investigations. Crude extracts and essential oils of *M. communis* seem to be rich in polyphenols and terpenoids (Ben Hsouna et al., 2014), natural constituents of several plant portions that mediate a remarkable antioxidant activity along with strong antimicrobial effects against several pathogens (Aleksic and Knezevic, 2014). A wide plethora of scientific studies have also shown the significant properties of peel and juice pomegranate (*P. granatum* L.) extracts, in particular their anti-inflammatory and antimicrobial effects derived from the high content of polyphenols, mainly including ellagitannins and anthocyanins (Ismail et al., 2012; Pagliarulo et al., 2016; Ferrazzano et al., 2017). Most of the studies have investigated the antimicrobial activity of natural extracts against planktonic forms. In comparison, the experimental evidences of their antibiofilm effects are still few. Furthermore, the current antibiotic therapies showed very limited effectiveness to contrast the biofilm infection (Aparna and Yadav, 2008). Given the requirement to discover novel agents, preferably natural, with antibiofilm activity, as well as activity against oral biofilms, the aim of this study has been to define the antibiofilm profile of characterized polyphenolic extracts derived from myrtle leaf and pomegranate peel against *S. mutans*, *S. oralis*, *S. mitis*, and *R. dentocariosa* clinical isolates, important representative members of the dental plaque. Dental plaque bacteria are among the main microorganisms causing biofilm-related infections (from dental caries to systemic diseases). In particular, several studies have revealed that *S. mutans* represents about the 20–40% of the cultivable flora in biofilms removed from carious lesion (Rosenbloom and Tinanoff, 1991; Koo et al., 2013) and that *S. oralis* is a cariogenic bacterium significantly concurring in dental plaque formation (Jung et al., 2016). Recent reports also suggest that *S. mitis* and *R. dentocariosa* are common inhabitants of biofilms in the oral cavity that could be opportunistic pathogens, causing dental caries and periodontal pathologies (Peros et al., 2011; Banas et al., 2016). These reasons led us to consider the selected pathogenic bacterial strains as good candidates for the study of *in vitro* biofilm models useful in identifying new antibiofilm natural agents. The development of new knowledge about biofilm interferers/inhibitors could highlight novel, effective, and low-cost antibiofilm compounds that may find useful medical and environmental applications in the future.

MATERIALS AND METHODS

Polyphenolic Extracts

The hydroethanolic extracts tested in this study were prepared with a solid–liquid solvent-extraction method from samples of dry myrtle leaf and dry pomegranate fruit peel, harvested from plants growing in the southern Italy countryside in the Salerno and Avellino areas, respectively. In particular, the preparation procedure of myrtle (*M. communis* L.) polyphenolic extract is described by Sateriale et al. (2020). Briefly, the myrtle leaf powder was mixed with a solution of ethanol:water (50:50), reaching a final concentration of 0.1 g ml^{-1}. The suspension was stirred at room temperature (RT) for 30 min, using a rotary shaker, and centrifuged at 10,000 rpm for 15 min at RT. Then the supernatant was filtered through a single-use vacuum filtration unit (Sterilcup®/Steriltop® Filtration System, Merck-Millipore, Darmstadt, Germany) with a 0.45 μm porosity membrane, by using a water vacuum pump. The polyphenolic extract of *P. granatum* L. fruit peel was prepared according to Pagliarulo et al. (2016), with some minor changes. Pomegranate peel powder (5 g) was homogenized in 25 ml of ethanol:water (50:50) solution for 30 min at RT in the dark. After centrifugation (10,000 rpm for 15 min at RT), the supernatant was filtered by the vacuum filtration systems (0.45 μm porosity membrane) described for myrtle extracts.

Extract volume was reduced by a rotavapor (Heidolph 36001270 Hei-VAP Precision Rotary Evaporator) and finally lyophilized. The resuspension of lyophilized polyphenols in fresh solvent was carried out before each antimicrobial test, adjusting the concentration according to the requirements of the performed assays.

Bacterial Isolates and Growth Conditions

The antibiofilm activity of polyphenolic extracts was assessed against the *S. mutans* ATCC 25175 (LGC Standards, United Kingdom) strain, isolated from carious dentin, and against the clinical isolates of *S. oralis* SO1, *S. mitis* SM2, and *R. dentocariosa* RD1, obtained from samples of dental plaque from children with tooth decay, provided by the Pediatric Dentistry Department of "Federico II" University, Naples, Italy. Permission to take dental plaque samples was acquired according to the local planning authorities. Furthermore, approval for this study was granted by the ethics committee of the "Federico II" University, Naples, Italy (protocol number 101/14). The isolation of bacterial strains was carried out by culture techniques. The use of selective growth media allowed us to isolate representative colonies from dental plaque samples. The detailed identification of isolates was subsequently performed by mass spectrometry using the matrix-assisted laser desorption/ionization (MALDI) mass spectrometer (Bruker Daltonics, MALDI Biotyper, Fremont, CA, United States), a high-throughput proteomic technique for identification of a variety of bacterial species (Neville et al., 2011; Sogawa et al., 2011), and by a biochemical phenotyping method in a BD Phoenix Automated Microbiology System (Becton Dickinson, BD Franklin Lakes, NJ, United States), according to the manufacturer's instruction.

Oral bacterial isolates were aerobically cultured at 37°C in brain heart infusion (BHI) agar/broth (Condalab, Torrejón de Ardoz, Madrid, Spain) and Columbia CNA agar base with 5% sheep blood and with colistin and nalidixic acid (Condalab, Torrejón de Ardoz, Madrid, Spain).

Bacterial isolates were kept in agar media at 4°C and were stored frozen at −80°C in BHI broth with 10% glycerol (v/v) (Carlo Erba, Reagents, Milan, Italy). Working cultures were activated in broth medium at 37°C for 15–18 h before use.

Biofilm *in vitro* Reproduction

Tube Method

A qualitative and semiquantitative evaluation of biofilm formation was carried out, adapting the "tube method" (TM) described by Christensen et al. (1985) and Ansari et al. (2014). In brief, the bacterial isolates were subcultured in 5 ml of BHI broth tubes, by adjusting turbidity to an optical density (OD) of 0.5 at A_{600nm}, and aerobically incubated for 48 h at 37°C. Subsequently, the medium was discarded, and the tubes were washed with phosphate buffer saline (1xPBS, pH 7.3) and dried. The bacterial cells adherent to the tubes were then stained with crystal violet (2%) for 1 min. After removal of the stain excess, tubes were washed with deionized water, dried in an inverted position, and observed for biofilm formation. The isolates were considered as positive when a visible biofilm lined the wall and bottom of the tube, while a simple ring formation at the liquid interface was not indicative of biofilm formation. Based on the careful observation by the operator, the microbial isolates have been classified as negative (0), when no visible biofilm was observed; weakly positive (+), when a visible biofilm was observed; moderately positive (+ +), when a twice darker visible biofilm was observed with respect to weakly positive cases; and strongly positive (+ + +), when a three times darker visible biofilm was observed with respect to weakly positive cases. Each microorganism suspension at 0.5 $OD_{600\ nm}$ was inoculated in a ratio of 1:1:1:1 in mixed culture to form a multispecies biofilm.

Tissue Culture Plate Method

The biofilm biomass measurement of selected oral isolates was evaluated by the quantitative assay known as "tissue culture plate method" (TCPM), similar to that described by Costa et al. (2013). BHI broth (10 ml) was inoculated with test microorganisms from overnight cultures at 37°C for 24 h. After aerobic incubation, each fresh culture was further adjusted by reaching the OD at 0.5, by spectrophotometric reading at $A_{600\ nm}$, and aliquots of 0.2 ml of starter culture were dispensed, in six replicates, into each well of a 96-well flat-bottomed microplate for tissue cultures in hydrophilic polystyrene (Nunc™ MicroWell 96-well microplates, Thermo Scientific, Denmark). Each microorganism suspension at 0.5 $OD_{600\ nm}$ was inoculated in a ratio of 1:4 with others to form a multispecies biofilm. Sterile BHI broth was used as negative control. The culture plates were incubated at 37°C for 3–6–9–12–18–24–36–48 h, without shaking. Different plates were used for different incubation times. For incubation times longer than 3 h, non-adherent bacteria were removed at regular intervals (T_3–T_6–T_9–T_{12}–T_{18}–T_{24}–T_{36}–T_{48}), new fresh BHI broth medium was added, and plates were further

incubated for the remaining time, according to the established total incubation period. After each incubation, the bacterial culture was removed, and the wells were washed with 0.2 ml of 1xPBS (pH 7.3) three times to remove free-floating bacteria. The biofilms adherent to the wells were fixed with 0.2 ml of 85% ethanol (Sigma-Aldrich, Merck KGaA, Darmstadt, Germany) for 15 min and stained with 0.2% crystal violet (Sigma-Aldrich, Merck KGaA, Darmstadt, Germany) for 5 min. The stain excess was washed with deionized water, and plates were dried in a thermostat at a temperature of 30°C for 10 min upside down. The OD of the purple-stained solution was recorded at 600 nm wavelength by a microplate reader (Bio-Rad microplate reader, Model 680). Based on the measurement of OD (OD_I) compared to the OD of sterile BHI broth used as negative control (OD_C), the microbial isolates have been classified as non-adherent ($OD_I \leq OD_C$), weakly adherent ($OD_C < OD_I \leq 2^*OD_C$), moderately adherent ($2^*OD_C < OD_I \leq 4^*OD_C$), and strongly adherent ($4^*OD_C < OD_I$).

In vitro Antibiofilm Assays With Polyphenolic Extracts

Biofilm Formation Inhibition Assay

To evaluate the ability of the myrtle and pomegranate hydroethanolic polyphenolic extracts to inhibit biofilm formation, some modifications to the tissue culture plate method have been proposed. In particular, a volume of 0.1 ml of extracts, at sub-MIC (1/4 MIC and 1/2 MIC), MIC, and over-MIC (2 MIC and 4 MIC) concentrations, was added to each well of a 96-well microplate. The same volume of BHI broth was added to replace the extracts in the negative control. Finally, 0.1 ml of each single and mixed bacterial culture, with 0.5 OD at $A_{600\ nm}$ wavelength, was pipetted to each well, reaching a final volume of 0.2 ml. BHI (0.2 ml) broth was added in wells without bacterial culture as a blank. The plates were wrapped loosely and aerobically incubated at 37°C for 24 h without shaking to allow the cells to attach to the surface. After the incubation, the content of each well was removed, and all the subsequent steps of the above-mentioned TCPM have been performed. After staining with crystal violet, reading at $A_{600\ nm}$ by a microplate reader was performed. Results were given as a percentage of biofilm formation inhibition, applying the following formula, according to Bakkiyaraj et al. (2013):

$$\text{Biofilm formation inhibition\%} = \left(\frac{OD_{control} - OD_{assay}}{OD_{control}}\right)^* 100$$

where $OD_{control}$ is the mean OD measured for bacterial biofilms grown without extracts, while OD_{assay} is the mean OD measured for bacterial biofilms grown in the presence of myrtle and pomegranate hydroalcoholic polyphenolic extracts, as single agents and in binary combination.

The lowest concentration of each extract, or extract binary combination, that produced biofilm inhibition was considered to be the minimum biofilm inhibition concentration (MBIC).

Biofilm Eradication Assay

To assess the effects of myrtle and pomegranate hydroethanolic polyphenolic extracts upon mature 1-day biofilms, some adaptations of the TCPM biofilm formation protocol were performed. In particular, aliquots of 0.2 ml of single/mixed starter bacterial culture (with adjusted OD at 0.5 $OD_{600\ nm}$) were dispensed, in six replicates, into each well of a 96-well flat-bottomed microplate. BHI broth (0.2 ml) was added into wells without bacterial culture as a blank. The plates were wrapped loosely and aerobically incubated at 37°C for 24 h without shaking, to allow the cells to attach to the surface. Following incubation, the content of each well was removed, and a volume of 0.1 ml of extracts was added, at MBIC and over-MBIC (2 MBIC, 3 MBIC, and 4 MBIC) concentrations. The same volume of BHI broth was added as a negative control. Finally, 0.1 ml of fresh BHI broth was added to each well, reaching a final volume of 0.2 ml. Fresh BHI broth (0.2 ml) was added in wells without bacteria culture as a blank. The plates were again aerobically incubated at 37°C for 24 h. After the second incubation, the washings with PBS, the staining with 0.2% crystal violet, and the final washing with distilled water were performed before reading the plates at $A_{600\ nm}$ wavelength. Results for this test were given as a percentage of biofilm disruption, calculated by the following formula, according to Bakkiyaraj et al. (2013):

$$\textit{Biofilm disruption\%} = \left(\frac{OD_{control} - OD_{assay}}{OD_{control}}\right)^* 100$$

where $OD_{control}$ is the mean OD measured for 1-day bacterial biofilms without extracts, while OD_{assay} is the mean OD measured for 1-day bacterial biofilms treated with myrtle and pomegranate hydroalcoholic polyphenolic extracts, as single agents and in binary combination.

The lowest concentration of each extract, or binary combination of extracts, that is able to destroy (eradicate) preformed biofilms was considered to be the minimum biofilm eradication concentration (MBEC).

Biofilm Visualization Through Microscopy Techniques

Light microscopy analysis

The ability of myrtle and pomegranate polyphenolic hydroalcoholic extracts (50% v/v) in binary combination to inhibit biofilm formation has been confirmed by a microscopic technique similar to that described by Chaieb et al. (2011), with minor modifications. Briefly, the biofilm of each separate bacterial strain and also that of the multispecies biofilm formed by *S. mutans*, *S. oralis*, *S. mitis*, and *R. dentocariosa* were grown on glass cover slides (1 cm^2) placed in 24-well polystyrene plates (Nunc^{TM} MicroWell 96-well microplates, Thermo Fisher Scientific, Denmark). In particular, aliquots of 0.2 ml of single/mixed starter bacterial culture (with an adjusted OD at 0.5 OD_{600nm}) were dispensed on the cover glass, and then the wells were filled with different concentrations of extracts (0, 20, 40 $\mu g\ \mu l^{-1}$), reaching a final volume of 0.4 ml in each well, before aerobic incubation at 37°C for 24 h. For negative control, bacterial cultures without extracts were used. After incubation, wells were emptied, washed with PBS, fixed with 90% ethanol for

15 min, and completely dried at 30°C. Then biofilms were stained with 1% crystal violet (Sigma-Aldrich, Merck KGaA, Darmstadt, Germany) for 20 min at RT. The excess dye was washed with distilled water. Finally, dried stained glass pieces were placed on slides and were observed with a trinocular light microscope (Motic B1 Series, Model B1-223 A) at 40X magnification with 40X/0.65/S (WD 0.53 mm) objective.

Fluorescence microscopy analysis

Biofilm architecture, in the absence and in the presence of myrtle and pomegranate hydroalcoholic extracts in binary combination, was evaluated by fluorescence microscopy analysis. The performed method, adapted from Singh et al. (2012), consisted in assessing single and polymicrobial biofilms on glass coverslips (1 cm^2) immersed in bacterial culture (0.5 $OD_{600\ nm}$) in 24-well plates. In particular, aliquots of 0.2 ml of single/mixed starter bacterial cultures were dispensed on the cover glass, and then the wells were filled with different concentrations of extracts (0, 20, and 40 $\mu g\ \mu l^{-1}$), reaching a final volume of 0.4 ml in each well, before. Bacterial cultures without extracts were used as negative control. After aerobic incubation at 37°C for 24 h, mature-biofilm wells were emptied, washed with PBS, fixed with 90% ethanol for 15 min, and completely dried at 30°C. Then biofilms were stained with 1 mM propidium iodide (PI; product code 81845, Sigma-Aldrich, Merck KGaA, Darmstadt, Germany) for 15 min at RT. The excess of dye was washed with distilled water. Finally, biofilms were observed with a fluorescent microscope Nikon Eclipse Ti-S (Nikon, Florence, Italy) equipped with a digital camera DS-Qi2 (Nikon, Florence, Italy) and the acquisition and image analysis software NIS-Elements C (Nikon, Florence, Italy). Digital images were acquired using the 40X objective. PI (excitation wavelength, 543 nm; fluorescence emission wavelength, 617 nm) emits red fluorescence. All fluorescence images were analyzed by Fiji ImageJ software (National Institutes of Health, Bethesda, MD) to obtain the mean fluorescence intensities from biofilms.

Statistical Data Analysis

All experiments were performed in triplicate, with independent microbial cultures for antimicrobial assays. The results obtained were analyzed and graphically reported by using GraphPad Prism 6 software, validating the statistical significance by the one-way ANOVA test with Tukey correction and the two-way ANOVA test with Bonferroni and Dunnett corrections. In all cases, $p < 0.05$ were considered statistically significant.

RESULTS

Biofilm Production by *S. mutans* ATCC 25175, *S. oralis* SO1, *S. mitis* SM2, and *R. dentocariosa* RD1 Oral Isolates

In this study, *S. mutans* ATCC 25175, *S. oralis* SO1, *S. mitis* SM2, and *R. dentocariosa* RD1 biofilm-forming potential was qualitatively and quantitatively analyzed using the TM and the TCPM. The assigned adherence levels are shown in **Table 1**. A multispecies biofilm with the mentioned oral isolates was also set up and screened. To quantify the differences between the biofilm-forming ability of oral isolates over time, biofilm formation was monitored using crystal violet staining with regular intervals. **Figure 1** shows the microplate measurements generated after static incubations at 37°C from 3 to 48 h (T_3–T_6–T_9–T_{12}–T_{18}–T_{24}–T_{36}–T_{48}).

In vitro Antibiofilm Activity of Myrtle Leaf and Pomegranate Peel Polyphenolic Extracts, as Single Agents and in Binary Combination, Against *S. mutans* ATCC 25175, *S. oralis* SO1, *S. mitis* SM2, and *R. dentocariosa* RD1 Oral Isolates

The antibiofilm activity of polyphenolic hydroethanolic extracts of myrtle leaf (MLE) and pomegranate peel (PPE), also in binary combination (MLE + PPE, 1:1 ratio), was measured against *S. mutans* ATCC 25175, *S. oralis* SO1, *S. mitis* SM2, and *R. dentocariosa* RD1 oral isolates at several concentrations, including sub-MIC (1/4 MIC and 1/2 MIC), MIC, and over-MIC (2 MIC and 4 MIC) concentrations, in order to assess the impact of the natural extracts upon biofilm formation of dental plaque pathogens involved in caries disease etiology.

MBIC values, which ranged between 10 $\mu g\ \mu l^{-1}$ (MLE + PPE vs. *S. oralis* SO1 and *S. mitis* SM2) and 40 $\mu g\ \mu l^{-1}$ (MLE vs. *S. mutans* ATCC 25175 and *R. dentocariosa* RD1, together with PPE vs. *S. mutans* ATCC 25175, *S. mitis* SM2, and *R. dentocariosa* RD1) (**Table 2**), were assigned to the lowest concentrations of antimicrobial agents required to inhibit the formation of biofilms, while MBEC values, assigned to the lowest concentration of each antimicrobial agent that is able to destroy (eradicate) preformed biofilms, ranged between 40 $\mu g\ \mu l^{-1}$ (MLE + PPE vs. *S. mutans* ATCC 25175, *S. oralis* SO1, and *S. mitis* SM2) and 120 $\mu g\ \mu l^{-1}$ (MLE vs. *S. mutans* ATCC 25175 and *R. dentocariosa* RD1, together with PPE vs. *S. mutans* ATCC 25175, *S. mitis* SM2, and *R. dentocariosa* RD1) (**Table 2**).

The ability of the MLE, PPE, and MLE + PPE binary combination to disrupt preformed biofilms of *S. mutans* ATCC 25175, *S. oralis* SO1, *S. mitis* SM2, and *R. dentocariosa* RD1 was tested at MBIC and over-MBIC concentrations (2 MBIC, 3 MBIC, and 4 MBIC).

Biofilm inhibition and eradication activity of myrtle and pomegranate polyphenolic extracts, as single agents and in binary combination, on single-species and multispecies mature biofilms of *S. mutans* ATCC 25175, *S. oralis* SO1, *S. mitis* SM2, and *R. dentocariosa* RD1 oral isolates are reported in **Figures 2**, **3**, respectively.

Regarding the effect on biofilm formation, the hydroethanolic (50% v/v) polyphenolic extracts of *M. communis* L. leaf and *P. granatum* L. fruit peel produced a significant ($p < 0.05$) inhibition of *S. mutans* ATCC 25175, *S. oralis* SO1, *S. mitis* SM2, and *R. dentocariosa* RD1 biomass with respect to untreated control, as shown in **Figure 2**. In detail, both myrtle and pomegranate extracts, also in binary combination, at sub-MIC concentrations caused a slight or not significant decrease for all oral isolates, ranging from 1.2% (PPE vs. four-species

TABLE 1 | Biofilm adherence levels of *S. mutans* ATCC 25175, *S. oralis* SO1, *S. mitis* SM2, and *R. dentocariosa* RD1 oral isolates, in pure and mixed cultures.

Bacterial isolate	Mean control $OD_{600\ nm}$	Mean bacterial isolate $OD_{600\ nm}$	Bacterial adherence level
S. mutans ATCC 25175	0.057 ± 0.005	0.506 ± 0.045	Strongly adherent
S. oralis SO1	0.057 ± 0.005	0.224 ± 0.022	Moderately adherent
S. mitis SM2	0.057 ± 0.005	0.111 ± 0.011	Weakly adherent
R. dentocariosa RD1	0.057 ± 0.005	0.227 ± 0.020	Moderately adherent
Mixed culture (1:1:1:1 ratio)	0.057 ± 0.005	0.607 ± 0.028	Strongly adherent

$OD_{600\ nm}$, optical density detected at a wavelength of 600 nm by a microplate reader.

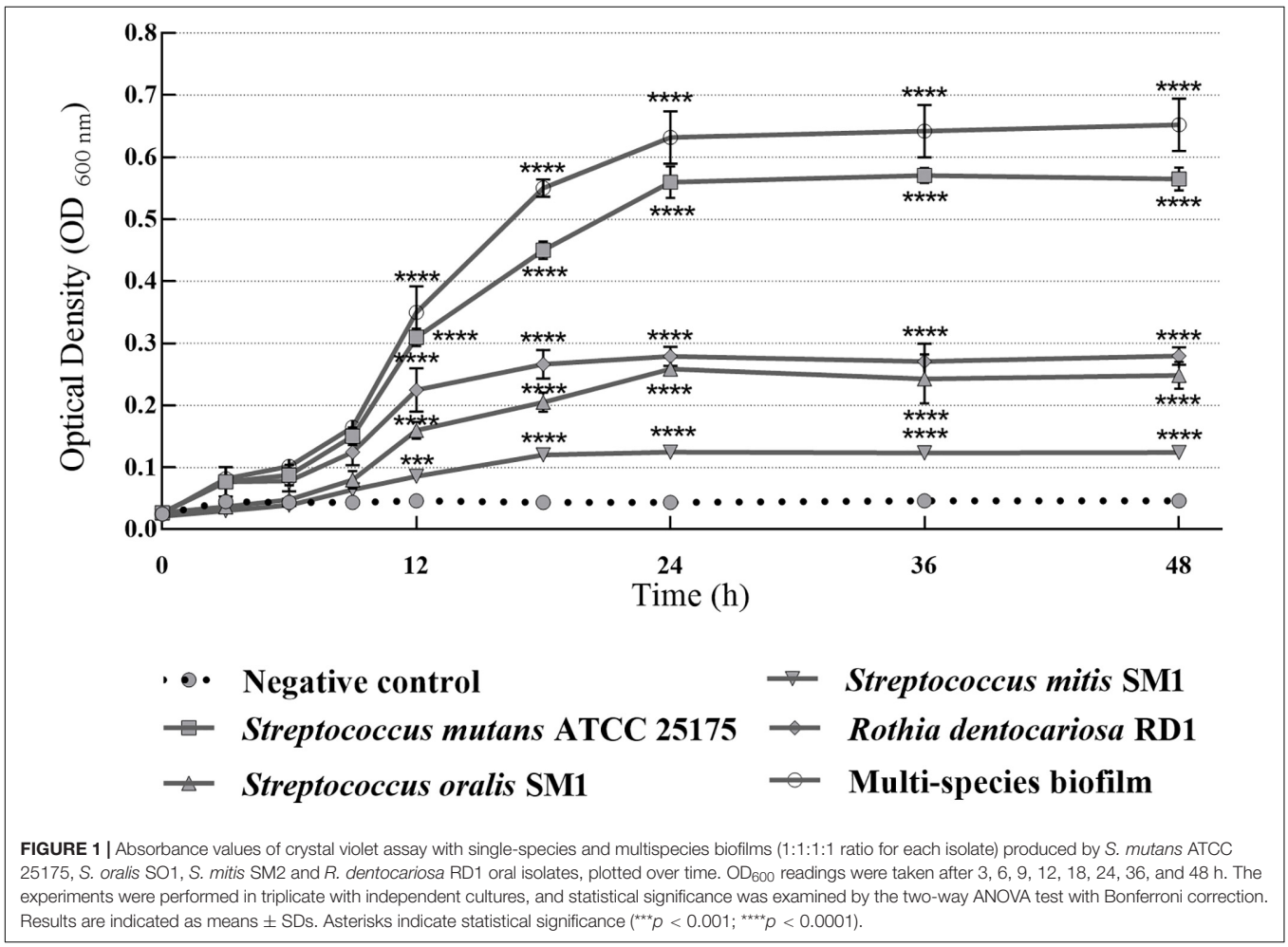

FIGURE 1 | Absorbance values of crystal violet assay with single-species and multispecies biofilms (1:1:1:1 ratio for each isolate) produced by *S. mutans* ATCC 25175, *S. oralis* SO1, *S. mitis* SM2 and *R. dentocariosa* RD1 oral isolates, plotted over time. OD_{600} readings were taken after 3, 6, 9, 12, 18, 24, 36, and 48 h. The experiments were performed in triplicate with independent cultures, and statistical significance was examined by the two-way ANOVA test with Bonferroni correction. Results are indicated as means ± SDs. Asterisks indicate statistical significance (***$p < 0.001$; ****$p < 0.0001$).

biofilm) to 35.7% (MLE + PPE vs. *S. mitis* biofilm) with respect to the control (**Figure 2**), while both produced a significant ($p < 0.05$) inhibition of biofilm formation at MIC and over-MIC concentrations, with inhibition percentages reaching up to 97.3% for MLE + PPE binary combination against the *S. mitis* biofilm (**Figure 2**). The ability of the MLE, PPE, and MLE + PPE binary combination to disrupt preformed biofilms of *S. mutans* ATCC 25175, *S. oralis* SO1, *S. mitis* SM2, and *R. dentocariosa* RD1 was tested at MBIC and over-MBIC concentrations (2 MBIC, 3 MBIC, and 4 MBIC). It was found that preformed biofilms of all tested oral isolates were significantly disrupted at over-MBIC concentrations (**Figure 3**).

Detection of *S. mutans* ATCC 25175, *S. oralis* SO1, *S. mitis* SM2, *R. dentocariosa* RD1, and Multispecies Biofilm Architecture in the Absence and in the Presence of Myrtle Leaf and Pomegranate Peel Polyphenolic Extracts

Microscopy techniques allowed us to visually confirm the effects of the polyphenolic extracts against single-species and multispecies biofilms produced by oral pathogens.

In particular, light microscopy images (**Figure 4**) show the morphology of the mature biofilms (24 h) of *S. mutans* ATCC 25175, *S. oralis* SO1, *S. mitis* SM2, and *R. dentocariosa*

TABLE 2 | Quantitative evaluation of effects of myrtle and pomegranate polyphenolic extracts, used individually and in binary combinations, against *S. mutans* ATCC 25175, *S. oralis* SO1, *S. mitis* SM2, and *R. dentocariosa* RD1 biofilms.

Antibacterial agent	*S. mutans* ATCC 25175		*S. oralis* SO1		*S. mitis* SM2		*R. dentocariosa* RD1	
	MBIC ($\mu g\ \mu l^{-1}$)	MBEC ($\mu g\ \mu l^{-1}$)	MBIC ($\mu g\ \mu l^{-1}$)	MBEC ($\mu g\ \mu l^{-1}$)	MBIC ($\mu g\ \mu l^{-1}$)	MBEC ($\mu g\ \mu l^{-1}$)	MBIC ($\mu g\ \mu l^{-1}$)	MBEC ($\mu g\ \mu l^{-1}$)
MLE	40.00	120.00	20.00	40.00	20.00	40.00	40.00	120.00
PPE	40.00	120.00	20.00	80.00	40.00	120.00	40.00	120.00
MLE + PPE (1:1 ratio)	20.00	40.00	10.00	40.00	10.00	40.00	20.00	80.00

MLE, myrtle leaf 50% ethanolic extracts; PPE, pomegranate peel 50% ethanolic extracts; MBIC, minimum biofilm inhibition concentration; MBEC, minimum biofilm eradication concentration.

RD1, in single species and multispecies, grown in the absence and in the presence of the binary combination of myrtle leaf 50% ethanolic extracts and pomegranate peel 50% ethanolic extracts (MLE + PPE). The images of single-species biofilm treated with MLE + PPE at increasing concentrations (**Figures 4A2,A3,B2,B3,C2,C3,D2,D3**) show a gradual reduction in biofilm mass at 20 and 40 $\mu g\ \mu l^{-1}$ extract concentrations, compared to their respective untreated controls (**Figures 4A1,B1,C1,D1**). The extracts also demonstrated the ability to inhibit the multispecies biofilm formation with respect to the unexposed control (**Figures 4E1–E3**).

The effects of the binary combination of MLE and PPE on the architecture of biofilms formed by *S. mutans*, *S. oralis*, *S. mitis*, and *R. dentocariosa*, in single and mixed cultures, were analyzed also by fluorescence microscopy with PI-based fluorescent staining, as shown in **Figure 5**.

In fluorescence microscopy images, we can observe a large fraction of red PI-stained areas in single-species and multispecies biofilms on untreated glass (**Figures 5A1,B1,C1,D1,E1**), while the fractions of red-stained areas tended to decrease progressively on treated surfaces with the extracts at increasing concentrations with respect to untreated controls (**Figures 5A2,A3,B2,B3,C2,C3,D2,D3,E2,E3**). PI is a fluorescent intercalating agent widely used to stain microbial cells, also encapsulated in a biofilm matrix, and nucleic acids, including extracellular DNA (eDNA), which is one of the most abundant components of the exopolysaccharide matrix (Whitchurch et al., 2002). To confirm the decrease of red PI-stained areas in single-species and multispecies biofilms on the surfaces treated with the extracts, a quantitative analysis of the relative fluorescence intensity was performed. In particular, *S. mutans* single culture showed a significant decrease of relative fluorescence intensity in the presence of myrtle leaf and pomegranate peel polyphenolic extracts with respect to the control [control: 61.78 ± 10.57 vs. MLE + PPE ($10 + 10\ \mu g\ \mu l^{-1}$): 15.44 ± 7.62, $p < 0.05$; and control: 61.78 ± 10.57 vs. MLE + PPE ($20 + 20\ \mu g\ \mu l^{-1}$): 7.93 ± 1.12, $p < 0.001$] (**Figure 5A4**). Similar results were obtained for *S. oralis* [control: 33.02 ± 8.2 vs. MLE + PPE ($10 + 10\ \mu g\ \mu l^{-1}$): 7.01 ± 4.16, $p < 0.05$; and control: 33.02 ± 8.2 vs. MLE + PPE ($20 + 20\ \mu g\ \mu l^{-1}$): 1.68 ± 1.19, $p < 0.05$] (**Figure 5B4**); *S. mitis* [control: 23.78 ± 6.45 vs. MLE + PPE ($10 + 10\ \mu g\ \mu l^{-1}$): 5.06 ± 2.24, $p < 0.05$; and control: 23.78 ± 6.45 vs. MLE + PPE ($20 + 20\ \mu g\ \mu l^{-11}$): 2.18 ± 0.17, $p < 0.05$] (**Figure 5C4**); *R. dentocariosa* [control: 52.33 ± 12.13 vs. MLE + PPE ($10 + 10\ \mu g\ \mu l^{-1}$): 12.49 ± 4.75, $p < 0.05$; and control: 52.33 ± 12.13 vs. MLE + PPE ($20 + 20\ \mu g\ \mu l^{-1}$): 3.9 ± 0.48, $p < 0.001$] (**Figure 5D4**); and also the mixture [control: 68.2 ± 8.71 vs. MLE + PPE ($10 + 100\ \mu g\ \mu l^{-1}$): 22.26 ± 6.92, $p < 0.001$; and control: 68.2 ± 8.71 vs. MLE + PPE ($20 + 20\ \mu g\ \mu l^{-1}$): 19.25 ± 1.58, $p < 0.001$] (**Figure 5E4**).

In addition, the morphology of biofilms on treated glass appeared altered with respect to control, with more intense fluorescent signals. This suggests the presence of dead microbial cells with compromised membranes: PI can easily cross them and intercalate in greater quantity into double-stranded nucleic acids by emitting a clearer red signal (Rosenberg et al., 2019).

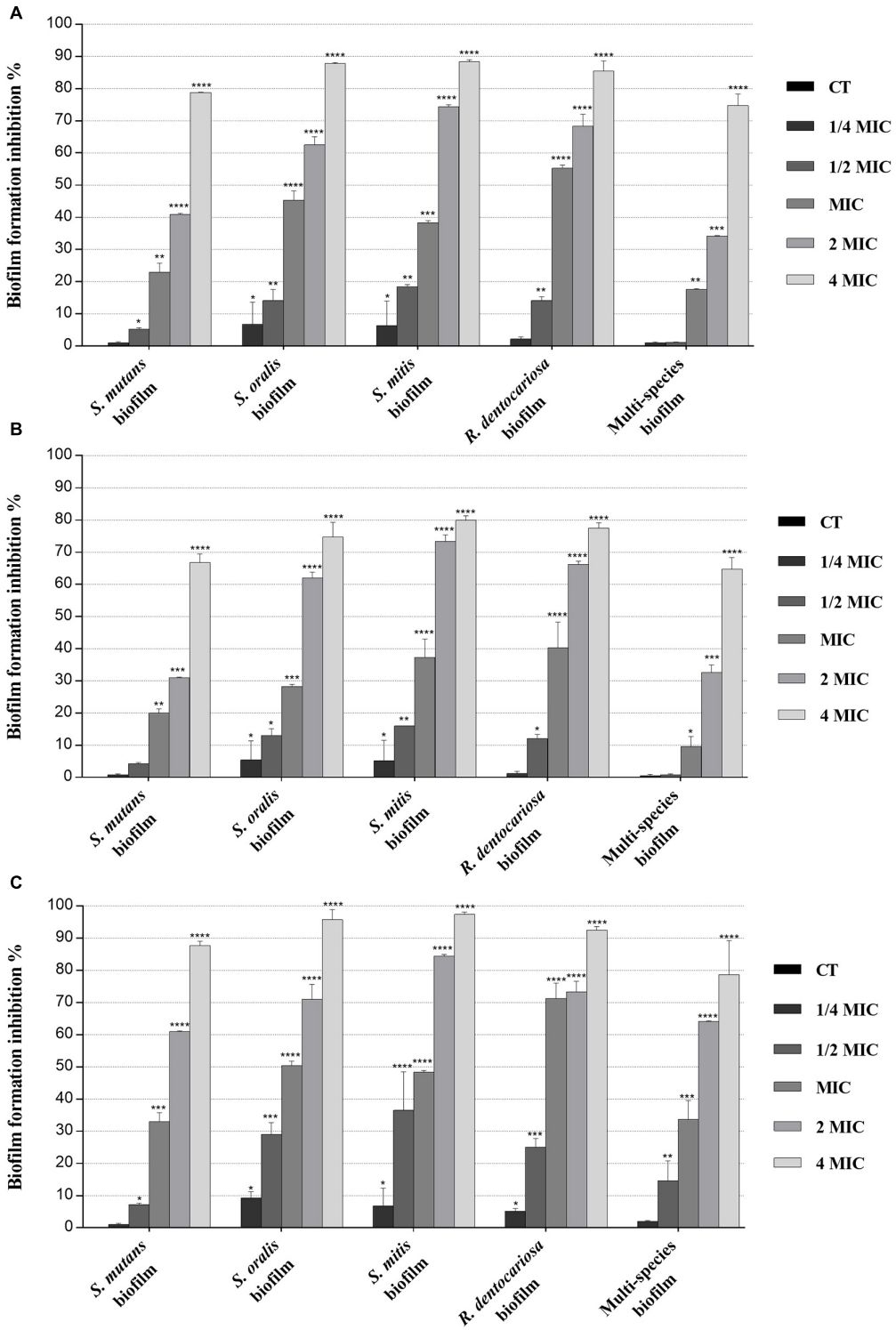

FIGURE 2 | Inhibitory effect of myrtle and pomegranate polyphenolic extracts, used individually and in binary combinations, on single-species and multispecies biofilm formation by *S. mutans* ATCC 25175, *S. oralis* SO1, *S. mitis* SM2, and *R. dentocariosa* RD1 oral isolates. Figure shows the inhibition percentage values of *S. mutans* ATCC 25175, *S. oralis* SO1, *S. mitis* SM2, and *R. dentocariosa* RD1 in single-species and multispecies biofilm (1:1:1:1 ratio for each isolate) detected, in the presence of sub-MIC (1/4 MIC and 1/2 MIC), MIC, and over-MIC (2 and 4 MIC) concentrations of myrtle leaf 50% hydroethanolic extract (MLE) **(A)**; pomegranate peel 50% hydroethanolic extract (PPE) **(B)**; myrtle leaf 50% hydroethanolic extract in combination with pomegranate peel 50% hydroethanolic extract (MLE + PPE) added in a 1:1 ratio **(C)**. The experiments were performed in triplicate with independent cultures, and statistical significance was examined by the two-way ANOVA test with Dunnett correction. Results are indicated as means ± SDs. Asterisks indicate statistical significance (*$p < 0.05$; **$p < 0.01$;***$p < 0.001$; ****$p < 0.0001$).

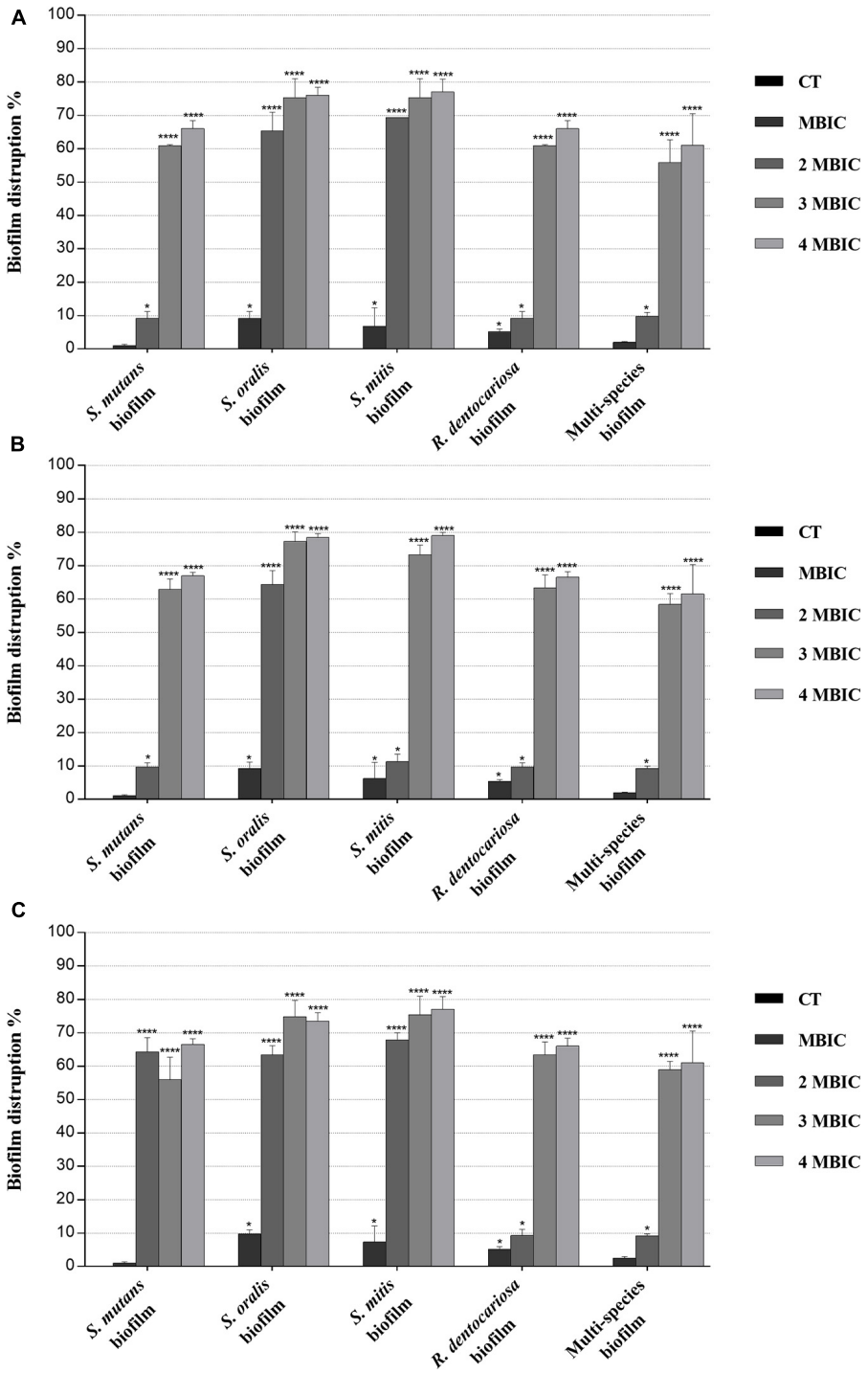

FIGURE 3 | Biofilm eradication activity of myrtle and pomegranate polyphenolic extracts, also in binary combination, on single-species and multispecies mature biofilms of *S. mutans* ATCC 25175, *S. oralis* SO1, *S. mitis* SM2, and *R. dentocariosa* RD1 oral isolates. Figure shows the disruption percentage values of *S. mutans* ATCC 25175, *S. oralis* SO1, *S. mitis* SM2, and *R. dentocariosa* RD1 oral isolates in single and multispecies biofilms (1:1:1:1 ratio for each isolate) detected in the presence of MBIC and over-MBIC (2 MBIC, 3 MBIC, and 4 MBIC) concentrations of myrtle leaf 50% hydroethanolic extract (MLE) **(A)**; pomegranate peel 50% hydroethanolic extract (PPE) **(B)**; myrtle leaf 50% hydroethanolic extract in combination with pomegranate peel 50% hydroethanolic extract (MLE + PPE) added in a 1:1 ratio **(C)**. The experiments were performed in triplicate with independent cultures, and statistical significance was examined by the two-way ANOVA test with Dunnett correction. Results are indicated as means ± SDs. Asterisks indicate statistical significance (*$p < 0.05$; ****$p < 0.0001$).

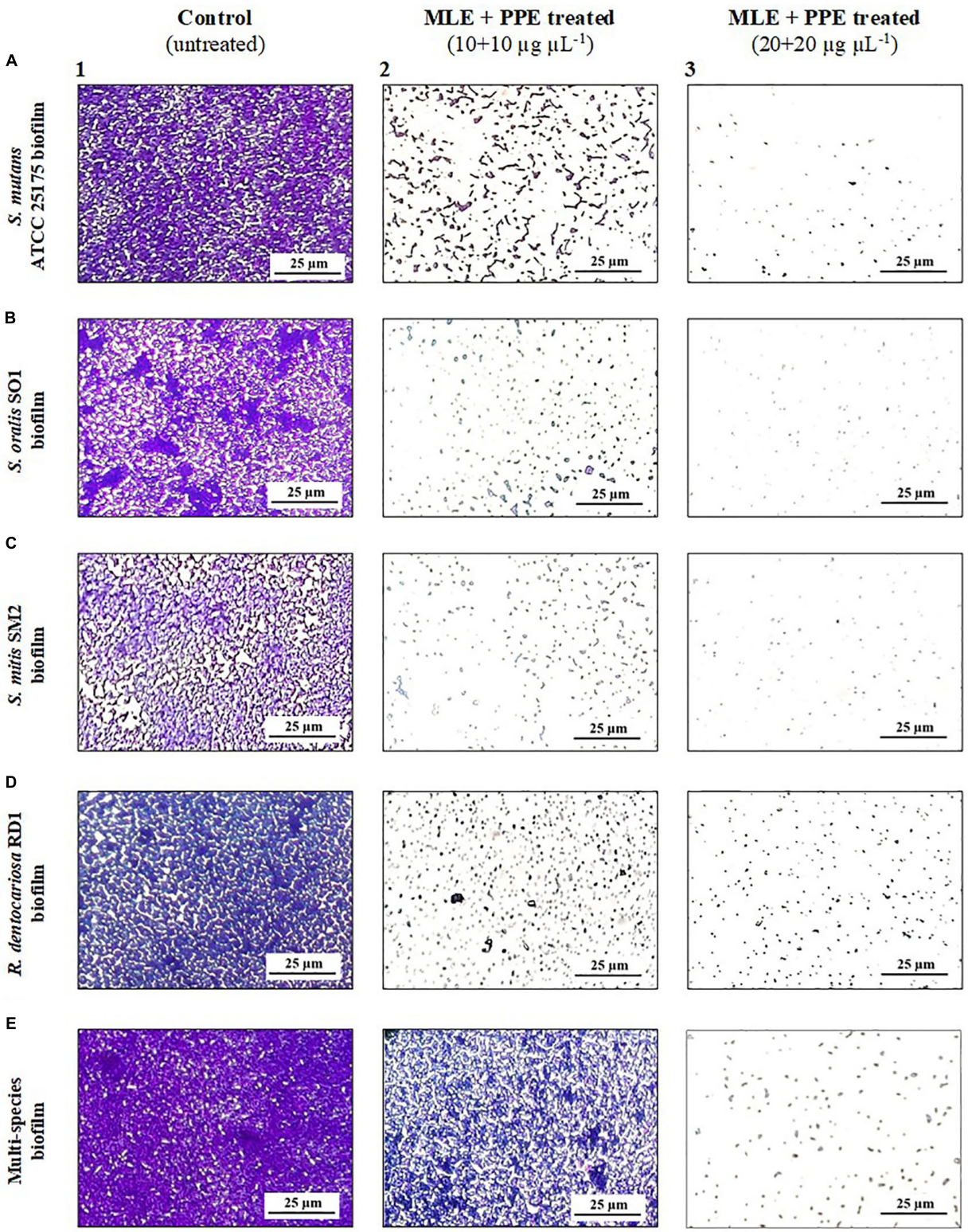

FIGURE 4 | Light microscopy images of mature *S. mutans* ATCC 25175 **(A)**, *S. oralis* SO1 **(B)**, *S. mitis* SM2 **(C)**, *R. dentocariosa* RD1 **(D)**, and multispecies **(E)** biofilms (1:1:1:1 ratio for each isolate) grown with and without treatment with myrtle extract in binary combination with pomegranate extract. Crystal violet staining; MLE + PPE, myrtle leaf 50% ethanolic extracts in binary combination with pomegranate peel 50% ethanolic extracts (1:1 ratio).

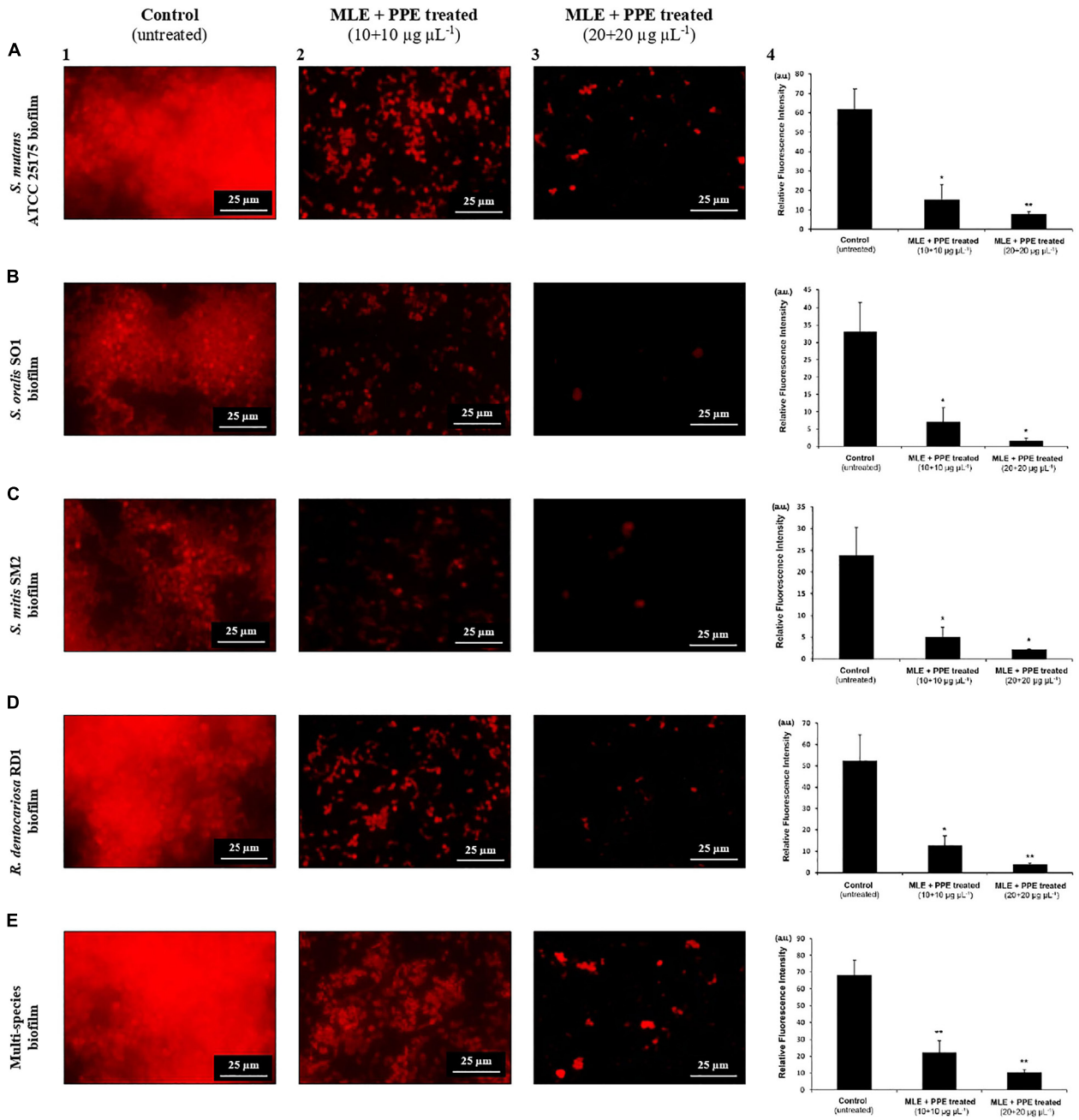

FIGURE 5 | Fluorescence microscopy images of mature *S. mutans* ATCC 25175 **(A)**, *S. oralis* SO1 **(B)**, *S. mitis* SM2 **(C)**, *R. dentocariosa* RD1 **(D)**, and multispecies **(E)** biofilms (1:1:1:1 ratio for each isolate) grown with and without treatment with myrtle extract in binary combination with pomegranate extract. PI staining; MLE + PPE, myrtle leaf 50% ethanolic extract in binary combination with pomegranate peel 50% ethanolic extract (1:1 ratio). Relative fluorescence intensity of biofilm architecture in the *S. mutans* ATCC 25175 (A4), *S. oralis* SO1 (B4), *S. mitis* SM2 (C4), *R. dentocariosa* RD1 (D4) and multispecies (E4) biofilms is reported in arbitrary unit (a.u.). Data are expressed as mean ± SE. $^{**}p < 0.001$,$^{*}p < 0.05$ compared to the control group.

DISCUSSION

In a previous work, the authors demonstrated that hydroalcoholic polyphenolic extracts of *M. communis* L. leaf and *P. granatum* L. fruit peel showed the ability to inhibit the growth and survival of cariogenic bacteria of dental plaque (Sateriale et al., 2020). Moreover, their remarkable synergistic effects, also in association with amoxicillin, have been demonstrated (Sateriale et al., 2020). The characterization of the hydroalcoholic pomegranate peel extract showed that the most abundant phenolic compounds include pedunculagin 1, punicalin, ellagic acid hexose, ellagic acid pentose, and ellagic acid deoxesose (Pagliarulo et al., 2016),

while gallic acid derivatives, tannins, myricetin, and quercetin derivatives are the most abundant phenolic compounds in hydroalcoholic extracts prepared from myrtle leaf (Sateriale et al., 2020). These results allowed us to design the goals of this study and to evaluate the antibiofilm activity of the same natural extracts in order to encourage their use as alternative options to prevent and treat oral infectious diseases, including biofilm-related ones.

Since adherence on oral surfaces is the first crucial step in biofilm formation in the oral cavity (Lendenmann et al., 2000), before analyzing the antibiofilm effects of myrtle and pomegranate extracts against dental plaque bacteria, the first objective of this work was to determine the ability of *S. mutans* ATCC 25175, *S. oralis* SO1, *S. mitis* SM2, and *R. dentocariosa* RD1 oral isolates to adhere and then to form biofilms. The results obtained by TM and TCPM methods showed the ability to form biofilm both on polystyrene tube walls and on polypropylene surface of 96-well microtiter plates, for all tested oral isolates. No oral isolates were indeed found to be negative for the TM test. In particular, *S. mutans* strain was shown to be strongly positive (+ + +), as well as the multispecies biofilm, while *S. oralis* and *R. dentocariosa* isolates were moderately positive (+ +), and finally the *S. mitis* isolate was weakly positive (+) (**Supplementary Table S1**). These results were confirmed by the quantification of microbial biofilm biomass through the recording of the OD (**Table 1**) at 600 nm by a microtiter reader. Interestingly, the high OD values measured for the *S. mutans* single biofilm (mean $OD_{600\ nm}$ of 0.506 ± 0.045) and for the multispecies biofilm (mean $OD_{600\ nm}$ of 0.607 ± 0.028) allow their classification as strongly adherent microbial isolates. *S. oralis* and *R. dentocariosa* isolates were moderately adherent, while the *S. mitis* isolate was weakly adherent. Both TM and TCPM proved to be effective methods to assess *in vitro* microbial biofilm formation by oral pathogens. However, given several disadvantages related to TM, in terms of major quantity of needed material for each sample and minor number of samples to test simultaneously, TCPM was preferred for subsequent assays. Crystal violet staining is a commonly used technique to quantify biofilm formation, thanks to its relatively easy execution, its reproducibility, and its ability to rapidly analyze multiple samples simultaneously (Stepanović et al., 2007; Agarwal et al., 2011; Liu et al., 2018). Considering these advantages and the interconnection between EPS production and microbial biomass amount in biofilms (Yallop et al., 2000), this staining has been selected as an adequate method to assess biofilm formation in the absence and in the presence of the natural extracts tested in this study. The first 12 h of biofilm formation was shown to correspond to the first adhesion stage, as indicated by the observed increase of OD values. With the increase in cell proliferation and the generation of extracellular matrix, the exponential growth was reached, coming to the plateau (or stationary phase) at about 18 h of monitoring, up to 48 h. No oral isolates showed significant differences in biofilm formation amount between 24 and 48 h of growth. These results, in accordance with other studies (Servetas et al., 2016; Mira et al., 2019), allow us to confirm that 24 h are enough to observe a stable biofilm growth by *S. mutans* ATCC 25175, *S. oralis* SO1, *S. mitis* SM2, and *R. dentocariosa* RD1 oral isolates and by their multispecies biofilm.

Subsequently, the antibiofilm activity of polyphenolic extracts against *S. mutans* ATCC 25175, *S. oralis* SO1, *S. mitis* SM2, and *R. dentocariosa* RD1 oral isolates was measured. Both 50% hydroethanolic myrtle leaf polyphenolic extracts (MLE) and pomegranate peel polyphenolic extracts (PPE) were able to inhibit the formation of biofilms made by all mentioned oral isolates, as well as to disrupt preformed 1-day biofilms. Interestingly, the binary combination of myrtle and pomegranate extracts (MLE + PPE) inhibited the biofilm formation and eradicated mature biofilm at lower concentrations with respect to the extracts individually tested.

These results suggest that the antibiofilm activity of polyphenolic myrtle leaf and pomegranate peel extracts, especially in binary combination, against *S. mutans* ATCC 25175, *S. oralis* SO1, *S. mitis* SM2, and *R. dentocariosa* RD1 oral isolates is in line with other studies that demonstrated the ability of *P. granatum* L. fruit peel and *M. communis* L. leaf extracts to inhibit the biofilm formation process and to disrupt preformed biofilms (Bakkiyaraj et al., 2013; Mansouri et al., 2013). The potential of the tested natural extracts in our study to prevent microbial adhesion could be closely linked to the antibiofilm properties of the extracted polyphenolic compounds. Interestingly, flavanols and flavonoids, such as rutin from myrtle extract, exhibited strong sortase inhibitory activity, thus interfering with the aptitude of bacteria to adhere to surfaces (Kang et al., 2006). In general, among the mechanisms underlying the antibacterial activity of polyphenols are the damage to the cytoplasmic membrane and the inhibition of nucleic acids and of energy metabolism but also the inhibition of cell membrane synthesis and cell wall synthesis (Cushnie and Lamb, 2011). As for the mechanisms behind the antibiofilm effects of polyphenols, although they are still unclear, they could be attributable to multiple factors acting in concert. The adhesion process to the surface can be influenced mainly by the physicochemical properties of the surface, but also by the bacterial characteristics and by environmental factors. The alteration of the bacterial surface could interfere with the normal cell–substrate interactions and compromise the attack phase and the normal biofilm development process (Simões et al., 2007). The researches on plant polyphenol antibiofilm activity have revealed several activities leading to biofilm suppression, for example, by affecting the bacterial regulatory mechanisms, such as quorum sensing (Silva et al., 2016) or by damaging the stability of the bacterial cytoplasmic membrane after inhibition of lipid metabolism (Rozalski et al., 2013). In addition, polyphenols could exert an aggregatory effect on bacterial cells, thus determining a preferred interaction of bacterial cells between themselves rather than with the surface (Cushnie et al., 2007). This could explain the ability of polyphenolic extracts to eradicate preformed biofilms, but future studies are needed to clarify their mechanisms of action. Regarding the synergistic antibiofilm effects of myrtle and pomegranate extracts, they could depend on their different polyphenolic contents and relative mechanisms of action. In particular, recent literature data showed that flavonoids, such as quercetin of myrtle extract, are

able to inhibit the activities of glucosyltransferases and F-ATPase, and the acid production by *S. mutans* cells, thus significantly affecting biofilm development and acidogenicity (Duarte et al., 2006), while gallic acid and tannins showed suppressive effect on *S. mutans* biofilm formation by inhibition of glucosyltransferase and fructosyltransferase (Sendamangalam et al., 2011). On the other hand, the mechanisms of action linked to antibiofilm activity of pomegranate polyphenolic extracts implicate both the precipitation of vital proteins involved in the formation of biofilms, such as adhesins, and the alteration of the cell surface charge thereby interfering with cell–substratum interactions and biofilm development, mediated by ellagic acid and ellagitannins, respectively (Liu et al., 2008).

In addition, to our knowledge, several studies demonstrated that pomegranate peel extracts do not exert cytotoxic effects on human fibroblast (Eid et al., 2015) and that could interfere with gingival fibroblast viability only at high concentrations (Celiksoy et al., 2020). Moreover, literature data reported that phytocompounds from *M. communis* L. leaves induce apoptosis only in cancer cell lines, but not in non-transformed human fibroblasts (Asgarpanah and Ariamanesh, 2015). In addition, the absence of cytotoxicity of myrtle derivatives is confirmed also by studies in humans. For example, the use myrtle paste was shown to be effective for increasing the quality of life of patients who suffer from painful oral condition, such as aphthous stomatitis, without toxic effects on mouth epithelial (Babaee et al., 2010). However, further research, including cytotoxicity assays and *in vivo* studies, is required to reach the practical application of these natural antimicrobials in clinical use to counteract oral biofilms.

In conclusion, this study opens toward new perspectives in using natural antimicrobial combined therapies against oral pathogens able to form biofilm. Although only some of the bacterial species forming the complex oral plaque community have been taken into consideration in this study, our data encourage the promotion of clinical trials for the development of innovative natural tools in the prophylaxis and treatment of biofilm-related oral diseases.

DATA AVAILABILITY STATEMENT

The raw data supporting the conclusions of this article will be made available by the authors, without undue reservation.

AUTHOR CONTRIBUTIONS

DS and CaP conceived the work. RI contributed to microscopy analyzes. RC, ChP, EV, MV, PS, and MP were involved in the data analysis, wrote and critically reviewed the manuscript. All authors read and approved the final manuscript.

FUNDING

This study was funded by the FRA 2019-2020.

ACKNOWLEDGMENTS

We would like to thank Prof. Gianmaria Fabrizio Ferrazzano, Department of Neuroscience, Reproductive and Oral Sciences, Section of Paediatric Dentistry, University of Naples Federico II, Naples, Italy, for kindly providing the dental plaque samples.

SUPPLEMENTARY MATERIAL

The Supplementary Material for this article can be found online at: https://www.frontiersin.org/articles/10.3389/fmicb.2020.592265/full#supplementary-material

REFERENCES

Agarwal, R. K., Singh, S., Bhilegaonkar, K. N., and Singh, V. P. (2011). Optimization of microtitre plate assay for the testing of biofilm formation ability in different *Salmonella* serotypes. *Int. Food Res. J.* 18:1493.

Ahmad, I., and Aqil, F. (2009). *New Strategies Combating Bacterial Infection*. Hoboken, NJ: John Wiley & Sons.

Ahmad, I., and Beg, A. Z. (2001). Antimicrobial and phytochemical studies on 45 Indian medicinal plants against multi-drug resistant human pathogens. *J. Ethnopharmacol.* 74, 113–123. doi: 10.1016/S0378-8741(00)00335-4

Aleksic, V., and Knezevic, P. (2014). Antimicrobial and antioxidative activity of extracts and essential oils of *Myrtus communis* L. *Microbiol. Res.* 169, 240–254. doi: 10.1016/j.micres.2013.10.003

Ansari, M. A., Khan, H. M., Khan, A. A., Cameotra, S. S., Saquib, Q., and Musarrat, J. (2014). Gum arabic capped-silver nanoparticles inhibit biofilm formation by multi-drug resistant strains of *Pseudomonas aeruginosa*. *J. Basic Microbiol.* 54, 688–699. doi: 10.1002/jobm.201300748

Aparna, M. S., and Yadav, S. (2008). Biofilms: microbes and disease. *Braz. J. Infect. Dis.* 12, 526–530. doi: 10.1590/S1413-86702008000600016

Asgarpanah, J., and Ariamanesh, A. (2015). Phytochemistry and pharmacological properties of *Myrtus communis* L. *Indian J. Traditional Knowl.* 14, 82–87.

Babaee, N., Mansourian, A., Momen-Heravi, F., Moghadamnia, A., and Momen-Beitollahi, J. (2010). The efficacy of a paste containing *Myrtus communis* (Myrtle) in the management of recurrent aphthous stomatitis: A randomized controlled trial. *Clin. Oral Investig.* 14, 65–70. doi: 10.1007/s00784-009-0267-3

Bakkiyaraj, D., Nandhini, J. R., Malathy, B., and Pandian, S. K. (2013). The anti-biofilm potential of pomegranate (*Punica granatum* L.) extract against human bacterial and fungal pathogens. *Biofouling* 29, 929–937. doi: 10.1080/08927014.2013.820825

Banas, J. A., Zhu, M., Dawson, D. V., Blanchette, D. R., Drake, D. R., Gu, H., et al. (2016). Acidogenicity and acid tolerance of *Streptococcus oralis* and *Streptococcus mitis* isolated from plaque of healthy and incipient caries teeth. *J. Oral Microbiol.* 8:32940. doi: 10.3402/jom.v8.32940

Ben Hsouna, A., Hamdi, N., Miladi, R., and Abdelkafi, S. (2014). Myrtus communis essential oil: Chemical composition and antimicrobial activities against food spoilage pathogens. *Chem. Biodivers.* 11, 571–580. doi: 10.1002/cbdv.201300153

Byers, H. L., Tarelli, E., Homer, K. A., and Beighton, D. (2000). Isolation and characterisation of sialidase from a strain of *Streptococcus oralis*. *J. Med. Microbiol.* 49, 235–244. doi: 10.1099/0022-1317-49-3-235

Caraher, E., Reynolds, G., Murphy, P., McClean, S., and Callaghan, M. (2007). Comparison of antibiotic susceptibility of *Burkholderia cepacia* complex

organisms when grown planktonically or as biofilm in vitro. *Eur. J. Clin. Microbiol. Infect. Dis.* 26, 213–216. doi: 10.1007/s10096-007-0256-x

Celiksoy, V., Moses, R. L., Sloan, A. J., Moseley, R., and Heard, C. M. (2020). Evaluation of the in vitro oral wound healing effects of pomegranate (*Punica granatum*) rind extract and punicalagin, in combination with Zn (II). *Biomolecules* 10:1234. doi: 10.3390/biom10091234

Chaieb, K., Kouidhi, B., Jrah, H., Mahdouani, K., and Bakhrouf, A. (2011). Antibacterial activity of Thymoquinone, an active principle of *Nigella sativa* and its potency to prevent bacterial biofilm formation. *BMC Complement. Altern. Med.* 11:29. doi: 10.1186/1472-6882-11-29

Chambless, J. D., Hunt, S. M., and Stewart, P. S. (2006). A three-dimensional computer model of four hypothetical mechanisms protecting biofilms from antimicrobials. *Appl. Environ. Microbiol.* 72, 2005–2013. doi: 10.1128/AEM.72.3.2005-2013.2006

Christensen, G. D., Simpson, W. A., Younger, J. J., Baddour, L. M., Barrett, F. F., Melton, D. M., et al. (1985). Adherence of coagulase-negative staphylococci to plastic tissue culture plates: A quantitative model for the adherence of staphylococci to medical devices. *J. Clin. Microbiol.* 22, 996–1006. doi: 10.1128/jcm.22.6.996-1006.1985

Costa, E. M., Silva, S., Tavaria, F. K., and Pintado, M. M. (2013). Study of the effects of chitosan upon *Streptococcus mutans* adherence and biofilm formation. *Anaerobe* 20, 27–31. doi: 10.1016/j.anaerobe.2013.02.002

Costerton, W., Veeh, R., Shirtliff, M., Pasmore, M., Post, C., and Ehrlich, G. (2003). The application of biofilm science to the study and control of chronic bacterial infections. *J. Clin. Investig.* 112, 1466–1477. doi: 10.1172/JCI200320365

Cowan, M. M. (1999). Plant products as antimicrobial agents. *Clin. Microbiol. Rev.* 12, 564–582. doi: 10.1128/cmr.12.4.564

Cushnie, T. P. T., and Lamb, A. J. (2011). Recent advances in understanding the antibacterial properties of flavonoids. *Int. J. Antimicrob. Agents* 38, 99–107. doi: 10.1016/j.ijantimicag.2011.02.014

Cushnie, T. P. T., Hamilton, V. E. S., Chapman, D. G., Taylor, P. W., and Lamb, A. J. (2007). Aggregation of *Staphylococcus aureus* following treatment with the antibacterial flavonol galangin. *J. Appl. Microbiol.* 103, 1562–1567. doi: 10.1111/j.1365-2672.2007.03393.x

Duarte, S., Gregoire, S., Singh, A. P., Vorsa, N., Schaich, K., Bowen, W. H., et al. (2006). Inhibitory effects of cranberry polyphenols on formation and acidogenicity of *Streptococcus mutans* biofilms. *FEMS Microbiol. Lett.* 257, 50–56. doi: 10.1111/j.1574-6968.2006.00147.x

Eid, H. A., Abo-Alazm, E. A., Mosleh, M. M., Alshahrani, M. A., Taha, T. H., El-Deeb, N. M., et al. (2015). Assessing the effects of different plant extracts on primary dental plaque colonizer and human fibroblast cells. *Asian J. Dentistry* 2:1025.

Ferrazzano, G. F., Scioscia, E., Sateriale, D., Pastore, G., Colicchio, R., Pagliuca, C., et al. (2017). In vitro antibacterial activity of pomegranate juice and peel extracts on cariogenic bacteria. *BioMed Res. Int.* 2017:2152749. doi: 10.1155/2017/2152749

Gibbons, S. (2005). Plants as a source of bacterial resistance modulators and anti-infective agents. *Phytochem. Rev.* 4, 63–78. doi: 10.1007/s11101-005-2494-9

Ismail, T., Sestili, P., and Akhtar, S. (2012). Pomegranate peel and fruit extracts: a review of potential anti-inflammatory and anti-infective effects. *J. Ethnopharmacol.* 143, 397–405. doi: 10.1016/j.jep.2012.07.004

Jung, J. E., Cai, J. N., Cho, S. D., Song, K. Y., and Jeon, J. G. (2016). Influence of fluoride on the bacterial composition of a dual-species biofilm composed of *Streptococcus mutans* and *Streptococcus oralis*. *Biofouling* 32, 1079–1087. doi: 10.1080/08927014.2016.1230607

Kang, S. S., Kim, J. G., Lee, T. H., and Oh, K. B. (2006). Flavonols inhibit sortases and sortase-mediated *Staphylococcus aureus* clumping to fibrinogen. *Biol. Pharm. Bull.* 29, 1751–1755. doi: 10.1248/bpb.29.1751

Keng, T. C., Ng, K. P., Tan, L. P., Chong, Y. B., Wong, C. M., and Lim, S. K. (2012). Rothia dentocariosa repeat and relapsing peritoneal dialysis-related peritonitis: a case report and literature review. *Renal Fail.* 34, 804–806. doi: 10.3109/0886022X.2012.678208

Khan, S. T., Ahamed, M., Musarrat, J., and Al-Khedhairy, A. A. (2014). Anti-biofilm and antibacterial activities of zinc oxide nanoparticles against the oral opportunistic pathogens Rothia dentocariosa and Rothia mucilaginosa. *Eur. J. Oral Sci.* 122, 397–403. doi: 10.1111/eos.12152

Koo, H., Falsetta, M. L., and Klein, M. I. (2013). The exopolysaccharide matrix: a virulence determinant of cariogenic biofilm. *J. Dent. Res.* 92, 1065–1073. doi: 10.1177/0022034513504218

Leid, J. G., Shirtliff, M. E., Costerton, J. W., and Stoodley, P. (2002). Human leukocytes adhere to, penetrate, and respond to *Staphylococcus aureus* biofilms. *Infect. Immun.* 70, 6339–6345. doi: 10.1128/IAI.70.11.6339-6345.2002

Lemos, J. A., Palmer, S. R., Zeng, L., Wen, Z. T., Kajfasz, J. K., Freires, I. A., et al. (2019). The Biology of *Streptococcus mutans*. *Microbiol. Spect.* 7:GPP3-0051-2018. doi: 10.1128/microbiolspec.gpp3-0051-2018

Lendenmann, U., Grogan, J., and Oppenheim, F. G. (2000). Saliva and dental pellicle–a review. *Adv. Dent. Res.* 14, 22–28. doi: 10.1177/08959374000140010301

Liu, L., Xu, Y., Cui, F., Xia, Y., Chen, L., Mou, X., et al. (2018). Monitoring of bacteria biofilms forming process by in-situ impedimetric biosensor chip. *Biosens. Bioelectron.* 112, 86–92. doi: 10.1016/j.bios.2018.04.019

Liu, Y., Gallardo-Moreno, A. M., Pinzon-Arango, P. A., Reynolds, Y., Rodriguez, G., and Camesano, T. A. (2008). Cranberry changes the physicochemical surface properties of E. coli and adhesion with uroepithelial cells. *Coll. Surf. B Biointerf.* 65, 35–42. doi: 10.1016/j.colsurfb.2008.02.012

Mansouri, S., Safa, A., Najar, S. G., and Najar, A. G. (2013). Inhibitory activity of Iranian plant extracts on growth and biofilm formation by *Pseudomonas aeruginosa*. *Malaysian J. Microbiol.* 9, 176–183.

Marsh, P. D. (2004). Dental plaque as a microbial biofilm. *Caries Res.* 38, 204–211. doi: 10.1159/000077756

Mira, A., Buetas, E., Rosier, B., Mazurel, D., Villanueva-Castellote, Á, Llena, C., et al. (2019). Development of an in vitro system to study oral biofilms in real time through impedance technology: validation and potential applications. *J. Oral Microbiol.* 11:1609838. doi: 10.1080/20002297.2019.1609838

Mitchell, J. (2011). *Streptococcus mitis*: walking the line between commensalism and pathogenesis. *Mol. Oral Microbiol.* 26, 89–98. doi: 10.1111/j.2041-1014.2010.00601.x

Neville, S. A., Lecordier, A., Ziochos, H., Chater, M. J., Gosbell, I. B., Maley, M. W., et al. (2011). Utility of matrix-assisted laser desorption ionization-time of flight mass spectrometry following introduction for routine laboratory bacterial identification. *J. Clin. Microbiol.* 49, 2980–2984. doi: 10.1128/JCM.00431-11

Nishikawara, F., Nomura, Y., Imai, S., Senda, A., and Hanada, N. (2007). Evaluation of cariogenic bacteria. *Eur. J. Dent.* 1, 31–39.

Pagliarulo, C., De Vito, V., Picariello, G., Colicchio, R., Pastore, G., Salvatore, P., et al. (2016). Inhibitory effect of pomegranate (*Punica granatum* L.) polyphenol extracts on the bacterial growth and survival of clinical isolates of pathogenic Staphylococcus aureus and *Escherichia coli*. *Food Chem.* 190, 824–831. doi: 10.1016/j.foodchem.2015.06.028

Peros, K., Mestrovic, S., Anic-Milosevic, S., and Slaj, M. (2011). Salivary microbial and nonmicrobial parameters in children with fixed orthodontic appliances. *Angle Orthodontist* 81, 901–906. doi: 10.2319/012111-44.1

Raghavendran, K., Mylotte, J. M., and Scannapieco, F. A. (2007). Nursing home-associated pneumonia, hospital-acquired pneumonia and ventilator-associated pneumonia: The contribution of dental biofilms and periodontal inflammation. *Periodontology* 2000, 164–177. doi: 10.1111/j.1600-0757.2006.00206.x

Rosenberg, M., Azevedo, N. F., and Ivask, A. (2019). Propidium iodide staining underestimates viability of adherent bacterial cells. *Sci. Rep.* 9:6483. doi: 10.1038/s41598-019-42906-3

Rosenbloom, R. G., and Tinanoff, N. (1991). Salivary *Streptococcus mutans* levels in patients before, during, and after orthodontic treatment. *Am. J. Orthod. Dentofacial Orthopedics* 32, 1079–1087. doi: 10.1016/0889-5406(91)70046-Y

Rozalski, M., Micota, B., Sadowska, B., Stochmal, A., Jedrejek, D., Wieckowska-Szakiel, M., et al. (2013). Antiadherent and antibiofilm activity of *Humulus lupulus* L. derived products: New pharmacological properties. *BioMed Res. Int.* 2013:101089. doi: 10.1155/2013/101089

Sateriale, D., Facchiano, S., Colicchio, R., Pagliuca, C., Varricchio, E., Paolucci, M., et al. (2020). *In vitro* synergy of polyphenolic extracts from honey, myrtle and pomegranate against oral pathogens, *S. mutans* and *R. dentocariosa*. *Front. Microbiol.* 11:1465. doi: 10.3389/fmicb.2020.01465

Savoia, D. (2012). Plant-derived antimicrobial compounds: alternatives to antibiotics. *Future Microbiol.* 7, 979–990. doi: 10.2217/fmb.12.68

Sendamangalam, V., Choi, O. K., Kim, D., and Seo, Y. (2011). The anti-biofouling effect of polyphenols against *Streptococcus mutans*. *Biofouling* 27, 13–19. doi: 10.1080/08927014.2010.535897

Servetas, S. L., Carpenter, B. M., Haley, K. P., Gilbreath, J. J., Gaddy, J. A., and Scott Merrell, D. (2016). Characterization of key *Helicobacter* pylori regulators identifies a role for arsrs in biofilm formation. *J. Bacteriol.* 198, 2536–2548. doi: 10.1128/JB.00324-16

Silva, L. N., Zimmer, K. R., Macedo, A. J., and Trentin, D. S. (2016). Plant natural products targeting bacterial virulence factors. *Chem. Rev.* 116, 9162–9236. doi: 10.1021/acs.chemrev.6b00184

Simões, L. C., Simþoes, M., Oliveira, R., and Vieira, M. J. (2007). Potential of the adhesion of bacteria isolated from drinking water to materials. *J. Basic Microbiol.* 47, 174–183. doi: 10.1002/jobm.200610224

Singh, N., Nayyar, A., Bhattacharjee, G., Singh, A. K., and Pruthi, V. (2012). Assessment of dentifrices against *Candida biofilm*. *Appl. Biochem. Biotechnol.* 167, 1688–1698. doi: 10.1007/s12010-012-9574-2

Slobodníková, L., Fialová, S., Rendeková, K., Kováč, J., and Mučaji, P. (2016). Antibiofilm activity of plant polyphenols. *Molecules* 21:E1717. doi: 10.3390/molecules21121717

Sogawa, K., Watanabe, M., Sato, K., Segawa, S., Ishii, C., Miyabe, A., et al. (2011). Use of the MALDI BioTyper system with MALDI-TOF mass spectrometry for rapid identification of microorganisms. *Anal. Bioanal. Chem.* 400, 1905–1911. doi: 10.1007/s00216-011-4877-7

Stepanović, S., Vuković, D., Hola, V., Di Bonaventura, G., Djukić, S., Ćirković, I., et al. (2007). Quantification of biofilm in microtiter plates: overview of testing conditions and practical recommendations for assessment of biofilm production by staphylococci. *APMIS* 115, 891–899. doi: 10.1111/j.1600-0463.2007.apm_630.x

Wenzel, R. P. (2007). Health care–associated infections: major issues in the early years of the 21st century. *Clin. Infect. Dis.* 45(Suppl. 1), S85–S88. doi: 10.1086/518136

Whalan, R. H., Funnell, S. G. P., Bowler, L. D., Hudson, M. J., Robinson, A., and Dowson, C. G. (2006). Distribution and genetic diversity of the ABC transporter lipoproteins PiuA and PiaA within *Streptococcus pneumoniae* and related streptococci. *J. Bacteriol.* 188, 1031–1038. doi: 10.1128/JB.188.3.1031-1038.2006

Whitchurch, C. B., Tolker-Nielsen, T., Ragas, P. C., and Mattick, J. S. (2002). Extracellular DNA required for bacterial biofilm formation. *Science* 295, 1487–1487. doi: 10.1126/science.295.5559.1487

WHO (2014). *Antimicrobial Resistance. Global Report on Surveillance*. Geneva: World Health Organization.

Yallop, M. L., Paterson, D. M., and Wellsbury, P. (2000). Interrelationships between rates of microbial production, exopolymer production, microbial biomass, and sediment stability in biofilms of intertidal sediments. *Microb. Ecol.* 39, 116–127. doi: 10.1007/s002489900186

Yang, C.-Y., Hsueh, P.-R., Lu, C.-Y., Tsai, H.-Y., Lee, P.-I., Shao, P.-L., et al. (2009). *Rothia dentocariosa* Bacteremia in children: report of two cases and review of the literature. *J. Form. Med. Assoc.* 37, 292–295. doi: 10.1016/s0929-6646(09)60364-8

Conflict of Interest: PS was employed by CEINGE.

The remaining authors declare that the research was conducted in the absence of any commercial or financial relationships that could be construed as a potential conflict of interest.

frontiers in Microbiology

OPINION
published: 11 November 2020
doi: 10.3389/fmicb.2020.592283

New Functional Criterion for Evaluation of Homologous MDR Pumps

Pavel A. Nazarov[1,2]*, *Alexandra I. Sorochkina*[1] and *Marina V. Karakozova*[3]

[1] Department of Bioenergetics, Belozersky Institute of Physico-Chemical Biology, Lomonosov Moscow State University, Moscow, Russia, [2] Laboratory of Molecular Genetics, Moscow Institute of Physics and Technology, Dolgoprudny, Russia, [3] Center of Life Sciences, Skolkovo Institute of Science and Technology, Moscow, Russia

Keywords: paralog, antibacterial drug, AcrAB-TolC, SkQ1, multidrug pump

INTRODUCTION

In recent years, bacterial resistance has become increasingly important for health care. With a simultaneous decrease in the number of newly registered antibacterial drugs, resistance to them is growing at an ever-higher rate, which makes the development of new drugs an expensive and ineffective undertaking. Therefore, creation of effective new antibacterial drugs is the most important task of modern Drug Development. Recently, several antibacterial drugs have been discovered (Khailova et al., 2015; Ling et al., 2015; Dibrov et al., 2017; Nazarov et al., 2017; Imai et al., 2019; Luther et al., 2019); however, for all of them, there are restrictions on the spectrum of action on bacteria. Some of them are active only toward gram-negative bacteria (Imai et al., 2019; Luther et al., 2019), while others toward gram-positive (Ling et al., 2015). However, for one of them (Khailova et al., 2015; Nazarov et al., 2017), the spectrum of action opened up as the antibiotic was being studied, from acting only toward gram-positive bacteria (Khailova et al., 2015), to acting on any bacteria, with the exception of those which had a certain AcrAB-TolC multidrug resistance pump (Nazarov et al., 2017, 2019).

The tripartite efflux system AcrAB-TolC is the main drug efflux transporter complex in *Escherichia coli* (Tam et al., 2020), which extrudes multiple antibiotics (erythromycin, oxacillin, ciprofloxacin, etc.), dyes (rhodamine 6G, ethidium, acridine, etc.), bile salts, detergents (SDS, taurocholate, berberine, tetraphenylphosphonium, etc.) and small organic molecules (hexane, indole, cyclohexane, etc.) (Pos, 2009). AcrAB–TolC is comprised of the outer membrane protein TolC, the periplasmic adaptor protein AcrA, and the inner membrane transporter AcrB from the resistance-nodulation-cell division (RND) superfamily (Shi et al., 2019).

Mitochondria-targeted antioxidant SkQ1 (decyl triphenylphosphonium-conjugated plastoquinone) is a member of a new class of antibiotics that directly affect bacterial bioenergetics. The use of synthetic non-targeted compounds has its own advantages and seems to be quite promising (Hards and Cook, 2018; Nazarov, 2018). SkQ1 is one of the most researched mitochondria-targeted antioxidants, and although the protective effect of SkQ1 and SkQR1 in acute bacterial infection has been well studied in an *in vitro* inflammation model and in an *in vivo* rat model of acute pyelonephritis in the presence of bacterial lysate (Plotnikov et al., 2013), it was believed that SkQ1 lacks antibiotic properties (Anisimov et al., 2011). However, although no antibacterial effect was observed against the classical model gram-negative bacterium *Escherichia coli*, an antibacterial effect was observed against another classical model gram-positive bacterium *Bacillus subtilis* (Khailova et al., 2015). In further studies (Nazarov et al., 2017), it was found that SkQ1 is effective as an antibacterial agent toward all the studied gram-positive bacteria, regardless of the structure of the bacterial cell envelope. Moreover, upon removal of any of the proteins of the AcrAB-TolC

OPEN ACCESS

Edited by:
Rodolfo García-Contreras, National Autonomous University of Mexico, Mexico

Reviewed by:
Divakar Sharma, Indian Institute of Technology Delhi, India
Anima Nanda, Sathyabama Institute of Science and Technology, India
Bernardo Franco, University of Guanajuato, Mexico

***Correspondence:**
Pavel A. Nazarov
nazarovpa@gmail.com; pasha@genebee.msu.ru

Specialty section:
This article was submitted to Antimicrobials, Resistance and Chemotherapy, a section of the journal Frontiers in Microbiology

Received: *06 August 2020*
Accepted: *20 October 2020*
Published: *11 November 2020*

Citation:
Nazarov PA, Sorochkina AI and Karakozova MV (2020) New Functional Criterion for Evaluation of Homologous MDR Pumps. Front. Microbiol. 11:592283. doi: 10.3389/fmicb.2020.592283

pump in *E. coli*, the bacterium completely lost its resistance against SkQ1 which became comparable to that of gram-positive bacteria (**Figure 1**). It should be noted that, according to modern concepts, the AcrAB-TolC pump contains not only the AcrA, AcrB, and TolC proteins, but also the small accessory protein AcrZ (Hobbs et al., 2012; Du et al., 2014). However, in the case of resistance to SkQ1, the deletion of the *acrZ* gene did not affect the resistance of *E. coli* (Nazarov et al., 2019). This suggested that the resistance depends on the presence of the AcrAB-TolC pump, but this observation turned to be preliminary. At this time, however, we can confirm that SkQ1 is expelled from cells by only one multidrug resistance pump under normal conditions. This fact makes SkQ1 an interesting and effective tool for studying pump performance, especially that of TolC-containing pumps.

SkQ1-BASED ANALYSIS OF PROTEINS COMPRISING TolC-CONTAINING PUMPS

In our studies (Nazarov et al., 2017, 2019), we analyzed all pumps containing TolC in relation to SkQ1 under conditions close to physiological in the cell. Although the important contribution of protein topogenesis and quality control of protein complexes to mitochondrial function is known (Luzikov, 2009), the topogenesis of bacterial membrane proteins is only beginning to be intensively studied (Mercier et al., 2020). However, the quality control of the assembled complexes is often not fully understood, therefore the effect of the absence of a pump component and its contribution to the formation of the bacterial membrane infrastructure cannot be precisely estimated. For example, deletion of TolC is known to cause changes in the expression of a number of membrane proteins, such as OmpF (Rosner and Martin, 2009) and can lead to metabolic shut-down (Dhamdhere and Zgurskaya, 2010). However, for most proteins of TolC-containing pumps, the effect on the phenotype has not been adequately studied.

Analysis of deletion mutants showed that loss of resistance occurs in the case of deletion of any of the proteins of the AcrAB-TolC pump (except AcrZ), thereby confirming the dependence of the resistance on the presence of the AcrAB-TolC pump in the bacterial membrane. Another important finding was the fact that under physiological conditions, none of the remaining pumps replaced the AcrAB-TolC function in its absence. This strikingly distinguishes bacterial pumps from eukaryotic ones, where pleiotropy is observed (Knorre et al., 2014), which may be one of the reasons for the greater resistance of both yeast and other eukaryotic cells to SkQ1.

Another important conclusion is the confirmation of the necessity of the AcrA protein for the functioning of the AcrAB-TolC pump. Although TolC protein interacts with both AcrA protein and AcrB protein (Symmons et al., 2009) and TolC can bind AcrB directly, in accordance with the current paradigm, the formation of the tripartite complex is initiated by TolC-AcrB binding and only stabilized by AcrA binding (Tikhonova et al., 2011), but without AcrA, the complex does not work properly. This observation is the first confirmation of the necessity of the AcrA protein in the formation of an active AcrAB-TolC pump. Moreover, this apparently excludes a significant role of the amino acid residues of the AcrA and TolC proteins in the formation of the active center of the AcrAB-TolC pump, since the AcrAD-TolC pump containing AcrA, TolC, and AcrD protein homologous to AcrB protein (66% sequence identity) is unable to pump out SkQ1 from bacterial cells (Nazarov et al., 2019).

ALL *ESCHERICHIA COLI* STRAINS DEMONSTRATED IDENTICAL RESISTANCE TO SkQ1

Escherichia coli strains are the most studied bacterial species with over a thousand complete or partial genome sequences, making them excellent subjects for analysis. Many of the *E. coli* strains have a long history of laboratory evolution and have undergone random or targeted mutagenesis. Strain B was described by d'Herelle at the Pasteur Institute in Paris in 1918 and strain K-12 was first isolated at Stanford University in 1922 (Karakozova and Nazarov, 2018). The genes coding for multidrug resistance pumps, such as AcrAB-TolC, are not essential, so multiple point mutations, partial or complete deletions are expected to occur in this class of genes. However, when analyzing the sequences of different laboratory strains, attention is drawn to the fact that the sequences of all three proteins AcrA, AcrB and TolC are identical for all strains and do not contain even a single substitution, despite the fact that the strains were isolated on different continents, countries, cities and research institutes (Karakozova and Nazarov, 2018). This suggests that we can assume identical resistance for all studied strains, which was confirmed in laboratory studies (Nazarov et al., 2019). Thus, despite the fact that the genes of the AcrAB-TolC pump are not essential, natural selection is aimed at maintaining the conservation of the amino acid sequences of these proteins, apparently due to their important function of clearing the bacterial cell from toxic components and the involvement of the AcrAB-TolC pump in the continuous "cleaning" of bacterial cells (Karakozova and Nazarov, 2018). Thus, significant substitutions in the sequences may lead to the loss of important functions in cell physiology of *E. coli* bacteria. This observation was confirmed in a recent work (Bhattacharyya et al., 2020), which demonstrated the key role of individual amino acid residues of AcrA and TolC in "necrosignal" recognition that activates swarm-specific resistance in an *E. coli* population. Thus, it can be assumed that the AcrAB-TolC pump may not only remove certain molecules from the cell, but also is a keystone element in regulatory processes important for the physiology of bacteria.

On the other hand, the nature of bacterial resistance to SkQ1 makes it possible to compare the level of resistance in independent experiments under different experimental conditions, normalizing the resistance to that of the *E. coli* strains.

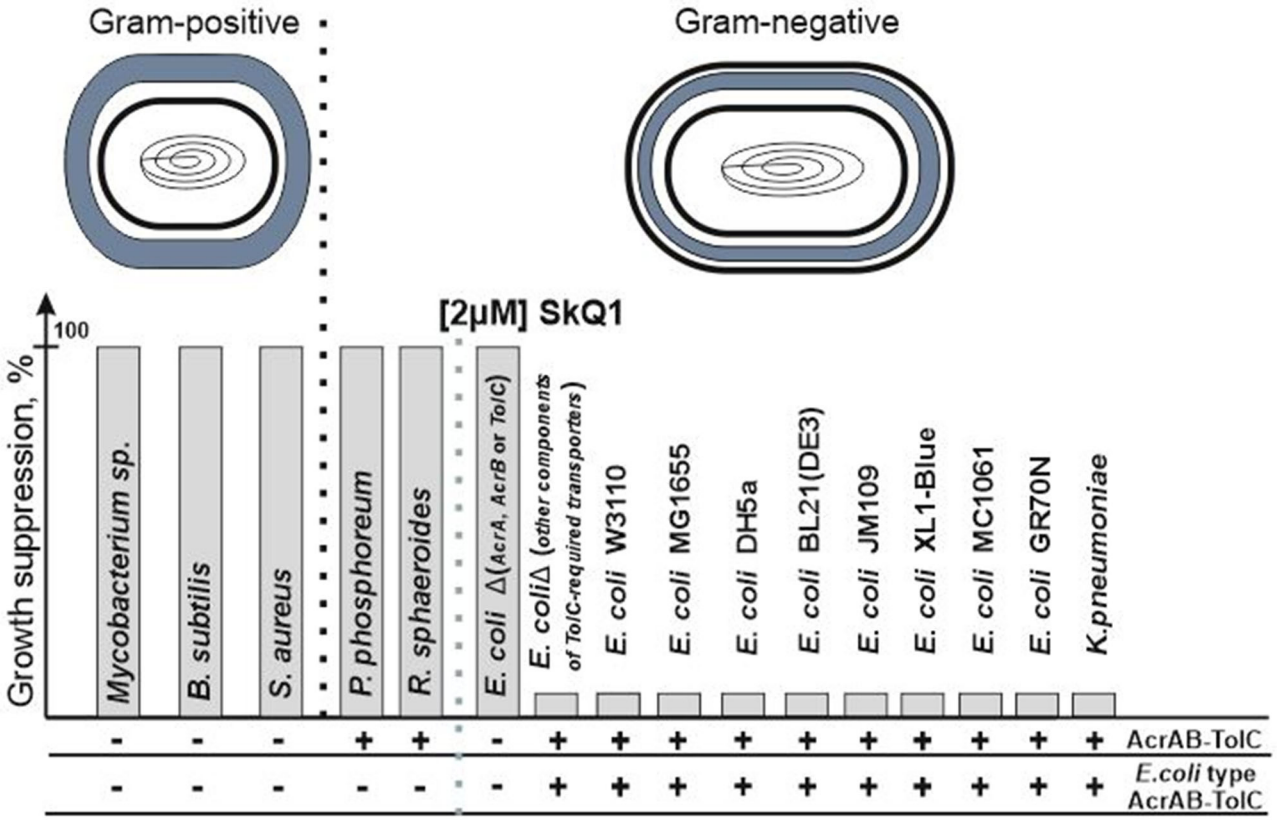

FIGURE 1 | SkQ1 resistance does not depend on the structure of the cell wall. The presence of all genes encoding AcrAB-TolC pump's proteins in the genome (AcrAB-TolC) and the presence of proteins similar (the identity is higher than the identity between the sequences of AcrD and AcrB proteins) to those from *E. coli* (*E. coli* type AcrAB-TolC) among them are marked as (+). Since AcrAB-TolC deletion mutants do not contain all proteins of the AcrAB-TolC pump and therefore the pump cannot be assembled in their cells, these bacteria are designated as (–). Deletions of genes encoding other TolC-containing pumps' proteins (for example, the AcrD gene from the AcrAD-TolC pump or the MdtE/MdtF genes from the MdtEF-TolC pump) did not lead to growth suppression.

AcrAB-TolC PUMP DOES NOT ENSURE SkQ1 RESISTANCE

We might assume that the presence of the AcrAB-TolC pump means that cells will be resistant to SkQ1, but this is not the case. Gram-negative bacteria *Rhodobacter sphaeroides* and *Photobacterium phosphoreum* that demonstrated sensitivity to SkQ1 also contained an AcrAB-TolC pump. This seeming paradox turned out to be easy to explain. AcrB protein sequences from *Rhodobacter sphaeroides* and *Photobacterium phosphoreum* demonstrate only 33 and 65% identity, respectively, to the AcrB protein sequence from *E. coli* (Nazarov et al., 2019). As mentioned above, sequence identity between AcrB and AcrD proteins is 66%, but the AcrAD-TolC pump cannot substitute for the AcrAB-TolC pump ability to remove SkQ1 from cells. It should be emphasized that when analyzing the entire tripartite complex, the overall sequence similarity between AcrAB-TolC pumps from different bacteria will decrease due to the difference in the sequences of other proteins (AcrA and TolC), while when comparing AcrAB-TolC and AcrAD-TolC from *E. coli,* the overall sequence similarity will increase. This allows us to assume that with <66% sequence identity of the AcrB protein, resistance to SkQ1 cannot be expected.

DISCUSSION

It is known that a conclusion that two or more genes or proteins are homologous is a conjecture, not an experimental fact (Koonin and Galperin, 2003). We can talk about homology, similarity, sequence identity, but the most important thing for comparing two protein pumps is whether we can say that they are functionally identical. A 33% identity may look quite significant, and if it met the criteria for homologous sequences (Koonin and Galperin, 2003), and the similarity extended over a long stretch of sequence, we would say that these are homologous protein sequences. However, we would not be able to say that these were functionally identical proteins because we missed one very important criterion – that of functional identity. It is clear that pumps can function on a variety of substrates, and

sequence changes can and appear to lead to changes in substrate specificity. While this is a relatively rare documented property, pumps appear to have a set of unique substrates, by which we mean a molecule or a group of molecules with similar structural patterns that are recognized by only one pump in a cell. If a unique pump substrate is available, a functionally identical pump will remove it regardless of its sequence identity. Lack of substrate specificity for unique substrates will indicate that the pump is no longer the same. Since SkQ1 is a unique substrate for AcrAB-TolC, the main MDR pump of *E. coli*, the loss of the ability to recognize and remove SkQ1 by bacteria is an evidence of the lack of a functional AcrAB-TolC pump. The ability to recognize and remove a unique substrate, however, does not guarantee the availability of a functional pump, and requires sequence comparison and application of criteria for sequence analysis (Koonin and Galperin, 2003).

However, what if SkQ1 was a unique substrate only for the *E. coli* AcrAB-TolC pump, and this was not applicable to other bacteria? Then we would observe resistance in the *E. coli* bacteria and sensitivity in all other gram-negative bacteria, as in the case of *R. sphaeroides* and *P. phosphoreum*. However, this is not supported by evidence, and the bacteria *Klebsiella pneumoniae* having an identity of 91.5% also demonstrates resistance comparable to *E. coli* (**Figure 1**) (Nazarov et al., 2019), which confirms the existence of a previously missing criterion for functionally homologous proteins.

Thus, proteins AcrB and AcrD from *E. coli* are genetic and functional paralogs, and proteins AcrB from *E. coli* and *K. pneumoniae* are genetic and functional orthologs. In turn, the AcrB proteins from *E. coli*, *R. sphaeroides*, and *P. phosphoreum* may be genetically orthologous, but functionally they are paralogs. Therefore, the presence of a similar pump cannot be a necessary and sufficient condition for establishing the presence of resistance for bacteria and the functional test is required.

AUTHOR CONTRIBUTIONS

PN: funding acquisition. PN, AS, and MK: writing. All authors have read and agreed to the published version of the manuscript.

FUNDING

The reported study was funded by the Russian Foundation for Basic Research (RFBR), project number 20-015-00537.

REFERENCES

Anisimov, V. N., Egorov, M. V., Krasilshchikova, M. S., Lyamzaev, K. G., Manskikh, V. N., Moshkin, M. P., et al. (2011). Effects of the mitochondria-targeted antioxidant SkQ1 on lifespan of rodents. *Aging* 3, 1110–1119. doi: 10.18632/aging.100404

Bhattacharyya, S., Walker, D. M., and Harshey, R. M. (2020). Dead cells release a 'necrosignal' that activates antibiotic survival pathways in bacterial swarms. *Nat. Commun*. 11:4157. doi: 10.1038/s41467-020-17709-0

Dhamdhere, G., and Zgurskaya, H. I. (2010). Metabolic shutdown in Escherichia coli cells lacking the outer membrane channel TolC. *Mol. Microbiol*. 77, 743–754. doi: 10.1111/j.1365-2958.2010.07245.x

Dibrov, P., Dibrov, E., Maddaford, T. G., Kenneth, M., Nelson, J., Resch, C., et al. (2017). Development of a novel rationally designed antibiotic to inhibit a nontraditional bacterial target. *Can. J. Physiol. Pharmacol*. 95, 595–603. doi: 10.1139/cjpp-2016-0505

Du, D., Wang, Z., James, N. R., Voss, J. E., Klimont, E., Ohene-Agyei, T., et al. (2014). Structure of the AcrAB-TolC multidrug efflux pump. *Nature* 509, 512–515. doi: 10.1038/nature13205

Hards, K., and Cook, G. M. (2018). Targeting bacterial energetics to produce new antimicrobials. *Drug Resist. Updat*. 36, 1–12. doi: 10.1016/j.drup.2017.11.001

Hobbs, E. C., Yin, X., Paul, B. J., Astarita, J. L., and Storz, G. (2012). Conserved small protein associates with the multidrug efflux pump AcrB and differentially affects antibiotic resistance. *Proc. Natl. Acad. Sci. U. S. A*. 109, 16696–16701. doi: 10.1073/pnas.1210093109

Imai, Y., Meyer, K. J., Iinishi, A., Favre-Godal, Q., Green, R., Manuse, S., et al. (2019). A new antibiotic selectively kills Gram-negative pathogens. *Nature* 576, 459–464. doi: 10.1038/s41586-019-1791-1

Karakozova, M. V., and Nazarov, P. A. (2018). Conserved sequences of genes coding for the multidrug resistance pump AcrAB-TolC of Escherichia coli suggest their involvement into permanent cell "cleaning". *Bull. RSMU* 2, 32–36. doi: 10.24075/brsmu.2018.024

Khailova, L. S., Nazarov, P. A., Sumbatyan, N. V., Korshunova, G. A., Rokitskaya, T. I., Dedukhova, V. I., et al. (2015). Uncoupling and toxic action of alkyltriphenylphosphonium cations on mitochondria and the bacterium Bacillus subtilis as a function of alkyl chain length. *Biochemistry* 80, 1589–1597. doi: 10.1134/S000629791512007X

Knorre, D. A., Markova, O. V., Smirnova, E. A., Karavaeva, I. E., Sokolov, S. S., and Severin, F. F. (2014). Dodecyltriphenylphosphonium inhibits multiple drug resistance in the yeast Saccharomyces cerevisiae. *Biochem. Biophys. Res. Commun*. 450, 1481–1484. doi: 10.1016/j.bbrc.2014.07.017

Koonin, E. V., and Galperin, M. Y. (2003). *Sequence - Evolution - Function: Computational Approaches in Comparative Genomics*. Boston: Kluwer Academic.

Ling, L. L., Schneider, T., Peoples, A. J., Spoering, A. L., Engels, I., Conlon, B. P., et al. (2015). A new antibiotic kills pathogens without detectable resistance. *Nature* 517, 455–459. doi: 10.1038/nature14098

Luther, A., Urfer, M., Zahn, M., Müller, M., Wang, S. Y., Mondal, M., et al. (2019). Chimeric peptidomimetic antibiotics against Gram-negative bacteria. *Nature* 576, 452–458. doi: 10.1038/s41586-019-1665-6

Luzikov, V. N. (2009). Principles of control over formation of structures responsible for respiratory functions of mitochondria. *Biochemistry* 74, 1443–1456. doi: 10.1134/S0006297909130021

Mercier, E., Wintermeyer, W., and Rodnina, M. V. (2020). Co-translational insertion and topogenesis of bacterial membrane proteins monitored in real time. *EMBO J.* 39:e104054. doi: 10.26226/morressier.5ebd45acffea6f735881aef4

Nazarov, P. A. (2018). Alternatives to antibiotics: phage lytic enzymes and phage therapy. *Bull. RSMU* 7, 5–15. doi: 10.24075/brsmu.2018.002

Nazarov, P. A., Kotova, E. A., Skulachev, V. P., and Antonenko, Y. N. (2019). Genetic variability of the AcrAB-TolC multidrug efflux pump underlies SkQ1 resistance in gram-negative bacteria. *Acta Nat*. 11, 93–98. doi: 10.32607/20758251-2019-11-4-93-98

Nazarov, P. A., Osterman, I. A., Tokarchuk, A. V., Karakozova, M. V., Korshunova, G. A., Lyamzaev, K. G., et al. (2017). Mitochondria-targeted antioxidants as highly effective antibiotics. *Sci. Rep*. 7:1394. doi: 10.1038/s41598-017-00802-8

Plotnikov, E. Y., Morosanova, M. A., Pevzner, I. B., Zorova, L. D., Manskikh, V. N., Pulkova, N. V., et al. (2013). Protective effect of mitochondria-targeted antioxidants in an acute bacterial infection. *Proc. Natl. Acad. Sci. U. S. A*. 110, E3100–E3108. doi: 10.1073/pnas.1307096110

Pos, K. M. (2009). Drug transport mechanism of the AcrB efflux pump. *Biochim. Biophys. Acta*. 1794, 782–793. doi: 10.1016/j.bbapap.2008.12.015

Rosner, J. L., and Martin, R. G. (2009). An excretory function for the *Escherichia coli* outer membrane pore TolC: upregulation of marA and soxS transcription and Rob activity due to metabolites accumulated in tolC mutants. *J. Bacteriol.* 191, 5283–5292. doi: 10.1128/JB.00507-09

Shi, X., Chen, M., Yu, Z., Bell, J. M., Wang, H., Forrester, I., et al. (2019). *In situ* structure and assembly of the multidrug efflux pump AcrAB-TolC. *Nat. Commun*. 10:2635. doi: 10.1038/s41467-019-10512-6

Symmons, M. F., Bokma, E., Koronakis, E., Hughes, C., and Koronakis, V. (2009). The assembled structure of a complete tripartite bacterial multidrug eflux pump. *Proc. Natl. Acad. Sci. U. S. A*. 106, 7173–7178. doi: 10.1073/pnas.0900693106

Tam, H. K., Malviya, V. N., Foong, W. E., Herrmann, A., Malloci, G., Ruggerone, P., et al. (2020). Binding and transport of carboxylated drugs by the multidrug transporter AcrB. *J. Mol. Biol.* 432, 861–877. doi: 10.1016/j.jmb.2019.12.025

Tikhonova, E. B., Yamada, Y., and Zgurskaya, H. I. (2011). Sequential mechanism of assembly of multidrug efflux pump AcrAB-TolC. *Chem. Biol.* 18, 454–463. doi: 10.1016/j.chembiol.2011.02.011

Conflict of Interest: The authors declare that the research was conducted in the absence of any commercial or financial relationships that could be construed as a potential conflict of interest.

frontiers in Microbiology

ORIGINAL RESEARCH
published: 17 November 2020
doi: 10.3389/fmicb.2020.606185

Porphyrin-Loaded Lignin Nanoparticles Against Bacteria: A Photodynamic Antimicrobial Chemotherapy Application

*Nidia Maldonado-Carmona[1,2], Guillaume Marchand[3], Nicolas Villandier[1], Tan-Sothea Ouk[1], Mariette M. Pereira[2], Mário J. F. Calvete[2], Claude Alain Calliste[3], Andrzej Żak[4,5], Marta Piksa[5], Krzysztof J. Pawlik[5], Katarzyna Matczyszyn[6] and Stéphanie Leroy-Lhez[1]**

[1] PEIRENE Laboratory, Faculty of Sciences and Techniques, University of Limoges, Limoges, France, [2] Laboratory of Catalysis and Fine Chemistry, Department of Chemistry, University of Coimbra, Coimbra, Portugal, [3] PEIRENE Laboratory, Faculty of Pharmacy, University of Limoges, Limoges, France, [4] Electron Microscopy Laboratory, Wrocław University of Science and Technology, Wrocław, Poland, [5] Institute of Immunology and Experimental Therapy, Polish Academy of Sciences, Wrocław, Poland, [6] Advanced Materials Engineering and Modelling Group, Faculty of Chemistry, Wrocław University of Science and Technology, Wrocław, Poland

OPEN ACCESS

Edited by:
Rodolfo García-Contreras, National Autonomous University of Mexico, Mexico

Reviewed by:
Eliana Alves, University of Aveiro, Portugal
Virginia Aiassa, National University of Córdoba, Argentina

***Correspondence:**
Stéphanie Leroy-Lhez
stephanie.lhez@unilim.fr

Specialty section:
This article was submitted to Antimicrobials, Resistance and Chemotherapy, a section of the journal Frontiers in Microbiology

Received: *14 September 2020*
Accepted: *20 October 2020*
Published: *17 November 2020*

Citation:
Maldonado-Carmona N, Marchand G, Villandier N, Ouk T-S, Pereira MM, Calvete MJF, Calliste CA, Żak A, Piksa M, Pawlik KJ, Matczyszyn K and Leroy-Lhez S (2020) Porphyrin-Loaded Lignin Nanoparticles Against Bacteria: A Photodynamic Antimicrobial Chemotherapy Application. Front. Microbiol. 11:606185. doi: 10.3389/fmicb.2020.606185

The need for alternative strategies to fight bacteria is evident from the emergence of antimicrobial resistance. To that respect, photodynamic antimicrobial chemotherapy steadily rises in bacterial eradication by using light, a photosensitizer and oxygen, which generates reactive oxygen species that may kill bacteria. Herein, we report the encapsulation of 5,10,15,20-tetrakis(4-hydroxyphenyl)-21H,23H-porphyrin into acetylated lignin water-dispersible nanoparticles (**THPP@AcLi**), with characterization of those systems by standard spectroscopic and microscopic techniques. We observed that **THPP@AcLi** retained porphyrin's photophysical/photochemical properties, including singlet oxygen generation and fluorescence. Besides, the nanoparticles demonstrated enhanced stability on storage and light bleaching. **THPP@AcLi** were evaluated as photosensitizers against two Gram-negative bacteria, *Escherichia coli* and *Pseudomonas aeruginosa*, and against three Gram-positive bacteria, *Staphylococcus aureus*, *Staphylococcus epidermidis*, and *Enterococcus faecalis*. **THPP@AcLi** were able to diminish Gram-positive bacterial survival to 0.1% when exposed to low white LED light doses (4.16 J/cm^2), requiring concentrations below 5 μM. Nevertheless, the obtained nanoparticles were unable to diminish the survival of Gram-negative bacteria. Through transmission electron microscopy observations, we could demonstrate that nanoparticles did not penetrate inside the bacterial cell, exerting their destructive effect on the bacterial wall; also, a high affinity between acetylated lignin nanoparticles and bacteria was observed, leading to bacterial flocculation. Altogether, these findings allow to establish a photodynamic antimicrobial chemotherapy alternative that can be used effectively against Gram-positive topic infections using the widely available natural polymeric lignin as a drug carrier. Further research, aimed to inhibit the growth and survival of Gram-negative bacteria, is likely to enhance the wideness of acetylated lignin nanoparticle applications.

Keywords: tetrapyrrolic compounds, valorized lignin, nanoparticles, photodynamic antimicrobial therapy, antimicrobial alternatives

INTRODUCTION

Antimicrobial resistance (AMR) upraise is one of the greatest challenges that modern medicine and chemistry are facing. After the "golden age of antibiotics," the decay on the discovery rate of new and more efficient molecules was conjugated with the appearance of antimicrobial-resistant strains. AMR alone is expected to cause 10 million deaths by 2050, with an accumulative cost of 100 trillion USD (O'Neill, 2016). However, this prediction only accounts for developed countries, and this number is expected to be higher and still to be determined, with the greatest impact on developing countries. The World Health Organization has devised a global action plan (WHO, 2015) emphasizing the necessity to find new antimicrobial alternatives and to improve disinfection processes, while exploring therapeutic approaches that are less prone to generate resistance (Lewis, 2013; Regiel-Futyra et al., 2017).

In that respect, photodynamic therapy (PDT) has revealed to be a suitable alternative. PDT is the conjugation of light and a photosensitizer molecule, generating reactive oxygen species (ROS) from either molecular oxygen in the media (Type II mechanism) or a substrate (Type I mechanism) (Josefsen and Boyle, 2012). When these ROS are directed against microorganisms, the process is addressed as photodynamic antimicrobial chemotherapy (PACT) (Wainwright, 2019). These *in situ*-generated ROS are able to destroy biomacromolecules, including proteins, membrane lipids, and nucleic acids, through a non-specific target mechanism (Wainwright et al., 2017). Commonly in PDT addressed against cancer, desired photosensitizers are molecules with strong absorption bands near the infrared range (700–900 nm), which coincides with the skin transparent wavelengths, and permit light to reach deeper through the skin (Josefsen and Boyle, 2012). In contrast, most of the applications of PACT are at surfaces or topic applications, thus photosensitizing molecules are not limited to absorption in the infrared range. Recent PACT applications have been developed for usage under white light (Nzambe Ta keki et al., 2016; Ringot et al., 2018; Aroso et al., 2019; Khaldi et al., 2019), blue light (Buchovec et al., 2016), and even solar light (Jia et al., 2019). Currently, PACT applications are actively pursued by several research groups, with applications in dentistry as a complement of systemic antibiotic treatments (de Freitas et al., 2016; Bechara Andere et al., 2018), as a non-invasive treatment against *Helicobacter pylori* (Baccani et al., 2019), and even as an environment-friendly alternative for active food packaging (i.e., biodegradable coatings for strawberries disinfection), food disinfection (i.e., curcumin derivatives for lettuce and mung beans disinfection), and other agronomical applications (i.e., porphyrinic insecticides and pesticides) (Riou et al., 2014; Buchovec et al., 2016; Glueck et al., 2017; Martinez et al., 2017).

In parallel, organic matrices (e.g., cellulose, chitosan, cyclodextrin) have been used for the transport and encapsulation of small molecules, with some examples of conjugating photosensitizers, enabling bacterial eradication and, in some cases, demonstrating a synergistic effect with the organic matrix (Hsieh et al., 2019; Maldonado-Carmona et al., 2020). In this regard, an organic matrix that has been neglected is lignin. Lignin is a natural aromatic polymer, representing up to 20–35% of the total lignocellulosic biomass, and it is usually a by-product of the paper industry. It is a polymer of p-coumaryl alcohol, coniferyl alcohol, and sinapyl alcohol units, whose proportions vary according to its botanic origin (Faix, 1991). Due to its chemical nature, it can withstand several chemical modifications, either through the creation of new chemically active sites or through the substitution of the already available ones (Calvo-Flores and Dobado, 2010; Duval and Lawoko, 2014; Wang et al., 2016; Figueiredo et al., 2018; Marchand et al., 2018). In addition to chemical modifications, different methods for the preparation of lignin-based nanomaterials had been developed. One of the main applications given to these nano-objects is the loading and release of active substances.

Understandably, lignin has not been widely used as a photosensitizing molecule's vehicle mainly due to the widely known antioxidant activity of lignin (Ponomarenko et al., 2015; Yang et al., 2016). To the best of our knowledge, only one approach is reported in literature using lignin-coated noble metal nanoparticles for *Staphylococcus aureus* and *Escherichia coli* photo-induced disinfection (Rocca et al., 2018). Another report has been found where lignin was linked to a phenyl porphyrin, resulting in a biopolymer with increased fluorescence, but no photodynamic approach was implied (Tse et al., 2019). Besides, lignin nanoparticles are demonstrated to be innocuous to *Chlamydomonas reinhardtii*, an aquatic microorganism, and to *Saccharomyces cerevisiae*, a eukaryotic cell model (Frangville et al., 2012). Additionally, they are demonstrated to be innocuous against Caco-2 cells (Alqahtani et al., 2019), a human colon carcinoma cell line. Among all the possible lignin modifications, lignin acetylation is widely described in the literature (Qian et al., 2014b). For instance, recent reports have demonstrated that acetylated Kraft and Organosolv lignins (**AcLi**) work as weak photosensitizers (Marchand et al., 2018) and that **AcLi** is also able to form spherical nanoparticles (Qian et al., 2014a,b; Marchand et al., 2020), further demonstrating the capability to transport active molecules (Zhou et al., 2019; Marchand et al., 2020).

Considering all the above, here we report the encapsulation of commercial 5,10,15,20-tetrakis(4-hydroxyphenyl)-21*H*,23*H*-porphyrin (**THPP**) inside acetylated lignin nanoparticles (**@AcLi**). The nanoparticles were characterized through transmission electron microscopy (TEM), dynamic light scattering (DLS), zeta potential, UV-vis absorption and fluorescence, and electron paramagnetic resonance (EPR) in order to evaluate their capacity to generate singlet oxygen. The nanoparticles were tested against three Gram-positive bacteria, *S. aureus* CIP 76.25, *Staphylococcus epidermidis* CIP 109562, and *Enterococcus faecalis* CIP 76.1170, and against two Gram-negative bacteria, *E. coli* CIP 53.126 and *Pseudomonas aeruginosa* CIP 76.110, under white LED light irradiation. Additionally, **THPP**-loaded **@AcLi** (**THPP@AcLi**) were evaluated for their stability over long storage periods, and their properties were assessed at different pH ranges.

MATERIALS AND METHODS

Materials and Microbiological Strains

Kraft lignin was kindly donated by the Université du Québec à Trois-Rivières, Canada. **THPP**, acetic anhydride, dry pyridine, and other reagents were purchased at Sigma-Aldrich (Lyon, France) and used as received, without further purification. *E. coli* CIP 53.126, *E. faecalis* CIP 76.1170, *P. aeruginosa* CIP 76.110, *S. aureus* CIP 76.25, and *S. epidermidis* CIP 109562 were obtained from the Institute Pasteur Collection (Institute Pasteur, Paris, France). All bacterial strains were kept frozen as small aliquots (100 µl), at −78°C, with glycerol 50% as cryopreservant. A whole aliquot was used for each culture, avoiding defrosting of the other samples. *P. aeruginosa* was grown in Luria–Bertani (LB) broth (tryptone 10 g/L, sodium chloride 10 g/L, yeast extract 5 g/L), while all the other bacterial strains were routinely growth at trypto-casein soy medium (TS, Biokar; tryptone 17 g/L, papaic digest of soybean meal 3 g/L, glucose 2.5 g/L, dipotassium phosphate 2.5 g/L, sodium chloride 2 g/L), prepared as a broth (LBB and TSB) or as a solid media (LBA and TSA; 1.7% agar) according to standard procedures. Saline solution (0.9% NaCl) and phosphate buffer pH 7 (PB pH 7, NaH_2PO_4 6.045 g/L, Na_2HPO_4 10.5 g/L) were routinely prepared and sterilized.

Preparation of Acetylated Lignin

AcLi was prepared according to previous publications (Marchand et al., 2018). A kraft lignin solution (50 mg/ml) was prepared in an acetic anhydride/dry pyridine (1:1) mixture and stirred at 25°C, under a calcium chloride ($CaCl_2$) trap, for 48 h. Then, the reaction mixture was poured onto 500 ml distilled water, and the precipitate was filtrated, dissolved on chloroform, and washed three times with distilled water. The organic phase was dried with $MgSO_4$ and evaporated to dryness.

Acetylated Lignin Characterization

Acetylated lignin was dissolved in acetonitrile, and its UV-vis absorption spectrum was recorded on a spectrophotometer Specord 210 Lambda (Analytik Jena) on quartz cells. FT-IR spectrum of materials was obtained using a Frontier PerkinElmer spectrometer in the attenuation total reactance analysis mode. Spectra were collected between 600 and 4,000 cm^{-1} after placing the pure product on a diamond crystal plate.

Preparation and Quantification of Acetylated Lignin Nanoparticles

Nanoparticles were prepared as previously described (Figueiredo et al., 2017). Acetylated lignin nanoparticles were prepared starting from an acetylated lignin solution (2 mg/ml) in acetone. For **THPP** encapsulation, **THPP** (0.2 mg/ml) was added in the acetonic solution. The AcLi solution was dialyzed on a regenerated cellulose membrane rod (Fisherbrand, 12–14 kDa) against distilled water for 24 h. After dialysis, nanoparticles were centrifuged at 10,000 × *g* for 1 h. Then, nanoparticles were washed with distilled water and centrifuged again. Finally, nanoparticles were suspended in distilled water and stored for further use. Routinely, after the harvest of **THPP@AcLi**, a small amount of nanoparticles was dissolved in acetone, and **THPP** quantification was done using the Soret band absorption (λ_{max} 419 nm, ε = 388,500 L/mol cm). Similarly, nanoparticles were dissolved in acetonitrile for AcLi quantification. The volume of dissolved nanoparticles was always below 3%, regarding the final volume on organic solvent. For **THPP@AcLi** analysis in aqueous media, nanoparticles were diluted on an appropriated buffer and their spectra were recorded. Spectra were collected between 200 and 800 nm. The encapsulation rate was calculated, as the ratio of the amount of **THPP** inside the nanoparticles, to the initial amount (Eq. 1):

$$Encapsulation\ rate\ (\%) = \frac{C_{THPP} V_{Np} MW_{THPP}}{THPP_i} \times 100 \qquad (1)$$

where C_{THPP} was the observed concentration of **THPP** in the final volume of nanoparticles (V_{Np}), considering the molecular weight of **THPP** (MW_{THPP}) and the initial mole number of **THPP** (**THPP**$_i$).

Apparent Size and Zeta Potential Analysis

Nanoparticle size was analyzed through DLS on a Zetasizer Nano-ZS (Malvern Instrument). Three measurements were performed on each sample at 20°C using a light scattering angle of 173° and a refractive index of 1.59 for lignins. Nanoparticles were diluted on distilled water for each DLS determination. The obtained DLS raw data were fit to a Gaussian model, excluding the values with less than 1% of presence. The obtained data were validated through the analysis of their R square coefficient and through the analysis of the residuals with a D'Agostino–Pearson Omnibus K2 test. With this statistical approach, we obtained the mean size (geometrical mean) and the standard deviation (σ), which allowed us to approximate the range where 95% of the nanoparticles were found (2σ). Zeta potential was obtained with the same equipment, and nanoparticles were diluted on an appropriated aqueous solution for each determination.

Transmission Electron Microscopy Observations

The samples were observed using the TEM, model H-800 (Hitachi), using an accelerating voltage of 150 kV. For nanoparticle imaging, a dense suspension of nanoparticles in water was used. Two microliters of each sample were deposited on carbon on the copper grid. The excess of liquid was carefully blotted with a filter paper and air-dried for 1 h. For bacterial and interaction observations, an overnight culture of *S. aureus* in TSB was washed with PB pH 7.4 (5,000 × *g*, 5 min) three times. Then, bacteria were carefully suspended on a minimal volume of buffer. After deposition of the 2 µl of the sample on grid and blotting, the samples were fixed and negative stained with 2 µl drop of 2% uranyl acetate deposited on the grid. The stain was blotted after 60 s, and the samples were air-dried for 1 h. For the interaction observations, 150 µl from the bacterial suspension was mixed with 150 µl of the nanoparticle suspension. Light irradiation was done with the 2 µl mixed sample on the TEM grid, under an incandescent lamp, with

light irradiation of around 2,500 lux for 5 min. After that, the samples were blotted and fixed as described above. The scheme of the preparation process is shown in **Supplementary Material 1**. For nanoparticle size determination, ImageJ Fiji (Schindelin et al., 2012; Schneider et al., 2012) software was used (Thresholding default, size 0.01–1.00 μm^2, circularity 0.06–1.00).

Stability of 5,10,15,20-Tetrakis(4-Hydroxyphenyl)-21H,23H-Porphyrin Inside Acetylated Lignin Nanoparticles

The stability of the encapsulation was tested over time. For this, a suspension of **THPP@AcLi** at 100 μM was prepared and divided in small 500-μl fractions, which were stored at 25°C in the dark. When analyzed, samples were centrifuged (10,000 × *g*, 30 min) and the supernatant was retired. The pelleted nanoparticles were resuspended in distilled water, and both nanoparticles and supernatants were analyzed by UV-vis absorption spectroscopy. The stability of the nanoparticles was followed through the changes of the Soret band absorption (λ_{max} 430 nm) over time in both nanoparticles and supernatants.

Singlet Oxygen Detection by Electron Paramagnetic Resonance

Measurements were recorded as described elsewhere (Riou et al., 2014). The samples were exposed to a 20 W halogen lamp, with a light irradiation of 20,000 lux. The intensity of illumination was measured by a lux meter (Digital Lux Tester YF-1065). EPR spectra were recorded with a Bruker Model ESP300E spectrometer operating at room temperature. Routinely, a fresh solution of 25 mM 2,2,6,6-tetramethylpiperidine (**TEMP**) was prepared in phosphate buffer pH 7.4. Acetylated lignin nanoparticle suspension was prepared at a concentration of 4 mg/ml of AcLi, while **THPP@AcLi** suspension was diluted at 120 μM of **THPP** or 0.2 mg/ml of AcLi. For singlet oxygen detection, 50 μl of the fresh **TEMP** solution were mixed with 50 μl of the nanoparticle suspension. The solution obtained was immediately transferred into quartz capillaries (100 μl) and placed at 20 cm from the source of illumination with a light intensity of 270 $\mu E/(s\ m^2)$ during periods of 5 min. A dark control was prepared, and rose Bengal in dimethylformamide (DMF) was used as a standard. EPR spectra were performed under the following conditions: modulation frequency, 100 kHz; microwave frequency, 9.78 GHz; microwave power, 4 mW; modulation amplitude, 0.987 G; time constant, 10.24 ms; scans number, 2.

Fluorescence Quantum Yield

Fluorescence quantum yield was calculated as described elsewhere (Vinagreiro et al., 2020). The fluorescence emission spectra were recorded in a Horiba Scientific Spectrofluorometer Fluoromax-4. The spectra were collected from 550 up to 800 nm using standard quartz cuvettes of 1 cm of optical path. Fluorescence quantum yields (Φ_F) were obtained by comparing the area of integrated fluorescence of the samples (F_s) with that of the reference (F_{ref}) compound, with known Φ_F, corrected by the absorption of sample (A_s) and reference (A_{ref}) at the excitation wavelength and by the refractive index of the solvents used for the sample (η_s) and reference (η_{ref}) solutions (Eq. 2).

$$\Phi_F = \Phi_F^{ref} \frac{F_s A_{ref} \eta_s^2}{F_{ref} A_s \eta_{ref}^2} \quad (2)$$

Tetraphenylporphyrin (**TPP**) in toluene (Φ_F ref = 0.11) was used as standard (Pineiro et al., 1998). The absorbance of the sample at the excitation wavelength was around 0.01.

Photobleaching Quantum Yield

Photobleaching experiments were done at similar conditions as those carried away for the microbiological experiments and following the procedure stated elsewhere (Vinagreiro et al., 2020). **THPP@AcLi** were diluted to a final concentration of 10 μM in PB pH 7. A volume of 200 μl (V_{irr}) was deposited on a flat-bottom 96-well plate (l = 1 cm) and irradiated, ensuring that all the light went through the solution. The samples were irradiated for a time Δ_t using a white LED light with emission (λ_{Em}) at 447 nm and output power P_0 of 1 mW. The actual light power absorbed was determined for each compound and properly taken into account in the calculation of the photobleaching quantum yield, as described in the **Supplementary Material 2** (Schaberle, 2018). Photobleaching quantum yield (Φ_{pb}) is defined as the ratio between the rate of disappearance of photosensitizer molecules (v_d) and the rate of absorption of photons (v_P) (Eq. 3).

$$\Phi_{Pb} = \frac{v_d}{v_p} = \frac{V_{irr} N_A h c \Delta A_{Soret}}{\varepsilon_{Soret} l \lambda_{Em} P (1 - 10^{-A_0}) \Delta_t} \quad (3)$$

where A_0 is the initial absorption at the Soret band. The Soret band absorbance was found to decrease, and its decay was followed during the light exposure.

Photodynamic Antimicrobial Chemotherapy Bacteriostatic Effect

The bacteriostatic effect was evaluated against planktonic bacteria in the middle of the exponential phase of growth. An aliquot of bacteria was inoculated in 5 ml of TSB or LB and incubated for 16 h, 37°C, 100 rpm. The OD_{600} was measured for the resulting culture, and it was diluted at an OD_{600} = 0.05 in 5 ml of fresh TSB or LB. Bacteria subcultures were incubated under the same previous conditions, during 2 h for *E. coli*, and 3 h for the other bacteria. Bacteria were washed with sterile PB pH 7 (5,000 × *g*, 5 min), and 100 μl were diluted in 10 ml of PB pH 7 for a final concentration of $\sim 10^6$ CFU/ml. Onto a 96-well plate, a volume of 50 μl of bacterial suspension was mixed with 50 μl of a solution with **THPP@AcLi** or **@AcLi**, at geometrically decreasing concentrations, ranging from 50 to 0.010 μM and 1.6 mg/ml to 6.25 μg/ml, respectively. The plate was irradiated under white LED light (1.2 mW/cm^2) for 1 h. A volume of 100 μl of TSB media was added to each well, and the initial OD_{595} (S_i) was acquired using an iMark multiplate reader (Bio-Rad). The plate was incubated at 37°C in the dark for 6 h, and then its OD_{595}

was measured again (S_t). Appropriated controls were prepared, a sample without bacteria and treatment (B_0) was used as a blank, while a sample without treatment was used as growth control and addressed as concentration zero (G_i) and followed over time (G_t). Normalized bacterial growth (G_B) was obtained according to Eq. 4.

$$G_B = \frac{S_t - S_i}{G_t - G_i} \quad (4)$$

A second 96-well plate was prepared, with bacteria and nanoparticles at the same concentrations and conditions and kept away from the light. Bacterial growth was allowed and monitored as the light-irradiated plate, becoming the dark control.

Photodynamic Antimicrobial Chemotherapy Bactericidal Effect

The bactericidal effect was evaluated against planktonic bacteria in the middle of the exponential phase of growth. An aliquot of bacteria was inoculated in 5 ml of TSB or LB and incubated for 16 h, 37°C, 100 rpm. The OD_{600} was measured and diluted at an OD_{600} = 0.05 in 5 ml of fresh TSB or LB. Bacteria subcultures were incubated under the same previous conditions for 2 h for *E. coli* and 3 h for the other bacteria. Bacteria were washed with sterile PB pH 7 (5,000 × *g*, 5 min) and suspended in 10 ml of PB pH 7 for a final concentration of $\sim 10^8$ CFU/ml. Onto a 96-well plate, a volume of 50 μl of bacterial suspension was mixed with 50 μl of a solution with **THPP@AcLi**, at geometrically decreasing concentrations, ranging from 2.5 to 0.010 μM, while **@AcLi** was only tested at 1.6 mg/ml, the highest concentration tested at the PACT bacteriostatic effect. Appropriated controls were prepared; a sample without nanoparticle treatment was used as a survival control. The plate was irradiated under white LED light (1.2 mW/cm^2) for 1 h. Besides, a second identical plate was prepared and kept away from light. Then, the solution on the wells was serially diluted on 900 μl of saline solution, and 50 μl were spread on TSA or LBA plates using an automatic plater EasySpiral (Interscience). Petri dishes were incubated at 37°C, in the dark, for 16 h. Colony-forming units (CFUs) were counted using a colony counter Scan 100 (Interscience). Bacterial survival was calculated, comparing the number of viable bacteria after the treatment (CFU/ml$_{Treatment}$) with the number of viable bacteria without treatment (CFU/ml$_{Control}$) (Eq. 5).

$$Bacterial\ survival\ (\%) = \frac{CFU/mL_{Treatment}}{CFU/mL_{Control}} \times 100 \quad (5)$$

Statistical Analysis

Experiments were performed at least in triplicate. The results were analyzed with GraphPad Prism 6.01. Biological data were analyzed with a two-way ANOVA using a Sidak's test for multiple comparisons with 95% of the cohort. The obtained DLS raw data were fit to a Gaussian model, excluding the values with less than 1% of presence. The obtained data were validated through the analysis of their R square coefficient and through the analysis of the residuals with a D'Agostino–Pearson Omnibus K2 test. With this statistical approach, we obtained the mean size (geometrical mean) and the standard deviation (σ), which allowed us to approximate the range of size that have 95% of the nanoparticles (D_{95}).

RESULTS

Preparation of Acetylated Lignin Nanoparticles and Their Physicochemical Characterization

AcLi was prepared as previously described (Marchand et al., 2018), and their chemical properties are discussed in **Supplementary Material 3**. Acetylated lignin nanoparticles were prepared as previously described (Figueiredo et al., 2017; Marchand et al., 2020) from an acetone solution (**Figure 1**). **THPP** encapsulation was done at similar conditions, through the addition of **THPP** into the acetone solution. In both cases, the acetone solution was dialyzed against water. The thereof obtained nanoparticles were centrifuged and suspended in distilled water.

THPP@AcLi suspension was analyzed with UV-vis absorption spectroscopy (**Figure 2**), and the spectroscopic data were summarized in **Table 1**. Due to the low aqueous solubility of **THPP**, the UV-vis spectrum of **THPP@AcLi** was compared with the spectra of **THPP** in dimethylsulfoxide (DMSO) and in a mixture of PB and DMSO (95/5 v/v), with the last simulating biological aqueous conditions. **THPP@AcLi** kept the typical porphyrin UV-vis absorption profile: one intense Soret band and four Q-bands at higher wavelengths. When compared with **THPP**, a red-shift of the Soret band in **THPP@AcLi** (λ = 430.5 nm) was observed compared with the observed Soret band in pure DMSO (λ = 424.5 nm). The observed red-shift and diminished absorbance that occurred were due to a solvatochromic effect and/or π-π interactions with the lignin aromatic core. Additionally, these features could also be due to the formation of **THPP** J-aggregates, as it has been previously described that, in the presence of water, **THPP** aggregates show a red-shifted Soret band with a diminished absorbance (Zannotti et al., 2018). **THPP** proneness to aggregate in aqueous medium was further corroborated with the observed wide and diminished Soret band for **THPP** in 5% DMSO. In addition, the appearance of extra bands at 457 nm (B-band) and at 701.5 nm (Q_c) indicates the presence of protonated **THPP** (**THPPH$_2^{2+}$**) species inside the nanoparticles (Zannotti et al., 2018; Leroy-Lhez et al., 2019). Moreover, it seems that encapsulation of **THPP** inside **AcLi** nanoparticles reduced the aggregated state when compared to **THPP** dissolved in a mixture of aqueous media/organic solvent, where we observed a broad Soret band with diminished absorption.

Given the presence of **THPPH$_2^{2+}$** species, further investigations on the effect of the pH on the loaded nanoparticles were deemed necessary. Thus, UV-vis absorption spectra of **THPP@AcLi** nanoparticles were recorded at several pH values using different buffers (0.1 M), as displayed in **Figure 3**. The **THPP@AcLi** UV-vis absorption profile remained stable at pH values above 4, as the proportion between the **THPP** and its protonated species **THPPH$_2^{2+}$** (expressed as ratio A_{457}/A_{430}) remained constant. Upon pH acidification, a change in the

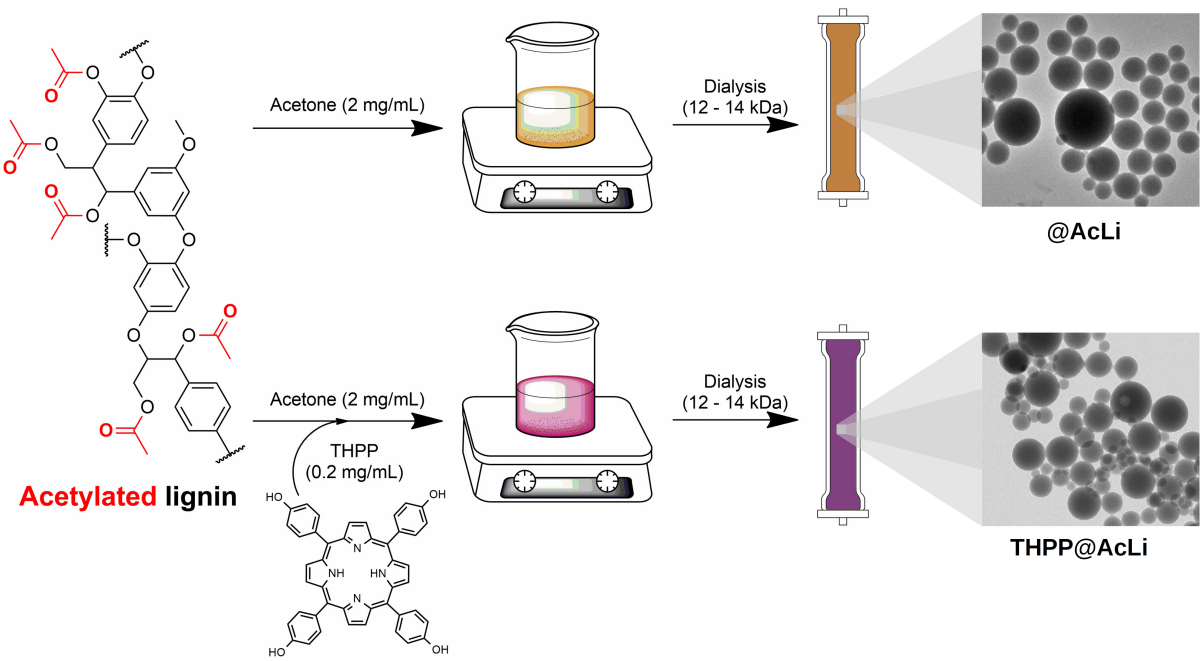

FIGURE 1 | Preparation of acetylated lignin nanoparticles **(@AcLi)** and 5,10,15,20-tetrakis(4-hydroxyphenyl)-21*H*,23*H*-porphyrin (**THPP**)-loaded **@AcLi** (**THPP@AcLi**).

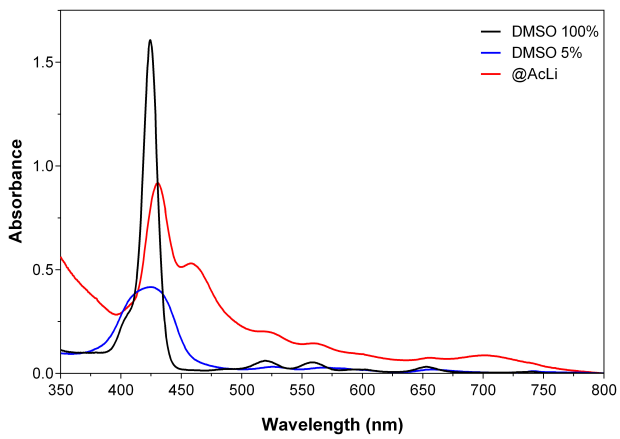

FIGURE 2 | Comparison of the UV-vis spectra of 5,10,15,20-tetrakis (4-hydroxyphenyl)-21*H*,23*H*-porphyrin **(THPP)** 5 μM in DMSO (DMSO 100%) in a mixture of PB pH 7 and DMSO 5% (DMSO 5%) and as **THPP**-loaded acetylated lignin nanoparticles **(THPP@AcLi)**, suspended in PB pH 7.

UV-vis absorption profile can be observed by a decrease of the absorbance at 430 nm with concomitant increase of the absorbance at 457 nm, reaching its maximum at pH 2, as depicted by the evolution of the ratio A_{457}/A_{430} (**Figure 3** inset, left axis). This, along with an increase of the absorbance at 701.5 nm, suggested an increased presence of protonated porphyrin $\mathbf{THPPH_2}^{2+}$ at values below pH 4. This experiment seems to corroborate the presence of both **THPP** and $\mathbf{THPPH_2}^{2+}$ species inside nanoparticles. Interestingly, neither at basic pH do the $\mathbf{THPPH_2}^{2+}$ related bands disappear, which either suggests the stability of the initial mixture or the solvent inaccessibility inside the nanoparticles. The last one has been previously analyzed through computational analysis on **@AcLi** formation, where nanoparticles have a lower solvent accessible surface area than lignin dissolved in organic solvent (Marchand et al., 2020). Nevertheless, **THPP** encapsulated inside **@AcLi** appears to be stable on a wide pH range (ca. 4–10), with its absorbance remaining unaffected by changes in the surrounding media.

Additionally, we could determine the amount of **THPP** encapsulated inside the nanoparticles through UV-vis quantification in acetone, as previously reported (Marchand et al., 2020). Our results demonstrated that up to 87.6% of the initial amount of **THPP** was encapsulated inside **@AcLi**; thus, the encapsulation process is not only sustainable but highly effective, allowing a good recovery of our photosensitizing molecule.

The size and shape of nanoparticles were also analyzed through two different methods, DLS and TEM. DLS indirectly permits to know the hydrodynamic size and the polydispersity index (PDI). The hydrodynamic size takes into account the presence of salts and water molecules surrounding the nanoparticles; thus, the size obtained is apparent and depends on the interaction of nanoparticles with the surrounding media. On the other hand, TEM observations directly analyze the size of opaque nanoparticles without taking into account the influence of the media; however, TEM observations need specialized software for image processing. In order to fully characterize the nanoparticles, both methods were compared for **THPP@AcLi** and **@AcLi** (**Figure 4**), with the results being summarized

TABLE 1 | Absorption bands of **THPP** 5 μM in DMSO 100%, PB and DMSO 5%, and as **THPP@AcLi** suspended in PB pH 7.

	Soret band		λ_{max} B	λ_{max} Q_1	λ_{max} Q_2	λ_{max} Q_3	λ_{max} Q_4	λ_{max} Q_C
	λ_{max}	ε_{max} (L/mol cm)						
DMSO	424.5	3.214×10^5		519.5	558.5	594.5	653	
PB pH 7 DMSO 5%	424.5	8.320×10^4		526	568.5	599.5	657	
PB pH 7 **@AcLi**	430.5	1.836×10^5	457	516.5	559.5	596.5	656	701.5

THPP, *5,10,15,20-tetrakis(4-hydroxyphenyl)-21H,23H-porphyrin;* ***THPP@AcLi, THPP****-loaded acetylated lignin nanoparticles.*

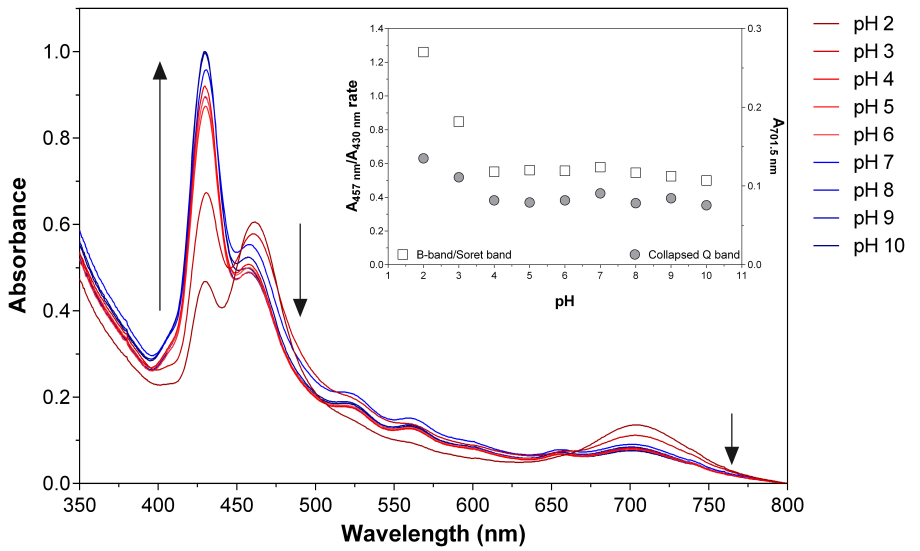

FIGURE 3 | Absorption spectra of 5.87 μM 5,10,15,20-tetrakis(4-hydroxyphenyl)-21*H*,23*H*-porphyrin-loaded acetylated lignin nanoparticles **(THPP@AcLi)** suspensions at different pHs [0.1 M glycine-HCl buffer (pH 2 and pH 3), 0.1 M acetate buffer (pH 4 and pH 5), 0.1 M phosphate buffer (0.1 M pH 6, pH 7, and pH 8), 0.1 M glycine-NaOH buffer (pH 9 and pH 10)]. The black arrows depict the changes found through increasing the pH of the media. Inset, the ratio of absorbance values at 457 and 430.5 nm (squares, left axis) and the absorbance at 701.5 nm (circles, right axis) are depicted as a function of pH.

in **Table 2**. The results obtained were compared under the assumption that the nanoparticle populations follow a Gaussian distribution. DLS and TEM analysis obtained similar size values for both nanoparticles (approximately 200 nm). In both cases, **@AcLi** were slightly smaller than **THPP@AcLi**, by less than 10 nm. When analyzed, the PDI values obtained were below 0.2, which indicates that the degree of size dispersion was in the desired range of reported nanoparticles (Danaei et al., 2018), as high PDI values describe a wide distribution in the size of the population and is associated to flocculation of the samples. The wideness of the size of the nanoparticles was analyzed through the comparison of the range where 95% of the nanoparticles were found (D_{95}). Both TEM and DLS analysis provided evidence that both populations had similar distributions, between 30 and 380 nm. These results were slightly different from those obtained by previous experiences (Marchand et al., 2020), where loaded nanoparticles have a smaller size than non-loaded nanoparticles. However, these differences could be due to differences in the workup of nanoparticles, as in the present work, nanoparticles are centrifuged at 10,000 × *g*.

In addition to size, another important parameter to characterize is the zeta potential. The zeta potential helps to describe both the apparent charge of a nanoparticle, as well as the stability of a colloidal suspension. As the apparent charge of a suspended particle, the zeta potential is deeply related to the presence of ions in the surrounding media and to its pH. Additionally, it allows us to understand the interactions of the particles with themselves and with other nano molecules that may lead to flocculation. Thus, the zeta potentials of **@AcLi** and **THPP@AcLi** were measured in PB pH 7 (−23.42 ± 2.17 and −17.00 ± 1.67, respectively). A negative charge was observed for both nanoparticles, and no significant difference was found between them (two-way ANOVA, Sidak's multiple comparison test, $P > 0.05$). As the values obtained for both nanoparticles were similar, it could be assumed that **THPP** did not exert an effect on the charge of the nanoparticle and in its zeta potential. Thus, for further analysis, nanoparticle zeta potential was measured at different pH values in 0.1 M buffers (**Figure 5**). Interestingly, both types of nanoparticles had a similar behavior, with an increase on the zeta potential value at pH 2, reaching a plateau and then decreasing at basic pH 9 and 10. However, we could observe that the addition of **THPP** into **@AcLi** nanoparticles leads to an increase on the zeta potential (Two-way ANOVA, Sidak's multiple comparison test, $P < 0.05$), excepting pH 7

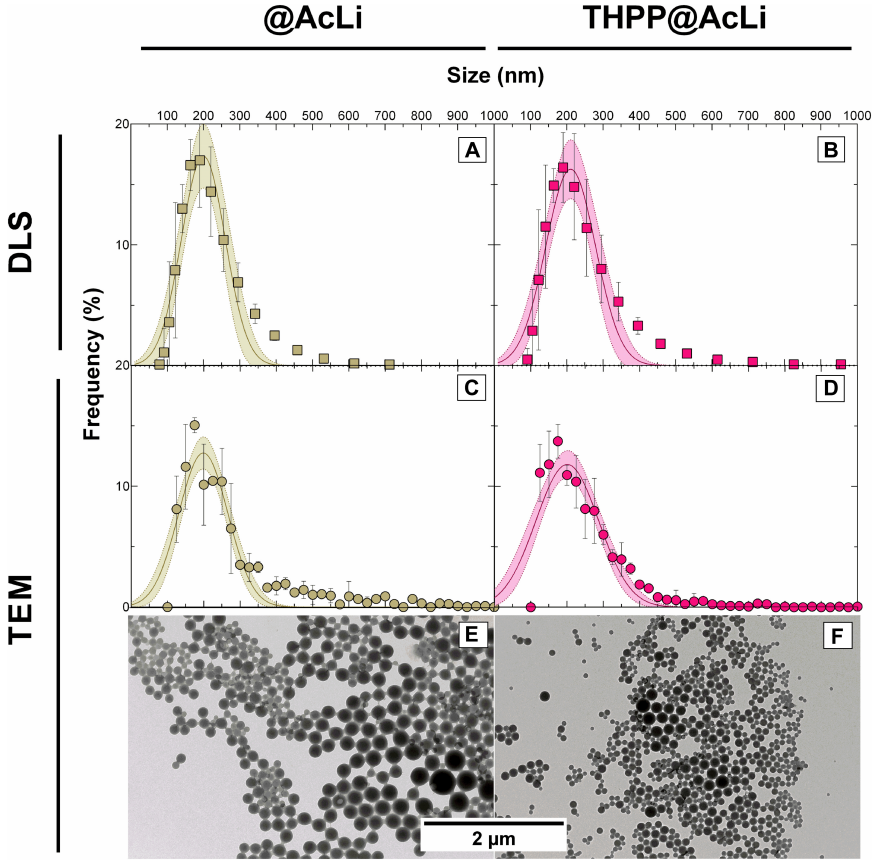

FIGURE 4 | Size distribution of acetylated lignin nanoparticles **(@AcLi)** and 5,10,15,20-tetrakis(4-hydroxyphenyl)-21*H*,23*H*-porphyrin-loaded @AcLi (**THPP@AcLi)** measured through dynamic light scattering (DLS) **(A,B)** and through transmission electron microscopy (TEM) **(C,D)**. Also, the spherical shape of nanoparticles is observed for both **(E,F)**.

and pH 8 (two-way ANOVA, Sidak's multiple comparison test, $P > 0.05$). The magnitude of the zeta potential can predict the stability of a colloidal suspension, being that suspensions with higher magnitudes of zeta potential tend to be more stable and less likely to flocculate (Kumar and Dixit, 2017). Thus, our findings indicate that at acidic pH, **@AcLi** are more likely to flocculate, reaching their highest stability in basic pH. As we found differences between **THPP@AcLi** and **@AcLi**, **THPP** exerts an effect in the apparent charge of the nanoparticles, increasing the likeness of nanoparticle flocculation, when compared with **@AcLi.**

To further demonstrate the viability of our process, we tested the stability of **THPP@AcLi** by monitoring the UV-vis absorption spectra of the nanoparticles suspended in PB pH 7, over 60 days, when stored in the dark at 25°C (**Supplementary Material 4**). **THPP@AcLi** demonstrated a high stability, with negligible **THPP** leaking, after 60 days of storage (9%). Additionally, the UV-vis profile did not change over time. Thus, **THPP@AcLi** withstood suspension in aqueous media in the dark and at 25°C, which makes it suitable for storage, without specific conditions in order to preserve the stability of the formulation.

TABLE 2 | Size of nanoparticles determined by DLS and TEM, expressed as the Gaussian mean and the distribution of 95% of the nanoparticles (D_{95}).

	DLS				TEM		
	Mean size (nm)	**Range (D_{95})**	**R^2 Gaussian model fitting**	**PDI**	**Mean size (nm)**	**Range (D_{95})**	**R^2 Gaussian model fitting**
@AcLi	199.6	79.02–320.18	0.9160	0.189	198.7	130.7–266.7	0.8410
THPP@AcLi	210.8	73.4–348.2	0.9154	0.176	200.6	114.16–287.4	0.8637

***@AcLi**, acetylated lignin nanoparticles; DLS, dynamic light scattering; PDI, polydispersity index; TEM, transmission electron microscopy; **THPP,** 5,10,15,20-tetrakis(4-hydroxyphenyl)-21H,23H-porphyrin; **THPP@AcLi, THPP**-loaded @AcLi.*

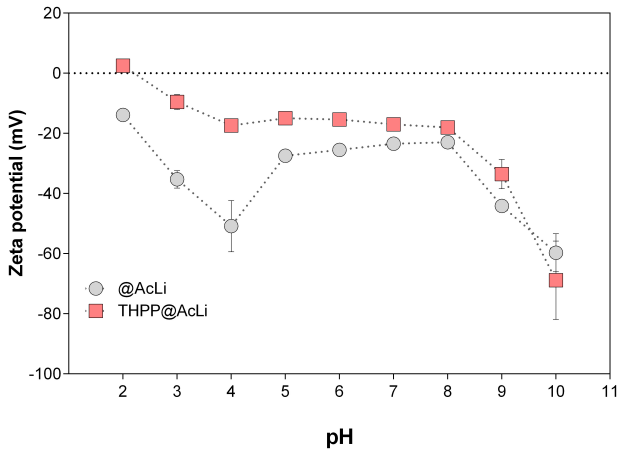

FIGURE 5 | The pH effect on the zeta potential of acetylated lignin nanoparticles **(@AcLi)** and 5,10,15,20-tetrakis(4-hydroxyphenyl)-21*H*,23*H*-porphyrin-loaded @AcLi **(THPP@AcLi)** [0.1 M glycine-HCl buffer (pH 2 and pH 3), 0.1 M acetate buffer (pH 4 and pH 5), 0.1 M phosphate buffer (0.1 M pH 6, pH 7, and pH 8), 0.1 M glycine-NaOH buffer (pH 9 and pH 10)].

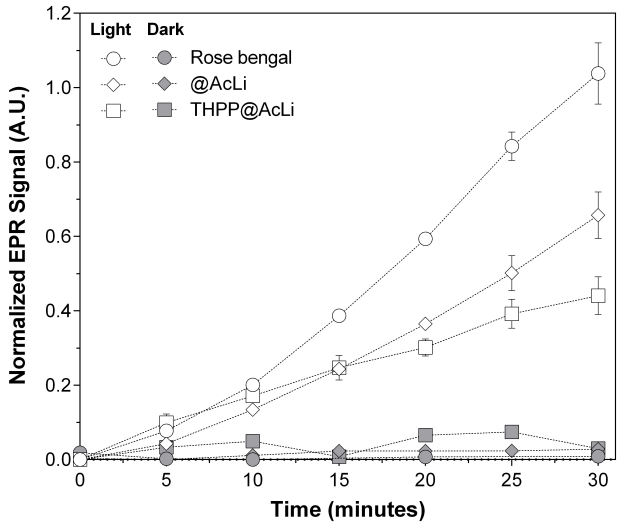

FIGURE 6 | Monitoring of singlet oxygen production, as 2,2,6,6-tetramethylpiperidine-1-oxyl (TEMPO) radical detection through electron paramagnetic resonance (EPR) of acetylated lignin nanoparticles **(@AcLi)** [2 mg/ml] (diamonds) and 5,10,15,20-tetrakis(4-hydroxyphenyl)-21*H*,23*H*-porphyrin-loaded @AcLi **(THPP@AcLi)** [**THPP** 60 μM, **AcLi** 100 μg/ml] (squares). Rose bengal [1.5 μM] (circles) was used as a reference. Singlet oxygen production was measured as a function of time under light irradiation (white symbols) or dark incubation (gray symbols).

Acetylated Lignin Nanoparticles Singlet Oxygen Production

It has been demonstrated that AcLi can produce ROS, specifically, singlet oxygen and superoxide anion (Marchand et al., 2018). We extrapolate these observations to the particular case of **@AcLi**, acting as photosensitizers in aqueous media and producing ROS. The singlet oxygen generated by **@AcLi** and **THPP@AcLi** was monitored by **TEMP** quenching, which easily

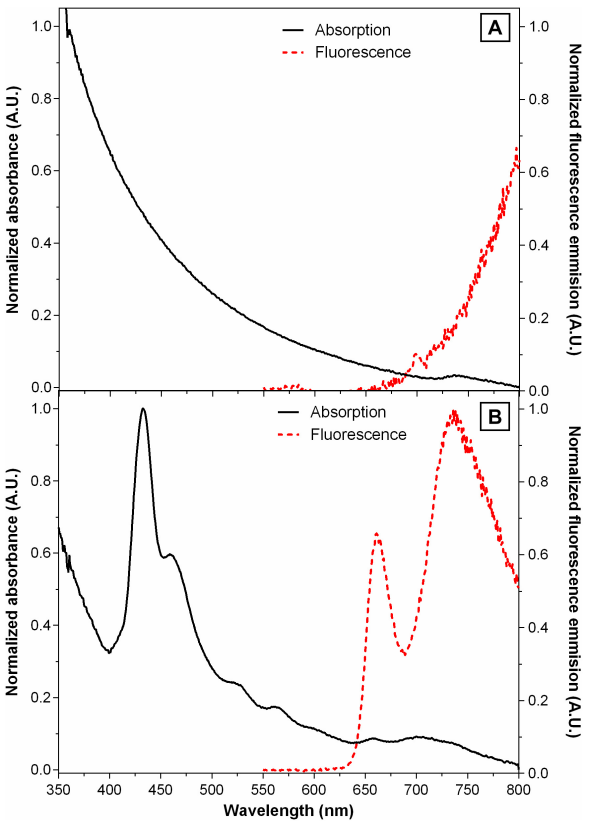

FIGURE 7 | Normalized UV-vis absorption spectra (black lines) and fluorescence emission spectra (red lines) of **(A)** acetylated lignin nanoparticles **(@AcLi)** [30 μg/ml] and **(B)** 5,10,15,20-tetrakis(4-hydroxyphenyl)-21*H*,23*H*-porphyrin-loaded **@AcLi (THPP@AcLi)** [**THPP** 2.5 μM, **AcLi** 30 μg/ml]; recorded in PB 0.1 M pH 7, room temperature, λ_{ex} = 425 nm.

reacts with singlet oxygen to form 2,2,6,6-tetramethylpiperidine-1-oxyl (**TEMPO**), a stable radical that can be detected with EPR spectroscopy (Riou et al., 2014; Marchand et al., 2018). In **Figure 6**, the nanoparticle suspensions in PB pH 7.4 of **@AcLi** (2 mg/ml) and **TPPOH@AcLi** (100 μg/ml lignin, 60 μM **THPP**) were compared, with or without light irradiation [halogen lamp, 270 μE/(s m^2)]. Rose bengal (1.5 μM, DMF), a well-known photosensitizer and singlet oxygen generator, was used as a reference. It is worth mentioning that the concentration of **@AcLi** nanoparticles was 20 times superior to that of **THPP@AcLi** but showed similar singlet oxygen generation, meaning that **THPP@AcLi** is approximately 20 times more efficient at producing singlet oxygen under the tested conditions. Both **@AcLi** and **THPP@AcLi** singlet oxygen was light-driven, corroborated by the differences observed between the dark and light irradiated samples, after 30 min (two-way ANOVA, Sidak's multiple comparison test, $P < 0.01$). The more efficient generation of singlet oxygen of **THPP@AcLi**, compared with **@AcLi**, demonstrated that **THPP** keeps its photosensitizing activity after encapsulation. Remarkably, the singlet oxygen produced by the encapsulated **THPP** is able to diffuse outside the nanoparticles, react with TEMP, and form the more stable TEMPO radical.

Acetylated Lignin Nanoparticle Fluorescence

It has been previously documented that molecular aggregation due to water coordination is a fluorescence quencher for porphyrins (Zannotti et al., 2018), a quantum phenomenon that is competitive with singlet oxygen production. To evaluate the extent of this issue, the fluorescent emission spectra of **@AcLi** (30 μg/ml) and **THPP@AcLi** (**THPP** 2.5 μM, **AcLi** 30 μg/ml) were measured as suspended in PB pH 7, with excitation at 425 nm (**Figure 7**).

Previous reports indicate that different chemical derivatives of lignin are fluorescent (Donaldson and Radotic, 2013). However, most of these observations have been done in organic solvents, where lignin is deployed without aggregation. Reports in the literature indicate that the fluorescence of lignin depends on the degree of aggregation, as the architecture of the nano-objects affects the interaction of the fluorophores (Xue et al., 2020). However, most of the studies on lignin fluorescence have been done with excitation wavelengths on the UV region, where lignin was known to strongly absorb. In our studies, we aimed at exciting the porphyrin, thus using excitation wavelength in the 400–500 nm range, where lignin did not absorb significantly. Thus, it is not surprising that a defined fluorescence band was not found for **@AcLi**; therefore, AcLi contribution to the fluorescence of **THPP@AcLi** was negligible in the tested conditions.

The **THPP@AcLi** emission spectrum, after excitation at 425 nm, showed two main peaks, a defined peak at 663 nm and a stronger less defined peak at around 733 nm. Additional experiments (**Supplementary Material 5**) showed that the peak found at 663 nm corresponds to **THPP** emission, while the peak at 733 nm could correspond to both **THPP** and $\mathbf{THPPH_2}^{2+}$ centered emission, as evidenced by the corresponding excitation spectra. The calculated quantum yield (Φ_F) for **THPP@AcLi** is 0.0016 ± 0.0001, a value that is lower than the one reported for **THPP** (Φ_F = 0.17, DMF) (Ormond and Freeman, 2013). Nevertheless, the obtained fluorescence still represents a success, as previous experiments have demonstrated that the fluorescence of **THPP** in aqueous media (Φ_F = 0.00071, PB pH 7, with 2.5% DMSO) is almost completely quenched. Thus, the encapsulation of **THPP@AcLi** partially prevented the quenching of **THPP** in aqueous medium and additionally avoided the usage of organic solvents to increase the availability of **THPP**.

Porphyrin's fluorescence is sensitive to the medium, especially to the pH (Zannotti et al., 2018; Leroy-Lhez et al., 2019). Previously in this work, we have demonstrated that **THPP@AcLi** were resistant to the fluctuation of pH in the media, according to UV-vis absorption and zeta potential studies. To further corroborate our findings, the fluorescence emission of **THPP@AcLi** was also recorded at different pH values (**Figure 8**). We could observe a pronounced decrease of fluorescence intensity with pH at 663 nm (**Figure 8**, inset), while the intensity of the fluorescence of the second band remained stable. Concomitantly, a red-shift of the wavelength of emission for this second band was also observed (from 733 nm at pH 10 to 745 nm at pH 2). This was not surprising as the peak at 663 nm is related to **THPP**, which in acidic media transforms into the protonated species $\mathbf{THPPH_2}^{2+}$; meanwhile, the second peak was related to both species and was thus affected by the equilibrium between **THPP** and $\mathbf{THPPH_2}^{2+}$ as a function of pH. Therefore, at a low pH value, $\mathbf{THPPH_2}^{2+}$ must be the predominant species, characterized by an emission at higher wavelength than **THPP**. However, when Φ_F was calculated for the whole pH range, it was found that besides variations on the emission profile, Φ_F remained stable (∼0.16) (**Supplementary Material 6**). This is consistent with our previous results, where we observed changes on the absorption spectra at acidic conditions. Nevertheless, the global quantum yield remained stable at different pHs.

Photodynamic Antimicrobial Chemotherapy Effect of Porphyrin-Loaded Nanoparticles Against Bacteria

The nanoparticles were tested against five bacterial strains, three Gram-positive (*S. aureus*, *S. epidermidis*, and *E. faecalis*) and two Gram-negative (*E. coli* and *P. aeruginosa*). The highest concentration of **THPP** encapsulated in **@AcLi** was 50 μM, corresponding to 0.33 mg/ml of **AcLi.** For **@AcLi**, the highest concentration used was 1.6 mg/ml; reports in the literature indicate that at this concentration, lignin nanoparticles were innocuous to human cells (Alqahtani et al., 2019). The results found in this study showed that **@AcLi** have a bacteriostatic effect at 1.6 mg/ml; nevertheless, **@AcLi** do not have a bactericidal effect at the highest concentration tested (**Supplementary Material 7**).

First, **THPP@AcLi** were evaluated as bacteriostatic agents, analyzing its capability to arrest bacterial growth. **THPP@AcLi** demonstrated a high capacity to diminish the growth of Gram-positive bacteria, after 1 h of irradiation, under a white LED light dose (4.16 J/cm^2). For Gram-positive inactivation, concentrations as low as 0.078 μM were enough to diminish growth at around 85% (**Figure 9A**). On the other hand, **THPP@AcLi** was not able to diminish the growth of Gram-negative *E. coli* but seemed to exert a bacteriostatic non-photodynamic effect on *P. aeruginosa* (**Figure 9B**). The most sensitive strain was *S. epidermidis*, followed by *E. faecalis* and, lastly, *S. aureus*. Usually, in PACT, low dark toxicities are desired, as it ensures that the antimicrobial effect is only triggered by light irradiation. Our results fulfill this necessity, as when using 0.640 μM of **THPP@AcLi**, the bacterial growth of *E. faecalis* was less than 10% after light irradiation; meanwhile, at dark incubation, the bacterial growth in the dark was around 85%. Similar results were found with *S. aureus* and *S. epidermidis* (**Supplementary Material 8**).

Although it can be addressed that growth arrest was due to the cellular death, it can also be provoked by a decrease on the bacterial metabolism or due to cellular damage, which may be overcome with enough recovery time. The difference between bacteriostatic and bactericidal effect is dose-dependent. Thus, the bacterial survival was assessed under similar conditions. As previously observed, **THPP@AcLi** was not effective against Gram-negative bacteria (**Supplementary Material 8**). Indeed, **THPP@AcLi** was unable to diminish the Gram-negative bacterial survival rate at 50 μM either at light (white LED light dose,

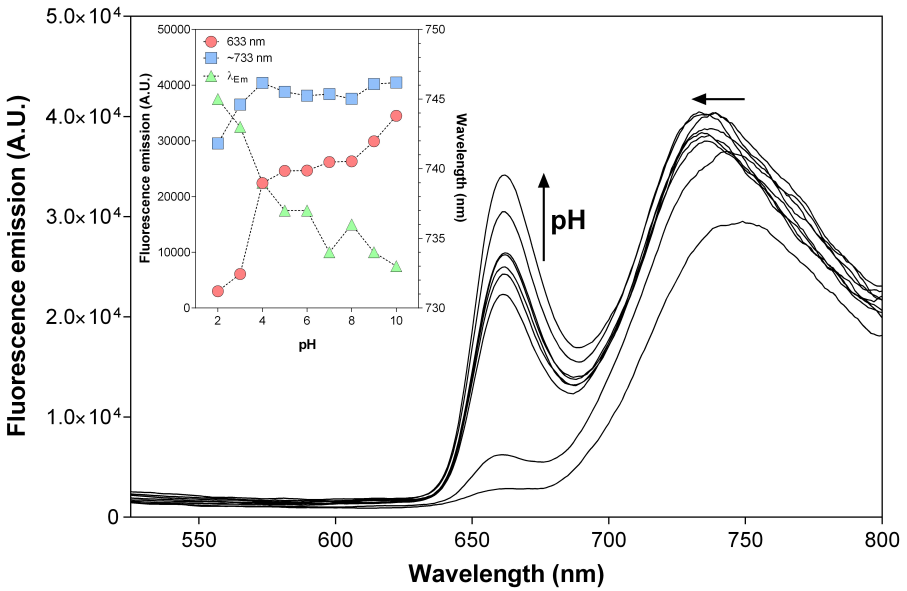

FIGURE 8 | Emission spectra of 5,10,15,20-tetrakis(4-hydroxyphenyl)-21*H*,23*H*-porphyrin-loaded acetylated lignin nanoparticles **(THPP@AcLi)** [3 μM], as a function of pH [0.1 M glycine-HCl buffer (pH 2 and pH 3), 0.1 M acetate buffer (pH 4 and pH 5), 0.1 M phosphate buffer (0.1 M pH 6, pH 7, and pH 8), 0.1 M glycine-NaOH buffer (pH 9 and pH 10)]; recorded at room temperature, λ_{Ex} = 425 nm. Inset: evolution of the fluorescence intensities recorded at 663 nm (red circles), the maximum emission at around 733 (blue squares), and the wavelength for the maximum emission found for the ∼733 nm band (green triangles) as a function of pH.

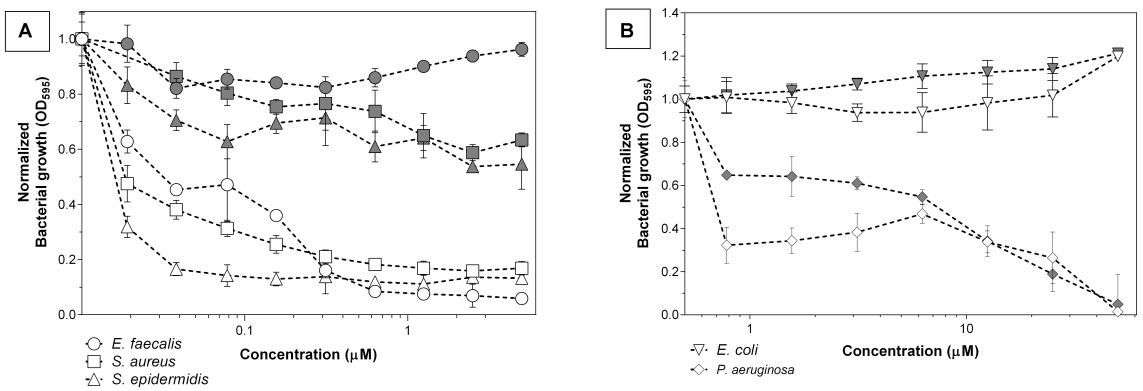

FIGURE 9 | Bacteriostatic effect of 5,10,15,20-tetrakis(4-hydroxyphenyl)-21*H*,23*H*-porphyrin-loaded acetylated lignin nanoparticles **(THPP@AcLi)** after light irradiation (white LED light dose, 4.16 J/cm^2, white symbols) or dark incubation (gray symbols) against **(A)** three Gram-positive bacteria and **(B)** two Gram-negative bacteria.

4.16 J/cm^2) or dark conditions (two-way ANOVA, Sidak's multiple comparisons test, $P > 0.05$).

Otherwise, several concentrations were tested for **THPP@AcLi** against the Gram-positive strains. They demonstrated a great efficiency at killing bacteria, being able to destroy up to 99.9999% of *E. faecalis* (**Figure 10**). Previous experiments (**Figure 9**) demonstrated a low dark chemotoxic effect for **THPP@AcLi**; in agreement, similar results were found on the bacterial survival rate (**Supplementary Material 10**), with differences between the light and dark conditions of several orders of magnitude. We found an efficient bactericidal effect at concentrations as low as 2.5 μM of **THPP@AcLi** and just 4.16 J/cm^2 of white LED light dose.

Our previous experiments had demonstrated that **THPP@AcLi** were stable at a wide range of pH. This is important for antibacterial applications. Usually, bacteria are viable within a limited range of pH values; with pathogenic bacteria being viable at a range between 5.5 and 8 (Madigan et al., 2014). However, bacterial metabolism provokes changes in the pH in different ways. Excretion of organic acids, such as propionic acid and isopropylic acid, can decrease the pH of the surrounding media, while amine compounds, formed through the degradation of amino acids and proteins, can increase the pH of the bacterial surrounding media (MacFaddin, 2000). Additionally, the pH of the medium has been found to influence the efficiency of several antibiotics (Yang et al., 2014). PACT is usually addressed as a

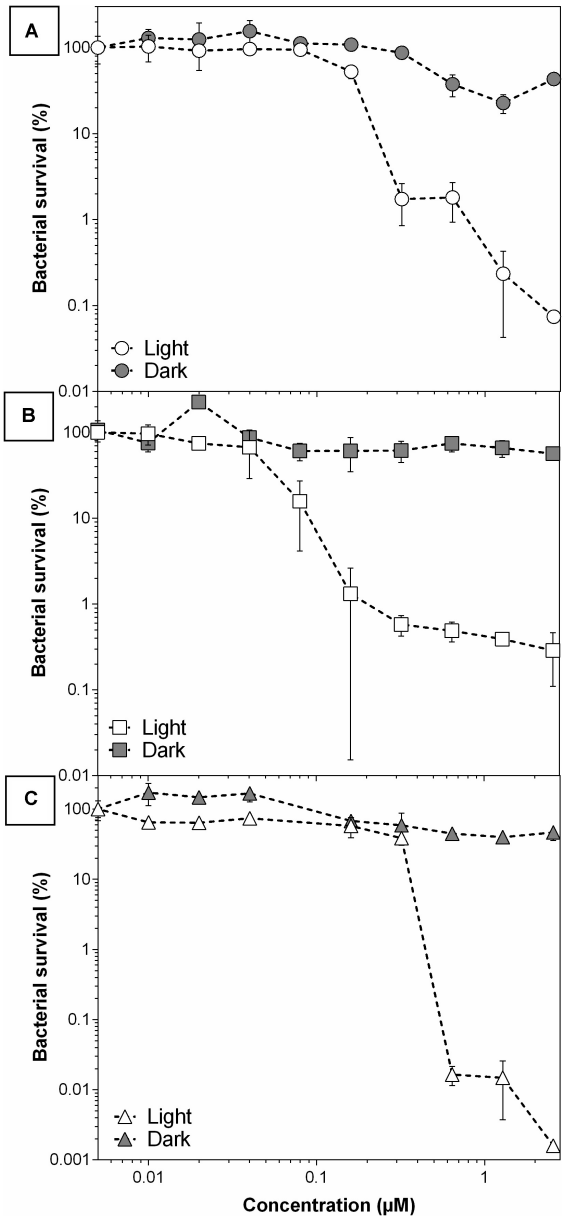

FIGURE 10 | 10 | Bacterial survival of **(A)** *S. aureus*, **(B)** *S. epidermidis*, and **(C)** *E. faecalis*, with 5,10,15,20-tetrakis(4-hydroxyphenyl)-21*H*,23*H*-porphyrin-loaded acetylated lignin nanoparticle **(THPP@AcLi)** treatment at different concentrations after light dose (4.16 J/cm^2) or dark incubation.

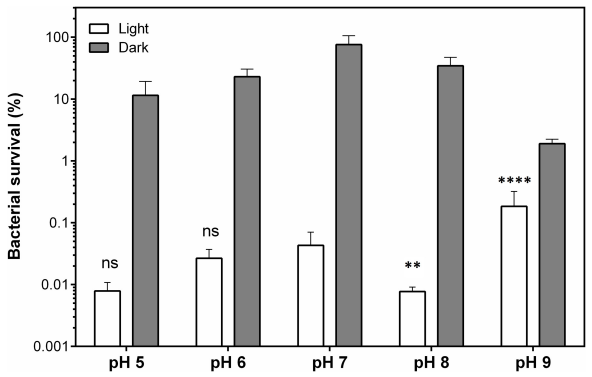

FIGURE 11 | Bacterial survival of *S. aureus*, as a function of pH, when treated with 5,10,15,20-tetrakis(4-hydroxyphenyl)-21*H*,23*H*-porphyrin-loaded acetylated lignin nanoparticles **(THPP@AcLi)** 2.5 μM under light irradiation (white LED light dose, 4.16 J/cm^2) or dark incubation. A two-way ANOVA analysis was made, with a Sidak's multiple comparison test, to analyze the differences found between pH 7 and the other pH conditions tested (ns, non-significant $P > 0.05$; $^{**}P < 0.01$; $^{****}P < 0.0001$). At all pH conditions, a difference was found between the light and dark conditions ($P < 0.0001$).

topical treatment or for surface disinfection due to the difficulty of irradiating the inside of a living being (Wainwright et al., 2017). Thus, a formulation that works on a wide range of pH is desirable, as it can withstand the changes provoked by bacteria or the conditions found on several surfaces.

In that perspective, **THPP@AcLi** was tested against *S. aureus* on aqueous media from pH 5 to pH 9, at a concentration of 2.5 μM, where we had previously observed a decrease of bacterial survival of at least 99.9% (**Figure 11**). Other pH conditions were tested, but as the bacterial controls demonstrated being unviable, these results were not included in the analysis. **THPP@AcLi** was able to diminish bacterial survival at all the pH conditions, through an effective photodynamic effect observed, with differences between light irradiation and dark incubation samples (two-way ANOVA, Sidak's multiple comparisons test, $P < 0.0001$). When compared with the PACT effect obtained at pH 7, no differences were found at pH 5 and pH 6 ($P > 0.05$). Nevertheless, at pH 8, the PACT effect had a slight improvement ($P < 0.01$), while at pH 9, the bacterial survival increased up to 0.184 ($P < 0.0001$). Although statistically there were some differences found, in general, the PACT effect permitted a bacterial survival below 0.2%. The fluctuation of the values found could be attributed to either the pH effect on the cells or the buffer composition, as three buffers with different compositions were used for this experiment. Thus, **THPP@AcLi** PACT effect was stable at a wide range of pH. Their stability corresponded to our previous observations, where their photophysical characteristics remained relatively stable at different pH conditions. This good correlation between the photophysical properties and their biological applications enhanced the applications spectra for **@AcLi** loaded with a photosensitizer.

In order to further demonstrate the stability of **THPP@AcLi**, their resistance to light irradiation was assessed. **THPP@AcLi** were exposed to light irradiation periods before incubation with bacteria under conditions similar to previously done PACT experiments. Afterward, the irradiated nanoparticles were mixed with *S. aureus* bacteria and the PACT irradiation was carried out, as routinely for bacterial eradication. A non-irradiated control was used, and bacterial survival was reported after *S. aureus* photodynamic eradication (**Figure 12A**). The **THPP@AcLi** withstood the light irradiation, remaining as effective as the previously non-irradiated sample (0 J/cm^2). This would allow nanoparticles to remain functional after long irradiation periods or after several cycles of usage. To analyze the effect of light irradiation on **THPP@AcLi**, nanoparticles were irradiated under

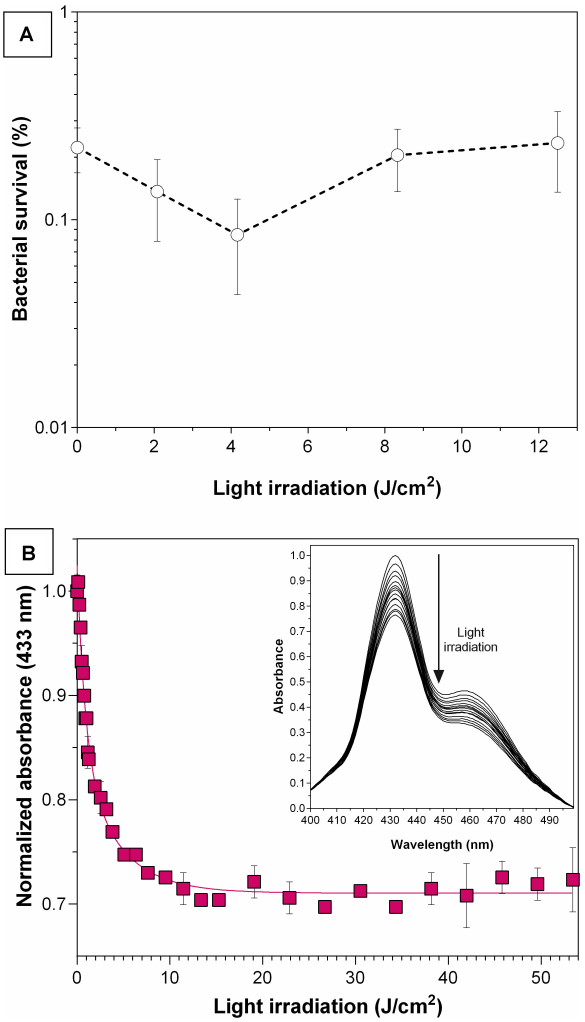

FIGURE 12 | Effect on 5,10,15,20-tetrakis(4-hydroxyphenyl)-21*H*,23*H*-porphyrin-loaded acetylated lignin nanoparticles **(THPP@AcLi)** of previous light irradiation. **(A)** Photoeradication of *S. aureus* (white LED light dose, 4.16 J/cm^2), with nanoparticles previously irradiated with white LED light. As a control, a non-irradiated sample was used (0 J/cm^2). **(B) THPP@AcLi** absorbance at 433 nm was monitored through its irradiation with white LED light (1 mW/cm^2). Inset: the spectra between 400 and 500 nm are observed for the whole irradiation time.

similar conditions and the absorbance at 433 nm was monitored after irradiation in order to evaluate potential degradation due to light-driven self-annihilation (**Figure 12B**). Interestingly, the absorption of the Soret band diminished quickly and then reached a plateau, with around 73.32% of the original absorbance found, even after 7 h of constant irradiation (1 mW/cm^2). By analyzing the UV-vis absorption spectra, a decrease on the B-band intensity at 457 nm was also observed, with changes in the ratio between this and the Soret band (initial A_{437}/A_{452} 0.465, final A_{437}/A_{452} 0.334). As the B-band can be attributed to the protonated molecule $\mathbf{THPPH_2}^{2+}$ according to the literature (Zannotti et al., 2018; Leroy-Lhez et al., 2019), we can conclude that this species was more sensitive to photobleaching than the non-protonated one.

5,10,15,20-Tetrakis(4-Hydroxyphenyl)-21H,23H-Porphyrin Inside Acetylated Lignin Nanoparticle Interaction With Bacteria

In this work, the stability of **THPP@AcLi** photophysical properties has been demonstrated, being effective against Gram-positive bacteria at different pH values, even after previous light irradiation. However, the previous experiments had not clarified how bacteria are eradicated, as is less likely that the photosensitizer gets in direct contact with bacteria. The uptake of porphyrins and other photosensitizers by bacteria had been widely studied (Ferro et al., 2007; Orekhov et al., 2018), but our results suggested that **THPP@AcLi** do not leak out the photosensitizer. In order to have an insight into the interaction between bacteria and **THPP@AcLi**, we made TEM observations over a mixture of bacteria and nanoparticles. *S. aureus* cells were observed without typical chemical fixation (**Figure 13A**). The observed cells did not have the characteristic round shape found for staphylococci bacteria; rather, they had a "squashed" shape likely due to the acidic uranyl acetate fixation/staining. When nanoparticles were mixed, a spontaneous binding was observed, as no incubation time elapsed for the first observation (**Figure 13B**). Interestingly, the amount of observable free nanoparticles was low when compared to the observed bound nanoparticles. Nanoparticles were observed surrounding the surface of bacteria. The attached nanoparticles were observed as spheres, with only a partial merge within the bacterial membrane. This suggested that nanoparticles do not penetrate inside the cell but remained in the outskirts of the membrane. Preparations made from a mixture of bacteria and nanoparticles, done 30 min ahead, still presented this pattern. Thus, the penetration of nanoparticles inside bacteria is not time dependent. The mixture of nanoparticles and bacteria was irradiated *in situ* over the copper grid with an incandescent bulb light (2,500 lux, 5 min) and was observed at TEM. After light irradiation, bacteria were scarce and cellular debris was observed throughout the place. Bacteria were also found surrounded by **THPP@AcLi** (**Figures 13C,D**). In some cases, bacteria were observed while spilling their cellular contents (**Figure 13D**). The cellular contents include proteins and nucleic acids, which are transparent to the TEM, but we were able to observe them after being contrasted with uranyl acetate, observable at TEM, as black debris. The TEM observations suggest that bacteria suffered extensive damage on their cellular wall when exposed to light and **THPP@AcLi**. As presumably nanoparticles were unable to completely penetrate inside the cell, a local ROS production against the cellular wall was likely to trigger the photodynamic effect. Insufficient damage to the bacterial wall may provoke an arrest on the bacterial growth, which corresponds to our previous observations of a large bacteriostatic effect for **THPP@AcLi**.

An interesting observation was the spontaneous binding of THPP@AcLi with bacteria. It had been previously observed that lignin nanoparticles worked as flocculants, capturing

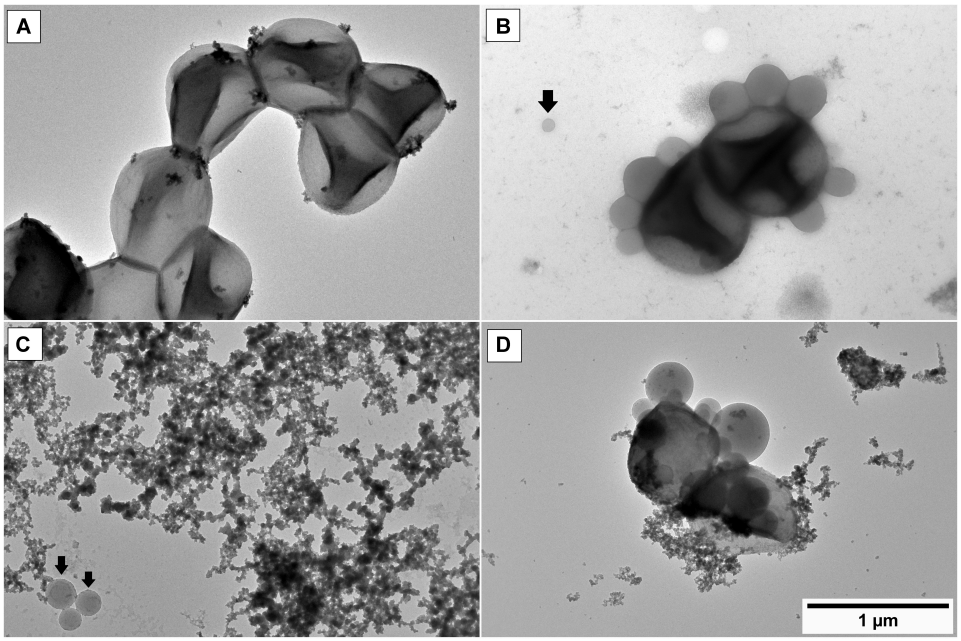

FIGURE 13 | Transmission electron microscopy (TEM) observations of **(A)** *S. aureus* cells *in vivo*; **(B)** *S. aureus* and 5,10,15,20-tetrakis(4-hydroxyphenyl)-21*H*,23*H*-porphyrin-loaded acetylated lignin nanoparticles **(THPP@AcLi)**, the black arrow indicates a non-bound nanoparticle; **(C)** and **(D)** *S. aureus* and **THPP@AcLi** after light irradiation (incandescent bulb, 2,500 luxes, 5 min).

E. coli and *S. aureus* (Yin et al., 2018). This effect was observed in our experiments, where the mixture of bacteria and nanoparticles quickly flocculated to the bottom of the flask. The high affinity of bacteria and THPP@AcLi may work as a synergic system. Although we had observed through EPR a low production of singlet oxygen for THPP@AcLi, the tight interaction between bacteria and nanoparticles results in a higher concentration of ROS at the cellular level. Thus, both flocculant and photodynamic effect could be a promising alternative as a PACT system. Such system could find wide applications in wastewater purification, a complex media with biological and chemical pollutants that require disinfection before release into the environment. Purification of wastewater usually comprises physical methods, involving sedimentation, aeration, and filtration, and at these steps, lignin could be used as an alternative.

DISCUSSION

Our results demonstrate that **THPP** encapsulation into @AcLi is an easy, effective, and reproducible method, increasing the value of lignin as a biopolymer with biomedical applications. Besides, this encapsulation method may be suitable for a wide range of molecules, which are our current subject of study.

The effect of aggregation on porphyrins and tetrapyrrolic compounds has been addressed as one of the main issues for biological applications of both PDT and PACT, as aggregation quenches ROS production, diminishing their efficiency and potential (Liu et al., 2018). The present work has produced a formulation that efficiently delivers **THPP** into an aqueous media, with less aggregation than the non-encapsulated **THPP**. Besides, **THPP** inside **@AcLi** is able to withstand a wide pH range without being affected, as demonstrated by its UV-vis absorption and fluorescence emission properties. Additionally, the pH stability is extended to its physicochemical properties, as its zeta potential, and the changes in the pH of the media do not affect their efficiency against bacteria.

Lignin nanoparticles are currently under research as vehicles for small molecules, with reports of nanoparticles being able to diffuse the small molecules over time or over pH changes (Zhou et al., 2019). Nevertheless, we were able to demonstrate that **THPP@AcLi** are stable over time, releasing less than 10% of **THPP** into the surrounding media after 60 days of observations. However, the stable encapsulation of **THPP** inside nanoparticles leads to the question if ROS generated by **THPP** would be able to escape from the nanoparticles and actually produce an observable macroscopic effect. Through EPR, we detected singlet oxygen generation for **@AcLi** and for **THPP@AcLi**. However, the evidence has demonstrated that **THPP@AcLi** singlet oxygen generation is mostly due to **THPP**, as **THPP@AcLi** is 20 times more efficient at producing singlet oxygen than **@AcLi**. Then, singlet oxygen generated by **THPP** was able to diffuse through the**@AcLi**.

Although it has been indicated that a light dose of 4.16 J/cm^2 is necessary to kill bacteria, recent reports have indicated that the UV-vis absorbance of PACT and PDT molecules need to be taken into account for a corrected light dose (Schaberle, 2018). With this correction done (**Supplementary Material 2**), **THPP@AcLi** is only able to absorb 65% of the white LED light irradiated on it,

resulting in a corrected light dose of 2.71 J/cm^2. Our experiments had demonstrated that the nanoparticles were stable under light doses 20 times higher than the corrected light dose, and thus higher doses could be applied on bacteria, while maintaining their efficiency.

In regard to bacterial eradication, **THPP@AcLi** was only able to diminish the bacterial growth and survival of Gram-positive bacteria. This is not surprising, as PACT has been described as more effective against Gram-positive bacteria than against Gram-negative ones (Huang et al., 2012). The differences in the efficiency were addressed to be due to the impermeability of its double membrane, a common problem with the development of successful antibiotic treatments (Nikaido, 2003). Interestingly, PACT applications on Gram-negative bacteria had overcome this obstacle through the usage of cationic photosensitizers (Ragàs et al., 2010; Cieplik et al., 2018; Aroso et al., 2019) or photosensitizers linked to antimicrobial peptides (Le Guern et al., 2017, 2018), which have a high affinity for the anionic heads of the lipopolysaccharides, facilitating the interaction between bacteria and photosensitizer. Interestingly, in our work, we observed that although nanoparticles have a negative charge, they seem to strongly interact with bacteria, demonstrated by TEM observations. Thus, further investigations are underway with cationic molecules inside **@AcLi**, aiming for Gram-negative bacteria eradication. Additionally, lignin modifications could lead to the construction of cationic lignin nanoparticles. Nevertheless, we had observed strong spontaneous interactions between nanoparticles and bacteria. It has been previously addressed that lignin nanoparticles were prone to act as flocculant agents, working as a physical method for water disinfection (Yin et al., 2018). Our strategy combines physical decontamination and a light-driven chemotoxic effect, a combination that could be ideal for wastewater decontamination. Wastewater is a complex mixture that needs to be purified before being released into the environment. Acetylated lignin nanoparticles could be used for light-driven water purification and, at the same time, for physical removal of bacteria and bacterial debris.

This work represents a cornerstone on lignin applications, as it is the first time it has been used on PACT applications. The present work, although able to eradicate Gram-positive bacteria, was unable to affect the survival of Gram-negative bacteria. Our future work comprises the modification of lignin with "sticky" moieties and the encapsulation of cationic porphyrins, hoping to obtain a wide-range formulation for antibacterial and antibiofilm purposes. Additionally, our future work aims to enhance the comprehension of the mechanism of the interaction between THPP/AcLi/bacteria through porphyrin uptake experiments and flow cytometry.

CONCLUSION

Acetylated lignin nanoparticles were able to encapsulate a porphyrinic compound, **THPP**. Additionally, the encapsulation system was stable at a wide pH range, conserving its physical and photophysical properties, without leaking the encapsulated compound. Furthermore, it was demonstrated that this system was able to produce ROS and exert a photodynamic eradication effect on three Gram-positive strains. The photodynamic eradication could be due to a synergic effect of the flocculant properties of lignin nanoparticles and the light-driven ROS production of **THPP**. The encapsulation of further photosensitizers is likely to improve the presented results, and this strategy is currently under study for water decontamination and other applications.

DATA AVAILABILITY STATEMENT

The raw data supporting the conclusions of this article will be made available by the authors, without undue reservation, to any qualified researcher.

AUTHOR CONTRIBUTIONS

NM-C, GM, and NV participated on the preparation of the raw material and the nanoparticles. NM-C, GM, and SL-L participated on the characterization of the physico-chemical properties of the raw material and the nanoparticles. NM-C and CC measured the singlet oxygen production through EPR. NM-C and T-SO designed and performed the microbiological experiments. NM-C, KP, AŻ, and KM designed and performed the TEM observations. NM-C, MMP, and MC designed and performed the fluorescence spectroscopy experiments. All authors discussed the results and commented on the manuscript.

FUNDING

This project has received funding from the European Union's Horizon 2020 Research and Innovation Program under the Marie Skłodowska-Curie grant agreement no. 764837. The transmission electron microscopy imaging was funded from the National Science Centre (PL) under "Miniatura" grant no. 2019/03/X/NZ3/02100.

ACKNOWLEDGMENTS

NM-C would like to acknowledge the support of Dr. Fábio A. Schaberle regarding the fluorescence spectroscopy and photobleaching experiments.

SUPPLEMENTARY MATERIAL

The Supplementary Material for this article can be found online at: https://www.frontiersin.org/articles/10.3389/fmicb.2020.606185/full#supplementary-material

REFERENCES

Alqahtani, M. S., Alqahtani, A., Al-Thabit, A., Roni, M., and Syed, R. (2019). Novel lignin nanoparticles for oral drug delivery. *J. Mater. Chem. B* 7, 4461–4473. doi: 10.1039/c9tb00594c

Aroso, R. T., Calvete, M. J. F., Pucelik, B., Dubin, G., Arnaut, L. G., Pereira, M. M., et al. (2019). Photoinactivation of microorganisms with sub-micromolar concentrations of imidazolium metallophthalocyanine salts. *Eur. J. Med. Chem.* 184:111740. doi: 10.1016/j.ejmech.2019.111740

Baccani, I., Faraoni, P., Marini, M., Gnerucci, A., Orsini, B., Pecile, P., et al. (2019). Synergistic effect of photodynamic therapy at 400 nm and doxycycline against *Helicobacter pylori*. *Fut. Microbiol.* 14, 1199–1205. doi: 10.2217/fmb-2019-0129

Bechara Andere, N. M. R., Dos Santos, N. C. C., Araujo, C. F., Mathias, I. F., Rossato, A., de Marco, A. C., et al. (2018). Evaluation of the local effect of nonsurgical periodontal treatment with and without systemic antibiotic and photodynamic therapy in generalized aggressive periodontitis. A randomized clinical trial. Photodiagnosis Photodyn. *Ther.* 24, 115–120. doi: 10.1016/j.pdpdt.2018.09.002

Buchovec, I., Lukseviciute, V., Marsalka, A., Reklaitis, I., and Luksiene, Z. (2016). Effective photosensitization-based inactivation of Gram (-) food pathogens and molds using the chlorophyllin–chitosan complex: towards photoactive edible coatings to preserve strawberries. *Photochem. Photobiol. Sci.* 15, 506–516. doi: 10.1039/C5PP00376H

Calvo-Flores, F. G., and Dobado, J. A. (2010). Lignin as renewable raw material. *ChemSusChem* 3, 1227–1235. doi: 10.1002/cssc.201000157

Cieplik, F., Deng, D., Crielaard, W., Buchalla, W., Hellwig, E., Al-Ahmad, A., et al. (2018). Antimicrobial photodynamic therapy–what we know and what we don't. *Crit. Rev. Microbiol.* 44, 571–589. doi: 10.1080/1040841X.2018.1467876

Danaei, M., Dehghankhold, M., Ataei, S., Hasanzadeh Davarani, F., Javanmard, R., Dokhani, A., et al. (2018). Impact of particle size and polydispersity index on the clinical applications of lipidic nanocarrier systems. *Pharmaceutics* 10:57. doi: 10.3390/pharmaceutics10020057

de Freitas, L. M., Calixto, G. M. F., Chorilli, M., Giusti, J. S. M., Bagnato, V. S., Soukos, N. S., et al. (2016). Polymeric nanoparticle-based photodynamic therapy for chronic periodontitis *in Vivo*. *Int. J. Mol. Sci.* 17:769. doi: 10.3390/ijms17050769

Donaldson, L. A., and Radotic, K. (2013). Fluorescence lifetime imaging of lignin autofluorescence in normal and compression wood. *J. Microsc.* 251, 178–187. doi: 10.1111/jmi.12059

Duval, A., and Lawoko, M. (2014). A review on lignin-based polymeric, micro- and nano-structured materials. *React. Funct. Polym.* 85, 78–96. doi: 10.1016/j.reactfunctpolym.2014.09.017

Faix, O. (1991). Classification of lignins from different botanical origins by FT-IR spectroscopy. *Holzforschung* 45, 21–28. doi: 10.1515/hfsg.1991.45.s1.21

Ferro, S., Ricchelli, F., Monti, D., Mancini, G., and Jori, G. (2007). Efficient photoinactivation of methicillin-resistant *Staphylococcus aureus* by a novel porphyrin incorporated into a poly-cationic liposome. *Int. J. Biochem. Cell Biol.* 39, 1026–1034. doi: 10.1016/j.biocel.2007.02.001

Figueiredo, P., Lintinen, K., Hirvonen, J. T., Kostiainen, M. A., and Santos, H. A. (2018). Properties and chemical modifications of lignin: Towards lignin-based nanomaterials for biomedical applications. *Prog. Mater. Sci.* 93, 233–269. doi: 10.1016/j.pmatsci.2017.12.001

Figueiredo, P., Lintinen, K., Kiriazis, A., Hynninen, V., Liu, Z., Bauleth-Ramos, T., et al. (2017). *In vitro* evaluation of biodegradable lignin-based nanoparticles for drug delivery and enhanced antiproliferation effect in cancer cells. *Biomaterials* 121, 97–108. doi: 10.1016/j.biomaterials.2016.12.034

Frangville, C., Rutkevièius, M., Richter, A. P., Velev, O. D., Stoyanov, S. D., and Paunov, V. N. (2012). Fabrication of environmentally biodegradable lignin nanoparticles. *ChemPhysChem* 13, 4235–4243. doi: 10.1002/cphc.201200537

Glueck, M., Schamberger, B., Eckl, P., and Plaetzer, K. (2017). New horizons in microbiological food safety: Photodynamic decontamination based on a curcumin derivative. *Photochem. Photobiol. Sci.* 16, 1784–1791. doi: 10.1039/C7PP00165G

Hsieh, Y. H., Chuang, W. C., Yu, K. H., Jheng, C. P., and Lee, C. I. (2019). Sequential photodynamic therapy with phthalocyanine encapsulated chitosan-tripolyphosphate nanoparticles and flucytosine treatment against *Candida tropicalis*. *Pharmaceutics* 11:16. doi: 10.3390/pharmaceutics11010016

Huang, L., Xuan, Y., Koide, Y., Zhiyentayev, T., Tanaka, M., and Hamblin, M. R. (2012). Type I and Type II mechanisms of antimicrobial photodynamic therapy: An *in vitro* study on Gram-negative and Gram-positive bacteria. *Laser* 44, 490–499. doi: 10.1002/lsm.22045.Type

Jia, R., Tian, W., Bai, H., Zhang, J., Wang, S., and Zhang, J. (2019). Sunlight-driven wearable and robust antibacterial coatings with water-soluble cellulose-based photosensitizers. *Adv. Healthc. Mater.* 8:1801591. doi: 10.1002/adhm.201801591

Josefsen, L. B., and Boyle, R. W. (2012). Unique diagnostic and therapeutic roles of porphyrins and phthalocyanines in photodynamic therapy, imaging and theranostics. *Theranostics* 2, 916–966. doi: 10.7150/thno.4571

Khaldi, Z., Nzambe Takeki, J. K., Ouk, T.-S., Lucas, R., and Zerrouki, R. (2019). Synthesis and photo-bactericidal properties of a cationic porphyrin grafted onto kraft pulp fibers. *J. Porphyr. Phthalocyanines* 23, 489–496. doi: 10.1142/S1088424619500330

Kumar, A., and Dixit, C. K. (2017). "Methods for characterization of nanoparticles," in *Advances in Nanomedicine for the Delivery of Therapeutic Nucleic Acids*, eds C. Ramesh, N. Gupta, and S. Nimesh (Netherlands: Elsevier), 43–58. doi: 10.1016/B978-0-08-100557-6.00003-1

Le Guern, F., Ouk, T. S., Ouk, C., Vanderesse, R., Champavier, Y., Pinault, E., et al. (2018). Lysine analogue of polymyxin B as a significant opportunity for photodynamic antimicrobial chemotherapy. *ACS Med. Chem. Lett.* 9, 11–16. doi: 10.1021/acsmedchemlett.7b00360

Le Guern, F., Sol, V., Ouk, C., Arnoux, P., Frochot, C., and Ouk, T. S. (2017). Enhanced photobactericidal and targeting properties of a cationic porphyrin following the attachment of polymyxin B. *Bioconjug. Chem.* 28, 2493–2506. doi: 10.1021/acs.bioconjchem.7b00516

Leroy-Lhez, S., Rezazgui, O., Issawi, M., Elhabiri, M., Calliste, C. A., and Riou, C. (2019). Why are the anionic porphyrins so efficient to induce plant cell death? A structure-activity relationship study to solve the puzzle. *J. Photochem. Photobiol. A Chem.* 368, 276–289. doi: 10.1016/j.jphotochem.2018.09.050

Lewis, K. (2013). Platforms for antibiotic discovery. *Nat. Rev. Drug Discov.* 12, 371–387. doi: 10.1038/nrd3975

Liu, D., Li, L., Chen, J., Chen, Z., Jiang, L., Yuan, C., et al. (2018). Dissociation of zinc phthalocyanine aggregation on bacterial surface is key for photodynamic antimicrobial effect. *J. Porphyr. Phthalocyanines* 22, 1–10. doi: 10.1142/S1088424618500888

MacFaddin, J. F. (2000). *Biochemical Tests for Identification of Medical Bacteria*, 3rd Edn. Pennsylvania: Williams and Wilkins.

Madigan, M. T., Martinko, J. F., Bender, K. S., Buckley, D. H., Stahl, D. A., and Brock, T. (2014). *Brock Biology of Microorganisms*, 14th Edn. London: Pearson Education Limited.

Maldonado-Carmona, N., Ouk, T. S., Calvete, M. J. F., Pereira, M. M., Villandier, N., and Leroy-Lhez, S. (2020). Conjugating biomaterials with photosensitizers: Advances and perspectives for photodynamic antimicrobial chemotherapy. *Photochem. Photobiol. Sci.* 19, 445–461. doi: 10.1039/c9pp00398c

Marchand, G., Calliste, C. A., Williams, R. M., McLure, C., Leroy-Lhez, S., and Villandier, N. (2018). Acetylated lignins: A potential bio-sourced photosensitizer. *ChemistrySelect* 3, 5512–5516. doi: 10.1002/slct.201801039

Marchand, G., Fabre, G., Maldonado-Carmona, N., Villandier, N., and Leroy-Lhez, S. (2020). Acetylated lignin nanoparticles as a prospective vehicle for photosensitizing molecules. *Nanoscale Adv.* 2020, D0NA00615G. doi: 10.1039/D0NA00615G

Martinez, A. F. C., de Almeida, L. G., Moraes, L. A. B., and Cônsoli, F. L. (2017). Tapping the biotechnological potential of insect microbial symbionts: new insecticidal porphyrins. *BMC Microbiol.* 17:143. doi: 10.1186/s12866-017-1054-y

Nikaido, H. (2003). Molecular basis of bacterial outer membrane permeability revisited. *Microbiol. Mol. Biol. Rev.* 67, 593–656. doi: 10.1128/MMBR.67.4.593-656.2003

Nzambe Ta keki, J. K., Ouk, T.-S., Zerrouki, R., Faugeras, P.-A., Sol, V., and Brouillette, F. (2016). Synthesis and photobactericidal properties of a neutral porphyrin grafted onto lignocellulosic fibers. *Mater. Sci. Eng.* 62, 61–67. doi: 10.1016/j.msec.2016.01.028

O'Neill, J. (2016). *Tackling drug-resistant infections globally: Final report and recommendations*. United Kingdom: Government of the United Kingdom.

Orekhov, P. S., Kholina, E. G., Bozdaganyan, M. E., Nesterenko, A. M., Kovalenko, I. B., and Strakhovskaya, M. G. (2018). Molecular mechanism of uptake of cationic photoantimicrobial phthalocyanine across bacterial membranes revealed by molecular dynamics simulations. *J. Phys. Chem. B* 122, 3711–3722. doi: 10.1021/acs.jpcb.7b11707

Ormond, A. B., and Freeman, H. S. (2013). Effects of substituents on the photophysical properties of symmetrical porphyrins. *Dye. Pigment.* 96, 440–448. doi: 10.1016/j.dyepig.2012.09.011

Pineiro, M., Carvalho, A. L., Pereira, M. M., Gonsalves, A. M. d'A. R, Arnaut, L. G., and Formosinho, S. J. (1998). Photoacoustic measurements of porphyrin triplet-state quantum yields and singlet-oxygen efficiencies. *Chem. A Eur. J.* 4, 2299–2307. doi: 10.1002/(SICI)1521-3765(19981102)4:11<2299::AID-CHEM2299<3.0.CO;2-H

Ponomarenko, J., Lauberts, M., Dizhbite, T., Lauberte, L., Jurkjane, V., and Telysheva, G. (2015). Antioxidant activity of various lignins and lignin-related phenylpropanoid units with high and low molecular weight. *Holzforschung* 69, 795–805. doi: 10.1515/hf-2014-0280

Qian, Y., Deng, Y., Li, H., and Qiu, X. (2014a). Reaction-free lignin whitening via a self-assembly of acetylated lignin. *Ind. Eng. Chem. Res.* 53, 10024–10028. doi: 10.1021/ie5010338

Qian, Y., Deng, Y., Qiu, X., Li, H., and Yang, D. (2014b). Formation of uniform colloidal spheres from lignin, a renewable resource recovered from pulping spent liquor. *Green Chem.* 16, 2156–2163. doi: 10.1039/c3gc42131g

Ragàs, X., Sánchez-García, D., Ruiz-González, R., Dai, T., Agut, M., Hamblin, M. R., et al. (2010). Cationic porphycenes as potential photosensitizers for antimicrobial photodynamic therapy. *J. Med. Chem.* 53, 7796–7803. doi: 10.1021/jm1009555

Regiel-Futyra, A., Dąbrowski, J. M., Mazuryk, O., Śpiewak, K., Kyzioł, A., Pucelik, B., et al. (2017). Bioinorganic antimicrobial strategies in the resistance era. *Coord. Chem. Rev.* 351, 76–117. doi: 10.1016/j.ccr.2017.05.005

Ringot, C., Saad, N., Brégier, F., Bressollier, P., Poli, E., Chaleix, V., et al. (2018). Antibacterial activity of a photosensitive hybrid cellulose fabric. *Photochem. Photobiol. Sci.* 17, 1780–1786. doi: 10.1039/C8PP00212F

Riou, C., Calliste, C. A., Da Silva, A., Guillaumot, D., Rezazgui, O., Sol, V., et al. (2014). Anionic porphyrin as a new powerful cell death inducer of Tobacco Bright Yellow-2 cells. *Photochem. Photobiol. Sci.* 13:621. doi: 10.1039/c3pp50315a

Rocca, D. M., Vanegas, J. P., Fournier, K., Becerra, M. C., Scaiano, J. C., and Lanterna, A. E. (2018). Biocompatibility and photo-induced antibacterial activity of lignin-stabilized noble metal nanoparticles. *RSC Adv.* 8, 40454–40463. doi: 10.1039/C8RA08169G

Schaberle, F. A. (2018). Assessment of the actual light dose in photodynamic therapy. Photodiagnosis Photodyn. *Ther.* 23, 75–77. doi: 10.1016/j.pdpdt.2018.06.009

Schindelin, J., Arganda-Carreras, I., Frise, E., Kaynig, V., Longair, M., Pietzsch, T., et al. (2012). Fiji: an open-source platform for biological-image analysis. *Nat. Methods* 9, 676–682. doi: 10.1038/nmeth.2019

Schneider, C. A., Rasband, W. S., and Eliceiri, K. W. (2012). NIH Image to ImageJ: 25 years of image analysis. *Nat. Methods* 9, 671–675. doi: 10.1038/nmeth.2089

Tse, H.-Y., Cheng, S.-C., Yeung, C. S., Lau, C.-Y., Wong, W.-H., Dong, C., et al. (2019). Development of a waste-derived lignin-porphyrin bio-polymer with enhanced photoluminescence at high water fraction with wide pH range and heavy metal sensitivity investigations. *Green Chem.* 21, 1319–1329. doi: 10.1039/C8GC02904K

Vinagreiro, C. S., Zangirolami, A., Schaberle, F. A., Nunes, S. C. C., Blanco, K. C., Inada, N. M., et al. (2020). Antibacterial photodynamic inactivation of antibiotic-resistant bacteria and biofilms with nanomolar photosensitizer concentrations. *ACS Infect. Dis.* 6, 1517–1526. doi: 10.1021/acsinfecdis.9b00379

Wainwright, M. (2019). Photoantimicrobials and PACT: what's in an abbreviation? *Photochem. Photobiol. Sci.* 18, 12–14. doi: 10.1039/C8PP00390D

Wainwright, M., Maisch, T., Nonell, S., Plaetzer, K., Almeida, A., Tegos, G. P., et al. (2017). Photoantimicrobials—are we afraid of the light? *Lancet Infect. Dis.* 17, 49–55e. doi: 10.1016/S1473-3099(16)30268-7

Wang, C., Kelley, S. S., and Venditti, R. A. (2016). Lignin-based thermoplastic materials. *ChemSusChem* 9, 770–783. doi: 10.1002/cssc.201501531

WHO (2015). *Global action plan on antimicrobial resistance*. Geneva,: World Health. Organnization.

Xue, Y., Qiu, X., and Ouyang, X. (2020). Insights into the effect of aggregation on lignin fluorescence and its application for microstructure analysis. *Int. J. Biol. Macromol.* 154, 981–988. doi: 10.1016/j.ijbiomac.2020.03.056

Yang, L., Wang, K., Li, H., Denstedt, J. D., and Cadieux, P. A. (2014). The influence of urinary pH on antibiotic efficacy against bacterial uropathogens. *Urology* 84:48. doi: 10.1016/j.urology.2014.04.048

Yang, W., Owczarek, J. S., Fortunati, E., Kozanecki, M., Mazzaglia, A., Balestra, G. M., et al. (2016). Antioxidant and antibacterial lignin nanoparticles in polyvinyl alcohol/chitosan films for active packaging. *Ind. Crops Prod.* 94, 800–811. doi: 10.1016/j.indcrop.2016.09.061

Yin, H., Liu, L., Wang, X., Wang, T., Zhou, Y., Liu, B., et al. (2018). A novel flocculant prepared by lignin nanoparticles-gelatin complex from switchgrass for the capture of *Staphylococcus aureus* and *Escherichia coli*. *Colloids Surf. A Physicochem. Eng. Asp.* 545, 51–59. doi: 10.1016/j.colsurfa.2018.02.033

Zannotti, M., Giovannetti, R., Minofar, B., Øeha, D., Plaèková, L., D'Amato, C. A., et al. (2018). Aggregation and metal-complexation behaviour of THPP porphyrin in ethanol/water solutions as function of pH. Spectrochim. *Acta Part A Mol. Biomol. Spectrosc.* 193, 235–248. doi: 10.1016/j.saa.2017.12.021

Zhou, M., Wang, D., Yang, D., Qiu, X., and Li, Y. (2019). Avermectin loaded nanosphere prepared from acylated alkali lignin showed anti-photolysis property and controlled release performance. *Ind. Crops Prod.* 137, 453–459. doi: 10.1016/j.indcrop.2019.04.037

Conflict of Interest: The authors declare that the research was conducted in the absence of any commercial or financial relationships that could be construed as a potential conflict of interest.

frontiers in Microbiology

ORIGINAL RESEARCH
published: 17 November 2020
doi: 10.3389/fmicb.2020.571691

Inhibition of the Citrus Canker Pathogen Using a Photosensitizer Assisted by Sunlight Irradiation

Libin Jiang[1], Yurong Liu[1], Xianyuan Xu[2], Dan Su[1], Huasong Zou[2], Jianyong Liu[1], Cai Yuan[3] and Mingdong Huang[1]**

[1] College of Chemistry, Fuzhou University, Fuzhou, China, [2] State Key Laboratory of Ecological Pest Control for Fujian and Taiwan Crops, Fujian University Key Laboratory for Plant–Microbe Interaction, College of Plant Protection, Fujian Agriculture and Forestry University, Fuzhou, China, [3] College of Biological Science and Engineering, Fuzhou University, Fuzhou, China

Citrus canker, induced by bacterial infection, seriously affects the growth and productivity of citrus around the world and has attracted strong research interest. The current treatment for this disease uses copper salts to inactivate the pathogenic bacteria: *Xanthomonas citri subsp. citri* (*Xcc*) strain. However, copper salts may have a negative impact on the environment or plant. In this work, we identify a chemical compound, 2,6-diiodo-1,3,5,7-tetramethyl-8-(P-benzoic acid)-4,4′-difluoroboradiazaindacene (DIBDP), to inactivate the pathogenic *Xcc* strain (*29-1*). DIBDP is activated by sunlight and generates reactive oxygen species to kill the bacteria. In order to overcome the degradation of DIBDP under sunlight, an adjuvant agent was identified to limit the photodegradation of DIBDP by forming a photosensitizer complex (PSC). This complex demonstrated significant antimicrobial activity to *Xcc 29-1*, which was 64-fold more potent than the copper biocides. The antimicrobial efficacy of PSC on citrus leaves infected by *Xcc 29-1* also was much stronger than copper agent and, at the same time, the PSC was safe to the host exposed to sunlight. Thus, this PSC is a promising antibacterial agent to control citrus canker disease.

Keywords: citrus canker, photosensitizer, antimicrobial activity, photodegradation, sunlight

OPEN ACCESS

Edited by:
Bertha González-Pedrajo, National Autonomous University of Mexico, Mexico

Reviewed by:
Yong-Qiang He, Guangxi University, China
Yunzeng Zhang, Yangzhou University, China

****Correspondence:***
Cai Yuan
cyuan@fzu.edu.cn
Mingdong Huang
HMD_lab@fzu.edu.cn

Specialty section:
This article was submitted to Antimicrobials, Resistance and Chemotherapy, a section of the journal Frontiers in Microbiology

Received: *11 June 2020*
Accepted: *16 September 2020*
Published: *17 November 2020*

Citation:
Jiang L, Liu Y, Xu X, Su D, Zou H, Liu J, Yuan C and Huang M (2020) Inhibition of the Citrus Canker Pathogen Using a Photosensitizer Assisted by Sunlight Irradiation. Front. Microbiol. 11:571691. doi: 10.3389/fmicb.2020.571691

INTRODUCTION

Citrus canker is one of the most serious quarantine diseases worldwide (Gottwald et al., 2002; Brunings and Gabriel, 2003). The canker causes necrotic lesions on leaves, twigs, and fruit, and leads to defoliation and fruit drop in severe cases (Schubert et al., 2001). The canker is caused by the bacterial pathogen *Xanthomonas citri subsp. citri* (*Xcc*), which enters the plant through the stomata or wounds, and invades into the intercellular space in the apoplast (Brunings and Gabriel, 2003; Ryan et al., 2011). The canker spreads out to remote areas, helped by the leaf miner fly or during wind-blown rain (Bock et al., 2005). Although millions of dollars are spent annually on prevention, quarantines, eradication programs, and disease control, citrus canker remains a serious challenge (Graham et al., 2004; Behlau et al., 2016).

Photodynamic therapy is a clinically used method for tumor eradication (Agostinis et al., 2011; Shi et al., 2019). This method has also been used as a new and promising strategy to eradicate a wide

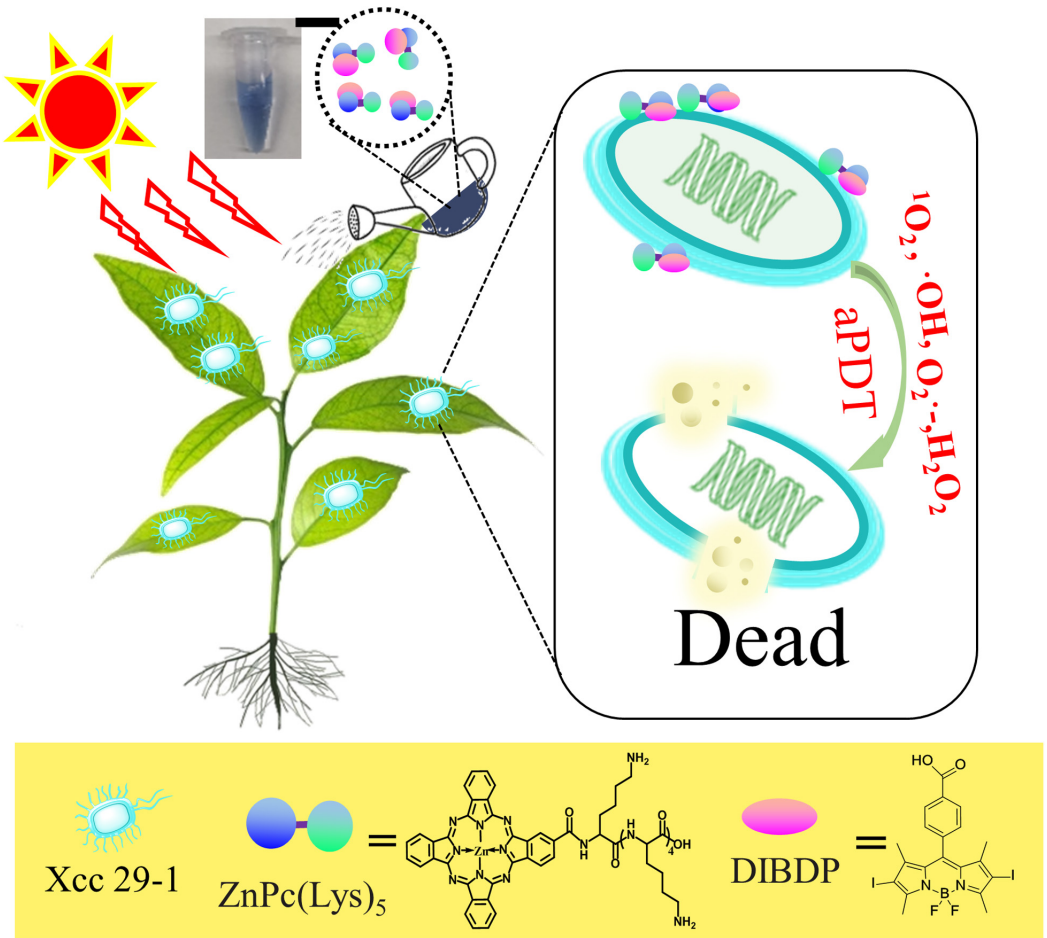

GRAPHICAL ABSTRACT | TOC: A photosensitizer complex (PSC) was developed to kill the pathogen for citrus canker, *Xanthomonas citri subsp. citri*, under sunlight irradiation, using reactive oxygen species. The PSC is safe to the host leaves and to environment.

spectrum of microorganisms, including bacteria, yeasts, molds, viruses, and parasites (Hamblin and Hasan, 2004; Wainwright et al., 2017), and is named antimicrobial photodynamic therapy (aPDT) (Huang et al., 2010). This therapy requires the presence of a small amount of photosensitizer (PS), typically at a micromolar range concentration. Photosensitizers are often organic dyes, absorb light with long wavelengths (to promote tissue penetration), and transfers light energy to surrounding oxygen, ultimately leading to the generation of reactive oxygen species (ROS), such as singlet oxygen and free radicals (Wainwright, 1998; Huang et al., 2012; Carrera et al., 2016). The ROS causes significant toxicity, leading to death of nearby cells (Sperandio et al., 2013). A strong advantage of aPDT is its very high efficiency to kill the microorganisms, leading to very low chance of them developing resistance (Pedigo et al., 2009; Giuliani et al., 2010; Maisch, 2015).

The translation application of clinical PDT to agricultural PDT to inactivate the citrus canker pathogen has proven to be a major challenge. In clinical PDT, long wavelength light (>630 nm) is used to reach deep tissue (up to ∼10 mm). Photosensitizers satisfying this requirement usually have aromatic rings with a high degree of π electron dislocation in their molecular structure, e.g., porphyrin and phthalocyanine. Such photosensitizers may not be optimal for agriculture PDT, where the light source is sunlight with maximal irradiation at 520 nm (Kim et al., 2015). Thus, a new type of photosensitizer must be found for agricultural PDT.

Organic dye Boron Dipyrromethene (BODIPY), 4,4-difluoro-4-bora-3a,4a-diaza-s-indacene, was discovered in 1968 by Treibs and Kreuzer (Kreuzer, 1968), and consists of two pyrrole units linked by a methine bridge and a BF2 group that connect both pyrrolic nitrogen atoms (**Figure 1A**). BODIPY derivatives possess remarkable properties, such as high extinction coefficients and high fluorescence quantum yields, and are widely used in many fields, such as in fluorescent markers for bio-imaging and potential photosensitizers in PDT (Loudet and Burgess, 2007; Durantini et al., 2018). Most importantly, BODIPY has an absorption spectrum maximal absorption around 540 nm, close to the Sun's maximal irradiation at sea level (∼520 nm), and thus can be a candidate for agricultural PDT.

Here, we report an effective and facile method based on aPDT to control citrus canker. We develop a BODIPY-based

antibacterial agent that is quite stable under sunlight and highly effective toward *Xanthomonas citri subsp. citri*. This antibacterial agent is about 64 times more effective than the copper agent, representing a new alternative pesticide that controls plant diseases caused by the citrus canker pathogen.

MATERIALS AND METHODS

Materials and Instruments

Reagents and Materials

All chemical reagents used were of analytical grade and purchased from Sigma-Aldrich Co., Ltd. (St. Louis, United States) or Sinopharm Chemical Reagent Co., Ltd (Shanghai, China). Pentalysine β-carboxyl phthalocyanine zinc ($ZnPc(Lys)_5$), tetra-carboxyl phthalocyanine zinc ($Pc(COOH)_4$), and β-carbonyl phthalocyanine zinc (CPZ) were synthesized as described in previous studies (Chen et al., 2006; Dumoulin et al., 2010; Li et al., 2012). Chromatographic purification was performed on silica gel (Qingdao Ocean, Qingdao, Shandong, China, 200–300 mesh) columns with the indicated eluents.

Light Source and Instruments

Two different types of light sources were used in the current study. One light source was a LM-LED light (Bridgelux led, Mid Atlantic, United States) which emitted light ranging from 480 to 580 nm with a predominant central wavelength of 520 nm. Light emission spectra of the LM-LED grow light was measured using a FLS 980 fluorescence spectrometer (Edinburgh Instruments, United Kingdom) (**Supplementary Figure 1**). The other light source was a solar simulator (Newport 91160) with flux approximating natural sunlight irradiance from 295 to 2500 nm.

^{1}H-NMR spectra were recorded on an AVANE III 400 (1H, 400 MHz) instrument (Bruker, Karlsruhe, Germany) in $CDCl_3$. Chemical shifts were expressed in ppm relative to TMS (0 ppm). Electronic absorption spectra and fluorescence spectra were obtained using a microplate reader (SpectraMax i3x, Molecular Devices Corporation, California, United States).

Bacteria Strain and Plants

The *Xanthomonas citri subsp. citri strains 29-1* (*Xcc 29-1*) was cultivated in nutrient broth medium (NB) or nutrient broth supplemented with 1.5% agar (NA) at 28°C, as described in our previous publication (Zou et al., 2011). Honey murcott plants were grown in small pots with sterile soil. Antimicrobial studies were performed in a quarantine greenhouse facility (Fujian University Key Laboratory for Plant–Microbe Interaction, Fuzhou, China) under controlled temperatures (28–35°C) and a relative humidity of 80%.

Experimental Procedure

Synthesis of DIBDP, Compound 3

2,6-Diiodo-1,3,5,7-tetramethyl-8-(P-benzoic acid)-4,4′-difluoro-boradiazaindacene (DIBDP, Compound 3) was prepared using a method similar to ones previously reported (Zhang et al., 2008; Guo et al., 2013). All the reactions were carried out under the atmosphere of nitrogen. The compound 4-carboxylbenzaldehyde (Compound 1, 0.52 g, 3.47 mmol) and 2,4-dimethylpyrrole (0.63 g, 6.63 mmol) were added to anhydrous dichloromethane (500 ml) together with two drops of trifluoroacetic acid. The mixture was stirred overnight at an ambient temperature and was followed by the addition of 2,3-dichloro-5,6-dicyano-p-benzoquinone (DDQ, 0.62 g, 2.74 mmol) in anhydrous dichloromethane and further stirred continuously for 4 h. Under an ice-water bath, triethylamine (18 ml, 0.13 mole) and $BF_3{\cdot}Et_2O$ (18 ml, 0.15 mole) were added dropwise into the mixture, and stirred overnight at an ambient temperature. The reaction was monitored by thin-layer chromatography (TLC). After the completion of the reaction, the mixture was washed with saturated $NaHCO_3$ aqueous solution, followed by water. The organic fraction was dried over anhydrous Na_2SO_4 and then concentrated to dryness under vacuum. The crude product was purified by silica gel column chromatography using CH_2Cl_2/petroleum ether (1:2, v/v) as the eluent to make Compound 2 an orange-yellow solid (0.40 g, 39%). Next, I_2 (0.31 g, 1.21 mmol) and HIO_4 (0.17 g, 0.98 mmol) were added to a mixture of Compound 2 (0.19 g, 0.53 mmol) in absolute ethanol (200 ml), and then stirred under an atmosphere of nitrogen for 6 h at 60°C. The mixture was concentrated under reduced pressure after the reaction was completed, as monitored by thin-layer chromatography (TLC). Then, the residue was purified by silica gel column chromatography using CH_2Cl_2/petroleum ether (1:3, v/v) as the eluent to give DIBDP as a red solid (0.25 g, 85%), and confirmed by ^{1}H NMR (400 MHz, $CDCl_3$).

Photostability Measurement of DIBDP

The DIBDP (10 μM) in PBS was illuminated using the LM-LED light source at a light dosage of 4 mW/cm^2 or the solar simulator at a power density of 80 mW/cm^2. The ultraviolet-visible spectrum of DIBDP was monitored at 540 nm on a microplate reader.

Preparation of Stable Photosensitizer Complex (PSC) Under Light Irradiation

To prepare a stable photosensitizer complex under light irradiation, three adjuvants (1 mM in DMSO) – pentalysine β-carboxyl phthalocyanine zinc ($ZnPc(Lys)_5$), tetra-carboxyl phthalocyanine zinc ($Pc(COOH)_4$), and β-carbonyl phthalocyanine zinc (CPZ), were respectively mixed with DIBDP (1 mM in DMSO) at a molar ratio of 1:1. The mixed solutions were added into PBS buffer up to 1 ml, followed by stirring for 2 h. The DMSO was then removed by dialysis against proper solvents (PBS or DI water) overnight at room temperature. The stability of the samples was evaluated using the ultraviolet-visible spectrum of DIBDP with illumination.

A similar procedure was employed to optimize the amount of adjuvant $ZnPc(Lys)_5$ needed. DIBDP was mixed with the adjuvant at different molar ratios (10:1, 5:1, 2:1, 1:1, 1:2, 1:5, and 1:10). The absorbance value of DIBDP at 540 nm was monitored during constant illumination for 720 s. The photodegradation rate of DIBDP was assessed using the photodegradation rate constant K, following the formula: $N_t = N_0{*}e^{-kt}$ (Eggeling et al., 1999; Demchenko, 2020). Here, N_t

and N_0 was residual DIBDP of the experimental and control group, respectively, and K was the photodegradation rate constant. This is a popular kinetic approach used to quantify photobleaching, based on the assumption that photobleaching is a quasiunimolecular reaction, and the concentration of the dye molecule shows an exponential decrease in time from the initial concentration.

Antimicrobial Studies of PSC on *Xcc 29-1*

Xcc 29-1 was cultivated in nutrient broth medium at 28°C until reaching10^8 CFU/ml, and then diluted to $\sim 10^6$ CFU/ml in PBS. The diluted *Xcc 29-1* suspension was added into 96-well plates with 200 μl per well and incubated with the PSC solution at different concentrations ($10^{-4.5}$ M, 10^{-5} M, $10^{-5.5}$ M, 10^{-6} M, $10^{-6.5}$ M, 10^{-7} M, $10^{-7.5}$ M, 10^{-8} M, $10^{-8.5}$ M, 10^{-9} M and $10^{-9.5}$ M, respectively). Four replicates at each concentration were tested. The plate was illuminated using the solar simulator to a power density of 80 mW/cm^2 (1 min). The number of alive bacteria was evaluated by colony counting method. Bacterial solution (100 μl) from each well was serially diluted to 10^{-1} to 10^{-5} in PBS and spread onto nutrient broth agar plates. After incubation at 28°C for 48 h, the colonies were counted and the survival percentage was calculated as the average number of colonies of the treated plates divided by the average number of colonies of the control plate.

Determination of MIC Against *Xcc 29-1*

The antibacterial potential of PSC was compared to copper sulfate and copper hydroxide. Minimum inhibitory concentration (MIC) values were measured using the double dilution method according to our previously reported work or others with some modifications (Liu et al., 2018; Rodrigues et al., 2018). *Xcc 29-1* was grown in NB medium at 28°C with constant shaking at 200 rpm to an O.D 600 of 0.3 and was adjusted to a concentration of 10^6 colony-forming units ([CFU]/ml). 100 μl of such nutrient broth was pipetted into a set of wells in a 96-well microplate. In another set of wells, 100 μl of a 248 μg/ml stock of PSC was added and serially diluted to concentrations of 124, 62, 31, 15.5, 7.75, 3.9, 1.9, 0.97, 0.48, 0.24, and 0.12 μg/ml. Copper sulfate or copper hydroxide concentration gradient (2,000, 1,000, 500, 250, 125, 62.5, 31.25, 15.6, 7.8, 3.9, and 1.96 μg/ml) were also set up. The first column of wells containing only broth was used as negative control. A 100 μl aliquot of 5×10^6 CFU/ml bacteria suspension was added to each well. Then, the PSC was illuminated by the solar simulator to a light dosage of 4.8 J/cm^2. The microplate was incubated in 28°C at 200 rpm. After 24 h, the MIC concentration was established as the lowest concentration of the compound in which *Xcc 29-1* did not grow. All determinations were conducted in three replicates and repeated three times.

Antibacterial Mechanism of PSC

Morphologies change of Xcc 29-1 treated by PSC

The morphologies of *Xcc 29-1* treated by PSC were observed using a scanning electron microscope (SEM). The specimens of *Xcc 29-1* were prepared by the procedure of fixation, dehydration, and coating. For details, *Xcc 29-1* was harvested by being centrifuged at 6,000 *g* for 10 min and washed twice with sterile phosphate buffered saline (PBS). For fixation, the bacteria were fixed with pre-cooling 2.5% (v/v) glutaraldehyde in PBS overnight at 4°C, then washed by PBS twice. For dehydration, the bacteria were soaked sequentially in a series of ethanol (30, 50, 70, 90, and 100%) for about 10–15 min at each concentration. For the coating and observation, the dehydrated bacteria were placed onto silicon wafers and dried at 37°C overnight. Then, prepared specimens were sprayed with gold before observation on a scanning electron microscope (SEM).

ROS measurement of PSC

Detection of ROS was performed using the probe 2,7-dichlorofluorescein diacetate (DCFH-DA), which can be transformed into 2,7-dichlorofluorescein (DCF, ex 488 nm, em 525 nm) in the present ROS. Ascorbic acid is a well-known water-soluble antioxidant and is a chemically scavenged singlet oxygen (Chou and Khan, 1983). In the present study, PSC (5 μM) and DCFH-DA (100 μM) were added to 96-well plates with or without ascorbic acid (100 μM), giving total volumes of 200 μl. The solutions were irradiated using the solar simulator at a power density of 80 mW/cm^2 for 8 min. DCF fluorescence intensity (excited at 488 nm) was monitored on a microplate reader (PerkinElmer Instruments).

Stability Studies of the PSC on Leaves

Plant leaves of approximately the same size were placed in a 12-well plate, and 20 μl of PSC stock solution (50 μM) was pipetted onto the leaves, forming liquid droplets. The leaves were illuminated using the solar simulator at a power density of 80 mW/cm^2 for different amounts of time. The PSC solutions on leaves were then recovered. The leaves were further washed with DMSO solution. The DIBDP in the combined solutions was quantified by measuring the absorption at 540 nm. We have carried out a control experiment to show that DMSO extraction on plain leaves did not display 540 nm absorption.

Antimicrobial Studies of the PSC on Leaves

Puncture inoculation

In order to determine the curative activities of PSC in citrus plants, well growing citrus leaves were chosen and inoculated using the puncture method. Fully extended leaves (n = 15) were randomly divided into three groups and 10 pin-holes were punctured per leaf. *Xcc 29-1* cells at a final concentration of 10^8 CFU/ml were infiltrated into citrus leaves with degreasing cotton. A total of 1 day after inoculation, the PSC solution at 30 μg/ml (50 μM) and copper sulfate solution at 1 mg/ml were uniformly sprayed onto the leaves until dripping down, whereas PBS solution was uniformly sprayed onto the negative control leaves. The leaves of the PSC group were illuminated by the solar simulator with a power density of 80 mW/cm^2 for 10 min. At 7 and 14 days after spraying, using a macroscopic lesion for observation, the disease development was recorded and disease incidence was calculated. The disease incidence of puncture inoculation was calculated by dividing the total infected leaves with total inoculated.

Spray infection

In these preventive assays, the leaves of sweet orange were kept under greenhouse conditions and were sprayed with either the PSC solution at 30 μg/ml or copper sulfate solution at 1 mg/ml. Upon drying of the leaf surface (∼2 h), the Xcc 29-1 culture suspensions (10^8 CFU/ml) were sprayed on leaves (18 leaves per strain and randomly divided into three groups) until fully covered with bacterial suspension. A PBS treatment was setup as a negative control. Each group had three replicates. The PSC treatment group was illuminated by the solar simulator at a power density of 80 mW/cm^2 for 10 min. At 30 days post-inoculation, the disease severity of each group was measured regarding the number of citrus canker lesions per cm^2, and foliar area were measured using digital images from Adobe Photoshop software (Adobe Systems Inc., San Jose, CA, United States).

In the curative assays, the PSC solution (30 μg/ml) or copper sulfate solution (1 mg/ml) at 10 μl/lesion were added to 35-day-old canker lesions of leaves, which generated in the preventive tests. The PSC treatment group was illuminated by the solar simulator with a power density of 80 mW/cm^2 for 10 min. After a day, the treated leaves were disinfested by immersion in 70% ethanol for 1 min, followed by washing with sterilized distilled water for 1 min. Each individual lesion (with a size ∼4 mm^2) was cut out and smashed in 1 ml PBS with a sterile glass rod. The bacterial suspension (100 μl) was serially diluted to 10^{-1} to 10^{-5} in PBS and spread onto nutrient broth agar plates. After incubation at 28°C for 48 h, the number of cfu were counted and transformed to log10 cfu/lesion.

RESULTS

Design and Characteristic of DIBDP

We chose a DIBDP photosensitizer (**Figure 1A**) to study its ability to inactivate bacteria based on the following considerations. First, this photosensitizer has a strong photodynamic effect due to the presence of iodine atoms. The heavy atoms (iodine) facilitate intersystem crossing of excited photons, therefore promoting the generation of singlet oxygen (a type of ROS) in high efficiency. Secondly, the compound has a maximal adsorption at 540 nm in its UV-VIS absorption spectrum (**Figure 1B**), which matches the maximal

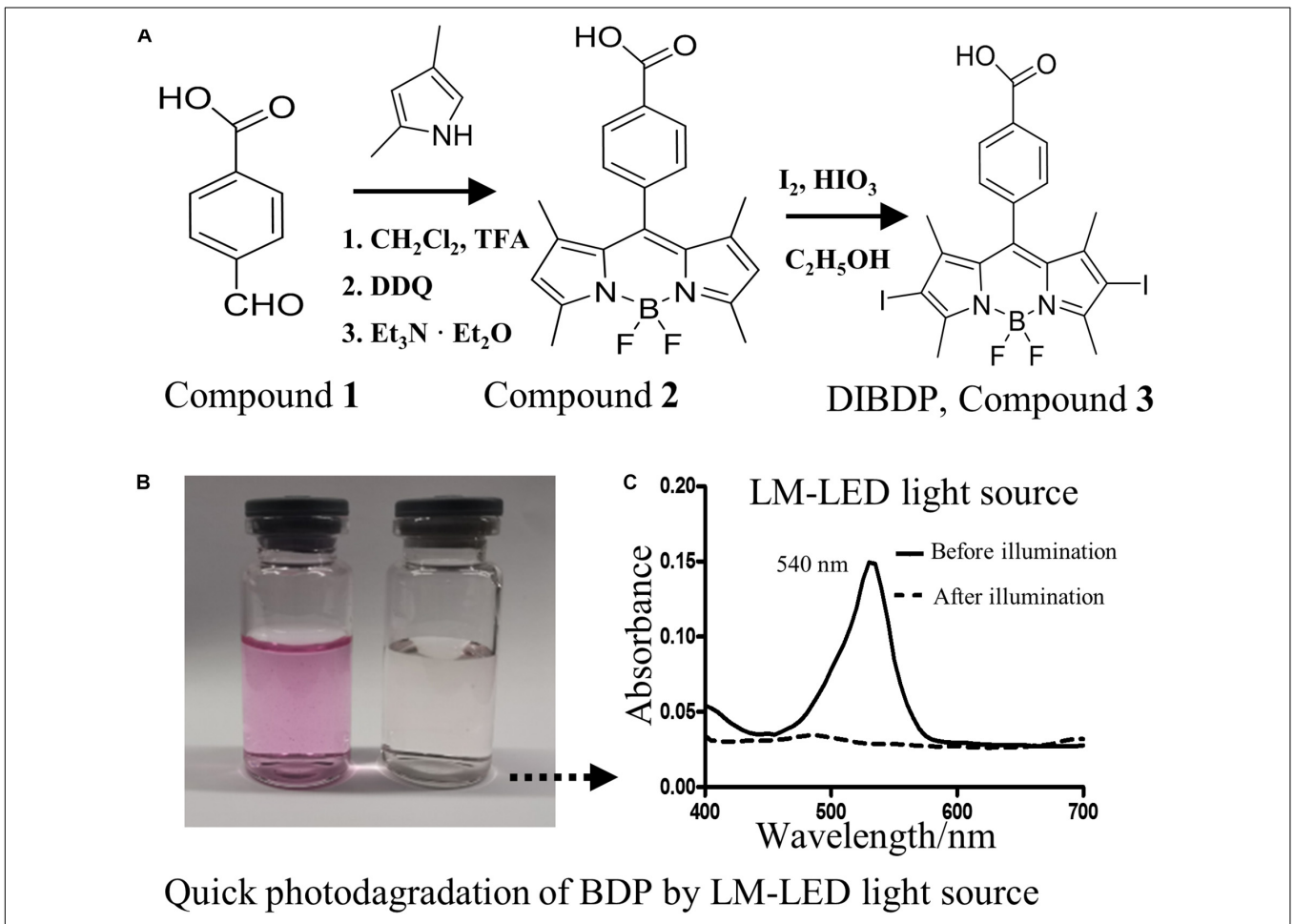

FIGURE 1 | (A) Synthesis scheme for the target compound DIBDP. **(B)** Color change before (left) and after (right) light illumination. **(C)** UV-VIS absorption spectrum of DIBDP at 10 μM in PBS before and after light illumination at a dose of 0.25 J/cm^2 (520 nm, 4 mW/cm^2).

emission wavelength of sunlight (Kim et al., 2015). This DIBDP compound was synthesized chemically in high yield (**Figure 1A**), and its structure was fully confirmed by proton NMR spectrum (**Supplementary Figure 2**).

However, we found that the DIBDP degraded rapidly under light illumination. The DIBDP at a concentration of 10 μM completely degraded in 1 min with the illumination of an LED light source (4 mW/cm^2) or a solar simulator (80 mW/cm^2) (**Figure 1C** and **Supplementary Figure 3**).

Optimization of a Photosensitizer Complex (PSC) Stable Under Sunlight

To meet the challenge of photodegradation, we searched for an adjuvant to increase the DIBDP photostability under sunlight.

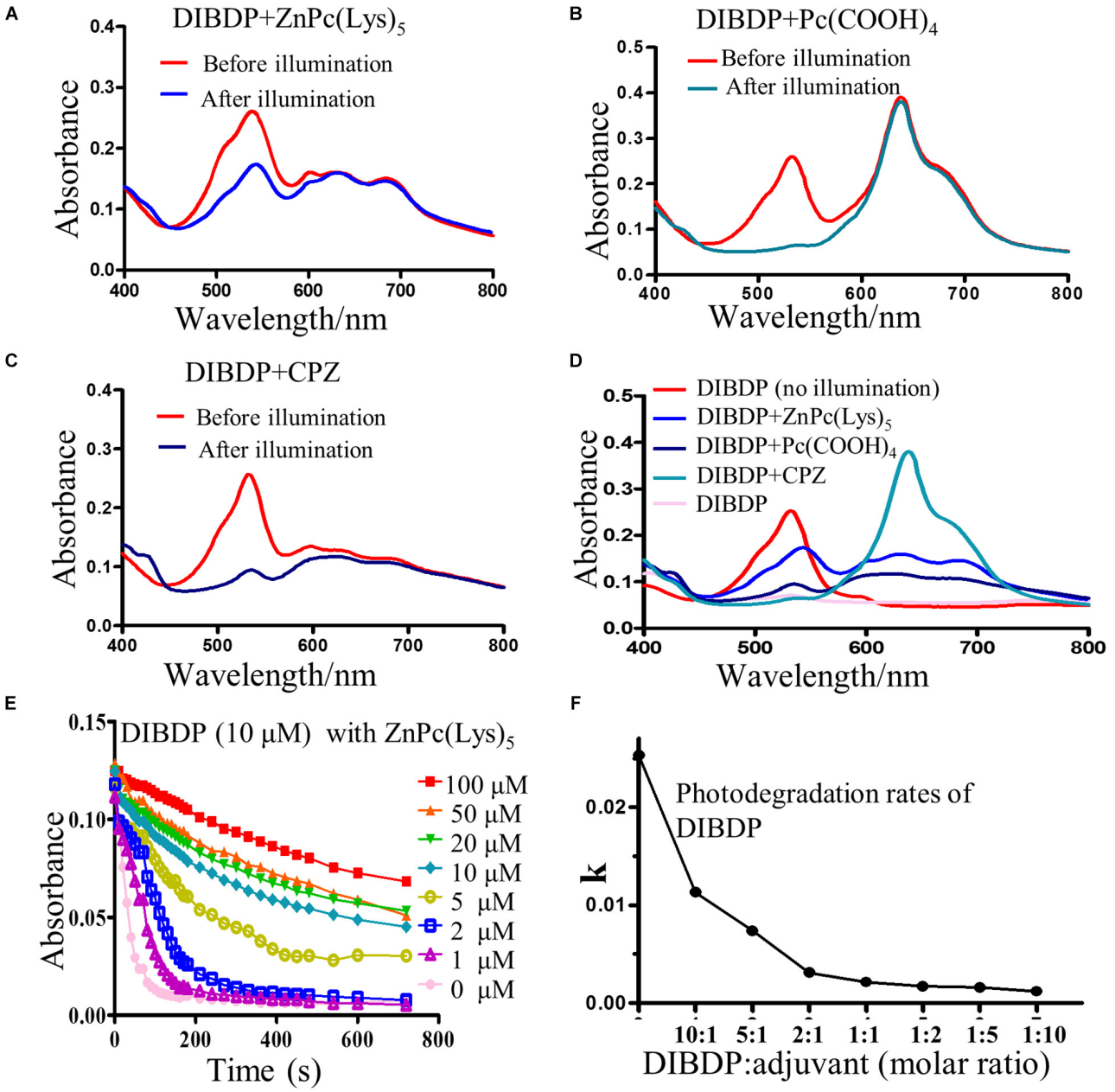

FIGURE 2 | Optimization of a complex (PSC) for resistance to photodegradation under sunlight irradiation. **(A–C)**: The absorbance spectrum of DIBDP with three adjuvants at 1:1 molar ratio in PBS buffer before or after light irradiation (520 nm, 1 min at 4 mW/cm^2); [**(A)**, pentalysine β-carboxyl phthalocyanine zinc (ZnPc(Lys)$_5$]; **(B)** tetra-carboxyl phthalocyanine zinc (Pc(COOH)$_4$); [**(C)** β-carbonyl phthalocyanine zinc (CPZ)]. **(D)** Comparison of the stabilizing effects of three adjuvants. **(E)** Typical photodegradation kinetics to optimize molar ratio of DIBDP (10 μM) and the adjuvant (ZnPc(Lys)$_5$) (1 μM to 100 μM) by monitoring absorbance value of DIBDP at 540 nm for 720 s with a LM-LED light source (4 mW/cm^2). **(F)** The quantification of **(E)** into photodegradation rate constant (k).

In our previous work, we found that a compound named zinc phthalocyanine is quite resistant to photodegradation, despite being an organic dye (Jia et al., 2018). In this work, we studied a series of this type of compound to see if they can stabilize the DIBDP we chose. We selected a number of zinc phthalocyanine compounds, mixed them with the DIBDP, and measured the photodegradation rates of the mixtures at different molar ratios. We chose three compounds with different characteristics: β-carbonylphthalocyanine zinc (CPZ), tetra-carboxyphthalocyanine zinc ($Pc(COOH)_4$), and pentalysine β-carboxyl phthalocyanine zinc ($ZnPc(Lys)_5$). Fortunately, we did identify a compound ($ZnPc(Lys)_5$) that stabilized the photobleaching of DIBDP (**Figures 2A–D**).

In order to optimize the amount of the adjuvant needed, we mixed the DIBDP (10 μM) with different amounts of the adjuvant (1 μM to 100 μM) and measured the photodegradation rate. **Figure 2E** showed the effect of the adjuvant on the DIBDP photobleaching rates. Illumination of DIBDP in solutions leads to quick photobleaching: more than 90% degradation in 100 s and almost complete degradation in 200 s for 10 μM of DIBDP at a light illumination condition of 4 mW/cm^2. The degradation of DIBDP reduced with the increase of adjuvant concentration. Even a small amount of adjuvant (1 μM) reduced the photodegradation rate of DIBDP by 50% (**Figure 2E**), demonstrating the power of this method. At the 1:1 molar ratio, the photodegradation rate reduced nearly 12-fold. In addition, PSC showed a similar result under the condition of sunlight (**Supplementary Figures 4A,B**). In the following experiments, we selected a molar ratio of DIBDP:adjuvant of 1:2, which led to the optimal 15-fold reduction of DIBDP photodegradation (**Figure 2F**). This agent is here named photosensitizer complex or PSC. We want to point out that the adjuvant agent, zinc phthalocyanine, has absorption at the far red region (Kobayashi et al., 2003), and thus does not interfere with the photodynamic effect of the DIBPD. The minimum inhibitory concentration (MIC) of zinc salt or its metal against bacteria was very high (500 μg/ml, or 3.12 mM) (Goncalves et al., 2017; Gugala et al., 2019), much higher than the concentration of adjuvant that we used here. Thus, it is unlikely that the antimicrobial efficacy of PSC observed here was due to the zinc salt in the adjuvant. Stability of PSC on leaves upon light illumination.

We also evaluated the stability of PSC on citrus leaves using the solar simulator (**Supplementary Figure 5**). The DIBDP itself on leaves again led to quick photobleaching and almost complete degradation in 6 min. On the other hand, PSC showed excellent resistance with over 60% of intact BDP left at 40 min. With longer light illumination, the PSC solution evaporated completely and become a solid film after 25 min, and the PSC solid was no longer degraded.

Antibacterial Efficacy of PSC Under Sunlight

The antibacterial effect of the PSC against the *Xcc 29-1* bacteria strain was measured using the colony counting method with light illumination from a solar simulator at the power of 80 mW/cm^2. The IC_{50} of the PSC was measured to be 0.26 μM, which was 7.3-fold lower than that of DIBDP alone (1.9 μM), showing enhanced antimicrobial activity in the presence of the adjuvant agent (**Figure 3A**).

Copper salts are currently used to control the infection by Xcc, even though their potencies are low. We measured the minimum inhibitory concentration (MIC) of the PSC toward the *Xcc 29-1* strain, together with the positive control copper sulfate and copper hydroxide, two widely used agents to control citrus canker. The PSC showed a 64-fold lower MIC against *Xcc 29-1* (MIC 7.75 μg/ml) compared to copper sulfate (MIC 500 μg/ml) or copper hydroxide (MIC 830 μg/ml) (**Figure 3B**). These results demonstrated that the PSC was much more potent against *Xcc 29-1* than the copper salts.

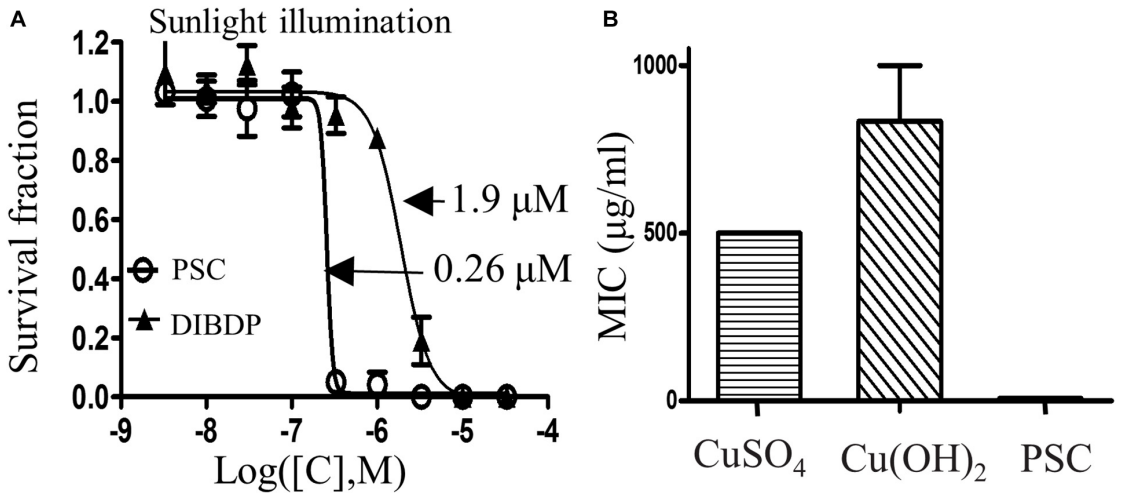

FIGURE 3 | Antimicrobial effects of PSC on *Xcc 29-1*. **(A)** The photoinactivation of DIBDP or PSC against *Xcc 29-1* under sunlight irradiation with the solar simulator at a power density of 80 mW/cm^2 (1 min). **(B)** Minimum inhibitory concentration (MIC) of PSC, $CuSO_4$, and $Cu(OH)_2$ against *Xcc 29-1*.

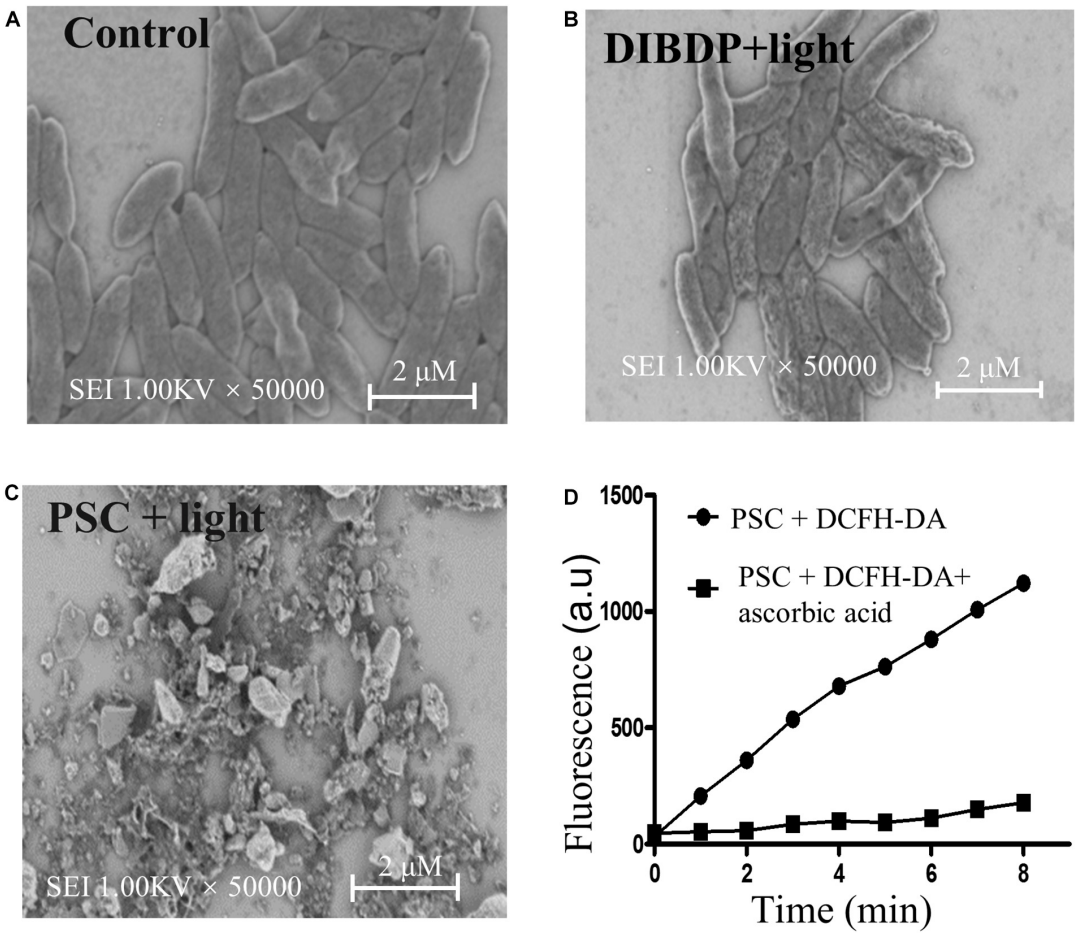

FIGURE 4 | Antibacterial mechanism of PSC. SEM images of *Xcc 29-1* before **(A)** and after treatment with DIBDP **(B)** or PSC **(C)** at 10 μM followed by sunlight irradiation. **(D)** Fluorescence of DCFH-DA (100 μM) was activated by ROS generated by PSC (5 μM), but quenched by ascorbic acid (100 μM).

Antibacterial Mechanism of PSC

To further study how the PSC damage bacteria cell's surface morphology, scanning electron microscopy (SEM) was performed on *Xcc 29-1* after incubation with PSC with illumination. As shown in **Figure 4A**, *Xcc 29-1* without treatment displayed characteristic straight rods with smooth outer surfaces. In contrast, the morphology of the bacteria cell showed membrane deformation and surface collapse after treatment with DIBDP at a concentration of 10 μM and light irradiation (**Figure 4B**). With treatment of PSC, the bacteria practically broke down into debris, as shown by SEM (**Figure 4C**). These results confirmed the severe damage of *Xcc 29-1* induced by aPDT under light irradiation, and the PSC enhanced antimicrobial activity compared to free DIBDP.

Next, we measured the generation of ROS from the PSC using the probe DCFH-DA, which has no fluorescence but is converted to fluorescent species (DCF) in the presence of ROS. As shown in **Figure 4D**, the DCF fluorescence intensity was gradually increased as the irradiation time was prolonged. Such fluorescence was suppressed in the presence of ascorbic acid, which is a relatively specific quencher for singlet oxygen ($^1O_2$). These experiments demonstrated that PSC inactivated the pathogen using ROS, most likely by singlet oxygen.

Effect of PSC on Citrus Canker Development

In order to evaluate the antimicrobial activity of the PSC on plants infected with citrus canker, both puncture inoculation and spray infection methods were carried out, using 30 μg/ml PSC for treatment, based on the MIC value measured above. Copper sulfate (1 mg/ml) was used as control.

A puncture inoculation plant model was established by inoculating *Xcc 29-1* bacteria on perforated leaves. Lesion development on the leaves was monitored daily up to 14 days after inoculation. In our assay, a solution of the PSC (30 μg/ml) was uniformly sprayed onto the leaves after the application of *Xcc 29-1* inoculum. The solvent (PBS) and copper sulfate (1 mg/ml) were used as the negative and positive control, respectively (**Figure 5A**). After the inoculation of *Xcc 29-1* bacteria for 5 days, the leaves began to show spongy pustules. On the 7th day, these pustules darkened and thickened into a light tan to brown corky

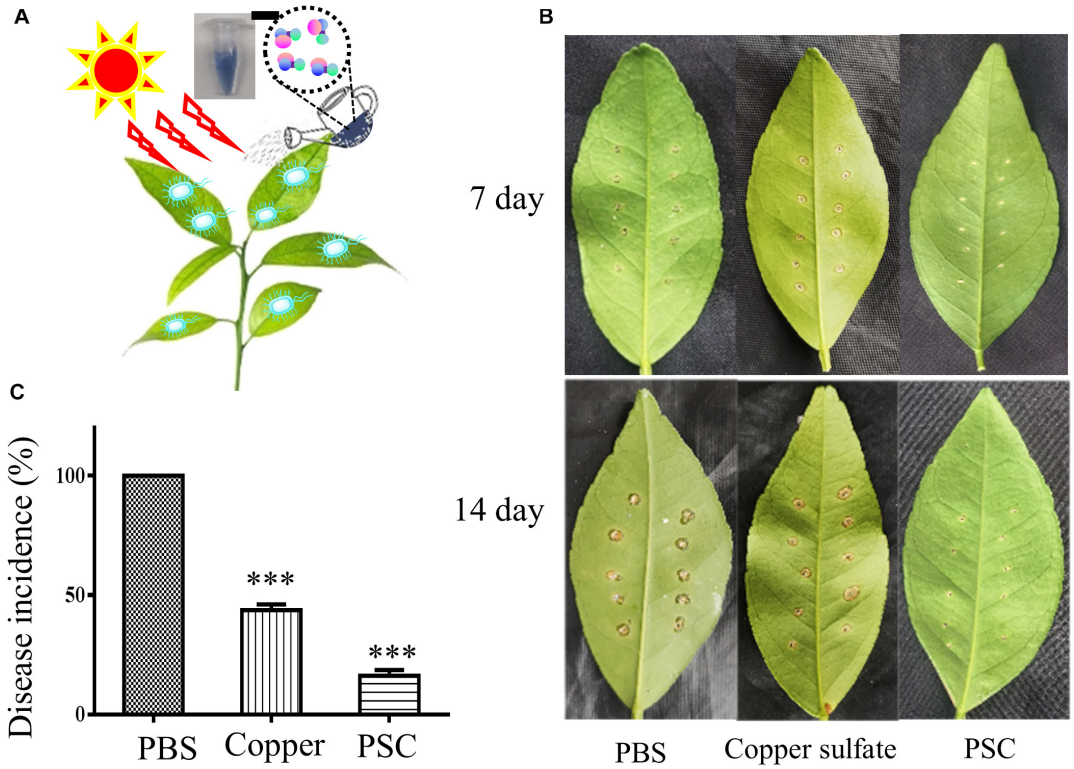

FIGURE 5 | Antimicrobial effect of PSC on citrus plants infected with *Xcc* bacteria. **(A)** A photosensitizer complex (PSC) was developed to kill the pathogen for citrus canker, *Xanthomonas citri subsp. citri*, under sunlight irradiation, using reactive oxygen species. **(B)** Representative Honey murcott leaves treated with PBS, copper sulfate, or PSC at 7 and 14 day using the puncture inoculation method. **(C)** Quantitative results of three treated groups. All bars represent standard error of the mean (SEM). The data were analyzed for statistical differences using one-way ANOVA (***$P < 0.001$).

canker, which was rough to the touch (**Figure 5B**). These corky cankers were further aggravated and all the punctures developed into severe corky cankers by the 14th day. The PSC treatment remarkably reduced lesion development over time compared with the controls. In addition, the PSC treatment showed results superior to the copper sulfate treatment group. The copper control group had 45% punctures that developed into corky cankers by the 14th day and showed severe damage to the citrus leaves. The PSC treatment significantly reduced the incidence of canker lesions, with only 16% of punctures deteriorating into cankers (**Figure 5C**).

We also evaluated the preventive and curative effects of the PSC based on spray infection, which reflected the natural infection process of citrus canker. It took about 30 days post spread inoculation with wild type Xcc 29-1 for the canker lesion to develop. The lesions had a typical brownish corky-like appearance. The number of citrus canker lesions/cm^2 on leaves treated with PBS was an average of 5.07 lesions/cm^2, while the PSC treatment group had only an average of 0.26 lesions/cm^2 on the leaves (**Figures 6A,B**). These results clearly indicated that the PSC ($P < 0.001$) strongly prevented canker development and is useful for the control of canker in citrus fruit plantations. In our control, copper salt also showed decent effect in preventing the development of citrus canker lesions (**Figure 6**). For the curative assay, we applied either PSC or copper to the infected leaves, and measured the amount of bacteria on 15 lesions in each group by CFU counting. The result showed the amount of bacterial population on the leaves of trees treated with PSC was reduced by 95%, similar to the copper treatment, demonstrating that PSC is a promising agent to control citrus canker (**Figure 6C**).

The above results indicated that PSC killed *Xcc 29-1* in plants under sunlight at a concentration much lower than copper (30 μg/ml vs. 1 mg/ml). In addition, we observed no adverse effects at all of PSC on the normal plant leaves at the doses used to kill *Xcc 29-1* bacteria, demonstrating the safety of PSC.

DISCUSSION

There is strong interest in understanding the pathogenesis of *Xcc* and its interaction with its host in hope to find new agents to intervene with citrus canker formation (Ference et al., 2018). We identified a number of novel genes of *Xcc* (Song et al., 2015; Xia et al., 2016) that are related to its virulence. One of them encodes an extracellular endoglucanase on *Xcc* (BglC3) and is required for the full virulence of *Xcc* (Xia et al., 2016). In addition, a response regulator (VemR) was found to be important in the flagellum-derived cell motility of *Xcc* (Wu et al., 2019). Deletion of this gene (*vemR*) reduced not only cell motility, but also the exopolysaccharide production,

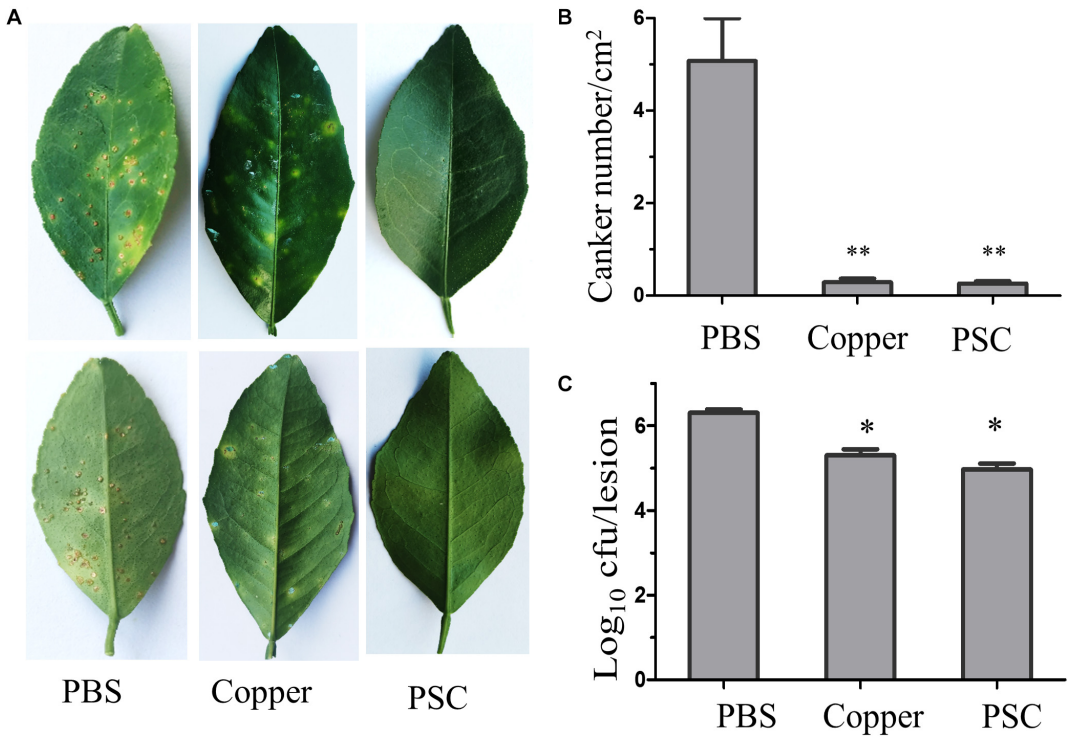

FIGURE 6 | Preventive **(A,B)** and curative **(C)** effects of PSC in citrus canker control. **(A)** The canker lesions developed on leaf surface 30 days after being spread with *Xcc 29-1* (top panel, PBS group) but had much less infection in the group treated with either copper sulfate (1 mg/ml) or PSC (30 μg/ml). The quantitation of canker number was shown in **(B)**. **(C)** The number of CFU in each lesion at 35-day-old canker lesions after treatments with either copper salt or PSC. All bars represent standard error of the mean (SEM). The data were analyzed for statistical differences using one-way ANOVA (*$P < 0.05$, **$P < 0.01$).

leading to lower virulence. This VemR was also an RpoN2 cognate activator and positively regulated the transcription of the rod gene *flgG* in the bacteria (Wu et al., 2019). These works identified critical genes on *Xcc* for citrus infection that could be valuable targets to control citrus canker. In another strategy to control citrus canker, an *Xcc* resistant strain of citrus was generated by engineering of the *Xcc*-susceptibility gene *CsLOB1* of citrus using CRISPR/Cas9-mediated promoter editing (Peng et al., 2017). The current management methods of citrus canker mainly include the applications of copper agents to kill or inhibit pathogenic bacteria, insecticide to control the leaf miner fly which rapidly spreads canker diseases (Leite and Mohan, 1990), or biological control agents such as bacteriophages (Balogh et al., 2008; Ibrahim et al., 2017). Bacteriophage suffers from having a short active period caused mainly by the detrimental effects of sunlight UV irradiation, seriously affecting its control effect (Ji et al., 2006).

Copper bactericide is the main agent used in large quantities despite its low antibacterial efficacy (Marin et al., 2019). Long-term use of copper bactericides results in a harmful impact on the environment, plants, and safety human (Zhu and Alva, 1993; Lin et al., 2010). In addition, the multiple and independent applications of chemical pesticides have led to the emergence of resistance genes identified in Argentina and Florida, United States (Behlau et al., 2011, 2013). Aggressive measures to remove infected trees can only prevent the diffusion of the pathogen to some extent and cannot completely control citrus canker (Sosnowski et al., 2009). The lack of effective control methods seriously damage the citrus industry and result in significant economic losses. Therefore, it is desirable to develop an effective and ecologically friendly anti-microbial technology to replace copper pesticides.

In the present study, we developed a photosensitizer complex (PSC) to inactivate *Xcc 29-1* under sunlight. The result showed that *Xcc 29-1* was effectively inactivated at a MIC value of 7.75 μg/ml PSC, much lower than the copper sulfate control (500 μg/ml).

Our results of PSC showed low toxicity to leaves when exposed to sunlight. Such safety to leaves could be due to the low concentration (μM range) of PSC used during aPDT. Moreover, the lifetime of single oxygen in tissues is very short (<40 ns) and its action distance is limited (less than 20 nm) (Moan, 1990). In addition, the leaf cuticle of the citrus leaves appears to be more resistant to aPDT using PSC. Such resistance in plants is in major contrast to animal cells and microorganisms, which are more vulnerable to insults from PDT.

The development of bacterial resistance to aPDT was considered unlikely due to the multi-target mechanism of photoinactivation (Tavares et al., 2010; Martins et al., 2018). Thus, the application of aPDT to control citrus canker could be a safe alternative to copper for the effective control of canker in citrus fruit plantations. In the long run, PSC will be degraded over

time in the environment, which should reduce the risk of its accumulation. Future studies will include field trials' evaluation and investigation of its environmental fate on non-target species.

CONCLUSION

In conclusion, we successfully prepared a photosensitizer complex (PSC) and demonstrated its antibacterial effects using a solar simulator on citrus leaves. The PSC was prepared by simple mixing; the optimum mixing ratio of DIBDP and adjuvant agent was 1:2. Under sunlight irradiation, PSC had more enhanced antimicrobial activity than single DIBDP. Compared to the traditional antibacterial agent copper salts, PSC showed a lower MIC concentration (MIC 7.75 μg/ml) against *Xcc 29-1* comparable to copper standards (MIC 500 μg/ml). The PSC showed much strong efficacy than the copper agent and had lower toxicity to leaves, demonstrating that PSC is a promising agent to control citrus canker.

DATA AVAILABILITY STATEMENT

All datasets presented in this study are included in the article/**Supplementary Material**.

AUTHOR CONTRIBUTIONS

LJ carried out the experiments and drafted the manuscript. YL, XX, and DS assisted in the experiments. HZ and JL provided key reagents and expertise necessary for this interdisciplinary work. CY and MH conceived and designed the project, analyzed data, and wrote the manuscript. All authors contributed to the article and approved the submitted version.

FUNDING

This research work was financially supported by grants from the National Key R&D Program of China (2017YFE0103200), National Natural Science Foundation of China (31370737, 31400637, 31570745, and 31670739), and Natural Science Foundation of Fujian Province (2018J01897 and 2018J01729).

SUPPLEMENTARY MATERIAL

The Supplementary Material for this article can be found online at: https://www.frontiersin.org/articles/10.3389/fmicb.2020.571691/full#supplementary-material

REFERENCES

Agostinis, P., Berg, K., Cengel, K. A., Foster, T. H., Girotti, A. W., Gollnick, S. O., et al. (2011). Photodynamic therapy of cancer: an update. *CA Cancer J. Clin.* 61, 250–281.

Balogh, B., Canteros, B. I., Stall, R. E., and Jones, J. B. (2008). Control of citrus canker and citrus bacterial spot with bacteriophages. *Plant Dis.* 92, 1048–1052. doi: 10.1094/pdis-92-7-1048

Behlau, F., Canteros, B. I., Minsavage, G. V., Jones, J. B., and Graham, J. H. (2011). Molecular characterization of copper resistance genes from *Xanthomonas citri* subsp. citri and *Xanthomonas alfalfae* subsp. citrumelonis. *Appl. Environ. Microbiol.* 77, 4089–4096. doi: 10.1128/aem.03043-10

Behlau, F., Fonseca, A. E., and Belasque, J. (2016). A comprehensive analysis of the Asiatic citrus canker eradication programme in Sao Paulo state, Brazil, from 1999 to 2009. *Plant Pathol.* 65, 1390–1399. doi: 10.1111/ppa.12503

Behlau, F., Hong, J. C., Jones, J. B., and Graham, J. H. (2013). Evidence for acquisition of copper resistance genes from different sources in citrus-associated xanthomonads. *Phytopathology* 103, 409–418. doi: 10.1094/phyto-06-12-0134-r

Bock, C. H., Parker, P. E., and Gottwald, T. R. (2005). Effect of simulated wind-driven rain on duration and distance of dispersal of *Xanthomonas axonopodis* pv. citri from canker-infected citrus trees. *Plant Dis.* 89, 71–80. doi: 10.1094/pd-89-0071

Brunings, A. M., and Gabriel, D. W. (2003). *Xanthomonas citri*: breaking the surface. *Mol. Plant Pathol.* 4, 141–157. doi: 10.1046/j.1364-3703.2003.00163.x

Carrera, E. T., Dias, H. B., Corbi, S. C. T., Marcantonio, R. A. C., Bernardi, A. C. A., Bagnato, V. S., et al. (2016). The application of antimicrobial photodynamic therapy (aPDT) in dentistry: a critical review. *Laser Phys.* 26:123001. doi: 10.1088/1054-660x/26/12/123001

Chen, J. C., Chen, N. S., Huang, J. F., Wang, J. D., and Huang, M. D. (2006). Derivatizable phthalocyanine with single carboxyl group: synthesis and purification. *Inorg. Chem. Commun.* 9, 313–315. doi: 10.1016/j.inoche.2005.12.002

Chou, P. T., and Khan, A. U. (1983). L-ascorbic acid quenching of singlet delta molecular oxygen in aqueous media: generalized antioxidant property of vitamin C. *Biochem. Biophys. Res. Commun.* 115, 932–937. doi: 10.1016/s0006-291x(83)80024-2

Demchenko, A. P. (2020). Photobleaching of organic fluorophores: quantitative characterization, mechanisms, protection. *Methods Appl. Fluoresc.* 8:022001. doi: 10.1088/2050-6120/ab7365

Dumoulin, F., Durmus, M., Ahsen, V., and Nyokong, T. (2010). Synthetic pathways to water-soluble phthalocyanines and close analogs. *Coord. Chem. Rev.* 254, 2792–2847. doi: 10.1016/j.ccr.2010.05.002

Durantini, A. M., Heredia, D. A., Durantini, J. E., and Durantini, E. N. (2018). BODIPYs to the rescue: potential applications in photodynamic inactivation. *Eur. J. Med. Chem.* 144, 651–661. doi: 10.1016/j.ejmech.2017.12.068

Eggeling, C., Rigler, W. J., and Seidelc, R. (1999). "Photostability of fluorescent dyes for single-molecule spectroscopy: mechanisms and experimental methods for estimating photobleaching in aqueous solution," in *Applied Fluorescence in Chemistry, Biology and Medicine*, eds W. Rettig, B. Strehmel, S. Schrader, and H. Seifert (Berlin: Springer), 193–240. doi: 10.1007/978-3-642-59903-3_10

Ference, C. M., Gochez, A. M., Behlau, F., Wang, N., Graham, J. H., and Jones, J. B. (2018). Recent advances in the understanding of *Xanthomonas citri* ssp. citri pathogenesis and citrus canker disease management. *Mol. Plant Pathol.* 19, 1302–1318.

Giuliani, F., Martinelli, M., Cocchi, A., Arbia, D., Fantetti, L., and Roncucci, G. (2010). In vitro resistance selection studies of RLP068/Cl, a new Zn(II) phthalocyanine suitable for antimicrobial photodynamic therapy. *Antimicrob. Agents Chemother.* 54, 637–642. doi: 10.1128/aac.00603-09

Goncalves, R. C., Da Silva, D. P., Signini, R., and Naves, P. L. F. (2017). Inhibition of bacterial biofilms by carboxymethyl chitosan combined with silver, zinc and copper salts. *Int. J. Biol. Macromol.* 105, 385–392. doi: 10.1016/j.ijbiomac.2017.07.048

Gottwald, T. R., Graham, J. H., and Schubert, T. S. (2002). Citrus canker: the pathogen and its impact. *Plant Health Progress* doi: 10.1094/PHP-2002-0812-01-RV

Graham, J. H., Gottwald, T. R., Cubero, J., and Achor, D. S. (2004). *Xanthomonas axonopodis* pv. citri: factors affecting successful eradication of citrus canker. *Mol. Plant Pathol.* 5, 1–15. doi: 10.1046/j.1364-3703.2004.00197.x

Gugala, N., Vu, D., Parkins, M. D., and Turner, R. J. (2019). Specificity in the susceptibilities of *Escherichia coli*, *Pseudomonas aeruginosa* and *Staphylococcus*

aureus clinical isolates to six metal antimicrobials. *Antibiotics* 8:51. doi: 10.3390/antibiotics8020051

Guo, S., Zhang, H. L., Huang, L., Guo, Z. D., Xiong, G., and Zhao, J. Z. (2013). Porous material-immobilized iodo-Bodipy as an efficient photocatalyst for photoredox catalytic organic reaction to prepare pyrrolo[2,1-a]isoquinoline. *Chem. Commun.* 49, 8689–8691. doi: 10.1039/c3cc44486d

Hamblin, M. R., and Hasan, T. (2004). Photodynamic therapy: a new antimicrobial approach to infectious disease? *Photochem. Photobiol. Sci.* 3, 436–450. doi: 10.1039/b311900a

Huang, L., Dai, T., and Hamblin, M. R. (2010). Antimicrobial photodynamic inactivation and photodynamic therapy for infections. *Methods Mol. Biol.* 635, 155–173. doi: 10.1007/978-1-60761-697-9_12

Huang, L., Xuan, Y., Koide, Y., Zhiyentayev, T., Tanaka, M., and Hamblin, M. R. (2012). Type I and Type II mechanisms of antimicrobial photodynamic therapy: an in vitro study on gram-negative and gram-positive bacteria. *Lasers Surg. Med.* 44, 490–499. doi: 10.1002/lsm.22045

Ibrahim, Y. E., Saleh, A. A., and Al-Saleh, M. A. (2017). Management of asiatic citrus canker under field conditions in saudi arabia using bacteriophages and acibenzolar-S-methyl. *Plant Dis.* 101, 761–765. doi: 10.1094/pdis-08-16-1213-re

Ji, P., Campbell, H. L., Kloepper, J. W., Jones, J. B., Suslow, T. V., and Wilson, M. (2006). Integrated biological control of bacterial speck and spot of tomato under field conditions using foliar biological control agents and plant growth-promoting rhizobacteria. *Biol. Control* 36, 358–367. doi: 10.1016/j.biocontrol.2005.09.003

Jia, Y., Li, J., Chen, J., Hu, P., Jiang, L., Chen, X., et al. (2018). Smart photosensitizer: tumor-triggered oncotherapy by self-assembly photodynamic nanodots. *ACS Appl. Mater. Interfaces* 10, 15369–15380. doi: 10.1021/acsami.7b19058

Kim, K., Park, H., and Lim, K. M. (2015). Phototoxicity: its mechanism and animal alternative test methods. *Toxicol. Res.* 31, 97–104. doi: 10.5487/tr.2015.31.2.097

Kobayashi, N., Ogata, H., Nonaka, N., and Luk'yanets, E. A. (2003). Effect of peripheral substitution on the electronic absorption and fluorescence spectra of metal-free and zinc phthalocyanines. *Chemistry* 9, 5123–5134. doi: 10.1002/chem.200304834

Kreuzer, A. T. F. (1968). Difluorboryl-komplexe von di- und tripyrrylmethenen. *Liebigs Ann. Chem.* 718, 208–223. doi: 10.1002/jlac.19687180119

Leite, R. P., and Mohan, S. K. (1990). Integrated management of the citrus bacterial canker disease caused by *Xanthomonas-Campestris* Pv citri in the State of Parana, Brazil. *Crop. Protection* 9, 3–7. doi: 10.1016/0261-2194(90)90038-9

Li, L., Luo, Z., Chen, Z., Chen, J., Zhou, S., Xu, P., et al. (2012). Enhanced photodynamic efficacy of zinc phthalocyanine by conjugating to heptalysine. *Bioconjug. Chem.* 23, 2168–2172. doi: 10.1021/bc3002997

Lin, Y., He, Z., Rosskopf, E. N., Conn, K. L., Powell, C. A., and Lazarovits, G. (2010). A nylon membrane bag assay for determination of the effect of chemicals on soilborne plant pathogens in soil. *Plant Dis.* 94, 201–206. doi: 10.1094/pdis-94-2-0201

Liu, D. F., Li, L. S., Chen, J. C., Chen, Z., Jiang, L. G., Yuan, C., et al. (2018). Dissociation of zinc phthalocyanine aggregation on bacterial surface is key for photodynamic antimicrobial effect. *J. Porphyr. Phthalocyanines* 22, 925–934. doi: 10.1142/s1088424618500888

Loudet, A., and Burgess, K. (2007). BODIPY dyes and their derivatives: syntheses and spectroscopic properties. *Chem. Rev.* 107, 4891–4932. doi: 10.1021/cr078381n

Maisch, T. (2015). Resistance in antimicrobial photodynamic inactivation of bacteria. *Photochem. Photobiol. Sci.* 14, 1518–1526. doi: 10.1039/c5pp00037h

Marin, V. R., Ferrarezi, J. H., Vieira, G., and Sass, D. C. (2019). Recent advances in the biocontrol of *Xanthomonas* spp. *World J. Microbiol. Biotechnol.* 35:72.

Martins, D., Mesquita, M. Q., Neves, M., Faustino, M. A. F., Reis, L., Figueira, E., et al. (2018). Photoinactivation of *Pseudomonas* syringae pv. actinidiae in kiwifruit plants by cationic porphyrins. *Planta* 248, 409–421. doi: 10.1007/s00425-018-2913-y

Moan, J. (1990). On the diffusion length of singlet oxygen in cells and tissues. *J. Photochem. Photobiol.* 6, 343–347. doi: 10.1016/1011-1344(90)85104-5

Pedigo, L. A., Gibbs, A. J., Scott, R. J., and Street, C. N. (2009). "Absence of bacterial resistance following repeat exposure to photodynamic therapy," in *Proceedings of the 12th World Congress of the International Photodynamic Association: Photodynamic Therapy: Back to the Future*, (Washington, DC: SPIE).

Peng, A. H., Chen, S. C., Lei, T. G., Xu, L. Z., He, Y. R., Wu, L., et al. (2017). Engineering canker-resistant plants through CRISPR/Cas9-targeted editing of the susceptibility gene CsLOB1 promoter in citrus. *Plant Biotechnol. J.* 15, 1509–1519. doi: 10.1111/pbi.12733

Rodrigues, J. P., Peti, A. P. F., Figueiro, F. S., Rocha, I. D., Acquaro, V. R., Silva, T. G., et al. (2018). Bioguided isolation, characterization and media optimization for production of Lysolipins by actinomycete as antimicrobial compound against *Xanthomonas citri* subsp. citri. *Mol. Biol. Rep.* 45, 2455–2467. doi: 10.1007/s11033-018-4411-5

Ryan, R. P., Vorholter, F. J., Potnis, N., Jones, J. B., Van Sluys, M. A., Bogdanove, A. J., et al. (2011). Pathogenomics of *Xanthomonas*: understanding bacterium-plant interactions. *Nat. Rev. Microbiol.* 9, 344–355. doi: 10.1038/nrmicro2558

Schubert, T. S., Rizvi, S. A., Sun, X., Gottwald, T. R., Graham, J. H., and Dixon, W. N. (2001). Meeting the challenge of eradicating citrus canker in florida-again. *Plant Dis.* 85, 340–356. doi: 10.1094/pdis.2001.85.4.340

Shi, X., Zhang, C. Y., Gao, J., and Wang, Z. (2019). Recent advances in photodynamic therapy for cancer and infectious diseases. *Wiley Interdiscip. Rev. Nanomed. Nanobiotechnol.* 11:e1560.

Song, X., Guo, J., Ma, W. X., Ji, Z. Y., Zou, L. F., Chen, G. Y., et al. (2015). Identification of seven novel virulence genes from *Xanthomonas citri* subsp citri by Tn5-based random mutagenesis. *J. Microbiol.* 53, 330–336. doi: 10.1007/s12275-015-4589-3

Sosnowski, M. R., Fletcher, J. D., Daly, A. M., Rodoni, B. C., and Viljanen-Rollinson, S. L. H. (2009). Techniques for the treatment, removal and disposal of host material during programmes for plant pathogen eradication. *Plant Pathol.* 58, 621–635. doi: 10.1111/j.1365-3059.2009.02042.x

Sperandio, F. F., Huang, Y. Y., and Hamblin, M. R. (2013). Antimicrobial photodynamic therapy to kill Gram-negative bacteria. *Recent Pat. Antiinfect. Drug. Discov.* 8, 108–120. doi: 10.2174/1574891x113089990012

Tavares, A., Carvalho, C. M., Faustino, M. A., Neves, M. G., Tome, J. P., Tome, A. C., et al. (2010). Antimicrobial photodynamic therapy: study of bacterial recovery viability and potential development of resistance after treatment. *Mar. Drugs* 8, 91–105. doi: 10.3390/md8010091

Wainwright, M. (1998). Photodynamic antimicrobial chemotherapy (PACT). *J. Antimicrob. Chemother.* 42, 13–28. doi: 10.1093/jac/42.1.13

Wainwright, M., Maisch, T., Nonell, S., Plaetzer, K., Almeida, A., Tegos, G. P., et al. (2017). Photoantimicrobials-are we afraid of the light? *Lancet Infect. Dis.* 17, e49–e55.

Wu, W., Zhao, Z., Luo, X., Fan, X., Zhuo, T., Hu, X., et al. (2019). Response regulator VemR regulates the transcription of flagellar rod gene flgG by interacting with sigma(54) factor RpoN2 in *Xanthomonas citri* ssp. citri. *Mol. Plant Pathol.* 20, 372–381. doi: 10.1111/mpp.12762

Xia, T., Li, Y. J., Sun, D. L., Zhuo, T., Fan, X. J., and Zou, H. S. (2016). Identification of an extracellular endoglucanase that is required for full virulence in *Xanthomonas citri* subsp. citri. *PLoS One* 11:e0151017. doi: 10.1371/journal.pone.0151017

Zhang, X., Xiao, Y., and Qian, X. (2008). Highly efficient energy transfer in the light harvesting system composed of three kinds of boron-dipyrromethene derivatives. *Org. Lett.* 10, 29–32. doi: 10.1021/ol702381j

Zhu, B., and Alva, A. K. (1993). Trace-metal and cation-transport in a sandy soil with various amendments. *Soil Sci. Soc. Am. J.* 57, 723–727. doi: 10.2136/sssaj1993.03615995005700030016x

Zou, H. S., Yuan, L. A., Guo, W., Li, Y. R., Che, Y. Z., Zou, L. F., et al. (2011). Construction of a Tn5-tagged mutant library of *Xanthomonas oryzae* pv. oryzicola as an invaluable resource for functional genomics. *Curr. Microbiol.* 62, 908–916. doi: 10.1007/s00284-010-9804-1

Conflict of Interest: The authors declare that the research was conducted in the absence of any commercial or financial relationships that could be construed as a potential conflict of interest.

frontiers in Microbiology

REVIEW
published: 01 December 2020
doi: 10.3389/fmicb.2020.606404

Mesenchymal Stromal Cells as Potential Antimicrobial for Veterinary Use—A Comprehensive Review

Keith A. Russell[1†], *Livia C. Garbin*[2†], *Jonathan M. Wong*[1†] *and Thomas G. Koch*[1*]

[1] *Department of Biomedical Sciences, Ontario Veterinary College, University of Guelph, Guelph, ON, Canada,* [2] *Clinical Veterinary Sciences Department, School of Veterinary Medicine, Faculty of Medical Sciences, The University of the West Indies, St. Augustine, West Indies*

The emergence of "superbugs" resistant to antimicrobial medications threatens populations both veterinary and human. The current crisis has come about from the widespread use of the limited number of antimicrobials available in the treatment of livestock, companion animal, and human patients. A different approach must be sought to find alternatives to or enhancements of present conventional antimicrobials. Mesenchymal stromal cells (MSC) have antimicrobial properties that may help solve this problem. In the first part of the review, we explore the various mechanisms at work across species that help explain how MSCs influence microbial survival. We then discuss the findings of recent equine, canine, and bovine studies examining MSC antimicrobial properties in which MSCs are found to have significant effects on a variety of bacterial species either alone or in combination with antibiotics. Finally, information on the influence that various antimicrobials may have on MSC function is reviewed. MSCs exert their effect directly through the secretion of various bioactive factors or indirectly through the recruitment and activation of host immune cells. MSCs may soon become a valuable tool for veterinarians treating antimicrobial resistant infections. However, a great deal of work remains for the development of optimal MSC production conditions and testing for efficacy on different indications and species.

Keywords: veterinary medicine, antimicrobial resistance (AMR), animal models, mesenchymal stem (stromal) cell, cellular therapy

OPEN ACCESS

Edited by:
Rodolfo García-Contreras, National Autonomous University of Mexico, Mexico

Reviewed by:
Claire Masterson, National University of Ireland Galway, Ireland
Caleb Perez, National Autonomous University of Mexico, Mexico

***Correspondence:**
Thomas G. Koch
tkoch@uoguelph.ca

†These authors have contributed equally to this work

Specialty section:
This article was submitted to Antimicrobials, Resistance and Chemotherapy, a section of the journal Frontiers in Microbiology

Received: *14 September 2020*
Accepted: *10 November 2020*
Published: *01 December 2020*

Citation:
Russell KA, Garbin LC, Wong JM and Koch TG (2020) Mesenchymal Stromal Cells as Potential Antimicrobial for Veterinary Use—A Comprehensive Review. Front. Microbiol. 11:606404. doi: 10.3389/fmicb.2020.606404

1. INTRODUCTION

Antimicrobial resistance (AMR) is a growing concern in all clinical populations, with few treatment options for those afflicted. Resistance is caused by unnecessary or superfluous antimicrobial use or even misuse associated with suboptimal dosage or duration (Guardabassi et al., 2018). In the last few years, the American Veterinary Medical Association (AVMA), Federation of Veterinarians of Europe (FVE), and Canadian Veterinary Medical Association (CVMA) have released a joint statement on responsible and judicious use of antimicrobials and have published guidelines for appropriate veterinary antimicrobial use[1]. Further, many federal agencies around the world are moving to reduce overall use of antimicrobials in animals. For example, Canada has restricted

[1]https://www.avma.org/resources-tools/avma-policies/joint-avma-fve-cvma-statement-responsible-and-judicious-use-antimicrobials (accessed September 3, 2020).

the sale of medically important antimicrobials for veterinary use by changing their status to prescription drugs[2]. Clinicians may want to consider alternative or complementary strategies in order to treat microbial infections.

Mesenchymal stromal cells (MSCs) have long been explored in regenerative medicine as raw material for engineering tissues or as immunomodulatory agents for treatment of inflammatory diseases (Devireddy et al., 2017). More recently, MSCs have shown promise as a potential treatment to address AMR. MSCs have antimicrobial properties whose mechanisms are still being uncovered. They are known to both secrete antimicrobial molecules that directly interact with pathogens as well as other factors that boost the antimicrobial activity of host immune cells (Maxson et al., 2012; Alcayaga-Miranda et al., 2017). In proof of concept studies, MSCs have shown strong synergy with existing antibiotic treatments to penetrate biofilm infections (Johnson et al., 2017) as well as capacity to serve as antifungal (Yang et al., 2013; Arango et al., 2018), antiviral (Kang et al., 2005; Kniazev et al., 2012; Khatri et al., 2018), and antiparasitic (Spekker et al., 2013) agents.

Over-prescription of broad-spectrum antibiotics in both human and veterinary medicine are creating a growing need for novel methods of disease treatment (Shallcross and Davies, 2014; Martin et al., 2015). In 2015, the WHO recognized the growing threat of AMR and recommended a global action plan built around the interdisciplinary "One Health" approach to combat AMR at the Animal-Human-Ecosystems interface (World Health Organization, 2017). Recommendations include an overall reduction of medically-important antimicrobials in the treatment of food-producing animals and the complete restriction of such antimicrobials for reasons of growth promotion or prophylactic use. If MSC antimicrobial properties can translate into viable treatment options, they could supplant much of the antimicrobials currently in use in animals. In this review, we will explore the veterinary literature regarding MSCs as antimicrobials. Although this is an emerging field of study, we will outline possible mechanisms and examine potential synergism to be found in combination therapies as well as possible deleterious effects of such an approach.

2. ANTIMICROBIAL EFFECT OF MSCS

MSCs have demonstrated antimicrobial effects both *in vitro* and *in vivo* with many different mechanisms implicated throughout the literature. Elucidating mechanisms can be challenging due to the fact that mechanisms can vary across donor species as well as target species of bacteria (Meisel et al., 2014; Mezey and Nemeth, 2015; Maria Holban et al., 2016; Rodríguez-Milla et al., 2020). Other variables can further impact the MSC phenotype and frustrate efforts to find consistency across studies such as MSC tissue source and the use of preconditioning protocols (Mezey and Nemeth, 2015; Cortés-Araya et al., 2018; Taguchi et al., 2019). Preconditioning, also known as activating or priming, MSCs through various culture conditions is commonly used to modulate or enhance desirable MSC properties. A number of preconditioning methods have been employed over the years including hypoxia, serum deprivation, and exposure to antagonistic substances to improve MSCs' ability to differentiate or modulate immune cells. Conditions promoting antimicrobial activity are being examined with exposure to cytokines, target bacteria, bacterial components, vitamins, and antibiotics improving both direct and indirect antimicrobial effects (Gupta et al., 2012; Guerra et al., 2017; Johnson et al., 2017; Cahuascanco et al., 2019; Yagi et al., 2020).

2.1. Direct Mechanisms of Antimicrobial Effects of MSC

Antimicrobial peptides (AMPs) are key components to MSC antimicrobial efficacy (**Figure 1**, **Table 1**). AMPs are short strings of amino acids co-expressed in clusters as a natural defense to bacteria, yeasts, fungi, and cancer cells (Vizioli and Salzet, 2002; Neshani et al., 2019). Over 1,200 known AMPs exist and are produced by organisms ranging from prokaryotes to higher animals (Lai and Gallo, 2009). AMPs primarily facilitate microbial killing through disruption of the microbial cell membrane. In addition, AMPs also modulate host innate immune cells mounting an orchestrated defense to microbes (Lai and Gallo, 2009). Several AMPs have been identified to be secreted by MSCs contributing to their overall antimicrobial function, with species-dependent expression of specific AMPs. Among the more broadly studied families of AMPs are cathelicidin, defensin, and lipocalin.

Cathelicidins are a major family of AMPs with prominent roles in innate immunity. Notably, cathelicidins across different species can vary their mechanism of action, albeit bacterial membrane disruption, and cell lysis generally occur (Schneider et al., 2016; Scheenstra et al., 2019). In humans, cathelicidin LL-37 has been implicated in the direct bacterial killing effects of MSCs (Guerra et al., 2017; Ren et al., 2019). LL-37 has bactericidal properties as well as the ability to decrease cytokine and endotoxin levels in septic models. Investigators identified LL-37 activity as crucial to MSC antimicrobial activity *in vitro* as well as in an *in vivo* mouse model using human MSCs (Krasnodembskaya et al., 2010). Yagi et al. (2020) further found LL-37 activity from adipose-derived MSCs was dependent on 1,25-dihydroxy vitamin D3. 1,25-dihydroxy vitamin D3 supplementation enhanced LL-37 production relative to MSCs under standard culture conditions, whereas treatment with a vitamin D receptor inhibitor nullified the antibacterial response. *In vivo* studies using allogenic murine MSCs have also implicated cathelicidin as a key AMP for bacterial killing (Johnson et al., 2017). Cathelicidin acts through TLR2/4-IRAK-4-dependent pathways in order to establish effective killing of mycobacteria (Naik et al., 2017). Interestingly, *M. tuberculosis* (Mtb) has developed a survival mechanism that disrupts this pathway and suppresses the antimicrobial effect of BM-MSCs via downregulation of *CAMP* gene expression (Naik et al., 2017). This suggests that a panel of AMPs might be necessary to overwhelm the defenses of certain microbes.

[2]https://www.canada.ca/en/public-health/services/antibiotic-antimicrobial-resistance/animals/actions/responsible-use-antimicrobials.html (accessed September 3, 2020).

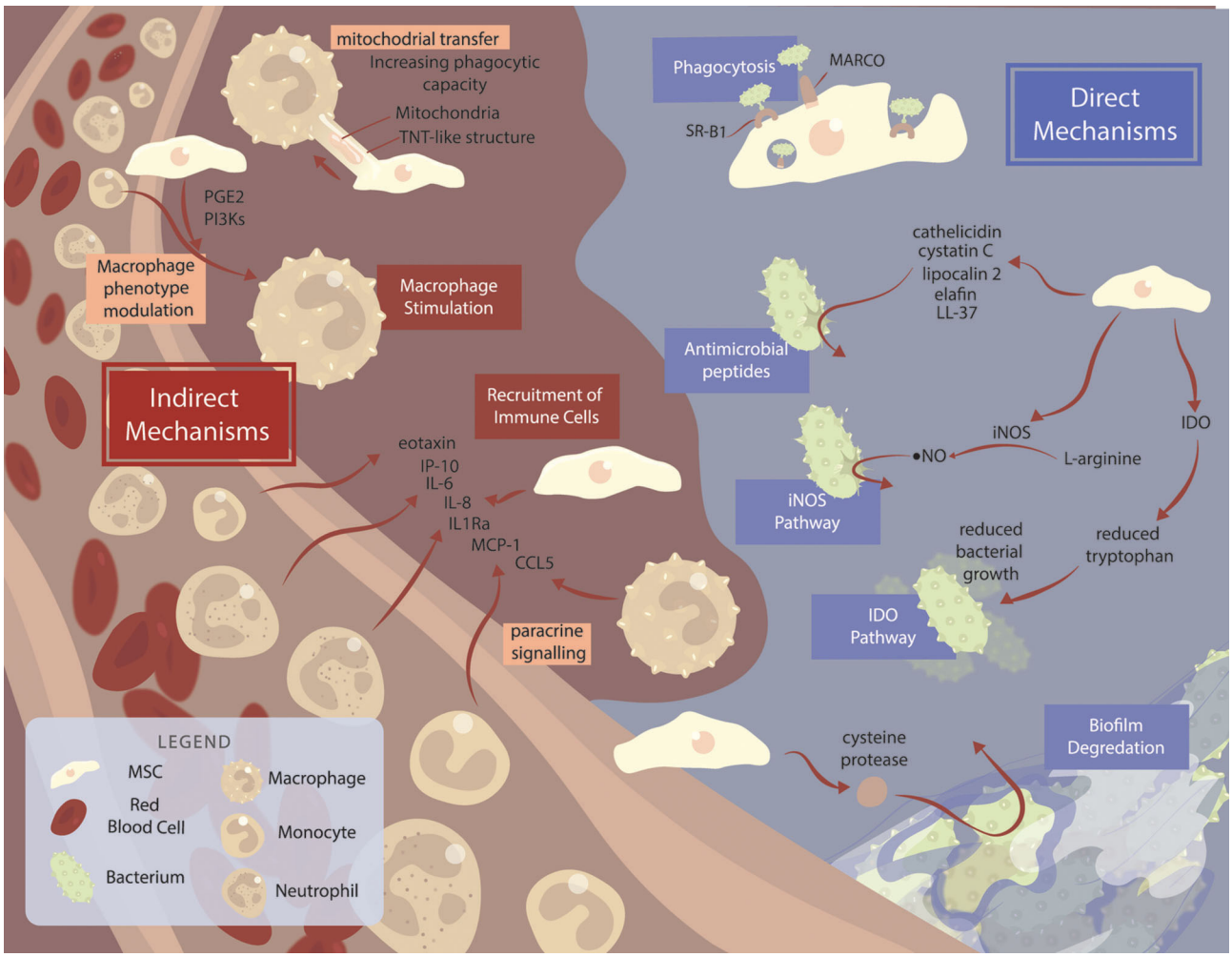

FIGURE 1 | Mechanisms of mesenchymal stromal cell-mediated killing across species. Summary of the major mechanisms and pathways used by MSCs. MSCs are often able to exhibit antimicrobial properties without stimulation, although various factors can improve MSC functionality. Direct mechanisms of MSC-mediated bacterial killing (blue background) include MARCO and SR-B1 receptor-mediated phagocytosis, antimicrobial peptide production, and IDO and iNOS pathways. Degradation of bacterial biofilms via cysteine protease secretion acts as a method of improving antibiotic function in combination therapy. Indirect mechanisms (brown background) include MSC bacterial killing via immune cell recruitment, and macrophage stimulation.

β-defensins are cysteine-rich cationic proteins with sizes ranging from 18 to 145 amino acids (Kim, 2014). These molecules similarly form pores in bacteria resulting in lysis (Esfandiyari et al., 2019). The presence of β-defensins have not always been detected in human MSC studies. Sutton et al. (2016) found no presence of β-defensin 2 or β-defensin 3 after MSC exposure to *P. aeruginosa*, *S. aureus*, and *Streptococcus pneumonia*, and attributed all bactericidal effect to LL-37 release. Conversely, Ren et al. (2019) identified human β-defensin 2 in both *P. aeruginosa*-stimulated and unstimulated MSCs. Other investigators identified β-defensin secretion from human MSCs via TLR-4 signaling as the key mechanism of paracrine *in vitro* antibacterial effect after *E. coli* exposure (Sung et al., 2016). Sung et al. also demonstrated similar β-defensin secretion from human MSCs treating *E. coli* in a mouse model. In cows, AMP gene expression of β-defensin 4A (bBD-4A) in addition to NK-lysine 1 (NK1) was found in fetal MSCs, while cathelicidin 2, hepcidin, and IDO expression were not found (Cahuascanco et al., 2019). Co-culture with *S. aureus* increased gene expression of bBD-4A and NK1.

Lipocalin 2 is an AMP that works by sequestering iron-laden siderophores, thus depriving bacteria of iron and limiting bacterial growth (Flo et al., 2004). Higher expression of lipocalin 2 was found in syngeneic murine MSCs after exposure to gram-negative bacterial pneumonia in an *in vivo* mouse model (Gupta et al., 2012). When lipocalin 2 was blocked in this study, the bacterial clearance effect observed with MSCs was lost. Expression of lipocalin 2 could be upregulated through MSC activation with LPS and TNFα. In horses, it was also found that LPS stimulation led to increased lipocalin 2 expression in equine MSCs (Cortés-Araya et al., 2018). In another equine MSC study, lipocalin 2 was also detected along with cathelicidin, cystatin C,

TABLE 1 | Mechanisms of MSC antimicrobial effects.

MSC origin	Study type (model)	MSC pre-activation	Bacteria	Mechanism	Outcome	Reference
Direct mechanisms						
Equine PB	*In vitro*	No	*E. coli* and *S. aureus*	Cystatin C, elafin, lipocalin 2, cathelicidin secretion	MSC and MSC conditioned media inhibited bacterial growth.	Harman et al., 2017
Human CB	*In vitro/in vivo* (mouse)	Yes	*E. coli*	β-defensin secretion	*In vitro*: growth of bacteria was significantly inhibited by MSCs or their conditioned medium. siRNA mediated knockdown of TLR-4 abolished antibacterial effects of MSCs. *In vivo*: intratracheal transplantation of MSCs reduced alveolar congestion, hemorrhage, neutrophil infiltration, and wall thickening 1 day post-*E. coli* intratracheal inoculation.	Sung et al., 2016
Human BM	*In vitro/in vivo* (mouse)	No	*E. coli*, *P. aeruginosa*, *S. aureus*	LL-37 secretion	*In vitro*: MSC and MSC conditioned media decreased bacterial growth in comparison to controls. *In vivo*: MSCs reduced bacterial growth in lung homogenates and bronchoalveolar lavage fluid.	Krasnodembskaya et al., 2010
Murine AT	*In vivo*	Yes	*S. aureus*	Cathelicidin secretion	Administration of antibiotics or MSC alone did not significantly reduce bacterial burden at wound site. TLR3 ligand-activated MSC with antibiotic therapy was the only treatment that significantly reduced bacterial burden at wound site.	Johnson et al., 2017
Murine BM	*In vitro*	No	*M. smegmatis*, *M. bovis*	Cathelicidin secretion	MSCs induced killing of *M. smegmatis* and *M.bovis* but were unable to kill *M. tuberculosis*.	Naik et al., 2017
Equine PB	*In vitro*	No	*P. aeruginosa*, *A. viridans*, *A. baumannii*, *S. epidermis*, *S. aureus*, MRSA	Cysteine protease secretion	MSC conditioned media inhibited bacterial growth for all bacteria tested. Cysteine protease secretion was found to inhibit biofilm formation as well as improve efficacy of antibiotics against mature biofilms of MRSA.	Marx et al., 2020
Human BM, CB	*In vitro*	No	*M. tuberculosis*	Direct phagocytosis, nitric oxide secretion	Phagocytosed bacteria did not replicate within MSCs, while showing a decline in numbers over 7 days	Khan et al., 2017
Human BM	*In vitro*	Yes	*S. aureus*, *S. epidermis*, *E. faecium*, group B streptococci, *T. gondii*, human cytomegalovirus	Indoleamine 2,3-dioxygenase pathway	MSCs exhibited broad-spectrum antimicrobial effector function. Addition of IDO inhibitors or tryptophan restored bacterial growth.	Meisel et al., 2011
Murine BM	*In vitro*	Yes	*S. aureus*, *S. epidermis*, *T. gondii*	iNOS pathway	Failed to inhibit *S. aureus* and *S. epidermis*. Intracellular growth of *Toxoplasma gondii* parasites was attenuated, with inhibitory effect being partially blocked by the iNOS-specific inhibitor NGMMA.	Meisel et al., 2011
Indirect mechanisms						
Human BM	*In vitro/in vivo* (rat)	No	*E. coli*	Macrophage differentiation into M1-like and M2-like macrophages	MSCs enhanced human macrophage phagocytosis of unopsonized bacteria and enhanced bacterial killing when compared with untreated macrophages. PGE2 and PI3K were key mediators of M1 macrophage induction.	Rabani et al., 2018

(Continued)

TABLE 1 | Continued

MSC origin	Study type (model)	MSC pre-activation	Bacteria	Mechanism	Outcome	Reference
Human PDL	*In vitro*	Yes	None	RANTES, eotaxin, IP-10, MCP-1, IL-6, IL-8, and IL-1ra	*P. gingivalis* total protein extract pre-treatment induced higher secretion of inflammatory markers and chemokines. Increased recruitment of neutrophil-differentiated human promyelocytic leukemia HL-60 cells was seen with increased production of intracellular reactive oxygen species.	Misawa et al., 2019
Murine AT	*In vivo*	Yes	*S. aureus*	Chemokine CCL2 release	Increased neutrophil phagocytosis, monocyte recruitment, M2 macrophage induction.	Johnson et al., 2017
Human BM	*In vivo* (mouse)	No	*E. coli*	Mitochondrial transfer from MSCs to macrophages	MSC administration was associated with enhanced alveolar macrophage phagocytosis.	Jackson et al., 2016

E. coli, Escherichia coli; S. aureus, Staphylococcus aureus; MSC, mesenchymal stromal cell; AT, adipose tissue; BM, bone marrow; CB, cord blood; EM, endometrium; PB, peripheral blood; PDL, periodontal ligament; TLR-4, Toll-like receptor 4; P. aeruginosa, Pseudomonas aeruginosa; TLR-3, Toll-like receptor 3; M. smegmatis, Mycobacterium smegmatis; M. bovis, Mycobacterium bovis; MCP-1, monocyte chemoattractant protein-1; CCL5, chemokine ligand 5; IL-6, interleukin 6; IL-8, interleukin 8; IRPA, imipenem-resistant P. aeruginosa; LPS, lipopolysaccharide; PGE2, prostaglandin E2; PI3K, phosphatidylinositol 3-kinase; RANTES, regulated on activation normal T cell expressed and secreted; IP-10, interferon γ inducible protein 10; P. gingivalis, Porphyromonas gingivalis; IL-1ra, interleukin 1 receptor antagonist; CCL2, chemokine ligand 2; M. tuberculosis, Mycobacterium tuberculosis; S. epidermis, Staphylococcus epidermidis; E. faecium, Enterococcus faecium; A. viridans, Aerococcus viridans; A. baumannii, Acinetobacter baumannii; NGMMA, N-G-monomethyl-L-arginine; MRSA, methicillin-resistant S. aureus; IDO, indoleamine 2,3-doxygenase; PMN, polymorphonuclear neutrophil granulocytes; NET, neutrophil extracellular trap.

and elafin (Harman et al., 2017). While AMPs are significant to MSCs' response to microbial challenge, they are not the only mechanisms at work.

Indoleamine 2,3-dioxygenase (IDO) expression in MSCs has also been involved in response to bacteria in humans. IDO acts to reduce local tryptophan levels thus inducing broad-spectrum antimicrobial activity (Däubener et al., 2009). MSCs stimulated with the inflammatory cytokines TNFα, IL1β, and IFNγ upregulated IDO expression, resulting in a reduction of bacterial growth (Meisel et al., 2011). TNFα and IL1β alone failed to restrict bacterial growth, yet both cytokines upregulated the IFNγ-mediated IDO-activity. Notably, addition of IDO inhibitors or tryptophan restored bacterial growth, confirming IDO as a key mechanism of antimicrobial effect. In contrast, IDO expression by murine MSCs was not found in *in vivo* mouse studies (Meisel et al., 2011). The authors found murine MSCs were unable to inhibit *S. aureus* growth due to the lack of IDO but were effective at inhibiting intracellular growth of *T. gondii* parasites via the inducible nitric oxide synthase mechanism (Meisel et al., 2011). Interestingly, infection with human cytomegalovirus (HCMV) suppressed human MSCs' ability to induce bacterial and parasitic killing, due to HCMV's ability to inhibit the IFN-γ pathway (Meisel et al., 2014). Relevantly, while some researchers have found no expression of IDO in equine MSCs (Carrade et al., 2012), others have found that upregulation of IDO expression can be induced by priming equine MSCs with exposure to the TLR3 agonist poly I:C (Cassano et al., 2018). As antimicrobial effects of IDO in equine cells have not been assessed, future studies are warranted to further explore this mechanism in an equine population.

Another mechanism at play is MSCs' ability to phagocytose Mtb (Khan et al., 2017). Direct internalization of Mtb relies on the macrophage receptor with collagenous structure (MARCO) and SR-B1 receptors. Rapamycin exposure increased lipidation of microtubule-associated light chain-3. Furthermore, no change in viability was seen *in vitro* after 7 days of infection, and internalized Mtb counts decreased over 7 days. They also found nitric oxide (NO) secretion by MSCs which further restricted Mtb growth. Bacterial internalization has also been noted in other studies, where human MSCs were found to internalize *S. aureus* (Josse et al., 2014; Guerra et al., 2017). Guerra et al. noted correlations between production of IL-6 by MSC and bacterial internalization, although mechanistic studies were not performed to clarify this relationship.

Biofilm development is a hallmark of antibiotic resistance. Biofilms are a bacteria-produced polymer matrix, resulting in increased resistance to disinfectants, antibiotics, and immune cells (Wu et al., 2015). Recent evidence has suggested MSCs have potential in breaking down biofilms, which is clinically relevant as infections that reach the biofilm stage have increased antimicrobial tolerance by 100–1,000-fold (Olsen, 2015). As a consequence, reaching effective antibiotic levels *in vivo* becomes unattainable due to the associated side effects and toxicity (Olsen, 2015). MSCs present a strategy to increase efficacy of conventional antibiotics via degradation of the biofilm layer and increased antibiotic penetration. Marx et al. investigated the *in vitro* effects of the MSC conditioned media (CM) against a variety of bacteria. Investigators found inhibition of biofilm formation and growth in *P. aeruginosa*, *S. aureus*, and *S. epidermidis*, although this was not consistent against all bacterial strains (Marx et al., 2020). In extension to these

findings, the presence of cysteine protease was identified in the equine MSC CM, which was found to inhibit MRSA biofilms via reduction of extracellular protein content and allowed for better penetration of conventional antibiotics (Marx et al., 2020). These preliminary findings suggest potential for MSC-antibiotic combination therapy, although further studies must be done to confirm clinical treatment viability.

2.2. Indirect Mechanisms of Antimicrobial Effects of MSC

MSCs have further demonstrated the ability to interact with the host immune system via paracrine factors and direct cell-cell interactions. Macrophages are key immunological players, having roles in tissue repair, homeostasis, and bacterial autophagy (Bah and Vergne, 2017; Doster et al., 2018). Furthermore, macrophages can be induced into the anti-inflammatory M2 phenotype or the pro-inflammatory M1 phenotype (Jayasingam et al., 2020). Johnson et al. (2017) identified M2 macrophage induction by activated allogeneic murine MSCs in infected tissues, whereas untreated infected tissues had a M1 dominant macrophage population. Bacterial killing has been attributed to the ability of MSCs to induce the M1 macrophage phenotype. Notably in this study, treatment with non-activated MSCs resulted in a mixed population of M1 and M2 macrophages. M2 macrophages were hypothesized to improve wound healing, which was consistent with the improved physical and histological appearance of the activated MSC treatment group when compared with the other treatment groups (Johnson et al., 2017). Similar findings were shared by Rabani et al. (2018) where non-activated human MSCs were in the same way capable of affecting macrophage phenotype, inducing a mixed population of M2 and M1 macrophages in a rat model. It was found that MSC modulation of human macrophages was dependent on prostaglandin E2 and phosphatidylinositol 3-kinase, which resulted in effective phagocytosis of unopsonised bacteria (Rabani et al., 2018). MSC administration can also result in enhanced alveolar macrophage phagocytosis as shown in a recent mouse study (Jackson et al., 2016). A tunneling nanotube (TNT)-like structure was used to transfer mitochondria from human MSCs to macrophages both *in vitro* and *in vivo*, which resulted in improved macrophage phagocytic capacity and bioenergetics (Jackson et al., 2016). Direct MSC-macrophage cell contact was found to optimize mitochondrial transfer, although blockage of MSC TNT formation via cytochalasin B did not fully abrogate mitochondrial transfer due to exosome-mediated mitochondrial transfer. *In vivo* studies found TNT formation was required for antimicrobial efficacy of MSCs, implying cell contact-dependent transfer is key for macrophage polarization. Similar results were seen in a rodent model using human MSCs, where MSCs enhanced macrophage phagocytosis of *E. coli*, and further enhancements in phagocytic activity were seen with addition of endotoxin and TNFα (Devaney et al., 2015). Lee et al. proposed another mechanism for macrophage stimulation. Allogeneic human MSCs were found to release keratinocyte growth factor (KGF) onto KGF receptors on human monocytes, resulting in enhanced bacterial clearance and decreased apoptosis of monocytes in an *ex vivo* lung model (Lee et al., 2013b). Other studies identified high levels of CCL2 released by MSCs *in vitro*, which is known to induce recruitment of inflammatory monocytes (Johnson et al., 2017). Higher levels of CCL2 were released by poly I:C-activated MSCs compared to non-activated MSCs.

Neutrophils have demonstrated similar phagocytic enhancements seen in macrophages. MSCs were found to enhance polymorphonuclear neutrophil granulocyte (PMN) bacterial uptake via secretion of IL-6, IL-8, and MIF cytokines (Brandau et al., 2014). These molecules bind to receptors CXCR1 and CXCR2 on neutrophils to mediate PMN recruitment and activation (Lazennec and Richmond, 2010; McDonald and Kubes, 2011). Neutrophils are further known to produce neutrophil extracellular traps (NET) which aid in preventing spread of bacteria and mediate killing (Hirschfeld, 2014). Chow et al. identified increased NET area produced per cell after incubation with CM from poly I:C-activated human MSCs when compared to non-activated MSC or control neutrophils in a mouse model (Chow et al., 2020), albeit NET formation was seen in all groups. Neutrophil phagocytosis was also seen in this study, with a similar activation-augmented effect.

Furthermore, activation of MSCs has been shown to enhance other immune regulatory properties. Human periodontal ligament-derived MSCs (PDLSC) stimulated with *P. gingivalis* total protein extract (PgPE) secreted inflammatory markers and chemokines including RANTES, eotaxin, IFNγ, inducible protein 10 (IP-10), IL-6, IL-8, and interleukin receptor antagonist protein (IL-1ra) (Misawa et al., 2019). The authors concluded PDLSCs were key in recruiting immune cells to infected tissues, with unstimulated MSCs having negligible levels of chemokines. MSC exposure to *S. typhimurium* and *L. acidophilus* has also resulted in higher transcription of immunomodulatory genes COX2, IL-6, and IL-8 as well as increased PGE2 secretion (Kol et al., 2014). These findings are supported in equine populations where in addition to AMP expression, investigators identified upregulated expression of immunomodulatory genes MCP-1, IL-6, IL-8, and CCL5 in equine MSCs after bacterial challenge, thus pointing to immune cell recruitment and activation as mechanisms of microbial killing (Cortés-Araya et al., 2018). MSCs have further been found to increase immunomodulatory activity after minocycline exposure. Minocycline induced phosphorylation of transcriptional nuclear factor-kB (NFkB) in human MSCs, resulting in decreased LL-37 production, increased IL-6 production, and overall net reductions in *S. aureus* bacterial load (Guerra et al., 2017). While it is surprising that lower LL-37 production would lead to reduced bacterial survival, it shows that combining antibiotics with MSCs must be examined closely for both synergistic and antagonistic effects as will be discussed below.

2.3. Examples of Antimicrobial Effect of MSC in Domestic Animals and Models

When looking at an overview of the MSC antibacterial research undertaken in the veterinary field, it is useful to look first at the broad strokes of the different approaches to this problem that

research groups have taken. A good place to start is to examine what source of MSCs were used. It could be argued that all of the studies to be discussed here were guided by the clinical practicality of using allogeneic cells or cell-free preparations over autologous cells as they have been repeatedly shown to be well-tolerated (Zhang et al., 2015; Bogatcheva and Coleman, 2019). If the aim is to supplement or replace antibiotics, then an off-the-shelf cellular product is preferred. When looking at the broader field of MSC study historically, the most common source tissues from which MSCs are isolated are BM and adipose tissue (AT) (Xu et al., 2017). It should come as no surprise that these sources were also most common in this subset of studies. Ease of isolation was likely a factor in choosing BM or AT for some (Johnson et al., 2017; Cortés-Araya et al., 2018; Cahuascanco et al., 2019; Bujňáková et al., 2020; Peralta et al., 2020) and peripheral blood (PB) for others (Harman et al., 2017; Marx et al., 2020). Still, potency and lack of immunogenicity were also cited as reasons for choosing certain tissue sources, which led more than one group to isolate MSCs from fetal sources of BM, AT, or the amniotic membrane (Cahuascanco et al., 2019; Lange-Consiglio et al., 2019; Peralta et al., 2020). Although fetal and perinatal tissue-derived MSCs have been reported to be superior to their adult-derived counterparts in their proliferative potential and hypoimmunogenicity (Deus et al., 2020), it is as yet unclear what effect, if any, their more primitive state might have on their antimicrobial activity.

Another trend in the field of MSC study that can be seen reflected among these studies is the move toward cell-free therapies using the secretome and CM of the cells. MSCs are known to secrete a wide range of potentially therapeutic biomolecules and factors into the extracellular space including growth factors, cytokines, chemokines, extracellular vesicles, and the aforementioned AMPs. The specific makeup of the secretome can vary depending on tissue source and in response to environmental conditions (Al Naem et al., 2020). Consequently, the secretome can be influenced by culture conditions that activate or precondition MSCs to respond to the clinical problem at hand as discussed above. In the articles reviewed here, only two of the studies took strictly a cellular approach (Johnson et al., 2017; Peralta et al., 2020), one assessed both cells and CM (Harman et al., 2017), while the rest worked only with CM (Cortés-Araya et al., 2018; Cahuascanco et al., 2019; Lange-Consiglio et al., 2019; Bujňáková et al., 2020; Marx et al., 2020). Co-culturing equine PB-MSCs with either *E. coli* or *S. aureus*, Harman et al. compared direct contact with transwell separation and found that both the cells and the paracrine factors alone had an inhibitory effect albeit somewhat muted in the case of the transwell setup (Harman et al., 2017). Follow-up experiments with CM from unstimulated MSCs indicated that at least some of the antibacterial factors were secreted constitutively and were not as a result of direct bacterial stimulation. Using cell-free preparations has advantages over using the cells themselves. It removes some safety risks associated with live cell transplantations including immune compatibility and tumorigenicity (Vizoso et al., 2017). CM can also be concentrated for higher potency or lyophilized for cheaper and easier shipment and storage (Bogatcheva and Coleman, 2019). Harman investigated the effects of lyophilization/reconstitution as well as heat inactivation, proteinase K treatment, and freezing/thawing on their equine PB-MSC CM and found that its antimicrobial potency remained regardless of processing method employed (Harman et al., 2017). Cahuascanco et al. (2019) evaluated the effects of concentrating (4x) CM or using CM from activated fetal bovine AT- and BM-MSCs. While the concentrated CM was not directly compared to the non-concentrated CM, the activated CM significantly reduced *S. aureus* proliferation over the 3 h tested both when concentrated and not. MSCs were activated with pre-exposure to *S. aureus*. Activation or preconditioning of MSCs is not unique to antimicrobial studies. It is a strategy that has been used to enhance specific MSC properties including *in vivo* survival and immunomodulation (Lee and Kang, 2020). For example, to bolster immunomodulatory activity, previous studies have employed the TLR3 and TLR4 receptor agonists LPS (Yan et al., 2014; Liu et al., 2016; Kink et al., 2019) and poly I:C (Rashedi et al., 2016; Qiu et al., 2017; Kim et al., 2018). These immune receptor agonists were used similarly to prime canine (Johnson et al., 2017) and equine (Cortés-Araya et al., 2018) MSCs to boost antimicrobial activity as well.

Breaking it down by species, the antimicrobial properties of equine MSCs have been evaluated in recent years although no *in vivo* work has been undertaken to date. As mentioned briefly above, Harman et al. (2017) looked at the effects of PB-MSCs and CM on both *E. coli* and *S. aureus*. Equine dermal fibroblasts were used as control cells as they are known to secrete antimicrobial peptides. In both direct contact and transwell coculture experiments, the MSCs were shown to have an inhibitory effect on both bacterial species equal to or greater than the fibroblasts. They further investigated what secreted AMPs could be responsible for these effects and found cystatin C, elafin, lipocalin 2, and cathelicidin to be expressed at higher levels than fibroblast controls but not β-defensin 1 found in other species. Some of these findings were partially confirmed in a similar equine study that found expression of lipocalin 2, but not β-defensin 1 in equine MSCs derived from bone marrow, endometrium, and adipose tissue (Cortés-Araya et al., 2018). These four AMPs alone could only account for part of the effect as there was still considerable effect after blocking AMP activity (Harman et al., 2017). According to the authors, although the effect of the AMPs are not immediately bactericidal, they depolarize bacterial cell membranes and may serve to increase the efficacy of conventional antibiotics. The authors further identified differential mechanisms used by MSCs to target different bacterial species, where factors >10 kDa inhibited growth of *E. coli* and factors >30 kDa inhibited growth of *S. aureus*. Some caution must be observed when drawing conclusions based on this study alone since penicillin/streptomycin and gentamicin were added to the cell media. Use of these antibiotics certainly may have influenced the results to some extent, although the fractionation experiments clearly show other factors at work (Harman et al., 2017). To build on these findings and correcting for the earlier design flaw, this research group turned more recently to the greater challenges of potentially treating biofilms and multidrug resistant (MDR) bacteria (Marx et al., 2020). Antibiotic-free CM from both equine

PB-MSCs and dermal fibroblasts were measured with DMEM or DMEM with antibiotics as controls. In the initial experiments, four bacterial species commonly associated with skin wounds as well as *S aureus* were tested in three different states: planktonic and developing or established biofilms. For planktonic bacterial cocultures, there was significantly better inhibition of bacterial growth in the antibiotic treatment than MSC CM with which only some inhibition was seen in 4/5 of the species. Separately, MSC CM was shown to diminish developing and mature biofilms in most cases often as effectively as antibiotics. However, when looking at the biofilms of methicillin-resistant *S. aureus* (MRSA), only MSC CM was capable of significant growth inhibition. This growth reduction was attributed in part to cysteine protease activity of cathepsins and others seen highly expressed in a protease array. This mechanism was validated by the use of a protease inhibitor, which reduced the MSC CM's inhibitory effect. Cysteine proteases degrade extracellular proteins and, in this case, could allow better penetration of antimicrobials into biofilms. This reasoning set up the final experiment where penicillin/streptomycin only disrupted mature MRSA biofilms when pretreated with MSC CM and not with oxacillin or penicillin/streptomycin itself (Marx et al., 2020).

Turning to canines, *in vivo* studies involving multidrug resistant (MDR) bacteria were recently conducted by Johnson et al. (2017). While the experiments were split between murine and canine models, the canine study is notable in that an observational pilot study was run evaluating poly I:C-activated allogeneic AT-MSCs in client-owned dogs with spontaneous MDR chronic wound infections. A series of three intravenous administrations at 2 week intervals of preactivated allogeneic canine AT-MSCs (2×10^6/kg body weight) were given to 7 dogs. Antibiotic therapy continued throughout the trial and bacterial cultures were obtained from the wound sites starting prior to treatment and continuing every 2 weeks thereafter. After 8 weeks, 5 of the dogs had completely cleared infections of either methicillin resistant *S. pseudointermedius* (MRSP) or a combination of *P. aeruginosa* (PA) and *E. coli* (**Table 2**). The other 2 dogs did show clinical improvement with one of them eliminating 2 MDR species, but not MRSP. No adverse reactions to the treatments were noted. The authors argue that there are direct and indirect mechanisms at play in activated MSC suppression of wound infections. The findings of the murine experiments showed that MSCs secrete not only AMPs to interact directly with bacteria but also secrete factors that enhance bacterial clearance through activation of host innate immune cells as mentioned. Neutrophils co-cultured with activated MSCs were shown to phagocytose bacteria at higher levels. In addition, monocytes co-cultured with activated MSCs were shown to migrate to wound sites more and promote the M2 phenotype of macrophages in infected tissues (Johnson et al., 2017). The authors conclude that the synergism between MSCs (or MSC-secreted AMPs) and antibiotics could offer a solution to attenuate a variety of MDR bacterial infections without leading to further resistance. Another study examining the antimicrobial effects of canine MSCs is notable in that it introduces an underexamined area of MSC antimicrobial research: how MSCs may block communication among bacteria, otherwise known as quorum sensing (QS). QS is important to biofilm formation and differentiation, and when disrupted can lead to bacteria being more susceptible to antibiotics (Diggle et al., 2007). Using a QS reporter strain of *E. Coli* that bioluminesces when QS signaling is elicited, the authors were able to detect antibiofilm effect of canine BM-MSC CM. A previous study by the group that ran proteomic analysis on the CM allowed for the authors to posit specific components to explain the antimicrobial effects observed including the AMPs apolipoprotein B and D, amyloid-β peptide, cathepsin B, and protein S100-A4 (Humenik et al., 2019). While proteins and peptides picked from the known content of the CM could suggest plausible cause for the antimicrobial effects detected, it should be emphasized that it is merely speculative at this point as no further experiments were designed to test these candidates in any way.

TABLE 2 | Patient data from 7 pet dogs with spontaneous, chronic infections with MDR bacteria treated with activated MSC.

Dog	Infection site	Infection duration	Organism(s)	Bacteriologic response (8 wks)	Clinical Response (8 wks)
1	Post-operative stifle infection	12 months	MRSP	Eliminated	Resolved
2	Post-operative stifle infection	6 mos	MRSP	Eliminated	Resolved
3	Draining tract stifle	4 mos	MRSP	Eliminated	Resolved
4	Soft tissue injury-paw	4 weeks	PA, EC	Eliminated	Resolved
5	Infected bone plate	3 mos	MRSP, EC, Crny, Kleb	Eliminated (except MRSP)	Improved
6	Cervical abscess from pacemaker lead	24 mos	MRSP- 2 strains	Unchanged	Improved
7	Deep pyoderma-paws	9 mos	MRSP	Eliminated	Resolved

PA, Pseudomonas aeruginosa; EC, Escherichia coli; MRSP, methicillin resistant Staphylococcus pseudointermedius; Crny, Corynebacterium sp.; Kleb, Klebsiella sp. From Johnson et al. (2017). Licensed under CC BY 4.0. No changes were made. To view a copy of this license, visit http://creativecommons.org/licenses/by/4.0/.

In bovine studies, two recent independent articles examining MSC therapies for mastitis in dairy cows indicate that MSCs may become a useful tool for production animals as well (Lange-Consiglio et al., 2019; Peralta et al., 2020). In the first study, four-fold concentrated CM reconstituted from lyophilized allogeneic non-primed bovine amniotic tissue-derived MSC CM were used for both *in vitro* and *in vivo* studies (Lange-Consiglio et al., 2019). The *in vivo* study enrolled 48 dairy cows with either acute or chronic mastitis and compared CM versus antibiotic treatment. Cows were treated intramammarily with CM or antibiotics twice daily on 3 consecutive days. No significant differences were found between the two treatment groups regarding somatic cell counts (SCC, a milk quality indicator) in milk samples, and there was no mastitis recurrence in any of the CM-treated animals compared to a 67 and 100% relapse rate in acute and chronic antibiotic-treated control cases, respectively. The *in*

vitro study had *S. aureus*-inoculated bovine mammary epithelial cell cultures set up with 10% MSC CM added at the time of inoculation, 4 h later, or not at all. After 24 h, epithelial cell survival rates were 90% for cultures when supplemented by CM at time 0, 61% when supplemented at 4 h, and 0% when no CM was added (Lange-Consiglio et al., 2019). In the second study, *S. aureus* mastitis was experimentally induced in 15 Holstein Friesian cows who were then treated intramammarily twice within 10 days with either allogeneic non-primed bovine AT-MSCs (2.5×10^7/dose), antibiotics, or ringer lactate (negative control; vehicle) (Peralta et al., 2020). As in the Lange-Consiglio et al. paper just discussed, no differences were seen in SCC. However, there were significantly fewer CFU in the MSC-treated cows compared to the negative control between days 6 and 10 (Peralta et al., 2020). One question not examined in this paper is why they opted for a cellular treatment when this research group is the very same that tested the different formulations (e.g., concentrated or activated) of bovine MSC CM against *S. aureus* discussed above (Cahuascanco et al., 2019).

3. EFFECTS OF ANTIMICROBIALS ON MSC FUNCTION

Antimicrobials have not only been used in medicine to treat infections but also prophylactically in cell culture (Skubis et al., 2017). It has been observed that antimicrobials can have an effect on MSCs during culture and even in local tissue cells after therapeutic implementation. Thus, until more is known, the therapeutic properties of MSCs can be potentially affected by some antimicrobials (Skubis et al., 2017). While no study has yet examined conventional antimicrobials' effect on MSC antimicrobial function, it is still worth examining their influence on other functions.

Experimentally, different classes of antimicrobials did have a significant effect on MSCs from different sources (**Table 3**). Aminoglycosides, such as gentamycin are widely used in equine practice, including in regional limb perfusion (Rubio-Martínez and Cruz, 2006) and intraosseous applications (Parker et al., 2010). Potential toxic osteonecrosis secondary to intraosseous perfusion of gentamicin raised questions in terms of the potential toxic effects of this antibiotic on stem cells (Parker et al., 2010). In fact, osteogenesis and chondrogenesis of human BM-MSCs decreased significantly when cultured with gentamicin in a dose-dependent manner (Chang et al., 2006). This has been observed in osteoblasts with the use of other aminoglycosides as well, such as tobramycin (Rathbone et al., 2011) and amikacin but only when using higher concentrations (>2,000 μg/mL) (Rathbone et al., 2011). In equine BM-MSCs, on the other hand, gentamicin had no effect on cell viability *in vitro*, but it reduced total RNA levels at higher concentrations (500 μg/mL) (Parker et al., 2012). In this same study, fluoroquinolones such as enrofloxacin also caused significant reduction in BM-MSC viability and total RNA levels (Parker et al., 2012). Finally, in AT-MSCs, antibiotics such as amphotericin affected growth and differentiation of these cells within 24 h of culture (Skubis et al., 2017), which was also observed with chloramphenicol use (Turani et al., 2015).

Although many antimicrobials have an inhibitory effect, other classes of antimicrobials can potentiate MSC differentiation (Lee et al., 2013a). Tetracyclines, such as doxycycline was shown to enhance chondrogenic differentiation of human BM-MSCs, which was further confirmed *in vivo* (Lee et al., 2013a). In addition, oxytetracycline was shown to promote cartilage differentiation in pre-chondrocyte cell lines, promoting chondrogenesis in a dose-dependent manner (Hojo et al., 2010). Polypeptide antibiotics such as bacitracin potentiated osteogenic differentiation of human BM-MSCs in a dose-dependent manner, increasing intracellular alkaline phosphatase (ALP), collagen and mineralization, and upregulating the level of osteogenic genes (Li et al., 2018). Amphotericin B (AmB) and AmB-Cu improved osteogenesis of AT-MSCs in the presence of osteogenic-induction factors, including dexamethasone, β-glycerophosphate and L-ascorbic acid compared to control and penicillin-streptomycin treated cells (Skubis et al., 2017).

Antimicrobials were also demonstrated to potentially induce immunomodulatory effects of MSCs. This was observed with the use of minocycline in human BM-MSCs (Hou et al., 2013). This effect was later confirmed in an *in vivo* study, where hydrogel loaded with minocycline enhanced the wound healing phenotype of human BM-MSCs in culture compared to hydrogel alone in a rat wound model (Guerra et al., 2017).

Other antimicrobials did not have a measurable effect on MSCs. Cephalosporins such as ceftiofur did not present noticeable effects until higher concentrations were used (at 500 μg/mL), which caused reduction in total RNA obtained in equine BM-MSCs, suggesting toxic effects. In the same study, different concentrations of penicillin overall did not present a significant effect in cells (Parker et al., 2012).

It is important to consider that the combination of penicillin-streptomycin is frequently used in cell culture to avoid contamination. This combination of antibiotics is used when cells are expanded and selected in preparation for experiments, including experiments that aim to investigate antimicrobial effects in MSCs (Parker et al., 2012). Although the assumption is that the effects of using such antibiotics could be considered negligible, penicillin-streptomycin has been demonstrated to cause significant change in gene expression, cell regulation, and growth rate (Cohen et al., 2006; Ryu et al., 2017). Such influence can interfere directly with how cells respond to different stimuli *in vitro* and consequently, experimental results (Ryu et al., 2017). It is possible that the use of penicillin-supplemented media could influence a cell population's response (or lack of response) to certain antimicrobials during the experiments reported here through selection bias.

3.1. Mechanisms of Antimicrobial Effects on MSC Function

Mesenchymal stem cell behavior and expression of healing properties is governed by signaling pathways such as mitogen-activated protein kinase (MAPK/ERK), transcriptional nuclear factor-kB (NF-kB), and c-Jun NH2-terminal kinase (JNK/SAPK)

TABLE 3 | Effects of different antimicrobials in MSCs.

#	Antibiotic class	Antibiotic	Species	Study type	Aim	Outcomes	References
1	β-lactams	Penicillin	Horse	*In vitro*	To investigate the effects of commonly used antibiotics in equine practice on BM-MSCs viability and gene expression.	Dose-dependent effect. Increased mRNA expression of TNC and COL1A1 at 50 μg/mL. No effect observed in BM-MSCs viability, total RNA concentration or mRNA expression at higher concentrations (up to 500 μg/mL).	Parker et al., 2012
2	Cephalosporins	Ceftiofur	Horse	*In vitro*	As described in row 1.	Dose-dependent effect. Increased mRNA expression of TNC and reduced TGF-βR2 expression at 50 μg/mL. Reduced total RNA concentrations at 500 μg/mL.	Parker et al., 2012
3	Aminoglycosides	Gentamicin	Horse	*In vitro*	As described in row 1.	Dose-dependent effect. Reduced mRNA expression of BCl2 and COL1A2 at 50 μg/mL. Reduced total RNA concentrations at 500 μg/mL.	Parker et al., 2012
4		Amikacin	Horse	*In vitro*	As described in row 1.	Dose-dependent effect. Increased mRNA expression of matrix components and decreased BCl2 expression at 50 μg/mL. Reduced BM-MSC viability and total RNA concentration at 500 μg/mL.	Parker et al., 2012
5	Quinolones	Enrofloxacin	Horse	*In vitro*	As described in row 1.	Dose-dependent effect. Reduced BM-MSC viability and total RNA concentrations at 200 μg/mL and 500 μg/mL. Increase in mRNA COL1A2 expression at 50 μg/mL.	Parker et al., 2012
6	Tetracyclines	Doxycycline	Human	*In vitro/in vivo*	To test if doxycycline reduces MMP, enhances chondrogenesis of human BM-MSCs and improves cartilage repair in an osteochondral defect model in rats	Enhanced chondrogenesis of BM-MSCs *in vitro/in vivo*.	Lee et al., 2013a
7		Minocycline	Human	*In vitro/in vivo*	To evaluate the beneficial effects of BM-MSCs and minocycline in an autoimmune encephalomyelitis mice model.	Increased immunomodulatory effect when applied with BM-MSCs *in vivo*.	Hou et al., 2013
8	Polypeptide antibiotics	Bacitracin	Human	*In vitro*	To investigate whether bacitracin affects osteogenic differentiation of BM-MSCs and the molecular mechanisms involved.	Increased osteogenic differentiation of BM-MSCs.	Li et al., 2018

AT-MSC, adipose tissue-derived mesenchymal stromal cell; BCl2, apoptosis regulator; BM-MSC, bone marrow-derived mesenchymal stromal cell; COL1A1, collagen type 1 α-1; COL1A2, collagen type 1 α-2, TGF-βR2, transforming growth factor β receptor 2; TNC, tenascin C.

explained in detail elsewhere (Zhong et al., 2012; Choi et al., 2014; Lu et al., 2016). Such pathways are stimulated by pro-inflammatory cytokines, triggering the pro-healing phenotype in MSCs. Certain antibiotics have been shown to interfere with such pathways in MSCs (Guerra et al., 2017). One study demonstrated that the NF-kB pathway may be activated through the interaction of minocycline in MSCs, leading to the increase in IL-6 and VEGF observed (Guerra et al., 2017). The activation of the NF-kB pathway with the use of minocycline may occur due to the stimulation of TNF receptor family. Stimulation of TNF receptors leads to NF-kB cytoplasmic phosphorylation and IkB kinase ε (IKKε) nuclear translocation, which may be responsible for the minocycline-induced enhancement of VEGF and IL-6 production in MSCs (Guerra et al., 2017). The authors speculated that the increase in IL-6 could be related to increased internalization of *S. aureus* observed in MSCs treated with minocycline (Guerra et al., 2017). In addition, the activation of the NF-kB pathway is correlated with cleavage of complement protein C5 to C5a and C5b in MSCs. These complement proteins ultimately lead to the formation of a Membrane Attack Complex (MAC) that induces cell death in microorganisms (Manthey et al., 2009; Lappas et al., 2012). However, minocycline was observed to inhibit this specific effect (Guerra et al., 2017).

Regarding osteogenic differentiation, bacitracin has been shown to increase osteogenic differentiation in BM-MSCs (Li et al., 2018). Studies demonstrated that bacitracin activated the transcription of the bone morphogenetic protein-2 (BMP-2) gene, an essential gene in the BMP-2/SMAD signaling axis, leading to the phosphorylation of SMAD1/5/9, which was significantly increased in bacitracin-treated cells (Li et al., 2018).

For chondrogenesis, cordycepin showed a regulatory effect in chondrogenic differentiation of MSCs. The increase in gene expression of chondrogenic genes was mediated by inhibition of Nrf2 and activation of BMP signaling (Cao et al., 2016).

However, as mentioned, some antibiotics may have a deleterious effect on cell differentiation. The mechanism of action of streptomycin is connected to its binding to the 30S subunit of the bacterial ribosome. It also possesses affinity to the ribosomes in eukaryotic cells. Streptomycin may act on eukaryotic cells through disruption of protein synthesis, affecting mitochondrial activity by binding to certain RNAs or by interfering with miRNAs' action (Li and Yue, 2019). This indicates that addition of streptomycin may change gene expression profiles in cells, thereby affecting the differentiation process.

Most antibiotics used either in clinical practice or cell culture seem to have some effect in MSCs. Such effects can be advantageous in certain cases when specific differentiation processes are targeted. With few exceptions, most antimicrobials seem to interfere with MSC proliferation, migration, and differentiation capacity. While these effects are usually concentration-dependent, clinicians and researchers should be conscious about the effects of antimicrobials and their implications in the clinical use of MSCs. More research into conventional antimicrobials' effect on MSC antimicrobial effect may be warranted, though the use of MSC CM may circumvent the problem altogether.

4. CONCLUSIONS

MSCs have shown promising efficacy in treating infections in proof-of-principle studies and small clinical case-studies. These observations warrant further study of MSCs' potential to replace or ameliorate current antimicrobial therapies. MSCs appear to exert their antimicrobial effects through a variety of mechanisms to induce microbial killing including AMP secretion, promotion of the host immune system, and direct phagocytosis. At this point, the number of studies examining MSCs as antimicrobials is quite limited in the veterinary space. However, piecing together the evidence from the few that exist suggests that MSCs can become a clinically important broad-spectrum antimicrobial effective in treating planktonic bacteria, biofilms, and MDR strains of bacteria alone or more likely in combination with conventional antimicrobials.

Much work remains to be done in order to determine the best approach to optimizing production conditions and MSC antimicrobial product formulation(s). Although preconditioning of MSCs with various stimulants has proven effective in inducing a more antimicrobial phenotype, comparison of these activation methods could be explored in more depth. While it is true that part of the overall effect comes from direct cell-cell contact, important for future clinical and commercial considerations is the confirmation that MSC secreted factors can be frozen, concentrated, and lyophilized for less expensive long-term storage without loss of antimicrobial activity. Fractionation of this cell-free product may also become an important step for improving potency or targeting certain species of bacteria.

There is also considerable justification to expand the focus to more veterinary species. Specific conditions that could be targeted include sepsis, pneumonia, urinary tract infections, and bloodstream infections. From a clinical perspective, veterinary patients merit continued efforts to improve their quality of care in and of themselves, and they may serve as powerful preclinical models of analogous human infections as in other areas of MSC research. From a "One Health" perspective, it is arguably even more important for human health that MSCs or cell-free preparations have the potential to curtail the use of antibiotics and decrease AMR in livestock where misuse may be most prevalent and pernicious. As this area of veterinary MSC research is only just emerging, there are a multitude of different research questions left to address.

AUTHOR CONTRIBUTIONS

KR, LG, and JW wrote sections of the manuscript. All authors contributed to manuscript revision, read, and approved the submitted version.

FUNDING

Funding was generously provided by the NSERC Discovery Grant, Equine Guelph, and the MITACS Accelerate Program.

ACKNOWLEDGMENTS

We would like to thank Naomi Robson and Robson Visuals for the scientific illustration presented as **Figure 1**. We would also like to thank Dr. Scott Weese for his feedback during the writing of this manuscript.

REFERENCES

Al Naem, M., Bourebaba, L., Kucharczyk, K., Röcken, M., and Marycz, K. (2020). Therapeutic mesenchymal stromal stem cells: isolation, characterization and role in equine regenerative medicine and metabolic disorders. *Stem Cell Rev. Rep*. 16, 301–322. doi: 10.1007/s12015-019-09932-0

Alcayaga-Miranda, F., Cuenca, J., and Khoury, M. (2017). Antimicrobial activity of mesenchymal stem cells: current status and new perspectives of antimicrobial peptide-based therapies. *Front. Immunol*. 8:339. doi: 10.3389/fimmu.2017.00339

Arango, J. C., Puerta-Arias, J. D., Pino-Tamayo, P. A., Arboleda-Toro, D., and González, Á. (2018). Bone marrow–derived mesenchymal stem cells transplantation alters the course of experimental paracoccidioidomycosis by exacerbating the chronic pulmonary inflammatory response. *Med. Mycol*. 56, 884–895. doi: 10.1093/mmy/myx128

Bah, A., and Vergne, I. (2017). Macrophage autophagy and bacterial infections. *Front. Immunol*. 8:1483. doi: 10.3389/fimmu.2017.01483

Bogatcheva, N. V., and Coleman, M. E. (2019). Conditioned medium of mesenchymal stromal cells: a new class of therapeutics. *Biochemistry* 84, 1375–1389. doi: 10.1134/S0006297919110129

Brandau, S., Jakob, M., Bruderek, K., Bootz, F., Giebel, B., Radtke, S., et al. (2014). Mesenchymal stem cells augment the anti-bacterial activity of neutrophil granulocytes. *PLoS ONE* 9:e106903. doi: 10.1371/journal.pone.0106903

Bujňáková, D., Čuvalová, A., Čížek, M., Humenik, F., Salzet, M., and Čížková, D. (2020). Canine bone marrow mesenchymal stem cell conditioned media affect bacterial growth, biofilm-associated *Staphylococcus aureus* and AHL-dependent quorum sensing. *Microorganisms* 8:1478. doi: 10.3390/microorganisms8101478

Cahuascanco, B., Bahamonde, J., Huaman, O., Jervis, M., Cortez, J., Palomino, J., et al. (2019). Bovine fetal mesenchymal stem cells exert antiproliferative effect against mastitis causing pathogen *Staphylococcus aureus*. *Vet. Res*. 50:25. doi: 10.1186/s13567-019-0643-1

Cao, Z., Dou, C., Li, J., Tang, X., Xiang, J., Zhao, C., et al. (2016). Cordycepin inhibits chondrocyte hypertrophy of mesenchymal stem cells through PI3K/Bapx1 and notch signaling pathway. *BMB Rep*. 49, 548–553. doi: 10.5483/BMBRep.2016.49.10.071

Carrade, D. D., Lame, M. W., Kent, M. S., Clark, K. C., Walker, N. J., and Borjesson, D. L. (2012). Comparative analysis of the immunomodulatory properties of equine adult-derived mesenchymal stem cells. *Cell Med*. 4, 1–12. doi: 10.3727/215517912X647217

Cassano, J. M., Schnabel, L. V., Goodale, M. B., and Fortier, L. A. (2018). Inflammatory licensed equine MSCs are chondroprotective and exhibit enhanced immunomodulation in an inflammatory environment. *Stem Cell Res. Ther*. 9, 1–13. doi: 10.1186/s13287-018-0840-2

Chang, Y., Goldberg, V. M., and Caplan, A. I. (2006). Toxic effects of gentamicin on marrow-derived human mesenchymal stem cells. *Clin. Orthop. Relat. Res*. 452, 242–249. doi: 10.1097/01.blo.0000229324.75911.c7

Choi, H., Nguyen, H. N., and Lamb, F. S. (2014). Inhibition of endocytosis exacerbates TNF-α-induced endothelial dysfunction via enhanced JNK and p38 activation. *Am. J. Physiol. Heart Circul. Physiol*. 306, H1154–H1163. doi: 10.1152/ajpheart.00885.2013

Chow, L., Johnson, V., Impastato, R., Coy, J., Strumpf, A., and Dow, S. (2020). Antibacterial activity of human mesenchymal stem cells mediated directly by constitutively secreted factors and indirectly by activation of innate immune effector cells. *Stem Cells Transl. Med*. 9, 235–249. doi: 10.1002/sctm.19-0092

Cohen, S., Samadikuchaksaraei, A., Polak, J. M., and Bishop, A. E. (2006). Antibiotics reduce the growth rate and differentiation of embryonic stem cell cultures. *Tissue Eng*. 12, 2025–2030. doi: 10.1089/ten.2006.12.2025

Cortés-Araya, Y., Amilon, K., Rink, B. E., Black, G., Lisowski, Z., Donadeu, F. X., et al. (2018). Comparison of antibacterial and immunological properties of mesenchymal stem/stromal cells from equine bone marrow, endometrium, and adipose tissue. *Stem Cells Dev*. 27, 1518–1525. doi: 10.1089/scd.2017.0241

Däubener, W., Schmidt, S. K., Heseler, K., Spekker, K. H., and MacKenzie, C. R. (2009). Antimicrobial and immunoregulatory effector mechanisms in human endothelial cells. *Thromb. Haemost*. 102, 1110–1116. doi: 10.1160/TH09-04-0250

Deus, I. A., Mano, J. F., and Custódio, C. A. (2020). Perinatal tissues and cells in tissue engineering and regenerative medicine. *Acta Biomater*. 110, 1–14. doi: 10.1016/j.actbio.2020.04.035

Devaney, J., Horie, S., Masterson, C., Elliman, S., Barry, F., O'Brien, T., et al. (2015). Human mesenchymal stromal cells decrease the severity of acute lung injury induced by *E. coli* in the rat. *Thorax* 70, 625–635. doi: 10.1136/thoraxjnl-2015-206813

Devireddy, L. R., Boxer, L., Myers, M. J., Skasko, M., and Screven, R. (2017). Questions and challenges in the development of mesenchymal stromal/stem cell-based therapies in veterinary medicine. *Tissue Eng. Part B* 23, 462–470. doi: 10.1089/ten.teb.2016.0451

Diggle, S. P., Crusz, S. A., and Cámara, M. (2007). Quorum sensing. *Curr. Biol*. 17, R907–R910. doi: 10.1016/j.cub.2007.08.045

Doster, R. S., Rogers, L. M., Gaddy, J. A., and Aronoff, D. M. (2018). Macrophage extracellular traps: a scoping review. *J. Innate Immun*. 10, 3–13. doi: 10.1159/000480373

Esfandiyari, R., Halabian, R., Behzadi, E., Sedighian, H., Jafari, R., and Imani Fooladi, A. A. (2019). Performance evaluation of antimicrobial peptide ll-37 and hepcidin and β-defensin-2 secreted by mesenchymal stem cells. *Heliyon* 5:e02652. doi: 10.1016/j.heliyon.2019.e02652

Flo, T. H., Smith, K. D., Sato, S., Rodriguez, D. J., Holmes, M. A., Strong, R. K., et al. (2004). Lipocalin 2 mediates an innate immune response to bacterial infection by sequestrating iron. *Nature* 432, 917–921. doi: 10.1038/nature03104

Guardabassi, L., Apley, M., Olsen, J. E., Toutain, P.-L., and Weese, S. (2018). Optimization of antimicrobial treatment to minimize resistance selection. *Microbiol. Spectr*. 6, 1–36. doi: 10.1128/9781555819804.ch30

Guerra, A. D., Rose, W. E., Hematti, P., and Kao, W. J. (2017). Minocycline modulates NFκB phosphorylation and enhances antimicrobial activity against *Staphylococcus aureus* in mesenchymal stromal/stem cells. *Stem Cell Res. Ther*. 8:171. doi: 10.1186/s13287-017-0623-1

Gupta, N., Krasnodembskaya, A., Kapetanaki, M., Mouded, M., Tan, X., Serikov, V., et al. (2012). Mesenchymal stem cells enhance survival and bacterial clearance in murine *Escherichia coli* pneumonia. *Thorax* 67, 533–539. doi: 10.1136/thoraxjnl-2011-201176

Harman, R. M., Yang, S., He, M. K., and Van de Walle, G. R. (2017). Antimicrobial peptides secreted by equine mesenchymal stromal cells inhibit the growth of bacteria commonly found in skin wounds. *Stem Cell Res. Ther*. 8:157. doi: 10.1186/s13287-017-0610-6

Hirschfeld, J. (2014). Dynamic interactions of neutrophils and biofilms. *J. Oral Microbiol*. 6:26102. doi: 10.3402/jom.v6.26102

Hojo, H., Yano, F., Ohba, S., Igawa, K., Nakajima, K., Komiyama, Y., et al. (2010). Identification of oxytetracycline as a chondrogenic compound using a cell-based screening system. *J. Bone Miner. Metab*. 28, 627–633. doi: 10.1007/s00774-010-0179-y

Hou, Y., Ryu, C., Park, K., Kim, S., Jeong, C., and Jeun, S.-S. (2013). Effective combination of human bone marrow mesenchymal stem cells and minocycline in experimental autoimmune encephalomyelitis mice. *Stem Cell Res. Ther*. 4:77. doi: 10.1186/scrt228

Humenik, F., Cizkova, D., Cikos, S., Luptakova, L., Madari, A., Mudronova, D., et al. (2019). Canine bone marrow-derived mesenchymal stem cells: genomics, proteomics and functional analyses of paracrine factors. *Mol. Cell. Proteom*. 18, 1824–1835. doi: 10.1074/mcp.RA119.001507

Jackson, M. V., Morrison, T. J., Doherty, D. F., McAuley, D. F., Matthay, M. A., Kissenpfennig, A., et al. (2016). Mitochondrial transfer via tunneling nanotubes is an important mechanism by which mesenchymal stem cells enhance macrophage phagocytosis in the *in vitro* and *in vivo* models of ARDS. *Stem Cells* 34, 2210–2223. doi: 10.1002/stem.2372

Jayasingam, S. D., Citartan, M., Thang, T. H., Mat Zin, A. A., Ang, K. C., and Ch'ng, E. S. (2020). Evaluating the polarization of tumor-associated macrophages into M1 and M2 phenotypes in human cancer tissue: technicalities and challenges in routine clinical practice. *Front. Oncol*. 9:1512. doi: 10.3389/fonc.2019.01512

Johnson, V., Webb, T., Norman, A., Coy, J., Kurihara, J., Regan, D., et al. (2017). Activated mesenchymal stem cells interact with antibiotics and host innate immune responses to control chronic bacterial infections. *Sci. Rep*. 7:9575. doi: 10.1038/s41598-017-08311-4

Josse, J., Velard, F., Mechiche Alami, S., Brun, V., Guillaume, C., Kerdjoudj, H., et al. (2014). Increased internalization of staphylococcus aureus and cytokine expression in human Wharton's jelly mesenchymal stem cells. *Bio Med. Mater. Eng*. 24(1 Suppl.), 27–35. doi: 10.3233/BME-140971

Kang, H. S., Habib, M., Chan, J., Abavana, C., Potian, J. A., Ponzio, N. M., et al. (2005). A paradoxical role for IFN-γ in the immune properties of mesenchymal stem cells during viral challenge. *Exp. Hematol*. 796–803. doi: 10.1016/j.exphem.2005.03.012

Khan, A., Mann, L., Papanna, R., Lyu, M.-A., Singh, C. R., Olson, S., et al. (2017). Mesenchymal stem cells internalize mycobacterium tuberculosis through scavenger receptors and restrict bacterial growth through autophagy. *Sci. Rep*. 7, 1–15. doi: 10.1038/s41598-017-15290-z

Khatri, M., Richardson, L. A., and Meulia, T. (2018). Mesenchymal stem cell-derived extracellular vesicles attenuate influenza virus-induced acute lung injury in a pig model. *Stem Cell Res. Ther*. 9:17. doi: 10.1186/s13287-018-0774-8

Kim, D. S., Lee, W. H., Lee, M. W., Park, H. J., Jang, I. K., Lee, J. W., et al. (2018). Involvement of TLR3-dependent PGES expression in immunosuppression by human bone marrow mesenchymal stem cells. *Stem Cell Rev. Rep*. 14, 286–293. doi: 10.1007/s12015-017-9793-6

Kim, J. M. (2014). Antimicrobial proteins in intestine and inflammatory bowel diseases. *Intest. Res*. 12, 20–33. doi: 10.5217/ir.2014.12.1.20

Kink, J. A., Forsberg, M. H., Reshetylo, S., Besharat, S., Childs, C. J., Pederson, J. D., et al. (2019). Macrophages educated with exosomes

from primed mesenchymal stem cells treat acute radiation syndrome by promoting hematopoietic recovery. *Biol. Blood Marrow Transpl.* 25, 2124–2133. doi: 10.1016/j.bbmt.2019.07.026

Kniazev, O. V., Ruchkina, I. N., Parfenov, A. I., Konopliannikov, A. G., and Sagynbaeva, V. E. (2012). [complete elimination of cytomegalovirus without antiviral therapy after systemic transplantation of mesenchymal bone marrow stromal cells in a patient with ulcerative colitis]. *Exp. Clin. Gastroenterol.* 118–123.

Kol, A., Foutouhi, S., Walker, N. J., Kong, N. T., Weimer, B. C., and Borjesson, D. L. (2014). Gastrointestinal microbes interact with canine adipose-derived mesenchymal stem cells *in vitro* and enhance immunomodulatory functions. *Stem Cells Dev.* 23, 1831–1843. doi: 10.1089/scd.2014.0128

Krasnodembskaya, A., Song, Y., Fang, X., Gupta, N., Serikov, V., Lee, J.-W., et al. (2010). Antibacterial effect of human mesenchymal stem cells is mediated in part from secretion of the antimicrobial peptide LL-37. *Stem Cells* 28, 2229–2238. doi: 10.1002/stem.544

Lai, Y., and Gallo, R. L. (2009). AMPed up immunity: how antimicrobial peptides have multiple roles in immune defense. *Trends Immunol.* 30, 131–141. doi: 10.1016/j.it.2008.12.003

Lange-Consiglio, A., Gusmara, C., Manfredi, E., Idda, A., Soggiu, A., Greco, V., et al. (2019). Antimicrobial effects of conditioned medium from amniotic progenitor cells *in vitro* and *in vivo*: toward tissue regenerative therapies for bovine mastitis. *Front. Vet. Sci.* 6:443. doi: 10.3389/fvets.2019.00443

Lappas, M., Woodruff, T. M., Taylor, S. M., and Permezel, M. (2012). Complement c5a regulates prolabor mediators in human placenta. *Biol. Reprod.* 86, 1–9. doi: 10.1095/biolreprod.111.098475

Lazennec, G., and Richmond, A. (2010). Chemokines and chemokine receptors: new insights into cancer-related inflammation. *Trends Mol. Med.* 16, 133–144. doi: 10.1016/j.molmed.2010.01.003

Lee, B.-C., and Kang, K.-S. (2020). Functional enhancement strategies for immunomodulation of mesenchymal stem cells and their therapeutic application. *Stem Cell Res. Ther.* 11:397. doi: 10.1186/s13287-020-01920-3

Lee, H., O'Malley, M., Friel, N., and Chu, C. (2013a). Effects of doxycycline on mesenchymal stem cell chondrogenesis and cartilage repair. *Osteoarthr. Cartil.* 21, 385–393. doi: 10.1016/j.joca.2012.11.010

Lee, J. W., Krasnodembskaya, A., McKenna, D. H., Song, Y., Abbott, J., and Matthay, M. A. (2013b). Therapeutic effects of human mesenchymal stem cells in *ex vivo* human lungs injured with live bacteria. *Am. J. Respir. Crit. Care Med.* 187, 751–760. doi: 10.1164/rccm.201206-0990OC

Li, H., Nie, B., Du, Z., Zhang, S., Long, T., and Yue, B. (2018). Bacitracin promotes osteogenic differentiation of human bone marrow mesenchymal stem cells by stimulating the bone morphogenetic protein-2/Smad axis. *Biomed. Pharmacother.* 103, 588–597. doi: 10.1016/j.biopha.2018.04.084

Li, H., and Yue, B. (2019). Effects of various antimicrobial agents on multi-directional differentiation potential of bone marrow-derived mesenchymal stem cells. *World J. Stem Cells* 11, 322–336. doi: 10.4252/wjsc.v11.i6.322

Liu, G.-Y., Liu, Y., Lu, Y., Qin, Y.-R., Di, G.-H., Lei, Y.-H., et al. (2016). Short-term memory of danger signals or environmental stimuli in mesenchymal stem cells: implications for therapeutic potential. *Cell. Mol. Immunol.* 13, 369–378. doi: 10.1038/cmi.2015.11

Lu, Z.-Y., Chen, W.-C., Li, Y.-H., Li, L., Zhang, H., Pang, Y., et al. (2016). TNF-α enhances vascular cell adhesion molecule-1 expression in human bone marrow mesenchymal stem cells via the NF-κB, ERK and JNK signaling pathways. *Mol. Med. Rep.* 14, 643–648. doi: 10.3892/mmr.2016.5314

Manthey, H. D., Woodruff, T. M., Taylor, S. M., and Monk, P. N. (2009). Complement component 5a (c5a). *Int. J. Biochem. Cell Biol.* 41, 2114–2117. doi: 10.1016/j.biocel.2009.04.005

Maria Holban, A., Bleotu, C., Carmen Chifiriuc, M., and Lazar, V. (2016). Phenotypic and genetic evaluation of the influence of *Pseudomonas aeruginosa* culture fractions on the human mesenchymal stem cells viability, apoptotic pathways and cytokine profile. *Curr. Stem Cell Res. Ther.* 12, 175–180. doi: 10.2174/1574888X10666151026114817

Martin, M. J., Thottathil, S. E., and Newman, T. B. (2015). Antibiotics overuse in animal agriculture: a call to action for health care providers. *Am. J. Publ. Health* 105, 2409–2410. doi: 10.2105/AJPH.2015.302870

Marx, C., Gardner, S., Harman, R. M., and de Walle, G. R. V. (2020). The mesenchymal stromal cell secretome impairs methicillin-resistant *Staphylococcus aureus* biofilms via cysteine protease activity in the equine model. *Stem Cells Transl. Med.* 9, 746–757. doi: 10.1002/sctm.19-0333

Maxson, S., Lopez, E. A., Yoo, D., Danilkovitch-Miagkova, A., and LeRoux, M. A. (2012). Concise review: role of mesenchymal stem cells in wound repair. *Stem Cells Transl. Med.* 1, 142–149. doi: 10.5966/sctm.2011-0018

McDonald, B., and Kubes, P. (2011). Cellular and molecular choreography of neutrophil recruitment to sites of sterile inflammation. *J. Mol. Med.* 89, 1079–1088. doi: 10.1007/s00109-011-0784-9

Meisel, R., Brockers, S., Heseler, K., Degistirici, Ö., Bülle, H., Woite, C., et al. (2011). Human but not murine multipotent mesenchymal stromal cells exhibit broad-spectrum antimicrobial effector function mediated by indoleamine 2,3-dioxygenase. *Leukemia* 25, 648–654. doi: 10.1038/leu.2010.310

Meisel, R., Heseler, K., Nau, J., Schmidt, S. K., Leineweber, M., Pudelko, S., et al. (2014). Cytomegalovirus infection impairs immunosuppressive and antimicrobial effector functions of human multipotent mesenchymal stromal cells. *Mediat. Inflamm.* 2014:898630. doi: 10.1155/2014/898630

Mezey, É., and Nemeth, K. (2015). Mesenchymal stem cells and infectious diseases: smarter than drugs. *Immunol. Lett.* 168, 208–214. doi: 10.1016/j.imlet.2015.05.020

Misawa, M. Y. O., Silvério Ruiz, K. G., Nociti, F. H., Albiero, M. L., Saito, M. T., Nóbrega Stipp, R., et al. (2019). Periodontal ligament-derived mesenchymal stem cells modulate neutrophil responses via paracrine mechanisms. *J. Periodontol.* 90, 747–755. doi: 10.1002/JPER.18-0220

Naik, S. K., Padhi, A., Ganguli, G., Sengupta, S., Pati, S., Das, D., et al. (2017). Mouse bone marrow sca-1 + CD44 + mesenchymal stem cells kill avirulent mycobacteria but not mycobacterium tuberculosis through modulation of cathelicidin expression via the p38 mitogen-activated protein kinase-dependent pathway. *Infect. Immun.* 85:e00471-17. doi: 10.1128/IAI.00471-17

Neshani, A., Zare, H., Akbari Eidgahi, M. R., Kamali Kakhki, R., Safdari, H., Khaledi, A., et al. (2019). LL-37: review of antimicrobial profile against sensitive and antibiotic-resistant human bacterial pathogens. *Gene Rep.* 17:100519. doi: 10.1016/j.genrep.2019.100519

Olsen, I. (2015). Biofilm-specific antibiotic tolerance and resistance. *Eur. J. Clin. Microbiol. Infect. Dis.* 34, 877–886. doi: 10.1007/s10096-015-2323-z

Parker, R. A., Bladon, B. M., McGovern, K., and Smith, K. C. (2010). Osteomyelitis and osteonecrosis after intraosseous perfusion with gentamicin. *Vet. Surg.* 39, 644–648. doi: 10.1111/j.1532-950X.2010.00685.x

Parker, R. A., Clegg, P. D., and Taylor, S. E. (2012). The *in vitro* effects of antibiotics on cell viability and gene expression of equine bone marrow-derived mesenchymal stromal cells. *Equine Vet. J.* 44, 355–360. doi: 10.1111/j.2042-3306.2011.00437.x

Peralta, O. A., Carrasco, C., Vieytes, C., Tamayo, M. J., Mu noz, I., Sepulveda, S., et al. (2020). Safety and efficacy of a mesenchymal stem cell intramammary therapy in dairy cows with experimentally induced *Staphylococcus aureus* clinical mastitis. *Sci. Rep.* 10, 1–12. doi: 10.1038/s41598-020-59724-7

Qiu, Y., Guo, J., Mao, R., Chao, K., Chen, B.-L., He, Y., et al. (2017). TLR3 preconditioning enhances the therapeutic efficacy of umbilical cord mesenchymal stem cells in TNBS-induced colitis via the TLR3-Jagged-1-Notch-1 pathway. *Mucos. Immunol.* 10, 727–742. doi: 10.1038/mi.2016.78

Rabani, R., Volchuk, A., Jerkic, M., Ormesher, L., Garces-Ramirez, L., Canton, J., et al. (2018). Mesenchymal stem cells enhance NOX2-dependent reactive oxygen species production and bacterial killing in macrophages during sepsis. *Eur. Respir. J.* 51, 1–14. doi: 10.1183/13993003.02021-2017

Rashedi, I., Gomez-Aristizabal, A., Wang, X.-H., Viswanathan, S., and Keating, A. (2016). TLR3 or TLR4 activation enhances mesenchymal stromal cell-mediated treg induction via notch signaling. *Stem Cells.* 35, 265–275. doi: 10.1002/stem.2485

Rathbone, C. R., Cross, J. D., Brown, K. V., Murray, C. K., and Wenke, J. C. (2011). Effect of various concentrations of antibiotics on osteogenic cell viability and activity. *J. Orthop. Res.* 29, 1070–1074. doi: 10.1002/jor.21343

Ren, Z., Zheng, X., Yang, H., Zhang, Q., Liu, X., Zhang, X., et al. (2019). Human umbilical-cord mesenchymal stem cells inhibit bacterial growth and alleviate antibiotic resistance in neonatal imipenem-resistant *Pseudomonas aeruginosa* infection. *Innate Immun.* 26, 215–221. doi: 10.1177/1753425919883932

Rodríguez-Milla, M. Á., Morales-Molina, A., Perisé-Barrios, A. J., Cejalvo, T., and García-Castro, J. (2020). AKT and JUN are differentially activated in mesenchymal stem cells after infection with human and canine oncolytic adenoviruses. *Cancer Gene Ther.* 1–12. doi: 10.1038/s41417-020-0184-9

Rubio-Martínez, L. M., and Cruz, A. M. (2006). Antimicrobial regional limb perfusion in horses. *J. Am. Vet. Med. Assoc.* 228, 706–712. doi: 10.2460/javma.228.5.706

Ryu, A. H., Eckalbar, W. L., Kreimer, A., Yosef, N., and Ahituv, N. (2017). Use antibiotics in cell culture with caution: genome-wide identification of antibiotic-induced changes in gene expression and regulation. *Sci. Rep*. 7:7533. doi: 10.1038/s41598-017-07757-w

Scheenstra, M. R., van den Belt, M., Tjeerdsma-van Bokhoven, J. L. M., Schneider, V. A. F., Ordonez, S. R., van Dijk, A., et al. (2019). Cathelicidins PMAP-36, LL-37 and CATH-2 are similar peptides with different modes of action. *Sci. Rep*. 9:4780. doi: 10.1038/s41598-019-41246-6

Schneider, V. A. F., Coorens, M., Ordonez, S. R., Tjeerdsma-van Bokhoven, J. L. M., Posthuma, G., van Dijk, A., et al. (2016). Imaging the antimicrobial mechanism(s) of cathelicidin-2. *Sci. Rep*. 6:32948. doi: 10.1038/srep 32948

Shallcross, L. J., and Davies, D. S. C. (2014). Antibiotic overuse: a key driver of antimicrobial resistance. *Br. J. Gen. Pract*. 64, 604–605. doi: 10.3399/bjgp14X682561

Skubis, A., Gola, J., Sikora, B., Hybiak, J., Paul-Samojedny, M., Mazurek, U., et al. (2017). Impact of antibiotics on the proliferation and differentiation of human adipose-derived mesenchymal stem cells. *Int. J. Mol. Sci*. 18:2522. doi: 10.3390/ijms18122522

Spekker, K., Leineweber, M., Degrandi, D., Ince, V., Brunder, S., Schmidt, S. K., et al. (2013). Antimicrobial effects of murine mesenchymal stromal cells directed against *Toxoplasma gondii* and *Neospora caninum*: role of immunity-related GTPases (IRGs) and guanylate-binding proteins (GBPs). *Med. Microbiol. Immunol*. 202, 197–206. doi: 10.1007/s00430-012-0281-y

Sung, D. K., Chang, Y. S., Sung, S. I., Yoo, H. S., Ahn, S. Y., and Park, W. S. (2016). Antibacterial effect of mesenchymal stem cells against *Escherichia coli* is mediated by secretion of beta- defensin- 2 via toll-like receptor 4 signaling. *Cell. Microbiol*. 18, 424–436. doi: 10.1111/cmi. 12522

Sutton, M. T., Fletcher, D., Ghosh, S. K., Weinberg, A., Van Heeckeren, R., Kaur, S., et al. (2016). Antimicrobial properties of mesenchymal stem cells: therapeutic potential for cystic fibrosis infection, and treatment. *Stem Cells Int*. 2016, 1–12. doi: 10.1155/2016/5303048

Taguchi, T., Borjesson, D. L., Osmond, C., and Griffon, D. J. (2019). Influence of donor's age on immunomodulatory properties of canine adipose tissue-derived mesenchymal stem cells. *Stem Cells Dev*. 28, 1562–1571. doi: 10.1089/scd.2019.0118

Turani, M., Banfalvi, G., Peter, A., Kukoricza, K., Kiraly, G., Talas, L., et al. (2015). Antibiotics delay *in vitro* human stem cell regrowth. *Toxicol. In vitro* 29, 370–379. doi: 10.1016/j.tiv.2014.10.013

Vizioli, J., and Salzet, M. (2002). Antimicrobial peptides from animals: focus on invertebrates. *Trends Pharmacol. Sci*. 23, 494–496. doi: 10.1016/S0165-6147(02)02105-3

Vizoso, F. J., Eiro, N., Cid, S., Schneider, J., and Perez-Fernandez, R. (2017). Mesenchymal stem cell secretome: toward cell-free therapeutic strategies in regenerative medicine. *Int. J. Mol. Sci*. 18:1852. doi: 10.3390/ijms18091852

World Health Organization (2017). *WHO Guidelines on Use of Medically Important Antimicrobials in Food-Producing Animals*.

Wu, H., Moser, C., Wang, H.-Z., Høiby, N., and Song, Z.-J. (2015). Strategies for combating bacterial biofilm infections. *Int. J. Oral Sci*. 7, 1–7. doi: 10.1038/ijos.2014.65

Xu, L., Liu, Y., Sun, Y., Wang, B., Xiong, Y., Lin, W., et al. (2017). Tissue source determines the differentiation potentials of mesenchymal stem cells: a comparative study of human mesenchymal stem cells from bone marrow and adipose tissue. *Stem Cell Res. Ther*. 8:275. doi: 10.1186/s13287-017-0716-x

Yagi, H., Chen, A. F., Hirsch, D., Rothenberg, A. C., Tan, J., Alexander, P. G., et al. (2020). Antimicrobial activity of mesenchymal stem cells against *Staphylococcus aureus*. *Stem Cell Res. Ther*. 11:293. doi: 10.1186/s13287-020-01807-3

Yan, H., Wu, M., Yuan, Y., Wang, Z. Z., Jiang, H., and Chen, T. (2014). Priming of Toll-like receptor 4 pathway in mesenchymal stem cells increases expression of B cell activating factor. *Biochem. Biophys. Res. Commun*. 448, 212–217. doi: 10.1016/j.bbrc.2014.04.097

Yang, R., Liu, Y., Kelk, P., Qu, C., Akiyama, K., Chen, C., et al. (2013). A subset of IL-17 + mesenchymal stem cells possesses anti- candida albicans effect. *Cell Res*. 23, 107–121. doi: 10.1038/cr.2012.179

Zhang, J., Huang, X., Wang, H., Liu, X., Zhang, T., Wang, Y., et al. (2015). The challenges and promises of allogeneic mesenchymal stem cells for use as a cell-based therapy. *Stem Cell Res. Ther*. 6:234. doi: 10.1186/s13287-015-0240-9

Zhong, X., Li, X., Liu, F., Tan, H., and Shang, D. (2012). Omentin inhibits TNF-α-induced expression of adhesion molecules in endothelial cells via ERK/NF-κB pathway. *Biochem. Biophys. Res. Commun*. 425, 401–406. doi: 10.1016/j.bbrc.2012.07.110

Conflict of Interest: The authors declare that the research was conducted in the absence of any commercial or financial relationships that could be construed as a potential conflict of interest.

frontiers in Microbiology

ORIGINAL RESEARCH
published: 09 December 2020
doi: 10.3389/fmicb.2020.591426

High-Throughput Identification of Antibacterials Against *Pseudomonas aeruginosa*

*Shijia Li, Pengfei She, Linying Zhou, Xianghai Zeng, Lanlan Xu, Yaqian Liu, Lihua Chen and Yong Wu**

Department of Laboratory Medicine, The Third Xiangya Hospital, Central South University, Changsha, China

Antibiotic resistance is a growing public health concern, though the constant development of new antibiotics. The combination of high-throughput screening and drug repurposing is an effective way to develop new therapeutic uses of drugs. In this study, we screened a drug library consisting of 1,573 drugs already approved by the Food and Drug Administration and 903 drugs from the natural product library, to identify antimicrobials against *Pseudomonas aeruginosa*. A high-throughput screening assay based on microtiter plate was used to screen 39 drugs that inhibit the planktonic or biofilm formation of *P. aeruginosa* while most of them are antibiotics. The antimicrobial activities of these drugs were evaluated by phenotypic analysis. Further studies showed the combined therapy of tetracycline antibiotics demeclocycline hydrochloride (DMCT) and the novel antimicrobial peptide SAAP-148 has an effective synergistic antibacterial effect on *P. aeruginosa* PAO1 and *P. aeruginosa* ATCC27853. Moreover, the time-kill curve assay and murine model of cutaneous abscesses further confirmed the synergistic effect. In addition, the combination of DMCT and SAAP-148 has the potential to combat clinically isolated multidrug-resistant (MDR) *P. aeruginosa* strains. Our results clearly indicate that DMCT and SAAP-148 combined therapy could be an effective method to combat MDR *P. aeruginosa*-related infections.

Keywords: *Pseudomonas aeruginosa*, demeclocycline hydrochloride, SAAP-148, high-throughput screening, drug combination

OPEN ACCESS

Edited by:
Bertha González-Pedrajo, National Autonomous University of Mexico, Mexico

Reviewed by:
Kaushiki Mazudar, University of Maryland, Baltimore, United States
Jorge Andres Olivares Pacheco, Pontificia Universidad Católica de Valparaíso, Chile

***Correspondence:**
Yong Wu
wuyong_zn@csu.edu.cn

Specialty section:
This article was submitted to Antimicrobials, Resistance and Chemotherapy, a section of the journal Frontiers in Microbiology

Received: *04 August 2020*
Accepted: *16 November 2020*
Published: *09 December 2020*

Citation:
Li S, She P, Zhou L, Zeng X, Xu L, Liu Y, Chen L and Wu Y (2020) High-Throughput Identification of Antibacterials Against Pseudomonas aeruginosa. Front. Microbiol. 11:591426. doi: 10.3389/fmicb.2020.591426

INTRODUCTION

Pseudomonas aeruginosa is a Gram-negative opportunistic pathogen usually widespread in clinical settings (Rahme et al., 1995), causing life-threatening infections in diverse patient populations (Djapgne et al., 2018). *P. aeruginosa* can grow as single cell in planktonic form or in a physiologically different biofilm form (She et al., 2019). Bacterial biofilm is a bacterial community that contains a large number of densely packed cells (Prindle et al., 2015), and it is difficult to remove with antibacterial agents due to its antibiotic or biocide resistance relative to planktonic cells (Mah and O'Toole, 2001; Chu et al., 2016). As *P. aeruginosa* is prone to intrinsic and acquired antibiotic resistance that's why it has become one of the most difficult opportunistic pathogens to treat, and can cause many serious infections in immunocompromised and hospitalized patients (Pendleton et al., 2013; Sousa and Pereira, 2014). Moreover, the formation of biofilm makes *P. aeruginosa* infection chronic.

Antibiotics can be considered as the greatest medical intervention in human history (Pletzer et al., 2018). Although the current global health assessment shows that the number of infections caused by bacteria resistant to many antibiotics has increased significantly (Almaaytah et al., 2019). Drug discovery is a key process to discover compounds and molecules that may develop into clinical therapeutic drugs. However, this development process is expensive and full of risks of failure (Trombetta et al., 2018). Therefore, there is an urgent need to replace antibiotics or change current treatment methods to prevent further resistance and/or improve the effects of existing antibiotics (Hayes et al., 2019). Repurposing drugs that have been applied to humans is a promising method that can reduce the cost and time usually associated with traditional drug discovery strategies, and is more likely to produce bioavailable and safe compounds, which can be more convenient and faster to enter clinical trials (Ashburn and Thor, 2004; Mullard, 2012).

In addition to drug repurposing, one of the drugs that have been intensively studied for the successful development of antibiotics in the past decade is antimicrobial peptides (Mishra et al., 2017), which has received increasing attention as potential novel antibiotics (Fosgerau and Hoffmann, 2015). At present, more and more synthetic antibacterial peptides are reported. One of the presumed advantages of AMPs is that the evolution of bacterial resistance is much slower than that of traditional antibiotics, which is a very desirable characteristic (Yu et al., 2018). The antimicrobial peptide SAAP-148 is an LL-37-inspired peptide developed by de Breij's team (de Breij et al., 2018). They confirmed that SAAP-148 has a wide range of antibacterial activity against Gram-positive and Gram-negative bacteria, including *P. aeruginosa*, so it is an ideal drug to combat fighting difficult-to-treat infections. Since the use of antibiotics can easily lead to bacterial resistance, the combined use of antimicrobials is an attractive option with many advantages, including potential synergistic effects. Therefore, the combined use of antimicrobials can improve the efficacy of either monotherapy (Brooks and Brooks, 2014). The combination therapy can also potentially reduce the concentration required to treat bacterial infection, hereby reducing future antibiotic resistance. In the absence of evidence-based treatment options, combinations are increasingly employed to enhance the antibacterial effects of available drugs against multidrug-resistant strains (Tängdén, 2014).

In this work, we used a high-throughput screening assay to screen FDA-approved products to identify drugs with novel antimicrobial activity against *P. aeruginosa* planktonic or biofilms. After verifying the antibacterial effect through phenotypic experiments, we chose the tetracycline antibiotic DMCT for further analysis. We evaluated the antibacterial activity of DMCT used in combination with SAAP-148, and tested against *P. aeruginosa* PAO1, ATCC27853 and current clinical bacterial strains through checkerboard assay and time-kill assay. Finally, the effectiveness of the combined therapy was verified by the *in vivo* experiment of the murine cutaneous abscess model.

MATERIALS AND METHODS

Bacterial Isolates, Cultural Conditions, and Reagents

The strains used are laboratory strain PAO1 (ATCC15692), a widely used and well-characterized wound isolate, and *P. aeruginosa* ATCC27853 (Holloway, 1955; Schmidt et al., 1996). The clinical isolates used in this study were obtained from the sputum or pus of inpatients at the Third Xiangya Hospital of Central South University (Changsha, Hunan, China). *P. aeruginosa* strains were grown in Luria broth (LB) (Solarbio, Shanghai, China) at 37°C with constant shaking (180 rpm), and the peptides were synthesized by GL Biochem (Shanghai, China).

High-Throughput Screening

A library of 2,476 FDA approved drugs was purchased from MedChem Express (Monmouth Junction, NJ, United States), and preliminary analysis was performed in a 96-well microtiter plate (Corning costar, Cambridge, MA, United States). *P. aeruginosa* PAO1 strain was used for high-throughput screening. Briefly, overnight cultures of *P. aeruginosa* PAO1 were suspended in MH broth to 1×10^6 CFU/ml. Hundred microliter of bacterial suspension was added to 96 μl of MH broth, and 4 μl of screening drugs from the drug library was added to wells of a 96-well microtiter plate, achieving a concentration of 100 μM. The plate was then incubated at 37°C for 24 h. After treatment, we used the turbidimeter to determine the survival rate of planktonic cells at an optical density (OD) of 630 nm (Campbell, 2011; Sun et al., 2016) and classified the drugs that reduce the turbidity of culture by more than 50% as compared with the untreated control as the plate was gently washed with $1 \times$ PBS after the culture was removed. The inhibition rate of biofilm formation was determined by measuring at 570 nm of 0.5% (w/V) crystal violet dissolved in ethanol. Experimental assays were performed twice. The second screening reduced the drug concentration to 30 μM. The screening procedure was the same as the initial screen. Experimental assays were performed in triplicate.

Antimicrobial Susceptibility Assay

According to the Clinical and Laboratory Standards Institute (CLSI) guidelines (Institute, 2006), the *in vitro* antibacterial activity of selected drugs was evaluated by microdilution broth sensitivity test (Institute, 2006). The MIC values of the selected drug were determined by the wells with the lowest concentration and no visible bacterial growth. To determine MBC, bacterial cultures from the wells were mixed gently and streaked on blood agar plates, and then the plates were incubated at 37°C for 24 h. The MBC value was defined as the minimum drug concentration without bacterial colony growth on the plate after 24 h of incubation (Huang et al., 2012). The assay was conducted in triplicate.

Frequency of Resistance

The spontaneous resistance frequency was performed based on the modified method reported by Peter A. Smith with slight

adaptations (Smith et al., 2018). Five independent colonies from PAO1 were scraped off and established an overnight culture. The cultures were concentrated to 1×10^9 CFU/ml by centrifuging and resuspending in 100 μl. The concentrated bacterial cell suspensions were then spread on MH agar containing drugs at 4–8-times the MIC. The MH plates were prepared from Mueller Hinton II cation adjusted broth (BBLTM 212322) and SeaKem LE Agarose (17 g/L; Lonza) as per manufactures instructions. The resistance frequency was calculated by dividing the number of colonies formed after a 48 h incubation at 37°C by the initial viable cell count. Testing was performed in triplicate.

Biofilm Determination

For *P. aeruginosa* determination, bacterial cultures were grown overnight and diluted 1:100 in MH broth (Included 1% glucose). 200 μl of the diluted cultures were added to each well of the microtiter plate and incubated at 37°C for 24 h. After the incubation, the cultures in the wells were aspirated and rinsed, 100 μl of MH broth and 100 μl of the selected drug were added to each well, and incubated for 37°C for 24 h. Then washed away the liquid in the well and determined the remaining biofilm by XTT assay. In short, XTT and phenazine methyl sulfate were diluted to a concentration of 0.2 and 0.02 mg/ml with 1 × PBS, respectively, and then mixed (MACKLIN, Shanghai, China). Then 200 μl of the mixture was then added to the wells, and measured the contents at OD490 nm after incubating for 3 h in the dark at 37°C (Nesse et al., 2015). MBEC50/MBEC70 was defined as the lowest concentration for a specific drug to inhibit 50%/70% growth of biofilms compared to the untreated group (Gomes et al., 2009).

Checkerboard Assay

The efficacy of individual drug and the combined therapy with SAAP-148 were evaluated by using the microdilution checkerboard assay (Odds, 2003). According to the MIC, the maximum concentration of the drug is twice the MIC value. Overnight cultures were diluted in MH broth to reach a final concentration of approximately 5×10^5 CFU/ml. The fractional inhibitory concentration index (FICI) is measured by dividing the combined MIC by the MIC of a single antibacterial agent. FICI $\leq$ 0.5 designated indicates synergy; 0.5 < FICI < 1.0 designated partial synergy; FICI = 1.0 designated additivity; 1.0 < FICI < 4.0 designated indifference; and FICI $\geq$ 4.0 designated antagonism (Pachón-Ibáñez et al., 2011).

Time-Kill Assay

To confirm the synergistic effects of DMCT and SAAP-148 on PAO1 and ATCC27853, a time-kill assay was carried out. The overnight bacterial cells were diluted into 10 ml aliquots in a burette with a density of 1×10^6 CFU/ml. 10 ml of MH broth containing 1/2×, 1× or 2 × MIC drugs was inoculated individually or in combination with a final concentration of 1×10^5 CFU/ml. The negative control was contained with equal amount of saline. During the incubation period, 100 μl of each sample was taken at 0, 2, 4, 8, 12, and 24 h of incubation at 37°C. Each sample was serially diluted 10-fold in aliquots and plated on blood agar, incubated overnight at 37°C for colony counts.

Hemolysis Assay

The hRBCs were collected from the Department of Clinical Laboratory of the Third Xiangya Hospital. 2 ml hRBCs were washed 3 times using 1 × PBS followed by centrifugation for 5 min at 1,000 rpm at 4°C. The hRBCs were then added to SAAP-148 containing 1 × PBS (1.5625 μM to 200 μM) for a final hRBCs concentration of 5% (vol/vol). After incubation for 1 h at 37°C, the samples were centrifuged at 1,000 rpm for 5 min, then 100 μl of the supernatant was added to the 96-well plate and the absorbance was measured at 450 nm. The hRBC samples with 0.1% Triton X-100 or 1% DMSO were used as positive and negative controls, respectively. Three replicates were evaluated under this condition.

Cutaneous Mouse Infection Model

The mice used in this study were purchased from Hunan Slake Jingda Experimental Animal, Co., Ltd. (Hunan, China). All mice were 6-week-old, female CD-1, weighing about 25 ± 3 g during the experiment. The infection model has been slightly modified, as described in previous reports (Pletzer et al., 2018). The bacterial cultures used in the infection model were washed twice with 1 × PBS and then suspended in saline. To produce a repeatable abscess, 100 μl bacterial suspension was injected into the right side of the dorsum to achieve a final concentration of about 1×10^9 CFU/mice. The treatment was delivered directly into the subcutaneous space to the infected area (100 μl) at 1 h post-infection. The development of infection was monitored daily. Skin abscesses (including all empyema) were excised and regimented homogenized in 1 × PBS by an automatic tissue homogenizer (Servicebio KZ-II, Wuhan, China). Bacterial count was quantified by serial dilution. Hematoxylin and eosin (H&E) staining is used for histopathological analysis of skin abscesses. The experiment was performed at least three times, with 2–4 animals in each group.

Statistical Analysis

Statistical analysis was performed using GraphPad Prism 6.0. Statistical significance was analyzed by the ANOVA test. $P < 0.05$ was considered a statistically significant difference.

RESULTS

Identification of Screening Drugs That Are Bactericidal Against *P. aeruginosa*

The high-throughput *in vitro* screening identified FDA-approved drugs that effectively inhibit *P. aeruginosa* PAO1 planktonic or biofilm cell. We identified the growth inhibitors of PAO1 through 96-well microtiter plate-based high-throughput screening of 2,476 compounds belonging to the compound library. The initial screening drug concentration was

100 μM, and we identified 67 compounds that inhibit PAO1 plankton or biofilm by > 50%, as determined by turbidometry (**Supplementary Table S1**). The second screening reduced the concentration of 67 compounds to 30 μM, and a total of 39 drugs with an inhibition rate of ≥ 50% were screened out (**Table 1**). Not surprisingly, most of the compounds are known as antibiotics.

Evaluation of Antibacterial Effects of Selected Drugs on *P. aeruginosa*

To further understand the effect of screening drugs on *P. aeruginosa*, a series of phenotypic experiments were conducted. The MIC and MBC assays were determined (**Table 1**). Since most of the selected drugs inhibited the formation of the PAO1 biofilms, we next evaluate whether they have the ability to eradicate pre-formed biofilms. Quantitative analysis using XTT assay revealed that 18 of the 39 drugs significantly attenuated metabolic activity due to biofilm disruption at the concentration ≤ 64 μM **(Figure 1**).

The mutation is a common mechanism by which bacteria develop resistance to antibiotics (Fajardo-Cavazos and Nicholson, 2016). The spontaneous resistance frequencies of selected drugs were measured at 4 × and 8 × MIC, to investigate the development of resistant mutants when PAO1 is

TABLE 1 | Drugs with activity against *P. aeruginosa* PAO1 planktonic and biofilm.

Drug	Class	% planktonic inhibition at 30 μ M	% biofilm inhibition at 30 μ M	MIC (μ M)	MBC (μ M)
Tosufloxacin	Fluoroquinolone	100	100	3.125	6.25
Sitafloxacin	Fluoroquinolone	100	98.5	1.5625	3.125
Tobramycin	Aminoglycoside	99.5	96.2	0.78125	3.125
Sisomicin	Aminoglycoside	100	97.7	0.78125	6.25
Amikacin	Aminoglycoside	100	99.6	1.5625	6.25
Azlocillin	Penicillin	100	93	6.25	12.5
Gemifloxacin	Fluoroquinolone	100	97.6	3.125	3.125
Netilmicin	Aminoglycoside	100	96.2	3.125	6.25
Cefozopran	Cephalosporin	100	91.7	0.78125	1.5625
Cefepime	Cephalosporin	100	93.3	1.5625	3.125
Prulifloxacin	Fluoroquinolone	100	97	3.125	6.25
Doripenem	Carbapenem	100	96.3	1.5625	6.25
Colistin	Polymyxin	100	99.8	1.5625	12.5
Ceftazidime	Cephalosporin	100	97	1.5625	3.125
Danofloxacin	Fluoroquinolone	98.2	94.3	6.25	12.5
Piperacillin	Penicillin	100	98.6	1.5625	6.25
Mezlocillin	Mezlocillin	98.4	90.8	25	50
Ceftriaxone	Cephalosporin	100	97	6.25	25
Cefmenoxime	Cephalosporin	100	97.8	3.125	6.25
Lomefloxacin	Fluoroquinolone	100	100	6.25	12.5
Pazufloxacin	Fluoroquinolone	99.2	94.8	6.25	12.5
Aztreonam	Monolactam	100	93.4	6.25	12.5
Garenoxacin	Quinolone	100	95.6	6.25	25
Gatifloxacin	Quinolone	100	98.9	6.25	25
Sparfloxacin	Quinolone	99.1	92.1	6.25	25
Demeclocycline	Tetracycline	100	99.6	12.5	> 50
Rifaximin	Ansamycin	100	99.5	12.5	> 50
Streptomycin	Aminoglycoside	100	97.5	3.125	6.25
Paromomycin	Aminoglycoside	100	94.3	12.5	25
Levofloxacin	Quinolone	100	97.6	12.5	12.5
Pefloxacin	Quinolone	100	93.4	12.5	25
Besifloxacin	Fluoroquinolone	100	92	12.5	25
Enoxacin	Fluoroquinolone	100	91.1	12.5	50
Bekanamycin	Aminoglycoside	100	99.4	12.5	50
Erythromycin	Monobactam	98.8	88.4	50	50
Telithromycin	Macrolide	100	< 80	50	> 50
Azithromycin	Macrolide	100	95	50	> 50
Nedaplatin	Cancer	81	< 80	50	> 50
Chlorhexidine	Fungicide	100	98.8	12.5	25

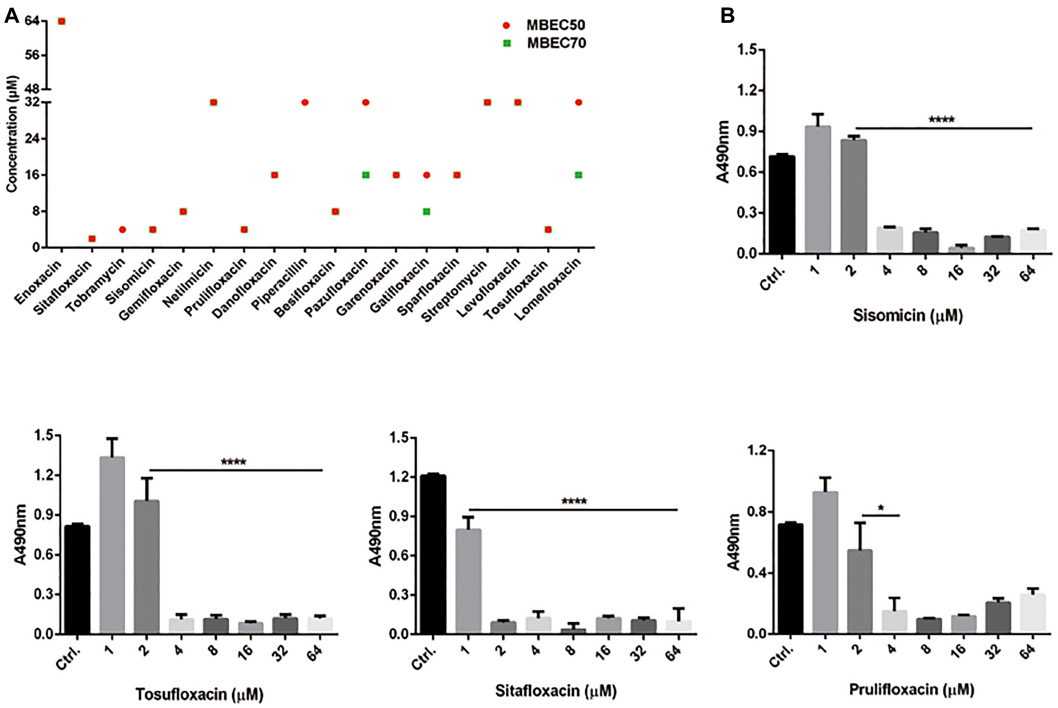

FIGURE 1 | Minimum biofilm eradication concentrations of drugs against *P. aeruginosa* PAO1 Biofilms. **(A)** Biofilm eradication by selected drugs detected by XTT assay. Biofilms cultured for 24 h were treated with selected drugs at the specified concentrations. After incubation, removed planktonic cells and stained biofilms with XTT/PMS solution. The red circle and the green square represent the MBEC50 and MBEC70 of 18 drugs, respectively. **(B)** The effect of representative drugs on the biofilm eradication of PAO1, data representing three independent experiments performed in duplicate. $^{*}P < 0.05$; $^{****}P < 0.0001$.

treated with each drug (**Table 2**). These data may have a certain guiding role in the selection of medication.

Synergistic Antibacterial Effect of Drug Combination Against *P. aeruginosa*

The emergence of antibiotic resistance has become a serious public health concern worldwide. Finding novel antimicrobial agents and therapies based on synergistic combinations are essential to combat drug-resistant bacteria. AMPs are one of the most promising antibiotic agents. Therefore, several antimicrobial peptides were selected to determine the antimicrobial activity against PAO1. According to the antibacterial effect of AMPS, SAAP-148 inhibited the growth of PAO1 at low concentrations among selected AMPs. In addition, the cytotoxicity of SAAP-148 was tested by measuring the ability to cause hRBC lysis. We found that SAAP-148 has little hemolytic activity at high concentrations (200 μM) **(Supplementary Figure S1)**. We finally regarded SAAP-148 as an optimized antimicrobial peptide for further detailed research (**Supplementary Table S2**).

SAAP-148 is a novel antibacterial peptide with broad-spectrum antibacterial effect. The microdilution checkerboard assay was used to evaluate the synergistic effects of the selected drugs and SAAP-148 (**Table 3**). The combination of SAAP-148 and DMCT has a significant synergistic effect on PAO1, with a FICI of 0.5 (**Figure 2**). In addition, we measured another laboratory strain *P. aeruginosa* ATCC27853 by checkerboard assay, synergistic effects or addictive effects can be seen among *P. aeruginosa* ATCC27853 and MDR clinical strains when using the combination of SAAP-148 and DMCT (**Supplementary Table S3** and **Figure 2**).

Time-Kill Curve Assay for the *P. aeruginosa*

The time-kill assays were performed in order to confirm the synergistic effects of SAAP-148 and DMCT against PAO1 and ATCC27853. As shown in **Figure 3**, the SAAP-148 (1/2 × MIC) and DMCT (1/2 × MIC) alone did not induce cell death after 24 h incubation. The combination of DMCT(1/2 × MIC) and SAAP-148 (1/2 × MIC) showed a reduced viable count (> 3log10 CFU/ml) compared to that of the initial inoculum. Although the regrowth was observed at 24 h, the combined treatment was still at least ≥ 5log10 CFU/ml lower than the level of growth control at 24 h (**Figure 3**). Overall, combination therapy can significantly reduce the bacterial count compared with DMCT and SAAP-148 monotherapy.

Therapeutic Efficacy of DMCT Combined With SAAP-148 *in vivo*

Finally, we used murine model of cutaneous abscesses to determine the *in vivo* efficacy of the combination therapy.

TABLE 2 | Spontaneous resistance frequencies of *P. aeruginosa* PAO1.

Drug	Spontaneous resistance frequency (SD)
	4 × MIC
Amikacin	4.35×10^{-6} ($\pm$ 1.67×10^{-6})
Netilmicin	1.08×10^{-6} ($\pm$ 0.17×10^{-6})
Sisomicin	2.57×10^{-7} ($\pm$ 0.9×10^{-7})
Streptomycin	6.49×10^{-6} ($\pm$ 1.33×10^{-6})
Tobramycin	1.87×10^{-6} ($\pm$ 0.62×10^{-6})
Tosufloxacin	0.87×10^{-7} ($\pm$ 0.31×10^{-7})
Gemifloxacin	6.73×10^{-7} ($\pm$ 1.4×10^{-7})
Chlorhexidine	1.33×10^{-8} ($\pm$ 0.58×10^{-8})
Lomefloxacin	2.28×10^{-6} ($\pm$ 0.76×10^{-6})
Gatifloxacin	1.23×10^{-7} ($\pm$ 0.38×10^{-7})
Telithromycin	2.94×10^{-6} ($\pm$ 0.9×10^{-6})
Bekanamycin	9.44×10^{-6} ($\pm$ 7.56×10^{-6})
Rifaximin	0.87×10^{-6} ($\pm$ 0.16×10^{-6})
Aztreonam	0.33×10^{-8} ($\pm$ 0.58×10^{-8})
Pefloxacin	1.37×10^{-7} ($\pm$ 1.06×10^{-7})
Garenoxacin	3×10^{-8} ($\pm$ 3.61×10^{-8})
Enoxacin	2.27×10^{-7} ($\pm$ 0.75×10^{-7})
Sparfloxacin	1.27×10^{-7} ($\pm$ 0.15×10^{-7})
	8 × MIC
Ceftazidime	1.6×10^{-6} ($\pm$ 0.02×10^{-6})
Paromomycin	2.41×10^{-6} ($\pm$ 0.37×10^{-6})
Cefmenoxime	5.17×10^{-7} ($\pm$ 3.15×10^{-7})
Danofloxacin	4.13×10^{-7} ($\pm$ 0.4×10^{-7})
Mezlocillin	2.11×10^{-5} ($\pm$ 0.12×10^{-5})
	4 × MIC
Sitafloxacin	/
Colistin	/
Prulifloxacin	/
Pazufloxacin	/
Besifloxacin	/
Levofloxacin	/

/means no colony growth on the plate at 4 × MIC after 48 h incubation at 37°C, drugs that are not listed indicate that the colony is covered with the plate at 4 × MIC after 48 h incubation at 37°C.

Infections with high bacterial loads ($> 10^7$ CFU/ml bacteria) are rarely mentioned, especially those associated with biofilms or abscesses, but deserve more attention (Pletzer et al., 2018). The effects of different drugs concentrations were determined through preliminary experiments, with reference to the pharmacokinetics or empirically test (Agwuh and Macgowan, 2006; de Breij et al., 2018). We finally determined appropriate concentration that reduces abscess areas enough to observe the synergistic effect between SAAP-148 and DMCT (**Supplementary Figure S2**). The combination of DMCT and SAAP-148 against PAO1 were about 36 times lower than the saline control group and showed synergistic effects over the monotherapy (**Figure 4**). Similarly, DMCT (5 mg/kg) or SAAP-148 (10 mg/kg) could not inhibit the growth of abscess alone, but abscess size was notably diminished when used in combination. Consistent with these results, histopathological analysis showed that compared with monotherapy, the group of mice treated with the combination therapy significantly reduced the inflammation of the skin abscess, or even disappeared.

These important observations prove that antimicrobial monotherapy is usually ineffective when *P. aeruginosa* develops high-density infections. In addition, combination therapy can significantly enhance the efficacy of bacterial infections.

DISCUSSION

The purpose of this work was to find possible inhibitors against *P. aeruginosa*, which is notorious for its increased resistance. The thirty-nine drugs were selected through high-throughput screening, and their antibacterial effects on *P. aeruginosa* were further evaluated through phenotypic experiments. In addition, we showed that the combination of antimicrobial peptide SAAP-148 and DMCT showed a strong antimicrobial effect on both the standard strain of *P. aeruginosa* and the clinically isolated strain of MDR.

High-throughput screening has become an important approach in finding target drugs. Moreover, the plans of repurposing existing drugs that are currently being used as treatments for other diseases is also attractive (Miró-Canturri et al., 2019). Successful repurposing screens have produced candidates for Zika virus and Ebola virus (Johansen et al., 2015; Barrows et al., 2016). In this study, we screened these drugs like many other studies in order to find drugs that can inhibit *P. aeruginosa*. It has been listed by the World Health Organization as an important pathogen that poses a "serious" threat to human health (Shankar, 2014). The ability to form intrinsic resistant biofilms is posing another major threat to human health, as several infections include catheter-related infections and wounds directly related to biofilms. Therefore, we focused on finding drugs that have inhibitory effects on biofilms. Among the selected drugs, 37 drugs inhibited biofilm formation by more than 80% at the concentration of 30 μM. We further screened out 18 of 39 drugs that disrupt the preformed biofilms (**Figure 1**). The destruction of biofilm is the key to the treatment of chronic infection of *P. aeruginosa*. These drugs may play an important role in the treatment of biofilm diseases.

We found that the combination of DMCT and SAAP-148 has a synergistic effect on *P. aeruginosa*. SAAP-148 is derived from the classical AMP LL-37 with improved antimicrobial and antibiofilm activities. Compared with many antimicrobial peptides in the preclinical and clinical stages, SAAP-148 has higher *in vitro* bactericidal efficacy under physiological conditions. SAAP-148 showed broad antibacterial activity against both Gram-positive and Gram-negative bacteria of MDR and could interact with cell membrane and permeate rapidly. In particular, SAAP-148 can kill persister cells and eradicate biofilm without selective resistance. DMCT is a tetracycline derivative antibiotic produced by Lederle et al. (McCormick et al., 1957). DMCT kill bacteria by binding to ribosomes inhibiting protein synthesis. It is used as a

TABLE 3 | FICs of selected drugs and SAAP-148 alone or in combination against PAO1.

Drug	MIC (μ M)		$MIC_{Incombination}/MIC_{singly}$	FICI	Outcome
	Singly	Combination			
Demeclocycline	12.5	3.125	0.25	0.5	Synergy
SAAP-148	6.25	1.5625	0.25		
Azlocillin	6.25	3.125	0.5	0.75	Partial Synergy
SAAP-148	6.25	1.5625	0.25		
Mezlocillin	25	6.25	0.25	0.75	Partial Synergy
SAAP-148	6.25	3.125	0.5		
Ceftriaxone	6.25	3.125	0.5	0.75	Partial Synergy
SAAP-148	6.25	1.5625	0.25		
Cefepime	1.5625	0.78125	0.5	0.75	Partial Synergy
SAAP-148	6.25	1.5625	0.25		
Pazufloxacin	6.25	1.5625	0.25	0.75	Partial Synergy
SAAP-148	6.25	3.125	0.5		
Prulifloxacin	3.125	1.5625	0.5	1	Additivity
SAAP-148	6.25	3.125	0.5		
Sisomicin	0.78125	0.3906	0.5	1	Additivity
SAAP-148	6.25	3.125	0.5		
Aztreonam	6.25	3.125	0.5	1	Additivity
SAAP-148	6.25	3.125	0.5		
Sparfloxacin	6.25	3.125	0.5	1.5	Indifference
SAAP-148	6.25	6.25	1		
Pefloxacin	12.5	6.25	0.5	1	Additivity
SAAP-148	6.25	3.125	0.5		
Besifloxacin	12.5	6.25	0.5	1	Additivity
SAAP-148	6.25	3.125	0.5		
Azithromycin	50	25	0.5	1	Additivity
SAAP-148	6.25	3.125	0.5		
Chlorhexidine	12.5	6.25	0.5	1	Additivity
SAAP-148	6.25	3.125	0.5		
Netilmicin	3.125	1.5625	0.5	1	Additivity
SAAP-148	6.25	3.125	0.5		
Piperacillin	1.5625	0.78125	0.5	1	Additivity
SAAP-148	6.25	3.125	0.5		
Cefozopran	0.78125	0.78125	1	1.5	Indifference
SAAP-148	6.25	3.125	0.5		
Sitafloxacin	1.5625	1.5625	1	2	Indifference
SAAP-148	6.25	6.25	1		
Amikacin	1.5625	0.78125	0.5	1.5	Indifference
SAAP-148	6.25	6.25	1		
Gemifloxacin	3.125	1.5625	0.5	1	Additivity
SAAP-148	6.25	3.25	0.5		
Cefmenoxime	3.125	1.5625	0.5	1	Additivity
SAAP-148	6.25	3.125	0.5		
Lomefloxacin	6.25	3.125	0.5	1	Additivity
SAAP-148	6.25	3.125	0.5		
Garenoxacin	6.25	3.125	0.5	1	Additivity
SAAP-148	6.25	3.125	0.5		
Gatifloxacin	6.25	3.125	0.5	1	Additivity
SAAP-148	6.25	3.125	0.5		
Levofloxacin	12.5	6.25	0.5	1.5	Indifference
SAAP-148	6.25	6.25	1		
Enoxacin	12.5	6.25	0.5	1.5	Indifference

(Continued)

TABLE 3 | Continued

Drug	MIC (μ M)		$MIC_{Incombination}/MIC_{singly}$	FICI	Outcome
	Singly	Combination			
SAAP-148	6.25	6.25	1		
Danofloxacin	6.25	3.125	0.5	1.5	Indifference
SAAP-148	6.25	6.25	1		
Tosufloxacin	3.125	1.5625	0.5	1.5	Indifference
SAAP-148	6.25	6.25	1		
Streptomycin	3.125	1.5625	0.5	1.5	Indifference
SAAP-148	6.25	6.25	1		
Doripenem	1.5625	1.5625	1	2	Indifference
SAAP-148	6.25	6.25	1		
Colistin	1.5625	0.78125	0.5	1.5	Indifference
SAAP-148	6.25	6.25	1		
Ceftazidime	1.5625	1.5625	1	2	Indifference
SAAP-148	6.25	6.25	1		
Rifaximin	12.5	6.25	0.5	1.5	Indifference
SAAP-148	6.25	6.25	1		
Erythromycin	50	50	1	2	Indifference
SAAP-148	6.25	6.25	1		
Telithromycin	50	25	0.5	1.5	Indifference
SAAP-148	6.25	6.25	1		
Bekanamycin	12.5	6.25	0.5	1.5	Indifference
SAAP-148	6.25	6.25	1		
Tobramycin	0.78125	0.78125	1	2	Indifference
SAAP-148	6.25	6.25	1		
Paromomycin	12.5	12.5	1	2	Indifference
SAAP-148	6.25	6.25	1		

FICI is the fractional inhibitory concentration index.

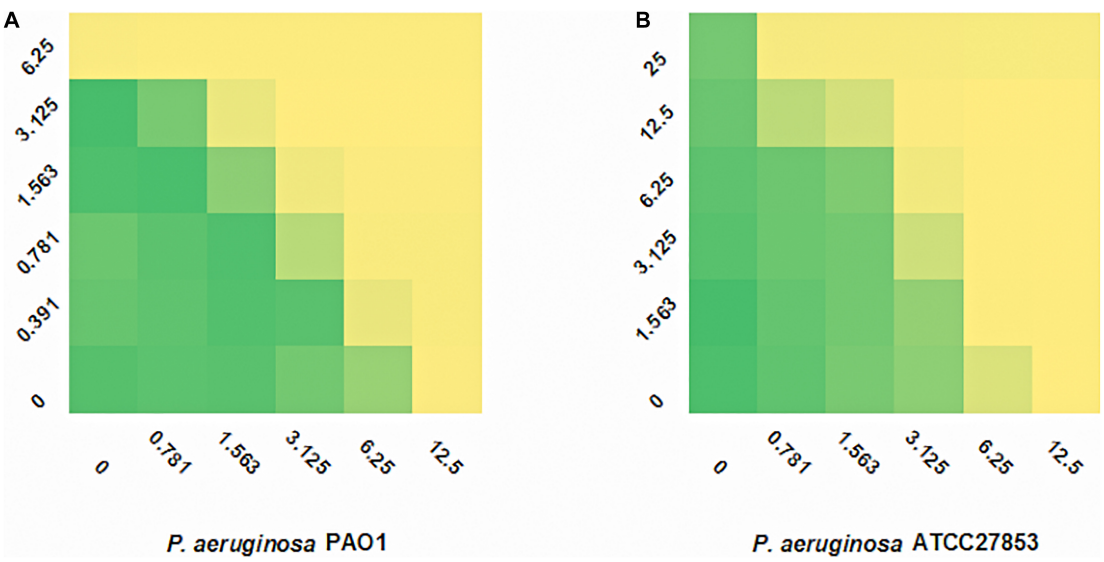

FIGURE 2 | FIC indexes of DMCT/SAAP-148 combination. Fractional inhibitory concentration (FIC) testing of DMCT and SAAP-148 alone and combination against PAO1 **(A)** and ATCC27853 **(B)**.

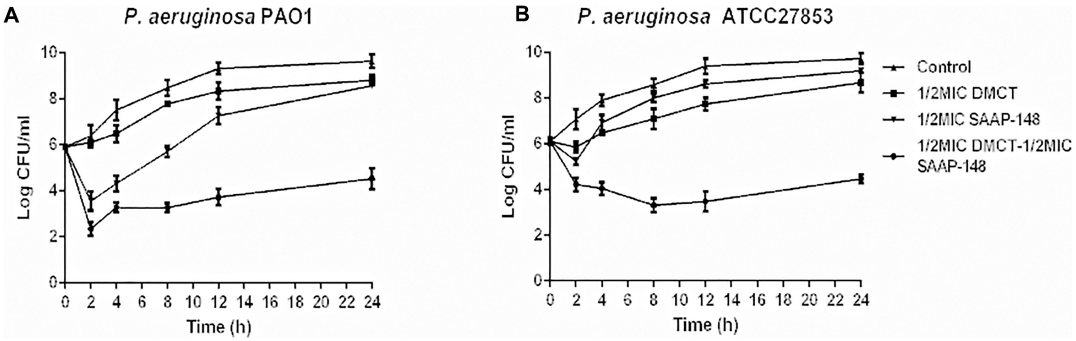

FIGURE 3 | Time-kill curves for DMCT and SAAP-148 alone or combination against *P. aeruginosa*. Time-kill assay using one-second the MIC of each agent (6.25 μM of DMCT, 3.125 μM of SAAP-148) alone and in combination for PAO1 **(A)** and ATCC27853 **(B)**. The data were presented as mean ± SD.

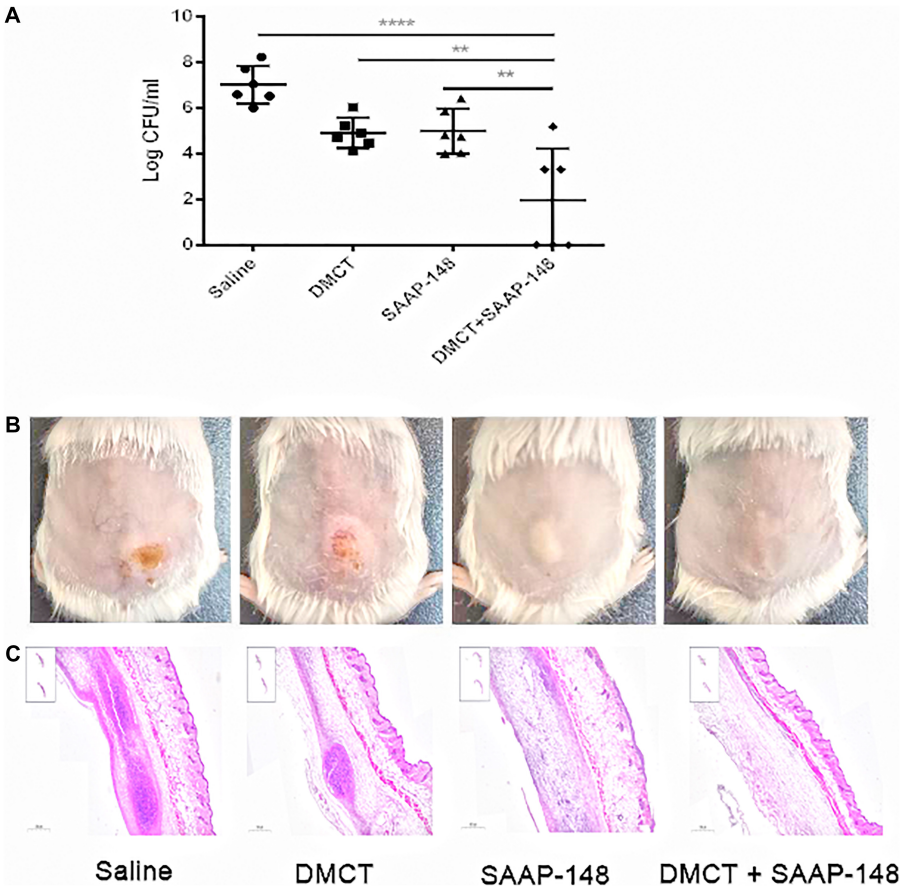

FIGURE 4 | DMCT and SAAP-148 combinatorial therapy in a murine cutaneous abscess model. CD-1 female mice were injected with 1×10^9 CFU/ml *P. aeruginosa* PAO1 and treated 1 h post-infection with saline (control), DMCT, SAAP-148, or DMCT + SAAP-148 combination. Drugs concentrations for all conditions were as follows: DMCT, 5 mg/kg and SAAP-148, 10 mg/kg. Infected abscess lumps and pus were excised to determine CFU by 3 days post-infection. Counted CFU/ml data is expressed **(A)**. An entire dorsal back abscess and representative results are shown at 3 days after therapy for PAO1 **(B)**. **(C)** Histological results (H&E stain, 3×, down panels) are shown at 3 days after therapy for mono- or combined therapy. All experiments were performed three times with 2–4 mice per group. Statistical analysis was performed using one-way ANOVA, Kruskal–Wallis test with Dunn's correction (two-sided). The asterisk indicates significant differences. $^{**}P < 0.01$; $^{****}P < 0.0001$.

broad-spectrum antibiotic, but may be more often used to treat chronic syndrome of inappropriate secretion of antidiuretic hormone (SIADH) (Miell et al., 2015). According to reports, DMCT is expected to be used as a contrast agent for intraoperative detection of brain tumors (Sarkar et al., 2020). In our study, we collected 6 MDR clinical isolate strains of *P. aeruginosa* for combination therapy. It is worth noting that we found that the combination of DMCT and SAAP-148 has a synergistic effect on these strains (**Supplementary Table S3**). It is known that the killing of bacteria by SAAP-148 involves the rapid interaction of peptides with the bacterial membrane and subsequent permeabilization, leading to the death of bacteria. Thus, we infer that the mode of action of SAAP-148 likely facilitates the penetration of DMCT to the bacteria, and at the next step, the interaction of DMCT and SAAP-148 causes death of bacteria.

The bacterial skin and soft tissue infections (SSTIs) are a very common problem. The bacteria that often cause SSTI are methicillin-resistant Staphylococcus aureus (MRSA), but gram-negative bacteria are becoming more and more important in global SSTI (Ruef, 2008; Mansour et al., 2016). The SENTRY Antimicrobial Surveillance Program (North America) reported that 10.8% of the major pathogens isolated from SSTI include *P. aeruginosa* (Rennie et al., 2003). SSTIs can lead to cutaneous abscesses, and recurring abscesses cause difficult-to-treat infections. According to our research, highly synergistic interactions between DMCT and SAAP-148 were observed against a high bacterial load-containing abscess model of PAO1. In our cutaneous abscess model, DMCT or SAAP-148 alone showed a moderate effect on bacterial load. The abscess area of the monotherapy group was similar to that of the saline control group (**Figure 4**). On the contrary, DMCT combined with SAAP-148 could inhibit abscess and reduce PAO1 bacterial load. There is a good correlation between bacterial burden reduction and combination therapy. Topical application of the peptide SAAP-148 in hypromellose gel at a dose up to 300 mg/day per animal, proved to be safe without any adverse effects (de Breij et al., 2018). As an ancient antibacterial drug, the safety of DMCT *in vivo* animal research and clinical application has been fully proved, though DMCT is more widely used in non-antibacterial fields. In the screening trial, subjects were given DMCT 600 mg/day by oral therapy for pustules treatment (Plewig and Schöpf, 1975). The combination of antibiotics and antimicrobial peptides targeting bacterial membrane can effectively treat infection and reduce the severity of skin abscess.

In summary, we used high-throughput screening methods to identify drugs that have bactericidal activity against *P. aeruginosa*. A total of 39 compounds were identified as potential drugs against PAO1, which were further confirmed by phenotypic experiments. It was also concluded that the combination therapy resulted in a significant reduction in the effective concentrations of DMCT and SAAP-148 needed to inhibit *P. aeruginosa* and reduce its toxicity. Our results proved that DMCT in combination with SAAP-148 proved to be an attractive option for the development of antimicrobial combined therapy.

DATA AVAILABILITY STATEMENT

The original contributions presented in the study are included in the article/**Supplementary Material**, further inquiries can be directed to the corresponding author.

ETHICS STATEMENT

The animal study was reviewed and approved by the Clinical samples collection and animal experiments were conducted under the approval of the Ethics Committee of the Third Xiangya Hospital, Central South University (No. 2019-S021). Strains were isolated from clinical samples routinely collected from patients, and the identification of patients was not needed. Therefore, the need for written informed consent was waived and oral informed consent was obtained.

AUTHOR CONTRIBUTIONS

YW, PS, and SL conducted the experimental design for this study. SL was the main completer of the experiment, analyzed the results of the experiment, and wrote the manuscript. LC provided reagents and methods needed for the study. LZ, XZ, LX, and YL performed some supplementary experiments. YW supervised the entire study. All the authors read and approved the final manuscript.

FUNDING

This work was supported by the National Natural Science Foundation of China (grant no. 82072350).

ACKNOWLEDGMENTS

We thank Mingqiang Qiao (College of Life Sciences of Nankai University, Tianjin, China) for providing the *P. aeruginosa* PAO1 strain (ATCC15692).

SUPPLEMENTARY MATERIAL

The Supplementary Material for this article can be found online at: https://www.frontiersin.org/articles/10.3389/fmicb.2020.591426/full#supplementary-material

REFERENCES

Agwuh, K. N., and Macgowan, A. (2006). Pharmacokinetics and pharmacodynamics of the tetracyclines including glycylcyclines. *J. Antimicrob. Chemother.* 58, 256–265. doi: 10.1093/jac/dkl224

Almaaytah, A., Abualhaijaa, A., and Alqudah, O. (2019). The evaluation of the synergistic antimicrobial and antibiofilm activity of AamAP1-Lysine with conventional antibiotics against representative resistant strains of both Gram-positive and Gram-negative bacteria. *Infect. Drug Resist.* 12, 1371–1380. doi: 10.2147/idr.S204626

Ashburn, T., and Thor, K. B. (2004). Drug repositioning: identifying and developing new uses for existing drugs. *Nat. Rev. Drug Discov.* 3, 673–683. doi: 10.1038/nrd1468

Barrows, N., Campos, R., Powell, S., Prasanth, K., Schott-Lerner, G., Soto-Acosta, R., et al. (2016). A screen of FDA-approved drugs for inhibitors of Zika virus infection. *Cell Host Microbe* 20, 259–270. doi: 10.1016/j.chom.2016.07.004

Brooks, B., and Brooks, A. (2014). Therapeutic strategies to combat antibiotic resistance. *Adv. Drug Deliv. Rev.* 78, 14–27. doi: 10.1016/j.addr.2014.10.027

Campbell, J. (2011). High-throughput assessment of bacterial growth inhibition by optical density measurements. *Curr. Protoc. Chem. Biol.* 3:100115. doi: 10.1002/9780470559277.ch100115

Chu, M., Zhang, M., Liu, Y., Kang, J., Chu, Z., Yin, K., et al. (2016). Role of berberine in the treatment of methicillin-resistant *Staphylococcus aureus* infections. *Sci. Rep.* 6:24748. doi: 10.1038/srep24748

de Breij, A., Riool, M., Cordfunke, R., Malanovic, N., de Boer, L., Koning, R., et al. (2018).). The antimicrobial peptide SAAP-148 combats drug-resistant bacteria and biofilms. *Sci. Transl. Med.* 10:eaan4044. doi: 10.1126/scitranslmed.aan4044

Djapgne, L., Panja, S., Brewer, L., Gans, J., Kane, M., Woodson, S., et al. (2018). The *Pseudomonas aeruginosa* PrrF1 and PrrF2 small regulatory RNAs promote 2-Alkyl-4-quinolone production through redundant regulation of the mRNA. *J. Bacteriol.* 200, e704–e717. doi: 10.1128/jb.00704-17

Fajardo-Cavazos, P., and Nicholson, W. (2016). Cultivation of *Staphylococcus epidermidis* in the human spaceflight environment leads to alterations in the frequency and spectrum of spontaneous rifampicin-resistance mutations in the rpoB gene. *Front. Microbiol.* 7:999. doi: 10.3389/fmicb.2016.00999

Fosgerau, K., and Hoffmann, T. (2015). Peptide therapeutics: current status and future directions. *Drug Discov. Today* 20, 122–128. doi: 10.1016/j.drudis.2014.10.003

Gomes, F., Teixeira, P., Azeredo, J., and Oliveira, R. (2009). Effect of farnesol on planktonic and biofilm cells of *Staphylococcus epidermidis*. *Curr. Microbiol.* 59, 118–122. doi: 10.1007/s00284-009-9408-9

Hayes, K., Cotter, L., and O'Halloran, F. (2019). In vitro synergistic activity of erythromycin and nisin against clinical Group B *Streptococcus* isolates. *J. Appl. Microbiol.* 127, 1381–1390. doi: 10.1111/jam.14400

Holloway, B. W. (1955). Genetic recombination in *Pseudomonas aeruginosa*. *J. Gen. Microbiol.* 13, 572–581. doi: 10.1099/00221287-13-3-572

Huang, R., Li, M., and Gregory, R. (2012). Effect of nicotine on growth and metabolism of *Streptococcus mutans*. *Eur. J. Oral Sci.* 120, 319–325. doi: 10.1111/j.1600-0722.2012.00971.x

Institute, C. (2006). *Methods for Dilution Antimicrobial Susceptibility Tests for Bacteria That Grow AerobicallyCLSIApproved Standard - Seventh Edition*. CLSI Document M7-A72006. Wayne, PA: CLSI.

Johansen, L. M., DeWald, L. E., Shoemaker, C. J., Hoffstrom, B. G., Lear-Rooney, C. M., Stossel, A., et al. (2015). A screen of approved drugs and molecular probes identifies therapeutics with anti-Ebola virus activity. *Sci. Transl. Med.* 7:290ra289. doi: 10.1126/scitranslmed.aaa5597

Mah, T., and O'Toole, G. (2001). Mechanisms of biofilm resistance to antimicrobial agents. *Trends Microbiol.* 9, 34–39. doi: 10.1016/s0966-842x(00)01913-2

Mansour, S., Pletzer, D., de la Fuente-Núñez, C., Kim, P., Cheung, G., Joo, H., et al. (2016). Bacterial abscess formation is controlled by the stringent stress response and can be targeted therapeutically. *EBioMedicine* 12, 219–226. doi: 10.1016/j.ebiom.2016.09.015

McCormick, J., Sjolander, N., Hirsch, U., Jensen, E., and Doerschuk, A. (1957). A new family of antibiotics: the demethyltetracyclines. *J. Am. Chem. Soc.* 79, 4561–4563. doi: 10.1021/ja01573a089

Miell, J., Dhanjal, P., and Jamookeeah, C. (2015). Evidence for the use of demeclocycline in the treatment of hyponatraemia secondary to SIADH: a systematic review. *Int. J. Clin. Pract.* 69, 1396–1417. doi: 10.1111/ijcp.12713

Miró-Canturri, A., Ayerbe-Algaba, R., and Smani, Y. J. F. I. M. (2019). Drug repurposing for the treatment of bacterial and fungal infections. *Front. Microbiol.* 10:41. doi: 10.3389/fmicb.2019.00041

Mishra, B., Reiling, S., Zarena, D., and Wang, G. (2017). Host defense antimicrobial peptides as antibiotics: design and application strategies. *Curr. Opin. Chem. Biol.* 38, 87–96. doi: 10.1016/j.cbpa.2017.03.014

Mullard, A. (2012). Drug repurposing programmes get lift off. *Nat. Rev. Drug Discov.* 11, 505–506. doi: 10.1038/nrd3776

Nesse, L., Berg, K., and Vestby, L. K. (2015). Effects of norspermidine and spermidine on biofilm formation by potentially pathogenic *Escherichia coli* and *Salmonella enterica* wild-type strains. *Appl. Environ. Microbiol.* 81, 2226–2232. doi: 10.1128/aem.03518-14

Odds, F. (2003). Synergy, antagonism, and what the chequerboard puts between them. *J. Antimicrob. Chemother.* 52:1. doi: 10.1093/jac/dkg301

Pachón-Ibáñez, M., Ribes, S., Domínguez, M., Fernández, R., Tubau, F., Ariza, J., et al. (2011). Efficacy of fosfomycin and its combination with linezolid, vancomycin and imipenem in an experimental peritonitis model caused by a *Staphylococcus aureus* strain with reduced susceptibility to vancomycin. *Eur. J. Clin. Microbiol. Infect. Dis.* 30, 89–95. doi: 10.1007/s10096-010-1058-0

Pendleton, J., Gorman, S., and Gilmore, B. (2013). Clinical relevance of the ESKAPE pathogens. *Expert Rev. Anti. Infect. Ther.* 11, 297–308. doi: 10.1586/eri.13.12

Pletzer, D., Mansour, S., and Hancock, R. (2018). Synergy between conventional antibiotics and anti-biofilm peptides in a murine, sub-cutaneous abscess model caused by recalcitrant ESKAPE pathogens. *PLoS Pathog.* 14:e1007084. doi: 10.1371/journal.ppat.1007084

Plewig, G., and Schöpf, E. (1975). Anti-inflammatory effects of antimicrobial agents: an in vivo study. *J. Investig. Dermatol.* 65, 532–536. doi: 10.1111/1523-1747.ep12610281

Prindle, A., Liu, J., Asally, M., Ly, S., Garcia-Ojalvo, J., and Süel, G. J. N. (2015). Ion channels enable electrical communication in bacterial communities. *Nature* 527, 59–63. doi: 10.1038/nature15709

Rahme, L., Stevens, E., Wolfort, S., Shao, J., Tompkins, R., and Ausubel, F. J. S. (1995). Common virulence factors for bacterial pathogenicity in plants and animals. *Science* 268, 1899–1902. doi: 10.1126/science.7604262

Rennie, R., Jones, R., and Mutnick, A. (2003). Occurrence and antimicrobial susceptibility patterns of pathogens isolated from skin and soft tissue infections: report from the SENTRY antimicrobial surveillance program (United States and Canada, 2000). *Diagn. Microbiol. Infect. Dis.* 45, 287–293. doi: 10.1016/s0732-8893(02)00543-6

Ruef, C. J. I. (2008). Complicated skin and soft-tissue infections–consider gram-negative pathogens. *Infection* 36:295. doi: 10.1007/s15010-008-3408-8

Sarkar, S., Li, Y., Mirzaei, R., Rawji, K., Poon, C., Wang, J., et al. (2020). Demeclocycline reduces the growth of human brain tumor-initiating cells: direct activity and through monocytes. *Front Immunol.* 11:272. doi: 10.3389/fimmu.2020.00272

Schmidt, K., Tümmler, B., and Römling, U. (1996). Comparative genome mapping of *Pseudomonas aeruginosa* PAO with *P. aeruginosa* C, which belongs to a major clone in cystic fibrosis patients and aquatic habitats. *J. Bacteriol.* 178, 85–93. doi: 10.1128/jb.178.1.85-93.1996

Shankar, P. R. (2014). Antimicrobial resistance: global report on surveillance. *Austral. Med. J.* 7:237.

She, P., Wang, Y., Liu, Y., Tan, F., Chen, L., Luo, Z., et al. (2019). Effects of exogenous glucose on *Pseudomonas aeruginosa* biofilm formation and antibiotic resistance. *MicrobiologyOpen* 8:e933. doi: 10.1002/mbo3.933

Smith, P. A., Koehler, M. F. T., Girgis, H. S., Yan, D., Chen, Y., Chen, Y., et al. (2018). Optimized arylomycins are a new class of Gram-negative antibiotics. *Nature* 561, 189–194.

Sousa, A., and Pereira, M. J. P. (2014). *Pseudomonas aeruginosa* diversification during infection development in cystic fibrosis lungs-a review. *Pathogens* 3, 680–703. doi: 10.3390/pathogens3030680

Sun, W., Weingarten, R., Xu, M., Southall, N., Dai, S., Shinn, P., et al. (2016). Rapid antimicrobial susceptibility test for identification of new therapeutics and drug combinations against multidrug-resistant bacteria. *Emerg. Microbes Infect.* 5:e116. doi: 10.1038/emi.2016.123

Tängdén, T. (2014). Combination antibiotic therapy for multidrug-resistant Gram-negative bacteria. *Ups J. Med. Sci.* 119, 149–153. doi: 10.3109/03009734.2014.899279

Trombetta, R., Dunman, P., Schwarz, E., Kates, S., and Awad, H. (2018). A high-throughput screening approach to repurpose FDA-approved drugs for bactericidal applications against *Staphylococcus aureus* small-colony variants. *mSphere* 3, e422–e418. doi: 10.1128/mSphere.00422-18

Yu, G., Baeder, D. Y., Reogoes, R. R., and Rolff, J. (2018). Predicting drug resistance evolution: insights from antimicrobial peptides and antibiotics. *Proc. R. Soc.* 285:20172687. doi: 10.1098/rspb.2017.2687

Conflict of Interest: The authors declare that the research was conducted in the absence of any commercial or financial relationships that could be construed as a potential conflict of interest.

frontiers in Microbiology

ORIGINAL RESEARCH
published: 18 December 2020
doi: 10.3389/fmicb.2020.579621

Isolation and Characterization of Fengycins Produced by *Bacillus amyloliquefaciens* JFL21 and Its Broad-Spectrum Antimicrobial Potential Against Multidrug-Resistant Foodborne Pathogens

Long-Zhen Lin[1,2†], Qian-Wang Zheng[1,2†], Tao Wei[1,2], Zi-Qian Zhang[1,2], Chao-Fan Zhao[1,2], Han Zhong[1,2], Qing-Yuan Xu[1,2], Jun-Fang Lin[1,2] and Li-Qiong Guo[1,2*]*

[1] Department of Bioengineering, College of Food Science, South China Agricultural University, Guangzhou, China,
[2] Research Center for Micro-Ecological Agent Engineering and Technology of Guangdong Province, Guangzhou, China

The continuing emergence and development of pathogenic microorganisms that are resistant to antibiotics constitute an increasing global concern, and the effort in new antimicrobials discovery will remain relevant until a lasting solution is found. A new bacterial strain, designated JFL21, was isolated from seafood and identified as *B. amyloliquefaciens*. The antimicrobial substance produced by *B. amyloliquefaciens* JFL21 showed low toxicity to most probiotics but exhibited strong antimicrobial activities against multidrug-resistant foodborne pathogens. The partially purified antimicrobial substance, Anti-JFL21, was characterized to be a multiple lipopeptides mixture comprising the families of surfactin, fengycin, and iturin. Compared with commercially available polymyxin B and Nisin, Anti-JFL21 not only could exhibit a wider and stronger antibacterial activity toward Gram-positive pathogens but also inhibit the growth of a majority of fungal pathogens. After further separation through gel filtration chromatography (GFC), the family of surfactin, fengycin, and iturin were obtained, respectively. The results of the antimicrobial test pointed out that only fengycin family presented marked antimicrobial properties against the indicators of *L. monocytogenes*, *A. hydrophila*, and *C. gloeosporioides*, which demonstrated that fengycins might play a major role in the antibacterial and antifungal activity of Anti-JFL21. Additionally, the current study also showed that the fengycins produced by *B. amyloliquefaciens* JFL21 not only maintained stable anti-*Listeria* activity over a broad pH and temperature range, but also remained active after treatment with ultraviolet sterilization, chemical reagents, and proteolytic enzymes. Therefore, the results of this study suggest the new strain and its antimicrobials are potentially useful in food preservation for the biological control of the multidrug-resistant foodborne pathogens.

Keywords: fengycin, *Bacillus amyloliquefaciens*, antimicrobial activity, multidrug-resistant foodborne pathogens, probiotics, lipopeptides

OPEN ACCESS

Edited by:
Mariano Martinez-Vazquez, National Autonomous University of Mexico, Mexico

Reviewed by:
Maria José Saavedra, Universidade de Trás os Montes e Alto Douro, Portugal
Piyush Baindara, University of Missouri, United States
Rodolfo García-Contreras, National Autonomous University of Mexico, Mexico

***Correspondence:**
Jun-Fang Lin
linjf@scau.edu.cn
Li-Qiong Guo
guolq@scau.edu.cn

† These authors have contributed equally to this work

Specialty section:
This article was submitted to Antimicrobials, Resistance and Chemotherapy, a section of the journal Frontiers in Microbiology

Received: *03 July 2020*
Accepted: *02 December 2020*
Published: *18 December 2020*

Citation:
Lin L-Z, Zheng Q-W, Wei T, Zhang Z-Q, Zhao C-F, Zhong H, Xu Q-Y, Lin J-F and Guo L-Q (2020) Isolation and Characterization of Fengycins Produced by Bacillus amyloliquefaciens JFL21 and Its Broad-Spectrum Antimicrobial Potential Against Multidrug-Resistant Foodborne Pathogens. Front. Microbiol. 11:579621. doi: 10.3389/fmicb.2020.579621

INTRODUCTION

Foodborne diseases have been a serious global public health issue and most of them are caused by foodborne pathogens such as *Salmonella*, *Shigella*, *Vibrio*, *Escherichia coli* O157, *Yersinia enterocolitica*, *Listeria monocytogenes*, *Staphylococcus aureus*, and *Aspergillus flavus*, etc. (World Health Organization, 2015; European Food Safety Authority, 2018; Tack et al., 2019). According to the data reported by the World Health Organization (WHO), foodborne diseases have caused approximate 600 million illness and 420, 000 deaths in the world and at least $100 billion costs in low- and middle-income countries every year, and the actual number of cases is also likely to be underestimated due to the high failure rate of reporting foodborne diseases worldwide (World Health Organization, 2015, 2019). Although antibiotics are essential to treat infections caused by foodborne pathogens, their overuse and misuse has been linked to the emergence and spread of multiple resistant strains during the past decades and has led to public awareness (Garedew et al., 2015; Kuch et al., 2018; U.S. Centers for Disease Control and Prevention, 2019). According to the government data of U.S. Centers for Disease Control and Prevention (CDC), antibiotic-resistant infections from foodborne germs (bacteria and fungi) still cause more than 2.8 million illnesses and 35,000 deaths in the United States each year despite attempts to combat the problem (U.S. Centers for Disease Control and Prevention, 2019). Thus, there is an urgent need for alternatives to antibiotics to fight against the foodborne pathogens.

In recent years, many studies have shown that the cyclic lipopeptides (CLPs) produced by *Bacillus* spp. have potent antimicrobial activity against antibiotic-resistant strains and can be generally divided into three main families: surfactin, fengycin, and iturin (Chi et al., 2015; Jemil et al., 2017; Perez et al., 2017; Piewngam et al., 2018). Due to their specific amphiphilic structure, CLPs primarily destroy target organisms by directly disrupting the integrity of the plasma membrane or cell wall in a detergent-like manner, and thus display a lower propensity to develop resistance than do conventional antibiotics (Banat et al., 2010; Mandal et al., 2013; Singh and Abraham, 2014; Patel et al., 2015; Ndlovu et al., 2017). Besides, CLPs are biodegradable, biocompatible, eco-friendly, relatively non-toxic, and resistant to extreme conditions of temperatures, pH, and salinity (Pradhan et al., 2013; Ben Ayed et al., 2017). Because of these attractive characteristics, naturally produced antimicrobial CLPs have received increasing attention as promising new antibiotic candidates for food, pharmaceutical, and biomedical applications.

Considering the increasingly prominent problems of antibiotic contamination and food safety, this research aimed to search for candidate *Bacillus* strains that could produce a potent antimicrobial agent to combat various foodborne pathogens with multi-drug resistant profiles. Besides, FITR, HPLC, and MALDI-TOF MS analysis were exploited to identify the structural characteristics of the partially purified antimicrobial substances Anti-JFL21. Moreover, the different lipopeptide families in Anti-JFL21 was further separated, and the effective antimicrobial family was elucidated. what's more, the fengycins stability after the treatment of heating, pH change, ultraviolet sterilization, enzymes, and chemical reagents was determined to evaluate the possible incorporation in the food production chain.

MATERIALS AND METHODS

Microorganisms and Cultivation Conditions

In this study, the three *Bacillus* isolates named JFL21, LQG17, and LQG36, with excellent antimicrobial properties were, respectively, isolated from the gut of hairtail, fermented soybean, and pickle purchased from Guangzhou farmers market. *Bacillus subtilis* 168, one of the model organisms of the *Bacillus* genus, was purchased from the Bacillus Genetic Stock Center (BGSC). The thirty-three indicator strains used for evaluation of antibacterial and antifungal activity were selected for their importance as probiotics or pathogens in food and seafood products. The source and culture conditions of the thirty-three indicator strains are listed in **Table 1**. The bacterial or fungal cultures were preserved in 25% glycerol at −80°C.

Measurement of Drug Resistance of Probiotics and Pathogens

Drug resistance of probiotics and pathogens were determined according to the agar disk diffusion assay (Xu et al., 2014; Perez et al., 2017). Briefly, Sterile Oxford cups (10 mm × 6 mm × 8 mm, height × inner diameter × outer diameter) were placed on the assay medium seeded with the fresh culture suspension of different indicator strains (about 10^8 colony forming units/mL for bacterial cells and 10^6 spores/mL for fungal strains). Each cup was added with 100 μL of commonly used antibiotics (100 μg/mL) (**Table 1**). Besides, the same amount of sterile water, anhydrous ethanol, DMSO, and 0.01 mol/L HCl that applied to prepare antibiotics were used as the negative control to subtract the inhibitory activity of the solvents. After incubation 24 h at 37°C for bacteria and 7 days at 28°C for fungal strains, the inhibition zones were measured and recorded as a mean diameter (mm). All tests were conducted in triplicate.

Identification of Bacterial Strain and Phylogenetic Analysis

Genomic DNA from the *Bacillus* spp. was extracted using the HiPure Bacterial DNA Kit (Magen, China) according to the manufacturer's protocol. The 16S rRNA gene fragment from each of the isolates was amplified using universal primers 27F (5′-AGAGTTTGATCCTGGCTCAG-3′) and 1492R (5′-TACGGTTACCTTGTTACGACTT-3′) according to the method described by Dimkić et al. (2017). The amplified product was purified with the QIAquick PCR purification kit (Qiagen, Germany) and sent for sequencing to Tianyi Huiyuan Bioscience & Technology Inc. (Guangzhou, China). The sequences obtained were deposited in GenBank under the accession numbers MT159453 for *Bacillus* sp. JFL21,

TABLE 1 | Drug resistance of representative bacterial pathogens, pathogenic fungi, and probiotics in food and seafood products.[a]

Indicator microorganisms	Source[b]	Media[c]	T(°C)	Antibiotic sensitivity[d]											
				1	2	3	4	5	6	7	8	9	10	11	12
Lactic acid bacteria (Probiotics)															
Lactobacillus plantarum	Yogurt	MRS	37	+++	++	−	−	+++	−	+++	−	+++	−	−	−
Pediococcus pentosaceus	Tilapia gut	MRS	37	++	++	−	−	+++	−	+++	−	++	−	−	−
Lactobacillus casei	Pickle	MRS	37	+++	−	−	+++	−	−	−	−	++	−	−	−
Lactococcus lactis	*Pleurotus eryngii*	MRS	37	+++	++	+++	++	+++	++	+++	−	++	−	−	−
Leuconostoc mesenteroides	Shrimp gut	MRS	37	+++	+++	+++	+++	+++	++	+++	++	+++	−	−	−
Gram-positive pathogen															
Listeria monocytogenes	ATCC 19111	BHI	37	+++	−	+++	−	++	−	++	++	+++	−	−	−
Staphylococcus aureus	ATCC 12600	TSA	37	+++	++	+++	++	+++	+++	++	++	+++	−	−	−
Staphylococcus epidermidis	ATCC 14990	BHI	37	−	++	++	−	−	+	+	+	+++	+	−	−
Staphylococcus warneri	ATCC 27836	TSA	37	−	−	+++	+	−	++	−	−	++	−	−	−
Staphylococcus haemolyticus	ATCC 29970	TSA	37	+++	−	+++	+++	−	++	−	−	+++	−	−	−
Bacillus cereus	ATCC 14579	TSA	37	+	++	+	+	++	++	+	+++	+++	−	−	−
Gram-negative pathogen															
Vibrio parahaemolyticus	ATCC 17802	BHI	37	++	−	−	−	−	+	−	+	++	−	−	−
Vibrio harveyi	ATCC 33843	TSA	37	+++	−	++	−	−	−	+	+++	+++	−	−	−
Vibrio vulnificus	ATCC 27562	BHI	37	+++	−	−	−	−	+	+++	+	+	−	−	−
Vibrio campbellii	ATCC 33863	TSA	37	−	++	+++	−	−	+	−	−	++	−	−	−
Pseudomonas aeruginosa	ATCC 10145	TSA	37	−	−	+++	−	−	−	−	−	+++	−	−	−
Aeromonas hydrophila	ATCC 7966	TSA	37	−	+++	+++	++	−	++	+	−	++	−	−	−
Indicator microorganisms	**Source[b]**	**Media[c]**	**T(°C)**	**Antibiotic sensitivity[d]**											
				1	2	3	4	5	6	7	8	9	10	11	12
Escherichia coli O157:H7	ATCC 35150	TSA	37	+++	+	++	−	−	++	+	−	++	−	−	−
Salmonella choleraesuis	ATCC 10708	TSA	37	+	+++	++	−	−	+	−	+	+	−	−	−
Salmonella typhimurium	CMCC(B) 50115	TSA	37	+++	−	+++	−	−	++	−	+	+	−	−	−
Shigella flexneri	ATCC 29903	TSA	37	+++	+++	+++	−	−	+	++	−	+	−	−	−
Yersinia enterocolitica	ATCC 9610	TSA	37	−	−	−	−	−	++	+	++	+++	−	−	−
Proteus mirabilis	ATCC 29906	TSA	37	+++	+	−	−	−	+	−	++	−	−	−	−
Cronobacter sakazakii	ATCC 51329	TSA	37	+++	++	+	−	−	++	+	+	++	+	−	−
Klebsiella pneumoniae	ATCC 13883	TSA	37	−	+++	+++	++	++	++	++	−	++	−	−	−
Enterobacter aerogenes	CMCC(B) 45103	TSA	37	−	−	+++	−	−	+	−	−	++	−	−	−
Pathogenic fungi															
Rhizopus oryzae	GIM 3.126	PDA	28	−	−	−	−	−	−	−	−	−	−	−	−
Aspergillus niger	Grape	PDA	28	−	−	−	−	−	−	−	−	−	−	−	++
Aspergillus flavus	GIM 3.18	PDA	28	−	−	−	−	−	−	−	−	−	−	−	−
Aspergillus fumigatus	GIM 3.19	PDA	28	−	−	−	−	−	−	−	−	−	−	+++	−
Peronophythora litchii	Litchi	PDA	28	−	−	−	−	−	−	−	−	−	−	−	++
Colletotrichum gloeosporioides	Mango	PDA	28	−	−	−	−	−	−	−	−	−	−	−	−
Penicillium polonicum	Orange	PDA	28	−	−	−	−	−	−	−	−	−	−	+++	−

[a] *The experimental concentration of each antibiotic was 100 ug/ml. 1, Ampicillin; 2, chloramphenicol; 3, Tetracycline; 4, Chlorotetracycline; 5, Erythromycin; 6, kanamycin; 7, Azithromycin; 8, Apramycin; 9, Gentamicin; 10, Spectinomycin; 11, Benomyl; 12, Actidione.* [b] *ATCC, American Type Culture Collection; CMCC, National Center for Medical Culture Collections; Rhizopus oryzae, Aspergillus flavus, and Aspergillus fumigatus were purchased from Guangdong Culture Collection Center; The other indicator bacteria were isolated from different food samples and stored in our laboratory.* [c] *MRS, de Man, Rogosa and Sharpe medium; TSA, Trypticase Soya Agar; BHI, Brain Heart Infusion; PDA, Potato Dextrose Agar.* [d] *The inhibition zone (IZ) were measured based on the agar disk diffusion assay. −: Sensitivity, IZ ≤ 9; +: Slight resistance, 9 ≤ IZ < 15 mm; ++: Moderate resistance, 15 ≤ IZ < 21 mm; +++: High resistance, IZ ≥ 21 mm.*

MT159454 for *Bacillus* sp. LQG17, and MT159455 for *Bacillus* sp. LQG36. The homology comparison of the obtained sequences with previously sequenced genes in the GenBank database was performed, using the National Center for Biotechnology Information's Blast search program (Bethesda, United States). The most closely related sequences of strain types were aligned using Clustal W software, and phylogenetic trees were constructed in MEGA version 7 using the Neighbor-joining method with 1,000 bootstrap repetitions (Dimkić et al., 2017; Perez et al., 2017).

Production of Antimicrobial Compounds

An inoculum of the glycerol stock of each of the *Bacillus* strains was streaked onto a Luria-Bertani (LB) plate which was incubated for 24 h at 37°C. A single colony was then inoculated into LB broth medium at 30°C and 200 r/min for 16 h (approximately 5×10^7 CFU/mL) to prepare seed cultures. A 1% (v/v) of inoculum was transferred into a 1 L shake flask containing 400 ml of Landy medium which was composed of the following: glucose 20 g/L, yeast extract 1 g/L, L-glutamic acid 5 g/L, KCl 0.5 g/L, $MgSO_4$ 0.5 g/L, KH_2PO_4 1 g/L, L-phenylalanine 2 mg/L, $MnSO_4$

5 mg/L, $FeSO_4$ 0.15 mg/L, $CuSO_4$ 0.16 mg/L. The initial pH was adjusted to 7.0 and submerged fermentation was carried out in the rotary shaker at 30°C and 200 r/min for 48 h to produce the antimicrobial substance. After fermentation, the culture was centrifuged at 10,000 × *g* for 15 min at 4°C to remove microbial cells. The cell-free supernatants (CFS) was further sterilized by filtration through a cellulose filter with a pore size of 0.45 μm. Thereafter the filtered CFS (100 μL) from different *Bacillus* strains was tested for antimicrobial activity against thirty-three indicator strains (**Table 1**) using the agar disk diffusion assay mentioned above. The same amount of uninoculated Landy medium was used as negative control.

Extraction and Partial Purification of the Antimicrobial Compounds

The partial purification of the antimicrobial substance was carried out by a combination of acid precipitation and methanol extraction method (Sharma et al., 2015; Ndlovu et al., 2017). Briefly, the filtered CFS was adjusted to pH 2.0 by the addition of 6N HCl and allowed to precipitate at 4°C overnight. The acid precipitate was then harvested by centrifugation at 10,000 × *g* for 15 min at 4°C, and the pellet was washed twice with the 100 mL pH 2.0 distilled water (prepared through a MilliQ system from Millipore, Billerica, United States). This pellet was then resuspended in distilled water by raising the pH to 7.0, lyophilized, and solvent-extracted with methanol. The methanol-soluble fraction was dried using a rotary vacuum evaporator at 45°C. After the removal of methanol, a minimum quantity of methanol was added to dissolve the antimicrobial compound, which was again lyophilized and weighed for quantification. The crude extract from the CFS of *Bacillus* sp. JFL21 and *Bacillus* sp. LQG17 was designated as Anti-JFL21 and Anti-LQG17, respectively.

Determination of the Antimicrobial Activity of Anti-JFL21 and Anti-LQG17

Anti-JFL21 and Anti-LQG17 were prepared with methanol at the final concentration of 1 mg/mL and then tested for antimicrobial activity against the thirty-three indicator strains. Besides, the remaining supernatant after the extraction of Anti-JFL21 or Anti-LQG17 were separately readjusted to pH 7, and the antimicrobial experiment was also carried out to verify whether the antimicrobial substances were sufficiently extracted. Antimicrobial activity was measured by implementing the agar disk diffusion assay mentioned above. Meanwhile, the antimicrobial spectrum of Anti-JFL21 and Anti-LQG17 against bacteria and fungi was compared to those of Nisin (1 mg/mL, Sigma) and polymyxin B (1 mg/mL, Sigma). The same amount of sterile water, methanol, and 0.02 mol/L HCl that applied to prepare samples were used as negative controls.

Fourier Transformation Infra-Red (FTIR) Analysis

Fourier transformation infra-red spectroscopy analysis was performed to identify the structural groups of the purified biosurfactant using a Bruker Vertex 70v FTIR spectrometer (Bruker, Germany). In this experiment, 1 mg of Anti-JFL21 was ground with 100 mg of KBr in a pestle and pressed with load for 30 s to obtain translucent pellets. The FTIR spectra were collected at a frequency range from 4000 to 500 cm^{-1} (Sharma et al., 2015).

Reversed-Phase HPLC Analysis

The powder of Anti-JFL21 and Anti-LQG17 was dissolved in an aqueous solution of 40% methanol at 1 mg/mL and filtered using a 0.22 μm pore filter (Millipore, United States). A 20 μL aliquot was injected into an Inertsil ODS-SP C18 column (4.6 mm ID × 25 cm L, 5 μm particle diameter) in the HPLC system (Shimadzu, Japan) to separate and identify the isoforms, according to published methods with some modifications (Yang et al., 2015). In brief, the equal volumes of 1 mg/mL standard surfactin, fengycin and iturin (purity of 90% or greater, Sigma-Aldrich, United States) were fully mixed and used to confirm the RP-HPLC fraction groups of three lipopeptide families. The mobile phases consisted of water (A) and acetonitrile (B), and all of them contained 0.1% trifluoroacetic acid (TFA). The detailed gradient strategy for the acetonitrile-water mobile phase system was as follows: 0–3 min, 45% acetonitrile to 50% acetonitrile; 3–8 min, 50% acetonitrile to 80% acetonitrile; 8–25 min, 80% acetonitrile to 100% acetonitrile; 25–30 min, 100% acetonitrile. The total flow rate of the mobile phases was kept at 0.8 mL/min, and the products were monitored by absorbance at 215 nm. All HPLC solvents were prepared fresh daily and filtered under vacuum before use.

Matrix-Assisted Laser Desorption Ionization – Time of Flight Mass Spectrometry (MALDI-TOF MS) Analysis

Anti-JFL21 was further subjected to MALDI-TOF MS analysis and the methanol solvent was used as a negative control. The experiments were conducted using an ultrafleXtreme™ MALDI-TOF MS instrument (Bruker Daltonics, Germany) equipped with a 337 nm pulsed nitrogen laser. All tested samples (2 μL) were mixed with an equal volume of the matrix (a saturated solution of α-cyano-4-hydroxycinnamic acid in 50% acetonitrile with 0.1% TFA), as described previously (Kim et al., 2010; Piewngam et al., 2018). The sample was spotted onto the gold-coated plate and air-dried. Then the target plate was loaded into an ultrafleXtreme™ MALDI-TOF MS instrument (Bruker Daltonics, Germany). The mass spectrum was analyzed in the range of 500–3500 Da. MALDI-TOF MS/MS coupled with LIFT mode in the same spectrometer was used to analyze the fragment ions of the selected precursor ions for further characterization of the amino acid sequence. Other identification score criteria used were those recommended by the manufacturer.

Isolation and Purification of Different Lipopeptides Family

To clarify which lipopeptide classes were responsible for antibacterial and antifungal activity, the family of iturin, fengycin,

and surfactin were separated through Sephadex LH-20 gel filtration chromatography (GFC) (Kim et al., 2010; Zhang et al., 2013). *L. monocytogenes*, *A. hydrophila*, and *C. gloeosporioides* were used as indicator strains for quantifying antimicrobial effects since they were found to be the most sensitive indicator among Gram-positive pathogens, Gram-negative pathogens, and fungal pathogens, respectively. Briefly, the dried Anti-JFL21 was dissolved in 40% methanol (v/v) and prepared to a final concentration of 15 mg/mL, and filtered through a 0.2 μm membrane. To separate and purify the three lipopeptide family of Anti-JFL21, the filtrate (2 mL) of Anti-JFL21 was applied to a Sephadex LH-20 column (16 mm ID × 100 cm L) and fractionated by size-exclusion chromatography by using 40% methanol as eluent. A total of 100 fractions was collected (3 mL/tube) using a fraction collector (model DBS 100; Shanghai Hu Xi Analysis Instrument Factory Co. Ltd., Shanghai, China), and the flow rate of the eluent was kept at 0.5 mL/min. Then, each fraction was further detected using a UV spectrophotometer at 215 nm and analyzed by RP-HPLC, and tested for the antimicrobial activity.

Determination of the Minimal Inhibitory Concentration of the Fengycins From Different Sources

After separation through GFC, the isolated active fractions containing only fengycin were pooled and dried with a vacuum freeze dryer. To further evaluate and compare the antimicrobial efficacy of fengycins isolated from Anti-JFL21 with the commercial fengycins standard (Sigma-Aldrich, United States), the minimal inhibitory concentration (MIC) was measured according to the agar disk diffusion assay (Sharma et al., 2015). *L. monocytogenes*, *A. hydrophila*, and *C. gloeosporioides* were used as indicator microorganisms, which were typically representative of Gram-positive pathogen, Gram-negative pathogen, and fungal pathogen, respectively. In brief, fengycins and its commercial standard was dissolved in methanol at a final concentration of 0.8 mg/mL and diluted by two-fold dilution to a variety of concentrations. Samples of different concentrations were then used for measuring of the antimicrobial activity against indicator strains and the MIC value was defined as the lowest concentration of samples that inhibits the visible growth of a tested strain after a chosen incubation period. The same amount of methanol was used as negative controls and the experiments were repeated independently three times.

Biochemical Characterization of Fengycins

The powder of fengycins isolated from Anti-JFL21 was then dissolved in sterile phosphate-buffered saline (PBS) at pH 7.0 at a final concentration of 1 mg/mL and used for investigating the effect of temperature, pH, ultraviolet sterilization. The effect of temperature, pH, ultraviolet sterilization, enzymes, and chemical reagents on the antimicrobial activity of anti-JFL21 was evaluated by the agar disk diffusion assay using *L. monocytogenes* as an indicator strain (Sabaté and Audisio, 2013; Chalasani et al., 2015; Lee et al., 2016). The untreated sample was used as positive controls and its activity was defined as 100%. Negative controls were also performed without fengycins to subtract the inhibitory activity of the enzymes and chemical reagents.

In brief, the aliquots of fengycins were separately incubated under ultraviolet sterilization or in a water bath at different temperatures (37, 60, 80, and 100℃) for 2 h, and the residual antimicrobial activity was determined after cooling the treated samples to room temperature. Besides, the effect of pH on fengycins activity was examined over a pH range of 1.0–13.0 by adding 1N NaOH or HCl as appropriate. After incubation in the various pH for 2 h at 25°C, the samples were neutralized to pH 7.0 and its residual activity was measured. To evaluate stability to different enzymes, fengycins were incubated at 37°C for 2 h with 1 mg/mL (final concentration) of the following enzymes (Sigma, United States): cellulase, α-amylase, proteinase K, papain, bromelain, trypsin, and pepsin. The enzymes after incubation were inactivated by heating at 80°C for 10 min and then residual antimicrobial activities were measured. Also, the effects of various chemical reagents (EDTA, SDS, $ZnSO_4$, and $MnCl_2$) on fengycins activity were assayed after preincubating the fengycins with 1 mM (final concentration) of these reagents at 25°C and 100 r/min for 2 h.

Statistical Analysis

The diameters of the zones of inhibition against various indicator strains were expressed as mean values ± SD. All the assays were repeated at least in three separate experiments. The student's *t*-test was utilized to determine the statistically significant difference in the residual anti-*Listeria* activity after the various treatments. The *P*-values of less than 0.05 ($p < 0.05$) were considered significant.

RESULTS

Measurement of Drug Resistance of the Probiotics and Pathogens

To investigate the drug resistance of probiotics and pathogens used in this study, the inhibitory effects of the twelve commonly used antibiotics against thirty-three indicator strains were examined. The negative controls (sterile water, anhydrous ethanol, DMSO, and 0.01 mol/L HCl) did not show any antimicrobial ability against all the indicator strains (data not shown), which suggest that the solvents itself did not affect the antimicrobial activity of the antibiotics against the tested indicator strains. As presented in **Table 1**, all the pathogenic microorganisms used in this study were resistant to several different antibiotics, indicating all of them were multidrug-resistant. In particular, all pathogens except for *C. sakazakii* and *K. pneumoniae* were resistant to at least six antibiotics. Furthermore, conventional antibiotics usually did not have selective antimicrobial effects, and they inhibit the growth of probiotics as well as pathogens. Thus, it is important to develop alternative antibiotics that are less toxic to most probiotics but can inhibit or kill pathogens extensively and potently.

Characterization of *Bacillus* Strains Isolated From Fermented Food and Seafood Products

A phylogenetic tree based on the 16S rDNA sequences of the four *Bacillus* spp. was constructed and shown in **Figure 1**. As can be seen, the strain *Bacillus* sp. JFL21 was assigned in a node with 99.86% of support with *B. amyloliquefaciens* DSM 7, while the strain *Bacillus* sp. LGQ17 was clustered together with the members of other *B. subtilis* groups supported by a sequence similarity of 99.93%. Moreover, *Bacillus* sp. LGQ36 was designated as *B. halotolerans* ATCC 25096 because their 16S rDNA gene sequences were 100% identical.

Comparison of the Antimicrobial Activities of Metabolites From Different *Bacillus* spp.

As presented in **Figures 2**, **3**, the CFS produced by *B. subtilis* LGQ17 and *B. halotolerans* LGQ36 had an obvious inhibitory effect on the majority of indicators except for pathogenic fungi, while the CFS produced by *B. amyloliquefaciens* JFL21 exhibited a marked antimicrobial activity toward the majority of indicators except for probiotics. Among them, the CFS produced by *B. amyloliquefaciens* JFL21 exhibited broader inhibitory spectrum toward pathogens but showed no inhibitory effect on probiotics, and thus has higher application value. However, the CFS produced by *B. subtilis* 168 failed to show any antibacterial or antifungal effect against all indicators, which may be due to its poor capability to produce antimicrobial substances. Based on the antimicrobial spectrum and inhibitory efficacy, the antimicrobial substance produced by *B. amyloliquefaciens* JFL21 and *B. subtilis* LGQ17 were selected for the additional extraction and characterization.

Inhibitory Spectrum of the Bioactive Substance Produced From *B. amyloliquefaciens* JFL21 and *B. subtilis* LGQ17

As showed in **Table 2**, Anti-JFL21 exhibited significant antibacterial and antifungal activity against most indicators while Anti-LQG17 showed a weak antibacterial effect against a few indicators. To further check whether the antimicrobial substances were adequately extracted, the remaining supernatant after the extraction of Anti-JFL21 or Anti-LQG17 were also tested for the antimicrobial activity. The result revealed that the remaining supernatant after the extraction of Anti-LQG17 (CFS-LQG17) still has an obvious antibacterial effect on many indicators, which indicated Anti-LQG17 maybe not the primary

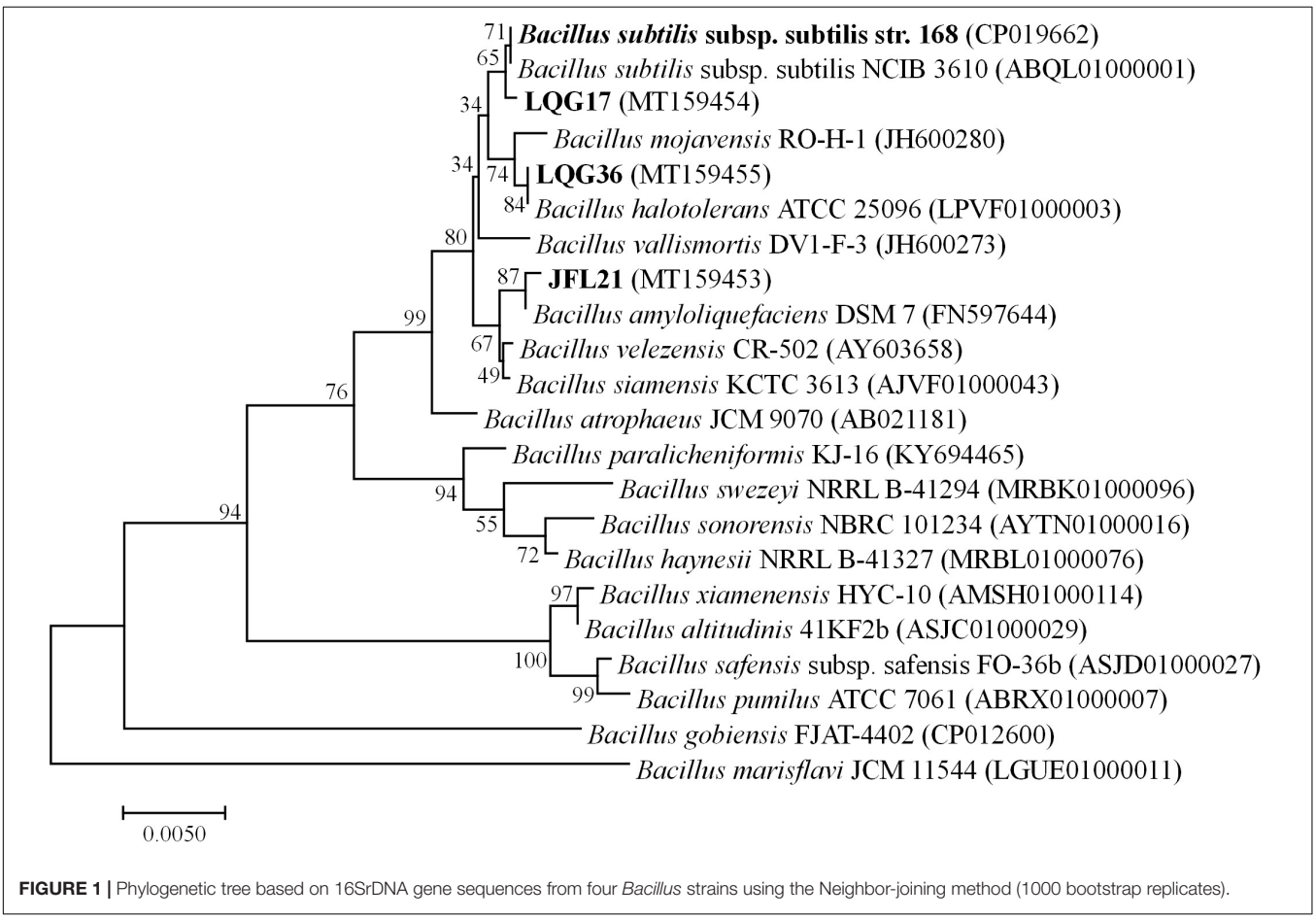

FIGURE 1 | Phylogenetic tree based on 16SrDNA gene sequences from four *Bacillus* strains using the Neighbor-joining method (1000 bootstrap replicates).

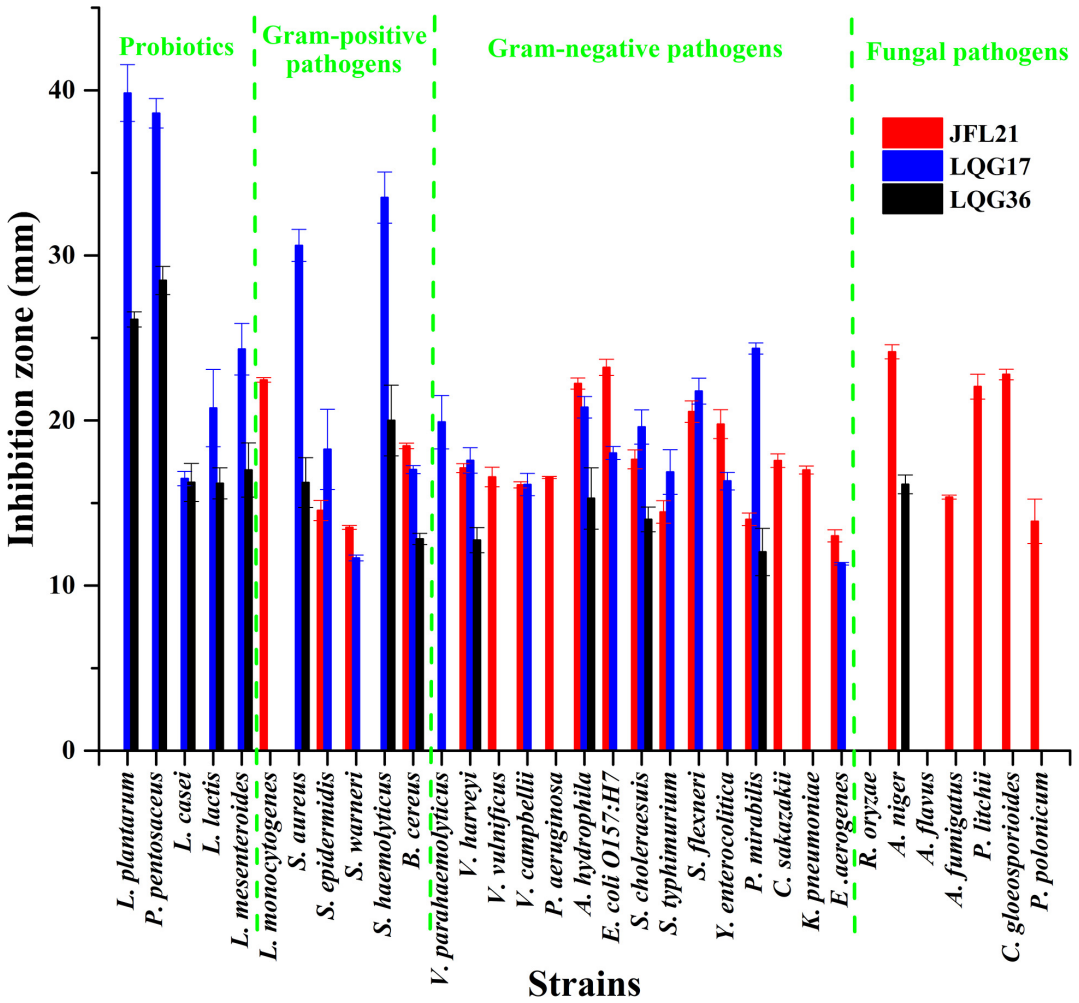

FIGURE 2 | Antimicrobial spectrum of cell-free supernatants from different *Bacillus* strains. JFL21, LQG17, and LQG36 were referred to as the cell-free supernatants produced by *Bacillus amyloliquefaciens* JFL21, *Bacillus natto* LQG17, and *Bacillus halotolerans* LQG36, respectively.

antimicrobial substances produced by *B. subtilis* LGQ17 and the main active ingredients need to be clarified by subsequent experiments. However, the remaining supernatant after the extraction of Anti-JFL21 (CFS- JFL21) did not inhibit the growth of every indicator (data not shown), confirming the antimicrobial substances were sufficiently extracted from the CFS of *B. amyloliquefaciens* JFL21. Additionally, the antimicrobial activity of Anti-JFL21 was also compared with those of commercially available nisin and polymyxin B, which were represented as bacteriocin and lipopeptide, respectively (**Table 2**). As can be observed, Anti-JFL21 not only exhibited unique advantages in inhibiting the growth of a broad range of fungal pathogens but also showed a wider and stronger antibacterial activity toward Gram-positive pathogens when compared with polymyxin B and Nisin. What's more, although Anti-JFL21 also inhibited the growth of some probiotics, the inhibitory activity against probiotics was significantly lower when compared to pathogens. These results suggest that Anti-JFL21 could be expected to a promising alternative source of biological preservatives in the food industry for controlling various multidrug-resistant foodborne pathogens and extending the shelf-life of food products.

Structure Analysis of Crude Lipopeptides by FTIR

Fourier transformation infra-red spectral peaks of Anti-JFL21 were exhibited in **Figure 4**. The broader absorption peak of 3315.36 cm^{-1} indicates the presence of –OH or –NH groups. Peaks at 2926.82 cm^{-1}, 2854.89 cm^{-1}, 1451.67 cm^{-1}, and 1402.66 cm^{-1} confirm the –C–H stretching (−CH3, −CH2) of the aliphatic chain of the lipid. A similar stretching for –C–H of lipid was also found by Pradhan et al. (2013) and Al-Wahaibi et al. (2014). The presence of amide bond (617.81 cm^{-1}), N–H bending of secondary amides (1544.54 cm^{-1}), and the carbonyl group (C = O) of amide (1658.17 cm^{-1}) confirms the peptide fraction in the sample. C–O bending of esters was characterized by the peaks at 1236.79 cm^{-1} and 1068.77 cm^{-1}. The same bending and stretching were reported for peptide groups in the

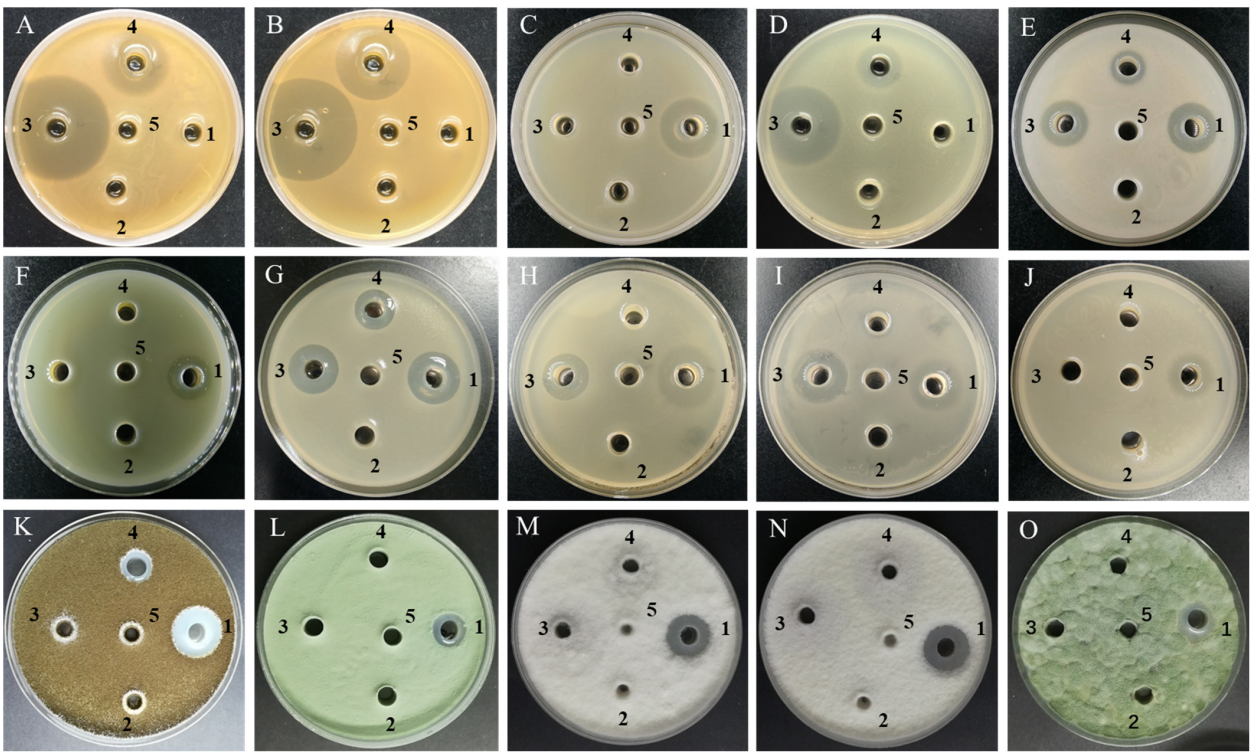

FIGURE 3 | Antimicrobial activity of cell-free supernatants from different *Bacillus* strains against some representative indicator microorganisms. **(A)** *L. plantarum*; **(B)** *L. pentosus*; **(C)** *L. monocytogenes*; **(D)** *S. aureus*; **(E)** *B. cereus*; **(F)** *P. aeruginosa*; **(G)** *A. hydrophila*; **(H)** *E. coli* O157:H7; **(I)** *S. typhimurium*; **(J)** *C. sakazakii*; **(K)** *A. niger*; **(L)** *A. fumigatus*; **(M)** *P. litchii*; **(N)** *C. gloeosporioides*; **(O)** *P. polonicum*; 1–4, the cell-free supernatants produced by *Bacillus amyloliquefaciens* JFL21, *Bacillus subtilis* 168, *Bacillus subtilis* LQG17, and *Bacillus halotolerans* LQG36, respectively; 5, the uninoculated Landy medium.

previous research (Pradhan et al., 2013; Sharma et al., 2015; Varjani and Upasani, 2016). Thus, the nature of the antimicrobial substance produced by *B. amyloliquefaciens* JFL21 was speculated as cyclic lipopeptide compounds.

Lipopeptides Quantification by RP-HPLC Analysis

The reversed-phase HPLC (RP-HPLC) analysis was carried out to characterize the structural properties of Anti-JFL21 and Anti-LGQ17, and the results were presented in **Figure 5**. The peaks at retention time 4.86, 8.37, and 18.81 min maybe methanol solvent or impurity peak (**Figure 5A**). The retention times of iturin, fengycin, and surfactin were identified in the ranges of 6.5–13, 13–18, and 18–27 min, respectively, according to our previous results (**Figure 5B**). For the lipopeptides extract Anti-JFL21, three peaks clusters were observed on the RP-HPLC profile which exhibited similar retention times as the three standard groups (**Figure 5C**). The RP-HPLC profiles of Anti-JFL21 showed the major peaks which corresponded to iturin and fengycin families, while traces of surfactin families were also detected but the content was relatively low. Furthermore, the peaks of the iturin and fengycin families in Anti-JFL21 were relatively more than those of the three standards, which may be due to the more analogs or homologs of three lipopeptide families in Anti-JFL21. Meanwhile, RP-HPLC analysis also revealed that Anti-LGQ17 was mainly composed of four surfactin analogs (**Figure 5D**). These results suggested that different *Bacillus* species could synthesize different CLPs family, and the antimicrobial properties of these CLPs exhibited significant differences.

Identification of the Active Compounds by MALDI-TOF MS

To determine the accurate molecular mass, Anti-JFL21 was further subjected to MALDI-TOF MS analysis. Anti-LGQ17 was not selected for further analysis since it did not show significant antimicrobial activity. As shown in **Figure 5**, the MALDI-TOF MS analysis result of Anti-JFL21 showed two well-resolved groups of peaks at *m/z* values range of 1029.28–1109.59 Da (**Figure 6A**) and 1421.79–1513.88 Da (**Figure 6B**), which could be, respectively, attributed to the isomers of iturin and fengycin, as previously described (Torres et al., 2015; Yang et al., 2015; Sarwar et al., 2018). As can be observed in **Figure 6A**, the protonated molecular ion ($[M + H]^+$) peaks of the iturin A homologs were detected at *m/z* 1029.28, 1043.59, 1057.60, and 1071.62 Da, and the peaks with the differences of 14 Da may correspond to the molecular weight of one CH_2 group. Besides, peaks in the *m/z* of 1065.57, 1079.58, and 1093.60 Da may be assigned as the sodium adducts ($[M + Na]^+$) of C_{14}, C_{15}, and C_{16} homologs of iturin A, and *m/z* = 1109.59 Da could be attributed to the potassium adducts ($[M + K]^+$) for C_{16} iturin. However,

TABLE 2 | Inhibition spectrum of Anti-JFL21 and Anti-LQG17[a].

Indicator strains	Inhibition zone (mm)				
	Anti-JFL21 (1 mg/mL)	Anti-LQG17 (1 mg/mL)	CFS-LQG17 (100 ul)[b]	Polymyxin B (1 mg/mL)	Nisin (1 mg/mL)
Probiotics					
L. plantarum	14.36 ± 1.22	12.46 ± 0.89	29.24 ± 0.87	–	15.07 ± 0.35
P. pentosaceus	–	–	26.12 ± 0.56	–	14.13 ± 0.62
L. casei	13.22 ± 0.67	–	–	–	21.76 ± 0.96
L. lactis	–	–	15.33 ± 2.25	–	17.34 ± 0.74
L. mesenteroides	–	–	20.59 ± 1.37	–	19.51 ± 1.69
G^+ pathogen					
L. monocytogenes	22.96 ± 0.74	–	–	–	–
S. aureus	14.51 ± 1.48	–	25.22 ± 1.14	–	–
S. epidermidis	13.22 ± 0.46	–	14.12 ± 0.57	12.17 ± 0.31	17.15 ± 0.54
S. warneri	12.98 ± 0.51	–	13.02 ± 0.79	14.22 ± 1.04	–
S. haemolyticus	–	–	18.02 ± 0.66	–	–
B. cereus	19.80 ± 0.25	12.99 ± 0.49	14.88 ± 0.42	–	–
G^- pathogen					
V. parahaemolyticus	–	–	21.12 ± 0.85	15.34 ± 1.63	–
V. harveyi	15.65 ± 1.20	–	–	22.45 ± 0.19	–
V. vulnificus	–	–	–	–	–
V. campbellii	14.55 ± 1.67	–	–	16.42 ± 0.47	–
P. aeruginosa	20.25 ± 0.57	–	–	–	–
A. hydrophila	22.72 ± 0.34	11.98 ± 0.73	20.96 ± 0.08	21.13 ± 0.87	–
E. coli O157:H7	21.45 ± 0.96	–	13.08 ± 1.45	15.36 ± 0.95	–
S. choleraesuis	19.65 ± 0.42	–	12.66 ± 0.75	15.74 ± 0.32	–
S. typhimurium	17.94 ± 1.03	–	–	15.89 ± 0.45	–
S. flexneri	15.73 ± 2.86	–	20.02 ± 0.17	15.93 ± 0.22	–
Y. enterocolitica	16.85 ± 2.51	–	–	17.96 ± 2.01	–
P. mirabilis	20.71 ± 0.11	10.02 ± 1.15	17.46 ± 0.32	–	–
C. sakazakii	20.57 ± 0.92	–	–	14.86 ± 1.15	–
K. pneumoniae	17.34 ± 0.34	–	–	17.03 ± 0.84	–
E. aerogenes	16.58 ± 1.54	–	–	14.65 ± 0.73	–
Pathogenic fungi					
R. oryzae	–	–	–	–	–
A. niger	21.76 ± 0.15	–	–	–	–
A. flavus	18.28 ± 0.75	–	–	–	–
A. fumigatus	20.13 ± 0.68	–	–	–	–
P. litchii	16.55 ± 0.91	–	–	–	–
C. gloeosporioides	22.24 ± 0.49	–	–	–	–
P. polonicum	19.21 ± 1.13	–	–	–	–

[a] *–: no inhibition zone;* [b] *CFS-LQG17: the remaining supernatant after the extraction of Anti-LQG17.*

the absence of a typical peak of surfactin (e.g., *m/z* 1008, 1022, 1034, 1046, and 1058) may be due to its low relative content in the sample, which is consistent with the results of RP-HPLC analysis. On the other hand, several fengycin homologs were detected as $[M + H]^+$ at *m/z* 1421.79, 1435.81, 1449.84, 1463.86, 1477.89, and 1491.91 Da (**Figure 6B**), which may correspond to the different fatty acid length. Moreover, the $[M + Na]^+$ and $[M + K]^+$ adducts of fengycin isoforms were also observed at *m/z* 1471.82, 1485.84, 1499.86, and 1513.88 Da (**Figure 6B**). Compared with the groups of fengycin peaks of Anti-JFL21, the commercial fengycin standard was also identified with many of the same ions of $[M + H]^+$, $[M + Na]^+$, and $[M + K]^+$, such as the 1463.81, 1477.84, 1485.80, 1491.85, 1499.81, and 1505.87 Da (**Figure 6C**). In addition, the difference between the ion of 1447.81 Da detected in the commercial fengycin standard and the 1449.84 Da identified in Anti-JFL21 only 2 Da, which may be due to the presence of a double bond in fatty acids chain (Pathak et al., 2012; Sa et al., 2018). The major *m/z* peaks of Anti-JFL21 and the fengycin standard were summarized in the **Table 3**.

Characterization of Fengycin Isoforms by MALDI-TOF MS/MS

In the earlier literature, fengycins have been mainly divided into fengycin A and fengycin B, which are characterized by the existence of Ala and Val residues at position 6 of the peptide ring, respectively (Vanittanakom et al., 1986; Wang et al., 2004). Recently, a new variant of fengycin, termed as fengycin A2 or fengycin B2 with the presence of Val instead of Ile at position 10 was also observed (Pathak et al., 2012; Cochrane and Vederas, 2016). Since many fengycin isoforms may have the same nominal mass and molecular formula, it is difficult for MALDI-TOF

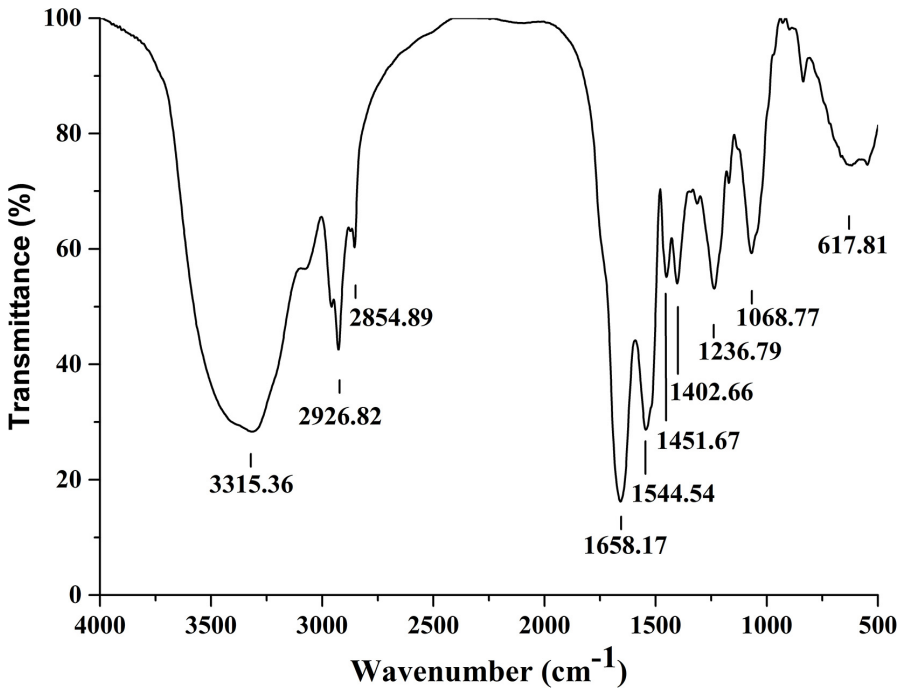

FIGURE 4 | Fourier transformation infra-red spectra analysis of the lipopeptides mixture Anti-JFL21 obtained from *Bacillus amyloliquefaciens* JFL21.

MS to definitely discriminate different fengycin isomers. To obtain more precise amino acid sequence information, the fengycin protonated parent ions ($[M + H]^+$) of Anti-JFL21 together with the commercial fengycin standard were selected for further MALDI-TOF MS/MS analysis. The representative MS/MS spectra of the precursor ion of 1477 Da from Anti-JFL21 compared to the fengycin standard was displayed in **Figure 7**.

In the MS/MS spectrum of the precursor ion of 1477.88 Da (**Figure 7A**), it can be quickly identified as C_{18} fengycin A2 (Ala^6, Val^{10}), C_{17} fengycin A1 (Ala^6, Ile^{10}), C_{15} fengycin B1 (Val^6, Ile^{10}) and C_{16} fengycin B2 (Val^6, Val^{10}) based on the presence of four typical paired product ions of 952 and 1066 Da, 966 and 1080 Da, 980 and 1094 Da, and 994 and 1108 Da, respectively (Wang et al., 2004; Pathak et al., 2012). Similarly, two paired product ions of 966 and 1080 Da, and 994 and 1108 Da were appeared in MS/MS spectrum of the parent ion at *m/z* 1477.84 Da (**Figure 7B**), which enable it to be assigned corresponding to C_{17} fengycin A1 and C_{15} fengycin B1. Unlike Anti-JFL21, the fengycin standard were failed to detect the two paired specific fingerprint ions of 952 and 1066 Da, and 980 and 1094 Da (**Figure 7B** and **Table 3**), which indicated the fengycin standard was only composed of fengycin A1 and fengycin B1. Besides, the product ion of 1378 Da may be resulted from the loss of Val while a series of fragment ions at *m/z* 389 Da, 226 Da, and 115 Da may specifically represented the sequence of Pro-Gln-Tyr, Pro-Gln, and Pro-H_2O, respectively (Yu et al., 2012; Yang et al., 2015). In addition, other fengycin precursor peaks, fingerprint ions, and structural assignments were summarized and showed in **Table 3**.

Isolation and Purification of Lipopeptides

To assess the antimicrobial contribution of individual lipopeptide classes, Anti-JFL21 was subjected to further isolation and purification by GFC. As shown in **Figure 8**, the spectrophotometer analysis at 215 nm indicated the possible presence of lipopeptides in the fractions from 13 to 66, which was also confirmed by RP-HPLC (data not shown). Besides, RP-HPLC results revealed that the fractions in the range of 13–18, 19–42, and 43–72 were mainly identified as single surfactin, fengycin, and iturin families, respectively (**Supplementary Figure 1**). The fractions containing fengycins exhibited the primary antimicrobial activity against *L. monocytogenes*, *A. hydrophila*, and *C. gloeosporioides*, whereas the rest of the fractions comprising only surfactins or iturins did not present any antagonistic effect on the three indicator strains (**Figure 8** and **Supplementary Figure 2**). These results demonstrated that fengycins play a key role in antimicrobial activity.

Comparison of Minimal Inhibitory Concentration of the Fengycins Isolated From Anti-JLF21 and the Commercial Fengycins Standard

To compare the antimicrobial efficacy of the fengycins isolated from Anti-JFL21 with the commercial fengycins standard, their MIC was determined and compared using *L. monocytogenes*, *A. hydrophila*, and *C. gloeosporioides* as the indicator strains (**Table 4**). The result showed that the fengycins isolated from Anti-JFL21 could display the antimicrobial effect toward *L. monocytogenes*, *A. hydrophila*, and *C. gloeosporioides* at a low

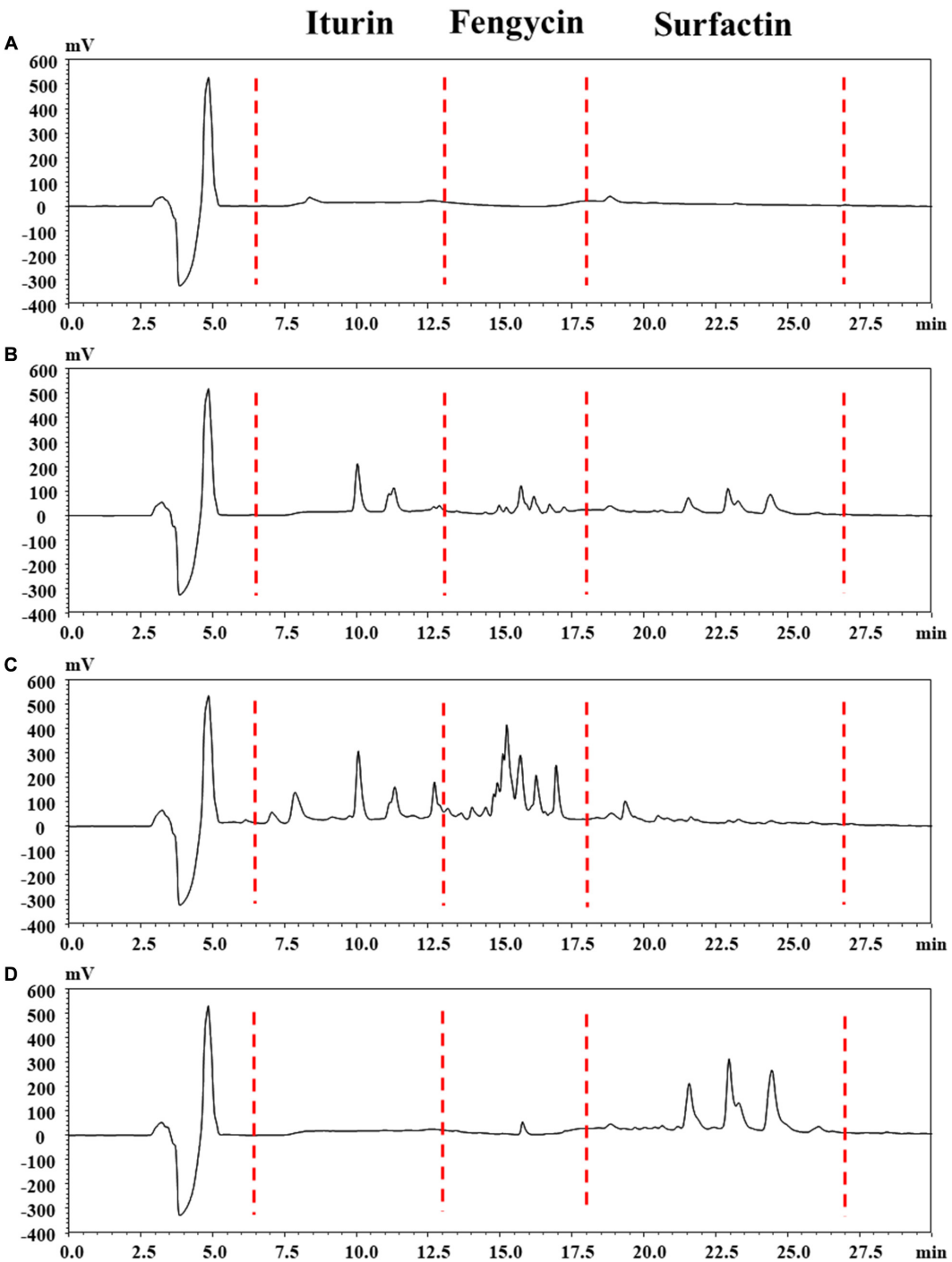

FIGURE 5 | Reversed phase HPLC chromatogram analysis of the lipopeptides mixture Anti-JFL21 and Anti-LQG17. **(A)** methyl alcohol; **(B)** complexes with final concentrations of 0.33 mg/mL of commercial standard iturin, fenycin, and surfactin; **(C)** 1 mg/mL Anti-JFL21 obtained from *Bacillus amyloliquefaciens* JFL21; **(D)** 1 mg/mL Anti-LQG17 obtained from *Bacillus natto* LQG17.

MIC range of 25–50 ug/mL. Besides, the commercial fengycins standard was found to active against *C. gloeosporioides* at low MIC concentration (25 ug/mL) but fail to inhibit the growth of *L. monocytogenes* and *A. hydrophila* even at the highest tested concentration (800 μg/ml). These results suggest that the fengycins isolated from Anti-JFL21 are more efficient in inhibiting pathogenic bacteria as compared to the commercial fengycins standard, which may be contributed to the greater variety of structural analogs, especially in the variation at position 10 (Val/Ile) (**Table 3**).

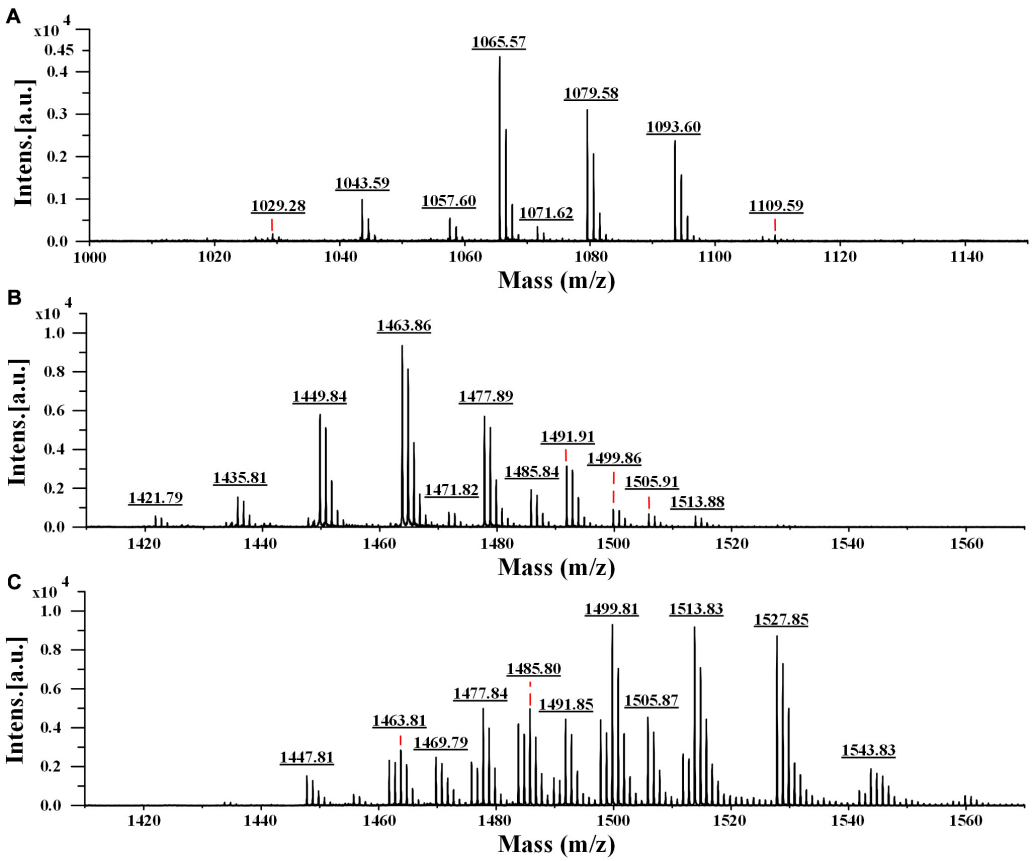

FIGURE 6 | MALDI-TOF MS analysis of the lipopeptides mixture Anti-JFL21 and the commercial fengycin standard. **(A)** the peaks of Anti-JFL21 in the range of *m/z* = 1000–1150 Da; **(B)** the peaks of Anti-JFL21 in the range of *m/z* = 1410–1570 Da; **(C)** the peaks of the commercial fengycin standard in the range of *m/z* = 1410–1570 Da.

Biochemical Characterization of Fengycins

To evaluate the possible application in the food industry, the antimicrobial stability of fengycins produced by *B. amyloliquefaciens* JFL21 under various conditions was determined. *L. monocytogenes*, an important foodborne pathogen was used as an indicator strain. As shown in **Table 5**, the fengycins did not show loss of its inhibitory activity against *L. monocytogenes* after the treatment for 2 h under the ultraviolet sterilization, over a pH range of 5.0 to 9.0, or at temperatures below 80℃. Although there was a very significant reduction in the activity after incubation for 2 h at 100℃, pH 1.0, and pH 13.0, the residual activity remained 90, 85, and 72%, respectively. Thus, our results indicate that the fengycins were resistant to the various harsh conditions and the sterilization process such as commercial pasteurization and ultraviolet sterilization, and thus can be used as a natural preservative in the food industry.

DISCUSSION

The increased emergence and evolution of multiple drug-resistant foodborne pathogens in recent decades has become a worldwide vexing problem of public concern. In this work, antibiotics susceptibility test results indicated that all foodborne pathogens used in the current study were multidrug-resistant according to the recent drug-resistance definition (**Table 1**; Magiorakos et al., 2012). Likewise, Lee et al. (2017) disclosed that 27 (82%) of 33 *L. monocytogenes* isolates collected from ready-to-eat seafood and food processing environments were resistant to at least four antibiotics. Besides, a high proportion of multidrug-resistant isolates from food was also commonly reported in other foodborne pathogens such as *Y. enterocolitica* (66/70, 94.3%) (Ye et al., 2015), *Salmonella* (30/42, 71.4%) (Tirziu et al., 2015), and *S. aureus* (62/93, 66.67%) (Ma et al., 2018). Thus, the development of new antimicrobial agents or other alternative strategies is required promptly.

Bacillus is an important genus producing a wide array of bioactive secondary metabolites, including lipopeptides, polyketides, lantibiotics, siderophores, lytic enzymes, and peptides (Cawoy et al., 2015; Dimkić et al., 2017). Moreover, the majority of *Bacillus* spp. such as *B. subtilis*, *B. amyloliquefaciens*, and *B. licheniformis* have been generally recognized as safe microorganisms for application in the food industry and considered to be important biological control agents (Torres et al., 2015; Lastochkina et al., 2019). In this study, three *Bacillus*

TABLE 3 | Possible assignments of major *m/z* peaks of Anti-JFL21 and the commercial fengycin standard[a].

Samples	Detected precursor ions (*m/z*)			Two fingerprint ions (*m/z*)	Possible assignment[b]	Amino acid at position 6 and 10
	$[M + H]^+$	$[M + Na]^+$	$[M + K]^+$			
Anti-JFL21	1029.28	–	–	/	C_{13} iturin A	/
	1043.59	1065.57	–	/	C_{14} iturin A	/
	1057.60	1079.58	–	/	C_{15} iturin A	/
	1071.62	1093.60	1109.59	/	C_{16} iturin A	/
	1421.79	–	–	952.25, 1066.42	C_{14} fengycin A2	Ala^6, Val^{10}
	1435.81	–	–	952.35, 1066.44 966.37, 1080.48	C_{15} fengycin A2 C_{14} fengycin A1	Ala^6, Val^{10} Ala^6, Ile^{10}
	1449.84	1471.82	–	952.30, 1066.41 966.31, 1080.40 980.34, 1094.45	C_{16} fengycin A2 C_{15} fengycin A1 C_{14} fengycin B2	Ala^6, Val^{10} Ala^6, Ile^{10} Val^6, Val^{10}
	1463.86	1485.84	–	952.32, 1066.44 966.35, 1080.46	C_{17} fengycin A2 C_{16} fengycin A1	Ala^6, Val^{10} Ala^6, Ile^{10}
	1477.89	1499.86	–	952.43, 1066.50 966.37, 1080.48 980.39, 1094.51 994.39, 1108.52	C_{18} fengycin A2 C_{17} fengycin A1 C_{16} fengycin B2 C_{15} fengycin B1	Ala^6, Val^{10} Ala^6, Ile^{10} Val^6, Val^{10} Val^6, Ile^{10}
	1491.91	1513.88	–	952.26, 1066.18 966.19, 1080.16 980.20, 1094.20 994.35, 1108.50	C_{19} fengycin A2 C_{18} fengycin A1 C_{17} fengycin B2 C_{16} fengycin B1	Ala^6, Val^{10} Ala^6, Ile^{10} Val^6, Val^{10} Val^6, Ile^{10}
	1505.91	–	–	980.39, 1094.47 994.42, 1108.53	C_{18} fengycin B2 C_{17} fengycin B1	Val^6, Val^{10} Val^6, Ile^{10}
fengycin standard	1447.81	1469.79	–	966.45, 1080.55 994.47, 1108.55	*C_{15} fengycin A1 *C_{13} fengycin B1	Ala^6, Ile^{10} Val^6, Ile^{10}
	1463.81	1485.80	–	966.37, 1080.46 994.38, 1108.48	C_{16} fengycin A1 C_{14} fengycin B1	Ala^6, Ile^{10} Val^6, Ile^{10}
	1477.84	1499.81	–	966.39, 1080.47 994.40, 1108.49	C_{17} fengycin A1 C_{15} fengycin B1	Ala^6, Ile^{10} Val^6, Ile^{10}
	1491.85	1513.83	–	966.34, 1080.45 994.33, 1108.44	C_{18} fengycin A1 C_{16} fengycin B1	Ala^6, Ile^{10} Val^6, Ile^{10}
	1505.87	1527.85	1543.83	994.34, 1108.46	C_{17} fengycin B1	Val^6, Ile^{10}

[a] *–, no detected; /, not tested or studied; *, indicates one double bond in the fatty acid chain.* [b] *Possible assignments based on Pathak et al. (2012), Torres et al. (2015); Yang et al. (2015), and Sarwar et al. (2018).*

isolates from various food sources, namely *B. amyloliquefaciens* JFL21, *B. subtilis* LQG17, and *B. halotolerans* LQG36 were obtained and their antimicrobial properties were compared. Results revealed that the CFS produced by these *Bacillus* strains exhibited different inhibitory spectrum or inhibitory efficacy against the thirty-three indicators (**Figures 2**, **3**), which suggested that different *Bacillus* species or isolates may be capable of producing different kinds or amounts of bioactive metabolites. Hence, screening and characterization of the *Bacillus* spp. with remarkable biological properties still receives a great scientific interest due to the application potential of these strains and their active metabolites (Li et al., 2015).

In recent years, CLPs have received considerable attention because of their efficient biosurfactant and antimicrobial properties (Perez et al., 2017; Sarwar et al., 2018). In this work, the lipopeptides mixture Anti-JFL21 not only exhibited strong antimicrobial activities against the majority of multidrug-resistant foodborne pathogens but also showed relatively low toxicity to most probiotics (**Figures 2**, **3**). This may be since all probiotics used in this study belongs to lactic acid bacteria (LAB), and Anti-JFL21 have a relatively weak inhibitory effect on LAB. The similar phenomenon was also observed by Lee et al. (2016), who reported that the lipopeptides mixture containing four surfactin and four bacillomycin D analogs, inhibited the growth of many Gram-positive pathogens (e.g., *B. cereus* and *L. monocytogenes*) and fungal pathogen (e.g., *A. nidulans* and *F. moniliforme*), but it did not inhibit LAB such as *L. plantarum* and *L. lactis*. Moreover, Todorov et al. (2018) also found that *L. plantarum* has a natural high resistance to a glycopeptide antibiotic when compared to *L. monocytogenes*, which was attributed to the presence of D-Ala-D-Lactate in its peptidoglycan rather than in the D-Ala-D-Ala dipeptide. Thus, it is speculated that the weak inhibitory effect of lipopeptides Anti-JFL21 on LAB may be due to the difference of cell wall composition between LAB and other indicator bacteria. However, the specific mechanism of the relatively weak bacteriostatic effect of CLPs on LAB still needs to be further explored.

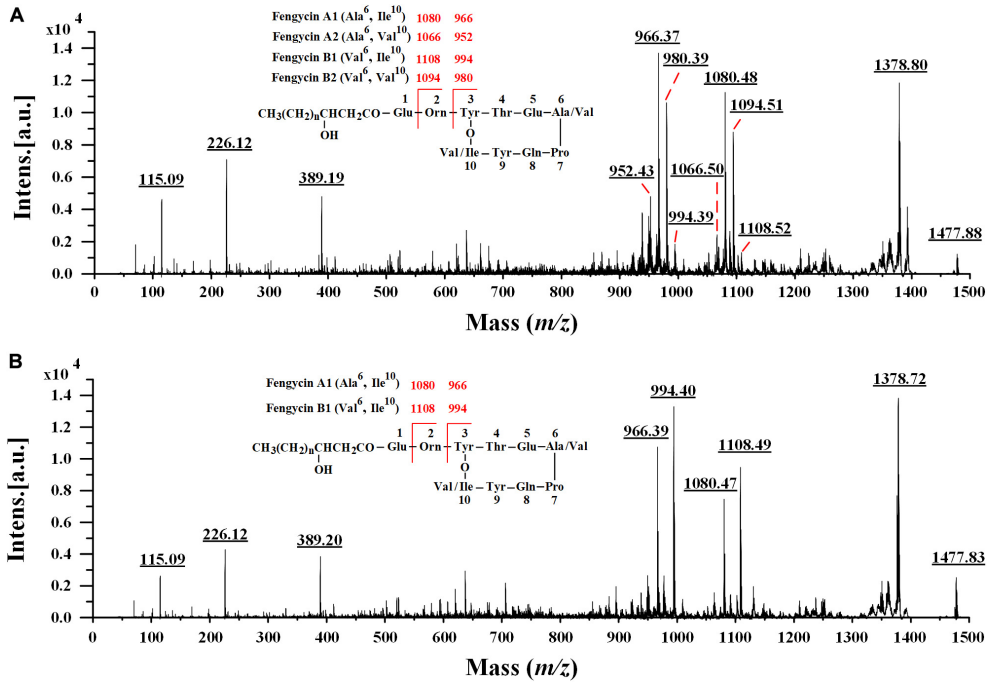

FIGURE 7 | Comparison of MALDI-TOF MS/MS spectra of the lipopeptides mixture Anti-JFL21 and the commercial fengycin standard. MS/MS spectra of the precursor ion of 1477.88 Da from Anti-JFL21 **(A)** compared to the precursor ion of 1477.84 Da from the commercial fengycin standard **(B)**.

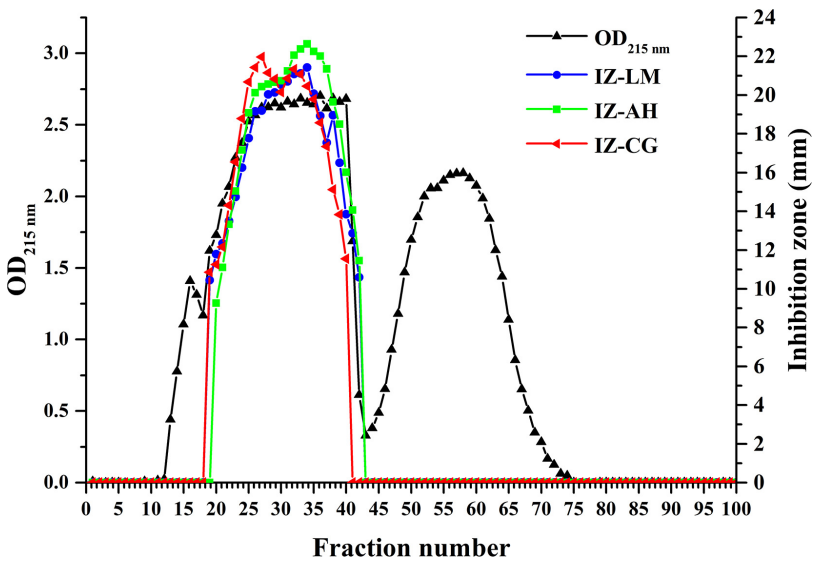

FIGURE 8 | Gel filtration chromatography and antimicrobial activity of the different fractions separated from the lipopeptides mixture Anti-JFL21 produced by *Bacillus amyloliquefaciens* JFL21. IZ-LM, IZ-AH, and IZ-CG were referred to as the inhibition zone of the different fractions separated from Anti-JFL21 against *L. monocytogenes*, *A. hydrophila*, and *C. gloeosporioides*, respectively.

Historically, the elucidation of specific effective antimicrobial components is crucial to the accuracy of the drug application or antiseptic addition. In this research, the family of surfactin, fengycin, and iturin were successfully separated by GFC, and the results of the antimicrobial test demonstrated that fengycins might play a major role in the antibacterial and antifungal activity of Anti-JFL21 (**Figure 8** and **Supplementary Figures 1,2**). To our knowledge, this study is the first report that fengycin is a primary active compound of *B. amyloliquefaciens* against a broad range of foodborne pathogens including Gram-positive pathogens, Gram-negative pathogens, and fungal pathogens. However, unlike some previous studies, which displayed that

TABLE 4 | Minimum inhibitory concentration of different fengycin sources against some representative indicator strains.

Indicator strains	MIC (ug/ml)	
	Fengycins isolated from Anti-JFL21	The commercial Fengycins standard
L. monocytogenes	25	>800
A. hydrophila	50	>800
C. gloeosporioides	25	25

TABLE 5 | Effect of enzymes, chemical reagents, and physical factors on fengycins anti-*Listeria* activity[a].

Factors	Treatment for 2 h	Relative activity (%)[a]
Control	Untreated	100
pH	1	85 ± 3.8**
	3	93 ± 2.6*
	5	99 ± 1.1
	7	102 ± 1.6
	9	101 ± 0.7
	11	88 ± 3.2**
	13	72 ± 5.9**
Heat	37°C	99 ± 1.9
	60°C	100 ± 0.5
	80°C	97 ± 1.5
	100°C	90 ± 4.3*
Light	Ultraviolet	101 ± 0.3
Enzymes (1 mg/mL)	Cellulase	104 ± 2.6
	α-Amylase	99 ± 1.4
	Proteinase K	98 ± 0.5
	Papain	100 ± 2.7
	Bromelain	101 ± 1.0
	Trypsin	100 ± 0.2
	Pepsin	98 ± 5.3
Chemical reagents (1 mM)	EDTA	102 ± 2.4
	SDS	97 ± 1.8
	$MnCl_2$	100 ± 1.1
	$ZnSO_4$	92 ± 6.4

[a] *The relative antimicrobial activity was measured by using L. monocytogenes as an indicator strain. Values are given as mean ± SD from triplicate determinations (n = 3). The value represents the mean ± SE of triple determinations. *p < 0.05, **p < 0.01.*

surfactin and iturin presented important antibacterial and antifungal activity, respectively (Loiseau et al., 2015; Narendra Kumar et al., 2017; Sudarmono et al., 2019). Surfactins produced by *B. subtilis* LQG17 showed a weak antibacterial effect against few bacterial indicators, and surfactins and iturins produced by *B. amyloliquefaciens* JFL21 were not able to inhibit either bacteria or fungi. This may be due to the production and structural diversity of each lipopeptide family are influenced by the various *Bacillus* species or isolates (Sabaté and Audisio, 2013; Fan et al., 2017; Sudarmono et al., 2019), and the effective isoforms of surfactin and iturin synthesized by *B. subtilis* LQG17 or *B. amyloliquefaciens* JFL21 was few or not enough to reach the antimicrobial concentration. This phenomenon was also found by Sabaté and Audisio (2013), who reported that the surfactin produced by *B. subtilis* C4 inhibited the *L. monocytogenes* with a concentration of 0.125 mg/mL while 1 mg/mL of the surfactin produced by *B. subtilis* M1 was necessary to inhibit the pathogen.

Indeed, it is well known that different isoforms and homologs of the lipopeptide family could exhibit different properties and activities, which depend in particular on the chain length (Ben Ayed et al., 2014). In this work, RP-HPLC and MALDI-TOF MS analysis also revealed that each lipopeptide family produced by *B. amyloliquefaciens* JFL21 was composed of different isoforms and fengycins exhibited variation in the length of the β-hydroxy-fatty acid from 14 to 19 carbons units (**Figure 6B** and **Table 3**). Our results are consistent with previous works reported by Jemil et al. (2017) and Perez et al. (2017) that showed the co-production of different homologous compounds of each lipopeptide family. However, the quantity of fengycin isoforms may be different in the various *Bacillus* species or isolates. For example, *B. subtilis* N6–34 could produce multiple fengycin homologs with chain lengths from C_{15} to C_{17} whereas *B. amyloliquefaciens* S13-3 only synthesize C_{16} fengycin variant (Yamamoto et al., 2015; Sa et al., 2018).

Except for the difference of the fatty acid chain length, fengycin isoforms also vary in the lactone rings of amino acid composition. According the previous literature, the variations at position 6 (Ala/Val), and variations at position 10 (Val/Ile) were mostly observed (Pathak et al., 2012; Cochrane and Vederas, 2016). Since the precursor ions mainly cleaved at the Glu–Orn and Orn–Tyr bonds, resulting in the specific octapeptide ring ions at *m/z* 952 and 1066 Da, 966 and 1080 Da, 980 and 1094 Da, and 994 and 1108 Da, respectively (Wang et al., 2004; Pathak et al., 2012; Yang et al., 2015; Sa et al., 2018). Moreover, the extra stability of the charged octapeptide ring system suppressed further fragmentation along the peptide backbone, and thus these specific product ions have been used as diagnostics for identifying fengycin variants with the amino acids replacement within the macrocyclic moiety (Pathak et al., 2012). Based on these specific product ions, the fengycin identified in the lipopeptides mixture Anti-JFL21 was readily assigned as four fenycin variants (fengycin A1, A2, B1, and B2) with chain lengths from C_{13} to C_{19}, whereas the commercial fengycin standard was determined as two fenycin variants (fengycin A1 and B1) with lengths from C_{13} to C_{18}. In addition, the MALDI-TOF MS/MS analysis revealed that a precursor ion of fengycin could be simultaneously identified as multiple fengycin variants, which indicated that it is a mixture of structural analogs and the further component purification are still required to obtain the mono variant or isoform.

Previously, fengycin was mainly characterized by strong antifungal activities against a wide range of plant pathogens, especially filamentous fungi (Guo et al., 2014; Fan et al., 2017; Zihalirwa Kulimushi et al., 2017). Nevertheless, it is particularly noteworthy that the fengycin produced by *B. amyloliquefaciens* JFL21 not only exhibited a remarkable antifungal activity comparable to the commercial fengycin standard but also showed stronger antibacterial efficacy against Gram-positive and Gram-negative foodborne pathogen as compared to the commercial fengycin standard (**Table 4**). This may be due to the commercial fengycin standard only contained two fengycin variants with the variations at position 6 (Ala/Val), whereas the fengycin identified in the present study was composed of four fengycin variants with the variations not only at position 6 (Ala/Val) but also at position 10 (Val/Ile) (**Table 3**). In addition, the various content

combinations of homologs or isoforms may also lead to the different antimicrobial properties (Sabaté and Audisio, 2013; Kaur et al., 2017; Sa et al., 2018). However, to better clarify the structure-function relationships, the separation, characterization, and antimicrobial test of specific fengycin variants or isoforms are still highly necessary in the future study.

In general, an antimicrobial substance in a food item is by itself not likely to ensure complete safety, and therefore often used in combination with either other antimicrobial compounds, chemical reagents, or technologies such as ultraviolet sterilization, heat, and various pH pressure (Zacharof and Lovitt, 2012; Lee et al., 2016). The current study shows that the fengycins produced by *B. amyloliquefaciens* JFL21 not only maintained anti-*Listeria* activity over a broad pH and temperature range, but it was also active after treatment with ultraviolet sterilization, chemical reagents, and proteolytic enzymes (**Table 5**). The similar properties of highly thermostable and resistant to many proteolytic enzymes and a broad range of pH were also found in other *Bacillus*-derived antimicrobial CLPs such as surfactin (Sabaté and Audisio, 2013) and a lipopeptide mixture (Ben Ayed et al., 2014).

To date, the active mechanism of fengycins is less well known compared with iturins and surfactins. The possible mechanism for the antifungal activity of fengycins is that they interact with sterol and phospholipid molecules in membranes and thus alter the structure and permeability of the fungal cell membrane (Farzand et al., 2019; Hanif et al., 2019). However, the mechanism of interaction may vary and depend on the structural features of fengycins and pathogen species (Kaur et al., 2017; Sarwar et al., 2018). Recently, Piewngam et al. (2018) firstly revealed that β-OH-C_{17} fengycin B could potentially be used as quorum-sensing blockers to combat antibiotic-resistant *S. aureus*, which laid the foundation for probiotic *Bacillus* to comprehensively eradicate intestinal *S. aureus* colonization. Consequently, extensive studies are still required for fully understanding and characterizing the exact antimicrobial role of fengycins toward individual foodborne pathogen.

CONCLUSION

In this study, three *Bacillus* strains with excellent antimicrobial properties named JFL21, LQG17, and LQG36, were isolated from food or seafood sources and identified closely related to the species of *B. amyloliquefaciens*, *B. subtilis*, and *B. halotolerans*, respectively. Besides, the model organism *B. subtilis* 168 was also exploited to compare the antimicrobial properties with the three *Bacillus* strains. The results showed that the capacity to produce antimicrobial substances varied greatly among different *Bacillus* species or isolates. Among them, the antimicrobial substances produced by *B. amyloliquefaciens* JFL21 was low toxicity to most probiotics but exhibited strong and extensive antimicrobial activities against multidrug-resistant foodborne pathogens, and thus have more application potential. Subsequently, the FITR, HPLC, and MALDI-TOF MS analysis revealed that the partially purified antimicrobial compounds, Anti-JFL21, was composed of multiple lipopeptides of the surfactin, fengycin, and iturin families. After the separation of different lipopeptide classes, the result of this work demonstrated that fengycins not only play a critical role in antimicrobial activity but also remain highly stable against a variety of enzymes, chemical reagents, and extreme conditions. To the best of our knowledge, this study is the first report that fengycin is a primary active compound of *B. amyloliquefaciens* against a broad range of foodborne pathogenic microorganisms including Gram-positive pathogens, Gram-negative pathogens, and fungal pathogens.

DATA AVAILABILITY STATEMENT

The original contributions presented in the study are included in the article/**Supplementary Material**, further inquiries can be directed to the corresponding author/s.

AUTHOR CONTRIBUTIONS

L-ZL, L-QG, and J-FL conceived and designed this experiment. L-ZL performed data analysis and was a major contributor in drafting the work. Q-WZ and TW helped revise the manuscript critically. L-ZL and Q-WZ carried out the antimicrobial experiment. L-ZL and Z-QZ performed the purification, characterization, and comparison of the antimicrobial metabolites from different *Bacillus*. HZ and C-FZ performed the isolation and purification of lipopeptides. TW and Q-YX performed the biochemical characterization of fengycin. All authors reviewed and approved the submitted manuscript to be published.

FUNDING

This study was funded by the National Natural Science Foundation of China (Grant number 31901693), the Key-Area Research and Development Program of Guangdong Province (Grant numbers 2018B020205003, 2018B020205001, and 2020B020226006), and Guangdong Basic and Applied Basic Research Foundation (Grant number 2020A1515010756).

SUPPLEMENTARY MATERIAL

The Supplementary Material for this article can be found online at: https://www.frontiersin.org/articles/10.3389/fmicb.2020.579621/full#supplementary-material

Supplementary Figure 1 | Reversed-phase HPLC analysis of the different fractions separated from the lipopeptides mixture Anti-JFL21. **(A)** fraction 16; **(B)** fraction 30; **(C)** fraction 55.

Supplementary Figure 2 | Antimicrobial activity of different lipopeptide components separated from the lipopeptides mixture Anti-JFL21 by Sephadex LH-20 gel column chromatography. **(A–C)** *L. monocytogenes*; **(D–F)** *A. hydrophila*; **(G–I)** *C. gloeosporioides*; CK, 1 mg/mL Anti-JFL21; 13–18, the fractions from 11 to 18; 25–30, the fractions from 25 to 30; 55–60, the fractions from 55 to 60.

REFERENCES

Al-Wahaibi, Y., Joshi, S., Al-Bahry, S., Elshafie, A., Al-Bemani, A., and Shibulal, B. (2014). Biosurfactant production by *Bacillus subtilis* B30 and its application in enhancing oil recovery. *Colloids Surf. B Biointerfaces* 114, 324–333. doi: 10.1016/j.colsurfb.2013.09.022

Banat, I. M., Franzetti, A., Gandolfi, I., Bestetti, G., Martinotti, M. G., Fracchia, L., et al. (2010). Microbial biosurfactants production, applications and future potential. *Appl. Microbiol. Biotechnol.* 87, 427–444. doi: 10.1007/s00253-010-2589-0

Ben Ayed, H., Hmidet, N., Béchet, M., Chollet, M., Chataigné, G., Leclère, V., et al. (2014). Identification and biochemical characteristics of lipopeptides from *Bacillus mojavensis* A21. *Process Biochem.* 49, 1699–1707. doi: 10.1016/j.procbio.2014.07.001

Ben Ayed, H., Hmidet, N., Béchet, M., Jacques, P., and Nasri, M. (2017). Identification and natural functions of cyclic lipopeptides from *Bacillus amyloliquefaciens* An6. *Eng. Life Sci.* 17, 536–544. doi: 10.1002/elsc.201600050

Cawoy, H., Debois, D., Franzil, L., De Pauw, E., Thonart, P., and Ongena, M. (2015). Lipopeptides as main ingredients for inhibition of fungal phytopathogens by *Bacillus subtilis/amyloliquefaciens*. *Microb. Biotechnol.* 8, 281–295. doi: 10.1111/1751-7915.12238

Chalasani, A. G., Gunaseelan, D., Sushma, N., Ramkrishna, S., and Utpal, R. (2015). An antimicrobial metabolite from *Bacillus* sp.: significant activity against pathogenic bacteria including multidrug-resistant clinical strains. *Front. Microbiol.* 6:1335. doi: 10.3389/fmicb.2015.01335

Chi, Z., Rong, Y. J., Li, Y., Tang, M. J., and Chi, Z. M. (2015). Biosurfactins production by *Bacillus amyloliquefaciens* R3 and their antibacterial activity against multi-drug resistant pathogenic *E. coli*. *Bioprocess Biosyst. Eng.* 38, 853–861. doi: 10.1007/s00449-014-1328-9

Cochrane, S. A., and Vederas, J. C. (2016). Lipopeptides from *Bacillus* and *Paenibacillus* spp.: a gold mine of antibiotic candidates. *Med. Res. Rev.* 36, 4–31. doi: 10.1002/med.21321

Dimkić, I., Stanković, S., Nišavić, M., Petković, M., Ristivojević, P., Fira, D., et al. (2017). The profile and antimicrobial activity of *Bacillus* lipopeptide extracts of five potential biocontrol strains. *Front. Microbiol.* 8:925. doi: 10.3389/fmicb.2017.00925

European Food Safety Authority (2018). The European Union summary report on trends and sources of zoonoses, zoonotic agents and food-borne outbreaks in 2017. *EFSA J.* 16, 1–262. doi: 10.2903/j.efsa.2018.5500

Fan, H. Y., Ru, J. J., Zhang, Y. Y., Wang, Q., and Li, Y. (2017). Fengycin produced by *Bacillus subtilis* 9407 plays a major role in the biocontrol of apple ring rot disease. *Microbiol. Res.* 199, 89–97. doi: 10.1016/j.micres.2017.03.004

Farzand, A., Moosa, A., Zubair, M., Khan, R. A., Massawe, C. V., Tahir, A. H., et al. (2019). Suppression of *Sclerotinia sclerotiorum* by the induction of systemic resistance and regulation of antioxidant pathways in tomato using fengycin produced by *Bacillus amyloliquefaciens* FZB42. *Biomolecules* 9:613. doi: 10.3390/biom9100613

Garedew, L., Hagos, Z., Addis, Z., Tesfaye, R., and Zegeye, B. (2015). Prevalence and antimicrobial susceptibility patterns of *Salmonella* isolates in association with hygienic status from butcher shops in Gondar town, Ethiopia. *Antimicrob. Resist. Infect. Control* 4:21. doi: 10.1186/s13756-015-0062-7

Guo, Q. G., Dong, W. X., Li, S. Z., Lu, X. Y., Wang, P. P., Zhang, X. Y., et al. (2014). Fengycin produced by *Bacillus subtilis* NCD-2 plays a major role in biocontrol of cotton seedling damping-off disease. *Microbiol. Res.* 169, 533–540. doi: 10.1016/j.micres.2013.12.001

Hanif, A., Zhang, F., Li, P. P., Li, C. C., Xu, Y. J., Zubair, M., et al. (2019). Fengycin produced by *Bacillus amyloliquefaciens* FZB42 inhibits *Fusarium graminearum* growth and mycotoxins biosynthesis. *Toxins* 11:295. doi: 10.3390/toxins11050295

Jemil, N., Manresa, A., Rabanal, F., Ben Ayed, H., Hmidet, N., and Nasri, M. (2017). Structural characterization and identification of cyclic lipopeptides produced by *Bacillus methylotrophicus* DCS1 strain. *J. Chromatogr. B* 1060, 374–386. doi: 10.1016/j.jchromb.2017.06.013

Kaur, P. K., Joshi, N., Singh, I. P., and Saini, H. S. (2017). Identification of cyclic lipopeptides produced by *Bacillus vallismortis* R2 and their antifungal activity against *Alternaria alternata*. *J. Appl. Microbiol.* 122, 139–152. doi: 10.1111/jam.13303

Kim, P. I., Ryu, J., Kim, Y. H., and Chi, Y. T. (2010). Production of biosurfactant lipopeptides Iturin A, fengycin and surfactin A from *Bacillus subtilis* CMB32 for control of *Colletotrichum gloeosporioides*. *J. Microbiol. Biotechnol.* 20, 138–145. doi: 10.4014/jmb.0905.05007

Kuch, A., Goc, A., Belkiewicz, K., Filipello, V., Ronkiewicz, P., Gołębiewska, A., et al. (2018). Molecular diversity and antimicrobial susceptibility of *Listeria monocytogenes* isolates from invasive infections in Poland (1997–2013). *Sci. Rep.* 8:14562. doi: 10.1038/s41598-018-32574-0

Lastochkina, O., Seifikalhor, M., Aliniaeifard, S., Baymiev, A., Pusenkova, L., Garipova, S., et al. (2019). *Bacillus* spp.: efficient biotic strategy to control postharvest diseases of fruits and vegetables. Plants 8:97. doi: 10.3390/plants8040097

Lee, D. Y., Ha, J. H., Lee, M. K., and Cho, Y. S. (2017). Antimicrobial susceptibility and serotyping of *Listeria monocytogenes* isolated from ready-to-eat seafood and food processing environments in Korea. *Food Sci. Biotechnol.* 26, 287–291. doi: 10.1007/s10068-017-0038-x

Lee, M. H., Lee, J., Nam, Y. D., Lee, J. S., Seo, M. J., and Yi, S. H. (2016). Characterization of antimicrobial lipopeptides produced by *Bacillus* sp. LM7 isolated from chungkookjang, a Korean traditional fermented soybean food. *Int. J. Food Microbiol.* 221, 12–18. doi: 10.1016/j.ijfoodmicro.2015.12.010

Li, X., Yang, H., Zhang, D. L., Li, X., Yu, H. M., and Shen, Z. Y. (2015). Overexpression of specific proton motive force-dependent transporters facilitate the export of surfactin in *Bacillus subtilis*. *J. Ind. Microbiol. Biotechnol.* 42:93. doi: 10.1007/s10295-014-1527-z

Loiseau, C., Schlusselhuber, M., Bigot, R., Bertaux, J., Berjeaud, J. M., and Verdon, J. (2015). Surfactin from *Bacillus subtilis* displays an unexpected anti-*Legionella* activity. *Appl. Microbiol. Biotechnol.* 99, 5083–5093. doi: 10.1007/s00253-014-6317-z

Ma, Y., Zhao, Y. Y., Tang, J. N., Tang, C., Chen, J., and Liu, J. (2018). Antimicrobial susceptibility and presence of resistance & enterotoxins/enterotoxin-likes genes in *Staphylococcus aureus* from food. *CyTA J. Food* 16, 76–84. doi: 10.1080/19476337.2017.1340341

Magiorakos, A. P., Srinivasan, A., Carey, R. B., Carmeli, Y., Falagas, M. E., Giske, C. G., et al. (2012). Multidrug-resistant, extensively drug-resistant and pandrug-resistant bacteria: an international expert proposal for interim standard definitions for acquired resistance. *Clin. Microbiol. Infect.* 18, 268–281. doi: 10.1111/j.1469-0691.2011.03570.x

Mandal, S. M., Barbosa, A. E. A. D., and Franco, O. L. (2013). Lipopeptides in microbial infection control: scope and reality for industry. *Biotechnol. Adv.* 31, 338–345. doi: 10.1016/j.biotechadv.2013.01.004

Narendra Kumar, P., Swapna, T. H., Khan, M. Y., Reddy, G., and Hameeda, B. (2017). Statistical optimization of antifungal iturin A production from *Bacillus amyloliquefaciens* RHNK22 using agro-industrial wastes. *Saudi J. Biol. Sci.* 24, 1722–1740. doi: 10.1016/j.sjbs.2015.09.014

Ndlovu, T., Rautenbach, M., Vosloo, J. A., Khan, S., and Khan, W. (2017). Characterisation and antimicrobial activity of biosurfactant extracts produced by *Bacillus amyloliquefaciens* and *Pseudomonas aeruginosa* isolated from a wastewater treatment plant. *AMB Express* 7:108. doi: 10.1186/s13568-017-0363-8

Patel, S., Ahmed, S., and Eswari, J. S. (2015). Therapeutic cyclic lipopeptides mining from microbes: latest strides and hurdles. *World J. Microbiol. Biotechnol.* 31, 1177–1193. doi: 10.1007/s11274-015-1880-8

Pathak, K. V., Keharia, H., Gupta, K., Thakur, S. S., and Balaram, P. (2012). Lipopeptides from the banyan endophyte, *Bacillus subtilis* K1: mass spectrometric characterization of a library of fengycins. *J. Am. Soc. Mass Spectrom* 23:1716. doi: 10.1007/s13361-012-0437-4

Perez, K. J., Viana, J. D. S., Lopes, F. C., Pereira, J. Q., Dos Santos, D. M., Oliveira, J. S., et al. (2017). *Bacillus* spp. Isolated from puba as a source of biosurfactants and antimicrobial lipopeptides. Front. Microbiol. 8:61. doi: 10.3389/fmicb.2017.00061

Piewngam, P., Zheng, Y., Nguyen, T. H., Dickey, S. W., Joo, H.-S., Villaruz, A. E., et al. (2018). Pathogen elimination by probiotic *Bacillus* via signalling interference. *Nature* 562, 532–537. doi: 10.1038/s41586-018-0616-y

Pradhan, A. K., Pradhan, N., Mall, G., Panda, H. T., Sukla, L. B., Panda, P. K., et al. (2013). Application of lipopeptide biosurfactant isolated from a halophile: *Bacillus tequilensis* CH for inhibition of biofilm. *Appl. Biochem. Biotechnol.* 171, 1362–1375. doi: 10.1007/s12010-013-0428-3

Sa, R. B., An, X., Sui, J. K., Wang, X. H., Ji, C., Wang, C. Q., et al. (2018). Purification and structural characterization of fengycin homologues produced by *Bacillus subtilis* from poplar wood bark. *Aust. Plant Pathol.* 47, 259–268. doi: 10.1007/s13313-018-0552-1

Sabaté, D. C., and Audisio, M. C. (2013). Inhibitory activity of surfactin, produced by different *Bacillus subtilis* subsp. *subtilis* strains, against *Listeria monocytogenes* sensitive and bacteriocin-resistant strains. *Microbiol. Res.* 168, 125–129. doi: 10.1016/j.micres.2012.11.004

Sarwar, A., Hassan, M. N., Imran, M., Iqbal, M., Majeed, S., Brader, G., et al. (2018). Biocontrol activity of surfactin A purified from *Bacillus* NH-100 and NH-217 against rice bakanae disease. *Microbiol. Res.* 209, 1–13. doi: 10.1016/j.micres.2018.01.006

Sharma, D., Ansari, M. J., Gupta, S., Al Ghamdi, A., Pruthi, P., and Pruthi, V. (2015). Structural characterization and antimicrobial activity of a biosurfactant obtained from *Bacillus pumilus* DSVP18 grown on potato peels. *Jundishapur J. Microbiol.* 8:e21257. doi: 10.5812/jjm.21257

Singh, N., and Abraham, J. (2014). Ribosomally synthesized peptides from natural sources. *J. Antibiot.* 67, 277–289. doi: 10.1038/ja.2013.138

Sudarmono, P., Wibisana, A., Listriyani, L. W., and Sungkar, S. (2019). Characterization and synergistic antimicrobial evaluation of lipopeptides from *Bacillus amyloliquefaciens* isolated from oil-contaminated soil. *Int. J. Microbiol.* 2019:3704198. doi: 10.1155/2019/3704198

Tack, D. M., Marder, E. P., Griffin, P. M., Cieslak, P. R., Dunn, J., Hurd, S., et al. (2019). Preliminary incidence and trends of infections with pathogens transmitted commonly through food - foodborne diseases active surveillance network, 10 U.S. sites, 2015-2018. *MMWR Morb. Mortal. Wkly. Rep.* 68, 369–373. doi: 10.15585/mmwr.mm6816a2

Tirziu, E., Lazar, R., Sala, C., Nichita, I., Morar, A., Seres, M., et al. (2015). *Salmonella* in raw chicken meat from the Romanian seaside: frequency of isolation and antibiotic resistance. *J. Food Prot.* 78, 1003–1006. doi: 10.4315/0362-028x.jfp-14-460

Todorov, S. D., De Paula, O. L., Camargo, A. C., Lopes, D. A., and Nero, L. A. (2018). Combined effect of bacteriocin produced by *Lactobacillus plantarum* ST8SH and vancomycin, propolis or EDTA for controlling biofilm development by *Listeria monocytogenes*. *Rev. Argent. Microbiol.* 50, 48–55. doi: 10.1016/j.ram.2017.04.011

Torres, M. J., Petroselli, G., Daz, M., Erra-Balsells, R., and Audisio, M. C. (2015). *Bacillus subtilis* subsp. *subtilis* CBMDC3f with antimicrobial activity against Gram-positive foodborne pathogenic bacteria: UV-MALDI-TOF MS analysis of its bioactive compounds. *World J. Microbiol. Biotechnol.* 31, 929–940. doi: 10.1007/s11274-015-1847-9

U.S. Centers for Disease Control and Prevention (2019). *Antibiotic Resistance Threats in the United States, 2019*. Available online at: https://www.cdc.gov/drugresistance/pdf/threats-report/2019-ar-threats-report-508.pdf (accessed March 27, 2020).

Vanittanakom, N., Loeffler, W., Koch, U., and Jung, G. (1986). Fengycin–a novel antifungal lipopeptide antibiotic produced by *Bacillus subtilis* F-29-3. *J. Antibiot.* 39, 888–901. doi: 10.7164/antibiotics.39.888

Varjani, S. J., and Upasani, V. N. (2016). Carbon spectrum utilization by an indigenous strain of *Pseudomonas aeruginosa* NCIM 5514: production, characterization and surface active properties of biosurfactant. *Bioresour. Technol.* 221, 510–516. doi: 10.1016/j.biortech.2016.09.080

Wang, J. Q., Liu, J. Z., Wang, X. L., Yao, J., and Yu, Z. S. (2004). Application of electrospray ionization mass spectrometry in rapid typing of fengycin homologues produced by *Bacillus subtilis*. *Lett. Appl. Microbiol.* 39, 98–102. doi: 10.1111/j.1472-765X.2004.01547.x

World Health Organization (2015). *WHO Estimates of the Global Burden of Foodborne Diseases: Foodborne Disease Burden Epidemiology Reference Group 2007-2015*. Available online at: http://apps.who.int/iris/bitstream/handle/10665/199350/9789241565165_eng.pdf (accessed April 25, 2019).

World Health Organization (2019). *International Food Safety Conference*. Available online at: https://www.who.int/news-room/events/international-food-safety-conference (accessed March 27, 2020).

Xu, H.-M., Rong, Y.-J., Zhao, M.-X., Song, B., and Chi, Z.-M. (2014). Antibacterial activity of the lipopetides produced by *Bacillus amyloliquefaciens* M1 against multidrug-resistant *Vibrio* spp. isolated from diseased marine animals. *Appl. Microbiol. Biotechnol.* 98, 127–136. doi: 10.1007/s00253-013-5291-1

Yamamoto, S., Shiraishi, S., and Suzuki, S. (2015). Are cyclic lipopeptides produced by *Bacillus amyloliquefaciens* S13-3 responsible for the plant defence response in strawberry against *Colletotrichum gloeosporioides*? *Lett. Appl. Microbiol.* 60, 379–386. doi: 10.1111/lam.12382

Yang, H., Li, X., Li, X., Yu, H., and Shen, Z. (2015). Identification of lipopeptide isoforms by MALDI-TOF-MS/MS based on the simultaneous purification of iturin, fengycin, and surfactin by RP-HPLC. *Anal. Bioanal. Chem.* 407, 2529–2542. doi: 10.1007/s00216-015-8486-8

Ye, Q. H., Wu, Q. P., Hu, H. J., Zhang, J. M., and Huang, H. X. (2015). Prevalence, antimicrobial resistance and genetic diversity of *Yersinia enterocolitica* isolated from retail frozen foods in China. *FEMS Microbiol. Lett.* 362:fnv197. doi: 10.1093/femsle/fnv197

Yu, S. M., Oh, B. T., and Lee, Y. H. (2012). Biocontrol of green and blue molds in postharvest satsuma mandarin using *Bacillus amyloliquefaciens* JBC36. *Biocontrol Sci. Technol.* 22, 1181–1197. doi: 10.1080/09583157.2012.719150

Zacharof, M. P., and Lovitt, R. W. (2012). Investigation of shelf life of potency and activity of the *Lactobacilli* produced bacteriocins through their exposure to various physicochemical stress factors. *Probiotics Antimicrob. Proteins* 4, 187–197. doi: 10.1007/s12602-012-9102-2

Zhang, B., Dong, C. J., Shang, Q. M., Cong, Y., Kong, W. J., and Li, P. L. (2013). Purification and partial characterization of Bacillomycin L produced by *Bacillus amyloliquefaciens* K103 from lemon. *Appl. Biochem. Biotechnol.* 171, 2262–2272. doi: 10.1007/s12010-013-0424-7

Zihalirwa Kulimushi, P., Argüelles Arias, A., Franzil, L., Steels, S., and Ongena, M. (2017). Stimulation of fengycin-type antifungal lipopeptides in *Bacillus amyloliquefaciens* in the presence of the maize fungal pathogen *Rhizomucor variabilis*. *Front. Microbiol.* 8:850. doi: 10.3389/fmicb.2017.00850

Conflict of Interest: The authors declare that the research was conducted in the absence of any commercial or financial relationships that could be construed as a potential conflict of interest.

frontiers in Microbiology

ORIGINAL RESEARCH
published: 13 January 2021
doi: 10.3389/fmicb.2020.612367

Inactivation Effect of Violet and Blue Light on ESKAPE Pathogens and Closely Related Non-pathogenic Bacterial Species – A Promising Tool Against Antibiotic-Sensitive and Antibiotic-Resistant Microorganisms

Katharina Hoenes[1], Richard Bauer[2], Tobias Meurle[1], Barbara Spellerberg[2] and Martin Hessling[1]*

[1] Institute of Medical Engineering and Mechatronics, Ulm University of Applied Sciences, Ulm, Germany, [2] Institute of Medical Microbiology and Hygiene, University Hospital Ulm, Ulm, Germany

OPEN ACCESS

Edited by:
Rodolfo García-Contreras, National Autonomous University of Mexico, Mexico

Reviewed by:
Brock Aaron Arivett, Middle Tennessee State University, United States
Bernardo Franco, University of Guanajuato, Mexico

***Correspondence:**
Katharina Hoenes
katharina.hoenes@thu.de

Specialty section:
This article was submitted to Antimicrobials, Resistance and Chemotherapy, a section of the journal Frontiers in Microbiology

Received: *30 September 2020*
Accepted: *11 December 2020*
Published: *13 January 2021*

Citation:
Hoenes K, Bauer R, Meurle T, Spellerberg B and Hessling M (2021) Inactivation Effect of Violet and Blue Light on ESKAPE Pathogens and Closely Related Non-pathogenic Bacterial Species – A Promising Tool Against Antibiotic-Sensitive and Antibiotic-Resistant Microorganisms. Front. Microbiol. 11:612367. doi: 10.3389/fmicb.2020.612367

Due to the globally observed increase in antibiotic resistance of bacterial pathogens and the simultaneous decline in new antibiotic developments, the need for alternative inactivation approaches is growing. This is especially true for the treatment of infections with the problematic ESKAPE pathogens, which include *Enterococcus faecium, Staphylococcus aureus, Klebsiella pneumoniae, Acinetobacter baumannii, Pseudomonas aeruginosa*, and *Enterobacter* species, and often exhibit multiple antibiotic resistances. Irradiation with visible light from the violet and blue spectral range is an inactivation approach that does not require any additional supplements. Multiple bacterial and fungal species were demonstrated to be sensitive to this disinfection technique. In the present study, pathogenic ESKAPE organisms and non-pathogenic relatives are irradiated with visible blue and violet light with wavelengths of 450 and 405 nm, respectively. The irradiation experiments are performed at 37°C to test a potential application for medical treatment. For all investigated microorganisms and both wavelengths, a decrease in colony forming units is observed with increasing irradiation dose, although there are differences between the examined bacterial species. A pronounced difference can be observed between Acinetobacter, which prove to be particularly light sensitive, and enterococci, which need higher irradiation doses for inactivation. Differences between pathogenic and non-pathogenic bacteria of one genus are comparatively small, with the tendency of non-pathogenic representatives being less susceptible. Visible light irradiation is therefore a promising approach to inactivate ESKAPE pathogens with future fields of application in prevention and therapy.

Keywords: visible light irradiation, photoinactivation, antimicrobial blue light, ESKAPE pathogens, non-pathogen, 405 nm, 450 nm

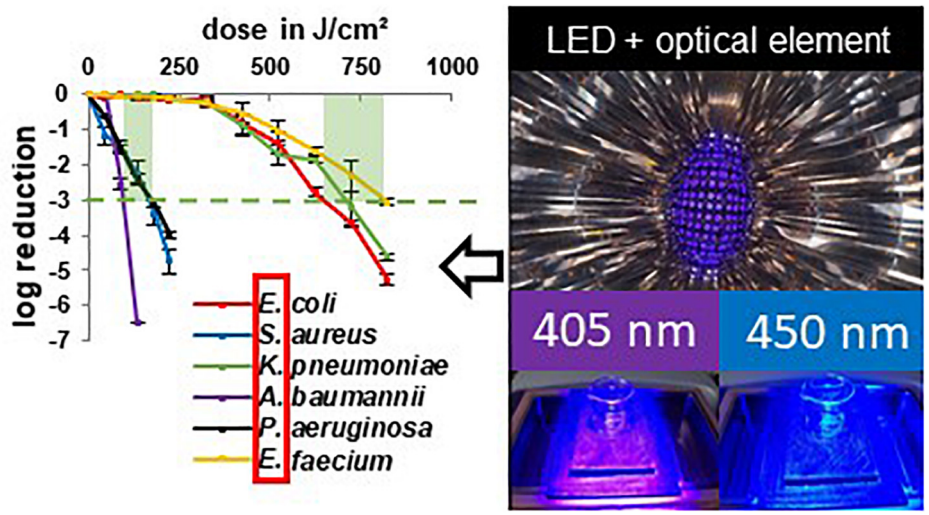

GRAPHICAL ABSTRACT |

INTRODUCTION

Hospital acquired infections (HAIs) challenge the health care sector (World Health Organization, 2017) and affect millions of patients each year. The increasing development of antibiotic resistances is worsening the situation creating an urgent need for establishing new anti-infective strategies. Consequently, to expedite the utilization of new technologies is critical, as the increasing prevalence of multidrug resistant microorganisms in hospitals became a serious threat for public health (Boucher et al., 2009). Most of the ESKAPE pathogens appear on the World Health Organization (WHO) list of the most problematic microbial species resulting in an appeal to concentrate research efforts on this topic. For 2007, the European Centre for Disease and Control (ECDC) estimated the death of 25,000 patients in the European Union, Norway and Iceland and an additional 900 million Euros hospital costs due to five selected antibiotic-resistant species (European center for disease prevention and control, 2009), completely intersecting with the ESKAPE pathogens. In 2016, HAI developed in 8.4% of patients staying in an intensive care unit for more than 2 days (European center for disease prevention and control, 2018).

Among research efforts to find alternative antimicrobial approaches, light-based technologies experience an intensified investigation (Mulani et al., 2019). Especially irradiation treatment with wavelengths in the range of visible light is often indicated as a possible antibiotic alternative (Wang et al., 2017; Hamblin and Abrahamse, 2019). Indeed, there seem to be multiple advantages. Due to current progress in the development of light emitting diodes (LED) this method is easily available, durable, sustainable and cost-effective. Several implementations in hospital-associated applications have been suggested. The equipment of endotracheal tubes with blue LEDs might intervene, where other antimicrobial approaches are struggling for many years to prevent ventilator associated pneumonia (VAP; Sicks et al., 2020). Endoscopically delivered light reduced gastric *Helicobacter pylori* infection (Ganz et al., 2005), urinary tract infection could successfully be treated in a rat model (Huang et al., 2018) and biofilm growth on catheter material was demonstrated to be reduced by the influence of irradiation (Vollmerhausen et al., 2017). The development of a light diffusing fiber delivery system (Shehatou et al., 2019), a minimally invasive ingestible capsule (Romano et al., 2016), the investigation of a continuous surface disinfection of hospital rooms during the patient's presence (Maclean et al., 2013) and a whole range of different patents (Ahmed et al., 2018), demonstrate simultaneously the emerging significance of light-based technologies and their applicability.

The mechanisms for visible light inactivation is based on endogenous photosensitizers present in bacterial cells, which absorb photons of a certain wavelength converting the photosensitizers into an excited state. Those can interact with ambient oxygen to form reactive oxygen species (ROS) (Hamblin and Abrahamse, 2020), which cause damage to several intracellular targets (Dai et al., 2013; Adair and Drum, 2016; Kim and Yuk, 2017; Djouiai et al., 2018; Chu et al., 2019; Hyun and Lee, 2020). The violet wavelength of 405 nm was proven to be especially effective (Maclean et al., 2008; Endarko et al., 2012) tracing back to endogenous porphyrins, which are recognized as responsible photosensitizers (Ashkenazi et al., 2003; Hamblin et al., 2005; Lipovsky et al., 2009). The blue wavelength of 450 nm also has a considerable inactivation impact, albeit weaker than for 405 nm (Hessling et al., 2017; Plavskii et al., 2018; Tomb et al., 2018) but may be preferable for clinical applications due to higher tissue penetration depth and lower absorption by blood. For 450 nm flavins are considered as responsible photosensitizer (Cieplik et al., 2014; Plavskii et al., 2018; Hoenes et al., 2019).

It has been noticed that differences exist in the way, in which microbial genera react to the exposure to visible light of the same wavelength (Hessling et al., 2017; Tomb et al., 2018). However, the underlying causes are not totally resolved. Varying compositions and concentrations of endogenous photosensitizers might play a role, as those are the responsible mediators between light and bacterial damage. Due to differing investigation methods, the comparison of test results for different strains is problematic. It is hard to determine if variables arise from biological factors or the different treatment and environmental properties. Parameters like pH of the culture medium (Kjeldstad et al., 1984), specific culture conditions and growth phase (Keshishyan et al., 2015; Abana et al., 2017; Biener et al., 2017; Fyrestam et al., 2017) as well as pH, salt concentration and temperature during irradiation (Ghate et al., 2015; Keshishyan et al., 2015; McKenzie et al., 2016), have been demonstrated to influence bacterial inactivation. Barneck et al. (2016) found that the irradiation effect is dose-dependent and that different irradiation intensities did not play a role concerning the inactivation result at a specific dose, independent of the irradiation time. Nevertheless, this was only a single study, so it might be risky to rely on the dose-dependency when comparability is desired.

Our aim was therefore to perform all our investigations on pathogenic and non-pathogenic representatives of different genera with the same test protocol. In this study, we wanted to examine whether pathogenic bacterial species and closely related non-pathogenic species respond in the same manner to visible light irradiation at wavelengths of 405 and 450 nm. Therefore, a pathogenic strain and a non-pathogenic relative were investigated in comparison. To come up with new methods capable to cope with ESKAPE pathogens we chose those 6 species for our experiments. In total, we thus investigated 11 strains, as no non-pathogenic *Klebsiella* strain is available.

MATERIALS AND METHODS

Bacterial Strains and Cultivation

Enterococcus moraviensis (DSM 15919), *Staphylococcus carnosus* (DSM 20501), *Acinetobacter kookii* (DSM 29071), *Pseudomonas stutzeri* (DSM 5190), *Escherichia coli* (DSM 1607), and *Enterococcus faecium* (DSM 17050) were obtained from DSMZ (Deutsche Sammlung für Mikroorganismen und Zellkulturen, Braunschweig, Germany). *Staphylococcus aureus* (ATCC 43300), *Klebsiella pneumoniae* (ATCC 700603), *Acinetobacter baumannii* (ATCC 19606), and *Pseudomonas aeruginosa* (ATCC 27853) were obtained from American Type Culture Collection (ATCC, Manassas, VA, United States). *Escherichia coli* BSU1286 was obtained from the Institute of Medical Microbiology and Hygiene (University Hospital Ulm, Germany). All strains were cultivated to mid-exponential phase and then centrifuged at 7,000 *g* for 5 min. The resultant pellet was resuspended in phosphate buffered saline (PBS) and washed in PBS, before the suspension was diluted to the desired population density between 5×10^7 and 10^8 colony forming units per ml (CFU/ml) for experimental use. All experiments were conducted in PBS to avoid the possible photosensitizing impact and absorbance of medium ingredients. Media that were used for cultivation are listed in **Table 1**.

TABLE 1 | Overview of the strains investigated in this study in this study and their specific media.

strain	Pathogenicity	Resistances	Medium reference	Ingredients per 1000 ml
E. moraviensis, *S. carnosus*	-	–	M92	30 g tryptic soy broth (Sigma-Aldrich Chemie GmbH, München, Germany), 3 g yeast extract (Merck KGaA, Darmstadt, Germany)
A. kookii	-	–	M220	15 g peptone from casein (VWR international, Leuven Belgium), 5 g peptone from soymeal (Sigma-Aldrich Chemie GmbH, München, Germany), 5 g sodium chloride (VWR international, Leuven Belgium)
P. stutzeri	-	–	M1	5 g peptone from casein (VWR international, Leuven Belgium), 3 g meat extract (VWR international, Leuven Belgium)
E. coli HB101 K12	-	–	LB	10 g tryptone (VWR international, Leuven, Belgium), 5 g yeast extract (Merck KgaA, Darmstadt, Germany), 10 g sodium chloride (VWR international, Leuven Belgium)
E. faecium	+	VRE	THY	36.4 g Todd–Hewitt Broth (Oxoid, Basingstoke, United Kingdom), 5 g yeast extract (BD, Sparks, MD, United States)
S. aureus	+	MRSA	THY	36.4 g Todd–Hewitt Broth (Oxoid, Basingstoke, United Kingdom), 5 g yeast extract (BD, Sparks, MD, United States)
K. pneumoniae	+	ESBL	THY	36.4 g Todd–Hewitt Broth (Oxoid, Basingstoke, United Kingdom), 5 g yeast extract (BD, Sparks, MD, United States)
A. baumannii	+	–	LB	10 g tryptone (Gibco, Detroit, MI), 5 g yeast extract (BD, Sparks, MD, United States), 10 g sodium chloride (AppliChem, Darmstadt, Germany)
P. aeruginosa	+	–	THY	36.4 g Todd–Hewitt Broth (Oxoid, Basingstoke, United Kingdom), 5 g yeast extract (BD, Sparks, MD, United States)
E. coli	+	ESBL	LB	10 g tryptone (Gibco, Detroit, MI), 5 g yeast extract (BD, Sparks, MD, United States), 10 g sodium chloride (AppliChem, Darmstadt, Germany)

ESBL, extended spectrum beta-lactamases; MRSA, methicillin resistant S. aureus; VRE, vancomycin resistant enterococcus. The declaration of biosafety level served as indicator for the pathogenicity.

Irradiation Setup

Two different wavelengths were applied for irradiation. Due to safety regulations the strains were investigated in two groups and in two laboratories with test setups slightly adapted to laboratory conditions, but with the same parameters. A truncated hollow pyramid with a high reflective inside, already described before in Hoenes et al., 2019, ensured that the sample area was irradiated homogenously. LEDs were mounted to a heat sink, which was actively cooled with a fan during experiments to avoid heating the sample (**Figure 1**). Experiments were performed in separate vessels with 11 mm diameter. For irradiation at the violet wavelength, LEDs with a peak wavelength of 405 nm were applied. The second wavelength was chosen from the blue wavelength range at 450 nm. For both wavelengths, an intensity of 20 mW/cm^2 was selected. Irradiation intensity was measured by means of an optical power meter OPM150 (Qioptiq, Göttingen, Germany).

As we wanted to refer to therapeutic applications taking place at or in the human body the experiments were conducted at 37°C. For pathogenic microorganisms, the whole setup was placed inside an incubator. Samples of non-pathogenic strains were heated by a temperature regulated water bath ICC basic (IKA, Staufen, Germany), with tempered water passing the lower third of the vessel continuously. The sample temperature was checked at each sampling interval with an infrared thermometer (Raytek Fluke Process Instruments GmbH, Berlin, Germany).

Samples were drawn in certain time intervals with increasing doses and plated on nutrient agar. The media used for agar plates have been the same as the cultivation media for non-pathogenic and sheep blood agar plates (TSA + SB, Oxoid, Basingstoke, United Kingdom) for pathogenic strains. After incubation at 37°C for 24–48 h grown colonies were enumerated manually. The resultant count was converted to CFU/ml and expressed as log reduction in comparison to the starting concentration. Each experiment was performed in triplicates and repeated at least three times.

RESULTS

In this study we wanted to evaluate the irradiation susceptibility of different microbial genera and potential differences between closely related pathogenic and non-pathogenic bacterial species. In **Figure 2** the inactivation results for the wavelengths 405 and 450 nm are depicted for two different species in each illustration - one pathogenic and one non-pathogenic of a certain genus, to compare whether there are differences in their inactivation profile. The dotted lines portray the non-pathogenic representative, while the solid lines represent the

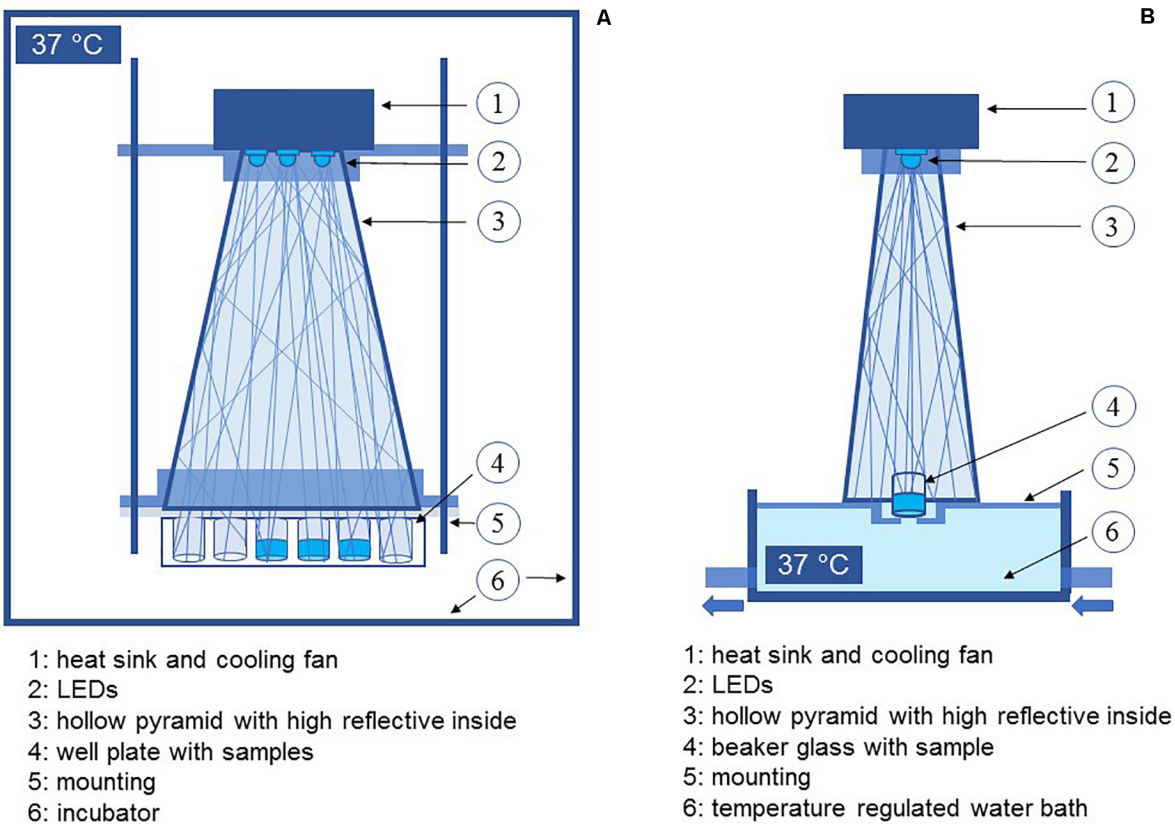

FIGURE 1 | Schematic depiction of the experimental setup for experiments with pathogenic bacteria **(A)** and non-pathogenic bacteria **(B)**.

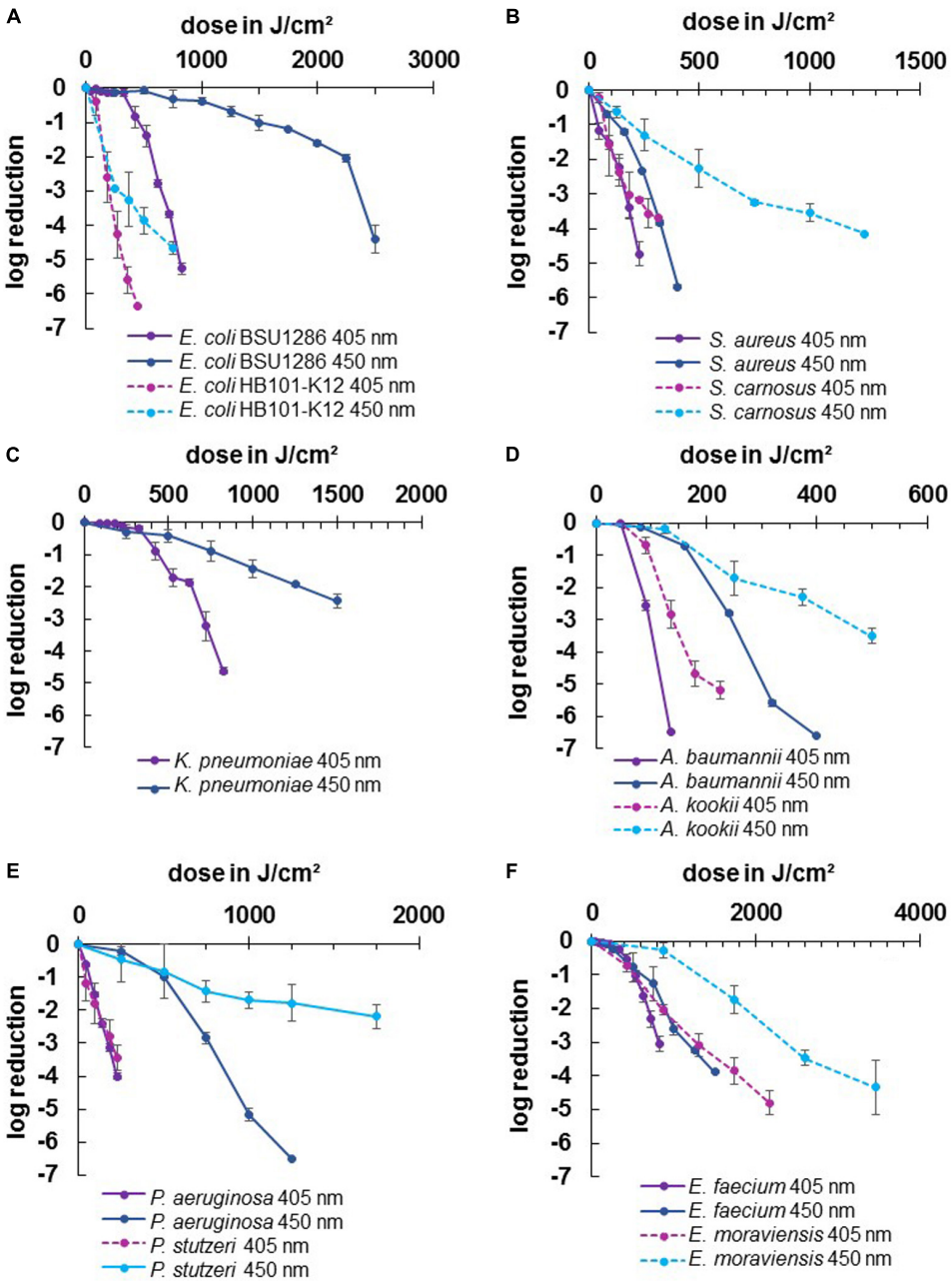

FIGURE 2 | Inactivation results for pathogenic ESKAPE-strains and non-pathogenic relatives for 405 and 450 nm: *E. coli* BSU1286/*E. coli* HB101 K12 **(A)**, *S. aureus*/*S. carnosus* **(B)**, *K. pneumoniae* **(C)**, *A. baumannii*/*A. kookii* **(D)**, *P. aeruginosa*/*P. stutzeri* **(E)**, *E. faecium*/*E. moraviensis* **(F)**. Error bars represent standard deviation of three independent experiments.

pathogenic species. There was no considerable decrease in most non-irradiated controls. However, the *E. moraviensis* control was reduced by 1.38 log at the end of the longer 450 nm experiment at 48 h. Therefore, the log decrease in the control at this strain was subtracted from the irradiation value at each sampling point to demonstrate the sole light impact. Likewise, *A. kookii* results were corrected in this manner. For all other strains, the decrease in the control was so low to not perceptibly affect the irradiation results.

For all tested strains, the violet wavelength of 405 nm exhibited a stronger inactivation effect compared to the blue wavelength of 450 nm (**Figure 2**). However, comparing the two wavelengths between pathogenic and non-pathogenic species, there were two cases in which 450 nm on the pathogenic strain was as effective as 405 nm on the non-pathogenic strain at a similar dose. For *S. aureus* we achieved 3.84 log reduction at 320 J/cm^2 with 450 nm while *S. carnosus* required 315 J/cm^2 of 405 nm to be inactivated by 3.70 log (**Figure 2B**). Likewise, for *E. faecium* 3.26

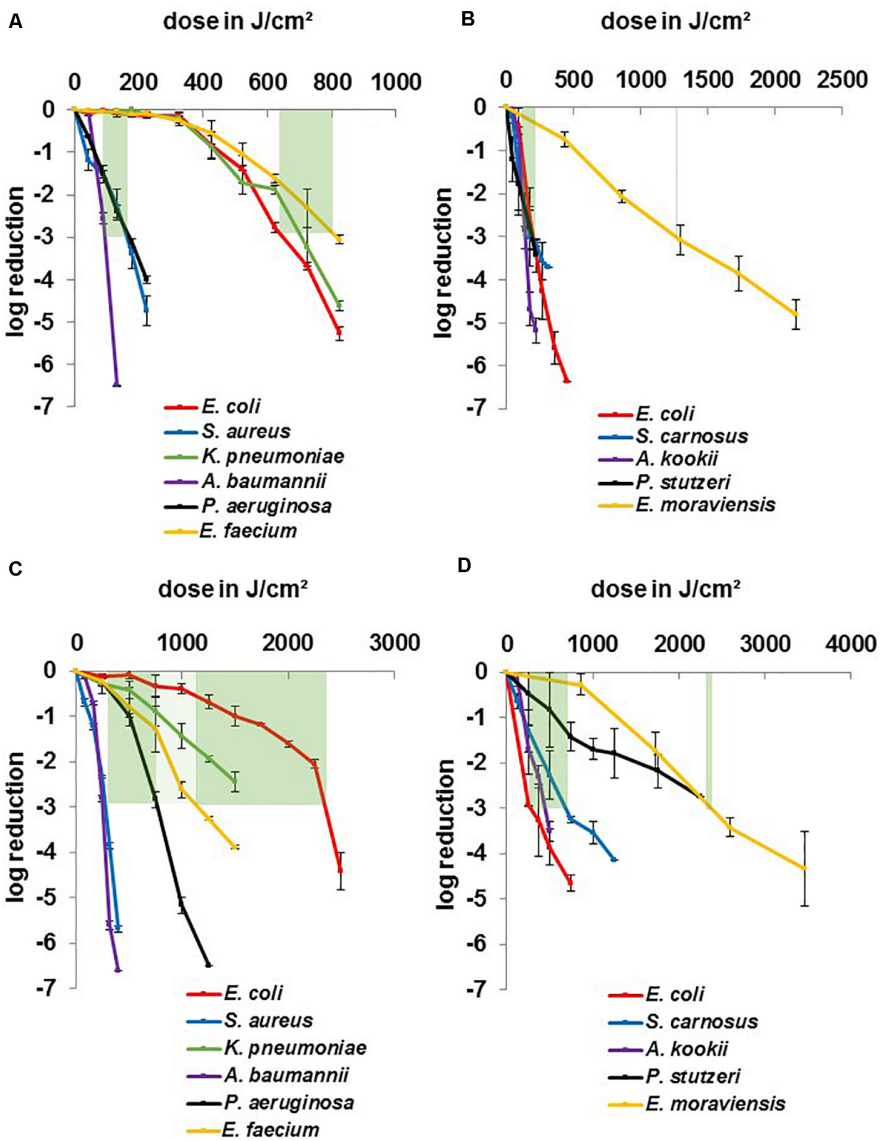

FIGURE 3 | Inactivation results for pathogenic ESKAPE-strains and non-pathogenic relatives for 405 and 450 nm grouped by wavelength: pathogenic strains at 405 nm **(A)**, non-pathogenic strains at405 nm **(B)**, pathogenic strains at 450 nm **(C)**, non-pathogenic strains at 450 nm **(D)**. Green bars mark a dose range for similar behaving microorganisms for a 3 log reduction. Error bars represent standard deviation of three independent experiments.

log at 1250 J/cm^2 was achieved with 450 nm, while *E. moraviensis* was reduced by 3.08 log when exposed to 1296 J/cm^2 of 405 nm (**Figure 2F**).

All strains exhibited the typical behavior for visible light inactivation with a non-monoexponential shape, showing a linear relationship of inactivation and dose in a semi-logarithmic representation. In some cases, a so called "shoulder" occured at lower doses indicating the ability of bacteria to overcome small damages. This slow initial reaction particularly became apparent for 450 nm irradiation of *E. coli* BSU1286, showing a slow decrease up to a dose of 2250 J/cm^2, followed by a steeper slope (**Figure 2A**). In addition, at 450 nm *P. aeruginosa* illustrated a distinct development of this behavior (**Figure 2E**).

Both applied wavelengths were successful at inactivating the strains investigated here. However, the doses necessary to achieve a certain log reduction were varying, especially between different genera. The highest dose of 450 nm irradiation for a reduction of 3 or more log levels, had to be applied to *E. coli* BSU1286, with 2500 J/cm^2 for 4.4 log reduction (**Figure 2A**). Meanwhile, only 320 J/cm^2 of 450 nm had to be applied to *A. baumannii* for a 5.60 log reduction. Concerning 405 nm Acinetobacter likewise appeared to be the most susceptible genus with only 225 J/cm^2 exposure that was necessary to reduce the non-pathogenic representative *A. kookii* by 5.19 log (**Figure 2D**). The microorganisms most difficult to diminish with 405 nm have been enterococci with *E. faecium* being inactivated by 3.06 log

at 825 J/cm^2 and *E. moraviensis* requiring 1296 J/cm^2 for 3.08 log reduction (**Figure 2F**).

The difference in the effectiveness of the two wavelengths compared has been most apparent for pseudomonads (**Figure 2E**). For *P. aeruginosa* in addition the extensive development of a shoulder at 450 nm was observable, whereas the 405 nm inactivation progress illustrated an almost straight line, representing an exponential decline. Furthermore, the pathogen *E. coli* representative showed huge susceptibility differences between the two wavelengths, which is essentially caused by the low inactivation efficiency at 450 nm in this case (**Figure 2A**).

For 405 nm the non-pathogenic and pathogenic representatives of the same species exhibited similar behavior. Non-pathogenic strains tended to be rather less susceptible to 405 nm irradiation, becoming apparent when directly opposing log reductions. Indicating the non-pathogenic strain following by the pathogenic, reductions of 3.16/4.74 log at 225 J/cm^2 for staphylococci, 0.69/2.55 log at 90 J/cm^2 for Acinetobacter, 2.06/3.05 at 864/825 J/cm^2 for enterococci, and 3.43/4.01 log at 225 J/cm^2 for pseudomonads respectively, have been achieved. Only for *E. coli* the proportions are inverted with 6.36/0.84 log at 450/425 J/cm^2, with the disparity being especially vast here. For the pathogenic *E. coli* strain BSU1286 a dose of 825 J/cm^2 was necessary to reach a reduction of 5.26 log, which means that an approximately doubled dose was needed for the same reduction compared to the non-pathogenic relative (**Figure 2A**).

The same trend as for 405 nm became apparent for 450 nm. Likewise, the non-pathogenic strain was less susceptible than its pathogenic relative. Here we achieved log reductions of 2.27/5.69 at 500/400 J/cm^2 for staphylococci, 2.30/6.61 at 375/400 J/cm^2 for Acinetobacter, 1.73/3.89 log at 1728/1500 J/cm^2 for enterococci, and 1.78/5.17 log at 1250 J/cm^2 for pseudomonads, again first naming the non-pathogenic followed by the pathogenic strain. Again, the pathogenic *E. coli* strain was in contrary much less susceptible than the non-pathogenic strain with 4.66/0.33 log reduction at 750 J/cm^2 of 450 nm. To reach an inactivation of 4.41 log the suspension had to be exposed to 2500 J/cm^2 of 450 nm (**Figure 2A**).

Altogether, the least differences between pathogenic and non-pathogenic relative occurred for pseudomonads referring to the wavelength of 405 nm (**Figure 2E**). However, concerning 450 nm irradiation *Pseudomonas* together with *Escherichia* are the genera at which the differences between pathogenic and non-pathogenic strains investigated became most evident, albeit in opposite direction. Contemplating the general strain differences across all microorganisms, the differences at 450 nm irradiation had been more evident than for 405 nm.

In **Figure 3** where data have been categorized concerning better comparability of different genera, it becomes apparent that 3 strains especially stand out regarding their insusceptibility. *K. pneumoniae*, *E. coli* BSU1286, and *E. faecium* (**Figure 3A**) provide a strong contrast compared to the other pathogen representatives at 405 nm and clearly divide the microorganisms in two different susceptibility groups. To achieve a 3 log reduction, the dose ranges of 100–175 J/cm^2 compared to 650–800 J/cm^2 had to be applied, respectively. Non-pathogenic strains (**Figure 3B**) lie closer together with a range of 125–200 J/cm^2 with only *E. moraviensis* as outlier with around 1200 J/cm^2 of 405 nm. Yet it is necessary to mention here, that a non-pathogenic *Klebsiella* strain was not available for testing.

A similar distribution is observable for the non-pathogenic strains at 450 nm (**Figure 3D**) with a dose range of 350–750 J/cm^2 and *E. moraviensis* as well as *P. stutzeri* at around 2400 J/cm^2, though it has to be noted that the field had widened at this wavelength. While *E. coli* and *E. moraviensis* required a doubled dose comparing 405 to 450 nm, *S. carnosus* and *A. kookii* exhibited even more reduced susceptibility at 450 nm, while still lying in the range of 2 to 5-fold dose increase, which is found in the literature comparing 405 and 450 nm (Hessling et al., 2017; Tomb et al., 2018). *P. stutzeri* required even the 12-fold dose at 450 nm compared to 405 nm, which is an unusual finding regarding the literature and was likewise not observed for the pathogenic *P. aeruginosa*.

The 450 nm dose range of the more susceptible pathogenic group (**Figure 3C**) was 250–750 J/cm^2, indicating a 2 to 5-fold increase at the blue wavelength. Similarly, as for the non-pathogenic strains, it is observable that *P. aeruginosa* especially required higher doses at 450 nm, as mentioned before. *E. faecium* had not pulled apart extremely, but *K. pneumoniae* and *E. coli* BSU1286 spread the field to a dose range of 1,200–2,400 J/cm^2. Overall, for pathogenic strains at 450 nm the dose distribution for different genera is evenly distributed. While the susceptibility tendencies of different genera are still visible, no similar clear separable categories as for 405 nm could be drawn.

DISCUSSION

Photoinactivation with visible light has recently received increased interest due to the demand for the development of new disinfection technologies. Multiple studies investigating single bacterial species with a certain test setup at a specific wavelength have been published. However, extensive differences were observed in these data collections probably caused by a lack of uniform methodologies (Hessling et al., 2017; Tomb et al., 2018). Only few studies compare multiple strains with the same test protocol. Therefore, we aimed to investigate all ESKAPE pathogens under comparable conditions, including the comparison of related pathogenic and non-pathogenic species. As literature data about non-pathogenic microorganisms are still scarce we mainly concentrated on the pathogenic representatives for a comparison with the literature data to evaluate the achieved results.

Maclean et al. (2009) investigated 405 nm irradiation at 10 mW/cm^2 against a broad range of microorganisms including all ESKAPE-pathogens. Their findings concerning the sensitivity of different genera is comparable to the results obtained here. *A. baumannii*, *S. aureus*, and *P. aeruginosa* are more susceptible to visible light, while for *E. coli*, enterococci and *K. pneumoniae* higher doses are necessary for 1 log reduction (**Figure 2**). Compared to our results there is a factor of approximately 2 in the dose for 1 log reduction of *E. coli*, enterococci and *K. pneumoniae* compared to Maclean et al. (2009), but the tendencies are similar, including the necessity of an exposure of about 300 J/cm^2 for enterococci until inactivation progress is

noticeable. In addition, the inactivation dose of 42.9 J/cm^2 for 1 log reduction of *P. aeruginosa* is comparable to the 57.1 J/cm^2 result achieved here.

Gupta et al. (2015) investigated clinical isolates from infectious hip and knee arthroplasties including all ESKAPE species except *A. baumannii* at 123 mW/cm^2 of 405 nm irradiation. The study indicated the dose needed to reach an approximate 5 log reduction, which was their measured maximum. With 441.9 J/cm^2 for a calculated 1 log average inactivation their results fit well to the calculated 492.2 J/cm^2 for 1 log *E. coli* BSU1286 inactivation achieved here. For *K. pneumoniae* and *S. aureus* the averaged 1 log exposures were lower than in this study, even though clinical isolates were used by Gupta et al. (2015), which are often considered to be more challenging to inactivate. For *E. faecium* Halstead et al. (2016) delivered a value of 393 J/cm^2 for 1 log reduction for a clinical isolate at 400 nm irradiation, while the strain investigated here required 525 J/cm^2.

Concluding, the results for the necessary dose at 405 nm irradiation in this study are relatively high, especially concerning the inactivation of Enterobacteriaceae - including *Klebsiella* and *Escherichia* – and enterococci. For *S. aureus* there are several studies coming to similar conclusions with doses between 50.2 and 61.6 for a 1 log reduction (Enwemeka et al., 2008; Guffey et al., 2013; McKenzie et al., 2016). Furthermore, our data is in agreement with the literature that *Acinetobacter baumannii*, declared as one of the most problematic species in the WHO priority list (World Health Organization, 2017), is the most susceptible ESKAPE pathogen at 405 nm irradiation.

Irradiation around 450 nm has not been tested as extensively as 405 nm, hence the literature data available to compare with the results obtained here are limited. As expected, the doses required for inactivation have been higher at 450 nm for all strains investigated compared to 405 nm. Interestingly, a linear fit applied to the 450 nm data of *E. faecium* and *K. pneumoniae* delivered coefficients of 0.9453 and 0.9534, respectively, while "shoulders" existed for 405 nm irradiation. In contrast, for *S. aureus* and *P. aeruginosa* a linear fit was suitable at 405 nm, whereas a distinct "shoulder" appeared at 450 nm treatment. It was noticed before (Schmid et al., 2019) that there seems to be a correlation between the length of the wavelength, the duration of the slow initial inactivation and the occurrence of a shoulder. Webb and Brown (1976) already described similar observations concerning the wavelength dependency of the shoulder-effect in 1976 for *E. coli*.

For *P. aeruginosa* two very diverse literature results for 450 nm irradiation exist. Tomb et al. (2018) reported 91.9 J/cm^2 (Keshishyan et al., 2015) and 428.6 J/cm^2 (Decarli et al., 2016) for a 1 log reduction at 450 and 460 nm, respectively. We measured 0.98 log at 500 J/cm^2 and can therefore reproduce the value from the second study, although the first study was conducted at 37°C and the second at room temperature. Even though longer wavelengths were considered to have less impact on bacteria, the wavelength of 460 nm is probably not very different from 450 nm, as the flavin absorption peak is relatively broad. For *S. carnosus* we previously determined an increase of 12% for the required dose at 460 nm compared to 450 nm when conducting an action spectrum (Hoenes et al., 2019).

Lui et al. (2016) investigated *E. faecalis* at 455 nm irradiation for drinking water disinfection and found a required exposure dose of 410 J/cm^2 for a 1 log reduction. With 0.78 log at 500 J/cm^2 our results for *E. faecium* are comparable.

Some studies were conducted on pathogenic *E. coli* at wavelengths between 450 and 455 nm (Lipovsky et al., 2010; Keshishyan et al., 2015; Lui et al., 2016) ranging from approximately 100–300 J/cm^2 for 1 log inactivation but none of them is close to our results with 1500 J/cm^2 for 1.00 log. Within this study the *E. coli* strain stands out, although the majority of the data for all strains investigated here already rank at the upper end of visible light inactivation data.

The investigated *S. aureus* strain however was inactivated by 1.22 log at 160 J/cm^2 of 450 nm, while literature data suggest a 1 log dose of around 300 J/cm^2 at 450 nm at 37°C (Keshishyan et al., 2015), 400 J/cm^2 at 455 nm (Lipovsky et al., 2010), or 300 J/cm^2 at 460 nm (Decarli et al., 2016) for methicillin-sensitive strains.

To our knowledge, there are no data available for the inactivation of any *Acinetobacter* or *Klebsiella* strain with 450 nm light.

However, it is difficult to compare the data on bacterial inactivation of different research groups. Due to the lack of uniform test setups and protocols influences might occur that are not apparent at first sight. In this study, special attention was paid to a homogenous irradiation intensity by applying a reflective pyramid structure. Depending on the light source arrangement, without a homogenizing technique, great variations in intensity can occur due to the punctiform emission of LEDs, making it difficult to relate the achieved bacterial impact to a certain dose applied over time. A specificity for the results of this study is the investigation at 37°C, directing at achieving a benchmark for applications at human body temperature. As most literature data were obtained at room temperature (with varying degree of monitoring and regulation), this can make a direct comparison difficult. The research groups that obtained data at different temperatures tend to suggest that lower temperatures are favorable for visible light inactivation (McKenzie et al., 2014; Keshishyan et al., 2015; Kumar et al., 2015). This might partly explain the ranking of our data at the upper end compared to available reference values at room temperature.

This study is part of an ongoing development of an enhanced endotracheal tube. A potential protoype was presented earlier (Sicks et al., 2020). Utilizing the antimicrobial effects of photoinactivation and the applicability without adding external photosensitizers we aim to equip endotracheal tubes with a light source for prevention of VAP. The susceptibility investigation of ESKAPE microorganisms at the body core temperature of 37°C forms the foundation for further experiments under more realistic conditions. Data of this universal scientific state are nevertheless important and can likewise be used for multiple further medical developments. Catheter based approaches were already suggested (Vollmerhausen et al., 2017; Huang et al., 2018) as well as an ingestible capsule (Romano et al., 2016) against gastric ulcer, but also (burn) wound treatment is conceivable (Dai et al., 2013; Halstead et al., 2016).

It has been discussed before whether the Gram properties of microorganisms affect their susceptibility towards visible light

(Maclean et al., 2009). We could not detect any tendency, as staphylococci and enterococci, the two Gram positive species investigated, exhibited very different inactivation behavior and belonged to different groups of susceptibility for both 405 and 450 nm (**Figure 3**). Confirmative, there was no distinction found between the entirety of Gram positive and Gram negative species by Tomb et al. (2018) when reviewing literature data, with both groups requiring around 200 J/cm^2 of 405 nm irradiation in average for a 1 log reduction. The same absence of a clear difference between Gram properties was noticed in Hessling et al. (2017).

Except from the *E. coli* strains the irradiation at both wavelengths indicated a lower susceptibility for the non-pathogenic representatives investigated. Abana et al. (2017) investigated various *E. coli* strains, including a non-pathogenic strain, on their 455 nm light inactivation behavior. Comparable to our results the non-pathogenic strain was the most susceptible with approximately 2 log reduction at 120 J/cm^2. Lacombe et al. (2016) however did not detect differences in response to 405 nm between pathogenic and non-pathogenic *E. coli* strains. Nevertheless, the majority of non-pathogenic strains have been less susceptible in our study. In the supplementary material of the review of Tomb et al. (2018) we found a reference to a *P. stutzeri* investigation, achieving a 1 log reduction at 60 J/cm^2 of 405 nm. Our result with 3.43 log reduction at 225 J/cm^2 of 405 nm can be converted to 67.4 J/cm^2 necessary for 1 log reduction by a linear fit at log scale, which matches perfectly.

Virulence factors have been a recent topic of investigation within light-based approaches, as it was found that they will be destroyed by antimicrobial photodynamic inactivation (aPDI) using external photosensitizers for irradiation treatment (Kömerik et al., 2000; Tubby et al., 2009; Kato et al., 2013; Pourhajibagher et al., 2018). Bartolomeu et al. (2016) even found in their study investigating 6 *S. aureus* strains with varying properties, that those producing endotoxins were more susceptible to the aPDI treatment. Tang et al. (2007) noticed a stronger inactivation by irradiation for a MRSA strain compared with the corresponding ATCC strain, ascribed to the altered penicillin binding protein, which lead to a more permeable cell wall. A ROS induced impairment of factors for antimicrobial resistance or virulence, not only integral for the pathogenic properties but also fulfilling physiological performance in the microorganisms (Peterson, 1996), might therefore contribute to an additional reduction in viability. However, there might exist differences comparing aPDI and visible light irradiation, which is solely based on endogenous photosensitizers. In this study we therefore investigated whether similar tendencies are detectable for 405 and 450 nm irradiation without external dyes and if virulence plays a role for the behavior concerning irradiation.

The American Society for Microbiology (ASM) published a study, on important criteria for choosing appropriate surrogates for pathogens (Sinclair et al., 2012). For testing disinfection methods, it is recommended to choose a strain that is rather resistant compared to the target microorganisms, and thus testing a kind of worst case scenario. This criterion is fulfilled for all our non-pathogenic strains, besides *E. coli*.

The ASM further recommends to achieve a performance of 99.9% reduction in bactericidal tests (American Society for Microbiology, 2019). All investigated strains in this study reached this goal for irradiation with both 405 nm and 450 nm, besides *K. pneumoniae* and *P. stutzeri* at 450 nm for which the applied maximum dose of 1500 J/cm^2 and 2250 J/cm^2 led to a 2.44 log and a 2.75 log inactivation, respectively. The kinetics of the inactivation curves however suggest that 3 log can be reached at higher doses.

CONCLUSION

To our best knowledge, this has been the first time that all ESKAPE pathogens have been investigated within one study and therefore with the same test methodology, not only on their susceptibility to 405 nm but also to 450 nm. All strains in this study could be inactivated significantly with both wavelengths.

It has also been the first time that related pathogenic and non-pathogenic bacterial species have been directly compared. In our investigation, non-pathogenic strains tend to be less susceptible than the pathogenic representatives at both wavelengths, with the differences being more pronounced at 450 nm. As non-pathogenic relatives are rather more difficult to inactivate, it is considered valid to choose non-pathogenic surrogates for the investigation of visible light photoinactivation.

An exception was noticed for *E. coli* BSU1286, where the pathogenic strain was far less susceptible, not only compared to the non-pathogenic relative, but also compared to all other strains and to the available literature data.

DATA AVAILABILITY STATEMENT

The raw data supporting the conclusions of this article will be made available by the authors, without undue reservation.

AUTHOR CONTRIBUTIONS

KH co-designed the study, analyzed the effect of 405 and 450 nm on non-pathogenic microorganisms, and wrote the manuscript. RB analyzed the effect of 405 and 450 nm on pathogenic microorganisms and edited the manuscript. TM constructed the irradiation setup, helped with the experiments on non-pathogenic microorganisms and edited the manuscript. BS and MH designed the study, supervised the study, and edited the manuscript. All authors contributed to the article and approved the submitted version.

FUNDING

This work was supported by the German Federal Ministry of Education and Research (grant 13N15140) which is gratefully acknowledged.

REFERENCES

American Society for Microbiology. (2019). *Antimicrobial Agents and Chemotherpy, Instructions to Authors*. Available online at: https://aac.asm.org/sites/default/files/additional-assets/AAC-ITA.pdf (accessed September 07, 2020).

Abana, C. M., Brannon, J. R., Ebbott, R. A., Dunigan, T. L., Guckes, K. R., Fuseini, H., et al. (2017). Characterization of blue light irradiation effects on pathogenic and nonpathogenic *Escherichia coli*. *Microbiologyopen* 6:e00466. doi: 10.1002/mbo3.466

Adair, T. L., and Drum, B. E. (2016). RNA-Seq reveals changes in the *Staphylococcus aureus* transcriptome following blue light illumination. *Genomics Data* 9, 4–6. doi: 10.1016/j.gdata.2016.05.011

Ahmed, I., Fang, Y., Lu, M., Yan, Q., El-Hussein, A., Hamblin, M. R., et al. (2018). Recent patents on light-based anti-infective approaches. *Recent Pat. Antiinfect. Drug Discov.* 13, 70–88. doi: 10.2174/1872213X11666171108104104

Ashkenazi, H., Malik, Z., Harth, Y., and Nitzan, Y. (2003). Eradication of *Propionibacterium acnes* by its endogenic porphyrins after illumination with high intensity blue light. *FEMS Immunol. Med. Microbiol.* 35, 17–24. doi: 10.1111/j.1574-695X.2003.tb00644.x

Barneck, M. D., Rhodes, N. L., de La Presa, M., Allen, J. P., Poursaid, A. E., Nourian, M. M., et al. (2016). Violet 405-nm light: a novel therapeutic agent against common pathogenic bacteria. *J. Surg. Res.* 206, 316–324. doi: 10.1016/j.jss.2016.08.006

Bartolomeu, M., Rocha, S., Cunha, Â, Neves, M. G., Faustino, M. A., and Almeida, A. (2016). Effect of photodynamic therapy on the virulence factors of *Staphylococcus aureus*. *Front. Microbiol.* 7:267. doi: 10.3389/fmicb.2016.00267

Biener, G., Masson-Meyers, D. S., Bumah, V. V., Hussey, G., Stoneman, M. R., Enwemeka, C. S., et al. (2017). Blue/violet laser inactivates methicillin-resistant *Staphylococcus aureus* by altering its transmembrane potential. *J. Photochem. Photobiol. B Biol.* 170, 118–124. doi: 10.1016/j.jphotobiol.2017.04.002

Boucher, H. W., Talbot, G. H., Bradley, J. S., Edwards, J. E., Gilbert, D., Rice, L. B., et al. (2009). Bad bugs, no drugs: no ESKAPE! An update from the Infectious Diseases Society of America. *Clin. Infect. Dis.* 48, 1–12. doi: 10.1086/595011

Chu, Z., Hu, X., Wang, X., Wu, J., Dai, T., and Wang, X. (2019). Inactivation of *Cronobacter sakazakii* by blue light illumination and the resulting oxidative damage to fatty acids. *Can. J. Microbiol.* 65, 922–929. doi: 10.1139/cjm-2019-0054

Cieplik, F., Späth, A., Leibl, C., Gollmer, A., Regensburger, J., Tabenski, L., et al. (2014). Blue light kills *Aggregatibacter actinomycetemcomitans* due to its endogenous photosensitizers. *Clin. Oral Investig.* 18, 1763–1769. doi: 10.1007/s00784-013-1151-8

Dai, T., Gupta, A., Huang, Y.-Y., Yin, R., Murray, C. K., Vrahas, M. S., et al. (2013). Blue light rescues mice from potentially fatal *Pseudomonas aeruginosa* burn infection: efficacy, safety, and mechanism of action. *Antimicrob. Agents Chemother.* 57, 1238–1245. doi: 10.1128/AAC.01652-12

Decarli, M. C., Carvalho, M. T., Corrêa, T. Q., Bagnato, V. S., and de Souza, C. W. (2016). Different Photoresponses of Microorganisms: from Bioinhibition to Biostimulation. *Curr. Microbiol.* 72, 473–481. doi: 10.1007/s00284-015-0976-6

Djouiai, B., Thwaite, J. E., Laws, T. R., Commichau, F. M., Setlow, B., Setlow, P., et al. (2018). Role of DNA repair and protective components in *Bacillus subtilis* spore resistance to inactivation by 400-nm-Wavelength Blue Light*. *Appl. Environ. Microbiol.* 84:e01604-18. doi: 10.1128/AEM.01604-18

Endarko, E., Maclean, M., Timoshkin, I. V., MacGregor, S. J., and Anderson, J. G. (2012). High-intensity 405 nm light inactivation of *Listeria monocytogenes*. *Photochem. Photobiol.* 88, 1280–1286. doi: 10.1111/j.1751-1097.2012.01173.x

Enwemeka, C. S., Williams, D., Hollosi, S., Yens, D., and Enwemeka, S. K. (2008). Visible 405 nm SLD light photo-destroys methicillin-resistant *Staphylococcus aureus* (MRSA) in vitro. *Lasers Surg. Med.* 40, 734–737. doi: 10.1002/lsm.20724

European center for disease prevention and control (2009). *The Bacterial Challenge: Time to React a Call to Narrow the Gap Between Multidrug-Resistant bacteria in the EU and the Development of New Antibacterial Agents*. Luxembourg: Publications Office.

European center for disease prevention and control (2018). *Healthcare-Associated Infections in Intensive Care Units: Annual Epidemiological Report for 2016*. Stockholm: ECDC.

Fyrestam, J., Bjurshammar, N., Paulsson, E., Mansouri, N., Johannsen, A., and Östman, C. (2017). Influence of culture conditions on porphyrin production in *Aggregatibacter actinomycetemcomitans* and *Porphyromonas gingivalis*. *Photodiagnosis Photodyn. Ther.* 17, 115–123. doi: 10.1016/j.pdpdt.2016.11.001

Ganz, R. A., Viveiros, J., Ahmad, A., Ahmadi, A., Khalil, A., Tolkoff, M. J., et al. (2005). *Helicobacter pylori* in patients can be killed by visible light. *Lasers Surg. Med.* 36, 260–265. doi: 10.1002/lsm.20161

Ghate, V., Leong, A. L., Kumar, A., Bang, W. S., Zhou, W., and Yuk, H.-G. (2015). Enhancing the antibacterial effect of 461 and 521 nm light emitting diodes on selected foodborne pathogens in trypticase soy broth by acidic and alkaline pH conditions. *Food Microbiol.* 48, 49–57. doi: 10.1016/j.fm.2014.10.014

Guffey, J. S., Payne, W., Jones, T., and Martin, K. (2013). Evidence of resistance development by *Staphylococcus aureus* to an In Vitro, multiple stage application of 405 nm light from a Supraluminous Diode Array. *Photomed. Laser Surg.* 31, 179–182. doi: 10.1089/pho.2012.3450

Gupta, S., Maclean, M., Anderson, J. G., MacGregor, S. J., Meek, R. M., and Grant, M. H. (2015). Inactivation of micro-organisms isolated from infected lower limb arthroplasties using high-intensity narrow-spectrum (HINS) light. *Bone Joint J.* 97-B, 283–288. doi: 10.1302/0301-620X.97B2.35154

Halstead, F. D., Thwaite, J. E., Burt, R., Laws, T. R., Raguse, M., Moeller, R., et al. (2016). Antibacterial activity of blue light against nosocomial wound pathogens growing planktonically and as mature biofilms. *Appl. Environ. Microbiol.* 82, 4006–4016. doi: 10.1128/AEM.00756-16

Hamblin, M. R., and Abrahamse, H. (2019). Can light-based approaches overcome antimicrobial resistance? *Drug Dev. Res.* 80, 48–67. doi: 10.1002/ddr.21453

Hamblin, M. R., and Abrahamse, H. (2020). Oxygen-independent antimicrobial Photoinactivation: type III Photochemical Mechanism?. *Antibiotics* 9:53. doi: 10.3390/antibiotics9020053

Hamblin, M. R., Viveiros, J., Yang, C., Ahmadi, A., Ganz, R. A., and Tolkoff, M. J. (2005). *Helicobacter pylori* accumulates photoactive porphyrins and is killed by visible light. *Antimicrob. Agents Chemother.* 49, 2822–2827. doi: 10.1128/AAC.49.7.2822-2827.2005

Hessling, M., Spellerberg, B., and Hoenes, K. (2017). Photoinactivation of bacteria by endogenous photosensitizers and exposure to visible light of different wavelengths - a review on existing data. *FEMS Microbiol. Lett.* 364:fnw270. doi: 10.1093/femsle/fnw270

Hoenes, K., Wenzel, U., Spellerberg, B., and Hessling, M. (2019). Photoinactivation sensitivity of *Staphylococcus carnosus* to visible-light irradiation as a function of wavelength. *Photochem. Photobiol.* 96, 156–169. doi: 10.1111/php.13168

Huang, Y.-Y., Wintner, A., Seed, P. C., Brauns, T., Gelfand, J. A., and Hamblin, M. R. (2018). Antimicrobial photodynamic therapy mediated by methylene blue and potassium iodide to treat urinary tract infection in a female rat model. *Sci. Rep.* 8:7257. doi: 10.1038/s41598-018-25365-0

Hyun, J.-E., and Lee, S.-Y. (2020). Antibacterial effect and mechanisms of action of 460–470 nm light-emitting diode against *Listeria monocytogenes* and *Pseudomonas fluorescens* on the surface of packaged sliced cheese. *Food Microbiol.* 86:103314. doi: 10.1016/j.fm.2019.103314

Kato, I. T., Prates, R. A., Sabino, C. P., Fuchs, B. B., Tegos, G. P., Mylonakis, E., et al. (2013). Antimicrobial photodynamic inactivation inhibits *Candida albicans* virulence factors and reduces in vivo pathogenicity. *Antimicrob. Agents Chemother.* 57, 445–451. doi: 10.1128/AAC.01451-12

Keshishyan, E. S., Zaporozhtseva, Z. V., Zenina, O. M., and Zrodnikov, V. S. (2015). Photodynamic inactivation of bacteria in vitro under the effect of blue light. *Bull. Exp. Biol. Med.* 158, 475–477. doi: 10.1007/s10517-015-2788-x

Kim, M.-J., and Yuk, H.-G. (2017). Antibacterial Mechanism of 405-Nanometer Light-Emitting Diode against *Salmonella* at Refrigeration Temperature. *Appl. Environ. Microbiol.* 83:e02582-16. doi: 10.1128/AEM.02582-16

Kjeldstad, B., Johnsson, A., and Sandberg, S. (1984). Influence of pH on porphyrin production in *Propionibacterium acnes*. *Arch. Dermatol. Res.* 276, 396–400. doi: 10.1007/BF00413361

Kömerik, N., Wilson, M., and Poole, S. (2000). The effect of photodynamic action on two virulence factors of gram-negative bacteria. *Photochem. Photobiol.* 72, 676–680. doi: 10.1562/0031-865520000720676TEOPAO2.0.CO2

Kumar, A., Ghate, V., Kim, M.-J., Zhou, W., Khoo, G. H., and Yuk, H.-G. (2015). Kinetics of bacterial inactivation by 405nm and 520nm light emitting diodes and the role of endogenous coproporphyrin on bacterial susceptibility. *J. Photochem. Photobiol. B Biol.* 149, 37–44. doi: 10.1016/j.jphotobiol.2015.05.005

Lacombe, A., Niemira, B. A., Sites, J., Boyd, G., Gurtler, J. B., Tyrell, B., et al. (2016). Reduction of bacterial pathogens and potential surrogates on the surface

of almonds using high-intensity 405-Nanometer Light. *J. Food Prot.* 79, 1840–1845. doi: 10.4315/0362-028X.JFP-15-418

Lipovsky, A., Nitzan, Y., Friedmann, H., and Lubart, R. (2009). Sensitivity of *Staphylococcus aureus* strains to broadband visible light. *Photochem. Photobiol.* 85, 255–260. doi: 10.1111/j.1751-1097.2008.00429.x

Lipovsky, A., Nitzan, Y., Gedanken, A., and Lubart, R. (2010). Visible light-induced killing of bacteria as a function of wavelength: implication for wound healing. *Lasers Surg. Med.* 42, 467–472. doi: 10.1002/lsm.20948

Lui, G. Y., Roser, D., Corkish, R., Ashbolt, N. J., and Stuetz, R. (2016). Point-of-use water disinfection using ultraviolet and visible light-emitting diodes. *Sci. Total Environ.* 553, 626–635. doi: 10.1016/j.scitotenv.2016.02.039

Maclean, M., Booth, M. G., Anderson, J. G., MacGregor, S. J., Woolsey, G. A., Coia, J. E., et al. (2013). Continuous decontamination of an intensive care isolation room during patient occupancy using 405 nm light technology. *J. Infect. Prevent.* 14, 176–181. doi: 10.1177/1757177413483646

Maclean, M., MacGregor, S. J., Anderson, J. G., and Woolsey, G. (2008). High-intensity narrow-spectrum light inactivation and wavelength sensitivity of *Staphylococcus aureus*. *FEMS Microbiol. Lett.* 285, 227–232. doi: 10.1111/j.1574-6968.2008.01233.x

Maclean, M., MacGregor, S. J., Anderson, J. G., and Woolsey, G. (2009). Inactivation of bacterial pathogens following exposure to light from a 405-nanometer light-emitting diode array. *Appl. Environ. Microbiol.* 75, 1932–1937. doi: 10.1128/AEM.01892-08

McKenzie, K., Maclean, M., Grant, M. H., Ramakrishnan, P., MacGregor, S. J., and Anderson, J. G. (2016). The effects of 405 nm light on bacterial membrane integrity determined by salt and bile tolerance assays, leakage of UV-absorbing material and SYTOX green labelling. *Microbiology* 162, 1680–1688. doi: 10.1099/mic.0.000350

McKenzie, K., Maclean, M., Timoshkin, I. V., MacGregor, S. J., and Anderson, J. G. (2014). Enhanced inactivation of *Escherichia coli* and *Listeria monocytogenes* by exposure to 405nm light under sub-lethal temperature, salt and acid stress conditions. *Int. J. Food Microbiol.* 170, 91–98. doi: 10.1016/j.ijfoodmicro.2013.10.016

Mulani, M. S., Kamble, E. E., Kumkar, S. N., Tawre, M. S., and Pardesi, K. R. (2019). Emerging strategies to combat ESKAPE Pathogens in the era of antimicrobial resistance: a review. *Front. Microbiol.* 10:539. doi: 10.3389/fmicb.2019.00539

Peterson, J. W. (1996). *Bacterial Pathogenesis*. Texas: University of Texas Medical Branch at Galveston.

Plavskii, V. Y., Mikulich, A. V., Tretyakova, A. I., Leusenka, I. A., Plavskaya, L. G., Kazyuchits, O. A., et al. (2018). Porphyrins and flavins as endogenous acceptors of optical radiation of blue spectral region determining photoinactivation of microbial cells. *J. Photochem. Photobiol. B Biol.* 183, 172–183. doi: 10.1016/j.jphotobiol.2018.04.021

Pourhajibagher, M., Rokn, A. R., Rostami-Rad, M., Barikani, H. R., and Bahador, A. (2018). Monitoring of virulence factors and metabolic activity in Aggregatibacter Actinomycetemcomitans cells surviving Antimicrobial Photodynamic Therapy via Nano-Chitosan Encapsulated Indocyanine Green. *Front. Phys.* 6:124. doi: 10.3389/fphy.2018.00124

Romano, G., Tortora, G., Calusi, S., Orsini, B., Gnerucci, A., and Fusi, F. (2016). Minimally invasive ingestible device to perform anti-bacterial phototherapy in the stomach. *Phys. Med.* 32:215. doi: 10.1016/j.ejmp.2016.07.724

Schmid, J., Hoenes, K., Vatter, P., and Hessling, M. (2019). Antimicrobial Effect of Visible Light-Photoinactivation of *Legionella rubrilucens* by Irradiation at 450, 470, and 620 nm. *Antibiotics* 8:187. doi: 10.3390/antibiotics8040187

Shehatou, C., Logunov, S. L., Dunman, P. M., Haidaris, C. G., and Klubben, W. S. (2019). Characterizing the Antimicrobial Properties of 405 nm Light and the Corning® Light-Diffusing Fiber Delivery System. *Lasers Surg. Med.* 51, 887–896. doi: 10.1002/lsm.23132

Sicks, B., Hönes, K., Spellerberg, B., and Hessling, M. (2020). Blue LEDs in endotracheal tubes may prevent ventilator-associated Pneumonia. *Photobiomodul. Photomed. Laser Surg.* 38, 571–576. doi: 10.1089/photob.2020.4842

Sinclair, R. G., Rose, J. B., Hashsham, S. A., Gerba, C. P., and Haas, C. N. (2012). Criteria for selection of surrogates used to study the fate and control of pathogens in the environment. *Appl. Environ. Microbiol.* 78, 1969–1977. doi: 10.1128/AEM.06582-11

Tang, H. M., Hamblin, M. R., and Yow, C. M. (2007). A comparative in vitro photoinactivation study of clinical isolates of multidrug-resistant pathogens. *J. Infect. Chemother.* 13, 87–91. doi: 10.1007/s10156-006-0501-8

Tomb, R. M., White, T. A., Coia, J. E., Anderson, J. G., MacGregor, S. J., and Maclean, M. (2018). Review of the comparative susceptibility of microbial species to Photoinactivation Using 380-480 nm Violet-Blue Light. *Photochem. Photobiol.* 94, 445–458. doi: 10.1111/php.12883

Tubby, S., Wilson, M., and Nair, S. P. (2009). Inactivation of staphylococcal virulence factors using a light-activated antimicrobial agent. *BMC Microbiol.* 9:211. doi: 10.1186/1471-2180-9-211

Vollmerhausen, T. L., Conneely, A., Bennett, C., Wagner, V. E., Victor, J. C., and O'Byrne, C. P. (2017). Visible and UVA light as a potential means of preventing *Escherichia coli* biofilm formation in urine and on materials used in urethral catheters. *J. Photochem. Photobiol. B Biol.* 170, 295–303. doi: 10.1016/j.jphotobiol.2017.04.018

Wang, Y., Wang, Y., Wang, Y., Murray, C. K., Hamblin, M. R., Hooper, D. C., et al. (2017). Antimicrobial blue light inactivation of pathogenic microbes: state of the art. *Drug Resist. Updates* 3, 1–22. doi: 10.1016/j.drup.2017.10.002

Webb, R. B., and Brown, M. S. (1976). Sensitivity of strains of *Escherichia coli* differing in repair capability to far UV, near UV and visible radiations. *Photochem. Photobiol.* 24, 425–432. doi: 10.1111/j.1751-1097.1976.tb06849.x

World Health Organization (2017). *Global Priority List of Antibiotic-Resistant Bacteria to Guide Research, Discovery, and Development of New Antibiotics*. Available online at: https://www.who.int/medicines/publications/global-priority-list-antibiotic-resistant-bacteria/en/ (accessed September 14, 2020).

Conflict of Interest: The authors declare that the research was conducted in the absence of any commercial or financial relationships that could be construed as a potential conflict of interest.

frontiers in Microbiology

ORIGINAL RESEARCH
published: 14 January 2021
doi: 10.3389/fmicb.2020.616797

The Antibacterial and Antibiofilm Activity of Telithromycin Against *Enterococcus* spp. Isolated From Patients in China

Yanpeng Xiong[1†], Junwen Chen[1†], Xiang Sun[1†], Guangjian Xu[1], Peiyu Li[1], Qiwen Deng[1,2], Zhijian Yu[1,2], Zhong Chen[1,2] and Jinxin Zheng[1,2*]*

[1] Department of Infectious Diseases and Shenzhen Key Laboratory for Endogenous Infections, Shenzhen Nanshan People's Hospital, Shenzhen University of School Medicine, Shenzhen, China, [2] Quality Control Center of Hospital Infection Management of Shenzhen, Shenzhen Nanshan People's Hospital of Guangdong Medical University, Shenzhen, China

OPEN ACCESS

Edited by:
Rodolfo García-Contreras, National Autonomous University of Mexico, Mexico

Reviewed by:
Zhangya Pu, Xiangya Hospital, Central South University, China
Corina-Diana Ceapa, National Autonomous University of Mexico, Mexico

***Correspondence:**
Zhong Chen
cchen17@fudan.edu.cn
Jinxin Zheng
jinxinzheng@fudan.edu.cn

[†]These authors have contributed equally to this work

Specialty section:
This article was submitted to Antimicrobials, Resistance and Chemotherapy, a section of the journal Frontiers in Microbiology

Received: 13 October 2020
Accepted: 14 December 2020
Published: 14 January 2021

Citation:
Xiong Y, Chen J, Sun X, Xu G, Li P, Deng Q, Yu Z, Chen Z and Zheng J (2021) The Antibacterial and Antibiofilm Activity of Telithromycin Against Enterococcus spp. Isolated From Patients in China. Front. Microbiol. 11:616797. doi: 10.3389/fmicb.2020.616797

Telithromycin has been reported to possess robust *in vitro* antibacterial activity against many species of gram-positive bacteria, and telithromycin is also effective against *Staphylococcus aureus* biofilms. However, the *in vitro* antimicrobial susceptibility of telithromycin against clinical enterococci isolates in China is rarely reported and the impacts of telithromycin on the biofilm formation and eradication of enterococci remain elusive. Therefore, this study aimed to explore the inhibitory effects of telithromycin on planktonic cells and biofilms of *Enterococcus* strains. A total of 280 *Enterococcus faecalis* and 122 *Enterococcus faecium* isolates were collected from individual inpatients in China. The 50% minimum inhibitory concentration (MIC_{50}) values of telithromycin against the *E. faecalis* and *E. faecium* strains carrying erythromycin-resistant methylase (*erm*) genes such as the *ermA*, *ermB,* or *ermC*, were 2 and 4 μg/mL, respectively. In addition, these isolates were typed using multilocus sequence typing (MLST) based on housekeeping genes. The predominant sequence types (STs) of *E. faecalis* were ST16, ST30, and ST179, and the main STs of *E. faecium* isolates were ST18, ST78, and ST80. Among these major STs, 87.1% (135/158) of *E. faecalis* and 80.4% (41/51) of *E. faecium* carried *erm* genes. Furthermore, at the subinhibitory concentrations (1/4 and 1/8 × MIC) of telithromycin, the biofilm formation of 16 *E. faecalis* isolates were inhibited by approximately 35%. Moreover, treatment with 8 × MIC of telithromycin or ampicillin led to an almost 40% reduction in the established biofilms of *E. faecalis* isolates, whereas vancomycin or linezolid with 8 × MIC had minimal effects. The combination of telithromycin and ampicillin resulted in an almost 70% reduction in the established biofilms of *E. faecalis*. In conclusion, these results revealed that telithromycin significantly decreased the planktonic cells of both *E. faecalis* and *E. faecium*. In addition, the data further demonstrated that telithromycin has the robust ability to inhibit *E. faecalis* biofilms and the combination of telithromycin and ampicillin improved antibiofilm activity. These *in vitro* antibacterial and antibiofilm activities suggest that telithromycin could be a potential candidate for the treatment of enterococcal infections.

Keywords: telithromycin, *Enterococcus faecalis*, *Enterococcus faecium*, erythromycin-resistance, MIC, MLST, biofilm

INTRODUCTION

Enterococci are gram-positive cocci which are commonly found in the gastrointestinal tracts of nearly all land animals, including humans (Fiore et al., 2019). Although a core member of the microbiome, enterococci are capable of resulting in various infectious diseases, such as urinary tract infections, wound infections, intra-abdominal and pelvic regions infections, and bloodstream infections (Murray and Weinstock, 1999; Richards et al., 2000; Mohamed and Huang, 2007). Enterococci are now the third most common nosocomial pathogen. Statistics showed that enterococci caused almost 15% of hospital-acquired infections in the United States between 2011 and 2014 (Weiner et al., 2016), an increase of 12% from 2006 to 2007 (Hidron et al., 2008). In addition, enterococci are also responsible for 5–20% of cases of infective endocarditis (Megran, 1992). *Enterococcus faecalis*, the most common species of *Enterococcus* in the clinical setting, causes 85 to 90% of human enterococcal infections, while *Enterococcus faecium* is responsible for 5 to 10% of the remainder (Jett et al., 1994; Jones et al., 2004). Because *E. faecalis* and *E. faecium* usually carry a range of intrinsic and acquired resistance genes, these *Enterococcus* strains are frequently resistant to many commonly used antibiotics, such as glycopeptides (vancomycin and teicoplanin), beta-lactams (ampicillin, penicillin), aminoglycoside (gentamicin or streptomycin), and macrolides (van Harten et al., 2017; Ch'ng et al., 2019). Of note, the widespread emergence of vancomycin-resistant enterococci (VRE) has caused further concern due to the high mortality rate (Eliopoulos, 1997). In 2013, almost 70% of clinical *E. faecium* isolates in the United States displayed vancomycin resistance, while this was up to 20% in Europe (Mendes et al., 2016). In contrast, *E. faecalis* isolates are less frequently resistant to vancomycin (<10%) (Sievert et al., 2013).

Besides antibiotic resistance, enterococci are also known for their ability to form biofilms which is a population of cells growing on a surface and surrounded by a matrix of macromolecules like polysaccharides, proteins, lipids, and extracellular DNA (Jakubovics and Burgess, 2015). The term biofilm was introduced into medicine in 1982 by Costerton as *Staphylococcus aureus* biofilms were observed on a cardiac pacemaker lead (Marrie et al., 1982). Bacteria that are not innately resistant to antibiotics can also become resistant by forming persistent biofilms that lead to chronic infections (Lebeaux et al., 2014). In today's healthcare environment, the diversity of biofilm-associated infections has risen with time, it is suggested that biofilms are present in more than 65% of all bacterial infections (Costerton et al., 1999; Lewis, 2001). Especially, due to a sharp increase in the number of patients receiving implanted medical devices in recent years, the rates of infection are 40% for ventricular assist devices, 10% for ventricular shunts, and 4% for mechanical heart valves, pacemakers, and defibrillators (Darouiche, 2004). Biofilms serve as a new nidus for bacterial dissemination and as a reservoir for antimicrobials resistant genes. Additionally, biofilms protect bacteria from detergent solutions, antimicrobial agents, environmental stress, and effectively make bacteria 10 to 1000-fold more resistant to antibiotic treatment, making their eradication extremely difficult (Lewis, 2001). Therefore, biofilm infections are becoming increasingly difficult to effectively treat due to the decreasing efficacy of antibiotics (Paganelli et al., 2012; van Harten et al., 2017). Enterococci frequently cause biofilm-associated infections such as catheter-related bloodstream infections, urinary tract infections, and infective endocarditis (Arias and Murray, 2012). Among *Enterococcus* species, *E. faecalis* isolates usually have a higher capacity of producing biofilms than *E. faecium* isolates and the prevalence of *E. faecalis* biofilms varies in different regions (Mohamed and Huang, 2007). For example, in Sardinia, biofilm production was identified among 87% of *E. faecalis* clinical isolates and 16% of *E. faecium* clinical isolates (Duprè et al., 2003). In Rome, 80% of *E. faecalis* and 48% of *E. faecium* isolates from infected patients were able to form biofilms (Baldassarri et al., 2001). Other study showed similar results and indicated that *E. faecalis* (95%) isolates produced biofilms more often than *E. faecium* (29%) (Di Rosa et al., 2006). In contrast with planktonic cells, biofilm-embedded enterococci are involved in multidrug resistance and may even be untreatable with conventional antibiotics (Lewis, 2001). Therefore, there is an urgent need to identify novel treatments for enterococcal infections.

Telithromycin (HMR 3647), a semi-synthetic derivative of erythromycin, belongs to a new chemical class of antibiotics called ketolides that have been added to the macrolide-lincosamide-streptogramin class of antibiotics (Douthwaite and Champney, 2001). Telithromycin has been approved by the U.S. Food and Drug Administration (FDA) to treat several infectious diseases, such as community-acquired pneumonia, acute exacerbations of chronic bronchitis, and acute maxillary sinusitis (Nguyen and Chung, 2005). The antimicrobial action of telithromycin, and probably that of the other 14-member-ring macrolides, is compounded by binding to 23S rRNA and blocking protein synthesis at the early stages (Menninger, 1995). Macrolides resistance is dominantly explained by the prevalence of *erm* genes in a wide spectrum of gram-positive bacteria (Westh et al., 1995). *erm* gene classes can encode a series of methyltransferase that specifically methylate the N-6 position of adenosine 2058 (A2058) or neighboring nucleotides in domain V of 23S rRNA within the large ribosomal subunit (Weisblum, 1995; Vester and Douthwaite, 2001), this prevents interaction with macrolides. In addition, erythromycin-resistant enterococci often exhibit macrolide-lincosamide-streptogramin B (MLSB) antibiotic resistance phenotypes due to the presence of *erm* genes. However, compared with MLSB antibiotics like erythromycin, telithromycin has an additional target site at position A752 in domain II of 23S rRNA. U747 methylation promotes G748 methylation, resulting in the increased binding of telithromycin to ribosomes and enhanced telithromycin susceptibility (Shoji et al., 2015). Telithromycin has been found to conquer *erm*-mediated resistance in *S. pneumonia*

Abbreviations: AMP, ampicillin; CIP, ciprofloxacin; DOX, doxycycline; ERY, erythromycin; LZD, linezolid; MICs, minimum inhibitory concentrations; MIN, minocycline; MLST, multilocus sequence type; NIT, nitrofurantoin; PCR, polymerase chain reaction; STs, sequence types; TEC, tetracycline; TED, tedizolid; TEL, telithromycin; TET, tetracycline; VAN, vancomycin.

and *S. aureus* (Van Laethem and Sternon, 2003; Sun et al., 2018), and it also showed less efficacy against erythromycin-resistant *Enterococcus* isolates from different regions (TEL, MIC ≥ 4 μg/mL) (Singh et al., 2000; Min et al., 2011). However, the antimicrobial impacts of telithromycin on *Enterococcus* carrying *erm* genes remain less clear in China. Moreover, a previous study reported that telithromycin exhibited effective antibiofilm activity against *S. aureus in vitro* (Zheng et al., 2020). Therefore, the effect of telithromycin on *Enterococcus* biofilms should be further investigated.

In this study, the *in vitro* antibacterial activity of telithromycin was tested against enterococcal clinical isolates from inpatients in Shenzhen Nanshan People's Hospital, and then the antibacterial activity of telithromycin was further compared with that of other antimicrobials. In addition, the multilocus sequence types (MLSTs) and *erm* genes expression in enterococci were detected by PCR assay. Moreover, the effect of telithromycin on the biofilms of *E. faecalis* isolates was further explored.

MATERIALS AND METHODS

Bacterial Isolates and Growth Conditions

A total of 280 *E. faecalis* and 122 *E. faecium* strains were isolated from individual patients at Shenzhen Nanshan People's Hospital from 2011 to 2015. Bacterial isolates were determined by standard methods using a VITEK 2 system (Biomérieux, Marcy l'Etoile, France). *E. faecalis* ATCC 29212 and OG1RF (ATCC 47077) were tested as quality control strains. The isolates were cultured overnight in tryptic soy broth (TSB) (Oxoid, Basingstoke, United Kingdom) at 37°C with a shaker at 220 rpm. Telithromycin (TEL), erythromycin (ERY), ampicillin (AMP), vancomycin (VAN), tetracycline (TET), doxycycline (DOX), minocycline (MIN), ciprofloxacin (CIP), nitrofurantoin (NIT), linezolid (LZD), tedizolid (TED), and tetracycline (TEC) were purchased from MCE (Princeton, NJ, United States).

Antimicrobials Susceptibility Testing

Antimicrobial susceptibilities of *Enterococcus* to several clinical antibiotics, including TEL, ERY, AMP, VAN, TET, DOX, MIN, CIP, NIT, LZD, TED, and TEC were tested with the VITEK 2 system. The MICs of AMP, VAN, TEL, and ERY were determined by the broth macrodilution method in cation-adjusted Mueller-Hinton broth (CAMHB) according to the 2019 Clinical and Laboratory Standards Institute (CLSI) guidelines[1]. The isolates were cultured overnight in TSB at 37°C with a shaker at 220 rpm, then the strains were diluted at 1:200 [2.0–3.0 × 10^7 colony-forming units (CFU) ml^{-1}], and inoculated into 96 polystyrene microtiter plates with 200 μL of CAMHB containing the indicated concentrations of antibiotics. As the MIC breakpoint of telithromycin against enterococci has not been established, the MIC value of telithromycin against *S. aureus* (≤1, 2, ≥4 μg/mL) was based on the 2019 CLSI guidelines. Four MIC levels were thus employed for telithromycin in the antimicrobial susceptibility analysis (≤1, 2, 4, ≥8 μg/mL). The used concentrations of indicated antibiotics are given in the figure legends and **Supplementary Table 4**. All experiments were performed at least three times.

Detection of ERY Resistance Genes

DNA was extracted from all clinical enterococcal isolates with lysis buffer as templates for PCR according to the manufacturer's instructions (Takara Bio Inc., Japan). As described previously (Bai et al., 2018), PCR analysis was performed to detect *ermA*, *ermB*, and *ermC* genes, and the primers used for PCR amplification were as follows:

ermA: sense: 5′- TCTAAAAAGCATGTAAAAGAAA-3′ and antisense: 5′- CGATACTTTTTGTAGTCCTTC-3′; *ermB*: sense: 5′-CCGTTTACGAAATTGGAACAGGTAAAGGGC-3′ and antisense: 5′-GAATCGAGACTTGAGTGTGC-3′; *ermC*: sense: 5′-GCTAATATTGTTTAAATCGTCAATTCC-3′ and antisense: 5′- GGATCAGGAAAAGGACATTTTAC -3′.

Multilocus Sequence Type

The genotypes of the enterococcal isolates were analyzed by MLST. Seven pairs of housekeeping genes: *gdh, gyd, pstS, gki, aroE, xpt,* and *yqiL* for *E. faecalis,* and *atpA, ddl, gdh, purK, gyd, pstS,* and *adk* for *E. faecium* were amplified by PCR. As previously reported (Zheng et al., 2017), the purified PCR products were sequenced, and the results were submitted to the MLST database[2] for comparison, and the sequence types (STs) of enterococci were determined. The primers used for PCR amplification are listed in **Supplementary Tables 5, 6**.

Inhibition and Eradication of *E. faecalis* Biofilms

A detailed protocol has been previously reported (Zheng et al., 2020). As for the inhibition experiments, *E. faecalis* isolates were cultured overnight in TSB at 37°C with a shaker at 220 rpm, then the strains were diluted at 1:200 [2.0–3.0 × 10^7 colony-forming units (CFU) ml^{-1}], and inoculated into 96 polystyrene microtiter plates with 200 μL of TSBG (TSB with 0.5% glucose) containing the indicated concentration of antibiotics. TSBG without antimicrobials was used as an untreated control. After incubation for 24 h, the biofilm biomasses were washed three times with ddH_2O before and after crystal violet staining, the stained biofilms were detected by optical density (OD_{570}). Solithromycin was used as a positive control (Wang et al., 2020). As for the eradication assays of the established biofilms, *E. faecalis* isolates were cultivated in tryptic TSB medium at 37°C for 24 h to form matured biofilms, then they were treated with antimicrobials (8 × MIC) for 48 h with the medium replaced daily. TSBG without antimicrobials was used as an untreated control. Biofilm biomasses were stained and then detected. The used concentrations of indicated antibiotics are given in the figure legends and **Supplementary Table 4**. All data are representative of three independent experiments.

[1]https://eucast.org/clinical_breakpoints/

[2]http://efaecalis.mlst.net/ and http://efaecium.mlst.net/

Detecting the Adherent Cells in the Established Biofilms

The adherent cells in the established biofilms of *E. faecalis* were identified by the CFU numbers as described previously (Zheng et al., 2019). Briefly, the *E. faecalis* isolates were inoculated into 24 polystyrene microtiter plates with TSBG and formed mature biofilms after 24 h of static incubation. The supernatant was discarded and plates were washed, fresh TSBG containing antimicrobials was added, and TSBG without antimicrobials was used as an untreated control. After 48 h of static incubation with the medium being replaced daily, the supernatant was discarded and the remaining adherent cells in the established biofilms were collected by scratching the wall of the wells with a flat end toothpick. Finally, the bacteria were centrifuged and the numbers of CFU were determined. The used concentrations of indicated antibiotics were given in the figure legends and **Supplementary Table 4**. All data are representative of three independent experiments.

Time-Kill Curve Assay

Two *E. faecalis* 16C3 and 16C6 isolates were cultured in TSB at 37°C for 16 h, then diluted 200 times with TSB and antibiotics were added to make the final concentrations at 4 × MIC. A colony count was performed after 0, 1, 3, and 24 h. Data are representative of three independent experiments.

Statistical Analysis

The SPSS software (version 19.0) and GraphPad Prism software (version 5.0) were used for statistical analysis. For multiple comparisons, one-way analysis of variance (ANOVA) and a *post hoc*-Dunnett test were applied to analyze the data. All experiments were repeated at least three times. Sample size, n, for each experiment is given in the figure legends. Results are shown as mean ± SEM. Value differences were considered significant when $^{*}p < 0.05$ (not significant $p > 0.05$, $^{**}p < 0.01$, $^{***}p < 0.001$).

RESULTS

In vitro Antibacterial Activity of Telithromycin Against Enterococci Isolates

Enterococcus faecalis isolates ($n = 280$) and *E. faecium* isolates ($n = 122$) were retrospectively collected from different clinical specimens in China, including urine, wound secretions, blood, bile, phlegm, and other sources (**Supplementary Figures 1A,B**). The *in vitro* antibacterial activity of telithromycin against clinical isolates of *E. faecalis* and *E. faecium* are summarized in **Tables 1**, **2**. As expected, these clinical isolates of enterococci showed a high frequency of resistance to erythromycin (ERY, MIC ≥ 8 μg/mL) and some commonly used tetracycline antibiotics, including tetracycline (TET, MIC ≥ 16 μg/mL), doxycycline (DOX, MIC ≥ 16 μg/mL), and minocycline (MIN, MIC ≥ 16 μg/mL), whereas they remained highly susceptible to vancomycin (VAN, MIC ≤ 4 μg/mL), nitrofurantoin (NIT, MIC ≤ 32 μg/mL), and linezolid (LZD, MIC ≤ 2 μg/mL).

In addition, as shown in **Tables 1**, **2**, both *E. faecalis* and *E. faecium* isolates had a high MIC_{50}/MIC_{90} (the MIC values for 50% or 90% of bacterial growth inhibition) of ERY (>256/>256 μg/mL). However, the MIC_{50}/MIC_{90} values of telithromycin against the *E. faecalis* and *E. faecium* strains were 2/8 μg/mL and 4/8 μg/mL, respectively. Moreover, 75.7% (212/280) of *E. faecalis* isolates were shown with ERY MIC ≥ 8 μg/mL, whereas only 11.8% (33/280) of *E. faecalis* isolates were shown with telithromycin MIC ≥ 8 μg/mL (**Table 1**). Similarly, among 122 *E. faecium* isolates, 85.2% (104/122) of strains had a high resistance to ERY (MIC ≥ 8 μg/mL), whereas 40% (49/122) of strains were shown with telithromycin MIC ≥ 8 μg/mL (**Table 2**), suggesting that *Enterococcus* isolates were more susceptible to telithromycin than ERY. Interestingly, it was found that there was a high susceptibility rate of 99.6% (274/275) for *E. faecalis* isolates toward ampicillin (MIC ≤ 8 μg/mL), whereas there was a high resistant rate of 87.5% (98/112) for *E. faecium* isolates to ampicillin (MIC ≥ 16 μg/mL). These results indicate that the antibacterial activity of telithromycin against *Enterococcus* was better than that of ERY.

Telithromycin Against the *Enterococcus* Clinical Isolates Harboring *erm* Genes

Next, this study further examined the effects of *E. faecalis* and *E. faecium* isolates carrying *erm* genes on the sensitivity of telithromycin. At first, the presence of *ermA*, *ermB,* or *ermC* in *Enterococcus* isolates was detected by PCR assays. As shown in **Table 3**, the rates of *E. faecalis* strains harboring *ermA* and *ermB* genes were 3.9 and 67.1%, respectively. However, there were no *ermC*-positive *E. faecalis* isolates. Additionally, among 122 *E. faecium* isolates, the rates of *E. faecium* isolates carrying *ermA*, *ermB,* and *ermC* gene were 9.8, 32.8, and 45.9%, respectively (**Table 4**). Furthermore, telithromycin MIC_{50}/MIC_{90} values of *ermA* and *ermB*-positive *E. faecalis* strains or *E. faecium* strains both were 4/8 μg/mL, and *ermC*-positive *E. faecium* strains had a telithromycin MIC_{50}/MIC_{90} of 8/8 μg/mL (**Tables 3**, **4**). As mentioned, the MIC_{50}/MIC_{90} values of telithromycin against *E. faecalis* and *E. faecium* strains were 2/8 and 4/8 μg/mL, respectively (**Tables 1**, **2**), suggesting that the presence of *erm* genes slight impacted telithromycin susceptibility in the *Enterococcus* isolates.

Relationship Between Telithromycin MICs Distribution and ST Clonality

Subsequently, MLST was performed to determine the ST distribution of *E. faecalis* and *E. faecium* isolates. As shown in **Supplementary Tables 1, 2**, ST16, ST30, and ST179 were the predominant STs in 44 STs detected from *E. faecalis* isolates. In total, 25 STs were identified in *E. faecium* isolates, the main STs were ST18, ST78, and ST80. In addition, the relationships between telithromycin and ERY MICs distributions in the predominant ST isolates are shown in **Tables 5**, **6**. The data indicated that *E. faecalis* with telithromycin MIC ≤ 1, 2, 4,

TABLE 1 | *In vitro* antibacterial activity of TEL compared with that of various antibiotics against *E. faecalis* isolates.

Antibiotic	No. isolates	Resistance rate (%)	MIC (μg/mL) breakpoints	NO.	TEL MIC (μg/mL)						ERY MIC (μg/mL)			
					≤0.5	1	2	4	≥8	MIC_{50}/MIC_{90}	≤0.5	1–4	≥8	MIC_{50}/MIC_{90}
Total	280	–	–	–	116	7	27	97	33	2/8	10	58	212	>256/>256
Ampicillin	275	0.4	≤8	274	130	6	26	83	29	2/8	8	55	211	>256/>256
			≥16	1	0	0	0	1	0	4/4	0	0	1	–
Vancomycin	280	0	≤4	278	115	7	27	96	33	2/8	10	58	210	>256/>256
			8–16	2	1	0	0	1	0	0.125/4	0	0	2	>256/>256
			≥32	0	0	0	0	0	0	–	0	0	0	–
Tetracycline	276	83.7	≤4	39	33	3	1	2	0	0.06/1	7	17	15	4/>256
			8	6	3	0	0	2	1	0.06/4	1	1	4	128/>256
			≥16	231	79	4	25	91	32	4/8	2	39	190	>256/>256
Doxycycline	280	78.9	≤4	40	36	1	2	1	0	0.06/0.125	7	19	14	2/>256
			8	19	7	2	3	6	1	2/4	1	2	16	128/>256
			≥16	221	73	4	22	90	32	4/8	2	37	182	>256/>256
Minocycline	280	73.2	≤4	43	37	2	2	2	0	0.06/2	7	21	15	2/>256
			8	32	11	0	9	9	3	2/4	1	5	26	>256/>256
			≥16	205	68	5	16	86	30	4/8	2	32	171	>256/>256
Ciprofloxacin	252	26.6	≤1	151	68	3	11	51	18	2/8	5	25	121	>256/>256
			2	34	22	1	2	8	1	0.125/4	1	12	21	128/>256
			≥4	67	24	3	14	20	6	2/8	2	12	53	>256/>256
Nitrofurantoin	254	1.2	≤32	247	102	6	26	84	29	2/8	9	52	186	>256/>256
			64	4	2	0	0	2	0	0.5/4	0	0	4	>256/>256
			≥128	3	3	0	0	0	0	0.03/0.25	0	2	1	4/>128
Linezolid	280	5.4	≤2	214	87	6	21	75	25	2/8	9	44	161	>256/>256
			4	51	23	1	6	17	4	2/4	1	11	39	>256/>256
			≥8	15	6	0	0	5	4	4/8	0	3	12	>256/>256

MIC, minimum inhibitory concentration; TEL, telithromycin; ERY, erythromycin; MIC_{50}/MIC_{90}, the MIC values for 50% or 90% of bacterial growth inhibition.

≥8 μg/mL accounted for 26.6% (42/158), 9.5% (15/158), 47.5% (75/158), 16.4% (26/158) and that the rates of *E. faecium* isolates with telithromycin MIC ≤ 1, 2, 4, ≥8 μg/mL were 15.7% (8/51), 2% (1/51), 23.5% (12/51), 58.8% (30/51), respectively. However, the ERY-resistant rates of *E. faecalis* and *E. faecium* isolates with the top three STs reached 98.7% (156/158) and 94.1% (48/51), respectively. Moreover, among the predominant STs isolates, 87.1% (135/158) of *E. faecalis* and 80.4% (41/51) of *E. faecium* were shown alongside the *erm* genes carriage (**Tables 5**, **6**), demonstrating clonal clustering toward these predominant STs.

The Effects of Telithromycin Against Biofilm Formation and Eradication of *E. faecalis* Clinical Isolates

Many studies have demonstrated that *E. faecalis* isolates have a higher capacity of producing biofilms than *E. faecium* (Duprè et al., 2003; Sandoe et al., 2003; Zheng et al., 2017), thus *E. faecalis* isolates are usually chosen for biofilm analysis. Among our 280 *E. faecalis* isolates, 16 *E. faecalis* isolates showed a higher biofilm-forming ability, these specific 16 strains were thus tested for biofilm formation. The isolation sites of the 16 *E. faecalis* strains are listed in **Supplementary Table 3**. The inhibitory effect of telithromycin on the biofilm formation of these 16 *E. faecalis* isolates was determined by crystal violet staining. The MIC values of AMP, VAN, LZD, and telithromycin against these isolates are listed in **Supplementary Table 4**. As shown in **Figure 1**, 1/2 × MIC, 1/4 × MIC, or 1/8 × MIC of telithromycin could inhibit the biofilm formation of the 16 *E. faecalis* isolates.

Finally, to dissect the effect of telithromycin on the established biofilms of *E. faecalis* isolates. Here, eight specific *E. faecalis* isolates were chosen for analysis by crystal violet staining. As shown in **Figures 2A,B**, the established biofilms of *E. faecalis* reduced by almost 40% after treatment with 8 × MIC of telithromycin or ampicillin, whereas 8 × MIC of vancomycin or linezolid only showed slight effects. Due to the high susceptibility rate of the *E. faecalis* isolates toward ampicillin (**Table 1**), the effects of telithromycin combined with ampicillin on the established biofilms of these eight *E. faecalis* isolates were further evaluated. The data showed that the combination of telithromycin and ampicillin resulted in an approximate 70% reduction in the established biofilms than with telithromycin or ampicillin alone (**Figures 2C,D**). Additionally, a colony-forming unit (CFU) assay was performed to quantify the viable cells of the established biofilms. Consistently, the data further confirmed that telithromycin combined with ampicillin could kill more than 70% of adherent cells in the established biofilms than telithromycin or ampicillin alone (**Figures 2E,F**). Therefore, these results suggest that the combination of telithromycin and ampicillin is an effective way to reduce the established biofilms in the *E. faecalis* isolates.

TABLE 2 | *In vitro* antibacterial activity of TEL compared with that of various antibiotics against *E. faecium* isolates.

Antibiotic	No. isolates	Resistance rate (%)	MIC (μg/mL) breakpoints	No.	TEL MIC (μg/mL)						ERY MIC (μg/mL)			
					≤0.5	1	2	4	≥8	MIC_{50}/MIC_{90}	≤0.5	1–4	≥8	MIC_{50}/MIC_{90}
Total	122	–	–	–	25	2	12	34	49	4/8	6	12	104	>256/>256
Ampicillin	112	87.5	≤8	14	11	0	0	3	0	0.06/4	1	6	7	8/>128
			≥16	98	13	2	12	29	42	4/8	5	6	87	>128/>256
Vancomycin	120	0.0	≤4	116	23	2	12	31	48	4/8	6	11	99	128/>256
			8–16	4	2	0	0	2	0	0.06/4	0	1	3	8/>256
			≥32	0	0	0	0	0	0	–	0	0	0	–
Teicoplanin	115	0.9	≤8	114	24	2	12	33	43	4/8	6	12	96	>128/>256
			16	0	0	0	0	0	0	–	0	0	0	–
			≥32	1	0	0	0	0	1	8	0	0	1	>256/>256
Tetracycline	119	46.2	≤4	45	11	1	1	16	16	4/8	1	6	38	>128/>256
			8	19	3	0	1	3	12	8/8	2	0	17	>256/>256
			≥16	55	10	1	10	14	20	4/8	3	5	47	>256/>256
Doxycycline	120	38.3	≤4	62	15	1	4	22	20	4/8	4	8	50	>128/>256
			8	12	1	0	4	1	6	4/8	0	0	12	>256/>256
			≥16	46	9	1	4	8	24	8/8	2	4	40	>128/>256
Minocycline	120	27.5	≤4	66	16	1	4	22	23	4/8	4	8	54	>128/>256
			8	21	3	1	6	4	7	2/8	1	1	19	>256/>256
			≥16	33	6	0	2	7	18	8/8	1	3	29	>128/>256
Ciprofloxacin	113	9.7	≤1	29	10	1	7	8	3	2/4	1	5	23	>256/>256
			2	4	1	0	0	1	2	4/8	1	0	3	>256/>256
			≥4	80	13	1	5	24	37	4/8	3	7	70	>128/>256
Nitrofurantoin	114	57.0	≤32	11	2	0	3	2	4	4/8	1	1	9	>256/>256
			64	38	6	1	5	12	14	4/8	1	4	33	>256/>256
			≥128	65	16	1	4	18	26	4/8	4	7	54	>128/>256
Linezolid	122	2.4	≤2	116	22	2	12	32	48	4/8	6	10	100	>128/>256
			4	3	2	0	0	1	0	0.06/4	0	1	2	8/>256
			≥8	3	1	0	0	1	1	4/8	0	1	2	>256/>256

MIC, minimum inhibitory concentration; TEL, telithromycin; ERY, erythromycin; MIC_{50}/MIC_{90}, the MIC values for 50% or 90% of bacterial growth inhibition.

TABLE 3 | *In vitro* activity of TEL against *E. faecalis* isolates with ERY-specific resistant genes.

Erythromycin resistance genes		No. (%)	TEL MIC (μg/mL)						ERY MIC (μg/mL)			
			≤0.5	1	2	4	≥8	MIC_{50}/MIC_{90}	≤0.5	1–4	≥8	MIC_{50}/MIC_{90}
Total		280	116	7	27	97	33	2/8	10	58	212	>256/>256
ermA	+	11 (3.9)	1	0	0	6	4	4/8	0	0	11	>256/>256
	–	269 (96.1)	115	7	27	91	29	2/8	10	58	201	>256/>256
ermB	+	188 (67.1)	39	4	23	92	30	4/8	1	8	179	>256/>256
	–	92 (32.9)	77	3	4	5	3	0.06/2	9	50	33	2/>256
ermC	+	0 (0)	0	0	0	0	0	–	0	0	0	–
	–	280 (100)	116	7	27	97	33	2/8	10	58	212	>256/>256

MIC, minimum inhibitory concentration; TEL, telithromycin; ERY, erythromycin; +, positive; –, negative; MIC_{50}/MIC_{90}, the MIC values for 50% or 90% of bacterial growth inhibition.

DISCUSSION

Enterococci species are commensal bacteria in the human gastrointestinal tract with the ability to cause various nosocomial infections. They not only have multiple inherent antimicrobial resistances, but are also able to acquire mutations and/or new resistance genes (Cetinkaya et al., 2000; Raza et al., 2018). Telithromycin, a novel ketolide antimicrobial agent, can be utilized for the treatment of respiratory infections. It retains its activity against most macrolide-resistant strains of *Streptococcus pneumoniae* and *Streptococcus pyogenes* (Spiers and Zervos, 2004; Wolter et al., 2008; Togami et al., 2009; Uzun et al., 2014). In addition, the efficacy of telithromycin against *Enterococcus* has been studied worldwide (Baltch et al., 2001; Bonnefoy et al., 2001; Mensa et al., 2003; Min et al., 2011), and it has been proven to be more effective against enterococci

TABLE 4 | *In vitro* activity of TEL against *E. faecium* isolates with ERY-specific resistant genes.

Erythromycin resistance genes		No. (%)	TEL MIC (μg/mL)						ERY MIC (μg/mL)			
			≤0.5	1	2	4	≥8	MIC_{50}/MIC_{90}	≤0.5	1–4	≥8	MIC_{50}/MIC_{90}
Total		122	25	2	12	34	49	4/8	6	12	104	≥0.25–256
ermA	+	12 (9.8)	2	0	2	3	5	4/8	0	2	10	128/>256
	−	110 (90.2)	23	2	10	31	44	4/8	6	10	94	>128/>256
ermB	+	40 (32.8)	2	0	3	21	14	4/8	0	2	38	128/>256
	−	82 (67.2)	23	2	9	13	35	4/8	6	10	66	>128/>256
ermC	+	56 (45.9)	5	2	7	10	32	8/8	0	1	55	>256/>256
	−	66 (54.1)	20	0	5	24	17	4/8	6	11	49	>128/>256

MIC, minimum inhibitory concentration; TEL, telithromycin; ERY, erythromycin; +, positive; −, negative; MIC_{50}/MIC_{90}, the MIC values for 50% or 90% of bacterial growth inhibition.

TABLE 5 | TEL MIC values of predominant STs in *E. faecalis* isolates with the *ermB* gene.

ST	No. (%)	TEL MIC (μg/mL)						ERY MIC (μg/mL)				*ermB*
		≤0.5	1	2	4	≥8	MIC_{50}/MIC_{90}	≤0.5	1–4	≥8	MIC_{50}/MIC_{90}	
ST16	78 (27.9)	18	3	9	36	12	4/8	0	6	72	>256/>256	67
ST30	8 (2.9)	7	0	1	0	0	0.125/2	0	2	6	128/>256	6
ST179	72 (25.7)	14	0	5	39	14	4/8	2	7	63	>256/>256	62

MIC, minimum inhibitory concentration; TEL, telithromycin; ERY, erythromycin; MIC_{50}/MIC_{90}, the MIC values for 50% or 90% of bacterial growth inhibition.

TABLE 6 | TEL MIC values of predominant STs in *E. faecium* isolates carrying the *ermB* and *ermC* genes.

ST	No. (%)	TEL MIC (μg/mL)						ERY MIC (μg/mL)				*ermB*	*ermC*
		≤0.5	1	2	4	≥8	MIC_{50}/MIC_{90}	≤0.5	1–4	≥8	MIC_{50}/MIC_{90}		
ST18	18 (12.3)	3	0	0	0	15	8/8	0	1	17	>256/>256	1	17
ST78	26 (21.3)	4	1	0	9	12	4/8	3	1	22	128/>256	16	3
ST80	7 (5.7)	0	0	1	3	3	4/8	0	0	7	>128/>128	4	0

MIC, minimum inhibitory concentration; TEL, telithromycin; ERY, erythromycin; MIC_{50}/MIC_{90}, the MIC values for 50% or 90% of bacterial growth inhibition.

than some of first- and second-generation macrolides. For instance, telithromycin was found to be more potent against enterococci than erythromycin in a mouse peritonitis model (Singh et al., 2000). The MIC_{50}/MIC_{90} of telithromycin were 8/32 μg/mL against vancomycin-resistance enterococci strains, whereas erythromycin and clarithromycin were completely inactive (Hamilton-Miller and Shah, 1998). In this study, the MIC_{50}/MIC_{90} of ERY were >256/>256 μg/mL, and the resistance rate of ERY reached more than 75% in both *E. faecalis* and *E. faecium* isolates (**Tables 1**, **2**). However, the MIC_{50}/MIC_{90} of telithromycin in *E. faecalis* and *E. faecium isolates* were found to be as low as 2/8 and 4/8 μg/mL, respectively (**Tables 1**, **2**). This study thus delineated additional evidence to support the fact that telithromycin could be a promising antimicrobial drug for use against enterococci. Of note, the majority of clinical *E. faecalis* isolates remain susceptible to β-lactams which are inhibitors of cell wall synthesis, and time-kill curve studies demonstrated that telithromycin (4 × MIC) combined with ampicillin (4 × MIC) could kill more than 100 times more planktonic cells in comparison to telithromycin or ampicillin alone in two *E. faecalis* isolates (**Supplementary Figures 2A,B**), suggesting that the combination of telithromycin and ampicillin could improve bactericidal activities against *E. faecalis*.

Ever since erythromycin has been clinically applied, the MLSB resistance phenotype has been widely found in erythromycin-resistant isolates of many bacteria species. For instance, Weisblum B et al. demonstrated that erythromycin-resistant *S. aureus* was related to the MLSB resistance phenotype after the clinical application of erythromycin (Weisblum and Demohn, 1969). This MLSB phenotype was determined by the *erm* genes producing erythromycin-resistant methylases, which induced methylation at specific adenosine residues on the 23S rRNA, thus leading to the resistance of the newly synthesized ribosome to MLSB antibiotics (Westh et al., 1995; Ackermann and Rodloff, 2003). Previous studies have described that the emergence of high-level erythromycin resistance narrowed the clinical application of macrolides and their application might result in a poor prognosis, more severe recurrence, and higher mortality for the treatment of bacterial infections (Min et al., 2011; Celik et al., 2014). While the chemical structure of telithromycin is derived from erythromycin, telithromycin has a low potential for drug-drug interaction, and is less likely to induce MLSB

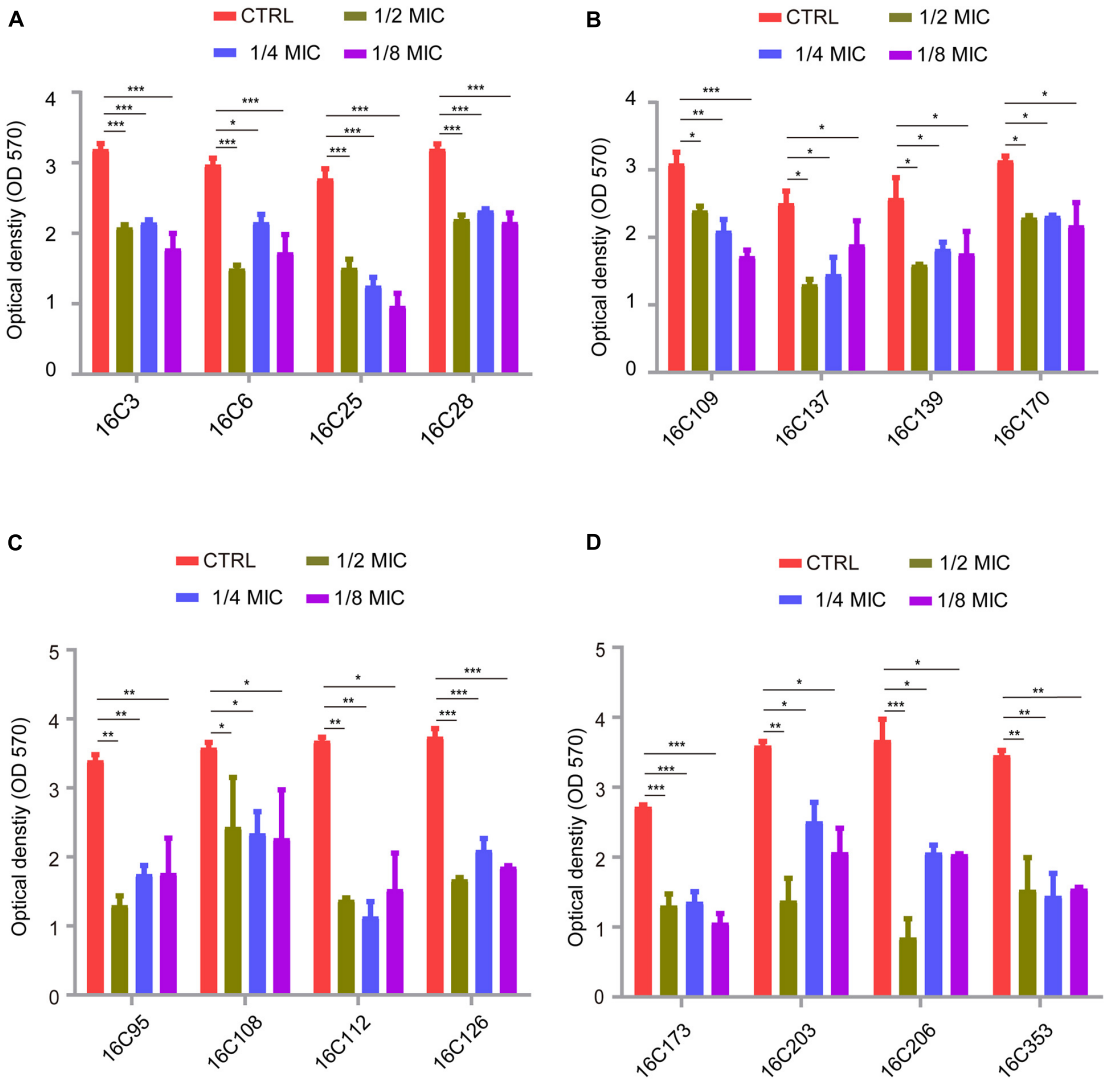

FIGURE 1 | Telithromycin inhibiting biofilm formation of 16 *E. faecalis* isolates. **(A,B)** The four isolates per group were treated with TEL at 1/2 ×, 1/4 ×, and 1/8 × MICs, respectively. All of the eight isolates with the TEL MIC at 8 μg/mL. **(C,D)** The eight isolates of the two groups were treated with TEL at 1/2 ×, 1/4 ×, and 1/8 × MICs. The MICs were 0.25, 0.5, 0.125, 0.125, 0.5, 0.125, 0.25, and 0.25 μg/mL, respectively. TSBG without antimicrobials was used as an untreated control. The data were presented as the mean ± SEM ($n = 3$ experiments), one-way analysis of variance (ANOVA), and a *post hoc*-Dunnett test, $^{*}p < 0.05$, $^{**}p < 0.01$, $^{***}p < 0.001$, compared with the CTRL group.

resistance than macrolides with a 14- or 15-member ring (Benes, 2004). In this study, the *ermA* and *ermB* genes were found in ERY-resistant isolates of *E. faecalis*, and *ermA*, *ermB,* and *ermC* genes were detected in *E. faecium* isolates (**Tables 3**, **4**). However, telithromycin remained active against enterococci with *erm* genes. Recombination is involved in the genetic variation of resistance and virulence determinants, which might promote the hospital adaptation of *Enterococcus* bacteria such as *E. faecalis* and *E. faecium* (Homan et al., 2002; Ruiz-Garbajosa et al., 2006). In this study, *E. faecalis* isolates were grouped into 44 distinct STs, with the predominant STs being ST16 and ST179, which belonged to the clonal complex (CC16) (Bai et al., 2018). In addition, 25 STs were determined in *E. faecium* isolates, among which ST18 and ST78 were the main positive STs (**Tables 5**, **6**). These results further confirmed that the presence of *erm* genes had minimal effects on the sensitivity of the predominant ST strains to telithromycin, suggesting its potential application for the treatment of some multi-resistant enterococci infections.

Evidence continues to accrue documenting the crucial role of biofilm formation in enterococcal infection (Ch'ng et al., 2019). The majority of clinical *E. faecalis* isolates are capable of forming biofilms on inanimate and living surfaces, which may promote antibiotic tolerance and reduce susceptibility to environmental influences or antimicrobial pressures (Paganelli et al., 2012; Holmberg and Rasmussen, 2016). Thus, targeting the biofilm formation of *E. faecalis* may potentially contribute to the treatment of enterococcal infections. As previously described, telithromycin could be considered as a novel inhibitor of

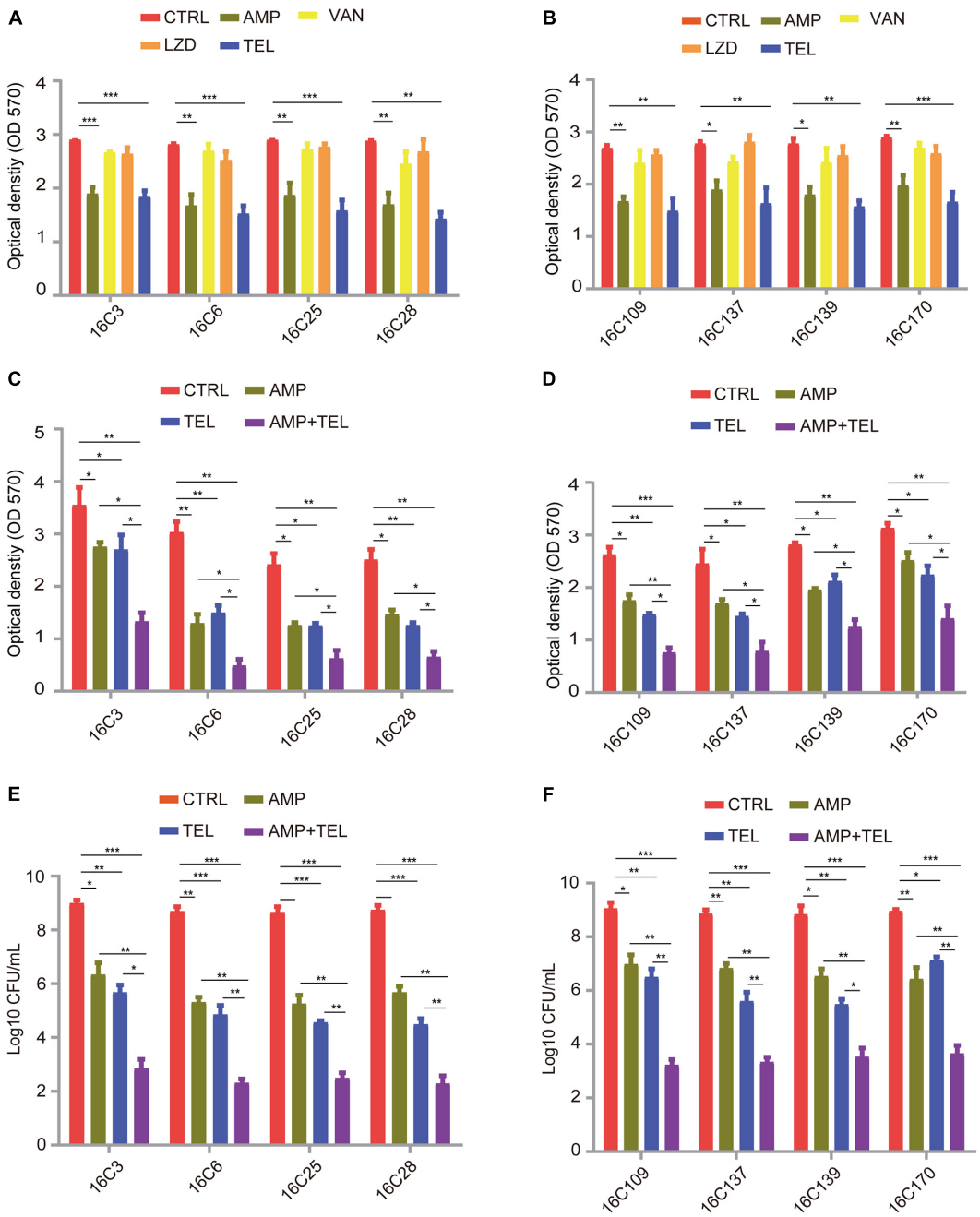

FIGURE 2 | Telithromycin alone or combined with ampicillin eradicating the established biofilms of eight *E. faecalis* isolates. **(A,B)** A total of eight isolates formed mature biofilms for 24 h, then treated with AMP, VAN, LZD, or TEL at 8 × MICs for 48 h. The MICs of AMP, VAN, and TEL for these isolates were 2, 1, and 8 μg/mL, respectively. The MICs of LZD for 16C3, 16C6, 16C25, and 16C28 isolates were 4 μg/mL, the MICs for 16C109, 16C137, 16C139, and 16C170 were 2 μg/mL. **(C,D)** A total of eight isolates formed mature biofilms for 24 h, then were treated with AMP and TEL alone or TEL combined with AMP at 8 × MICs for 48 h. The MICs of AMP and TEL for these isolates were 2 and 8 μg/mL, respectively. **(E,F)** A total of eight isolates formed mature biofilms for 24 h, then were treated with AMP and TEL alone or TEL combined with AMP at 8 × MICs for 48 h. Then the adherent cells in these established biofilms were detected by the CFU numbers. The MICs of AMP and TEL for these isolates were 2 and 8 μg/mL, respectively. TSBG without antimicrobials was used as an untreated control throughout. The data were presented as the mean ± SEM ($n = 3$ experiments), one-way analysis of variance (ANOVA), and *post hoc*-Dunnett test, $^{*}p < 0.05$, $^{**}p < 0.01$, $^{***}p < 0.001$, compared with the CTRL group.

S. aureus biofilms, which may be a result of the decreased expression of biofilm formation-related genes (Woo et al., 2017; Zheng et al., 2020), but there are no available data on the contribution of telithromycin susceptibility to biofilm phenotype in *E. faecalis*. The present study firstly showed that subinhibitory concentrations of telithromycin could inhibit the

biofilm formation of 16 *E. faecalis* isolates (**Figure 1**). However, the data regarding biofilm formation inhibition does not show a dose-dependent effect. Therefore, further investigation is needed to characterize the inhibitory effect of telithromycin on the biofilm formation of *E. faecalis*.

Because biofilm prevention is not always possible, the removal of pre-existing enterococcal biofilms remains a necessity. Although the antibiofilm activity of antibiotics is likely hampered by poor penetration or slowed cell division in metabolically dormant biofilms, the use of antibiotics as first-line treatment for biofilm-associated infections is commonplace (Stewart, 2002). For example, the most recommended antibiotic treatment of endocarditis caused by *E. faecalis* involves ampicillin combined with gentamicin for 4–6 weeks (Habib et al., 2015). In this study, both telithromycin and ampicillin exhibited promising biofilm-inhibiting activity (40% reduction) in *E. faecalis* (**Figures 2A,B**), these results are consistent with those previously reported in the *in vitro* activities of telithromycin or ampicillin against *S. aureus* or *E. faecalis* biofilms (Di Domenico et al., 2019; Zheng et al., 2020). Notably, treatment with an 8 × MIC telithromycin/ampicillin combination exhibited a visible reduction (∼70%) in mature *E. faecalis* biofilms (**Figures 2C,D**) and killed 70% of adherent cells in the established biofilms (**Figures 2E,F**). Therefore, the combination of telithromycin with ampicillin as an anti-adherence or anti-biofilm strategy appears to be much more promising for the treatment of biofilm-associated enterococcal infections.

Accumulating evidence has revealed that there is a lower likelihood of resistance developing through the clinical use of telithromycin. For example, spontaneous resistance to telithromycin was at a low frequency *in vitro*. Telithromycin does not induce MLSB resistance and it shows low potential in selecting resistance or cross-resistance (Felmingham, 2001). In addition, pharmacodynamic studies suggested that telithromycin was generally well tolerated and a once-daily 800 mg oral dose of telithromycin maintains an effective concentration in plasma for the treatment of respiratory tract infections involving the key respiratory pathogens (Drusano, 2001; Namour et al., 2001). However, information regarding kill kinetics and post-antibiotic effects for telithromycin against enterococci is limited. Thereafter, there is inadequate clinical evidence to suggest an optimal dosage regimen for telithromycin against enterococci. The present study demonstrated the antimicrobial susceptibility and antibiofilm activity of telithromycin against *Enterococcus* isolates *in vitro*, suggesting that this compound might be useful, alone or in combination, in some difficult to treat enterococcal infections. The further results of *in vivo* studies should provide some evidence to support such a possibility.

CONCLUSION

In summary, this study presents the effective antimicrobial activity of telithromycin against clinical enterococci isolates from China in comparison to that of ERY. Importantly, this study further demonstrated that telithromycin could inhibit the biofilm formation of *E. faecalis* and that telithromycin combined with ampicillin resulted in enhanced antimicrobial and antibiofilm activity. To our knowledge, this is the first study to present new insight into the antibiofilm activity of telithromycin against enterococci and provide further evidence for the potential clinical application of telithromycin/ampicillin combination for the treatment of *Enterococcus* infections.

DATA AVAILABILITY STATEMENT

The original contributions presented in the study are included in the article/**Supplementary Material**, further inquiries can be directed to the corresponding authors.

AUTHOR CONTRIBUTIONS

YX conducted the PCR analyses, MLST analysis, biofilms inhibition and eradication of *E. faecalis*, and drafted the manuscript. JC collected the bacterial isolates, performed the antimicrobials susceptibility tests, and gene manipulation. XS participated in gene manipulation, MLST analysis, and the inhibition of *E. faecalis* biofilms. GX and PL participated in the collection of bacterial isolates, MLST analysis, and the inhibition and eradication of *E. faecalis* biofilms. ZY and QD participated in the collection of bacterial isolates, and the inhibition and eradication of *E. faecalis* biofilms. ZC and JZ designed the study, analyzed the experimental data, and revised the manuscript. All authors have read and approved the manuscript.

FUNDING

This work was supported by the following grants: the collection of bacterial isolates, antimicrobials susceptibility tests, PCR analyses, and MLST analysis were supported by the Science, Technology and Innovation Commission of Shenzhen Municipality of Key Funds (JCYJ20180508162403996) and basic research funds (JCYJ20180302144721183, JCYJ20180302144340004, JCYJ20180302144345028, and JCYJ20180302144431923). The inhibition and eradication of *E. faecalis* biofilms were supported by the Sanming Project of Medicine in Shenzhen (No. SMGC201705029) and the Shenzhen Nanshan District Scientific Research Program of the People's Republic of China (Nos. 2019042, 2019051, 2019046, 2019027, and 2019040); provincial medical fund of Guangdong (2018116164215307), and Shenzhen Key Medical Discipline Construction Fund (No. SZXK06162).

ACKNOWLEDGMENTS

The authors would like to thank Yang Wu (Key Laboratory of Medical Molecular Virology of Ministries of Education and Health, School of Basic Medical Science and Institutes of Biomedical Sciences, Shanghai Medical College, Fudan University) for his excellent technical support and suggestions.

The authors would also like to thank Ms. Cynthia Brast (University of Florida, Gainesville, FL, United States) for reviewing the manuscript. This manuscript has been released as a pre-print at ResearchSquare https://www.researchsquare.com/article/rs-24213/v1 (Yanpeng et al., 2020).

SUPPLEMENTARY MATERIAL

The Supplementary Material for this article can be found online at: https://www.frontiersin.org/articles/10.3389/fmicb.2020.616797/full#supplementary-material

REFERENCES

Ackermann, G., and Rodloff, A. C. (2003). Drugs of the 21st century: telithromycin (HMR 3647)–the first ketolide. *J. Antimicrob. Chemother.* 51, 497–511. doi: 10.1093/jac/dkg123

Arias, C. A., and Murray, B. E. (2012). The rise of the Enterococcus: beyond vancomycin resistance. *Nat. Rev. Microbiol.* 10, 266–278. doi: 10.1038/nrmicro2761

Bai, B., Hu, K., Li, H., Yao, W., Li, D., Chen, Z., et al. (2018). Effect of tedizolid on clinical Enterococcus isolates: in vitro activity, distribution of virulence factor, resistance genes and multilocus sequence typing. *FEMS Microbiol. Lett.* 3:365. doi: 10.1093/femsle/fnx284

Baldassarri, L., Cecchini, R., Bertuccini, L., Ammendolia, M. G., Iosi, F., Arciola, C. R., et al. (2001). Enterococcus spp. produces slime and survives in rat peritoneal macrophages. *Med. Microbiol. Immunol.* 190, 113–120. doi: 10.1007/s00430-001-009698

Baltch, A. L., Smith, R. P., Ritz, W. J., and Bopp, L. H. (2001). Inhibitory and bactericidal effects of telithromycin (HMR 3647, RU 56647) and five comparative antibiotics, used singly and in combination, against vancomycin-resistant and vancomycin-susceptible enterococci. *Chemotherapy* 47, 250–260. doi: 10.1159/000048531

Benes, J. (2004). Telithromycin. *Klin. Mikrobiol. Infekc. Lek.* 10, 16–21.

Bonnefoy, A., Guitton, M., Delachaume, C., Le Priol, P., and Girard, A. M. (2001). In vivo efficacy of the new ketolide telithromycin (HMR 3647) in murine infection models. *Antimicrob. Agents Chemother.* 45, 1688–1692. doi: 10.1128/aac.45.6.1688-1692.2001

Celik, S., Cakirlar, F. K., and Torun, M. M. (2014). Presence of vancomycin, aminoglycosides, and erythromycin resistance genes in enterococci isolated from clinical samples in Turkey. *Clin. Lab.* 60, 1801–1806. doi: 10.7754/clin.lab.2014.140211

Cetinkaya, Y., Falk, P., and Mayhall, C. G. (2000). Vancomycin-resistant enterococci. *Clin. Microbiol. Rev.* 13, 686–707. doi: 10.1128/cmr.13.4.686-707.2000

Ch'ng, J. H., Chong, K. K. L., Lam, L. N., Wong, J. J., and Kline, K. A. (2019). Biofilm-associated infection by enterococci. *Nat. Rev. Microbiol.* 17, 82–94. doi: 10.1038/s41579-018-0107-z

Costerton, J. W., Stewart, P. S., and Greenberg, E. P. (1999). Bacterial biofilms: a common cause of persistent infections. *Science* 284, 1318–1322. doi: 10.1126/science.284.5418.1318

Darouiche, R. O. (2004). Treatment of infections associated with surgical implants. *N. Engl. J. Med.* 350, 1422–1429. doi: 10.1056/NEJMra035415

Di Domenico, E. G., Rimoldi, S. G., Cavallo, I., D'Agosto, G., Trento, E., Cagnoni, G., et al. (2019). Microbial biofilm correlates with an increased antibiotic tolerance and poor therapeutic outcome in infective endocarditis. *BMC Microbiol.* 19:228. doi: 10.1186/s12866-019-15961592

Di Rosa, R., Creti, R., Venditti, M., D'Amelio, R., Arciola, C. R., Montanaro, L., et al. (2006). Relationship between biofilm formation, the enterococcal surface protein (Esp) and gelatinase in clinical isolates of Enterococcus faecalis and Enterococcus faecium. *FEMS Microbiol. Lett.* 256, 145–150. doi: 10.1111/j.1574-6968.2006.00112.x

Douthwaite, S., and Champney, W. S. (2001). Structures of ketolides and macrolides determine their mode of interaction with the ribosomal target site. *J. Antimicrob. Chemother.* 48, 1–8. doi: 10.1093/jac/48.suppl_2.1

Drusano, G. (2001). Pharmacodynamic and pharmacokinetic considerations in antimicrobial selection: focus on telithromycin. *Clin. Microbiol. Infect.* 7, 24–29.

Duprè, I., Zanetti, S., Schito, A. M., Fadda, G., and Sechi, L. A. (2003). Incidence of virulence determinants in clinical Enterococcus faecium and Enterococcus faecalis isolates collected in Sardinia (Italy). *J. Med. Microbiol.* 52, 491–498. doi: 10.1099/jmm.0.050385030

Eliopoulos, G. M. (1997). Vancomycin-resistant enterococci. Mechanism and clinical relevance. *Infect. Dis. Clin. North Am.* 11, 851–865. doi: 10.1016/s0891-5520(05)7039370397

Felmingham, D. (2001). Microbiological profile of telithromycin, the first ketolide antimicrobial. *Clin. Microbiol. Infect.* 7, 2–10.

Fiore, E., Van Tyne, D., and Gilmore, M. S. (2019). Pathogenicity of Enterococci. *Microbiol. Spectr.* 4:7. doi: 10.1128/microbiolspec.GPP3-00532018

Habib, G., Lancellotti, P., Antunes, M. J., Bongiorni, M. G., Casalta, J. P., Del Zotti, F., et al. (2015). 2015 ESC Guidelines for the management of infective endocarditis: The Task Force for the Management of Infective Endocarditis of the European Society of Cardiology (ESC). *Eur. Heart J.* 36, 3075–3128. doi: 10.1093/eurheartj/ehv319

Hamilton-Miller, J. M., and Shah, S. (1998). Comparative in-vitro activity of ketolide HMR 3647 and four macrolides against gram-positive cocci of known erythromycin susceptibility status. *J. Antimicrob. Chemother.* 41, 649–653. doi: 10.1093/jac/41.6.649

Hidron, A. I., Edwards, J. R., Patel, J., Horan, T. C., Sievert, D. M., Pollock, D. A., et al. (2008). NHSN annual update: antimicrobial-resistant pathogens associated with healthcare-associated infections: annual summary of data reported to the National Healthcare Safety Network at the Centers for Disease Control and Prevention, 2006-2007. *Infect. Control. Hosp. Epidemiol.* 29, 996–1011. doi: 10.1086/591861

Holmberg, A., and Rasmussen, M. (2016). Mature biofilms of Enterococcus faecalis and Enterococcus faecium are highly resistant to antibiotics. *Diagn. Microbiol. Infect. Dis.* 84, 19–21. doi: 10.1016/j.diagmicrobio.2015.09.012

Homan, W. L., Tribe, D., Poznanski, S., Li, M., Hogg, G., Spalburg, E., et al. (2002). Multilocus sequence typing scheme for Enterococcus faecium. *J. Clin. Microbiol.* 40, 1963–1971. doi: 10.1128/jcm.40.6.1963-1971.2002

Jakubovics, N. S., and Burgess, J. G. (2015). Extracellular DNA in oral microbial biofilms. *Microbes Infect.* 17, 531–537. doi: 10.1016/j.micinf.2015.03.015

Jett, B. D., Huycke, M. M., and Gilmore, M. S. (1994). Virulence of enterococci. *Clin. Microbiol. Rev.* 7, 462–478. doi: 10.1128/cmr.7.4.462

Jones, M. E., Draghi, D. C., Thornsberry, C., Karlowsky, J. A., Sahm, D. F., and Wenzel, R. P. (2004). Emerging resistance among bacterial pathogens in the intensive care unit–a European and North American Surveillance study (2000-2002). *Ann. Clin. Microbiol. Antimicrob.* 3:14. doi: 10.1186/1476-0711-314

Lebeaux, D., Ghigo, J. M., and Beloin, C. (2014). Biofilm-related infections: bridging the gap between clinical management and fundamental aspects of recalcitrance toward antibiotics. *Microbiol. Mol. Biol. Rev.* 78, 510–543. doi: 10.1128/mmbr.0001314

Lewis, K. (2001). Riddle of biofilm resistance. *Antimicrob. Agents Chemother.* 45, 999–1007. doi: 10.1128/aac.45.4.999-1007.2001

Marrie, T. J., Nelligan, J., and Costerton, J. W. (1982). A scanning and transmission electron microscopic study of an infected endocardial pacemaker lead. *Circulation* 66, 1339–1341. doi: 10.1161/01.cir.66.6.1339

Megran, D. W. (1992). Enterococcal endocarditis. *Clin. Infect. Dis.* 15, 63–71. doi: 10.1093/clinids/15.1.63

Mendes, R. E., Castanheira, M., Farrell, D. J., Flamm, R. K., Sader, H. S., and Jones, R. N. (2016). Longitudinal (2001-14) analysis of enterococci and VRE causing invasive infections in European and US hospitals, including a contemporary (2010-13) analysis of oritavancin in vitro potency. *J. Antimicrob. Chemother.* 71, 3453–3458. doi: 10.1093/jac/dkw319

Menninger, J. R. (1995). Mechanism of inhibition of protein synthesis by macrolide and lincosamide antibiotics. *J. Basic Clin. Physiol. Pharmacol.* 6, 229–250. doi: 10.1515/jbcpp.1995.6.3-4.229

Mensa, J., García-Vázquez, E., and Vila, J. (2003). Macrolides, ketolides and streptogramins. *Enferm. Infecc. Microbiol. Clin.* 21:219.

Min, Y. H., Yoon, E. J., Kwon, A. R., Shim, M. J., and Choi, E. C. (2011). Alterations in regulatory regions of erm(B) genes from clinical isolates of

enterococci resistant to telithromycin. *Arch. Pharm. Res.* 34, 2149–2154. doi: 10.1007/s12272-011-12191214

Mohamed, J. A., and Huang, D. B. (2007). Biofilm formation by enterococci. *J. Med. Microbiol.* 56, 1581–1588. doi: 10.1099/jmm.0.4733147330

Murray, B. E., and Weinstock, G. M. (1999). Enterococci: new aspects of an old organism. *Proc. Assoc. Am. Physicians* 111, 328–334. doi: 10.1046/j.1525-1381.1999.99241.x

Namour, F., Wessels, D. H., Pascual, M. H., Reynolds, D., Sultan, E., and Lenfant, B. (2001). Pharmacokinetics of the new ketolide telithromycin (HMR 3647) administered in ascending single and multiple doses. *Antimicrob. Agents Chemother.* 45, 170–175. doi: 10.1128/aac.45.1.170-175.2001

Nguyen, M., and Chung, E. P. (2005). Telithromycin: the first ketolide antimicrobial. *Clin. Ther.* 27, 1144–1163. doi: 10.1016/j.clinthera.2005.08.009

Paganelli, F. L., Willems, R. J., and Leavis, H. L. (2012). Optimizing future treatment of enterococcal infections: attacking the biofilm? *Trends Microbiol.* 20, 40–49. doi: 10.1016/j.tim.2011.11.001

Raza, T., Ullah, S. R., Mehmood, K., and Andleeb, S. (2018). Vancomycin resistant Enterococci: A brief review. *J. Pak. Med. Assoc.* 68, 768–772.

Richards, M. J., Edwards, J. R., Culver, D. H., and Gaynes, R. P. (2000). Nosocomial infections in combined medical-surgical intensive care units in the United States. *Infect. Control. Hosp. Epidemiol.* 21, 510–515. doi: 10.1086/501795

Ruiz-Garbajosa, P., Bonten, M. J., Robinson, D. A., Top, J., Nallapareddy, S. R., Torres, C., et al. (2006). Multilocus sequence typing scheme for Enterococcus faecalis reveals hospital-adapted genetic complexes in a background of high rates of recombination. *J. Clin. Microbiol.* 44, 2220–2228. doi: 10.1128/jcm.025962595

Sandoe, J. A. T., Witherden, I. R., Cove, J. H., Heritage, J., and Wilcox, M. H. (2003). Correlation between enterococcal biofilm formation in vitro and medical-device-related infection potential in vivo. *J. Med. Microbiol.* 52, 547–550. doi: 10.1099/jmm.0.052015200

Shoji, T., Takaya, A., Sato, Y., Kimura, S., Suzuki, T., and Yamamoto, T. (2015). RlmCD-mediated U747 methylation promotes efficient G748 methylation by methyltransferase RlmAII in 23S rRNA in Streptococcus pneumoniae; interplay between two rRNA methylations responsible for telithromycin susceptibility. *Nucleic Acids Res.* 43, 8964–8972. doi: 10.1093/nar/gkv609

Sievert, D. M., Ricks, P., Edwards, J. R., Schneider, A., Patel, J., Srinivasan, A., et al. (2013). Antimicrobial-resistant pathogens associated with healthcare-associated infections: summary of data reported to the National Healthcare Safety Network at the Centers for Disease Control and Prevention, 2009-2010. *Infect. Control. Hosp. Epidemiol.* 34, 1–14. doi: 10.1086/668770

Singh, K. V., Zscheck, K. K., and Murray, B. E. (2000). Efficacy of telithromycin (HMR 3647) against enterococci in a mouse peritonitis model. *Antimicrob. Agents Chemother.* 44, 3434–3437. doi: 10.1128/aac.44.12.3434-3437.2000

Spiers, K. M., and Zervos, M. J. (2004). Telithromycin. *Expert Rev. Anti. Infect. Ther.* 2, 685–693. doi: 10.1586/14789072.2.5.685

Stewart, P. S. (2002). Mechanisms of antibiotic resistance in bacterial biofilms. *Int. J. Med. Microbiol.* 292, 107–113. doi: 10.1078/1438-42214196

Sun, X., Lin, Z. W., Hu, X. X., Yao, W. M., Bai, B., Wang, H. Y., et al. (2018). Biofilm formation in erythromycin-resistant Staphylococcus aureus and the relationship with antimicrobial susceptibility and molecular characteristics. *Microb. Pathog.* 124, 47–53. doi: 10.1016/j.micpath.2018.08.021

Togami, K., Chono, S., Seki, T., and Morimoto, K. (2009). Distribution characteristics of telithromycin, a novel ketolide antimicrobial agent applied for treatment of respiratory infection, in lung epithelial lining fluid and alveolar macrophages. *Drug Metab. Pharmacokinet* 24, 411–417. doi: 10.2133/dmpk.24.411

Uzun, B., Güngör, S., Pektaş, B., Aksoy Gökmen, A., Yula, E., Koçal, F., et al. (2014). [Macrolide-lincosamide-streptogramin B (MLSB) resistance phenotypes in clinical Staphylococcus isolates and investigation of telithromycin activity]. *Mikrobiyol. Bul.* 48, 469–476. doi: 10.5578/mb.7748

van Harten, R. M., Willems, R. J. L., Martin, N. I., and Hendrickx, A. P. A. (2017). Multidrug-Resistant Enterococcal Infections: New Compounds, Novel Antimicrobial Therapies? *Trends Microbiol.* 25, 467–479. doi: 10.1016/j.tim.2017.01.004

Van Laethem, Y., and Sternon, J. (2003). [Telithromycin, first ketolide]. *Rev. Med/. Brux* 24, 42–46.

Vester, B., and Douthwaite, S. (2001). Macrolide resistance conferred by base substitutions in 23S rRNA. *Antimicrob. Agents Chemother.* 45, 1–12. doi: 10.1128/aac.45.1.1-12.2001

Wang, Y., Xiong, Y., Wang, Z., Zheng, J., Xu, G., Deng, Q., et al. (2020). Comparison of solithromycin with erythromycin in Enterococcus faecalis and Enterococcus faecium from China: antibacterial activity, clonality, resistance mechanism, and inhibition of biofilm formation. *J. Antibiot.* doi: 10.1038/s41429-020-00374372 [Online ahead of print].

Weiner, L. M., Webb, A. K., Limbago, B., Dudeck, M. A., Patel, J., Kallen, A. J., et al. (2016). Antimicrobial-Resistant Pathogens Associated With Healthcare-Associated Infections: Summary of Data Reported to the National Healthcare Safety Network at the Centers for Disease Control and Prevention, 2011-2014. *Infect. Control. Hosp. Epidemiol.* 37, 1288–1301. doi: 10.1017/ice.2016.174

Weisblum, B. (1995). Erythromycin resistance by ribosome modification. *Antimicrob. Agents Chemother.* 39, 577–585. doi: 10.1128/aac.39.3.577

Weisblum, B., and Demohn, V. (1969). Erythromycin-inducible resistance in Staphylococcus aureus: survey of antibiotic classes involved. *J. Bacteriol.* 98, 447–452. doi: 10.1128/jb.98.2.447-452.1969

Westh, H., Hougaard, D. M., Vuust, J., and Rosdahl, V. T. (1995). Prevalence of erm gene classes in erythromycin-resistant Staphylococcus aureus strains isolated between 1959 and 1988. *Antimicrob. Agents Chemother.* 39, 369–373. doi: 10.1128/aac.39.2.369

Wolter, N., Smith, A. M., Farrell, D. J., Northwood, J. B., Douthwaite, S., and Klugman, K. P. (2008). Telithromycin resistance in Streptococcus pneumoniae is conferred by a deletion in the leader sequence of erm(B) that increases rRNA methylation. *Antimicrob. Agents Chemother.* 52, 435–440. doi: 10.1128/aac.010741077

Woo, S. G., Lee, S. Y., Lee, S. M., Lim, K. H., Ha, E. J., and Eom, Y. B. (2017). Activity of novel inhibitors of Staphylococcus aureus biofilms. *Folia Microbiol.* 62, 157–167. doi: 10.1007/s12223-016-0485484

Yanpeng, X., Junwen, C., Xiang, S., Guangjian, X., Peiyu, L., Qiwen, D., et al. (2020). In vitro antibacterial activity of telithromycin against Enterococcus spp. isolated from China. *BMC Microbiol.* 2020:24213. doi: 10.21203/rs.3.rs-24213/v1

Zheng, J. X., Sun, X., Lin, Z. W., Qi, G. B., Tu, H. P., Wu, Y., et al. (2019). In vitro activities of daptomycin combined with fosfomycin or rifampin on planktonic and adherent linezolid-resistant isolates of Enterococcus faecalis. *J. Med. Microbiol.* 68, 493–502. doi: 10.1099/jmm.0.000945

Zheng, J. X., Tu, H. P., Sun, X., Xu, G. J., Chen, J. W., Deng, Q. W., et al. (2020). In vitro activities of telithromycin against Staphylococcus aureus biofilms compared with azithromycin, clindamycin, vancomycin and daptomycin. *J. Med. Microbiol.* 69, 120–131. doi: 10.1099/jmm.0.001122

Zheng, J. X., Wu, Y., Lin, Z. W., Pu, Z. Y., Yao, W. M., Chen, Z., et al. (2017). Characteristics of and Virulence Factors Associated with Biofilm Formation in Clinical Enterococcus faecalis Isolates in China. *Front. Microbiol.* 8:2338. doi: 10.3389/fmicb.2017.02338

Conflict of Interest: The authors declare that the research was conducted in the absence of any commercial or financial relationships that could be construed as a potential conflict of interest.

frontiers in Microbiology

REVIEW
published: 26 January 2021
doi: 10.3389/fmicb.2021.609459

Futuristic Non-antibiotic Therapies to Combat Antibiotic Resistance: A Review

Manoj Kumar[1], Devojit Kumar Sarma[1], Swasti Shubham[1], Manoj Kumawat[1], Vinod Verma[2], Praveen Balabaskaran Nina[3], Devraj JP[4], Santosh Kumar[4], Birbal Singh[5] and Rajnarayan R. Tiwari[1]*

[1] ICMR-National Institute for Research in Environmental Health, Bhopal, India, [2] Stem Cell Research Centre, Department of Hematology, SGPGIMS, Lucknow, India, [3] Department of Epidemiology and Public Health, Central University of Tamil Nadu, Thiruvarur, India, [4] ICMR- National Institute of Nutrition, Hyderabad, India, [5] ICAR-Indian Veterinary Research Institute, Regional Station, Palampur, India

The looming problem of resistance to antibiotics in microorganisms is a global health concern. The drug-resistant microorganisms originating from anthropogenic sources and commercial livestock farming have posed serious environmental and health challenges. Antibiotic-resistant genes constituting the environmental "resistome" get transferred to human and veterinary pathogens. Hence, deciphering the origin, mechanism and extreme of transfer of these genetic factors into pathogens is extremely important to develop not only the therapeutic interventions to curtail the infections, but also the strategies to avert the menace of microbial drug-resistance. Clinicians, researchers and policymakers should jointly come up to develop the strategies to prevent superfluous exposure of pathogens to antibiotics in non-clinical settings. This article highlights the present scenario of increasing antimicrobial-resistance in pathogenic bacteria and the clinical importance of unconventional or non-antibiotic therapies to thwart the infectious pathogenic microorganisms.

Keywords: antibiotic resistance, gene transfer, health problems, alternative therapies, drug-resistance

OPEN ACCESS

Edited by:
Israel Castillo-Juárez, Colegio de Postgraduados (COLPOS), Mexico

Reviewed by:
José Rivera-Chávez, Universidad Nacional Autónoma de México, Mexico
Miguel Cocotl-Yañez, National Autonomous University of Mexico, Mexico

****Correspondence:***
Manoj Kumar
manoj15ndri@gmail.com

Specialty section:
This article was submitted to Antimicrobials, Resistance and Chemotherapy, a section of the journal Frontiers in Microbiology

Received: *23 September 2020*
Accepted: *04 January 2021*
Published: *26 January 2021*

Citation:
Kumar M, Sarma DK, Shubham S, Kumawat M, Verma V, Nina PB, Devraj JP, Kumar S, Singh B and Tiwari RR (2021) Futuristic Non-antibiotic Therapies to Combat Antibiotic Resistance: A Review. Front. Microbiol. 12:609459. doi: 10.3389/fmicb.2021.609459

HIGHLIGHTS

- Drug-resistant Staphylococci, Enterococci and Streptococci are the major pathogens that increase morbidity, mortality and healthcare costs.
- Frenzied use of antibiotics as growth-promoters in some food animals is the prime driver of dissemination of antibiotic-resistant genes.
- Alternative therapies like stem cell-AMPs, CRISPR-Cas, probiotics, nanobiotics etc., should be explored to combat antibiotic resistant infections.

INTRODUCTION

Discovery of antibiotics to treat infectious diseases had a phenomenal impact on human and animal health since 1940s. However, haphazard use of antibiotics and disinfectants has led to unprecedented health problems worldwide. This condition had its origin when microorganisms started developing genes that provide resistance toward residual antibiotics. The resistant genes

augment the survival of pathogens in multiple environments, which not only limit the treatment options for infectious diseases, but also increase the morbidity and mortality by disseminating multiple drug resistant bacteria in human and animal. Antibiotic resistance, due to ESKAPE pathogens are found to be associated with high risk of mortality and morbidity leading to greater economic cost particularly in ICU settings of developing countries (Founou et al., 2017). The problem is aggravated further due to slow-pace inventions in the development of novel antibiotics (Nordmann et al., 2012; Kumar et al., 2016; Singh et al., 2017).

It is speculated that human deaths caused by drug-resistant microorganisms could rise from approximately 700,000 per year to 10 million per year by 2050 (World Health Organization, 2014). According to Laxminarayan et al. (2016), the world's largest consumer of antibiotics have created conditions that promote drug-resistant infections. Poor public health conditions, lack of awareness about drug-resistant bacteria among the public, high incidence of diseases, easy availability of antibiotics and their haphazard use are the major factors aggravating the problem.

Vikesland et al. (2019) have summarized the mode of actions of some of the widely available antibiotics, which are the key drivers of development of antimicrobial resistance and subsequently transfer of resistant genes among pathogens; this condition is more prevalent in low- and high-income countries. Hence in order to have a stable and efficient drug-delivery system, use of CRISPR-Cas systems, nanotechnology-based approach – such as nanoparticles or nanocrystals as carriers of antibiotics, antibacterial and anti-viral chemical compounds (e.g., retinoid analogs), and synthetic and natural AMPs need to be considered (Lima et al., 2019; Pacios et al., 2020). Also for infections caused by multi-drug resistant pathogens, bacteriophages, mutant and bioengineered lytic phages and lytic endolysins alone or in combination with antibiotics need to be considered (Pacios et al., 2020).

Gupta et al. (2019) in their study have emphasized the potential of nanomaterials and nanoparticle-based approaches as self-therapeutic agents and drug-delivery vehicles as expected strategies against antimicrobial resistance.

In view of the dearth of developments in new antibiotics, there is an upsurge in use of computational and *in silico* tools to identify novel therapeutic targets (Sharma S. et al., 2019), and use of sustainable plant- and animal-origin and engineered products natural (Bérdy, 2012) and microorganisms (Kumar et al., 2016; Singh et al., 2016) as powerful supplementary therapeutics against infectious agents. Further advances in our understanding of properties and interactions among drug candidates, bacteria and metabolic pathways will pave the way to development of superior antimicrobial agents. Since combinatorial approaches have not proved to be vastly effective to develop potent drug molecules, development of antibiotics from already existing natural scaffolds could be an alternative short-term remedy against antibiotic resistance (Rossiter et al., 2017). Therefore, in the existing scenario, exploration and utilization of natural resources including probiotics and their metabolites will acquire eminence to deliver functional bio-molecules against MDR infections.

In the present review, we have highlighted the salient features of supplemental non-antibiotic therapies such as mesenchymal stem cell–derived AMPs, bacterial films and quorum-sensing inhibitors, immunotherapeutic, FMT and microbial or probiotic-based treatments.

DRUG RESISTANCE AS A CONTINUED PROCESS

Microorganisms are highly astute and evolve mechanisms swiftly to endure and proliferate in environments turning unfavorable. Although antibiotic-resistance started appearing soon after the clinical introduction of antibiotics, the problem was slow and ignored initially as a matter of low distress. Sulfonamide-resistant *Streptococcus pyogenes* appeared in the human clinical settings in early the 1930s, while penicillin-resistant *S. pyogenes* was noted in the 1940s. Emergence of multidrug-resistant bacteria was highlighted in the 1950s (Levy and Marshall, 2004; **Table 1**).

Two distinct pathways, namely vertical evolution (mutations which cause antibiotic tolerance transmittable to offspring), and horizontal evolution (acquisition of inheritable antibiotic-resistance genes from other bacteria via conjugation, transduction or transformation) are regarded as prime modes of development of antibiotic-resistance. The comprehensive genomic analysis of human and animal pathogens has shown that horizontal gene transfer is an important mechanism of transfer of antibiotic-resistant genes among microorganisms (Martínez et al., 2017).

The antibiotic resistance, though a grave concern, was overlooked for a long period (Martínez et al., 2017). However, incidences that attracted the attention of clinicians and biochemists included detection of bacteria carrying extended spectrum β-lactamases (ESBL) imparting resistance to penicillins and cephalosporins, extensively drug-resistant (XDR) *Mycobacterium tuberculosis*, and multidrug-resistant *Acinetobacter baumannii*, Enterobacteriaceae, *Neisseria gonorrhoeae*, and *Pseudomonas aeruginosa* (Wright, 2010a,b).

A decade ago, the New Delhi metallo-β-lactamase 1 (NDM-1) was first identified in a single isolate of *Klebsiella pneumoniae* and *Escherichia coli*, both isolated from a patient admitted in a hospital in New Delhi, India (Yong et al., 2009). Third-generation cephalosporin-resistant *E. coli* infections are accountable for the utmost disease burden and more than half of these infections occur in the community. This indicates that to reduce the burden of antimicrobial resistance (AMR), antimicrobial stewardship should be limited not only to the hospitals, but it is necessary to the primary care system including prescribers and interventions (OECD, 2019).

Antibiotic-resistance is a globally admitted problem in clinical and health sectors, but more severe is in developing countries such as India (Ganguly et al., 2011). The crude mortality owing to infectious diseases in India was 416.75 per 100,000 persons, which was twice the rate prevailing in United States (roughly 200 per 100,000 persons; (Armstrong et al., 1999). It has been observed that there is a significant surge in the global consumption of antibiotics (increased by 65%, 21.1–34.8 billion DDDs (defined

TABLE 1 | Overview of the development of bacterial resistance against common antibiotics.

Antibiotic class	Mechanism of Action	Examples of antibiotics	Year introduced to the market	Year antibiotic resistance identified
Penicillins (β-Lactam)	Inhibition of bacterial cell wall synthesis.	Penicillin	1943	1940,1965, 1967,1976 (Ventola, 2015)
		Ampicillin	1961	1962,1964 (Fischer et al., 2010; Ravina, 2011)
		Amoxicillin	1972	1977 (Fischer et al., 2010; Roy, 2011)
		Methicillin	1960	1960 (Jevons, 1961)
Cephalosporins (β-Lactam)		Cefotaxime	1980	1983 (Knothe et al., 1983)
		Ceftaroline	2010	2011 (FDA, 2010; CDC, 2013)
	Avibactam inhibits serine β-lactamases enzyme	Ceftazidime (3rd Generation cephalosporins)	1984	1987 (Burwen et al., 1994; Fischer et al., 2010; Humphries et al., 2015)
		Ceftazidime–avibactam	2015	2015 (FDA, 2015; Humphries et al., 2015)
Aminoglycosides	Protein biosynthesis inhibition	Streptomycin	1944	1946 (Youmans and Williston, 1946; Crofton and Mitchison, 1948; Schatz et al., 2005)
		Tobramycin	1967	1981 (Fischer et al., 2010)
		Amikacin	1976	1981 (Bongaerts and Kaptijn, 1981; John et al., 1982; Levine et al., 1985)
		Gentamicin	1963	1973 (Greene et al., 1973; Fischer et al., 2010)
		Neomycin	1952	1950 (Waisbren and Spink, 1950; Fischer et al., 2010)
		Kanamycin	1957	1967 (Umezawa et al., 1957)
Chloramphenicol		Chloramphenicol	1948	1960 (Smith and Worrel, 1949; Fischer et al., 2010; Lewis, 2013)
Glycopeptides	Cell wall synthesis inhibition	Vancomycin	1972	1988 (Anderson et al., 1961; Leclercq et al., 1988; Uttley, 1988; Murray, 2000; Depardieu et al., 2003; Sievert et al., 2008)
		Teicoplanin (derivative of Vancomycin)	1984	1986 (Johnson et al., 1990; Butler et al., 2014)
Ansamycins	RNA synthesis inhibition	Rifampin	1968	1972 (Tsukamura, 1972; Sensi, 1983; Telenti et al., 1993; Lesch, 2007)
Sulfonamides	DNA synthesis inhibition	Prontosil	1936, 1935	1942 (Lesch, 2007; Simon, 2011)
		Sulfamethoxazole	1961	1960 (Akiba et al., 1960; Stamm and Hooton, 1993; Andrew, 2013)
Tetracyclines	Protein biosynthesis inhibition	Tetracycline	1950	1959 (Ramsey and Edwards, 1961; Fischer et al., 2010)
Macrolide		Erythromycin	1953	1956 (Finland et al., 1956)
		Azithromycin	1980	2011 (Soge et al., 2012)
Oxazolidinones		Linezolid	2000	2001 (Tsiodras et al., 2001; Li and Corey, 2013; Török et al., 2016)
Quinolones	DNA synthesis inhibition	Ciprofloxacin	1987	2007 (Castanheira et al., 2007)
		Levofloxacin	1996	1996 (CDC, 2013)
Lipopeptides	Cell wall synthesis disruption disrupting multiple aspects of bacterial cell membrane function	Daptomycin	2003	2004 (Mangili et al., 2005)
		Bacitracin	1945	1955 (Weinberg, 1967; Mary, 2007)
		Aztreonam	1984, 1986	1986 (Res et al., 2017)
		Imipenem	1985	1996 (Troillet et al., 1997; Fischer et al., 2010)
Lincosamides	Interfering with the synthesis of proteins	Clindamycin	1966	1971 (Watanakunakorn, 1976; Troillet et al., 1997)

daily doses) during 2000 to 2015, which was mainly driven by low- and middle- income countries) (Klein et al., 2018). Recently, Klein et al., used an indicator (Drug Resistance Index, DRI) to elucidate the effectiveness of antibiotic therapy by combining antibiotic consumption and resistance (Klein et al., 2019). A highest DRI for low and middle- income countries was observed by using data from 41 countries on antibiotic uses and resistance in WHO priority pathogens. **Figure 1** depicts the global consumption and DRI along with the drug resistance pattern in WHO priority pathogens against selected antibiotics in some countries.

The surge in antibiotic-resistance might be due to poor public health systems, prevalence of infectious diseases and use of antibiotics without prescription of medical and veterinary specialists (Baquero et al., 2008). The threat is aggravated in poor or developing countries where medical services are scanty. Further, self-medication is a common practice as antibiotics are sold without restrictions in chemists' shop, and the users are unaware of the consequences of overuse of antibiotics (Planta, 2007; Wellington et al., 2013; **Figure 2**).

ANTIBIOTICS USAGE AND ITS CONSEQUENCE

The notion that antibiotics are safe to humans and veterinary health has changed. Besides killing microorganisms, the antibiotics interrupt human and animal health. Though antibiotics are recommended for human use after rigorous clinical trials of efficacy and safety, from a perspective of microorganisms, they pose health threats to humans. Medical professionals and regulatory agencies are dubious that some antibiotics over the long-term use could have debilitating health effects in humans (Merchant et al., 2018).

For instance, the fluoroquinolones, being safe to most people, are prescribed by medical doctors all over the world. The phenomenal side effects of antibiotics have urged

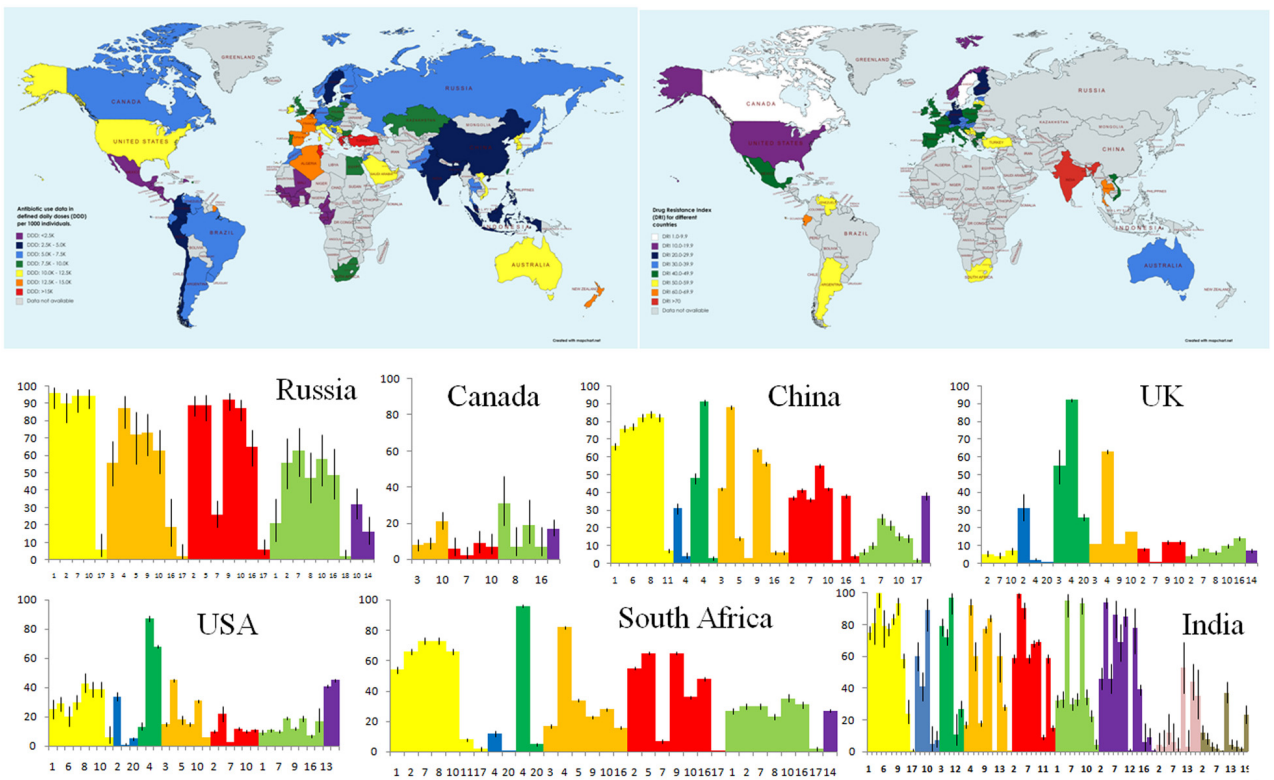

WHO priority pathogens

Species name	Colour	Species name	Colour
Acinetobacter baumannii		*Pseudomonas aeruginosa*	
Enterococcus faecalis		*Staphylococcus aureus*	
Enterococcus faecium		*Salmonella paratyphi*	
Escherichia Coli		*Salmonella typhi*	
Klebsiella pneumoniae			

Antibiotic name	Code no	Antibiotic name	Code no	Antibiotic name	Code no
Amikacin	1	Ceftazidime	8	Penicillins	15
Aminoglycosides	2	Cephalosporins (3rd generation)	9	Piperacillin-tazobactam	16
Aminoglycosides (High - level)	3	Fluoroquinolones	10	Polymyxins	17
Aminopenicillins	4	Glycylcyclines	11	Rifampicin	18
Amoxicillin-clavulanate	5	Linezolid	12	Trimethoprim-sulfamethoxazole	19
Ampicillin sulbactam	6	Macrolides	13	Vancomycin	20
Carbapenems	7	Oxacillin (MRSA)	14		

FIGURE 1 | Country wide Antibiotic consumption rate (in defined daily doses (DD) per 1000 individuals) and Drug Resistance Index (DRI) along with prevalence of antibiotic resistance in some selected countries. [Data for antibiotic consumption rate (up to 2015) and prevalence of antibiotic resistance in the selected countries are retrieved from The Center for Disease Dynamics, Economics and Policy (The Center for Disease Dynamics, 2020). Drug Resistance Index map has been created from the data derived from Klein et al. (2019)].

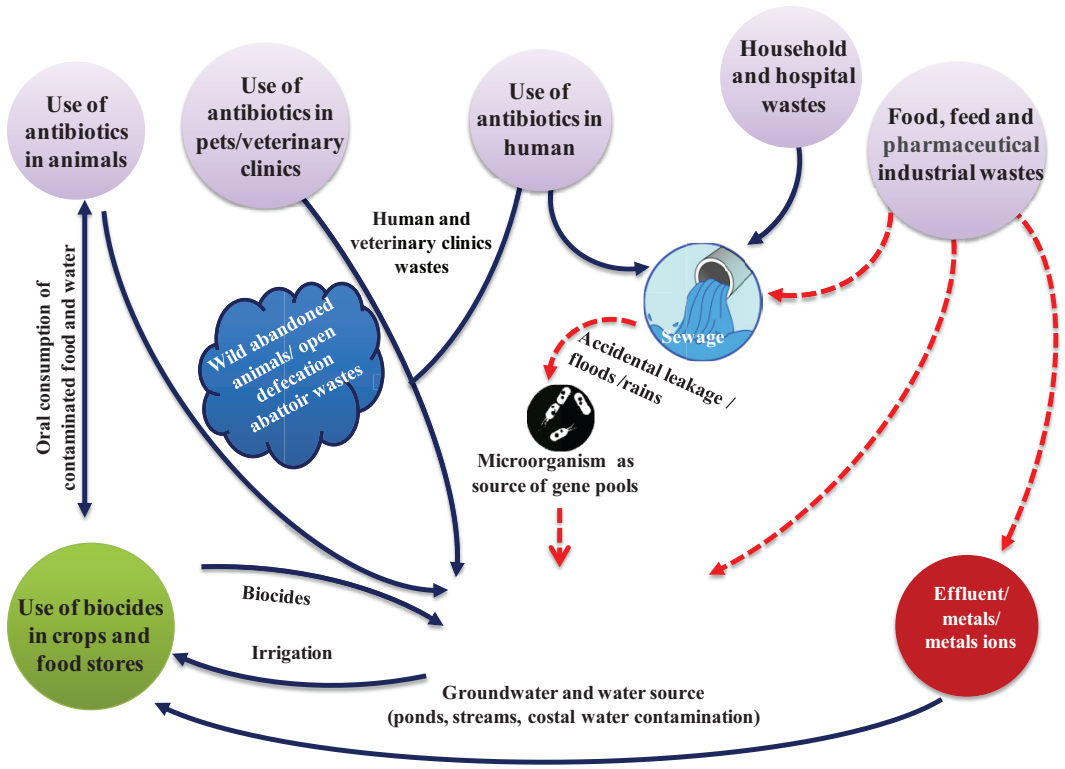

FIGURE 2 | Factors leading to rapid development and use of antibiotics increasing antibiotic-resistance among pathogens, and the routes by which resistant pathogens enter human and animal food chain. Antibiotic-resistant bacteria from humans and animals enter water sources used for drinking or irrigation. Residual antibiotics released from industries alter the natural soil and water microbiota.

health professionals and regulatory agencies to reassess their use in biomedical and veterinary segments. Side effects of fluoroquinolones, such as muscles and tendons damage, neuropsychiatric disorders and mitochondrial toxicity, are the compelling examples that antibiotics do to humans other than treating infections. Even though effective treatment of fluoroquinolone-associated disability (FQAD) is difficult, it is not so effective. Hence, in view of repeated incidences of FQAD, it is warned that the antibiotics should be prescribed exclusively for serious infections (Merchant et al., 2018).

LIVESTOCK AS A MAJOR CONTRIBUTOR OF ANTIBIOTIC-RESISTANCE

Use of antimicrobials in animal feeding as growth-promoters is strongly correlated with emergence and spread of antimicrobial-resistant bacteria, making it difficult to treat infectious diseases. Many food-producing animals, especially the poultry, pigs and cattle are treated with antibiotics to prevent infections and to compensate for unhygienic conditions in commercial livestock farms. For instance, the antibiotic use in livestock in India is fourth highest in the world after China (23%), the United States (13%), and Brazil (9%) (Sivaraman, 2018). In United States, 80% of sold antibiotics are used in livestock alone (Mullard, 2015; Van Boeckel et al., 2015; FDA, 2017; Goutard et al., 2017). Nevertheless, non-therapeutic use of antibiotics in animal husbandry due to its contribution to increase antibiotic-resistant bacterial infections is of immense public health concern (Resistance, 2004).

The livestock act as a source that spreads resistant microorganisms into environment, for example, through contaminated bio wastes, milk or meat, or by direct contact with animals and humans working in animal farms. Similarly, the zoonotic pathogens act as donors of antimicrobial-resistant genes to human pathogens. As animals and livestock products are transported across the world, AMR distressing the food supply of one country poses threats in other places. For instance, after use of avoparcin, a glycopeptide antibiotic used as animal growth-promoter in Europe, vancomycin-resistant enterococci (VRE) spread in animal feed and meat (Wegener et al., 1999). Consequently, the avoparcin was banned in food-producing animals in European Union, and reduction has been noted in the incidences of VRE in humans and animals (Bates, 1997). Similarly, the spread of ciprofloxacin-resistant *Salmonella*, *Campylobacter* and *E. coli,* which have caused human infections difficult to treat, can be attributed to a significant extent to the use of fluoroquinolones (e.g., enrofloxacin) in milch and meat animals. There are several instances where drug-resistant bacteria spread worldwide via travel and food trade mode.

Bacteria develop resistance toward antibiotics when exposed to low doses over long periods. A common practice is to feed low-dose antibiotics to the livestock to promote body weight gain. In addition, antibiotics are also used arbitrarily to prevent diseases in crowded herds or flocks. Such practices contribute to emergence and spread of resistance to antibiotics. These practices lead to massive accumulation of antibiotics in the environment, and acquisition of resistance in microorganisms coming in contact with them (Allen, 2014). Many countries including European Union have imposed a ban on use of some antibiotics in feed or as growth promoters (Heuer et al., 2011).

In addition to the development of resistance to drugs due to mutations in genes, the microorganisms originating from non-clinical environments are the prime candidates expressing resistance toward antibiotics (Martinez et al., 2008). Therefore, attention is focused on understanding the sources and molecular mechanisms involved in acquisition of resistance.

However, it is difficult to determine the route and quantity of resistance factors from animals to humans and thus prove that animals act as reservoirs of resistant genes. This is further complicated by the spontaneously present resistance genes in the environment. For example, resistance to naturally occurring antibiotics is known to occur much before the progress of agriculture. The metallo-β-lactamases (of which NDM is one especially annoying example) have a very old origin, so ancient is the fact that no detectable sequence homology remains between different classes of these genes (Hall et al., 2004; Bebrone, 2007). Horizontal gene transfer is thought to play a significant role in the development of metallo-β-lactamases, but whether that process has been accelerated by using of antibiotics in agriculture is not known.

SCALE OF ANTIBIOTIC USE IN HUMAN AND ANIMALS

As per 2010 statistical data, India with the consumption of 12.9×10^9 units (10.7 units/person) was the largest consumer of antibiotics, followed by China, which used 10.0×10^9 units (7.5 units per person), while the United States used 6.8×10^9 units (22.0 units per person) (Van Boeckel et al., 2017). Seventy-six percent of the overall rise in antibiotic use during the decade 2000 to 2010 was noted in BRICS countries (Brazil, Russia, India, China, and South Africa) (Van Boeckel et al., 2015).

Among five major rising national economies i.e., BRICS countries, 23% of the rise in the retail antibiotic sales was attributed to India, while around 57% of the increase in medical sector was in China. Overall, in India, the pattern of antibiotic use is changing with decline in the use of ampicillin and co-trimoxazole and increase in quinolone consumption. The above scale-up in antibiotic use in India was due to swift economic growth, increasing incomes and incidences of infectious diseases (Laxminarayan and Chaudhury, 2016; Laxminarayan et al., 2016).

Several strategies are adopted to enhance animal production to maximize profits and fulfill the need of animal-origin foods. The global estimate of antimicrobial use in food-producing animals was at 63,151 (±1,560) tons in 2010, and was projected to rise by 67%, to 105,596 (±3,605) tons, by the year 2030. Out of this, 60% of the rise is estimated to be due to rising number of animals reared for food production. The remaining 34% rise was due to a shift in farming practices, with a larger proportion of animals projected to be the integral component of intensive farming systems by 2030. It is envisaged that, by 2030, the antimicrobial consumption in Asia could roughly reach 51,851 tons, representing 82% of the current global antimicrobial consumption in food animals in 2010. However, animal's antimicrobial consumption is expected to grow by 99% by 2030 in the BRICS countries, whereas human antimicrobial consumption is expected to grow by 13% over the same period (Van Boeckel et al., 2015).

ANTIBIOTIC-RESISTANT GENES (ARGs) AS ENVIRONMENTAL CONTAMINANTS

Antibiotics of human-origin enter the environment through a several routes. Antibiotics and their metabolites are released from hospitals through biological wastes (urine, feces, sputum, placenta, tissues and organs). Likewise, the antibiotics and antibiotic-resistant pathogens are released into environment through abandoned animals (e.g., cattle in India), stray animals (dogs, pigs, and birds) and open human defecation such as in slum area. From the wastewater treatment plants, the untreated antibiotics end up in sludge disseminated on fields as fertilizer or can be released as runoff directly into water (Hughes et al., 2012; Wellington et al., 2013). Sometimes, the wastewater is treated by releasing it into wetlands, thereby releasing antibiotics into water that directly or indirectly enter human and animals food chain (Scholz and Lee, 2005). A marked correlation has been noted between the routes of dispersal of antibiotics and resistant bacteria entering the human body (Baquero et al., 2008).

Impact of ARGs present in water on animal and human health needs further studies as does its use as a bacteriological indicator in terms of concentration and prevalence. Numerous decisive questions need to be answered in that aspect (Durso and Cook, 2018). There is a need to discover (1) whether the antibiotic resistance in real pathogens increases the risk of disease complications or results in increased cost of treatments of infections, and (2) whether presence of ARG in fecal indicators correlates in some way with high risk of horizontal gene transfer to pathogens still needs to be studied. At last, (3) the role of ARGs in environments in the emergence of antibiotic resistant pathogens needs to be assessed. There is a need to extensively study the interplay of environmental factors in relation to emergence of resistance which ultimately lead to evolve conceptual models for the role of environment in emergence and dissemination of resistance (Bengtsson-Palme et al., 2017).

People encounter with resistant microorganisms through various routes including drinking contaminated water, consuming contaminated vegetables, crops, fish, and meat.

The bacteria once entered human body then transfer the ARGs to microflora inhabiting the host (Wellington et al., 2013).

GUT MICROBIOTA AS A RESERVOIR FOR ARGs

Among various mechanisms facilitating the transfer of ARGs, the conjugative drug transfer of genetic determinants *viz*. plasmids and transposons, and transduction are important. However, the quantum and mechanism of ARG transfer from gut resistome to pathogens are still unknown. The macrolide-resistant genes *ermB*, *ermF*, and *ermG* and the tetracycline-resistant genes *tetM* and *tetQ* are likely to spread among other bacteria (Salyers et al., 2004). The ARGs from gut microorganisms tend to get transferred to related bacteria. For instance, the β-lactamase *cblA* present in Bacteroides is one of the most abundant ARGs in the microbiota of healthy persons as well as patients (Forslund et al., 2013). This gene hardly transfers to food-borne or opportunistic pathogens, such as Enterobacteriaceae, even though functional metagenomic analysis indicates that this gene β-lactamase is resistant to human *E. coli* (Sommer et al., 2009; Buelow et al., 2014).

It has been noted that transfer of resistant genes between unrelated bacteria, for example between anaerobic gut commensals (e.g., Bacteroides) and Gram-negative facultative anaerobic opportunistic pathogens (e.g., *Enterobacter*) does not occur readily. Even then conjugative transfer of ARGs from Bacteroides to *E. coli* is possible under controlled laboratory environment (Guiney and Davis, 1978; Privitera et al., 1979), however, within the gut, the conditions are adverse for such gene transfer.

With the use of metagenomics as a tool, it is possible to detect pathogens in the fecal samples (Loman et al., 2013), and track fluctuations in individual patients (Buelow et al., 2014). Probably, the diagnostic relevance of resistome profiling by metagenomic analysis is limited, performing sequencing and analyzing the metagenomic data are time-consuming processes (Singh et al., 2008).The advancement in high-throughput genomic sequencing technologies enabled rapid and reliable mapping of resistome in gut microbiome. This will guide the choice of antibiotics for curtailing infections, at least partially, by the composition and relative abundance of the ARGs in gene reservoir in patients. To fully assess the risks that are associated with the selection of ARGs in GI or genitourinary commensals, profiling of their ARGs and study of horizontal gene transfer is required.

The normal human microbiota is one of the main reservoirs of ARGs that can be transferred to pathogenic bacteria, which come in contact during disease progression. Dissemination of resistant microorganisms and ARGs occurs between humans during direct contact and spread into human-associated environments.

Studies have shown that multidrug-resistant uropathogenic *E. coli* (UPEC) share the same genetic lineages with the *E. coli* that infects poultry; this suggests that there is a high likelihood of food-borne transmissions of antibiotic-resistant UPEC and its genetic matter. To accurately quantify the contribution of food or food animals, to evaluate the impact of environmental samples as reservoirs for antibiotic-resistant bacteria and to plot their route of transmission to humans, modern technological tools such as whole genome sequencing (WGS) and metagenomics should be used. Such approaches will help develop focused public health interventions to prevent the infections.

ALTERNATIVE NON-ANTIBIOTIC STRATEGIES TO COMBAT ANTIBIOTIC-RESISTANT PATHOGENS

It is imperative to evolve alternative non-antibiotic strategies that are safer to humans and livestock and effective against infectious pathogens (Singh et al., 2014; Kumar et al., 2016). Use of bacteriophage (Kadouri et al., 2013; Shatzkes et al., 2017a,b), antimicrobial peptides (AMPs) or bacteriocins (Cotter et al., 2013; Kumar et al., 2016; Garcia-Gutierrez et al., 2019), antimicrobial adjuvants, fecal microbiota transplant (FMT) and competitive exclusion of pathogens through genetically modified probiotics and postbiotics are the prospective alternative unconventional strategies (**Figure 3**). In this context, research should also be carried out in finding ideal targets for new inhibitory molecules like bacterial secretion system and two component system. Bacterial secretion system is a highly specialized nano-mechanical system analogous to "nano-syringes" that are capable of direct delivery of substances in eukaryotic cells. This makes it a very desirable tool for nano-therapeutics and targeted drug delivery system. Of the six families known (type I–VI secretion systems), only the type III, IV, and VI systems have been shown to facilitate direct delivery into the cytoplasm of a target cell (Walker et al., 2017). Such targeted delivery of antimicrobials may reduce the rapidity of antimicrobial resistance evolution. In addition, Bacterial type III secretion system (T3SS) is an attractive target for developing antibacterial as it is essential in the pathogenesis of many Gram-negative bacteria (Mcshan and De Guzman, 2015). On the other hand, two component system (TCS) are global regulatory elements unique to bacteria that are essential for growth and virulence. The fact that they are not present in eukaryotic cells makes them a potentially attractive target for future antimicrobials. Several TCS involved in cell cycle and cell envelope integrity have been identified and show promise as targets for novel antimicrobials in a bid to alleviate MDR (Cardona et al., 2018).

STEM CELL-DERIVED ANTIMICROBIAL PEPTIDES

Mesenchymal stem cells (MSCs) have been extensively studied for several decades to develop a safe and promising therapeutic product against a broad range of chronic diseases. MSCs exhibit promising ability to promote immunomodulation, tissue healing and control of excessive inflammation (Harman et al., 2017). Recently, it was established that human MSCs synthesize factors that behave as antimicrobial peptides (AMPs) that eradicate the bacteria through multiple mechanisms including inhibition

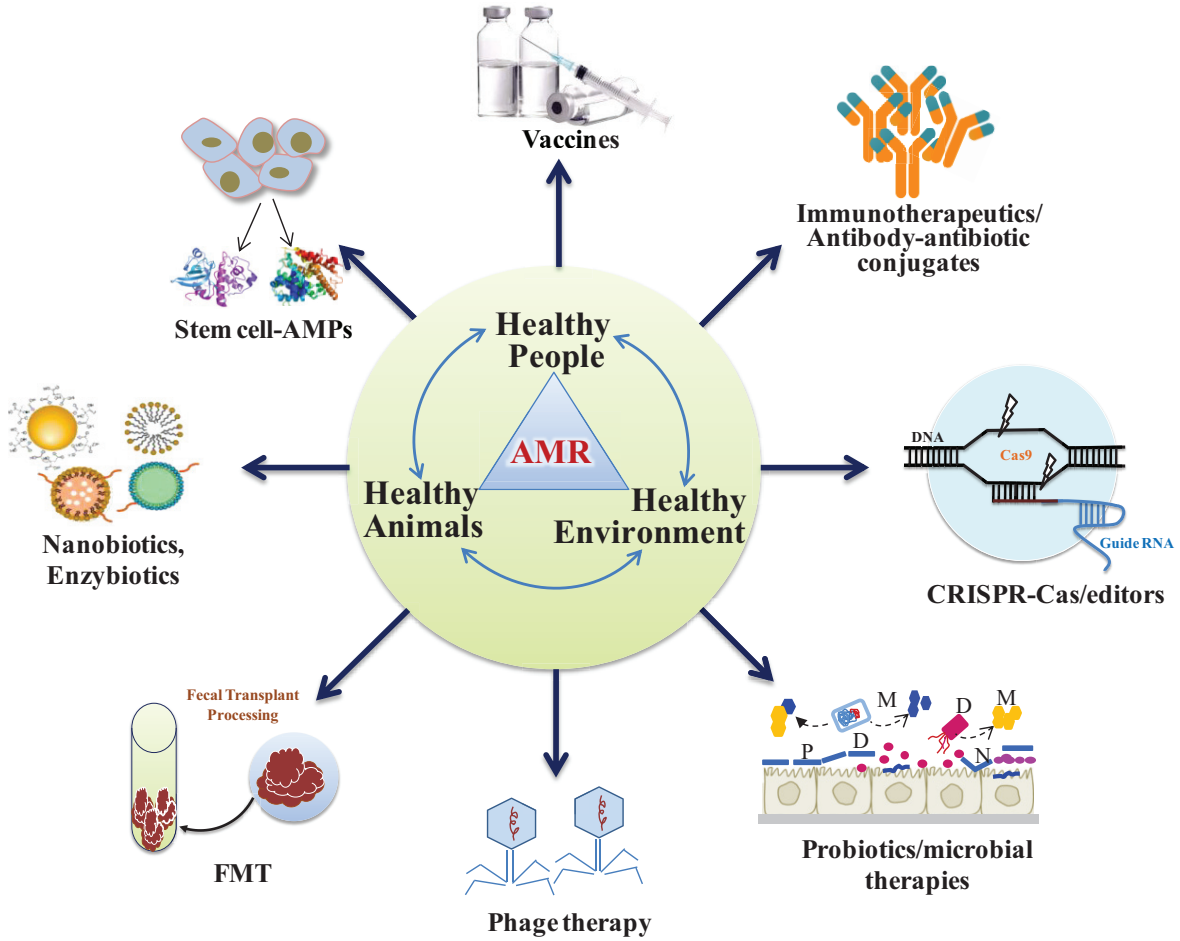

FIGURE 3 | Alternative non-antibiotic strategies to prevent antimicrobial-resistant infections in animals and humans. Probiotics and phages act as microbiome-modifying therapies to defend against drug-resistant pathogens. Healthy people, healthy animals and healthy environment constitute as One Health Concept to keep environment healthy (P, prebiotics; D, designer or engineered probiotics; M, microbial metabolites; FMT, fecal microbiota transplantation).

of bacterial cell wall synthesis (Alcayaga-Miranda et al., 2017; Cortes-Araya et al., 2018; Marx et al., 2020). Therefore, secretome from MSCs, which significantly reduces the bacterial infections including the antibiotic-resistant MRSA, represents a hopeful approach or supportive treatment in future against various related infections.

Conditioned medium containing AMPs named as lipocal, hepcidin and LL-37 derived from human bone marrow (BM) and umbilical-cord MSCs (hUCMSCs) was found to exhibit antibacterial effects against drug resistant clinical pathogens such as *E. coli*, *S. aureus* and *K. pneumonia* (Mccarthy et al., 2020). hUMSCs possessed direct antagonistic activities against imipenem-resistant *P. aeruginosa* isolated from human infants (Ren et al., 2020).

HEMOFILTRATION DEVICES

Suppressing the cytokine storm is important to prevent organ damage in several cases of critical illnesses and infections. Hemofiltration or renal replacement therapies used in intensive clinical care settings utilize the devices that bind to and remove circulating bacterial products, inflammatory mediators and cytokines (Liu et al., 2018) and some pathogens circulating in blood. Such devices, for example, extracorporeal pathogen removal filters are at various stages of development. Two of the more fascinating devices include the mannose-binding lectins (Mccrea et al., 2014) or bound heparin (Kang et al., 2014). It is thought that if substantial reduction in the pathogenic bacterial load is achieved by these hemofilters, the host immune system will be able to tackle the remaining pathogens even in cases of multidrug resistance.

Hemofiltration is useful in curtail the adverse effects of infections in infants and aged patients. It was found to reduce the serum levels of bile acid microbial metabolites namely, total bilirubin, direct bilirubin, total bile acids, lactate and IL-6 in patients suffering from bacterial sepsis and hepatic dysfunction (Cui et al., 2018). Various devises are available in markets for hemofiltration.

QUORUM-SENSING INHIBITORS

Formation of biofilms and quorum sensing are the two important attributes of bacterial species enhancing the chances of their survival under adverse environments. Quorum sensing is one of the main methods of intracellular communication between bacteria. An array of natural and synthetic molecules can block quorum sensing, which are under study in experimental models with interesting results. Several classes of compounds with potential quorum-sensing inhibitions are reported (Saeki et al., 2020). Whether quorum sensing inhibitors could ever be of practical clinical significance in preventing infections is a subject of considerable ponders (Kang et al., 2014; Brackman and Coenye, 2015).

CRISPR-Cas AGAINST ANTIMICROBIAL RESISTANT PATHOGENS

Clustered regularly interspaced short palindromic repeats (CRISPR)-cas is a distinctive adaptive immune feature in archaea and bacteria that provides protection against invading bacteriophages (Barrangou et al., 2007). Short sequences from bacteriophages or plasmids called as spacers are inserted into the bacterial genome as CRISPR array; the guide RNAs from the spacers will be utilized by the Cas protein machinery for specific targeting of the invading nucleic acid carrying the same sequence (Pursey et al., 2018; Shabbir et al., 2019). CRISPR-Cas systems are classified into two classes: class I comprises of types I, III, and IV, while class II consists of types II, V, and VI (Pursey et al., 2018). In Class I, multiple Cas proteins participate in DNA recognition and cleavage, whereas in class II, a single multi-domain Cas protein recognizes and cleaves the DNA (Pursey et al., 2018). The later (type II CRISPR-Cas9 system) has revolutionized molecular biology in the last decade and is used in genome editing of prokaryotes and eukaryotes. Several groups have shown the use of CRISPR-Cas9 in selective removal of AMR genes from bacterial populations (Bikard et al., 2014; Citorik et al., 2014). Phagemids and conjugative plasmids have been shown to deliver CRISPR-Cas for selective targeting of AMR genes in plasmids and chromosome, respectively (Bikard et al., 2014). Removal of AMR genes results in the sensitization of the bacteria to antibiotics (Citorik et al., 2014). CRISPR-Cas9 phagemids can kill specific bacteria *in vivo* (Bikard et al., 2014; Citorik et al., 2014). Delivering CRISPR-Cas through temperate phages can provide selective advantage to re-sensitized bacteria (Yosef et al., 2015). A synthetic biology strategy that utilizes engineering phage genomes in *Saccharomyces cerevisiae* has been shown to modulate the phage host spectrum (Ando et al., 2015). To circumvent the loading and packing efficiency in phage-based delivery, a successful non-viral editing strategy involving nano-sized CRISPR complexes (polymer-derivatized Cas9 complexed with single guide RNA) has been developed. Nanosized CRISPR complexes can effectively target the mec-A gene involved in methicillin-resistance inside the methicillin-resistant *S. aureus* (Kang et al., 2017). Despite the promise, there are some major challenges in the use of CRISPR-Cas9 system against AMR genes. These include perturbations in the microbial community after the removal of AMR bacteria, narrow host range of CRISPR-Cas vectors, resistance due to anti-CRISPR genes, and legislation (Pursey et al., 2018).

DEVELOPMENT AND USE OF IMMUNOTHERAPEUTIC AND VACCINES

As health authorities, clinicians and drug developers struggle with the emerging antimicrobial resistance (AMR) crisis, vaccines are considered as a potential solution. Immunotherapeutic are the biomolecules that boost the immune system of host and confer immunity against infectious agents. One of the most widely used immunotherapeutic agents is pegfilgrastim, a granulocyte colony-stimulating factor (G-CSF). It is used to increase the severely decreased neutrophil count in patients undergoing chemotherapy (Molineux, 2004).

Notably, it is important to maintain an appropriate neutrophil count in the blood so that the immune system can combat infections. Similar therapy is also used in animals in the form of pegbovigrastim, a bovine G-CSF used in cattle before parturition to improve immunity and reduce the incidences of mastitis. The advantage of immunotherapeutic agents lies in the fact that they boost the internal immune system. However, the disadvantage is the precise determination of timing of delivery.

Developments in new recombinant vaccine technology have been instrumental in reducing primary and secondary bacterial infections that would have necessitated the use of various antibiotics. Vaccines continue to be one of the most significant ways to prevent infections. A few of vaccines against deadly pathogenic bacteria, for example, *Clostridium difficile* (Phase III), *Mycobacterium tuberculosis* (Phase II), Group B *Streptococcus* (Phase II), *S. aureus* (Phase II) are in mid-stage clinical development by pharma companies.

PHAGE THERAPIES

Failure of currently available antibiotics to treat some infections is worrying biomedical problem (Wright et al., 2019; Pacios et al., 2020). Phage therapy is extensively investigated as an alternative therapy to combat bacterial infections. This therapy was introduced in the early 1920s in Georgia and later on in whole Eastern Europe and also western countries (Wittebole et al., 2014). Even though there are several challenges, the bacteriophage therapy has potential to be used as a substitute for antimicrobial agents against drug-resistant pathogens in future. The technique is gaining popularity in present scenario because phages are ubiquitous, host-specific

and harmless and can be administered orally along with food (Wittebole et al., 2014).

Recombinant phages are developed to deliver antimicrobial proteins in target bacteria. The therapy can be used topically on open wounds (Wright et al., 2009), or given intravenously in case of systemic infections. However, there are some serious concerns associated with phage therapy. The major one is their fine specificity toward host bacterium species. This precludes their applications as empiric therapy for acute infections.

Further, it is essential that pathogen must be identified before selecting a phage as therapeutic strategy. Developing and establishing a complete library of phages for every plausible infectious bacteria will be a big challenge (Wittebole et al., 2014). In addition, the therapy requires knowledge of the target sites. As it is likely that bacteria might develop resistance to phages, the phage libraries should be continuously screened for their efficacy to curtail bacterial pathogens.

Bacteriophage lysins, the extremely specific peptidoglycan hydrolases, were the base for their investigation as antibacterial agents and they were also named "enzybiotics" (Nelson et al., 2001). Owing to their modular structure, synthesis and use of bioengineered lysins with designed properties such as higher lytic activities or broader spectrum bacteriophages lysins are promising prospects. Lysins can be engineered to kill several pathogens including Gram-negative bacteria. These enzymes have attractive features that they do not activate an adverse immune response and raise of resistance is very unlikely.

As multidrug-resistant pathogens become a greater and more widespread threat, engineered lysins represent a newer modality of therapy, which is powerful and readily available to fight antimicrobial resistance (Vazquez et al., 2018).

FECAL MICROBIOTA TRANSPLANT (FMT)

Fecal microbiota transplant therapy is known by a variety of names as fecal bacteriotherapy, fecal transfusion, fecal transplant, fecal enema, human probiotic infusion, and stool transplant. But, in veterinary medicine, it is known as "transformation" used for treatment of ruminant animals such as sheep, cow, etc. (Depeters and George, 2014). The introduction of FMT into mainstream medicine was first described in 1958 to treat four ill patients suffering from pseudomembranous colitis (Eiseman et al., 1956). However, the first use of fecal enema therapy was described by Ge Hong in fourth-century China (Zhang et al., 2012). FMT is the process of transplantation of a suspension of fecal matter containing commensal bacteria from a healthy individual donor using various routes including enema, nasogastric, nasoduodenal and colonoscopy into intestinal lumen of the recipients (Bakken et al., 2011; Smits et al., 2013). Few studies have shown that FMT is an effective treatment regimen for people with *C. difficile* infection along with other gastrointestinal diseases, such as irritable bowel syndrome, colitis, constipation, diarrhea and several other neurological conditions such as Parkinson's, multiple sclerosis, etc. However, the safety and efficacy of FMT therapy is related to ethical issues; therefore, appropriate clinical trials, data and deep scientific research are needed for its approval as therapy owning to its new hope to save the humanity from antibiotic resistance menace.

Clinical trials have revealed that autologous FMT (aFMT) is better than probiotic therapy and induced a speedy and almost complete recovery of GI microbiota in antibiotics-perturbed human patients (Suez et al., 2018). Intention-to-treat clinical trial involving 22 patients in donor FMT group revealed that 20 of 22 (90.9%) patients achieved clinical cure from *Cl. difficile* infection. The success rate of clinical recovery was higher than aFMT (62.5%), and donor FMT restored the gut microbial diversity and functioning of the recipients comparable to the donors (Kelly et al., 2016). High-intensity FMT treatment in adult patients with mild to moderate ulcerative colitis (UC) resulted in high likelihood of remission at 8 weeks of the treatment. Though further research is suggested, it was observed that FMT had better outcomes than the aFMT (Costello et al., 2019).

NANOANTIBIOTICS

Nanoparticulate materials can either be used to deliver antimicrobial substances or may contain antimicrobial substances. The metal and metal oxide-based nanoparticles and antibiotics, due to less toxicity and enhanced antibacterial, antiviral and anticancer efficacy, are regarded as promising therapeutic candidates for future applications in biomedical sciences (Fernandez-Moure et al., 2017; Muzammil et al., 2018). Their size provides them with unique properties such as an increased surface area to volume ratio, which makes them efficient drug carriers and enhance their solubility, compatibility as well as ease of delivery (Wang et al., 2017). Nanoparticles, in addition to acting as carriers for targeted drug delivery, can have antibacterial properties of their own via several mechanisms such as disruption of bacterial wall, biofilm inhibition, modulation of immune response in host, generation of reactive oxygen species and damage to key DNA and protein molecules of the resistant bacteria (Baptista et al., 2018). Due to these diverse mechanisms of action, nano-antibiotics are likely to be effective against antibiotic resistant bacteria. Recently researchers demonstrated that bismuth nanoparticles exhibit broad anticandidal activity and slow down the spread of the multidrug-resistant *Candida auris* strains in the healthcare-settings (Vazquez-Munoz et al., 2020). However, detailed study of pharmacokinetics, precision of action and controllability of the nanoantibiotics need to be conducted to ensure its efficacy and safety in clinical settings.

PROBIOTICS, POSTBIOTICS AND SYNBIOTICS

Identification of novel animal-origin probiotics, and postbiotics, the non-viable microbial probiotics or probiotic metabolites that have biological activities in host (Tsilingiri et al., 2012; Aguilar-Toalá et al., 2018), and using them as alternative therapeutic combinations may facilitate the development of improved dosing

regimens and strategies to prevent economic loss due to enteric infections.

Probiotics, the live microorganisms or microbial feed supplements primarily comprise of two classes of lactic acid-producing microorganisms: the Bifidobacteria and lactic acid bacteria (LAB) including species of *Enterococcus*, *Lactobacillus*, *Lactococcus*, *Pediococcus*, *Vagococcus*, *Aerococcus*, *Carnobacterium*, *Streptococcus,* and *Weissella.* Most LAB, since generally regarded as safe status, and abundance of some genera in GI tract, mammary gland and feminine genitourinary tract (Singh and Madhup, 2013) are regarded as alternative health-promoting strategies. Advances in next generation sequencing and genetic engineering has enabled scientists to develop future strategies, such as bioengineered probiotics or pharmabiotics, which may become a bio-therapeutic or prophylactic strategy against bacterial infection. Bioengineered probiotics with manifold immunogenic properties could be a possible option against antibiotics. Engineered or recombinant probiotics could be personalized to deliver drugs, therapeutic proteins and gene therapy vectors with great competence, with a higher degree of site specificity than common drug administration regimes.

Vaccinations using recombinant probiotics against *Yersinia pseudotuberculosis*, *Salmonella enterica*, enterotoxigenic *E. coli*, and *Streptococcus pneumonia* (Wu and Chung, 2007; Daniel et al., 2009; Hernani et al., 2011; Kajikawa, 2012) have generated desirable immune responses in murine models. Recombinant probiotic bacteria *Lactobacillus acidophilus* and *Lactobacillus gasseri* were used to deliver protective antigen and exhibit anti-protective antigen antibody and T-cell–mediated responses against *Bacillus anthracis* (Mohamadzadeh et al., 2009). These promising therapies deserve further assessment before they are recommended for human use.

ONE HEALTH MODEL TO TACKLE AMR

Prevention of AMR is associated with the One Health concept. Since antibiotic resistance genes are persistent in environmental and human–animal health interfaces, an approach which deals with all the three areas is required, which highlights the concept of "One Health approach" (Chee-Sanford et al., 2009). The One Health approach is defined as "the mutual attempt of various disciplines- working locally nationally, and worldwide – to accomplish optimal health for humans, livestock and our environment" (Fletcher, 2015). This approach perceives that human health is linked to the health of animals and the environment and is applicable to the crisis of antibiotic resistance as well. Dissemination of ARGs through livestock is due to use of many antibiotics in animal rearing, in sub-therapeutic doses and with elongated exposure periods, these production systems generate perfect milieu for bacteria for horizontal gene transfer that confers resistance. ARGs can consequently be transmitted to human-adapted pathogens or other gut microorganisms. Since the antibiotics used for both animals and human beings are similar or closely related, as are most of the animal and human pathogenic bacteria, similar patterns of antimicrobial-resistance are likely to emerge, in addition transmission of such resistance through genetic transfer between animal and human pathogens is highly possible, either directly or via the environment.

The One Health approach for dealing with AMR, encircling all three pillars (human health, animal health, and environmental health), will depend on sound knowledge about the interactions and the ways how these components interrelate in the transmission to humans.

OUTLOOK AND CHALLENGES

While pressure is to increase production from the livestock sector, maintaining human and animal health is also essential. Even though the overall burden of drug-resistance is difficult to estimate, it seems reasonable to believe that the burden will be high in vulnerable groups such as immune-compromised elderly persons, patients and the neonates.

Indeed, antibiotics therapies have transformed treatments against bacterial and fungal infections. However, widespread infections are posing threats to human and animal health with several pathogens developing resistant to available antibiotics. The normal role of antibiotics in social context of the microbial communities is not clear. While some examples such as ARGs dissemination between environmental and pathogenic bacteria are evident, the intricacy of the mechanisms and relative paucity of the observations made so far are lacking. Processes and relative paucity of studies indicate that knowledge is still missing in the field.

Novel branded antibiotics, namely besifloxacin, ceftobiprole, ceftaroline, dalbavancin, delafloxacin, omadacycline, ozenoxacin, oritavancin, telavancin, and tedizolid are effective against drug-resistant Gram-positive infectious bacteria (Koulenti et al., 2019). However, it is likely that pathogens may develop resistance against these antibiotics as well. It is, therefore, imperative to use combinations of non-antibiotic therapies against infectious pathogens.

Developing alternative methods of producing animal-origin foods is one way to minimize environmental pollution and development of superbugs and AMR genes (Singh, 2020). We strongly posit that there is need to screen and utilize natural plant (Wright, 2017) and animal products (Singh et al., 2019) as alternative therapeutics. In addition, cutting edge molecular approaches, nanotechnology-oriented methods (Vikesland et al., 2019), genome and proteome databases of stem cells and microorganisms (Sharma R. et al., 2019) to identify potential bio-molecules as futuristic antimicrobial candidates against drug-resistant pathogens. Bioengineered microorganism or probiotics as drug-delivery vehicles, and their metabolites (Kumar et al., 2016) is another viable option to curb drug-resistant pathogens.

In conclusion, antibiotic resistance can affect the people or animals at any stage of life. It is advisable to develop alternative therapies to lessen the dependence on chemical therapeutics. The efficacy of antibiotics is waning since they became a part of modern medicine before seven decades. Experts from diverse fields such as clinical research, microbiology, genetics and computational engineering, imaging and modeling should work in combination to evolve strategies and develop novel

therapeutics to tackle the problem. Clinicians should avoid unnecessary prescription and over prescription of antibiotics to the patients having normal infections and advise the patients to follow good hygiene such as hand washing and appropriate infection control measures.

AUTHOR CONTRIBUTIONS

All authors listed have made a substantial, direct and intellectual contribution to the work, and approved it for publication.

REFERENCES

Aguilar-Toalá, J., Garcia-Varela, R., Garcia, H., Mata-Haro, V., González-Córdova, A., Vallejo-Cordoba, B., et al. (2018). Postbiotics: An evolving term within the functional foods field. *Trends Food Sci. Technol.* 75, 105–114. doi: 10.1016/j.tifs.2018.03.009

Akiba, T., Koyama, K., Ishiki, Y., Kimura, S., and Fukushima, T. (1960). On the mechanism of the development of multiple drug-resistant clones of *Shigella*. *Japan. J. Microbiol.* 4, 219–227. doi: 10.1111/j.1348-0421.1960.tb00170.x

Alcayaga-Miranda, F., Cuenca, J., and Khoury, M. (2017). Antimicrobial Activity of Mesenchymal Stem Cells: Current Status and New Perspectives of Antimicrobial Peptide-Based Therapies. *Front. Immunol.* 8:339. doi: 10.3389/fimmu.2017.00339

Allen, H. K. (2014). Antibiotic resistance gene discovery in food-producing animals. *Curr. Opin. Microbiol.* 19, 25–29. doi: 10.1016/j.mib.2014.06.001

Anderson, R., Higgins, H. Jr., and Pettinga, C. (1961). Symposium: how a drug is born. *Cinc. J. Med.* 42, 49–60.

Ando, H., Lemire, S., Pires, D. P., and Lu, T. K. (2015). Engineering Modular Viral Scaffolds for Targeted Bacterial Population Editing. *Cell Syst.* 1, 187–196. doi: 10.1016/j.cels.2015.08.013

Andrew, W. (2013). *Pharmaceutical manufacturing encyclopedia*. New York: Springer, 305.

Armstrong, G. L., Conn, L. A., and Pinner, R. W. (1999). Trends in infectious disease mortality in the United States during the 20th century. *JAMA* 281, 61–66. doi: 10.1001/jama.281.1.61

Bakken, J. S., Borody, T., Brandt, L. J., Brill, J. V., Demarco, D. C., Franzos, M. A., et al. (2011). Treating Clostridium difficile infection with fecal microbiota transplantation. *Clin. Gastroenterol. Hepatol.* 9, 1044–1049.

Baptista, P. V., Mccusker, M. P., Carvalho, A., Ferreira, D. A., Mohan, N. M., Martins, M., et al. (2018). Nano-Strategies to Fight Multidrug Resistant Bacteria-"A Battle of the Titans". *Front. Microbiol.* 9:1441. doi: 10.3389/fmicb.2018.01441

Baquero, F., Martínez, J.-L., and Cantón, R. (2008). Antibiotics and antibiotic resistance in water environments. *Curr. Opin. Biotechnol.* 19, 260–265. doi: 10.1016/j.copbio.2008.05.006

Barrangou, R., Fremaux, C., Deveau, H., Richards, M., Boyaval, P., Moineau, S., et al. (2007). CRISPR provides acquired resistance against viruses in prokaryotes. *Science* 315, 1709–1712. doi: 10.1126/science.1138140

Bates, J. (1997). Epidemiology of vancomycin-resistant enterococci in the community and the relevance of farm animals to human infection. *J. Hosp. Infect.* 37, 89–101. doi: 10.1016/s0195-6701(97)90179-1

Bebrone, C. (2007). Metallo-β-lactamases (classification, activity, genetic organization, structure, zinc coordination) and their superfamily. *Biochemical. Pharmacol.* 74, 1686–1701. doi: 10.1016/j.bcp.2007.05.021

Bengtsson-Palme, J., Kristiansson, E., and Larsson, D. J. (2017). Environmental factors influencing the development and spread of antibiotic resistance. *FEMS Microbiol. Rev.* 42:fux053.

Bérdy, J. (2012). Thoughts and facts about antibiotics: where we are now and where we are heading. *J. Antibiot.* 65, 385–395. doi: 10.1038/ja.2012.27

Bikard, D., Euler, C. W., Jiang, W., Nussenzweig, P. M., Goldberg, G. W., Duportet, X., et al. (2014). Exploiting CRISPR-Cas nucleases to produce sequence-specific antimicrobials. *Nat. Biotechnol.* 32, 1146–1150. doi: 10.1038/nbt.3043

Bongaerts, G. P., and Kaptijn, G. M. (1981). Aminoglycoside phosphotransferase-II-mediated amikacin resistance in *Escherichia coli*. *Antimicrob. Agents Chemother.* 20, 344–350. doi: 10.1128/aac.20.3.344

Brackman, G., and Coenye, T. (2015). Inhibition of Quorum Sensing in Staphylococcus spp. *Curr. Pharm. Des.* 21, 2101–2108. doi: 10.2174/1381612821666150310101014

Buelow, E., Gonzalez, T. B., Versluis, D., Oostdijk, E. A., Ogilvie, L. A., Van Mourik, M. S., et al. (2014). Effects of selective digestive decontamination (SDD) on the gut resistome. *J. Antimicrob. Chemother.* 69, 2215–2223. doi: 10.1093/jac/dku092

Burwen, D. R., Banerjee, S. N., Gaynes, R. P., and System, N. N. I. S. (1994). Ceftazidime resistance among selected nosocomial gram-negative bacilli in the United States. *J. Infect. Dis.* 170, 1622–1625. doi: 10.1093/infdis/170.6.1622

Butler, M. S., Hansford, K. A., Blaskovich, M. A., Halai, R., and Cooper, M. A. (2014). Glycopeptide antibiotics: back to the future. *J. Antibiot.* 67, 631–644. doi: 10.1038/ja.2014.111

Cardona, S. T., Choy, M., and Hogan, A. M. (2018). Essential Two-Component Systems Regulating Cell Envelope Functions: Opportunities for Novel Antibiotic Therapies. *J. Membr. Biol.* 251, 75–89. doi: 10.1007/s00232-017-9995-5

Castanheira, M., Pereira, A. S., Nicoletti, A. G., Pignatari, A. C., Barth, A. L., and Gales, A. C. (2007). First report of plasmid-mediated qnrA1 in a ciprofloxacin-resistant *Escherichia coli* strain in Latin America. *Antimicrob Agents Chemother.* 51, 1527–1529. doi: 10.1128/aac.00780-06

CDC (2013). *Office of Infectious Disease Antibiotic Resistance Threats in the United States, 2013*. Atlanta, GA: Centers for Disease Control and Prevention.

Chee-Sanford, J. C., Mackie, R. I., Koike, S., Krapac, I. G., Lin, Y. F., Yannarell, A. C., et al. (2009). Fate and transport of antibiotic residues and antibiotic resistance genes following land application of manure waste. *J. Environ. Qual.* 38, 1086–1108. doi: 10.2134/jeq2008.0128

Citorik, R. J., Mimee, M., and Lu, T. K. (2014). Sequence-specific antimicrobials using efficiently delivered RNA-guided nucleases. *Nat. Biotechnol.* 32:1141. doi: 10.1038/nbt.3011

Cortes-Araya, Y., Amilon, K., Rink, B. E., Black, G., Lisowski, Z., Donadeu, F. X., et al. (2018). Comparison of Antibacterial and Immunological Properties of Mesenchymal Stem/Stromal Cells from Equine Bone Marrow, Endometrium, and Adipose Tissue. *Stem Cells Dev.* 27, 1518–1525. doi: 10.1089/scd.2017.0241

Costello, S. P., Hughes, P. A., Waters, O., Bryant, R. V., Vincent, A. D., Blatchford, P., et al. (2019). Effect of Fecal Microbiota Transplantation on 8-Week Remission in Patients With Ulcerative Colitis: A Randomized Clinical Trial. *JAMA* 321, 156–164. doi: 10.1001/jama.2018.20046

Cotter, P. D., Ross, R. P., and Hill, C. (2013). Bacteriocins - a viable alternative to antibiotics? *Nat. Rev. Microbiol.* 11, 95–105. doi: 10.1038/nrmicro2937

Crofton, J., and Mitchison, D. A. (1948). Streptomycin resistance in pulmonary tuberculosis. *Br. Med. J.* 2, 1009–1015. doi: 10.1136/bmj.2.4588.1009

Cui, Y., Xiong, X., Wang, F., Ren, Y., Wang, C., and Zhang, Y. (2018). Continuous hemofiltration improves the prognosis of bacterial sepsis complicated by liver dysfunction in children. *BMC Pediatr.* 18:269. doi: 10.1186/s12887-018-1243-3

Daniel, C., Sebbane, F., Poiret, S., Goudercourt, D., Dewulf, J., Mullet, C., et al. (2009). Protection against Yersinia pseudotuberculosis infection conferred by a Lactococcus lactis mucosal delivery vector secreting LcrV. *Vaccine* 27, 1141–1144. doi: 10.1016/j.vaccine.2008.12.022

Depardieu, F., Bonora, M. G., Reynolds, P. E., and Courvalin, P. (2003). The vanG glycopeptide resistance operon from Enterococcus faecalis revisited. *Mol. Microbiol.* 50, 931–948. doi: 10.1046/j.1365-2958.2003.03737.x

Depeters, E. J., and George, L. W. (2014). Rumen transfaunation. *Immunol. Lett.* 162, 69–76. doi: 10.1016/j.imlet.2014.05.009

Durso, L. M., and Cook, K. L. (2018). One health and antibiotic resistance in agroecosystems. *EcoHealth* 16, 414–419. doi: 10.1007/s10393-018-1324-7

Eiseman, B., Owens, J. C., and Swan, H. (1956). Hypothermia in general surgery. *N. Engl. J. Med.* 255, 750–755.

FDA (2010). *Forest Announces FDA Approval of Teflaro (ceftaroline fosamil) for the Treatment of Community-Acquired Bacterial Pneumonia and Acute Bacterial Skin and Skin Structure Infection* [Online]. Available online at: https://www.businesswire.com/news/home/20101029006328/en/Forest-Announces-FDA-Approval-Teflaro%E2%84%A2-ceftaroline-fosamil (accessed on October 30, 2010).

FDA (2015). *AVYCAZ safely and effectively [Online]. Forest Pharmaceuticals: FDA*. Available online at: https://www.accessdata.fda.gov/drugsatfda_docs/label/2015/206494s000lbl.pdf (accessed on Feb 2015 2015).

FDA (2017). *Antimicrobials sold or distributed for use in food-producing animals*. Maryland: FDA.

Fernandez-Moure, J. S., Evangelopoulos, M., Colvill, K., Van Eps, J. L., and Tasciotti, E. (2017). Nanoantibiotics: a new paradigm for the treatment of surgical infection. *Nanomedicine* 12, 1319–1334. doi: 10.2217/nnm-2017-0401

Finland, M., Jones, W. F. Jr., and Nichols, R. L. (1956). Development of resistance and cross-resistance in vitro to erythromycin, carbomycin, spiramycin, oleandomycin and streptogramin. *Proc. Soc. Exp. Biol. Med.* 93, 388–393. doi: 10.3181/00379727-93-22766

Fischer, J., Ganellin, C. R., Ganesan, A., and Proudfoot, J. (2010). *Analogue-based drug discovery*. Hoboken, NJ: Wiley-VCH.

Fletcher, S. (2015). Understanding the contribution of environmental factors in the spread of antimicrobial resistance. *Environ. Health Prev. Med.* 20, 243–252. doi: 10.1007/s12199-015-0468-0

Forslund, K., Sunagawa, S., Kultima, J. R., Mende, D. R., Arumugam, M., Typas, A., et al. (2013). Country-specific antibiotic use practices impact the human gut resistome. *Genome Res.* 23, 1163–1169. doi: 10.1101/gr.155465.113

Founou, R. C., Founou, L. L., and Essack, S. Y. (2017). Clinical and economic impact of antibiotic resistance in developing countries: A systematic review and meta-analysis. *PLoS One* 12:e0189621. doi: 10.1371/journal.pone.0189621

Ganguly, N., Arora, N., Chandy, S., Fairoze, M., Gill, J., Gupta, U., et al. (2011). Global antibiotic resistance partnership (GARP): India Working Group. *Indian J. Med. Res.* 134, 281–294.

Garcia-Gutierrez, E., Mayer, M. J., Cotter, P. D., and Narbad, A. (2019). Gut microbiota as a source of novel antimicrobials. *Gut Microbes* 10, 1–21. doi: 10.1080/19490976.2018.1455790

Goutard, F. L., Bordier, M., Calba, C., Erlacher-Vindel, E., Góchez, D., De Balogh, K., et al. (2017). Antimicrobial policy interventions in food animal production in South East Asia. *BMJ* 358:j3544. doi: 10.1136/bmj.j3544

Greene, W. H., Moody, M., Schimpff, S., Young, V. M., and Wiernik, P. H. (1973). *Pseudomonas aeruginosa* resistant to carbenicillin and gentamicin. *Ann. Intern. Med.* 79, 684–689.

Guiney, D. G., and Davis, C. E. (1978). Identification of a conjugative R plasmid in *Bacteroides* ochraceus capable of transfer to *Escherichia coli*. *Nature* 274, 181–182. doi: 10.1038/274181a0

Gupta, A., Mumtaz, S., Li, C.-H., Hussain, I., and Rotello, V. M. (2019). Combatting antibiotic-resistant bacteria using nanomaterials. *Chem. Soc. Rev.* 48, 415–427. doi: 10.1039/c7cs00748e

Hall, B. G., Salipante, S. J., and Barlow, M. (2004). Independent Origins of Subgroup Bl+ B2 and Subgroup B3Metallo-β-Lactamases. *J. Mole. Evolut.* 59, 133–141.

Harman, R. M., Yang, S., He, M. K., and Van De Walle, G. R. (2017). Antimicrobial peptides secreted by equine mesenchymal stromal cells inhibit the growth of bacteria commonly found in skin wounds. *Stem Cell Res. Ther.* 8:157.

Hernani, M. D. L., Ferreira, P. C., Ferreira, D. M., Miyaji, E. N., Ho, P. L., and Oliveira, M. L. (2011). Nasal immunization of mice with Lactobacillus casei expressing the pneumococcal surface protein C primes the immune system and decreases pneumococcal nasopharyngeal colonization in mice. *FEMS Immunol. Med. Microbiol.* 62, 263–272. doi: 10.1111/j.1574-695x.2011.00809.x

Heuer, H., Schmitt, H., and Smalla, K. (2011). Antibiotic resistance gene spread due to manure application on agricultural fields. *Curr. Opin. Microbiol.* 14, 236–243. doi: 10.1016/j.mib.2011.04.009

Hughes, S. R., Kay, P., and Brown, L. E. (2012). Global synthesis and critical evaluation of pharmaceutical data sets collected from river systems. *Environ. Sci. Technol.* 47, 661–677. doi: 10.1021/es3030148

Humphries, R. M., Yang, S., Hemarajata, P., Ward, K. W., Hindler, J. A., Miller, S. A., et al. (2015). First Report of Ceftazidime-Avibactam Resistance in a KPC-3-Expressing *Klebsiella pneumoniae* Isolate. *Antimicrob. Agents Chemother.* 59, 6605–6607. doi: 10.1128/aac.01165-15

Jevons, M. P. (1961). "Celbenin"-resistant staphylococci. *Br. Med. J.* 1:24.

John, J. F. Jr., Mcneill, W. F., Price, K. E., and Kresel, P. A. (1982). Evidence for a chromosomal site specifying amikacin resistance in multiresistant *Serratia marcescens*. *Antimicrob. Agents Chemother.* 21, 587–591. doi: 10.1128/aac.21.4.587

Johnson, A. P., Uttley, A. H., Woodford, N., and George, R. C. (1990). Resistance to vancomycin and teicoplanin: an emerging clinical problem. *Clin. Microbiol. Rev.* 3, 280–291. doi: 10.1128/cmr.3.3.280

Kadouri, D. E., To, K., Shanks, R. M., and Doi, Y. (2013). Predatory bacteria: a potential ally against multidrug-resistant Gram-negative pathogens. *PLoS One* 8:e63397. doi: 10.1371/journal.pone.0063397

Kajikawa, A. (2012). [Protection against *Salmonella* via immunization with recombinant lactic acid bacteria]. *Nihon. Rinsho.* 70, 1293–1297.

Kang, J. H., Super, M., Yung, C. W., Cooper, R. M., Domansky, K., Graveline, A. R., et al. (2014). An extracorporeal blood-cleansing device for sepsis therapy. *Nat. Med.* 20, 1211–1216. doi: 10.1038/nm.3640

Kang, Y. K., Kwon, K., Ryu, J. S., Lee, H. N., Park, C., and Chung, H. J. (2017). Nonviral Genome Editing Based on a Polymer-Derivatized CRISPR Nanocomplex for Targeting Bacterial Pathogens and Antibiotic Resistance. *Bioconjug. Chem.* 28, 957–967. doi: 10.1021/acs.bioconjchem.6b00676

Kelly, C. R., Khoruts, A., Staley, C., Sadowsky, M. J., Abd, M., Alani, M., et al. (2016). Effect of Fecal Microbiota Transplantation on Recurrence in Multiply Recurrent Clostridium difficile Infection: A Randomized Trial. *Ann. Intern. Med.* 165, 609–616. doi: 10.7326/m16-0271

Klein, E. Y., Tseng, K. K., Pant, S., and Laxminarayan, R. (2019). Tracking global trends in the effectiveness of antibiotic therapy using the Drug Resistance Index. *BMJ Global. Health* 4:e001315. doi: 10.1136/bmjgh-2018-001315

Klein, E. Y., Van Boeckel, T. P., Martinez, E. M., Pant, S., Gandra, S., Levin, S. A., et al. (2018). Global increase and geographic convergence in antibiotic consumption between 2000 and 2015. *Pro. Natl. Acad. Sci.* 115, E3463–E3470.

Knothe, H., Shah, P., Krcmery, V., Antal, M., and Mitsuhashi, S. (1983). Transferable resistance to cefotaxime, cefoxitin, cefamandole and cefuroxime in clinical isolates of *Klebsiella pneumoniae* and *Serratia marcescens*. *Infection* 11, 315–317. doi: 10.1007/bf01641355

Koulenti, D., Song, A., Ellingboe, A., Abdul-Aziz, M. H., Harris, P., Gavey, E., et al. (2019). Infections by multidrug-resistant Gram-negative Bacteria: What's new in our arsenal and what's in the pipeline? *Int. J. Antimicrob. Agents* 53, 211–224. doi: 10.1016/j.ijantimicag.2018.10.011

Kumar, M., Yadav, A. K., Verma, V., Singh, B., Mal, G., Nagpal, R., et al. (2016). Bioengineered probiotics as a new hope for health and diseases: an overview of potential and prospects. *Fut. Microbiol.* 11, 585–600. doi: 10.2217/fmb.16.4

Laxminarayan, R., and Chaudhury, R. R. (2016). Antibiotic resistance in India: drivers and opportunities for action. *PLoS medicine* 13:e1001974. doi: 10.1371/journal.pmed.1001974

Laxminarayan, R., Matsoso, P., Pant, S., Brower, C., Rottingen, J. A., Klugman, K., et al. (2016). Access to effective antimicrobials: a worldwide challenge. *Lancet* 387, 168–175.

Leclercq, R., Derlot, E., Duval, J., and Courvalin, P. (1988). Plasmid-mediated resistance to vancomycin and teicoplanin in Enterococcus faecium. *N. Engl. J. Med.* 319, 157–161. doi: 10.1056/nejm198807213190307

Lesch, J. E. (2007). *The first miracle drugs: how the sulfa drugs transformed medicine*. USA: Oxford University Press.

Levine, J. F., Maslow, M. J., Leibowitz, R. E., Pollock, A. A., Hanna, B. A., Schaeffer, S., et al. (1985). Amikacin-resistant gram-negative bacilli: correlation of occurrence with amikacin use. *J. Infect. Dis.* 151, 295–300. doi: 10.1093/infdis/151.2.295

Levy, S. B., and Marshall, B. (2004). Antibacterial resistance worldwide: causes, challenges and responses. *Nat. Med.* 10:S122.

Lewis, K. (2013). Platforms for antibiotic discovery. *Nat. Rev. Drug Discov.* 12, 371–387. doi: 10.1038/nrd3975

Li, J. J., and Corey, E. J. (2013). *Drug discovery: practices, processes, and perspectives*. Netherland: John Wiley & Sons.

Lima, R., Del Fiol, F. S., and Balcão, V. M. (2019). Prospects for the use of new technologies in combating multidrug-resistant bacteria. *Front. Pharmacol.* 10:692. doi: 10.3389/fphar.2019.00692

Liu, Y., Chen, X., Wang, D., Li, H., Huang, J., Zhang, Z., et al. (2018). Hemofiltration Successfully Eliminates Severe Cytokine Release Syndrome Following CD19 CAR-T-Cell Therapy. *J. Immunother.* 41, 406–410. doi: 10.1097/cji.0000000000000243

Loman, N. J., Constantinidou, C., Christner, M., Rohde, H., Chan, J. Z., Quick, J., et al. (2013). A culture-independent sequence-based metagenomics approach to the investigation of an outbreak of Shiga-toxigenic *Escherichia coli* O104:H4. *JAMA* 309, 1502–1510. doi: 10.1001/jama.2013.3231

Mangili, A., Bica, I., Snydman, D. R., and Hamer, D. H. (2005). Daptomycin-resistant, methicillin-resistant Staphylococcus aureus bacteremia. *Clin. Infect. Dis.* 40, 1058–1060.

Martínez, J. L., Coque, T. M., Lanza, V. F., De La Cruz, F., and Baquero, F. (2017). Genomic and metagenomic technologies to explore the antibiotic resistance mobilome. *Anna. N. Y. Acad. Sci.* 1388, 26–41. doi: 10.1111/nyas.13282

Martinez, J. L., Fajardo, A., Garmendia, L., Hernandez, A., Linares, J. F., Martínez-Solano, L., et al. (2008). A global view of antibiotic resistance. *FEMS Microbiol. Rev.* 33, 44–65.

Marx, C., Gardner, S., Harman, R. M., and Van De Walle, G. R. (2020). The mesenchymal stromal cell secretome impairs methicillin-resistant Staphylococcus aureus biofilms via cysteine protease activity in the equine model. *Stem Cells Transl. Med.* 9, 746–757. doi: 10.1002/sctm.19-0333

Mary, C. P. (2007). *Antibiotic use on the farm hurts people—and doesn't help the bottom line*. US: Discover Magazine.

Mccarthy, S. D., Horgan, E., Ali, A., Masterson, C., Laffey, J. G., Macloughlin, R., et al. (2020). Nebulized Mesenchymal Stem Cell Derived Conditioned Medium Retains Antibacterial Properties Against Clinical Pathogen Isolates. *J. Aerosol. Med. Pulm. Drug. Deliv.* 33, 140–152. doi: 10.1089/jamp.2019.1542

Mccrea, K., Ward, R., and Larosa, S. P. (2014). Removal of Carbapenem-Resistant *Enterobacteriaceae* (CRE) from blood by heparin-functional hemoperfusion media. *PLoS One* 9:e114242. doi: 10.1371/journal.pone.0114242

Mcshan, A. C., and De Guzman, R. N. (2015). The bacterial type III secretion system as a target for developing new antibiotics. *Chem. Biol. Drug Design* 85, 30–42. doi: 10.1111/cbdd.12422

Merchant, S., Proudfoot, E. M., Quadri, H. N., Mcelroy, H. J., Wright, W. R., Gupta, A., et al. (2018). Risk factors for *Pseudomonas aeruginosa* infections in Asia-Pacific and consequences of inappropriate initial antimicrobial therapy: A systematic literature review and meta-analysis. *J. Global. Antimicrobial. Resist.* 14, 33–44. doi: 10.1016/j.jgar.2018.02.005

Mohamadzadeh, M., Duong, T., Sandwick, S. J., Hoover, T., and Klaenhammer, T. R. (2009). Dendritic cell targeting of Bacillus anthracis protective antigen expressed by Lactobacillus acidophilus protects mice from lethal challenge. *Proc. Natl. Acad. Sci. U. S. A.* 106, 4331–4336. doi: 10.1073/pnas.0900029106

Molineux, G. (2004). The design and development of pegfilgrastim (PEG-rmetHuG-CSF, Neulasta§). *Curr. Pharmaceut. Design* 10, 1235–1244. doi: 10.2174/1381612043452613

Mullard, A. (2015). *2014 FDA drug approvals*. Berlin: Nature Publishing Group.

Murray, B. E. (2000). Vancomycin-resistant enterococcal infections. *N. Engl. J. Med.* 342, 710–721.

Muzammil, S., Hayat, S., Fakhar, E. A. M., Aslam, B., Siddique, M. H., Nisar, M. A., et al. (2018). Nanoantibiotics: Future nanotechnologies to combat antibiotic resistance. *Front. Biosci.* 10, 352–374. doi: 10.2741/e827

Nelson, D., Loomis, L., and Fischetti, V. A. (2001). Prevention and elimination of upper respiratory colonization of mice by group A streptococci by using a bacteriophage lytic enzyme. *Proc. Natl. Acad. Sci. U S A* 98, 4107–4112. doi: 10.1073/pnas.061038398

Nordmann, P., Dortet, L., and Poirel, L. (2012). Carbapenem resistance in *Enterobacteriaceae*: here is the storm! *Trends Mole. Med.* 18, 263–272. doi: 10.1016/j.molmed.2012.03.003

OECD (2019). *Antimicrobial resistance. Tackling the burden in the European Union. Briefing note for EU/EAA countries* [Online]. Available online at: https://www.oecd.org/health/health-systems/AMR-Tackling-the-Burden-in-the-EU-OECD-ECDC-Briefing-Note-2019.pdf (accessed on March 18, 2019 2019).

Pacios, O., Blasco, L., Bleriot, I., Fernandez-Garcia, L., Gonzalez Bardanca, M., Ambroa, A., et al. (2020). Strategies to Combat Multidrug-Resistant and Persistent Infectious Diseases. *Antibiotics* 9:65. doi: 10.3390/antibiotics9020065

Planta, M. B. (2007). The role of poverty in antimicrobial resistance. *J. Am. Board Fam. Med.* 20, 533–539. doi: 10.3122/jabfm.2007.06.070019

Privitera, G., Dublanchet, A., and Sebald, M. (1979). Transfer of multiple antibiotic resistance between subspecies of *Bacteroides* fragilis. *J. Infect. Dis.* 139, 97–101. doi: 10.1093/infdis/139.1.97

Pursey, E., Sunderhauf, D., Gaze, W. H., Westra, E. R., and Van Houte, S. (2018). CRISPR-Cas antimicrobials: Challenges and future prospects. *PLoS Pathog* 14:e1006990. doi: 10.1371/journal.ppat.1006990

Ramsey, C. H., and Edwards, P. R. (1961). Resistance of *Salmonella*e isolated in 1959 and 1960 to tetracyclines and chloramphenicol. *Appl. Microbiol.* 9, 389–391. doi: 10.1128/aem.9.5.389-391.1961

Ravina, E. (2011). *The evolution of drug discovery: from traditional medicines to modern drugs*. New York: John Wiley & Sons.

Ren, Z., Zheng, X., Yang, H., Zhang, Q., Liu, X., Zhang, X., et al. (2020). Human umbilical-cord mesenchymal stem cells inhibit bacterial growth and alleviate antibiotic resistance in neonatal imipenem-resistant *Pseudomonas aeruginosa* infection. *Innate Immun.* 26, 215–221. doi: 10.1177/1753425919883932

Res, R., Hoti, K., and Charrois, T. L. (2017). Pharmacists' perceptions regarding optimization of antibiotic prescribing in the community. *J. Pharm. Pract.* 30, 146–153. doi: 10.1177/0897190015623883

Resistance, A. (2004). *Federal Agencies Need to Better Focus Efforts to Address Risk to Humans from Antibiotic Use in Animals. Report to Congressional Requesters*. Washington, DC: US General Accounting Office.

Rossiter, S. E., Fletcher, M. H., and Wuest, W. M. (2017). Natural products as platforms to overcome antibiotic resistance. *Chem. Rev.* 117, 12415–12474. doi: 10.1021/acs.chemrev.7b00283

Roy, J. (2011). *An introduction to pharmaceutical sciences: Production, chemistry, techniques and technology*. Netherland: Elsevier.

Saeki, E. K., Kobayashi, R. K. T., and Nakazato, G. (2020). Quorum sensing system: Target to control the spread of bacterial infections. *Microb. Pathog.* 142:104068. doi: 10.1016/j.micpath.2020.104068

Salyers, A. A., Gupta, A., and Wang, Y. (2004). Human intestinal bacteria as reservoirs for antibiotic resistance genes. *Trends Microbiol.* 12, 412–416. doi: 10.1016/j.tim.2004.07.004

Schatz, A., Bugie, E., and Waksman, S. A. (2005). Streptomycin, a substance exhibiting antibiotic activity against gram-positive and gram-negative bacteria 1944. *Clin. Orthop. Relat. Res.* 437, 3–6. doi: 10.1097/01.blo.0000175887.98112.fe

Scholz, M., and Lee, B. H. (2005). Constructed wetlands: a review. *Int. J. Environ. Stud.* 62, 421–447.

Sensi, P. (1983). History of the development of rifampin. *Rev. Infect. Dis.* 5, S402–S406.

Shabbir, M. A. B., Shabbir, M. Z., Wu, Q., Mahmood, S., Sajid, A., Maan, M. K., et al. (2019). CRISPR-cas system: biological function in microbes and its use to treat antimicrobial resistant pathogens. *Anna. Clin. Microbiol. Antimicr.* 18:21.

Sharma, S., Gupta, J., Prabhakar, P. K., Gupta, P., Solanki, P., and Rajput, A. (2019). Phytochemical repurposing of natural molecule: Sabinene for identification of novel therapeutic benefits using in silico and in vitro approaches. *ASSAY Drug Devel. Technol.* 17, 339–351. doi: 10.1089/adt.2019.939

Sharma, R., Pielstick, B. A., Bell, K. A., Nieman, T. B., Stubbs, O. A., Yeates, E. L., et al. (2019). A novel, highly-related jumbo family of bacteriophages that were isolated against Erwinia. *Front. Microbiol.* 10:1533. doi: 10.3389/fmicb.2019.01533

Shatzkes, K., Connell, N. D., and Kadouri, D. E. (2017a). Predatory bacteria: a new therapeutic approach for a post-antibiotic era. *Fut. Med.* 12, 469–472. doi: 10.2217/fmb-2017-0021

Shatzkes, K., Tang, C., Singleton, E., Shukla, S., Zuena, M., Gupta, S., et al. (2017b). Effect of predatory bacteria on the gut bacterial microbiota in rats. *Scient. Rep.* 7:43483.

Sievert, D. M., Rudrik, J. T., Patel, J. B., Mcdonald, L. C., Wilkins, M. J., and Hageman, J. C. (2008). Vancomycin-resistant Staphylococcus aureus in the United States, 2002–2006. *Clin. Infect. Dis.* 46, 668–674.

Simon, C. (2011). *Sulfanilamide (and its relatives).* [Online]. Available online at: http://www.chm.bris.ac.uk/motm/sulfanilamide2/sulfanilamideh.htm (accessed on May 30, 2011).

Singh, B., Gautam, S. K., Verma, V., Kumar, M., and Singh, B. (2008). Metagenomics in animal gastrointestinal ecosystem: Potential biotechnological prospects. *Anaerobe* 14, 138–144. doi: 10.1016/j.anaerobe.2008.03.002

Singh, K. (2020). *Nanosensors for Food Safety and Environmental Monitoring Nanotechnology for Food, Agriculture, and Environment*. New York: Springer, 63–84.

Singh, P., Kim, Y. J., Zhang, D., and Yang, D. C. (2016). Biological Synthesis of Nanoparticles from Plants and Microorganisms. *Trends Biotechnol.* 34, 588–599. doi: 10.1016/j.tibtech.2016.02.006

Singh, R., Smitha, M. S., and Singh, S. P. (2014). The role of nanotechnology in combating multi-drug resistant bacteria. *J. Nanosci. Nanotechnol.* 14, 4745–4756. doi: 10.1166/jnn.2014.9527

Singh, S., and Madhup, S. (2013). Clinical profile and antibiotics sensitivity in childhood urinary tract infection at Dhulikhel Hospital. *Kathmandu Univ. Med. J.* 11, 319–324. doi: 10.3126/kumj.v11i4.12541

Singh, S., Singh, D. B., Singh, S., Shukla, R., Ramteke, P. W., and Misra, K. (2019). Exploring medicinal plant legacy for drug discovery in post-genomic era. *Proc. Natl. Acad. Sci. India Sec. B Biol. Sci.* 89, 1141–1151. doi: 10.1007/s40011-018-1013-x

Singh, S. B., Young, K., and Silver, L. L. (2017). What is an "ideal" antibiotic? Discovery challenges and path forward. *Biochem. Pharmacol.* 133, 63–73. doi: 10.1016/j.bcp.2017.01.003

Sivaraman. (2018). *Antibiotic Use in Food Animals: India Overview*. Vellore: Christian Medical College.

Smith, G. N., and Worrel, C. S. (1949). Enzymatic reduction of chloramphenicol. *Arch. Biochem.* 24, 216–223.

Smits, L. P., Bouter, K. E., De Vos, W. M., Borody, T. J., and Nieuwdorp, M. (2013). Therapeutic potential of fecal microbiota transplantation. *Gastroenterology* 145, 946–953.

Soge, O. O., Harger, D., Schafer, S., Toevs, K., Raisler, K. A., Venator, K., et al. (2012). Emergence of increased azithromycin resistance during unsuccessful treatment of *Neisseria gonorrhoeae* infection with azithromycin (Portland, OR, 2011). *Sex Transm. Dis.* 39, 877–879. doi: 10.1097/olq.0b013e31826 85d2b

Sommer, M. O., Dantas, G., and Church, G. M. (2009). Functional characterization of the antibiotic resistance reservoir in the human microflora. *Science* 325, 1128–1131. doi: 10.1126/science.1176950

Stamm, W. E., and Hooton, T. M. (1993). Management of urinary tract infections in adults. *N. Engl. J. Med.* 329, 1328–1334.

Suez, J., Zmora, N., Zilberman-Schapira, G., Mor, U., Dori-Bachash, M., Bashiardes, S., et al. (2018). Post-Antibiotic Gut Mucosal Microbiome Reconstitution Is Impaired by Probiotics and Improved by Autologous FMT. *Cell* 174, 1406–1423. doi: 10.1016/j.cell.2018.08.047

Telenti, A., Imboden, P., Marchesi, F., Lowrie, D., Cole, S., Colston, M. J., et al. (1993). Detection of rifampicin-resistance mutations in Mycobacterium tuberculosis. *Lancet* 341, 647–650. doi: 10.1016/0140-6736(93) 90417-f

The Center for Disease Dynamics (2020). *Resistance Map* [Online. Available online at: https://resistancemap.cddep.org/AntibioticUse.php. (accessed on November 30, 2020).

Török, E., Moran, E., and Cooke, F. (2016). *Oxford handbook of infectious diseases and microbiology*. Oxford: Oxford University Press.

Troillet, N., Samore, M. H., and Carmeli, Y. (1997). Imipenem-resistant *Pseudomonas aeruginosa*: risk factors and antibiotic susceptibility patterns. *Clin. Infect. Dis.* 25, 1094–1098. doi: 10.1086/516092

Tsilingiri, K., Barbosa, T., Penna, G., Caprioli, F., Sonzogni, A., Viale, G., et al. (2012). Probiotic and postbiotic activity in health and disease: comparison on a novel polarised ex-vivo organ culture model. *Gut* 61, 1007–1015. doi: 10.1136/gutjnl-2011-300971

Tsiodras, S., Gold, H. S., Sakoulas, G., Eliopoulos, G. M., Wennersten, C., Venkataraman, L., et al. (2001). Linezolid resistance in a clinical isolate of Staphylococcus aureus. *Lancet* 358, 207–208.

Tsukamura, M. (1972). The pattern of resistance development to rifampicin in Mycobacterium tuberculosis. *Tubercle* 53, 111–117. doi: 10.1016/0041-3879(72)90027-x

Umezawa, H., Ueda, M., Maeda, K., Yagishita, K., Kondo, S., Okami, Y., et al. (1957). Production and isolation of a new antibiotic: kanamycin. *J. Antibiot.* 10, 181–188.

Uttley, A. C. (1988). Vancomycin-resistant enterococci. *Lancet* 2, 57–58.

Van Boeckel, T. P., Brower, C., Gilbert, M., Grenfell, B. T., Levin, S. A., Robinson, T. P., et al. (2015). Global trends in antimicrobial use in food animals. *Proc. Natl. Acad. Sci.* 112, 5649–5654.

Van Boeckel, T. P., Glennon, E. E., Chen, D., Gilbert, M., Robinson, T. P., Grenfell, B. T., et al. (2017). Reducing antimicrobial use in food animals. *Science* 357, 1350–1352.

Vazquez, R., Garcia, E., and Garcia, P. (2018). Phage Lysins for Fighting Bacterial Respiratory Infections: A New Generation of Antimicrobials. *Front. Immunol.* 9:2252. doi: 10.3389/fimmu.2018.02252

Vazquez-Munoz, R., Lopez, F. D., and Lopez-Ribot, J. L. (2020). Bismuth Nanoantibiotics Display Anticandidal Activity and Disrupt the Biofilm and Cell Morphology of the Emergent Pathogenic Yeast Candida auris. *Antibiotics* 2020:461. doi: 10.3390/antibiotics9080461

Ventola, C. L. (2015). The antibiotic resistance crisis: part 1: causes and threats. *P T* 40, 277–283.

Vikesland, P., Garner, E., Gupta, S., Kang, S., Maile-Moskowitz, A., and Zhu, N. (2019). Differential Drivers of Antimicrobial Resistance across the World. *Acc. Chem. Res.* 52, 916–924. doi: 10.1021/acs.accounts.8b00643

Waisbren, B. A., and Spink, W. W. (1950). A clinical appraisal of neomycin. *Ann. Intern. Med.* 33, 1099–1119. doi: 10.7326/0003-4819-33-5-1099

Walker, B. J., Stan, G. V., and Polizzi, K. M. (2017). Intracellular delivery of biologic therapeutics by bacterial secretion systems. *Exp. Rev. Mol. Med.* 19:e6.

Wang, L., Hu, C., and Shao, L. (2017). The antimicrobial activity of nanoparticles: present situation and prospects for the future. *Int. J. Nanomed.* 12, 1227–1249. doi: 10.2147/ijn.s121956

Watanakunakorn, C. (1976). Clindamycin therapy of Staphylococcus aureus endocarditis. *Am. J. Med.* 60, 419–425. doi: 10.1016/0002-9343(76)90758-0

Wegener, H. C., Aarestrup, F. M., Jensen, L. B., Hammerum, A. M., and Bager, F. (1999). Use of antimicrobial growth promoters in food animals and Enterococcus faecium resistance to therapeutic antimicrobial drugs in Europe. *Emerg. Infect. Dis.* 5:329. doi: 10.3201/eid0503.990303

Weinberg, E. D. (1967). *"Bacitracin," in Antibiotics*. Netherland: Springer, 90–101.

Wellington, E. M., Boxall, A. B., Cross, P., Feil, E. J., Gaze, W. H., Hawkey, P. M., et al. (2013). The role of the natural environment in the emergence of antibiotic resistance in Gram-negative bacteria. *Lancet Infect. Dis.* 13, 155–165.

Wittebole, X., De Roock, S., and Opal, S. M. (2014). A historical overview of bacteriophage therapy as an alternative to antibiotics for the treatment of bacterial pathogens. *Virulence* 5, 226–235. doi: 10.4161/viru.25991

World Health Organization (2014). *Antimicrobial resistance: global report on surveillance*. Geneva: World Health Organization.

Wright, A., Hawkins, C., Änggård, E., and Harper, D. (2009). A controlled clinical trial of a therapeutic bacteriophage preparation in chronic otitis due to antibiotic−resistant *Pseudomonas aeruginosa*; a preliminary report of efficacy. *Clin. Otolaryngol.* 34, 349–357. doi: 10.1111/j.1749-4486.2009.01973.x

Wright, G. D. (2010a). Antibiotic resistance in the environment: a link to the clinic? *Curr. Opin. Microbiol.* 13, 589–594. doi: 10.1016/j.mib.2010.08.005

Wright, G. D. (2010b). Q&A: Antibiotic resistance: where does it come from and what can we do about it? *BMC Biol.* 8:123. doi: 10.1186/1741-7007-8-123

Wright, G. D. (2017). Opportunities for natural products in 21 st century antibiotic discovery. *Nat. Product Rep.* 34, 694–701. doi: 10.1039/c7np00019g

Wright, R. C., Friman, V.-P., Smith, M. C., and Brockhurst, M. A. (2019). Resistance evolution against phage combinations depends on the timing and order of exposure. *MBio* 10, 1652–e1619.

Wu, C. M., and Chung, T. C. (2007). Mice protected by oral immunization with Lactobacillus reuteri secreting fusion protein of *Escherichia coli* enterotoxin subunit protein. *FEMS Immunol. Med. Microbiol.* 50, 354–365. doi: 10.1111/j.1574-695x.2007.00255.x

Yong, D., Toleman, M. A., Giske, C. G., Cho, H. S., Sundman, K., Lee, K., et al. (2009). Characterization of a new metallo-β-lactamase gene, blaNDM-1, and a novel erythromycin esterase gene carried on a unique genetic structure in *Klebsiella pneumoniae* sequence type 14 from India. *Antimicrobial. Agents Chemother.* 53, 5046–5054. doi: 10.1128/aac.00774-09

Yosef, I., Manor, M., Kiro, R., and Qimron, U. (2015). Temperate and lytic bacteriophages programmed to sensitize and kill antibiotic-resistant bacteria. *Proc. Natl. Acad. Sci. U. S. A.* 112, 7267–7272. doi: 10.1073/pnas.1500107112

Youmans, G. P., and Williston, E. H. (1946). Effect of streptomycin on experimental infections produced in mice with streptomycin resistant strains of M. *tuberculosis var. hominis*. *Proc. Soc. Exp. Biol. Med.* 63, 131–134. doi: 10.3181/00379727-63-15523

Zhang, F., Luo, W., Shi, Y., Fan, Z., and Ji, G. (2012). Should we standardize the 1,700-year-old fecal microbiota transplantation? *Am. J. Gastroenterol.* 107:1755. doi: 10.1038/ajg.2012.251

Conflict of Interest: The authors declare that the research was conducted in the absence of any commercial or financial relationships that could be construed as a potential conflict of interest.

frontiers in Microbiology

ORIGINAL RESEARCH
published: 04 February 2021
doi: 10.3389/fmicb.2021.633467

Isopropoxy Benzene Guanidine Kills *Staphylococcus aureus* Without Detectable Resistance

Xiufeng Zhang[1,2†], Wenguang Xiong[1,2†], Xianfeng Peng[3], Yixing Lu[1,2], Jie Hao[1,2], Zonghua Qin[3] and Zhenling Zeng[1,2]*

[1] National Risk Assessment Laboratory for Antimicrobial Resistance of Animal Original Bacteria, Guangdong Provincial Key Laboratory of Veterinary Pharmaceutics Development and Safety Evaluation, College of Veterinary Medicine, South China Agricultural University, Guangzhou, China, [2] Guangdong Laboratory for Lingnan Modern Agriculture, Guangzhou, China, [3] Guangzhou Insighter Biotechnology Co., Ltd., Guangzhou, China

Serious infections caused by multidrug-resistant *Staphylococcus aureus* clearly urge the development of new antimicrobial agents. Drug repositioning has emerged as an alternative approach that enables us to rapidly identify effective drugs. We first reported a guanidine compound, isopropoxy benzene guanidine, had potent antibacterial activity against *S. aureus.* Unlike conventional antibiotics, repeated use of isopropoxy benzene guanidine had a lower probability of resistance section. We found that isopropoxy benzene guanidine triggered membrane damage by disrupting the cell membrane potential and cytoplasmic membrane integrity. Furthermore, we demonstrated that isopropoxy benzene guanidine is capable of treating invasive MRSA infections *in vivo* studies. These findings provided strong evidence that isopropoxy benzene guanidine represents a new chemical lead for novel antibacterial agent against multidrug-resistant *S. aureus* infections.

Keywords: isopropoxy benzene guanidine, multidrug-resistant *Staphylococcus aureus*, membrane damage, resistance section, transcriptome

OPEN ACCESS

Edited by:
Rodolfo García-Contreras, National Autonomous University of Mexico, Mexico

Reviewed by:
Kui Zhu, China Agricultural University, China
Yuan Liu, Yangzhou University, China

****Correspondence:***
Zhenling Zeng
zlzeng@scau.edu.cn

† These authors have contributed equally to this work

Specialty section:
This article was submitted to Antimicrobials, Resistance and Chemotherapy, a section of the journal Frontiers in Microbiology

Received: *25 November 2020*
Accepted: *11 January 2021*
Published: *04 February 2021*

Citation:
Zhang X, Xiong W, Peng X, Lu Y, Hao J, Qin Z and Zeng Z (2021) Isopropoxy Benzene Guanidine Kills Staphylococcus aureus Without Detectable Resistance. Front. Microbiol. 12:633467. doi: 10.3389/fmicb.2021.633467

INTRODUCTION

Antibiotic resistance is one of the most prominent public health challenges (Årdal et al., 2019). *Staphylococcus aureus* is the most clinically important multidrug-resistant pathogen and a leading cause of bacteremia, endocarditis, osteomyelitis and skin, and soft tissue infections (Tacconelli et al., 2018; Turner et al., 2019). The alarming increase in the prevalence of global spread clones in *S. aureus* resistant to nearly all antibiotics is a major public health concern (Lakhundi and Zhang, 2018). Hence, there is a dire need to develop novel antimicrobial compounds, as well as are tolerated with low propensity for resistance development (Nambiar et al., 2014).

Nowadays, antimicrobial drug discovery is under constant challenge. The decreasing rate and huge cost of antibiotic discovery has led to alternative strategies being introduced to the clinic (Antibiotics Currently in Global Clinical Development, 2019). Repurposing drugs has emerged as an innovation stream of pharmaceutical development and gained great success in treating various infectious diseases (Austin and Gadhia, 2017; Pushpakom et al., 2019). The majority of recently approved agents against *S. aureus* infections have been developed from existing drug classes, including tetracycline, fluoroquinolone, and pleuromutilin (Talbot et al., 2019). In order to rescue last-resort antibiotics, researchers synthesized vancomycin derivatives by respective or combined modifications, which greatly improved

the antibacterial activity or changed the antimicrobial mechanism (Okano et al., 2017; Guan et al., 2018).

As guanidine had strong organic bases and presented hydrophilic in nature, guanidine compounds have been discovered as new promising drugs in both synthetic and medicinal chemistry (Saczewski and Balewski, 2013; Massimba-Dibama et al., 2015). Liu reported that metformin restored tetracyclines susceptibility against multidrug resistant bacteria by promoting intracellular accumulation of doxycycline (Liu Y. et al., 2020). In our previous study, we screened a guanidine compound isopropoxy benzene guanidine (IBG) as anti-*Enterococci* agent by disrupting their cell membrane potential (Zhang et al., 2019). This compound showed low cytotoxicity against human lung epithelial cells and was well tolerated by mice red blood cells. In this study, we characterized the response of *S. aureus* ATCC 29213 to IBG using phenotypic assays and transcriptomics. The probability of IBG on resistance selection was estimated by serial passage assay and whole genome sequencing. The *in vivo* treatment efficacy of IBG was investigated in a mouse septicemia model.

MATERIALS AND METHODS

Bacterial Strains, Growth Conditions

Staphylococcus aureus strain ATCC 29213, methicillin-resistant *S. aureus* (MRSA) ATCC 43300, 105 clinical *S. aureus* isolates (including 55 MRSA strains), and 8 Gram-negative strains were used in this study. *Acinetobacter baumannii* and *Klebsiella pneumonia* were grown in Cation-Adjusted Mueller-Hinton (MH) broth, all other strains were grown in MH broth. Multilocus sequence typing (MLST) was conducted according to the reference MLST database.

Antimicrobial Agents and Chemicals

Vancomycin (VAN), gentamicin, ciprofloxacin (CIP), linezolid, and amikacin were purchased from Sangon Biotech (Shanghai, China). Isopropoxy benzene guanidine (IBG) (batch number 20150506, content 99.9%) was synthesized by Guangzhou Insighter Biotechnology (Guangzhou, China). Dimethyl Sulphoxide (DMSO) (Dmreagent, Tianjing, China) was utilized as solvent to dissolve IBG. Anti-infective detergent benzalkonium chloride (BAC) was purchased from Aladdin Industrial Corporation (Shanghai, China). SYTOX® green nucleic acid stain agents and 3,3′-diethyloxacarbocyanine iodide [$DiOC_2(3)$] (Thermo Fisher Scientific, Germany) were used as molecular probes.

Antibacterial Test

The MIC and MBC of IBG were determined by broth microdilution according to CLSI guidelines (Clinical and Laboratory Standards Institute, 2018). The MBC was defined as the lowest concentration where a 99.9% colony count reduction was observed (Mohammad et al., 2015). The presence of fetal bovine serum (Tianhang Biotechnology, Zhejiang, China) on IBG activity against *S. aureus* was also tested. Experiments were performed in triplicates.

Antibiotic Synergy Test

The checkerboard method was used for determining synergy of IBG with conventional antibiotics (Falagas et al., 2019). The interaction between two compounds was defined as synergy if FICI < 0.5, addition if $0.5 \leq$ FICI ≤ 1, no interaction if $1 <$ FICI ≤ 4, antagonism if FICI > 4.

Killing Kinetics Assay

The time-dependent killing for *S. aureus* ATCC 29213 and MRSA 43300 with IBG, VAN at 10 × MIC was investigated previously (AbdelKhalek et al., 2016). The OD_{600nm} was measured to determine bacterial lysis when *S. aureus* (OD_{600nm} ∼0.4) treated with 10 × MIC of IBG, VAN, and BAC (positive control) for 4 h (Kim et al., 2018). All the experiments were replicated.

Resistance Studies

In order to select IBG-resistant mutants, $\sim 10^{10}$ CFU of *S. aureus* ATCC 29213 cells were plated onto MH agar containing 2.5×, 5×, and 10×MIC of IBG. After 48 h of incubation at 37°C, resistant colonies were calculated and the MICs of IBG were determined. When this approach proved unsuccessful, development of resistant mutants by serial passage in liquid medium was conducted previously (Ling et al., 2015). The bacteria culture (OD_{600} = 0.01) was treated with IBG or CIP at different concentrations. Cells were incubated at 37°C and passaged at 24 h intervals in the presence of IBG or CIP. The MIC was determined by broth microdilution. Experiments were performed with three replicates (SP1, SP2, and SP3).

The genomic DNA from the strains with elevated MIC of IBG was extracted using a Hipure bacterial DNA kit (Magen, Shanghai, China). A paired-end sequencing library (2 bp × 250 bp) was created using a VAHTS Universal DNA Library Prep kit for Illumina® (Illumina, San Diego, CA, United States) and sequenced on an Illumina HiSeq system (Illumina Inc.). Processed reads were *de novo* assembled into draft genomes using CLC Genomics Workbench 10.1 (CLC Bio, Aarhus, Denmark) and annotated by using Prokka pipeline. These genomes were subjected to SNP analysis by utilizing snippy pipeline. *S. aureus* ATCC 29213 genome of the starting strain was used as a reference genome in SNP analysis.

Membrane Potential Assay

To examine the perturbation of the cell membrane of *S. aureus* by IBG, the membrane potential of the cells was measured by fluorescence spectrometry using fluorescent probe $DiOC_2(3)$, as described previously (Wang et al., 2017). Bacterial cells were energized by the addition of glucose to establish a proton motive force (negative and basic inside the cell). This led to an increase in fluorescence associated with aggregation of the $DiOC_2(3)$. Upon addition of the ionophore CCCP, the $\Delta\psi$ was dissipated and the fluorescence intensity dropped to the level before addition of glucose. All assays were performed at least twice.

Membrane Permeability Assay

To confirm the integrity of the bacterial membranes, we performed an assay based on the uptake of the fluorescent

dye with SYTOX Green (Kim et al., 2018). The fluorescence was measured using a multifunctional microplate reader, with excitation and emission wavelengths of 485 and 525 nm, respectively. All experiments were conducted in duplicate.

Transmission Electron Microscopy

Morphological appearance of the cell membrane of *S. aureus* (ATCC 29213) treated with 10 × MIC IBG was observed using a JEOL 1200EX transmission electron microscopy (TEM) (Li et al., 2016).

Transcriptome Analysis

Staphylococcus aureus ATCC 29213 cells (OD_{600}∼0.4) were treated with 10 × MIC IBG for 4 h. Then bacteria was collected and preserved with RNA protect (Qiagen, United States). Total RNA of each sample was extracted using TRIzol Reagent (Invitrogen)/RNeasy Mini Kit (Qiagen). Control samples were collected from an antibiotic-free culture. RNA sequencing was conducted by High-Throughput Sequencing Facility at the GENWIZ lnc (Jiangsu, China). Raw sequence data were underwent quality control using Cutadapt (V1.9.1) and FastQC (V0.10.1). Clean data were aligned with the reference genome of *S. aureus* NCTC 8325 (NCBI accession number NC_007795.1) *via* software Bowtie2 (v2.1.0) and the gene expression level were estimated by HTSeq (v0.6.1p1). The calculation of fragment per kilobase of exon per million fragments mapped (FPKM) for all genes were performed through Cufflinks (v2.2.1) software. Differential expression genes (DEGs) were screened out by using the DESeq Bioconductor package and defined as those with a change in expression of >twofold and a corresponding false discovery rate (FDR) of <0.05. The gene ontology terms and functional pathways were annotated *via* Gene Ontology (GO) and Kyoto Encyclopedia of Genes and Genome (KEGG), respectively. Cell-PLoc 2.0 was used to analyze the subcellular localization of DEGs (Chou and Shen, 2010).

Mouse Sepsis Protection Model

Animal studies were carried out at animal laboratory center of South China Agricultural University and approved by the Animal Research Committee of South China Agricultural University (2018030). All animal studies were performed with specific-pathogen-free female KM mice (Southern Medical University, Guangdong, China), 6–8-weeks old, weighing 20 ± 2 g.

A mouse septicemia protection assay was used to assess *in vivo* treatment efficacy of IBG (Thangamani et al., 2016). KM female mice were treated intraperitoneally with a dose of 40 mg/kg IBG. After 24 h, KM female mice were infected with 0.1 ml of bacterial suspension (MRSA YXMC004P) *via* tail vein injection, a concentration that achieves about 90% mortality within 18 days after infection. At 0.5 h and 24 h post infection, mice (18 per group) were treated with 40 mg/kg IBG, 15 mg/kg VAN and PBS via intraperitoneal injection. Mice were monitored for 18 days after MRSA infection and the statistical analysis was performed by non-parametric log-rank test.

Statistical Analyses

Statistical analysis was performed using GraphPad Prism 5 and SPSS software. All data were presented as the mean ± s.d.

Data Availability

The whole-genome resequencing for eight *S. aureus* strains involved in resistance studies have been deposited in GenBank under accession numbers: VUKQ00000000, VUKK00000000, VUKL00000000, VUKM00000000, VUKO00000000, VUKP00000000, VUKR00000000, and VUKS00000000. RNA-seq data have been deposited in the NCBI's Sequence Read Archive with accession number PRJNA557004.

RESULTS

Antimicrobial Activity of IBG

The structure of IBG was shown in **Figure 1A**. IBG exhibited potent activity against all tested *S. aureus* with the MIC range of 0.125–4 μg/ml (**Table 1**). However, IBG was inactive against Gram-negative bacteria (**Supplementary Table 1**). Besides, in the presence of 10% FBS, the MIC range increased eightfold. The MBC range for IBG against *S. aureus* strains harboring different MLST types was 4–8-fold of their MICs (**Table 2**). The kill kinetics of IBG was similar to VAN, which greatly reduced the number of bacteria within 4 h (**Figures 1B,C**). However, IBG and VAN did cause *S. aureus* lysis (**Figure 1D**). In addition, IBG exhibited addition activity (0.5 < FICI < 1) with gentamicin or amikacin when tested against *S. aureus* ATCC 29213, MRSA ATCC 43300 (**Supplementary Figure 1**).

IBG Had a Low Probability of Resistance Selection in *S. aureus*

We were unable to obtain IBG-resistant mutants by plating 10^{10} CFU of *S. aureus* ATCC 29213 on agar containing 2.5×, 5× or 10× MIC of IBG. Similarly, serial passage of three independent *S. aureus* 29,213 cultures for 100 days treated with IBG yielded only putative mutants with two or fourfold greater resistance to IBG, whereas serial passage in CIP for 100 days generated strains that were 512-fold more resistant (**Figure 1E** and **Table 3**). A total of 24 mutation genes were identified and most mutations genes encoded products related to catalytic activity, binding and proton transmembrane transporter activity (**Supplementary Table 2**). In addition, *atpE*, *pcrA*, and *walR* genes were responsible for the reduced susceptibility of IBG.

IBG Disrupted Cell Membrane in Multiple Ways

A large reduction in the magnitude of the generated membrane potential was observed in the IBG-treated group, compared to that of the untreated cells and cells in the presence of ampicillin (**Figure 2A**). Therefore, IBG involved disruption of the inner membrane of bacteria. The membrane disruption properties of IBG were monitored by the SYTOX Green uptake. The fluorescence value clearly increased treated with IBG, even at a concentration of 1× MIC, which indicated IBG could cause

TABLE 1 | Activity of IBG against *Staphylococcus aureus*.

Organism	IBG MIC (μg/ml)	VAN MIC (μg/ml)
S. aureus ATCC 29213 (MSSA)	4	1
S. Aureus 29213 + 10% FBS	32	1
MRSA ATCC 43300	4	1
MRSA 43300 + 10% FBS	32	1
Clinical MSSA (50)	0.125–4	0.5–1
Clinical MRSA (55)	2–4	0.5–1

IBG, isopropoxy benzene guanidine; VAN, vancomycin; FBS, fetal bovine serum; -, undetected. MIC, Minimum inhibitory concentration; MSSA, methicillin-sensitive S. aureus; MRSA, methicillin-resistant S. aureus.

TABLE 2 | MBC of IBG against *Staphylococcus aureus*.

Organism	MLST	Spa type	MIC (μg/ml)	MBC (μg/ml)
MSSA ATCC 29213			4	16
MRSA ATCC 43300			4	16
MSSA GDM4P080P	9	899	4	32
MSSA GDE5P004P	9	1775	2	16
MSSA 131372	22	–	4	16
MSSA 131373	7	–	4	16
MSSA 131374	188	–	4	16
MSSA 131390	59	–	4	16
MSSA 131391	5	–	4	16
MSSA 131403	944	–	4	16
MSSA 131440	15	–	4	16
MSSA 131447	6	–	0.125	1
MSSA 131448	88	–	4	16
MSSA 131449	188	–	4	16
MRSA THPS19-2	9	899	4	32
MRSA GDT4P196P	9	1939	4	16
MRSAGDC6P096P	398	34	4	16
MRSA SHP6P028P	398	571	2	8
MRSA 131371	338	–	4	16
MRSA 131404	45	–	4	16
MRSA 131405	59	–	4	16
MRSA 131436	1	–	4	16

MBC, Minimum bactericidal concentration; IBG, isopropoxy benzene guanidine; –, undetected; MIC, Minimum inhibitory concentration; MSSA, methicillin-sensitive S. aureus; MRSA, methicillin-resistant S. aureus.

the damage of cell plasma membrane (**Figure 2B**). TEM results showed that IBG treatment caused remarkable morphological changes in *S. aureus* cells, such as mesosome-like structures, cells with ruptured wall and cytoplasmic membrane were found. Even worse, the cytoplasmic contents of some cells were released to the extracellular medium (**Figure 2C**).

IBG Regulated the Expression of Membrane Related Genes

The principal component analysis (PCA) analysis revealed that IBG successfully separated treated samples from untreated samples (**Figure 3A**). Compared to the control group, IBG treatment led to an up-regulation of 230 and down-regulation of 214 DEGs (**Figure 3B**). According to the GO and KEGG enrichment analysis, IBG treatment caused the changed expression of genes involved in basic metabolic processes, including purine metabolism, pyrimidine metabolism, amino sugar and nucleotide sugar metabolism, alanine, aspartate and glutamate metabolism (**Figures 3C,D**). Notably, more than a third of DEGs (159/444) located on cell membrane, which mostly related to membrane transport function (**Figure 3E**). These genes were associated with osmotolerance, including those encoding efflux pumps, enzymes involved in ABC transporters, cation transporters and phosphotransferase system (PTS) (**Figures 4A–C**). Specifically, virulence, purine and pyrimidine biosynthesis pathway related genes in *S. aureus* were down-regulated under IBG treatment (**Figures 4D–F**).

IBG Rescued Mice From MRSA Septicemic Infection

Mice were infected with MRSA at a dose (3.0×10^6 CFU/mouse) that led to a 83.3% mortality (**Supplementary Figure 2**). The

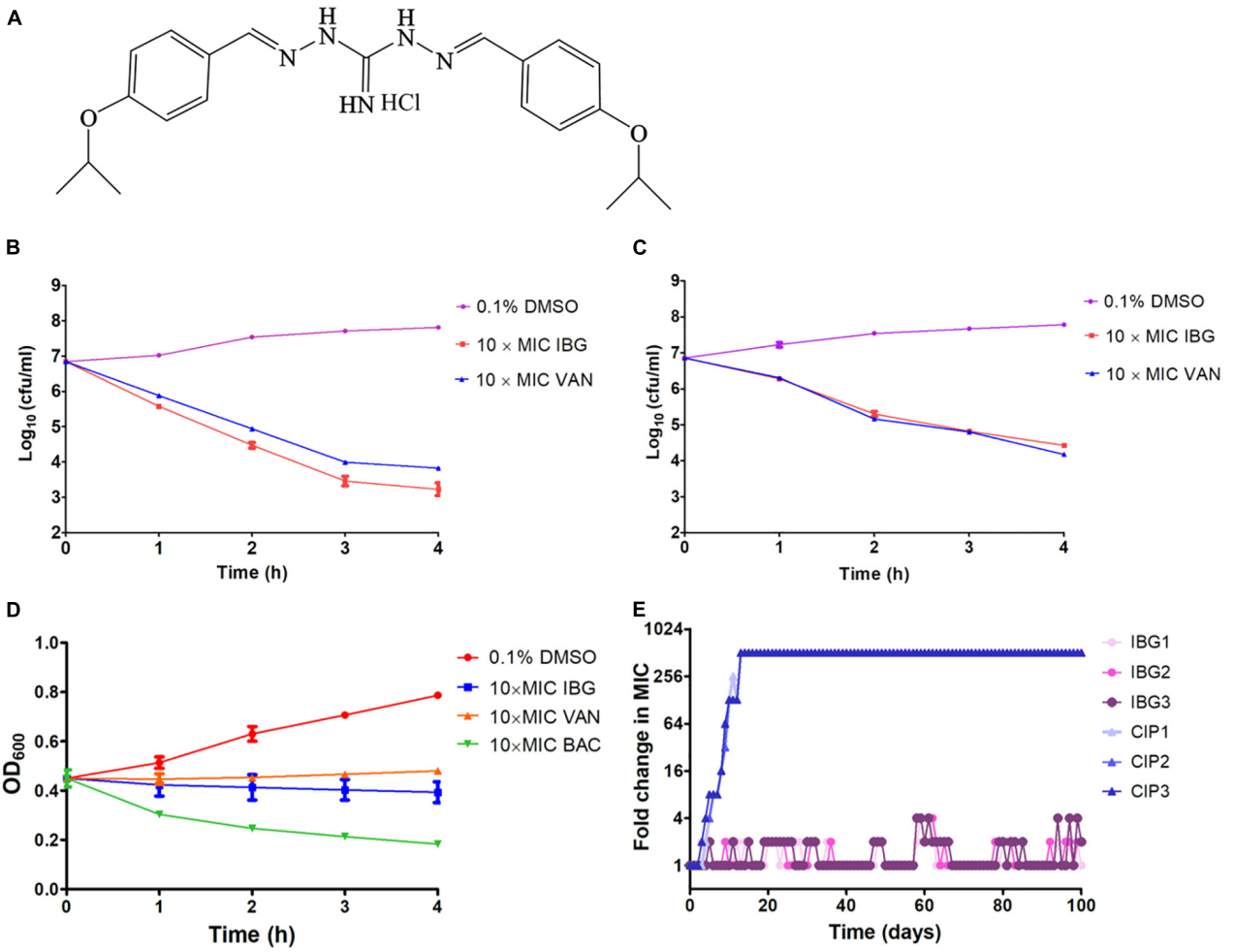

FIGURE 1 | IBG inhibits *S. aureus* growth without detectable mutant development. **(A)** Structure of IBG. **(B)** Viability of *S. aureus* ATCC 29213 treated with IBG or VAN. **(C)** Viability of MRSA ATCC 43300 treated with IBG or VAN for 4 h. **(D)** IBG treatment could not result in *S. aureus* ATCC 29213 lysis; **(E)** Appearance of spontaneous IBG and CIP-resistant *S. aureus* mutants over 100 days of serial passages. IBG, isopropoxy benzene guanidine; VAN, vancomycin; CIP, ciprofloxacin; Individual data points (n = 3 biologically independent experiments) and mean ± SD. are shown.

survival rate of infected mice was 66.6 and 83.3% treated with IBG or VAN, respectively. These results suggested that IBG was efficacious in protecting mice from septicemic MRSA infection.

DISCUSSION

Staphylococcus aureus infections pose a significant challenge to public health due to the diminishing arsenal of effective antibiotics available. The development of novel antibacterial discovery has not kept pace with the rapid emergence of bacterial resistance to numerous antibiotics. Some researchers have proved that repurposing drug was the less time-consuming and more financially way to identify new antibiotics (Austin and Gadhia, 2017). In this study, we found that a guanidine compound displayed potent bactericidal activity against *S. aureus* by targeting cell membrane.

We demonstrated that IBG possessed antibacterial activity against multi-resistant *S. aureus*, including MRSA. Compared to the robenidine analog 16 (3-OCH_3) and 26 [4-$CH(CH_3)_2$] reported previously (Abraham et al., 2016), IBG only had the isopropoxy group [3-$OCH(CH_3)_2$] replacement in benzene ring, but showed the most active against MRSA. This finding was consistent with the antimicrobial activity of IBG against *Enterococci* (Zhang et al., 2019). Additionally, IBG maintained their activity against *S. aureus* isolates exhibiting resistance to different class of antibiotics, which indicated cross-resistance between IBG and these antibiotics is unlikely to occur.

Antibiotic resistance can evolve through sequential accumulation of multiple mutations. Hence, we performed laboratory evolution experiments to assess the propensity of bacteria to develop drug resistance (Toprak et al., 2011). We found that MIC of IBG was almost unchanged over 100 days, whereas the MIC of CIP quickly increased, which is consistent with the report that quinolones can easily induce bacteria

TABLE 3 | Antimicrobial susceptibility of *S. aureus* ATCC 29213 mutants isolated by serial passage for 100 days.

Mutant strain	Mutated gene	MIC (μg/ml)				
		IBG	VAN	LNZ	CIP	GEN
SP1-1		4	1	1	0.25	0.5
SP1-58	*pnp_1*, *atpE*, *walR*, *pcrA*, *ybiV*, *Org1_01939*, *Org1_01695*, *Org1_01489*	8	2	0.5	0.25	0.5
SP1-99	*rsmG*, *atpE*, *dtd3*,*walR*, *pcrA*, *Org1_01695*, *Org1_01489*, *prkC*, *lip2*, *mnhG1*	8	2	0.5	0.5	0.5
SP2-1		4	1	1	0.25	0.5
SP2-58	*rpoE*, *atpE*, *walR*, *pcrA*, *ybiV*, *Org1_01695*, *Org1_01701*, *Org1_01489*, *Org1_01939*, *Org1_00143*, *pnp_1*	16	2	0.5	0.5	0.5
SP2-100	*nusG*, *atpE*, *pcrA*, *isdG_2*, *Org1_00312*	8	2	1	0.25	0.5
SP3-1		4	1	1	0.25	0.5
SP3-34	*atpE*, *walR*, *pcrA*, *ybiV*, *Org1_01489*, *lip2*	8	2	1	0.5	0.5
SP3-66	*Org1_00874*, *atpE*, *Org1_00657*, *walR*, *pcrA*, *ybiV*, *Org1_01695*, *Org1_01489*, *Org1_01939*, *Org1_00143*, *pnp_1*	8	2	0.5	0.25	0.5
SP3-100	*Org1_00874*, *atpE*, *Org1_00657*, *walR*, *pcrA*, *ybiV*, *sasA*, *Org1_01939*, *Org1_00143*, *tcaR*, *pnp_1*, *glpK*	8	2	0.5	0.25	0.5

MIC, minimum inhibitory concentration; IBG, isopropoxy benzene guanidine; VAN, vancomycin; LNZ, linezolid; CIP, ciprofloxacin; GEN, gentamicin. SP1, SP2, and SP3 indicate three independent S. aureus 29213 cultures. Kb, S. aureus 29213 cells treated with 0.1% DMSO.

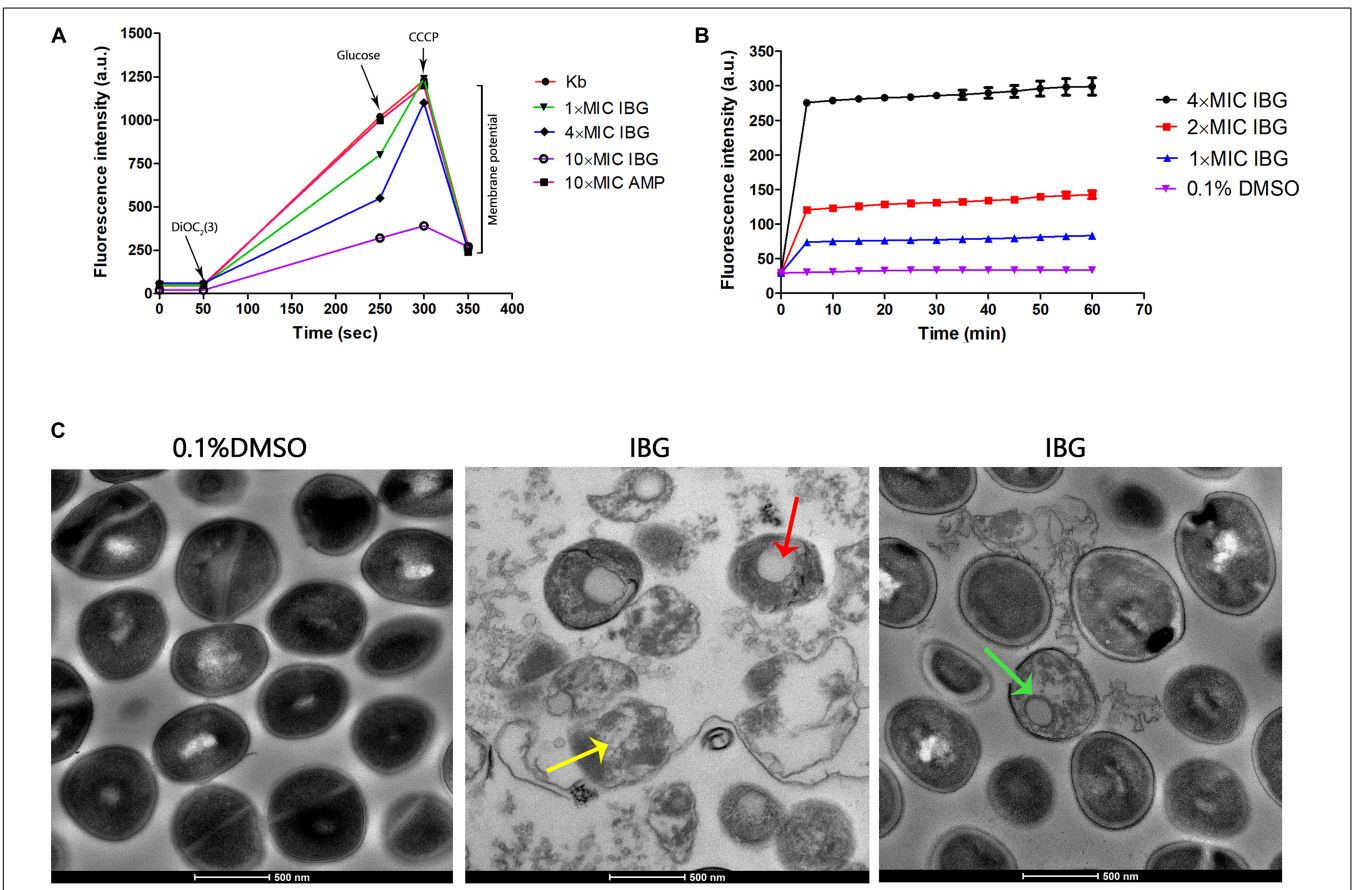

FIGURE 2 | IBG exerts its antibacterial action on the cell membrane of *S. aureus*. **(A)** IBG dissipates the membrane potential of *S. aureus* ATCC 29213. *P* values were determined using a non-parametric one-way ANOVA. *P* values of (*$\leq$0.05) (**$P \leq 0.01$) are considered as significant. **(B)** Uptake of SYTOX Green by exponential-phase *S. aureus* ATCC 29213 cells treated with IBG. **(C)** Transmission electron micrographs of *S. aureus* cells in response to IBG. Scale bars, 500 nm. These arrows indicate damage to the cell membrane by IBG. Kb, *S. aureus* ATCC 29213 control cell treated with 0.1% DMSO.

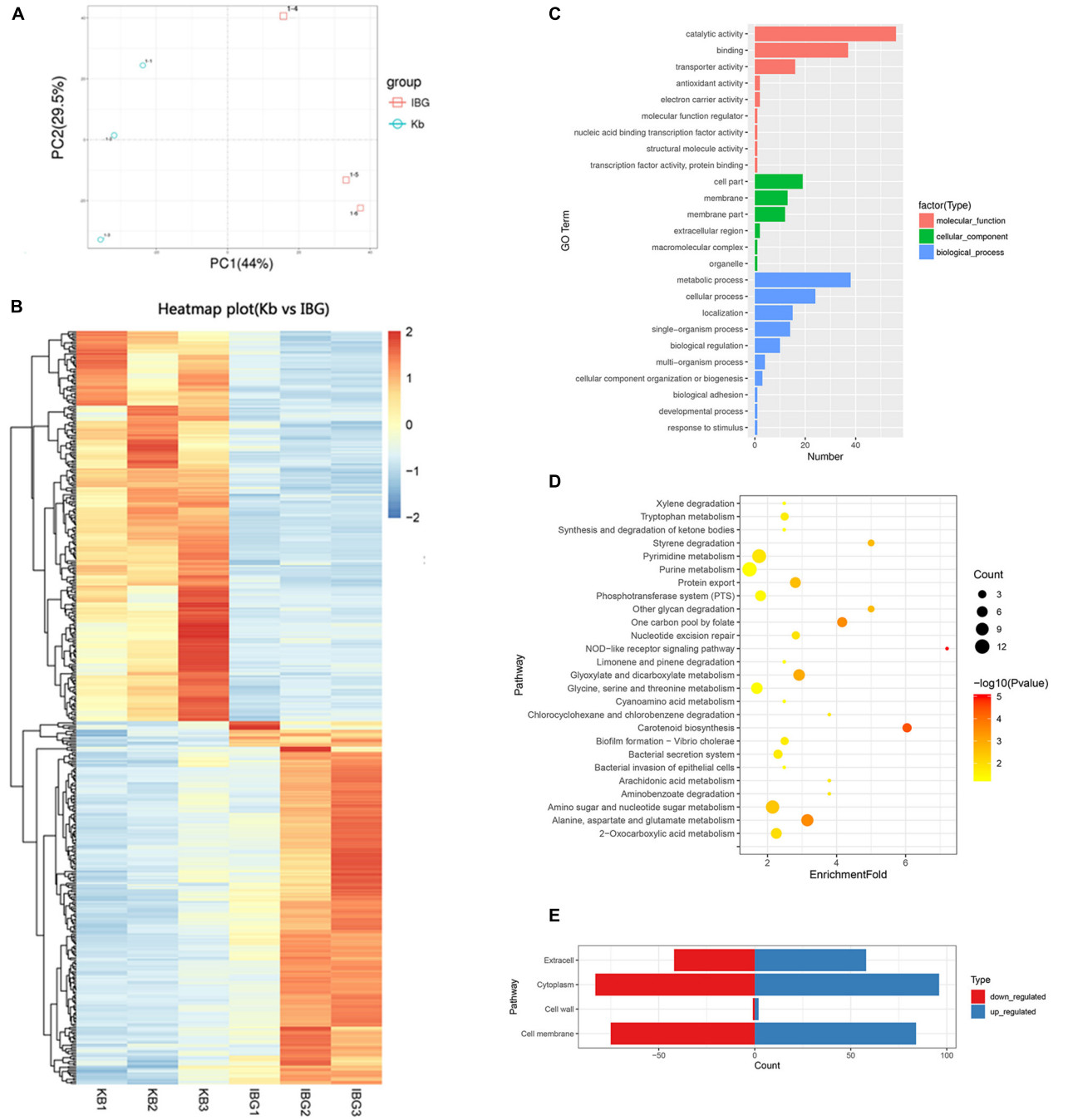

FIGURE 3 | Transcriptome analysis of DEGs in response to IBG stress. **(A)** PCA results. **(B)** Heat map representation of DEGs; **(C)** Go enrichment analysis of DEGs. **(D)** KEGG enrichment analysis of DEGs. **(E)** Subcellular localization of DEGs. DEGs, different expression genes; While all selected genes in RNA-seq data had FDR value of <0.05, which meant significant difference.

to develop drug resistance (Ling et al., 2015). These results demonstrated that *S. aureus* cannot easily develop resistance to IBG. To identify the genetic changes responsible for IBG resistance, we performed whole-genome sequence of seven hyposensitive *S. aureus* strains to IBG. All strains had two mutation genes (*aptE* and *pcrA*) and six of them had a mutation in *walR* gene. Gene *atpE* encodes subunit C of the ATP synthase which utilizes energy stored in the transmembrane electrochemical gradient to synthesize ATP and has been reported to involve in antibiotic resistance (Lamontagne Boulet et al., 2018). PcrA is an ATP-driven 3′–5′ DNA helicase which is involved in DNA repair and plasmid rolling circle replication (Dillingham et al., 2001; Mhashal et al., 2016). Mutations in *walR* locus in *S. aureus* have been shown to relate to reduced

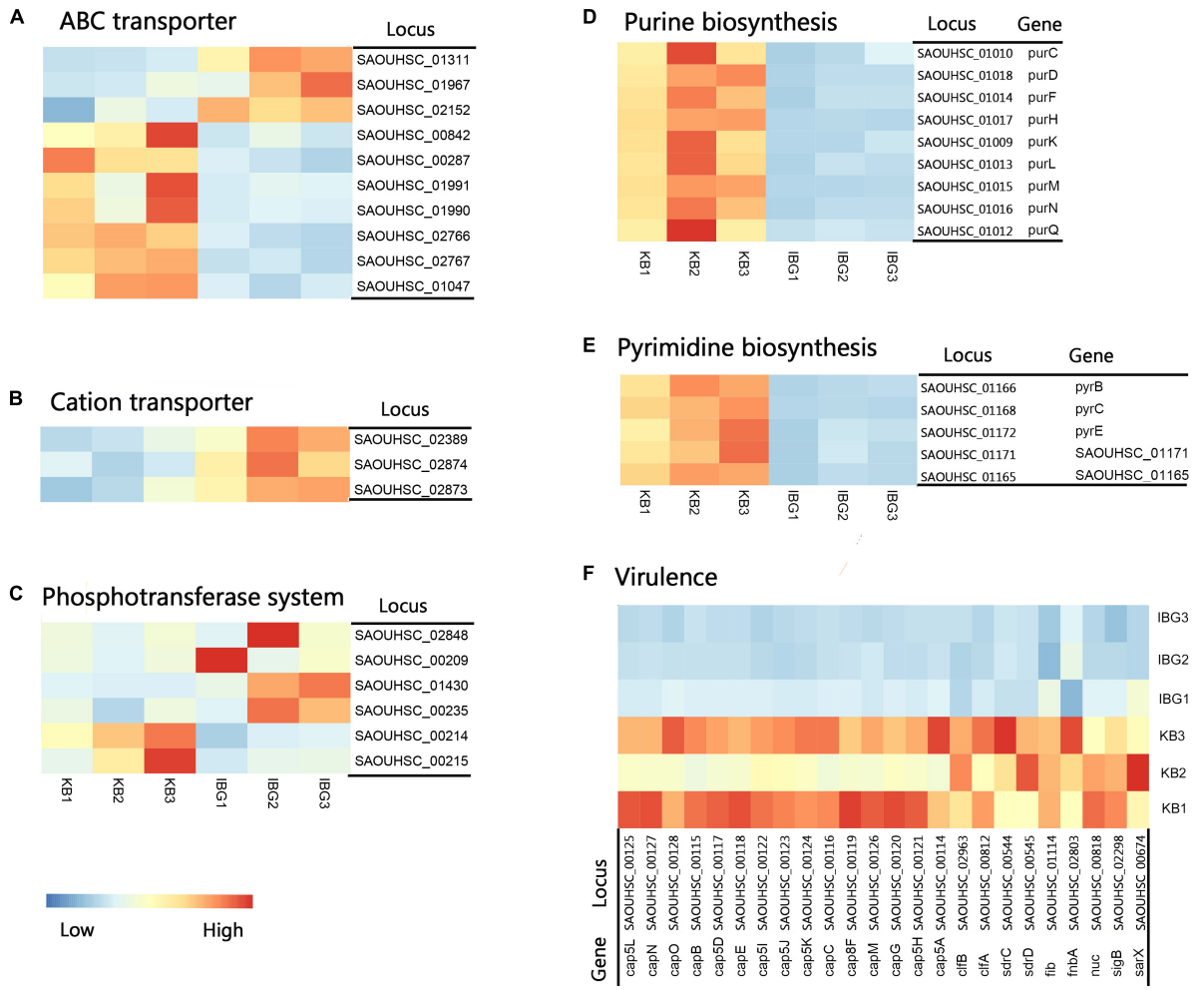

FIGURE 4 | Heat map representation of DEGs involved in main pathways. **(A)** DEGs related to ABC transporters. **(B)** DEGs involved in cation transporters; **(C)** DEGs related to phosphotransferase system. **(D)** DEGs involved in purine biosynthesis pathway. **(E)** DEGs involved in pyrimidine biosynthesis pathway. **(F)** DEGs involved in virulence. All genes represented have a >twofold change in expression treated with IBG relative to their expression in control samples.

susceptibility of vancomycin, which was also found in our study. WalR is a member of the two-component regulatory system WalKR that regulates genes involved in antibiotic resistance, autolysis, biofilm formation and cell wall metabolism (Howden et al., 2011). In addition, there is a *rpoE* mutation in the day 34 of SP2. RpoE (δ factor) is the DNA-dependent RNA polymerase (RNAP) subunit and works as a part of transcription machinery in *S. aureus*. It has been reported that *rpoE* can be involved in orchestrating the ability of *S. aureus* to react and adapt to environmental changes and play a critical role in virulence (Weiss et al., 2014).

We previously confirmed that IBG displayed potent bactericidal activity against *Enterococcus* by disrupting the cell membrane potential[12]. This was also observed in *S. aureus*. The results showed IBG could disrupt the bacterial cell membranes. Similar findings were reported in a previous study in which MRSA strains were treated with robenidine analog NCL195 or techniques (Muthaiyan et al., 2012; Ogunniyi et al., 2017). Moreover, the micrograph indicated that the ultra-structural changes caused by IBG treatment might be irreversible. Perturbation of its structure by IBG maybe the crucial reason for its lethal action on *S. aureus*. However, death is not accompanied by a decline in culture absorbance.

Analysis of transcriptomic changes caused by IBG showed that the expression of genes associated with ABC transport and PTS transporter were remarkable changed. It was found that these transporter systems were associated with nutrient uptake and the export of toxins and antibiotics (Fleury et al., 2009; Liu M. et al., 2020). This may hint the disruption of the membrane potential could hinder the establishment and maintenance of essential energy sources for cell functioning. In addition, IBG treatment also repressed virulence and nucleotide biosynthesis. The down-regulation of virulence factor genes including *sigB*, capsules polysaccharides, might be very likely as a secondary effect for bacteria to survive (Shinji et al., 2011; Tuchscherr et al., 2015; Wang et al., 2019). Purine and pyrimidine biosynthesis pathway

genes, crucial for cell growth *via* DNA and RNA synthesis, were down-regulated in IBG treatment group (Li et al., 2018). This was probably induced by the derived effects of increased membrane permeability. Its membrane-targeting actions toward bacteria might contribute to the lack of drug resistance during prolonged laboratory culture in its presence.

The effect with IBG was decreased at 10% FBS, which suggests a high level of protein binding of IBG. This was also observed in robenidine analogs (Abraham et al., 2016). But it does not necessarily render these compounds ineffective *in vivo*. Our results showed IBG could used as a therapeutic agent against mice MRSA systemic infection. Furthermore, IBG demonstrated additive activity when combined with antibiotics traditionally used to treat systemic MRSA infections. This is important given the emergence of resistance to systemic antimicrobials currently used in the clinic; pairing these antibiotics with IBG may improve the morbidity associated with bacterial infections and stymie the rate at which resistance to these antibiotics arises.

CONCLUSION

In the summary, we first identified that IBG possesses potent antimicrobial activity against clinical isolates of *S. aureus* by targeting cell membrane. IBG had a low probability of resistance selection and considerable efficacy. IBG has the promising potential to become a new class of antimicrobials for the treatment of Gram-positive bacterial infections.

DATA AVAILABILITY STATEMENT

The datasets presented in this study can be found in online repositories. The names of the repository/repositories and accession number(s) can be found in the article/**Supplementary Material**.

ETHICS STATEMENT

The animal study was reviewed and approved by the Animal Research Committee of South China Agricultural University (2018030). Animal studies were carried out at the animal laboratory center of South China Agricultural University.

AUTHOR CONTRIBUTIONS

ZZ conceived and designed the project. XZ and WX drafted the manuscript. XP and ZQ worked on the synthesis of compound IBG. YL and JH preformed the antimicrobial susceptibility tests, time-kill assay, and checkerboard assay. XZ carried out the RAN-Seq and data analysis. All authors read and approved the final manuscript.

FUNDING

The work was supported by the National Natural Science Foundation of China (Grant No. 31672608).

SUPPLEMENTARY MATERIAL

The Supplementary Material for this article can be found online at: https://www.frontiersin.org/articles/10.3389/fmicb.2021.633467/full#supplementary-material

REFERENCES

AbdelKhalek, A., Ashby, C. R. Jr., Patel, B. A., Talele, T. T., and Seleem, M. N. (2016). *In vitro* antibacterial activity of rhodanine derivatives against pathogenic clinical isolates. *PLoS One* 11:e164227. doi: 10.1371/journal.pone.0164227

Abraham, R. J., Stevens, A. J., Young, K. A., Russell, C., Qvist, A., Khazandi, M., et al. (2016). Robenidine analogues as Gram-positive antibacterial agents. *J. Med. Chem*. 59, 2126–2138. doi: 10.1021/acs.jmedchem.5b01797

Antibiotics Currently in Global Clinical Development (2019). *Tracking the Pipeline of Antibiotics in Development*. Available online at: pewtrusts.org/antibiotic-pipeline

Årdal, C., Balasegaram, M., Laxminarayan, R., McAdams, D., Outterson, K., Rex, J. H., et al. (2019). Antibiotic development – economic, regulatory and societal challenges. *Nat. Rev. Microbiol*. 18, 267–274. doi: 10.1038/s41579-019-0293-3

Austin, B. A., and Gadhia, A. D. (2017). New therapeutic uses for existing drugs. *Adv. Exp. Med. Biol*. 1031, 233–247. doi: 10.1007/978-3-319-67144-4_14

Chou, K., and Shen, H. (2010). Cell-PLoc 2.0: an improved package of web-servers for predicting subcellular localization of proteins in various organisms. *Nat. Sci*. 02, 1090–1103. doi: 10.4236/ns.2010.210136

Clinical and Laboratory Standards Institute (2018). *Performance Standards for Antimicrobial Susceptibility Testing, M100*. 28th Edn. Wayne, PA: Clinical and Laboratory Standards Institute.

Dillingham, M. S., Soultanas, P., Wiley, P., Webb, M. R., and Wigley, D. B. (2001). Defining the roles of individual residues in the single-stranded DNA binding site of PcrA helicase. *Proc. Natl. Acad. Sci. U.S.A*. 98, 8381–8387. doi: 10.1073/pnas.131009598

Falagas, M. E., Voulgaris, G. L., Tryfinopoulou, K., Giakkoupi, P., Kyriakidou, M., Vatopoulos, A., et al. (2019). Synergistic activity of colistin with azidothymidine against colistin-resistant *Klebsiella pneumoniae* clinical isolates collected from inpatients in Greek hospitals. *Int. J. Antimicrob. Agents* 53, 855–858. doi: 10.1016/j.ijantimicag.2019.02.021

Fleury, B., Kelley, W. L., Lew, D., Gotz, F., Proctor, R. A., and Vaudaux, P. (2009). Transcriptomic and metabolic responses of *Staphylococcus aureus* exposed to supra-physiological temperatures. *Int. J. Antimicrob. Agents* 9:76. doi: 10.1186/1471-2180-9-76

Guan, D., Chen, F., Faridoon, Liu, J., Li, J., Lan, L., et al. (2018). Design and synthesis of pyrophosphate-targeting vancomycin derivatives for combating vancomycin-resistant *Enterococci*. *Chemmedchem* 13, 1644–1657. doi: 10.1002/cmdc.201800252

Howden, B. P., McEvoy, C. R., Allen, D. L., Chua, K., Gao, W., Harrison, P. F., et al. (2011). Evolution of multidrug resistance during *Staphylococcus aureus* infection involves mutation of the essential two component regulator WalKR. *PLoS Pathog.* 7:e1002359. doi: 10.1371/journal.ppat.1002359

Kim, W., Zhu, W., Hendricks, G. L., Van Tyne, D., Steele, A. D., Keohane, C. E., et al. (2018). A new class of synthetic retinoid antibiotics effective against bacterial persisters. *Nature* 556, 103–107. doi: 10.1038/nature26157

Lakhundi, S., and Zhang, K. (2018). Methicillin-resistant *Staphylococcus aureus*: molecular characterization, evolution, and epidemiology. *Clin. Microbiol. Rev*. 31, e18–e20. doi: 10.1128/CMR.00020-18

Lamontagne Boulet, M., Isabelle, C., Guay, I., Brouillette, E., Langlois, J. P., Jacques, P. E., et al. (2018). Tomatidine is a lead antibiotic molecule that targets *Staphylococcus aureus* ATP synthase subunit c. *Antimicrob. Agents Chemother.* 62, e02197-17. doi: 10.1128/aac.02197-17

Li, J., Ahn, J., Liu, D., Chen, S., Ye, X., and Ding, T. (2016). Evaluation of ultrasound-induced damage to *Escherichia coli* and *Staphylococcus aureus* by flow cytometry and transmission electron microscopy. *Appl. Environ. Microbiol.* 82, 1828–1837. doi: 10.1128/aem.03080-15

Li, L., Abdelhady, W., Donegan, N. P., Seidl, K., Cheung, A., Zhou, Y. F., et al. (2018). Role of purine biosynthesis in persistent methicillin-resistant *Staphylococcus aureus* infection. *J. Infect. Dis.* 218, 1367–1377. doi: 10.1093/infdis/jiy340

Ling, L. L., Schneider, T., Peoples, A. J., Spoering, A. L., Engels, I., Conlon, B. P., et al. (2015). A new antibiotic kills pathogens without detectable resistance. *Nature* 517, 455–459. doi: 10.1038/nature14098

Liu, M., Feng, M., Yang, K., Cao, Y., Zhang, J., Xu, J., et al. (2020). Transcriptomic and metabolomic analyses reveal antibacterial mechanism of astringent persimmon tannin against methicillin-resistant *Staphylococcus aureus* isolated from pork. *Food Chem.* 309:125692. doi: 10.1016/j.foodchem.2019.125692

Liu, Y., Jia, Y., Yang, K., Li, R., Xiao, X., Zhu, K., et al. (2020). Metformin restores tetracyclines susceptibility against multidrug resistant bacteria. *Adv. Sci.* 7:1902227. doi: 10.1002/advs.201902227

Massimba-Dibama, H., Mourer, M., Constant, P., Daffe, M., and Regnouf-de-Vains, J. B. (2015). Guanidinium compounds with sub-micromolar activities against *Mycobacterium tuberculosis*. *Synth. Charact. Biol. Eval.* 23, 5410–5418. doi: 10.1016/j.bmc.2015.07.053

Mhashal, A. R., Choudhury, C. K., and Roy, S. (2016). Probing the ATP-induced conformational flexibility of the PcrA helicase protein using molecular dynamics simulation. *J. Mol. Model.* 22:54. doi: 10.1007/s00894-016-2922-3

Mohammad, H., Reddy, P. V., Monteleone, D., Mayhoub, A. S., Cushman, M., and Seleem, M. N. (2015). Synthesis and antibacterial evaluation of a novel series of synthetic phenylthiazole compounds against methicillin-resistant *Staphylococcus aureus* (MRSA). *Eur. J. Med. Chem.* 94, 306–316. doi: 10.1016/j.ejmech.2015.03.015

Muthaiyan, A., Martin, E. M., Natesan, S., Crandall, P. G., Wilkinson, B. J., and Ricke, S. C. (2012). Antimicrobial effect and mode of action of terpeneless cold-pressed Valencia orange essential oil on methicillin-resistant *Staphylococcus aureus*. *J. Appl. Microbiol.* 112, 1020–1033. doi: 10.1111/j.1365-2672.2012.05270.x

Nambiar, S., Laessig, K., Toerner, J., Farley, J., and Cox, E. (2014). Antibacterial drug development: challenges, recent developments, and future considerations. *Clin. Pharmacol. Ther.* 96, 147–149. doi: 10.1038/clpt.2014.116

Ogunniyi, A. D., Khazandi, M., Stevens, A. J., Sims, S. K., Page, S. W., Garg, S., et al. (2017). Evaluation of robenidine analog NCL195 as a novel broad-spectrum antibacterial agent. *Plos One* 12:e0183457. doi: 10.1371/journal.pone.0183457

Okano, A., Isley, N. A., and Boger, D. L. (2017). Peripheral modifications of [Ψ[CH(2)NH]Tpg(4)]vancomycin with added synergistic mechanisms of action provide durable and potent antibiotics. *Proc. Natl. Acad. Sci. U.S.A.* 114, E5052–E5061. doi: 10.1073/pnas.1704125114

Pushpakom, S., Iorio, F., Eyers, P. A., Escott, K. J., Hopper, S., Wells, A., et al. (2019). Drug repurposing: progress, challenges and recommendations. *Nat. Rev. Drug Discov.* 18, 41–58. doi: 10.1038/nrd.2018.168

Saczewski, F., and Balewski, L. (2013). Biological activities of guanidine compounds, 2008 – 2012 update. *Expert Opin. Ther. Pat.* 23, 965–995. doi: 10.1517/13543776.2013.788645

Shinji, H., Yosizawa, Y., Tajima, A., Iwase, T., Sugimoto, S., Seki, K., et al. (2011). Role of fibronectin-binding proteins A and B in in vitro cellular infections and *in vivo* septic infections by *Staphylococcus aureus*. *Infect. Immun.* 79, 2215–2223. doi: 10.1128/iai.00133-11

Tacconelli, E., Carrara, E., Savoldi, A., Harbarth, S., Mendelson, M., Monnet, D. L., et al. (2018). Discovery, research, and development of new antibiotics: the WHO priority list of antibiotic-resistant bacteria and tuberculosis. *Lancet Infect. Dis.* 18, 318–327. doi: 10.1016/s1473-3099(17)30753-3

Talbot, G. H., Jezek, A., Murray, B. E., Jones, R. N., Ebright, R. H., Nau, G. J., et al. (2019). The infectious diseases society of America's 10 x '20 initiative (10 new systemic antibacterial agents US food and drug administration approved by 2020): is 20 x '20 a possibility? *Clin. Infect. Dis.* 69, 1–11. doi: 10.1093/cid/ciz089

Thangamani, S., Mohammad, H., Abushahba, M. F., Sobreira, T. J., Hedrick, V. E., Paul, L. N., et al. (2016). Antibacterial activity and mechanism of action of auranofin against multi-drug resistant bacterial pathogens. *Sci. Rep.* 6:22571. doi: 10.1038/srep22571

Toprak, E., Veres, A., Michel, J., Chait, R., Hartl, D. L., and Kishony, R. (2011). Evolutionary paths to antibiotic resistance under dynamically sustained drug selection. *Nat. Genet.* 44, 101–105. doi: 10.1038/ng.1034

Tuchscherr, L., Bischoff, M., Lattar, S. M., Noto Llana, M., Pfortner, H., Niemann, S., et al. (2015). Sigma factor SigB is crucial to mediate *Staphylococcus aureus* adaptation during chronic infections. *PLoS Pathog.* 11:e1004870. doi: 10.1371/journal.ppat.1004870

Turner, N. A., Sharma-Kuinkel, B. K., Maskarinec, S. A., Eichenberger, E. M., Shah, P. P., Carugati, M., et al. (2019). Methicillin-resistant *Staphylococcus aureus:* an overview of basic and clinical research. *Nat. Rev. Microbiol.* 17, 203–218. doi: 10.1038/s41579-018-0147-4

Wang, X., Wu, H., Niu, T., Bi, J., Hou, H., Hao, H., et al. (2019). Downregulated expression of virulence factors induced by benzyl isothiocyanate in *Staphylococcus aureus*: a transcriptomic analysis. *Int. J. Mol. Sci.* 20:5441. doi: 10.3390/ijms20215441

Wang, Y., Mowla, R., Guo, L., Ogunniyi, A. D., Rahman, T., De Barros Lopes, M. A., et al. (2017). Evaluation of a series of 2-napthamide derivatives as inhibitors of the drug efflux pump AcrB for the reversal of antimicrobial resistance. *Bioorg. Med. Chem. Lett.* 27, 733–739. doi: 10.1016/j.bmcl.2017.01.042

Weiss, A., Ibarra, J. A., Paoletti, J., Carroll, R. K., and Shaw, L. N. (2014). The delta subunit of RNA polymerase guides promoter selectivity and virulence in *Staphylococcus aureus*. *Infect. Immun.* 82, 1424–1435. doi: 10.1128/iai.01508-14

Zhang, X., Han, D., Pei, P., Hao, J., Lu, Y., Wan, P., et al. (2019). In vitro antibacterial activity of isopropoxy benzene guanidine against multidrug-resistant *Enterococci*. *Infect. Drug Resist.* 12, 3943–3953. doi: 10.2147/IDR.S234509

Conflict of Interest: XP and ZQ was employed by company Guangzhou Insighter Biotechnology Co., Ltd.

The remaining authors declare that the research was conducted in the absence of any commercial or financial relationships that could be construed as a potential conflict of interest.

frontiers in Microbiology

ORIGINAL RESEARCH
published: 09 February 2021
doi: 10.3389/fmicb.2020.605962

Synergistic Combination of Linezolid and Fosfomycin Closing Each Other's Mutant Selection Window to Prevent Enterococcal Resistance

Lifang Jiang[1,2], Na Xie[1,2], Mingtao Chen[1,2], Yanyan Liu[3], Shuaishuai Wang[1,2], Jun Mao[1,2], Jiabin Li[3] and Xiaohui Huang[1,2]**

[1] Department of Basic and Clinical Pharmacology, School of Pharmacy, Anhui Medical University, Hefei, China, [2] Anhui Province Key Laboratory of Major Autoimmune Diseases, School of Pharmacy, Anhui Institute of Innovative Drugs, Anhui Medical University, Hefei, China, [3] Department of Infectious Diseases, The First Affiliated Hospital of Anhui Medical University, Hefei, China

OPEN ACCESS

Edited by:
Fabian Cieplik,
University Medical Center Regensburg, Germany

Reviewed by:
Divakar Sharma,
Indian Institute of Technology Delhi, India
Haruyoshi Tomita,
Gunma University, Japan

***Correspondence:**
Xiaohui Huang
math2088@163.com
Jiabin Li
lijiabin@ahmu.edu.cn

Specialty section:
This article was submitted to Antimicrobials, Resistance and Chemotherapy, a section of the journal Frontiers in Microbiology

Received: 14 September 2020
Accepted: 30 December 2020
Published: 09 February 2021

Citation:
Jiang L, Xie N, Chen M, Liu Y, Wang S, Mao J, Li J and Huang X (2021) Synergistic Combination of Linezolid and Fosfomycin Closing Each Other's Mutant Selection Window to Prevent Enterococcal Resistance. Front. Microbiol. 11:605962. doi: 10.3389/fmicb.2020.605962

Enterococci, the main pathogens associated with nosocomial infections, are resistant to many common antibacterial drugs including β-lactams, aminoglycosides, etc. Combination therapy is considered an effective way to prevent bacterial resistance. Preliminary studies in our group have shown that linezolid combined with fosfomycin has synergistic or additive antibacterial activity against enterococci, while the ability of the combination to prevent resistance remains unknown. In this study, we determined mutant prevention concentration (MPC) and mutant selection window (MSW) of linezolid, fosfomycin alone and in combination including different proportions for five clinical isolates of *Enterococcus* and characterized the resistance mechanism for resistant mutants. The results indicated that different proportions of linezolid combined with fosfomycin had presented different MPCs and MSWs. Compared with linezolid or fosfomycin alone, the combination can restrict the enrichment of resistant mutants at a lower concentration. A rough positive correlation between the selection index (SI) of the two agents in combination and the fractional inhibitory concentration index (FICI) of the combination displayed that the smaller FICI of linezolid and fosfomycin, the more probable their MSWs were to close each other. Mutations in ribosomal proteins (L3 and L4) were the mechanisms for linezolid resistant mutants. Among the fosfomycin-resistant mutants, only two strains have detected the MurA gene mutation related to fosfomycin resistance. In conclusion, the synergistic combination of linezolid and fosfomycin closing each other's MSW could effectively suppress the selection of enterococcus resistant mutants, suggesting that the combination may be an alternative for preventing enterococcal resistance. In this study, the resistance mechanism of fosfomycin remains to be further studied.

Keywords: MPC, MSW, linezolid, fosfomycin, *Enterococcus*

INTRODUCTION

Enterococci are one of prominent causes of hospital acquired infection, especially in urinary tract, soft tissue, and device-associated infections (Fiore et al., 2019; García-Solache and Rice, 2019). *Enterococcus faecalis and Enterococcus faecium* are the main pathogenic bacteria of enterococcal infections (Gilmore et al., 2013). Both the two species shown intrinsic resistance to common antibiotics historically used as front-line agents, making enterococcal infection to be a serious threat to public health (Mercuro et al., 2018; Torres et al., 2018; Haghi et al., 2019). Combination therapy is recommended as an effective method to combat bacterial resistance (Tyers and Wright, 2019). Clinical studies also shown that patients treated with antibacterial combination therapy can obtain good clinical effect and lower mortality rates (Falagas et al., 2014; Ni et al., 2015). Currently, a variety of synergistic and effective combinations against enterococcal infections have been reported (Leone et al., 2016; Mercuro et al., 2018). However, most studies were aimed at exploring the antibacterial activity of the combination *in vitro* or *in vivo* (Mercuro et al., 2018). There are few researches about combinations that can effectively prevent enterococcal resistance.

One approach to predict bacterial resistance to antimicrobials *in vitro* was determination of the mutant prevention concentration (MPC) and mutant selection window (MSW). The MSW comprises a specific drug concentration range in which mutant strains with reduced susceptibility can be selected (Drlica and Zhao, 2007; Blondeau, 2009). It has been confirmed in many antibiotics such as fluoroquinolones (Strukova et al., 2016), oxazolidinones (Alieva et al., 2018), aminoglycosides (Ni et al., 2016). MPC is defined as the lowest concentration that blocks the emergence of first-step resistant mutants in a large susceptible population, usually more than 10^{10} colony forming unit (CFU)/mL bacteria (Drlica, 2003). Maintaining the drug concentration above MPC can effectively restrict the selection resistant subpopulations (Zinner et al., 2008; Alieva et al., 2018). In practice, high exposure was related to higher incidence of side effects. Fortunately, combination therapy at a low concentration could prevent the selection of resistant mutants by narrowing or closing the MSW (Díez-Aguilar et al., 2015; Ni et al., 2016). Theoretically, the more likely the combination is to shut off each other's MSW at the same time, the stronger its ability to prevent bacterial resistance. Therefore, finding a combination that can close each other's MSW at the same time to achieve therapeutic effect with lower dose was the key to preventing enterococcal resistance.

Linezolid is used as the first-line drug for the treatment of severe gram-positive infections, instead of vancomycin (Zahedi Bialvaei et al., 2017). Although, some studies have shown that the frequency of spontaneous resistance to linezolid was low in enterococci (L. Drago et al., 2008). Unfortunately, in recent years, the increasing number of linezolid resistant enterococci had been reported worldwide (Sassi et al., 2019; Zou and Xia, 2020). Even, some studies revealed that prolonged linezolid therapy was regarded as a risk factor for the obtaining of linezolid resistant *E. faecium* clinical isolates (Smith et al., 2018). And high linezolid consumption facilitates the development of linezolid resistant *E. faecalis* (Bai et al., 2019). In addition, with the increase in exposure and treatment time, linezolid may cause higher rates of adverse reactions such as thrombocytopenia and neuropathy (Bayram et al., 2017; Tsuji et al., 2017; Lee and Caffrey, 2018). Considering the limitations of linezolid monotherapy, the use of a combination strategy may be a good approach. Fosfomycin acts on bacterial cell walls and shows good antibacterial activity against gram-positive and gram-negative bacteria including multi-drug resistant bacteria. Fosfomycin, due to its unique mechanism of action, has a synergistic effect with a variety of antibiotics and is not easy to produce cross-resistance (Falagas et al., 2016). The previous study of our group confirmed that linezolid combined with fosfomycin has an *in vitro* synergistic effect on *Enterococcus and Staphylococcus aureus* (Chen et al., 2018; Qi et al., 2019). However, the ability of the combination to prevent enterococcus resistance remains to be studied.

Understanding the mechanism of bacterial resistance is of great significance for guiding the rational application of antibiotics, preventing bacterial drug resistance and effective anti-infection treatment. However, the mechanisms of bacterial resistance are complex. On the one hand, bacteria can become resistant by acquiring either exogenous resistance genes or chromosomal mutations (Durão et al., 2018). On the other hand, the drug-resistant phenotype of bacteria can also be expressed through changes in protein levels (Sharma et al., 2019a,b). Although, the drug resistance mechanism of clinically isolated linezolid-resistant enterococci (Hua et al., 2019; Zou and Xia, 2020) or fosfomycin-resistant enterococci has been reported (Zhang et al., 2019). But, mechanisms responsible for linezolid or fosfomycin resistant mutants selected from the MSW are still lacking. The emergence of first-step mutants during the MPC measurement offers the possibility to explore the mechanisms of resistance in the molecular level.

To support the clinical application of this combination, this study is the first *in vitro* to evaluate the ability of linezolid combined with fosfomycin in different proportions to prevent enterococcal resistance by determining the MSW of the two agents when used alone or in combination. Similarly, this study conducted a preliminary exploration of the resistance mechanism of linezolid or fosfomycin resistant mutants.

MATERIALS AND METHODS

Bacterial Isolates

Number of 43 non-duplicate clinical isolates of *Enterococcus* were isolated from urine, blood, bile, pus, and excrement between January and October 2018 in the First Affiliated Hospital of Anhui Medical University. Among them, 20 strains of *Enterococcus faecium*, 23 strains of *Enterococcus faecalis*. All strains were identified by the automated VITEK-2 system (BioMerieux, Marcy l'Etoile, France). *Enterococcus faecalis* ATCC 29212 was used as the quality control strain. In addition, these strains were not specifically isolated for this research but were part of the routine hospital laboratory procedure. This study was approved by the First Affiliated Hospital of Anhui Medical University institutional review board.

Antimicrobial Agents and Medium

Linezolid and fosfomycin were purchased from the National Institute for Food and Drug Control of China (Beijing, China). Mueller–Hinton broth (MHB, Oxoid, England) was used for culturing bacteria and Mueller-Hinton agar (MHA, Oxoid, England) was used for culturing bacteria, performing agar dilution method and quantifying colony counts.

Determination of Antimicrobial Susceptibility

The minimum inhibitory concentration (MIC) for the two drugs was determined by agar dilution according to Clinical and Laboratory Standards Institute (Clsi, 2019) guidelines. Briefly, Mueller Hinton agar (MHA; Oxoid, England) plates containing a series of 2-fold concentration increments of each agent were prepared. The agar plates containing fosfomycin needs to add glucose-6-phosphate and makes the final concentration 25 mg/L. Then, $\sim 10^5$ colony-forming units (CFU) of bacterial cells were inoculated with an autoclaved replicator and incubated at 37°C for 24 h. The MIC was defined as the lowest drug concentration in which no visible colonies grew. *Enterococcus faecalis* ATCC 29212 was used as the quality control strain in each batch of tests. The experiment was replicated three times.

Checkerboard Assays

Checkerboard assay was used for the synergy testing. Tests were performed on 96-well plates according to our previous study (Qi et al., 2019), the two drugs were diluted with Mueller-Hinton Broth into a series of concentrations based on the MICs for each tested isolate. In brief, linezolid ranging between 1/64 × MIC and 2 × MIC was dispensed in each column. Then, fosfomycin supplemented with 25 mg/L of glucose-6-phosphate ranging from 1/64 × MIC to 2 × MIC was added in every row. Then, each well was inoculated with an equal volume of 1×10^6 CFU/mL bacterial suspension. Plates were incubated at 37°C for 24 h and visually inspected for turbidity to determine the growth. All the experiments were performed in triplicate.

Synergy was evaluated by the fractional inhibitory concentration index (FICI): FICI = (MIC of drug A in combination/MIC of drug A alone) + (MIC of drug B in combination/MIC of drug B alone). The FICI value was interpreted as follows: FICI $\leq$ 0.5, synergy; 0.5 < FICI $\leq$ 1, additivity; 1 < FICI $\leq$ 4, indifference; FICI > 4, antagonism (Davis et al., 2020).

MIC99%

According to the results of checkerboard assay, five isolates (*Enterococcus faecium*: NO.1, NO.5; *Enterococcus faecalis*: NO.6, NO.22, NO.43) with different value of FICI were selected for the MSW studies. For the five selected strains, the $MIC_{99\%}$ of linezolid and Fosfomycin were determined repeatedly by the agar plate methods reported in previous research (Xu et al., 2018). In short, bacterial suspension was inoculated on agar plates including linear drug concentrations with 20% per sequential decrease from each MIC, and those plates without drug used for blank controls. The fosfomycin-containing agar plates were required to supplement with glucose-6-phosphate at a final concentration of 25 mg/L. The plates were incubated at 35°C for 24 h, and then the colonies growing on different plates were counted. Finally, calculate the inhibition percentage (y) and plot against different antibacterial agent concentrations (x) to gain a regression equation. Accordingly, their $MIC_{99\%}$ were, respectively, calculated according to their individual equations.

MPC Alone or in Combination

Linezolid, fosfomycin, and linezolid-fosfomycin combination MPCs for five isolates (NO.1, NO.5, NO.6, NO.22, and NO.43) were determined according to the method reported in previous studies (Wentao et al., 2018). In brief, bacterial cells were grown overnight in fresh Mueller-Hinton broth (MHB) with violently shaking at 35°C and followed by 10-fold dilution with MHB, incubated at 35°C for 6 h. The growth was centrifuged (4000 × *g* for 10 min) to yield a high-density culture containing cells of $\sim 10^{10}$ CFU/ml. One hundred microliter culture (approximate $\sim 10^9$ cell) was placed onto Mueller-Hinton agar plates with 2-fold increasing concentrations. Also, the glucose-6-phosphate at a final concentration of 25 mg/L need to be added into agar plates containing fosfomycin. Then, the plates were incubated at 35°C for 72 h. The preliminary MPC was recorded as the lowest antimicrobial concentration that prevented bacterial growth. Further, the exact MPC was determined by linear antimicrobial concentration with 20% per sequential decrease from preliminary MPC. Based on the FICI value of the combination, thirteen different composition ratios (Linezolid: Fosfomycin, from 64:1 to 1:64) were designed for the combination MPCs studies. The MPCs of different proportions of linezolid combined with fosfomycin were determined according to above methods and procedures. For each strain, colonies that grew in the highest linezolid or fosfomycin concentration were passaged five times on drug-free agars, and then their MICs were determined by the agar dilution methods to check for mutants and stored for further testing (Díez-Aguilar et al., 2015). All MPC studies were performed in three times.

Characterization of Resistance Mechanisms

Five original strains and their corresponding mutant derivatives recovered from the single-drug MPC studies were sequenced and compared. DNA was harvested using TIANamp bacteria DNA Kit (Tiangen, Beijing, China). The possible mechanisms of linezolid resistance were screened by polymerase chain reaction (PCR) using previously reported primers and conditions: the 23S rRNA domain (Gawryszewska et al., 2017), ribosomal protein (L3 and L4) domain (Lee et al., 2017), the methyltransferase gene *cfr* (Doern et al., 2016), and ABC-type transporter gene *optrA* (Wang et al., 2015). Meanwhile, resistance genes related to fosfomycin (*fosB, MurA, glpT, and uhpT*) were also amplified by PCR (Fu et al., 2016; Zhang et al., 2019). All PCR positive products were subjected to sequencing analysis. The primers (listed in **Supplementary Table 1**) used for the sequencing reaction were the same as those used for PCR. The nucleotide sequences were compared with the *E. faecalis* ATCC29212 strain

(no. CP008816.1) and *E. faecium* ZY11 strain (no. CP038995.1). The nucleotide sequence comparison was completed by BLAST[1] and SnapGene Viewer (Version 5.1).

Nucleotide Sequence Accession Numbers

The sequences for strains the have been deposited in GenBank with the following accession numbers: GenBank accession MW301818-MW301829 (rplC and rplD gene related sequences); GenBank MW281777-MW281785 (23S RNA gene related sequences); GenBank MW357580-MW357581 (*MurA* gene related sequences).

Statistical Analysis

All statistical analyses were performed with GraphPad Prism, version 7.0 (GraphPad Software Inc., San Diego, CA, United States). One-way ANOVA was performed to assess the changes in MPC of linezolid or fosfomycin, used alone and in combination. *P*-values < 0.05 were considered statistically significant.

RESULTS

Antimicrobial Susceptibility Testing

Among the 43 Enterococcus isolates, 37 isolates (86.0%) were susceptible to linezolid, 23 isolates (53.0%) were susceptible to fosfomycin. The MIC90 for linezolid and fosfomycin were 2 and 128 mg/L, respectively (**Supplementary Table 2**).

In vitro Synergy Testing With the Checkerboard Method

The FICI values of all tested strains (**Supplementary Table 2**) illustrated that linezolid showed synergy or additivity in combination with fosfomycin against most of the tested strains (69.8%). No antagonistic effect was detected against all isolates evaluated.

$MIC_{99\%}$ Alone, MPC of Single Drugs and Combinations

For the five selected isolates with different FICI values, their $MIC_{99\%}$ alone, MPC alone of the two antimicrobial agents were listed on **Table 1**. For the five tested isolates, the MPCs of linezolid used alone ranged from 8.0 to 25.6 mg/L, while MPC/MIC ratio was in the range of 3–6. The MPC value of fosfomycin used alone was 1228.8 to 2321.1 mg/L, and the ratio of MPC/MIC was 13 to 20. However, linezolid combined with Fosfomycin can limit the enrichment of enterococcal resistant mutants at a lower concentration (**Table 2**). Furthermore, different proportions of linezolid and fosfomycin in a combination would present different MPCs. Compared with the MPC of linezolid or fosfomycin alone, the MPC of both two agents in combination were significantly reduced ($P < 0.05$) (**Supplementary Figures 1, 2**).

[1]http://blast.ncbi.nlm.nih.gov/Blast.cgi

TABLE 1 | $MIC_{99\%}$s and MPCs of two antimicrobial agents alone for five selected *Enterococcus* strains.

Isolates	MIC (mg/L)		$MIC_{99\%}$ (mg/L)		MPC (mg/L)		FICI
	LIN	FOS	LZD	FOS	LZD	FOS	
NO.1	2	128	2.0	126.2	8.5	2321.1	0.625
NO.5	2	128	1.9	126.8	8.0	2321.1	0.5
NO.6	2	128	1.9	120.3	10.4	1774.9	0.375
NO.22	8	128	7.8	112.3	25.6	2321.1	0.312
NO.43	2	64	1.9	64.0	8.5	1228.8	1.0

MIC, minimum inhibitory concentration; MIC99%, a minimal concentration that inhibits colony formation by 99%; MPC, mutant prevention concentration; LZD, linezolid; FOS, fosfomycin; FICI, fractional inhibitory concentration index.

SI Values of Two Drugs When Used Alone or Combined in Different Proportions

The width of the mutant selection window (MSW) is termed as selection index (SI), which can be expressed as the ratio of MPC to $MIC_{99\%}$. Closing MSW implied that SI were less than or equal to one. Based on the MSW theory, a combination in which SI of each agent was less than or equal to one would be efficacious to prevent antimicrobial resistance. The SI values of the two agents used alone or in combination with different proportions were showed in **Figure 1**. It can be clearly observed from the **Figure 1**: (1) For each strain, the SI values of fosfomycin alone were significantly higher than that of linezolid alone. It means that the MSW of Fosfomycin was larger than the MSW of linezolid. However, the MSW of fosfomycin was firstly to be closed when combined with linezolid. (2) Linezolid combined with fosfomycin in different ratios, the SI values of the two were different. (3) For the isolates with the value of FICI ≤ 0.5 (NO.22, NO.6, and NO.5), the combination of linezolid and fosfomycin can simultaneously close each other's MSW within a certain ratio rang. The smaller FICI, the wider range of the combination to close each other's mutation selection window (**Figures 1B–D**). But, for the NO.1 and NO.43 strain (with FICI > 0.5), in any composition ratio, the combination of linezolid and fosfomycin cannot shut down each other's MSW at the same time, (**Figures 1A,E**). Above experimental data and analyses showed that a roughly positive correlations between SI and FICI suggested that the smaller the FICI value of linezolid and fosfomycin was, the more probable the combination was to close each other's MSW (SI was less than or equal to one).

Characterization of Linezolid or Fosfomycin Resistance Mechanisms

The sequencing results and MIC determination results of the resistant mutants and its parent strains were presented in **Tables 3**, **4**. As shown in **Table 3**, linezolid-resistant mutants showed low-level resistance to linezolid, and its MIC value was 8 to 32 mg/L. Mutations in the *rplC* gene encoding ribosomal protein L3 or the *rplD* gene encoding ribosomal protein L4 were detected in the linezolid-resistant mutants of each strain (**Table 3**). Nucleotide substitutions of nt608, nt609, nt613, nt614 led to substitution of Glu by Gly at amino acid of rplD. In

TABLE 2 | MPCs of linezolid and fosfomycin in combinations with thirteen different proportions.

Isolates	MPCs of two antimicrobial agents in combinations with thirteen different proportions (mg/L) (LZD: FOS)												
	64:1	32:1	16:1	8:1	4:1	2:1	1:1	1:2	1:4	1:8	1:16	1:32	1:64
NO.1	6.9/0.11	6.4/0.2	5.9/0.4	5.3/0.7	3.7/0.9	3.5/1.5	3.5/3.5	2.7/5.9	5.3/21.3	4.8/38.4	3.5/55.5	2.7/172.5	2.0/128.0
NO.5	6.9/0.11	5.3/0.17	5.3/0.3	6.4/0.8	5.3/1.3	5.3/2.7	3.2/3.2	2.9/5.9	4.8/19.2	2.9/23.5	2.7/42.7	2.9/93.9	1.9/119.5
NO.6	6.9/0.11	5.9/0.18	3.2/0.2	2.7/0.3	2.4/0.6	2.7/1.3	2.4/2.4	2.4/4.8	4.8/19.2	2.7/21.3	1.6/27.7	1.6/51.2	1.7/119.5
NO.22	21.3/0.33	21.3/0.67	21.3/1.3	20.3/2.5	18.1/4.5	17.1/8.5	14.9/14.9	6.4/12.8	6.9/27.7	6.4/51.2	6.9/110.9	5.9/187.7	5.9/375.5
NO.43	6.4/0.1	5.9/0.18	5.9/0.37	4.8/0.6	5.3/1.3	4.8/2.4	4.8/4.8	3.7/7.5	3.2/11.7	2.4/19.2	2.4/38.4	2.9/93.9	1.9/119.5

MPC, mutant prevention concentration; LZD, linezolid; FOS, fosfomycin.

the NO.1-LM strain, a mutation of nt610 (A → T) and nt610 (T → C) resulted the amino acid changes of *rplC*. Moreover, four of five linezolid resistant mutants presented mutations both in *rplC* and *rplD* gene. Except for the detection of the *rplC* gene mutation encoding ribosomal protein L3 in the NO.22 strain, no gene mutation was detected in the other parental strains. As fosfomycin mutant derivatives (**Table 4**), compared with their parent strains, four of five showed highly resistant to fosfomycin (MICs rang 1024 to 2048 mg/L). The sequencing results showed that a nucleotide substitution at nt465 (A → G) in strain NO.1-FM and at nt1163 (A → C), nt1216 (T → A) in strain NO.5-FM, resulted the amino acid changes of *MurA*. However, some fosfomycin mutants and their parents did not successfully amplify several drug-resistant gene related fragments.

DISCUSSION

In this study, the FICI values of 43 strains indicated that linezolid-fosfomycin combination showed synergistic or additive effect on 69.8% of the tested strains and no antagonistic effects was observed. Consistent with this experiment, the synergistic antibacterial activity of the linezolid-fosfomycin combination against *Staphylococcus aureus* and *Enterococcus* was also confirmed *in vitro* time-killing curve (Chai et al., 2016; Chen et al., 2018; Qi et al., 2019). However, research on the combination to prevent resistance was still lacking.

Mutant prevention concentration and mutant selection window are special parameters that may provide useful information about the necessary drug concentration required in the infection area, in order to avoid the emergence of resistance, particular in case of high bacterial load (Vassilara et al., 2017). For the five strains, the MPCs of fosfomycin alone were 13 to 20-fold than their MICs, which implied that the MSW of fosfomycin was very wider. This results also showed in the MPC study of fosfomycin against *Staphylococcus aureus* (Mei et al., 2015), *Escherichia coli* (Pan et al., 2017), and *Pseudomonas aeruginosa* (Díez-Aguilar et al., 2015). Moreover, all MPC values of five selected strains exceed 1000 mg/L. However, according to the pharmacokinetic study of fosfomycin, a 4-g intravenous infusion reaches C_{max} (peak concentration) of 200–250 mg/L and an 8-g dose C_{max} of 260–450 mg/L (Roussos et al., 2009). It means that when fosfomycin monotherapy was used, the concentration at the infected site easily falls into the MSW, which may cause to the occurrence of bacterial resistance. The paradox is that fosfomycin resistance develops readily *in vitro* but less so *in vivo* (Falagas et al., 2016). The apparent discrepancy between *in vitro* and *in vivo* may partly explained by the function of immune system. Handel et al. revealed that an immune response greatly narrows the MSW and decreases the emergence of resistance despite a large drug-induced decline of bacteria numbers (Handel et al., 2009). Concern about the clinical application of fosfomycin is that resistance may appear during monotherapy. Currently, Fosfomycin is generally recommended in combination with other antibacterial drugs to treat bacterial infections (Falagas et al., 2018). As the results of linezolid MPC alone, the MPC values were 8.0 to 10.4 mg/L in the four linezolid-susceptible isolates (NO.1, NO.5, NO.6, and NO.43). This is a slightly higher than the MPC of clinically isolated enterococci reported in other studies (Zinner et al., 2008; Allen and Bierman, 2009). Some studies showed that maintaining drug concentrations above its MPC throughout therapy can severely restrict the acquisition of linezolid resistant mutants (Zinner et al., 2018; Alieva et al., 2019). The *in vitro* pharmacodynamics of linezolid against a clinical isolate of *E. faecium* (MIC1.8 mg/L and MPC 7 mg/L) demonstrated that an AUC24/MIC ratio >200 h (AUC_{24},24 h area under the curve) was estimated to restrict the selection of linezolid-resistant enterococci (Zinner et al., 2008). However, this estimated value is twice the value provided by a 600 mg clinical dose of twice-daily linezolid (Zinner et al., 2008). Increasing the dose of linezolid can achieve its therapeutic effect, while this will increase the risk of adverse and toxic effects. Therefore, linezolid monotherapy may be not a wise choice to prevent bacterial resistance and improve drug safety.

Combinations including individual drug constituents with smaller MSWs may have better ability in preventing the evolution of resistance (Ni et al., 2016). For the five tested strains, the MSW of fosfomycin monotherapy was much larger than that of linezolid. Interestingly, the MSW of fosfomycin was prior to be closed in the two agents of the combination. Furthermore, the combination of linezolid and fosfomycin in different ratios can effectively suppress the enrichment of enterococcal resistant mutants at a lower concentration. Compared with linezolid or fosfomycin alone, the MPC values of the two antibacterial drugs were significantly reduced when the two drugs combined in different proportions ($P < 0.05$). It may suggest that the MSW of one antimicrobial agent in combination can be narrowed or even close by increasing the proportion of another agent whether it's synergy or not. This has also confirmed by many previous studies

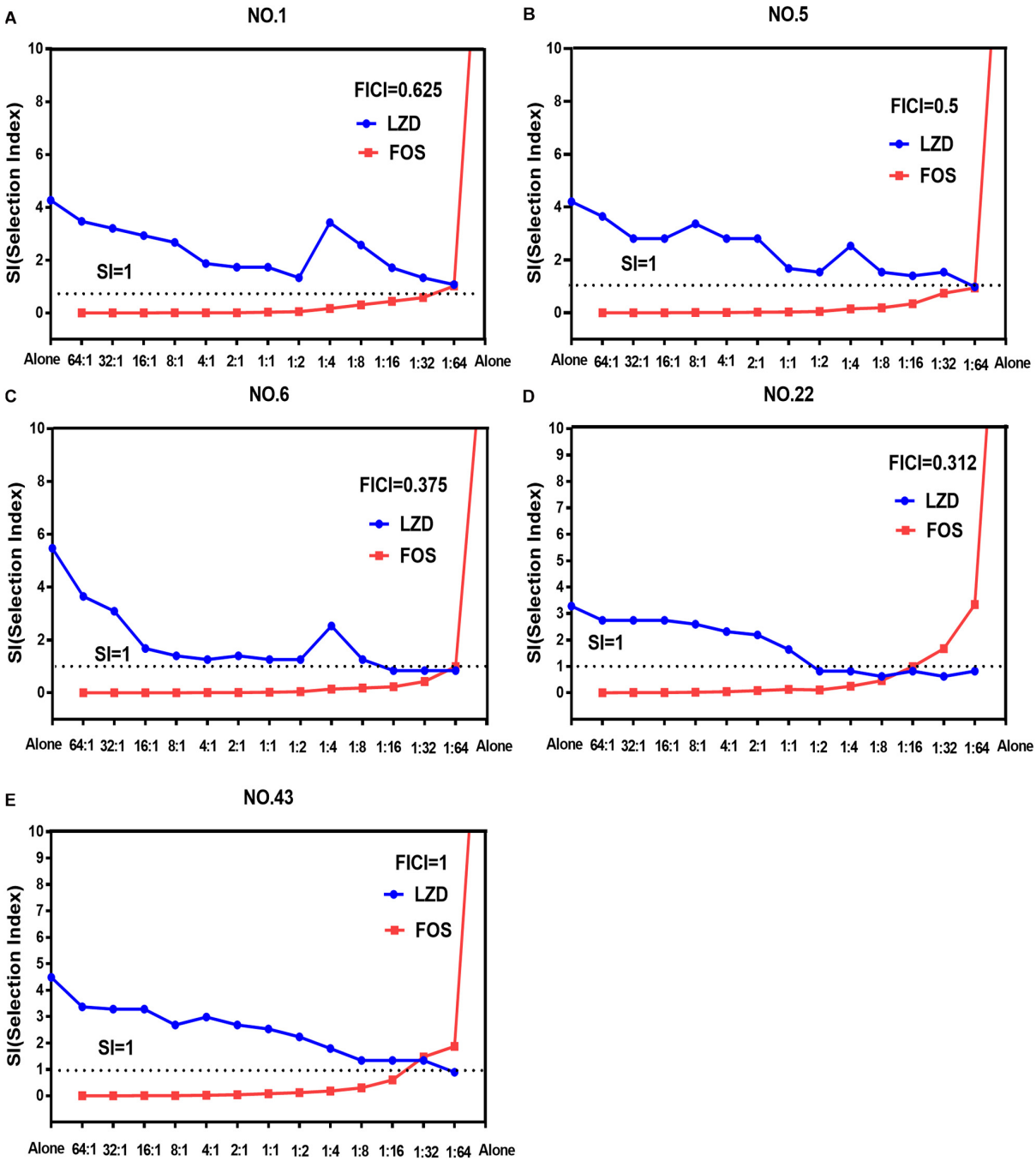

FIGURE 1 | Mutant selection indexes (SIs) of linezolid and fosfomycin when the two agents used alone or in combination with different ratios (linezolid: fosfomycin) against five enterococci. **(A)** NO.1 strain; **(B)** NO.5 strain; **(C)** NO.6 strain; **(D)** NO.22 strain; **(E)** NO.43 strain; LZD, linezolid; FOS, fosfomycin; FICI, fractional inhibitory concentration index; that the SIs of two agents in a combination including thirteen proportions were simultaneously less than or equal to one represented their MSWs were closed each other.

on combinations such as minocycline and amikacin (Wentao et al., 2018) or gentamicin, tigecycline and amikacin (Ni et al., 2016), fosfomycin and tobramycin (Díez-Aguilar et al., 2015). However, something may be different when it is discussed that the combination of linezolid and fosfomycin simultaneously closes each other's mutation selection window. Closing MSW mean that mutant selection index (SI, the ratio of MPC to MIC99%) were less than or equal to one. For the selected isolates with FICI $\leq$ 0.5 (NO.5, NO.6, and NO.22), both the SI of linezolid and fosfomycin in combination were simultaneously less than or equal to one within a certain range of proportions (**Figures 1B–D**). In addition, the more significant synergistic effect between linezolid

TABLE 3 | MIC values of linezolid and resistance mechanisms in linezolid resistant-mutants obtained from the MPC study of linezolid alone.

Isolates	Resistance gene					Linezolid MIC (mg/L)
	rplC	*rplD*	*cfr*	*optrA*	23s RNA	
NO.1	–	–	–	–	–	2
NO.1-LM	A610T(Lys192Asn)/T611C(Ser193Pro) /615A(194Ser)	Insert(610A)/A613G(Glu166Gly)	–	–	–	16
NO.5	–	–	–	–	–	2
NO.5-LM	T18A(Ile6Asn)/T604C/T607A	Insert(610A/T611)/A614G(Glu167Gly)	–	–	–	8
NO.6	–	–	–	–	–	2
NO.6-LM	–	A609G(Glu165Gly)	–	–	–	8
NO.22	A606T/insert(8C/9A)	–	–	–	–	8
NO.22-LM	A605T/insert(8C)	A608G(Glu165Gly)	–	–	–	32
NO.43	–	–	–	–	–	2
NO.43-LM	A605T	C349T	–	–	–	8

"–" undetected; the isolates of NO.1, NO.5, NO.6, NO.22, and NO.43 are the parent strains and the isolates of NO.1-LM, NO.5-LM, NO.6-LM, NO.22-LM, and NO.43-LM are their corresponding linezolid resistant-mutants recovered from the MPC study of linezolid alone; rplC gene, encoding ribosomal protein L3; rplD gene, encoding ribosomal protein L4.

and fosfomycin was, the wider extent of the two drugs closing their MSW was. But for the tested strains with FICI > 0.5 (NO.1 and NO.43), the two agents in combination cannot close each other's mutation selection window at the same time in any composition ratio. Based on the above results (**Figures 1A–E**), we found a rough positive correlation between SI and FICI, which displayed that the smaller FICI was, the more probable the combination was to close each other's MSW (SI was less than or equal to one). Similar to our results, Xu et al. (2018) revealed that the smaller FICIs of two agents in combinations were, the more probable their MSWs were to close each other. In accordance with the MSW theory, the synergistic combination of linezolid and fosfomycin simultaneously closing their MSW has a great potency to prevent enterococcal resistance.

Could the synergistic combination of linezolid and fosfomycin completely prevent resistance? Combination efficacy was complicated by many factors, including the proportion of drugs in the combination. Although a lot of combinations have been reported to prevent bacterial resistance, while different proportions of two drugs in combination rarely determined. In this study, thirteen proportions of linezolid and fosfomycin in combination was designed and the results show that different ratios of linezolid and fosfomycin in a combination would present different MPCs and SIs. Taking into account the difference in the pharmacokinetics of linezolid and fosfomycin *in vivo*, the ratios of two drugs in blood and infectious sites may be different even if the two agents administrated at fixed ratio, which would result in different effects in preventing resistance (Xu et al., 2018). Therefore, it is preferable to select a combination of two antimicrobials that can close each other's mutation selection window in a wide range of proportions. However, even though the linezolid-fosfomycin combination presented evidently synergistic activities against enterococcus NO.22 and NO.6, only proportions against NO.22 (1:2 to 1:16) and NO.6 (1:16 to 1:64) could close each other's MSW (**Figures 1C,D**). Thereby, it was best to choose the combination with the small FICI value as much as possible to prevent enterococcal resistance. Ideally, the maximum FICI value was better less than 0.5.

TABLE 4 | MIC values of fosfomycin and resistance mechanisms in fosfomycin resistant-mutants obtained from the fosfomycin MPC study.

Isolates	Resistance gene				Fosfomycin MIC (mg/L)
	MurA	*uhpT*	*glpT*	*fosB*	
NO.1	–	–	–	–	128
NO.1-FM	A465G(Cys210Arg)/C754T/	–	–	–	2048
NO.5	–	–	–	–	128
NO.5-FM	A1163C(Leu344Val)/ T1216A(Asp361Val)/C1091T	–	–	–	2048
NO.6	–	–	–	–	128
NO.6-FM	–	–	–	–	1024
NO.22	–	–	–	–	128
NO.22-FM	–	–	–	–	512
NO.43	–	–	–	–	128
NO.43-FM	–	–	–	–	1024

"–" undetected; the isolates of NO.1, NO.5, NO.6, NO.22, and NO.43 are the parent strains and the isolates of NO.1-FM, NO.5-FM, NO.6-FM, NO.22-FM, and NO.43-FM are their corresponding fosfomycin resistant-mutants obtained from the MPC study of fosfomycin alone.

The common mechanisms of *Enterococcus* resistance to linezolid include point mutations in chromosome 23S rRNA genes or genes encoding L3, L4, and L22 ribosomal proteins (Mendes et al., 2014; Wang et al., 2014). Other important mechanisms include plasmid-mediated chloramphenicol-florfenicol resistance *cfr* gene or ribosome protection gene *optrA* and *poxtA* (Wang et al., 2014; Park et al., 2020; Ruiz-Ripa et al., 2020). Correspondingly, several mechanisms have been proposed to be related to fosfomycin resistance including fosfomycin forming an inactive adduct (Falagas et al., 2018), fosfomycin modification enzyme (Cassir et al., 2014), mutations in the chromosomal genes encoding fosfomycin transporters (Fu et al., 2016; Xu et al., 2017) and mutations in the target enzyme *MurA* (Falagas et al., 2016). In order to explore the resistance mechanism of linezolid resistant mutants or fosfomycin resistant

mutants, several related genes were amplified in this experiment. All linezolid resistant mutants showed low levels resistance to linezolid. Moreover, only mutations in *rplC* gene encoding ribosomal proteins L3 or *rplD* gene encoding ribosomal proteins L4 were detected in the linezolid resistant mutants. The outcomes are in accord with recent study which reported that the L3 and L4 mutations are associated with low-level linezolid resistance in enterococci (Chen et al., 2013). Differently, Hua et al. (2019) held that since the L3 and L4 mutations did not simultaneously occur in the same strain, they play a negligible role in linezolid resistance. But, in this study, four linezolid resistant mutants had both ribosomal protein L3 and L4 mutations. For the mechanism of resistance to fosfomycin, sequencing analyses detected distinct mutations in the *MurA* gene of the two fosfomycin resistant mutants. The bacterial enzyme *MurA* catalyzes the transfer of enolpyruvate from Phosphoenolpyruvate (PEP) to uridine diphospho-N-acetylglucosamine (UNAG), which is the first step of bacterial cell wall biosynthesis (Kurnia et al., 2019). The mutations detected in *MurA* have been shown to reduce the affinity of fosfomycin (Fu et al., 2016; Xu et al., 2017). Recently study shown that the mutations in the fosfomycin target enzyme *MurA* were related to the resistance mechanisms clinically isolated enterococci (Zhang et al., 2019). However, the mechanism of three fosfomycin resistant mutants to fosfomycin remains unclear. The mechanism that governs fosfomycin resistance in enterococci requires further study.

Limitations of This Study

Firstly, although different ratios of linezolid and fosfomycin were designed in this study, the static concentration *in vitro* could not truly reflect the dynamic process of the drug *in vivo*. And we neglected the influence of *in vivo* immunity on resistance selection. The MSW hypothesis and the MPC concept have been applied to a planktonic mode of bacterial growth and not for biofilms, which are one of the causes of bacterial resistance (Cantón and Morosini, 2011). These findings need to be further verified in dynamic model of pharmacokinetics and pharmacodynamics *in vitro* (Golikova et al., 2017), animal models (Pan et al., 2017), bacterial biofilm (Siala et al., 2018; Sharma et al., 2019c). Secondly, only five strains of *Enterococcus* were used in MSW and MPC studies. Thirdly, mutations in drug-resistant gene from chromosome preliminarily verified the applicability of MSW theory to linezolid and fosfomycin. However, under clinical conditions, enterococci can acquire resistance via chromosomal mutations and lateral gene transfer. Our study could not reflect the entire complex clinical situation, because MPCs/MSWs derived from chromosomal mutations but not lateral gene transfer (Ni et al., 2016). Furthermore, the relationship between a mutation and drug resistance is not always a simple one-to-one correspondence. Although many mutations contributing to antibiotic resistance have been identified, the relationship between the mutations and the related phenotypic changes in charge of resistance has yet to be fully elucidated (Suzuki et al., 2014). Taking into,account the complexity of bacterial resistance mechanisms, it is necessary to use proteomics (Vranakis et al., 2014; Yan et al., 2018) and other methods (Hua et al., 2018) to further elaborate the specific mechanisms.

CONCLUSION

Linezolid combined with fosfomycin could validly restrict the enrichment of resistant enterococci at low concentrations, compared with the two drugs alone. The synergistic combination of linezolid and fosfomycin may have better ability in preventing the evolution of resistance in clinic and provide a new option for clinical treatment of enterococcal infection.

DATA AVAILABILITY STATEMENT

The datasets presented in this study can be found in online repositories. The names of the repository/repositories and accession number(s) can be found below: GenBank, accession: MW301818-MW301829, MW281777-MW281785, and MW357580-MW357581.

AUTHOR CONTRIBUTIONS

XH and JL conceived the idea and designed the study. LJ performed the study, analyzed the data, and wrote the manuscript. NX, MC, and YL provided technical support. SW and JM revised the manuscript. All authors read and approved the final version of the manuscript.

FUNDING

This study was supported by the National Natural Science Foundation of China (81173133), the Fund of Excellent Talents in Colleges and Universities of Anhui Province, China (gxbjZD06), and the Fund of Academic Leaders of Anhui Province, China (2015D068).

ACKNOWLEDGMENTS

We thank Department of Infectious Diseases, The First Affiliated Hospital of Anhui Medical University for its assistance.

SUPPLEMENTARY MATERIAL

The Supplementary Material for this article can be found online at: https://www.frontiersin.org/articles/10.3389/fmicb.2020.605962/full#supplementary-material

Supplementary Figure 1 | The MPC of linezolid when it used alone or combined with fosfomycin in thirteen proportions (linezolid: fosfomycin) against five enterococci. **(A)** NO.1 strain; **(B)** NO.5 strain; **(C)** NO.6 strain; **(D)** NO.22 strain; **(E)** NO.43 strain; MPC, mutant prevention concentration; *p-value < 0.05; **p-value < 0.001; ***p-value < 0.0001.

Supplementary Figure 2 | The MPC of fosfomycin when it used alone or combined with linezolid in thirteen proportions (linezolid: fosfomycin) against five enterococci. **(A)** NO.1 strain; **(B)** NO.5 strain; **(C)** NO.6 strain; **(D)** NO.22 strain; **(E)** NO.43 strain; MPC, mutant prevention concentration; ***p-value < 0.0001.

REFERENCES

Alieva, K. N., Golikova, M. V., Portnoy, Y. A., Dovzhenko, S. A., Kobrin, M. B., Zinner, S. H., et al. (2019). Concentration-dependent enrichment of resistant *Enterococcus faecium* exposed to linezolid in an in vitro dynamic model. *J. Chemother.* 30, 364–370. doi: 10.1080/1120009x.2018.1533267

Alieva, K. N., Strukova, E. N., Golikova, M. V., Portnoy, Y. A., Zinner, S. H., and Firsov, A. A. (2018). Time inside the mutant selection window as a predictor of *staphylococcal* resistance to linezolid. *J. Antibiot.* 71, 514–521. doi: 10.1038/s41429-017-0016-9

Allen, G. P., and Bierman, B. C. (2009). In vitro analysis of resistance selection by linezolid in vancomycin-susceptible and -resistant *Enterococcus faecalis* and *Enterococcus faecium*. *Int. J. Antimicrob. Agents* 34, 21–24. doi: 10.1016/j.ijantimicag.2008.12.011

Bai, B., Hu, K., Zeng, J., Yao, W., Li, D., Pu, Z., et al. (2019). Linezolid consumption facilitates the development of linezolid resistance in *Enterococcus faecalis* in a tertiary-care hospital: a 5-year surveillance study. *Microb. Drug Resist.* 25, 791–798. doi: 10.1089/mdr.2018.0005

Bayram, N., Duzgol, M., Kara, A., Ozdemir, F. M., and Devrim, I. (2017). Linezolid-related adverse effects in clinical practice in children. *Arch. Argent. Pediatr.* 115, 470–475. doi: 10.5546/aap.2017.eng.470

Blondeau, J. M. (2009). New concepts in antimicrobial susceptibility testing: the mutant prevention concentration and mutant selection window approach. *Vet. Dermatol.* 20, 383–396. doi: 10.1111/j.1365-3164.2009.00856 x

Cantón, R., and Morosini, M.-I. (2011). Emergence and spread of antibiotic resistance following exposure to antibiotics. *FEMS Microbiol. Rev.* 35, 977–991. doi: 10.1111/j.1574-6976.2011.00295.x

Cassir, N., Rolain, J., and Brouqui, P. (2014). A new strategy to fight antimicrobial resistance: the revival of old antibiotics. *Front. Microbiol.* 5:551. doi: 10.3389/fmicb.2014.00551

Chai, D., Liu, X., Wang, R., Bai, Y., and Cai, Y. (2016). Efficacy of linezolid and fosfomycin in catheter-related biofilm infection caused by methicillin-resistant *Staphylococcus aureus*. *Biomed. Res. Int.* 2016, 1–7. doi: 10.1155/2016/6413982

Chen, H., Li, L., Liu, Y., Wu, M., Xu, S., Zhang, G., et al. (2018). In vitro activity and post-antibiotic effects of linezolid in combination with fosfomycin against clinical isolates of *Staphylococcus aureus*. *Volume* 11, 2107–2115. doi: 10.2147/IDR.S175978

Chen, H., Wu, W., Ni, M., Liu, Y., Zhang, J., Xia, F., et al. (2013). Linezolid-resistant clinical isolates of enterococci and Staphylococcus cohnii from a multicentre study in China: molecular epidemiology and resistance mechanisms. *Int. J. Antimicrob. Agents* 42, 317–321. doi: 10.1016/j.ijantimicag.2013.06.008

Clsi. (2019). *Performance Standards for Antimicrobial Susceptibility Testing; Twenty-ninth Informational Supplement (M100)*. Wayne, PA: Clinical and Laboratory Standards Institute.

Davis, H., Brown, R., Ashcraft, D., and Pankey, G. (2020). In vitro synergy with fosfomycin plus doxycyclin against linezolid and vancomycin-resistant *Enterococcus faecium*. *J. Global Antimicrob. Resist.* 22, 78–83. doi: 10.1016/j.jgar.2020.01.014

Díez-Aguilar, M., Morosini, M. I., Tedim, A. P., Rodríguez, I., Aktaş, Z., Cantón, R. et al. (2015). Antimicrobial activity of fosfomycin-tobramycin combination against *Pseudomonas aeruginosa* isolates assessed by time-kill assays and mutant prevention concentrations. *Antimicrob. Agents Chemother.* 59, 6039–6045. doi: 10.1128/AA

Doern, C. D., Park, J. Y., Gallegos, M., Alspaugh, D., and Burnham, C. D. (2016). Investigation of linezolid resistance in *Staphylococci* and *Enterococci*. *J. Clin. Microbiol.* 54, 1289–1294. doi: 10.1128/JCM.01929-15

Drago, L., Nicola, L., and De Vecchi, E. (2008). A comparative in-vitro evaluation of resistance selection after exposure to teicoplanin, vancomycin, linezolid and quinupristin–dalfopristin in *Staphylococcus aureusan Enterococcus spp*. *Clin. Microbiol. Infect.* 14, 608–611. doi: 10.1111/j.1469-0691.2008.01993.x

Drlica, K. (2003). The mutant selection window and antimicrobial resistance. *J. Antimicrob. Chemother.* 52, 11–17. doi: 10.1093/jac/dkg269

Drlica, K., and Zhao, X. (2007). Mutant selection window hypothesis updated. *Clin. Infect. Dis.* 44, 681–688. doi: 10.1086/511642

Durão, P., Balbontín, R., and Gordo, I. (2018). Evolutionary mechanisms shaping the maintenance of antibiotic resistance. *Trends Microbiol.* 26, 677–691. doi: 10.1016/j.tim.2018.01.005

Falagas, M. E., Athanasaki, F., Voulgaris, G. L., Triarides, N. A., and Vardakas, K. Z. (2018). Resistance to fosfomycin: Mechanisms, Frequency and Clinical Consequences. *Int. J. Antimicrob. Agents* 53, 22–28. doi: 10.1016/j.ijantimicag.2018.09.013

Falagas, M. E., Lourida, P., Poulikakos, P., Rafailidis, P. I., and Tansarli, G. S. (2014). Antibiotic treatment of infections due to carbapenem-resistant *Enterobacteriaceae*: systematic evaluation of the available evidence. *Antimicrob. Agents Chemother.* 58, 654–663. doi: 10.1128/AAC.01222-13

Falagas, M. E., Vouloumanou, E. K., Samonis, G., and Vardakas, K. Z. (2016). Fosfomycin. *Clin. Microbiol. Rev.* 29, 321–347. doi: 10.1128/CMR.00068-15

Fiore, E., Van Tyne, D., and Gilmore, M. S. (2019). Pathogenicity of *Enterococci*. *Microbiol. Spectr.* 7, 31298205. doi: 10.1128/microbiolspec.GPP3-0053-2018

Fu, Z., Ma, Y., Chen, C., Guo, Y., Hu, F., Liu, Y., et al. (2016). Prevalence of fosfomycin resistance and mutations in *murA, glpT*, and *uhpT* in methicillin-resistant *Staphylococcus aureus* strains isolated from blood and cerebrospinal fluid samples. *Front. Microbiol.* 6:1544. doi: 10.3389/fmicb.2015.01544

García-Solache, M., and Rice, L. B. (2019). The *Enterococcus*: a model of adaptability to its environment. *Clin. Microbiol. Rev.* 32, e18–e58. doi: 10.1128/CMR.00058-18

Gawryszewska, I., żabicka, D., Hryniewicz, W., and Sadowy, E. (2017). Linezolid-resistant enterococci in Polish hospitals: species, clonality and determinants of linezolid resistance. *Eur. J. Clin. Microbiol.* 36, 1279–1286. doi: 10.1007/s10096-017-2934-7

Gilmore, M. S., Lebreton, F., and van Schaik, W. (2013). Genomic transition of enterococci from gut commensals to leading causes of multidrug-resistant hospital infection in the antibiotic era. *Curr. Opin. Microbiol.* 16, 10–16. doi: 10.1016/j.mib.2013.01.006

Golikova, M. V., Strukova, E. N., Portnoy, Y. A., Dovzhenko, S. A., Kobrin, M. B., Zinner, S. H., et al. (2017). Predicting effects of antibiotic combinations using MICs determined at pharmacokinetically derived concentration ratios: in vitro model studies with linezolid- and rifampicin-exposed *Staphylococcus aureus*. *J. Chemother.* 29, 267–273. doi: 10.1080/1120009X.2017.1281093

Haghi, F., Lohrasbi, V., and Zeighami, H. (2019). High incidence of virulence determinants, aminoglycoside and vancomycin resistance in enterococci isolated from hospitalized patients in northwest iran. *BMC Infect. Dis.* 19:744. doi: 10.1186/s12879-019-4395-3

Handel, A., Margolis, E., and Levin, B. R. (2009). Exploring the role of the immune response in preventing antibiotic resistance. *J. Theor. Biol.* 256, 655–662. doi: 10.1016/j.jtbi.2008.10.025

Hua, R., Xia, Y., Wu, W., Yan, J., and Yang, M. (2018). Whole transcriptome analysis reveals potential novel mechanisms of low-level linezolid resistance in *Enterococcus faecalis*. *Gene* 647, 143–149. doi: 10.1016/j.gene.2018.01.008

Hua, R., Xia, Y., Wu, W., Yang, M., and Yan, J. (2019). Molecular epidemiology and mechanisms of 43 low-level linezolid-resistant *Enterococcus faecalis* strains in chongqing. *China. Ann. Lab. Med.* 39, 36–42. doi: 10.3343/alm.2019.39.1.36

Kurnia, D., Apriyanti, E., Soraya, C., and Satari, M. H. (2019). Antibacterial flavonoids against oral bacteria of *Enterococcus Faecalis* ATCC 29212 from Sarang semut (myrmecodia pendans) and its inhibitor activity against enzyme mura. *Curr. Drug Discov. Technol.* 16, 290–296. doi: 10.2174/1570163815666180828113920

Lee, E. Y., and Caffrey, A. R. (2018). Thrombocytopenia with tedizolid and linezolid. *Antimicrob. Agents Chemother.* 62, e1417–e1453. doi: 10.1128/AAC.01453-17

Lee, S., Huh, H. J., Song, D. J., Shim, H. J., Park, K. S., Kang, C., et al. (2017). Resistance mechanisms of linezolid-nonsusceptible enterococci in Korea: low rate of 23S rRNA mutations in *Enterococcus faecium*. *J. Med. Microbiol.* 66, 1730–1735. doi: 10.1099/jmm.0.000637

Leone, S., Noviello, S., and Esposito, S. (2016). Combination antibiotic therapy for the treatment of infective endocarditis due to enterococci. *Infection* 44, 273–281. doi: 10.1007/s15010-015-0836-0

Mei, Q., Ye, Y., Zhu, Y. L., Cheng, J., Chang, X., Liu, Y. Y., et al. (2015). Testing the mutant selection window hypothesis in vitro and in vivo with Staphylococcus aureus exposed to fosfomycin. *Eur. J. Clin. Microbiol.* 34, 737–744. doi: 10.1007/s10096-014-2285-6

Mendes, R. E., Deshpande, L. M., and Jones, R. N. (2014). Linezolid update: stable in vitro activity following more than a decade of clinical use and summary of associated resistance mechanisms. *Drug Resist. Updat.* 17, 1–12. doi: 10.1016/j.drup.2014.04.002

Mercuro, N. J., Davis, S. L., Zervos, M. J., and Herc, E. S. (2018). Combatting resistant enterococcal infections: a pharmacotherapy review. *Expert Opin. Pharmaco.* 19, 979–992. doi: 10.1080/14656566.2018.1479397

Ni, W., Cai, X., Wei, C., Di, X., Cui, J., Wang, R., et al. (2015). Efficacy of polymyxins in the treatment of carbapenem-resistant *Enterobacteriaceae* infections: a systematic review and meta-analysis. *Braz. J. Infect. Dis.* 19, 170–180. doi: 10.1016/j.bjid.2014.12.004

Ni, W., Wei, C., Zhou, C., Zhao, J., Liang, B., Cui, J., et al. (2016). Tigecycline-amikacin combination effectively suppresses the selection of resistance in clinical isolates of *KPC ProducingKlebsiella pneumoniae*. *Front. Microbiol.* 7:1304. doi: 10.3389/fmicb.2016.01304

Pan, A. J., Mei, Q., Ye, Y., Li, H. R., Liu, B., and Li, J. B. (2017). Validation of the mutant selection window hypothesis with fosfomycin against *Escherichia coli* and *Pseudomonas aeruginosa:* an in vitro and in vivo comparative study. *J. Antibiot.* 70, 166–173. doi: 10.1038/ja.2016.124

Park, K., Jeong, Y. S., Chang, J., Sung, H., and Kim, M. (2020). Emergence of *optrA* -mediated linezolid-nonsusceptible *Enterococcus faecalis* in a tertiary care hospital. *Ann. Lab. Med.* 40, 321–325. doi: 10.3343/alm.2020.40.4.321

Qi, C., Xu, S., Wu, M., Zhu, S., Liu, Y., Huang, H., et al. (2019). Pharmacodynamics of linezolid-plus-fosfomycin against vancomycin-susceptible and -resistant *Enterococci* in vitro and in vivo of a galleria mellonella larval infection model. *Volume* 12, 3497–3505. doi: 10.2147/IDR.S219117

Roussos, N., Karageorgopoulos, D. E., Samonis, G., and Falagas, M. E. (2009). Clinical significance of the pharmacokinetic and pharmacodynamic characteristics of fosfomycin for the treatment of patients with systemic infections. *Int. J. Antimicrob. Agents* 34, 506–515. doi: 10.1016/j.ijantimicag.2009.08.013

Ruiz-Ripa, L., Feßler, A. T., Hanke, D., Eichhorn, I., Azcona-Gutiérrez, J. M., Pérez-Moreno, M. O., et al. (2020). Mechanisms of linezolid resistance among enterococci of clinical origin in spain—detection of optrA- and cfr(D)-carrying e. faecalis. *Micro Organ.* 8:1155. doi: 10.3390/microorganisms8081155

Sassi, M., Guérin, F., Zouari, A., Beyrouthy, R., Auzou, M., Fines-Guyon, M., et al. (2019). Emergence of optrA-mediated linezolid resistance in enterococci from France, 2006–16. *J. Antimicrob. Chemother.* 74, 1469–1472. doi: 10.1093/jac/dkz097

Sharma, D., Garg, A., Kumar, M., and Khan, A. U. (2019a). Proteome profiling of carbapenem-resistant K. pneumoniae clinical isolate (NDM-4): Exploring the mechanism of resistance and potential drug targets. *J. Proteomics.* 200, 102–110. doi: 10.1016/j.jprot.2019.04.003

Sharma, D., Garg, A., Kumar, M., Rashid, F., and Khan, A. U. (2019b). Down-regulation of flagellar, fimbriae, and Pili proteins in carbapenem-resistant *Klebsiella pneumoniae* (NDM-4) clinical isolates: a novel linkage to drug resistance. *Front. Microbiol.* 10:2865. doi: 10.3389/fmicb.2019.02865

Sharma, D., Misba, L., and Khan, A. U. (2019c). Antibiotics versus biofilm: an emerging battleground in microbial communities. *Antimicrob. Resist. Infect. Control* 8:76. doi: 10.1186/s13756-019-0533-3

Siala, W., Rodriguez-Villalobos, H., Fernandes, P., Tulkens, P. M., and Van Bambeke, F. (2018). Activities of combinations of antistaphylococcal antibiotics with fusidic acid against staphylococcal biofilms inin vitro static and dynamic models. *Antimicrob. Agents Chemother.* 62, e518–e598. doi: 10.1128/AAC.00598-18

Smith, T. T., Tamma, P. D., Do, T. B., Dzintars, K. E., Zhao, Y., Cosgrove, S. E., et al. (2018). Prolonged linezolid use is associated with the development of linezolid-resistant *Enterococcus faecium*. *Diagn. Micr. Infec. Dis.* 91, 161–163. doi: 10.1016/j.diagmicrobio.2018.01.027

Strukova, E. N., Portnoy, Y. A., Romanov, A. V., Edelstein, M. V., Zinner, S. H., Firsov, A. A. et al. (2016). Searching for the optimal predictor of ciprofloxacin resistance in *Klebsiella pneumoniae* by using in vitro dynamic models. *Antimicrob. Agents Chemother.* 60, 1208–1215. doi: 10.1128/AAC.02334-15

Suzuki, S., Horinouchi, T., and Furusawa, C. (2014). Prediction of antibiotic resistance by gene expression profiles. *Nat. Commun.* 5:5792. doi: 10.1038/ncomms6792

Torres, C., Alonso, C. A., Ruiz-Ripa, L., León-Sampedro, R., Del Campo, R., Coque, T. M. et al. (2018). Antimicrobial resistance in *Enterococcus spp*. of animal origin. *Microbio. Spectr.* 6:30051804. doi: 10.1128/microbiolspec.arba-0032-2018

Tsuji, Y., Holford, N. H. G., Kasai, H., Ogami, C., Heo, Y., Higashi, Y., et al. (2017). Population pharmacokinetics and pharmacodynamics of linezolid-induced thrombocytopenia in hospitalized patients. *Brit. J. Clin. Pharmaco.* 83, 1758–1772. doi: 10.1111/bcp.13262

Tyers, M., and Wright, G. D. (2019). Drug combinations: a strategy to extend the life of antibiotics in the 21st century. *Nat. Rev. Microbio.* 17, 141–155. doi: 10.1038/s41579-018-0141-x

Vassilara, F., Galani, I., Souli, M., Papanikolaou, K., Giamarellou, H., Papadopoulos, A. et al. (2017). Mechanisms responsible for imipenem resistance among *Pseudomonas aeruginosa* clinical isolates exposed to imipenem concentrations within the mutant selection window. *Diagn. Micr. Infec. Dis.* 88, 276–281. doi: 10.1016/j.diagmicrobio.2017.04.005

Vranakis, I., Goniotakis, I., Psaroulaki, A., Sandalakis, V., Tselentis, Y., Gevaert, K., et al. (2014). Proteome studies of bacterial antibiotic resistance mechanisms. *J. Proteomics* 97, 88–99. doi: 10.1016/j.jprot.2013.10.027

Wang, L., He, Y., Xia, Y., Wang, H., and Liang, S. (2014). Investigation of mechanism and molecular epidemiology of linezolid-resistant *Enterococcus faecalis* in China. *Infect. Genet. Evol.* 26, 14–19. doi: 10.1016/j.meegid.2014.05.001

Wang, Y., Lv, Y., Cai, J., Schwarz, S., Cui, L., Hu, Z., et al. (2015). A novel gene, *optrA*, that confers transferable resistance to oxazolidinones and phenicols and its presence in *Enterococcus faecalis* and of human and animal origin. *J. Antimicrob. Chemotehr.* 70, 2182–2190. doi: 10.1093/jac/dkv116

Wentao, N., Guobao, L., Jin, Z., Junchang, C., Rui, W., Zhancheng, G., et al. (2018). In vitro activity of minocycline combined with aminoglycosides against *Klebsiella pneumoniae* carbapenemase-producing *K. pneumoniae*. *J. Antibiot.* 71, 506–513. doi: 10.1038/s41429-017-0024-9

Xu, S., Fu, Z., Zhou, Y., Liu, Y., Xu, X., and Wang, M. (2017). Mutations of the transporter proteins *GlpT* and *UhpT* confer fosfomycin resistance in *Staphylococcus aureus*. *Front. Microbiol.* 8:914. doi: 10.3389/fmicb.2017.00914

Xu, X., Xu, L., Yuan, G., Wang, Y., Qu, Y., and Zhou, M. (2018). Synergistic combination of two antimicrobial agents closing each other's mutant selection windows to prevent antimicrobial resistance. *Sci. Rep.* 8:7237. doi: 10.1038/s41598-018-25714-z

Yan, J., Xia, Y., Yang, M., Zou, J., Chen, Y., Zhang, D., et al. (2018). Quantitative proteomics analysis of membrane proteins in *Enterococcus faecalis* with low-level linezolid-resistance. *Front. Microbiol.* 9:1698. doi: 10.3389/fmicb.2018.01698

Zahedi Bialvaei, A., Rahbar, M., Yousefi, M., Asgharzadeh, M., and SamadiKafil, H. (2017). Linezolid: a promising option in the treatment of Gram-positives. *J. Antimicrob. Chemotehr.* 72, 354–364. doi: 10.1093/jac/dkw450

Zhang, X., Bi, W., Chen, L., and Zhang, Y. (2019). Molecular mechanisms and epidemiology of fosfomycin resistance in *Enterococci* isolated from patients at a teaching hospital in China from 2013 to 2016. *J. Global Antimicrob. Resis.* 20, 191–196. doi: 10.1016/j.jgar.2019.08.006

Zinner, S. H., Gilbert, D., Lubenko, I. Y., Greer, K., and Firsov, A. A. (2008). Selection of linezolid-resistant *Enterococcus faecium* in an in vitro dynamic model: protective effect of doxycycline. *J. Antimicrob. Chemotehr.* 61, 629–635. doi: 10.1093/jac/dkm542

Zinner, M. V. G. E., Yury, A., and Portnoy, A. A. F. (2018). Predicting antibiotic combination effects on the selection of resistant *Staphylococcus aureus*: in vitro model studies with linezolid and gentamicin. *Int. J. Antimicrob. Agents* 52, 854–860. doi: 10.1016/j.ijantimicag.2018.09.005

Zou, J., and Xia, Y. (2020). Molecular characteristics and risk factors associated with linezolid-resistant *Enterococcus faecalis* infection in southwest china. *J. Global Antimicrob. Resis.* 22, 504–510. doi: 10.1016/j.jgar.2020.03.027

Conflict of Interest: The authors declare that the research was conducted in the absence of any commercial or financial relationships that could be construed as a potential conflict of interest.

frontiers in Microbiology

ORIGINAL RESEARCH
published: 19 February 2021
doi: 10.3389/fmicb.2021.611560

Synthesis, Characterization, Antibacterial and Wound Healing Efficacy of Silver Nanoparticles From *Azadirachta indica*

*Gandhimathi Chinnasamy[1], Smitha Chandrasekharan[1], Tong Wey Koh[2] and Somika Bhatnagar[1]**

[1] Plant Transformation and Tissue Culture, Temasek Life Sciences Laboratory, Singapore, Singapore, [2] Diabetes and Neurodegeneration, Temasek Life Sciences Laboratory, Singapore, Singapore

OPEN ACCESS

Edited by:
Mariano Martinez-Vazquez, Institute of Chemistry, National Autonomous University of Mexico, Mexico

Reviewed by:
Madhuree Kumari, Indian Institute of Science (IISc), India
Rodolfo García-Contreras, National Autonomous University of Mexico, Mexico

***Correspondence:**
Somika Bhatnagar
somika@tll.org.sg

Specialty section:
This article was submitted to Antimicrobials, Resistance and Chemotherapy, a section of the journal Frontiers in Microbiology

Received: *29 September 2020*
Accepted: *21 January 2021*
Published: *19 February 2021*

Citation:
Chinnasamy G, Chandrasekharan S, Koh TW and Bhatnagar S (2021) Synthesis, Characterization, Antibacterial and Wound Healing Efficacy of Silver Nanoparticles From Azadirachta indica. Front. Microbiol. 12:611560. doi: 10.3389/fmicb.2021.611560

Bacteria are the causative agents of numerous diseases. Ever increasing number of bacterial infections has generated the need to find new antibiotic materials and new ways to combat bacterial infections. Our study investigated *Azadirachta indica* (AI) as an alternate source of antibiotic compounds. Phytochemical and GC-MS analysis revealed presence of flavonoids, phenolic compounds, terpenoids and terpenes. Aqueous extracts of leaves were used to synthesize silver nanoparticles (AI-AgNPs), as established by colorimetric confirmation with maximum absorbance peak at 400 nm. Optimized reaction parameters produced high yield of stable AI-AgNPs, which were characterized by UV-Vis spectroscopy, energy-dispersive X-ray spectroscopy, scanning electron microscopy, and transmission electron microscopy. Results confirmed particle diameter of 33 nm and spherical shape of AI-AgNPs. Fourier transform infrared spectroscopy inferred the presence of functional groups in bioactive constituents involved in conversion of silver ions into elemental silver by acting as capping and reducing agents during formation of AI-AgNPs. X-ray diffraction revealed their crystalline nature. Toxicity studies on *Drosophila* validated normal egg laying capacity and eclosion of F1 generation on AI-AgNPs (100 μg/mL). DPPH (65.17%) and ABTS (66.20%) assays affirmed strong radical scavenging effect of AI-AgNPs (500 μg/mL). The antibacterial activity of AI-AgNPs (1,000 μg/mL) was confirmed by disc diffusion assay with zone of inhibition against *Bacillus cereus* (17.7 mm), *Escherichia coli* (18.7 mm), *Pseudomonas aeruginosa* (10.3 mm), and *Staphylococcus aureus* (17.7 mm). Minimum inhibitory concentration and minimum bactericidal concentration values for AI-AgNPs ranged between 390 and 780 μg/mL. Higher bacterial suppression by AI-AgNPs in comparison with AI-extract was further divulged by prominent damage to the bacterial cell walls, disintegration of cell membranes and outflow of intercellular content as evident in SEM images. AI-AgNPs were loaded on PF127 (biocompatible-biodegradable polymer) to form a viscous, spreadable, hydrogel that demonstrated enhanced antibacterial properties in disc diffusion assay (13–18.7 mm). When topically applied on mice, AI-AgNPs-PF127 hydrogel did not show symptoms of skin irritation. Application of

AI-AgNPs-PF127 hydrogel on wound sites in mice, significantly increased the wound contraction rate. Our studies present a simple green route to synthesize AI-AgNPs with enhanced antibacterial and free-radical scavenging efficacy; and AI-AgNPs-PF127 hydrogel as a low-toxic, eco-friendly delivery vehicle with potential in wound healing.

Keywords: antibacterial, antioxidant, wound healing, hydrogel, silver nanoparticles, green synthesis, *Azadirachta indica*

INTRODUCTION

Bacteria are the causative agents of numerous diseases often leading to death and disruption due to damaged crops, spoiled food products, and contaminated equipment (Baranwal et al., 2018). Bacterial infections increase the medical costs and create pressure on health care systems due to long stays in hospitals, treatment failures, persistence of infections and delayed healing of wounds often leading to amputation and increased mortality (WHO, 2020). There is a pressing need to develop new antibiotic material and new strategies to combat bacterial infections. Chemically synthesized drugs have many side effects; hence medicinal plants are being evaluated for curative role owing to their easy availability and non-toxicity for therapeutic use while being effective in curbing bacterial infections (Chinnasamy et al., 2019). Effectiveness of metal nanoparticles (1–100 nm) in combating infectious diseases is an exciting area of research with wide applications (Zazo et al., 2016; Lee et al., 2019). Physical and chemical routes to synthesize nanoparticles involve expensive apparatus and reagents, high voltage, high temperatures, and toxic solvents which leave hazardous residues and by-products raising safety and health concerns for environment and humans (Kumar and Yadav, 2009). Phyto-nanotechnology has gained considerable attention as an alternative, simple, rapid, easily scalable, and cost-effective route where nanoparticles are synthesized using extracts from plants, viruses, algae, fungi, and bacteria (Thakkar et al., 2010; Ahmad et al., 2019). Use of plant extracts has advantage of biocompatibility as they are rich in bioactive compounds which are amicable to extraction by water as an inert solvent and further act as reducing and capping agents in the synthesis of nanoparticles (Noruzi, 2015). Among the different metals in use such as gold, copper, iron, titanium, zinc; silver is the most prevalent one in therapeutic applications owning to inherent antimicrobial properties. Silver nanoparticles synthesized from plants that are ubiquitous in secondary metabolites, have been documented for their intrinsic property of antibacterial inhibition in foodborne pathogens and antibiotic resistant bacteria (Jain and Mehata, 2017; Loo et al., 2018). Among the various drug delivery systems, thermo-sensitive hydrogels are materials of choice for tissue engineering and wound healing applications due to their water holding capacity, uniform dispersion of therapeutic agents and their release in a controlled manner (Huang et al., 2019). Thermo-reversible Pluronic F-127 with sol-gel transition at body temperatures has been found to enhance topical wound healing (Arafa et al., 2018). *Azadirachta indica* (AI) commonly known as neem, is a tropical tree that originated in Indian sub-continent and its distribution has spread worldwide. United Nations acknowledged the importance of this tree and entitled it as "Tree of the 21st century." It is a revered home remedy and find multiple uses as leaf juice to kill intestinal worms, twigs for cleaning teeth, bark paste, and gum for topical application to treat leprosy and skin ailments, seed oil as mosquito repellent and leaves are known for anti-inflammatory, antipyretic, antimalarial, anticancer and antidiabetic properties (Kumar and Navaratnam, 2013; Sarah et al., 2019). In the current studies, we utilized leaves of neem plant for synthesizing silver nanoparticles (AI-AgNPs) and evaluated them for antioxidant activity and antibacterial potency against four species of bacteria. *Bacillus cereus* causes gastrointestinal illness; *Escherichia coli* causes cholecystitis, urinary tract infection, traveler's diarrhea, neonatal meningitis, pneumonia; *Pseudomonas aeruginosa* survives on medical devices such as ventilators, catheters, and often causes infections in hospital-patients and *Staphylococcus aureus* causes skin infections, bone and join infections, bacteremia, and sepsis. As many basic biological and physiological properties are upto 65% conserved between humans and *Drosophila melanogaster*, we evaluated the toxic response of orally administered AI-AgNPs in *Drosophila.* Thermo-sensitive hydrophilic PF127 was used as a non-toxic biocompatible hydrogel carrier for AI-AgNPs in topical applications on mice skin towards wound healing.

MATERIALS AND METHODS

Materials

Bacillus cereus ATCC 14579, *E. coli* ATCC 25922, *P. aeruginosa* ATCC 15442, and *S. aureus* ATCC 23235 were purchased from American Type Culture Collection (Rockville, MD, United States). Leaves of neem were collected from the premises of Temasek Life Sciences Laboratory, Singapore. Chemicals were procured from Sigma-Aldrich, Singapore.

Identification of Bioactive Compounds (GC-MS Analysis)

To prepare samples for gas chromatography-mass spectroscopy (GC-MS) analysis, neem leaves were lyophilized in liquid nitrogen using a mortar and pestle to obtain fine powder. 1 g of this powder was weighed and dissolved in either 1 mL of hexane or 1 mL of ethyl acetate along with 1 μL (10 mg/mL) of camphor (internal standard). After vortex, the slush was incubated on a horizontal shaker at 30 rpm for 2 h. The mixture was centrifuged at 4,200 rpm for 25 min at

15°C and the separated organic layer was dried in anhydrous sodium sulphate to remove traces of water. For phytochemical analysis the organic extract was transferred into 2 mL glass vial and loaded in a GC system (Agilent 7890A) with a Mass Selective Detector (MSD, Agilent Technologies 5975C Inert XL) and HP-5MS UI column (30 m × 0.25 mm – 0.25 μm). Experimental conditions of the system were as follows: injection volume – 2 μL; splitless injection; oven program 50°C (1 min hold) at 8°C min^{-1} to 300°C (5 min hold). Spectral analysis of data was by MSD Chem Station Data Analysis software (Agilent Technologies).

Synthesis and Characterization of AI-AgNPs

Nanoparticles were synthesized and characterized according to our previous paper, Chinnasamy et al. (2019). Briefly, washing of leaves under running water ensured removal of dust, pests, and spores, if any. Air dried leaves were homogenized into powder in a blender. Aqueous extract was prepared by adding 10 g of leaf powder to 100 mL of distil water (1:10 ratio) and heating in a water bath at 50°C for 30 min. The solution was cooled to room temperature (RT, 25°C), filtered through Whatman filter paper (No. 1), labelled as AI-extract and used for synthesis of nanoparticles. 5 mL of AI-extract was slowly added into 45 mL of silver nitrate ($AgNO_3$, 1 mM) in an Erlenmeyer flask. The resultant mixture was adjusted to pH 7 and incubated on a rotary shaker at 200 rpm, in dark, at RT for 24 h. During this period, visual observations were made to detect any change in colour. Aliquots were taken out at regular intervals of 6 h to measure the absorbance by UV-Visual spectrophotometer (2100 pro UV-Vis, GE). Thereafter, the nanoparticle suspension was centrifuged at 4,500 rpm for 20 min to collect AI-AgNPs as a pellet. To ensure removal of unreacted silver ions and any unbound phyto-constituent, this pellet was washed thrice with distil water, air-dried, and stored at RT for further use. The stability of AI-AgNPs in five different reagents namely distil water, PBS buffer, NaCl (0.9%), Dulbecco's modified eagle medium (DMEM), and complete medium (CM) was determined by measuring absorbance in wavelength range of 100–900 nm. On-shelf stability in distil water as a storage solution was tested over an additional period of 28 days by measuring absorbance in wavelength range of 100–900 nm.

AI-AgNPs were subjected to UV-Vis spectroscopy (UV1601, Shimadzu), scanning electron microscopy (SEM, JEOL JEM-6360 OLV), energy-dispersive X-ray spectroscopy (EDX), and transmission electron microscopy (TEM, JEOL JEM-1230) for characterization of shape, size morphology and elemental composition. Fourier transform infrared spectroscopy (FTIR, Thermo Fischer Scientific) recorded the absorption spectra in the range of 4,000–400 cm^{-1} to identify the presence of functional groups involved in bio-reduction. X-ray diffraction (XRD, D8 X-ray diffractometer, Brucker BioScience Corporation) of samples exposed to Cu-Kα radiation over an angular range of 20°–80° (2θ) determined the crystalline nature of AI-AgNPs.

Toxicity Studies of AI-AgNPs on *Drosophila melanogaster*

Fly Strain and Medium Preparation

White eyed fly strain, w^{1118} (Bloomington stock #3605) was used for the toxicity studies that included viability, development, and egg to adult survivorship. Flies were maintained on standard culture medium (fly food composed of bacto agar, corn meal flour, brewer's yeast, dextrose and nipagin). The treatment medium consisted of standard culture medium infused separately with AI-extract and AI-AgNPs; both in 5 different doses (10, 25, 50, 100, and 250 μg/mL).

Rate of Eclosion

Freshly emerged flies were kept for mating for 24 h in vials containing standard culture medium. The eggs laid in 4 h were transferred on treatment medium (50 eggs per treatment) and reared until eclosed (growth from egg to adult stage). Observations were recorded as percentage eclosion.

Egg Laying Capacity

Freshly emerged flies were grown on treatment medium for 10 days. This was followed by mating of flies for 24 h on standard culture medium. The egg laying capacity (of 50 female flies per treatment) was determined by counting the numbers of eggs laid in 4 h.

Rate of Eclosion of F1 Flies

Freshly emerged flies were grown on treatment medium for 10, 20, and 30 days. This was followed by mating of flies for 24 h on standard culture medium. The eggs were collected and grown on standard culture medium (50 eggs per treatment) until eclosed to determine the percentage of F1 flies eclosion.

TEM Image

The third instar larvae were grown on treatment medium AI-AgNPs (100 μg/mL) and the intestinal midguts were dissected under a microscope and treated with PBS. Samples were fixed in glutaraldehyde (2.5%) for 24 h and ossified with osmium tetroxide (1%) for 4 h. This was followed by dehydration with alcohol series (30–100%, 15 min each) and fixation with epoxy resin for 24 h. Resin blocks were sectioned into 20–30 μm thick tissue slices using an ultrathin tissue sectioner. Sections fixed on copper grid were stained with lead citrate before viewing under TEM to mark the presence of AI-AgNPs.

Free Radical Scavenging Assay

The free radical scavenging activity was determined by DPPH (2,2-diphenyl-1-picryhydrazil) radical and ABTS {2,2′-Azino-bis-(3-ethylbensothiazoline-6-sulfonic-acid)} radical assays using standard spectrophotometry method. In separate experiments, 100 μL of test samples in different concentrations (100–500 μg/mL) were mixed either with 100 μL of DPPH (0.1 mM) or 100 μL of ABTS master mix (10 mL of 7.4 mM ABTS + 10 mL

of 2.45 mM ammonium persulfate). After incubation at room temperature for 30 min in dark, the absorbance (A) of resultant solutions were taken at 515 nm for DPPH and 734 nm for ABTS. A blank (solution without samples) was taken as control and butylated hydroxytoluene (BHT) as a reference. The percentage of free radical scavenging was calculated by following equation:

$$\text{Percentage of radical scavanging} = \frac{(\text{A of Control} - \text{A of Sample})}{\text{A of Control}} \times 100$$

Antibacterial Activity

Disc Diffusion Method

Antibacterial activity of AI-extract and AI-AgNPs against four bacterial species was examined by Kirby-Bauer disk diffusion susceptibility test (Bauer et al., 1966). Single colonies of bacteria were picked and incubated overnight in Mueller-Hinton broth (MHB) at 250 rpm at 37°C. Absorbency of the bacterial suspension was measured at 600 nm by a spectrophotometer and adjusted to a concentration of 1×10^6 CFU/mL. Mueller-Hinton Agar (MHA) plates seeded with bacterial suspension were inoculated aseptically with 6 mm sterile paper discs infused separately with sterile distil water (control), Rifampicin (reference), silver nitrate, AI-extract or AI-AgNPs at a concentration of 1,000 μg/mL. The plates were incubated for 24 h at 37°C and visually examined for zone of inhibition (ZOI) around the discs which was the measure of bioactivity of the disc content. Another set of bacterial plates were similarly prepared to test the effect of AI-AgNPs-PF127 hydrogel.

Determination of MIC and MBC of AI-AgNPs

Minimum inhibitory concentration (MIC) was measured as the lowest concentration of AI-AgNPs sufficient to inhibit the growth of bacteria and was tested by broth micro dilution method as recommended by the guidelines of CLSI (2012). The MIC test was performed in a 96 well microtiter plate as described by Klancnik et al. (2010). Bacterial suspensions grown overnight in MHB were adjusted to a concentration of 1×10^6 CFU/mL. From a stock solution of AI-AgNPs (50 mg/mL) serial two-fold dilutions were prepared in MHB. This diluted series were inoculated with bacterial suspensions along with untreated control samples. The final volume in each well was 100 μL. The plates were sealed to prevent evaporation and incubated for 24 h at 37°C. Bacterial growth was measured at 600 nm in a microplate reader (Tecan-Spark). Minimum bactericidal concentration (MBC) endpoint is defined as the lowest concentration of antibacterial agent that completely kills the bacterial population. For determination of MBC, aliquots from each well of overnight microtiter plate were seeded on MHA plates without AI-AgNPs and incubated for 24 h at 37°C.

Bacterial Imaging by SEM

AI-extract and AI-AgNP were separately added to bacterial cultures (1×10^6 CFU/mL) in 6-well-plate and incubated for 6 h at 37°C. Plain MHB was used as control. The samples were centrifugated at 3,000 × *g* for 30 min to obtain bacterial pellets. These pellets were thoroughly washed and fixed in glutaraldehyde (2.5%, 30 min), followed by dehydration with ethanol series (30–100%, 15 min each step) and overnight drying in amyl acetate. Samples were then sputter coated with gold and visualized under SEM.

Wound Healing Study on Mice

AI-AgNPs-PF127 Hydrogel Preparation

Pluronic F-127 hydrogel (PF127, 30% w/v) was prepared in ice cold PBS. Treatment hydrogels were prepared by adding three different concentration of AI-AgNPs (0.3, 1, and 3 mg) to PF127 hydrogel. The mixtures were kept on rotary shaker overnight (in cold room), to get a clear solution and obtained gels were stored in refrigerator at 4°C for future studies.

Evaluation of Physiochemical Properties of AI-AgNPs-PF127 Hydrogel

Physical appearance of the PF127 and treatment hydrogels were visually observed for characteristics such as colour, homogeneity, and consistency. pH was measured by a standard pH meter after diluting the hydrogels to 1% with distil water. Viscosity of the hydrogels was measured at 4°C by an ostwald viscometer. To analyze the spreadability, 50 μL of hydrogels were pressed slightly between two glass slides and left undisturbed for 10 min (as per El-Houssieny and Hamouda, 2010). Diameter of the spread samples was then measured.

Skin Irritation Test

To evaluate toxicity of treatment hydrogel on mice, the skin irritation test was performed following the method of Mohamad et al. (2014). After shaving the hair, 20 μL of pristine PF127 hydrogel and 20 μL of 3 mg AI-AgNPs-PF127 hydrogel was applied on back of mice. Skin responses were noted at 1, 6, 24, and 48 h.

In vivo Wound Healing Activity

Animal experiments were carried out with an approved protocol from the Institutional Animal Care and Use Committee (IACUC), Nanyang Technological University, Singapore (ARF-SBS/NIE-A0367NTU). Pathogen-free, healthy, adult male albino mice with the body weight around 25–30 g were maintained under 12 h day/12 h night cycle in standard lab conditions. Animals were fed with typical rodent diet and distil water throughout this experiment. After one-week of acclimatization, the mice were anesthetized using 5% v/v isoflurane/air and maintained at 2.5% v/v isoflurane/air. Dorsal skin was shaved, disinfected with 70% ethyl alcohol and 6 mm (diameter) of full thickness excision wounds were created. Mice were divided into four groups each comprising of six mice. Group I: control, Group II: pristine PF127 hydrogel, Group III: 0.3 mg AI-AgNPs-PF127 hydrogel, and Group IV: 1.0 mg AI-AgNPs-PF127 hydrogel. 20 μL of respective hydrogel samples were smeared onto the wound site on 1st day and the wounds were covered with Tegaderm and opsite flexifix transparent wound dressing material. Wound areas were examined on 3rd, 5th, 7th, and 10th

day after the surgical procedure and evaluated for the percentage of wound contraction as per the following equation:

$$\text{Percentage of wound contraction} = \frac{\text{Wound area day 1} - \text{Wound area day } n}{\text{Wound area day 1}} \times 100$$

Statistical Analysis

All the experiments were repeated thrice. Data was represented as mean value ± standard deviation. The data was analyzed using Student's *t*-test. Values $p \leq 0.001$ were considered statistically significant.

RESULTS

Identification of Bioactive Compounds (GC-MS Analysis)

AI leaves as source of bioactive compounds to synthesize AgNPs made it a simple sustainable method as they were easily available in sufficient quantities throughout the year. The compounds identified by GC-MS analysis have been tabulated in **Table 1**.

Synthesis and Characterization of AI-AgNPs

The efficacy of biosynthesized AgNPs is dependent on the parameters of its preparation like – pH, temperature, concentration of extract, concentration of silver nitrate – which can be manipulated to our advantage to produce AgNPs of well-defined shape, structure, and size distribution to cater to wound healing applications. The change in color of solution from transparent to brown within 5 min of addition of aqueous AI-extract to $AgNO_3$ established synthesis of AI-AgNPs (**Figure 1A**). This was further validated by the presence of a maximum absorbance peak at 400 nm in the UV-Vis spectroscopy. Optimized reaction parameters for synthesis of stable AI-AgNPs were addition of 5 mL of AI-extract to 45 mL of $AgNO_3$ (1 mM) at pH 7 and incubation at 25°C in dark at 200 rpm for 18 h. AI-AgNPs were stable in all the five solutions tested (**Figure 1B**) and during the 28-days test period in distil water at RT (**Figure 1C**). Results from SEM (**Figure 1D**) and

TABLE 1 | Phytochemical composition of leaves of *Azadirachta indica* identified by GC-MS analysis.

No.	Name of the Compound	Chemical formula	Relative abundance (%) in extractions by		Activity
			Ethyl acetate	Hexane	
1	Ethyl propionate	$C_5H_{10}O_2$	39.69	-	Antimicrobial
2	2-Hexenal	$C_6H_{10}O$	-	4.70	Antioxidant
3	Ethyl butyrate	$C_6H_{12}O_2$	2.51	-	Antioxidant
4	Trimethylbenzene	C_9H_{12}	0.75	-	Antimicrobial
5	Methyleugenol	$C_{11}H_{14}O_2$	0.30	-	Anti-inflammatory
6	Dihydroactinidiolide	$C_{11}H_{16}O_2$	0.38	-	Antibacterial, antioxidant
7	2-Butyl-1-octanol	$C_{12}H_{26}O$	-	0.40	Antimicrobial
8	Elixene	$C_{15}H_{24}$	-	1.43	Antibacterial
9	α-Copaene	$C_{15}H_{24}$	-	2.95	Antimicrobial
10	γ-Gurjunene	$C_{15}H_{24}$	-	2.16	Antibacterial
11	Caryophyllene	$C_{15}H_{24}$	-	23.22	Antimicrobial, antioxidant
12	γ-Elemene	$C_{15}H_{24}$	0.44	40.98	Anti-inflammatory
13	Humulene	$C_{15}H_{24}$	-	2.73	Anti-inflammatory, analgesic
14	β-Cubebene	$C_{15}H_{24}$	-	0.94	Antimicrobial
15	Alloaromadendrene	$C_{15}H_{24}$	-	1.46	Antioxidant, antiaging
16	δ-Cadinene	$C_{15}H_{24}$	-	0.80	Antioxidant
17	α-Selinene	$C_{15}H_{24}$	-	1.35	Antioxidant, analgesic
18	Caryophyllene oxide	$C_{15}H_{24}O$	0.40	-	Anti-inflammatory, analgesic
19	Dodecanoic acid, trimethylsilyl ester	$C_{15}H_{32}O_2Si$	2.02	-	Antibacterial
20	Tetradecanoic acid, trimethylsilyl ester	$C_{17}H_{36}O_2Si$	1.44	-	Antibacterial
21	Oleic acid	$C_{18}H_{34}O_2$	1.10	-	Antioxidant
22	Hexadecanoic acid, trimethylsilyl ester	$C_{19}H_{40}O_2Si$	42.75	-	Anti-inflammatory
23	Phytol	$C_{20}H_{40}O$	2.27	4.38	Antioxidant, analgesic
24	Phytol, acetate	$C_{22}H_{42}O_2$	-	2.92	Antioxidant
25	Silane, [(3,7,11,15-tetramethyl-2-hexadecenyl)oxy]trimethyl	$C_{23}H_{48}OSi$	5.90	-	Antimicrobial
26	Heptacosane	$C_{27}H_{56}$	-	1.94	Antibacterial
27	α-Tocopherol	$C_{29}H_{50}O_2$	-	7.64	Antioxidant, wound healing

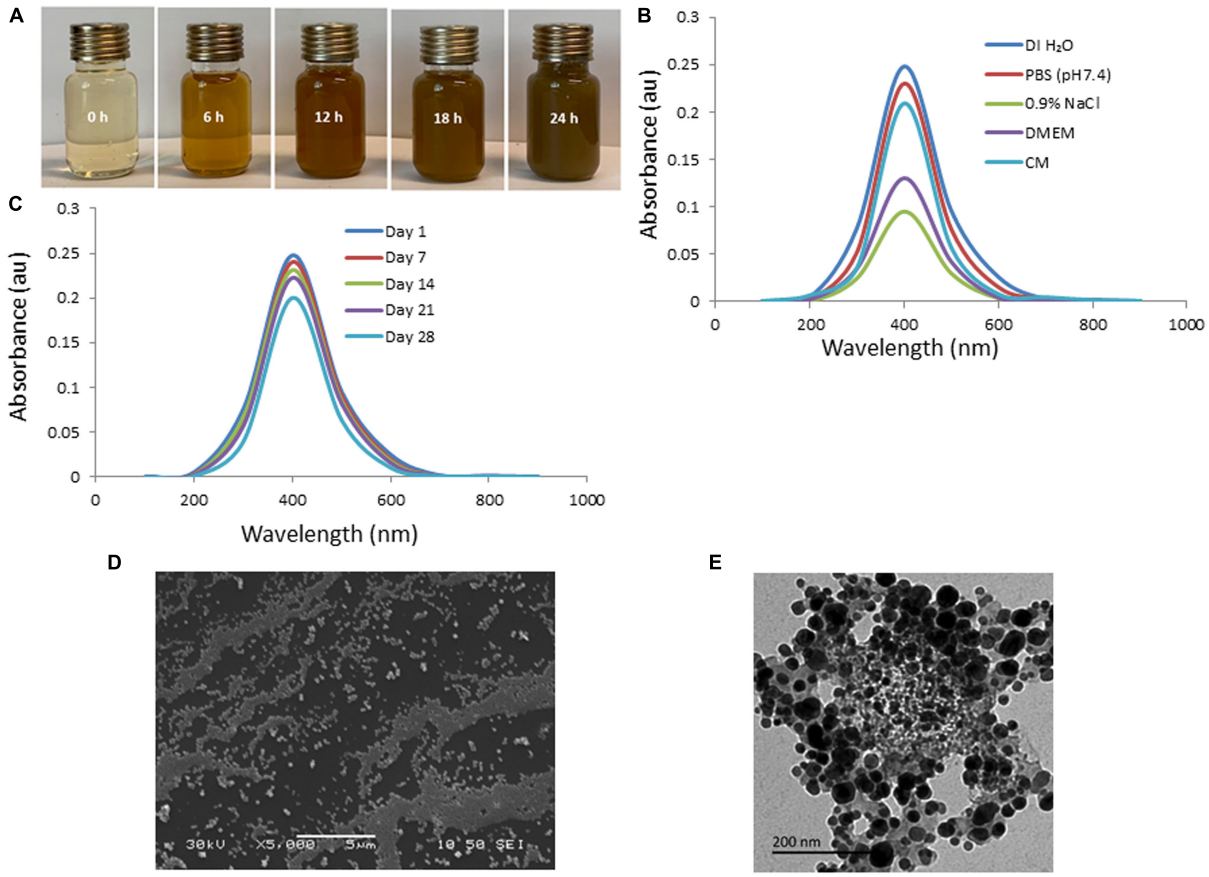

FIGURE 1 | Green synthesis and characterization of AI-AgNPs: **(A)** Change in color during formation, **(B)** Absorption spectra in different test solutions, **(C)** On-shelf stability at various time intervals in UV-Vis spectroscopy analysis, **(D)** SEM image, and **(E)** TEM image.

TEM (**Figure 1E**) images substantiate AI-AgNPs were of the particle diameter 33.20±3.79 nm and spherical in shape. The presence of elemental silver was represented as strong signal at 3 KeV peak in EDX analysis (**Figure 2A**) and the particle diameter size range was represented in **Figure 2B**. Fourier transform infrared (FTIR) inferred the involvement of functional groups present in bioactive constituents in conversion of silver ions into elemental silver by acting as capping and reducing agents. Comparative analysis of FTIR spectra of AI-extract and AI-AgNPs (**Figure 2C**) depict the shift in peaks from 3254 to 3211 cm^{-1} corresponding to NH or OH stretching vibration of amino or phenolic/hydroxyl, from 2,252 to 2,048 cm^{-1} corresponding to –C=C– stretching vibration of alkenes, from 1,612 to 1,550 cm^{-1} corresponding to –C=O– stretching vibration of amides characteristic of –COOH and from 1,408 to 1,445 cm^{-1} corresponding to -N-H- bending vibration of primary amines. The peak obtained around 1,700 to 1,300 cm^{-1} disclosed formation of AI-AgNPs. This result implied that hydroxyl/phenolic, carbonyl, amide and amino groups were involved in the reduction of silver ion to AI-AgNPs formation. The crystalline nature of AI-AgNPs was evident from XRD pattern where four characteristic peaks were observed at 2θ values of 39.24°, 44.12°, 63.52°, and 77.80° corresponding to crystal facets of (1 1 1), (2 0 0), (2 2 0), and (3 1 1) of face-centered cubic silver (**Figure 2D**).

Toxicity Study of AI-AgNPs on *Drosophila*

Rate of Eclosion

To test whether the AI-extract and AI-AgNPs have any adverse effects on physiology and development, we grew *Drosophila* on treatments media containing five different doses of the preparations. The adult flies eclosion rate confirmed that the changes in treatments upto 250 µg/mL were insignificant when compared with the control (**Figure 3A**).

Egg Laying Capacity

No significant change in egg laying capacity of flies was observed in treatments upto 100 µg/mL. $p \leq 0.001$ significant difference was observed in 250 µg/mL of AI-AgNPs treated group as compared with control groups (**Figure 3B**). Therefore, the treatment did not affect reproductive functions.

Rate of Eclosion of F1 Flies

Percentage eclosion of F1 adult flies did not unfurl any significant difference in the treated and control groups on the 10^{th}, 20^{th}, and

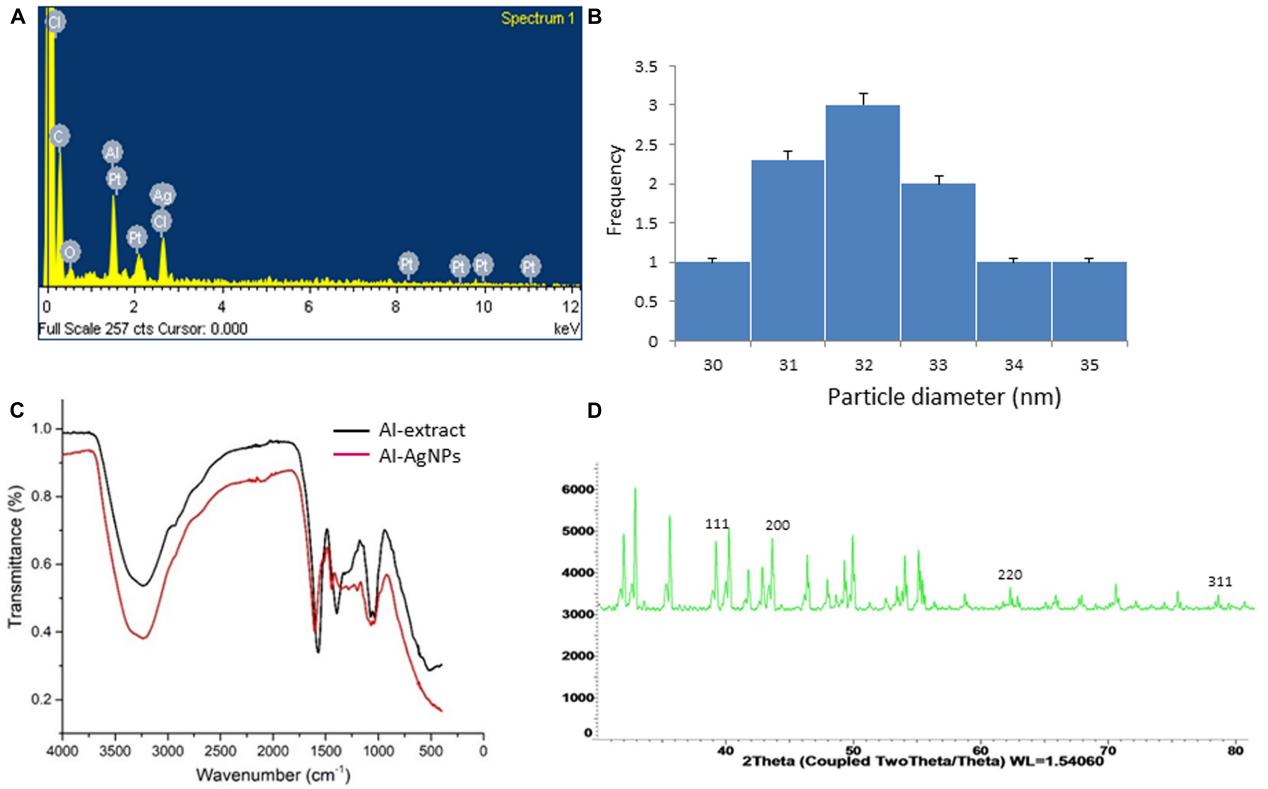

FIGURE 2 | Analysis of surface and content of Al-AgNPs: **(A)** EDX analysis, **(B)** Particle size distribution, **(C)** FTIR spectral analysis, comparison with Al-extract, and **(D)** X-ray powder diffraction analysis.

30th day in medium with up to 100 μg/mL of Al-extract or Al-AgNPs. However, at 250 μg/mL Al-AgNPs treated group shows significant difference ($p \leq 0.001$) in the F1 flies eclosion rate as compared with the control group on 30th day (**Figures 3C,D**). Hence, Al-extract did not affect development and overall viability at all tested doses, while Al-AgNPs showed no adverse effect at doses below 250 μg/mL.

TEM Image

To investigate whether the ingested Al-AgNPs were retained by the digestive system of the flies, we examined fly intestines by TEM. The control group was devoid of any particles (**Figure 4A**). Al-AgNPs were spotted adhering to the microvilli of intestinal lumen and within the cells of intestinal wall in the treated group (**Figure 4B**), indicating that abundant uptake of the particles had occurred.

Free Radical Scavenging Assay

Free radical scavenging effect was observed in a concentration-dependent manner. At 100 μg/mL of Al-extract showed 14.45% radical scavenging in DPPH assay and 13.4% radical scavenging in ABTS assay; these values increased to 33.73% and 36.46% at 500 μg/mL. Interestingly, 100 μg/mL of the Al-AgNPs obtained 40.02% radical scavenging in DPPH and 42.71% radical scavenging in ABTS assay, which increased to 65.17% and 66.20% at 500 μg/mL. The results confirmed two-fold increase in radical scavenging for Al-AgNPs as compared to Al-extract (**Table 2**).

Antibacterial Activity

Disc Diffusion Assay

Preliminary screening for bioactivity of Al-AgNPs on agar plates inoculated with a confluent lawn of bacterial cells proved that growth of all the strains was inhibited though to a varied degree. As tabulated in **Table 3**, diameter of ZOI reports higher inhibition in *B. cereus*, *E. coli*, and *S. aureus* at 17.7, 18.7, and 17.7 mm, respectively as compared to *P. aeruginosa* at 10.3 mm. **Figure 5A** is representative of the effectiveness of Al-AgNPs in *S. aureus*. Additionally, this antibacterial efficiency was retained and enhanced in the Al-AgNPs-PF127 hydrogel as evident from **Figure 5B** for *E. coli* and corroborated by diameter of ZOI measured for *B. cereus*, *E. coli, P. aeruginosa,* and *S. aureus* at 18.7, 20, 13, and 20 mm respectively in **Table 3**.

MIC and MBC of Al-AgNPs

Disc diffusion assay results were further validated by determining the least inhibitory effect of Al-AgNPs as MIC and the concentration of least biocidal agent required to kill 99.9% of bacteria as MIB when cultured on bacterial media. MIC and MBC values ranged from 390 to 780 μg/mL as represented in **Table 3**.

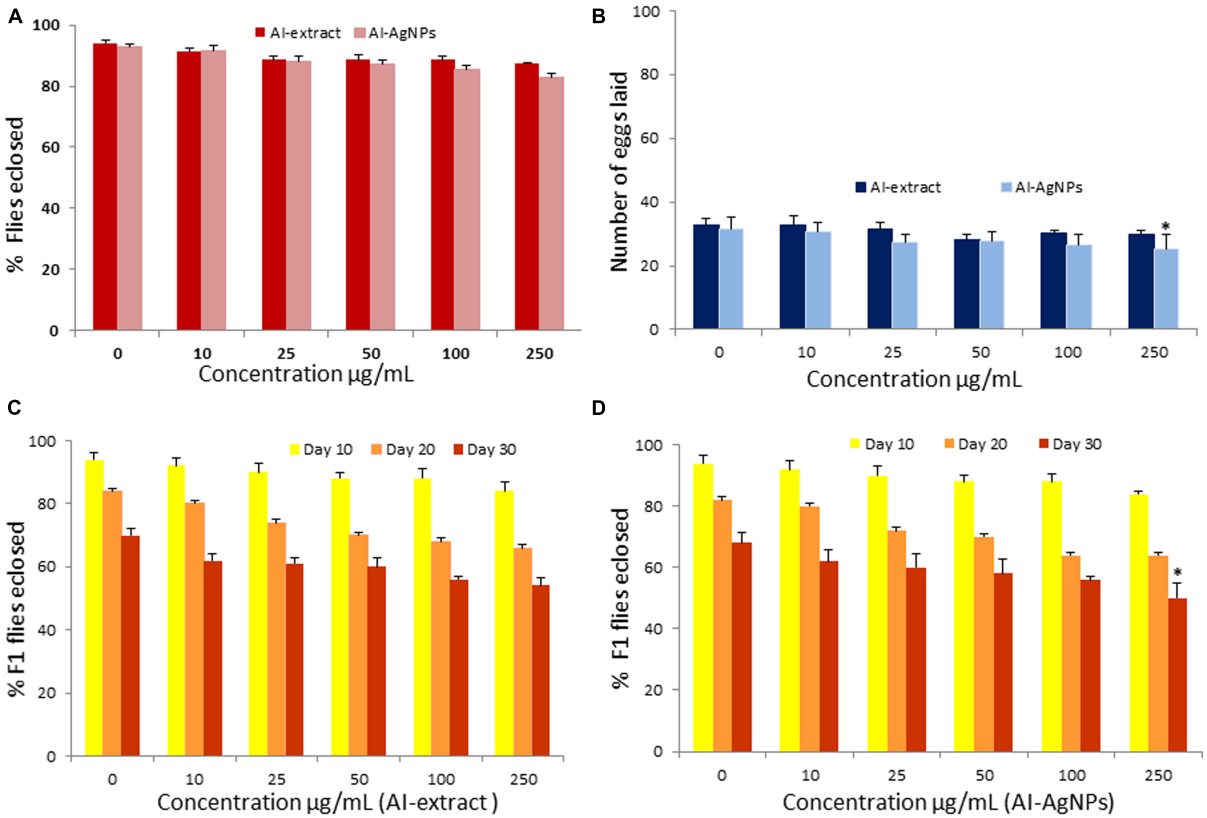

FIGURE 3 | Toxicity effect of Al-AgNPs on *Drosophila*: **(A)** Flies eclosion, **(B)** Egg laying capacity, **(C)** F1 Flies eclosion in Al-extract, and **(D)** F1 Flies eclosion in Al-AgNPs (*$p \leq 0.001$ considered statistically significant).

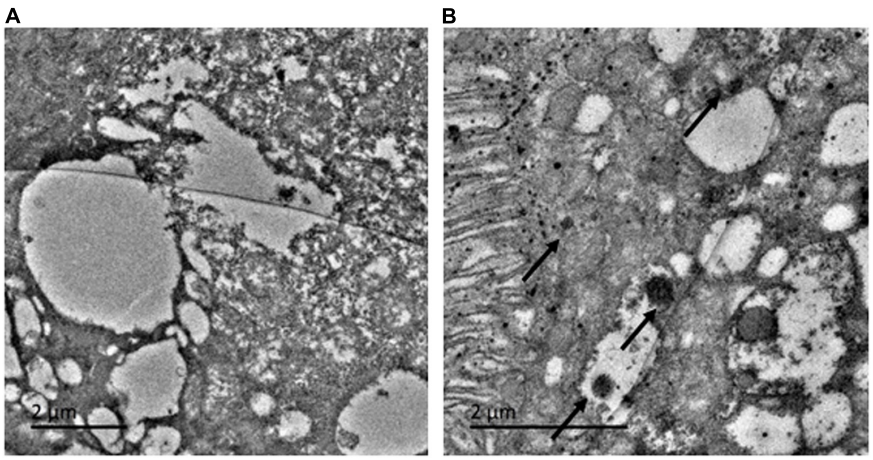

FIGURE 4 | Toxicity effect on *Drosophila* in larval intestinal midgut: **(A)** Control and **(B)** Al-AgNPs treated medium.

Mechanism of Antibacterial Action

Bacterial cells observed under SEM, revealed that in comparison with the intact cells in control (**Figure 6A**) and slightly disrupted cells in Al-extract (**Figure 6B**); a sub-lethal concentration of Al-AgNPs can result in damaged cell membranes, shrunken cytoplasm and leakage of cell content (**Figure 6C**).

Wound Healing Activity

Evaluation of Al-AgNPs-PF127 Hydrogel

Due to the presence of Al-AgNPs, the Al-AgNPs-PF127 hydrogel appeared pale ash brown, while the pristine PF127 hydrogel was transparent. pH of the two hydrogels were 5.7–5.8. They exhibited impressive features in terms of sol-gel transition

TABLE 2 | Antioxidant activity of AI-Extract and AI-AgNPs.

Conc (μg/ml)	% DPPH radical scavenging			% ABTS radical scavenging		
	AI-extract	AI-AgNPs	BHT	AI-extract	AI-AgNPs	BHT
100	14.45 ± 1.99	40.02 ± 1.57	60.03 ± 1.65	13.4 ± 1.36	42.71 ± 1.39	61.38 ± 1.12
200	20.46 ± 0.71	47.58 ± 2.65	62.84 ± 1.22	19.82 ± 0.99	49.94 ± 2.31	64.25 ± 2.01
300	24.30 ± 1.21	51.85 ± 1.82	68.19 ± 1.72	26.73 ± 1.13	54.26 ± 2.69	68.62 ± 2.24
400	31.83 ± 1.87	59.43 ± 0.92	78.79 ± 1.16	32.32 ± 2.73	59.92 ± 2.27	77.98 ± 2.11
500	33.73 ± 1.44	65.17 ± 1.21	86.93 ± 1.08	36.46 ± 2.64	66.20 ± 1.52	88.02 ± 1.37

TABLE 3 | Determination of diameter of Zone of Inhibition (ZOI), Minimum Inhibitory Concentration (MIC) and Minimum Bactericidal Concentration (MBC) of AI-AgNPs and AI-AgNPs-PF127 hydrogel tested against bacterial species.

Name of the bacterial species	ZOI for AI-AgNPs (mm)	ZOI for AI-AgNPs-PF127 hydrogel (mm)	MIC for AI-AgNPs (μg/mL)	MBC for AI-AgNPs (μg/mL)
Bacillus cereus	17.7 ± 1.24	18.7 ± 0.94	390	390
Escherichia coli	18.7 ± 1.15	20.0 ± 1.0	780	780
Pseudomonas aeruginosa	10.3 ± 0.50	13.0 ± 0.46	780	780
Staphylococcus aureus	17.7 ± 0.47	20.0 ± 0.47	390	390

between 22 and 37°C, being liquid at 4°C and hydrogel at 37°C. Viscosity of the hydrogels increased with the increase in temperature. Spreadability of the hydrogels was in the range of 6.0–7.7 cm. Except for slight difference in colour, other characteristics of PF127 were retained in AI-AgNPs-PF127 hydrogel.

Skin Irritation Test

AI-AgNPs-PF127 hydrogel did not produce any undesirable side effects such as skin redness, dryness, or flakiness when applied on skin of mice. The skin of both control and treated animals appeared normal.

Wound Healing Study

The quantitative analysis of wound healing involved measuring the initial wound size (1st day) along with healing towards wound closure (10th day). The healing rate in terms of percentage wound contraction was 23.12, 42.33, 56.11, and 60.42 on 3rd, 5th, 7th, and 10th day for control group. Animals treated with pristine PF127 hydrogel showed 25.46, 50.11, 67.54, and 75.77 wound contraction, test group 0.3 mg AI-AgNPs-PF127 hydrogel displayed 27.22, 52.32, 75.44, and 85.52 and test group 1.0 mg AI-AgNPs-PF127 hydrogel reached 24.25, 56.43, 85.23, and 94.54 wound contraction rate on 3rd, 5th, 7th, and 10th day, respectively (**Figure 7A**). The results showcased near complete wound closure with 1.0 mg AI-AgNPs-PF127 hydrogel on 10th day, thus confirming its healing potential (**Figure 7B**). 1 mg of AI-AgNPs-PF127 hydrogel treated group had significantly faster healing effect as compared to control group.

DISCUSSION

Traditional medicinal plants are being explored as source of new drugs against increasing number of antibiotic resistant bacteria (Anand et al., 2019). All parts of a neem plant are used in traditional and folk remedies for a variety of ailments and hence are commercially exploited today in both pharmacology and cosmetic industry. Our preliminary phytochemical screening of neem leaves confirmed the presence of flavonoids, phenolic compounds and terpenoids. GC-MS analysis of AI-extract further revealed elemene, caryophyllene, tocopherol, 2-hexanal, and phytol in extraction with hexane (a non-polar solvent) and ethyl propionate, hexadecanoic acid, trimethylsilyl ester and Silane,[(3,7,11,15-tetramethyl-2-hexadecenyl)oxy]trimethyl in extraction with ethyl acetate (a polar solvent). These phyto-chemicals are known for analgesic, anti-inflammatory, antimicrobial, antioxidant, and wound healing activities. GC-MS analysis of supercritical carbon dioxide extraction of seed and steam-solvent extraction of crude oil from leaves of neem elucidated different phytochemicals (Sonale et al., 2018; Babatunde et al., 2019).

Silver nanoparticles have garnered prominent position in disease management due to their unique properties owing to small dimension and large surface area, mechanical and thermal stability, chemical inertness, electrical conductivity, biosensor, and antimicrobial activity (Rai et al., 2014). The green synthesis of AI-AgNPs was evident from change in colour of solution which is attributed to surface plasma resonance phenomenon. A clear dominant peak at 400 nm in UV-Vis spectroscopy and microscopic evaluation (SEM, TEM) established the particle size (∼33 nm) and spherical shape of synthesized AI-AgNPs, which was in accordance with the literature (Zhang et al., 2016). Optimized conditions of reactants concentration and ratio, temperature, pH, light, and duration resulted in high yield of AI-AgNPs. Quality and quantity of biosynthesized AgNPs depend on reaction parameters and their properties are often governed by the presence of secondary metabolites (Singh et al., 2016). Detection of functional groups such as phenolic/hydroxyl, amide,

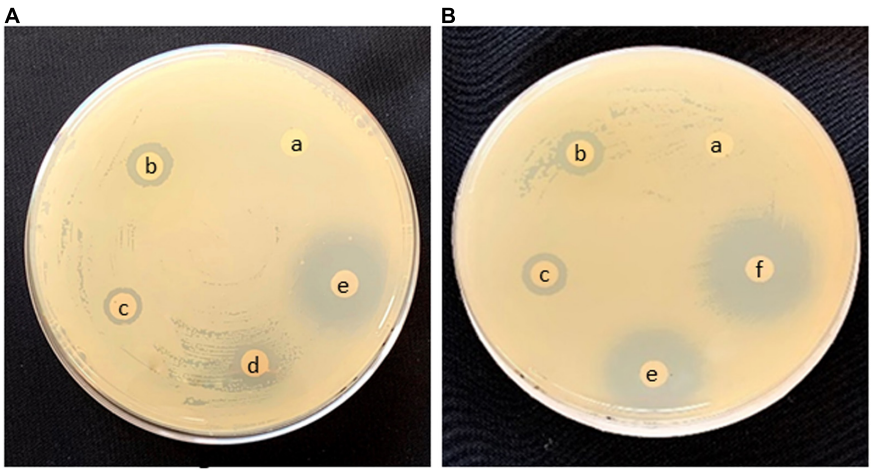

FIGURE 5 | Antimicrobial effect in Disc diffusion assay of **(A)** *S. aureus* and **(B)** *E. coli* **(a)** control, **(b)** rifampicin, **(c)** $AgNO_3$, **(d)** Al-extract, **(e)** Al-AgNPs, and **(f)** Al-AgNPs-PF127 hydrogel.

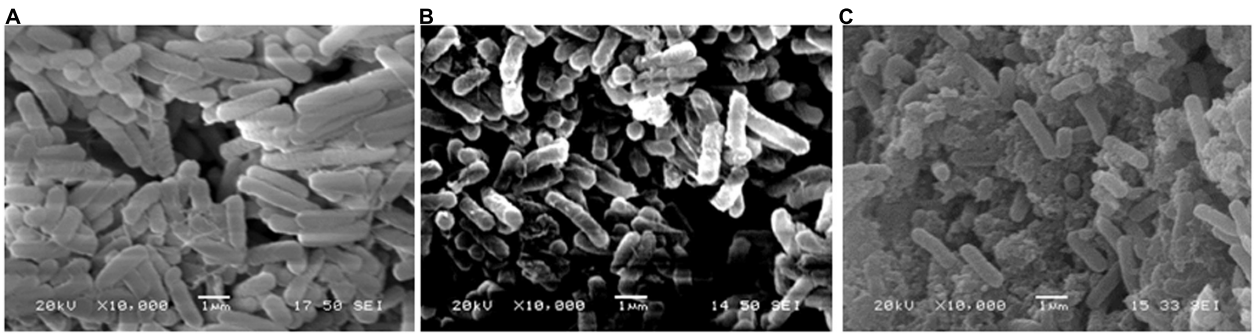

FIGURE 6 | Antibacterial activity in SEM image of *E. coli*: **(A)** control, **(B)** Al-extract, and **(C)** Al-AgNPs.

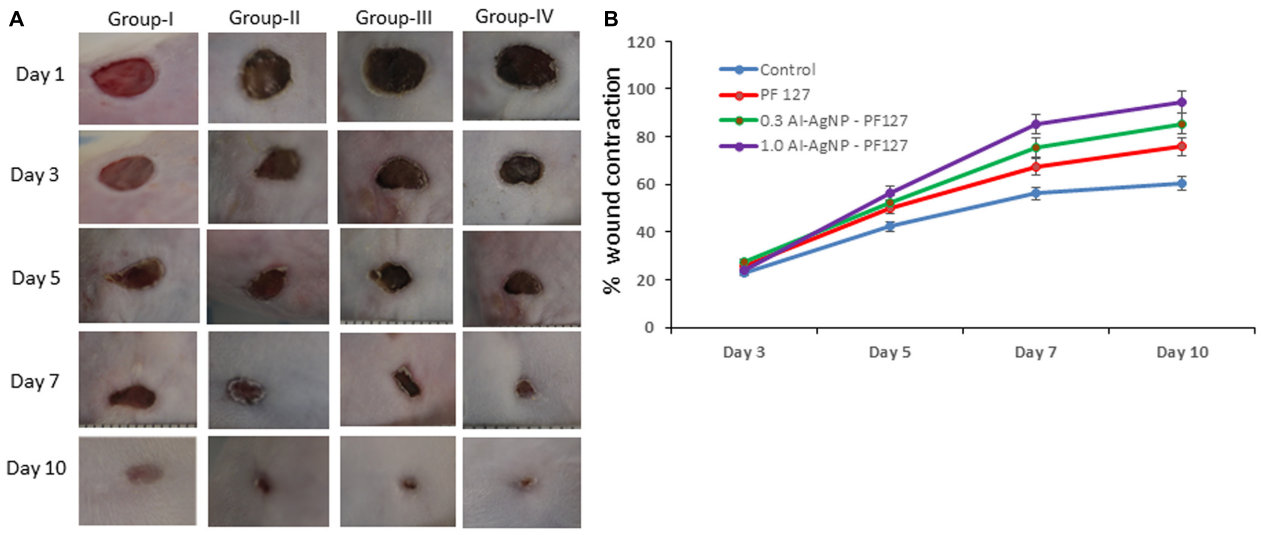

FIGURE 7 | Wound healing process in mice: **(A)** Image represents effect on control (group-I), pristine PF127 hydrogel (group-II), 0.3 mg Al-AgNPs-PF127hydrogel (group-III) and 1.0 mg Al-AgNPs-PF127 hydrogel (group-IV) and **(B)** percentage wound contraction with time.

and amine in FTIR spectra indicated that alkaloids/flavonoids/terpenoids present in AI-extract played the role of reducing agents during the formation of AI-AgNPs. Alkaloids, flavonoids, steroids, terpenoids and tannins are present in neem extract (Thakurta et al., 2007; Sarah et al., 2019); this supported our FTIR findings.

The antibacterial property of AgNPs is harnessed in medical devices, wound dressing, and food packaging; thus, it is important to analyze their toxicity and determine the safe dosage to mitigate any detrimental effect on health. *Drosophila* has been increasing utilized as an *in vivo* model organism for studying human diseases, as nearly 75% of human disease-causing genes have a functional homolog in *Drosophila*; in addition, it has a short life cycle, high reproduction rate, and ease of cultivation in a cost-effective manner (Ong et al., 2015; Vecchio, 2015). Effect of ingesting chemically synthesized AgNPs, studied on emergence of adult flies and lifespan of their progeny in a dose dependent manner, observed normal behavior until 50 μg/mL of AgNPs (Raj et al., 2017). In our toxicity study, exposure to doses upto 100 μg/mL did not have any significant effect on survival, development, and growth of parent as well as F1 generation flies. Similar effect of chicken egg-protein based AgNPs (100 μg/mL) on hatchability, viability, development, and pigmentation was reported by Thiyagarajan et al. (2018). This proved the enhanced safety in using biologically synthesized AgNPs over chemically synthesized AgNPs. Our TEM image displayed AI-AgNPs attached to the intestinal microvilli, lumen, and cytoplasm of midgut epithelial cells of larvae. Though the presence of AI-AgNPs did not result in any obvious phenotypic deviation in features from those of control flies, in future, we plan to further extend our toxicity study on reactive oxygen species (ROS) at gene expression level.

Neem extract is rich in phytochemicals which are inherent hydrogen donors, oxygen quenchers and redox agents that can deactivate free radicals or activate antioxidant enzymes to disrupt this oxidation reaction chain (Septiyani and Wibowo, 2019). The nature of DPPH and ABTS to easily accept a hydrogen molecule or electron from an antioxidant moiety under stable conditions was exploited to determine the radical scavenging activity of AI-extract. When AI-AgNPs were biosynthesized with polyphenol rich AI-extract, their ability to reduce free radical scavenging enhanced up to two-fold in a dose dependent manner.

The synergistic interactions between the Ag^+ ions and phytochemicals present in the plant extract resulted in formation and stability of bioactive AI-AgNPs molecules that displayed better antibacterial efficacy than AI-extract. AI-AgNPs are easily penetrable into the bacterial cell wall due to their small size and larger exposed surface area for interaction with cell wall components. Morones et al. (2005) suggested that the amount of AgNPs present on and within the bacteria could be explained by the alterations produced by the AgNPs on the membrane morphology of the bacteria. Bacterial cell machinery comprises of sulphur and phosphorus moieties that are basic in nature. The affinity of acidic silver to these molecules present in cellular matrix within bacterial proteins and DNA, binds with oxygen molecules to form sulphydryl groups (S-H) which accelerates the disintegration of respiratory and replication framework of the pathogen resulting in cell death. Proteomic analysis of silver regulated membrane proteins in *P. aeruginosa* exposed to silver nitrate and AgNPs proved that the silver binding proteins for both AgNPs and Ag^+ ions had a similar pattern, however, the bio-uptake of Ag^+ ions and the accumulation of ROS was found to be greater in cells exposed to AgNPs (Yan et al., 2018). Though the mechanism of action of both Ag^+ ions and AgNPs are similar in nature the effectiveness on target site corresponds to the lower concentration of AgNPs required leading to less agglomeration. MIC and MBC values are estimated to determine the inhibitory capability of AgNPs against a test organism. Micro dilution assay of AgNPs provides a better understanding of its bioactivity due to the dispersed AgNPs in a culture broth in comparison with the diffused AgNPs in a disc diffusion agar plate. It also functions as resistance surveillance especially in antibiotic resistant bacteria (Wiegand et al., 2008). In our study, MIC and MBC values of AI-AgNPs depicted a concentration dependent growth inhibitory effect on all the four strains of bacteria. SEM images of bacterial cells depicted morphologically deteriorating cell structures with dismembered bacterial bodies and increased oozing cytoplasmic contents from control to AI-extract to AI-AgNPs treatment. GC-MS results comprehended a polyphenol rich plant extract formulate an intact, stable polyphenol-nanoparticle conjugate that can adsorb oxygen molecules to release silver ion to adhere on bacterial membrane. The underlying mechanism of dispersion of silver ions by AgNP was illustrated to that of a Trojan-horse-type model that continuously releases Ag^+ ions from the conjugate matrix into the pathogen (Hsiao et al., 2015). Comparative analysis of bio-uptake of Ag^+ ions in AgNP treated *E. coli* cells found a higher density of internalized Ag^+ ions and ROS than extracellular. The internalized Ag^+ ions hamper the respiratory chain and induces oxidative stress in the bacteria by disruption of membrane-specific enzymes, peroxidation of lipids and development of structural lesions in DNA molecules (Long et al., 2017). Various antibacterial mechanism of action of AgNPs can be summarized as cell membrane adhesion and damage, generation of ROS and cell stress, loss of stability of cellular proteins and RNA, leakage of DNA from nucleus, and alternation of cell signaling pathway (Baranwal et al., 2018).

Untreated wound is susceptible to infections caused by bacteria such as *S. aureus*. Broad-spectrum antimicrobial activity of AgNPs has stimulated the development of AgNPs-based dressing for wound healing. Tian et al. (2007) reported that AgNPs were able to treat inflammation through cytokine modulation and induce wound healing with decreased scar formation. Frankova et al. (2016) also substantiated that AgNPs treated group displays decreased release of growth factors and inflammatory cytokines (which are secreted from immune cells), in human dermal keratinocytes. Our studies proved the potential for AI-AgNPs in bacterial cell disruption which together with its free-radical scavenging ability can be utilized for development of wound dressings. ROS is actively involved in wound healing, when present in low concentrations it fights the invading microbe, however, an imbalance in the oxidative-antioxidant respiratory system can result in excessive production of ROS (Sanchez et al., 2018) and an over accumulation in cells can

be antagonistic in would healing. Thus, we tested AI-AgNPs in a dose-dependent manner. Conventional dry dressings material such as gauze, plasters, bandages are making way for plant- based wound dressings incorporated films, foams, and gels (Krishnan and Thomas, 2019). Pluronics (Poloxamers) is an exciting thermosensitive polymer that has a critical solution temperature (CST) below the human physiological temperature thus, it exists as a gel state on the body at 37°C. Being a biocompatible and biodegradable polymer material, with excellent mechanical and thermo-sensitive properties, PF127 hydrogel finds applications as drug carriers in cancer and skin diseases (Akash and Rehman, 2015; Chatterjee et al., 2019). Measurement of viscosity is an important parameter in gel preparations meant for topical medication of wound to complete the filling (Mekkawy et al., 2013). AI-AgNPs-PF127 hydrogel exhibited similar viscosity as PF127 hydrogel. This indicated inclusion of AgNPs with PF127 polymer linkage of the formulated hydrogels did not alter flow behavior. Uniform distribution of the gel on the skin is dependent on the spreadability. Spreadability of ideal formulation was found to be 5.7–8.6 cm (El-Kased et al., 2017) which was met by AI-AgNPs-PF127 hydrogel. The pH of the AI-AgNPs-PF127 hydrogel was between 5.5-5.8. Commonly used hydrogels for wound healing applications have pH in range 4.3–6.8 (El-Kased et al., 2017). Further, AI-AgNPs-PF127 hydrogel did not cause any skin irritation in mice, which progresses it to the testing on wounds. Healing of the wound is a complex process that involves synchronous arrangement among various chemical constituents to allow reconstruction of the impaired tissues and to repair the normal skin functions (Diegelmann and Evans, 2004). ZOI results confirmed greater magnitude of bacterial inhibition by AI-AgNPs-PF127 hydrogel than AI-AgNPs. Similar result of a higher antibacterial activity of amino acid loaded PF127 than control was explained based on accumulation of intracellular ROS in bacterial cells (Santos et al., 2020). AI-AgNPs-PF127 hydrogel is able to restrict the infectivity of both Gram positive and Gram negative bacterial types and provide a sterile environment possible to aid active wound healing. The antagonistic effect of AI-AgNPs-PF127 hydrogel on bacterial growth and survival, couple with timely release of AI-AgNPs upon application make it feasible as a wound dressing. Liu et al. (2010) validated that the topical application of AgNPs stimulated wound-healing process included remodeling, re-epithelialization, and wound contraction processes. According to Diniz et al. (2020), a wound takes more than 14 days to heal completely with application of chemically synthesized AgNPs, loaded on gelatin hydrogel. Interestingly our result showed that AI-AgNPs-PF127 hydrogel led to better healing effect in just 10 days. This was due to continuous release of AI-AgNPs from hydrogel, which timely entered the physiological system and interacted with inflammatory cells present in the wound sites. This slow release ensured no damage to the normal cells while prolonging the wound healing effect.

In summary, our studies have shown green synthesized AI-AgNPs as effective antibacterial and antioxidant agents with enhanced and sustained effects when compared to the leaf-extracts alone. These AI-AgNPs did not have any significant toxic effect on development and reproduction of *Drosophila* when used as a feed additive. The development and application of AI-AgNPs-PF127 hydrogel improved wound contraction rate in mice. AI-AgNPs-PF127 hydrogel did not show any signs of skin irritation in mice. Biosynthesized neem silver nanoparticles loaded PF127 hydrogel as a promising alternative candidate for smart, ecofriendly delivery system in cases of bacterial infections and wound healing.

DATA AVAILABILITY STATEMENT

The raw data supporting the conclusions of this article will be made available by the authors, upon reasonable request.

ETHICS STATEMENT

The animal study was reviewed and approved by Institutional Animal Care and Use Committee (IACUC), Nanyang Technological University, Singapore (ARF-SBS/NIE-A0367NTU).

AUTHOR CONTRIBUTIONS

SB conceived and developed the idea of work and provided guidance. GC, SC, and TK designed the experiments. GC and SC performed the experiments and prepared the manuscript. SB and TK edited the manuscript. All authors reviewed and approved the final manuscript.

ACKNOWLEDGMENTS

We thank Prof David Becker, NTU, Singapore for providing guidance and support. We acknowledge the support from Temasek Life Sciences Laboratory, Singapore.

REFERENCES

Ahmad, F., Ashraf, N., Ashraf, T., Zhou, R. B., and Yin, D. C. (2019). Biological synthesis of metallic nanoparticles (MNPs) by plants and microbes: their cellular uptake, biocompatibility, and biomedical applications. *Appl. Microbiol. Biotechnol.* 103, 2913–2935. doi: 10.1007/s00253-019-09675-5

Akash, M. S. H., and Rehman, K. (2015). Recent progress in biomedical applications of Pluronic (PF127): pharmaceutical perspectives. *J. Control Release* 209, 120–138. doi: 10.1016/j.jconrel.2015.04.032

Anand, U., Jacobo-Herrera, N., Altemimi, A., and Lakhssassi, N. (2019). A comprehensive review on medicinal plants as antimicrobial therapeutics: potential avenues of biocompatible drug discovery. *Metabolites*. 9:258. doi: 10.3390/metabo9110258

Arafa, M. G., El-Kased, R. F., and Elmazar, M. M. (2018). Thermoresponsive gels containing gold nanoparticles as smart antibacterial and wound healing agents. *Sci. Rep.* 8:13674. doi: 10.1038/s41598-018-31895-4

Babatunde, D. E., Otusemade, G. O., Efeovbokhan, V. E., Ojewumi, M. E., Bolade, O. P., and Owoeye, T. F. (2019). Chemical composition of steam and solvent

crude oil extracts from Azadirachta indica leaves. *Chem. Data Collection.* 20:100208. doi: 10.1016/j.cdc.2019.100208

Baranwal, A., Srivastava, A., Kumar, P., Bajpai, V. K., Maurya, P. K., and Chandra, P. (2018). Prospects of nanostructure materials and their composites as antimicrobial agents. *Front. Microbiol.* 9:422. doi: 10.3389/fmicb.2018.00422

Bauer, A., Kirby, W., Sherris, J. C., and Turck, M. (1966). Antibiotic susceptibility testing by a standardized single disk method. *Am. J. Clin. Pathol.* 45, 493–496. doi: 10.1093/ajcp/45.4_ts.493

Chatterjee, S., Hui, P. C., Kan, C., and Wang, W. (2019). Dual-responsive (pH/temperature) Pluronic F-127 hydrogel drug delivery system for textile-based transdermal therapy. *Sci. Rep.* 9:11658. doi: 10.1038/s41598-019-48254-6

Chinnasamy, G., Chandrasekharan, S., and Bhatnagar, S. (2019). Biosynthesis of silver nanoparticles from Melia azedarach: Enhancement of antibacterial, wound healing, antidiabetic and antioxidant activities. *Int. J. Nanomed.* 14, 9823–9836. doi: 10.2147/IJN.S231340

CLSI (2012). *Performance Standards for Antimicrobial Susceptibility Testing; Twenty-Second Informational Supplement*. Wayne, PA: The Clinical and Laboratory Standards Institute.

Diegelmann, R. F., and Evans, M. C. (2004). Wound healing: An overview of acute, fibrotic and delayed healing. *Front. Biosci.* 9:283–289. doi: 10.2741/1184

Diniz, F. R., Maia, R., Rannier, L., Andrade, L. N., Chaud, V., da Silva, M., et al. (2020). Silver nanoparticles-composing alginate/gelatine hydrogel improves wound healing In Vivo. *Nanomaterials* 10:390. doi: 10.3390/nano10020390

El-Houssieny, B. M., and Hamouda, H. M. (2010). Formulation and evaluation of clotrimazole from pluronic F127 gels. *Drug Discov. Ther.* 4, 33–43.

El-Kased, R. F., Amer, R. I., Attia, D., and Elmazar, M. M. (2017). Honey-based hydrogel: in vitro and comparative in vivo evaluation for burn wound healing. *Sci. Rep.* 7:9692. doi: 10.1038/s41598-017-08771-8

Frankova, J., Pivodova, V., Vágnerova, H., Juranova, J., and Ulrichova, J. (2016). Effects of silver nanoparticles on primary cell cultures of fibroblasts and keratinocytes in a wound-healing model. *J. Appl. Biomater Funct. Mater.* 14, e137–e142. doi: 10.5301/jabfm.5000268

Hsiao, I. L., Hsieh, Y. K., Wang, C. F., Chen, I. C., and Huang, Y. J. (2015). Trojan-horse mechanism in the cellular uptake of silver nanoparticles verified by direct intra- and extracellular silver speciation analysis. *Environ. Sci. Technol.* 49, 3813–3821. doi: 10.1021/es504705p

Huang, H., Qi, X., Chen, Y., and Wu, Z. (2019). Thermo-sensitive hydrogels for delivering biotherapeutic molecules: A review. *Saudi Pharma. J.* 27, 990–999. doi: 10.1016/j.jsps.2019.08.001

Jain, S., and Mehata, M. S. (2017). Medicinal plant leaf extract and pure flavonoid mediated green synthesis of silver nanoparticles and their enhanced antibacterial property. *Sci. Rep.* 7:15867. doi: 10.1038/s41598-017-15724-8

Klancnik, A., Piskernik, S., Jersek, B., and Mozina, S. S. (2010). Evaluation of diffusion and dilution methods to determine the antibacterial activity of plant extracts. *J. Microbiol. Methods.* 81, 121–126. doi: 10.1016/j.mimet.2010.02.004

Krishnan, K. A., and Thomas, S. (2019). Recent advances on herb-derived constituents-incorporated wound-dressing materials: a review. *Polym. Adv. Technol.* 30, 823–838. doi: 10.1002/pat.4540

Kumar, V., and Yadav, S. K. (2009). Plant-mediated synthesis of silver and gold nanoparticles and their applications. *J. Chem. Technol. Biotechnol.* 84, 151–157. doi: 10.1002/jctb.2023

Kumar, V. S., and Navaratnam, V. (2013). Neem (Azadirachta indica): prehistory to contemporary medicinal uses to humankind. *Asian Pac. J. Trop. Biomed.* 3, 505–514. doi: 10.1016/S2221-1691(13)60105-7

Lee, N. Y., Ko, W. C., and Hsueh, P. R. (2019). Nanoparticles in the treatment of infections caused by multidrug-resistant organisms. *Front. Pharmacol.* 10:1153. doi: 10.3389/fphar.2019.01153

Liu, X., Lee, P. Y., Ho, C. M., Lui, V. C., Chen, Y., Che, C. M., et al. (2010). Silver nanoparticles mediate differential responses in keratinocytes and fibroblasts during skin wound healing. *Chem. Med. Chem.* 5, 468–475. doi: 10.1002/cmdc.200900502

Long, Y. M., Hu, L. G., Yan, X. T., Zhao, X. C., Zhou, Q. F., Cai, Y., et al. (2017). Surface ligand controls silver ion release of nanosilver and its antibacterial activity against *Escherichia coli*. *Int. J. Nanomed.* 12, 3193–3206. doi: 10.2147/IJN.S132327

Loo, Y. Y., Rukayadi, Y., Nor-Khaizura, M. A., Kuan, C. H., Chieng, B. W., Nishibuchi, M., et al. (2018). In vitro antimicrobial activity of green synthesized silver nanoparticles against selected gram-negative foodborne pathogens. *Front. Microbiol.* 9:1555. doi: 10.3389/fmicb.2018.01555

Mekkawy, A., Fathy, M., and El-Shanawany, S. (2013). Formulation and in vitro evaluation of fluconazole topical gels. *Br. J. Pharm. Res.* 3, 293–313.

Mohamad, N., Mohd Amin, M. C., Pandey, M., Ahmad, N., and Rajab, N. F. (2014). Bacterial cellulose/acrylic acid hydrogel synthesized via electron beam irradiation: accelerated burn wound healing in an animal model. *Carbohydr. Polym.* 114, 312–320. doi: 10.1016/j.carbpol.2014.08.025

Morones, J. R., Elechiguerra, J. L., Camacho, A., Holt, K., Kouri, J. B., Ramírez, J. T., et al. (2005). The bactericidal effect of silver nanoparticles. *Nanotechnology.* 16, 2346–2353. doi: 10.1088/0957-4484/16/10/059

Noruzi, M. (2015). Biosynthesis of gold nanoparticles using plant extracts. *Bioprocess Biosyst. Eng.* 38, 1–14. doi: 10.1007/s00449-014-1251-0

Ong, C., Yung, L. Y., Cai, Y., Bay, B. H., and Baeg, G. H. (2015). Drosophila melanogaster as a model organism to study nanotoxicity. *Nanotoxicology.* 9, 396–403. doi: 10.3109/17435390.2014.940405

Rai, M., Kon, K., Ingle, A., Duran, N., Galdiero, S., and Galdiero, M. (2014). Broad-spectrum bioactivities of silver nanoparticles: the emerging trends and future prospects. *Appl. Microbiol.Biotechnol.* 98, 1951–1961. doi: 10.1007/s00253-013-5473-x

Raj, A., Shah, P., and Agrawal, N. (2017). Dose-dependent effect of silver nanoparticles (AgNPs) on fertility and survival of drosophila: an in-vivo study. *PLoS One* 12:e0178051. doi: 10.1371/journal.pone.0178051

Sanchez, M. C., Lancel, S., Boulanger, E., and Neviere, R. (2018). Targeting oxidative stress and mitochondrial dysfunction in the treatment of impaired wound healing: a systematic review. *Antioxidants* 7:98. doi: 10.3390/antiox7080098

Santos, D. C., Goes, J. M. R., de Souza, C. V., Bispo, D. F., Otubo, L., Andrade, G. R. S., et al. (2020). Green synthesis of silver nanostructures with amino acid modified Pluronic F127 for antibacterial applications. *Appl. Surf. Sci.* 505:144449. doi: 10.1016/j.apsusc.2019.144449

Sarah, R., Tabassum, B., Idrees, N., and Hussain, M. K. (2019). "Bio-active compounds isolated from neem tree and their applications," in *Natural bio-active compounds*. Singapore: Springer Nature, 509–528. doi: 10.1007/978-981-13-7154-7_17

Septiyani, R., and Wibowo, C. (2019). Identification of active compounds and testing the antioxidant properties of neem leaf extract. *AIP Confer. Proc.* 2094, 0200341–0200347. doi: 10.1063/1.5097503

Singh, P., Kim, Y. J., Zhang, D., and Yang, D. C. (2016). Biological synthesis of nanoparticles from plants and microorganisms. *Trends Biotechnol.* 34, 588–599. doi: 10.1016/j.tibtech.2016.02.006

Sonale, R. S., Ramalakshmi, K., and Udaya Sankar, K. (2018). Characterization of neem (Azadirachta indica A. Juss) seed volatile compounds obtained by supercritical carbon dioxide process. *J. Food Sci. Technol.* 55, 1444–1454. doi: 10.1007/s13197-018-3060-y

Thakkar, K. N., Mhatre, S. S., and Parikh, R. Y. (2010). Biological synthesis of metallic nanoparticles. *Nanomedicine.* 6, 257–262. doi: 10.1016/j.nano.2009.07.002

Thakurta, P., Bhowmik, P., Mukherjee, S., Hajra, T. K., Patra, A., and Bag, P. K. (2007). Antibacterial, antisecretory and antihemorrhagic activity of Azadirachta indica used to treat cholera and diarrhea in India. *J. Ethnopharmacol.* 111, 607–612. doi: 10.1016/j.jep.2007.01.022

Thiyagarajan, K., Bharti, V. K., Tyagi, S., Tyagi, P. K., Ahuja, A., Kumar, K., et al. (2018). Synthesis of non-toxic, biocompatible, and colloidal stable silver nanoparticle using egg-white protein as capping and reducing agents for sustainable antibacterial application. *RSC Adv.* 8, 23213–23229. doi: 10.1039/c8ra03649g

Tian, J., Wong, K., Ho, C. M., Lok, C. N., Yu, W. Y., Che, C. M., et al. (2007). Topical delivery of silver nanoparticles promotes wound healing. *Chem. Med. Chem.* 2, 129–136. doi: 10.1002/cmdc.200600171

Vecchio, G. (2015). A fruit fly in the nanoworld: Once again Drosophila contributes to environment and human health. *Nanotoxicology.* 9, 135–137. doi: 10.3109/17435390.2014.911985

WHO (2020). *Antimicrobial resistance*. Geneva: World Health Organization.

Wiegand, I., Hilpert, K., and Hancock, R. (2008). Agar and broth dilution methods to determine the minimal inhibitory concentration (MIC) of

antimicrobial substances. *Nat. Protoc.* 3, 163–175. doi: 10.1038/nprot.2007.521

Yan, X., He, B., Liu, L., Qu, G., Shi, J., Hu, L., et al. (2018). Antibacterial mechanism of silver nanoparticles in *Pseudomonas aeruginosa*: proteomics approach. *Metallomics*. 10, 557–564. doi: 10.1039/c7mt00328e

Zazo, H., Colino, C. I., and Lanao, J. M. (2016). Current applications of nanoparticles in infectious diseases. *Control Release* 224, 86–102. doi: 10.1016/j.jconrel.2016.01.008

Zhang, X. F., Liu, Z. G., Shen, W., and Gurunathan, S. (2016). Silver nanoparticles: Synthesis, characterization, properties, applications, and therapeutic approaches. *Int. J. Mol. Sci*. 17:1534. doi: 10.3390/ijms17091534

Conflict of Interest: The authors declare that the research was conducted in the absence of any commercial or financial relationships that could be construed as a potential conflict of interest.

frontiers in Microbiology

REVIEW
published: 22 February 2021
doi: 10.3389/fmicb.2021.616979

Review: Lessons Learned From Clinical Trials Using Antimicrobial Peptides (AMPs)

*Gabrielle S. Dijksteel[1,2], Magda M. W. Ulrich[1,2,3], Esther Middelkoop[1,2] and Bouke K. H. L. Boekema[1]**

[1] Association of Dutch Burn Centres, Beverwijk, Netherlands, [2] Department of Plastic, Reconstructive and Hand Surgery, Amsterdam Movement Sciences, Amsterdam UMC, Vrije Universiteit Amsterdam, Amsterdam, Netherlands, [3] Department of Pathology, Amsterdam UMC, Vrije Universiteit Amsterdam, Amsterdam, Netherlands

Antimicrobial peptides (AMPs) or host defense peptides protect the host against various pathogens such as yeast, fungi, viruses and bacteria. AMPs also display immunomodulatory properties ranging from the modulation of inflammatory responses to the promotion of wound healing. More interestingly, AMPs cause cell disruption through non-specific interactions with the membrane surface of pathogens. This is most likely responsible for the low or limited emergence of bacterial resistance against many AMPs. Despite the increasing number of antibiotic-resistant bacteria and the potency of novel AMPs to combat such pathogens, only a few AMPs are in clinical use. Therefore, the current review describes (i) the potential of AMPs as alternatives to antibiotics, (ii) the challenges toward clinical implementation of AMPs and (iii) strategies to improve the success rate of AMPs in clinical trials, emphasizing the lessons we could learn from these trials.

Keywords: antimicrobial peptide, clinical trial, resistance, infection, cytotoxicity, mechanism of action, improvement strategies, peptide modifications

OPEN ACCESS

Edited by:
Mariano Martinez-Vazquez, National Autonomous University of Mexico, Mexico

Reviewed by:
Sónia Gonçalves, University of Lisbon, Portugal
Peter Bergman, Karolinska Institutet (KI), Sweden

***Correspondence:**
Bouke K. H. L. Boekema
bboekema@burns.nl

Specialty section:
This article was submitted to Antimicrobials, Resistance and Chemotherapy, a section of the journal Frontiers in Microbiology

Received: *13 October 2020*
Accepted: *29 January 2021*
Published: *22 February 2021*

Citation:
Dijksteel GS, Ulrich MMW, Middelkoop E and Boekema BKHL (2021) Review: Lessons Learned From Clinical Trials Using Antimicrobial Peptides (AMPs). Front. Microbiol. 12:616979. doi: 10.3389/fmicb.2021.616979

INTRODUCTION

Antibiotic resistance is a global concern in health care as (new) resistance mechanisms are emerging and spreading globally. Resistant bacterial strains have been identified for various antibiotics in clinical use. For example, shortly after the emergence of penicillin-resistant *Staphylococcus aureus* in 1940 (Abraham and Chain, 1940), several pathogenic bacteria became resistant not only to penicillin but also to semi-synthetic penicillin, cephalosporins and newer carbapenems (Kumarasamy et al., 2010). In addition, the decline in the approval of new antibiotics by regulatory bodies has further exacerbated this problem.

As alternatives to antibiotics, AMPs have been at the forefront of international efforts because they are less likely to induce bacterial resistance (Wimley and Hristova, 2011). AMPs are a diverse group of naturally occurring peptides of the innate defense system with activity against various pathogens such as yeast, fungi, viruses and bacteria (Zasloff, 2002; Beisswenger and Bals, 2005).

Abbreviations: AMPs, antimicrobial peptides; BPI, bactericidal permeability-increasing protein; β-hCG, human β-chorionic gonadotropin; FDA, Food and Drug Administration; GRAS, generally recognized as safe; hBD, human β-defensin; hLT-1-1, human lactoferrin; HNP, human neutrophil; HPMC, hydroxypropyl methylcellulose; IL, interleukin; LPS, lipopolysaccharide; LptD, lipopolysaccharide transport protein D; MDR, multi-drug resistant; STAMPS, specifically targeted antimicrobial peptides; TFA, trifluoroacetic acid; TLR, toll-like receptors.

To inactivate these pathogens, AMPs display a multi-hit, non-specific and rapid action, resulting in the slow or limited emergence of resistance (Wimley and Hristova, 2011). Additionally, some AMPs show synergistic interactions with conventional antibiotics (Steenbergen et al., 2009; Wu et al., 2020), which could decrease the selection of antibiotic resistant bacteria.

Around the same time as the discovery of the first antibiotic penicillin in 1928, the first AMP nisin was discovered in milk (Zhang and Zhong, 2015). This AMP was approved by the FDA of the United States as a food preservative in 1988 due to its heat stability and tolerance of low pH (Delves-Broughton et al., 1996; Cleveland et al., 2001). After the discovery of nisin, several other AMPs such as gramicidin, tyrocidine, alamethicin, purothionin, and defensins were isolated from bacteria, fungi, plants, invertebrates and vertebrates (Van Epps, 2006; Bahar and Ren, 2013). However, the clinical application of AMPs as antimicrobials was limited due to toxicity considerations and other problems, such as high production costs as compared to antibiotics (Fry, 2018).

The renewed interest in AMPs as a consequence of the increasing number of antibiotic resistant and tolerant bacteria has resulted in the FDA approval of gramicidin and polymyxin B as constituents in Neosporin® in 1955, colistin (polymyxin E) in 1962 and daptomycin in 2003 (Chen and Lu, 2020). Several naturally occurring and synthetic AMPs have been clinically investigated to combat pathogenic bacteria but since the approval of daptomycin no new AMPs have been approved as antimicrobials. To understand this innovation gap, we reviewed the literature to describe the potential of AMPs as alternative to antibiotics and the challenges toward clinical application of AMPs. Additionally, we provide an overview of the strategies that are currently available to facilitate the successful clinical implementation of AMPs using examples from clinical trials.

FUNCTION OF AMPs

Physiological Role of AMPs in the Skin

The skin is not only a physical barrier to the external environment. It is an active immune organ protecting the host from harmful toxins and pathogenic organisms (Salmon et al., 1994). The immune response of the skin involves various resident cells in the epidermis such as keratinocytes, melanocytes, Langerhans cells and γδ T cells, and in the dermis such as dendritic cells, macrophages, fibroblasts, mast cells, B and T cells, plasma cells and natural killer cells (Zasloff, 2002; Ryu et al., 2014; Lacey et al., 2016). These skin cells release several pro-inflammatory cytokines such as IL-17 and IL-22 and produce AMPs, which act as the first line of defense against microorganisms (**Figure 1**) (Liang et al., 2006). AMPs display a broad-spectrum of antimicrobial activity against yeast, fungi, viruses and bacteria. For example, the human cathelicidin LL-37 shows activity against various Gram-positive and Gram-negative bacteria, and antibiotic-resistant bacterial strains (Dean et al., 2011; Shurko et al., 2018). The same AMP also shows activity against fungi and some viruses such as influenza and HIV. Bergman et al. (2007) showed that LL-37 inhibits HIV-1 replication and suggested that this AMP contributes to the protection against HIV-1 infection. Furthermore, Luo et al. (2019) reported that LL-37 inhibits *Aspergillus fumigatus* infection via direct antifungal activity and reduction of excessive inflammation.

The ability to modulate the immune responses has been reported for several AMPs. LL-37 is a well-studied AMP with such immunomodulatory properties in humans. It acts as a chemoattractant for monocytes and promotes the production and release of various cytokines and chemokines that may direct the course and intensity of inflammation (Agier et al., 2015). Among others, LL-37 can reduce the inflammatory response via interaction with TLR. TLRs are widely expressed receptors on immune cells that recognize pathogenic-associated molecular patterns. LL-37 downregulates signaling through TLR4 by scavenging its ligand LPS (Larrick et al., 1995; Rosenfeld et al., 2006) as well as by disrupting the receptor complex function (Di Nardo et al., 2007; Brown et al., 2011). Furthermore, LL-37 potentially elongates the lifespan of neutrophils via the suppression of neutrophil apoptosis (Nagaoka et al., 2012), thereby enhancing host immunity. Additionally, Carretero et al. (2008) report that LL-37 activates and promotes angiogenesis and migration of keratinocytes, which results in an improved re-epithelialization and granulation tissue formation.

The antimicrobial and immunomodulatory effects of AMPs are necessary to maintain homeostasis of the skin function. Therefore, the production of AMPs is upregulated upon injury and infection (Miller et al., 2005; Sørensen et al., 2006). For example, in acne vulgaris several AMPs such as LL-37 and hBD-2 are upregulated by, e.g., keratinocytes in response to the *Propionibacterium acnes* (Nagy et al., 2006). As the *P. acnes* strains vary in their ability to stimulate inflammatory responses, upregulation of AMPs could be beneficial due to their antimicrobial and anti-inflammatory effects. In some skin conditions, for example in diabetic foot ulcers, the upregulation of AMPs such as hBD-2, 3, and 4 is often not sufficient to control the inflammation and wound infection (Rivas-Santiago et al., 2012). Therefore, such skin conditions require specialized care for proper healing.

Structure and Mechanism of Action

Antimicrobial peptides are usually small, consisting of 12–50 amino acids. They are composed of hydrophilic, hydrophobic and cationic residues (net charge +2 to +11). The cationicity and hydrophobicity of AMPs are critical for bactericidal activity. Together with the hydrophilic residues, the hydrophobic residues form an amphipathic structure for insertion into the bacterial membrane (Ebenhan et al., 2014). To form this structure, some AMPs (i.e., α-helical peptides such as melittin) undergo conformational changes upon interaction with bacterial membranes, while others already have a rigid amphipathic structure (i.e., β-sheet peptides such as β-defensins) to target bacterial membranes (Ebenhan et al., 2014). The positive charge of AMPs facilitates the initial binding of AMPs to the membrane surfaces via electrostatic interactions. Bacterial membranes consisting of negatively charged phospholipid headgroups

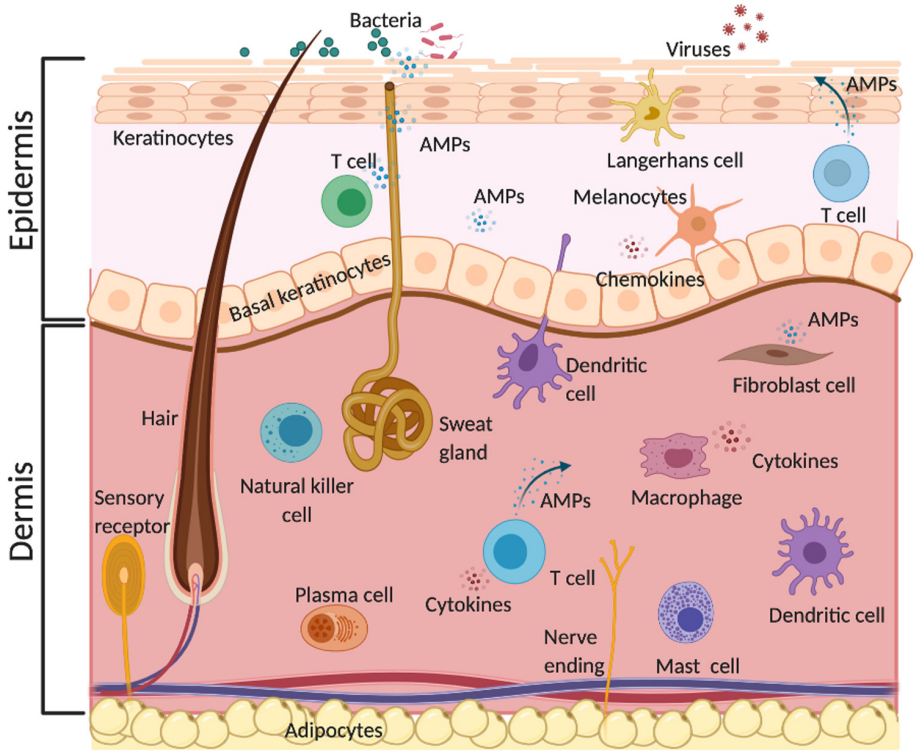

FIGURE 1 | Physiological role of AMPs in the skin. AMPs are produced by different resident skin cells. They act as the first line of innate immune defense against various pathogens such as bacteria, fungi, and viruses via direct and indirect antimicrobial activities and/or immunomodulatory effects. This illustration was created with BioRender.com.

such as phosphatidylglycerol, cardiolipin, or phosphatidylserine show high affinity for cationic AMPs (Matsuzaki, 1999). Contrarily, mammalian cell membranes that are enriched with zwitterionic phospholipids such as phosphatidylethanolamine, phosphatidylcholine, or sphingomyelin show low affinity for cationic AMPs due to their neutral net charge.

Most AMPs cause membrane disruption through non-specific interactions with the membrane surface. They are suggested to form micelles or pores, causing loss of membrane integrity and consequently leakage of intracellular components, resulting in cell death (Chan et al., 2006). Depending on the membrane topology and geometry of pores, pores can be described by three models, i.e., barrel-stave, toroidal and sinking-raft model (**Figure 2**). In the sinking-raft model, AMPs lie on the membrane surface and cause an increase in membrane curvature. Self-aggregation of the peptide causes the AMPs to sink into the membrane, creating transient pores (Brogden, 2005). In both the barrel-stave pore and toroidal pore, the peptide has a transmembrane topology. The main difference between these two models is that the formation of barrel-stave pores is driven by both hydrophobic and electrostatic interactions, whereas the formation of toroidal pores is mainly driven by electrostatic interactions (Bertelsen et al., 2012). As a result, toroidal pores are covered by phosphate headgroups, initiating changes in membrane curvature. The mechanism of action of AMPs that form micelles is not well-understood. It is believed that these AMPs act by a detergent-like mechanisms causing intrinsic perturbations of the membrane (Li et al., 2017).

Membrane disruptive AMPs might also kill bacteria using non-membrane disruptive pathways, and vice versa (Hale and Hancock, 2007). Additionally, they could act independently or in synergy with non-membrane disruptive AMPs. Non-membrane disruptive AMPs are able to transverse membranes to reach their intracellular target components. Such AMPs could inhibit protein-folding, proteases, cell division, the synthesis and metabolism of proteins, nucleic acids and cell walls (Le et al., 2017). Previously, Edgerton et al. (2000) showed that two AMPs with clearly different structures, i.e., histatin 5 and human neutrophil (HNP)-1, act on similar pathways. The role of these AMPs suggests that membrane and non-membrane disruptive AMPs serve as equally important peptides of the innate defense system to inactivate pathogens.

CLINICAL TRIALS USING AMPs

The results from pre-clinical studies using AMPs revealed that AMPs could be used for the prevention and treatment of various clinical conditions. For example, peptide coating of catheters using a novel peptide E6 prevented catheter associated infections in mouse models (Yu et al., 2017). PXL150 demonstrated efficacy against *Pseudomonas aeruginosa* in burn wounds in

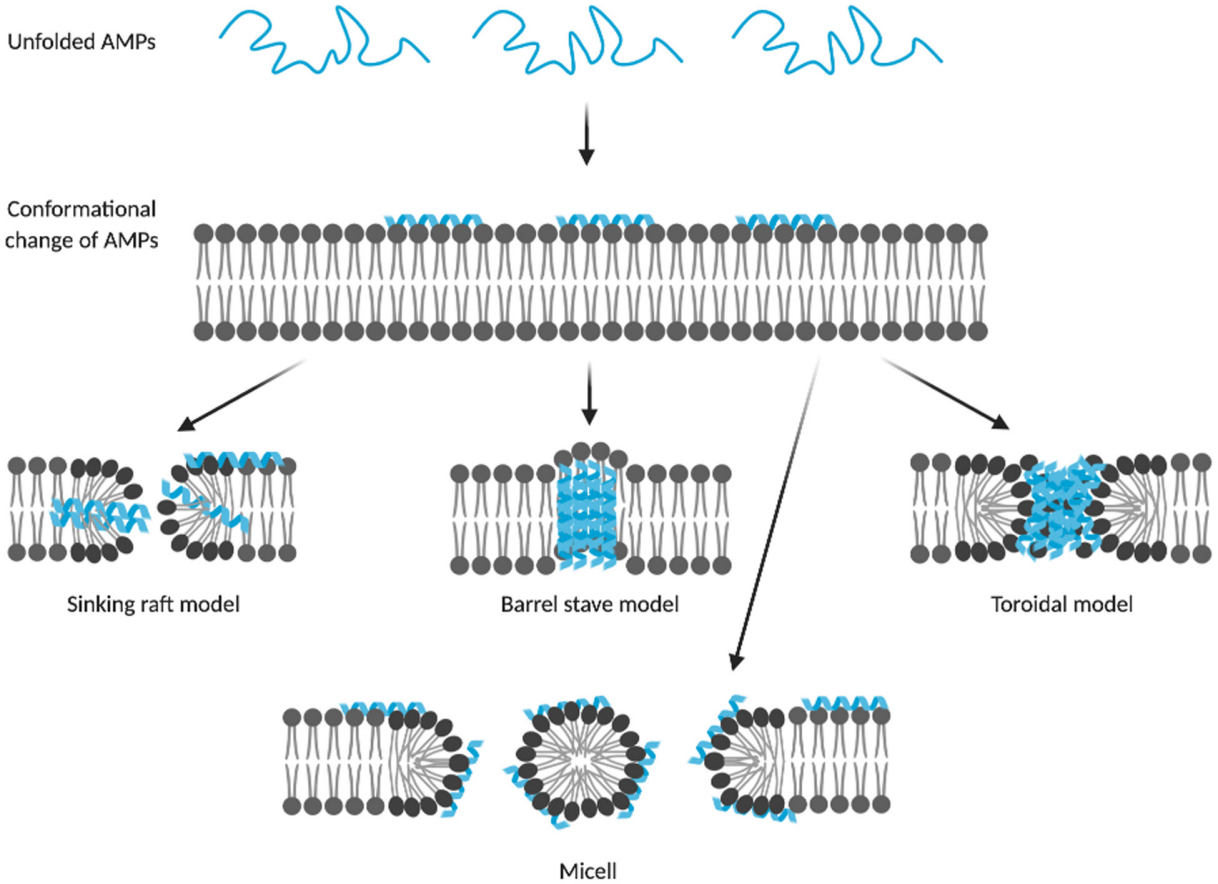

FIGURE 2 | Membrane disruptive models of AMPs. Membrane disruptive AMPs form micelles or pores on the bacterial membrane, resulting in leakage of the intercellular components and cell death. Membrane pores can be categorized by their membrane topology and geometry into the sinking raft, barrel stave and toroidal models. AMPs that form barrel stave and toroidal pores display a transmembrane topology, whereas AMPs of the sinking raft model cause self-aggregation to sink into the membrane, creating transient pores. AMPs that form toroidal pores are mainly driven by electrostatic interactions and as a result of these interactions, the pores are covered by phosphate headgroups. AMPs forming micelles show a detergent-like mechanism of action, causing membrane perturbation. This illustration was created with BioRender.com and Bahar and Ren, 2013.

mouse models (Björn et al., 2015). Both LL-37 and IDR-1 restored pulmonary function in mice with pneumonia (Hou et al., 2013). Also, nisin demonstrated *in vitro* efficacy against *Clostridium difficile* (Bartoloni et al., 2004). Furthermore, several AMPs including LL-37 displayed anti-biofilm activity *in vivo* (Chennupati et al., 2009; Segev-Zarko et al., 2015; Batoni et al., 2016). Based on promising pre-clinical results, numerous AMPs have been investigated in human clinical trials to demonstrate efficacy and safety. Several of these trials are still ongoing, others are completed, discontinued or approved. The successes and flaws of these clinically investigated AMPs are described in the following sections. Structural information, mechanism of action and the intended target of AMPs in clinical trials is provided in **Table 1**.

AMPs Approved for Clinical Use

Currently, nisin, gramicidin, polymyxins, daptomycin and melittin are in clinical use as alternative to antibiotics because of their antimicrobial potency (**Figure 3A**). Nisin, also known as nisin A, is composed of 34 amino acids and consists of dehydrated, unsaturated and thioether amino acids, forming five lanthionine rings. It is naturally produced by lactic acid bacteria such as *Lactococcus lactis* and shows a broad-spectrum of bactericidal activity (Stevens et al., 1991; Severina et al., 1998). *L. lactis* also produces nisin Z, F and Q, which differ by up to 10 amino acids from nisin A resulting in differences in physiochemical properties and antimicrobial activity (Piper et al., 2011). Among others, nisins inhibit cell wall synthesis through interactions with lipid II, a precursor molecule that is essential for bacterial cell-wall bio-synthesis. Nisins also form membrane pores causing cell lysis (Prince et al., 2016). Nisin A is approved as a food preservative and is GRAS (Delves-Broughton et al., 1996; Cleveland et al., 2001). In clinical trials, the effect of nisin A has been investigated using probiotics, i.e., the consumption of live microorganisms (e.g., *L. lactis*) that produce nisin A. The results of a systematic review of such trials indicated that these probiotics reduce infectious complications and may subsequently reduce intensive care unit mortality

TABLE 1 | Clinical trial(s) of AMPs under investigation and in clinical use.

Peptide name	Description	Target	Administration	Phase	Clinical Trial ID	Mechanism	MW (g/mol)	Length	Net charge	References
Nisin	Polycyclic lantibiotic	Gram-positive bacteria	Oral		NCT02928042; NCT02467972	Depolarization of cell membrane	3354	34	4	Prince et al., 2016
Gramicidin	Polycyclic peptide	Infected wounds and ulcers	Topical	III	NCT00534391	Membrane disruption/immunomodulation	1882	16	0	David and Rajasekaran, 2015
Polymyxin B	Cyclic polypeptide	Gram-negative bacteria	Topical	III	NCTOO490477; NCT00534391	Membrane disruption/immunomodulation	1204	10	5	Morrison and Jacobs, 1976
Polymyxin E (Colistin)	Cyclic polypeptide	*A. baumannii*/pneumonia	Intravenous	III	NCT01292031; NCT02573064	Membrane disruption/immunomodulation	1155	10	5	Yu et al., 2015
Daptomycin	Lipopeptide	Skin infection/bacteremia	Intravenous	III	NCT01922011; NCT00093067; NCT01104662; NCT02972983	Membrane disruption/immunomodulation	1621	13	0	Taylor and Palmer, 2016
LL-37	Human cathelicidin	Leg ulcers	Topical	II	EUCTR2012-002100-41	Membrane disruption/immunomodulation	4491	37	6	Brown et al., 2011
Melittin	α-helical peptide	Inflammation	Intradermal	I/II	NCT02364349, NCT01526031	Membrane disruption/immunomodulation	2846.5	26	5	Lee and Bae, 2016
Friulimicin	Cyclic lipopeptide	MRSA/pneumonia	Intravenous	I	NCT00492271	Membrane disruption	1303.5	12	−2	Schneider et al., 2009
Murepavadin (POL7080)	Analog of Protegrin	*P. aeruginosa, K. pneumoniae*	Intravenous	II	EUCTR2017-003933-27-EE	Binding to LptD	1553.8	14	5	Srinivas et al., 2010
Neuprex® (rBPI21)	Derivative of BPI	Pediatric meningococcemia	Intravenous	III	NCT00462904	Membrane disruption	∼21000	193		Schultz and Weiss, 2007
Iseganan (IB-367)	Analog of Protegrin	Pneumonia/oral mucositis	Topical	III	NCT00118781; NCT00022373	Membrane disruption	1900.3	17	4	Orlov et al., 1805
Surotomycin (CB-315)	Cyclic lipopeptide	*C. difficile*	Oral	III	NCT01597505	Membrane disruption	1680.8	13	−3	Alam et al., 2015
Pexiganan (MSI-78)	Analog of Magainin	Diabetic foot ulcers	Topical	III	NCT00563394; NCT00563433; NCT01590758; NCT01594762	Membrane disruption/immunomodulation	2477.2	22	9	Gottler and Ramamoorthy, 2009
XOMA-629 (XMP-629)	Derivative of BPI	Impetigo/acne rosacea	Topical	III		Immunomodulation	1158.4	9	3	Easton et al., 2009
Omiganan (MBI-226)	Derivative of Indolicidin	Antisepsis/catheter infection	Topical	III	NCT00231153; NCT00608959	Membrane disruption/immunomodulation	1779.2	12	5	Rubinchik et al., 2009
NVB-302	Lantibiotic	*C. difficile*	Oral	I	ISRCTN40071144	Inhibition of cell wall synthesis	1754.0	19	0	Crowther et al., 2013
OP-145	Derivative of LL-37	Chronic middle ear infection	Ear drops	I/II	ISRCTN84220089	Membrane disruption/immunomodulation	3093.8	24	6	Malanovic et al., 2015
P113 (PAC-113)	Fragment of Histatin-5	Oral candidiasis	Mouth rinse	II	NCT00659971	Membrane disruption/immunomodulation	1564.8	12	5	Woong et al., 2008

(Continued)

TABLE 1 | Continued

Peptide name	Description	Target	Administration	Phase	Clinical Trial ID	Mechanism	MW (g/mol)	Length	Net charge	References
LTX-109	Synthetic tripeptide	MRSA/impetigo	Topical	I/II	NCT01803035; NCT01158235	Membrane disruption	788.1	3	2	Isaksson et al., 2011; Sivertsen et al., 2014
EA-230	Oligopeptide	Sepsis	Intravenous	II	NCT03145220	Immunomodulation	415.5	4	0	Van Groenendael et al., 2018
SGX942 (Dusquetide)	Analog of IDR-1	Oral mucositis	Oral rinse	III	NCT03237325	Immunomodulation	553.7	5	2	Kudrimoti et al., 2016
hLF1-11	Fragment of human lactoferrin	Bacterial/fungal infections	Intravenous	I/II	NCT00430469	Membrane disruption/immunomodulation	1373.7	11	4	Nibbering et al., 2001; Welling et al., 2018
C16G2	Synthetic peptide	*Streptococcus mutans*	Mouth wash	II	NCT03004365	Membrane disruption	4077.4	35	10	Guo et al., 2015
Novexatin (NP213)	Cyclic Cationic peptide	Fungal nail infection	Topical	II	NCT02933879	Membrane disruption	1093.3	7	7	Mercer et al., 2020
Ramoplanin (NTI-851)	Glycolipodepsipeptide	*C. difficile*, VRE	Oral	III		Inhibition of cell wall synthesis	2568.1	17	2	Fulco and Wenzel, 2006
p2TA (AB103)	Synthetic peptide	Necrotic tissue infection	Intravenous	III		Immunomodulation	1037.2	8	−1	Bulger et al., 2014
D2A21	Synthetic peptide	Burn wound infections	Topical	III		Membrane disruption	2775.4	23	9	Muchintala et al., 2020
Melamine	Chimeric peptide	Contact lenses microbials	Topical	II/III		Membrane disruption	2786.6	29	15	Yasir et al., 2019, 2020
Mel4	Derivative of melamine	Contact lenses microbials	Topical	II/III	ACTRN12615000725550	Membrane disruption	2347.8	17	14	Yasir et al., 2020
LFF571	Semisynthetic thiopeptide	*C. difficile*	Oral	II	NCT01232595	Inhibition of protein synthesis	1366.6			Leeds et al., 2012
Delmitide (RDP58)	Derivative of HLA	Inflammatory bowel disease	Topical	II	ISRCTN84220089	Immunomodulation	1228.6	10	2	Travis et al., 2005
DPK-060	Derivative of Kininogen	Acute external otitis	Ear drops	II	NCT01447017	Membrane disruption/immunomodulation	2503.2	20	7	Håkansson et al., 2019
GSK1322322 (Lanopepden)	Synthetic hydrazide	Bacterial skin infection	Oral	II	NCT01209078	Peptide deformylase inhibitor	479.3			Peyrusson et al., 2015
PXL01	Analog of Lactoferrin	Postsurgical adhesions	Topical	II	NCT01022242	Immunomodulation	3061.6	25	5	Edsfeldt et al., 2017
AP-214	Derivative of α-MSH	Post-surgical organ failure	Intravenous	II	NCT00903604	Membrane disruption/immunomodulation	2433.9	19	7	Doi et al., 2008
PMX-30063 (Brilacidin)	Defensin mimetic	Acute bacterial skin infection	Intravenous	II	NCT01211470; NCT02052388	Membrane disruption/immunomodulation	936.9			Mensa et al., 2014
XF-73 (Exeporfinium chloride)	Derivative of porphyrin	*Staphylococcal* infection	Topical	II	NCT03915470	Membrane disruption	765.8			Ooi et al., 2009

(Continued)

TABLE 1 | Continued

Peptide name	Description	Target	Administration	Phase	Clinical Trial ID	Mechanism	MW (g/mol)	Length	Net charge	References
CZEN-002	Derivative of α-MSH	Antifungal	Topical	II		Immunomodulation	971.2	8	2	Csato et al., 1989
Ghrelin	Endogenous peptide	Chronic respiratory infection	Intravenous	II	NCT00763477	Immunomodulation	3314.9	28	5	Gualillo et al., 2003
Wap-8294A2 (Lotilibcin)	Produced by *Lysobacter species*	Gram-positive bacteria	Topical	I/II		Membrane disruption	1562.8	12	1	Itoh et al., 2017
PL-5	Synthetic peptide	Skin infections	Topical	I		Membrane disruption	2933.5	26	6	Miyake et al., 2004
IDR-1	Bactenecin	Infection prevention	Intravenous	I		Immunomodulation	1391.7	13	3	Yu et al., 2009

A. baumannii; Acinetobacter baumannii; BPI, bactericidal permeability increasing protein; C. difficile, Clostridium difficile; HLA, human leukocyte antigen; IDR, innate defense regulator; K. pneumoniae, Klebsiella pneumoniae; LptD, lipopolysaccharide transport protein D; MRSA, methicillin-resistant Staphylococcus aureus; MSH, melanocyte-stimulating hormone; P. aeruginosa, Pseudomonas aeruginosa; VRE, vancomycin-resistant Enterococci.

(Petrof et al., 2012). Minor but possible side effects of nisin A are itching (pruritus) and flushing of the skin, and nausea or vomiting. The safety profile together with the broad-spectrum of bactericidal activity, indicated that the application of nisin could extend beyond food-related bacteria (Blay et al., 2007; Shin et al., 2015). Applications of nisins in humans include dental-care and pharmaceutical products such as for the treatment of stomach ulcer and colon infections (Sakamoto et al., 2001; Mitra et al., 2019).

Gramicidin or gramicidin D is a mixture of gramicidin A, B and C making up 80, 6, and 14% of the mixture, respectively. These AMPs are hydrophobic linear polypeptides composed of 15 amino acids (Meikle et al., 2016). They are naturally produced by Gram-positive *Brevibacillus brevis* commonly found in soil (Van Epps, 2006). Gramicidins form ion-channels within the bacterial membrane, allowing the passive diffusion of Na^+ and K^+ along their concentration gradient (David and Rajasekaran, 2015). This results in membrane depolarization, osmotic swelling and lysis of bacterial cells. Gramicidin is effective against a variety of Gram-positive bacteria and is clinically used for ophthalmic purposes as a constituent in Neosporin®. In a clinical trial, patients suffering from hordeolum who received the ophthalmic solution containing gramicidin (Neosporin®) reported a comparable pain score as those who received a placebo treatment (Hirunwiwatkul and Wachirasereechai, 2005). Additionally, the duration of cure of these treatment groups was not statistically different (p = 0.988). The authors of this study suggested that the lack of statistically significant differences between the placebo and peptide-treated group could be due to the small sample size of 14 patients in each group (Hirunwiwatkul and Wachirasereechai, 2005). In another clinical study using a larger sample size of 91 patients, the effect of this ophthalmic solution on the duration of cure of bacterial-positive corneal ulcers was reported (Bosscha et al., 2004). An average of 12.5 days was required for complete re-epithelialization of these ulcers. This was more favorable compared to the duration of cure of ulcers treated with ofloxacin (13.7 days) and ciprofloxacin (14.4 days) (Prajna et al., 2001). These findings suggest that Neosporin® containing gramicidin could be used as an alternative to conventional antibiotics for such ophthalmic purposes. Another AMP in Neosporin® is polymyxin B.

Polymyxins (A, B, C, D, and E) are a group of cyclic polypeptides naturally produced by Gram-positive *Paenibacillus polymyxa*. They show activity against MDR Gram-negative bacteria such as *P. aeruginosa* and *Escherichia coli* (Zavascki et al., 2007). Polymyxins bind to the lipid A component of LPS on the outer membrane of Gram-negative bacteria (Morrison and Jacobs, 1976), which contributes to the insertion of the AMPs into the membrane. They can increase cell-permeability via a detergent-like mechanism, which causes cell death (Schroder et al., 1992). Polymyxins in clinical use are polymyxin B and E, which differ only by one amino acid from each other (Li et al., 2005; Falagas et al., 2006; Kwa et al., 2007). Polymyxin B is prescribed to treat eye infections, whereas polymyxin E is used to treat wound infections. These AMPs are recognized as crucial but last-resort treatment options because of their ability to induce adverse events. Nephrotoxicity and

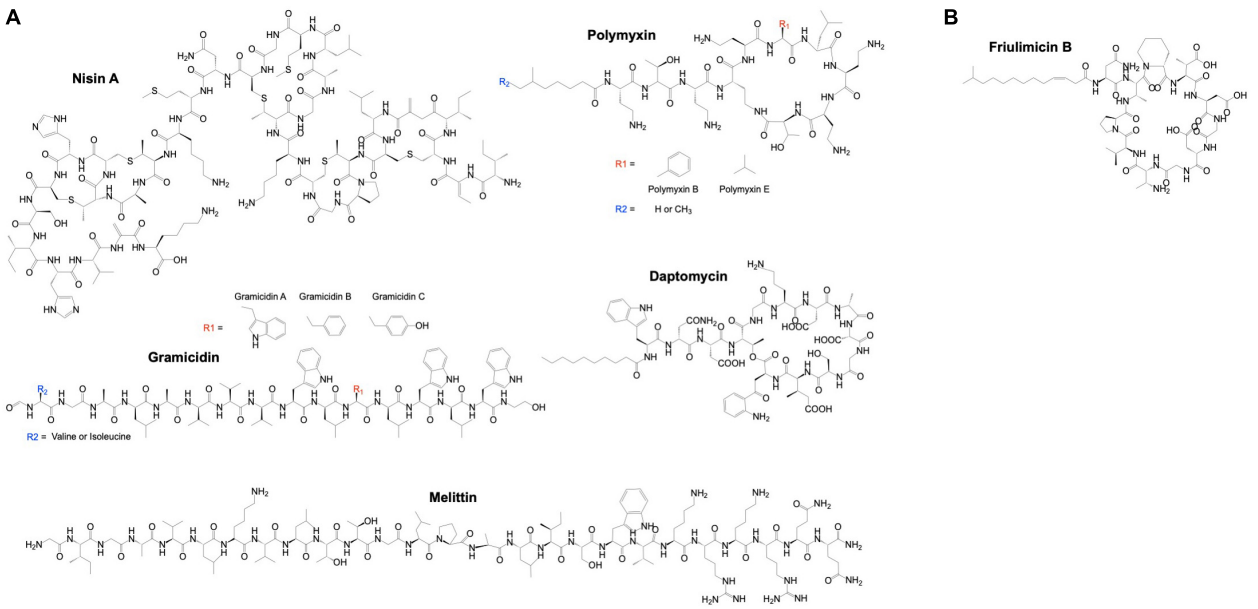

FIGURE 3 | Chemical structure of AMPs in clinical use. **(A)** A few α-helical (gramicidin and melittin) and cyclic AMPs (nisin A, polymyxin and daptomycin) have been approved for clinical use. **(B)** Despite the physiochemical similarities of the cyclic AMP friulimicin B with daptomycin, the Phase I clinical trial of friulimicin B was terminated due to unfavorable pharmacokinetics. ChemDraw version 19 was used to draw the chemical structure of AMPs.

neurotoxicity are the most common adverse events reported for polymyxins (Falagas and Kasiakou, 2006; Cisneros et al., 2019). To optimize the clinical use of polymyxins without such severe adverse effects, clinical trials are currently being executed, e.g., in combination with different antimicrobial agents. Minor side effects, such as blurred vision, watery eyes, and sensitivity to light, have been reported for Neosporin® containing two AMPs, gramicidin and polymyxin B, and an aminoglycoside antibiotic neomycin. Thus, not one agent but the mixture of three antimicrobial agents are responsible for these minor side effects.

Daptomycin is a cyclic lipopeptide consisting of 13 amino acids, which is naturally produced by the bacterium *Streptomyces roseosporus* (Ball et al., 2004). It shows bactericidal activity against Gram-positive bacteria, including antibiotic resistant strains (Jorgensen et al., 2003). Daptomycin inhibits cell wall synthesis, causes membrane depolarization and forms membrane pores, eventually causing cell death. A daily treatment of 4-6 mg/kg daptomycin is recommended in critically ill patients. For the treatment of bacteria with reduced susceptibility high dosages of 10 mg/kg can be prescribed, which are also well tolerated. In a phase I clinical trial, 2 of 5 healthy volunteers who received 4 mg/kg per 12 h of daptomycin (8 mg/kg per day) developed reversible myopathy (Dvorchik et al., 2003). Nonetheless, the number of incidence and the severity of myopathy were substantially decreased in healthy volunteers when the total dose of 8 mg/kg was administered once daily. Other studies reported that the development of myopathy was not related to the administration of daptomycin but to other factors such as concomitant medications, comorbidities and the number of surgical interventions (Galar et al., 2019). In a Phase IV clinical trial, the effect of daptomycin on the resolution of skin infections was compared to that of the standard of care, i.e., cloxacillin, nafcillin, oxacillin, flucloxacillin or vancomycin (Arbeit et al., 2004). The success rate of the daptomycin-treated patients was 71.5%, which was clinically and statistically comparable to the standard treatments with a success rate of 71.1%. In another clinical study, efficacy of daptomycin was demonstrated in a placebo-control trial. All patients also received a β-lactam therapy. In this study, the daptomycin treatment resulted in faster clearance of bacteremia than the control treatment (placebo + β-lactam therapy) (Cheng et al., 2018). Hence, combination therapy using daptomycin can improve the clinical success rate.

Melittin is the predominant (40–48%) component of venom from the European honeybee *Apis mellifera*. It is composed of 26 amino acids and adopts an α-helical conformation upon interaction with the membrane surface (Terwilligert and Eisenbergg, 1982). It possesses anti-inflammatory properties (Lee and Bae, 2016) and is therefore approved by the FDA for relieving pain and swelling associated with rheumatoid arthritis, tendinitis, bursitis and multiple sclerosis (Son et al., 2007; Alves et al., 2011). Melittin also forms membrane toroidal pores to inactivate pathogens. This was shown in several *in vitro* and animal experiments using cancer cells (Gajski and Garaj-Vrhovac, 2013), viruses (Memariani et al., 2020) and (resistant) bacteria (Park et al., 2006; Van Den Bogaart et al., 2008; Choi et al., 2015). Hence, similar to nisin, the clinical application of melittin could extend beyond the FDA-approved purposes. Side effects of melittin are redness and swelling of the skin at the side

of administration, itching, trouble breathing, nausea, sleepiness and low blood pressure.

Flaws of Some AMPs

Some clinical trials using AMPs were discontinued or terminated due to various reasons. For example, the Phase I clinical trial of friulimicin B in healthy volunteers was terminated due to its unfavorable pharmacokinetic profile. The nature of these unfavorable findings remains unknown and unexpected. Friulimicins (A, B, C, D, and E) are a group of naturally occurring peptides produced by *Actinoplanes friuliensis* and like daptomycin, they are cyclic lipopeptides (**Figure 3B**). Friulimicin B was clinically investigated and demonstrated efficacy in various murine infection models (Endermann et al., 2007). It has similar physiochemical properties and mechanism of action as daptomycin (Schneider et al., 2009) but has been found to trigger different stress responses in *Bacillus subtilis* as compared to daptomycin (Wecke et al., 2009). This might be related to differences in the pharmacokinetic profiles of these AMPs. Another AMP, Murepavadin (POL7080) failed unexpectedly in advanced clinical trials. Murepavadin is a 14 amino acid cyclic peptide that targets the LPS transport protein D (LptD) on the bacterial membrane to form pores (Srinivas et al., 2010). It was demonstrated to be safe in Phase I clinical trials in healthy volunteers and in subjects with an impaired renal function (Martin-Loeches et al., 2018). Safety and efficacy of murepavadin were demonstrated in Phase II clinical trials in patients with acute exacerbation of non-cystic fibrosis bronchiectasis or ventilator-associated bacterial pneumonia due to *P. aeruginosa* (Martin-Loeches et al., 2018). However, Phase III clinical trial of this AMP in patients with nosocomial pneumonia was prematurely ended due to higher than expected acute kidney injuries, i.e., 56% for the murepavadin plus ertapenem treated group versus 25–40% for the meropenem treated control group and according to the literature (BioSpace, 2019).

Besides pharmacokinetic and safety issues, several AMPs have failed Phase III clinical trials because of lack of clear efficacy or lack of superiority over conventional treatments. A clear example is demonstrated for the AMP Neuprex® (rBPI21) which is a recombinant α-helical peptide consisting of the first 193 amino acids of the N-terminus of BPI. Clinical studies showed that patients with meningococcemia or hemorrhage due to trauma who received Neuprex® had no toxic side effects and showed a trend toward improved outcomes, i.e., reduced bone marrow aplasia and deaths (Demetriades et al., 1999; Guinan et al., 2011). However, Neuprex® failed to show clear efficacy (p = 0.07) as compared to the placebo-treated group (Giroir et al., 2001). Similar to Neuprex®, at least five AMP that have completed advanced clinical trials, failed to show clear efficacy (i.e., iseganan and XOMA-629) or superiority over conventional treatments (i.e., surotomycin, pexiganan, and omiganan) (Gordon et al., 2005). Nevertheless, the latter AMPs could be potential alternatives to conventional antibiotics due to their favorable safety profile and low or limited ability to induce bacterial resistance. Since antibiotics are no longer routinely used to treat bacterial infections as a consequence of resistance development, the ability of AMPs to induce bacterial resistance, is a more important parameter to consider during clinical trials. Hence, instead of superiority trials, equivalence or non-inferiority trials in which AMPs cause a similar effect as the standard treatment, should become more common (Committee for Proprietary Medicinal Products, 2001). In two equivalence trials with systemic ofloxacin as the comparator, efficacy of topical pexiganan was determined in patients with diabetic foot ulcers (Lipsky et al., 2008). The combined results of these trials demonstrated that pexiganan was clinically comparable to this antibiotic. However, equivalence to ofloxacin was not acceptable as main evidence of efficacy and FDA approval of pexiganan. Additional clinical trials were required to demonstrate efficacy superior to a topical placebo cream plus standard treatment for diabetic foot ulcers. Of note, clinical trials are often not designed using placebo treatment only as control due to ethical reasons. In the additional trials, pexiganan plus standard treatment failed to meet the primary outcome, i.e., resolution of infection (Genetic Engineering, and Biotechnology News, 2016). Failure of AMPs in such trials may arise from stability issues, inappropriate drug administration or unknown interactions between the peptide and the standard treatment. Currently, the developers of pexiganan continue to evaluate the data to consider this peptide for the treatment of other clinical indications.

Challenges Toward Clinical Application of AMPs

The development of AMPs for clinical use is accompanied by several challenges such as high development and production costs, cytotoxic issues, reduced activity in clinically relevant environments and the emergence of bacterial resistance, despite the initial claims that they may not induce resistance. To begin with, the manufacturing costs of antibiotics are relatively inexpensive. For example, aminoglycoside production costs $0.80 per gram as compared to $50–400 per gram of amino acid for AMPs by solid phase synthesis (Marr et al., 2006). As a consequence, alternative methods are required to promote commercial-scale production.

Furthermore, AMPs acting on membranes are not completely selective to microbial cells and may be toxic for eukaryotic cells as well. Several AMPs cause hemolytic and/or cytotoxic effects at antimicrobial concentrations, limiting their wider utilization (Laverty, 2014; Bacalum and Radu, 2015). Polymyxins are an example of such AMPs: they are crucial antimicrobials to eradicate MDR Gram-negative bacteria but they may cause nephrotoxicity and neurotoxicity at antimicrobial concentrations (Falagas and Kasiakou, 2006).

Another drawback for the clinical implementation of AMPs is the low antimicrobial activity in clinically relevant environments. AMPs may lose their bactericidal activity under physiological salt conditions due to loss of electrostatic interactions between AMPs and cell membranes (Falanga et al., 2016; Mohamed et al., 2016). In the presence of serum, AMPs may bind to proteins such as albumin (Sivertsen et al., 2014; Li et al., 2017). Additionally, AMPs can be susceptible to proteolytic degradation (Perona and Craik, 1997; Thwaite et al., 2006; McCrudden et al., 2014). Also, Starr et al. (2016) suggested that host cells can interfere with

the activity of AMPs in a way similar to serum protein binding. This reduces the effective concentration of available AMPs to eradicate bacteria.

Although AMPs do not seem to induce bacterial resistance, resistance to AMPs has been reported. AMPs that require specific recognition molecules such as LPS, Lipid A, Lipid I/II and LptD, on the membrane surface of bacteria most likely develop resistance. For example, resistance to nisin involves mutations in bacterial cells that induce changes in membrane and cell wall composition and eventually prevents the binding of nisin to lipid II (Kramer et al., 2008). Alternatively, bacteria may inactivate nisin using dehydropeptide reductase, also known as nisinase (Bastos et al., 2015). Resistance to polymyxins and cross-resistance to AMPs have also been reported (Li and Nation, 2006; Valencia et al., 2009; Arcilla et al., 2016; Dobias et al., 2017). Resistance to polymyxins is mediated by the *mrc-1* gene encoding a phosphoethanolamine modification in lipid A, which prevents the initial binding of polymyxins to the bacterial membranes (Liu et al., 2016). This gene was initially isolated from Chinese livestock animals and has been identified in the human fecal microbiome, indicating that polymyxin resistance is horizontally transferable (Arcilla et al., 2016). Moreover, Li et al. (2007) reported that the *aps* AMP sensor/regulator system is important for *S. aureus* virulence *in vivo*. They show that AMPs may induce resistance mechanisms in MRSA via this system, which involves the D-alanylation of teichoic acids, the incorporation of lysophosphatidylglycerol in the bacterial membrane, the increase of lysine biosynthesis and AMP transport systems (Arcilla et al., 2016). Although the impact of bacterial resistance on the minimal inhibitory concentration of the AMPs (2–30-fold increase) is less dramatic than for antibiotics (100–1000-fold increase) (Andersson et al., 2016), the risk of bacterial resistance should be carefully investigated.

IMPROVEMENT STRATEGIES

The majority of the AMPs under clinical evaluation are positively charged analogs of naturally occurring AMPs and are limited to topical or intravenous applications for an effective bio-available concentration of the peptides. Importantly, the route of drug administration could markedly affect the efficacy of AMPs as efficacy is dependent on the bio-distribution and stability of the peptides (Benet, 1978). Analogs of naturally occurring AMPs have been prepared to overcome the challenges associated with high production costs, low bio-availability and efficacy, and cytotoxic effects of AMPs (**Figure 4**). Strategies to improve the performance of AMPs are described in the following sections.

Ultra-Short and/or Truncated AMPs

Efforts to reduce production costs include alternative peptide synthesis methods and the production of ultra-short and/or truncated AMPs. The latter has been pursued by several companies. The AMPs OP-145 (Nell et al., 2006), P113 (Woong et al., 2008), LTX-109 (Midura-Nowaczek and Markowska, 2014), and EA-230 (Van Groenendael et al., 2018) all consist of a lower number of amino acids as compared to their "original" peptide LL-37, histatin-5, bovine lactoferrin and loop-2 of β-hCG, respectively. Beside truncation of AMPs, the synthesis of ultra-short AMPs such as the 5-amino acid linear peptide SGX942 further reduces the production costs of AMPs (Kudrimoti et al., 2016). Alternatively, solution phase synthesis or by chemoenzymatic methods could be used for production of small AMPs (Bray, 2003). This remains challenging for large peptides and therefore a biotechnological approach is often considered, i.e., the production of AMPs in microorganisms (Ingham and Moore, 2007). Magainin, hBD-3, melittin and other AMPs have been synthesized using calmodulin as carrier protein (Ishida et al., 2016; Boto et al., 2018). This protein protects the producing bacterial cells, e.g., *E. coli* from the toxic effects of the AMPs and prevents degradation of the AMP during the production process. Alternative approaches to obtain AMPs from plants or bacterial ribosomes have been reviewed by Montesinos and Bardají (2008), and Rogers and Suga (2015), respectively.

Delivery Systems

To improve the bio-availability of AMPs, delivery systems can be used to administer the peptides. Nisin is readily degraded by enzymes in the gastrointestinal tract (Heinemann and Williams, 1966). To target *C. difficile*, a bacterium that can infect the colon (Le Lay et al., 2016), nisin requires a delivery vehicle to reach the colon without being digested and absorbed by the upper gastrointestinal tract. To achieve this, nisin has been encapsulated in pectin/HPMC compression coated tablets to form an enzymatically controlled delivery system (Ugurlu et al., 2007). Alternative systems such as liposomes, nanoparticles, and nisin-controlled gene expression in *Lactobacillus gasseri* have also shown to be successful delivery systems (Neu and Henrich, 2003; Taylor et al., 2007; Khan and Oh, 2016). Colon-specific delivery approaches such as pro-drugs and conjugates have been reviewed by Fang et al. (2017) and Mishra et al. (2017). These approaches have also been used to improve the *in vivo* bio-availability of different AMPs, for example Polymyxin E, which is administered as an inactive pro-drug that undergoes hydrolysis to release the active AMPs. Polymyxin E was also successfully integrated into hydrogels for the treatment of burn wound infections (Zhu et al., 2017). Please note that such delivery systems, may not only improve the bio-availability of the AMPs but may also improve the efficacy and reduce cytotoxicity, as a consequence of increased solubility and specificity, respectively (Mahlapuu et al., 2016; Kim et al., 2017; Nordström and Malmsten, 2017).

Chemical Modifications

The order and position of amino acids were found to play an important role in the biological activity of the hLT-1-1 peptide, according to its structure-activity relationship (Welling et al., 2018). Also, the α-helical content, the hydrophobicity and amphipathicity of AMPs may affect their bactericidal activity and cytotoxicity. Schmidtchen et al. (2014) reported that an increase in the hydrophobicity might induce hemolytic activity of AMPs. Another group showed that a reduction in the net positive charge of AMPs may not affect the bactericidal efficacy of AMPs but may reduce cytotoxic effects (Jiang et al., 2008). For higher bactericidal activity and less cytotoxic effects, the introduction of arginine was

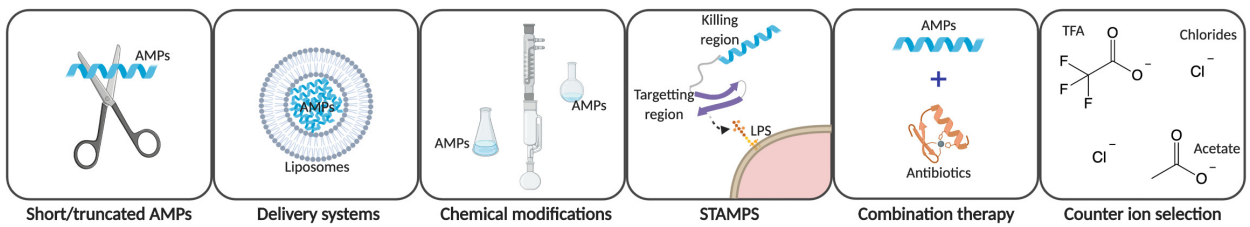

FIGURE 4 | Improvement strategies. Several strategies have been developed to reduce production costs and cytotoxic effects and to improve bio-availability and efficacy of AMPs. Short and/or truncated AMPs have been pursued by several companies to reduce the production costs, whereas the development of a delivery system and the introduction of chemical modifications are more common to improve the bio-availability and efficacy of AMPs *in vivo*. STAMPS, combination therapy with conventional antibiotics and the selection of a counter ion during the final step of peptide synthesis might not only improve efficacy but may also reduce cytotoxic effects of AMPs. This illustration was created with BioRender.com.

found to be superior to lysine for providing the positive charge of AMPs (Yang et al., 2018). To improve proteolytic stability, different approaches have been used such as the introduction of D-amino acids, cyclization, amidation or acetylation of the terminal regions (Strömstedt et al., 2009; Gentilucci et al., 2010; Chu et al., 2013). To increase the salt and serum stability of AMPs, tryptophan or β-naphthylalanine end-tagging of the terminal regions of AMPs could be considered (Chu et al., 2013; Pfalzgraff et al., 2018).

Specifically Targeted AMPs (STAMPS)

Due to the broad-spectrum activity and non-specific mechanisms of action of AMPs, these peptides may induce cytotoxic effects as well. To reduce these effects, STAMPS have been designed (Eckert et al., 2012). STAMPS selectively target and kill a specific pathogenic species without affecting the normal flora (Eckert et al., 2006). They consist of at least two regions, i.e., one or multiple targeting regions and a killing region linked by a spacer. The targeting region improves the activity of the AMPs by enhancing the initial binding of the peptide to the specific pathogenic determinants on the membrane (He et al., 2010). Using two are more targeting regions reduces the likelihood of bacterial resistance and improves efficacy (Sarma et al., 2018). Currently, C16G2 which is a synthetic AMP or STAMP, is under clinical investigation for the treatment of tooth decay by *Streptococcus mutans*. The N-terminus of C16G2, is the targeting region for *S. mutans* and the C-terminus is the killing region or AMP G2 (Kaplan et al., 2011). C16G2 demonstrated a strong safety profile and efficacy against *S. mutans* (Todd and Pierre, 2015).

Combination Therapy

To improve treatment outcomes, two or more antibiotics are often used in clinical practice. The same could be done for novel AMPs as many peptides show synergistic interactions with conventional antibiotics. This could not only reduce the amount of peptide needed for effective treatment and thus reduce costs but may also extend the lifetime of current antibiotics (Phee et al., 2015; Kampshoff et al., 2019). There are numerous examples of AMPs demonstrating synergism (Rand and Houck, 2004; Oo et al., 2010; Dosler et al., 2016; Alni et al., 2020). The combination of polymyxins with carbapenems or rifampicin suppresses the development of polymyxin resistance (Rodriguez et al., 2010; Lenhard et al., 2016). Also, Polymyxin B is used in combination with gramicidin and neomycin in Neosporin® due to their synergistic interactions, resulting in reduced resistance development and less cytotoxic effects (Booth et al., 1994; Tempera et al., 2009).

Counter-Ion Selection

The final step of AMP synthesis, which involves the cleavage and deprotection of the peptide chain with, e.g., TFA should be investigated to improve efficacy and reduce cytotoxicity. Counter-ions such as TFA anions are able to interact with positively charged AMPs and affect the hydrogen-bonding network along with the secondary structure (Blondelle et al., 1995; Gaussier et al., 2002). Also, TFA was shown to be cytotoxic for mammalian cells (Cornish et al., 1999). Previously, Sikora et al. (2018) studied the effect of three counter-ions, i.e., TFA anions, acetate and chlorides, on the bactericidal efficacy and cytotoxicity of a set of AMPs. They found that the peptide salts of acetate and chlorides seemed to be more potent antimicrobials than trifluoroacetates. However, trifluoroacetates have greater ability to promote α-helix formation in, e.g., LL-37 (Johansson et al., 1998). Additionally, acetate counter-ions seemed to be associated with high hemolytic activity (Sikora et al., 2018). In contrast, pexiganan acetate showed less cytotoxicity in cell viability assays and was the most stable salt for pexiganan (Desai, 2013; Sikora et al., 2018). Hence, superiority of one salt over another is peptide-dependent and should be taken into account.

CONCLUSION AND PERSPECTIVES

As a result of the increasing number of antibiotic resistant bacteria, there has been a renewed interest in AMPs as a potential alternative to conventional antibiotics. AMPs display clear advantages over conventional antibiotics to combat various infectious diseases. In particular,

(i) their broad spectrum of activity, (ii) multi-hit, non-specific and rapid mode of action, which results in limited emergence of resistance, (iii) the potential immunomodulatory properties and (iv) synergistic interactions with conventional antibiotics could eliminate the threat of MDR bacteria. Yet, until now, only a few AMPs (e.g., nisin, gramicidin, polymyxins, daptomycin, and melittin) have reached the clinic. Challenges toward clinical application of AMPs include cytotoxic effects, production costs, and problems related to peptide bio-availability and efficacy. To overcome these challenges, several strategies have been designed such as the preparation of ultra-short/truncated AMPs, delivery systems and STAMPS, chemical modifications and the careful selection of a counter-ion in the final step of AMP synthesis. Although not all AMPs in the clinical pipeline will reach the market, these strategies could improve the success rate of AMPs in clinical trials. Nonetheless, several AMPs in clinical trials have failed due to lack of clear efficacy or superiority over conventional antibiotics, while showing a trend toward improved clinical outcomes. Therefore, practical strategies should also be considered in future clinical testing of AMPs as we have learned the following lessons:

(1) The application of AMPs can extend beyond FDA-approved clinical indications;
(2) Defining the most optimal dose and administration regimen might reduce cytotoxic effects of AMPs;
(3) Efficacy of AMPs can be demonstrated in equivalence or non-inferiority trials with an antibiotic as comparator;
(4) Bacterial resistance development should be included as one of the primary outcome parameters in clinical trials of AMPs;
(5) The bio-availability and efficacy of AMPs can be improved using delivery systems and,
(6) The combination AMPs with conventional antibiotics or other compounds (e.g., AMPs) might result in an improved antimicrobial effect in clinical trials.

Taking these lessons into consideration, an increasing number of AMPs could reach the market as multi-functional, potent and long-lasting antimicrobials against various infectious diseases.

AUTHOR CONTRIBUTIONS

GD wrote a draft version of the manuscript. MU, EM, and BB contributed to the design of the review and revised the manuscript. All authors assisted with the interpretation of the findings, read, and approved the final manuscript.

FUNDING

This collaborative project was funded by the Ministry of Economic Affairs through two public–private partnership (PPP) allowances, made available by Health-Holland and Top Sector life Sciences & Health. One of the PPP allowances was co-funded by the Dutch Burns Foundation, Madam Therapeutics B.V., Avivia B.V., Leiden University Medical Center, Amsterdam University Medical Center and the Association of Dutch Burn Centers (LSHM17078-SGF) and the other PPP allowance was co-funded by the Dutch Burns Foundation, Madam Therapeutics B.V., Mölnlycke Health Care AB, Leiden University Medical Center, Amsterdam University Medical Center and the Association of Dutch Burn Centers (LSH-TKI40-43100-98-017). These funders were not involved in the study design, collection, analysis, interpretation of data, the writing of this article or the decision to submit it for publication.

REFERENCES

Abraham, E. P., and Chain, E. (1940). An enzyme from bacteria able to destroy penicillin. *Nature* 146:837. doi: 10.1038/146837a0

Agier, J., Efenberger, M., and Brzezińska-Blaszczyk, E. (2015). Cathelicidin impact on inflammatory cells. *Cent. Eur. J. Immunol.* 40, 225–235. doi: 10.5114/ceji.2015.51359

Alam, M. Z., Wu, X., Mascio, C., Chesnel, L., and Hurdle, J. G. (2015). Mode of action and bactericidal properties of surotomycin against growing and nongrowing *Clostridium difficile*. *Antimicrob. Agents Chemother.* 59, 5165–5170. doi: 10.1128/aac.01087-15

Alni, R. H., Tavasoli, F., Barati, A., Badarbani, S. S., Salimi, Z., and Babaeekhou, L. (2020). Synergistic activity of melittin with mupirocin: a study against methicillin-resistant *S. aureus* (MRSA) and methicillin-susceptible *S. aureus* (MSSA) isolates. *Saudi J. Biol. Sci.* 27, 2580–2585. doi: 10.1016/j.sjbs.2020.05.027

Alves, E. M., Heneine, L. G. D., Pesquero, J. L., and de Merlo, L. A. (2011). *Pharmaceutical Composition Containin an Apitoxin Fraction and Use Thereof.* Google Patents No: WO2011041865. International Research Report (Art. 21 (3)).

Andersson, D. I., Hughes, D., and Kubicek-Sutherland, J. Z. (2016). Mechanisms and consequences of bacterial resistance to antimicrobial peptides. *Drug Resist. Updat.* 26, 43–57. doi: 10.1016/j.drup.2016.04.002

Arbeit, R. D., Maki, D., Tally, F. P., Campanaro, E., and Eisenstein, B. I. (2004). The safety and efficacy of daptomycin for the treatment of complicated skin and skin-structure infections. *Clin. Infect. Dis.* 38, 1673–1681. doi: 10.1086/420818

Arcilla, M. S., van Hattem, J. M., Matamoros, S., Melles, D. C., Penders, J., de Jong, M. D., et al. (2016). Dissemination of the mcr-1 colistin resistance gene. *Lancet Infect. Dis.* 16, 147–149. doi: 10.1016/s1473-3099(15)00540-x

Bacalum, M., and Radu, M. (2015). Cationic antimicrobial peptides cytotoxicity on mammalian cells: an analysis using therapeutic index integrative concept. *Int. J. Pept. Res. Ther.* 21, 47–55. doi: 10.1007/s10989-014-9430-z

Bahar, A. A., and Ren, D. (2013). Antimicrobial peptides. *Pharmaceuticals* 6, 1543–1575. doi: 10.3390/ph6121543

Ball, L. J., Goult, C. M., Donarski, J. A., Micklefield, J., and Ramesh, V. (2004). NMR structure determination and calcium binding effects of lipopeptide antibiotic daptomycin. *Org. Biomol. Chem.* 2, 1872–1878. doi: 10.1039/b402722a

Bartoloni, A., Mantella, A., Goldstein, B. P., Dei, R., Benedetti, M., Sbaragli, S., et al. (2004). In-vitro activity of nisin against clinical isolates of *Clostridium difficile*. *J. Chemother.* 16, 119–121. doi: 10.1179/joc.2004.16.2.119

Bastos, M. D. C. D. F., Coelho, M. L. V., and Santos, O. C. D. S. (2015). Resistance to bacteriocins produced by gram-positive bacteria. *Microbiology* 161, 683–700. doi: 10.1099/mic.0.082289-0

Batoni, G., Maisetta, G., and Esin, S. (2016). Antimicrobial peptides and their interaction with biofilms of medically relevant bacteria. *Biochim. Biophys. Acta Biomembr.* 1858, 1044–1060. doi: 10.1016/j.bbamem.2015.10.013

Beisswenger, C., and Bals, R. (2005). Functions of antimicrobial peptides in host defense and immunity. *Curr. Protein Pept. Sci.* 6, 255–264. doi: 10.2174/1389203054065428

Benet, L. Z. (1978). Effect of route of administration and distribution on drug action. *J. Pharmacokinet. Biopharm.* 6, 559–585. doi: 10.1007/BF01062110

Bergman, P., Walter-Jallow, L., Broliden, K., Agerberth, B., and Soderlund, J. (2007). The antimicrobial peptide LL-37 inhibits HIV-1 replication. *Curr. HIV Res.* 5, 410–415. doi: 10.2174/157016207781023947

Bertelsen, K., Dorosz, J., Hansen, S. K., Nielsen, N. C., and Vosegaard, T. (2012). Mechanisms of peptide-induced pore formation in lipid bilayers investigated by oriented 31P solid-state NMR spectroscopy. *PLoS One* 7:e47745. doi: 10.1371/journal.pone.0047745

BioSpace (2019). *Polyphor Temporarily Halts Enrollment in the Phase III Studies of Murepavadin for the Treatment of Patients with Nosocomial Pneumonia*.

Björn, C., Noppa, L., Näslund Salomonsson, E., Johansson, A. L., Nilsson, E., Mahlapuu, M., et al. (2015). Efficacy and safety profile of the novel antimicrobial peptide PXL150 in a mouse model of infected burn wounds. *Int. J. Antimicrob. Agents* 45, 519–524. doi: 10.1016/j.ijantimicag.2014.12.015

Blay, G., Le Lacroix, C., Zihler, A., and Fliss, I. (2007). In vitro inhibition activity of nisin A, nisin Z, pediocin PA-1 and antibiotics against common intestinal bacteria. *Lett. Appl. Microbiol.* 45, 252–257. doi: 10.1111/j.1472-765X.2007.02178.x

Blondelle, S. E., Ostresh, J. M., Houghten, R. A., and Perez-Paya, E. (1995). Induced conformational states of amphipathic peptides in aqueous/lipid environments. *Biophys J.* 68, 351–359. doi: 10.1016/S0006-3495(95)80194-3

Booth, J. H., Benrimoj, S. I., and Nimmo, G. R. (1994). *In vitro* interactions of neomycin sulfate, bacitracin, and polymyxin B sulfate. *Int. J. Dermatol.* 33, 517–520. doi: 10.1111/j.1365-4362.1994.tb02872.x

Bosscha, M. I., Van Dissel, J. T., Kuijper, E. J., Swart, W., and Jager, M. J. (2004). The efficacy and safety of topical polymyxin B, neomycin and gramicidin for treatment of presumed bacterial corneal ulceration. *Br. J. Ophthalmol.* 88, 25–28. doi: 10.1136/bjo.88.1.25

Boto, A., De La Lastra, J. M. P., and González, C. C. (2018). The road from host-defense peptides to a new generation of antimicrobial drugs. *Molecules* 23:311. doi: 10.3390/molecules23020311

Bray, B. L. (2003). Large-scale manufacture of peptide therapeutics by chemical synthesis. *Nat. Rev. Drug Discov.* 2, 587–593. doi: 10.1038/nrd1133

Brogden, K. A. (2005). Antimicrobial peptides: pore formers or metabolic inhibitors in bacteria? *Nat. Rev. Microbiol.* 3, 238–250. doi: 10.1038/nrmicro1098

Brown, K. L., Poon, G. F. T., Birkenhead, D., Pena, O. M., Falsafi, R., Dahlgren, C., et al. (2011). Host defense peptide LL-37 selectively reduces proinflammatory macrophage responses. *J. Immunol.* 186, 5497–5505. doi: 10.4049/jimmunol.1002508

Bulger, E. M., Maier, R. V., Sperry, J., Joshi, M., Henry, S., Moore, F. A., et al. (2014). A novel drug for treatment of necrotizing soft-tissue infections: a randomized clinical trial. *JAMA Surg.* 149, 528–536. doi: 10.1001/jamasurg.2013.4841

Carretero, M., Escámez, M. J., García, M., Duarte, B., Holguín, A., Retamosa, L., et al. (2008). In vitro and in vivo wound healing-promoting activities of human cathelicidin LL-37. *J. Invest. Dermatol.* 128, 223–236. doi: 10.1038/sj.jid.5701043

Chan, D. I., Prenner, E. J., and Vogel, H. J. (2006). Tryptophan- and arginine-rich antimicrobial peptides: structures and mechanisms of action. *Biochim. Biophys. Acta Biomembr.* 1758, 1184–1202. doi: 10.1016/j.bbamem.2006.04.006

Chen, C. H., and Lu, T. K. (2020). Development and challenges of antimicrobial peptides for therapeutic applications. *Antibiotics* 9:24. doi: 10.3390/antibiotics9010024

Cheng, M. P., Lawandi, A., Butler-Laporte, G., Paquette, K., and Lee, T. C. (2018). Daptomycin versus placebo as an adjunct to beta-lactam therapy in the treatment of *Staphylococcus aureus* bacteremia: study protocol for a randomized controlled trial. *Trials* 19, 1–10. doi: 10.1186/s13063-018-2668-6

Chennupati, S. K., Chiu, A. G., Tamashiro, E., Banks, C. A., Cohen, M. B., Bleier, B. S., et al. (2009). Effects of an LL-37-derived antimicrobial peptide in an animal model of biofilm *Pseudomonas* sinusitis. *Am. J. Rhinol. Allergy* 23, 46–51. doi: 10.2500/ajra.2009.23.3261

Choi, J. H., Jang, A. Y., Lin, S., Lim, S., Kim, D., Park, K., et al. (2015). Melittin, a honeybee venom-derived antimicrobial peptide, may target methicillin-resistant *Staphylococcus aureus*. *Mol. Med. Rep.* 12, 6483–6490. doi: 10.3892/mmr.2015.4275

Chu, H. L., Yu, H. Y., Yip, B. S., Chih, Y. H., Liang, C. W., Cheng, H. T., et al. (2013). Boosting salt resistance of short antimicrobial peptides. *Antimicrob. Agents Chemother.* 57, 4050–4052. doi: 10.1128/AAC.00252-13

Cisneros, J. M., Rosso-Fernández, C. M., Roca-Oporto, C., De Pascale, G., Jiménez-Jorge, S., Fernández-Hinojosa, E., et al. (2019). Colistin versus meropenem in the empirical treatment of ventilator-associated pneumonia (Magic Bullet study): an investigator-driven, open-label, randomized, noninferiority controlled trial. *Crit. Care* 23:383. doi: 10.1186/s13054-019-2627-y

Cleveland, J., Montville, T. J., Nes, I. F., and Chikindas, M. L. (2001). Bacteriocins: safe, natural antimicrobials for food preservation. *Int. J. Food Microbiol.* 71, 1–20. doi: 10.1016/s0168-1605(01)00560-8

Committee for Proprietary Medicinal Products (2001). Points to consider on switching between superiority and non-inferiority. *Br. J. Clin. Pharmacol.* 52:223. doi: 10.1046/J.0306-5251.2001.01397-3.X

Cornish, J., Callon, K. E., Lin, C. Q. X., Xiao, C. L., Mulvey, T. B., Cooper, G. J. S., et al. (1999). Trifluoroacetate, a contaminant in purified proteins, inhibits proliferation of osteoblasts and chondrocytes. *Am. J. Physiol. Endocrinol. Metab.* 277, E779–E783. doi: 10.1152/ajpendo.1999.277.5.E779

Crowther, G. S., Baines, S. D., Todhunter, S. L., Freeman, J., Chilton, C. H., and Wilcox, M. H. (2013). Evaluation of NVB302 versus vancomycin activity in an in vitro human gut model of *Clostridium difficile* infection. *J. Antimicrob. Chemother.* 68, 168–176. doi: 10.1093/jac/dks359

Csato, M., Kenderessy, A. S., and Dobozy, A. (1989). Enhancement of *Candida albicans* killing activity of separated human epidermal cells by α-melanocyte stimulating hormone. *Br. J. Dermatol.* 121, 145–147. doi: 10.1111/j.1365-2133.1989.tb01415.x

David, J. M., and Rajasekaran, A. K. (2015). Gramicidin A: a new mission for an old antibiotic. *J. Kidney Cancer VHL* 2, 15–24. doi: 10.15586/jkcvhl.2015.21

Dean, S. N., Bishop, B. M., and van Hoek, M. L. (2011). Susceptibility of *Pseudomonas aeruginosa* biofilm to alpha-helical peptides: D-enantiomer of LL-37. *Front. Microbiol.* 2:128. doi: 10.3389/fmicb.2011.00128

Delves-Broughton, J., Blackburn, P., Evans, R. J., and Hugenholtz, J. (1996). Applications of the bacteriocin, nisin. *Antonie Van Leeuwenhoek Int. J. Gen. Mol. Microbiol.* 69, 193–202. doi: 10.1007/BF00399424

Demetriades, D., Smith, J. S., Jacobson, L. E., Moncure, M., Minei, J., Nelson, B. J., et al. (1999). Bactericidal/permeability-increasing protein (rBPI21) in patients with hemorrhage due to trauma: results of a multicenter phase II clinical trial. *J. Trauma Inj. Infect. Crit. Care* 46, 667–677. doi: 10.1097/00005373-199904000-00018

Desai, N. (2013). *Stable Pexiganan Formulation*. Google Patents No, WO/2013/188286. International Research Report (Art. 21 (3)).

Di Nardo, A., Braff, M. H., Taylor, K. R., Na, C., Granstein, R. D., McInturff, J. E., et al. (2007). Cathelicidin antimicrobial peptides block dendritic cell TLR4 activation and allergic contact sensitization. *J. Immunol.* 178, 1829–1834. doi: 10.4049/jimmunol.178.3.1829

Dobias, J., Poirel, L., and Nordmann, P. (2017). Cross-resistance to human cationic antimicrobial peptides and to polymyxins mediated by the plasmid-encoded MCR-1?. *Clin. Microbiol. Infect.* 23, 676.e1–676.e5. doi: 10.1016/j.cmi.2017.03.015

Doi, K., Hu, X., Yuen, P. S. T., Leelahavanichkul, A., Yasuda, H., Kim, S. M., et al. (2008). AP214, an analogue of α-melanocyte-stimulating hormone, ameliorates sepsis-induced acute kidney injury and mortality. *Kidney Int.* 73, 1266–1274. doi: 10.1038/ki.2008.97

Dosler, S., Karaaslan, E., and Alev Gerceker, A. (2016). Antibacterial and anti-biofilm activities of melittin and colistin, alone and in combination with antibiotics against gram-negative bacteria. *J. Chemother.* 28, 95–103. doi: 10.1179/1973947815Y.0000000004

Dvorchik, B. H., Brazier, D., DeBruin, M. F., and Arbeit, R. D. (2003). Daptomycin pharmacokinetics and safety following administration of escalating doses once daily to healthy subjects. *Antimicrob. Agents Chemother.* 47, 1318–1323. doi: 10.1128/AAC.47.4.1318-1323.2003

Easton, D. M., Nijnik, A., Mayer, M. L., and Hancock, R. E. W. (2009). Potential of immunomodulatory host defense peptides as novel anti-infectives. *Trends Biotechnol.* 27, 582–590. doi: 10.1016/j.tibtech.2009.07.004

Ebenhan, T., Gheysens, O., Kruger, H. G., Zeevaart, J. R., and Sathekge, M. M. (2014). Antimicrobial peptides: their role as infection-selective tracers for molecular imaging. *Biomed Res. Int.* 2014:867381. doi: 10.1155/2014/867381

Eckert, R., Brady, K. M., Greenberg, E. P., Qi, F., Yarbrough, D. K., He, J., et al. (2006). Enhancement of antimicrobial activity against *Pseudomonas aeruginosa* by coadministration of G10KHc and tobramycin. *Antimicrob. Agents Chemother.* 50, 3833–3838. doi: 10.1128/AAC.00509-06

Eckert, R., Sullivan, R., and Shi, W. (2012). Targeted antimicrobial treatment to re-establish a healthy microbial flora for long-term protection. *Adv. Dent. Res.* 24, 94–97. doi: 10.1177/0022034512453725

Edgerton, M., Koshlukova, S. E., Araujo, M. W. B., Patel, R. C., Dong, J., and Bruenn, J. A. (2000). Salivary histatin 5 and human neutrophil defensin 1 kill *Candida albicans* via shared pathways. *Antimicrob. Agents Chemother.* 44, 3310–3316. doi: 10.1128/AAC.44.12.3310-3316.2000

Edsfeldt, S., Holm, B., Mahlapuu, M., Reno, C., Hart, D. A., and Wiig, M. (2017). PXL01 in sodium hyaluronate results in increased PRG4 expression: a potential mechanism for anti-adhesion. *Ups. J. Med. Sci.* 122, 28–34. doi: 10.1080/03009734.2016.1230157

Endermann, R., Vente, A., and Labischinski, H. (2007). "Friulimicin B, a cyclic lipopeptide, exhibits potent efficacy in a murine pneumococcal pneumonia model," in *Poster Presentation at the 47th Interscience Conference on Antimicrobial Agents and Chemotherapy*, Chicago.

Falagas, M. E., and Kasiakou, S. K. (2006). Toxicity of polymyxins: a systematic review of the evidence from old and recent studies. *Crit. Care* 10:R27.

Falagas, M. E., Kasiakou, S. K., Tsiodras, S., and Michalopoulos, A. (2006). The use of intravenous and aerosolized polymyxins for the treatment of infections in critically ill patients: a review of the recent literature. *Clin. Med. Res.* 4, 138–146. doi: 10.3121/cmr.4.2.138

Falanga, A., Lombardi, L., Franci, G., Vitiello, M., Iovene, M. R., Morelli, G., et al. (2016). Marine antimicrobial peptides: nature provides templates for the design of novel compounds against pathogenic bacteria. *Int. J. Mol. Sci.* 17:785. doi: 10.3390/ijms17050785

Fang, Z., Wusgal, L., Cheng, H., and Liang, L. (2017). "Natural biodegradable medical polymers: therapeutic peptides and proteins," in *Science and Principles of Biodegradable and Bioresorbable Medical Polymers: Materials and Properties*, ed. X. C. Zhang (Amsterdam: Elsevier Inc), 321–350. doi: 10.1016/B978-0-08-100372-5.00011-8

Fry, D. E. (2018). Antimicrobial peptides. *Surg. Infect.* 19, 804–811. doi: 10.1089/sur.2018.194

Fulco, P., and Wenzel, R. P. (2006). Ramoplanin: a topical lipoglycodepsipeptide antibacterial agent. *Expert Rev. Anti. Infect. Ther.* 4, 939–945. doi: 10.1586/14787210.4.6.939

Gajski, G., and Garaj-Vrhovac, V. (2013). Melittin: a lytic peptide with anticancer properties. *Environ. Toxicol. Pharmacol.* 36, 697–705. doi: 10.1016/j.etap.2013.06.009

Galar, A., Muñoz, P., Valerio, M., Cercenado, E., García-González, X., Burillo, A., et al. (2019). Current use of daptomycin and systematic therapeutic drug monitoring: clinical experience in a tertiary care institution. *Int. J. Antimicrob. Agents* 53, 40–48. doi: 10.1016/j.ijantimicag.2018.09.015

Gaussier, H., Morency, H., Lavoie, M. C., and Subirade, M. (2002). Replacement of trifluoroacetic acid with HCl in the hydrophobic purification steps of pediocin PA-1: a structural effect. *Appl. Environ. Microbiol.* 68, 4803–4808. doi: 10.1128/aem.68.10.4803-4808.2002

Genetic Engineering, and Biotechnology News (2016). *Dipexium's Diabet. Foot Ulcer Candidate Fail. Phase III Trials*. Available online at: https://www.genengnews.com/news/dipexiums-diabetic-foot-ulcer-candidate-fails-phase-iii-trials/ (accessed September 30, 2020).

Gentilucci, L., De Marco, R., and Cerisoli, L. (2010). Chemical modifications designed to improve peptide stability: incorporation of non-natural amino Acids, pseudo-peptide bonds, and cyclization. *Curr. Pharm. Des.* 16, 3185–3203. doi: 10.2174/138161210793292555

Giroir, B. P., Scannon, P. J., and Levin, M. (2001). Bactericidal/permeability-increasing protein—Lessons learned from the phase III, randomized, clinical trial of rBPI21 for adjunctive treatment of children with severe meningococcemia. *Crit. Care Med.* 29, S130–S135. doi: 10.1097/00003246-200107001-00039

Gordon, Y. J., Romanowski, E. G., and McDermott, A. M. (2005). A review of antimicrobial peptides and their therapeutic potential as anti-infective drugs. *Curr. Eye Res.* 30, 505–515. doi: 10.1080/02713680590968637

Gottler, L. M., and Ramamoorthy, A. (2009). Structure, membrane orientation, mechanism, and function of pexiganan—a highly potent antimicrobial peptide designed from magainin. *Biochim. Biophys. Acta Biomembr.* 1788, 1680–1686. doi: 10.1016/j.bbamem.2008.10.009

Gualillo, O., Lago, F., Gómez-Reino, J., Casanueva, F. F., and Dieguez, C. (2003). Ghrelin, a widespread hormone: insights into molecular and cellular regulation of its expression and mechanism of action. *FEBS Lett.* 552, 105–109. doi: 10.1016/s0014-5793(03)00965-7

Guinan, E. C., Barbon, C. M., Kalish, L. A., Parmar, K., Kutok, J., Mancuso, C. J., et al. (2011). Bactericidal/permeability-increasing protein (rBPI21) and fluoroquinolone mitigate radiation-induced bone marrow aplasia and death. *Sci. Transl. Med.* 3:110ra118. doi: 10.1126/scitranslmed.3003126

Guo, L., Mclean, J. S., Yang, Y., Eckert, R., Kaplan, C. W., Kyme, P., et al. (2015). Precision-guided antimicrobial peptide as a targeted modulator of human microbial ecology. *Proc. Natl. Acad. Sci. U.S.A.* 112, 7569–7574. doi: 10.1073/pnas.1506207112

Håkansson, J., Ringstad, L., Umerska, A., Johansson, J., Andersson, T., Boge, L., et al. (2019). Characterization of the in vitro, ex vivo, and in vivo efficacy of the antimicrobial peptide DPK-060 used for topical treatment. *Front. Cell. Infect. Microbiol.* 9:174. doi: 10.3389/fcimb.2019.00174

Hale, J. D. F., and Hancock, R. E. W. (2007). Alternative mechanisms of action of cationic antimicrobial peptides on bacteria. *Expert Rev. Anti. Infect. Ther.* 5, 951–959. doi: 10.1586/14787210.5.6.951

He, J., Yarbrough, D. K., Kreth, J., Anderson, M. H., Shi, W., and Eckert, R. (2010). Systematic approach to optimizing specifically targeted antimicrobial peptides against *Streptococcus mutans*. *Antimicrob. Agents Chemother.* 54, 2143–2151. doi: 10.1128/AAC.01391-09

Heinemann, B., and Williams, R. (1966). Inactivation of nisin by pancreatin. *J. Dairy Sci.* 49, 312–314. doi: 10.3168/jds.S0022-0302(66)87854-2

Hirunwiwatkul, P., and Wachirasereechai, K. (2005). Effectiveness of combined antibiotic ophthalmic solution in the treatment of hordeolum after incision and curettage: a randomized, placebo-controlled trial: a pilot study. *J. Med. Assoc. Thail.* 88, 647–650.

Hou, M., Zhang, N., Yang, J., Meng, X., Yang, R., Li, J., et al. (2013). Antimicrobial peptide LL-37 and IDR-1 ameliorate MRSA pneumonia in vivo. *Cell. Physiol. Biochem.* 32, 614–623. doi: 10.1159/000354465

Ingham, A. B., and Moore, R. J. (2007). Recombinant production of antimicrobial peptides in heterologous microbial systems. *Biotechnol. Appl. Biochem.* 47:207. doi: 10.1042/ba20060207

Isaksson, J., Brandsdal, B. O., Engqvist, M., Flaten, G. E., Svendsen, J. S. M., and Stensen, W. (2011). A synthetic antimicrobial peptidomimetic (LTX 109): stereochemical impact on membrane disruption. *J. Med. Chem.* 54, 5786–5795. doi: 10.1021/jm200450h

Ishida, H., Nguyen, L. T., Gopal, R., Aizawa, T., and Vogel, H. J. (2016). Overexpression of antimicrobial, anticancer, and transmembrane peptides in *Escherichia coli* through a calmodulin-peptide fusion system. *J. Am. Chem. Soc.* 138, 11318–11326. doi: 10.1021/jacs.6b06781

Itoh, H., Tokumoto, K., Kaji, T., Paudel, A., Panthee, S., Hamamoto, H., et al. (2017). Total synthesis and biological mode of action of WAP-8294A2: a menaquinone-targeting antibiotic. *J. Org. Chem.* 83, 6924–6935. doi: 10.1021/acs.joc.7b02318

Jiang, Z., Vasil, A. I., Hale, J. D., Hancock, R. E. W., Vasil, M. L., and Hodges, R. S. (2008). Effects of net charge and the number of positively charged residues on the biological activity of amphipathic α-helical cationic antimicrobial peptides. *Biopolym. Pept. Sci. Sect.* 90, 369–383. doi: 10.1002/bip.20911

Johansson, J., Gudmundsson, G. H., Rottenberg, M. E., Berndt, K. D., and Agerberth, B. (1998). Conformation-dependent antibacterial activity of the naturally occurring human peptide LL-37. *J. Biol. Chem.* 273, 3718–3724. doi: 10.1074/jbc.273.6.3718

Jorgensen, J. H., Crawford, S. A., Kelly, C. C., and Patterson, J. E. (2003). *In vitro* activity of daptomycin against vancomycin-resistant *Enterococci* of various van types and comparison of susceptibility testing methods. *Antimicrob. Agents Chemother.* 47, 3760–3763. doi: 10.1128/AAC.47.12.3760-3763.2003

Kampshoff, F., Willcox, M. D. P., and Dutta, D. (2019). A pilot study of the synergy between two antimicrobial peptides and two common antibiotics. *Antibiotics* 8:60. doi: 10.3390/antibiotics8020060

Kaplan, C. W., Sim, J. H., Shah, K. R., Kolesnikova-Kaplan, A., Shi, W., and Eckert, R. (2011). Selective membrane disruption: mode of action of C16G2, a specifically targeted antimicrobial peptide. *Antimicrob. Agents Chemother.* 55, 3446–3452. doi: 10.1128/AAC.00342-11

Khan, I., and Oh, D. H. (2016). Integration of nisin into nanoparticles for application in foods. *Innov. Food Sci. Emerg. Technol.* 34, 376–384. doi: 10.1016/j.ifset.2015.12.013

Kim, S. H., Nguyen, T. H., and Maynard, H. D. (2017). Polymeric drug conjugates by controlled radical polymerization. *Comprehens. Biomater. II* 4, 493–505. doi: 10.1016/B978-0-08-100691-7.00020-3

Kramer, N. E., Hasper, H. E., van den Bogaard, P. T. C., Morath, S., de Kruijff, B., Hartung, T., et al. (2008). Increased D-alanylation of lipoteichoic and a thickened septum are main determinants in the nisin resistance mechanism of *Lactococcus lactis*. *Microbiology* 154, 1755–1762. doi: 10.1099/mic.0.2007/015412-0

Kudrimoti, M., Curtis, A., Azawi, S., Worden, F., Katz, S., Adkins, D., et al. (2016). Dusquetide: a novel innate defense regulator demonstrating a significant and consistent reduction in the duration of oral mucositis in preclinical data and a randomized, placebo-controlled Phase 2a clinical study. *J. Biotechnol.* 239, 115–125. doi: 10.1016/j.jbiotec.2016.10.010

Kumarasamy, K. K., Toleman, M. A., Walsh, T. R., Bagaria, J., Butt, F., Balakrishnan, R., et al. (2010). Emergence of a new antibiotic resistance mechanism in India, Pakistan, and the UK: a molecular, biological, and epidemiological study. *Lancet Infect. Dis.* 10, 597–602. doi: 10.1016/S1473-3099(10)70143-2

Kwa, A., Kasiakou, S. K., Tam, V. H., and Falagas, M. E. (2007). Polymyxin B: similarities to and differences from colistin (polymyxin E). *Expert Rev. Anti. Infect. Ther.* 5, 811–821. doi: 10.1586/14787210.5.5.811

Lacey, K. A., Geoghegan, J. A., and McLoughlin, R. M. (2016). The role of *Staphylococcus aureus* virulence factors in skin infection and their potential as vaccine antigens. *Pathogens* 5:22. doi: 10.3390/pathogens5010022

Larrick, J. W., Hirata, M., Balint, R. F., Lee, J., Zhong, J., and Wright, S. C. (1995). Human CAP18: a novel antimicrobial lipopolysaccharide-binding protein. *Infect. Immun.* 63, 1291–1297. doi: 10.1128/iai.63.4.1291-1297.1995

Laverty, G. (2014). Cationic antimicrobial peptide cytotoxicity. *SOJ Microbiol. Infect. Dis.* 2:112. doi: 10.15226/sojmid.2013.00112

Le, C. F., Fang, C. M., and Sekaran, S. D. (2017). Intracellular targeting mechanisms by antimicrobial peptides. *Antimicrob. Agents Chemother.* 61:e02340-16. doi: 10.1128/AAC.02340-16

Le Lay, C., Dridi, L., Bergeron, M. G., Ouellette, M., and Fliss, I. I. (2016). Nisin is an effective inhibitor of *Clostridium difficile* vegetative cells and spore germination. *J Med Microbiol* 65, 169–175. doi: 10.1099/jmm.0.000202

Lee, G., and Bae, H. (2016). Anti-inflammatory applications of melittin, a major component of bee venom: detailed mechanism of action and adverse effects. *Molecules* 21:616. doi: 10.3390/molecules21050616

Leeds, J. A., Sachdeva, M., Mullin, S., Dzink-Fox, J., and LaMarche, M. J. (2012). Mechanism of action of and mechanism of reduced susceptibility to the novel anti-*Clostridium difficile* compound LFF571. *Antimicrob. Agents Chemother.* 56, 4463–4465. doi: 10.1128/aac.06354-11

Lenhard, J. R., Nation, R. L., and Tsuji, B. T. (2016). Synergistic combinations of polymyxins. *Int. J. Antimicrob. Agents* 48, 607–613. doi: 10.1016/j.ijantimicag.2016.09.014

Li, J., Koh, J.-J., Liu, S., Lakshminarayanan, R., Verma, C. S., and Beuerman, R. W. (2017). Membrane active antimicrobial peptides: translating mechanistic insights to design. *Front. Neurosci.* 11:73. doi: 10.3389/fnins.2017.00073

Li, J., and Nation, R. L. (2006). Old polymyxins are back: is resistance close? *Clin. Infect. Dis.* 43, 663–664. doi: 10.1086/506571

Li, J., Nation, R. L., Milne, R. W., Turnidge, J. D., and Coulthard, K. (2005). Evaluation of colistin as an agent against multi-resistant gram-negative bacteria. *Int. J. Antimicrob. Agents* 25, 11–25. doi: 10.1016/j.ijantimicag.2004.10.001

Li, M., Cha, D. J., Lai, Y., Villaruz, A. E., Sturdevant, D. E., and Otto, M. (2007). The antimicrobial peptide-sensing system aps of *Staphylococcus aureus*. *Mol. Microbiol.* 66, 1136–1147. doi: 10.1111/j.1365-2958.2007.05986.x

Liang, S. C., Tan, X. Y., Luxenberg, D. P., Karim, R., Dunussi-Joannopoulos, K., Collins, M., et al. (2006). Interleukin (IL)-22 and IL-17 are coexpressed by Th17 cells and cooperatively enhance expression of antimicrobial peptides. *J. Exp. Med.* 203, 2271–2279. doi: 10.1084/jem.20061308

Lipsky, B. A., Holroyd, K. J., and Zasloff, M. (2008). Topical versus systemic antimicrobial therapy for treating mildly infected diabetic foot ulcers: a randomized, controlled, double-blinded, multicenter trial of pexiganan cream. *Clin. Infect. Dis.* 47, 1537–1545. doi: 10.1086/593185

Liu, Y.-Y., Wang, Y., Walsh, T. R., Yi, L.-X., Zhang, R., Spencer, J., et al. (2016). Emergence of plasmid-mediated colistin resistance mechanism MCR-1 in animals and human beings in China: a microbiological and molecular biological study. *Lancet Infect. Dis.* 16, 161–168. doi: 10.1016/s1473-3099(15)00424-7

Luo, X.-L., Li, J.-X., Huang, H.-R., Duan, J.-L., Dai, R.-X., Tao, R.-J., et al. (2019). LL37 inhibits Aspergillus fumigatus infection via directly binding to the fungus and preventing excessive inflammation. *Front. Immunol.* 10:283. doi: 10.3389/fimmu.2019.00283

Mahlapuu, M., Håkansson, J., Ringstad, L., and Björn, C. (2016). Antimicrobial peptides: an emerging category of therapeutic agents. *Front. Cell. Infect. Microbiol.* 6:194. doi: 10.3389/fcimb.2016.00194

Malanovic, N., Leber, R., Schmuck, M., Kriechbaum, M., Cordfunke, R. A., Drijfhout, J. W., et al. (2015). Phospholipid-driven differences determine the action of the synthetic antimicrobial peptide OP-145 on Gram-positive bacterial and mammalian membrane model systems. *Biochim. Biophys. Acta Biomembr.* 1848, 2437–2447. doi: 10.1016/j.bbamem.2015.07.010

Marr, A. K., Gooderham, W. J., and Hancock, R. E. (2006). Antibacterial peptides for therapeutic use: obstacles and realistic outlook. *Curr. Opin. Pharmacol.* 6, 468–472. doi: 10.1016/j.coph.2006.04.006

Martin-Loeches, I., Dale, G. E., and Torres, A. (2018). Murepavadin: a new antibiotic class in the pipeline. *Expert Rev. Anti. Infect. Ther.* 16, 259–268. doi: 10.1080/14787210.2018.1441024

Matsuzaki, K. (1999). Why and how are peptide-lipid interactions utilized for self-defense? Magainins and tachyplesins as archetypes. *Biochim. Biophys. Acta Biomembr.* 1462, 1–10. doi: 10.1016/S0005-2736(99)00197-2

McCrudden, M. T. C., McLean, D. T. F., Zhou, M., Shaw, J., Linden, G. J., Irwin, C. R., et al. (2014). The host defence peptide LL-37 is susceptible to proteolytic degradation by wound fluid isolated from foot ulcers of diabetic patients. *Int. J. Pept. Res. Ther.* 20, 457–464. doi: 10.1007/s10989-014-9410-3

Meikle, T. G., Conn, C. E., Separovic, F., and Drummond, C. J. (2016). Exploring the structural relationship between encapsulated antimicrobial peptides and the bilayer membrane mimetic lipidic cubic phase: studies with gramicidin A′. *RSC Adv.* 6, 68685–68694. doi: 10.1039/c6ra13658c

Memariani, H., Memariani, M., Moravvej, H., and Shahidi-Dadras, M. (2020). Melittin: a venom-derived peptide with promising anti-viral properties. *Eur. J. Clin. Microbiol. Infect. Dis.* 39, 5–17. doi: 10.1007/s10096-019-03674-0

Mensa, B., Howell, G., Scott, R., and DeGrado, W. (2014). Comparative mechanistic studies of brilacidin, daptomycin, and the antimicrobial peptide LL16. *Antimicrob. Agents Chemother.* 58, 5136–5145. doi: 10.1128/AAC.02955-14

Mercer, D. K., Robertson, J. C., Miller, L., Stewart, C. S., and O'Neil, D. A. (2020). NP213 (Novexatin®): a unique therapy candidate for onychomycosis with a differentiated safety and efficacy profile. *Med. Mycol.* 58, 1064–1072. doi: 10.1093/mmy/myaa015

Midura-Nowaczek, K., and Markowska, A. (2014). Antimicrobial peptides and their analogs: searching for new potential therapeutics. *Perspect. Med. Chem.* 6:PMC.S13215. doi: 10.4137/PMC.S13215

Miller, L. S., Sørensen, O. E., Liu, P. T., Jalian, H. R., Eshtiaghpour, D., Behmanesh, B. E., et al. (2005). TGF-α regulates TLR expression and function on epidermal keratinocytes. *J. Immunol.* 174, 6137–6143. doi: 10.4049/jimmunol.174.10.6137

Mishra, B., Reiling, S., Zarena, D., and Wang, G. (2017). Host defense antimicrobial peptides as antibiotics: design and application strategies. *Curr. Opin. Chem. Biol.* 38, 87–96. doi: 10.1016/j.cbpa.2017.03.014

Mitra, D., Yadav, A., Prithyani, S., John, L. E., Rodrigues, S., and Shah, R. (2019). The antiplaque efficacy of lantibiotic Nisin extract mouthrinse. *J. Indian Soc. Periodontol.* 23, 31–34. doi: 10.4103/jisp.jisp_326_18

Miyake, O., Ochiai, A., Hashimoto, W., and Murata, K. (2004). Origin and diversity of alginate lyases of families PL-5 and -7 in *Sphingomonas* sp. strain A1. *J. Bacteriol.* 186, 2891–2896. doi: 10.1128/JB.186.9.2891-2896.2004

Mohamed, M. F., Abdelkhalek, A., and Seleem, M. N. (2016). Evaluation of short synthetic antimicrobial peptides for treatment of drug-resistant and intracellular *Staphylococcus aureus*. *Sci. Rep.* 6, 1–14. doi: 10.1038/srep29707

Montesinos, E., and Bardají, E. (2008). Synthetic antimicrobial peptides as agricultural pesticides for plant-disease control. *Chem. Biodivers.* 5, 1225–1237. doi: 10.1002/cbdv.200890111

Morrison, D. C., and Jacobs, D. M. (1976). Binding of polymyxin B to the lipid A portion of bacterial lipopolysaccharides. *Immunochemistry* 13, 813–818. doi: 10.1016/0019-2791(76)90181-6

Muchintala, D., Suresh, V., Raju, D., and Sashidhar, R. B. (2020). Synthesis and characterization of cecropin peptide-based silver nanocomposites: its antibacterial activity and mode of action. *Mater. Sci. Eng. C* 110:110712. doi: 10.1016/j.msec.2020.110712

Nagaoka, I., Suzuki, K., Niyonsaba, F., Tamura, H., and Hirata, M. (2012). Modulation of neutrophil apoptosis by antimicrobial peptides. *ISRN Microbiol.* 2012:345791. doi: 10.5402/2012/345791

Nagy, I., Pivarcsi, A., Kis, K., Koreck, A., Bodai, L., McDowell, A., et al. (2006). Propionibacterium acnes and lipopolysaccharide induce the expression of antimicrobial peptides and proinflammatory cytokines/chemokines in human sebocytes. *Microb. Infect.* 8, 2195–2205. doi: 10.1016/j.micinf.2006.04.001

Nell, M. J., Tjabringa, G. S., Wafelman, A. R., Verrijk, R., Hiemstra, P. S., Drijfhout, J. W., et al. (2006). Development of novel LL-37 derived antimicrobial peptides with LPS and LTA neutralizing and antimicrobial activities for therapeutic application. *Peptides* 27, 649–660. doi: 10.1016/j.peptides.2005.09.016

Neu, T., and Henrich, B. (2003). New thermosensitive delivery vector and its use to enable nisin-controlled gene expression in *Lactobacillus gasseri*. *Appl. Environ. Microbiol.* 69, 1377–1382. doi: 10.1128/AEM.69.3.1377-1382.2003

Nibbering, P. H., Ravensbergen, E., Welling, M. M., van Berkel, L. A., van Berkel, P. H. C., Pauwels, E. K. J., et al. (2001). Human lactoferrin and peptides derived from Its N terminus are highly effective against infections with antibiotic-resistant bacteria. *Infect. Immun.* 69, 1469–1476. doi: 10.1128/IAI.69.3.1469-1476.2001

Nordström, R., and Malmsten, M. (2017). Delivery systems for antimicrobial peptides. *Adv. Colloid Interf. Sci.* 242, 17–34. doi: 10.1016/j.cis.2017.01.005

Oo, T. Z., Cole, N., Garthwaite, L., Willcox, M. D. P., and Zhu, H. (2010). Evaluation of synergistic activity of bovine lactoferricin with antibiotics in corneal infection. *J. Antimicrob. Chemother.* 65, 1243–1251. doi: 10.1093/jac/dkq106

Ooi, N., Miller, K., Hobbs, J., Rhys-Williams, W., Love, W., and Chopra, I. (2009). XF-73, a novel antistaphylococcal membrane-active agent with rapid bactericidal activity. *J. Antimicrob. Chemother.* 64, 735–740. doi: 10.1093/jac/dkp299

Orlov, D., Hong, T., Menzel, L. P., Azimov, R., Falla, T. J., Waring, A. J., et al. (1805). "Bactericidal mechanism of iseganan (IB-367), a rapidly acting antimicrobial protegrin peptide," in *Proceedings of the 41st Annual Interscience Conference on Antimicrobial Agents and Chemotherapy*, Chicago.

Park, S.-C., Kim, J.-Y., Shin, S.-O., Jeong, C.-Y., Kim, M.-H., Shin, S. Y., et al. (2006). Investigation of toroidal pore and oligomerization by melittin using transmission electron microscopy. *Biochem. Biophys. Res. Commun.* 343, 222–228. doi: 10.1016/j.bbrc.2006.02.090

Perona, J. J., and Craik, C. S. (1997). Evolutionary divergence of substrate specificity within the chymotrypsin-like serine protease fold. *J. Biol. Chem.* 272, 29987–29990. doi: 10.1074/jbc.272.48.29987

Petrof, E. O., Dhaliwal, R., Manzanares, W., Johnstone, J., Cook, D., and Heyland, D. K. (2012). Probiotics in the critically ill: a systematic review of the randomized trial evidence. *Crit. Care Med.* 40, 3290–3302. doi: 10.1097/CCM.0b013e318260cc33

Peyrusson, F., Butler, D., Tulkens, P. M., and Van Bambeke, F. (2015). Cellular pharmacokinetics and intracellular activity of the novel peptide deformylase inhibitor GSK1322322 against *Staphylococcus aureus* laboratory and clinical strains with various resistance phenotypes: studies with human THP-1 monocytes and J774 murine macrophages. *Antimicrob. Agents Chemother.* 59, 5747–5760. doi: 10.1128/AAC.00827-15

Pfalzgraff, A., Brandenburg, K., and Weindl, G. (2018). Antimicrobial peptides and their therapeutic potential for bacterial skin infections and wounds. *Front. Pharmacol.* 9:281. doi: 10.3389/fphar.2018.00281

Phee, L. M., Betts, J. W., Bharathan, B., and Wareham, D. W. (2015). Colistin and fusidic acid, a novel potent synergistic combination for treatment of multidrug-resistant *Acinetobacter baumannii* infections. *Antimicrob. Agents Chemother.* 59, 4544–4550. doi: 10.1128/aac.00753-15

Piper, C., Hill, C., Cotter, P. D., and Ross, R. P. (2011). Bioengineering of a nisin A-producing *Lactococcus lactis* to create isogenic strains producing the natural variants Nisin F, Q and Z. *Microb. Biotechnol.* 4, 375–382. doi: 10.1111/j.1751-7915.2010.00207.x

Prajna, N. V., George, C., Selvaraj, S., Lu, K. L., McDonnell, P. J., and Srinivasan, M. (2001). Bacteriologic and clinical efficacy of ofloxacin 0.3% versus ciprofloxacin 0.3% ophthalmic solutions in the treatment of patients with culture-positive bacterial keratitis. *Cornea* 20, 175–178. doi: 10.1097/00003226-200103000-00013

Prince, A., Sandhu, P., Kumar, P., Dash, E., Sharma, S., Arakha, M., et al. (2016). Lipid-II independent antimicrobial mechanism of nisin depends on its crowding and degree of oligomerization. *Sci. Rep.* 6, 1–15. doi: 10.1038/srep37908

Rand, K. H., and Houck, H. J. (2004). Synergy of daptomycin with oxacillin and other β-lactams against methicillin-resistant *Staphylococcus aureus*. *Antimicrob. Agents Chemother.* 48, 2871–2875. doi: 10.1128/AAC.48.8.2871-2875.2004

Rivas-Santiago, B., Trujillo, V., Montoya, A., Gonzalez-Curiel, I., Castañeda-Delgado, J., Cardenas, A., et al. (2012). Expression of antimicrobial peptides in diabetic foot ulcer. *J. Dermatol. Sci.* 65, 19–26. doi: 10.1016/j.jdermsci.2011.09.013

Rodriguez, C. H., De Ambrosio, A., Bajuk, M., Spinozzi, M., Nastro, M., Bombicino, K., et al. (2010). In vitro antimicrobials activity against endemic *Acinetobacter baumannii* multiresistant clones. *J. Infect. Dev. Ctries.* 4, 164–167. doi: 10.3855/jidc.604

Rogers, J. M., and Suga, H. (2015). Discovering functional, non-proteinogenic amino acid containing, peptides using genetic code reprogramming. *Org. Biomol. Chem.* 13, 9353–9363. doi: 10.1039/c5ob01336d

Rosenfeld, Y., Papo, N., and Shai, Y. (2006). Endotoxin (lipopolysaccharide) neutralization by innate immunity host-defense peptides: peptide properties and plausible modes of action. *J. Biol. Chem.* 281, 1636–1643. doi: 10.1074/jbc.M504327200

Rubinchik, E., Dugourd, D., Algara, T., Pasetka, C., and Friedland, H. D. (2009). Antimicrobial and antifungal activities of a novel cationic antimicrobial peptide, omiganan, in experimental skin colonisation models. *Int. J. Antimicrob. Agents* 34, 457–461. doi: 10.1016/j.ijantimicag.2009.05.003

Ryu, S., Song, P., Seo, C., Cheong, H., and Park, Y. (2014). Colonization and infection of the skin by *S. aureus*: immune system evasion and the response to cationic antimicrobial peptides. *Int. J. Mol. Sci.* 15, 8753–8772. doi: 10.3390/ijms15058753

Sakamoto, I., Igarashi, M., Kimura, K., Takagi, A., Miwa, T., and Koga, Y. (2001). Suppressive effect of *Lactobacillus gasseri* OLL 2716 (LG21) on *Helicobacter* pylori infection in humans. *J. Antimicrob. Chemother.* 47, 709–710. doi: 10.1093/jac/47.5.709

Salmon, J. K., Armstrong, C. A., and Ansel, J. C. (1994). The skin as an immune organ. *West. J. Med.* 160, 146–152.

Sarma, P., Mahendiratta, S., Prakash, A., and Medhi, B. (2018). Specifically targeted antimicrobial peptides: a new and promising avenue in selective antimicrobial therapy. *Indian J. Pharmacol.* 50, 1–3. doi: 10.4103/ijp.IJP_218_18

Schmidtchen, A., Pasupuleti, M., and Malmsten, M. (2014). Effect of hydrophobic modifications in antimicrobial peptides. *Adv. Colloid Interf. Sci.* 205, 265–274. doi: 10.1016/j.cis.2013.06.009

Schneider, T., Gries, K., Josten, M., Wiedemann, I., Pelzer, S., Labischinski, H., et al. (2009). The lipopeptide antibiotic friulimicin B inhibits cell wall biosynthesis through complex formation with bactoprenol phosphate. *Antimicrob. Agents Chemother.* 53, 1610–1618. doi: 10.1128/AAC.01040-08

Schroder, G., Brandenburg, K., and Seydel, U. (1992). Polymyxin B induces transient permeability fluctuations in asymmetric planar lipopolysaccharide/phospholipid bilayers. *Biochemistry* 31, 631–638. doi: 10.1021/bi00118a001

Schultz, H., and Weiss, J. P. (2007). The bactericidal/permeability-increasing protein (BPI) in infection and inflammatory disease. *Clin. Chim. Acta* 384, 12–23. doi: 10.1016/j.cca.2007.07.005

Segev-Zarko, L., Saar-Dover, R., Brumfeld, V., Mangoni, M. L., and Shai, Y. (2015). Mechanisms of biofilm inhibition and degradation by antimicrobial peptides. *Biochem. J.* 468, 259–270. doi: 10.1042/BJ20141251

Severina, E., Severin, A., and Tomasz, A. (1998). Antibacterial efficacy of nisin against multidrug-resistant grampositive pathogens. *J. Antimicrob. Chemother.* 41, 341–347. doi: 10.1093/jac/41.3.341

Shin, J. M., Ateia, I., Paulus, J. R., Liu, H., Fenno, J. C., Rickard, A. H., et al. (2015). Antimicrobial nisin acts against saliva derived multi-species biofilms without cytotoxicity to human oral cells. *Front. Microbiol.* 6:617. doi: 10.3389/fmicb.2015.00617

Shurko, J. F., Galega, R. S., Li, C., and Lee, G. C. (2018). Evaluation of LL-37 antimicrobial peptide derivatives alone and in combination with vancomycin against *S. aureus*. *J. Antibiot.* 71, 971–974. doi: 10.1038/s41429-018-0090-7

Sikora, K., Jaśkiewicz, M., Neubauer, D., Bauer, M., Bartoszewska, S., Barańska-Rybak, W., et al. (2018). Counter-ion effect on antistaphylococcal activity and cytotoxicity of selected antimicrobial peptides. *Amino Acids* 50, 609–619. doi: 10.1007/s00726-017-2536-9

Sivertsen, A., Isaksson, J., Leiros, H.-K. S., Svenson, J., Svendsen, J.-S., and Brandsdal, B. O. (2014). Synthetic cationic antimicrobial peptides bind with their hydrophobic parts to drug site II of human serum albumin. *BMC Struct. Biol.* 14:4. doi: 10.1186/1472-6807-14-4

Son, D. J., Lee, J. W., Lee, Y. H., Song, H. S., Lee, C. K., and Hong, J. T. (2007). Therapeutic application of anti-arthritis, pain-releasing, and anti-cancer effects of bee venom and its constituent compounds. *Pharmacol. Ther.* 115, 246–270. doi: 10.1016/j.pharmthera.2007.04.004

Sørensen, O. E., Thapa, D. R., Roupé, K. M., Valore, E. V., Sjöbring, U., Roberts, A. A., et al. (2006). Injury-induced innate immune response in human skin mediated by transactivation of the epidermal growth factor receptor. *J. Clin. Invest.* 116, 1878–1885. doi: 10.1172/JCI28422

Srinivas, N., Jetter, P., Ueberbacher, B. J., Werneburg, M., Zerbe, K., Steinmann, J., et al. (2010). Peptidomimetic antibiotics target outer-membrane biogenesis in *Pseudomonas aeruginosa*. *Science* 327, 1010–1013. doi: 10.1126/science.1182749

Starr, C. G., He, J., and Wimley, W. C. (2016). Host cell interactions are a significant barrier to the clinical utility of peptide antibiotics. *ACS Chem. Biol.* 11, 3391–3399. doi: 10.1021/acschembio.6b00843

Steenbergen, J. N., Mohr, J. F., and Thorne, G. M. (2009). Effects of daptomycin in combination with other antimicrobial agents: a review of in vitro and animal model studies. *J. Antimicrob. Chemother.* 64, 1130–1138. doi: 10.1093/jac/dkp346

Stevens, K. A., Sheldon, B. W., Klapes, N. A., and Klaenhammer, T. R. (1991). Nisin treatment for inactivation of *Salmonella* species and other gram-negative bacteria. *Appl. Environ. Microbiol.* 57, 3613–3615. doi: 10.1128/aem.57.12.3613-3615.1991

Strömstedt, A. A., Pasupuleti, M., Schmidtchen, A., and Malmsten, M. (2009). Evaluation of strategies for improving proteolytic resistance of antimicrobial peptides by using variants of EFK17, an internal segment of LL-37. *Antimicrob. Agents Chemother.* 53, 593–602. doi: 10.1128/AAC.00477-08

Taylor, S. D., and Palmer, M. (2016). The action mechanism of daptomycin. *Bioorganic Med. Chem.* 24, 6253–6268. doi: 10.1016/j.bmc.2016.05.052

Taylor, T. M., Gaysinsky, S., Davidson, P. M., Bruce, B. D., and Weiss, J. (2007). Characterization of antimicrobial-bearing liposomes by ζ-potential, vesicle size, and encapsulation efficiency. *Food Biophys.* 2, 1–9. doi: 10.1007/s11483-007-9023-x

Tempera, G., Mangiafico, A., Genovese, C., Giudice, E., Mastrojeni, S., Nicolosi, D., et al. (2009). In vitro evaluation of the synergistic activity of neomycin-polymyxin b association against pathogens responsible for otitis externa. *Int. J. Immunopathol. Pharmacol.* 22, 299–302. doi: 10.1177/039463200902200206

Terwilligert, T. C., and Eisenbergg, D. (1982). The structure of Melittin. *J. Biol. Chem.* 257, 6016–6022.

Thwaite, J. E., Hibbs, S., Titball, R. W., and Atkins, T. P. (2006). Proteolytic degradation of human antimicrobial peptide LL-37 by *Bacillus anthracis* may contribute to virulence. *Antimicrob. Agents Chemother.* 50, 2316–2322. doi: 10.1128/AAC.01488-05

Todd, P., and Pierre, K. (2015). *GlobeNewswire. C3 Jian Complet. Second Phase 2 Clin. Trial Anti-Cavity Drug.* Available online at: https://www.globenewswire.com/news-release/2015/07/13/751454/0/en/C3-Jian-Completes-Second-Phase-2-Clinical-Trial-of-Anti-Cavity-Drug.html (accessed September 18, 2020).

Travis, S., Yap, L. M., Hawkey, C., Warren, B., Lazarov, M., Fong, T., et al. (2005). RDP58 is a novel and potentially effective oral therapy for ulcerative colitis. *Inflamm. Bowel Dis.* 11, 713–719. doi: 10.1097/01.mib.0000172807.26748.16

Ugurlu, T., Turkoglu, M., Gurer, U. S., and Akarsu, B. G. (2007). Colonic delivery of compression coated nisin tablets using pectin/HPMC polymer mixture. *Eur. J. Pharm. Biopharm.* 67, 202–210. doi: 10.1016/j.ejpb.2007.01.016

Valencia, R., Arroyo, L. A., Conde, M., Aldana, J. M., Torres, M.-J., Fernández-Cuenca, F., et al. (2009). Nosocomial outbreak of infection with pan-drug-resistant *Acinetobacter baumannii* in a tertiary care university hospital. *Infect. Control Hosp. Epidemiol.* 30, 257–263. doi: 10.1086/595977

Van Den Bogaart, G., Guzmán, J. V., Mika, J. T., and Poolman, B. (2008). On the mechanism of pore formation by melittin. *J. Biol. Chem.* 283, 33854–33857. doi: 10.1074/jbc.M805171200

Van Epps, H. L. (2006). René dubos: unearthing antibiotics. *J. Exp. Med.* 203:259. doi: 10.1084/jem.2032fta

Van Groenendael, R., Kox, M., Van Eijk, L. T., and Pickkers, P. (2018). Immunomodulatory and kidney-protective effects of the human chorionic gonadotropin derivate EA-230. *Nephron* 140, 148–151. doi: 10.1159/000490772

Wecke, T., Zühlke, D., Mäder, U., Jordan, S., Voigt, B., Pelzer, S., et al. (2009). Daptomycin versus friulimicin B: in-depth profiling of *Bacillus subtilis* cell envelope stress responses. *Antimicrob. Agents Chemother.* 53, 1619–1623. doi: 10.1128/AAC.01046-08

Welling, M., Brouwer, C., Roscini, L., Cardinali, G., Corte, L., Casagrande Pierantoni, D., et al. (2018). Structure-activity relationship study of synthetic variants derived from the highly potent human antimicrobial peptide hLF(1-11). *Cohesive J. Microbiol. Infect. Dis.* doi: 10.31031/CJMI.2018.01.000512

Wimley, W. C., and Hristova, K. (2011). Antimicrobial peptides: successes, challenges and unanswered questions. *J. Membr. Biol.* 239, 27–34. doi: 10.1007/s00232-011-9343-0

Woong, S. J., Xuewei, S. L., Sun, J. N., and Edgerton, M. (2008). The P-113 fragment of histatin 5 requires a specific peptide sequence for intracellular translocation in *Candida albicans*, which is independent of cell wall binding. *Antimicrob. Agents Chemother.* 52, 497–504. doi: 10.1128/AAC.01199-07

Wu, C.-L., Hsueh, J.-Y., Yip, B.-S., Chih, Y.-H., Peng, K.-L., and Cheng, J.-W. (2020). Antimicrobial peptides display strong synergy with vancomycin against vancomycin-resistant *E. faecium*, *S. aureus*, and wild-type *E. coli*. *Int. J. Mol. Sci.* 21:4578. doi: 10.3390/ijms21134578

Yang, C. H., Chen, Y. C., Peng, S. Y., Tsai, A. P. Y., Lee, T. J. F., Yen, J. H., et al. (2018). An engineered arginine-rich α-helical antimicrobial peptide exhibits broad-spectrum bactericidal activity against pathogenic bacteria and reduces bacterial infections in mice. *Sci. Rep.* 8, 1–14. doi: 10.1038/s41598-018-32981-3

Yasir, M., Dutta, D., Hossain, K. R., Chen, R., Ho, K. K. K., Kuppusamy, R., et al. (2020). Mechanism of action of surface immobilized antimicrobial peptides against *Pseudomonas aeruginosa*. *Front. Microbiol.* 10:3053. doi: 10.3389/fmicb.2019.03053

Yasir, M., Dutta, D., and Willcox, M. D. P. (2019). Mode of action of the antimicrobial peptide Mel4 is independent of *Staphylococcus aureus* cell membrane permeability. *PLoS One* 14:e0215703. doi: 10.1371/journal.pone.0215703

Yu, H. B., Kielczewska, A., Rozek, A., Takenaka, S., Li, Y., Thorson, L., et al. (2009). Sequestosome-1/p62 is the key intracellular target of innate defense regulator peptide. *J. Biol. Chem.* 284, 36007–36011. doi: 10.1074/jbc.c109.073627

Yu, K., Lo, J. C. Y., Yan, M., Yang, X., Brooks, D. E., Hancock, R. E. W., et al. (2017). Anti-adhesive antimicrobial peptide coating prevents catheter associated infection in a mouse urinary infection model. *Biomaterials* 116, 69–81. doi: 10.1016/j.biomaterials.2016.11.047

Yu, Z., Qin, W., Lin, J., Fang, S., and Qiu, J. (2015). Antibacterial mechanisms of polymyxin and bacterial resistance. *Biomed. Res. Int.* 2015:679109. doi: 10.1155/2015/679109

Zasloff, M. (2002). Antimicrobial peptides of multicellular organisms. *Nature* 415, 389–395. doi: 10.1038/415389a

Zavascki, A. P., Goldani, L. Z., Li, J., and Nation, R. L. (2007). Polymyxin B for the treatment of multidrug-resistant pathogens: a critical review. *J. Antimicrob. Chemother.* 60, 1206–1215. doi: 10.1093/jac/dkm357

Zhang, J., and Zhong, J. (2015). The journey of nisin development in China, a natural-green food preservative. *Protein Cell* 6, 709–711. doi: 10.1007/s13238-015-0214-9

Zhu, C., Zhao, J., Kempe, K., Wilson, P., Wang, J., Velkov, T., et al. (2017). A hydrogel-based localized release of colistin for antimicrobial treatment of burn wound infection. *Macromol. Biosci.* 17:1600320. doi: 10.1002/mabi.201600320

Conflict of Interest: The authors declare that the research was conducted in the absence of any commercial or financial relationships that could be construed as a potential conflict of interest.

frontiers in Microbiology

ORIGINAL RESEARCH
published: 24 February 2021
doi: 10.3389/fmicb.2021.622410

Antimicrobial Photodynamic Therapy Combined With Antibiotic in the Treatment of Rats With Third-Degree Burns

Zhanjuan Zhao[1,2], Jinduo Ma[3], Yiyi Wang[4], Zehua Xu[5], Lu Zhao[6], Jianxi Zhao[7], Ge Hong[2] and Tianjun Liu[2]**

[1] College of Basic Medicine, Hebei University, Baoding, China, [2] Tianjin Key Laboratory of Biomedical Material, Institute of Biomedical Engineering, Chinese Academy of Medical Sciences and Peking Union Medical College, Tianjin, China, [3] College of Clinical Medicine, Hebei University, Baoding, China, [4] College of Bioscience and Resources Environment, Beijing University of Agriculture, Beijing, China, [5] College of Public Health, Hebei University, Baoding, China, [6] Medical Oncology, Affiliated Hospital of Hebei University, Baoding, China, [7] Department of Radiology, Affiliated Hospital of Hebei University, Baoding, China

OPEN ACCESS

Edited by:
Rodolfo García-Contreras, National Autonomous University of Mexico, Mexico

Reviewed by:
Grzegorz Szewczyk, Jagiellonian University, Poland
Ahmed El-Hussein, Cairo University, Egypt
Mai Bingjie, Shaanxi Normal University, China

***Correspondence:**
Ge Hong
hongge@bme.pumc.edu.cn
Tianjun Liu
liutj@bme.pumc.edu.cn

Specialty section:
This article was submitted to Antimicrobials, Resistance and Chemotherapy, a section of the journal Frontiers in Microbiology

Received: *28 October 2020*
Accepted: *06 January 2021*
Published: *24 February 2021*

Citation:
Zhao Z, Ma J, Wang Y, Xu Z, Zhao L, Zhao J, Hong G and Liu T (2021) Antimicrobial Photodynamic Therapy Combined With Antibiotic in the Treatment of Rats With Third-Degree Burns. Front. Microbiol. 12:622410. doi: 10.3389/fmicb.2021.622410

Cationic porphyrin conjugate, protoporphyrin IX-methyl ethylenediamine derivative (PPIX-MED) has a potent photosensitive antibacterial effect on clinically isolated bacteria, including methicillin-resistant *Staphylococcus aureus*, (MRSA), *Escherichia coli*, and *Pseudomonas aeruginosa*. This study investigated (i) the PPIX-MED-mediated antimicrobial photodynamic effect on these three species *in vitro* and (ii) the effect of antimicrobial photodynamic therapy (aPDT) combined with the use of an antibiotic on the healing *in vivo* of third-degree burns of rats with the wounds infected by these bacterial species. PPIX-MED exerted a potent inhibitory effect on the growth of the three bacterial species by producing reactive oxygen species when photoactivated. PPIX-MED-mediated antimicrobial photodynamic therapy (PPIX-MED-aPDT) had high bacterial photoinactivation ability *in vitro*, with a minimum inhibitory concentration of 15.6 μM PPIX-MED against each of the three types of bacteria and minimum bactericidal concentrations of 31.25 μM against MRSA and *E. coli* and 62.5 μM against *P. aeruginosa.* In rats with third-degree burns infected by a mixture of these bacteria, the bactericidal efficiency of PPIX-MED–aPDT-combined-with-antibiotic treatment was higher than that of antibiotic or aPDT treatment alone. This was confirmed by analysis of viable bacterial counts in wound tissue and blood. Enzyme-linked immunosorbent assay revealed that aPDT-combined-with-antibiotic treatment resulted in an obvious reduction in tumor necrosis factor-alpha and interleukin-6 levels compared with the no-treatment control group and the other treatment groups. Immunohistochemistry revealed that the expression of basic fibroblast growth factor and CD31 (a marker of neovascularization), expressed in burn wound tissue was higher in the aPDT-combined-with-antibiotic treatment group than in the other groups. PPIX-MED–aPDT has a promising bactericidal effect both *in vitro* and *in vivo*, and PPIX-MED–aPDT-combined-with-antibiotic treatment enhanced the healing of infected third-degree burns in rats.

Keywords: antimicrobial effect, antimicrobial photodynamic therapy, photosensitizer, cationic porphyrins, burned, rats

INTRODUCTION

Antimicrobial drugs are overused, misused, and widely applied prophylactically, which results in the emergence of drug-resistant microorganisms (Park et al., 2012). Multidrug-resistant bacterial infections are a major challenge to healthcare and an important cause of morbidity and mortality in hospitalized patients (Hamblin et al., 2002; Oda et al., 2004; Davies and Davies, 2010; Jernigan et al., 2020). The skin is the first line of defense against invading pathogens; it acts as a physical barrier against microbial invasion. Burning causes a rupture in the skin and other epithelial layers, which exposes the individual to infection as open wounds allow bacteria to enter and are suitable environments for their survival (Oyama et al., 2020). Infection is a common problem in cutaneous wounds and a critical complication in wound healing (Oyama et al., 2020). All wounds will have some bacterial colonization. Methicillin-resistant *Staphylococcus aureus* (MRSA), *Escherichia coli*, and *Pseudomonas aeruginosa* are early colonizers, accounting for the majority of burn wound infections (Cetik Yildiz et al., 2019). Burn healing is a complex process that involves clotting, inflammation, granulation tissue formation, epithelialization, collagen synthesis, and tissue remodeling (de Vasconcelos Catão et al., 2015). A delay or failure in the treatment of wounds can lead to progressive bacterial colonization until the development of a systemic infection (Oyama et al., 2020). As such, anti-infection treatment is important for burn patients (Mai et al., 2017).

Antibiotic treatment has side effects, which are themselves a threat to the health of burn patients. For deep burn wounds, antibiotic use may hinder the regeneration of skin tissue and the treatment of edema. Therefore, the development of novel antibacterial therapies, especially for burn infections caused by multidrug-resistant bacteria, is urgently required. One treatment shown in the literature to be lethal to microbial pathogens and to accelerate the healing of burns is antimicrobial photodynamic therapy (aPDT) (Seegers et al., 2003; Mai et al., 2017). aPDT involves three components: oxygen, a photosensitizer, and laser light with a wavelength matching the absorption of the photosensitizer. aPDT is based upon energy transfer from light to oxygen to produce reactive oxygen species that are lethal to microbial pathogens (Bhatti et al., 1998; Tavares et al., 2010). The antibacterial activity of aPDT results from oxidative damage produced by singlet oxygen and other reactive species; bacteria will not be able to develop resistance to it (Hamblin et al., 2003; Luan et al., 2009; Dai et al., 2010; Park et al., 2012).

The photosensitizer is the crucial element in aPDT. Cationic photosensitizers are capable of efficiently killing Gram-negative bacteria, inhibiting the secretion of inflammatory factors, and promoting wound healing after infection of burns (Mai et al., 2017; Huang et al., 2018). We hypothesized that the protoporphyrin IX (PPIX) conjugation, which is cationic, can exhibit significant phototoxic activities against Gram-negative and Gram-positive bacteria. A few reports have been published on the effect of aPDT on burn healing (Garcia et al., 2010; de Vasconcelos Catão et al., 2015; Jernigan et al., 2020). Rat burn wounds infected with bacteria can progress to invasive and life-threatening infections, such as bacteremia, abscesses, pneumonia, and sepsis (Mai et al., 2017). In the treatment of burn infections, antibiotic medication should be administered throughout the body instead of local administration, which leads to a low concentration of antibiotics at the burn site, making it impossible to kill the bacteria completely. Therefore, aPDT, a beneficial supplement to antibiotic treatment, can directly act on the infected lesions to effectively achieve antibacterial and cleansing results. At the same time, the low-level laser irradiation can also promote wound healing (de Vasconcelos Catão et al., 2015). aPDT can be used externally, but the body needs its immune system, possibly also antibiotics, to resist bacteria internally. Using aPDT to remove surface bacteria and antibiotics to inhibit bacteria in the body, a small quantity of antibiotic can have a therapeutic effect.

The principal aim of this study was to evaluate the effectiveness of aPDT *in vivo* on healing of experimental rat burn wounds infected with a mixture of pathogenic bacteria. The wounds were treated by aPDT using the photosensitizer PPIX-MED (**Figure 1**) with and without additional intravenous antibiotic treatment (Hamblin et al., 2002; Oda et al., 2004; Davies and Davies, 2010; Jernigan et al., 2020).

MATERIALS AND METHODS

Chemicals and Instruments

The compound PPIX-MED was synthesized in the Key Laboratory of Biomedical Material, Institute of Biomedical Engineering, Peking Union Medical College, and Chinese Academy of Medical Sciences. The chemical structure of this porphyrin derivative is shown in **Figure 2**. A stock solution (500 μM) was prepared by dissolution in dimethylsulfoxide (DMSO) and was stored at −20°C in the dark before use.

Ceftriaxone sodium is a broad-spectrum antibiotic, which was provided by Harbin Pharmaceutical Group (Harbin, China).

Light Source

A semiconductor 650-nm laser (7404, Industry, United States) was selected for this study, and the light spot energy density was determined with an optical power meter (LM1; Carl Zeiss, Germany).

Photobleaching

Photobleaching was conducted with a Multimode Microplate Spectrophotometer (Lv et al., 2013). Briefly, dye and buffer solutions were prepared immediately before measurements. Samples (200 μl) of 2×10^{-5} M dye in 96-well microtiter plates were sealed with cover slips to avoid evaporation. Photobleaching measurements at 300–800 nm were conducted for 30 min at ambient temperature, and data were recorded every 5 min. The delivered light energy was 0.2 J/cm^2 per min, and the total light energy density was 6 J/cm^2.

Measurement of the Quantum Yield of Singlet Oxygen

Singlet oxygen quantum yield ($[\Phi_\Delta]$) experiments were performed according to Álvarez-Micó et al. (2007). Briefly,

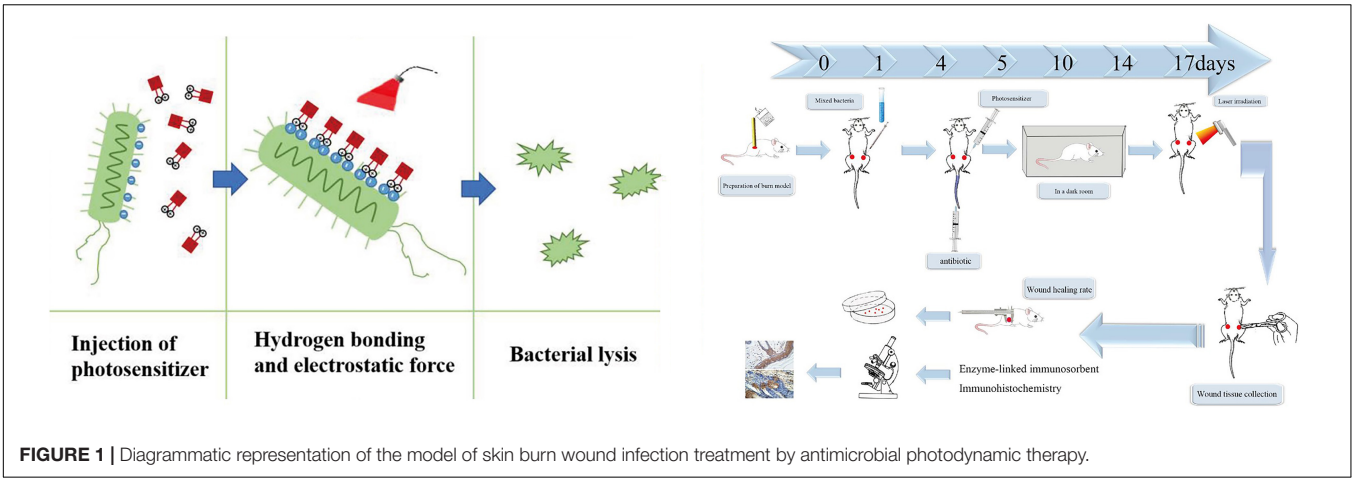

FIGURE 1 | Diagrammatic representation of the model of skin burn wound infection treatment by antimicrobial photodynamic therapy.

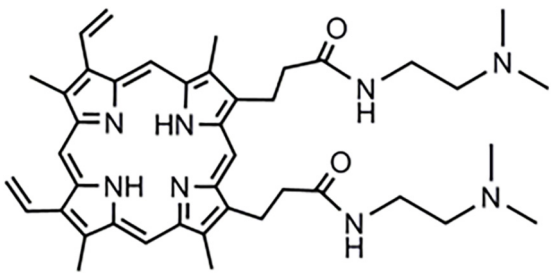

FIGURE 2 | Structure of ($C_{42}H_{54}N_8O_2$) dimethyl-8,13-divinyl-3,7,12,17-tetramethyl-21H, 23H-porphyrin-2,18-*bis*[-*N*-2-(dimethylamine)ethyl] propenamide (PPIX-MED).

$[\Phi_\Delta]$ was determined by the decomposition of 1,3-diphenyl isobenzofuran (DPBF) in DMSO; $[\Phi_\Delta]$ correlated with the decay of the absorption of DPBF at 410 nm (Lau et al., 2011). The sample was irradiated at 650 nm, 6 J/cm^2. Equation 1 was used to calculate the singlet oxygen generation, with 5,10,15,20-tetraphenylporphyrin (TPP) used as the reference ($[\Phi_\Delta^R] = 0.64$) (Álvarez-Micó et al., 2007).

$$\left[\Phi_\Delta^S = \Phi_\Delta^R \frac{K^S F^R}{K^R F^S}\right] \quad (1)$$

where $[\Phi_\Delta^R]$ is the singlet oxygen quantum yield for the reference, superscripts S and R indicate the sample and reference compound, respectively, K is the slope of the plot of change difference in absorbance of DPBF (at 410 nm) with irradiation time, and F is the absorption correction factor, which is given by $F = 1 - 10^{-OD}$, where OD is the absorbance at the irradiation wavelength.

Bacterial Culture

Three clinical bacterial strains – MRSA, *E. coli*, and *P. aeruginosa* – were isolated at the Tianjin Armed Police Hospital. Luria–Bertani (LB) medium was used to culture these bacterial strains. A single colony was used to inoculate 10 ml of liquid medium. The cells were grown at 37°C in aerobic conditions in a shaking incubator (200 rpm) until an optical density at 600 nm (OD_{600}) of approximately 0.7 was reached. The cells were then harvested by centrifugation and resuspended in an equal volume of phosphate-buffered saline (PBS) (Zhao et al., 2014).

Fibroblast Culture

Mouse fibroblast NIH 3T3 cells (SCSP-515) (Jainchill et al., 1969; Gong et al., 2018) were purchased from the Cell Bank of the Chinese Academy of Sciences (Shanghai, China). The cells were cultured in Dulbecco's modified Eagle's medium (Sigma-Aldrich, United Kingdom) containing 10% heat-inactivated fetal bovine serum (Gibco), penicillin (100 U/ml), and streptomycin (100 μg/ml) (Sigma-Aldrich) and incubated at 37°C in a humidified atmosphere of 5% CO_2 until the cell monolayer reached at least 80% confluence. The cells were washed with PBS and incubated for 3 min at 37°C with 0.05% trypsin and 0.02% ethylenediaminetetraacetic acid, seeded into 96-well cell culture plates (8×10^3–1×10^4 cells per well), and incubated overnight. All subsequent photoinactivation experiments involving these cells were performed in 96-well cell culture plates.

Cell Survival Assay

After 24 h of cell growth at 37°C in 5% CO_2, the cells were incubated with PPIX-MED at various concentrations (0, 3.9, 7.8, 15.6, and 31.25 μM) at 37°C for 30 min in the dark, then irradiated with 6 J/cm^2 light, and incubated overnight at 37°C. At 24 h after antimicrobial photodynamic therapy, 5 mg/ml 3-(4,5-dimethylthiazol-2-yl)2,5-diphenyl tetrazolium bromide (MTT) (Thermo Fisher, United States) was added to the cells, which were incubated at 37°C to allow cleavage of the tetrazolium ring by mitochondrial dehydrogenases and the formation of blue formazan crystals in living cells. After 3 h, the supernatant was removed, and the crystals were dissolved in DMSO. The absorption of formazan in each well was determined at 490 nm using a microplate reader (Thermo, Varioskan Flash Multimode Reader). All assays were performed in the dark (Kashef et al., 2012; Ahmed Alamoudi et al., 2018).

Dose-Dependent Photoinactivation Effects

The number of bacterial colonies is described in terms of the number of colony-forming units (CFU). Mixtures of 1×10^7 CFU/ml bacterial suspension and different concentrations of PPIX-MED (0, 3.9, 7.8, 15.6, and 31.25 μM) were added to a 96-well plate, incubated in the dark at 37°C for 30 min, and then irradiated with laser at 6 J/cm^2. After that, 100 μl of the mixture was taken from each well, and a gradient dilution (1×10^{-1}, 1×10^{-2}, 1×10^{-3}, 1×10^{-4}, and 1×10^{-5}) was spread on LB agar plates, which were incubated at 37°C for 18 h in the dark. Then, the number of CFU was counted. The experiment was repeated three times. Bacterial survival fractions were expressed as the ratio of the number of CFU of bacteria treated with light and photosensitizer to the number of CFU of untreated bacteria (Grinholc et al., 2008).

Uptake Assay

Uptake experiments were performed according to the method of Soukos et al. (1998). In general, 1 ml bacterial suspension was centrifuged (9000 × *g*, 1 min), and the cells were resuspended in PBS to OD_{600} = 0.7. PPIX-MED was added to final concentrations of 3.91–62.5 μM. The mixture was incubated in the dark for 30 min at ambient temperature and centrifuged at 9000 × *g* for 1 min; then, the cells were washed with PBS to remove residual photosensitizer. The bacterial pellet was dissolved in 1 ml 10% aqueous sodium lauryl sulfate solution and left for 24 h to fully release the absorbed photosensitizer. The uptake of photosensitizer by the bacteria was determined by a fluorescence assay. The PPIX-MED fluorescence was read (λ_{ex} = 406 nm, λ_{em} = 604 nm) and normalized as described above. A standard curve was obtained by plotting known concentrations of the target compound against the fluorescence intensity. The uptake amount was calculated by comparing the determined fluorescence intensity with the standard curve. A blank control group without photosensitizer was also used.

Determination of Minimum Inhibitory Concentration and Minimum Bactericidal Concentration

The three bacterial strains used in this study were treated with the same procedure; as an example, the treatment of MRSA is described in detail. Experiments were performed in 96-well flat-bottomed plates. Twenty microliters of MRSA suspension and 180 μl of the PPIX-MED compounds were added to each well. The final concentration of bacteria in the mixture was 10^6 CFU/ml. PPIX-MED was prepared at 1.95, 3.9, 7.8, 15.6, 31.25, 62.5, 125, 250, and 500 μM. The plates were kept in the dark for 30 min at 37°C and then exposed to light for 30 min or kept in the dark to provide dark control samples. Then, the samples were incubated in the dark at 37°C, and the number of CFU was evaluated after 18 h. Three sets of independent experiments were performed (Rodrigues et al., 2013).

Fractional Inhibitory Concentration Index

To determine the fractional inhibitory concentration index (FICI), ultrapure water was used to dissolve the ceftriaxone sodium and PPIX-MED so as to give stock concentrations of 4, 2, 0.5, and 0.25 MIC. Using the checkerboard design method, 50 μl of each drug was added at different concentrations in the horizontal and vertical columns of a 96-well plate, respectively. Then, 100 μl of bacterial (10^6 CFU/ml) suspension was added and mixed by slight shaking. The plates were kept in the dark for 30 min at 37°C and then exposed to light for 30 min. After light exposure, the samples were incubated in the dark at 37°C for 16–20 h. The MIC of each antimicrobial in the combination was read and interpreted using previously described methods. For each antimicrobial combination, we calculated the FICI by computing the ratio of the MIC of the combination divided by the MIC of the antimicrobial alone for each agent and then adding those two ratios together (see Equation 2). The FICI data were interpreted using the following criteria: synergy, FICI $\leq$ 0.5; indifference, FICI 0.5–4.0; and antagonism, FICI $>$ 4.0 (Barbee et al., 2014).

$$\mathrm{FICI} = \left[\frac{\mathrm{MIC_{A(with\ B)}}}{\mathrm{MIC_{A(alone)}}}\right] + \left[\frac{\mathrm{MIC_{B(with\ A)}}}{\mathrm{MIC_{B(alone)}}}\right] \quad (2)$$

Imaging by Confocal Laser Scanning Microscopy

The bacterial strains were suspended in PBS to an appropriate cell density (OD_{600} = 0.7), and then they were treated with 25 μM PPIX-MED for 30 min at room temperature. The cells were then harvested by centrifugation (9000 × *g*, 1 min), washed twice with PBS, and resuspended. One drop of this suspension was placed onto a confocal dish and allowed to dry. Fluorescent images were taken with a confocal laser scanning microscope (LSM510; Carl Zeiss), with excitation at 405 nm and emission at 650 nm (Zhao et al., 2014).

PPIX-MED–aPDT *in vivo*

Third-Degree Burn Wound Model and Establishment of Infection

The effects of PPIX-MED–aPDT on burn wound healing were evaluated using a rat model. All animal experiment procedures were experimented according to the National Institutes of Health Guide for Care and Use of Laboratory Animals, and the protocol was approved by the Laboratory Animal Management Committee/Laboratory Animal Welfare Ethics Committee, Institute of Radiation Medicine, Chinese Academy of Medical Sciences.

Sprague–Dawley rats from Beijing HFK Bioscience Co., Ltd., weighing about 220 g, were housed at one rat per cage and maintained in the dark except during aPDT treatment. The rats were first anesthetized via intraperitoneal injection of 1% sodium pentobarbital (80 mg/kg). Then, their back was shaved with an electric razor, followed by the use of a depilatory agent. In sterile conditions, a hollow round tube with a diameter of 30 mm was tightly attached to the back of the rat. Then, 50 ml of boiling water was poured into the empty pipe for 20 s. On each side, a burn

wound was made; the left and right sides were symmetrical. After the scalding, an abdominal injection of normal saline (40 ml/kg) was used to resist shock. Immediately after that, a suspension (50 μl) of mixed bacteria (10^9 CFU/ml MRSA, 5×10^8 CFU/ml *E. coli*, and 5×10^8 CFU/ml *P. aeruginosa*) in sterile PBS was inoculated onto the surface of each wound with a pipette tip and then smeared onto the wound surface with an inoculating loop. Then, the rats were used as wound model for mixed bacterial infection.

Photodynamic Treatment Protocol

Forty rats with burn wounds infected by mixed bacteria as described above were randomly divided into four groups: (A) no treatment (control group), (B) aPDT group (100 μl PPIX-MED each wound + laser treatment), (C) antibiotic group (intravenous injection of ceftriaxone 0.8 ml; ceftriaxone sodium was diluted to a concentration of 200 mg/kg in ultrapure water medium immediately before use), and (D) aPDT + antibiotic group (100 μl PPIX-MED each wound + laser therapy + intravenous injection of antibiotic 0.8 ml mixed treatment).

At 24 h after infection, 100 μl of PPIX-MED solution [four times of minimum bactericidal concentration (MBC) against *P. aeruginosa*] was injected under the eschar of the wound of rats in groups B and D. Then, after 30 min, these rats were illuminated with a 650-nm laser for 10 min (total light energy density 60 J/cm^2). On the next day, the same light dose was given to increase the effect of PPIX-MED–aPDT, but no more PPIX-MED was administered. This treatment is defined as one treatment. The above-mentioned treatment was repeated four times (total treatment days = 8). In groups C and D, the rats underwent a tail intravenous injection of ceftriaxone 0.8 ml once every 2 days; the above-mentioned treatment was repeated four times.

Bacterial Loads

To determine the bacterial counts in tissue samples at 4, 10, and 14 days post-infection, 10% tissue homogenates was serially diluted in PBS (1:10, 1:100, 1:1,000, 1:10,000, 1:100,000, and 1:1,000,000) and plated on a common broth–agar plate in triplicate. The plates were then incubated for at least 18 h at 37°C in a humidified atmosphere. Colony counts were expressed as $\log_{10}$ CFU per gram of tissue or milliliter of wound fluid.

The Rate of Wound Healing

After the treatment, wound healing was observed, and the width and length of the wounds were measured using a vernier caliper on days 5, 10, 14, and 17 post-infection. The rate of wound healing of each group after infection was recorded.

Blood Culture

After 4, 10, and 14 days post-infection, 1 ml of blood was extracted from the femoral vein of rats in sterile conditions, then placed in a test tube containing 9 ml of liquid LB medium, mixed thoroughly, and placed in an incubator at 37°C. After 3 days, 100 μl of ordinary coating inoculated on agar plates was taken and incubated for 24 h. If there was bacterial growth, the blood culture was considered positive.

Enzyme-Linked Immunosorbent Assay

ELISA was performed as described by Zhang et al. (2015). Resected skin tissue samples were frozen in liquid nitrogen, pulverized or homogenized, and digested in a tissue lysis reagent. Tumor necrosis factor (TNF-α) and interleukin-6 (IL-6) production at the skin injury site was quantified using ELISAs in accordance with the manufacturer's protocols (R&D Systems, Minneapolis, MN, United States).

Immunohistochemistry of Wound Tissue

After 4, 10, and 17 days post-infection, the skin granulation tissue at the forefront of the new epithelium was removed from the wound in aseptic conditions. Immunohistochemistry (IHC) was performed to evaluate the expression of basic fibroblast growth factor (bFGF) and CD31. Anti-bFGF (cat. no. ZA-0568) and anti-CD31 (cat. no. ZA-0558) were purchased from Cell Signaling Technology (Boston, MA, United States) and OriGene Technologies Inc. (Rockville, MD, United States), respectively. IHC was performed as previously described (Tan et al., 2019). PBS was used for the negative controls. Staining was observed under a Nikon microscope (Nikon Corporation).

Statistical Analysis

Data are presented as mean ± standard deviation ($\bar{x} + s$). The significance of differences between sample means was determined by least significant difference *t*-tests or χ^2 test using SPSS19.0 software (SPSS Inc., Chicago, IL, United States).

RESULTS

Photostability of PPIX-MED and Singlet Oxygen Yield

Photostability is a vital property of a photosensitizer and is determined by assessing photobleaching. Exposure of porphyrin derivatives to light may cause photochemical destruction of the tetrapyrrolic macrocycle, resulting in a decrease in the intensity of the Soret absorbance band at approximately 420 nm.

The maximum absorption of PPIX-MED (at 418 nm) decreased slightly over time, but after irradiation with 650-nm light (6 J/cm^2) for 30 min, the optical density of PPIX-MED changed by <1.9% (**Figure 3**). Thus, PPIX-MED is a photosensitizer with relatively high photostability.

An ideal photosensitizer should achieve a high singlet oxygen yield. In this study, DPBF was used as a reducing agent to trap singlet oxygen ($^1O_2$), and TPP was used as a reference compound to generate $^1O_2$. [Φ_Δ] for PPIX-MED reached 0.69 when a mixture of DPBF (2×10^{-5} mol/l) and PPIX-MED was irradiated with a 650-nm semiconductor laser (6 J/cm^2). The DPBF decay rate was higher in the presence of PPIX-MED than TPP, revealing that PPIX-MED was more efficient than TPP in producing singlet oxygen.

Uptake of PPIX-MED by Bacteria

The aPDT efficacy shows a high correlation with the amount of the photosensitizer taken up by bacteria; accordingly, a long-enough incubation time is required (Xuan et al., 2019). Bacterial

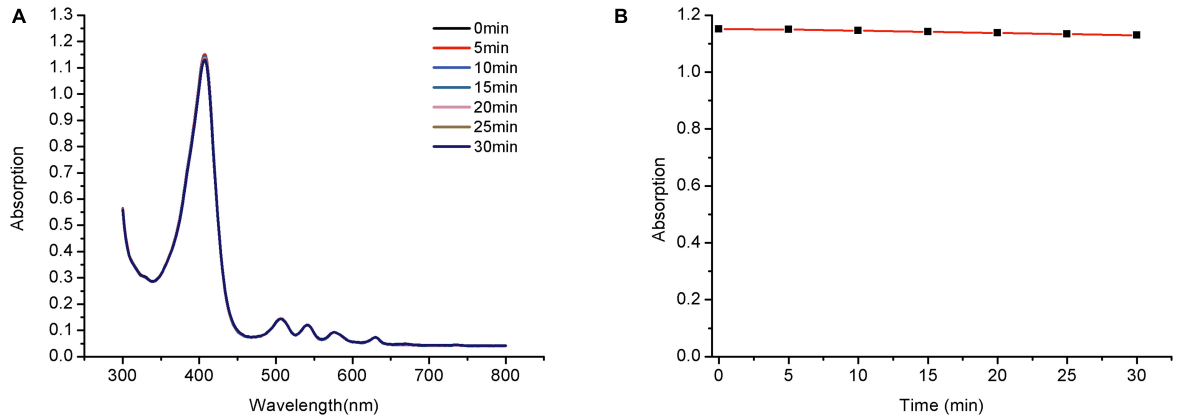

FIGURE 3 | Photobleaching of PPIX-MED. Photostability of PPIX-MED with irradiation time (2×10^{-5} mol/l PPIX-MED, 0.2 J/cm^2 per min). **(A)** The absorption spectrum of compound PPIX-MED from 0 to 30 min. **(B)** The absorbance change of compound PPIX-MED against irradiation time at the maximum absorption wavelength.

culture was incubated with PPIX-MED (6.25 μM) for 320 min, and the absorption of the photosensitizer by the bacteria was experimentally determined by spectrophotometry (Zhao et al., 2014). The uptake of PPIX-MED by the three bacterial species used in this study was dose- and time-dependent (**Figure 4**). **Figure 4B** shows that the three bacterial strains could absorb the maximum amount of the PPIX-MED in 30 min. Accordingly, 30 min was used as the incubation time for photoreaction and dark control reactions in subsequent *in vitro* and *in vivo* experiments in this work.

MIC and MBC Determinations

The MIC and the MBC of PPIX-MED toward the test bacteria were studied. Bacterial suspensions (10^6 CFU/ml) were incubated with PPIX-MED in the dark for 30 min at 37°C and then exposed to light (650 nm, 6 J/cm^2). The concentration of PPIX-MED required to make the suspensions change visibly from turbid to clear was regarded as the MIC, while the concentration at which five colonies or less were observed on plates was regarded as the MBC. As shown in **Table 1**, PPIX-MED had high bacterial photoinactivation ability, with an MIC of 15.6 μM for each of MRSA, *E. coli*, and *P. aeruginosa*. The MBC values were 31.25 μM for MRSA, 31.25 μM for *E. coli*, and 62.5 μM for *P. aeruginosa*. Meanwhile, the dark toxicity of PPIX-MED was relatively low, with MIC and MBC values > 500 μM for the three strains. From the MBC values, it can be concluded that PPIX-MED–aPDT is very effective against *E. coli*, *P. aeruginosa*, and MRSA. Thus, PPIX-MED is a good compound to evaluate in the treatment of bacterially infected burn wounds.

Fractional Inhibitory Concentration Index

The Etest results on the effect of combining ceftriaxone sodium with PPIX-MED–aPDT are summarized in **Table 2**. The average FICI for MRSA for ceftriaxone sodium in combination with

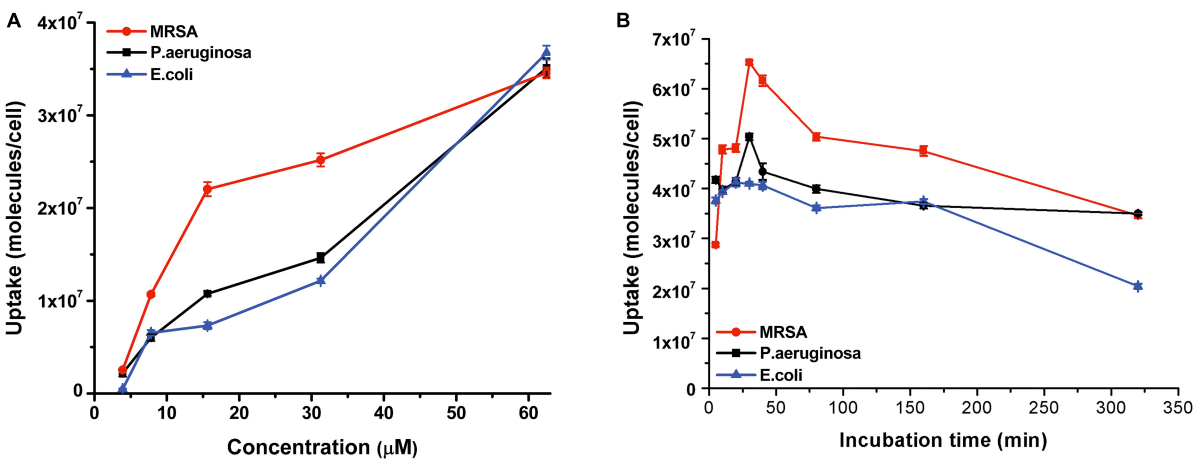

FIGURE 4 | PPIX-MED was taken up by three bacterial strains. **(A)** Bacterial culture was incubated with PPIX-MED (3.91–62.5 μM) in the dark for 30 min at ambient temperature. **(B)** Bacterial culture was incubated with PPIX-MED (6.25 μM) for 320 min.

TABLE 1 | Minimum inhibitory concentration (MIC, μM) and minimum bactericidal concentration (MBC, μM) of PPIX-MED against methicillin-resistant *Staphylococcus aureus*, *Pseudomonas aeruginosa*, and *Escherichia coli*.

PPIX-MED	6 J/cm^2		0 J/cm^2	
	MIC	MBC	MIC	MBC
MRSA	15.6	31.25	500	>500
P. aeruginosa	15.6	62.5	>500	>500
E. coli	15.6	31.25	>500	>500

PPIX-MED was 1.0. Thus, no synergy or antagonism was seen with the combination. The average FICI for *P. aeruginosa* was 0.625, indicating that an additive effect occurred with the combination, and the average FICI for *E. coli* was 0.75, again indicating an additive effect.

In vitro Photoinactivation of Bacteria Mediated by PPIX-MED

To delve into the photoinactivation effects of PPIX-MED against MRSA, *E. coli*, and *P. aeruginosa*, two experiments were performed: PPIX-MED treatment only and PPIX-MED + light treatment. **Figure 5A** shows the photodynamic efficacy of the photosensitizer against the three bacterial suspensions. In the PPIX-MED-only group, the bacterial survival rate decreased slightly, indicating that PPIX-MED alone had only a weak effect on the growth of the three bacterial strains tested in this study. When the bacterial suspensions were respectively incubated with PPIX-MED in the dark for 30 min at 37°C and then illuminated by the 650-nm laser (6 J/cm^2), the photoinactivation effect of PPIX-MED against MRSA, *E. coli*, and *P. aeruginosa* was PPIX-MED dose dependent. A sharp decrease in bacterial survival fraction was observed with an increase of the PPIX-MED concentration. The activity of the bacteria was largely inhibited in the concentration range 0–31.25 μM PPIX-MED, and the inhibition rate was >99% at 31.25 μM for *E. coli* and *P. aeruginosa* (which are Gram-negative bacteria) and 15.6 μM for MRSA (a Gram-positive bacterium). The results reveal that PPIX-MED displayed highly efficient photoinactivation toward these three bacterial species.

Phototoxicity of PPIX-MED Toward NIH 3T3 Cells

NIH 3T3 fibroblast cells were used as an example of normal mammalian cells to assess the phototoxicity of PPIX-MED via the MTT assay. NIH 3T3 cells were incubated with PPIX-MED in identical conditions to those used for MRSA, *E. coli*, and *P. aeruginosa*. The phototoxicity of PPIX-MED was concentration dependent (**Figure 5B**). In dark conditions, the cell survival of NIH 3T3 could reach >70% in the PPIX-MED concentration range 0–31.25 μM. After irradiation (6 J/cm^2), the NIH 3T3 cell activity exceeded 10.6% at 31.25 μM PPIX-MED, at which concentration the three bacterial strains were almost fully eliminated.

Confocal Laser Scanning Microscopy Images of Three Kinds of Bacteria Treated With PPIX-MED

Uptake of PPIX-MED by the three species of bacteria was examined by confocal laser scanning microscopy. Porphyrin conjugates emit red fluorescence at 650 nm when excited at 405 nm, which can be readily monitored with a fluorescence microscope system (Hamblin et al., 2003). The images in **Figure 6** confirm that PPIX-MED was internalized by the bacteria after incubation for only 30 min. The fluorescence imaging of *E. coli*, *P. aeruginosa*, or MRSA incubated with PPIX-MED was consistent with the dose-dependent photoinactivation effects.

In vivo Experiments

The Wounds and Healing Rates

To monitor the wound healing process, the leakage quantity of burn wounds, the presence of secretions, and healing range were observed at different times after infection. At 1 day after infection, the wounds of rats in the treated groups and the control group (no treatment) showed pale necrosis, the skin became hard and convex, and the wound surface showed bloody scabs and necrotic tissue coverage and congestion. At 4 days after infection, the untreated (control group) animals showed wound decay and ulceration. However, in the aPDT group and the aPDT-combined-with-antibiotic group, the skin was smooth, the wound scab was black and dry, and the wounds were better than in the antibiotic-only treatment group. At 10 days after infection, the wounds of the rats in the untreated control group were beginning to heal, but they were still very large and there was pus under the scab. Wound healing in the antibiotic-only treatment group was better than that in the untreated group. The scab did not fall off. It was gray, and there was pus underneath. In the aPDT and aPDT-combined-with-antibiotic treatment groups, all the scabs fell off, and new pink tissues were exposed.

TABLE 2 | Etest minimum inhibitory concentrations (median and range) of ceftriaxone sodium and PPIX-MED alone and in combination.

	MIC (μg/ml)				FICI▲	Interpretation
	MIC_A	$MIC_{A(withB)}$	MIC_B	$MIC_{B(withA)}$		
MRSA	128 μg/ml	64 μg/ml	16 μM	8 μM	1	Indifference
P. aeruginosa	32 μg/ml	16 μg/ml	32 μM	4 μM	0.625	Indifference
E. coli	64 μg/ml	16 μg/ml	32 μM	16 μM	0.75	Indifference

MIC_A, ceftriaxone sodium; MIC_B, PPIX-MED; $MIC_{A(withB)}$, ceftriaxone sodium with PPIX-MED; $MIC_{B(withA)}$, PPIX-MED with ceftriaxone sodium.

▲ *The fractional inhibitory concentration index (FICI) data were interpreted using the following criteria: synergistic effect, FICI ≤ 0.5; additive effect, FICI 0.5–1.0; irrelevant effect, FICI 1.0–2.0; and antagonistic effect, FICI ≥ 2.0.*

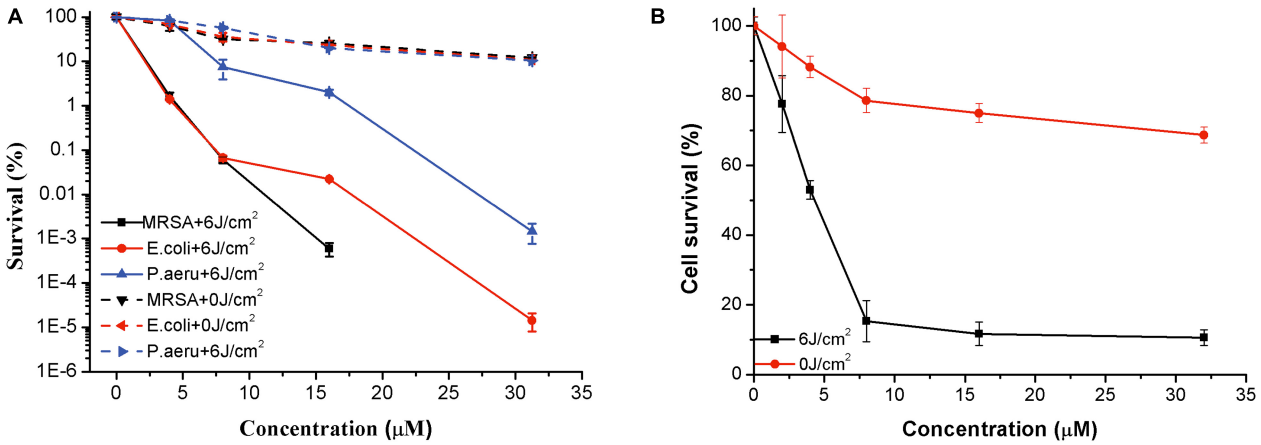

FIGURE 5 | Phototoxicity and dark toxicity of PPIX-MED against **(A)** three bacterial strains and **(B)** NIH 3T3 (mouse fibroblast) cells. Each bacterial species and the fibroblasts were respectively incubated with PPIX-MED (0–31.25 μM) for 30 min, followed by exposure to 650-nm laser light (6 J/cm^2) or darkness. The results are expressed as mean and standard deviation.

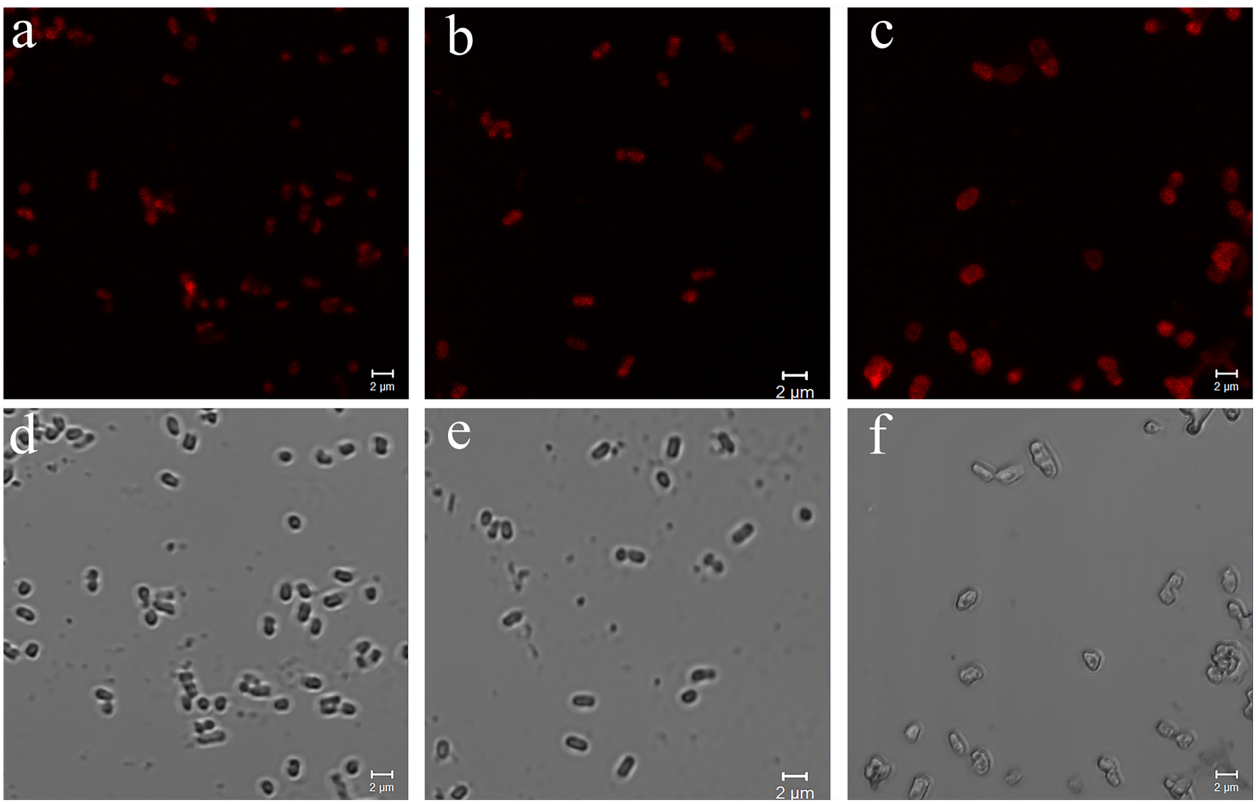

FIGURE 6 | Confocal laser scanning microscopy images of **(a)** *Pseudomonas aeruginosa*, **(b)** *Escherichia coli*, and **(c)** methicillin-resistant *Staphylococcus aureus* (MRSA) and optical images of **(d)** *P. aeruginosa*, **(e)** *E. coli*, and **(f)** MRSA. The strains were imaged after incubation for 30 min with PPIX-MED (15.6 μM) in phosphate-buffered saline. Excitation was at 405 nm. Scale bars = 2 μm.

For *in vivo* aPDT experiments, about five or 10 times the MIC is generally chosen as the working dose (Xu et al., 2016). On the basis of preliminary experiments, 187.5 mM of PPIX-MED, four times the MBC against *P. aeruginosa*, was chosen as the working dose for this study. The antibacterial effect of PPIX-MED–aPDT *in vivo* was analyzed. As shown in **Figure 7**, on days 5, 10, 14, and 17 post-infection, the wound healing rate of the treatment groups was higher than that of the untreated control group ($p < 0.01$). The rats in the aPDT + antibiotic therapy group exhibited faster wound healing than those in the antibiotic-therapy-only

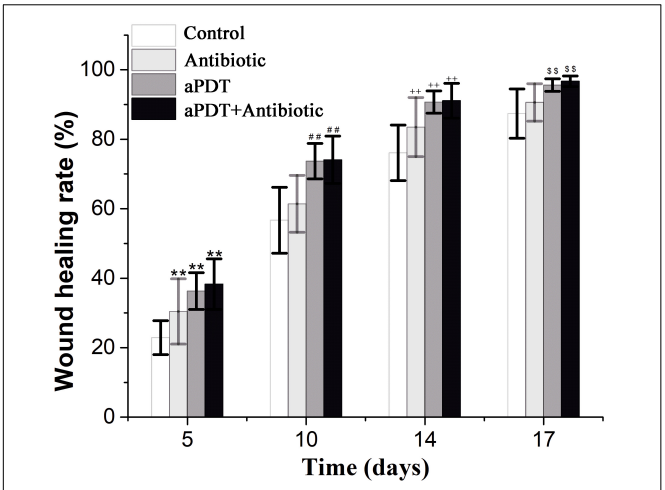

FIGURE 7 | Wound healing rate of each group on the 5th, 10th, 14th, and 17th day post-infection [$^{*}p < 0.05$, $^{**}p < 0.01$ vs. control group (5 days); $^{\#}p < 0.05$, $^{\#\#}p < 0.01$ vs. control group (10 days); $^{+}p < 0.05$, $^{++}p < 0.01$ vs. control group (14 days); $^{\$}p < 0.05$, $^{\$\$}p < 0.01$ vs. control group (17 days)].

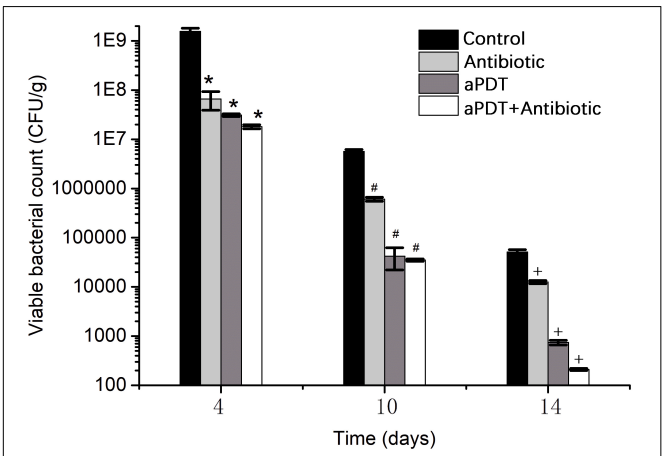

FIGURE 8 | The viability of bacteria in burn wound tissue of rats in each group on the 4th, 10th, and 14th day post-infection [$^{*}p < 0.05$ vs. control group (4 days); $^{\#}p < 0.05$ vs. control group (10 days); $^{+}p < 0.05$ vs. control group (14 days)].

group ($p < 0.01$) or the aPDT treatment group. On day 17 post-infection, the wounds in the aPDT + antibiotics group had healed (96.7 ± 1.5); the healing rate was significantly better than that in the antibiotic-only treatment group ($p < 0.01$) and the aPDT treatment group, respectively. The healing rate of the aPDT treatment group was superior to that of the antibiotic-only treatment group ($p < 0.01$). Therefore, aPDT combined with antibiotics was most efficient in the treatment of mixed bacterial infection of burn wounds, and aPDT treatment was also somewhat effective.

Viable Bacteria in Wound Tissue

The viability of bacteria in wound tissue was determined as an index of the bactericidal effect of PPIX-MED–aPDT treatment (**Figure 8**). The control group (i.e., wounds without any treatment) exhibited greater viability of MRSA, *P. aeruginosa*, and *E. coli* at each observation time point; on days 4, 10, and 14 post-infection, all the treatment groups exhibited an obvious reduction in bacterial viability compared with the controls ($p < 0.05$). In the treatment groups, bacterial viability decreased in the order aPDT + ceftriaxone group > aPDT group > ceftriaxone group. This suggests that PPIX-MED–aPDT has a bactericidal effect against MRSA, *P. aeruginosa*, and *E. coli* in burn wounds, and aPDT combined with antibiotics is more efficient in the treatment of burn infection.

TABLE 3 | Rate of detection of bacteria in blood cultures at 4, 10, and 14 days after infection ($\bar{x} + s$).

Groups	4 days	10 days	14 days
Control	100.0	100.0^{a}	80.0^{a}
Antibiotic	100.0	71.4$^{a▲}$	42.8$^{a▲}$
aPDT	88.9	33.3$^{b▲}$	11.1$^{b▲}$
aPDT + Antibiotic	70.0	0.0^{b}	0.0^{b}

At the same time, the difference in the α = 0.05 level between the different groups in the upper-right corner of the digital right angle was statistically significant; ▲ showing no difference between statistical significance (ignore the letters that are different).

Bacteria in Blood Culture and Animal Survival

As shown in **Table 3**, at 4 days after infection, the positive detection rate of bacteria in blood culture analysis for the aPDT + ceftriaxone (70%) and aPDT (88.9%) groups was lower than that in the ceftriaxone (100%) and control groups (100%). At 10 days, the aPDT + ceftriaxone (0%), aPDT (33.3%), and ceftriaxone groups (71.4%) showed a reduction of positive blood cultures compared with the control group (100%; $p = 0.004$). At 14 days, the rate of bacteria-positive blood cultures was still zero for the aPDT + ceftriaxone group and was 11.1% for the aPDT group and 42.8% for the ceftriaxone group; however, the rate in the control group remained high (80%).

In the control group, five rats died on days 1–4 post-infection. In the antibiotic treatment group, four rats died on days 1–3. In the aPDT treatment group, one rat died (on day 1). All rats in the aPDT + ceftriaxone group survived the experiment. These data indicate that PPIX-MED–aPDT was the most efficient approach to the treatment of mixed bacterial infection in a burn wound (**Figure 9**).

ELISA

ELISA was used to investigate tissue TNF-α and IL-6 concentrations in skin tissue after treatment (**Figure 10**). The TNF-α and IL-6 levels gradually decreased with time post-infection. The aPDT + antibiotics-treated group exhibited an obvious reduction in TNF-α and IL-6 levels ($p < 0.01$) compared with the no-treatment (control) group and the other treatment groups; at a given time point, the level of TNF-α and IL-6 in the groups was control > antibiotic > aPDT > aPDT + antibiotics. These results suggest that aPDT, especially when combined with antibiotic therapy, can inhibit the expression of IL-6 and TNF-α

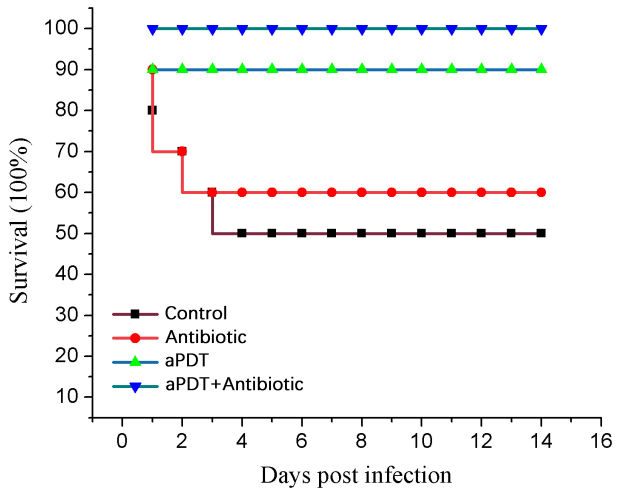

FIGURE 9 | Survival of treated and untreated rats.

in burn tissues, which will reduce the inflammatory reaction in the tissues and help with wound healing.

Expression of bFGF and CD31 in Burn Wound Tissue

Table 4 and **Figure 11** show the expression of bFGF at 4, 10, and 17 days post-infection in the various groups. At 4 days, the expression of bFGF in the antibiotic-only (36.33 ± 5.71), aPDT-only (50.50 ± 14.22), and aPDT + antibiotics (75.83 ± 23.25) treatment groups was higher than that in the control group (11.67 ± 2.07) ($p < 0.05$). At 10 days, the values were 41.33 ± 3.50, 91.00 ± 7.27, and 99.67 ± 9.27, respectively, compared with 16.67 ± 2.66 for the control group ($p < 0.05$). At day 17, the expression of bFGF in the antibiotic-only (48.33 ± 17.95), aPDT-only (51.83 ± 14.95), and aPDT + antibiotics (43.67 ± 4.97) groups remained higher than that in the control group (39.00 ± 5.90).

TABLE 4 | Expression of bFGF in tissues of burn wound sites as determined by immunochemistry.

Group	4 d	10 d	17 d
Control	11.67 ± 2.07[a]	16.67 ± 2.66[a]	39.00 ± 5.90
Antibiotic	36.33 ± 5.71[b]	41.33 ± 3.50[b]	48.33 ± 17.95
aPDT	50.50 ± 14.22[b]	91.00 ± 7.27[c]	51.83 ± 14.95
aPDT + Antibiotic	75.83 ± 23.25[c]	99.67 ± 9.27[c]	43.67 ± 4.97

The letter is completely different between $p < 0.05$.

At 4 and 10 days post-infection, the bFGF expression level in the aPDT + antibiotic group was obviously higher than that in the antibiotic and the aPDT treatment groups ($p < 0.01$). The expression of bFGF in the aPDT treatment group was higher than that in the antibiotic treatment group (4 days, $p > 0.05$; 10 days, $p < 0.01$). The expression level in the control and the antibiotic groups increased throughout the healing process. However, in the aPDT treatment group and the aPDT + antibiotic group, bFGF expression first increased and then decreased, being highest at 10 days post-infection among the timepoints that we measured: 99.7 ± 9.3 in the aPDT + antibiotic treatment group and 91.0 ± 7.3 in the aPDT group.

On days 4, 10, and 17 post-infection, the new blood vessel density (MVD), determined by the expression of CD31, was significantly higher in the treatment groups than in the control group ($p < 0.01$) (**Figure 12**). MVD in the aPDT + antibiotics group was significantly higher than that in the aPDT-only treatment group and the antibiotic-only group ($p < 0.01$). The

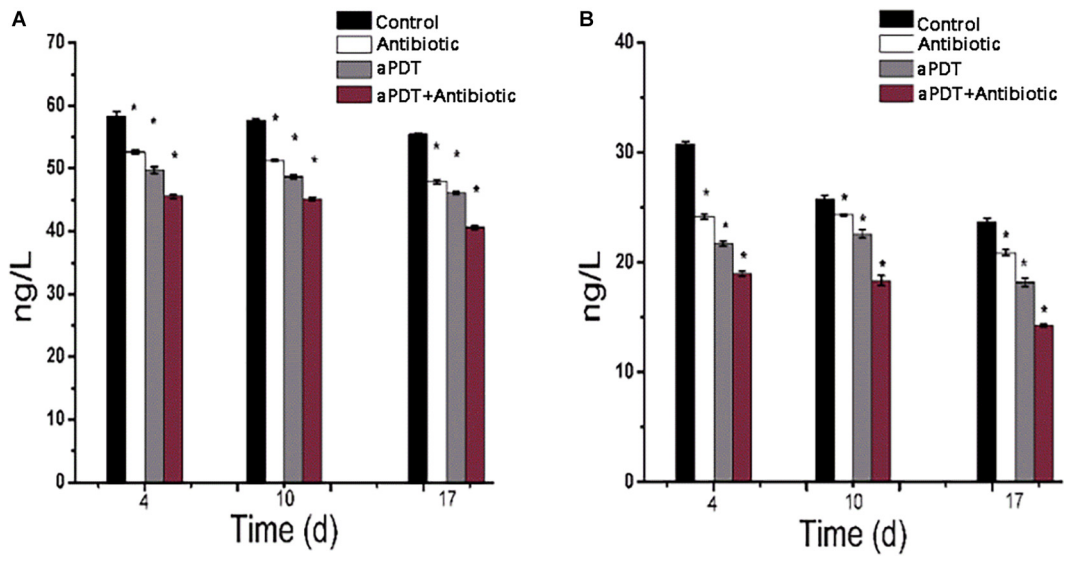

FIGURE 10 | Expression of TNF-α and IL-6 as determined by ELISA in burn wound tissue of rats. **(A)** TNF-α levels at 4, 10, and 17 days after infection. **(B)** IL-6 levels at 4, 10, and 17 days after infection.

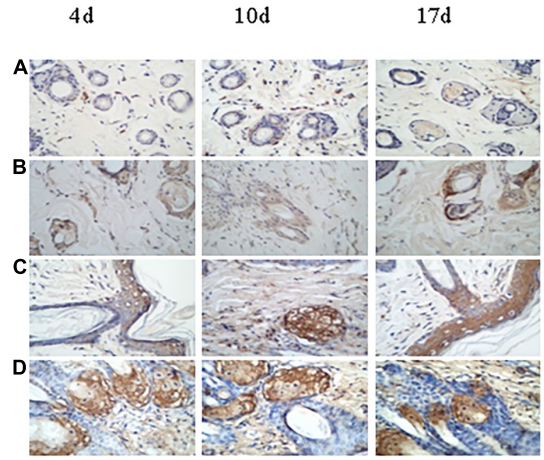

FIGURE 11 | Expression of bFGF in burn wound tissue by time (days post-infection) in treated and untreated rats. **(A)** Control group. **(B)** Antibiotic treatment group. **(C)** aPDT treatment group. **(D)** aPDT + antibiotic treatment group.

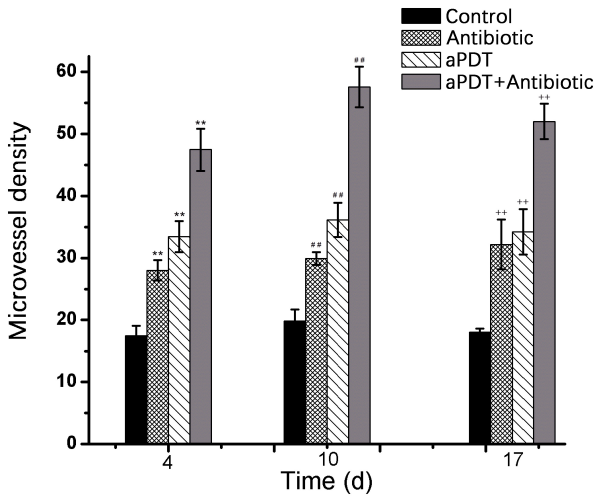

FIGURE 12 | Blood vessel density (measured by the expression of CD31) in tissues of burn wound sites as determined by immunochemistry [$^{*}p < 0.05$, $^{**}p < 0.01$ vs. control group (4 days); $^{\#}p < 0.05$, $^{\#\#}p < 0.01$ vs. control group (10 days); $^{+}p < 0.05$, $^{++}p < 0.01$ vs. control group (17 days)].

MVD in the aPDT-only treatment group was significantly higher than that in the antibiotics-only group ($p < 0.01$ at 4 and 10 days post-infection). The new MVD in the aPDT + antibiotic group reached its observed maximum on day 10.

Evaluation of Side Effects of Using aPDT + Antibiotics

We examined the potential *in vivo* toxicity of PPIX-MED–aPDT and aPDT + antibiotics treatments using the organ index in rats (**Table 5**). We harvested major organs: heart, liver, spleen, lung, kidney, and thymus. Compared with normal rats, we did not detect any overt signs of toxic side effects or changes in body weight or organ weight with the PPIX-MED–aPDT treatment, suggesting that the PPIX-MED–aPDT treatment was relatively safe to administer. However, the liver weight of the rats in the antibiotic treatment group and the aPDT + antibiotics group was lower than that in the other groups ($p < 0.01$), which may be caused by the toxicity of ceftriaxone sodium to the liver.

In control group rats, the body weight was lower than it was in the treatment groups. When dissecting the rats, many infections were observed on the spleen, and the small intestine adhered to the abdominal wall on both sides. Rats in the antibiotic-only treatment group also showed symptoms such as a grossly enlarged spleen and intestinal adhesions. These symptoms indicated that the experimental animals had different degrees of bacterial organ infections.

DISCUSSION

Complications caused by drug-resistant bacterial infection after burns are a major factor in the death of patients. Bacterial attachment to an open wound during the healing process is a prominent etiological factor of sepsis and multiple organ dysfunction syndrome (MODS), for example (Garcia et al., 2010). As such, anti-infection treatment is important for burn patients. Furthermore, the emergence of high antimicrobial resistance among bacterial pathogens has made the management of treatment of postoperative wound infections difficult (Andhoga et al., 2002; Nanda and Saravanan, 2009). Healing of burn wounds is a complex process that involves the response of several local and systemic tissues and is regulated by many different cellular and humoral factors. It normally proceeds in four overlapping phases: inflammation, granulation, matrix formation, and remodeling (Garcia et al., 2010).

In vitro (Thakuri et al., 2011; ElZorkany et al., 2019; Choi et al., 2020) and *in vivo* (de Vasconcelos Catão et al., 2015; Mai et al., 2017) studies have demonstrated that aPDT has anti-infection properties and effects on wound healing. A meta-analysis of aPDT indicated that it is highly effective in promoting tissue repair (Garcia et al., 2010; Mai et al., 2017). There are several reports in the literature on the beneficial effects of aPDT on local vascularization, edema, pain, and inflammation as well as the deposition and organization of both extracellular matrix and collagen (Garcia et al., 2010), but there are few published reports (Boluki et al., 2017) on the effect of aPDT-combined-with-antibiotic treatment on the healing of burns.

In our study, both aPDT alone and aPDT-combined-with-antibiotic treatment were used. We used a rat model with severe burns, infected by a mixture of pathogenic bacteria. Wounds treated with aPDT or aPDT combined with antibiotics healed in 5–17 days, faster than wounds in the control (untreated) group or the group treated with antibiotic alone. Moreover, half the rats in the control (untreated) group died within 4 days of infection, and 40% of the rats in the antibiotic-only treatment group died early in the experiment (days 1–3), but no rats in the aPDT + antibiotics treatment group died, and only one died in the aPDT-only group (on the first day after burning and infection). Immunohistochemical studies showed that aPDT

TABLE 5 | The organ index in rats after treatment.

Group	Weight (g)	Heart (mg/g)	Liver (mg/g)	Spleen (mg/g)	Lung (mg/g)	Kidney (mg/g)	Thymus index (mg/g)
Normal	286 ± 42	0.40 ± 0.02	4.05 ± 0.40	0.38 ± 0.10	0.70 ± 0.10	0.87 ± 0.10	0.18 ± 0.02
Control	263 ± 22	0.40 ± 0.10	4.60 ± 0.50	0.57 ± 0.10	0.73 ± 0.15	0.94 ± 0.20	0.16 ± 0.05
Antibiotic	283 ± 22	0.36 ± 0.05	3.50 ± 0.40▲	0.40 ± 0.20	0.70 ± 0.03	0.80 ± 0.04	0.17 ± 0.04
aPDT	292 ± 22	0.38 ± 0.03	4.20 ± 0.30	0.38 ± 0.07	0.60 ± 0.04	0.80 ± 0.05	0.17 ± 0.04
aPDT + Antibiotic	281 ± 16	0.38 ± 0.05	3.80 ± 0.40▲	0.42 ± 0.07	0.70 ± 0.04	0.86 ± 0.05	0.17 ± 0.03

Compared with control, ▲ means $p < 0.05$.

and aPDT combined with antibiotic promoted a high expression of bFGF before day 10; on day 10, the expression of bFGF was lower, whereas the expression level in the control group and the antibiotic-only group continued to increase at that timepoint. This may suggest that aPDT and aPDT combined with antibiotic can promote fibroblast proliferation that enhances wound healing (Garcia et al., 2010).

The viable bacteria in wound tissue and in blood were determined as an index of the bactericidal effects of aPDT and aPDT combined with antibiotics. On the 4th, 10th, and 14th day after infection, the aPDT-combined-with-antibiotics treatment group exhibited an obvious reduction in bacteria compared with the control group and the aPDT-only treatment group and the antibiotic-only group. This experiment confirmed that aPDT can significantly reduce the number of bacterial colonies under phase callus, increasing the rate of wound healing, and promote healing efficacy.

TNF-α is a crucial contributing factor to inflammation-mediated pathophysiology (Brüünsgaard and Pedersen, 2003; Ashcroft et al., 2012). The pleiotropic cytokine IL-6 is produced by macrophages, dendritic cells, mast cells, and other innate immune cells. TNF-α and IL-6 have long been considered as markers of inflammation (Nissen et al., 1996). In the present study, aPDT and aPDT-combined-with-antibiotic treatment decreased inflammation factor secretion; that is, it significantly reduced the scalded tissue concentration of TNF-α and IL-6. Neovascularization is an important part of granulation, providing nutrition and transporting metabolites to a wounded area, which plays an important role in the process of wound healing. Angiogenesis is critically important for the delivery of nutrients, oxygen, and inflammatory cells to the area of wound, which therefore contribute to promote wound healing (Salo et al., 2007). CD31 is a sensitive marker for the detection of neovascularization (Musumeci et al., 2015). The results here showed a higher expression of CD31 in the aPDT-combined-with-antibiotics group compared with the aPDT-only treatment group and the antibiotic-only group ($p < 0.01$). In the aPDT-combined-with-antibiotics group, the new blood vessel density reached its observed maximum on day 10 and was lower on day 14. The results showed that aPDT-combined-with-antibiotic treatment can promote neovascularization in burn wounds. Salo et al. (2007) showed that wound neovascularization is the main determinant of burn wound healing.

The major advantages of aPDT are its specific effect on target cells, a lack of collateral effects, activity only on exposure to light, and inability of bacteria to develop resistance to this type of killing (Zolfaghari et al., 2009; Sperandio et al., 2013). Further studies should be carried out to better understand the action of aPDT-combined-with-antibiotics in the healing process of third-degree burns because there is little literature on this subject. Moreover, it should be noted that the present safety evaluation of PPIX-MED is somewhat limited, and this should be expanded in a series of rigorous assessments before PPIX-MED is used clinically.

CONCLUSION

aPDT and aPDT-combined-with-antibiotic treatment showed beneficial effects in accelerating the healing process of bacterially infected third-degree burns of rats. These treatments stimulate macrophages to release chemical mediators, cytokines, and growth factors, which, in turn, stimulate and increase the production of connective tissue and create a new supply of blood vessels to nourish the wound site and promote remodeling. There was a histological tendency for better cicatrization after the use of aPDT combined with antibiotics in burn healing. The synergistic effect of aPDT-combined-with-antibiotic treatment could be promising for the management of third-degree burn skin infections.

DATA AVAILABILITY STATEMENT

The original contributions presented in the study are included in the article/supplementary material, further inquiries can be directed to the corresponding author/s.

ETHICS STATEMENT

The animal study was reviewed and approved by the Laboratory Animal Management Committee/Laboratory Animal Welfare Ethics Committee, Institute of Radiation Medicine, Chinese Academy of Medical Sciences.

AUTHOR CONTRIBUTIONS

TL and GH performed conceptualization. ZZ, TL, and GH performed data curation. ZZ and GH performed formal analysis. GH performed funding acquisition, project administration, and supervision. JZ, ZZ, and GH performed

investigation. LZ, TL, and GH performed methodology. ZZ, TL, and GH performed resources. ZX, YW, JM, and GH performed validation. ZZ and GH performed visualization and writing – original draft. ZZ, TL, and GH performed writing – review and editing. All authors contributed to the article and approved the submitted version.

FUNDING

This work was supported by the national Mega-project for Innovative Drugs (2019ZX09721001-006-001) and the medical and health science and technology innovation project of Chinese Academy of Medical Sciences (2019-I2M-1-005).

REFERENCES

Ahmed Alamoudi, W., Ahmad, F., Acharya, S., Haque, S., Alsamman, K., Herzallah, H. K., et al. (2018). A simplified colorimetric method for rapid detection of cell viability and toxicity in adherent cell culture systems. *J. Buon* 23, 1505–1513.

Álvarez-Micó, X., Calvete, M. J. F., Hanack, M., and Ziegler, T. J. C. R. (2007). A new glycosidation method through nitrite displacement on substituted nitrobenzenes. *Carbohydr. Res.* 342, 440–447. doi: 10.1016/j.carres.2006.11.017

Andhoga, J., Macharia, A., Maikuma, I., Wanyonyi, Z., Ayumba, B., and Kakai, R. (2002). Aerobic pathogenic bacteria in post-operative wounds at Moi teaching and referral hospital. *East Afr. Med. J.* 79, 640–644. doi: 10.4314/eamj.v79i12.8671

Ashcroft, G., Jeong, M., Ashworth, J., Hardman, M., Jin, W., Moutsopoulos, N., et al. (2012). Tumor necrosis factor-alpha (TNF-α) is a therapeutic target for impaired cutaneous wound healing. *Wound Repair Regen.* 20, 38–49. doi: 10.1111/j.1524-475X.2011.00748.x

Barbee, L., Soge, O., Holmes, K., and Golden, M. (2014). In vitro synergy testing of novel antimicrobial combination therapies against *Neisseria gonorrhoeae*. *J. Antimicrob. Chemother.* 69, 1572–1578. doi: 10.1093/jac/dkt540

Bhatti, M., MacRobert, A., Meghji, S., Henderson, B., and Wilson, M. (1998). A study of the uptake of toluidine blue O by *Porphyromonas gingivalis* and the mechanism of lethal photosensitization. *Photochem. Photobiol.* 68, 370–376. doi: 10.1111/j.1751-1097.1998.tb09694.x

Boluki, E., Kazemian, H., Peeridogaheh, H., Alikhani, M., Shahabi, S., Beytollahi, L., et al. (2017). Antimicrobial activity of photodynamic therapy in combination with colistin against a pan-drug resistant *Acinetobacter baumannii* isolated from burn patient. *Photodiagn. Photodyn. Ther.* 18, 1–5. doi: 10.1016/j.pdpdt.2017.01.003

Brüünsgaard, H., and Pedersen, B. (2003). Age-related inflammatory cytokines and disease. *Immunol. Allergy Clin. North Am.* 23, 15–39. doi: 10.1016/s0889-8561(02)00056-5

Cetik Yildiz, S., Demir, C., Cengiz, M., and Ayhanci, A. (2019). Protective properties of kefir on burn wounds of mice that were infected with *S. aureus*, *P. auroginasa* and *E. coli*. *Cell. Mol. Biol.* 65, 60–65. doi: 10.14715/cmb/2019.65.7.11

Choi, S., Oh, H., Kim, E., Lee, H., Kim, H., Choi, H., et al. (2020). In vitro bactericidal effects of photodynamic therapy combined with four tetracyclines against KCTC5009 in planktonic cultures. *Pathogens* 9:279. doi: 10.3390/pathogens9040279

Dai, T., Tegos, G., Zhiyentayev, T., Mylonakis, E., and Hamblin, M. (2010). Photodynamic therapy for methicillin-resistant *Staphylococcus aureus* infection in a mouse skin abrasion model. *Lasers Surg. Med.* 42, 38–44. doi: 10.1002/lsm.20887

Davies, J., and Davies, D. (2010). Origins and evolution of antibiotic resistance. *Microbiol. Mol. Biol. Rev.* 74, 417–433. doi: 10.1128/mmbr.00016-10

de Vasconcelos Catão, M., Nonaka, C., de Albuquerque, R., Bento, P., and de Oliveira Costa, R. (2015). Effects of red laser, infrared, photodynamic therapy, and green LED on the healing process of third-degree burns: clinical and histological study in rats. *Lasers Med. Sci.* 30, 421–428. doi: 10.1007/s10103-014-1687-0

ElZorkany, H., Youssef, T., Mohamed, M., and Amin, R. (2019). Photothermal versus photodynamic treatment for the inactivation of the bacteria *Escherichia coli* and *Bacillus cereus*: an in vitro study. *Photodiagn. Photodyn. Ther.* 27, 317–326. doi: 10.1016/j.pdpdt.2019.06.020

Garcia, V., de Lima, M., Okamoto, T., Milanezi, L., Júnior, E., Fernandes, L., et al. (2010). Effect of photodynamic therapy on the healing of cutaneous third-degree-burn: histological study in rats. *Lasers Med. Sci.* 25, 221–228. doi: 10.1007/s10103-009-0694-z

Gong, G., Cao, Y., Qian, H., Zhou, Y., Zhao, H., Li, L., et al. (2018). Assessment of the antitumor activity of a cyclopalladated ferrocene compound assisted by a dual-targeting drug delivery system. *Chem. Commun.* 54, 8312–8315. doi: 10.1039/c8cc03308k

Grinholc, M., Szramka, B., Kurlenda, J., Graczyk, A., and Bielawski, K. P. (2008). Bactericidal effect of photodynamic inactivation against methicillin-resistant and methicillin-susceptible *Staphylococcus aureus* is strain-dependent. *J. Photochem. Photobiol. B* 90, 57–63. doi: 10.1016/j.jphotobiol.2007.11.002

Hamblin, M., O'Donnell, D., Murthy, N., Contag, C., and Hasan, T. (2002). Rapid control of wound infections by targeted photodynamic therapy monitored by in vivo bioluminescence imaging. *Photochem. Photobiol.* 75, 51–57. doi: 10.1562/0031-8655(2002)075<0051:rcowib>2.0.co;2

Hamblin, M., Zahra, T., Contag, C., McManus, A., and Hasan, T. (2003). Optical monitoring and treatment of potentially lethal wound infections in vivo. *J. Infect. Dis.* 187, 1717–1725. doi: 10.1086/375244

Huang, L., Wang, M., Huang, Y., El-Hussein, A., Wolf, L., Chiang, L., et al. (2018). Progressive cationic functionalization of chlorin derivatives for antimicrobial photodynamic inactivation and related vancomycin conjugates. *Photochem. Photobiol. Sci.* 17, 638–651. doi: 10.1039/c7pp00389g

Jainchill, J. L., Aaronson, S. A., and Todaro, G. J. (1969). Murine sarcoma and leukemia viruses: assay using clonal lines of contact-inhibited mouse cells. *J. Virol.* 4, 549–553. doi: 10.1128/jvi.4.5.549-553.1969

Jernigan, J., Hatfield, K., Wolford, H., Nelson, R., Olubajo, B., Reddy, S., et al. (2020). Multidrug-resistant bacterial infections in U.S. hospitalized patients, 2012-2017. *New Engl. J. Med.* 382, 1309–1319. doi: 10.1056/NEJMoa1914433

Kashef, N., Ravaei Sharif Abadi, G., and Djavid, G. E. (2012). Photodynamic inactivation of primary human fibroblasts by methylene blue and toluidine blue O. *Photodiagn. Photodyn. Ther.* 9, 355–358. doi: 10.1016/j.pdpdt.2012.05.001

Lau, J. T., Lo, P. C., Fong, W. P., and Ng, D. K. (2011). Preparation and photodynamic activities of silicon(IV) phthalocyanines substituted with permethylated beta-cyclodextrins. *Chemistry* 17, 7569–7577. doi: 10.1002/chem.201100621

Luan, X., Qin, Y., Bi, L., Hu, C., Zhang, Z., Lin, J., et al. (2009). Histological evaluation of the safety of toluidine blue-mediated photosensitization to periodontal tissues in mice. *Lasers Med. Sci.* 24, 162–166. doi: 10.1007/s10103-007-0513-3

Lv, F., Li, Y., Cao, B., and Liu, T. (2013). Galactose substituted zinc phthalocyanines as near infrared fluorescence probes for liver cancer imaging. *J. Mater. Sci. Mater. Med.* 24, 811–819. doi: 10.1007/s10856-012-4820-2

Mai, B., Gao, Y., Li, M., Wang, X., Zhang, K., Liu, Q., et al. (2017). *Staphylococcus aureus*Photodynamic antimicrobial chemotherapy for and multidrug-resistant bacterial burn infection in vitro and in vivo. *Inter. J. Nanomed.* 12, 5915–5931. doi: 10.2147/ijn.S138185

Musumeci, G., Castorina, A., Magro, G., Cardile, V., Castorina, S., and Ribatti, D. (2015). Enhanced expression of CD31/platelet endothelial cell adhesion molecule 1 (PECAM1) correlates with hypoxia inducible factor-1 alpha (HIF-1α) in human glioblastoma multiforme. *Exper. Cell Res.* 339, 407–416. doi: 10.1016/j.yexcr.2015.09.007

Nanda, A., and Saravanan, M. (2009). Biosynthesis of silver nanoparticles from *Staphylococcus aureus* and its antimicrobial activity against MRSA and MRSE. *Nanomed. Nanotechnol. Biol. Med.* 5, 452–456. doi: 10.1016/j.nano.2009.01.012

Nissen, N., Polverini, P., Gamelli, R., and DiPietro, L. (1996). Basic fibroblast growth factor mediates angiogenic activity in early surgical wounds. *Surgery* 119, 457–465. doi: 10.1016/s0039-6060(96)80148-6

Oda, Y., Kagami, H., and Ueda, M. (2004). Accelerating effects of basic fibroblast growth factor on wound healing of rat palatal mucosa. *J. Oral Maxillof. Surg.* 62, 73–80. doi: 10.1016/j.joms.2003.05.007

Oyama, J., Fernandes, H. R.-M. Á, Lopes Lera-Nonose, D., Nesi-Reis, V., Galhardo, D. I., Alessi Aristides, S., et al. (2020). Photodynamic therapy in wound healing

in vivo: a systematic review. *Photodiagn. Photodyn. Ther.* 30:101682. doi: 10.1016/j.pdpdt.2020.101682

Park, J., Ahn, M., Kim, Y., Kim, S., Moon, Y., Ahn, S., et al. (2012). In vitro and in vivo antimicrobial effect of photodynamic therapy using a highly pure chlorin e6 against *Staphylococcus aureus* Xen29. *Biol. Pharm. Bull.* 35, 509–514. doi: 10.1248/bpb.35.509

Rodrigues, G., Dias-Baruffi, M., Holman, N., Wainwright, M., and Braga, G. (2013). In vitro photodynamic inactivation of *Candida* species and mouse fibroblasts with phenothiazinium photosensitisers and red light. *Photodiagn. Photodyn. Ther.* 10, 141–149. doi: 10.1016/j.pdpdt.2012.11.004

Salo, P., Bray, R., Seerattan, R., Reno, C., McDougall, J., and Hart, D. (2007). Neuropeptides regulate expression of matrix molecule, growth factor and inflammatory mediator mRNA in explants of normal and healing medial collateral ligament. *Regul. Peptid.* 142, 1–6. doi: 10.1016/j.regpep.2007.01.001

Seegers, H., Hood, V., Kidd, B., Cruwys, S., and Walsh, D. (2003). Enhancement of angiogenesis by endogenous substance P release and neurokinin-1 receptors during neurogenic inflammation. *J. Pharmacol. Exper. Therap.* 306, 8–12. doi: 10.1124/jpet.103.050013

Soukos, N. S., Ximenezfyvie, L. A., Hamblin, M. R., Socransky, S. S., and Hasan, T. (1998). Targeted antimicrobial photochemotherapy. *Antimicrob. Agents Chemother.* 42:2595. doi: 10.1128/aac.42.10.2595

Sperandio, F., Huang, Y., and Hamblin, M. (2013). Antimicrobial photodynamic therapy to kill Gram-negative bacteria. *Recent Pat. Anti Infec. Drug Discov.* 8, 108–120. doi: 10.2174/1574891x113089990012

Tan, Y., Wang, Q., Xie, Y., Qiao, X., Zhang, S., Wang, Y., et al. (2019). Identification of FOXM1 as a specific marker for triple-negative breast cancer. *Intern. J. Oncol.* 54, 87–97. doi: 10.3892/ijo.2018.4598

Tavares, A., Carvalho, C., Faustino, M., Neves, M., Tomé, J., Tomé, A., et al. (2010). Antimicrobial photodynamic therapy: study of bacterial recovery viability and potential development of resistance after treatment. *Mar. Drugs* 8, 91–105. doi: 10.3390/md8010091

Thakuri, P., Joshi, R., Basnet, S., Pandey, S., Taujale, S., and Mishra, N. (2011). Antibacterial photodynamic therapy on *Staphylococcus aureus* and *Pseudomonas aeruginosa* in-vitro. *Nepal Med. Coll. J.* 13, 281–284.

Xu, Z., Gao, Y., Meng, S., Yang, B., Pang, L., Wang, C., et al. (2016). Mechanism and in vivo evaluation: photodynamic antibacterial chemotherapy of lysine-porphyrin conjugate. *Front. Microbiol.* 7:242. doi: 10.3389/fmicb.2016.00242

Xuan, W., Huang, L., Wang, Y., Hu, X., Szewczyk, G., Huang, Y., et al. (2019). Amphiphilic tetracationic porphyrins are exceptionally active antimicrobial photosensitizers: in vitro and in vivo studies with the free-base and Pd-chelate. *J. Biophoton.* 12:e201800318. doi: 10.1002/jbio.201800318

Zhang, Y., Liang, D., Dong, L., Ge, X., Xu, F., Chen, W., et al. (2015). Anti-inflammatory effects of novel curcumin analogs in experimental acute lung injury. *Respir. Res.* 16:43. doi: 10.1186/s12931-015-0199-1

Zhao, Z., Li, Y., Meng, S., Li, S., Wang, Q., and Liu, T. (2014). Susceptibility of methicillin-resistant *Staphylococcus aureus* to photodynamic antimicrobial chemotherapy with α-D-galactopyranosyl zinc phthalocyanines: in vitro study. *Lasers Med. Sci.* 29, 1131–1138. doi: 10.1007/s10103-013-1488-x

Zolfaghari, P., Packer, S., Singer, M., Nair, S., Bennett, J., Street, C., et al. (2009). In vivo killing of *Staphylococcus aureus* using a light-activated antimicrobial agent. *BMC Microbiol.* 9:27. doi: 10.1186/1471-2180-9-27

Conflict of Interest: The authors declare that the research was conducted in the absence of any commercial or financial relationships that could be construed as a potential conflict of interest.

frontiers in Microbiology

ORIGINAL RESEARCH
published: 25 February 2021
doi: 10.3389/fmicb.2021.647289

New Insights Into the Antibacterial Mechanism of Cryptotanshinone, a Representative Diterpenoid Quinone From *Salvia miltiorrhiza* Bunge

Bo-Chen Chen[1†], Zhi-Shan Ding[2†], Jian-Sheng Dai[1], Ni-Pi Chen[1], Xing-Wen Gong[3], Lie-Feng Ma[4] and Chao-Dong Qian[1]*

[1] College of Life Science, Institute of Molecular Medicine, Zhejiang Chinese Medical University, Hangzhou, China, [2] College of Medical Technology, Zhejiang Chinese Medical University, Hangzhou, China, [3] Department of Biological Engineering, Zhejiang Gongshang University, Hangzhou, China, [4] College of Pharmaceutical Science, Zhejiang University of Technology, Hangzhou, China

OPEN ACCESS

Edited by:
Bertha González-Pedrajo, National Autonomous University of Mexico, Mexico

Reviewed by:
Maria José Saavedra, Universidade de Trás os Montes e Alto Douro, Portugal
Sergio Guerrero-Castillo, University Medical Center Hamburg-Eppendorf, Germany

***Correspondence:**
Chao-Dong Qian
zzdqcd@163.com

[†] These authors have contributed equally to this work and share first authorship

Specialty section:
This article was submitted to Antimicrobials, Resistance and Chemotherapy, a section of the journal Frontiers in Microbiology

Received: 29 December 2020
Accepted: 08 February 2021
Published: 25 February 2021

Citation:
Chen B-C, Ding Z-S, Dai J-S, Chen N-P, Gong X-W, Ma L-F and Qian C-D (2021) New Insights Into the Antibacterial Mechanism of Cryptotanshinone, a Representative Diterpenoid Quinone From Salvia miltiorrhiza Bunge. Front. Microbiol. 12:647289. doi: 10.3389/fmicb.2021.647289

The rapid rise of antibiotic resistance causes an urgent need for new antimicrobial agents with unique and different mechanisms of action. The respiratory chain is one such target involved in the redox balance and energy metabolism. As a natural quinone compound isolated from the root of *Salvia miltiorrhiza* Bunge, cryptotanshinone (CT) has been previously demonstrated against a wide range of Gram-positive bacteria including multidrug-resistant pathogens. Although superoxide radicals induced by CT are proposed to play an important role in the antibacterial effect of this agent, its mechanism of action is still unclear. In this study, we have shown that CT is a bacteriostatic agent rather than a bactericidal agent. Metabolome analysis suggested that CT might act as an antibacterial agent targeting the cell membrane. CT did not cause severe damage to the bacterial membrane but rapidly dissipated membrane potential, implying that this compound could be a respiratory chain inhibitor. Oxygen consumption analysis in staphylococcal membrane vesicles implied that CT acted as respiratory chain inhibitor probably by targeting type II NADH:quinone dehydrogenase (NDH-2). Molecular docking study suggested that the compound would competitively inhibit the binding of quinone to NDH-2. Consistent with the hypothesis, the antimicrobial activity of CT was blocked by menaquinone, and the combination of CT with thioridazine but not 2-n-heptyl-4-hydroxyquinoline-*N*-oxide exerted synergistic activity against *Staphylococcus aureus*. Additionally, combinations of CT with other inhibitors targeting different components of the bacterial respiratory chain exhibit potent synergistic activities against *S. aureus*, suggesting a promising role in combination therapies.

Keywords: cryptotanshinone, respiratory chain inhibitor, menaquinone, type II NADH:quinone dehydrogenase, metabolome analysis

INTRODUCTION

Infectious diseases remain a major threat to global health due to widespread antibiotic resistance among pathogens. Although improved preventive measures have reduced resistance in some bacteria, the discovery and development of new antimicrobial agents with a unique mechanism of action has been and will continue to be necessary for the treatment of infections caused by novel

drug-resistant pathogens. For a long time, the clinically used antibiotics mainly affect five major targets or biosynthetic pathways: the biosynthesis of DNA, RNA, proteins, peptidoglycan, and folic acid (Hurdle et al., 2011). Recently, the respiratory system has emerged as an attractive target for the development of new antibiotics, especially against multidrug-resistant tuberculosis (Hards and Cook, 2018; Iqbal et al., 2018). The mitochondrial respiratory systems of mammal usually consist of type I NADH dehydrogenase (NDH-1), succinate dehydrogenase, cytochrome bc_1 complex, cytochrome c oxidase, and ATP synthase. However, for adaption to different environments, the respiratory system of bacteria is far more diverse than that of mitochondria (Anraku, 1988). For instance, *Mycobacterium tuberculosis* can encode two distinct terminal oxidases as well as two types of NADH dehydrogenases, NDH-1 and type II NADH dehydrogenase (NDH-2) (Hards and Cook, 2018), while *Bacillus subtilis* possesses one NDH-2 and four types of terminal oxidases (Azarkina et al., 1999; Melo et al., 2004).

Numerous antimicrobial molecules targeting different components of the respiratory chain have been discovered. Thioridazine targets NDH-2 to block the electron transfer chain of bacteria and is effective against *Staphylococcus aureus* and *M. tuberculosis* (Weinstein et al., 2005; Schurig-Briccio et al., 2014). Bedaquiline and its analog TBAJ-876 kill *M. tuberculosis* by specifically inhibiting F_1F_0-ATP synthase (Andries, 2005; Koul et al., 2007; Sarathy et al., 2019). Lysocin E exerts its antimicrobial activity through a direct interaction with menaquinone (MK), which is the sole quinone in most of the Gram-positive bacteria, including *M. tuberculosis*, *S. aureus*, and *B. subtilis* (Hamamoto et al., 2015; Paudel et al., 2016; Boersch et al., 2018). Moreover, many compounds that target MK biosynthesis (Paudel et al., 2016; Boersch et al., 2018) and QcrB, a component of the cytochrome bc_1 complex (Foo et al., 2018; Iqbal et al., 2018; Lu et al., 2019), have been described. It is worth mentioning that bedaquiline was approved by the FDA in 2012 for the treatment of pulmonary multidrug-resistant tuberculosis in adults, and Q203, an imidazopyridine amide compound targeting the respiratory cytochrome bc_1 complex of *M. tuberculosis*, has recently entered clinical trials (Iqbal et al., 2018).

Over the past few decades, much attention has been directed to the study of plant-derived compounds due to their antibacterial activities, especially against multidrug-resistant pathogenic bacteria (Cha et al., 2014; Barbieri et al., 2017; Teng et al., 2018). Cryptotanshinone (CT), a representative diterpenoid quinone isolated from the root of *Salvia miltiorrhiza* Bunge (Dan Shen), is one of such compounds. It is the major active constituents of Danshentong capsules and Kecuoyintone gel, which are Chinese patent medicines used for the treatment of disorders such as acne vulgaris and other skin infections (Zhang et al., 2003; Zhao et al., 2007). CT exhibits antibacterial activity against a wide range of Gram-positive pathogenic bacteria (Lee et al., 1999; Lu, 2020). Clinically isolated methicillin-resistant *S. aureus* and vancomycin-resistant *S. aureus* were also reported to be sensitive to CT (Cha et al., 2014), making it an attractive new antibiotic candidate. However, little information has been obtained about the mode of action (MoA) of CT. It has only been speculated that superoxide radicals induced by CT might be important in the antibacterial activity of the agent (Lee et al., 1999; Feng et al., 2009).

To gain novel insight into the MoA of this compound, we conducted a comprehensive study using a model organism *B. subtilis* and an opportunistic pathogen *S. aureus*, the latter of which causes a wide range of hospital- and community-acquired infections (Al-Mebairik et al., 2016). We found that CT was a respiratory chain inhibitor probably by targeting NDH-2. Furthermore, we demonstrated that the phytochemical was strongly synergistic with several respiratory chain inhibitors.

MATERIALS AND METHODS

Chemicals and Bacterial Strains

Cryptotanshinone (≥98%, HPLC), menaquinone-4 (MK4), and NADH were purchased from Sigma–Aldrich (St. Louis, MO, United States). Reagents used in metabolomics: methanol, formic acid, and acetonitrile were purchased from CNW Technologies GmbH (Germany). Unless otherwise stated, all agents were dissolved in DMSO and then diluted to ensure a final DMSO concentration of ≤3.2% (vol/vol). *S. aureus* ATCC 25923, *S. aureus* ATCC 29213, *S. aureus* ATCC 43300, and *B. subtilis* 168 (Chen et al., 2018) were used in this study.

Antimicrobial Testing

The minimum inhibitory concentration (MIC)/minimum bactericidal concentration (MBC) was determined as described previously (Chen et al., 2018). Time-kill experiments were performed to evaluate the bactericidal/bacteriostasis activity of CT against *S. aureus* ATCC 43300 and *B. subtilis* 168 (Chen et al., 2018). Vancomycin was used as a positive control of bactericidal antibiotic, and DMSO (3.2%) was used as a negative control.

Untargeted Metabolomics Analysis

Overnight culture of *B. subtilis* was inoculated in Mueller–Hinton (MH) broth and incubated to early logarithmic phase. Bacterial cells were then diluted to OD_{600} = 0.2 with fresh MH broth, and treated with 16 μg/mL CT or 1.6% DMSO for 2 h. The cells were harvested by centrifugation, washed, and resuspended with ice-cold saline. The suspended cells were divided, pelleted, and then frozen rapidly in liquid nitrogen for 5 min, followed by storage at −80°C until analysis. An accurately weighed sample was resuspended in 1mL methanol:water (4:1 = v:v), added to 20 μL of 2-chloro-l-phenylalanine (0.3 mg/mL) dissolved in methanol as internal standard, and transferred to a 2.0-mL glass vial. A total of 200 μL of chloroform was added to each vial. The cells were then broken by sonication on an ice bath for 6 min at 500 W and centrifuged (16,000 × *g*, 4 °C) for 10 min. Quality control samples were prepared by mixing aliquots of all samples that served as a pooled sample. One milliliter of the supernatant was transferred to a 1.5-mL Eppendorf tube and dried in a freeze-concentration centrifugal dryer. The sample was then resuspended in 400 μL methanol: water (7:3 = v:v). After centrifugation, 150 μL of the supernatant was filtered through a 0.22 μm filter, followed by LC-MS analysis. ACQUITY UPLC I-Class system coupled with VION IMS QTOF mass

spectrometer (Waters Corporation, Milford, CT, United States) was used to analyze the metabolic profiling in both ESI positive and ESI negative ion modes. The acquired LC-MS raw data were analyzed by the progenesis QI software (Waters Corporation, Milford, CT, United States). Principal component analysis (PCA), partial least squares-discriminant analysis (PLS-DA), and orthogonal partial least-squares-discriminant analysis (OPLS-DA) were carried out to visualize the metabolic alterations among experimental groups, after mean centering and Pareto variance scaling, respectively. Variable importance in the projection (VIP) ranked the overall contribution of each variable to the OPLS-DA model, and those variables with VIP $>$ 1 were considered relevant for group discrimination. Student's *t*-test and fold change analyses were used to compare the difference of metabolites between the two groups.

Analysis of CT-Induced Release of Cytoplasmic Components

The intracellular concentration of potassium/magnesium in bacteria was determined as previously reported (Müller et al., 2016). Element concentrations were determined by iCAP 6300 Spectrometer (Thermo Fisher Scientific, United States) and normalized to the DMSO control. For analysis of ATP release, cells of *B. subtilis* 168 ($\sim 10^8$ CFU/mL) were resuspended in PBS and incubated with antibiotics at 37°C for 30 min. The samples were then centrifuged at 8,000 $\times$ *g* at 4°C for 10 min. A total of 100 μL of supernatant was mixed with an equal amount of working reagent from the BacTiter glow ATP detection Kit (Promega, United States) and incubated for 2 min. Luminescence was measured subsequently with a FLUOStar Omega (BMG LABTECH GmbH, Germany).

Propidium Iodide Stain

The cells of bacteria were grown to logarithmic phase and washed twice with PBS. The cell suspensions were then incubated with CT at 37°C for 2 h before centrifuging at 6,000 $\times$ *g* for 10 min. The acquired cells were resuspended in PBS and incubated with 30 μM propidium iodide (PI) at 37°C for 30 min. Fluorescence intensity was measured by an Accuri C6 flow cytometry with excitation at 490 nm and emission at 635 nm.

Determination of Membrane Potential

The effects of CT on bacterial membrane potential were determined first with a flow cytometer using fluorescent dye 3,3′-diethyloxacarbocyanine iodide [$DiOC_2(3)$] (Molecular Probes, Fisher Scientific). Bacteria grown to logarithmic growth phase were harvested and resuspended in PBS, and treated with drug and $DiOC_2(3)$ (10 μM) for 10 min at room temperature. Stained bacteria were assayed in a CytoFlex S flow cytometer (Beckman Coulter, United States) with a laser emitting at 485 nm. Fluorescence was observed in the green and red channels according to the instructions of the BacLight^{TM} Bacterial Membrane Potential Kit (Thermo Fisher Scientific, United States).

In investigating whether the effect of CT on bacterial membrane potential was time-dependent, the resuspended cells of bacteria in PBS were added into 96-well plates, incubated with 10 μM $DiOC_2(3)$ for 10 min in the dark, and the baseline recorded for 2 min using a FLUOstar Omega. Fluorescence intensity was measured at an excitation wavelength of 485 nm and two emission wavelengths, 530 nm (green) and 630 nm (red) (Saising et al., 2018). Subsequently, drugs were added, and fluorescence was measured for a specified time at room temperature.

Preparation of Inverted Membrane Vesicles

Membrane vesicles were isolated from the overnight cultures of *S. aureus* ATCC 43,300 (Lamontagne Boulet et al., 2018). The cells were suspended in KPN (20 mM potassium phosphate, 140 mM NaCl, pH 7.2), disrupted in a French press at 16,000 psi, and centrifuged at 6,000 $\times$ *g* for 30 min. The supernatant was centrifuged at 150,000 $\times$ *g* for 40 min using an ultracentrifuge (Optima XPN-100, Beckman, United States). The pellets were resuspended and centrifuged at 12,000 $\times$ *g* for 30 min. The supernatant containing membrane vesicles was stored at −80 °C. Protein concentration was estimated by a BCA protein assay kit (Beyotime Biotechnology, Shanghai, China) using bovine serum albumin as a standard.

ATP Synthesis Assay

Bacteria ($\sim 10^6$ CFU/mL) were preincubated with CT under stirring conditions for 10 min. Subsequently, 10 mM glucose (final concentration) was added, and the mixture further incubated for 30 min. Bacterial suspensions (100 μL) were then transferred into 96-well plates and mixed with an equal amount of working reagent from the BacTiter glow ATP detection Kit. Luminescence was finally measured with a FLUOStar Omega after incubation for 5 min. The effect of CT on ATP synthesis by membrane vesicles isolated from *S. aureus* was determined as previously described (Lamontagne Boulet et al., 2018).

Oxygen Consumption Assay

Oxygen consumption by membrane vesicles of *S. aureus* was measured polarographically with a clark-type polarographic electrode (Strathkelvin 782 dissolved oxygen meter, United Kingdom) (Weinstein et al., 2005). Membrane vesicles (0.2 mg/mL) were suspended in KPN buffer at 37°C, and 1 mM NADH was added to initiate respiration. Subsequently, CT was added to the reaction mixture, followed by the addition of dithiothreitol and ubiquinone-10. The result was expressed as the relative oxygen content, and the initial oxygen concentration was set as 100%.

Bacterial NADH/NAD$^+$ Ratios Assay

NADH/NAD$^+$ ratios were determined using an Amplite fluorimetric NAD/NADH ratio assay kit (AAT Bioquest, Inc., United States). Bacteria were grown to the early logarithmic phase and collected by centrifugation. The cell pellets were resuspended and treated with drug for 30 min at 37°C. The cells were pelleted at 6,000 $\times$ *g* for 5 min, washed, and resuspended with lysis buffer. Measurement of the

$NADH/NAD^+$ ratios in the supernatant was performed according to the manufacturer's instructions.

Molecular Docking Simulation

Molecular docking using Autodock 4.2 was employed to explore the mode of binding of CT with NDH-2. The X-ray crystal structure of NDH-2 from *S. aureus* (PDB ID: 4XDB) was retrieved from the Protein Data Bank[1]. All crystallographic water molecules and ions were removed from the protein structure. The 3-D structures of CT and ubiquinone-5 were retrieved from the PubChem database. The conformations were generated using the best conformational analysis method with CHARMM force field parameters. The obtained conformations were then docked into the binding site of NDH-2. The docked conformation with the lowest energy was used for the analysis of binding mode.

RESULTS

CT Is a Bacteriostatic Agent

To evaluate the bactericidal/bacteriostatic behavior of the agent, the MIC and MBC were determined for four strains (**Table 1**). The MICs of CT against tested bacteria ranged from 4 to 16 μg/mL. The MBC of CT for each strain was >64 μg/mL, and the MBC/MIC ratios were all higher than 4, indicating that CT is a bacteriostatic agent rather than a bactericidal agent (Clinical and Laboratory Standards Institute, 2009). To further examine the bacteriostatic activities of CT, time-kill assays against *S. aureus* ATCC 43300 and *B. subtilis* 168 were performed. As shown in **Figure 1**, less than one logarithmic unit of killing was observed at 4 × MIC of CT against two stains for 24 h, which was consistent with the bacteriostatic behavior revealed by the MBC/MIC analysis described above.

CT Induces Significant Changes in the Membrane Phospholipids

To obtain a first hint as to the antibacterial mechanism of CT, we conducted an untargeted metabolomics study.

[1]http://www.rcsb.org/

TABLE 1 | The MICs and MBCs of CT against reference strains.

Strains and compounds	MIC (μg/mL)	MBC (μg/mL)	MBC/MIC
***S. aureus* ATCC 29213**			
CT	16	>64	>4
Vancomycin	1	2	2
***S. aureus* ATCC 43300**			
CT	8	>64	>8
Vancomycin	2	2	1
***S. aureus* ATCC 25923**			
CT	8	>64	>8
Vancomycin	1	1	1
***B. subtilis* 168**			
CT	4	>64	>16
Vancomycin	0.5	>1	>2

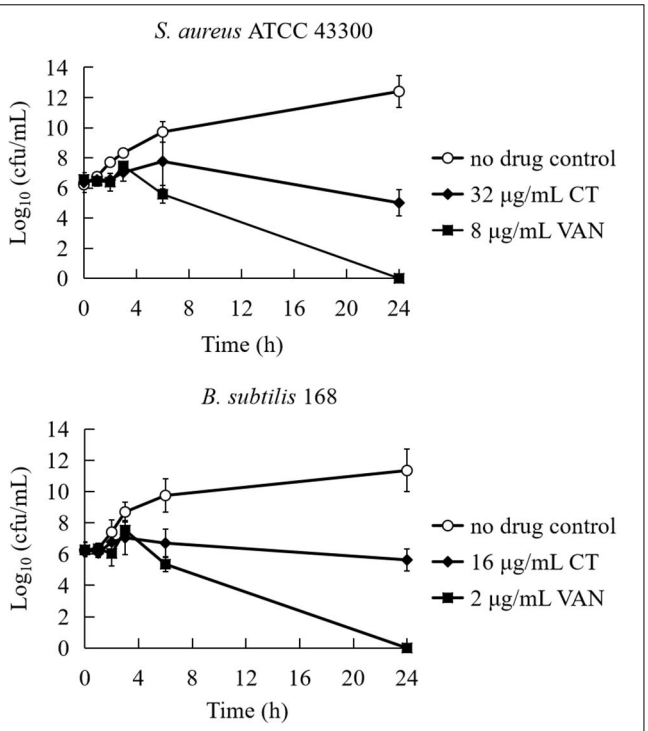

FIGURE 1 | Time-kill curves for *Bacillus subtilis* and *Staphylococcus aureus* treated with CT. The curves are viable cell concentrations plotted against time. MIC, minimum inhibitory concentration; VAN, vancomycin. DMSO (3.2%) is as a no drug control. Data represent the mean ± SD (n = 3).

PCA and heatmaps showed that the pooled biological quality control samples were tightly clustered together, indicating minimal technical variation. Under two treatment conditions, a total of 4,444 putative metabolites were identified. The PCA (**Supplementary Figure 1A**) and PLS-DA (**Supplementary Figure 1B**) showed that the untreated control and CT-treated samples were significantly separated. OPLS-DA (**Supplementary Figures 1C,D**) and two-tailed Student's t-test further revealed that 406 metabolites were significantly altered (VIP > 1, $p < 0.05$) following treatment with CT (**Supplementary Data Set 1**).

The most prominent changes associated with a specific metabolic pathway were mapped to KEGG pathways. Metabolites in purine metabolism, arginine biosynthesis, glycerophospholipid metabolism, sphingolipid metabolism, ABC transporters, biosynthesis of amino acids, and D-glutamine and D-glutamate metabolism were found to significantly differ between control and CT treatment ($p < 0.01$; **Supplementary Figure 2**). In general, CT dramatically decreased metabolites related to purine, pyrimidine, and amino acid metabolism. The relative abundance of nicotinamide adenine dinucleotide (NAD) was also significantly decreased in CT group ($\log_2$FC = −6.5; $p < 0.01$). Interestingly, CT induced significant changes in a wide range of the major membrane phospholipids in *B. subtilis*, including phosphatidylglycerol (PG), phosphatidylethanolamine (PE), and phospholipid acid (PA). More concretely, CT enriched a number of phospholipids {PE (15:0/15:0), PE (16:0/0:0), PE

[18:1(9Z)/0:0], Lyso PE (15:0/0:0), PA (10:0/17:0), PA (8:0/19:0), PA (P-16:0/13:0), and PA (P-16:0/12:0)} but decreased the levels of PG (15:0/0:0), PG (16:0/0:0)[U], and PG (17:0/0:0) (**Figure 2** and **Supplementary Data Set 2**). Many of metabolites affected by CT were related to glycerophospholipid, suggesting that CT might act as an antibacterial agent targeting the cell membrane.

CT Does Not Cause Severe Bacterial Membrane Damage but Dissipates Membrane Potential

Antimicrobial agents targeting cell membranes usually include membrane structure disruptors and respiratory chain inhibitors (Hurdle et al., 2011). To distinguish the type of action of CT, the effects of this compound on bacterial membrane integrity were investigated. We first investigated whether it causes the release of cytoplasmic components. As shown in **Figure 3A**, partial leakage of potassium and magnesium was observed when *B. subtilis* was treated with CT for 30 min. However, CT did not cause the release of ATP even after 120 min treatment with 32 μg/mL (**Figure 3B**), implying that CT does not cause severe membrane disruption. To confirm this finding, *S. aureus* and *B. subtilis* were stained with a fluorescent dye PI, an indicator of severe membrane disruption. When two strains were treated with nisin, marked increases in fluorescence were observed compared to the untreated cultures (**Figure 3C**). In contrast, incubation of cultures with 8 × MIC of CT for 120 min did not result in the uptake of PI (**Figure 3C**), indicating that CT did not cause serious damage to the bacterial membrane.

We then investigated the effect of CT on bacterial membrane potential. First, we evaluated the ability of CT to induce membrane depolarization using $DiOC_2(3)$. The green, fluorescent dye formed red fluorescent aggregates with increasing membrane potential. When the membrane potential is disrupted with a small molecule, the dye is released into the medium resulting in an increase in green fluorescence (Novo et al., 2000). As expected, the addition of CCCP to the suspensions of *B. subtilis* or *S. aureus* caused a marked increase in green fluorescence, while incubation of both strains with nigericin decreased the green fluorescence intensity (**Figures 4A,B**). Similar to CCCP, CT dissipated the membrane potential and led to a drastic increase in green fluorescence in two strains (**Figures 4A,B**). Further experiments showed that CT caused a dose-dependent and rapid dissipation of bacterial

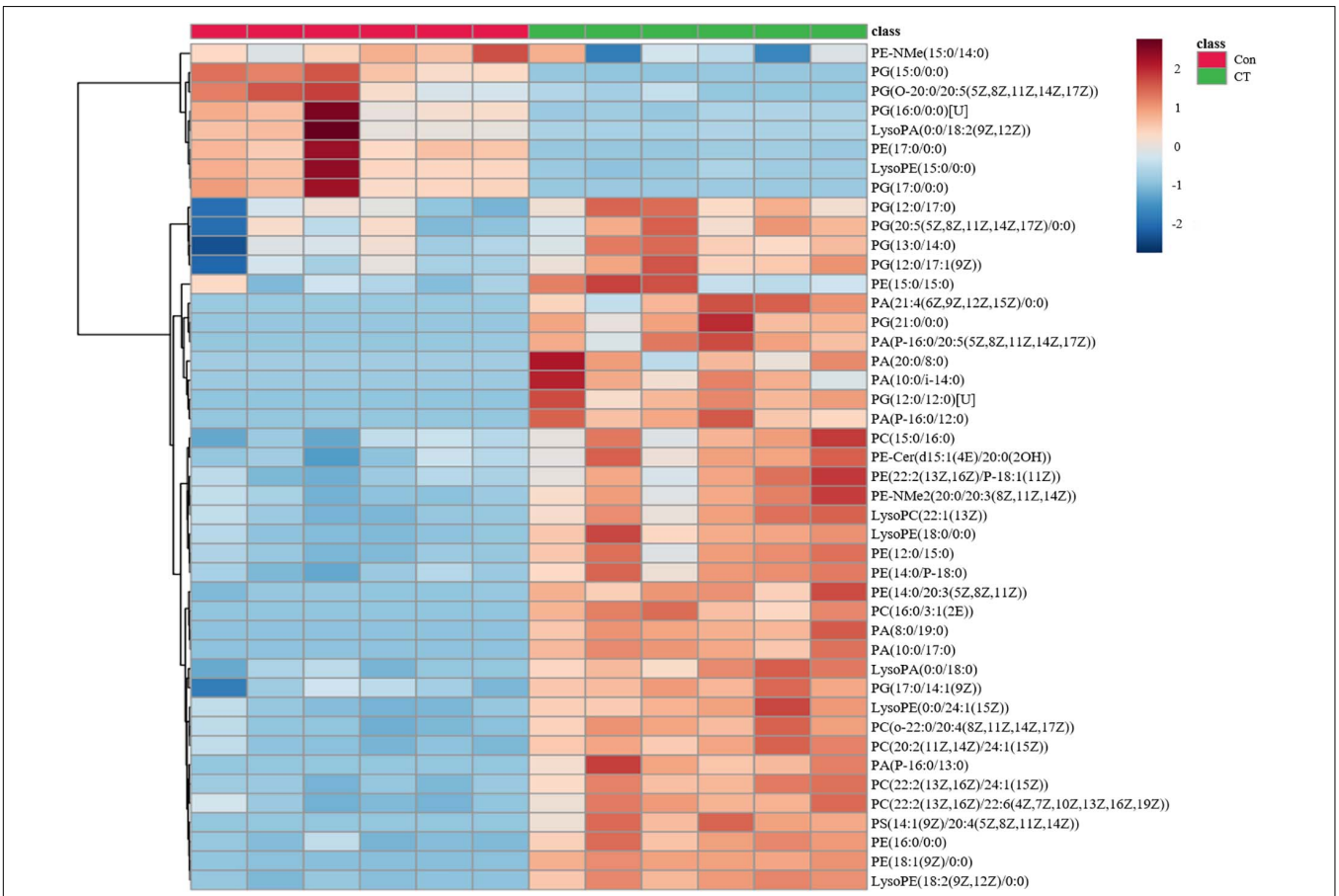

FIGURE 2 | CT significantly affects the glycerophospholipid metabolism of *Bacillus subtilis*. DMSO is as a control without drug (Con). Deep red represents the highest level, and deep blue represents the lowest level, with white representing equal levels. Each group is identified by green (CT) and red (DMSO) bars at the top of each column. Six biological replicates were tested for each sample.

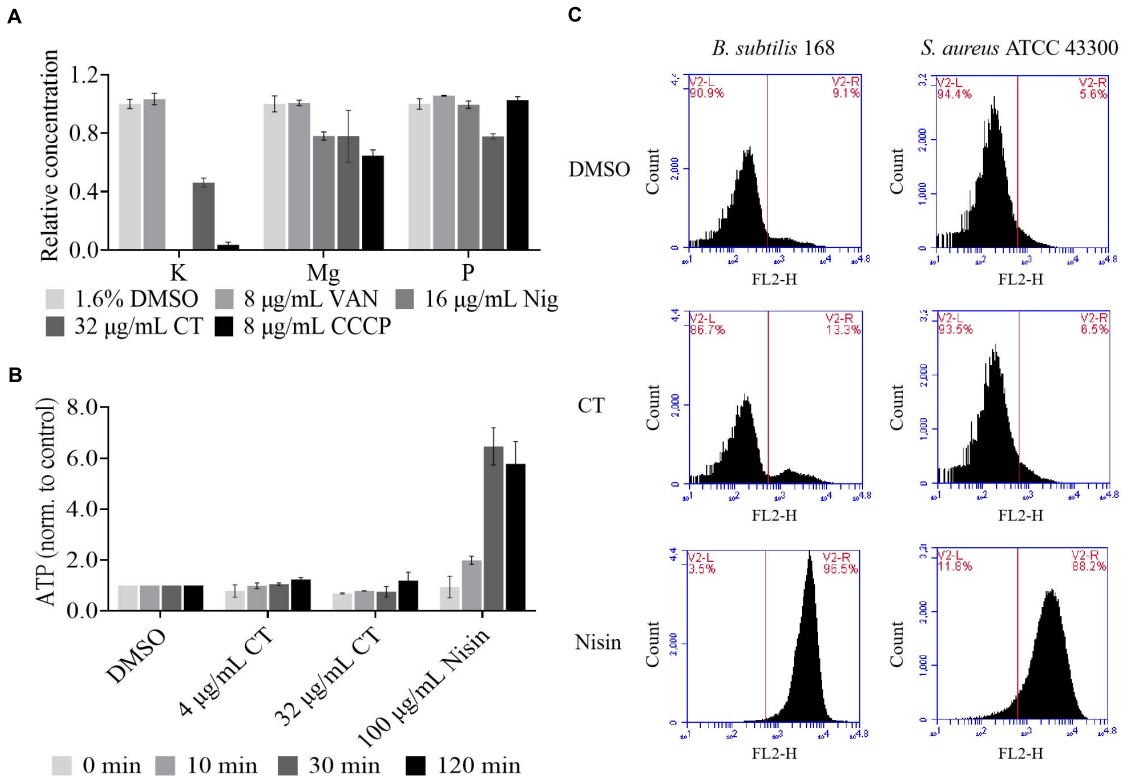

FIGURE 3 | Effect of CT on bacterial membrane integrity. **(A)** Determination of cellular element concentrations of *B. subtilis* 168 by inductively coupled plasma optical emission spectroscopy after CT treatment for 30 min. DMSO, non-drug treated control; VAN (vancomycin), negative control; Nig (nigericin), specific potassium ionophore; CCCP, depolarization agent. The experiments were carried out in triplicate in two independent replications. **(B)** Leakage of ATP following exposure of *B. subtilis* 168 to antimicrobial agents. Nisin, a pore-forming agent. Data are presented as mean ± SD of three independent experiments with triplicate measurements. **(C)** Staining with propidium iodide. Representative data from three independent cultures of *S. aureus* ATCC 43300 and *B. subtilis* 168 were shown following exposure to antimicrobial agents at 8 × MIC for 120 min.

membrane potential of within 1 min of the addition of this agent (**Figures 4C,D**). CT rapidly dissipated bacterial membrane potential without causing severe membrane damage, suggesting that this compound is a respiratory chain inhibitor.

CT Appears to Act as a Respiratory Chain Inhibitor Probably by Targeting NDH-2

The oxygen consumption of membrane vesicles derived from *S. aureus* was determined in a cell-free assay to test whether CT is a respiratory chain inhibitor. An immediate linear consumption of oxygen was observed when NADH was added to the staphylococcal membrane vesicles. The oxygen consumption was immediately inhibited by the addition of CT (**Figure 5A**), confirming that this agent is an inhibitor of respiratory systems. Similar results were observed with the addition of thioridazine (**Figure 5B**). As negative controls, vancomycin (**Figure 5C**) or DMSO (**Figure 5D**) did not inhibit the oxygen consumption initiated by NADH. Interestingly, respiration in the CT-arrested membranes was restored by the addition of dithiothreitol/ubiquinone-10. It was previously reported that there is no gene encoding type-1 NADH:quinone oxidoreductase, bc_1 complex, and cytochrome *c* oxidase in the genome of *S. aureus*, and that NDH-2 is the sole NADH:quinone oxidoreductase expressed in this strain (Schurig-Briccio et al., 2014). Thus, it was reasonable to speculate that the primary site of inhibition of respiration by CT is NDH-2. In agreement with the hypothesis, CT prevented efficient reoxidization of NADH to NAD^+, which resulted in a substantially increased NADH/NAD^+ ratio in CT-treated *S. aureus* (**Figure 5E**). The NAD^+ level in *B. subtilis* treated with CT also decreased significantly revealed by the metabonomic analysis described above.

To understand the interaction mode of CT binding to NDH-2, the molecular docking was performed. As shown in **Figure 6A**, ubiquinone interacted with Ala319, Gln320, Met323, Arg350, Thr352, Phe366, Ile382, and Ala386 *via* hydrophobic contact, and generated hydrogen bond interaction with flavin adenine dinucleotide (FAD), which is another important cofactor for NDH-2 (Schurig-Briccio et al., 2014). This observation was consistent with the proposal that the quinone binding cavity is near the *si*-side of FAD, and lined mostly by hydrophobic residues, namely, Tyr15, Ala319, Met323, Ile382, and Ala386 (Heikal et al., 2014; Sena et al., 2015). Intriguingly, CT was found to form a hydrogen bond with Arg385 (**Figure 6B**), which is located at the tunnel entrance of the quinone binding

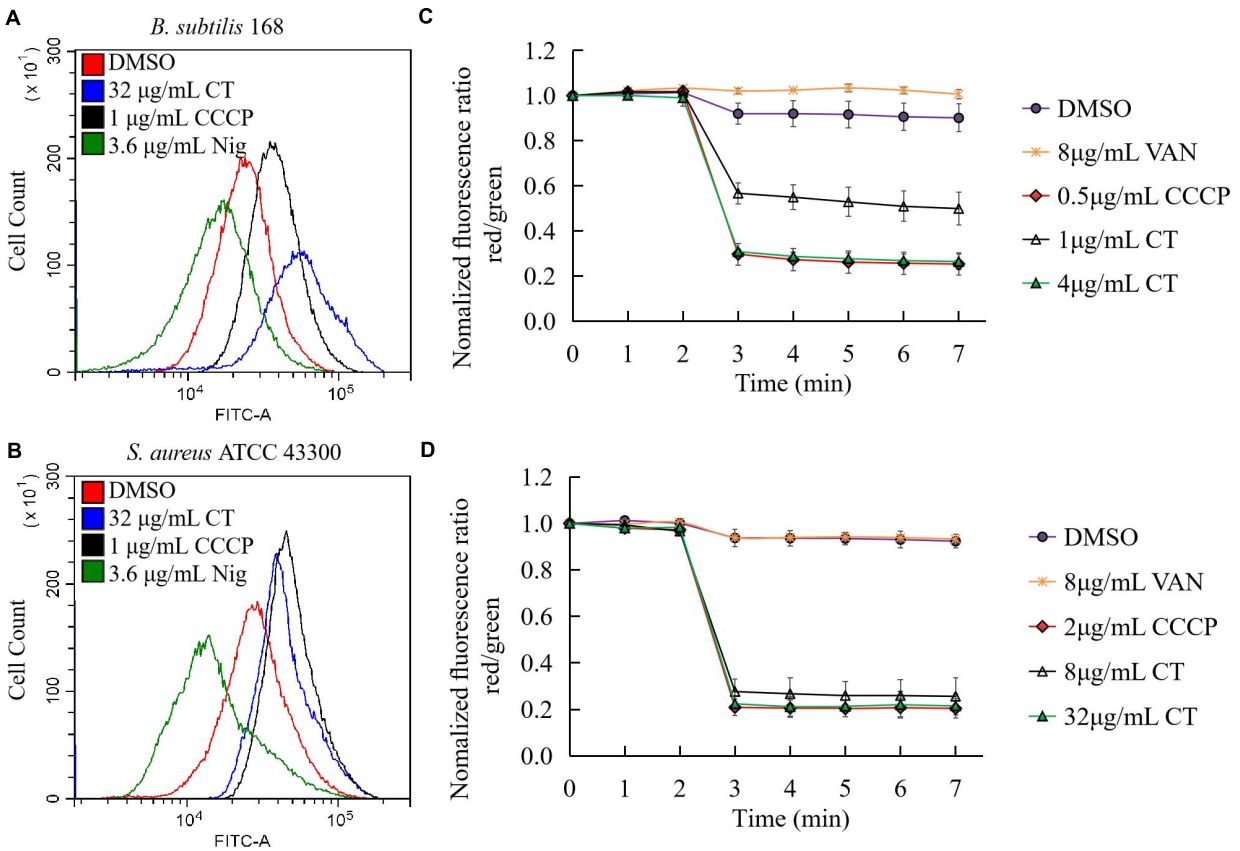

FIGURE 4 | Effect of CT on membrane potential of *B. subtilis* 168 **(A,C)** and *S. aureus* ATCC 43300 **(B,D)**. **(A,B)** Membrane potential estimation by flow cytometry using $DiOC_2(3)$ dye; Representative data from three independent cultures of both strains were shown following exposure to different agents for 10 min. **(C,D)** Fluorescence of $DiOC_2(3)$ was detected at an excitation wavelength of 485 nm and two emission wavelengths, 530 nm (green) and 630 nm (red), using a microplate reader. Addition of CT to the cell suspensions of bacteria is indicated by an arrow. Data are presented as mean ± SD of three independent experiments. DMSO (1.6%), non-drug treated control; CCCP, depolarization control; Nigericin, hyperpolarization control; VAN (vancomycin), negative control.

cavity in *S. aureus* NDH-2 (Sena et al., 2015). Besides, NDH-2 interacted with CT *via* hydrophobic contact through residues Gln320, Met323, Arg350, Ile382, and Lys389, which are partially overlapped with the binding sites of quinone. Thus, we speculated that CT could competitively inhibit the binding of quinone to NDH-2. In agreement with this hypothesis, supplementing CT-treated cultures with MK4 rescued the CT-treated bacteria (**Figure 6C** and **Table 2**). Interestingly, an antagonistic effect was observed in the combination of MK4 with 2-n-heptyl-4-hydroxyquinoline-*N*-oxide (HQNO), but not thioridazine (**Table 2**), both of which were reported to be NDH-2 inhibitors with different mechanisms (Schurig-Briccio et al., 2014; Sena et al., 2015).

CT Inhibits the Respiratory ATP Synthesis of Bacteria

Blocking the access of electrons into the respiratory chain achieved by inhibiting essential enzyme NDH-2 normally prevents the synthesis of ATP. Thus, we investigated the impact of inhibition of ATP synthesis by CT on cellular ATP levels. As shown in **Figure 7A**, a significant decrease in ATP levels was observed in CT-treated *B. subtilis* cells compared to the controls. The 50% inhibitory concentration (IC_{50}) of CT against *B. subtilis* was found to be 9.6 ± 1.3 μg/mL. However, CT did not significantly change ATP levels in *S. aureus* ATCC 43300 (**Supplementary Figure 3**). To eliminate the interference from ATP synthesized by phosphorylation at the substrate level, we determined the inhibitory activities of CT on ATP synthesis in staphylococcal membrane vesicles. As depicted in **Figure 7B**, CT showed remarkable inhibitory activity with an IC_{50} value of 107.1 ± 8.6 μg/mL, indicating that it possessed the ability to inhibit the respiratory ATP synthesis of *S. aureus*.

CT Interactions With Other Respiratory Chain Inhibitors

Synergistic interactions have been reported between molecules targeting different components of the bacterial respiratory chain (Berube and Parish, 2017; Foo et al., 2018; Iqbal et al., 2018; Lu et al., 2019). Thus, checkerboard assays for two-drug combinations were performed to determine the nature of interactions between CT with HQNO, thioridazine, 7-Methoxy-2-naphthol (MenA inhibitor) (Choi et al., 2016), or tomatidine

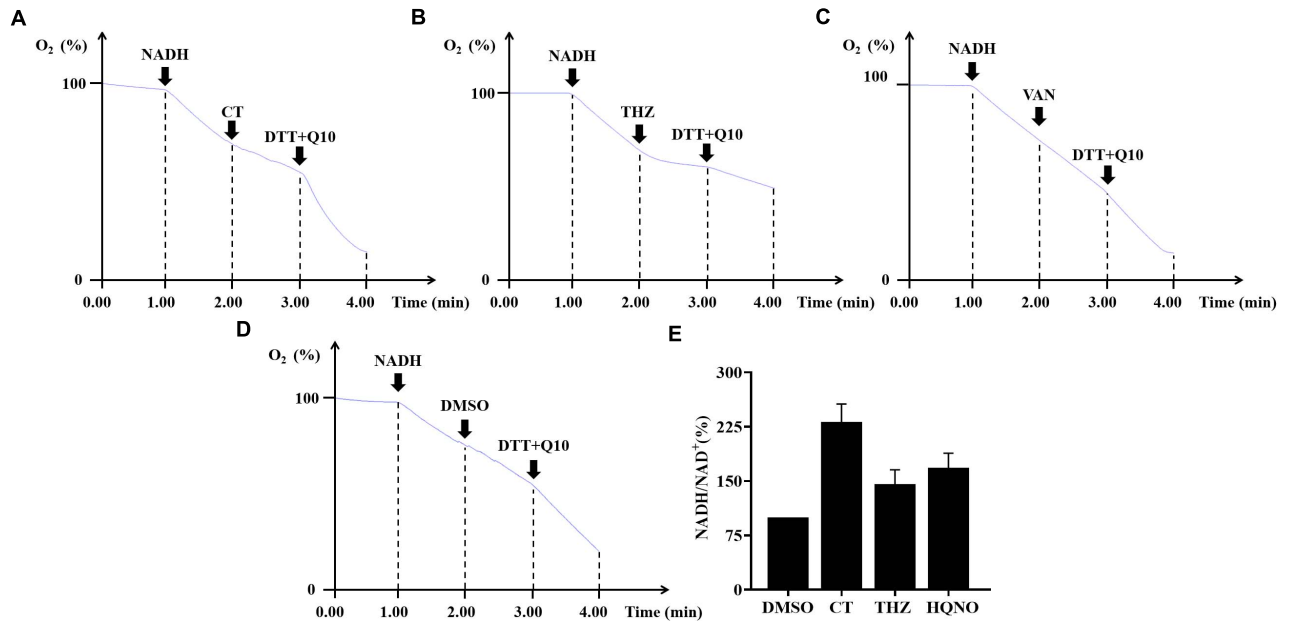

FIGURE 5 | The effects of CT on respiratory chain activity of bacteria. **(A–D)** Inhibition of oxygen consumption of staphylococcal membrane vesicles by CT. Respiration was initiated by the addition of 1 mM NADH. Thioridazine (THZ) was used as positive control. Vancomycin (VAN) and DMSO were used as negative control, respectively. CT, 80 μg/mL; THZ, 100 μg/mL; VAN, 64 μg/mL; DMSO, 2%; dithiothreitol (DTT), 2.85 mM; ubiquinone-10 (Q10), 40 μM. **(E)** Effect of CT on NADH/NAD^+ ratios. Intracellular NADH/NAD^+ ratios of *S. aureus* ATCC 43300 were determined by an Amplite fluorimetric NAD/NADH ratio assay kit. DMSO, 3.2%; CT, 32 μg/mL; thioridazine (THZ), 64 μg/mL; HQNO, 32 μg/mL.

(ATP Synthase inhibitor) (Lamontagne Boulet et al., 2018) in *S. aureus* ATCC 43300. As shown in **Table 3**, the interaction of CT with HQNO was additive with a fractional inhibitory concentration index (FICI) value of 0.75. The combinations of CT with 7-Methoxy-2-naphthol and thioridazine showed promising synergy with FICI values of 0.31 and 0.37, respectively. A strong synergy between CT and tomatidine with FICI of <0.19 was also observed.

DISCUSSION

Plant-derived antimicrobial agents have received much attention due to their effectiveness against drug-resistant strains. Thousands of compounds have been listed as antimicrobial phytochemicals (Ríos and Recio, 2005; Radulovic et al., 2013; Barbieri et al., 2017). However, most of the MICs of these plant metabolites are much higher than antibiotics commercially available, restricting their clinical application. One promising approach to improve the antimicrobial activity of phytochemicals involves the combination of different bioactive compounds. A deep understanding of the mechanism of drug action is conducive to the rational combination of antimicrobial agents. In this study, the antibacterial mechanism of CT and its effect of combination therapy were investigated.

Despite rapid technological progress, the identification of mechanisms of drug action is still a difficult task (Nonejuie et al., 2013; Zampieri, 2018; Martin et al., 2020). Metabolomics can detect dynamic changes in the abundance of thousands of small molecules in response to drug treatment and provide a deep insight into the mechanism of drug action (Zampieri, 2018). To obtain a first hint regarding the mechanism of action of CT, an untargeted metabolomics study of *B. subtilis* was conducted. The CT treatment induced significant changes in a wide range of glycerophospholipids. Similar alterations of the major membrane phospholipids were observed when bacteria were treated with surfactin or polymyxin B (Uttlová et al., 2016; Tran et al., 2018), both of which are membrane-damaging antimicrobials. Thus, we speculated that CT is also an antibacterial agent targeting the cell membrane. Unexpectedly, CT was subsequently proved to be a compound targeting the function of the membrane-associated respiratory chain rather than the organization of the bacterial membrane bilayer.

The most striking feature of *B. subtilis* cells treated with CT was the reduced level of PG accompanied by an increase in the content of PE and PA. These phospholipids vary not only in the length of fatty acids but also in the composition of their headgroups, which differ significantly in charge and propensity to form non-bilayer structures (Salzberg and Helmann, 2008). PA has been shown to stabilize and bind stronger than PG *via* H-bonds/electrostatic interactions with the membrane proteins, such as KcsA (Raja et al., 2007). PE was also reported to facilitate membrane association and insertion of monomeric KcsA, due to its small headgroup and extensive hydrogen bonding properties (Raja, 2011). Thus, we suggest that the increased levels of PA and PE contribute to the assembly and stabilization of membrane-bound respiratory chain proteins, which may counteract the destabilizing effect induced by CT. The altered compositions of

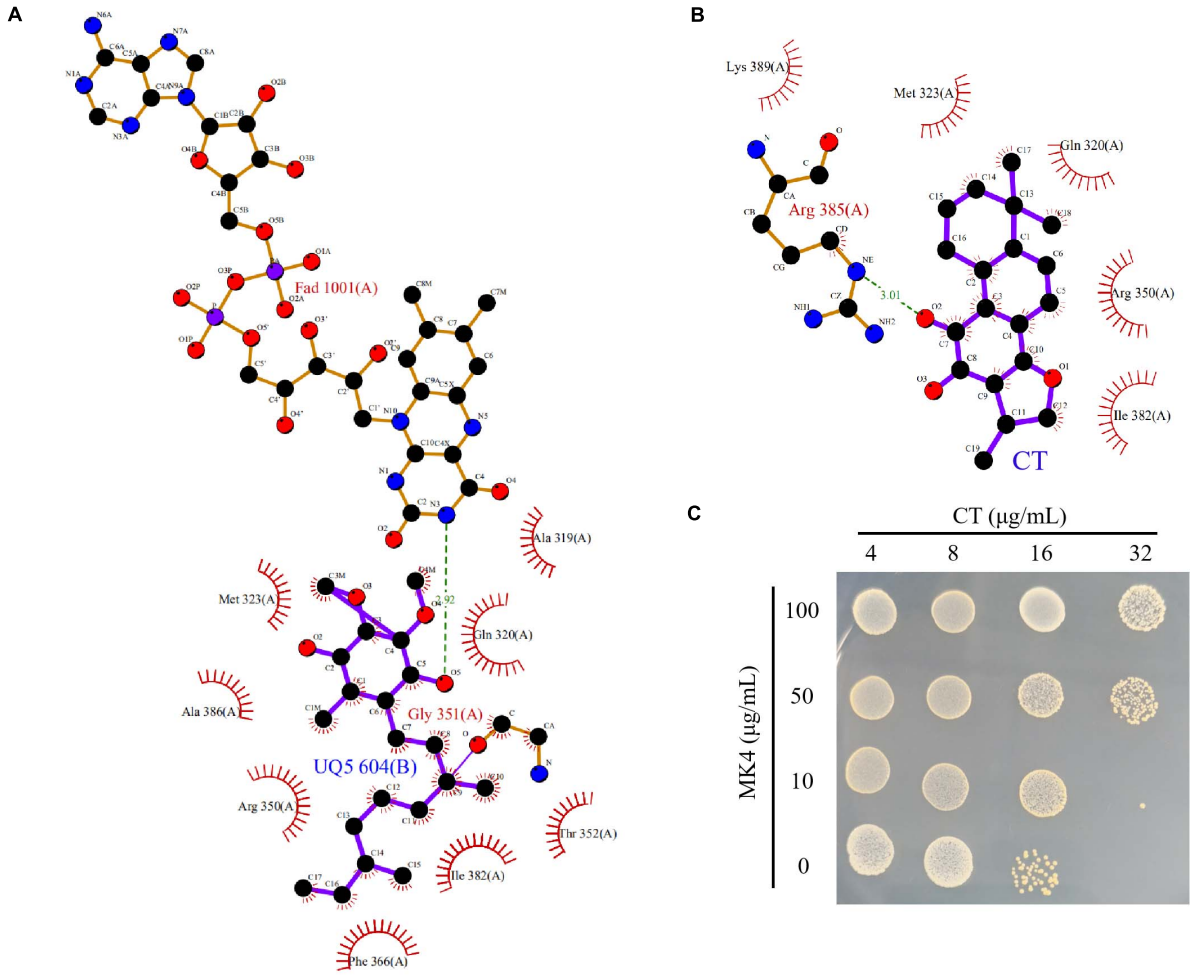

FIGURE 6 | CT competitively inhibits the binding of quinone to NDH-2. **(A)** Configuration for the interaction of ubiquinone-5 (UQ5) with NDH-2. **(B)** Configuration for the interaction of CT with NDH-2. **(C)** MK4 antagonizes the antibacterial activity of CT.

phospholipid may also impede entry of CT into the membrane, hindering access to its target. The relationship between the altered compositions of membrane phospholipid and the inhibition of the respiratory chain activity in bacteria treated with CT will need further study.

Cryptotanshinone rapidly dissipated bacterial membrane potential without causing severe membrane damage, suggesting that this compound is a respiratory chain inhibitor. It is documented that NADH produced in the cytoplasm of *S. aureus* is reoxidized to NAD^+ mainly by NDH-2, the sole type of NADH:quinone oxidoreductase expressed in this strain (Schurig-Briccio et al., 2014; Sena et al., 2015). Menaquinol generated from the corresponding menaquinone by NDH-2 is then directly oxidized by terminal oxidases (Schurig-Briccio et al., 2014). Taking advantage of the simple organization of the staphylococcal respiratory chain, we used the membrane vesicles derived from *S. aureus* to investigate the effect of CT on respiratory activity by oxygen consumption assay. The NADH-driven oxygen consumption was immediately inhibited by the addition of CT, confirming that this agent is an inhibitor of respiratory systems. Interestingly, respiration in the CT-arrested membranes was restored by the addition of dithiothreitol/ubiquinone-10, which donated electrons at the level of quinol:oxygen oxidoreductase. The recovery of oxygen consumption implied that the site of inhibition by CT is NDH-2, which is the only NADH dehydrogenase upstream of terminal quinol:oxygen oxidoreductase in *S. aureus* (Schurig-Briccio et al., 2014). This is supported by the observation that the $NADH/NAD^+$ ratio was substantially increased in CT-treated *S. aureus*.

Type II NADH dehydrogenase is a membrane bound protein with a non-covalently bound FAD as a cofactor, which catalyses the cytoplasmic oxidation of NADH and reduction of quinone in the membrane. The crystal structure of NDH-2 from *S. aureus* suggested that NADH and the quinone bind to different sites of the enzyme (Sena et al., 2015). The docking analysis showed that the binding sites of CT to NDH-2 partially overlap with that of quinone, implying that CT would competitively inhibit the binding of quinone to NDH-2. Consistent with this speculation,

TABLE 2 | Effects of menaquinone on antibacterial activity of CT.

Indicator strain	MIC (μg/mL)					
	CT	CT + MK4[a]	HQNO	HQNO + MK4[a]	THZ	THZ + MK4[a]
S. aureus ATCC 43300	8	>32	8	32	32	32
B. subtilis 168	4	>32	–	–	–	–

[a]*MK4 (menaquinone-4) concentration is 100 μg/mL.*

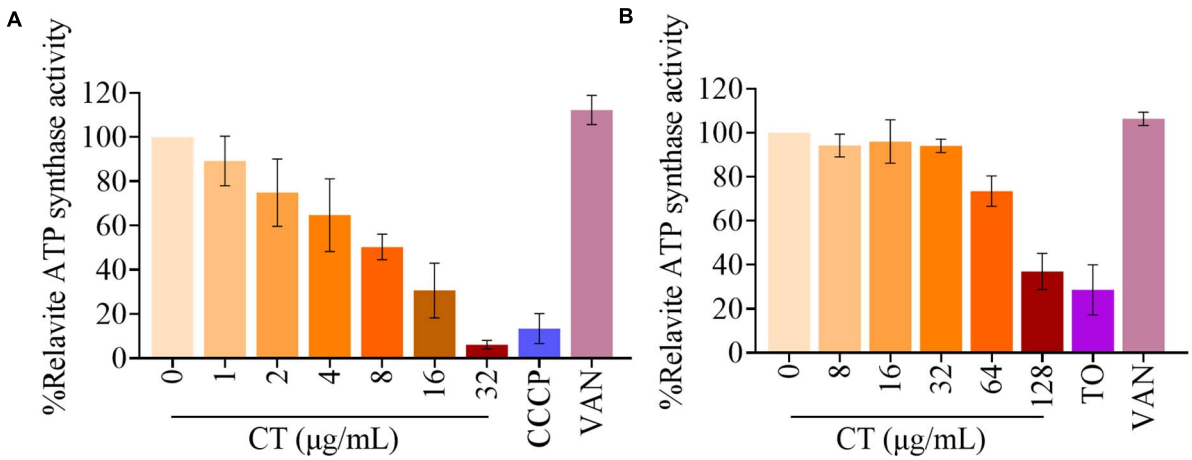

FIGURE 7 | Effect of CT on ATP synthesis. **(A)** Cellular ATP levels in *B. subtilis* 168 were measured in the presence of CT at specified concentration after the addition of 10 mM glucose for 30 min. Vancomycin (VAN, 2 μg/mL) and CCCP (8 μg/mL) were used as negative and positive control, respectively. **(B)** The ATP synthesis activity was determined in membrane vesicles isolated from *S. aureus* ATCC 43300 energized with NADH. Vancomycin (VAN, 32 μg/mL) and Tomatidine (TO, 64 μg/mL) were used as negative and positive control, respectively. Data from three independent experiments are presented as mean ± SD.

TABLE 3 | Interactions between CT and other respiratory chain inhibitors against *S. aureus* ATCC 43300.

Drug combination	Alone	Combination	FICI	Category[a]
CT	8	2	0.75	Additive
HQNO	8	4		
CT	8	1	0.37	Synergistic
Thioridazine	32	8		
CT	8	0.5	0.31	Synergistic
7-Methoxy-2-naphthol	512	128		
CT	8	0.25	<0.19	Synergistic
Tomatidine	>64	10		

[a]*FICI categories: ≤0.5, synergistic; >0.5 to ≤1, additive; >1 to < 4, no interaction; ≥4, antagonism.*

the antimicrobial activity of CT against *B. subtilis* and *S. aureus* was blocked by MK4. Some antimicrobial agents mainly targeting NDH-2 have been extensively described. Among them, HQNO was found to competitively inhibit binding of a quinone substrate for *S. aureus* NDH-2 (Sena et al., 2015; Petri et al., 2018), while phenothiazine compounds were reported to act as non-competitive inhibitors for quinone (Yano et al., 2006). In agreement with the literature, MK4 supplementation blocked the anti-*S. aureus* activity of HQNO but not phenothiazine thioridazine (**Table 2**). The observations that the combination of CT with thioridazine but not HQNO, exerted synergistic activity against *S. aureus* (**Table 3**), further implied that CT might act as a competitive inhibitor with respect to quinone.

Type II NADH dehydrogenase is an important enzyme in the respiratory system of many organisms, including *S. aureus* and *B. subtilis*. It is a primary entry point for electrons into the electron transport chain for generation of ATP, and is responsible for maintaining cellular NAD^+/NADH balance. Blocking the introduction of electrons into the respiratory chain achieved by inhibition of the enzyme NDH-2 can indirectly dissipate proton motive force, which is composed of the membrane potential and the transmembrane proton gradient. The proton motive force is essentially involved in the process of respiratory ATP synthesis and the active transport of solutes such as amino acids (Allen et al., 1991; Hards and Cook, 2018). This could be the reason why CT not only disrupted the NAD^+/NADH balance and proton motive force but also inhibited respiratory ATP synthesis.

CONCLUSION

In general, the direct and indirect evidence described above supports that CT is a respiratory chain inhibitor probably by targeting NDH-2, although more research is needed to confirm this. CT rapidly dissipates bacterial membrane potential and disrupts the NAD^+/NADH balance without causing significant membrane damage. Menaquinone antagonizes antibacterial activity of CT, while synergistic activities can be achieved by the

combinations of CT with thioridazine, 7-Methoxy-2-naphthol, or tomatidine, but not HQNO. All these observations are consistent with the finding that CT is a respiratory chain inhibitor. However, the mechanisms of its antibacterial activity should be investigated further.

DATA AVAILABILITY STATEMENT

The original contributions presented in the study are included in the article/**Supplementary Material**. Further inquiries can be directed to the corresponding author/s.

AUTHOR CONTRIBUTIONS

C-DQ, B-CC, and Z-SD designed the experiments. B-CC, J-SD, N-PC, X-WG, and L-FM conducted the experiments. C-DQ, B-CC, Z-SD, J-SD, N-PC, X-WG, and L-FM analyzed the data. C-DQ, B-CC, and Z-SD wrote the manuscript. All authors read and approved the final version of the manuscript.

FUNDING

This work was supported by the National Key Research and Development Program of China (Grant No. 2019YFC1708604) and Zhejiang Medical and Health Science and Technology Plan Project (Grant No. 2017KY498).

ACKNOWLEDGMENTS

The authors would like to thank the technical support from the Public Platform of Medical Research Center, Academy of Chinese Medical Science, Zhejiang Chinese Medical University.

SUPPLEMENTARY MATERIAL

The Supplementary Material for this article can be found online at: https://www.frontiersin.org/articles/10.3389/fmicb.2021.647289/full#supplementary-material

Supplementary Figure 1 | Score scatter plots of PCA, PLS-DA, OPLS-DA, and validation plots of OPLS-DA for two comparative groups. **(A)** PCA for CT/Con comparative group. **(B)** PLS-DA for CT/Con comparative group. **(C)** OPLS-DA for CT/Con comparative group. **(D)** Validation plots of OPLS-DA for CT/Con comparative group. CT, 16 μg/mL cryptotanshinone-treated group; Con, 1.6% DMSO-treated group.

Supplementary Figure 2 | Histogram of the different pathway −log (P = 10) values enriched in the CT-treated strain according to KEGG pathway analysis. The horizontal line (blue) at 1.3 indicates $P < 0.05$; the horizontal line (red) at 2 indicates $P < 0.01$.

Supplementary Figure 3 | Effect of CT on ATP synthesis. Cellular ATP levels in *S. aureus* ATCC 43300 were measured in the presence of CT at specified concentration after the addition of 10 mM glucose for 30 min. Vancomycin (VAN, 8 μg/mL) and CCCP (8 μg/mL) were used as negative and positive control, respectively.

Supplementary Data Set 1 | Y1-6 is cryptotanshinone-treated group.

Supplementary Data Set 2 | D1-6 is DMSO-treated group.

REFERENCES

Allen, N. E., Alborn, W. E., and Hobbs, J. N. (1991). Inhibition of membrane potential-dependent amino acid transport by daptomycin. *Antimicrob. Agents Chemother.* 35, 2639–2642. doi: 10.1128/AAC.35.12.2639

Al-Mebairik, N. F., El-Kersh, T. A., Al-Sheikh, Y. A., and Marie, M. A. M. (2016). A review of virulence factors, pathogenesis, and antibiotic resistance in Staphylococcus aureus. *Rev. Med. Microbiol.* 27, 50–56. doi: 10.1097/MRM.0000000000000067

Andries, K. (2005). A Diarylquinoline Drug Active on the ATP Synthase of Mycobacterium tuberculosis. *Science* 307, 223–227. doi: 10.1126/science.1106753

Anraku, Y. (1988). Bacterial Electron Transport Chains. *Annu. Rev. Biochem.* 57, 101–132. doi: 10.1146/annurev.bi.57.070188.000533

Azarkina, N., Siletsky, S., Borisov, V., von Wachenfeldt, C., Hederstedt, L., and Konstantinov, A. A. (1999). A Cytochrome bb'-type Quinol Oxidase in Bacillus subtilis Strain 168. *J. Biol. Chem.* 274, 32810–32817. doi: 10.1074/jbc.274.46.32810

Barbieri, R., Coppo, E., Marchese, A., Daglia, M., Sobarzo-Sánchez, E., Nabavi, S. F., et al. (2017). Phytochemicals for human disease: An update on plant-derived compounds antibacterial activity. *Microbiol. Res.* 196, 44–68. doi: 10.1016/j.micres.2016.12.003

Berube, B. J., and Parish, T. (2017). Combinations of Respiratory Chain Inhibitors Have Enhanced Bactericidal Activity against Mycobacterium tuberculosis. *Antimicrob. Agents Chemother.* 62:1677. doi: 10.1128/AAC.01677-17

Boersch, M., Rudrawar, S., Grant, G., and Zunk, M. (2018). Menaquinone biosynthesis inhibition: a review of advancements toward a new antibiotic mechanism. *RSC Adv.* 8, 5099–5105. doi: 10.1039/C7RA12950E

Cha, J.-D., Lee, J.-H., Choi, K. M., Choi, S.-M., and Park, J. H. (2014). Synergistic Effect between Cryptotanshinone and Antibiotics against Clinic Methicillin and Vancomycin-Resistant Staphylococcus aureus. *Evid. Based Compl. Altern. Med.* 2014, 1–16. doi: 10.1155/2014/450572

Chen, B.-C., Lin, C.-X., Chen, N.-P., Gao, C.-X., Zhao, Y.-J., and Qian, C.-D. (2018). Phenanthrene Antibiotic Targets Bacterial Membranes and Kills Staphylococcus aureus With a Low Propensity for Resistance Development. *Front. Microbiol.* 9:1593. doi: 10.3389/fmicb.2018.01593

Choi, S., Larson, M. A., Hinrichs, S. H., Bartling, A. M., Frandsen, J., and Narayanasamy, P. (2016). Discovery of bicyclic inhibitors against menaquinone biosynthesis. *Future Med. Chem.* 8, 11–16. doi: 10.4155/fmc.15.168

Clinical and Laboratory Standards Institute (2009). *Methods for dilution antimicrobial susceptibility tests for bacteria that grow aerobically. Approv. Stand. (8th ed.)*. Wayne, PA: CLSI, publication.

Feng, H., Xiang, H., Zhang, J., Liu, G., Guo, N., Wang, X., et al. (2009). Genome-Wide Transcriptional Profiling of the Response of Staphylococcus aureus to Cryptotanshinone. *J. Biomed. Biotechnol.* 2009, 1–8. doi: 10.1155/2009/617509

Foo, C. S., Lupien, A., Kienle, M., Vocat, A., Benjak, A., Sommer, R., et al. (2018). Arylvinylpiperazine Amides, a New Class of Potent Inhibitors Targeting QcrB of Mycobacterium tuberculosis. *MBio* 9:18. doi: 10.1128/mBio.01276-18

Hamamoto, H., Urai, M., Ishii, K., Yasukawa, J., Paudel, A., Murai, M., et al. (2015). Lysocin E is a new antibiotic that targets menaquinone in the bacterial membrane. *Nat. Chem. Biol.* 11, 127–133. doi: 10.1038/nchembio.1710

Hards, K., and Cook, G. M. (2018). Targeting bacterial energetics to produce new antimicrobials. *Drug Resist. Updat.* 36, 1–12. doi: 10.1016/j.drup.2017.11.001

Heikal, A., Nakatani, Y., Dunn, E., Weimar, M. R., Day, C. L., Baker, E. N., et al. (2014). Structure of the bacterial type II NADH dehydrogenase: a monotopic membrane protein with an essential role in energy generation. *Mol. Microbiol.* 91, 950–964. doi: 10.1111/mmi.12507

Hurdle, J. G., O'Neill, A. J., Chopra, I., and Lee, R. E. (2011). Targeting bacterial membrane function: an underexploited mechanism for treating persistent infections. *Nat. Rev. Microbiol.* 9, 62–75. doi: 10.1038/nrmicro2474

Iqbal, I., Bajeli, S., Akela, A., and Kumar, A. (2018). Bioenergetics of Mycobacterium: An Emerging Landscape for Drug Discovery. *Pathogens* 7:24. doi: 10.3390/pathogens7010024

Koul, A., Dendouga, N., Vergauwen, K., Molenberghs, B., Vranckx, L., Willebrords, R., et al. (2007). Diarylquinolines target subunit c of mycobacterial ATP synthase. *Nat. Chem. Biol.* 3, 323–324. doi: 10.1038/nchembio884

Lamontagne Boulet, M., Isabelle, C., Guay, I., Brouillette, E., Langlois, J.-P., Jacques, P. -É, et al. (2018). Tomatidine Is a Lead Antibiotic Molecule That Targets Staphylococcus aureus ATP Synthase Subunit C. *Antimicrob. Agents Chemother.* 62:2197. doi: 10.1128/AAC.02197-17

Lee, D.-S., Lee, S.-H., Noh, J.-G., and Hong, S.-D. (1999). Antibacterial Activities of Cryptotanshinone and Dihydrotanshinone I from a Medicinal Herb, Salvia miltiorrhiza Bunge. *Biosci. Biotechnol. Biochem.* 63, 2236–2239. doi: 10.1271/bbb.63.2236

Lu, G. (2020). The Mechanism in the Protection of Cryptotanshinone against Infection by Listeria monocytogenes.

Lu, X., Williams, Z., Hards, K., Tang, J., Cheung, C.-Y., Aung, H. L., et al. (2019). Pyrazolo[1,5- a]pyridine Inhibitor of the Respiratory Cytochrome bcc Complex for the Treatment of Drug-Resistant Tuberculosis. *ACS Infect. Dis.* 5, 239–249. doi: 10.1021/acsinfecdis.8b00225

Martin, J. K., Sheehan, J. P., Bratton, B. P., Moore, G. M., Mateus, A., Li, S. H.-J., et al. (2020). A Dual-Mechanism Antibiotic Kills Gram-Negative Bacteria and Avoids Drug Resistance. *Cell* 181, 1518–1532.e14. doi: 10.1016/j.cell.2020.05.005

Melo, A. M. P., Bandeiras, T. M., and Teixeira, M. (2004). New Insights into Type II NAD(P)H:Quinone Oxidoreductases. *Microbiol. Mol. Biol. Rev.* 68, 603–616. doi: 10.1128/MMBR.68.4.603-616.2004

Müller, A., Wenzel, M., Strahl, H., Grein, F., Saaki, T. N. V., Kohl, B., et al. (2016). Daptomycin inhibits cell envelope synthesis by interfering with fluid membrane microdomains. *Proc. Natl. Acad. Sci.* 113, E7077–E7086. doi: 10.1073/pnas.1611173113

Nonejuie, P., Burkart, M., Pogliano, K., and Pogliano, J. (2013). Bacterial cytological profiling rapidly identifies the cellular pathways targeted by antibacterial molecules. *Proc. Natl. Acad. Sci.* 110, 16169–16174. doi: 10.1073/pnas.1311066110

Novo, D. J., Perlmutter, N. G., Hunt, R. H., and Shapiro, H. M. (2000). Multiparameter Flow Cytometric Analysis of Antibiotic Effects on Membrane Potential, Membrane Permeability, and Bacterial Counts of Staphylococcus aureus andMicrococcus luteus. *Antimicrob. Agents Chemother.* 44, 827–834. doi: 10.1128/AAC.44.4.827-834.2000

Paudel, A., Hamamoto, H., Panthee, S., and Sekimizu, K. (2016). Menaquinone as a potential target of antibacterial agents. *Drug Discov. Ther.* 10, 123–128. doi: 10.5582/ddt.2016.01041

Petri, J., Shimaki, Y., Jiao, W., Bridges, H. R., Russell, E. R., Parker, E. J., et al. (2018). Structure of the NDH-2 – HQNO inhibited complex provides molecular insight into quinone-binding site inhibitors. *Biochim. Biophys. Acta Bioenerg.* 1859, 482–490. doi: 10.1016/j.bbabio.2018.03.014

Radulovic, N. S., Blagojevic, P. D., Stojanovic-Radic, Z. Z., and Stojanovic, N. M. (2013). Antimicrobial Plant Metabolites: Structural Diversity and Mechanism of Action. *Curr. Med. Chem.* 20, 932–952. doi: 10.2174/092986713805219136

Raja, M. (2011). Do Small Headgroups of Phosphatidylethanolamine and Phosphatidic Acid Lead to a Similar Folding Pattern of the K+ Channel? *J. Membr. Biol.* 242, 137–143. doi: 10.1007/s00232-011-9384-4

Raja, M., Spelbrink, R. E. J., de Kruijff, B., and Killian, J. A. (2007). Phosphatidic acid plays a special role in stabilizing and folding of the tetrameric potassium channel KcsA. *FEBS Lett.* 581, 5715–5722. doi: 10.1016/j.febslet.2007.11.039

Ríos, J. L., and Recio, M. C. (2005). Medicinal plants and antimicrobial activity. *J. Ethnopharmacol.* 100, 80–84. doi: 10.1016/j.jep.2005.04.025

Saising, J., Nguyen, M.-T., Härtner, T., Ebner, P., Al Mamun, Bhuyan, A., et al. (2018). Rhodomyrtone (Rom) is a membrane-active compound. *Biochim. Biophys. Acta Biomembr.* 1860, 1114–1124. doi: 10.1016/j.bbamem.2018.01.011

Salzberg, L. I., and Helmann, J. D. (2008). Phenotypic and Transcriptomic Characterization of Bacillus subtilis Mutants with Grossly Altered Membrane Composition. *J. Bacteriol.* 190, 7797–7807. doi: 10.1128/JB.00720-08

Sarathy, J. P., Ragunathan, P., Cooper, C. B., Upton, A. M., Grüber, G., and Dick, T. (2019). TBAJ-876 Displays Bedaquiline-Like Mycobactericidal Potency without Retaining the Parental Drug's Uncoupler Activity. *Antimicrob. Agents Chemother.* 64:1540. doi: 10.1128/AAC.01540-19

Schurig-Briccio, L. A., Yano, T., Rubin, H., and Gennis, R. B. (2014). Characterization of the type 2 NADH:menaquinone oxidoreductases from Staphylococcus aureus and the bactericidal action of phenothiazines. *Biochim. Biophys. Acta Bioenerg.* 1837, 954–963. doi: 10.1016/j.bbabio.2014.03.017

Sena, F. V., Batista, A. P., Catarino, T., Brito, J. A., Archer, M., Viertler, M., et al. (2015). Type-II NADH:quinone oxidoreductase from S taphylococcus aureus has two distinct binding sites and is rate limited by quinone reduction. *Mol. Microbiol.* 98, 272–288. doi: 10.1111/mmi.13120

Teng, Z., Li, M., Shi, D., Deng, X., and Wang, J. (2018). Synergistic interactions of cryptotanshinone and aminoglycoside antibiotics against Staphylococcus aureus in vitro. *J. Glob. Antimicrob. Resist.* 13, 264–265. doi: 10.1016/j.jgar.2018.05.013

Tran, T. B., Bergen, P. J., Creek, D. J., Velkov, T., and Li, J. (2018). Synergistic Killing of Polymyxin B in Combination With the Antineoplastic Drug Mitotane Against Polymyxin-Susceptible and -Resistant *Acinetobacter baumannii*: A Metabolomic Study. *Front. Pharmacol.* 9:359. doi: 10.3389/fphar.2018.00359

Uttlová, P., Pinkas, D., Bechyòková, O., Fišer, R., Svobodová, J., and Seydlová, G. (2016). Bacillus subtilis alters the proportion of major membrane phospholipids in response to surfactin exposure. *Biochim. Biophys. Acta Biomembr.* 1858, 2965–2971. doi: 10.1016/j.bbamem.2016.09.006

Weinstein, E. A., Yano, T., Li, L.-S., Avarbock, D., Avarbock, A., Helm, D., et al. (2005). Inhibitors of type II NADH:menaquinone oxidoreductase represent a class of antitubercular drugs. *Proc. Natl. Acad. Sci.* 102, 4548–4553. doi: 10.1073/pnas.0500469102

Yano, T., Li, L.-S., Weinstein, E., Teh, J.-S., and Rubin, H. (2006). Steady-state Kinetics and Inhibitory Action of Antitubercular Phenothiazines on Mycobacterium tuberculosis Type-II NADH-Menaquinone Oxidoreductase (NDH-2). *J. Biol. Chem.* 281, 11456–11463. doi: 10.1074/jbc.M508844200

Zampieri, M. (2018). From the metabolic profiling of drug response to drug mode of action. *Curr. Opin. Syst. Biol.* 10, 26–33. doi: 10.1016/j.coisb.2018.05.005

Zhang, G., Wu, Y., Zhang, H., and Gong, X. (2003). Comparative evaluation of Kecuo Yintong Cream with 1% clindamycin gel in the treatment of acne vulgaris. *J. Clin. Dermatol.* 32, 356–357.

Zhao, H., Zhang, H., and Shen, Y. (2007). Application of tanshinone capsules in dermatosis. *Med. Recapitul.* 13, 2048–2049.

Conflict of Interest: The authors declare that the research was conducted in the absence of any commercial or financial relationships that could be construed as a potential conflict of interest.

frontiers in Microbiology

ORIGINAL RESEARCH
published: 25 February 2021
doi: 10.3389/fmicb.2021.647611

In vitro Antibacterial Activity of an FDA-Approved H^+-ATPase Inhibitor, Bedaquiline, Against *Streptococcus mutans* in Acidic Milieus

Meng Zhang[1,2], Wenqian Yu[1], Shujing Zhou[3], Bing Zhang[1], Edward Chin Man Lo[2], Xin Xu[1] and Dongjiao Zhang[1]**

[1] Shandong Provincial Key Laboratory of Oral Tissue Regeneration, Shandong Engineering Laboratory for Dental Materials and Oral Tissue Regeneration, School and Hospital of Stomatology, Cheeloo College of Medicine, Shandong University, Jinan, China, [2] Faculty of Dentistry, University of Hong Kong, Sai Ying Pun, Hong Kong, [3] Department of Stomatology, Maternal and Child Health Hospital of Liaocheng City, Liaocheng, China

OPEN ACCESS

Edited by:
Rodolfo García-Contreras, National Autonomous University of Mexico, Mexico

Reviewed by:
Abdulrahman A. Balhaddad, Imam Abdulrahman Bin Faisal University, Saudi Arabia
Biao Ren, Sichuan University, China

***Correspondence:**
Xin Xu
xuxin@sdu.edu.cn
Dongjiao Zhang
djzhang1109@163.com

Specialty section:
This article was submitted to Antimicrobials, Resistance and Chemotherapy, a section of the journal Frontiers in Microbiology

Received: 30 December 2020
Accepted: 29 January 2021
Published: 25 February 2021

Citation:
Zhang M, Yu W, Zhou S, Zhang B, Lo ECM, Xu X and Zhang D (2021) In vitro Antibacterial Activity of an FDA-Approved H^+-ATPase Inhibitor, Bedaquiline, Against Streptococcus mutans in Acidic Milieus. Front. Microbiol. 12:647611. doi: 10.3389/fmicb.2021.647611

Background: Dental caries is an acid-related disease. Current anti-caries agents mainly focus on the bacteriostatic effect in a neutral environment and do not target acid-resistant microorganisms related to caries in acidic milieus.

Objectives: To assess the *in vitro* antibacterial activities of bedaquiline against oral pathogens in acidic milieus.

Methods: *Streptococcus mutans*, *Streptococcus sanguinis*, and *Streptococcus salivarius* were used to prepare the mono-/multiple suspension and biofilm. The MIC and IC_{50} of bedaquiline against *S. mutans* were determined by the broth microdilution method. Bedaquiline was compared regarding (i) the inhibitory activity in pH 4–7 and at different time points against planktonic and biofilm; (ii) the effect on the production of lactic acid, extracellular polysaccharide, and pH of *S. mutans* biofilm; (iii) the cytotoxicity effects; and (iv) the activity on H^+-ATPase enzyme of *S. mutans*.

Results: In pH 5 BHI, 2.5 mg/L (IC_{50}) and 4 mg/L (MIC) of bedaquiline inhibited the proliferation and biofilm generation of *S. mutans* and Mix in a dose-dependent and time-dependent manner, but it was invalid in a neutral environment. The lactic acid production, polysaccharide production, and pH drop range reduced with the incorporation of bedaquiline in a pH 5 environment. Its inhibitory effect (>56 mg/L) against H^+-ATPase enzyme in *S. mutans* and its non-toxic effect (<10 mg/L) on periodontal ligament stem cells were also confirmed.

Conclusion: Bedaquiline is efficient in inhibiting the proliferation and biofilm generation of *S. mutans* and other oral pathogens in an acidic environment. Its high targeting property and non-cytotoxicity also promote its clinical application potential in preventing caries. Further investigation of its specific action sites and drug modification are warranted.

Keywords: caries, antibacteria activity, *Streptococcus mutans*, acid resistance bacteria, acidic environment

INTRODUCTION

Dental caries is one of the most common oral diseases worldwide that affect oral health and general health (Smith AGC Kassebaum et al., 2017; Peres et al., 2019). The capability of caries-related pathogens to continuously metabolize carbohydrate in the acidic environment that they gradually create has been considered to be closely related to the initial development of dental decay (Selwitz et al., 2007). Numerous antibacterial agents, including quaternary ammonium monomer (Zhang et al., 2015; Ibrahim et al., 2020), fluoridated silver (Yin et al., 2020), and nanoparticle materials (Gao et al., 2016; Benoit et al., 2019), have been explored trying to inhibit those caries-related bacteria and balance plaque microecology (Pereira-Cenci et al., 2013). However, the conundrum is that it is difficult to target only caries-related microorganisms without interfering with normal microflora.

Acid resistance is one of the vital cariogenic properties of caries-related microorganisms (Lamont et al., 2018). When sufficient fermentable carbohydrates are overexposed, the balance between commensals and pathogens is disrupted. Large amounts of glucans, fructans (synthesize EPS), and lactic acid are produced by pathogens, which induce the pH of the local microenvironment to fall below 5.5 (Takahashi and Nyvad, 2011; Xiao et al., 2012; Bowen et al., 2018). In turn, this acidic environment provides a conditional cariogenic nest and further promotes microbial shifts toward pathogens with acid-resistant capability (Takahashi and Nyvad, 2011; Marsh and Zaura, 2017; Bowen et al., 2018). This favors the demineralization and disintegration of local mineralized tooth tissue and the onset of caries (Pitts et al., 2017). Therefore, this sort of anti-caries strategy that interferes with the acidic environment and inhibits the proliferation and metabolism of caries-related pathogens has been sought after by researchers to attempt to explore a way for the conundrum. Many novel pH-sensitivity biological materials have been applied to advance the feasibility of this strategy (Horev et al., 2015; Naha et al., 2019).

The proton pump FoF1-ATPase (also named H^+-ATPase) is a critical action enzyme involved in the acid-resistant mechanism for microbial (Liu et al., 2015). It is a ubiquitous and evolutionarily strong conserved membrane-bound macromolecular enzyme among prokaryotes and eukaryotes, it acts as the powerhouse of cell, and its transmembrane domain (Fo complex, subunit *c*) mediates the proton transport to resist low pH environment (Fillingame and Dmitriev, 2002). Hence, the FoF1-ATPase is a vital target for drugs that treat acid-related diseases (Spugnini and Fais, 2017; Abe et al., 2018), such as omeprazole targeting ATPase for gastric ulcer disease (Sachs, 1984), bedaquiline targeting Fo ring of *Mycobacterium tuberculosis* for tuberculosis (Preiss et al., 2015), and some proton pump inhibitions for cancer (Spugnini and Fais, 2017). However, dental caries is also an acid-related disease, and few studies have targeted H^+-ATPase of caries-related microorganisms to explore caries prevention. For human non-toxicity and safety concerns, a key factor to consider for screening new antibacterial drugs targeting the H^+-ATPase domain is the lack of eukaryotic homolog of the target.

During our continuous search for potential anti-caries agent, we identified bedaquiline, an antibiotic that was initially developed to specifically inhibit the mycobacterial ATP-synthase (Preiss et al., 2015) and does not recruit ATP synthesis-related toxicity in mammalian cells (Haagsma et al., 2009; Narang et al., 2019). The strong inhibitory effect of bedaquiline on *Streptococcus mutans* confirmed in preliminary experiments led us to propose that bedaquiline could be repurposed as a novel anti-caries agent, for the targeting H^+-ATPase. Therefore, here, the *in vitro* antibacterial activity of bedaquiline against *S. mutans* and multispecies genera (planktonic and biofilm) was investigated.

MATERIALS AND METHODS

Bacteria Inoculation and Biofilm Formation

S. mutans UA159 (ATCC10449) provided by Professor Mingwen Fan (Wuhan University, Wuhan, China), *Streptococcus sanguinis*, and *Streptococcus salivarius* isolated by Qiang Feng group (Shandong University, Jinan, China) were routinely inoculated in brain–heart infusion broth (BHI; BD Difco, United States) at an 37°C anaerobic incubator (90% N_2, 5% CO_2, 5% H_2; Whitley DG250 anaerobic workstation, United Kingdom). The prepared bacterial suspension [10^8 colony-forming units (CFUs)/ml, logarithmic phase] was obtained by transferring and incubating the overnight culture products of bacteria at a ratio of 1:40 for 3–6 h (*S. mutans* for 4 h; *S. sanguinis* for 6 h; *S. salivarius* for 3 h). For biofilm formation, the prepared bacterial suspension was inoculated into fresh BHI (1:100) with 1% (wt/vol) sucrose in multi-well cell (96-well and 24-well) culture plates for 24 h.

Minimum Inhibitory Concentration (MIC) and IC_{50} Concentration Assay

The MIC determination for bedaquiline (purchased from MedChemExpress) against planktonic *S. mutans* was conducted using the microdilution method in accordance with the Clinical Laboratory Standards Institute (CLSI) guideline (Pfaller and Diekema, 2012), with some modifications as described below. Bedaquiline powder was dissolved in DMSO to prepare a 10 mg/ml storage solution and then serially diluted in BHI medium to obtain 20, 10, 5, 2.5, 1.25, 0.625, and 0.3 mg/L working solution. One hundred microliters of serially diluted working solution with various concentrations of bedaquiline was mixed with 100 μl of the prepared bacterial suspension (10^7 CFU) in a 96-well plate. BHI with corresponding concentrations of DMSO were used as control and three parallel samples were set at each concentration. The plates were incubated anaerobically at 37℃ for 24 h. The optical density value of 600 nm ($OD_{600\ nm}$) was detected with a microplate reader (SPECTROstar Nano, BMG, Germany) to evaluate the growth status of bacteria.

The IC_{50} determination for bedaquiline against planktonic *S. mutans* was similar to the above procedure. Each well contained 1, 1.5, 2, 2.5, 3, 3.5, 4, 4.5, and 5 mg/L bedaquiline and 10^7 CFU bacterial suspension for incubation. The procedure

was also conducted on the control group and parallel samples. Meanwhile, the simplification procedure was set and performed to determine the MIC and IC_{50} of *S. sanguinis* and *S. salivarius* (only dosage concentrations of 1, 2, 2.5, 3, and 4 mg/L were tested). The MIC was defined as the lowest test concentration that substantially inhibited bacteria growth in the medium. The IC_{50} was defined as the concentration at which half visible bacteria grew in the medium.

Furthermore, the antibacterial effect of bedaquiline under different pH milieus (pH 4–7) was also investigated. Hydrochloric acid was used to prepare the pH of the BHI; the prepared bacterial suspension was mixed with acidic BHI incorporating 1–3 mg/L of bedaquiline (bacterial suspension: BHI medium = 1:100), and the $OD_{600\ nm}$ value was tested after 24 h of anaerobic culture at 37°C.

CFU Counts and Drop Assay

For CFU counts, bacterial suspension treated 0, 5, 10, 30 min, and 1, 2, 4, 6, and 8 h with bedaquiline in pH 5 BHI broth was serially diluted in PBS and plated 100 μl on BHI agar for incubation and CFU counts. In parallel, 10 μl of bacterial suspension at various time points was dropped on pH 7 BHI agar to visually detect the biomass.

Scanning Electron Microscopy (SEM) Imaging

For SEM imaging, 24-h incubated *S. mutans* and multispecies biofilms on coverslip disks in 24-well plate were used for processing and imaging (Zhang et al., 2015). Briefly, the biofilms were washed twice with PBS, fixed with 2.5% glutaraldehyde overnight, serially dehydrated with ethanol, gradient frozen, and dried for 12 h in freeze-dryers (Martin Christ, Germany). Then, the samples were sputter-coated with gold for SEM imaging.

Lactic Acid Measurement and pH Measurement

The biofilms for lactic acid measurement were incubated in 24-well plates with 1 ml of pH 5 BHI broth (Zhang et al., 2015). Follow the instructions (LA Assay Kit, Solarbio, China) to monitor the lactic acid production at $OD_{340\ nm}$. The supernatant of biofilm incubated in pH 5 BHI broth for 2, 4, 6, 8, and 16 h was used for pH measurement by Starter (Starter 3100, United States).

Furthermore, to evaluate the effect of bedaquiline on the lactic acid production of mature *S. mutans* biofilm (obtained by culturing in pH 7 BHI for 16 h), the shock assay was designed and performed. Based on the CFU count results of the antibacterial effect of bedaquiline with time gradient, the mature *S. mutans* biofilm was shocked for 2 h in pH 5 BHI with the incorporation of 2.5, 4, and 10 mg/L of bedaquiline, and then the lactic acid production of the shocked biofilms was detected as above. In parallel, pH changes of the shocked biofilms were recorded.

Polysaccharide Measurement

The biofilms were incubated in 24-well plates with 1 ml of pH 5 BHI broth. The water-insoluble extracellular polysaccharide of biofilms was determined by the anthrone method, the procedure referred to in Koo et al. (2003). Briefly, the cell pellet of biofilm was resuspended and washed thrice in sterile PBS and then resuspended using 4 ml of 0.4 M NaOH and centrifuged at 5,000 rpm for 3 min, and 200 μl of supernatant was mixed with 600 μl of freshly prepared anthrone–sulfuric acid solution [1 g/L (80% sulfuric acid)]. Simultaneously, 200 μl of freshly prepared dextran T 500 standard with various concentrations (0, 0.005, 0.01, 0.02, . . ., 0.09, and 0.1 mg/ml) were also mixed with 600 μl of freshly prepared anthrone–sulfuric acid solution for comparison. Put samples and standards in a 95°C dry bath for 6 min and immediately transfer them to the ice box for 15 min. Pipette 200 μl into a 96-well plate and detect the absorbance value of OD_{625nm}. Three parallel groups were set for each group. In addition, polysaccharide production assay of the shocked biofilms was also performed.

Live/Dead Bacteria Imaging

For live/dead imaging (Zhang et al., 2015), mature biofilms shocked in pH 5 BHI containing 2.5–10 mg/L of bedaquiline were stained following the manufacturer's instruction (Live/Dead Baclight™ Bacterial viability kits, Invitrogen™, United States). Briefly, the biofilms were stained with SYTO 9 for 15 min and then propidium iodide for 3 min. The labeled biofilms were imaged with a fluorescence microscope (Leica DMi8, Wetzlar, Germany) equipped with fully consistent exposure value (147), magnification (10×), and other parameters.

CCK8 Assay

The periodontal ligament stem cells (PDLSCs, P5) isolated and identified by our research group were activated and expanded for 48 h (5×10^5 live cells/ml), plating 3,000 cells/well in a 96-well plate. After monolayer culture overnight, the medium (DMEM + 10% FBS) containing different concentrations of bedaquiline (1–10 mg/L) and DMSO was replaced; culture is continued for 24, 48, and 72 h; and then the effect of bedaquiline on cell proliferation ($OD_{450\ nm}$) was tested with Cell counting kit-8 (CCK8, DOJINDO, Japan). Five parallel groups were set for each group (Ibrahim et al., 2020).

H^+-ATPase Activity Assay

Freshly activated *S. mutans* solution in stable phase (100 ml, 10^{10} CFU/ml) was prepared, and then the total protein was extracted by lysing the cell pellet with lysate and lysozyme. Protein concentration was obtained using the Bicinchoninic Acid Kit (BAC, Sigma-Aldrich, United States). An equal amount of 50 μg protein was dispensed and treated with 56–139 mg/L of bedaquiline or DMSO at 37℃ for 30 min (negative controls with a corresponding concentration of bedaquiline were also set), and then the activity of H^+-ATPase at 1, 10, and 30 min after substrate incorporation was detected with the H^+-ATPase assay kit (GMS50244.3, Genmed Scientifics Inc., United States, $OD_{340\ nm}$) (Iwamoto et al., 1991).

Statistical Analysis

IBM SPSS Statistics version 17.0 was used to perform the statistical analysis and graphs were drawn using GraphPad. All

experiments were independently repeated at least three times. One-way analysis of variance (ANOVA) and Tukey's test were performed to detect the significant effects of multiple groups. The *t*-test was performed for two groups. Differences were considered significant when $P < 0.05$.

RESULTS

Determination of the MIC and IC_{50} of Bedaquiline Against *S. mutans*

The activity of bedaquiline against *S. mutans* and multispecies suspension are summarized in **Figure 1**. In pH 7 BHI, 0.75–4 mg/L of bedaquiline (**Figure 1A**) and even 10 mg/L (data not shown) did not exhibit bacteriostatic effects, but exhibited excellent bacteriostatic effects in pH 5 BHI (**Figure 1A**). The bactericidal effect test at pH 4–7 BHI also evidenced that bedaquiline performed excellent bacteriostatic effect on *S. mutans* and Mix at pH 5 (**Figures 1B,C**). **Figures 1D,E** show the results of MIC and IC_{50} assay; bedaquiline demonstrated an MIC of 4 mg/L, with an IC_{50} of 2.5 mg/L against planktonic *S. mutans*. For *S. sanguinis*, MIC = 4 mg/L and IC_{50} = 2 mg/L. For *S. salivarius*, MIC = 4 mg/L and 2 mg/L < IC_{50} < 2.5 mg/L (**Supplementary Figures S1, S2**). Similar inhibitory concentrations were also presented in the assay with mixed multiple species (**Figure 1A**).

CFU count results showed that *S. mutans* grows and proliferates slowly in the first 6 h in the pH 5 BHI and remains in the 10^8 level (**Figure 2A**). After the incorporation of bedaquiline, the 2.5 mg/L group can reduce the bacteria amount to 10^6 levels within 10 min and stay at this level; the 4 mg/L group continued to decrease to 10^3 level in the first 2 h, reaching its limit of inhibition, but the inhibitory effect continued until 8 h; the 10 mg/L group achieved complete inhibition of bacteria within 30 min. The similar results of drop assay (**Supplementary Figure S3**) further provided an extra visual evidence for the dose-dependent and time-dependent effects of bedaquiline.

Inhibition of Biofilm Formation by Bedaquiline

The SEM images showed that the acidic environment itself affected biofilm formation (**Figures 2B,C**), and the incorporation of bedaquiline further inhibited the development of *S. mutans* and Mix biofilms to varying degrees (**Figure 2B**), but had no obvious effect on the formation of biofilms in a neutral environment (**Figure 2C**). The density of *S. mutans* biofilm formation with 2, 2.5, 3, and 4 mg/L of bedaquiline in pH 5 BHI gradually reduced in a dose-dependent manner. More intense inhibition of bedaquiline was shown in the Mix biofilm group.

Evaluation of the Lactic Acid Production of *S. mutans* Biofilm With Bedaquiline

Compared to the control group, *S. mutans* biofilms with 2.5 and 4 mg/L of bedaquiline in pH 5 BHI significantly reduced the lactic acid production ($P < 0.05$; **Figure 3B**). However, the incorporation of bedaquiline also significantly reduced the amounts of bacteria in the biofilm (**Figure 3A**), so the ratio of lactic acid production to $OD_{600\ nm}$ in the 2.5 mg/L group was not statistically different from the control group (**Figure 3C**).

The results of lactic acid production of the shocked biofilms showed that no significant differences were statistically obtained when the 2.5 and 4 mg/L groups were compared with the control group, even though the lactic acid production slightly decreased with increasing inhibitor concentration (**Supplementary Figure S4**).

Evaluation of the Water-Insoluble Polysaccharide Production of *S. mutans* Biofilm With Bedaquiline

The results of the water-insoluble extracellular polysaccharide production were similar to those of lactic acid. The polysaccharides in the 2.5 and 4 mg/L group decreased considerably ($P < 0.05$, **Figure 3E**), and the amounts of bacteria that make up the biofilm (OD_{600nm}) were also significantly inhibited (**Figure 3D**), which kept the ratio of the polysaccharide production to OD_{600nm} at a relatively conforming level ($P > 0.05$, **Figure 3F**). The yield of polysaccharides in shocked biofilms also showed a tendency to decrease slightly with increasing inhibitor concentration, but no statistical difference was shown (**Supplementary Figure S5**).

pH Dynamic Changes of the Medium of the Planktonic Bacteria and Shocked Biofilm After the Incorporation of Bedaquiline

The incorporation of bedaquiline retarded the pH drops (**Figure 4A**). The pH in the control group and the 1 mg/L group gradually dropped from 5.14 ± 0.01 to 4.25 ± 0.05 in 16 h, and the pH in the 2.5 mg/L group dropped slightly slowly to 4.59 ± 0.16 vs. that in the control group ($P = 0.02$). The pH in the 4 mg/L group dropped most slowly, staying at about 5.14 in 16 h. Moreover, the pH measurement of the shocked biofilms showed that no significant differences were obtained between the 2.5 and 4 mg/L group and the control group (data not shown).

Evaluation of the Live/Dead Bacteria Ratio in Shocked *S. mutans* Biofilm

Under a fluorescence microscope, green indicates live bacteria, red indicates dead bacteria, and yellow turned darker in the merge image when the proportion of dead bacteria was higher. As the concentration of incorporated bedaquiline increased, the area and depth of the yellow area increased (**Figure 4B**). However, even after treatment with the 10 mg/L group with complete bacteriostatic ability, the yellow brightness in the merge was only slightly dimmed.

Cytotoxicity Assessment of Bedaquiline

Cell viability in bedaquiline groups (1–10 mg/L) at 24and 48 h were not significantly different from the DMSO group (0.1%)

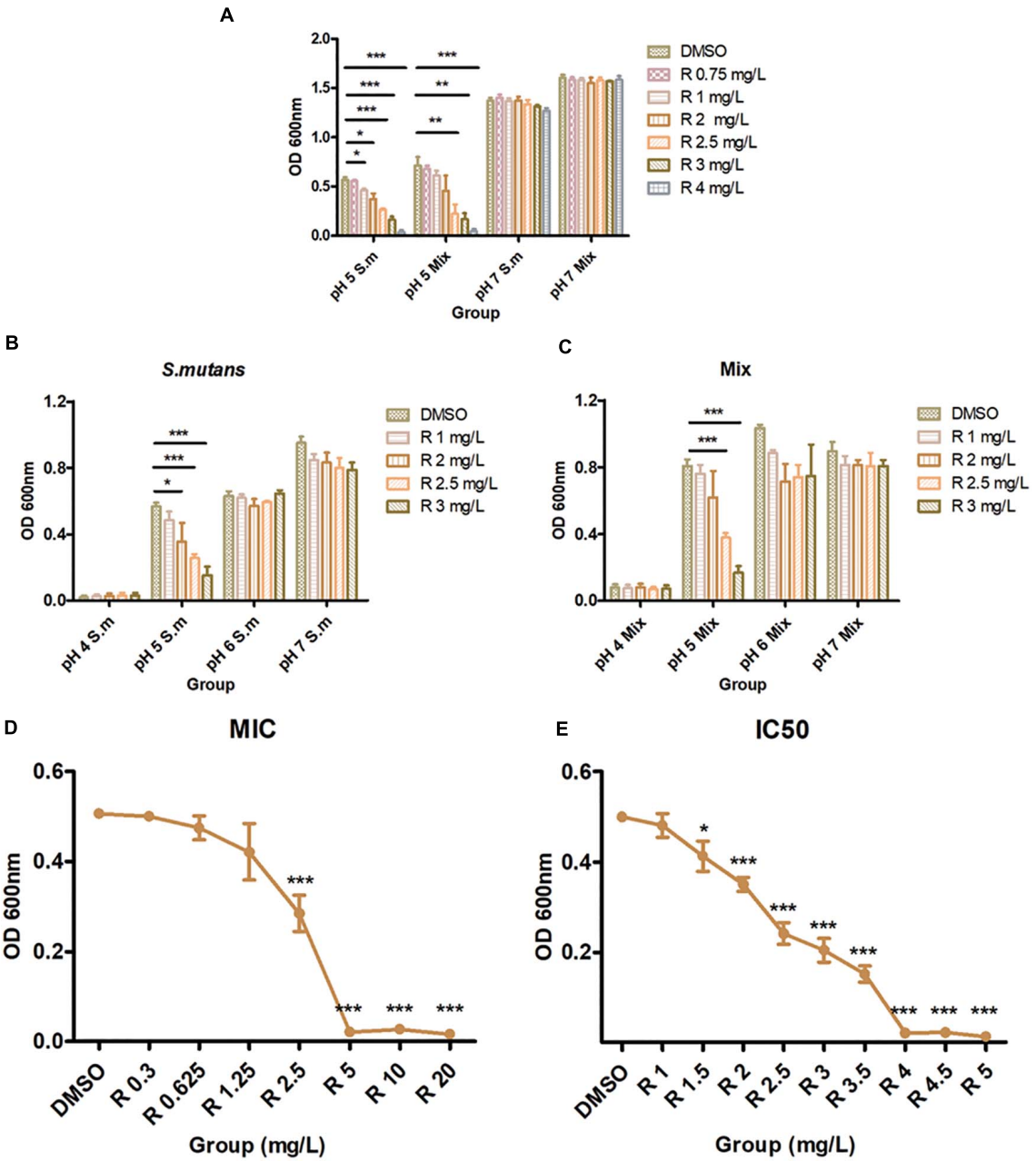

FIGURE 1 | Antibacterial properties of bedaquiline treatment. **(A)** In pH 5 and 7 BHI, the antibacterial effect of 0.75–4 mg/L of bedaquiline and DMSO against planktonic *S. mutans* and Mix (*S. mutans, S. sanguinis*, and *S. salivarius*). **(B)** In pH 4–7 BHI, the antibacterial effect of 1–3 mg/L of bedaquiline and DMSO against planktonic *S. mutans*. **(C)** In pH 4–7 BHI, the antibacterial effect of 1–3 mg/L of bedaquiline and DMSO against planktonic Mix. **(D)** The MIC assay of bedaquiline against planktonic *S. mutans* in pH 5 BHI. **(E)** The IC_{50} assay of bedaquiline against planktonic *S. mutans* in pH 5 BHI. *, **, and *** indicate statistically significant differences at $p < 0.05$, $p < 0.01$, and $p < 0.001$, respectively. Error bars are standard deviations.

and the control group ($P > 0.05$, **Figure 4C**). At 72 h, cell viability of bedaquiline groups and the DMSO group fluctuated to some extent, while statistics showed that there was no difference between the groups. However, the cell viability in the DMSO group at 72 h was reduced compared with the control group ($P = 0.055$), which indicated that 0.1% DMSO would bring some cytotoxicity with time, but bedaquiline below 10 mg/L did not show cytotoxicity.

Evaluation of the Inhibition of H^+-ATPase Activity by Bedaquiline

A total of 2.5 ml of 1 μg/μl total protein was extracted. The ≤56 mg/L of bedaquiline groups was the same as the DMSO group, and H^+-ATPase was gradually consumed by the substrate within 30 min, showing a slow downward trend (**Figure 5**). In the 69, 83, and 97 mg/L groups, H^+-ATPase activity at 0 min was inhibited to various extent, and as the concentration

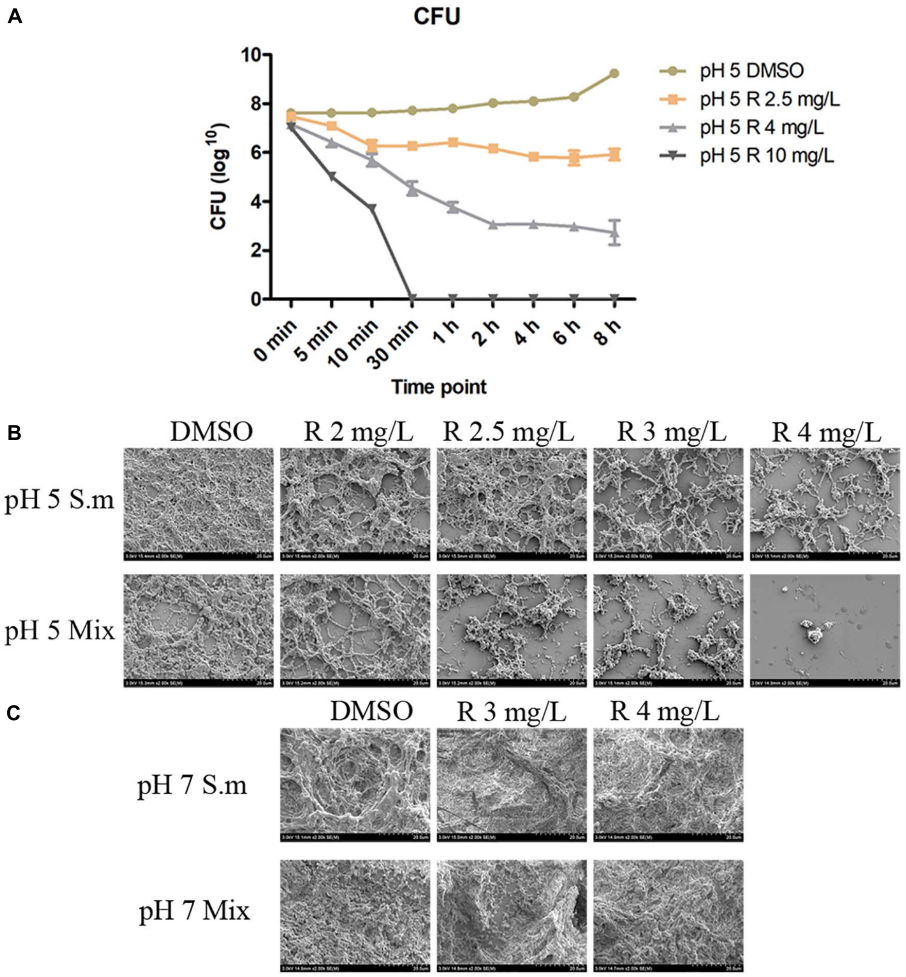

FIGURE 2 | The CFU count **(A)** of 2.5–10 mg/L of bedaquiline and DMSO against planktonic *S. mutans* in pH 5 BHI. Error bars are standard deviations. **(B,C)** Are anti-biofilm properties of bedaquiline (SEM). **(B)** In pH 5 BHI, anti-biofilm generation effect of 2–4 mg/L of bedaquiline and DMSO against *S. mutans* and Mix. **(C)** In pH 7 BHI, anti-biofilm generation effect of 3 and 4 mg/L of bedaquiline and DMSO against *S. mutans* and Mix.

increased, there was a gradual downward trend of the curve within 30 min. In the ≥97 mg/L groups, the curves were almost a horizontal line, indicating that the activity of H^+-ATPase had been completely inhibited, and there was no H^+-ATPase that could react with the substrate.

DISCUSSION

Here, we determined the antibacterial effects of bedaquiline against *S. mutans* and multiple species in acidic milieus, and its inhibitory effect on H^+-ATPase protein *in vitro*. These results evidenced that the way to inhibit H^+-ATPase, an acid-resistant functional protein, to resist caries-related microorganisms in an acidic caries environment is available. However, considering the use of bedaquiline is FDA approved for the treatment of MDR *M. tuberculosis*, the likelihood of antibiotic resistance among *M. tuberculosis* will increase if it is used directly as an anti-caries agent (Diacon et al., 2014). Therefore, subsequent research mainly focused on improving the feasibility of topical application of drugs by modifying bedaquiline and encapsulating it with nanomaterials to reduce its impact on the whole body.

Caries development is a consequence of dietary sugar-driven biofilm accumulation and localized acidification caused by deleterious microbes (Takahashi and Nyvad, 2011; Colombo and Tanner, 2019); this increased acidification is accompanied by the reduction in the levels and metabolic activity of beneficial bacteria, which preferentially grow at neutral pH (Teng et al., 2015; Johansson et al., 2016). At present, many antibacterial studies against dental caries mainly focus on their bactericidal effect in neutral microenvironment (Saputo et al., 2018; Qi et al., 2019; Ibrahim et al., 2020). Obviously, many innocent beneficial flora will be mutilated simultaneously by this bactericidal effect, destroying the local flora balance. A key point to remember is that those bacteria with acid-resistant capability (that is, caries-related bacteria) left behind by the conditional screening in acidic microenvironment are those we want to fight. Therefore, several novel pH-sensitive biological materials that load antibacterial

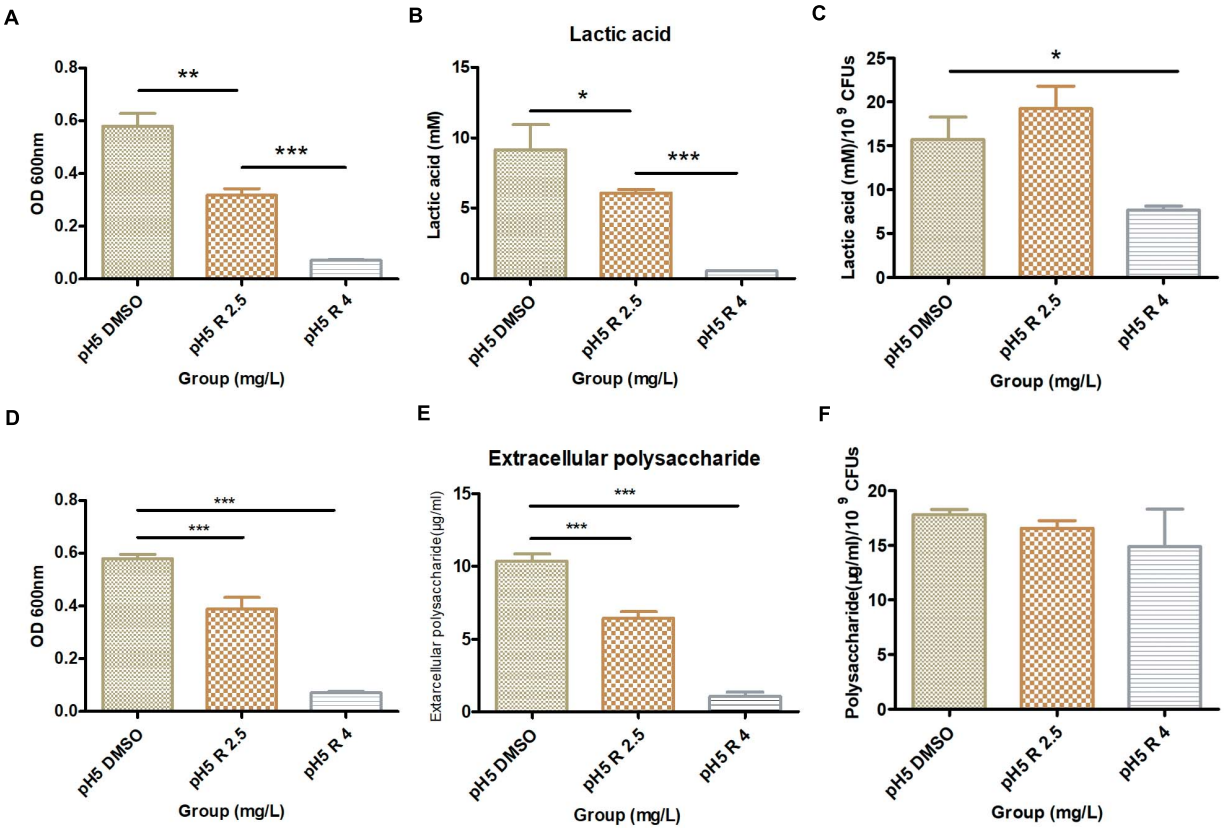

FIGURE 3 | Effect of 2.5 and 4.0 mg/L of bedaquiline and DMSO on lactic acid production and water-insoluble extracellular polysaccharide production within *S. mutans* biofilm in pH 5 BHI. **(A)** $OD_{600\ nm}$ value of *S. mutans* biofilm used for lactic acid detection. **(B)** Lactic acid production detection in different groups. **(C)** Lactic acid production/10^9 CFUs of different groups. **(D)** $OD_{600\ nm}$ value of *S. mutans* biofilm used for water-insoluble extracellular polysaccharide detection. **(E)** Extracellular polysaccharide detection in different groups. **(F)** Extracellular polysaccharide production/10^9 CFUs of different groups. *, **, and *** indicate statistically significant differences at $p < 0.05$, $p < 0.01$, and $p < 0.001$, respectively. Error bars are standard deviations.

drugs (Horev et al., 2015; Naha et al., 2019), antibacterial peptides with pH sensitivity (Zhang et al., 2015), and precision-guided antimicrobial peptides (Guo et al., 2015) have emerged to assist to overcome this. Here, in acidic milieus, bedaquiline in the low micromolar range [2.5 mg/L (IC_{50}), 4 mg/L (MIC); **Figure 1**] potently inhibited the proliferation of *S. mutans* and other caries-related bacteria, yet the antibacterial effect is not demonstrated in neutral milieus. It is favorable to maintain local biological balance by protecting healthy microflora and targeting only those caries-related microbiomes that are resistant to an acidic environment. Hence, bedaquiline is worth further exploration to assist in preventing dental caries.

The sucrose metabolism of microorganisms in the biofilm is closely related to the pH value in the local microenvironment (Xiao et al., 2012; Flemming et al., 2016; Hwang et al., 2016; Bowen et al., 2018). This extracellular matrix, including exopolysaccharides, glycoproteins, and lipoteichoic acid, has been increasingly recognized as essential for the cariogenic properties involved in surface adhesion, social interactions, and antimicrobial tolerance (Flemming et al., 2016; Bowen et al., 2018). Therefore, detecting the effect of antibacterial agent on microbial sucrose metabolism has been increasingly valued to assess its anti-caries potential, and commonly used indicators include lactic acid production, water-insoluble extracellular polysaccharide production, and pH monitoring (Zhang et al., 2015; Henley-Smith et al., 2018; Yu et al., 2019; Chen et al., 2020; Ibrahim et al., 2020). Consistent with many previous studies (Henley-Smith et al., 2018; Yu et al., 2019; Chen et al., 2020; Ibrahim et al., 2020), the incorporation of antibacterial agent, including bedaquiline, noticeably reduced both the lactic acid production and total water-insoluble extracellular polysaccharides compared to the control group (**Figure 3**); the drop in pH 5 was also significantly reduced (**Supplementary Figure S3**). However, the initial sugar production of pH 5 BHI in the control group in the present study is lower than that of pH 7 BHI in other research (Zhang et al., 2015; Yu et al., 2019), which may largely be related to the inhibitory effect of the acidic environment on the amount of bacteria and bacterial metabolism. In addition, the reduction extent in sugar production in the bedaquiline group is also not as great as in other studies, even in a similar situation where half of the bacterial biomass was suppressed (Zhang et al., 2015). Here, supplementary evidence shows that there is no difference in the proportion of sugar

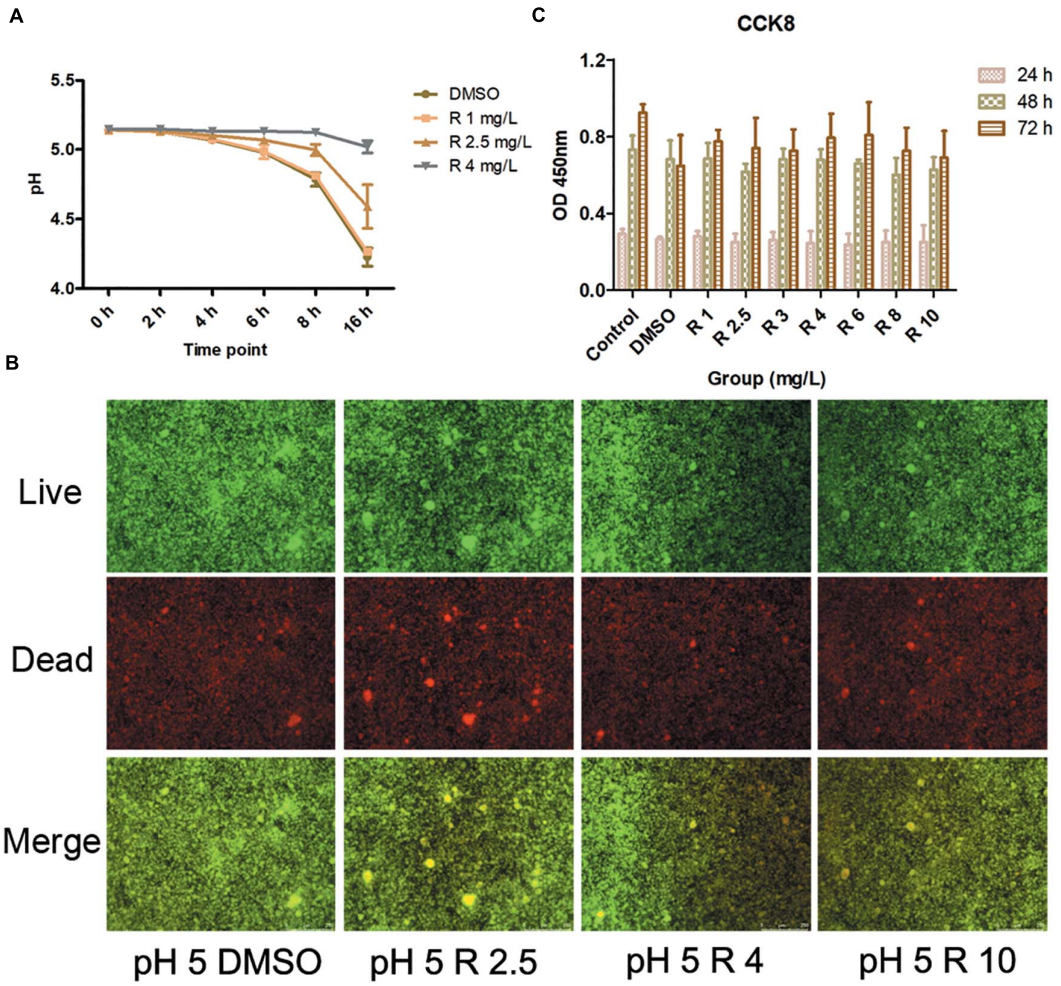

FIGURE 4 | (A) pH detection at 0–16 h culturation after the incorporation of 1–4 mg/L of bedaquiline and DMSO. **(B)** Live/dead bacteria stain imaging of *S. mutans* biofilm with 2.5, 4, and 10 μM of bedaquiline and DMSO treatment. **(C)** Cytotoxic effects of 1–10 mg/L of bedaquiline and DMSO on periodontal ligament stem cells at 24, 48, and 72 h.

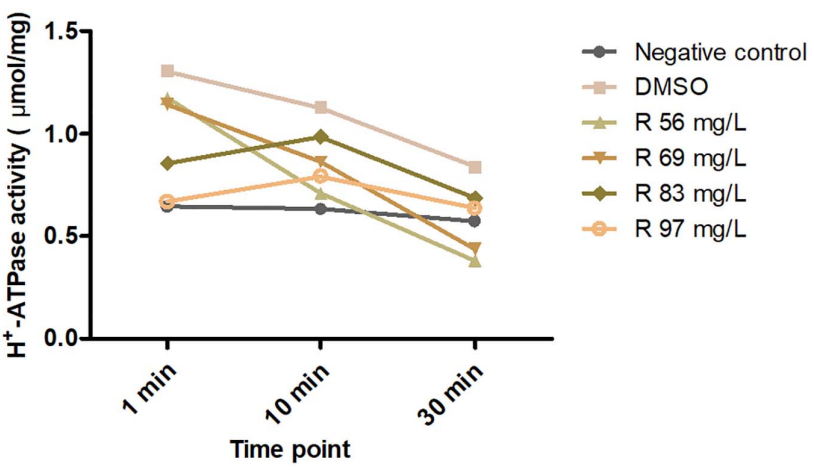

FIGURE 5 | Effects of 56–97 mg/L of bedaquiline and DMSO on H^+-ATPase activity of *S. mutans* at 0, 10, and 30 min.

production/$OD_{600\ nm}$ between the bedaquiline group and the control group. We speculate that the inhibitory effect of bedaquiline on sugar production may be mainly obtained by reducing the biomass of bacteria, but has no effect on sugar metabolism itself.

In addition, the present study shows that once the mature biofilm has been constructed, even the shock treatment with 10 mg/L of bedaquiline only causes the death of a small number of bacteria on the surface of the biofilm (**Figure 4B**), and there is no obvious change in the sugar yield and pH of the biofilm (**Supplementary Figures S4, S5**). This is consistent with the fact that biofilm itself is a complex and united small community; it is difficult to be attacked and influenced by some foreign drug molecules or agents, which is also a mechanism for its self-protection (Flemming et al., 2016; Bowen et al., 2018). This result also indicates that when bedaquiline is used as an anti-caries agent in the future, it should be directly applied on tooth surface or active lesion, or with the assist of novel biological nanomaterials to increase the permeability of bedaquiline to the biofilm (Naha et al., 2019).

The Fo protein of H^+-ATPase is utilized to pump out H^+ from cells, thereby maintaining the pH homeostasis and protecting cells from damage induced by acidic milieus. This mechanism is shared by various bacteria. Kuhnert's group (Kuhnert et al., 2004) found the transcriptionally upregulated H^+-ATPase in *S. mutans* confronted with a low pH environment, which confirms its critical role in acid resistance. Bedaquiline, an inhibitor of mycobacterial F1Fo-ATP synthase that binds to the enzyme's oligomeric *c* subunit of Fo protein (Andries et al., 2005; Koul et al., 2007; Preiss et al., 2015), has been approved by FDA for the treatment of drug-resistant *M. tuberculosis* disease (Diacon et al., 2009; Jones, 2013). Haagsma's group showed that ATP synthase isolated from human, mouse, and bovine mitochondria displayed extremely lower sensitivity for bedaquiline compared to that of mycobacterial ATP synthase (Haagsma et al., 2009), which indicates that bedaquiline is able to selectively inhibit ATP synthase in bacteria but not in mitochondria of normal cells (Fiorillo et al., 2016). This property contributes to its clinical usage as antibacterial agent due to toxicity issues and fatality concerns (Ferlazzo et al., 2018; Narang et al., 2019). Therefore, the potent inhibitory effect of bedaquiline on oral microorganisms and the non-toxic effect on PDLSCs in the present study laid a solid foundation for bedaquiline as a novel anti-caries agent.

The precise interaction of bedaquiline with the c-ring of Fo rotors and its mechanism of action have been explored and expounded by Preiss' group in mycobacterial ATP synthases (Preiss et al., 2015). They confirmed that the bedaquiline specifically interacts with nine residues on c-rings of *Mycobacterium phlei* (Gly^{62}, Leu^{63}, Glu^{65}, Ala^{66}, Ala^{67}, Tyr^{68}, Phe^{69}, Ile^{70}, and Leu^{72}) using X-ray crystallographic study. Among them, the glutamate residue with the strictly conserved bacterial ATP synthases (Glu^{65} in *M. phlei*, Glu^{53} in *S. mutans*) plays an essential role in binding and translocating H^+ and other ions during the ion translocation process (Pogoryelov et al., 2010; Hakulinen et al., 2012). Here, the inhibitory effect of bedaquiline on H^+-ATPase in *S. mutans* is confirmed (**Figure 5**); the conserved glutamate residue is presumed to be a key binding site for bedaquiline, but other potential binding sites in *S. mutans* need to be further studied.

Here, the inhibition effect of the H^+-ATPase inhibitor on caries-related pathogens in an acidic environment paves the way for the development of a novel anti-caries strategy option. However, since this study was conducted *in vitro*, and only a limited number of species were applied to research, it failed to accurately simulate the natural oral environment. Further *in vivo* research is needed to provide higher levels of evidence. Moreover, the inhibition effect of bedaquiline against *S. mutans* will definitely cause bacterial resistance over time, which is an issue that requires our continuous attention and cannot be ignored.

CONCLUSION

In conclusion, bedaquiline is efficient in inhibiting the proliferation and biofilm generation of *S. mutans* and other oral pathogens in an acidic environment. Its high targeting property and non-cytotoxicity promote its clinical application potential in preventing caries. Further mechanism exploration and drug modification are warranted to advance its feasibility.

DATA AVAILABILITY STATEMENT

The original contributions presented in the study are included in the article/**Supplementary Material**, further inquiries can be directed to the corresponding author/s.

AUTHOR CONTRIBUTIONS

DZ, XX, and EL conceived this study. MZ, WY, SZ, and BZ conducted the experiments. MZ and EL analyzed the data and wrote the manuscript. All authors contributed to the article and approved the submitted version.

FUNDING

This work was financially supported by the Construction Engineering Special Fund of Taishan Scholars (grant no: TS201511106) and the Fundamental Research Funds of Shandong University (grant no: 2018GN024).

ACKNOWLEDGMENTS

We would like to acknowledge Prof. Mingwen Fan (Wuhan University) and Prof. Qiang Feng (Shandong University) for providing experimental strains.

SUPPLEMENTARY MATERIAL

The Supplementary Material for this article can be found online at: https://www.frontiersin.org/articles/10.3389/fmicb.2021.647611/full#supplementary-material

REFERENCES

Abe, K., Irie, K., Nakanishi, H., Suzuki, H., and Fujiyoshi, Y. (2018). Crystal structures of the gastric proton pump. *Nature* 556, 214–218. doi: 10.1038/s41586-018-0003-8

Andries, K., Verhasselt, P., Guillemont, J., Göhlmann, H. W., Neefs, J. M., Winkler, H., et al. (2005). A diarylquinoline drug active on the ATP synthase of Mycobacterium tuberculosis. *Science* 307, 223–227. doi: 10.1126/science.1106753

Benoit, D. S. W., Sims, K. R., and Fraser, D. (2019). Nanoparticles for oral biofilm treatments. *ACS Nano.* 13, 4869–4875. doi: 10.1021/acsnano.9b02816

Bowen, W. H., Burne, R. A., Wu, H., and Koo, H. (2018). Oral biofilms: pathogens, matrix, and polymicrobial interactions in microenvironments. *Trends Microbiol.* 26, 229–242. doi: 10.1016/j.tim.2017.09.008

Chen, H., Tang, Y., Weir, M. D., Gao, J., Imazato, S., Oates, T. W., et al. (2020). Effects of S. mutans gene-modification and antibacterial monomer dimethylaminohexadecyl methacrylate on biofilm growth and acid production. *Dent. Mater.* 36, 296–309. doi: 10.1016/j.dental.2019.12.001

Colombo, A. P. V., and Tanner, A. C. R. (2019). The role of bacterial biofilms in dental caries and periodontal and peri-implant diseases: a historical perspective. *J. Dent. Res.* 98, 373–385. doi: 10.1177/0022034519830686

Diacon, A. H., Pym, A., Grobusch, M., Patientia, R., Rustomjee, R., Page-Shipp, L., et al. (2009). The diarylquinoline TMC207 for multidrug-resistant tuberculosis. *New Engl. J. Med.* 360, 2397–2405. doi: 10.1056/nejmoa0808427

Diacon, A. H., Pym, A., Grobusch, M. P., de los Rios, J. M., Gotuzzo, E., Vasilyeva, I., et al. (2014). Multidrug-resistant tuberculosis and culture conversion with bedaquiline. *New Engl. J. Med.* 371, 723–732.

Ferlazzo, G., Mohr, E., Laxmeshwar, C., Hewison, C., Hughes, J., Jonckheere, S., et al. (2018). Early safety and efficacy of the combination of bedaquiline and delamanid for the treatment of patients with drug-resistant tuberculosis in Armenia, India, and South Africa: a retrospective cohort study. *Lancet Infect. Dis.* 18, 536–544. doi: 10.1016/s1473-3099(18)30100-2

Fillingame, R. H., and Dmitriev, O. Y. (2002). Structural model of the transmembrane Fo rotary sector of H+-transporting ATP synthase derived by solution NMR and intersubunit cross-linking in situ. *Biochim. Biophys. Acta.* 1565, 232–245. doi: 10.1016/s0005-2736(02)00572-2

Fiorillo, M., Lamb, R., Tanowitz, H. B., Cappello, A. R., Martinez-Outschoorn, U. E., Sotgia, F., et al. (2016). Bedaquiline, an FDA-approved antibiotic, inhibits mitochondrial function and potently blocks the proliferative expansion of stem-like cancer cells (CSCs). *Aging* 8, 1593–1607. doi: 10.18632/aging.100983

Flemming, H. C., Wingender, J., Szewzyk, U., Steinberg, P., Rice, S. A., and Kjelleberg, S. (2016). Biofilms: an emergent form of bacterial life. *Nat. Rev. Microbiol.* 14, 563–575. doi: 10.1038/nrmicro.2016.94

Gao, L., Liu, Y., Kim, D., Li, Y., Hwang, G., Naha, P. C., et al. (2016). Nanocatalysts promote *Streptococcus mutans* biofilm matrix degradation and enhance bacterial killing to suppress dental caries in vivo. *Biomaterials* 101, 272–284. doi: 10.1016/j.biomaterials.2016.05.051

Guo, L., McLean, J. S., Yang, Y., Eckert, R., Kaplan, C. W., Kyme, P., et al. (2015). Precision-guided antimicrobial peptide as a targeted modulator of human microbial ecology. *PNAS* 112, 7569–7574. doi: 10.1073/pnas.1506207112

Haagsma, A. C., Abdillahi-Ibrahim, R., Wagner, M. J., Krab, K., Vergauwen, K., Guillemont, J., et al. (2009). Selectivity of TMC207 towards mycobacterial ATP synthase compared with that towards the eukaryotic homologue. *Antimicrob. Agents Chemother.* 53, 1290–1292. doi: 10.1128/aac.01393-08

Hakulinen, J. K., Klyszejko, A. L., Hoffmann, J., Eckhardt-Strelau, L., Brutschy, B., Vonck, J., et al. (2012). Structural study on the architecture of the bacterial ATP synthase Fo motor. *PNAS* 109, E2050–E2056.

Henley-Smith, C. J., Botha, F. S., Hussein, A. A., Nkomo, M., Meyer, D., and Lall, N. (2018). Biological activities of *Heteropyxis natalensis* against micro-organisms involved in oral infections. *Front. Pharmacol.* 9:291. doi: 10.3389/fphar.2018.00291

Horev, B., Klein, M. I., Hwang, G., Li, Y., Kim, D., Koo, H., et al. (2015). pH-activated nanoparticles for controlled topical delivery of farnesol to disrupt oral biofilm virulence. *ACS Nano.* 9, 2390–2404. doi: 10.1021/nn507170s

Hwang, G., Liu, Y., Kim, D., Sun, V., Aviles-Reyes, A., Kajfasz, J. K., et al. (2016). Simultaneous spatiotemporal mapping of in situ pH and bacterial activity within an intact 3D microcolony structure. *Sci. Rep.* 6:32841.

Ibrahim, M. S., Garcia, I. M., Vila, T., Balhaddad, A. A., Collares, F. M., Weir, M. D., et al. (2020). Multifunctional antibacterial dental sealants suppress biofilms derived from children at high risk of caries. *Biomater. Sci.* 8, 3472–3484. doi: 10.1039/d0bm00370k

Iwamoto, A., Omote, H., Hanada, H., Tomioka, N., Itai, A., Maeda, M., et al. (1991). Mutations in Ser174 and the glycine-rich sequence (Gly149, Gly150, and Thr156) in the beta subunit of *Escherichia coli* H(+)-ATPase. *J. Biol. Chem.* 266, 16350–16355. doi: 10.1016/s0021-9258(18)55304-7

Johansson, I., Witkowska, E., Kaveh, B., Lif Holgerson, P., and Tanner, A. C. (2016). The microbiome in populations with a low and high prevalence of caries. *J. Dent. Res.* 95, 80–86. doi: 10.1177/0022034515609554

Jones, D. (2013). Tuberculosis success. *Nat. Rev. Drug Discovery* 12, 175–176.

Kassebaum, N. J., Smith, A. G. C., Bernabé, E., Fleming, T. D., Reynolds, A. E., Vos, T., et al. (2017). Global, regional, and national incidence, prevalence, and years lived with disability for 328 diseases and injuries for 195 countries, 1990-2016: a systematic analysis for the Global Burden of Disease Study 2016. *Lancet (London, Engl.)* 390, 1211–1259.

Koo, H., Hayacibara, M. F., Schobel, B. D., Cury, J. A., Rosalen, P. L., Park, Y. K., et al. (2003). Inhibition of *Streptococcus mutans* biofilm accumulation and polysaccharide production by apigenin and tt-farnesol. *J. Antimicrob. Chemother.* 52, 782–789. doi: 10.1093/jac/dkg449

Koul, A., Dendouga, N., Vergauwen, K., Molenberghs, B., Vranckx, L., Willebrords, R., et al. (2007). Diarylquinolines target subunit c of mycobacterial ATP synthase. *Nat. Chem. Biol.* 3, 323–324. doi: 10.1038/nchembio884

Kuhnert, W. L., Zheng, G., Faustoferri, R. C., and Quivey, R. G. (2004). The F-ATPase operon promoter of *Streptococcus mutans* is transcriptionally regulated in response to external pH. *J. Bacteriol.* 186, 8524–8528. doi: 10.1128/jb.186.24.8524-8528.2004

Lamont, R. J., Koo, H., and Hajishengallis, G. (2018). The oral microbiota: dynamic communities and host interactions. *Nat. Rev. Microbiol.* 16, 745–759. doi: 10.1038/s41579-018-0089-x

Liu, Y., Tang, H., Lin, Z., and Xu, P. (2015). Mechanisms of acid tolerance in bacteria and prospects in biotechnology and bioremediation. *Biotechnol. Adv.* 33, 1484–1492. doi: 10.1016/j.biotechadv.2015.06.001

Marsh, P. D., and Zaura, E. (2017). Dental biofilm: ecological interactions in health and disease. *J. Clin. Periodontol.* 44(Suppl. 18), S12–S22. doi: 10.1111/jcpe.12679

Naha, P. C., Liu, Y., Hwang, G., Huang, Y., Gubara, S., Jonnakuti, V., et al. (2019). Dextran-Coated iron oxide nanoparticles as biomimetic catalysts for localized and pH-activated biofilm disruption. *ACS Nano.* 13, 4960–4971. doi: 10.1021/acsnano.8b08702

Narang, R., Kumar, R., Kalra, S., Nayak, S. K., Khatik, G. L., Kumar, G. N., et al. (2019). Recent advancements in mechanistic studies and structure activity relationship of FF ATP synthase inhibitor as antimicrobial agent. *Eur. J. Med. Chem.* 182:111644. doi: 10.1016/j.ejmech.2019.111644

Pereira-Cenci, T., Cenci, M. S., Fedorowicz, Z., and Azevedo, M. (2013). Antibacterial agents in composite restorations for the prevention of dental caries. *Cochrane Datab. Syst. Rev.* 12:CD007819. doi: 10.1002/14651858.CD007819.pub3

Peres, M. A., Macpherson, L. M. D., Weyant, R. J., Daly, B., Venturelli, R., Mathur, M. R., et al. (2019). Oral diseases: a global public health challenge. *Lancet (London, Engl.)* 394, 249–260.

Pfaller, M. A., and Diekema, D. J. (2012). Progress in antifungal susceptibility testing of *Candida* spp. by use of clinical and laboratory standards institute broth microdilution methods, 2010 to 2012. *J. Clin. Microbiol.* 50, 2846–2856. doi: 10.1128/jcm.00937-12

Pitts, N. B., Zero, D. T., Marsh, P. D., Ekstrand, K., Weintraub, J. A., Ramos-Gomez, F., et al. (2017). Dental caries. *Nat. Rev. Dis. Prime.* 3:17030.

Pogoryelov, D., Krah, A., Langer, J. D., Yildiz, Ö, Faraldo-Gómez, J. D., and Meier, T. (2010). Microscopic rotary mechanism of ion translocation in the Fo complex of ATP synthases. *Nat. Chem. Biol.* 6, 891–899. doi: 10.1038/nchembio.457

Preiss, L., Langer, J. D., Yildiz, Ö, Eckhardt-Strelau, L., Guillemont, J. E., Koul, A., et al. (2015). Structure of the mycobacterial ATP synthase Fo rotor ring in complex with the anti-TB drug bedaquiline. *Sci. Adv.* 1:e1500106. doi: 10.1126/sciadv.1500106

Qi, M., Chi, M., Sun, X., Xie, X., Weir, M. D., Oates, T. W., et al. (2019). Novel nanomaterial-based antibacterial photodynamic therapies to combat oral

bacterial biofilms and infectious diseases. *Int. J. Nanomed.* 14, 6937–6956. doi: 10.2147/ijn.s212807

Sachs, G. (1984). Pump blockers and ulcer disease. *New Engl. J. Med.* 310, 785–786. doi: 10.1056/nejm198403223101211

Saputo, S., Faustoferri, R. C., and Quivey, R. G. (2018). A drug repositioning approach reveals that *Streptococcus mutans* is susceptible to a diverse range of established antimicrobials and nonantibiotics. *Antimicrob. Agents Chemother.* 62:1.

Selwitz, R. H., Ismail, A. I., and Pitts, N. B. (2007). Dental caries. *Lancet (London, Engl.)* 369, 51–59.

Spugnini, E., and Fais, S. (2017). Proton pump inhibition and cancer therapeutics: a specific tumor targeting or it is a phenomenon secondary to a systemic buffering? *Semin. Cancer Biol.* 43, 111–118. doi: 10.1016/j.semcancer.2017.01.003

Takahashi, N., and Nyvad, B. (2011). The role of bacteria in the caries process: ecological perspectives. *J. Dent. Res.* 90, 294–303. doi: 10.1177/0022034510379602

Teng, F., Yang, F., Huang, S., Bo, C., Xu, Z. Z., Amir, A., et al. (2015). Prediction of early childhood caries via spatial-temporal variations of oral microbiota. *Cell Host Microbe* 18, 296–306. doi: 10.1016/j.chom.2015.08.005

Xiao, J., Klein, M. I., Falsetta, M. L., Lu, B., Delahunty, C. M., Yates, J. R., et al. (2012). The exopolysaccharide matrix modulates the interaction between 3D architecture and virulence of a mixed-species oral biofilm. *PLoS Pathogens* 8:e1002623. doi: 10.1371/journal.ppat.1002623

Yin, I. X., Zhao, I. S., Mei, M. L., Lo, E. C. M., Tang, J., Li, Q., et al. (2020). Synthesis and characterization of fluoridated silver nanoparticles and their potential as a non-staining anti-caries agent. *Int. J. Nanomed.* 15, 3207–3215. doi: 10.2147/ijn.s243202

Yu, S., Yun, E. J., Kim, D. H., Park, S. Y., and Kim, K. H. (2019). Anticariogenic activity of agarobiose and agarooligosaccharides derived from red macroalgae. *J. Agric. Food Chem.* 67, 7297–7303. doi: 10.1021/acs.jafc.9b01245

Zhang, K., Wang, S., Zhou, X., Xu, H. H., Weir, M. D., Ge, Y., et al. (2015). Effect of antibacterial dental adhesive on multispecies biofilms formation. *J. Dent. Res.* 94, 622–629. doi: 10.1177/0022034515571416

Conflict of Interest: The authors declare that the research was conducted in the absence of any commercial or financial relationships that could be construed as a potential conflict of interest.

frontiers in Microbiology

REVIEW
published: 13 April 2021
doi: 10.3389/fmicb.2021.640787

An Overview of Biological and Computational Methods for Designing Mechanism-Informed Anti-biofilm Agents

*Andy Y. An, Ka-Yee Grace Choi, Arjun S. Baghela and Robert E. W. Hancock**

Centre for Microbial Diseases and Immunity Research, University of British Columbia, Vancouver, BC, Canada

Bacterial biofilms are complex and highly antibiotic-resistant aggregates of microbes that form on surfaces in the environment and body including medical devices. They are key contributors to the growing antibiotic resistance crisis and account for two-thirds of all infections. Thus, there is a critical need to develop anti-biofilm specific therapeutics. Here we discuss mechanisms of biofilm formation, current anti-biofilm agents, and strategies for developing, discovering, and testing new anti-biofilm agents. Biofilm formation involves many factors and is broadly regulated by the stringent response, quorum sensing, and c-di-GMP signaling, processes that have been targeted by anti-biofilm agents. Developing new anti-biofilm agents requires a comprehensive systems-level understanding of these mechanisms, as well as the discovery of new mechanisms. This can be accomplished through omics approaches such as transcriptomics, metabolomics, and proteomics, which can also be integrated to better understand biofilm biology. Guided by mechanistic understanding, *in silico* techniques such as virtual screening and machine learning can discover small molecules that can inhibit key biofilm regulators. To increase the likelihood that these candidate agents selected from *in silico* approaches are efficacious in humans, they must be tested in biologically relevant biofilm models. We discuss the benefits and drawbacks of *in vitro* and *in vivo* biofilm models and highlight organoids as a new biofilm model. This review offers a comprehensive guide of current and future biological and computational approaches of anti-biofilm therapeutic discovery for investigators to utilize to combat the antibiotic resistance crisis.

Keywords: biofilms, antibiotic resistance, anti-biofilm agents, systems biology, virtual screening, machine learning, biofilm models, organoids

OPEN ACCESS

Edited by:
Mariano Martinez-Vazquez, National Autonomous University of Mexico, Mexico

Reviewed by:
Chris Waters, Michigan State University, United States
Cesar de la Fuente-Nunez, University of Pennsylvania, United States

***Correspondence:**
Robert E. W. Hancock
bob@hancocklab.com

Specialty section:
This article was submitted to Antimicrobials, Resistance and Chemotherapy, a section of the journal Frontiers in Microbiology

Received: *12 December 2020*
Accepted: *23 March 2021*
Published: *13 April 2021*

Citation:
An AY, Choi K-YG, Baghela AS and Hancock REW (2021) An Overview of Biological and Computational Methods for Designing Mechanism-Informed Anti-biofilm Agents. Front. Microbiol. 12:640787. doi: 10.3389/fmicb.2021.640787

INTRODUCTION

Bacterial biofilms are complex three-dimensional (3D) aggregates of microbes on surfaces including body surfaces, medical devices, and wounds. The National Institutes of Health estimate that biofilms are involved in 65-80% of all microbial infections and 80-90% of all chronic infections, making biofilms a significant healthcare issue (Attinger and Wolcott, 2012; Römling and Balsalobre, 2012; Jamal et al., 2018). Biofilm growth is an adaptive growth state and critically, biofilm

aggregates are highly (adaptively) antibiotic resistant when compared to the same bacteria in their free-floating planktonic form (Verderosa et al., 2019). With the growing antibiotic crisis fueled by antibiotic overuse and potentially accelerated by recent events such as COVID-19 (Strathdee et al., 2020), understanding biofilm formation, combatting antibiotic resistance, and developing new anti-biofilm agents are key priorities in health care.

Despite this necessity and priority, there are currently no approved anti-biofilm agents. Of the 82 registered clinical trials with known status (recruiting, active, completed, or terminated) on clinicaltrials.gov involving biofilm treatment or measurement, 25 involve testing a drug for anti-biofilm effects, mainly against oral biofilms. Most of these studies apply general antiseptics (e.g., chlorhexidine) or antibiotics (e.g., cefazolin), which are not biofilm-specific. However, there are currently two ongoing trials that are assessing anti-biofilm specific agents. The first is using nitric oxide, a known regulator for biofilms (Barraud et al., 2006), against chronic rhinosinusitis (Phase 2, NCT04163978). The other is using TRL1068, a human monoclonal antibody against the bacterial protein DNABII (which stabilizes DNA in the extracellular matrix of biofilms) (Xiong et al., 2017), against prosthetic joint infections (Phase 1, NCT04763759). Despite years of research, the fact that there are only two anti-biofilm candidates in the pipeline, and none approved, attests to the difficulty of creating anti-biofilm agents. This is likely due to a combination of a lack of priority given to this class of drugs, inaccurate biofilm models (that show efficacy *in vitro* and/or *in vivo* but not in humans) and an inadequate understanding of biofilm formation.

To accelerate discovery of novel anti-biofilm agents, we must leverage newer and more biologically relevant models, as well as new sequencing and computational technologies to better understand biofilm formation. Thus, in this review, we begin by describing current literature on biofilm formation and resistance, as well as the mechanisms of some existing anti-biofilm agents. We then describe how to employ a set of biological and computational methods to develop novel anti-biofilm agents to be used as a guide for investigators interested in anti-biofilm agent discovery. Most studies exploring biofilm mechanisms rely on omics studies, such as transcriptomics and proteomics, to uncover new genetic and protein targets for novel anti-biofilm agents to modulate. *In silico* screening can be used to screen for molecules from large databases that bind to and modulate these targets. Another approach is machine learning, in which algorithms are repetitively employed to predict the anti-biofilm activity of a molecule. Candidate molecules identified using machine learning or *in silico* screening can then be synthesized and validated in a variety of biological models, including biofilms grown in microtiter plates, flow cells, animal models, and human organoids. Successful candidates can then strengthen knowledge of biofilm formation mechanisms, further train machine learning algorithms, and ideally transition to clinical trials for human usage. Integrating multiple modalities of both lab and computational science can give investigators a better chance at developing a successful anti-biofilm agent (**Figure 1**).

THE CLINICAL RELEVANCE OF BIOFILMS

Biofilms can colonize biological or nonbiological surfaces, putting all patients, but especially the immunocompromised, surgical patients, individuals with major injuries or burns, and patients with implanted devices, at a high risk of developing biofilm infections. Critically, biofilms are associated with many or most chronic infections and are often associated with chronic inflammation, pain, and tissue damage. Biofilm-associated disease can affect virtually any organ system, most notably the cardiovascular (e.g., endocarditis), respiratory (e.g., cystic fibrosis), urinary (e.g., urinary tract infections), and oral (e.g., periodontitis) systems (Vestby et al., 2020). Implanted medical devices, such as catheters, stents, prosthetic heart valves, pacemakers, and artificial joints or limbs, are also common sites of biofilm formation (Bryers, 2008). Furthermore, planktonic bacteria can detach from the biofilm to spread throughout the body, causing bacteremia, colonizing other organ systems, forming thromboemboli, or triggering a septic episode (Fleming and Rumbaugh, 2018). Bacteria in biofilms are notoriously difficult to remove from abiotic surfaces such as door handles, beds, taps, showers, and other high-touch surfaces in the hospital setting, with such biofilms frequently containing multiple species of drug-resistant bacteria (Vickery et al., 2012). Persistence also occurs on biotic surfaces with chronic wounds. Biofilms colonize 60% of ulcers in diabetic patients, which can lead to limb amputation (James et al., 2008), and cause major problems in chronic rhinosinusitis (Karunasagar et al., 2018). The prevalence and persistence of biofilms can be attributed to a biofilm's ability to resist agents that would normally act against bacteria, including the host immune response and antibiotic treatment. Generally speaking, antibiotics have dramatically decreased mortality from infectious diseases. However, antibiotics have been almost exclusively developed and evaluated for efficacy against planktonic bacteria and are relatively ineffective against biofilms. Decades of research have sought an understanding of the biofilm processes that cause this resistance, with only moderate insights. Importantly, we need to understand unique biofilm biology in order to develop new anti-biofilm agents to specifically target biofilm processes and treat chronic infections.

Resistance describes a bacterium's ability to grow despite antibiotic treatment and is usually measured by the minimum inhibitory concentration (MIC, the lowest concentration of an antibiotic that inhibits bacterial growth). Biofilm resistance to antibiotics reflects the unique growth state of biofilms. First and foremost, biofilms undergo transcriptional reprogramming to the state that is intended to resist stress (de la Fuente-Núñez et al., 2013; Taylor et al., 2014). Since antibiotics are one type of stressor, it can be anticipated that alterations in the expression of genes in the resistome (encompassing all potential resistance mechanisms in any given bacterium) lead to decreased susceptibility, and that this likely involves multiple genes, as shown for other complex adaptive growth states such as swarming and surfing motility in *Pseudomonas aeruginosa* (Sun et al., 2018; Coleman et al., 2020). Our own current research is leading us to believe that this is also

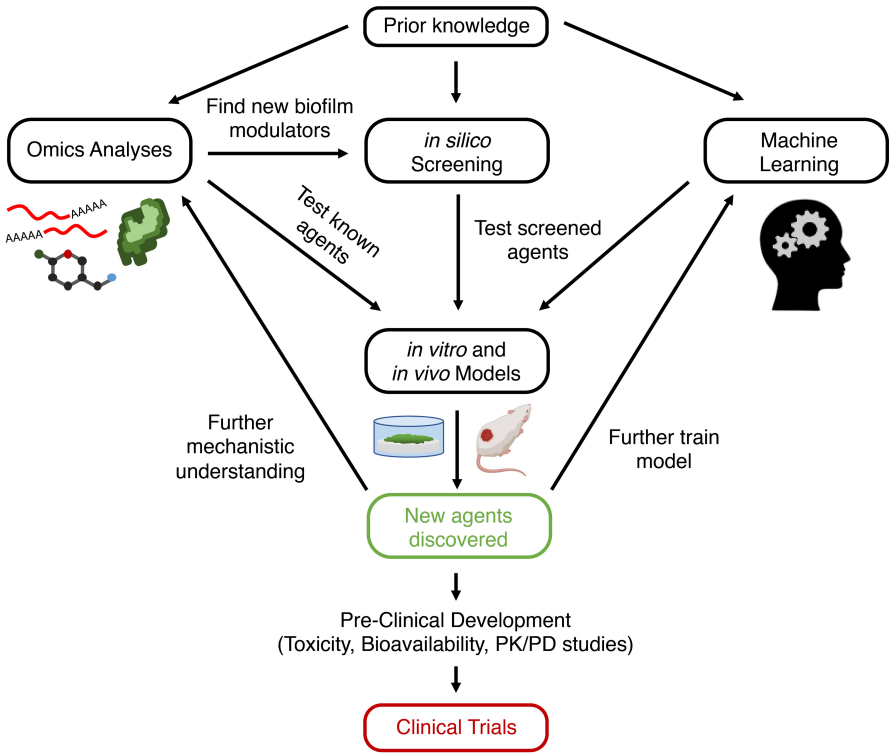

FIGURE 1 | Schematic view of approach for discovering new anti-biofilm agents. Prior knowledge leads to hypothesis generation and exploration of biofilm formation mechanisms. This can be probed using omics analyses, which can lead to the discovery of new anti-biofilm targets (genes, proteins, metabolites). Modulators of these targets (e.g., inhibitors of quorum sensing receptors) are screened directly using *in vitro* or *in vivo* models. Alternatively, *in silico* screening can be performed first on databases of compounds to identify those that bind to and modulate biofilm regulating proteins, which can then be validated with *in vitro* or *in vivo* models. Conversely, databases of known anti-biofilm agents can be used to train a machine learning model. The algorithm can then screen for putative anti-biofilm agents that are validated with *in vitro* and *in vivo* models. Finally, new agents that are discovered to be effective can undergo preclinical studies and then be entered into clinical trials and ultimately be used for human disease. In addition, these new agents can lead to further understanding of biofilm mechanisms, as well as providing additional data for optimization of machine learning models. Created with BioRender.com. PK, pharmacokinetics; PD, pharmacodynamics.

true for biofilms and there is considerable evidence supporting this perspective (Liao et al., 2013). This type of resistance is termed adaptive resistance or tolerance since it reverts as soon as the organisms are no longer growing as biofilms. It seems likely that at least some of the mechanisms involved are similar to those involved in resistance in planktonic cells (Hall and Mah, 2017) but exacerbated by the biofilm growth state, although unique regulatory genes and effectors might be involved. Evaluation of the resistome in planktonic cells has shown that mutations in numerous genes can lead to resistance to any given antibiotic (Breidenstein et al., 2008; Schurek et al., 2008; Gallagher et al., 2011; Coleman et al., 2020).

Other aspects of the biofilm growth state include increased cellular proximity, which has been shown to enhance horizontal gene transfer in biofilms compared to planktonic populations, resulting in faster acquisition of genetically resistant mutants in a biofilm (Molin and Tolker-Nielsen, 2003). In addition, the frequency of mutations appears to be enhanced in biofilms, perhaps due to increased oxidative stress (Driffield et al., 2008). Additional resistance of biofilms is conferred by the extracellular matrix, consisting of species-specific polysaccharides and proteins as well as extracellular DNA (Ciofu and Tolker-Nielsen, 2019). As a gel that loosely encapsulates and holds together the biofilm, the matrix may decrease the penetrance of certain but not all antibiotics (Singh et al., 2016). For example, the positively charged antibiotic tobramycin was sequestered by the matrix in *P. aeruginosa* biofilms, while the neutral antibiotic ciprofloxacin was able to penetrate (Tseng et al., 2013). Finally, nutrient gradients in a biofilm result in hypoxic regions within the biofilm, leading to less metabolically active bacteria (Stewart et al., 2016). These dormant bacteria can survive but not necessarily grow in the presence of antibiotics, a form of tolerance (Lebeaux et al., 2014). Antibiotics generally target active cells by inhibiting biosynthetic pathways; therefore, they are largely ineffective against dormant cells (Ciofu and Tolker-Nielsen, 2019). Thus, while active bacteria on the surface of biofilms may be eradicated by antibiotics, dormant persister cells are able to survive and become active once the antibiotic regimen is concluded, resulting in chronic infections (Høiby et al., 2010; Lebeaux et al., 2014). With all these mechanisms involved, biofilms are up to 1000-fold more resistant to multiple antibiotics than planktonic bacteria (Ceri et al., 1999).

Since resistance relies on the biofilm growth state, targeting biofilms, either by inhibiting formation or stimulating the

dispersal of mature biofilms, is an obvious path to overcoming resistance of biofilms to antibiotic therapies. Intriguingly, there are demonstrations that biofilm inhibitors can act synergistically with conventional antibiotics (de la Fuente-Núñez et al., 2015). Unfortunately, there is not a single approved treatment for biofilms presently, so this is an area that deserves attention. Critically, the first step to developing these therapies is understanding the mechanisms of biofilm formation.

BIOFILM FORMATION MECHANISMS AND EXISTING THERAPIES THAT TARGET THEM

Biofilms start as individual planktonic bacteria that can reversibly attach to surfaces. This can then lead to changes in gene expression that trigger irreversible binding, in part driven by the expression of particular adhesins. Concurrently, bacteria begin to secrete matrix components and the biofilm matures into a multilayer structure (Armbruster and Parsek, 2018). This complex process is regulated by multiple processes that have been extensively reviewed previously (Rabin et al., 2015; Tolker-Nielsen, 2015; Roy et al., 2018). Here we will highlight three major regulatory networks that appear to be somewhat conserved and are attractive targets for novel anti-biofilm agents, namely the stringent response, quorum sensing, and cyclic di-guanosine monophosphate (c-di-GMP) signaling.

The Stringent Response

All bacteria produce the nucleotide second-messengers/alarmones guanosine tetraphosphate and pentaphosphate [collectively (p)ppGpp] as part of the stringent stress response. Synthesis of these molecules is induced when a bacterial population is undergoing diverse nutritional stresses including limitations of carbon sources, amino acids, fatty acids, iron, and phosphate, but it is also clear that these molecules have important functions under normal growth conditions (Pletzer et al., 2020). Diverse enzymes mediate (p)ppGpp metabolism including ribosome-associated RelA synthase and SpoT in Gram negative bacteria and the bi-functional enzyme Rsh in Gram positives. The accumulation of (p)ppGpp results in a reprogramming of bacterial cells to adapt to nutrient deprivation, including decreasing macromolecular synthesis while upregulating stress accommodating pathways (Ross et al., 2016; Pletzer et al., 2020). The stringent response regulates biofilm formation in multiple Gram positive and Gram negative species (Balzer and McLean, 2002; He et al., 2012; de la Fuente-Núñez et al., 2014; Azriel et al., 2016; Liu et al., 2017). Mutants with deletions in (p)ppGpp synthases in *P. aeruginosa*, *S. aureus*, *E. coli*, *Salmonella*, *Listeria monocytogenes*, and *Enterococcus faecalis*, were either unable to form biofilms or formed poorly structured biofilms (Taylor et al., 2002; Chávez de Paz et al., 2012; de la Fuente-Núñez et al., 2014).

Due to its ubiquity in bacterial species and necessity for successful biofilm formation, (p)ppGpp is an excellent target for anti-biofilm therapies. Specific cationic amphipathic peptides, related to antimicrobial and host defense peptides, have preferential broad spectrum anti-biofilm activity which is mediated by binding directly to (p)ppGpp, marking it for degradation (de la Fuente-Núñez et al., 2014, 2015). While this class of peptides can have a variety of functions, including host immune system modulation, anti-inflammatory activity, wound healing, and direct antibacterial activity vs. planktonic bacteria (Haney et al., 2015), specific anti-biofilm activity was first observed with sub-inhibitory concentrations of LL-37 (Overhage et al., 2008) and subsequently with synthetic peptides such as IDR-1018 and the D-enantiomeric peptide DJK-5 (de la Fuente-Núñez et al., 2014, 2015). Excitingly, these peptides exhibit very broad spectrum activity against biofilms formed from all of the major antibiotic resistant pathogens in our society (collectively called the ESKAPE pathogens) (de la Fuente-Núñez et al., 2014, 2015; Pletzer et al., 2018), work against preformed biofilms and multispecies biofilms such as oral biofilms (Zhang et al., 2016; Wang et al., 2017), demonstrate synergy with conventional antibiotics *in vitro* (de la Fuente-Núñez et al., 2015) and *in vivo* (Pletzer et al., 2018), and work in several animal models. These peptides act in part against the stringent stress response and, in a murine abscess model, they also inhibit the transcription of (p)ppGpp-metabolizing enzyme SpoT, while it was proposed that there might be other or additional mechanisms explaining their action against biofilms (Pletzer et al., 2017; Salzer et al., 2020). Design features that discriminate such anti-biofilm peptides are different from those mediating activity against planktonic cells (de la Fuente-Núñez et al., 2014; Haney et al., 2018a). Thus, antibiofilm peptides are an attractive class of molecules that can be further optimized through rational design (see below) or synthesis of peptidomimetics (Gomes Von Borowski et al., 2018).

Instead of directly targeting (p)ppGpp, another method of stringent response modulation is through inhibition of (p)ppGpp synthetases, which is still a relatively unexplored field. The majority of known inhibitors are (p)ppGpp analogs such as Relacin (Wexselblatt et al., 2012) although these analogs have multiple off-target effects and low binding affinities (Wexselblatt et al., 2013). Given the recent characterization of synthetase structures, such as from *E. coli* (RelA) and *S. aureus* (RelP, RelQ), it will now be possible to use *in silico* screening methods to identify new inhibitors (Hall et al., 2020).

Quorum Sensing

Quorum sensing (QS) refers to the ability of bacteria within a population, such as a biofilm, to regulate gene expression based on cell density. QS is facilitated through small signaling molecules generated by bacteria that self-regulate their own expression through a positive feedback loop and are thus termed auto-inducers (Fetzner, 2015). Gram positive bacteria most commonly use auto-inducing cyclic peptides as auto-inducers, while Gram negative bacteria primarily use N-acyl homo-serine lactones (AHLs), quinolones, and fatty acids (Heeb et al., 2011; Schuster et al., 2013; Monnet et al., 2016; Zhou et al., 2017). Both Gram positive and negative bacteria can also use a furanosyl borate diester called autoinducer-2, suggesting the possibility of cross-talk between different species of bacteria in a community (De Keersmaecker et al., 2006). Auto-inducers are produced and at

a sufficient extracellular concentration are taken up and bind to their cognate receptors/transcription factors to exert their functions, including upregulating genes for virulence factors, antibiotic resistance, and biofilm formation (Liang et al., 2014).

Interfering with QS does not prevent biofilm formation but can have strong effects. For example, a *P. aeruginosa* mutant with a *lasI* deletion (which cannot produce the AHL 3-oxo-C12-HSL) has slower biofilm formation and flatter biofilms (Shih and Huang, 2002), while addition of 3-oxo-C12-HSL to this mutant allowed formation of biofilms structurally similar to wild type (Davies et al., 1998). Similarly, mutations in QS genes in *Burkholderia cepacia* and *Aeromonas hydrophila* also resulted in impaired biofilm formation (Huber et al., 2001; Lynch et al., 2002). QS interference can also result in biofilms that are more susceptible to antibiotic treatment and host immune responses. *P. aeruginosa* biofilms that were treated with QS inhibitors C-30 and C-56 furanones had increased sensitivity to tobramycin, while *lasI* mutants were more susceptible to kanamycin (Hentzer et al., 2002; Shih and Huang, 2002). *P. aeruginosa* with deletions in the Las and Rhl QS systems (*lasR, rhlA,* and *rhlR*) formed biofilms that were cleared more efficiently by polymorphonuclear cells compared to wild-type (Bjarnsholt et al., 2005; Gennip et al., 2009). Thus, therapies that inhibit QS (termed "quorum quenchers") represent a potential therapy targeting biofilms.

Quorum quenching can be divided into four mechanisms: (i) inhibiting auto-inducers from binding to their receptors, such as using halogenated furanones (Hentzer et al., 2002; Hentzer, 2003); (ii) decreasing production of auto-inducers by targeting their synthases, such as MvfR in *P. aeruginosa* (Starkey et al., 2014; Maura and Rahme, 2017); (iii) sequestering auto-inducers using cyclodextrans or antibodies (Park et al., 2007; Morohoshi et al., 2013); and (iv) degradation of auto-inducers using enzymes such as lactonases (Rémy et al., 2018). Most quorum quenchers that inhibit auto-inducer binding are derived from natural products (Rémy et al., 2018). However, QS systems are different across species, and generating broad-spectrum quorum quenchers might not be possible, and even different species sharing the same QS system may behave differently to a particular quorum quencher (Galloway et al., 2011). In the future, quorum quenchers might be used with conventional antibiotics since some quorum quenchers make biofilms more sensitive to conventional antibiotic use. However, while promising *in vitro* data is widely available, no quorum quenchers have been successfully tested in clinical trials for biofilm treatment (Hansen et al., 2005). It is also important to realize that quorum quenchers should be used only for specific species, since in some bacteria, such as *Vibrio cholerae*, QS actually represses biofilm formation to promote dispersal under high-density conditions. Thus, using a quorum quencher in this case could result in further aggregation of biofilms (Waters et al., 2014).

c-di-GMP Signaling

Signaling through c-di-GMP, a second-messenger molecule, is a significant player in controlling the transition from a motile to sessile (biofilm) lifestyle (Jenal et al., 2017). In most cases, high levels of c-di-GMP bind to downstream effectors such as transcriptional regulators, mRNA riboswitches, and protein adaptors to, among others, reduce the expression of motility (e.g., flagellar) genes and increase the expression of genes required for biofilm formation (Jenal et al., 2017). For example, in *P. aeruginosa*, higher c-di-GMP results in the increased expression of matrix components including adhesins (CdrA) and polysaccharides (Pel, Psl) (Borlee et al., 2010; Ha and O'Toole, 2015). The levels of c-di-GMP are controlled by multiple synthetic diguanylate cyclases and degradative phosphodiesterases, and both enzymes are heavily regulated by environmental cues, such as pathways regulated through QS (Srivastava and Waters, 2012). Thus, inhibiting diguanylate cyclases or activating phosphodiesterases to reduce the level of c-di-GMP may be another method of countering biofilms.

The fact that bacteria often have more than a dozen diguanylate cyclases and phosphodiesterases, which vary substantially between organisms, makes the possibility of drug development somewhat intimidating. However, various classes of diguanylate cyclases inhibitors have been developed. These include GTP or c-di-GMP analogs, which inhibit diguanylate cyclases in the active site and an allosteric site, respectively (Cho et al., 2020). Small molecule inhibitors of diguanylate cyclases have also been discovered using high-throughput *in vitro* and *in silico* screening (Cho et al., 2020), although activities tend to be modest. Stimulating activity of phosphodiesterases has been accomplished using nitric oxide donors such as sodium nitroprusside, leading to dispersal of *P. aeruginosa* biofilms (Barraud et al., 2006). Much like QS and the stringent response, the availability of structures of the specific proteins involved in regulating c-di-GMP pathways provides the necessary data to perform virtual screening for new inhibitors, as discussed below. A new avenue that works on a common property of bacteria is c-di-GMP sequestration using rationally designed peptides that mimic the structure of an effector protein to which c-di-GMP binds; such peptides have been shown to inhibit *P. aeruginosa* biofilm formation (Hee et al., 2020).

BIOINFORMATIC APPROACHES TO UNDERSTAND MECHANISM FOR NOVEL ANTI-BIOFILM AGENTS

A large proportion of current anti-biofilm agents have been developed by specifically targeting a process understood to regulate biofilm formation. Therefore, to develop new anti-biofilm agents, better understanding of biofilm formation is required to find new targets. Conversely, there are also existing anti-biofilm agents for which the precise mechanism of action is still unclear, and therefore understanding how these agents act on biofilms can provide new avenues and/or targets for modulation by new agents. Omics approaches such as transcriptomics, genomics, proteomics, and metabolomics are key to uncovering target genes, pathways, and processes required for biofilm formation. In general, each approach looks for differential abundance of biological molecules (nucleic acid, proteins, metabolites) between conditions. By comparing molecular changes between different conditions (e.g., bacteria in biofilms vs. planktonic growth, mutant vs. wild-type strains,

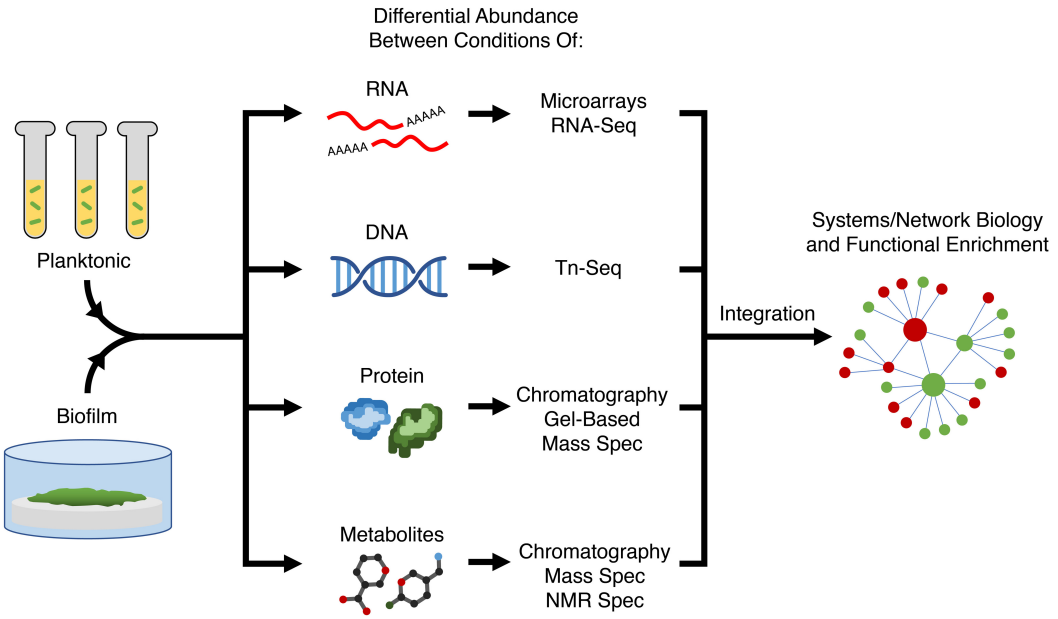

FIGURE 2 | Variety of omics approaches for elucidating biofilm mechanisms. Two or more conditions (e.g., planktonic vs. biofilm growth, presence or absence of an anti-biofilm agent, different biofilm substrates) are compared in terms of abundance of most biological molecules in the cell; with different methods being used to assess RNAs, transposon-insertions, proteins, and metabolites. Using systems or network biology, data from different modalities can be integrated to perform functional enrichment of genes and pathways required for biofilm formation to generate a holistic mechanistic view of biofilm formation. Tn-Seq, transposon insertion sequencing; Spec, spectroscopy; NMR, nuclear magnetic resonance.

± an anti-biofilm agent), one can hypothesize that the observed changes reflect the condition or treatment (**Figure 2**) and potentially reveal details about mechanisms and potential causes of resistance. These omics approaches yield a vast amount of data and thus a systems biology approach is needed for analysis. A common technique to group genes together is through pathway enrichment, using databases such as Kyoto Encyclopedia of Genes and Genomes (KEGG) or MetaCyc, and functional enrichment using gene ontology (GO) terms, in order to determine which pathways and functions are dysregulated and therefore potential targets for modulation (Kanehisa and Goto, 2000; Karp et al., 2002; Gene Ontology and Consortium, 2015).

Transcriptomics

RNA-Seq is a high-throughput technology employed to measure gene regulation and expression. Numerous studies have appeared in the literature using RNA-Seq (or its precursor microarray technology) to identify differentially expressed genes between planktonic and biofilm lifestyles for a variety of bacterial species including *P. aeruginosa* (Dötsch et al., 2012), *Klebsiella pneumoniae* (Guilhen et al., 2016), *Campylobacter jejuni* (Tram et al., 2020), *Bacillus licheniformis* (Sadiq et al., 2019), revealing that biofilm formation leads to hundreds of dysregulated genes (Amador et al., 2018). For example, RNA-Seq allowed for the identification of transcriptomic signatures specific to planktonic, biofilm, and biofilm-dispersed *K. pneumoniae* cells, highlighting underlying mechanisms involved in each bacterial lifestyle (Guilhen et al., 2016). RNA-Seq can also be used to study the effect of antibiotics and potential anti-biofilm agents on biofilm formation (Tan et al., 2015; Liu et al., 2018). Recently, Wu et al. (2020) probed the anti-biofilm effects of exopolysaccharide EPS273 on *P. aeruginosa* using RNA-Seq and found that EPS273 might mediate its effects by downregulating expression of genes in the PhoP-PhoQ two-component system and QS systems LasI/LasR and RhII/RhIR, which are involved in biofilm formation. These studies elucidated new pathways that can be targeted by novel therapies. As RNA-Seq costs decrease, technical methods improve, and better *in vitro* and *in vivo* models are developed for biofilm analysis, it is also now possible to perform dual RNA-Seq of both the host and pathogen to interrogate host-pathogen interactions (Westermann et al., 2017). To illustrate the potential applications of RNA-Seq for biofilm studies, we highlight two recent studies on complex adaptive lifestyles from our lab that employed RNA-Seq technologies.

Coleman et al. (2020) aimed to identify dysregulated genes that allowed *P. aeruginosa* to resist tobramycin while in the swarming state. Swarming motility is a coordinated surface-associated movement that occurs under conditions that mimic the surface of the human lung and has been proposed to allow for rapid colonization leading to biofilm formation in the cystic fibrosis lung. This adaptive growth state, like biofilm formation, leads to resistance to multiple antibiotics. RNA-Seq identified 29% (1581) of genes that were differentially expressed (DE) in swarming compared to swimming motility (behavior of bacteria in aqueous environments). From these, 26 DE genes were identified that were proven to be involved in swarming mediated resistance to tobramycin, demonstrating that adaptive resistance was multigenic. For example, genes in the *wbp* operon

involved in lipopolysaccharide synthesis were downregulated, indicating a new role in lipopolysaccharide alteration for adaptive tobramycin resistance. Thus, this approach highlights the mechanistic changes that occur to promote tobramycin resistance in swarming *P. aeruginosa*. A further 224 genes were DE between tobramycin-treated and untreated swarming *P. aeruginosa* and many downregulated genes were identified using GO as virulence factors and QS regulators, indicating while tobramycin might not kill swarming *P. aeruginosa*, it may still have clinical benefits in dampening virulence. A notable upregulated gene in swarming cells treated with tobramycin was *mexXY*, an efflux pump for aminoglycoside resistance indicating that tobramycin treatment further exacerbated resistance. A similar study evaluated the influence of ampicillin on *S. aureus* biofilms (Liu et al., 2018), revealing 530 DE genes including upregulation of several resistance pathways and genes encoding adhesion-promoting surface proteins in biofilms formed with vs. without sub-inhibitory ampicillin. The results collectively clarified important mechanisms by which biofilms resist ampicillin and how sub-inhibitory ampicillin enhances biofilm viability and biomass.

Alford et al. (2020) investigated the role of the nitrogen regulator NtrBC in biofilm formation and chronic infections. NtrBC was found to be not only required for swarming and biofilm formation, but also for dissemination to distal organs from a localized subcutaneous abscess in mice. RNA-Seq performed on *ntrB* and *ntrC* deletion mutants showed 790 and 1184 dysregulated genes, respectively, compared to wild-type in swarming conditions, with many involved in nitrogen and carbon metabolism as annotated by the KEGG database. In addition, there was downregulation of genes required for virulence in rat models of *Pseudomonas* lung infection, which matched the *in vivo* data of decreased dissemination. Thus, these results were consistent with the suggestion that NtrBC may be a new target for anti-biofilm therapies.

Transposon Insertion Sequencing

While most studies rely on mutants with deletions in specific genes to probe their functions in biofilm formation, transposon insertion sequencing (Tn-Seq) offers a high-throughput approach to identify multiple genes required to survive in a specific condition such as in a biofilm (Cain et al., 2020). Tn-Seq begins by creating a library of mutants with each cell carrying a promiscuous transposon inserted randomly into the genome, and in a library of such mutants, the function of each gene is disrupted in multiple mutants. These mutants can be grown and analyzed individually to elucidate the effect of the mutation on biofilm formation (Ueda and Wood, 2009) but a more efficient approach is to pool these mutants together and grow them collectively to determine which survive in different environments. Direct sequencing is performed on transposon-flanking regions to detect all genes with transposon insertions that exist in the population growing in a specific condition compared to a standard growth control. Mutants with a transposon disrupting a gene that is required for fitness in this condition will not grow well and therefore have decreased representation in the sequencing results. For example, if the mutant pool is sequenced from cells grown under planktonic and biofilm conditions, and a transposon-inserted gene is only detected in the planktonic condition, then that gene is required for biofilm formation (Cain et al., 2020). Genes identified to be required for biofilm formation can then be validated by growing the individual mutants. However, one limitation to pooling mutants for Tn-Seq is that genes encoding extracellular enzymes, proteins, matrix components, or autoinducers that are essential for biofilm formation may not be detected, since mutants of those genes can be cross-complemented by the extracellular components synthesized by non-mutants in the population. This method has incorporated new technologies in the last few years, such as sorting individual mutant cells using microfluidics and using inducible promoters to probe the function of essential genes (which cannot be analyzed using traditional Tn-Seq methods as disruption of essential genes results in non-viable mutants) as outlined in a recent review (Cain et al., 2020).

Poulsen et al. (2019) used Tn-Seq to identify 321 core essential genes shared across nine strains of *P. aeruginosa* isolated from human infections and the environment, as well as five different media replicating human sputum, serum, and urine, and conventional LB and M9 media. Considering that regulators of biofilm formation depend on both the stage of biofilm growth and the experimental setting, a similar approach could be performed on different biofilm stages ranging from initial adherence to dispersal, or different *in vitro* and *in vivo* biofilm models to identify "core essential genes" for biofilm formation shared across all settings. The pathways and proteins identified would be attractive targets for novel anti-biofilm agents. In another study, Morgan et al. (2019) found that interfering with biofilm genes in *P. aeruginosa* by deleting *lasR* (QS) or increasing c-di-GMP levels through deletion of the negative regulator *wspF* led, respectively, to decreased and increased biofilm formation, but surprisingly did not affect fitness in a murine chronic wound high-density infection model. Using Tn-Seq, they found 28 mutants that were absent in the chronic wound, with transposons in genes involved in anaerobic growth and metabolic functions, indicating their possible role in wound fitness. Fitness defects were later validated by growing transposon mutants individually. Thus, the ability to combat stressors in high-density populations is critical for maintaining a chronic infection, and forming biofilms does not appear to be the only way that bacteria can survive in chronic wounds, which has implications on how to approach developing therapies for chronic wounds.

Tn-Seq was also used to investigate the formation of persister cells that make biofilms difficult to eradicate. Cameron et al. (2018) generated 4,411 transposon mutants of *P. aeruginosa* and found 137 genes were needed for survival after fluoroquinolone treatment using Tn-Seq. They focused on *carB*, a subunit of the carbamoyl phosphate synthetase for pyrimidine and arginine synthesis, which was found to have the lowest survival rate when disrupted. The *carB* transposon mutant had increased intracellular ATP accumulation, and treatment with arsenate to reduce ATP levels restored antibiotic resistance in this strain. Thus, an agent that inhibits this synthetase, interferes with pyrimidine synthesis, or increases ATP levels would represent a novel method to prevent the formation of persister cells.

Proteomics

Proteomics can provide additional information on actual protein expression (which is not always coordinated with transcription due to post-transcriptional regulatory/modification mechanisms). While traditionally identified by gel electrophoresis, limitations in detection and quantification have led to the increasing popularity of liquid chromatography/mass spectrometry (LC-MS) methods that can analyze >80% of the proteome (Khemiri et al., 2016). Proteomics can also be done on "sub-proteomes" through specific extraction protocols that analyze proteins in the extracellular matrix (Gallaher et al., 2006), cell wall (Calvo et al., 2005), and bacterial surface (Solis et al., 2014), providing a level of functional detail that is not captured through genetic analyses. For example, to characterize the surface proteins expressed by *S. aureus*, cell shaving proteomics was performed by using proteases to selectively cleave surface exposed peptide epitopes, which were separated using LC-MS and matched to the original protein for identification (Solis et al., 2014). Characterizing matrix proteins can be accomplished by centrifugation and filtration of biofilms to eliminate cells from the biofilm matrix, followed by proteomic analysis (Couto et al., 2015). Furthermore, identifying temporal production of proteins can be accomplished through bio-orthogonal non-canonical amino acid tagging (BONCAT), in which azidohomoalanine (a methionine analog) is added to cultures and incorporated into newly formed proteins. Proteins containing azidohomoalanine can then be enriched for and characterized by LC-MS (Rothenberg et al., 2018). BONCAT has also recently been performed to identify metabolically active bacteria in cystic fibrosis microbiota (Valentini et al., 2020).

A recent study by Suryaletha et al. (2019) leveraged proteomics to identify proteins only expressed in biofilms when compared to planktonic growth of *Enterococcus faecalis*. GO and KEGG functional enrichment found enhanced production of proteins involved in glycolysis, the LuxS QS system, rhamnopolysaccharide synthesis, and arginine metabolism in biofilm growth, all of which would represent biofilm-selective targets for *Enterococcus* (Suryaletha et al., 2019). Similar studies were done comparing *Haemophilus influenzae* and *Mycobacterium tuberculosis* biofilm and planktonic forms to identify anti-biofilm protein targets (Gallaher et al., 2006; Wang et al., 2019). Erdmann et al. (2019) also aimed to uncover a "core proteome," much like a core essential genome discussed in the above section, through proteomics analyses of 27 clinical isolates of *P. aeruginosa* grown as biofilms or planktonic suspensions. Interestingly, proteomes from these clinical isolates were similar to each other during planktonic growth, but much more divergent in biofilms despite being grown under the same biofilm conditions. While no protein was selectively dysregulated in the biofilms of all isolates, 141 proteins were differentially expressed in at least 50% of the isolates. Functional enrichment showed increased expression of proteins involved in iron metabolism, fatty acid biosynthesis, and outer membrane protein synthesis, and decreased expression of proteins involved in translation, consistent with *in vivo* proteomic data of *P. aeruginosa* in cystic fibrosis patients (Wu et al., 2019). The proteome diversity across these isolates does not favor a "universal" *P. aeruginosa* biofilm-specific protein, although this might have reflected limited resolution, and argues that an anti-biofilm agent would likely need to target multiple effector proteins in order to have an effect on multiple *P. aeruginosa* isolates.

Finally, meta-proteomics provides a fascinating new area of proteomic research to uncover proteins required for multi-species populations. Most recently, this has been done on a community of four soil bacteria (*Stenotrophomonas rhizophila*, *Xanthomonas retroflexus*, *Microbacterium oxydans*, and *Paenibacillus amylolyticus*) that exhibited enhanced biofilm formation when co-cultivated compared to single species. Meta-proteomics identified the abundance of proteins for each species in key metabolic and energy pathways, such as amino acid metabolism and fermentation, that did not occur in single species communities, implicating both competitive and cooperative mechanisms of survival (Herschend et al., 2017). This technology may soon be applied to other multispecies biofilms, such as those found in healthcare or dental settings.

Metabolomics

Metabolomics analyzes differential production of small molecule metabolites and metabolism intermediates (e.g., carbohydrates, nucleotides, and amino acids). Bacterial populations are lysed, and the contents undergo either liquid, gas, or ion chromatography to separate the various metabolites by size or charge. This is followed by mass or nuclear magnetic resonance spectrometry of each of the separated fraction to identify metabolites. Metabolomics offers a snapshot of the functional changes that result from the transcriptomic and proteomic changes measured by the above methods. Furthermore, the analysis of metabolites that are consumed and secreted can be used to predict biofilm activity (Beale et al., 2013). Several metabolomic studies comparing planktonic and biofilm-associated bacteria have been undertaken (Yeom et al., 2013; Hasan et al., 2015; Wong et al., 2015; Harrison et al., 2019). For example, in *S. aureus*, arginine metabolites were found to be downregulated in biofilms when compared to planktonic samples, suggesting their consumption in the urea pathway (which uses arginine and arginine metabolites) to maintain pH balance in the biofilm environment (Stipetic et al., 2016). This is consistent with transcriptomic data showing upregulation of urea cycle proteins in biofilms (Resch et al., 2005). Thus, targeting the urea cycle might be a novel way of interfering with *S. aureus* biofilm formation.

Omics Integration

Each of these omics analyses on their own can analyze complex systems as a whole and provide a more comprehensive profile of the complex adaptive biofilm growth state when compared to a single-target reductionist approach. However, integration of these omics data can uncover new connections that might otherwise remain undetected through individual omics. In addition, the detection of dysregulation of a molecule, protein, or pathway by more than one omics method reinforces the observation that it is a key regulator or target for modulation. A variety of different integration methods are currently available, primarily for human studies (Lee et al., 2019; Misra et al., 2019),

although similar approaches have been recently considered for lactic acid bacteria (O'Donnell et al., 2020).

One approach is simply to create a protein-protein interaction network by inputting lists of DE genes and proteins, such as through the web-based platform NetworkAnalyst, which can annotate data from bacterial species such as *P. aeruginosa* and *E. coli* (Xia et al., 2015). Metabolomic data can be linked to this network through protein-metabolite interactors identified by MetaBridge (Hinshaw et al., 2018). Functional enrichment of these combined networks can highlight biologically relevant pathways derived from the combination of these omics analyses.

More complex integrative approaches are available such as through the R package mixOmic (Rohart et al., 2017). One of the issues with multi-omics data is the high dimensionality of each data source, since there can be thousands of genes and proteins in each omics data set. mixOmics can perform dimensional reduction by combining related factors in each dataset and highlighting the factors that provide the largest source of variation, creating a single factor matrix from multiple data matrices that can then be used for functional enrichment (Rohart et al., 2017).

With single-cell omics employed more frequently in other fields, single-cell technologies may be a potential future direction to analyze the heterogeneity of biofilms (Ma et al., 2019). For example, bulk RNA-Seq employed in most studies measures only the average gene expression; single-cell RNA-Seq for biofilms would measure gene expression of each cell, capturing the heterogeneity and pseudo-differentiation of biofilm cells. Regardless of the analysis method, whether it is single-omics or multi-omics, the data generated by these approaches have deepened understanding of biofilm formation and identified novel targets for modulating biofilm growth. The next logical step is to identify novel therapeutics that can act on these targets, which can be accomplished using *in silico* screens and models.

IN SILICO SCREENS AND MODELS FOR IDENTIFYING NOVEL ANTI-BIOFILM AGENTS

The above omics experiments indicate that several hundred proteins are apparently required for biofilm formation, each representing attractive candidates to modulate or inhibit using small molecules. While screening these compounds has been traditionally performed experimentally, computational (*in silico*) approaches represent an intriguing and potentially time-saving tool for designing and screening anti-biofilm agents. The appeal of deriving and screening agents computationally is multifold, including the ability to learn specific molecular properties associated with biofilm eradication and improved decision making in selecting candidate agents for validation (Vamathevan et al., 2019). Furthermore, *in silico* approaches are facilitated by increasing processing speeds and most importantly, large databases of putative molecules and their specific properties. *In silico* approaches that have been proposed include molecular docking screens, quantitative structure-activity relationship (QSAR) based modeling, and machine learning.

Virtual molecular docking screens rely on estimating the interaction between the 3D structures of targetable bacterial receptors and known ligands or small molecules. This approach was recently given a huge boost with major enhancements in the ability to computationally predict protein structures based on the primary sequence with amazing accuracy (Service, 2020). Interactions between specific receptor-target pairs are empirically scored by estimated hydrogen bonding, and electrostatic and hydrophobic interactions, with high scoring candidates representing novel targets (Schneider and Fechner, 2005; Dos Santos et al., 2018; Guedes et al., 2018). Of more recent interest are machine learning and QSAR methods, a suite of techniques enabling efficient screening and selection of agents in specific contexts, such as peptides targeting *E. coli* biofilms. These modeling frameworks have been reviewed previously (Tamay-Cach et al., 2016; Cardoso et al., 2019), largely by describing their general use in discovering antimicrobials. Furthermore, these two methods may be complementary, since virtual screens may generate compounds that can then be used to train machine learning models. In this section, we discuss virtual screening methods and machine learning methods for deriving candidate anti-biofilm agents and provide several examples of how they have been implemented.

Virtual Screening

Virtual molecular docking screens permit thousands of compounds in databases to be screened for binding against (and potentially modulating) protein targets identified by omics studies. The starting point is knowledge of the actual (crystallization or NMR derived) or predicted structure, and especially the active sites of the protein in question. Docking algorithms employ algorithms to iterate through possible binding conformations, which are typically optimized to maximize molecular interactions and minimize binding energy to a target protein. Several molecular docking tools have been published and also exist on web applications allowing easier accessibility for researchers, including HADDOCK, UCSF DOCK, and MTiOpenScreen (Allen et al., 2015; Labbé et al., 2015; van Zundert et al., 2016).

In the context of anti-biofilm agents, there are several recent studies that have described the use of molecular docking to screen molecules targeting QS proteins, diguanylate cyclases, (p)ppGpp synthetases, and other regulatory proteins (Fernicola et al., 2016; Kalia et al., 2017; Tiwari et al., 2018; Alves-Barroco et al., 2019; Ding et al., 2019; Mellini et al., 2019; Hall et al., 2020). More recently, Mellini et al. (2019) screened >1000 FDA-approved drugs for binding to PqsR, a previously crystallized protein involved in QS in *P. aeruginosa*. Exclusively screening FDA-approved drugs, an approach known as "drug repurposing," expedites clinical translation since the drugs' attributes in humans including toxicities are known. The authors identified five drugs that bind to PqsR with high affinity, and then validated these using *in vitro* biofilm and swarming motility assays. Similarly, Alves-Barroco et al. (2019) used the ZINC database to screen molecules against biofilm-regulatory protein BrpA from the bovine mastitis pathogen *Streptococcus dysgalactiae* subsp. *dysgalactiae*, employing the

Auto Dock Vina docking tool (Trott and Olson, 2010; Alves-Barroco et al., 2019). Because the crystallized structure of BrpA was unavailable, a BrpA homolog was submitted to Protein BLAST to identify structural templates. Nevertheless, the resultant molecules included ones with effective, albeit somewhat weak, anti-biofilm activity, providing a template for optimization. As more bacterial proteins are crystallized and solved, protein structural prediction algorithms become more accurate, databases of active anti-biofilm agents grow, and accessibility of docking software improves, the potential of virtual screening can increase dramatically and may soon become a standard technique employed after discovering a new protein target to uncover novel modulators of specific targets.

Machine Learning

While virtual docking screens rely on accurate 3D structures to predict activity, machine learning is a more flexible approach that focuses on the properties of the molecule itself rather than the target to infer anti-biofilm activity. Machine learning is a set of efficient and powerful statistical methods used to make predictions in various contexts, including the prediction of novel antimicrobial agents specifically targeted to biofilm infections. Generally, an algorithm is trained using large relevant datasets (training sets) in order to learn a relationship between the features describing the data and the prediction task at hand. In the context of small molecule anti-biofilm agents, these features (also termed molecular descriptors) include steric size, lipophilicity, and 3D structure, but there are hundreds of physical-chemical parameters that can be utilized (**Figure 3**). The goal of a good machine learning model is generalizability to unseen examples; thus, the accuracy of predictions is typically assessed on examples not used for training (a validation set). Several algorithms have been developed to extract complex linear and non-linear relationships and formulate them into predictive models, including Logistic Regression, Random Forest, Support Vector Machines (SVMs), and Neural Networks (Noble, 2006; LeCun et al., 2015).

In order to implement any machine learning technique to identify novel anti-biofilm agents, the prediction task must be established. The prediction task is often as simple as classifying an agent as "anti-biofilm" and "non-anti-biofilm," representing positive and negative training examples, respectively. Therefore, a set of agents, including small molecules, peptides, or existing antibiotic backbone structures, must be gathered and associated with a particular activity. Several databases comprising small molecules and peptides exist for these purposes, including SwissProt, PubChem, the Antimicrobial Peptide Database (APD), the Biofilm-active AMPs database (BaAMPS), aBiofilm, and the Data Repository of Antimicrobial Peptides (DRAMP) (Di Luca et al., 2015; Wang et al., 2016; Rajput et al., 2018; Kang et al., 2019; Kim S. et al., 2019; UniProt Consortium, 2019). BaAMPS was created to provide researchers a source of peptides to train machine learning models with antibiofilm activity (Di Luca et al., 2015). Gupta et al. (2016) used the BaAMPS database to select 178 anti-biofilm peptides for training an SVM model, whereas the non-anti-biofilm set was composed of randomly generated peptides from all SwissProt database sequences. Similarly, Sharma et al. (2016) used the BaAMPS database to select 80 anti-biofilm peptides to train an SVM model, while their non-anti-biofilm set included only QS peptides with no anti-biofilm/antimicrobial effects. However, while the model accurately predicted known anti-biofilm peptides, its ability to predict unknowns was not verified. Moreover, it is important to note that such validations assume a reproducible standardized assay for evaluation, with *in vitro* MIC compared to biofilm inhibitory concentration (BIC), and/or minimal biofilm inhibitory concentrations (MBIC) (Haney et al., 2018b). This has implications when implementing and comparing various machine learning models across studies, since the exact definition of anti-biofilm may differ.

Beyond the specific assays or mechanisms used to define anti-biofilm activity, an agent's molecular type (peptide, small molecule, lipid, etc.) and the specific bacterial species are also components of the prediction task. Whereas most machine learning pipelines used to predict anti-biofilm activity have been peptide based, smaller natural and synthetically derived molecules can also be modeled using machine learning. For example, machine learning models that predicted the anti-biofilm activity of naturally occurring essential oils were successfully implemented (Artini et al., 2018; Patsilinakos et al., 2019). Interestingly, Patsilinakos et al. (2019) assayed essential oils for two strains of *S. aureus* and two strains of *S. epidermidis* and used the results to train separate models for each strain. The anti-biofilm activity of each essential oil varied greatly for each strain, highlighting the value in training strain-specific machine learning models (Patsilinakos et al., 2019). Accordingly, the context in which machine learning models are trained can become quite specific, which must be considered when establishing the predictive scope and applicability of a machine learning model, and the need for drugs with broader spectra of activity.

To train a machine learning model, anti-biofilm agents of interest must have accurate numerical representations of physicochemical and 3D properties in the form of features/descriptors. The obvious assumption is that molecules with similar activities have similar physicochemical properties, whereby the approximate relationship between properties and activity are learned during the training of a machine learning model. Extracting features from molecules is an established discipline in itself, referred to as chemoinformatics. QSAR was an early chemoinformatics framework for extracting numerical descriptors from molecules, followed by training a simple machine learning algorithm (Cherkasov et al., 2014; Mitchell, 2014). There are a variety of diverse QSAR categories composed of hundreds of different descriptors extensively curated since inception, including topological, functional groups, and geometric (Danishuddin and Khan, 2016). Many examples of commercial and freely available software exist to extract feature descriptors for a variety of molecules (Sawada et al., 2014).

In this context, Haney et al. (2018a) trained a logistic regression model using seven QSAR descriptors to identify anti-biofilm peptides against methicillin resistant *S. aureus* (MRSA), derived from the widely studied 1018 peptide. The model was validated against a set of 100,000 semi-random peptides and predicted anti-biofilm potential of a previously

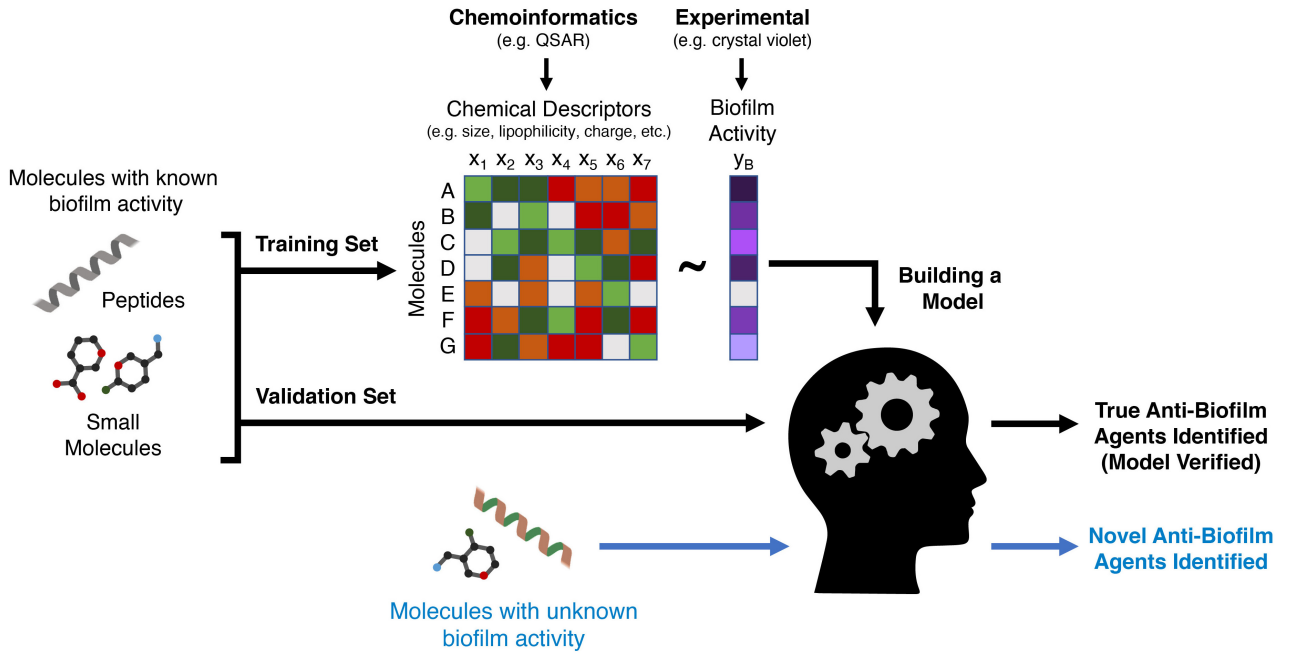

FIGURE 3 | A schematic of how machine learning can be used to discover new anti-biofilm agents. A training set comprising peptides or small molecules with known anti-biofilm activity (validated experimentally) are used to train a machine learning algorithm. Chemical features of these molecules (such as size or lipophilicity) can be generated using chemoinformatics methods such as QSAR. The algorithm then creates a mathematical relationship between a variety of features of each molecule and the anti-biofilm activity of the molecule. A second group of molecules (a validation set) with known anti-biofilm activity is then analyzed using the derived algorithm to ensure that it can accurately classify these molecules as having anti-biofilm activity or not. Finally, molecules for which anti-biofilm activity is not known, are then classified by the algorithm, with the output being potentially novel anti-biofilm agents that must then be validated with *in vitro* or *in vivo* models.

undescribed peptide 3002. *In vitro* validation showed that peptide 3002 had 8-fold enhanced anti-biofilm potency against MRSA biofilms when compared to 1018, and equivalent activity in a mouse abscess model. Thousands of descriptors were extracted from each peptide in the training set; however, computational prediction reduced this to a set of seven core descriptors that were ultimately used to train machine learning models. This strategy was employed to increase a machine learning model's generalizability by removing redundant descriptors and preventing overfitting.

Chemical graphs and fingerprints, which capture the atomic structure and connectivity of the molecule, are other approaches for representing molecules numerically for application in machine learning (Lo et al., 2018). These representations are typically appropriate for small molecules rather than peptides with complex and/or flexible secondary structures. Srivastava et al. (2020) trained a hybrid random forest model based on QSAR type descriptors and chemical fingerprints to identify potential anti-biofilm molecules. The authors extracted a 10,208-unit chemical fingerprint, which they combined with the QSAR descriptors to generate a hybrid classifier. Neural networks are a class of machine learning models that mimic the operations of neurons in the brain. Specifically, they allow the models to both learn features through hidden layers and then use them to perform the prediction task. Stokes et al. (2020) used a directed message passing deep neural network (Yang et al., 2019) to learn a type of chemical fingerprint based on the graph structure. Although the authors did not aim to discover an anti-biofilm agent, they predicted and validated the potential use of the antibiotic halicin for use against *E. coli* infections. Furthermore, this study represents a use of neural networks and feature learning which can be applied to identify novel anti-biofilm agents. In this regard, similar neural network approaches have been used to derive enhanced 9-amino-acid, broad-spectrum antimicrobial peptides, by relating descriptors to activity (Cherkasov et al., 2009). It is often stated in machine learning "garbage in, garbage out," meaning poor quality input data results in poor predictions. Accordingly, a large training set such as the one used by Cherkasov et al. (2009), a diverse set of accurately estimated features and descriptors, and robust modeling techniques are essential to predict novel anti-biofilm agents.

To assess the predictive ability of a trained machine learning model, a test or validation set is employed. This set includes agents where the anti-biofilm activity is known, thus the model's predictions can be compared for accuracy. Practically speaking, cross validation is often employed in which a subset of, for example, 80-90% of molecules with known activity is used for testing and the remainder for validation, and this is repeated iteratively using a different subset of molecules for validation. Finally, novel agents predicted as having anti-biofilm activity must be confirmed with *in vitro* or *in vivo* experiments as described in the next section. The application of machine learning to predict

anti-biofilm activity has often proven successful, as shown in the presented studies and broader studies identifying antimicrobial agents. Future directions in this field will include expanding databases of anti-biofilm agents and their respective potencies, as well as determining drug parameters such as pharmacokinetics/pharmacodynamics, bioavailability, and toxicity, to advance commercialization and provide an extensive repository of training and validation molecules for various prediction tasks. Whereas most studies have predicted anti-biofilm activity in a binary fashion, directly predicting potency may also generate better candidates. Expanding these resources will immensely benefit the community in building robust and generalizable machine learning models for novel anti-biofilm agents.

MODELS FOR ASSESSING NOVEL ANTI-BIOFILM AGENTS

The *in silico* methods described above can generate potential candidates. However, validation is required in accurate biofilm models to assess their anti-biofilm activity and clinical potential. An ideal biofilm model should provide high-throughput testing of multiple compounds against multiple species, be easily manipulatable, and to some extent resemble biofilms found in human infections and on abiotic surfaces such as medical devices. However, while no biofilm model exists that satisfies all three conditions, this section provides an overview and discussion of the advantages and limitations of current *in vitro* and *in vivo* based biofilm models to facilitate a decision on which biofilm model to use in different situations (**Figure 4**). These biofilm models can also be used for experiments to generate omics data as discussed earlier.

In vitro Biofilm Models

The purpose of an *in vitro* biofilm model is two-fold: (i) to provide a method of assessing the relative activities of a group of compounds and relating these to other compounds in the literature, and (ii) assessing the probability that compounds will work against biofilms in a relevant circumstance (e.g., a biofilm infection in a patient). Such *in vitro* models can be generally classified into closed, open, and tissue culture-based model systems. Closed or static models have no influx or efflux of nutrients, while dead cells, waste, and signaling byproducts will build up (Lebeaux et al., 2013). In addition, closed systems do not always reflect conditions found under some circumstances *in vivo*, such as shear stress from constant movement of liquids in the bloodstream or in medical devices such as catheters (Lebeaux et al., 2013). This issue might be somewhat overstated however, since biofilms in the body often occur on tissues (e.g., wounds, burns, skin, tissues, prosthetic joints, sinuses, bones, etc.), where it can be argued that there is minimal flow of liquids. Microtiter plate-based biofilm systems are classic examples of the closed model. Following on from the popular methods for determining minimal inhibitory concentration (MIC) for antimicrobials against planktonic bacteria (Wiegand et al., 2008), we have recently proposed a standardized method for assessing anti-biofilm activity (Haney et al., in press).

Microtiter plate biofilm assays are one of the most widely used *in vitro* model systems, where biofilms are grown on the bottom or the walls of a microtiter plate or on materials (e.g., microscope slides, silicone, titanium, and hydroxyapatite disks) placed within a microtiter plate (Vandecandelaere et al., 2016). They represent a relatively cheap and user-friendly system, with parallels to MIC assays, that can be easily used as a high-throughput screen, require only a small volume of reagents, provide researchers easy control over growing conditions (media type, temperature, humidity, and presence/absence of stress signals), and enable examination of various stages of biofilm development (Coenye and Nelis, 2010; Vandecandelaere et al., 2016). Numerous studies have used the microtiter biofilm system to understand biofilm formation on various biomedical materials and surfaces (Chin et al., 2006; Imamura et al., 2008; Silva et al., 2010; El-Ganiny et al., 2017; Wang et al., 2018), elucidate biofilm adaptation under different growth conditions (Strempel et al., 2017), screen for biofilm-deficient mutants (Tu Quoc et al., 2007; Okshevsky et al., 2018; Willett et al., 2019), and determine the efficacy of antimicrobial and antibiofilm therapies (Torres et al., 2018; Wang et al., 2018; Zhong et al., 2019). There are a wide range of relatively simple techniques to quantify the amount of biofilm in microtiter systems, including assessing colony forming unit (CFU) counts and staining of adhered bacteria. Staining methods such as crystal violet staining can be used to evaluate the total biomass, while tetrazolium-based dyes, resazurin, the BacTiter-Glo assay (which quantifies ATP production), or propidium iodide can be used to determine the residual number of metabolically active cells (Peeters et al., 2008; Vandecandelaere et al., 2016; Maiden et al., 2018; Wang et al., 2018).

There are several limitations to the aforementioned microtiter methods since they are closed models. The most profound of these is that many microtiter protocols involve adding the anti-biofilm agents along with planktonic bacteria during inoculation; therefore, it is difficult to differentiate between inhibition of planktonic growth, inhibition of the initial stages of biofilm development, killing of organisms in the biofilm growth state, or eradication/dispersal of mature biofilms (Haney et al., 2018b). Second, some staining methods make it difficult to discriminate between dead and live cells, since the most popular staining procedure, using crystal violet, stains the total biomass including matrix and dead cells (Peeters et al., 2008). To overcome these limitations, Haney et al. (2018b) described a simple, cost-effective, and reproducible procedure to assess the biofilm inhibition (addition at the time of bacterial addition) and eradication (delayed addition) abilities of antibiotics and anti-biofilm peptides, using common and relatively inexpensive materials. This high-throughput workflow combines a 96-well microtiter plate with crystal violet or tetrazolium chloride dye staining (Haney et al., 2018b). It should be mentioned that the medium leading to optimal biofilms growth varies substantially between species, so

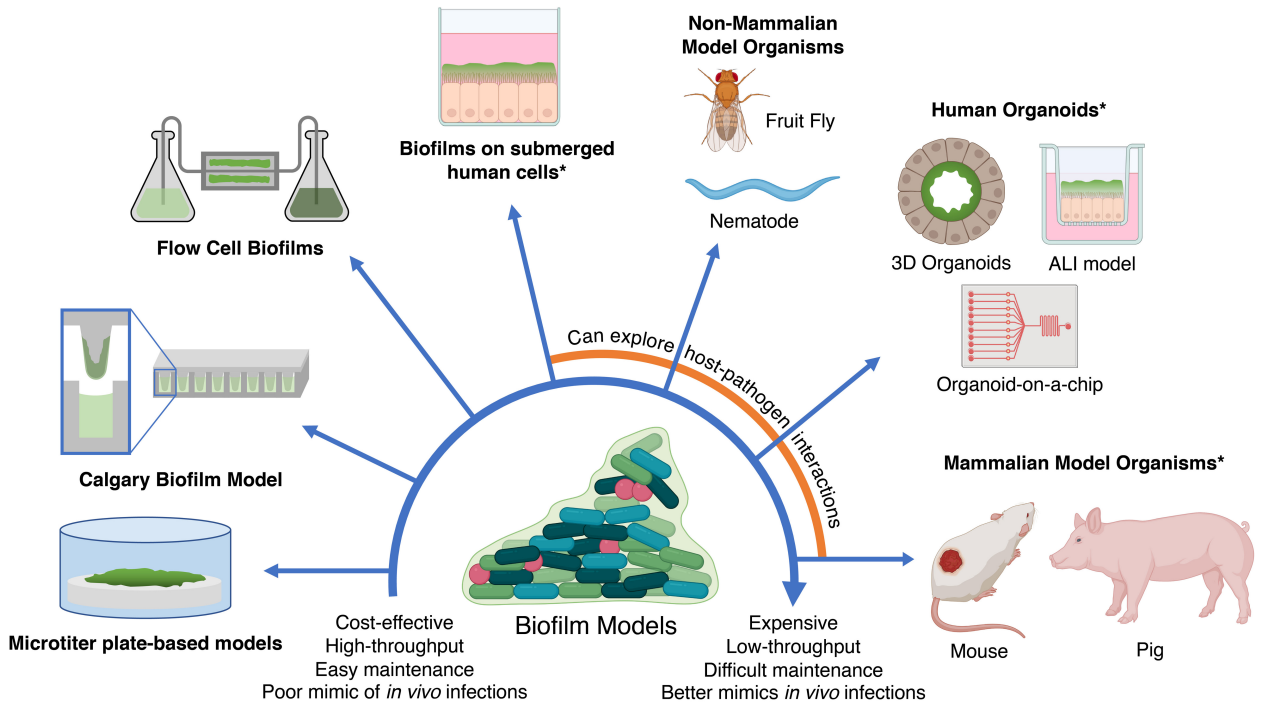

FIGURE 4 | *In vitro* and *in vivo* models for testing anti-biofilm agents. Simplistic models are easier to maintain and cost-effective; however, they fail to replicate *in vivo* infections as accurately as more expensive models such as *in vivo* animal models and human organoids. In addition, the use of human cells and mammalian models (indicated by asterisks) may require additional ethics approval. ALI, air-liquid interface. Created with BioRender.com.

this is one parameter that needs to be optimized in such microtiter systems.

Ceri et al. (1999) developed a rapid system to evaluate the biofilm eradication ability of certain compounds, called the Calgary Biofilm Device. This system involves a specialized top lid with pegs that fits over a conventional 96 well microtiter plate. Biofilm is first grown on the pegs, then the top lid is transferred into a second plate containing the compound of interest. Upon incubation, the amount of residual biofilm can be determined either through CFU count, optical density measurement, or microscopic techniques (Moskowitz et al., 2004). This method allows for the differentiation of biofilm from sedimented dead cells, thus also ascertaining biofilm eradication versus inhibition activity of compounds.

As mentioned above, biofilms in closed systems do not reflect situations where biofilms are exposed to the complex flow network of the circulatory, urinary, digestive, and respiratory systems, nor do they reflect biofilms in medical devices exposed to flowing liquid, such as catheters and intravenous lines (Waters et al., 2014). To understand the biofilm mechanisms and susceptibilities under conditions with constant flow, an open system should be used. However, such systems are considerably more technically complex.

Open systems have a constant flow of fresh medium, while wastes, signaling byproducts, and planktonic cells are constantly washed away, mimicking certain environments in human hosts and medical devices (Lebeaux et al., 2013; Azeredo et al., 2017). The environment of an open system can be controlled and adjusted by the researcher at any time during the experiment. For example, the flow and type of medium can be adjusted to create shear forces and nutrient composition that more closely reflect *in vivo* conditions (although shear forces vary depending on the clinical situation and are not always precisely known). This allows the study of physical and chemical resistance of biofilms. Flow cells are the most widely used open system, consisting of a series of growth chambers that are separately connected to a multichannel peristaltic pump, allowing the influx of fresh media and efflux of waste (Crusz et al., 2012). This system can be coupled with fluorescence or confocal laser scanning microscopy, enabling one to non-invasively visualize the development of a biofilm in real time and reconstruct 3D images of the biofilm structure, which cannot be done with microtiter assay methods (Heydorn et al., 2000; Millar et al., 2001; Mueller et al., 2006; Pamp et al., 2009). For example, Pihl et al. (2013) used flow cells and confocal laser scanning microscopy to model biofilm growth in catheters to show that rhamnolipids in the supernatant of *P. aeruginosa* play a role in reducing adherence and inducing dispersal of *S. epidermidis* to serum coated catheter surfaces. However, the construction and operation of a flow cell can be challenging and requires some expertise (Crusz et al., 2012) and it is less amenable to high-throughput analyses when compared to microtiter assays. Newer microfluidic models, also a type of open model, may alleviate this problem and are discussed below.

Although bacterial *in vitro* models are valuable tools for studying biofilms and screening for potential anti-biofilm agents under controlled conditions, there are some limitations. It

is essential to understand the impact of the host-microbe interaction (e.g., nutrient composition, host immunity, and stress factors) and recapitulate the timescale and complex physical and chemical environments bacteria may experience *in vivo*; all of these are absent in these *in vitro* models. These factors can greatly impact bacterial virulence and biofilm formation, which can hinder interpretations of antimicrobial efficacy (Palmer et al., 2007; Kolpen et al., 2010; Pearce et al., 2018; Pulkkinen et al., 2018). In addition, some bacteria found in *in vivo* biofilms are simply not culturable *in vitro* (Li et al., 2014). At least 92 species of bacteria were found in human dental plaque samples, of which eight were uncultivable but were associated with early stages of biofilm formation (Heller et al., 2016). Thus, it is important to also consider *in vivo* models, not only to validate *in vitro* results, but also to factor in the dynamic host-microbe relationships to form more biologically accurate biofilms for testing novel anti-biofilm agents.

In vivo Biofilm Models

In vivo biofilm models involve the use of living organisms, including both mammals and non-mammals (Lebeaux et al., 2013). While conventional mammalian models (e.g., mice, rats, and rabbits) are widely used to study *in vivo* biofilms and anti-biofilm agents, screening large numbers of potential antimicrobial candidates is costly, laborious, and ethically prohibited. To overcome these limitations, non-mammalian models, such as the nematode *Caenorhabditis elegans* (Millet and Ewbank, 2004) and fruit fly *Drosophila melanogaster* (Ferrandon et al., 2007), can be used to conduct initial candidate screening before moving to mammalian models.

Non-mammalian models have several advantages over mammalian models. First, such organisms have unique anatomy, but possess some similar immune responses when compared to mammals, and generally allow for easier monitoring of disease progression and the effects of antimicrobial agents (Antoshechkin and Sternberg, 2007; Lemaitre and Hoffmann, 2007; Ryu et al., 2010). Both *C. elegans* and *D. melanogaster* larvae are transparent, which allows for non-invasive monitoring of fluorescently tagged bacteria, host genes, or proteins in real-time (Bell et al., 2009; Kong et al., 2016). *C. elegans* also possess at least three of the innate immunity signaling pathways (p38 mitogen-activated protein kinase pathway, insulin/growth factor-1 pathway, and the transforming growth factor-β pathway) found in mammals (Mallo et al., 2002; Garsin et al., 2003; Troemel et al., 2006). *D. melanogaster* possess host defenses mechanisms such as Toll-like receptor pathways, host defense peptides, and reactive oxygen species (Dimarcq et al., 1994; Agaisse and Perrimon, 2004; Lemaitre and Hoffmann, 2007; Bell et al., 2009). Second, when compared to mammalian models, these non-mammalian models are more easily genetically manipulated from the perspective of both protocols and ethics, enabling investigation of the roles of host factors including immunity in biofilm formation (D'Argenio et al., 2001; Antoshechkin and Sternberg, 2007; Chakrabarti et al., 2012). Third, non-mammalian organisms are highly fertile with short reproduction times and easy maintenance (Antoshechkin and Sternberg, 2007; Jennings, 2011), making high-throughput candidate screens possible (Ewbank, 2002; Squiban and Kurz, 2011; Conery et al., 2014). However, there are profound differences in physiology, many immune responses, circulation, pharmacokinetics, and prospective delivery methods, and data gleaned are not useful in formal drug development. In addition, the short lifespan of *C. elegans* and *D. melanogaster* makes these models difficult for representing chronic infections, and the body temperatures of *C. elegans* (16-25°C) are not optimal for growth of many pathogens and do not reflect that of mammals (Kong et al., 2016). Thus, the use of mammalian models, which have a more complex immune system, relatively longer lifespan, and closer evolutionary relationship to humans, is required.

Mammalian *in vivo* models are indispensable tools to mimic human biofilm infection in the context of host-microbe interactions and to assess antimicrobial therapies before clinical trials (Festing, 2004). There are many well-established mouse (*Mus musculus*) models for biofilm-related diseases, including cystic fibrosis and chronic obstructive pulmonary disease-associated infections, urinary tract infections, intestinal infection, chronic skin/wound infections, chronic rhinosinusitis, and periodontitis (Coenye and Nelis, 2010). The small size, ease of handling and housing, short gestation period, and high reproductive rate of mice make such models attractive when compared to other mammalian models (Rumbaugh and Carty, 2011; Masopust et al., 2017). A recent study used a very simple cutaneous infection mouse model to demonstrate the efficacy of synthetic cationic peptides IDR-1018 and DJK-5, and their synergy with conventional antibiotics in all ESKAPE pathogens, as well as their relationships to the stringent response (Pletzer et al., 2017, 2018). Both peptides were effective in reducing abscess size and bacterial load, and showed synergy with several different antibiotics, in part through decreased (p)ppGpp synthesis due to *spoT* down-regulation. This abscess model can be used to evaluate other peptides and anti-biofilm agents for chronic wounds.

In addition, a large number of inbred mouse strains (which are genetically uniform to enhance reproducibility), outbred strains (which better represent genetic diversity in human hosts), and genetically modified strains are commercially available and well characterized (Thomas and Capecchi, 1987; Svenson et al., 2012; Masopust et al., 2017). Genetically modified strains allow investigators to induce immunodeficiency, humanize the immune system, and knock in/out specific genes to create phenotypes similar to certain human diseases (Criswell and Sack, 1990; Masopust et al., 2017; Gurumurthy and Lloyd, 2019). For example, a cystic fibrosis transmembrane conductance regulator (CFTR) knockout mouse model was used to study cystic fibrosis and the QS inhibiting effects of azithromycin against *P. aeruginosa* biofilms (Hoffmann et al., 2007).

Another mammalian model that more closely resembles humans than do mice, is the pig (*Sus scrofa domesticus*), especially in terms of their anatomy and immune system (Dawson, 2011; Meurens et al., 2012). Due to the close resemblance of porcine skin to human skin in terms of structure, immune responses, and the process of wound healing, the porcine model has been deemed the most relevant preclinical model of skin wound healing by the Wound Healing Society (Sullivan et al., 2001;

Gordillo et al., 2013). Gloag et al. (2019) used the porcine skin biofilm model to identify hyperbiofilm strain variants of *P. aeruginosa*, which were found to have mutations in the Wsp pathway (a chemosensory pathway involved in c-di-GMP regulation) and resistance to prophages in the wound. There are also recent developments to create *ex vivo* porcine skin models for use as a surrogate for live pigs, to improve ease of use and allow for high-throughput setups (Alves et al., 2018).

Although *in vivo* animal models are invaluable to investigate host-pathogen interactions, there are also some limitations. Interspecies differences still contribute to discrepancies in pharmacokinetic profiles, safety, and efficacy of therapeutic candidates between animal models and humans (Jansen et al., 2020). The growing awareness of animal welfare and related ethical issues encourages researchers to follow the 3Rs: Replace the use of animal models, Reduce the number of animals required for each experiment, and Refine experimental techniques to minimize animal suffering and improve animal welfare (Bailey and Balls, 2019; Hubrecht and Carter, 2019). To satisfy the first "R," an alternative model that can investigate host-pathogen interactions in the context of anti-biofilm therapies is tissue culture-based *in vitro* models.

Tissue Culture-Based Biofilm Models

Tissue culture-based are co-cultures of bacterial and human cells. Conventionally, submerged models are used, where a biofilm is grown over a monolayer of host cells submerged in medium (Coenye and Nelis, 2010). Compared to *in vivo* models, submerged monolayer models are cheaper, easier to manipulate, highly reproducible, and amenable to high-throughput screening, while still enabling investigation of host-pathogen interaction; however, they lack cell type complexity, commensal flora, nutrient gradients, shear forces, and immune components (Coenye and Nelis, 2010). For example, *Mycoplasma pneumoniae* biofilms grown on a monolayer of human bronchial epithelial cells were found to undergo similar architecture development as those grown on glass, but at a slower pace (Feng et al., 2020). However, the presence of complement significantly reduced the growth of *M. pneumoniae* on epithelial cells, suggesting that bacterial growth might be significantly different in a more complex system (Feng et al., 2020). In addition, most submerged models can only mimic acute infections, since culturing bacteria and host cells within a static condition leads to high cytotoxity (Kim et al., 2012). Hence, it is important to use alternative co-culture systems than submerged models that more closely resemble *in vivo* microenvironments.

A recent advance in tissue culture techniques is the development of host organoid systems, which overcome some of the limitations of submerged monolayer models (Barrila et al., 2018). Organoids are self-organized, multicellular structures that resemble miniature organs, and can be derived from immortalized cell lines, primary cells from healthy or diseased donors, induced pluripotent stem cells, embryonic stem cells, neonatal tissue stem cells, or *ex vivo* adult progenitors (Clevers, 2016). In general, organoid systems can be categorized into three main forms, in order of complexity: air-liquid interface (ALI) models, 3D spheroid organoids, and organoid-on-a chip models (Choi et al., 2020).

Air-liquid interface models are grown from a variety of different starting cells and differentiated on permeable filters to form sections of epithelium, with the apical region exposed to air and basal region submerged in medium (Choi et al., 2020). The dual exposure allows maturation of multiple cell types with different functions (e.g., mucin production, cilia movement) similar to those found *in vivo*, and there are ALI models for skin, lung, intestinal, gingival, and urothelial epithelium (Dvorak et al., 2011; Pezzulo et al., 2011; de Breij et al., 2012; Horsley et al., 2018; Brown et al., 2019; George et al., 2019). In addition, the presence of an apical and basal chamber provides a convenient platform for co-culture systems to investigate immune activity against biofilms on epithelium. Rudder et al. (2020) developed a triple co-culture ALI system, with upper respiratory tract epithelial cells, macrophages in the basal chamber, and donor nasal microbiota in the apical chamber, and found that diversity of microbial communities was altered by the addition of macrophages (Rudder et al., 2020). Similarly, a gingival epithelium ALI model studied oral biofilms formed by healthy microflora or microorganisms in gingivitis and periodontitis in the presence of primary peripheral blood mononuclear cells and CD14+ monocytes in the basal chamber (Brown et al., 2019). Recently, a miniaturized 96 well air-liquid interface human small airway epithelial model was developed, allowing ALI models to be used as a high-throughput screening platform (Bluhmki et al., 2020). An analogous skin model was established from N/TERT keratinocytes (Wu et al., 2021; de Breij et al., 2018), which enabled well-structured biofilms to be grown from *P. aeruginosa* and *S. aureus* and allowed for screening of the effects of various antibiofilm peptides and their influence of skin integrity.

A more complex system is 3D spheroid organoids, in which progenitor cells undergo stepwise directed differentiation with defined growth factor cocktails that activate and inhibit specific signaling pathways (Nickerson et al., 2001; Clevers, 2016; Gkatzis et al., 2018). Generally, 3D organoids mimic the *in vivo* architecture, multi-lineage differentiation, and organ development process of the natural epithelium in mammals (Sato and Clevers, 2013; Kim M. et al., 2019). Their enclosed nature can allow growth of bacteria that are unable to be cultured in other *in vitro* systems (Dutta et al., 2017; George et al., 2019). Furthermore, the ability of self-regeneration allows 3D organoids to be maintained and expanded over a long period of time to study chronic infections (Yamamoto et al., 2017; Sachs et al., 2019). Coupling the 3D organoids with microinjection and imaging techniques, Forbester et al. (2015) showed that *Salmonella enterica* serovar Typhimurium was able to invade the epithelial barrier and reside in vacuoles, similar to those found *in vivo* (Forbester et al., 2015).

While 3D organoids and ALIs better replicate *in vivo* conditions than other *in vitro* models, they still lack a dynamic mechanical and biochemical microenvironment with shear force and nutrient gradients as provided by flow cells. Combining these two technologies results in the organoid-on-a-chip model, which is a microfluidics platform where bacteria and/or host

cells grow in chambers perfused by microchannels (Kim et al., 2012). By strictly controlling intraluminal fluid flow to mimic peristalsis, Kim et al. (2012) developed a microfluidic model with intestinal epithelium that resembled the structure of intestinal villi and supported growth of *Lactobacillus rhamnosus* for >1 week without compromising host cell viability. Since only a small volume of cells and reagents are required, organoids-on-a-chip models appear to be a relatively cheaper and faster organoid screening method, although it requires a sophisticated, technically complex, and expensive platform to set up such experiments (Huh et al., 2011). Cells from microfluidic chambers can also be extracted for omics studies such as transcriptomics (Benam et al., 2016). Furthermore, microsensors embedded in the chip allow monitoring of events such as biofilm formation, cell migration, barrier function, protein production, and fluid pressure in real time (Bhatia and Ingber, 2014; Yu et al., 2019; Yuan et al., 2020). Yuan et al. (2020) developed an integrated system, combining gut-on-a-chip with optical coherence tomography, to visualize pathogenic *E. coli* mediated cellular changes in the presence or absence of probiotic protection of *Bifidobacterium breve* in real-time. Similarly, Sidar et al. (2019) incorporated 3D spheroid intestinal organoids with a microfluidics system to study intestinal secretion, absorption, transportation, and co-culture with intestinal microorganisms. Finally, a multifaceted combination of microchambers, microchannels, valves, pumps, and microsensors allows organoid-on-a-chip models to be tailored to specific needs for different experiments (Yu et al., 2019). For example, Ye et al. (2007) utilized a microfluidic device with eight drug gradient generators and parallel cell culture chambers to simultaneously test either eight different molecules or eight different concentrations of one molecule. This system has the potential to be used as a high-throughput screening system for antibiofilm agents. Organoid-on-a-chip models are relatively new, and their versatility makes them perhaps the closest to a biologically accurate model that still allows the ability of higher-throughput testing.

Each model has its own advantages and disadvantages, ranging from cost and ease of use to similarity to *in vivo* biofilms, with the latter point perhaps being the most important for success in developing an anti-biofilm agent that will be effective in humans. Furthermore, each of these models can also be used in conjunction with further omics analyses to better understand the mechanisms of the agents tested. With the advent of new technologies such as organoid-on-a-chip models, the prospects of creating a high-throughput, biologically relevant model for anti-biofilm agent testing are tantalizingly close.

CONCLUSION

In this review, we have provided a summary of current biological and computational strategies to develop new anti-biofilm agents. Omics analyses provide a systems biology approach to the complex interwoven processes of biofilm formation and are uncovering many potential protein targets and pathways required for biofilm formation in a variety of species. To find modulators for these targets, high-throughput screening using *in vitro* approaches have been used in the past to test potential modulators; however, with the increased availability of defined bacterial protein structures, recent approaches now more commonly involve an initial virtual screening of large databases of molecules before experimental validation, which is more cost-effective and less labor-intensive. Another approach to identify novel anti-biofilm agents is through machine learning, where a model is trained using a collection of known anti-biofilm and non-anti-biofilm molecules, learns patterns in the features of these molecules, and then applies those patterns to pick out potential anti-biofilm agents from databases. Finally, these new agents must be tested in biologically accurate biofilm models. While *in vitro* approaches such as microtiter assays are the easiest to work with, they poorly resemble actual *in vivo* infections in humans. However, animal models are more difficult to manage both ethically and logistically, and do not accurately resemble human physiology. The rise of organoid models such as relatively simple ALI models and more complex organoid-on-a-chip model can provide an *in vitro* approach that mimics human physiology yet retains the high-throughput characteristic of other *in vitro* models. Advances in this field may eventually result in organoids becoming the optimal model for growing and testing anti-biofilm agents.

Biofilm regulation is a complex process and while we have summarized key more-conserved biofilm regulation processes such as the stringent response, quorum sensing, and c-di-GMP signaling, not all processes have been highlighted here. However, the approaches we describe can equally be applied to motility regulation, small non-coding RNA regulation, and matrix synthesis, as well as new mechanisms discovered by methods outlined in this review. As mentioned before, there are no approved agents specifically targeting biofilms, despite biofilms being the most common form of infection and major reason for antibiotic resistance. We submit that anti-biofilm agents, when they do become introduced in the clinic, will likely be used in conjunction with conventional antibiotics as an "antibiotic sensitizer" by disrupting the biofilm and exposing individual bacteria to antibiotic therapy, or as a prophylactic measure to prevent biofilm formation on medical surfaces or prior to or after surgery. Our hope is that this review has provided a comprehensive introduction, for researchers interested in developing anti-biofilm agents, to the variety of technologies and models used for such an endeavor, as such agents are crucially needed in healthcare.

AUTHOR CONTRIBUTIONS

AA, AB, and K-YC contributed to writing and editing this manuscript. AA prepared the figures. RH supervised all authors, edited the manuscript, and provided critical insights and feedback. All authors read and approved the final version of the manuscript.

FUNDING

We acknowledge funding from a Canadian Institutes for Health Research grant FDN-154287 to RH. The content is solely the responsibility of the authors and does not necessarily represent the official views of the Canadian Institutes for Health Research. RH holds a Canada Research Chair in Health and Genomics and a UBC Killam Professorship. AA was supported by the Canadian Institutes of Health Research Frederick Banting and Charles Best Canada Graduate Scholarship and the Centre for Blood Research Graduate Student Award. K-YC was supported by the Michael Smith Foundation for Health Research and Lotte & John Hecht Memorial Foundation Research Trainee Award.

REFERENCES

Agaisse, H., and Perrimon, N. (2004). The roles of JAK/STAT signaling in *Drosophila* immune responses. *Immunol. Rev.* 198, 72–82. doi: 10.1111/j.0105-2896.2004.0133.x

Alford, M. A., Baghela, A., Yeung, A. T. Y., Pletzer, D., and Hancock, R. E. W. (2020). NtrBC regulates invasiveness and virulence of *Pseudomonas aeruginosa* during high-density infection. *Front. Microbiol.* 11:773. doi: 10.3389/fmicb.2020.00773

Allen, W. J., Balius, T. E., Mukherjee, S., Brozell, S. R., Moustakas, D. T., Lang, P. T., et al. (2015). DOCK 6: impact of new features and current docking performance. *J. Comput. Chem.* 36, 1132–1156. doi: 10.1002/jcc.23905

Alves, D. R., Booth, S. P., Scavone, P., Schellenberger, P., Salvage, J., Dedi, C., et al. (2018). Development of a high-throughput ex-vivo burn wound model using porcine skin, and its application to evaluate new approaches to control wound infection. *Front. Cell. Infect. Microbiol.* 8:196. doi: 10.3389/fcimb.2018.00196

Alves-Barroco, C., Roma-Rodrigues, C., Balasubramanian, N., Guimarães, M. A., Ferreira-Carvalho, B. T., Muthukumaran, J., et al. (2019). Biofilm development and computational screening for new putative inhibitors of a homolog of the regulatory protein BrpA in *Streptococcus dysgalactiae* subsp. *dysgalactiae*. *Int. J. Med. Microbiol.* 309, 169–181. doi: 10.1016/j.ijmm.2019.02.001

Amador, C. I., Sternberg, C., and Jelsbak, L. (2018). Application of RNA-seq and bioimaging methods to study microbe-microbe interactions and their effects on biofilm formation and gene expression. *Methods Mol. Biol.* 1734, 131–158. doi: 10.1007/978-1-4939-7604-1_12

Antoshechkin, I., and Sternberg, P. W. (2007). The versatile worm: genetic and genomic resources for *Caenorhabditis elegans* research. *Nat. Rev. Genet.* 8, 518–532. doi: 10.1038/nrg2105

Armbruster, C. R., and Parsek, M. R. (2018). New insight into the early stages of biofilm formation. *Proc. Natl. Acad. Sci. U.S.A.* 115, 4317–4319. doi: 10.1073/pnas.1804084115

Artini, M., Patsilinakos, A., Papa, R., Božoviæ, M., Sabatino, M., Garzoli, S., et al. (2018). Antimicrobial and antibiofilm activity and machine learning classification analysis of essential oils from different Mediterranean plants against *Pseudomonas aeruginosa*. *Mol. Basel Switz.* 23:482. doi: 10.3390/molecules23020482

Attinger, C., and Wolcott, R. (2012). Clinically addressing biofilm in chronic wounds. *Adv. Wound Care* 1, 127–132. doi: 10.1089/wound.2011.0333

Azeredo, J., Azevedo, N. F., Briandet, R., Cerca, N., Coenye, T., Costa, A. R., et al. (2017). Critical review on biofilm methods. *Crit. Rev. Microbiol.* 43, 313–351. doi: 10.1080/1040841X.2016.1208146

Azriel, S., Goren, A., Rahav, G., and Gal-Mor, O. (2016). The stringent response regulator DksA is required for *Salmonella enterica* serovar Typhimurium growth in minimal medium, motility, biofilm formation, and intestinal colonization. *Infect. Immun.* 84, 375–384. doi: 10.1128/IAI.01135-15

Bailey, J., and Balls, M. (2019). Recent efforts to elucidate the scientific validity of animal-based drug tests by the pharmaceutical industry, pro-testing lobby groups, and animal welfare organisations. *BMC Med. Ethics* 20:16. doi: 10.1186/s12910-019-0352-3

Balzer, G. J., and McLean, R. J. C. (2002). The stringent response genes *relA* and *spoT* are important for *Escherichia coli* biofilms under slow-growth conditions. *Can. J. Microbiol.* 48, 675–680. doi: 10.1139/w02-060

Barraud, N., Hassett, D. J., Hwang, S.-H., Rice, S. A., Kjelleberg, S., and Webb, J. S. (2006). Involvement of nitric oxide in biofilm dispersal of *Pseudomonas aeruginosa*. *J. Bacteriol.* 188, 7344–7353. doi: 10.1128/JB.00779-06

Barrila, J., Crabbé, A., Yang, J., Franco, K., Nydam, S. D., Forsyth, R. J., et al. (2018). Modeling host-pathogen interactions in the context of the microenvironment: three-dimensional cell culture comes of age. *Infect. Immun.* 86:e282-18. doi: 10.1128/IAI.00282-18

Beale, D. J., Barratt, R., Marlow, D. R., Dunn, M. S., Palombo, E. A., Morrison, P. D., et al. (2013). Application of metabolomics to understanding biofilms in water distribution systems: a pilot study. *Biofouling* 29, 283–294. doi: 10.1080/08927014.2013.772140

Bell, A. J., McBride, S. M. J., and Dockendorff, T. C. (2009). Flies as the ointment: *Drosophila* modeling to enhance drug discovery. *Fly* 3, 39–49. doi: 10.4161/fly.3.1.7774

Benam, K. H., Novak, R., Nawroth, J., Hirano-Kobayashi, M., Ferrante, T. C., Choe, Y., et al. (2016). Matched-comparative modeling of normal and diseased human airway responses using a microengineered breathing lung chip. *Cell Syst.* 3, 456.e4–466.e4. doi: 10.1016/j.cels.2016.10.003

Bhatia, S. N., and Ingber, D. E. (2014). Microfluidic organs-on-chips. *Nat. Biotechnol.* 32, 760–772. doi: 10.1038/nbt.2989

Bjarnsholt, T., Jensen, P. Ø, Burmølle, M., Hentzer, M., Haagensen, J. A. J., Hougen, H. P., et al. (2005). *Pseudomonas aeruginosa* tolerance to tobramycin, hydrogen peroxide and polymorphonuclear leukocytes is quorum-sensing dependent. *Microbiology* 151, 373–383. doi: 10.1099/mic.0.27463-0

Bluhmki, T., Bitzer, S., Gindele, J. A., Schruf, E., Kiechle, T., Webster, M., et al. (2020). Development of a miniaturized 96-Transwell air–liquid interface human small airway epithelial model. *Sci. Rep.* 10:13022. doi: 10.1038/s41598-020-69948-2

Borlee, B. R., Goldman, A. D., Murakami, K., Samudrala, R., Wozniak, D. J., and Parsek, M. R. (2010). *Pseudomonas aeruginosa* uses a cyclic-di-GMP-regulated adhesin to reinforce the biofilm extracellular matrix. *Mol. Microbiol.* 75, 827–842. doi: 10.1111/j.1365-2958.2009.06991.x

Breidenstein, E. B. M., Khaira, B. K., Wiegand, I., Overhage, J., and Hancock, R. E. W. (2008). Complex ciprofloxacin resistome revealed by screening a *Pseudomonas aeruginosa* mutant library for altered susceptibility. *Antimicrob. Agents Chemother.* 52, 4486–4491. doi: 10.1128/AAC.00222-08

Brown, J. L., Johnston, W., Delaney, C., Rajendran, R., Butcher, J., Khan, S., et al. (2019). Biofilm-stimulated epithelium modulates the inflammatory responses in co-cultured immune cells. *Sci. Rep.* 9:15779. doi: 10.1038/s41598-019-52115-7

Bryers, J. D. (2008). Medical biofilms. *Biotechnol. Bioeng.* 100, 1–18. doi: 10.1002/bit.21838

Cain, A. K., Barquist, L., Goodman, A. L., Paulsen, I. T., Parkhill, J., and van Opijnen, T. (2020). A decade of advances in transposon-insertion sequencing. *Nat. Rev. Genet.* 21, 526–540. doi: 10.1038/s41576-020-0244-x

Calvo, E., Pucciarelli, M. G., Bierne, H., Cossart, P., Albar, J. P., and Portillo, F. G. (2005). Analysis of the *Listeria* cell wall proteome by two-dimensional nanoliquid chromatography coupled to mass spectrometry. *Proteomics* 5, 433–443. doi: 10.1002/pmic.200400936

Cameron, D. R., Shan, Y., Zalis, E. A., Isabella, V., and Lewis, K. (2018). A genetic determinant of persister cell formation in bacterial pathogens. *J. Bacteriol.* 200:e303-18. doi: 10.1128/JB.00303-18

Cardoso, M. H., Orozco, R. Q., Rezende, S. B., Rodrigues, G., Oshiro, K. G. N., Cândido, E. S., et al. (2019). Computer-aided design of antimicrobial peptides: are we generating effective drug candidates? *Front. Microbiol.* 10:3097. doi: 10.3389/fmicb.2019.03097

Ceri, H., Olson, M. E., Stremick, C., Read, R. R., Morck, D., and Buret, A. (1999). The Calgary Biofilm Device: new technology for rapid determination of antibiotic susceptibilities of bacterial biofilms. *J. Clin. Microbiol.* 37, 1771–1776. doi: 10.1128/JCM.37.6.1771-1776.1999

Chakrabarti, S., Liehl, P., Buchon, N., and Lemaitre, B. (2012). Infection-induced host translational blockage inhibits immune responses and epithelial renewal in the *Drosophila* gut. *Cell Host Microbe* 12, 60–70. doi: 10.1016/j.chom.2012.06.001

Chávez de Paz, L. E., Lemos, J. A., Wickström, C., and Sedgley, C. M. (2012). Role of (p)ppGpp in biofilm formation by *Enterococcus faecalis*. *Appl. Environ. Microbiol.* 78, 1627–1630. doi: 10.1128/AEM.07036-11

Cherkasov, A., Hilpert, K., Jenssen, H., Fjell, C. D., Waldbrook, M., Mullaly, S. C., et al. (2009). Use of artificial intelligence in the design of small peptide antibiotics effective against a broad spectrum of highly antibiotic-resistant superbugs. *ACS Chem. Biol.* 4, 65–74. doi: 10.1021/cb800240j

Cherkasov, A., Muratov, E. N., Fourches, D., Varnek, A., Baskin, I. I., Cronin, M., et al. (2014). QSAR Modeling: where have you been? Where are you going to? *J. Med. Chem.* 57, 4977–5010. doi: 10.1021/jm4004285

Chin, M. Y. H., Busscher, H. J., Evans, R., Noar, J., and Pratten, J. (2006). Early biofilm formation and the effects of antimicrobial agents on orthodontic bonding materials in a parallel plate flow chamber. *Eur. J. Orthod.* 28, 1–7. doi: 10.1093/ejo/cji094

Cho, K. H., Tryon, R. G., and Kim, J.-H. (2020). Screening for diguanylate cyclase (DGC) inhibitors mitigating bacterial biofilm formation. *Front. Chem.* 8:264. doi: 10.3389/fchem.2020.00264

Choi, K.-Y. G., Wu, B. C., Lee, A. H.-Y., Baquir, B., and Hancock, R. E. W. (2020). Utilizing organoid and air-liquid interface models as a screening method in the development of new host defense peptides. *Front. Cell. Infect. Microbiol.* 10:228. doi: 10.3389/fcimb.2020.00228

Ciofu, O., and Tolker-Nielsen, T. (2019). Tolerance and resistance of *Pseudomonas aeruginosa* biofilms to antimicrobial agents—how *P. aeruginosa* can escape antibiotics. *Front. Microbiol.* 10:913. doi: 10.3389/fmicb.2019.00913

Clevers, H. (2016). Modeling development and disease with organoids. *Cell* 165, 1586–1597. doi: 10.1016/j.cell.2016.05.082

Coenye, T., and Nelis, H. J. (2010). *In vitro* and *in vivo* model systems to study microbial biofilm formation. *J. Microbiol. Methods* 83, 89–105. doi: 10.1016/j.mimet.2010.08.018

Coleman, S. R., Blimkie, T., Falsafi, R., and Hancock, R. E. W. (2020). Multidrug adaptive resistance of *Pseudomonas aeruginosa* swarming cells. *Antimicrob. Agents Chemother.* 64:e1999-19. doi: 10.1128/AAC.01999-19

Conery, A. L., Larkins-Ford, J., Ausubel, F. M., and Kirienko, N. V. (2014). High-throughput screening for novel anti-infectives using a *C. elegans* pathogenesis model. *Curr. Protoc. Chem. Biol.* 6, 25–37. doi: 10.1002/9780470559277.ch130160

Couto, N., Schooling, S. R., Dutcher, J. R., and Barber, J. (2015). Proteome profiles of outer membrane vesicles and extracellular matrix of *Pseudomonas aeruginosa* biofilms. *J. Proteome Res.* 14, 4207–4222. doi: 10.1021/acs.jproteome.5b00312

Criswell, L. A., and Sack, K. E. (1990). Tryptophan-induced eosinophilia-myalgia syndrome. *West. J. Med.* 153, 269–274.

Crusz, S. A., Popat, R., Rybtke, M. T., Cámara, M., Givskov, M., Tolker-Nielsen, T., et al. (2012). Bursting the bubble on bacterial biofilms: a flow cell methodology. *Biofouling* 28, 835–842. doi: 10.1080/08927014.2012.716044

Danishuddin, M., and Khan, A. U. (2016). Descriptors and their selection methods in QSAR analysis: paradigm for drug design. *Drug Discov. Today* 21, 1291–1302. doi: 10.1016/j.drudis.2016.06.013

D'Argenio, D. A., Gallagher, L. A., Berg, C. A., and Manoil, C. (2001). *Drosophila* as a model host for *Pseudomonas aeruginosa* infection. *J. Bacteriol.* 183, 1466–1471. doi: 10.1128/JB.183.4.1466-1471.2001

Davies, D. G., Parsek, M. R., Pearson, J. P., Iglewski, B. H., Costerton, J. W., and Greenberg, E. P. (1998). The involvement of cell-to-cell signals in the development of a bacterial biofilm. *Science* 280, 295–298. doi: 10.1126/science.280.5361.295

Dawson, H. (2011). "A comparative assessment of the pig, mouse and human genomes: structural and functional analysis of genes involved in immunity and inflammation," in *The Minipig in Biomedical Research*, eds. P. McAnulty, A. Dayan, N.-C. Ganderup, and K. Hastings (Boca Raton, FL: CRC Press), 323–342. doi: 10.1201/b11356-28

de Breij, A., Haisma, E. M., Rietveld, M., El Ghalbzouri, A., van den Broek, P. J., Dijkshoorn, L., et al. (2012). Three-dimensional human skin equivalent as a tool to study *Acinetobacter baumannii* colonization. *Antimicrob. Agents Chemother.* 56, 2459–2464. doi: 10.1128/AAC.05975-11

de Breij, A., Riool, M., Cordfunke, R. A., Malanovic, N., Boer, L., de, et al. (2018). The antimicrobial peptide SAAP-148 combats drug-resistant bacteria and biofilms. *Sci. Transl. Med.* 10:eaan4044. doi: 10.1126/scitranslmed.aan4044

De Keersmaecker, S. C. J., Sonck, K., and Vanderleyden, J. (2006). Let LuxS speak up in AI-2 signaling. *Trends Microbiol.* 14, 114–119. doi: 10.1016/j.tim.2006.01.003

de la Fuente-Núñez, C., Reffuveille, F., Fernández, L., and Hancock, R. E. W. (2013). Bacterial biofilm development as a multicellular adaptation: antibiotic resistance and new therapeutic strategies. *Curr. Opin. Microbiol.* 16, 580–589. doi: 10.1016/j.mib.2013.06.013

de la Fuente-Núñez, C., Reffuveille, F., Haney, E. F., Straus, S. K., and Hancock, R. E. W. (2014). Broad-spectrum anti-biofilm peptide that targets a cellular stress response. *PLoS Pathog.* 10:e1004152. doi: 10.1371/journal.ppat.1004152

de la Fuente-Núñez, C., Reffuveille, F., Mansour, S. C., Reckseidler-Zenteno, S. L., Hernández, D., Brackman, G., et al. (2015). D-enantiomeric peptides that eradicate wild-type and multi-drug resistant biofilms and protect against lethal *Pseudomonas aeruginosa* infections. *Chem. Biol.* 22, 196–205. doi: 10.1016/j.chembiol.2015.01.002

Di Luca, M., Maccari, G., Maisetta, G., and Batoni, G. (2015). BaAMPs: the database of biofilm-active antimicrobial peptides. *Biofouling* 31, 193–199. doi: 10.1080/08927014.2015.1021340

Dimarcq, J. L., Hoffmann, D., Meister, M., Bulet, P., Lanot, R., Reichhart, J. M., et al. (1994). Characterization and transcriptional profiles of a *Drosophila* gene encoding an insect defensin: a study in insect immunity. *Eur. J. Biochem.* 221, 201–209. doi: 10.1111/j.1432-1033.1994.tb18730.x

Ding, T., Li, T., and Li, J. (2019). Virtual screening for quorum-sensing inhibitors of *Pseudomonas fluorescens* P07 from a food-derived compound database. *J. Appl. Microbiol.* 127, 763–777. doi: 10.1111/jam.14333

Dos Santos, R. N., Ferreira, L. G., and Andricopulo, A. D. (2018). Practices in molecular docking and structure-based virtual screening. *Methods Mol. Biol.* 1762, 31–50. doi: 10.1007/978-1-4939-7756-7_3

Dötsch, A., Eckweiler, D., Schniederjans, M., Zimmermann, A., Jensen, V., Scharfe, M., et al. (2012). The *Pseudomonas aeruginosa* transcriptome in planktonic cultures and static biofilms using RNA sequencing. *PLoS One* 7:e31092. doi: 10.1371/journal.pone.0031092

Driffield, K., Miller, K., Bostock, J. M., O'Neill, A. J., and Chopra, I. (2008). Increased mutability of *Pseudomonas aeruginosa* in biofilms. *J. Antimicrob. Chemother.* 61, 1053–1056. doi: 10.1093/jac/dkn044

Dutta, D., Heo, I., and Clevers, H. (2017). Disease modeling in stem cell-derived 3D organoid systems. *Trends Mol. Med.* 23, 393–410. doi: 10.1016/j.molmed.2017.02.007

Dvorak, A., Tilley, A. E., Shaykhiev, R., Wang, R., and Crystal, R. G. (2011). Do airway epithelium air-liquid cultures represent the *in vivo* airway epithelium transcriptome? *Am. J. Respir. Cell Mol. Biol.* 44, 465–473. doi: 10.1165/rcmb.2009-0453OC

El-Ganiny, A. M., Shaker, G. H., Aboelazm, A. A., and El-Dash, H. A. (2017). Prevention of bacterial biofilm formation on soft contact lenses using natural compounds. *J. Ophthalmic Inflamm. Infect.* 7:11. doi: 10.1186/s12348-017-0129-0

Erdmann, J., Thöming, J. G., Pohl, S., Pich, A., Lenz, C., and Häussler, S. (2019). The core proteome of biofilm-grown clinical *Pseudomonas aeruginosa* isolates. *Cells* 8:1129. doi: 10.3390/cells8101129

Ewbank, J. J. (2002). Tackling both sides of the host-pathogen equation with *Caenorhabditis elegans*. *Microbes Infect.* 4, 247–256. doi: 10.1016/s1286-4579(01)01531-3

Feng, M., Burgess, A. C., Cuellar, R. R., Schwab, N. R., and Balish, M. F. (2020). Modelling persistent *Mycoplasma pneumoniae* biofilm infections in a submerged BEAS-2B bronchial epithelial tissue culture model. *J. Med. Microbiol.* 70. doi: 10.1099/jmm.0.001266

Fernicola, S., Paiardini, A., Giardina, G., Rampioni, G., Leoni, L., Cutruzzolà, F., et al. (2016). *In silico* discovery and *in vitro* validation of catechol-containing sulfonohydrazide compounds as potent inhibitors of the diguanylate cyclase PleD. *J. Bacteriol.* 198, 147–156. doi: 10.1128/JB.00742-15

Ferrandon, D., Imler, J.-L., Hetru, C., and Hoffmann, J. A. (2007). The *Drosophila* systemic immune response: sensing and signalling during bacterial and fungal infections. *Nat. Rev. Immunol.* 7, 862–874. doi: 10.1038/nri2194

Festing, M. F. W. (2004). Is the use of animals in biomedical research still necessary in 2002? Unfortunately, "yes". *Altern. Lab. Anim.* 32(Suppl. 1B), 733–739. doi: 10.1177/026119290403201s121

Fetzner, S. (2015). Quorum quenching enzymes. *J. Biotechnol.* 201, 2–14. doi: 10.1016/j.jbiotec.2014.09.001

Fleming, D., and Rumbaugh, K. (2018). The consequences of biofilm dispersal on the host. *Sci. Rep.* 8:10738. doi: 10.1038/s41598-018-29121-2

Forbester, J. L., Goulding, D., Vallier, L., Hannan, N., Hale, C., Pickard, D., et al. (2015). Interaction of *Salmonella enterica* serovar Typhimurium with intestinal organoids derived from human induced pluripotent stem cells. *Infect. Immun.* 83, 2926–2934. doi: 10.1128/IAI.00161-15

Gallagher, L. A., Shendure, J., and Manoil, C. (2011). Genome-scale identification of resistance functions in *Pseudomonas aeruginosa* using Tn-seq. *mBio* 2:e315-10. doi: 10.1128/mBio.00315-10

Gallaher, T. K., Wu, S., Webster, P., and Aguilera, R. (2006). Identification of biofilm proteins in non-typeable *Haemophilus influenzae*. *BMC Microbiol.* 6:65. doi: 10.1186/1471-2180-6-65

Galloway, W. R. J. D., Hodgkinson, J. T., Bowden, S. D., Welch, M., and Spring, D. R. (2011). Quorum sensing in Gram-negative bacteria: small-molecule modulation of AHL and AI-2 quorum sensing pathways. *Chem. Rev.* 111, 28–67. doi: 10.1021/cr100109t

Garsin, D. A., Villanueva, J. M., Begun, J., Kim, D. H., Sifri, C. D., Calderwood, S. B., et al. (2003). Long-lived *C. elegans daf-2* mutants are resistant to bacterial pathogens. *Science* 300:1921. doi: 10.1126/science.1080147

Gene Ontology and Consortium (2015). Gene ontology consortium: going forward. *Nucleic Acids Res.* 43, D1049–D1056. doi: 10.1093/nar/gku1179

Gennip, M. V., Christensen, L. D., Alhede, M., Phipps, R., Jensen, P. Ø, Christophersen, L., et al. (2009). Inactivation of the *rhlA* gene in *Pseudomonas aeruginosa* prevents rhamnolipid production, disabling the protection against polymorphonuclear leukocytes. *APMIS* 117, 537–546. doi: 10.1111/j.1600-0463.2009.02466.x

George, M. M., Rahman, M., Connors, J., and Stadnyk, A. W. (2019). Opinion: are organoids the end of model evolution for studying host intestinal epithelium/microbe interactions? *Microorganisms* 7:406. doi: 10.3390/microorganisms7100406

Gkatzis, K., Taghizadeh, S., Huh, D., Stainier, D. Y. R., and Bellusci, S. (2018). Use of three-dimensional organoids and lung-on-a-chip methods to study lung development, regeneration and disease. *Eur. Respir. J.* 52:1800876. doi: 10.1183/13993003.00876-2018

Gloag, E. S., Marshall, C. W., Snyder, D., Lewin, G. R., Harris, J. S., Santos-Lopez, A., et al. (2019). *Pseudomonas aeruginosa* interstrain dynamics and selection of hyperbiofilm mutants during a chronic infection. *mBio* 10:e1698-19. doi: 10.1128/mBio.01698-19

Gomes Von Borowski, R., Gnoatto, S. C. B., Macedo, A. J., and Gillet, R. (2018). Promising antibiofilm activity of peptidomimetics. *Front. Microbiol.* 9:2157. doi: 10.3389/fmicb.2018.02157

Gordillo, G. M., Bernatchez, S. F., Diegelmann, R., Di Pietro, L. A., Eriksson, E., Hinz, B., et al. (2013). Preclinical models of wound healing: is man the model? Proceedings of the Wound Healing Society Symposium. *Adv. Wound Care* 2, 1–4. doi: 10.1089/wound.2012.0367

Guedes, I. A., Pereira, F. S. S., and Dardenne, L. E. (2018). Empirical scoring functions for structure-based virtual screening: applications, critical aspects, and challenges. *Front. Pharmacol.* 9:1089. doi: 10.3389/fphar.2018.01089

Guilhen, C., Charbonnel, N., Parisot, N., Gueguen, N., Iltis, A., Forestier, C., et al. (2016). Transcriptional profiling of *Klebsiella pneumoniae* defines signatures for planktonic, sessile and biofilm-dispersed cells. *BMC Genomics* 17:237. doi: 10.1186/s12864-016-2557-x

Gupta, S., Sharma, A. K., Jaiswal, S. K., and Sharma, V. K. (2016). Prediction of biofilm inhibiting peptides: an *in silico* approach. *Front. Microbiol.* 7:949. doi: 10.3389/fmicb.2016.00949

Gurumurthy, C. B., and Lloyd, K. C. K. (2019). Generating mouse models for biomedical research: technological advances. *Dis. Model. Mech.* 12:dmm029462. doi: 10.1242/dmm.029462

Ha, D.-G., and O'Toole, G. A. (2015). c-di-GMP and its effects on biofilm formation and dispersion: a *Pseudomonas aeruginosa* review. *Microbiol. Spectr.* 3:MB-0003-2014. doi: 10.1128/microbiolspec.MB-0003-2014

Hall, C. W., and Mah, T.-F. (2017). Molecular mechanisms of biofilm-based antibiotic resistance and tolerance in pathogenic bacteria. *FEMS Microbiol. Rev.* 41, 276–301. doi: 10.1093/femsre/fux010

Hall, D. C., Król, J. E., Cahill, J. P., Ji, H.-F., and Ehrlich, G. D. (2020). The development of a pipeline for the identification and validation of small-molecule RelA inhibitors for use as anti-biofilm drugs. *Microorganisms* 8:1310. doi: 10.3390/microorganisms8091310

Haney, E. F., Brito-Sánchez, Y., Trimble, M. J., Mansour, S. C., Cherkasov, A., and Hancock, R. E. W. (2018a). Computer-aided discovery of peptides that specifically attack bacterial biofilms. *Sci. Rep.* 8:1871. doi: 10.1038/s41598-018-19669-4

Haney, E. F., Trimble, M. J., Cheng, J. T., Vallé, Q., and Hancock, R. E. W. (2018b). Critical assessment of methods to quantify biofilm growth and evaluate antibiofilm activity of host defence peptides. *Biomolecules* 8:29. doi: 10.3390/biom8020029

Haney, E. F., Mansour, S. C., Hilchie, A. L., de la Fuente-Núñez, C., and Hancock, R. E. W. (2015). High throughput screening methods for assessing antibiofilm and immunomodulatory activities of synthetic peptides. *Peptides* 71, 276–285. doi: 10.1016/j.peptides.2015.03.015

Haney, E. F., Trimble, M. J., and Hancock, R. E. W. (in press). Microtiter plate assays to assess antibiofilm activity against bacteria. *Nat. Protoc.*

Hansen, C. R., Pressler, T., Koch, C., and Høiby, N. (2005). Long-term azithromycin treatment of cystic fibrosis patients with chronic *Pseudomonas aeruginosa* infection; an observational cohort study. *J. Cyst. Fibros.* 4, 35–40. doi: 10.1016/j.jcf.2004.09.001

Harrison, A., Hardison, R. L., Wallace, R. M., Fitch, J., Heimlich, D. R., Bryan, M. O., et al. (2019). Reprioritization of biofilm metabolism is associated with nutrient adaptation and long-term survival of *Haemophilus influenzae*. *NPJ Biofilms Microbiomes* 5:33. doi: 10.1038/s41522-019-0105-6

Hasan, S., Danishuddin, M., and Khan, A. U. (2015). Inhibitory effect of *Zingiber* officinale towards *Streptococcus mutans* virulence and caries development: *in vitro* and *in vivo* studies. *BMC Microbiol.* 15:1. doi: 10.1186/s12866-014-0320-5

He, H., Cooper, J. N., Mishra, A., and Raskin, D. M. (2012). Stringent response regulation of biofilm formation in *Vibrio cholerae*. *J. Bacteriol.* 194, 2962–2972. doi: 10.1128/JB.00014-12

Hee, C.-S., Habazettl, J., Schmutz, C., Schirmer, T., Jenal, U., and Grzesiek, S. (2020). Intercepting second-messenger signaling by rationally designed peptides sequestering c-di-GMP. *Proc. Natl. Acad. Sci. U.S.A.* 117, 17211–17220. doi: 10.1073/pnas.2001232117

Heeb, S., Fletcher, M. P., Chhabra, S. R., Diggle, S. P., Williams, P., and Cámara, M. (2011). Quinolones: from antibiotics to autoinducers. *FEMS Microbiol. Rev.* 35, 247–274. doi: 10.1111/j.1574-6976.2010.00247.x

Heller, D., Helmerhorst, E. J., Gower, A. C., Siqueira, W. L., Paster, B. J., and Oppenheim, F. G. (2016). Microbial diversity in the early *in vivo*-formed dental biofilm. *Appl. Environ. Microbiol.* 82, 1881–1888. doi: 10.1128/AEM.03984-15

Hentzer, M. (2003). Attenuation of *Pseudomonas aeruginosa* virulence by quorum sensing inhibitors. *EMBO J.* 22, 3803–3815. doi: 10.1093/emboj/cdg366

Hentzer, M., Riedel, K., Rasmussen, T. B., Heydorn, A., Andersen, J. B., Parsek, M. R., et al. (2002). Inhibition of quorum sensing in *Pseudomonas aeruginosa* biofilm bacteria by a halogenated furanone compound. *Microbiology* 148, 87–102. doi: 10.1099/00221287-148-1-87

Herschend, J., Damholt, Z. B. V., Marquard, A. M., Svensson, B., Sørensen, S. J., Hägglund, P., et al. (2017). A meta-proteomics approach to study the interspecies interactions affecting microbial biofilm development in a model community. *Sci. Rep.* 7:16483. doi: 10.1038/s41598-017-16633-6

Heydorn, A., Nielsen, A. T., Hentzer, M., Sternberg, C., Givskov, M., Ersbøll, B. K., et al. (2000). Quantification of biofilm structures by the novel computer program COMSTAT. *Microbiol. Read. Engl.* 146(Pt 10), 2395–2407. doi: 10.1099/00221287-146-10-2395

Hinshaw, S. J., Lee, A. H. Y., Gill, E. E., and Hancock, R. E. W. (2018). MetaBridge: enabling network-based integrative analysis via direct protein interactors

of metabolites. *Bioinformatics* 34, 3225–3227. doi: 10.1093/bioinformatics/bty331

Hoffmann, N., Lee, B., Hentzer, M., Rasmussen, T. B., Song, Z., Johansen, H. K., et al. (2007). Azithromycin blocks quorum sensing and alginate polymer formation and increases the sensitivity to serum and stationary-growth-phase killing of *Pseudomonas aeruginosa* and attenuates chronic *P. aeruginosa* lung infection in *Cftr-/-* mice. *Antimicrob. Agents Chemother.* 51, 3677–3687. doi: 10.1128/AAC.01011-06

Høiby, N., Bjarnsholt, T., Givskov, M., Molin, S., and Ciofu, O. (2010). Antibiotic resistance of bacterial biofilms. *Int. J. Antimicrob. Agents* 35, 322–332. doi: 10.1016/j.ijantimicag.2009.12.011

Horsley, H., Dharmasena, D., Malone-Lee, J., and Rohn, J. L. (2018). A urine-dependent human urothelial organoid offers a potential alternative to rodent models of infection. *Sci. Rep.* 8:1238. doi: 10.1038/s41598-018-19690-7

Huber, B., Riedel, K., Hentzer, M., Heydorn, A., Gotschlich, A., Givskov, M., et al. (2001). The *cep* quorum-sensing system of *Burkholderia cepacia* H111 controls biofilm formation and swarming motility. *Microbiol. Read. Engl.* 147, 2517–2528. doi: 10.1099/00221287-147-9-2517

Hubrecht, R. C., and Carter, E. (2019). The 3Rs and humane experimental technique: implementing change. *Animal* 9:754. doi: 10.3390/ani9100754

Huh, D., Hamilton, G. A., and Ingber, D. E. (2011). From 3D cell culture to organs-on-chips. *Trends Cell Biol.* 21, 745–754. doi: 10.1016/j.tcb.2011.09.005

Imamura, Y., Chandra, J., Mukherjee, P. K., Lattif, A. A., Szczotka-Flynn, L. B., Pearlman, E., et al. (2008). *Fusarium* and *Candida albicans* biofilms on soft contact lenses: model development, influence of lens type, and susceptibility to lens care solutions. *Antimicrob. Agents Chemother.* 52, 171–182. doi: 10.1128/AAC.00387-07

Jamal, M., Ahmad, W., Andleeb, S., Jalil, F., Imran, M., Nawaz, M. A., et al. (2018). Bacterial biofilm and associated infections. *J. Chin. Med. Assoc.* 81, 7–11. doi: 10.1016/j.jcma.2017.07.012

James, G. A., Swogger, E., Wolcott, R., Pulcini, E., deLancey Secor, P., Sestrich, J., et al. (2008). Biofilms in chronic wounds. *Wound Repair Regen.* 16, 37–44. doi: 10.1111/j.1524-475X.2007.00321.x

Jansen, K., Pou Casellas, C., Groenink, L., Wever, K. E., and Masereeuw, R. (2020). Humans are animals, but are animals human enough? A systematic review and meta-analysis on interspecies differences in renal drug clearance. *Drug Discov. Today* 25, 706–717. doi: 10.1016/j.drudis.2020.01.018

Jenal, U., Reinders, A., and Lori, C. (2017). Cyclic di-GMP: second messenger extraordinaire. *Nat. Rev. Microbiol.* 15, 271–284. doi: 10.1038/nrmicro.2016.190

Jennings, B. H. (2011). *Drosophila* – a versatile model in biology & medicine. *Mater. Today* 14, 190–195. doi: 10.1016/S1369-7021(11)70113-4

Kalia, M., Singh, P. K., Yadav, V. K., Yadav, B. S., Sharma, D., Narvi, S. S., et al. (2017). Structure based virtual screening for identification of potential quorum sensing inhibitors against LasR master regulator in *Pseudomonas aeruginosa*. *Microb. Pathog.* 107, 136–143. doi: 10.1016/j.micpath.2017.03.026

Kanehisa, M., and Goto, S. (2000). KEGG: Kyoto Encyclopedia of Genes and Genomes. *Nucleic Acids Res.* 28, 27–30. doi: 10.1093/nar/28.1.27

Kang, X., Dong, F., Shi, C., Liu, S., Sun, J., Chen, J., et al. (2019). DRAMP 2.0, an updated data repository of antimicrobial peptides. *Sci. Data* 6:148. doi: 10.1038/s41597-019-0154-y

Karp, P. D., Riley, M., Paley, S. M., and Pellegrini-Toole, A. (2002). The MetaCyc database. *Nucleic Acids Res.* 30, 59–61. doi: 10.1093/nar/30.1.59

Karunasagar, A., Garag, S. S., Appannavar, S. B., Kulkarni, R. D., and Naik, A. S. (2018). Bacterial biofilms in chronic rhinosinusitis and their implications for clinical management. *Indian J. Otolaryngol. Head Neck Surg.* 70, 43–48. doi: 10.1007/s12070-017-1208-0

Khemiri, A., Jouenne, T., and Cosette, P. (2016). Proteomics dedicated to biofilmology: what have we learned from a decade of research? *Med. Microbiol. Immunol.* 205, 1–19. doi: 10.1007/s00430-015-0423-0

Kim, H. J., Huh, D., Hamilton, G., and Ingber, D. E. (2012). Human gut-on-a-chip inhabited by microbial flora that experiences intestinal peristalsis-like motions and flow. *Lab. Chip* 12:2165. doi: 10.1039/c2lc40074j

Kim, M., Mun, H., Sung, C. O., Cho, E. J., Jeon, H.-J., Chun, S.-M., et al. (2019). Patient-derived lung cancer organoids as *in vitro* cancer models for therapeutic screening. *Nat. Commun.* 10:3991. doi: 10.1038/s41467-019-11867-6

Kim, S., Chen, J., Cheng, T., Gindulyte, A., He, J., He, S., et al. (2019). PubChem 2019 update: improved access to chemical data. *Nucleic Acids Res.* 47, D1102–D1109. doi: 10.1093/nar/gky1033

Kolpen, M., Hansen, C. R., Bjarnsholt, T., Moser, C., Christensen, L. D., van Gennip, M., et al. (2010). Polymorphonuclear leucocytes consume oxygen in sputum from chronic *Pseudomonas aeruginosa* pneumonia in cystic fibrosis. *Thorax* 65, 57–62. doi: 10.1136/thx.2009.114512

Kong, C., Eng, S.-A., Lim, M.-P., and Nathan, S. (2016). Beyond traditional antimicrobials: a *Caenorhabditis elegans* model for discovery of novel anti-infectives. *Front. Microbiol.* 7:1956. doi: 10.3389/fmicb.2016.01956

Labbé, C. M., Rey, J., Lagorce, D., Vavruša, M., Becot, J., Sperandio, O., et al. (2015). MTiOpenScreen: a web server for structure-based virtual screening. *Nucleic Acids Res.* 43, W448–W454. doi: 10.1093/nar/gkv306

Lebeaux, D., Chauhan, A., Rendueles, O., and Beloin, C. (2013). From *in vitro* to *in vivo* models of bacterial biofilm-related infections. *Pathog. Basel Switz.* 2, 288–356. doi: 10.3390/pathogens2020288

Lebeaux, D., Ghigo, J.-M., and Beloin, C. (2014). Biofilm-related infections: bridging the gap between clinical management and fundamental aspects of recalcitrance toward antibiotics. *Microbiol. Mol. Biol. Rev.* 78, 510–543. doi: 10.1128/MMBR.00013-14

LeCun, Y., Bengio, Y., and Hinton, G. (2015). Deep learning. *Nature* 521, 436–444. doi: 10.1038/nature14539

Lee, A. H., Shannon, C. P., Amenyogbe, N., Bennike, T. B., Diray-Arce, J., Idoko, O. T., et al. (2019). Dynamic molecular changes during the first week of human life follow a robust developmental trajectory. *Nat. Commun.* 10:1092. doi: 10.1038/s41467-019-08794-x

Lemaitre, B., and Hoffmann, J. (2007). The host defense of *Drosophila melanogaster*. *Annu. Rev. Immunol.* 25, 697–743. doi: 10.1146/annurev.immunol.25.022106.141615

Li, L., Mendis, N., Trigui, H., Oliver, J. D., and Faucher, S. P. (2014). The importance of the viable but non-culturable state in human bacterial pathogens. *Front. Microbiol.* 5:258. doi: 10.3389/fmicb.2014.00258

Liang, H., Deng, X., Li, X., Ye, Y., and Wu, M. (2014). Molecular mechanisms of master regulator VqsM mediating quorum-sensing and antibiotic resistance in *Pseudomonas aeruginosa*. *Nucleic Acids Res.* 42, 10307–10320. doi: 10.1093/nar/gku586

Liao, J., Schurr, M. J., and Sauer, K. (2013). The MerR-like regulator BrlR confers biofilm tolerance by activating multidrug efflux pumps in *Pseudomonas aeruginosa* biofilms. *J. Bacteriol.* 195, 3352–3363. doi: 10.1128/JB.00318-13

Liu, H., Xiao, Y., Nie, H., Huang, Q., and Chen, W. (2017). Influence of (p)ppGpp on biofilm regulation in *Pseudomonas putida* KT2440. *Microbiol. Res.* 204, 1–8. doi: 10.1016/j.micres.2017.07.003

Liu, J., Yang, L., Hou, Y., Soteyome, T., Zeng, B., Su, J., et al. (2018). Transcriptomics study on *Staphylococcus aureus* biofilm under low concentration of ampicillin. *Front. Microbiol.* 9:2413. doi: 10.3389/fmicb.2018.02413

Lo, Y.-C., Rensi, S. E., Torng, W., and Altman, R. B. (2018). Machine learning in chemoinformatics and drug discovery. *Drug Discov. Today* 23, 1538–1546. doi: 10.1016/j.drudis.2018.05.010

Lynch, M. J., Swift, S., Kirke, D. F., Keevil, C. W., Dodd, C. E. R., and Williams, P. (2002). The regulation of biofilm development by quorum sensing in *Aeromonas hydrophila*. *Environ. Microbiol.* 4, 18–28. doi: 10.1046/j.1462-2920.2002.00264.x

Ma, Z., Chu, P. M., Su, Y., Yu, Y., Wen, H., Fu, X., et al. (2019). Applications of single-cell technology on bacterial analysis. *Quant. Biol.* 7, 171–181. doi: 10.1007/s40484-019-0177-6

Maiden, M. M., Hunt, A. M. A., Zachos, M. P., Gibson, J. A., Hurwitz, M. E., Mulks, M. H., et al. (2018). Triclosan is an aminoglycoside adjuvant for eradication of *Pseudomonas aeruginosa* biofilms. *Antimicrob. Agents Chemother.* 62:e146-18. doi: 10.1128/AAC.00146-18

Mallo, G. V., Kurz, C. L., Couillault, C., Pujol, N., Granjeaud, S., Kohara, Y., et al. (2002). Inducible antibacterial defense system in *C. elegans*. *Curr. Biol.* 12, 1209–1214. doi: 10.1016/s0960-9822(02)00928-4

Masopust, D., Sivula, C. P., and Jameson, S. C. (2017). Of mice, dirty mice, and men: using mice to understand human immunology. *J. Immunol.* 1950, 383–388. doi: 10.4049/jimmunol.1700453

Maura, D., and Rahme, L. G. (2017). Pharmacological inhibition of the *Pseudomonas aeruginosa* MvfR quorum-sensing system interferes with biofilm formation and potentiates antibiotic-mediated biofilm disruption. *Antimicrob. Agents Chemother.* 61:e1362-17. doi: 10.1128/AAC.01362-17

Mellini, M., Di Muzio, E., D'Angelo, F., Baldelli, V., Ferrillo, S., Visca, P., et al. (2019). *In silico* selection and experimental validation of FDA-approved drugs as anti-quorum sensing agents. *Front. Microbiol.* 10:2355. doi: 10.3389/fmicb.2019.02355

Meurens, F., Summerfield, A., Nauwynck, H., Saif, L., and Gerdts, V. (2012). The pig: a model for human infectious diseases. *Trends Microbiol.* 20, 50–57. doi: 10.1016/j.tim.2011.11.002

Millar, M. R., Linton, C. J., and Sherriff, A. (2001). "Use of a continuous culture system linked to a modified Robbins device or flow cell to study attachment of bacteria to surfaces," in *Methods in Enzymology*, ed. R. J. Doyle (Cambridge, MA: Academic Press), 43–62. doi: 10.1016/S0076-6879(01)37005-2

Millet, A. C., and Ewbank, J. J. (2004). Immunity in *Caenorhabditis elegans*. *Curr. Opin. Immunol.* 16, 4–9. doi: 10.1016/j.coi.2003.11.005

Misra, B. B., Langefeld, C., Olivier, M., and Cox, L. A. (2019). Integrated omics: tools, advances and future approaches. *J. Mol. Endocrinol.* 62, R21–R45. doi: 10.1530/JME-18-0055

Mitchell, J. B. O. (2014). Machine learning methods in chemoinformatics. *Wiley Interdiscip Rev. Comput. Mol. Sci.* 4, 468–481. doi: 10.1002/wcms.1183

Molin, S., and Tolker-Nielsen, T. (2003). Gene transfer occurs with enhanced efficiency in biofilms and induces enhanced stabilisation of the biofilm structure. *Curr. Opin. Biotechnol.* 14, 255–261. doi: 10.1016/S0958-1669(03)00036-3

Monnet, V., Juillard, V., and Gardan, R. (2016). Peptide conversations in gram-positive bacteria. *Crit. Rev. Microbiol.* 42, 339–351. doi: 10.3109/1040841X.2014.948804

Morgan, S. J., Lippman, S. I., Bautista, G. E., Harrison, J. J., Harding, C. L., Gallagher, L. A., et al. (2019). Bacterial fitness in chronic wounds appears to be mediated by the capacity for high-density growth, not virulence or biofilm functions. *PLoS Pathog.* 15:e1007511. doi: 10.1371/journal.ppat.1007511

Morohoshi, T., Tokita, K., Ito, S., Saito, Y., Maeda, S., Kato, N., et al. (2013). Inhibition of quorum sensing in gram-negative bacteria by alkylamine-modified cyclodextrins. *J. Biosci. Bioeng.* 116, 175–179. doi: 10.1016/j.jbiosc.2013.01.022

Moskowitz, S. M., Foster, J. M., Emerson, J., and Burns, J. L. (2004). Clinically feasible biofilm susceptibility assay for isolates of *Pseudomonas aeruginosa* from patients with cystic fibrosis. *J. Clin. Microbiol.* 42, 1915–1922. doi: 10.1128/jcm.42.5.1915-1922.2004

Mueller, L. N., de Brouwer, J. F. C., Almeida, J. S., Stal, L. J., and Xavier, J. B. (2006). Analysis of a marine phototrophic biofilm by confocal laser scanning microscopy using the new image quantification software PHLIP. *BMC Ecol.* 6:1. doi: 10.1186/1472-6785-6-1

Nickerson, C. A., Goodwin, T. J., Terlonge, J., Ott, C. M., Buchanan, K. L., Uicker, W. C., et al. (2001). Three-dimensional tissue assemblies: novel models for the study of *Salmonella enterica* serovar Typhimurium pathogenesis. *Infect. Immun.* 69, 7106–7120. doi: 10.1128/IAI.69.11.7106-7120.2001

Noble, W. S. (2006). What is a support vector machine? *Nat. Biotechnol.* 24, 1565–1567. doi: 10.1038/nbt1206-1565

O'Donnell, S. T., Ross, R. P., and Stanton, C. (2020). The progress of multi-omics technologies: determining function in lactic acid bacteria using a systems level approach. *Front. Microbiol.* 10:3084. doi: 10.3389/fmicb.2019.03084

Okshevsky, M., Louw, M. G., Lamela, E. O., Nilsson, M., Tolker-Nielsen, T., and Meyer, R. L. (2018). A transposon mutant library of *Bacillus cereus* ATCC 10987 reveals novel genes required for biofilm formation and implicates motility as an important factor for pellicle-biofilm formation. *MicrobiologyOpen* 7:e00552. doi: 10.1002/mbo3.552

Overhage, J., Campisano, A., Bains, M., Torfs, E. C. W., Rehm, B. H. A., and Hancock, R. E. W. (2008). Human host defense peptide LL-37 prevents bacterial biofilm formation. *Infect. Immun.* 76, 4176–4182. doi: 10.1128/IAI.00318-08

Palmer, K. L., Aye, L. M., and Whiteley, M. (2007). Nutritional cues control *Pseudomonas aeruginosa* multicellular behavior in cystic fibrosis sputum. *J. Bacteriol.* 189, 8079–8087. doi: 10.1128/JB.01138-07

Pamp, S. J., Sternberg, C., and Tolker-Nielsen, T. (2009). Insight into the microbial multicellular lifestyle via flow-cell technology and confocal microscopy. *Cytometry A* 75, 90–103. doi: 10.1002/cyto.a.20685

Park, J., Jagasia, R., Kaufmann, G. F., Mathison, J. C., Ruiz, D. I., Moss, J. A., et al. (2007). Infection control by antibody disruption of bacterial quorum sensing signaling. *Chem. Biol.* 14, 1119–1127. doi: 10.1016/j.chembiol.2007.08.013

Patsilinakos, A., Artini, M., Papa, R., Sabatino, M., Božoviæ, M., Garzoli, S., et al. (2019). Machine learning analyses on data including essential oil chemical composition and *in vitro* experimental antibiofilm activities against *Staphylococcus species*. *Mol. Basel Switz.* 24:890. doi: 10.3390/molecules24050890

Pearce, S. C., Coia, H. G., Karl, J. P., Pantoja-Feliciano, I. G., Zachos, N. C., and Racicot, K. (2018). Intestinal *in vitro* and *ex vivo* models to study host-microbiome interactions and acute stressors. *Front. Physiol.* 9:1584. doi: 10.3389/fphys.2018.01584

Peeters, E., Nelis, H. J., and Coenye, T. (2008). Comparison of multiple methods for quantification of microbial biofilms grown in microtiter plates. *J. Microbiol. Methods* 72, 157–165. doi: 10.1016/j.mimet.2007.11.010

Pezzulo, A. A., Starner, T. D., Scheetz, T. E., Traver, G. L., Tilley, A. E., Harvey, B.-G., et al. (2011). The air-liquid interface and use of primary cell cultures are important to recapitulate the transcriptional profile of *in vivo* airway epithelia. *Am. J. Physiol. Lung Cell. Mol. Physiol.* 300, L25–L31. doi: 10.1152/ajplung.00256.2010

Pihl, M., Arvidsson, A., Skepö, M., Nilsson, M., Givskov, M., Tolker-Nielsen, T., et al. (2013). Biofilm formation by *Staphylococcus epidermidis* on peritoneal dialysis catheters and the effects of extracellular products from *Pseudomonas aeruginosa*. *Pathog. Dis.* 67, 192–198. doi: 10.1111/2049-632X.12035

Pletzer, D., Blimkie, T. M., Wolfmeier, H., Li, Y., Baghela, A., Lee, A. H. Y., et al. (2020). The stringent stress response controls proteases and global regulators under optimal growth conditions in *Pseudomonas aeruginosa*. *mSystems* 5:e495-20. doi: 10.1128/mSystems.00495-20

Pletzer, D., Mansour, S. C., and Hancock, R. E. W. (2018). Synergy between conventional antibiotics and anti-biofilm peptides in a murine, sub-cutaneous abscess model caused by recalcitrant ESKAPE pathogens. *PLoS Pathog.* 14:e1007084. doi: 10.1371/journal.ppat.1007084

Pletzer, D., Wolfmeier, H., Bains, M., and Hancock, R. E. W. (2017). Synthetic peptides to target stringent response-controlled virulence in a *Pseudomonas aeruginosa* murine cutaneous infection model. *Front. Microbiol.* 8:1867. doi: 10.3389/fmicb.2017.01867

Poulsen, B. E., Yang, R., Clatworthy, A. E., White, T., Osmulski, S. J., Li, L., et al. (2019). Defining the core essential genome of *Pseudomonas aeruginosa*. *Proc. Natl. Acad. Sci. U.S.A.* 116, 10072–10080. doi: 10.1073/pnas.1900570116

Pulkkinen, K., Pekkala, N., Ashrafi, R., Hämäläinen, D. M., Nkembeng, A. N., Lipponen, A., et al. (2018). Effect of resource availability on evolution of virulence and competition in an environmentally transmitted pathogen. *FEMS Microbiol. Ecol.* 94:fiy060. doi: 10.1093/femsec/fiy060

Rabin, N., Zheng, Y., Opoku-Temeng, C., Du, Y., Bonsu, E., and Sintim, H. O. (2015). Biofilm formation mechanisms and targets for developing antibiofilm agents. *Future Med. Chem.* 7, 493–512. doi: 10.4155/fmc.15.6

Rajput, A., Thakur, A., Sharma, S., and Kumar, M. (2018). aBiofilm: a resource of anti-biofilm agents and their potential implications in targeting antibiotic drug resistance. *Nucleic Acids Res.* 46, D894–D900. doi: 10.1093/nar/gkx1157

Rémy, B., Mion, S., Plener, L., Elias, M., Chabrière, E., and Daudé, D. (2018). Interference in bacterial quorum sensing: a biopharmaceutical perspective. *Front. Pharmacol.* 9:203. doi: 10.3389/fphar.2018.00203

Resch, A., Rosenstein, R., Nerz, C., and Götz, F. (2005). Differential gene expression profiling of *Staphylococcus aureus* cultivated under biofilm and planktonic conditions. *Appl. Environ. Microbiol.* 71, 2663–2676. doi: 10.1128/AEM.71.5.2663-2676.2005

Rohart, F., Gautier, B., Singh, A., and Cao, K.-A. L. (2017). mixOmics: an R package for 'omics feature selection and multiple data integration. *PLoS Comput. Biol.* 13:e1005752. doi: 10.1371/journal.pcbi.1005752

Römling, U., and Balsalobre, C. (2012). Biofilm infections, their resilience to therapy and innovative treatment strategies. *J. Intern. Med.* 272, 541–561. doi: 10.1111/joim.12004

Ross, W., Sanchez-Vazquez, P., Chen, A. Y., Lee, J.-H., Burgos, H. L., and Gourse, R. L. (2016). ppGpp Binding to a site at the RNAP-DksA interface accounts for its dramatic effects on transcription initiation during the stringent response. *Mol. Cell* 62, 811–823. doi: 10.1016/j.molcel.2016.04.029

Rothenberg, D. A., Taliaferro, J. M., Huber, S. M., Begley, T. J., Dedon, P. C., and White, F. M. (2018). A proteomics approach to profiling the temporal translational response to stress and growth. *iScience* 9, 367–381. doi: 10.1016/j.isci.2018.11.004

Roy, R., Tiwari, M., Donelli, G., and Tiwari, V. (2018). Strategies for combating bacterial biofilms: a focus on anti-biofilm agents and their mechanisms of action. *Virulence* 9, 522–554. doi: 10.1080/21505594.2017.1313372

Rudder, C. D., Arroyo, M. C., Lebeer, S., and de Wiele, T. V. (2020). Dual and triple epithelial coculture model systems with donor-derived microbiota and THP-1 macrophages to mimic host-microbe interactions in the human sinonasal cavities. *mSphere* 5:e916-19. doi: 10.1128/mSphere.00916-19

Rumbaugh, K. P., and Carty, N. L. (2011). "*In vivo* models of biofilm infection," in *Biofilm Infections*, eds T. Bjarnsholt, P. Ø Jensen, C. Moser, and N. Høiby (New York, NY: Springer New York), 267–290. doi: 10.1007/978-1-4419-6084-9_16

Ryu, J.-H., Ha, E.-M., and Lee, W.-J. (2010). Innate immunity and gut-microbe mutualism in *Drosophila*. *Dev. Comp. Immunol.* 34, 369–376. doi: 10.1016/j.dci.2009.11.010

Sachs, N., Papaspyropoulos, A., Zomer-van Ommen, D. D., Heo, I., Böttinger, L., Klay, D., et al. (2019). Long-term expanding human airway organoids for disease modeling. *EMBO J.* 38:e100300. doi: 10.15252/embj.2018100300

Sadiq, F. A., Flint, S., Sakandar, H. A., and He, G. (2019). Molecular regulation of adhesion and biofilm formation in high and low biofilm producers of *Bacillus licheniformis* using RNA-Seq. *Biofouling* 35, 143–158. doi: 10.1080/08927014.2019.1575960

Salzer, A., Keinhörster, D., Kästle, C., Kästle, B., and Wolz, C. (2020). Small alarmone synthetases RelP and RelQ of *Staphylococcus aureus* are involved in biofilm formation and maintenance under cell wall stress conditions. *Front. Microbiol.* 11:575882. doi: 10.3389/fmicb.2020.575882

Sato, T., and Clevers, H. (2013). Growing self-organizing mini-guts from a single intestinal stem cell: mechanism and applications. *Science* 340, 1190–1194. doi: 10.1126/science.1234852

Sawada, R., Kotera, M., and Yamanishi, Y. (2014). Benchmarking a wide range of chemical descriptors for drug-target interaction prediction using a chemogenomic approach. *Mol. Inform.* 33, 719–731. doi: 10.1002/minf.201400066

Schneider, G., and Fechner, U. (2005). Computer-based de novo design of drug-like molecules. *Nat. Rev. Drug Discov.* 4, 649–663. doi: 10.1038/nrd1799

Schurek, K. N., Marr, A. K., Taylor, P. K., Wiegand, I., Semenec, L., Khaira, B. K., et al. (2008). Novel genetic determinants of low-level aminoglycoside resistance in *Pseudomonas aeruginosa*. *Antimicrob. Agents Chemother.* 52, 4213–4219. doi: 10.1128/AAC.00507-08

Schuster, M., Sexton, D. J., Diggle, S. P., and Greenberg, E. P. (2013). Acyl-homoserine lactone quorum sensing: from evolution to application. *Annu. Rev. Microbiol.* 67, 43–63. doi: 10.1146/annurev-micro-092412-155635

Service, R. F. (2020). 'The game has changed.' AI triumphs at protein folding. *Science* 370, 1144–1145. doi: 10.1126/science.370.6521.1144

Sharma, A., Gupta, P., Kumar, R., and Bhardwaj, A. (2016). dPABBs: a novel *in silico* approach for predicting and designing anti-biofilm peptides. *Sci. Rep.* 6:21839. doi: 10.1038/srep21839

Shih, P.-C., and Huang, C.-T. (2002). Effects of quorum-sensing deficiency on *Pseudomonas aeruginosa* biofilm formation and antibiotic resistance. *J. Antimicrob. Chemother.* 49, 309–314. doi: 10.1093/jac/49.2.309

Sidar, B., Jenkins, B. R., Huang, S., Spence, J. R., Walk, S. T., and Wilking, J. N. (2019). Long-term flow through human intestinal organoids with the gut organoid flow chip (GOFlowChip). *Lab. Chip* 19, 3552–3562. doi: 10.1039/C9LC00653B

Silva, S., Negri, M., Henriques, M., Oliveira, R., Williams, D., and Azeredo, J. (2010). Silicone colonization by non-*Candida albicans Candida* species in the presence of urine. *J. Med. Microbiol.* 59, 747–754. doi: 10.1099/jmm.0.017517-0

Singh, R., Sahore, S., Kaur, P., Rani, A., and Ray, P. (2016). Penetration barrier contributes to bacterial biofilm-associated resistance against only select antibiotics, and exhibits genus-, strain- and antibiotic-specific differences. *Pathog. Dis.* 74:ftw056. doi: 10.1093/femspd/ftw056

Solis, N., Parker, B. L., Kwong, S. M., Robinson, G., Firth, N., and Cordwell, S. J. (2014). *Staphylococcus aureus* surface proteins involved in adaptation to oxacillin identified using a novel cell shaving approach. *J. Proteome Res.* 13, 2954–2972. doi: 10.1021/pr500107p

Squiban, B., and Kurz, C. L. (2011). *C. elegans*: an all-in-one model for antimicrobial drug discovery. *Curr. Drug Targets* 12, 967–977. doi: 10.2174/138945011795677854

Srivastava, D., and Waters, C. M. (2012). A tangled web: regulatory connections between quorum sensing and cyclic Di-GMP. *J. Bacteriol.* 194, 4485–4493. doi: 10.1128/JB.00379-12

Srivastava, G. N., Malwe, A. S., Sharma, A. K., Shastri, V., Hibare, K., and Sharma, V. K. (2020). Molib: a machine learning based classification tool for the prediction of biofilm inhibitory molecules. *Genomics* 112, 2823–2832. doi: 10.1016/j.ygeno.2020.03.020

Starkey, M., Lepine, F., Maura, D., Bandyopadhaya, A., Lesic, B., He, J., et al. (2014). Identification of anti-virulence compounds that disrupt quorum-sensing regulated acute and persistent pathogenicity. *PLoS Pathog.* 10:e1004321. doi: 10.1371/journal.ppat.1004321

Stewart, P. S., Zhang, T., Xu, R., Pitts, B., Walters, M. C., Roe, F., et al. (2016). Reaction-diffusion theory explains hypoxia and heterogeneous growth within microbial biofilms associated with chronic infections. *NPJ Biofilms Microbiomes* 2:16012. doi: 10.1038/npjbiofilms.2016.12

Stipetic, L. H., Dalby, M. J., Davies, R. L., Morton, F. R., Ramage, G., and Burgess, K. E. V. (2016). A novel metabolomic approach used for the comparison of *Staphylococcus aureus* planktonic cells and biofilm samples. *Metabolomics* 12:75. doi: 10.1007/s11306-016-1002-0

Stokes, J. M., Yang, K., Swanson, K., Jin, W., Cubillos-Ruiz, A., Donghia, N. M., et al. (2020). A deep learning approach to antibiotic discovery. *Cell* 180, 688.e13–702.e13. doi: 10.1016/j.cell.2020.01.021

Strathdee, S. A., Davies, S. C., and Marcelin, J. R. (2020). Confronting antimicrobial resistance beyond the COVID-19 pandemic and the 2020 US election. *Lancet* 396, 1050–1053. doi: 10.1016/S0140-6736(20)32063-8

Strempel, N., Nusser, M., Neidig, A., Brenner-Weiss, G., and Overhage, J. (2017). The oxidative stress agent hypochlorite stimulates c-di-GMP synthesis and biofilm formation in *Pseudomonas aeruginosa*. *Front. Microbiol.* 8:2311. doi: 10.3389/fmicb.2017.02311

Sullivan, T. P., Eaglstein, W. H., Davis, S. C., and Mertz, P. (2001). The pig as a model for human wound healing. *Wound Repair Regen.* 9, 66–76. doi: 10.1046/j.1524-475x.2001.00066.x

Sun, E., Gill, E. E., Falsafi, R., Yeung, A., Liu, S., and Hancock, R. E. W. (2018). Broad-spectrum adaptive antibiotic resistance associated with *Pseudomonas aeruginosa* mucin-dependent surfing motility. *Antimicrob. Agents Chemother.* 62:e848-18. doi: 10.1128/AAC.00848-18

Suryaletha, K., Narendrakumar, L., John, J., Radhakrishnan, M. P., George, S., and Thomas, S. (2019). Decoding the proteomic changes involved in the biofilm formation of *Enterococcus faecalis* SK460 to elucidate potential biofilm determinants. *BMC Microbiol.* 19:146. doi: 10.1186/s12866-019-1527-2

Svenson, K. L., Gatti, D. M., Valdar, W., Welsh, C. E., Cheng, R., Chesler, E. J., et al. (2012). High-resolution genetic mapping using the mouse diversity outbred population. *Genetics* 190, 437–447. doi: 10.1534/genetics.111.132597

Tamay-Cach, F., Villa-Tanaca, M. L., Trujillo-Ferrara, J. G., Alemán-González-Duhart, D., Quintana-Pérez, J. C., González-Ramírez, I. A., et al. (2016). *In silico* studies most employed in the discovery of new antimicrobial agents. *Curr. Med. Chem.* 23, 3360–3373. doi: 10.2174/0929867323666161021141912

Tan, X., Qin, N., Wu, C., Sheng, J., Yang, R., Zheng, B., et al. (2015). Transcriptome analysis of the biofilm formed by methicillin-susceptible *Staphylococcus aureus*. *Sci. Rep.* 5:11997. doi: 10.1038/srep11997

Taylor, C. M., Beresford, M., Epton, H. A. S., Sigee, D. C., Shama, G., Andrew, P. W., et al. (2002). *Listeria monocytogenes relA* and *hpt* mutants are impaired in surface-attached growth and virulence. *J. Bacteriol.* 184, 621–628. doi: 10.1128/JB.184.3.621-628.2002

Taylor, P. K., Yeung, A. T. Y., and Hancock, R. E. W. (2014). Antibiotic resistance in *Pseudomonas aeruginosa* biofilms: towards the development of novel anti-biofilm therapies. *J. Biotechnol.* 191, 121–130. doi: 10.1016/j.jbiotec.2014.09.003

Thomas, K. R., and Capecchi, M. R. (1987). Site-directed mutagenesis by gene targeting in mouse embryo-derived stem cells. *Cell* 51, 503–512. doi: 10.1016/0092-8674(87)90646-5

Tiwari, V., Patel, V., and Tiwari, M. (2018). *In silico* screening and experimental validation reveal L-adrenaline as anti-biofilm molecule against biofilm-associated protein (Bap) producing *Acinetobacter baumannii*. *Int. J. Biol. Macromol.* 107, 1242–1252. doi: 10.1016/j.ijbiomac.2017.09.105

Tolker-Nielsen, T. (2015). Biofilm development. *Microbiol. Spectr.* 3:MB-0001-2014. doi: 10.1128/microbiolspec.MB-0001-2014

Torres, N. S., Montelongo-Jauregui, D., Abercrombie, J. J., Srinivasan, A., Lopez-Ribot, J. L., Ramasubramanian, A. K., et al. (2018). Antimicrobial and antibiofilm activity of synergistic combinations of a commercially available small compound library with colistin against *Pseudomonas aeruginosa*. *Front. Microbiol.* 9:2541. doi: 10.3389/fmicb.2018.02541

Tram, G., Klare, W. P., Cain, J. A., Mourad, B., Cordwell, S. J., Korolik, V., et al. (2020). RNA sequencing data sets identifying differentially expressed transcripts during *Campylobacter jejuni* biofilm formation. *Microbiol. Resour. Announc.* 9:e982-19. doi: 10.1128/MRA.00982-19

Troemel, E. R., Chu, S. W., Reinke, V., Lee, S. S., Ausubel, F. M., and Kim, D. H. (2006). p38 MAPK regulates expression of immune response genes and contributes to longevity in *C. elegans*. *PLoS Genet.* 2:e183. doi: 10.1371/journal.pgen.0020183

Trott, O., and Olson, A. J. (2010). AutoDock Vina: improving the speed and accuracy of docking with a new scoring function, efficient optimization, and multithreading. *J. Comput. Chem.* 31, 455–461. doi: 10.1002/jcc.21334

Tseng, B. S., Zhang, W., Harrison, J. J., Quach, T. P., Song, J. L., Penterman, J., et al. (2013). The extracellular matrix protects *Pseudomonas aeruginosa* biofilms by limiting the penetration of tobramycin. *Environ. Microbiol.* 15, 2865–2878. doi: 10.1111/1462-2920.12155

Tu Quoc, P. H., Genevaux, P., Pajunen, M., Savilahti, H., Georgopoulos, C., Schrenzel, J., et al. (2007). Isolation and characterization of biofilm formation-defective mutants of *Staphylococcus aureus*. *Infect. Immun.* 75, 1079–1088. doi: 10.1128/IAI.01143-06

Ueda, A., and Wood, T. K. (2009). Connecting quorum sensing, c-di-GMP, Pel polysaccharide, and biofilm formation in *Pseudomonas aeruginosa* through tyrosine phosphatase TpbA (PA3885). *PLoS Pathog.* 5:e1000483. doi: 10.1371/journal.ppat.1000483

UniProt Consortium (2019). UniProt: a worldwide hub of protein knowledge. *Nucleic Acids Res.* 47, D506–D515. doi: 10.1093/nar/gky1049

Valentini, T. D., Lucas, S. K., Binder, K. A., Cameron, L. C., Motl, J. A., Dunitz, J. M., et al. (2020). Bioorthogonal non-canonical amino acid tagging reveals translationally active subpopulations of the cystic fibrosis lung microbiota. *Nat. Commun.* 11:2287. doi: 10.1038/s41467-020-16163-2

Vamathevan, J., Clark, D., Czodrowski, P., Dunham, I., Ferran, E., Lee, G., et al. (2019). Applications of machine learning in drug discovery and development. *Nat. Rev. Drug Discov.* 18, 463–477. doi: 10.1038/s41573-019-0024-5

van Zundert, G. C. P., Rodrigues, J. P. G. L. M., Trellet, M., Schmitz, C., Kastritis, P. L., Karaca, E., et al. (2016). The HADDOCK2.2 web server: user-friendly integrative modeling of biomolecular complexes. *J. Mol. Biol.* 428, 720–725. doi: 10.1016/j.jmb.2015.09.014

Vandecandelaere, I., Van Acker, H., and Coenye, T. (2016). "A microplate-based system as *in vitro* model of biofilm growth and quantification," in *Bacterial Persistence: Methods and Protocols Methods in Molecular Biology*, eds J. Michiels and M. Fauvart (New York, NY: Springer), 53–66. doi: 10.1007/978-1-4939-2854-5_5

Verderosa, A. D., Totsika, M., and Fairfull-Smith, K. E. (2019). Bacterial biofilm eradication agents: a current review. *Front. Chem.* 7:824. doi: 10.3389/fchem.2019.00824

Vestby, L. K., Grønseth, T., Simm, R., and Nesse, L. L. (2020). Bacterial biofilm and its role in the pathogenesis of disease. *Antibiotics* 9:59. doi: 10.3390/antibiotics9020059

Vickery, K., Deva, A., Jacombs, A., Allan, J., Valente, P., and Gosbell, I. B. (2012). Presence of biofilm containing viable multiresistant organisms despite terminal cleaning on clinical surfaces in an intensive care unit. *J. Hosp. Infect.* 80, 52–55. doi: 10.1016/j.jhin.2011.07.007

Wang, C., Zhang, Q., Wang, Y., Tang, X., An, Y., Li, S., et al. (2019). Comparative proteomics analysis between biofilm and planktonic cells of *Mycobacterium tuberculosis*. *Electrophoresis* 40, 2736–2746. doi: 10.1002/elps.201900030

Wang, D., Haapasalo, M., Gao, Y., Ma, J., and Shen, Y. (2018). Antibiofilm peptides against biofilms on titanium and hydroxyapatite surfaces. *Bioact. Mater.* 3, 418–425. doi: 10.1016/j.bioactmat.2018.06.002

Wang, D., Shen, Y., Ma, J., Hancock, R. E. W., and Haapasalo, M. (2017). Antibiofilm effect of D-enantiomeric peptide alone and combined with EDTA *in vitro*. *J. Endod.* 43, 1862–1867. doi: 10.1016/j.joen.2017.06.037

Wang, G., Li, X., and Wang, Z. (2016). APD3: the antimicrobial peptide database as a tool for research and education. *Nucleic Acids Res.* 44, D1087–D1093. doi: 10.1093/nar/gkv1278

Waters, E. M., McCarthy, H., Hogan, S., Zapotoczna, M., O'Neill, E., and O'Gara, J. P. (2014). Rapid quantitative and qualitative analysis of biofilm production by *Staphylococcus epidermidis* under static growth conditions. *Methods Mol. Biol.* 1106, 157–166. doi: 10.1007/978-1-62703-736-5_14

Westermann, A. J., Barquist, L., and Vogel, J. (2017). Resolving host-pathogen interactions by dual RNA-seq. *PLoS Pathog.* 13:e1006033. doi: 10.1371/journal.ppat.1006033

Wexselblatt, E., Kaspy, I., Glaser, G., Katzhendler, J., and Yavin, E. (2013). Design, synthesis and structure-activity relationship of novel Relacin analogs as inhibitors of Rel proteins. *Eur. J. Med. Chem.* 70, 497–504. doi: 10.1016/j.ejmech.2013.10.036

Wexselblatt, E., Oppenheimer-Shaanan, Y., Kaspy, I., London, N., Schueler-Furman, O., Yavin, E., et al. (2012). Relacin, a novel antibacterial agent targeting the stringent response. *PLoS Pathog.* 8:e1002925. doi: 10.1371/journal.ppat.1002925

Wiegand, I., Hilpert, K., and Hancock, R. E. W. (2008). Agar and broth dilution methods to determine the minimal inhibitory concentration (MIC) of antimicrobial substances. *Nat. Protoc.* 3, 163–175. doi: 10.1038/nprot.2007.521

Willett, J. L. E., Ji, M. M., and Dunny, G. M. (2019). Exploiting biofilm phenotypes for functional characterization of hypothetical genes in *Enterococcus faecalis*. *NPJ Biofilms Microbiomes* 5:23. doi: 10.1038/s41522-019-0099-0

Wong, H. S., Maker, G. L., Trengove, R. D., and O'Handley, R. M. (2015). Gas chromatography-mass spectrometry-based metabolite profiling of *Salmonella enterica* serovar Typhimurium differentiates between biofilm and planktonic phenotypes. *Appl. Environ. Microbiol.* 81, 2660–2666. doi: 10.1128/AEM.03658-14

Wu, B. C., Haney, E. F., Akhoundsadegh, N., Pletzer, D., Trimble, M. J., Adriaans, A. E., et al. (2021). Human organoid biofilm model for assessing antibiofilm activity of novel agents. *NPJ Biofilms Microbiomes* 7:8. doi: 10.1038/s41522-020-00182-4

Wu, X., Siehnel, R. J., Garudathri, J., Staudinger, B. J., Hisert, K. B., Ozer, E. A., et al. (2019). *In vivo* proteome of *Pseudomonas aeruginosa* in airways of cystic fibrosis patients. *J. Proteome Res.* 18, 2601–2612. doi: 10.1021/acs.jproteome.9b00122

Wu, Z., Zheng, R., Zhang, J., and Wu, S. (2020). Transcriptional profiling of *Pseudomonas aeruginosa* PAO1 in response to anti-biofilm and anti-infection agent exopolysaccharide EPS273. *J. Appl. Microbiol.* 130, 265–277. doi: 10.1111/jam.14764

Xia, J., Gill, E. E., and Hancock, R. E. W. (2015). NetworkAnalyst for statistical, visual and network-based meta-analysis of gene expression data. *Nat. Protoc.* 10, 823–844. doi: 10.1038/nprot.2015.052

Xiong, Y. Q., Estellés, A., Li, L., Abdelhady, W., Gonzales, R., Bayer, A. S., et al. (2017). A human biofilm-disrupting monoclonal antibody potentiates antibiotic efficacy in rodent models of both *Staphylococcus aureus* and *Acinetobacter baumannii* infections. *Antimicrob. Agents Chemother.* 61:e904-17. doi: 10.1128/AAC.00904-17

Yamamoto, Y., Gotoh, S., Korogi, Y., Seki, M., Konishi, S., Ikeo, S., et al. (2017). Long-term expansion of alveolar stem cells derived from human iPS cells in organoids. *Nat. Methods* 14, 1097–1106. doi: 10.1038/nmeth.4448

Yang, K., Swanson, K., Jin, W., Coley, C., Eiden, P., Gao, H., et al. (2019). Analyzing learned molecular representations for property prediction. *J. Chem. Inf. Model.* 59, 3370–3388. doi: 10.1021/acs.jcim.9b00237

Ye, N., Qin, J., Shi, W., Liu, X., and Lin, B. (2007). Cell-based high content screening using an integrated microfluidic device. *Lab. Chip* 7, 1696–1704. doi: 10.1039/b711513j

Yeom, J., Shin, J.-H., Yang, J.-Y., Kim, J., and Hwang, G.-S. (2013). 1H NMR-based metabolite profiling of planktonic and biofilm cells in *Acinetobacter baumannii* 1656-2. *PLoS One* 8:e57730. doi: 10.1371/journal.pone.0057730

Yu, F., Hunziker, W., and Choudhury, D. (2019). Engineering microfluidic organoid-on-a-chip platforms. *Micromachines* 10:165. doi: 10.3390/mi10030165

Yuan, L., de Haan, P., Peterson, B. W., de Jong, E. D., Verpoorte, E., van der Mei, H. C., et al. (2020). Visualization of bacterial colonization and cellular layers in a gut-on-a-chip system using optical coherence tomography. *Microsc. Microanal.* 26, 1211–1219. doi: 10.1017/S143192762002454X

Zhang, T., Wang, Z., Hancock, R. E. W., de la Fuente-Núñez, C., and Haapasalo, M. (2016). Treatment of oral biofilms by a D-Enantiomeric peptide. *PLoS One* 11:e0166997. doi: 10.1371/journal.pone.0166997

Zhong, H., Xie, Z., Wei, H., Zhang, S., Song, Y., Wang, M., et al. (2019). Antibacterial and antibiofilm activity of Temporin-GHc and Temporin-GHd against cariogenic bacteria, *Streptococcus mutans*. *Front. Microbiol.* 10:2854. doi: 10.3389/fmicb.2019.02854

Zhou, L., Zhang, L.-H., Cámara, M., and He, Y.-W. (2017). The DSF family of quorum sensing signals: diversity, biosynthesis, and turnover. *Trends Microbiol.* 25, 293–303. doi: 10.1016/j.tim.2016.11.013

Conflict of Interest: RH has invented anti-biofilm peptides, related to those discussed here, and assigned these to his employer the University of British Columbia who filed for patent protection and licensed them to the ABT Innovations Inc., a company owned in part by RH.

The remaining authors declare that the research was conducted in the absence of any commercial or financial relationships that could be construed as a potential conflict of interest.

frontiers in Microbiology

ORIGINAL RESEARCH
published: 22 April 2021
doi: 10.3389/fmicb.2021.649757

Competence Mining of Vancomycin (VAN) in the Management of Infections Due to Bacterial Strains With High VAN Minimum Inhibitory Concentrations (MICs): A Novel Dosing Strategy Based on Pharmacokinetic/Pharmacodynamic Modeling

Xiangqing Song, Meizi Zeng, Yi Wu and Yong Pan*

Department of Pharmacy, Hunan Cancer Hospital, The Affiliated Cancer Hospital of Xiangya School of Medicine, Central South University, Changsha, China

OPEN ACCESS

Edited by:
Rodolfo García-Contreras, National Autonomous University of Mexico, Mexico

Reviewed by:
Juan M. Pericàs, Vall d'Hebron Research Institute (VHIR), Spain
Abrar Thabit, King Abdulaziz University, Saudi Arabia
Yang Yu, South China Agricultural University, China

***Correspondence:**
Xiangqing Song
sxqmaster@163.com

Specialty section:
This article was submitted to Antimicrobials, Resistance and Chemotherapy, a section of the journal Frontiers in Microbiology

Received: *05 January 2021*
Accepted: *30 March 2021*
Published: *22 April 2021*

Citation:
Song X, Zeng M, Wu Y and Pan Y (2021) Competence Mining of Vancomycin (VAN) in the Management of Infections Due to Bacterial Strains With High VAN Minimum Inhibitory Concentrations (MICs): A Novel Dosing Strategy Based on Pharmacokinetic/Pharmacodynamic Modeling. Front. Microbiol. 12:649757. doi: 10.3389/fmicb.2021.649757

The increasing emergence of bacterial strains with high VAN MICs ($BS_{H-VAN-M}$), such as *Enterococcus faecalis*, *Enterococcus faecium*, *Staphylococcus aureus*, *Staphylococcus epidermidis*, and *Streptococcus bovis*, results in growing concern that VAN is not effective against these isolates. Due to the limited data on VAN against $BS_{H-VAN-M}$ and the application limits of drugs currently considered to be effective for $BS_{H-VAN-M}$, exploration of "new usages for old drugs" is reasonable to improve and maximize the efficacy of existing antibiotics. This study aimed to construct a novel dosing strategy to mine the competence of VAN in the management of $BS_{H-VAN-M}$ infections. Herein, we optimized the traditional intermittent i.v. infusion (TIII) method to create an optimal two-step infusion (OTSI). With pharmacokinetic (PK)/pharmacodynamic (PD) modeling at the targeted ratio of the daily area under the concentration-time curve (AUC_{0-24}) to the minimum inhibitory concentration (MIC) (AUC_{0-24}/MIC) of 400, we used Monte Carlo simulations to evaluate the efficacy of 25 VAN regimens (including 15 OTSI regimens and 10 TIII regimens with daily doses of up to 6 g) to treat pneumonia, meningitis, sternal osteomyelitis, mastitis, pleuritis, bacteremia, and bacterial pericarditis resulting from isolates with MICs of ≤64 mg/L and to the current *E. faecalis*, *E. faecium*, *S. aureus*, *S. epidermidis*, and *S. bovis* populations with a pooled MIC distribution. Our data indicated that 4 g/day VAN, with an OTSI but not a TIII, for mastitis, pleuritis, bacteremia, and bacterial pericarditis due to isolates with MICs of ≤4 mg/L or to the current *E. faecalis*, *S. aureus*, *S. epidermidis*, and *S. bovis* populations

achieved the desired PK/PD exposure at the AUC_{0-24}/MIC target of 400. This study suggests the superiority and feasibility of OTSI relative to TIII for the competence mining of VAN against $BS_{H-VAN-M}$ from the perspective of PK/PD and provides a new resource for understanding how PK/PD modeling shapes the performance of VAN to meet the growing challenges of $BS_{H-VAN-M}$ infections.

Keywords: vancomycin, methicillin-resistant *Staphylococcus aureus*, MRSA, *Enterococcus*, pharmacokinetic/pharmacodynamic, Monte Carlo simulation

INTRODUCTION

The increasing emergence of bacterial strains with high VAN MICs ($BS_{H-VAN-M}$), such as *Staphylococcus aureus*, methicillin-resistant *Staphylococcus aureus* (MRSA), and *Enterococcus faecium* (The Micron Group, 2018; European Committee on Antimicrobial Susceptibility Testing (EUCAST), 2020), which are defined as any isolate displaying VAN MICs of ≥2 mg/L in the broth microdilution or of ≥1.5 mg/L in the *E*-test (Song et al., 2017), has posed significant public health threats and must be urgently addressed according to the antimicrobial resistance data released by the World Health Organization (WHO, 2017; Tacconelli et al., 2018). Infections due to these isolates not only cause growing concern that VAN is becoming disadvantageous (Sakoulas et al., 2004; Mavros et al., 2012) but also have severely limited treatment options.

Currently, some traditional drugs (e.g., daptomycin, linezolid, quinupristin-dalfopristin, tetracyclines, and chloramphenicol) and several newly approved agents (e.g., tedizolid, telavancin, oritavancin, and dalbavancin) for VAN-resistant *Enterococcus* (Barber et al., 2015), together with ceftaroline and tigecycline for MRSA (Gould, 2013), in monotherapy exhibit good activity. Unfortunately, however, they are limited due to either their significant shortcomings (Barber et al., 2015) [e.g., treatment-emergent side effects and drug interactions for daptomycin and linezolid (notably daptomycin) despite being well studied, higher morbidity and mortality and less tolerability for quinupristin-dalfopristin, and lack of sufficient documentation for tetracyclines and chloramphenicol] or the lack of sufficient clinical data. Worse, these drugs considered to be effective for $BS_{H-VAN-M}$ are still not available even in tertiary hospitals in some regions (e.g., our hospital). Likewise, combination therapies of daptomycin or VAN with a β-lactam, or daptomycin with trimethoprim-sulfamethoxazole, or linezolid with daptomycin (or VAN or gentamicin or fosfomycin), which are considered synergistic for $BS_{H-VAN-M}$ and may eventually prove to be more effective than monotherapy, particularly in "salvage" situations (Barber et al., 2015; Holubar et al., 2016; Chen et al., 2020), may also be limited since (1) the synergy of these combinations were derived mainly from retrospective studies or *in vitro* model, resulting in a lack of evidence of prospective randomized trials for a definitive answer on the synergy; and importantly (2) unavailability of daptomycin and linezolid in some hospitals is still an important factor that prevents this form of therapy. Antimicrobials, even novel and effective drugs, with a difficult balance of safety, efficacy, availability and other potential issues (e.g., cost and medical insurance protest), have often forced clinicians to rely on alternative options. Consequently, uncertainties remain for selecting the optimal treatment for $BS_{H-VAN-M}$ infections.

If the dilemma without better options in the presence of $BS_{H-VAN-M}$ infections can be broken through by optimizing the administration of the available drugs which have a currently reduced competency for such infections, it must be helpful for clinicians to treat such infections. Surprisingly, studies have shown that meropenem, with administration optimization, can still achieve sufficient PK/PD exposure against highly resistant bacterial isolates (Song et al., 2019), which has aroused substantial interest in exploring the "new usage for old drugs" to improve and maximize the performance of VAN against $BS_{H-VAN-M}$ infections. If successful, this exploration will have important significance in clinic, especially considering the rapid progress against the MIC creep phenomenon, delays in the development of new alternatives, and lack of better treatment options. Due to the lack of outcome data, the updated guidelines regarding VAN therapy issued in 2020 by the American Society of Health-System Pharmacists (called the 2020 VAN guidelines) (Rybak et al., 2020b) encourage investigators to ascertain whether VAN can provide sufficient PK/PD exposure for the isolates despite their having an MIC susceptibility breakpoint as low as 2 mg/L. Given that positive studies on these isolates have currently rarely been performed and few attempts have been made to mine the competence of VAN against the increasing number of $BS_{H-VAN-M}$ with MICs of ≥2 mg/L, this study aimed to construct a novel dosing strategy based on PK/PD modeling to exploit the maximum potentialities of VAN in the management of infections, especially for those resulting from isolates with MICs of ≥2 mg/L. We hope that our method will resolve the disadvantages of VAN in the growing presence of MIC creeping, especially in the absence of better alternatives.

MATERIALS AND METHODS

Design of a Novel Dosing Strategy

Drawing on our previous results on meropenem against highly resistant bacteria (Song et al., 2019) and the hypothesis stated by Pea et al. regarding the usefulness of continuous infusion for the treatment of borderline-susceptible pathogens (Pea and Viale, 2008), joint infusion mode with loading-rate rapid infusion (LRRI) and low-rate continuous infusion (LRCI) was speculated to be optimal and capable of yielding sufficient drug exposure for isolates with high MICs. Thus, the novel dosing strategy

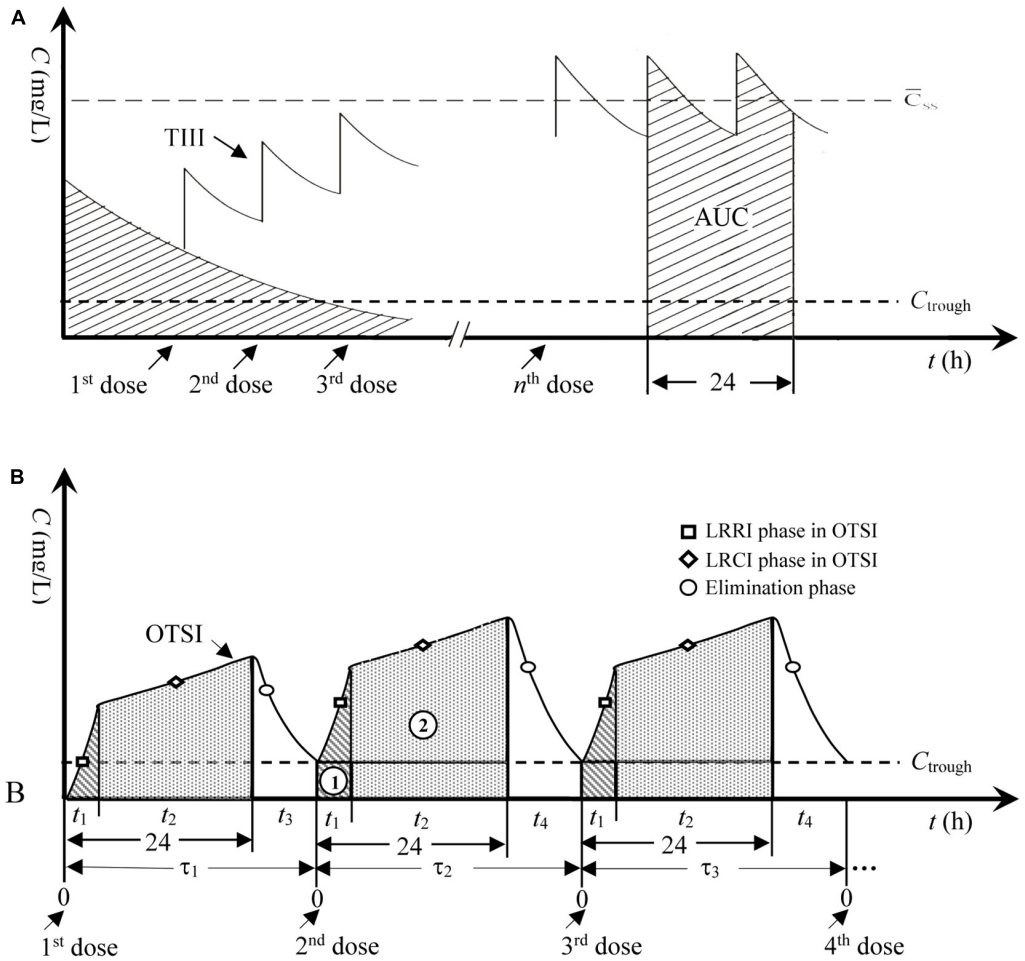

FIGURE 1 | Concentration-time profiles for TIII and OTSI. **(A)** TIII, traditional intermittent i.v. infusion; AUC, area under the concentration-time curve; $\bar{C}_{ss}$, mean steady-state plasma concentration. **(B)** OTSI, optimal two-step infusion; τ_1, dosing interval for the 2nd dose; τ_2, dosing interval for the 3rd dose; τ_3, dosing interval for the 4th dose; t_1, infusion time in the LRRI phase; t_2, infusion time in the LRCI phase; t_3, or t_4, duration in the elimination phase; ①, AUC in the LRRI phase; ②, AUC in the LRCI phase.

for VAN in this study represents an optimal two-step infusion (OTSI) mode, in which a portion of the VAN daily dose (D_{van}) was administered at an approved maximum rate of 10 mg/min (i.e., 600 mg/h) within t_1 in the LRRI phase to rapidly reach (but not limit) a trough serum concentration (C_{trough}) of 15–20 mg/L (herein set as 20 mg/L). This phase was immediately followed by administration of the remainder of the D_{van} via LRCI within t_2 to smoothly increase the concentration and maximize the daily area under the concentration-time curve (AUC_{0-24}), as illustrated in **Figure 1**. To reduce VAN accumulation, in the OTSI design, the latter dose should be administered when the concentration from the previous dose falls to the C_{trough} value.

Study Design

The PK/PD exposure, which is often considered an indicator of whether the infection is controllable or uncontrollable with antibacterial agents, of VAN was evaluated by Monte Carlo simulations (MCSs) and used to estimate the efficacy of VAN. The VAN-specific serum PK parameters [mainly the VAN clearance (CL_{van}) and distribution volume (V_d)] and microbiological susceptibility data for the targeted pathogens, together with the dosing parameters (mainly the dose, infusion duration, and rate), were incorporated into the mathematical model of the PK/PD index. MCSs were used to calculate the probabilities of target attainment (PTAs) at different MICs and the cumulative fractions of response (CFRs) for the targeted bacterial population with a pooled MIC distribution provided by each dosage regimen against the targeted bacterial species with doubling MICs between 0.125 and 64 mg/L for a given PK/PD target. A PTA or CFR of ≥90% and the causal dosage regimens were considered optimal.

VAN Dosage Regimens

In general, each dose of VAN does not exceed 2 g, and the daily dose does not exceed 4 g given its dose-dependent nephrotoxicity (del Mar Fernández de Gatta Garcia et al., 2007; Lodise et al., 2008; USP, 2018), even for continuous infusion

(Rybak et al., 2020b). However, to predict the interest of increasing the daily doses, simulations for higher doses (up to 6 g/day) were performed (del Mar Fernández de Gatta Garcia et al., 2007). In this study, 15 OTSI and 10 traditional intermittent i.v. infusion (TIII) regimens with daily doses of 2 g to up to 6 g for VAN were simulated, and the administration details for OTSI dosage regimens are shown in **Table 1**.

Reoptimization of the PK/PD Target and Calculation of the PK/PD Index

The 2020 VAN guidelines recommend a target AUC_{0-24}/MIC of 400–600 for a VAN MIC against MRSA of ≤1 mg/L (Rybak et al., 2020b). Herein, it should be noted that the upper limit of the AUC_{0-24}/MIC target of 600, associated with nephrotoxicity, depends on an assumptive MIC of 1 mg/L and an AUC_{0-24} of 600 as determined by the daily dose based on the formula $AUC_{0-24} = D_{van}/CL_{van}$ (Rybak et al., 2020a). For an MIC of <1 mg/L, a daily dose with an AUC_{0-24} of 600 may show an AUC_{0-24}/MIC of >600 and still reduced nephrotoxicity, implying that an AUC_{0-24}/MIC of >600 for a specific MIC at the permissible daily dose is acceptable due to high variability among MICs between strains. Although a target AUC_{0-24}/MIC of 400–600 is currently recommended as the primary PK/PD predictor for the treatment of serious MRSA infections, given that a VAN trough concentration of above 20 mg/L may be associated with increased risk of nephrotoxicity, a target AUC_{0-24}/MIC of ≥400 (with no upper limit at a permissible daily dose) based on a target C_{trough} of 15–20 mg/L (herein set as 20 mg/L) might be an ideal and reliable PK/PD predictor and was thus used as the optimal index in this study, as recommended by Kullar et al. (2011).

Of note, the AUC_{0-24}/MIC of ≥400 value used as an optimal target in this study might be more suitable for MRSA bloodstream infections (Rybak et al., 2020b). Therefore, for infections located at various sites, this value must be corrected

TABLE 1 | Simulated dosage regimens and administration details.

Models	TIII dosage regimens[a]	Administration details for OTSI dosage regimens						
		OTSI dosage regimens[a]	Volume of infusion solution (mL) [b]	LRRI for VAN		LRCI for VAN		Infusion operation (by microcomputer pumping)
				v_1 (mg/h)	t_1 (h)	v_2 (mg/h)	t_2 (h)	
2 g/day	0.5 g q 6 h or 1 g q 12 h	1.2 g LRRI + 0.8 g LRCI	500	600	2	36.36	22	2.5 mL/min (2 h) followed by 0.15 mL/min (22 h)
		1.8 g LRRI + 0.2 g LRCI	500	600	3	9.52	21	2.5 mL/min (3 h) followed by 0.04 mL/min (21 h)
		1.95 g LRRI + 0.05 g LRCI	500	600	3.25	2.41	20.75	2.5 mL/min (3.25 h) followed by 0.01 mL/min (20.75 h)
3 g/day	1 g q 8 h or 1.5 g q 12 h	1.2 g LRRI + 1.8 g LRCI	750	600	2	81.82	22	2.5 mL/min (2 h) followed by 0.34 mL/min (22 h)
		1.8 g LRRI + 1.2 g LRCI	750	600	3	57.14	21	2.5 mL/min (3 h) followed by 0.24 mL/min (21 h)
		2.0 g LRRI + 1.0 g LRCI	750	600	3.33	48.48	20.67	2.5 mL/min (3.33 h) followed by 0.20 mL/min (20.67 h)
4 g/day	1 g q 6 h or 2 g q 12 h	1.2 g LRRI + 2.8 g LRCI	1,000	600	2	127.27	22	2.5 mL/min (2 h) followed by 0.53 mL/min (22 h)
		1.8 g LRRI + 2.2 g LRCI	1,000	600	3	104.76	21	2.5 mL/min (3 h) followed by 0.44 mL/min (21 h)
		2.0 g LRRI + 2.0 g LRCI	1,000	600	3.33	96.86	20.67	2.5 mL/min (3.33 h) followed by 0.40 mL/min (20.67 h)
5 g/day	1.25 g q 6 h or 1.67 g q 8 h	1.2 g LRRI + 3.8 g LRCI	1,250	600	2	172.73	22	2.5 mL/min (2 h) followed by 0.72 mL/min (22 h)
		1.8 g LRRI + 3.2 g LRCI	1,250	600	3	152.38	21	2.5 mL/min (3 h) followed by 0.63 mL/min (21 h)
		2.0 g LRRI + 3.0 g LRCI	1,250	600	3.33	145.14	20.67	2.5 mL/min (3.33 h) followed by 0.60 mL/min (20.67 h)
6 g/day	1.5 g q 6 h or 2 g q 8 h	1.2 g LRRI + 4.8 g LRCI	1,500	600	2	218.18	22	2.5 mL/min (2 h) followed by 0.91 mL/min (22 h)
		1.8 g LRRI + 4.2 g LRCI	1,500	600	3	200.00	21	2.5 mL/min (3 h) followed by 0.83 mL/min (21 h)
		2.0 g LRRI + 4.0 g LRCI	1,500	600	3.33	193.52	20.67	2.5 mL/min (3.33 h) followed by 0.81 mL/min (20.67 h)

[a] according to the OTSI design, at the targeted C_{trough} of 20 mg/L and maximum limit of 2 g per dose (Lodise et al., 2008; Filippone et al., 2017), the dose of VAN administered in the LRRI phase ranges from 1.2 g (i.e., the minimum dose for the targeted C_{trough} according to the equation of C_{trough}) to 2 g (i.e., the maximum limit of per dose), [b] determined by the final concentration of 2.5–5 g/L for VAN (USP, 2018). t_1, infusion time in the LRRI phase; t_2, infusion time in the LRCI phase; v_1, zero-order infusion rate in the LRRI phase; v_2, zero-order infusion rate in the LRCI phase.

based on the VAN tissue permeability since VAN penetration into infected tissues or fluids, to provide pharmacologically active drug concentrations at the site of action, is critical for predicting therapeutic responses. Data on VAN tissue permeability was obtained from previously published studies on adult patients (preferably those describing infection studies when available) with normal renal function [i.e., creatinine clearance (CL_{cr}) $\geq$70 ml/min] or healthy volunteers (when the desired data from infected populations were unavailable), including those undergoing various surgeries. **Table 2** is a collection of data on VAN penetration coefficient into some common tissues (Massias et al., 1992; Cruciani et al., 1996; Albanèse et al., 2000; Kitzes-Cohen et al., 2000; Luzzati et al., 2000; Byl et al., 2003; Lodise et al., 2011). Considering the profiles of VAN tissue penetration, a corrected approximate value of AUC_{0-24}/MIC of $\geq$1,000 for pneumonia and meningitis, AUC_{0-24}/MIC of $\geq$667 for sternal osteomyelitis, AUC_{0-24}/MIC of $\geq$400 for mastitis, pleuritis and bacteremia, and AUC_{0-24}/MIC of $\geq$250 for bacterial pericarditis would indicate sufficient PK/PD exposure. Thus, these targets based on the target C_{trough} of 20 mg/L, were used to assess the PK/PD exposure of VAN for these infections. According to the previous version of the 2020 VAN guidelines issued in 2009 (called the 2009 VAN guidelines) (Rybak et al., 2009), the total AUC_{0-24}/MIC and the free VAN AUC_{0-24}/MIC (i.e., AUC_{0-24} × 50% protein binding/MIC) are interchangeably reported for VAN; thus, the AUC_{0-24}/MIC calculation refers to the total AUC_{0-24}/MIC in this study, and the formulas are as follows:

(i) Formulas for OTSI (Eq. 1 and Eq. 2) (see Appendix: derivation of equations):

$$C_{\text{trough}} = \frac{v_1}{CL_{\text{van}}} \cdot \left(1 - e^{-CL_{\text{van}}/V_{\text{d}} \cdot t_1}\right) \tag{1}$$

TABLE 2 | VAN for some common infections and the corresponding tissue penetration coefficient.

Infections	Corresponding infected tissues	VAN tissues penetration coefficient (i.e., ratio of the mean tissue/concomitant serum concentration or AUC)	References
Pneumonia	Lung or epithelial lining fluid	0.41	Cruciani et al. (1996), Lodise et al. (2011)
Meningitis	Cerebrospinal fluid	0.39	Albanèse et al. (2000)
Sternal osteomyelitis	Sternal bones	0.57	Massias et al. (1992)
Mastitis	Capsular tissue	1.06	Luzzati et al. (2000)
Bacterial pericarditis	Pericardium	1.6	Kitzes-Cohen et al. (2000)
Pleuritis	Pleural fluid	0.86	Byl et al. (2003)
Bacteremia	Bloodstream	1	NN

NN, not necessary.

$$\begin{aligned}
&\text{AUC}_{0\text{-}24}/\text{MIC} = \\
&\frac{e^{-\frac{CL_{van}}{V_d}(t_2-t_1)}\left\{t_2 \cdot e^{\frac{CL_{van}}{V_d}\cdot t_2}\left[CL_{van}\cdot v_2 \cdot e^{\frac{CL_{van}}{V_d}\cdot t_1}\right.\right.}{\left.\left.+CL_{van}\cdot v_1\left(e^{\frac{CL_{van}}{V_d}\cdot t_1}-1\right)+C_{trough}\cdot CL_{van}^2\cdot e^{\frac{CL_{van}}{V_d}\cdot t_1}\right]\right.} \\
&\left.+V_d\cdot v_2\cdot e^{\frac{CL_{van}}{V_d}\cdot t_1}\right\} \\
&+e^{-\frac{CL_{van}}{V_d}\cdot t_1}\left[t_1\cdot e^{\frac{CL_{van}}{V_d}\cdot t_1}\left(CL_{van}\cdot v_1 + C_{trough}\cdot CL_{van}^2\right)\right. \\
&\left.+V_d\cdot v_1\right] \\
&\frac{}{\text{MIC}\cdot CL_{van}^2} \\
&-\frac{V_d\,(v_2+v_1)}{\text{MIC}\cdot CL_{van}^2}
\end{aligned} \tag{2}$$

(ii) Formula for TIII (Eq. 3):

$$\text{AUC}_{0\text{-}24}/\text{MIC} = D_{\text{van}}/(CL_{\text{van}}\cdot\text{MIC}) \tag{3}$$

Eq. 3 was modified from the AUC_{0-24} formula derived from Moise-Broder et al. (2004a) as follows: AUC_{0-24} = dose per 24 h/[($\alpha \times CL_{cr} + \beta$) × γ] [i.e., $AUC_{0-24} = D_{van}/CL_{van}$ since the relationship of CL_{van} and CL_{cr} is linear in patients with various degrees of impaired renal function (Rodvold et al., 1988)],
where C_{trough} (mg/L) is the targeted trough serum concentration; AUC_{0-24} (mg·h/L) is the daily area under the concentration-time curve; MIC (mg/L) is the minimum inhibitory concentration; CL_{van} (L/h) is the VAN clearance; V_d (L) is the distribution volume at the steady state; t_1 (h) is the infusion time in the LRRI phase; t_2 (h) is the infusion time in the LRCI phase; v_1 (mg/h) is the zero-order infusion rate of 10 mg/min (i.e., 600 mg/h) in the LRRI phase; v_2 (mg/h) is the zero-order infusion rate in the LRCI phase, which is calculated as the dose in the LRCI phase divided by the infusion time [i.e., $(D_{van}-600 \times t_1)/t_2$)]; $\int$ is the integral operator; dt is the differential operator; e is the natural constant; ln is the natural logarithm; and α, β, γ are constants.

Key VAN Population PK Parameters

Previous studies have established various models for the key population PK parameters (mainly CL_{van} and V_d) for VAN among adult populations. However, some large cohort studies paid more attention to critically ill patients (Llopis-Salvia and Jiménez-Torres, 2006; Revilla et al., 2010; Roberts et al., 2011; Udy et al., 2013a; Mangin et al., 2014; Medellín-Garibay et al., 2017), as they are likely to show more PK variability than other populations due to their markedly varying physiological statuses (Roberts et al., 2014). However, PK changes to the antimicrobial volume of distribution, clearance, protein binding and tissue penetration in critically ill patients can be significantly different from those in other patient groups (Udy et al., 2013b), often resulting in insufficient antimicrobial concentrations in plasma and at the site of infection relative to those in the general population. Generally, accepted PK/PD targets may not be applicable for these patients (Roberts et al., 2014), potentially because it is more acceptable for these models to be used in critically ill patients. The population PK parameter models based

on systemically infected patients from the study conducted by Matzke et al. (1984) [i.e., CL_{van} (ml/min) = 3.66 + 0.689 × CL_{cr} (ml/min) and V_d (L) = 0.72 L/kg (if CL_{cr} > 60 ml/min) or V_d (L) = 0.89 L/kg (if 10 ml/min ≤ CL_{cr} ≤ 60 ml/min) or V_d (L) = 0.9 L/kg (if CL_{cr} < 10 ml/min)] were used for our analysis since these models can be utilized to devise dosing schedules for patients with any degree of renal impairment and with normal renal function (Matzke et al., 1984) and because they performed well with satisfactory precision and bias prediction errors among eleven models in an external validation evaluation (Sánchez et al., 2010). Herein, this study focused on only adult patients with normal renal function (i.e., CL_{cr} > 70 ml/min), and the estimations of CL_{van} of (3.84 ± 1.14) L/h and V_d of (48.82 ± 3.74) L based on the demographic characteristics of the subjects in the Matzke et al. study (Matzke et al., 1984) were used to predict the efficacy of VAN.

Microbiological Susceptibility Data

Based on the indications of VAN (USP, 2018) and the Antimicrobial Testing Leadership and Surveillance (ATLAS) database (The Micron Group, 2018), the targeted bacterial species with $BS_{H-VAN-M}$, including mainly *E. faecalis, E. faecium, S. aureus, S. epidermidis*, and *S. bovis*, were modeled to determine the competence of VAN for $BS_{H-VAN-M}$. The susceptibility data of these species, including the isolate numbers and the corresponding MIC frequency distributions, were derived from the ATLAS database between 2004 and 2018 (The Micron Group, 2018) and are displayed in **Table 3**.

MCSs (Evaluation of Dosage Schedules)

Oracle Crystal Ball (version 11.1.2; Decisioneering Inc., Denver, CO, United States), a leading spreadsheet (i.e., Excel)-based application for predictive modeling, forecasting, simulation, and optimization, was used to perform the MCSs to calculate the probability of each dosing regimen to achieve the given combined PK/PD target against isolates with MICs of 0.125, 0.25, 0.5, 1, 2, 4, 8, 16, 32, and 64 mg/L, which is referred to as the PTA. This method has been well described elsewhere (Moine et al., 2016; Song and Long, 2018). In general, MCSs includes the following five steps: (1) data inputting (i.e., inputting the simulation variables and their representative values into the Excel table cells), (2) distribution pattern settings of simulation variables (i.e., setting the distribution patterns of the simulation variables according to their characteristics), (3) predictive variable settings and calculation (i.e., setting the variable that can reflect the drug efficacy as the predictive variable and calculating its typical value based on the mathematical model of it established on the simulation variables), (4) simulation parameter settings and execution (i.e., setting the number of simulations and the confidence interval), and (5) simulation result analysis (including the sensitivity and trend analysis, report creation and extraction of data). Briefly, in this study, assumed lognormal distributions of CL_{van} (3.84 ± 1.14 L/h) and V_d (48.82 ± 3.74 L); custom distributions of MIC frequency distributions (e.g., for *E. faecalis*, MIC = 0.125, 0.25, 0.5, 1, 2, 4, 8, 16, 32, and 64 mg/L, probability = 0.23%, 0.71%, 10.95%, 57.96%, 25.84%, 1.64%, 0.55%, 0.18%, 0.21%, and 1.71%, respectively); C_{trough} (constant given values = 20 mg/L, probability = 100%); and the infusion time and infusion rate and dose (e.g., for the regimen of 1.2 g LRRI + 0.8 g LRCI, t_1 = 2 h, probability = 100%; t_2 = 22 h, probability = 100%; v_1 = 600 mg/h, probability = 100%; v_2 = 36.36 mg/h, probability = 100%; dose in LRRI phase = 1200 mg, probability = 100%; D_{van} = 2000 mg, probability = 100%) were used as the simulation variables incorporated into the mathematical model of the predictive variables (i.e., C_{trough} and AUC_{0-24}/MIC). The confidence interval was set to 95%. A 5,000-subject MCSs was performed on the predictive variable to obtain the PTA-predictive variable diagram, with the predictive variable as the abscissa and the PTA as the ordinate. The PTA at a given threshold of the predictive variable was obtained by specifying the abscissa as the given threshold. The overall expected value for the PTA (i.e., CFR) is related to PD target attainment in that it expresses the probability of a given dosage regimen achieving the desired exposures against an entire population of pathogens. Calculation of the CFR (Eq. 4) for each organism was performed by multiplying the PTA at each MIC by the percentage of isolates of each of the modeled organisms actually found at that MIC. A regimen with a PTA or CFR of ≥90% for the given PK/PD target was considered optimal.

$$\text{Eq. 4 : CFR} = \Sigma \text{PTA}_\text{i} \times \text{F}_\text{i} \quad (4)$$

where PTA_i is the probability of target attainment at a specific MIC value and F_i is the fraction of the targeted isolate actually found at that MIC in populations.

RESULTS

PTAs for the Targeted C_{trough} Values

PTAs versus the concentration profiles for simulations of the 15 OTSI regimens are presented in **Figure 2**. All of them achieved a PTA of ≥90% for the targeted C_{trough} of 20 mg/L, indicating that all regimens attained the predetermined C_{trough} target and thus laid the foundation to achieve the AUC_{0-24}/MIC target established for this targeted C_{trough}.

PTAs for the Targeted AUC_{0-24}/MIC Values

PTAs versus the various AUC_{0-24}/MIC targets for simulations of the tested regimens are displayed in **Figure 3**. All of the OTSI regimens and the TIII regimens with a daily dose of up to 6 g for the AUC_{0-24}/MIC target of 250 achieved a PTA of ≥90% at an MIC of up to 4 mg/L, while only the OTSI regimens with a daily dose of ≥4 g (e.g., 2 g LRRI + 2 g LRCI, 2 g LRRI + 3 g LRCI, 2 g LRRI + 4 g LRCI) for the AUC_{0-24}/MIC target of 400 achieved this PTA result for an MIC of up to 4 mg/L, indicating that VAN at 4 g/day can generate a sufficient PK/PD response for MICs of up to 4 mg/L at the AUC_{0-24}/MIC target of 400 when administered via OTSI for this dose. Surprisingly, 2 g/day VAN at the regimen of 1.95 g LRRI + 0.05 g LRCI still reached a PTA of ≥90% at an MIC of 2 mg/L. However, only OTSI regimens with a daily dose of ≥3 g obtained the optimal PTA for an MIC of up to 2 mg/L at an AUC_{0-24}/MIC of 667, but only a MIC of up to

TABLE 3 | MIC frequency distributions of isolates for the targeted bacterial species.

Bacterial species	Total (No.)	MIC (mg/L) frequency distributions [no. of the isolates (% of no.)]					
		≤0.0625	0.125	0.25	0.5	1	2
E. faecalis	26058	0(0.00)	61(0.23)	186 (0.71)	2854 (10.95)	15104 (57.96)	6734 (25.84)
E. faecium	12923	0(0.00)	35(0.27)	294 (2.28)	3646 (28.21)	3987 (30.85)	604 (4.67)
S. aureus	120172	0(0.00)	193(0.16)	983 (0.82)	36605 (30.46)	74052 (61.62)	8332 (6.93)
S. epidermidis	9641	0(0.00)	8(0.08)	25 (0.26)	140 (1.45)	3941 (40.88)	5405 (56.06)
S. bovis	39	0(0.00)	1(2.56)	19 (48.72)	15 (38.46)	3 (7.69)	1 (2.56)
		4	**8**	**16**	**32**	**64**	**≥128**
E. faecalis	26058	427(1.64)	143(0.55)	48 (0.18)	55 (0.21)	446 (1.71)	0 (0.00)
E. faecium	12923	171(1.32)	162(1.25)	97 (0.75)	379 (2.93)	3548 (27.45)	0 (0.00)
S. aureus	120172	7(0.01)	0(0.00)	0 (0.00)	0 (0.00)	0 (0.00)	0 (0.00)
S. epidermidis	9641	115(1.19)	7(0.07)	0 (0.00)	0 (0.00)	0 (0.00)	0 (0.00)
S. bovis	39	0(0.00)	0(0.00)	0 (0.00)	0 (0.00)	0 (0.00)	0 (0.00)

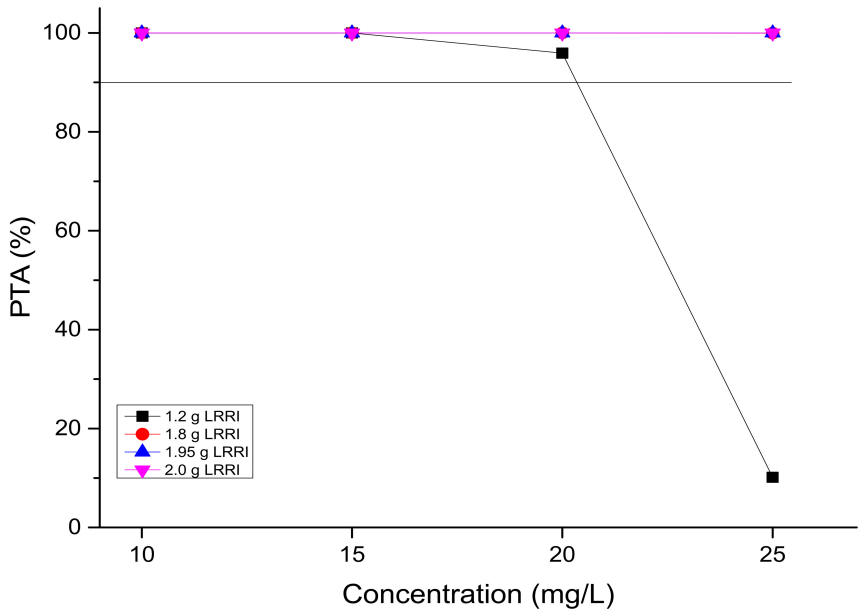

FIGURE 2 | PTAs for various C_{trough} targets. According to the OTSI design (see **Figure 1**), the C_{trough} target is determined by the dose administered in the LRRI phase for each OTSI regimen.

1 mg/L at an AUC_{0-24}/MIC of 1,000 of one independent regimen was applied. As expected, with the same daily dose, the OTSI regimens displayed superior PK/PD exposure relative to the TIII regimens regardless of the PD targets. **Table 4** summarizes the coverages of the tested regimens for the targeted bacterial isolate with different MICs at the condition of achieving ≥90% PTA.

CFRs for the Targeted Bacterial Species

The CFRs versus various targeted bacterial species for simulations of the tested regimens are displayed in **Figure 4**. No regimens achieved a CFR of ≥90% for the *E. faecium* population regardless of the PD targets. Based on currently pooled MIC distributions and an AUC_{0-24}/MIC of ≤400, the OTSI regimens, even at 2 g/day, yielded a CFR of ≥90% for the *E. faecalis, S. aureus, S. epidermidis*, and *S. bovis* populations. However, at an AUC_{0-24}/MIC of 667, the OTSI regimens with a daily dose of ≥3 g for these pathogen populations achieved the requisite CFR, while those with a daily dose of 2 g achieved the requisite CFR for only the *S. aureus and S. bovis* populations. Unfortunately, all OTSI regimens covered only the *S. aureus and S. bovis* populations at an AUC_{0-24}/MIC of 1,000. At the classical target of an AUC_{0-24}/MIC of 400, the TIII regimens with only ≥4 g/day achieved a CFR of ≥90% for the *E. faecalis, S. aureus, S. epidermidis*, and *S. bovis* populations. **Table 4** summarizes the coverages of the tested regimens for the targeted bacterial species with pooled MIC distributions at the condition of achieving ≥90% CFR.

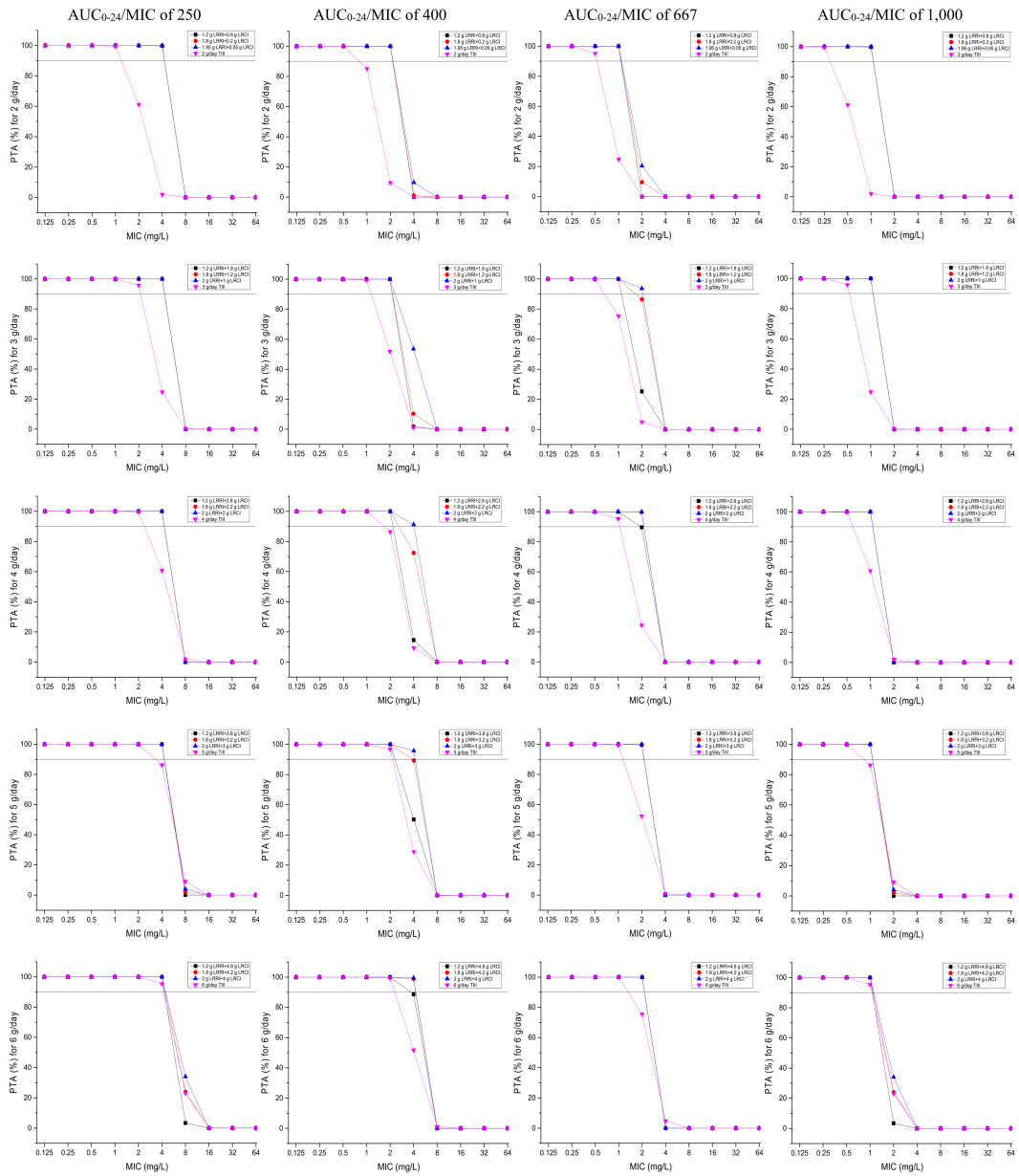

FIGURE 3 | PTAs for various AUC_{0-24}/MIC targets for MICs of up to 64 mg/L. Considering the profiles of VAN tissue penetration, simulating the target AUC_{0-24}/MIC of 1,000 is for predicting VAN exposure in lung interstitial fluid and cerebrospinal fluid (i.e., for pneumonia and meningitis), 667 is for predicting VAN exposure in sternal bones (i.e., for sternal osteomyelitis), 400 is for predicting VAN exposure in capsular tissue, pleural fluid, and bloodstream (i.e., for mastitis, pleuritis, and bacteremia), and 250 is for predicting VAN exposure in pericardium (i.e., for bacterial pericarditis).

DISCUSSION

To our knowledge, this study is the first to design OTSI method to exploit the maximum potentialities of VAN. Our data suggests great superiority and satisfactory PK/PD exposure of the dosing strategy of OTSI relative to that of TIII, especially for $BS_{H-VAN-M}$ of $\geq$2 mg/L and $\leq$4 mg/L, supporting that VAN in OTSI mode is still powerful for $BS_{H-VAN-M}$ of $\leq$4 mg/L and thus providing a temporary solution when better treatment options are unavailable.

Currently, it is still difficult to find an antimicrobial with a desired balance of safety, efficacy, availability, cost, and other potential issues for $BS_{H-VAN-M}$ despite the emergence of some current novel drugs (Gould, 2013; Barber et al., 2015). Importantly, the lack of clinical trials and experimental studies evaluating antimicrobial efficacy against $BS_{H-VAN-M}$ has forced clinicians to rely on alternative regimens extrapolated from PK/PD models, retrospective studies, and case reports (Yim et al., 2017). Currently, clinical data on the continued use of VAN in the setting of known $BS_{H-VAN-M}$ are quite

TABLE 4 | Coverage of the regimens for the isolates and/or for the targeted pathogen populations.

Models	Dosage regimen	Covered pathogen isolates and/or populations in various types of the infection at different PD targets			
		AUC_{0-24}/MIC of 250	AUC_{0-24}/MIC of 400	AUC_{0-24}/MIC of 667	AUC_{0-24}/MIC of 1,000
		Mainly for bacterial pericarditis	Mainly for mastitis, pleuritis, and bacteremia	Mainly for sternal osteomyelitis	Mainly for pneumonia and meningitis
2 g/day	1.2 g LRRI + 0.8 g LRCI	P_4 + EFS, SA, SE, SB	P_2 + EFS, SA, SE, SB	P_1 + SA, SB	P_1 + SA, SB
	1.8 g LRRI + 0.2 g LRCI	P_4 + EFS, SA, SE, SB	P_2 + EFS, SA, SE, SB	P_1 + SA, SB	P_1 + SA, SB
	1.95 g LRRI + 0.05 g LRCI	P_4 + EFS, SA, SE, SB	P_2 + EFS, SA, SE, SB	P_1 + SA, SB	P_1 + SA, SB
	2 g TIII	P_1 + SA, SB	$P_{0.5}$ + SB	$P_{0.5}$	$P_{0.25}$
3 g/day	1.2 g LRRI + 1.8 g LRCI	P_4 + EFS, SA, SE, SB	P_2 + EFS, SA, SE, SB	P_1 + SA, SB	P_1 + SA, SB
	1.8 g LRRI + 1.2 g LRCI	P_4 + EFS, SA, SE, SB	P_2 + EFS, SA, SE, SB	P_1 + EFS, SA, SE, SB	P_1 + SA, SB
	2.0 g LRRI + 1.0 g LRCI	P_4 + EFS, SA, SE, SB	P_2 + EFS, SA, SE, SB	P_1 + EFS, SA, SE, SB	P_1 + SA, SB
	3 g TIII	P_2 + EFS, SA, SE, SB	P_1 + SB	$P_{0.5}$ + SB	$P_{0.5}$ + SB
4 g/day	1.2 g LRRI + 2.8 g LRCI	P_4 + EFS, SA, SE, SB	P_2 + EFS, SA, SE, SB	P_1 + EFS, SA, SE, SB	P_1 + SA, SB
	1.8 g LRRI + 2.2 g LRCI	P_4 + EFS, SA, SE, SB	P_2 + EFS, SA, SE, SB	P_2 + EFS, SA, SE, SB	P_1 + SA, SB
	2.0 g LRRI + 2.0 g LRCI	P_4 + EFS, SA, SE, SB	P_4 + EFS, SA, SE, SB	P_2 + EFS, SA, SE, SB	P_1 + SA, SB
	4 g TIII	P_2 + EFS, SA, SE, SB	P_1 + EFS, SA, SE, SB	P_1 + SA, SB	$P_{0.5}$ + SB
5 g/day	1.2 g LRRI + 3.8 g LRCI	P_4 + EFS, SA, SE, SB	P_2 + EFS, SA, SE, SB	P_2 + EFS, SA, SE, SB	P_1 + SA, SB
	1.8 g LRRI + 3.2 g LRCI	P_4 + EFS, SA, SE, SB	P_2 + EFS, SA, SE, SB	P_2 + EFS, SA, SE, SB	P_1 + SA, SB
	2.0 g LRRI + 3.0 g LRCI	P_4 + EFS, SA, SE, SB	P_4 + EFS, SA, SE, SB	P_2 + EFS, SA, SE, SB	P_1 + SA, SB
	5 g TIII	P_2 + EFS, SA, SE, SB	P_2 + EFS, SA, SE, SB	P_1 + SA, SB	$P_{0.5}$ + SB
6 g/day	1.2 g LRRI + 4.8 g LRCI	P_4 + EFS, SA, SE, SB	P_2 + EFS, SA, SE, SB	P_2 + EFS, SA, SE, SB	P_1 + SA, SB
	1.8 g LRRI + 4.2 g LRCI	P_4 + EFS, SA, SE, SB	P_4 + EFS, SA, SE, SB	P_2 + EFS, SA, SE, SB	P_1 + SA, SB
	2.0 g LRRI + 4.0 g LRCI	P_4 + EFS, SA, SE, SB	P_4 + EFS, SA, SE, SB	P_2 + EFS, SA, SE, SB	P_1 + SA, SB
	6 g TIII	P_4 + EFS, SA, SE, SB	P_2 + EFS, SA, SE, SB	P_1 + SA, SB	P_1 + SA, SB

EFS, E. faecalis; SA, S. aureus; SE, S. epidermidis; SB, S. bovis. $P_{0.25}$, $P_{0.5}$, P_1, P_2, and P_4 signify the pathogen isolates with MICs of up to 0.25, 0.5, 1, 2, and 4 mg/L, respectively. Regimens with P_x (x = 0.25, 0.5, 1, 2, or 4) + y (y = EFS, SA, SE, SB, or a combination) signify that they are competent for the treatment of infections caused by the pathogen isolates actually found at that MIC if the exact MIC values are available and/or for the treatment of infections caused by the targeted pathogen populations identified with only bacterial species if the exact MIC values are unavailable.

rare. Some clinical and simulated studies have focused mainly on MRSA isolates with an MIC of 2 mg/L (still within the susceptibility range).

Clinically, despite the achievement of a target C_{trough} of 15 mg/L, VAN performed worse against MRSA bacteremia, intraabdominal infections and pneumonia caused by isolates with an MIC of 2 mg/L than against those with an MIC < 2 mg/L (Moise-Broder et al., 2004b; Sakoulas et al., 2004; Hidayat et al., 2006). Harigaya et al. (2009) demonstrated that VAN did not have bactericidal activity against MRSA pneumonia due to infection by isolates with an MIC of 1 mg/L regardless of whether 1–1.5 g of VAN was administered twice daily (i.e., 2–3 g/day) and of the assumptions of 100% VAN penetration in the lung and an AUC_{0-24}/MIC of 350 as the therapeutic target. Likewise, for MRSA meningitis due to strains with MICs of 2 mg/L, Sipahi et al. (2013) found that six (five of the six had MRSA isolates with a VAN MIC of 2 mg/L) out of eight patients (75%) with MRSA meningitis who received 500 mg VAN every 6 h (i.e., 2 g/day) as a 1 h infusion failed to achieve the clinical outcome, suggesting that VAN, at its standard daily dose and conventional dosing strategy, is unsatisfactory for such infections. Interestingly, our data indicated that even for bacteremia due to isolates with MICs of 2 mg/L, VAN at the standard 2 g/day can still produce adequate PK/PD exposure when administered using the regimen of 1.2 g LRRI + 0.8 g LRCI, 1.8 g LRRI + 0.2 g LRCI, or 1.95 g LRRI + 0.05 g LRCI, while worse outcomes were achieved when TIII was used; these results suggest the competence of VAN for such infections and the superiority of OTSI relative to TIII. Consistently, however, for pneumonia and meningitis due to isolates with MICs of 2 mg/L, VAN performed poorly (well only for those resulting from isolates with MICs of ≤1 mg/L) even at 6 g/day and with the OTSI strategy. The occurrence of this outcome may be due to the fact that VAN has poor profiles in terms of lung interstitial fluid and cerebrospinal fluid penetration. More recently, a review research for the penetration of VAN (15 mg/kg IV 1 h) into bone showed an average VAN concentration of 3.8 mg/L and 4.5 mg/L in cancellous and cortical bone, respectively (Thabit et al., 2019), suggesting that VAN reaches concentrations that exceed the MIC_{90} against *S. aureus* (1 mg/L) and thus implying that VAN will have good performance on bone infections due to such bacteria. However, in a case report, Lee et al. (2016) found that the infusion of even 1 g of VAN over 1 h every 12 h (i.e., 2 g/day) was unsuccessful for an infected patient who had lumbar osteomyelitis, discitis, and epidural abscess with persistent MRSA bacteremia resulted from isolates with an MIC of 1 mg/L. The occurrence of this result may be associated with the physiological and pathological status of the patient, slow bactericidal activity of VAN, inappropriate dosage regimen of VAN or a combination. However, our data showed that even

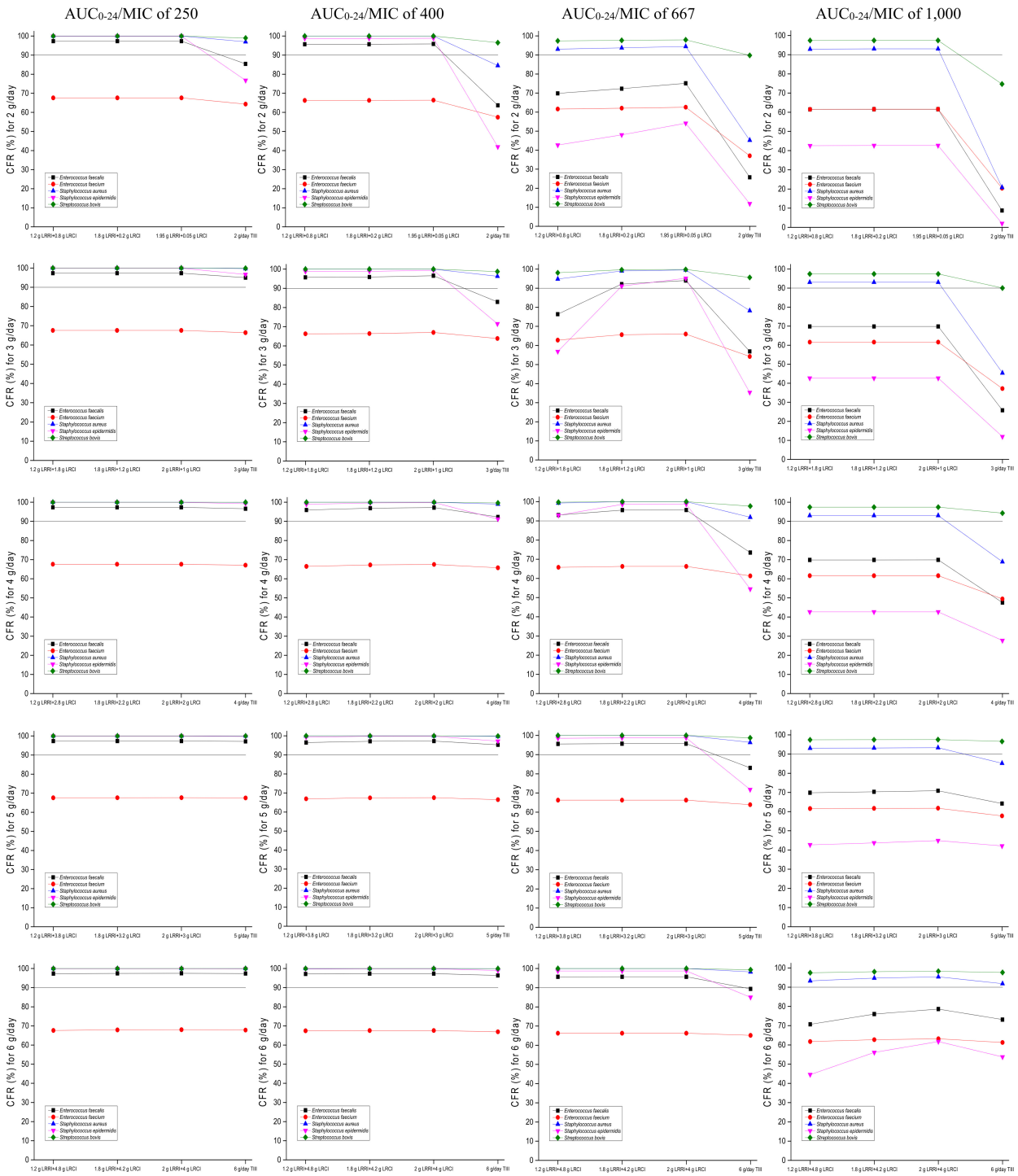

FIGURE 4 | CFRs of achieving AUC_{0-24}/MIC targets for the targeted bacterial species with pooled MIC distributions. Considering the profiles of VAN tissue penetration, simulating the target AUC_{0-24}/MIC of 1,000 is for predicting VAN exposure in lung interstitial fluid and cerebrospinal fluid (i.e., for pneumonia and meningitis), 667 is for predicting VAN exposure in sternal bones (i.e., for sternal osteomyelitis), 400 is for predicting VAN exposure in capsular tissue, pleural fluid, and bloodstream (i.e., for mastitis, pleuritis, and bacteremia), and 250 is for predicting VAN exposure in pericardium (i.e., for bacterial pericarditis).

though relatively poor bone penetration coefficient (0.57) of VAN was applied, 2 g/day VAN with a rational OTSI strategy (e.g., 1.2 g LRRI + 0.8 g LRCI) could still yield desirable PK/PD exposure for this complicated infection, and 4 g/day VAN with a rational OTSI regimen (e.g., 2 g LRRI + 2 g LRCI) performed well for this case due to isolates with an MIC of up to 2 mg/L. This

implied that for population in which VAN has good profiles of bone penetration, these optimal dosage regimens will show better PK/PD exposure performance, and this was also the case for VAN against other infected tissues. Unexpectedly, for bacterial pericarditis, 2 g/day VAN with a rational OTSI (e.g., 1.2 g LRRI + 0.8 g LRCI) achieved optimal PK/PD exposure for isolates with an MIC of up to 4 mg/L, indicating good activity at infected sites with strong VAN penetration and enrichment (e.g., the pericardium).

Likewise, in the simulated studies, poor VAN exposure at an MIC of 2 mg/L was also observed with a PTA of 90% as an acceptable PK/PD exposure target. By MCSs, Mohr et al. (Mohr and Murray, 2007) determined the PTAs for the targeted AUC_{0-24}/MIC of ≥400 using the PK data derived from the study conducted by Jeffres et al. (2006) and indicated that the PTA would be 100% at an MIC of 0.5 mg/L but 0% at an MIC of 2 mg/L despite that a high dose of VAN (i.e., C_{trough} > 15 mg/L but no detailed information on the simulated regimens) was used. Coincidentally, using MCSs, del Mar Fernández de Gatta Garcia et al. (2007) reported that 3–4 g/day VAN administered via the TIII strategy for an assumed MIC of 1 mg/L would reach a PTA of 90% at the targeted AUC_{0-24}/MIC of 400, thus questioning the dosage of 2 g/day as a standard schedule for such isolates. Interestingly, Setiawan et al. (2019) found that 2 g/day VAN with TIII obtained a PTA of 100% at an MIC of 0.5 mg/L but only 84.41% at an MIC of 1 mg/L; moreover, even 4 g/day VAN administered with TIII failed to achieve the optimal PTA for an MIC of 2 mg/L. Conversely, however, our data supported that at the above PK/PD target, 2 g/day VAN, with the regimen of 1.2 g LRRI + 0.8 g LRCI, 1.8 g LRRI + 0.2 g LRCI, or 1.95 g LRRI + 0.05 g LRCI, still produced a PTA of ≥90% at an MIC of 2 mg/L, suggesting the achievement of sufficient PK/PD exposure. Surprisingly, 4 g/day VAN, with the regimen of 2.0 g LRRI + 2.0 g LRCI, yielded a PTA of ≥90% (91.28%) for an MIC of up to 4 mg/L but failed with the regimen of 4 g/day administered with TIII. In addition, when administered via TIII and even at a high dose of 5 g/day, VAN cannot provide sufficient PK/PD exposure for *Enterococcus* isolates with MICs of 4 mg/L regardless of the infection, although these isolates are currently considered to be susceptible to VAN at this breakpoint. These findings show the superiority and feasibility of OTSI for the competence mining of VAN against $BS_{H-VAN-M}$. Of note, the achievement of such regimens for these MICs might be more agreeable for bacteremia, mastitis and pleuritis based on VAN tissue permeability and the derivation of the AUC_{0-24}/MIC target of 400 [derived mainly from MRSA bloodstream infections (Rybak et al., 2020b)].

However, the exact MIC values are often unavailable in empirical therapy. Fortunately, our data provided the CFRs for the targeted bacterial populations. In empirical therapy, 3–4 g/day VAN with an OTSI strategy, such as the preferred regimen of 2 g LRRI + 1 g LRCI or 2 g LRRI + 2 g LRCI, may be preferable for most common infections, including bacterial pericarditis, mastitis, pleuritis, bacteremia and sternal osteomyelitis, as these regimens produced a CFR of ≥90% for all of the targeted bacterial populations, including *E. faecalis*, *S. aureus*, *S. epidermidis*, and *S. bovis*, with the sole exception of *E. faecium*. However, for pneumonia and meningitis, even at the aggressive regimen of 6 g/day (2 g LRRI + 4 g LRCI), VAN was sufficient for infections due to only *S. aureus* and *S. bovis*; in theory, for such pathogen populations, the standard 2 g/day may result in similar PK/PD exposure and reduced nephrotoxicity relative to that at 6 g/day based on our data. **Table 5** summarizes some preferred VAN regimens for common infections based on our analysis.

Despite acquisition of target AUC_{0-24}/MIC by OTSI method, we were unable to demonstrate a microbiological or clinical superiority of these recommended VAN OTSI regimens based on MCSs as little data are currently available, either *in vivo* or *in vitro* experiments. However, in a study of *in vitro* pharmacodynamic model and MCSs (Eguchi et al., 2010), experimental verification of the efficacy of optimized two-step infusion therapy (OTIT), for meropenem but not for VAN, was performed. Surprisingly, the *in vitro* bactericidal effect of the optimal meropenem OTIT regimens is consistent with the bactericidal effect predicted by their respective PTA of these regimens derived from MCSs, especially for *Pseudomonas aeruginosa* isolates with meropenem MIC of ≤4 mg/L, which partly indicated the feasibility of MCSs method in predicting the efficacy of the regimens although the research object of this study was meropenem rather than VAN. However, despite this significative case of MCSs prediction, the

TABLE 5 | Preferred VAN regimen recommendations for some common infections.

Infections	Available for MIC [a]				Unavailable for MIC (i.e., in empirical therapy) [b]
	≤1 mg/L	>1 mg/L and ≤2 mg/L	>2 mg/L and ≤4 mg/L	>4 mg/L	
Bacterial pericarditis	1.95 g LRRI + 0.05 g LRCI	1.95 g LRRI + 0.05 g LRCI	1.95 g LRRI + 0.05 g LRCI	NA	1.95 g LRRI + 0.05 g LRCI
Mastitis, pleuritis, and bacteremia	1.95 g LRRI + 0.05 g LRCI	1.95 g LRRI + 0.05 g LRCI	2.0 g LRRI + 2.0 g LRCI	NA	1.95 g LRRI + 0.05 g LRCI
Sternal osteomyelitis	1.95 g LRRI + 0.05 g LRCI	2.0 g LRRI + 2.0 g LRCI	NA	NA	2.0 g LRRI + 1.0 g LRCI
Pneumonia and meningitis	1.95 g LRRI + 0.05 g LRCI	NA	NA	NA	1.95 g LRRI + 0.05 g LRCI

[a] determined by such a regimen that has a lower daily dose and a PTA of ≥90%; [b] determined by such a regimen that has a lower daily dose, a wider coverage of bacterial species and a CFR of ≥90%. NA, (VAN) not applicable.

recommended VAN OTSI regimens based on MCSs cannot be considered certainly effective against the target bacteria given the difference in action profiles among antibiotics and in resistance mechanisms among bacteria. In addition, modification of VAN delivery in severe infections may not be sufficient, by itself, to change the clinical outcome for critically ill patients, and the bacterial status like bacterial biofilm widely formed among various bacteria were also a barrier to effective anti-infection.

This study has some limitations. First, the desired regimens acquired by MCSs were not validated by experimental outcomes, which somewhat limits their generalization. However, further studies on this topic will be summarized in our next study. Second, the AUC_{0-24}/MIC target of >600 (e.g., 667 and 1,000) utilized in this study may be too high to increase VAN-induced nephrotoxicity. Regarding this, we need to correctly understand (1) the derivation of the value of 600, and (2) that these targets simulated herein are just used to simulate concentrations in sites other than the plasma (e.g., lung interstitial fluid and cerebrospinal fluid). Moreover, the dosing interval and a C_{trough} value of 20 mg/L designed for OTSI method ensure a theoretically low probability of drug accumulation; notwithstanding this optimal design, however, therapeutic monitoring of VAN should be recommended as a routine test, especially for patients with long medication time. Third, in consideration of the problem of VAN stability and low flow rate (especially in the LRCI phase), some experts consider that OTSI may not be implemented well clinically. However, the concern on the VAN stability is not a factor preventing the implementation of OTSI method since VAN displayed well chemical stability even during 24-h infusion (Masse et al., 2020). And, the low flow rate can be performed well with the recently developed microcomputer pumping method. Moreover, we can appropriately increase the total solvent volume of VAN to improve the velocity problem. Fourth, the PK models selected in this study may have been biased for assessing target attainment in different populations. Indeed, the inherent interindividual variability in the PK data contributes to the prediction bias. However, we believe that the use of these PK models together with PK/PD analysis based on MCSs still offers a definitive outcome to some extent since (1) the PK variability, which is often extensive, was considered by the lognormal distribution patterns settings of CL_{van} and V_d in MCSs, and (2) the PK models used in this study performed well with satisfactory precision and bias prediction errors when compared with some established models in the external validation evaluation (Sánchez et al., 2010). Finally, at the same PK/PD target, whether regimens with desirable PK/PD exposure to MRSA are also satisfactory against *Enterococcus* and whether regimens with acceptable PK/PD exposure for ordinary patients are also adequate for critically ill patients remains unknown, thereby limiting the extrapolation of optimal regimens to other $BS_{H-VAN-M}$ with different resistance mechanisms and to critically ill patients with marked PK variability. Notwithstanding its limitations, the study provides some tentative options for $BS_{H-VAN-M}$, especially in the absence of better alternatives. However, prospective validation of these limitations is desirable.

CONCLUSION

When faced with the daily challenge of infections due to isolates with high MICs, we should try to reduce the gap between the available medical evidence for using VAN and the dearth of alternative options, some of which have not been sufficiently explored and/or whose efficacy in certain situations remains debatable. The question of whether VAN can continue to be used for isolates with MICs of ≥2 mg/L (this study supports VAN, at an allowable daily dose and with a reasonable OTSI, for isolates with an MIC of up to 4 mg/L) is still not obsolete, and this study provides a new resource for understanding how PK/PD modeling shapes the power of VAN to meet the growing challenges of $BS_{H-VAN-M}$ infections. However, in the absence of control trials, the continued appraisal of VAN for use, along with the optimal dosage regimens in clinical experience, will provide additional important information on its utility against $BS_{H-VAN-M}$.

DATA AVAILABILITY STATEMENT

The original contributions presented in the study are included in the article/supplementary material, further inquiries can be directed to the corresponding author.

AUTHOR CONTRIBUTIONS

XS performed the model simulation and wrote the manuscript. MZ, YW, and YP conceptualized and supervised the manuscript. All authors approved the final version of the manuscript.

ACKNOWLEDGMENTS

The authors are grateful to the anti-infection experts at our hospital for their direction on VAN therapy. The authors thank all members of our hospital library for allowing access to their information resources.

REFERENCES

Albanèse, J., Léone, M., Bruguerolle, B., Ayem, M. L., Lacarelle, B., and Martin, C. (2000). Cerebrospinal fluid penetration and pharmacokinetics of vancomycin administered by continuous infusion to mechanically ventilated patients in an intensive care unit. *Antimicrob. Agents Chemother.* 44, 1356–1358. doi: 10.1128/aac.44.5.1356-1358.2000

Barber, K. E., King, S. T., Stover, K. R., and Pogue, J. M. (2015). Therapeutic options for vancomycin-resistant enterococcal bacteremia. *Expert Rev. Anti Infect. Ther.* 13, 363–377. doi: 10.1586/14787210.2015.1001839

Byl, B., Jacobs, F., Wallemacq, P., Rossi, C., de Francquen, P., Cappello, M., et al. (2003). Vancomycin penetration of uninfected pleural fluid exudate after continuous or intermittent infusion. *Antimicrob. Agents Chemother.* 47, 2015–2017. doi: 10.1128/aac.47.6.2015-2017.2003

Chen, H., Du, Y., Xia, Q., Li, Y., Song, S., and Huang, X. (2020). Role of linezolid combination therapy for serious infections: review of the current evidence. *Eur. J. Clin. Microbiol. Infect. Dis.* 39, 1043–1052. doi: 10.1007/s10096-019-03801-x

Cruciani, M., Gatti, G., Lazzarini, L., Furlan, G., Broccali, G., Malena, M., et al. (1996). Penetration of vancomycin into human lung tissue. *J. Antimicrob. Chemother.* 38, 865–869. doi: 10.1093/jac/38.5.865

del Mar Fernández de Gatta Garcia, M., Revilla, N., Calvo, M. V., Domínguez-Gil, A., et al. (2007). Pharmacokinetic/pharmacodynamic analysis of vancomycin in ICU patients. *Intensive Care Med.* 33, 279–285. doi: 10.1007/s00134-006-0470-5

Eguchi, K., Kanazawa, K., Shimizudani, T., Kanemitsu, K., and Kaku, M. (2010). Experimental verification of the efficacy of optimized two-step infusion therapy with meropenem using an in vitro pharmacodynamic model and Monte Carlo simulation. *J. Infect. Chemother.* 16, 1–9. doi: 10.1007/s10156-009-0001-8

European Committee on Antimicrobial Susceptibility Testing (EUCAST) (2020). *Antimicrobial wild type distributions of microorganisms*. Sweden: EUCAST.

Filippone, E. J., Kraft, W. K., and Farber, J. L. (2017). The Nephrotoxicity of Vancomycin. *Clin. Pharmacol. Ther.* 102, 459–469. doi: 10.1002/cpt.726

Gould, I. M. (2013). Treatment of bacteraemia: meticillin-resistant Staphylococcus aureus (MRSA) to vancomycin-resistant S. aureus (VRSA). *Int. J. Antimicrob. Agents* 42(Suppl.), S17–S21. doi: 10.1016/j.ijantimicag.2013.04.006

Harigaya, Y., Bulitta, J. B., Forrest, A., Sakoulas, G., Lesse, A. J., Mylotte, J. M., et al. (2009). Pharmacodynamics of vancomycin at simulated epithelial lining fluid concentrations against methicillin-resistant Staphylococcus aureus (MRSA): implications for dosing in MRSA pneumonia. *Antimicrob. Agents Chemother.* 53, 3894–3901. doi: 10.1128/AAC.01585-08

Hidayat, L. K., Hsu, D. I., Quist, R., Shriner, K. A., and Wong-Beringer, A. (2006). High-dose vancomycin therapy for methicillin-resistant Staphylococcus aureus infections: efficacy and toxicity. *Arch. Intern. Med.* 166, 2138–2144. doi: 10.1001/archinte.166.19.2138

Holubar, M., Meng, L., and Deresinski, S. (2016). Bacteremia due to Methicillin-Resistant Staphylococcus aureus: New Therapeutic Approaches. *Infect. Dis. Clin. North Am.* 30, 491–507. doi: 10.1016/j.idc.2016.02.009

Jeffres, M. N., Isakow, W., Doherty, J. A., McKinnon, P. S., Ritchie, D. J., Micek, S. T., et al. (2006). Predictors of mortality for methicillin-resistant Staphylococcus aureus health-care-associated pneumonia: specific evaluation of vancomycin pharmacokinetic indices. *Chest* 130, 947–955. doi: 10.1378/chest.130.4.947

Kitzes-Cohen, R., Farin, D., Piva, G., Ivry, S., Sharony, R., Amar, R., et al. (2000). Pharmacokinetics of vancomycin administered as prophylaxis before cardiac surgery. *Ther. Drug Monit.* 22, 661–667. doi: 10.1097/00007691-200012000-00004

Kullar, R., Davis, S. L., Levine, D. P., and Rybak, M. J. (2011). Impact of vancomycin exposure on outcomes in patients with methicillin-resistant Staphylococcus aureus bacteremia: support for consensus guidelines suggested targets. *Clin. Infect. Dis.* 52, 975–981. doi: 10.1093/cid/cir124

Lee, W.-S., Chen, Y.-C., Chen, H.-P., Chen, T.-H., and Cheng, C.-Y. (2016). Vertebral osteomyelitis caused by vancomycin-tolerant methicillin-resistant Staphylococcus aureus bacteremia: Experience with teicoplanin plus fosfomycin combination therapy. *J. Microbiol. Immunol. Infect.* 49, 600–603. doi: 10.1016/j.jmii.2013.09.002

Llopis-Salvia, P., and Jiménez-Torres, N. V. (2006). Population pharmacokinetic parameters of vancomycin in critically ill patients. *J. Clin. Pharm. Ther.* 31, 447–454. doi: 10.1111/j.1365-2710.2006.00762.x

Lodise, T. P., Drusano, G. L., Butterfield, J. M., Scoville, J., Gotfried, M., and Rodvold, K. A. (2011). Penetration of vancomycin into epithelial lining fluid in healthy volunteers. *Antimicrob. Agents Chemother.* 55, 5507–5511. doi: 10.1128/AAC.00712-11

Lodise, T. P., Lomaestro, B., Graves, J., and Drusano, G. L. (2008). Larger vancomycin doses (at least four grams per day) are associated with an increased incidence of nephrotoxicity. *Antimicrob. Agents Chemother.* 52, 1330–1336. doi: 10.1128/AAC.01602-07

Luzzati, R., Sanna, A., Allegranzi, B., Nardi, S., Berti, M., Barisoni, D., et al. (2000). Pharmacokinetics and tissue penetration of vancomycin in patients undergoing prosthetic mammary surgery. *J. Antimicrob. Chemother.* 45, 243–245. doi: 10.1093/jac/45.2.243

Mangin, O., Urien, S., Mainardi, J.-L., Fagon, J.-Y., and Faisy, C. (2014). Vancomycin pharmacokinetic and pharmacodynamic models for critically ill patients with post-sternotomy mediastinitis. *Clin. Pharmacokinet* 53, 849–861. doi: 10.1007/s40262-014-0164-z

Masse, M., Genay, S., Martin Mena, A., Carta, N., Lannoy, D., Barthélémy, C., et al. (2020). Evaluation of the stability of vancomycin solutions at concentrations used in clinical services. *Eur. J. Hosp. Pharm.* 27, 87–92e. doi: 10.1136/ejhpharm-2019-002076

Massias, L., Dubois, C., de Lentdecker, P., Brodaty, O., Fischler, M., and Farinotti, R. (1992). Penetration of vancomycin in uninfected sternal bone. *Antimicrob. Agents Chemother.* 36, 2539–2541. doi: 10.1128/aac.36.11.2539

Matzke, G. R., McGory, R. W., Halstenson, C. E., and Keane, W. F. (1984). Pharmacokinetics of vancomycin in patients with various degrees of renal function. *Antimicrob. Agents Chemother.* 25, 433–437. doi: 10.1128/aac.25.4.433

Mavros, M. N., Tansarli, G. S., Vardakas, K. Z., Rafailidis, P. I., Karageorgopoulos, D. E., and Falagas, M. E. (2012). Impact of vancomycin minimum inhibitory concentration on clinical outcomes of patients with vancomycin-susceptible Staphylococcus aureus infections: a meta-analysis and meta-regression. *Int. J. Antimicrob. Agents* 40, 496–509. doi: 10.1016/j.ijantimicag.2012.07.023

Medellín-Garibay, S. E., Romano-Moreno, S., Tejedor-Prado, P., Rubio-Álvaro, N., Rueda-Naharro, A., Blasco-Navalpotro, M. A., et al. (2017). Influence of Mechanical Ventilation on the Pharmacokinetics of Vancomycin Administered by Continuous Infusion in Critically Ill Patients. *Antimicrob. Agents Chemother.* 61:17. doi: 10.1128/AAC.01249-17

Mohr, J. F., and Murray, B. E. (2007). Point: Vancomycin is not obsolete for the treatment of infection caused by methicillin-resistant Staphylococcus aureus. *Clin. Infect. Dis.* 44, 1536–1542. doi: 10.1086/518451

Moine, P., Mueller, S. W., Schoen, J. A., Rothchild, K. B., and Fish, D. N. (2016). Pharmacokinetic and Pharmacodynamic Evaluation of a Weight-Based Dosing Regimen of Cefoxitin for Perioperative Surgical Prophylaxis in Obese and Morbidly Obese Patients. *Antimicrob. Agents Chemother.* 60, 5885–5893. doi: 10.1128/AAC.00585-16

Moise-Broder, P. A., Forrest, A., Birmingham, M. C., and Schentag, J. J. (2004a). Pharmacodynamics of vancomycin and other antimicrobials in patients with Staphylococcus aureus lower respiratory tract infections. *Clin. Pharmacokinet* 43, 925–942. doi: 10.2165/00003088-200443130-00005

Moise-Broder, P. A., Sakoulas, G., Eliopoulos, G. M., Schentag, J. J., Forrest, A., and Moellering, R. C. (2004b). Accessory gene regulator group II polymorphism in methicillin-resistant Staphylococcus aureus is predictive of failure of vancomycin therapy. *Clin. Infect. Dis.* 38, 1700–1705. doi: 10.1086/421092

Pea, F., and Viale, P. (2008). Should the currently recommended twice-daily dosing still be considered the most appropriate regimen for treating MRSA ventilator-associated pneumonia with vancomycin? *Clin. Pharmacokinet* 47, 147–152. doi: 10.2165/00003088-200847030-00001

Revilla, N., Martín-Suárez, A., Pérez, M. P., González, F. M., Fernández, and de Gatta, M. D. M. (2010). Vancomycin dosing assessment in intensive care unit patients based on a population pharmacokinetic/pharmacodynamic simulation. *Br. J. Clin. Pharmacol.* 70, 201–212. doi: 10.1111/j.1365-2125.2010.03679.x

Roberts, J. A., Abdul-Aziz, M. H., Lipman, J., Mouton, J. W., Vinks, A. A., Felton, T. W., et al. (2014). Individualised antibiotic dosing for patients who are critically ill: challenges and potential solutions. *Lancet Infect. Dis.* 14, 498–509. doi: 10.1016/S1473-3099(14)70036-2

Roberts, J. A., Taccone, F. S., Udy, A. A., Vincent, J.-L., Jacobs, F., and Lipman, J. (2011). Vancomycin dosing in critically ill patients: robust methods for improved continuous-infusion regimens. *Antimicrob. Agents Chemother.* 55, 2704–2709. doi: 10.1128/AAC.01708-10

Rodvold, K. A., Blum, R. A., Fischer, J. H., Zokufa, H. Z., Rotschafer, J. C., Crossley, K. B., et al. (1988). Vancomycin pharmacokinetics in patients with various degrees of renal function. *Antimicrob. Agents Chemother.* 32, 848–852. doi: 10.1128/aac.32.6.848

Rybak, M. J., Le, J., Lodise, T. P., Levine, D. P., Bradley, J. S., Liu, C., et al. (2020a). Executive Summary: Therapeutic Monitoring of Vancomycin for Serious Methicillin-Resistant Staphylococcus aureus Infections: A Revised Consensus Guideline and Review of the American Society of Health-System Pharmacists, the Infectious Diseases Society of America, the Pediatric Infectious Diseases Society, and the Society of Infectious Diseases Pharmacists. *Pharmacotherapy* 40, 363–367. doi: 10.1002/phar.2376

Rybak, M. J., Le, J., Lodise, T. P., Levine, D. P., Bradley, xJ. S., Liu, C., et al. (2020b). Therapeutic monitoring of vancomycin for serious methicillin-resistant Staphylococcus aureus infections: A revised consensus guideline and

review by the American Society of Health-System Pharmacists, the Infectious Diseases Society of America, the Pediatric Infectious Diseases Society, and the Society of Infectious Diseases Pharmacists. *Am. J. Health Syst. Pharm.* 77, 835–864. doi: 10.1093/ajhp/zxaa036

Rybak, M., Lomaestro, B., Rotschafer, J. C., Moellering, R., Craig, W., Billeter, M., et al. (2009). Therapeutic monitoring of vancomycin in adult patients: a consensus review of the American Society of Health-System Pharmacists, the Infectious Diseases Society of America, and the Society of Infectious Diseases Pharmacists. *Am. J. Health Syst. Pharm.* 66, 82–98. doi: 10.2146/ajhp080434

Sakoulas, G., Moise-Broder, P. A., Schentag, J., Forrest, A., Moellering, R. C., and Eliopoulos, G. M. (2004). Relationship of MIC and bactericidal activity to efficacy of vancomycin for treatment of methicillin-resistant Staphylococcus aureus bacteremia. *J. Clin. Microbiol.* 42, 2398–2402. doi: 10.1128/JCM.42.6.2398-2402.2004

Sánchez, J. L., Dominguez, A. R., Lane, J. R., Anderson, P. O., Capparelli, E. V., and Cornejo-Bravo, J. M. (2010). Population pharmacokinetics of vancomycin in adult and geriatric patients: comparison of eleven approaches. *Int. J. Clin. Pharmacol. Ther.* 48, 525–533. doi: 10.5414/cpp48525

Setiawan, E., Suwannoi, L., Montakantikul, P., and Chindavijak, B. (2019). Optimization of Intermittent Vancomycin Dosage Regimens for Thai Critically Ill Population Infected by MRSA in the Era of the "MIC Creep" Phenomenon. *Acta Med. Indones* 51, 10–18.

Sipahi, O. R., Bardak-Ozcem, S., Turhan, T., Arda, B., Ruksen, M., Pullukcu, H., et al. (2013). Vancomycin versus linezolid in the treatment of methicillin-resistant Staphylococcus aureus meningitis. *Surg. Infect.* 14, 357–362. doi: 10.1089/sur.2012.091

Song, K.-H., Kim, M., Kim, C. J., Cho, J. E., Choi, Y. J., Park, J. S., et al. (2017). Impact of Vancomycin MIC on Treatment Outcomes in Invasive Staphylococcus aureus Infections. *Antimicrob. Agents Chemother.* 61:16. doi: 10.1128/AAC.01845-16

Song, X., and Long, M. (2018). Pharmacodynamic model for β-lactam regimens used in surgical prophylaxis: model-based evaluation of standard dosing regimens. *Int. J. Clin. Pharm.* 40, 1059–1071. doi: 10.1007/s11096-018-0720-y

Song, X., Wu, Y., Cao, L., Yao, D., and Long, M. (2019). Is Meropenem as a Monotherapy Truly Incompetent for Meropenem-Nonsusceptible Bacterial Strains? A Pharmacokinetic/Pharmacodynamic Modeling With Monte Carlo Simulation. *Front. Microbiol.* 10:2777. doi: 10.3389/fmicb.2019.02777

Tacconelli, E., Carrara, E., Savoldi, A., Harbarth, S., Mendelson, M., Monnet, D. L., et al. (2018). Discovery, research, and development of new antibiotics: the WHO priority list of antibiotic-resistant bacteria and tuberculosis. *Lancet Infect. Dis.* 18, 318–327. doi: 10.1016/S1473-3099(17)30753-3

Thabit, A. K., Fatani, D. F., Bamakhrama, M. S., Barnawi, O. A., Basudan, L. O., and Alhejaili, S. F. (2019). Antibiotic penetration into bone and joints: An updated review. *Int. J. Infect. Dis.* 81, 128–136. doi: 10.1016/j.ijid.2019.02.005

The Micron Group (2018). *Antimicrobial Testing Leadership and Surveillance(ATLAS)-Antibacterials Database*. Boise: The Micron Group.

Udy, A. A., Covajes, C., Taccone, F. S., Jacobs, F., Vincent, J.-L., Lipman, J., et al. (2013a). Can population pharmacokinetic modelling guide vancomycin dosing during continuous renal replacement therapy in critically ill patients? *Int. J. Antimicrob. Agents* 41, 564–568. doi: 10.1016/j.ijantimicag.2013.01.018

Udy, A. A., Roberts, J. A., and Lipman, J. (2013b). Clinical implications of antibiotic pharmacokinetic principles in the critically ill. *Intensive Care Med.* 39, 2070–2082. doi: 10.1007/s00134-013-3088-4

USP (2018). *VANCOMYCIN Hydrochloride for Injection, USP PACKAGE INSERT*. Maryland: USP.

WHO (2017). *WHO publishes list of bacteria for which new antibiotics are urgently needed*. Geneva: WHO.

Yim, J., Smith, J. R., and Rybak, M. J. (2017). Role of Combination Antimicrobial Therapy for Vancomycin-Resistant Enterococcus faecium Infections: Review of the Current Evidence. *Pharmacotherapy* 37, 579–592. doi: 10.1002/phar.1922

Conflict of Interest: The authors declare that the research was conducted in the absence of any commercial or financial relationships that could be construed as a potential conflict of interest.

APPENDIX (DERIVATION OF EQUATIONS)

The two basic PK equations via i.v. infusion in the one-compartment model [derived from the book (Basic Pharmacokinetics and Pharmacodynamics: An Integrated Textbook and Computer Simulations, 1 edition. Hoboken, NJ, United States: Wiley; 2011) edited by Rosenbaum SE] are as follows:

(i) During infusion

$$C = \frac{v}{CL} \cdot (1 - e^{-CL/V \cdot t}) \quad (0 \le t \le t_{\text{inf}}) \tag{1}$$

C_{max} in every dose is achieved when t is equal to t_{inf}.

(ii) After completion of the infusion

$$C = C_{\max} \cdot e^{-CL/V \cdot t'} \quad \left(0 \le t' < \infty\right) \tag{2}$$

1. Derivation of C_{trough}

According to **Figure 1**, whether C can reach C_{trough} after the first dose is determined by Eq. 3:

$$C_{\text{trough}} = \frac{v_1}{CL} \cdot \left(1 - e^{-CL/V \cdot t_1}\right) \tag{3}$$

2. Derivation of AUC_{0-24}/MIC

According to the OTSI design, the change in concentration reaches a steady state from the second dose. Thus, the AUC_{0-24}/MIC at a steady state could be determined by an AUC_{0-24}/MIC produced from the second dose. In the second dose, due to the existence of a basal concentration of C_{trough},

$$C_{\text{LRRI}-2} = C_{\text{trough}} + \frac{v_1}{CL} \cdot (1 - e^{-CL/V \cdot t}) \quad (0 \le t \le t_1) \tag{4}$$

$$C_{\text{LRCI}-2} = C_{\text{trough}} + \frac{v_1}{CL} \cdot (1 - e^{-CL/V \cdot t_1}) + \frac{v_2}{CL} \cdot (1 - e^{-CL/V \cdot t}) \quad (0 \le t \le t_2) \tag{5}$$

According to **Figure 1**,

$$\text{AUC}_{0\text{-}24} = \text{AUC}_1 + \text{AUC}_2 \tag{6}$$

Due to the mathematical integral relationship of the AUC calculation with concentrations or the trapezoidal rule for the summation of curve area,

$$\text{AUC} = \int \text{Cdt} \tag{7}$$

According to Eqs. 4 and 5 as well as the definite integration of AUC_1 and AUC_2,

$$\text{AUC}_1 = \int_0^{t_1} \left[C_{\text{trough}} + \frac{v_1}{CL} \cdot \left(1 - e^{-CL/V \cdot t}\right)\right] dt \tag{8}$$

$$\text{AUC}_2 = \int_0^{t_2} \left[C_{\text{trough}} + \frac{v_1}{CL} \cdot \left(1 - e^{-CL/V \cdot t_1}\right) + \frac{v_2}{CL} \cdot \left(1 - e^{-CL/V \cdot t}\right)\right] dt \tag{9}$$

By transformation between the mathematical functions based on the online integral calculator (https://www.integral-calculator.com/),

$$\text{AUC}_1 = \frac{e^{-\frac{CL}{V} \cdot t_1} \left[t_1 \cdot e^{\frac{CL}{V} \cdot t_1} \left(CL \cdot v_1 + C_{trough} \cdot CL^2\right) + V \cdot v_1\right]}{CL^2} - \frac{V \cdot v_1}{CL^2} \tag{10}$$

$$\text{AUC}_2 = \frac{e^{-\frac{CL}{V}(t_2 - t_1)} \left\{t_2 \cdot e^{\frac{CL}{V} \cdot t_2} \left[CL \cdot v_2 \cdot e^{\frac{CL}{V} \cdot t_1} + CL \cdot v_1 \left(e^{\frac{CL}{V} \cdot t_1} - 1\right) + C_{trough} \cdot CL^2 \cdot e^{\frac{CL}{V} \cdot t_1}\right] + V \cdot v_2 \cdot e^{\frac{CL}{V} \cdot t_1}\right\}}{CL^2} - \frac{V \cdot v_2}{CL^2} \tag{11}$$

$$\text{AUC}_{0-24} = \frac{\begin{array}{l} e^{-\frac{CL}{V}(t_2 - t_1)} \left\{t_2 \cdot e^{\frac{CL}{V} \cdot t_2} \left[CL \cdot v_2 \cdot e^{\frac{CL}{V} \cdot t_1} + CL \cdot v_1 \left(e^{\frac{CL}{V} \cdot t_1} - 1\right) + C_{trough} \cdot CL^2 \cdot e^{\frac{CL}{V} \cdot t_1}\right] + V \cdot v_2 \cdot e^{\frac{CL}{V} \cdot t_1}\right\} \\ + e^{-\frac{CL}{V} \cdot t_1} \left[t_1 \cdot e^{\frac{CL}{V} \cdot t_1} \left(CL \cdot v_1 + C_{trough} \cdot CL^2\right) + V \cdot v_1\right] \end{array}}{CL^2} - \frac{V\left(v_2 + v_1\right)}{CL^2} \tag{12}$$

Notably,

$$\mathrm{AUC}_{0-24}/\mathrm{MIC} = \frac{\begin{array}{l} e^{-\frac{CL}{V}(t_2-t_1)}\left\{t_2 \cdot e^{\frac{CL}{V}\cdot t_2}\left[CL\cdot v_2\cdot e^{\frac{CL}{V}\cdot t_1} + CL\cdot v_1\left(e^{\frac{CL}{V}\cdot t_1}-1\right) + C_{trough}\cdot CL^2\cdot e^{\frac{CL}{V}\cdot t_1}\right] + V\cdot v_2\cdot e^{\frac{CL}{V}\cdot t_1}\right\} \\ +e^{-\frac{CL}{V}\cdot t_1}\left[t_1\cdot e^{\frac{CL}{V}\cdot t_1}\left(CL\cdot v_1 + C_{trough}\cdot CL^2\right) + V\cdot v_1\right] \end{array}}{\mathrm{MIC}\cdot CL^2} - \frac{V\,(v_2+v_1)}{\mathrm{MIC}\cdot CL^2} \tag{13}$$

Where C (mg/L) is the drug serum concentration; C_{max} (mg/L) is the peak concentration; v (mg/h) is the zero-order infusion rate; e is the natural constant; t (h) is the infusion time; t_{inf} (h) is the maximum of infusion time; t' (h) is the duration after infusion completion; t_1 (h) is the infusion time in the LRRI phase; t_2 (h) is the infusion time in the LRCI phase; C_{LRRI-2} (mg/L) is the drug serum concentration in the LRRI phase after the second dose; C_{LRCI-2} (mg/L) is the drug serum concentration in the LRCI phase after the second dose; AUC_{0-24} (mg·h/L) is the daily area under the concentration-time curve; AUC (mg·h/L) is the area under the concentration-time curve; AUC_1 (mg·h/L) is the area under the concentration-time curve in the LRRI phase; AUC_2 (mg·h/L) is the area under the concentration-time curve in the LRCI phase; AUC_{0-24}/MIC (h) is the daily area under the concentration-time curve to the minimum inhibitory concentration ratio; v_1 (mg/h) is the zero-order infusion rate in the LRRI phase; v_2 (mg/h) is the zero-order infusion rate in the LRCI phase, which is calculated as the dose in the LRCI phase divided by the infusion time [i.e., $(D\text{-}v_1 \times t_1)/t_2$]; $\int$ is the integral operator; dt is the differential operator; and ln is the natural logarithm.

frontiers in Microbiology

ORIGINAL RESEARCH
published: 17 August 2021
doi: 10.3389/fmicb.2021.649207

Probiotic Properties of *Bacillus proteolyticus* Isolated From Tibetan Yaks, China

*Zhibo Zeng[1†], Xiaoling He[1†], Feiran Li[1], Yan Zhang[1], Zonghao Huang[1], Yaping Wang[1], Kun Li[1,2], Yuhua Bao[3], Mudassar Iqbal[1,4], Muhammad Fakhar-e-Alam Kulyar[1] and Jiakui Li[1,5]**

[1] College of Veterinary Medicine, Huazhong Agricultural University, Wuhan, China, [2] College of Veterinary Medicine, Nanjing Agricultural University, Nanjing, China, [3] Tibet Autonomous Region Biological Drug Manufacturing Plant, Lhasa, China, [4] Faculty of Veterinary and Animal Sciences, The Islamia University of Bahawalpur, Bahawalpur, Pakistan, [5] College of Animals Husbandry and Veterinary Medicine, Tibet Agricultural and Animal Husbandry University, Linzhi, China

OPEN ACCESS

Edited by:
Mariano Martinez-Vazquez, National Autonomous University of Mexico, Mexico

Reviewed by:
Michael Leonidas Chikindas, Rutgers, The State University of New Jersey, United States
Murugan Kasi, Manonmaniam Sundaranar University, India

***Correspondence:**
Jiakui Li
lijk210@sina.com

[†] *These authors have contributed equally to this work*

Specialty section:
This article was submitted to Antimicrobials, Resistance and Chemotherapy, a section of the journal Frontiers in Microbiology

Received: *04 January 2021*
Accepted: *20 July 2021*
Published: *17 August 2021*

Citation:
Zeng Z, He X, Li F, Zhang Y, Huang Z, Wang Y, Li K, Bao Y, Iqbal M, Fakhar-e-Alam Kulyar M and Li J (2021) Probiotic Properties of Bacillus proteolyticus Isolated From Tibetan Yaks, China. Front. Microbiol. 12:649207. doi: 10.3389/fmicb.2021.649207

Yaks (*Bos grunniens*) live primarily in high-altitude hypoxic conditions and have a unique intestinal micro-ecosystem, remarkable adaptability, and strong climatic resistance. Accumulating evidence revealed the importance of probiotics in host metabolism, gut microbiota, growth performance, and health. The goal of this study was to screen out probiotics with excellent probiotic potential for clinical application. In this study, four strains of *Bacillus*, i.e., *Bacillus proteolyticus* (named Z1 and Z2), *Bacillus amyloliquefaciens* (named J), and *Bacillus subtilis* (named K), were isolated and identified. Afterward, their probiotic potential was evaluated. Antioxidant activity tests revealed that Z1 had the highest DPPH and hydroxyl radical scavenging activity, whereas Z2 had higher reducing power and inhibited lipid peroxidation. Additionally, the antibacterial testing revealed that all strains were antagonistic to three indicator pathogens, *Escherichia coli* C83902, *Staphylococcus aureus* BNCC186335, and *Salmonella enteritidis* NTNC13349. These isolates also had a higher hydrophobicity, autoaggregation, and acid and bile tolerance, all of which helped to survive and keep dangerous bacteria out of the host intestine. Importantly, all strains could be considered safe in terms of antibiotic susceptibility and lack of hemolysis. In conclusion, this is the first study to show that *B. proteolyticus* and *B. amyloliquefaciens* isolated from yaks have probiotic potential, providing a better foundation for future clinical use.

Keywords: yaks, antioxidant capacity, *Bacillus proteolyticus*, *Bacillus amyloliquefaciens*, probiotics

INTRODUCTION

Reactive oxygen species (ROS) is a single-electron reduction product of oxygen in the body, including superoxide anion, hydroxyl radical, and hydrogen peroxide (Mukherjee et al., 2014). Previous studies have shown that ultraviolet radiation, inflammatory cytokines, ionizing radiation, and chemicals are the primary sources of exogenous ROS production and intracellular oxidative metabolism that induce endogenous free radicals (Moné et al., 2011). Generally, there are antioxidant defense systems, including antioxidant enzymes and non-enzymatic antioxidants, in

most cells to eliminate free radicals, which are constantly generated. Oxidative stress is a series of damage processes of lipid peroxidation, protein denaturation, and DNA hydroxylation, all of which are primarily produced by oxygen free radicals when the body is unable to remove them. Previous studies have shown that oxidative stress is closely related to cancer, parkinsonism, diabetes mellitus, and multiple cardiovascular diseases (Pires et al., 2019).

Additionally, oxidative stress can also reduce production performance and meat quality, resulting in severe economic losses to the breeding industry, although some synthetic antioxidants such as butylated hydroxytoluene and tert-butylated hydroxyanisole are widely used to relieve oxidative stress (Hossain et al., 2020). These antioxidants are not currently recommended due to hepatic injury and carcinogenicity. Therefore, increasing research is devoted to finding safer and more natural antioxidants to alleviate the adverse effects of oxidative damage.

Increasing evidence suggested that probiotics have many health benefits to the host, such as maintaining intestinal flora balance, modulating immune responses, improving growth performance, and antimicrobial activities. Additionally, several recent studies have suggested the ability of the probiotic in enhancing antioxidant properties. Wang et al. reported that *Bacillus amyloliquefaciens* SC06 could significantly increase the antioxidant capacity of porcine intestinal epithelial cells to alleviate the oxidative stress induced by hydrogen peroxide (Wang et al., 2019). Probiotic representatives of species *Bacillus subtilis* and *Lactobacillus casei* can scavenge free radicals (*in vitro*) and reduce oxidative damage by improving lipid metabolism and reducing lipid peroxidation (Wang et al., 2018).

The Tibetan Plateau (average elevation 4,000 m) is the world's highest plateau. Low oxygen partial pressure and intense UV radiation characterize the frigid environment, which changes greatly from day to night (Li et al., 2020). Yak is an indigenous breed of the Qinghai–Tibet Plateau, and some researchers suggest that yaks have inhabited the region for millions of years (Li et al., 2015). Despite the fact that the hard-living environment might cause oxidative damage to the animal's body, the yak has thoroughly adapted to the harsh conditions of the Tibetan plateau. Therefore, microorganisms living in the intestines of yaks may also have antioxidant properties (Li et al., 2019a). However, there have been few studies on the oxidation resistance of probiotics in yaks. As a result, the goal of the present study was to evaluate if *Bacillus* isolated from yak possesses antioxidant capabilities.

MATERIALS AND METHODS

Isolation and Identification of *Bacillus* Strains

The fecal samples used in the present study were collected from the yaks of the Tibet Autonomous Region. The feces (2 g) were mixed with sterile phosphate-buffered saline and boiled for 15 min at 80°C. The supernatant (0.1 ml) was plated out in triplicate over Luria–Bertani (LB) agar and cultured for 24 h at 37°C under aerobic conditions. The suspected *Bacillus* strains with milky white were selected for purification and cultivation until the colony morphology was nearly comparable. Suspected strains were also tested by Gram staining and bacterial biochemical kits (Qingdao Haibo Biotechnology Co.). We used the technique of Wang et al. (2018) for conducting 16S rRNA sequencing to identify the bacteria species further. The isolated strains' genomic DNA was extracted using Bacterial DNA Isolation Kit (Tiangen Biotech Co., Ltd.) and 16S rRNA via universal PCR primers. Finally, the PCR products were transferred to Qingke Biotech Company (Wuhan, China) for sequencing. MEGA 6 software was used to perform BLAST analysis and build a phylogenic tree using the acquired gene sequences. Furthermore, new evidence suggested using draft genome sequencing or another suitable approach.

PCR Amplification of Antimicrobial Resistance Genes

To detect whether the four isolates carry the resistance genes, all strains had tested for *tet(K), tet(L), tet(M), tet(O), vanA,* and *vanB* genes (**Table 1**).

Resistance to Hydrogen Peroxide

The hydrogen peroxide tolerance test is an important part of the antioxidant test (Asad et al., 1998). We designed and experimented, as previously reported by Eiamphungporn, to assess the isolated strains' resistance to hydrogen peroxide, with few modifications (Eiamphungporn et al., 2003). The overnight cultures of isolated strains were inoculated at the level of 10^9 CFU/ml in LB broth containing 0, 0.4, 0.6, 0.8, and 1.2 mM H_2O_2 at 37°C for 8 h. Afterward, the cultured bacteria suspension was diluted by using isotonic saline and 0.1 ml of bacterial diluent in triplicate on LB agar. After incubation at 37°C for 24 h in a constant temperature incubator, the bacteria populations were visually counted on LB agar to assess bacterial viability at various hydrogen peroxide concentrations.

Hydroxyl Radical Scavenging Activity

The bacterial saline suspension (bacterial suspension) was incubated for 24 h and then centrifuged at 4°C for 10 min at 4,000 × *g*. The supernatant was discarded, and the remaining precipitate was then washed with sterile saline. After one more repeat, the bacterial suspension was allowed to be monitored at 600 nm on a UV spectrophotometer (UV1800, Shanghai AUCY Scientific Instrument Co., Ltd.) in order to obtain the value of 1.0.

The isolated strains were cultured for 24 h before being broken down for 20 min using an ultrasonic cell crusher (Shanghai Ji Pu Electronic Technology Co.) and centrifuged at 4°C for 10 min at 12,000 × *g* to obtain the bacteria-free extract. The sediment was discarded, and the supernatant was finally obtained.

The modified Fenton reaction method was used to evaluate the isolated strains' hydroxyl radical scavenging activity (Areskogh and Henriksson, 2011). The reaction system of Fenton was 4.5 ml containing 1.0 ml of brilliant green (0.435 mM), 2.0 ml of ferrous sulfate (0.5 mM), 1.5 ml of hydrogen peroxide (3.0%, w/v), 1.0 ml

of bacterial saline suspension and 1.0 ml of bacteria-free extract. The above reactants were mixed uniformly and then incubated at 37°C for 30 min in a thermostat water bath. The reaction mixture was centrifuged at 8,000 × *g* for 10 min at 4°C high-speed centrifuges (H2050R-1, Changsha, China). The absorbance of the resulting supernatant was monitored at 525 nm via a visible, ultraviolet spectrophotometer (UV1800, Shanghai AUCY Scientific Instrument Co., Ltd.). The hydroxyl radical scavenging activity (%) was calculated with the following formula:

$$\left[\frac{(AS - A0)}{A - A0}\right] \times 100\%$$

where A is the absorbance of the blank in the absence of H_2O_2, AS represents the absorbance of each sample, and A0 represents the absorbance of the supernatant without the samples.

DPPH Radical Scavenging Activity

The method of Wu, with some modifications, was used to evaluate the DPPH radical scavenging activity of isolated strains (Wu et al., 2014). Precisely, the reaction mixture, including 2.0 ml of 0.4 mM DPPH solution (diluted with 95% ethanol), 1.0 ml of bacterial saline suspension and 1.0 ml of bacteria-free extract was placed in darkness for 30 min at room temperature. Afterwards, the absorbance of the isolated supernatant was measured at 517 nm after centrifugation at 8,000 × *g* for 10 min. The DPPH radical scavenging activity (%) was calculated as

$$\left[1 - \frac{(AS - AB)}{AC}\right] \times 100\%$$

where AS represents the absorbance of the sample, AB represents the absorbance of the blank consisting of bacteria samples and ethanol and AC represents the absorbance of control consisting of DPPH solution and deionized water.

Reducing Power

The reducing power of the isolated strains was determined according to Oyaizu with minor modifications (Oyaizu, 1988). Each isolated strain's bacterial suspension (0.5 ml) and the bacteria-free extract (0.5 ml) were mixed with phosphate buffer solution (0.2 mol/L, pH 6.6) and 1% potassium ferricyanide

TABLE 1 | PCR primers used in this study.

Target gene	Primer pair	5′-3′,sequence	References
tet(K)	*tet(K)-F tet(K)-R*	TTAGGTGAAGGGTTAGGTCC GCAAACTCATTCCAGAAGCA	Aarestrup et al., 2000
tet(L)	*tet(L)-F tet(L)-R*	CATTTGGTCTTATTGGATCG ATTACACTTCCGATTTCGG	Aarestrup et al., 2000
tet(M)	*tet(M)-F tet(M)-R*	GTTAAATAGTGTTCTTGGAG CTAAGATATGGCTCTAACAA	Aarestrup et al., 2000
tet(O)	*tet(O)-F tet(O)-R*	GATGGCATACAGGCACAGAC CAATATCACCAGAGCAGGCT	Aarestrup et al., 2000
vanA	*vanA-F vanA-R*	GGGAAAACGACAATTGC GTACAATGCGGCCGTTA	Dutka-Malen et al., 1995
vanB	*vanB-F vanB-R*	GTGCTGCGAGATACCACAGA CGAACACCATGCAACATTTC	Ramos-Trujillo et al., 2003

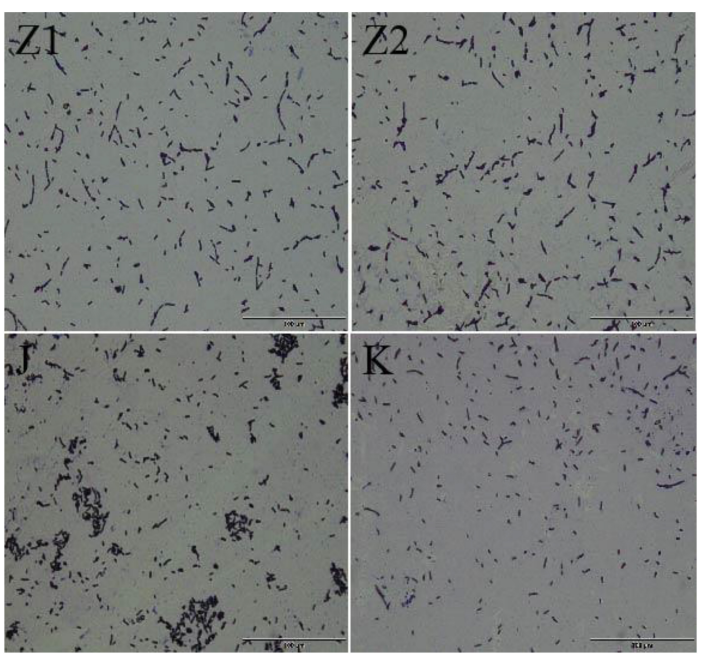

FIGURE 1 | Continued

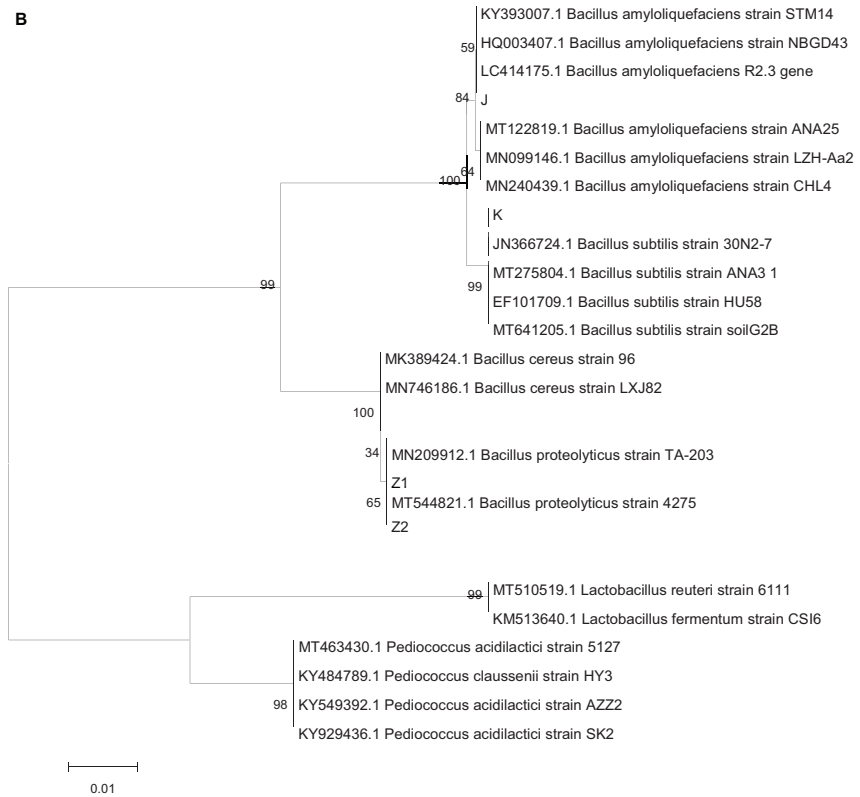

FIGURE 1 | (A) The diagram shows the results of Gram staining for four isolates: Z1 and Z2 (*Bacillus proteolyticus*), J (*Bacillus amyloliquefaciens*), and K (*Bacillus subtilis*). **(B)** Phylogenetic tree constructed by using a neighbor-joining method on the basis for 16S rRNA gene sequences. J (*Bacillus amyloliquefaciens*), K (*B. subtilis*), Z1 and Z2 (*B. proteolyticus*).

(2.5 ml, m/v) and incubated for 20 min at 50°C. The reaction mixture was then quickly cooled in ice water before being terminated with 2.5 ml of 10% trichloroacetic acid (w/v). The mixture reaction was centrifuged at 3,000 × *g* for 10 min, then the obtained supernatant (2 ml) was mixed with 1 ml of ferric chloride (0.1% m/v) and 2 ml of deionized water. The absorbance of the mixture was measured at 700 nm after 10 min. Instead of the sample, deionized water was used to substitute the control group. The higher absorbance value in this assay indicated that the reducing power of the sample had improved.

$$(\frac{AS - AB}{AB}) \times 100\%$$

where AS represents the absorbance of the sample and AB represents the absorbance of the blank.

Inhibition of Lipid Peroxidation

In the present study, the thiobarbituric acid (TBA) method was performed to assess the isolated strains to inhibit unsaturated linoleic acid peroxidation (Klimek et al., 1982). The linoleic acid emulsion (20 ml) was prepared by mixing linoleic acid (0.1 ml), Tween 20 (0.2 ml) and deionized water (19.7 ml). An aliquot of bacterial suspension (0.4 ml) and bacteria-free extract (0.4 ml) of isolated strains were mixed with 0.5 ml of phosphate buffer solution (0.02 mol/L, pH 7.4), 0.2 ml of 0.01% $FeSO_4$ (m/v), 1 ml of linoleic acid emulsion, and 0.02 ml of 0.01% ascorbic acid (m/v) and incubated at 37°C for 12 h. After that, the reaction solution (2 ml) was mixed with 2 ml of 0.8% thiobarbituric acid (TBA, m/v), 0.2 ml of 0.4% Tert-butyl para-cresol (BHT, m/v), and 0.2 ml of 4% trichloroacetic acid (TCA, m/v). The above mixture was allowed to cool quickly on ice water after incubating at 100°C for 30 min. Simultaneously, the obtained supernatant was centrifuged again for 10 min with the same conditions, and then the absorbance of the supernatant was measured at 523 nm. The inhibition rate of linoleic acid peroxidation was calculated by using the following equation:

$$\left(1 - \frac{AS}{AB}\right) \times 100\%$$

where AS represents the absorbance of the sample and AB represents the absorbance of the blank.

Heat Tolerance, pH, and Bile Salt

The overnight cultures of isolated strains were centrifuged at 3,000 × *g* for 10 min and then washed three times with phosphate-buffered saline (PBS) for further experiments. The medium was adjusted to pH 7.2 by adding 1% trypsin (m/v) or pH 2.5 with a hydrochloric acid solution containing 1% pepsin (m/v). After incubation for 0, 1, and 2 h, the isolated strains' viable cell number was counted using the plate count method.

Also, the cultures were inoculated into LB broth containing different bile salts (0.1, 0.2, 0.3, 0.4, and 0.5%) and hydrochloric acid concentrations (pH 2.0, pH 3.0, pH 4.0, and pH 5.0). Also, the LB broth without bile salts and hydrochloric acid (pH 7.0) were used as a control. In order to test heat resistance, the bacterial suspensions were heated at 40, 50, 60, 70, 80, 90, and 100°C for 15 min. During this procedure, bacterial suspension without heat treatment was used as a control. At the end, the absorbance of the culture was measured at 600 nm to calculate the survival rate according to the following equation:

$$Survival\ Rate = \frac{(Experimental\ Group\ OD - Blank\ Group\ OD)}{(Control\ Group\ OD) - Blank\ Group\ OD} \times 100\%$$

Antibiotic Susceptibility and Hemolytic Activity

Antibiotic sensitivity and hemolytic activity are important indicators to evaluate the safety of probiotics. In this assay, the disc diffusion method was used to assess the antibiotic sensitivity of the isolated strains (Kapse et al., 2018). Specifically, the four isolated strains (1×10^8 CFU/ml) were evenly spread onto LB agar plates with a sterile cotton swab. Then 12 drug-sensitive discs (ampicillin 10 μg, tetracycline 30 μg, gentamicin 10 μg, cefalexin 30 μg, enrofloxacin 10 μg, chloramphenicol 30 μg, norfloxacin 10 μg, erythromycin 15 μg, cefazolin 30 μg, vancomycin 30 μg, rifampin 5 μg, and lincomycin 2 μg) were used to evaluate the antibiotic sensitivity. After incubation at 37°C for 24 h, the inhibition zone diameter was measured using an electronic vernier caliper.

The hemolysis assay was processed according to the method (Liu et al., 2020). After overnight culture, all isolated strains were scribed on the LB agar plate containing sheep blood, and the *Staphylococcus aureus* BNCC186335 was used as a positive control. The hemolytic activity of the isolated strains was assessed via the presence of hemolytic rings after incubation at 37°C for 24 h.

Antimicrobial Activities

Standard strain: *Escherichia coli* C83902, *S. aureus* BNCC186335, and *Salmonella enteritidis* NTNC13349 were provided by the state key laboratory of agricultural microbiology, Huazhong Agricultural University, Wuhan, China.

In the present study, the agar diffusion test was used to evaluate all isolated strains' antimicrobial activity and three indicator pathogens (*E. coli* C83902, *S. aureus* BNCC186335, and *S. enteritidis* NTNC13349) were selected. LB liquid medium was used to raise these four strains, namely, Z1, Z2, J, and K, at 37°C for 24 h. Indicator pathogens (*E. coli*, *S. aureus*, and *S. enteritidis*) were activated in a 37°C LB liquid medium to rejuvenate. To test the antimicrobial activities, we refer to the method of Xia (Xia et al., 2019). Each of the three indicator bacteria (100 μl), *E. coli* (1.0×10^8 CFU/ml), *S. aureus* (1.0×10^8 CFU/ml), and *S. enteritidis* (1.0×10^8 CFU/mL), were evenly spread in LB agar plates with a sterile cotton swab. The sterilized Oxford cups (round glass or metal tubes with an inner diameter of 6 mm, an outer diameter of 8 mm, and a height of 10 mm) were lightly pressed in LB agar plates. Respectively, the bacterial suspensions of all isolated strains (1.0×10^8 CFU/mL) were injected into the Oxford cups with 100 μl. Finally, 100 μl of sterile water was added to the Oxford cup as a negative control group (Guo and Wang, 2017). There are three parallel spots for each strain. A vernier caliper measured inhibition areas after incubating at 37°C for 24 h.

TABLE 2 | Biochemical characterization of bacterial isolates.

Biochemical	Z1	Z2	J	K
Sodium citrate	+	+	+	+
Propionic acid	+	+	–	–
Fructose	+	+	+	+
Mannitol	–	–	+	+
Mannose	–	+	+	+
Galactose	–	–	–	–
Inulin	–	–	–	–
Rhamnose	–	–	–	–
Lactose	–	–	+	–
Myo-inositol	–	–	–	–
Salicin	–	–	–	–
Urea	–	–	–	–
Hydrogen sulfide	–	–	–	–
Dextrose	+	+	–	+
Sucrose	+	+	–	+
Xylose	–	+	–	–
Sorbitol	–	–	+	+
Catalase	–	–	–	–

"+" positive reaction and "–" negative reaction.
The results were based on a bacterial biochemical assay kit (Qingtao Haibo Biotechnology Co., Ltd.).

Autoaggregation Assay

The overnight cultures of isolated strains were centrifuged at 6,000 × *g* for 10 min at 4°C. Subsequently, the obtained bacterial cells were washed three times via PBS, and the concentration was adjusted to 10^8 CFU/ml. After incubation of bacterial suspension at 37°C, the optical density (OD600) values were measured at 2, 4, 8, 16, and 28 h. The autoaggregation ability was described as follows:

$$Auto - aggregation\ \% = \left(1 - \frac{Ax}{A0}\right) \times 100\%$$

where A0 is the optical density at 0 h, and Ax is the optical density at ×h (2, 4, 8, 16, 28 h).

Cell Surface Hydrophobicity Assay

The overnight cultures of isolated strains were centrifuged at 10,000 × *g* for 3 min at 4°C. Afterward, the obtained bacterial cells were washed three times using PBS, and then OD600 optical density values of the isolated strains were adjusted to 0.50 ± 0.05. An aliquot (3 ml) of bacterial suspension was combined with 3 ml of hexadecane and vortexed for 5 min at high speed. The mixture

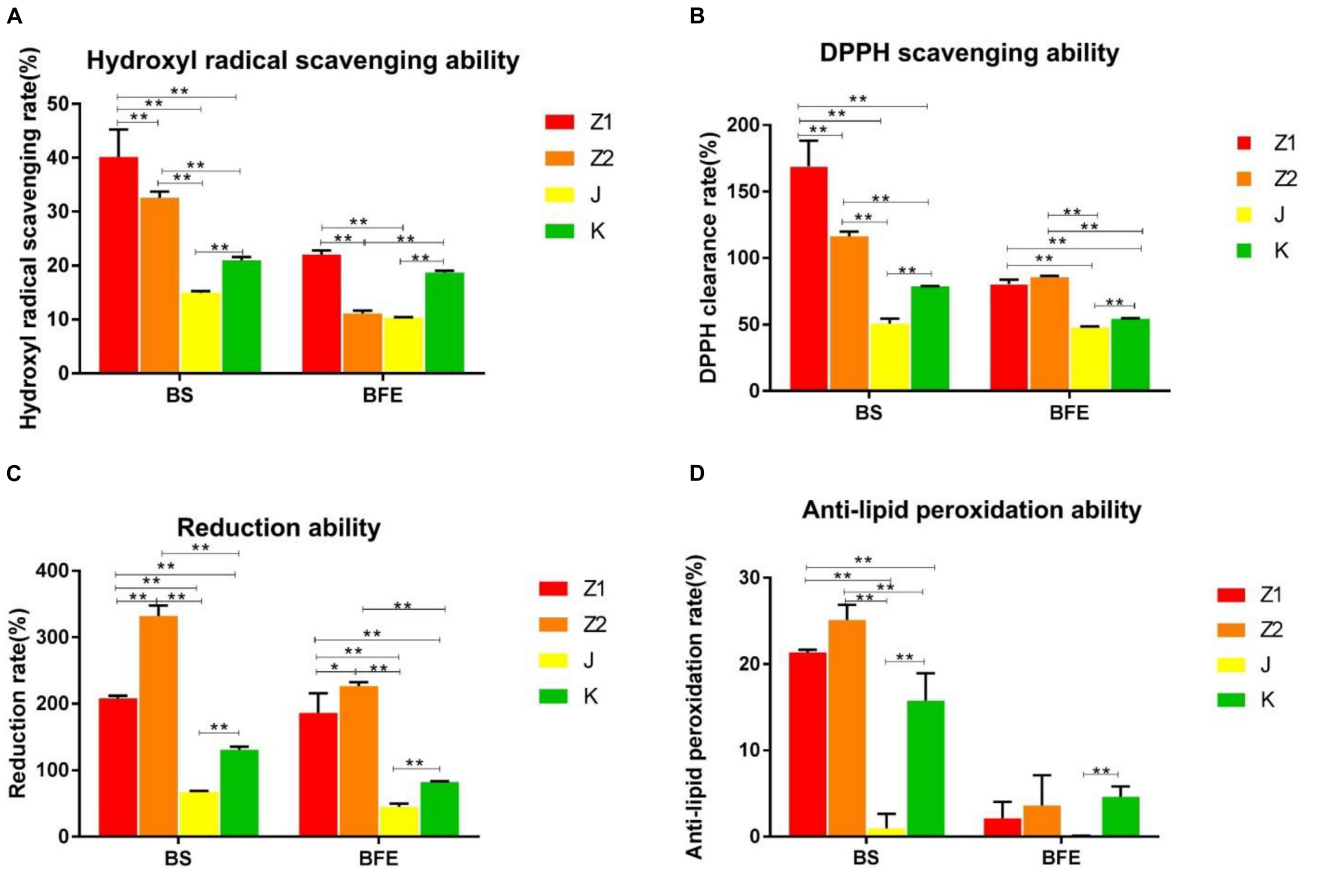

FIGURE 2 | (A,B) The scavenging ability of BS and BFE on hydroxyl radicals and DPPH. **(C,D)** The results of lipid peroxidation reducing ability inhibitory activity and anti-lipid peroxidation ability of BS and BFE. BS, bacterial saline suspension; BFE bacteria-free extract. The data were expressed as the mean ± SD. *$P < 0.05$, **$P < 0.01$.

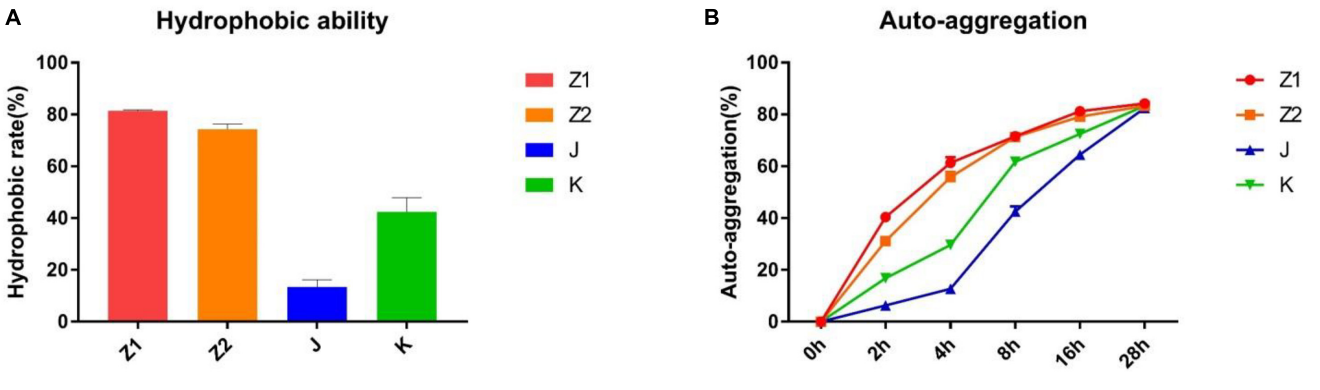

FIGURE 3 | The results of autoaggregation and cell surface hydrophobicity experiment. **(A)** Hydrophobic ability. **(B)** Autoaggregation ability.

was allowed to stand for 1 h, and then the organic solvent was discarded to obtain an aqueous phase. The percentage of surface hydrophobicity was described as follows:

$$Hydrophobicity\ \% = \left(1 - \frac{Ax}{A0}\right) \times 100\%$$

where A0 represents the optical density at 0 h, and Ax represents the optical density at ×h.

Statistical Analysis

All data were analyzed by one-way analysis of variance using SPSS 17.0 software. All data were expressed in mean ± SD, where SD is

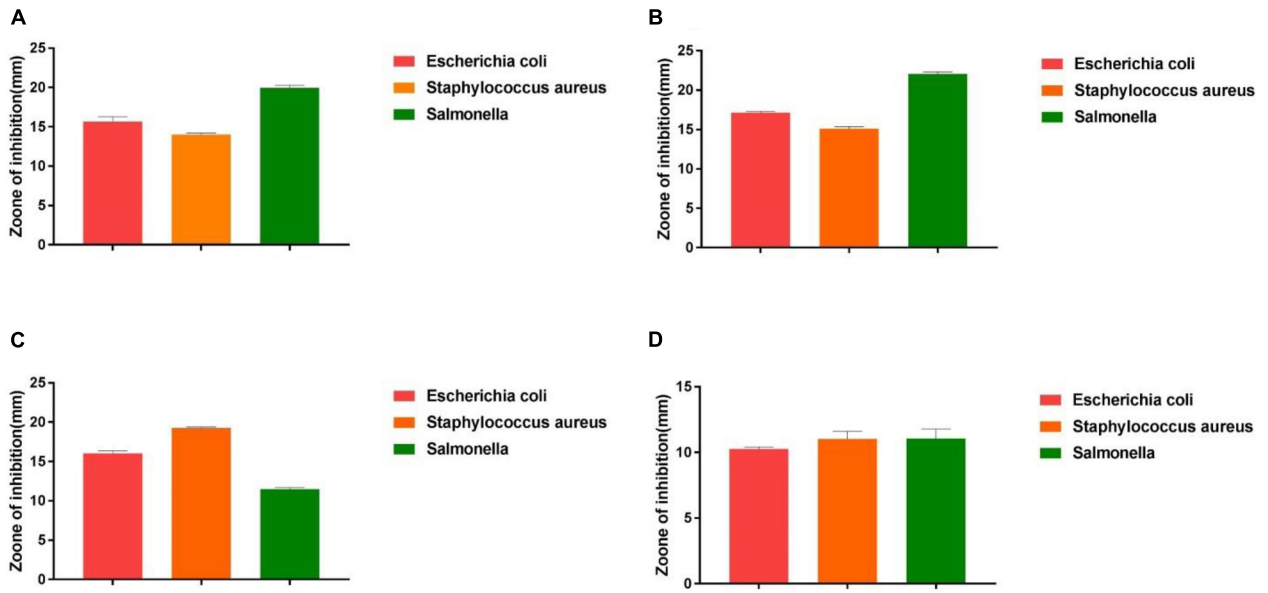

FIGURE 4 | The results of the antibacterial experiment. **(A)** The result shows the antimicrobial capacity of Z1. **(B)** The result shows the antimicrobial capacity of Z2. **(C)** The result shows the antimicrobial capacity of J. **(D)** The result shows the antimicrobial capacity of K.

TABLE 3 | The antibiotic susceptibility results of all strains.

Antibiotics	Z1	Z2	J	K
Ampicillin	R	R	S	R
Tetracycline	S	S	S	S
Gentamicin	S	S	S	S
Cefalexin	S	S	S	I
Enrofloxacin	S	S	S	S
Chloramphenicol	S	R	S	S
Norfloxacin	R	S	S	S
Erythromycin	I	I	S	I
Cefazolin	R	R	S	R
Vancomycin	S	S	S	S
Rifampin	R	R	R	R
Lincomycin	R	R	R	R

S, sensitive; R, resistant; I, intermediate.
The test result was based on NCCLS (Wayne, 2003).

the standard deviation. A level of probability value ($p < 0.05$) was considered statistically significant.

RESULTS

Species Isolation and Identification of the Bacteria

After screening milky white, large, and developed colonies on LB agar, 40 *Bacillus* strains were identified (**Supplementary Figure 1**). Unfortunately, following many inoculations, some strains showed a considerable decrease in vitality. So, we only selected stable and well-produced strains (Z1, Z2, J, K) for further study to avoid repetition. All the isolated strains were Gram-positive rod-shaped (**Figure 1A**) and catalase negative (**Table 2**). The phylogenic tree was constructed based on the 16S rRNA gene, using the neighbor-joining method with MEGA 7 software (**Figure 1B**).

Results of Antimicrobial Resistance Genes Tests

None of the isolated strains had tetracycline resistance genes, according to the findings. *tet(K), tet(L), tet(M), tet(O)* and vancomycin *van(A), van(B)*.

Hydroxyl and DPPH Radical Scavenging Activity

The radical scavenging activity of the isolated strains is shown in **Figures 2A,B**. The findings indicated that all of the isolated strains had strong radical scavenging activity and that various strains had high species specificity. The antioxidant capacity of the bacterial suspension was much higher than that of the nonbacterial extract. Specifically, the scavenging rate of the isolated strains for hydroxyl and DPPH radical were 14.67–46.05% and 46.15–190.04%, respectively. Interestingly, Z1 showed the highest hydroxyl and DPPH radicals scavenging activity among all the isolated strains (**Figures 2A,B**). On the contrary, J had the weakest scavenging ability for hydroxyl radical and DPPH radical (**Figures 2A,B**).

Reducing Power and Lipid Peroxidation Inhibition Activity

The lipid peroxidation inhibitory activity and reduction ability of different strains were similar to free radical scavenging activity results. The inhibition rate of lipid peroxidation of the isolated

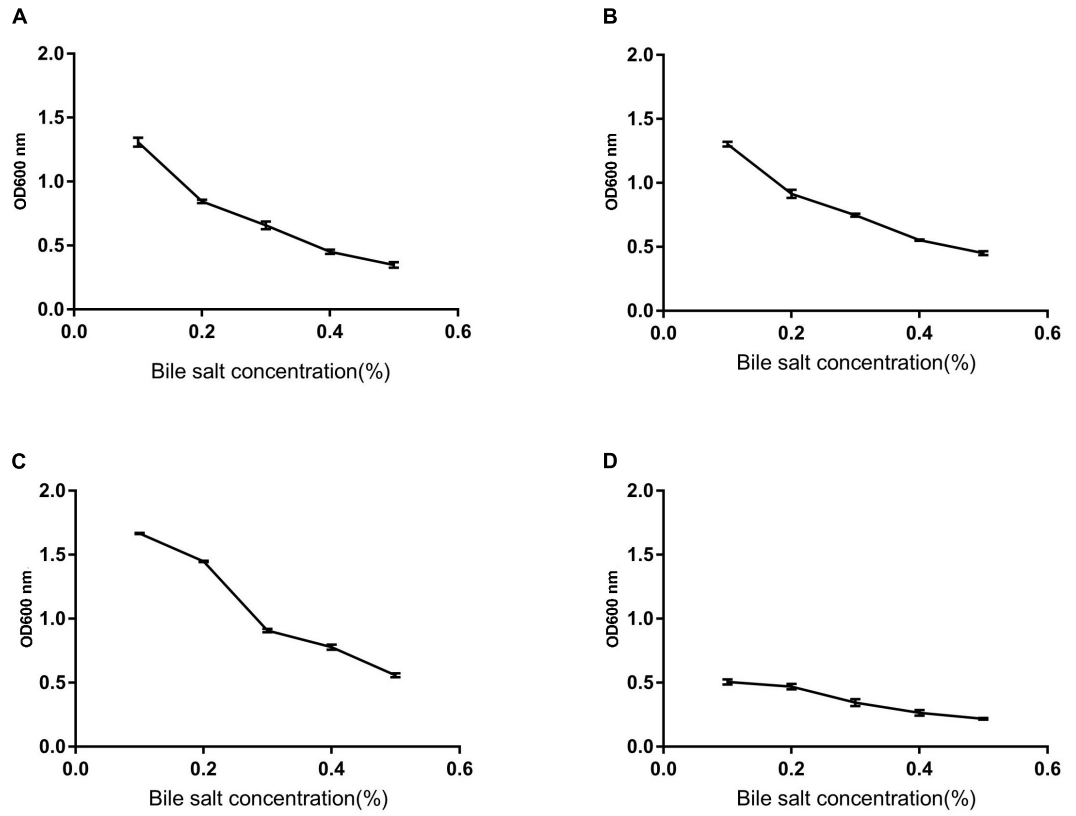

FIGURE 5 | The survival rate of strains under different bile salt concentrations. **(A)** The result determines tolerance to bile salts of Z1. **(B)** The result determines tolerance to bile salts of Z2. **(C)** The result determines tolerance to bile salts of J. **(D)** The result determines tolerance to bile salts of K.

strains varied from 2.9 to 26.77%. The results indicated that Z2 had the highest lipid peroxidation inhibition activity with an inhibition rate of 26.77%, while J had the lowest inhibition rate of 2.9% (**Figure 2D**). In addition, Z2 showed the most potent reducing power compared with other strains (**Figure 2C**).

Autoaggregation and Cell Surface Hydrophobicity

The ability of different strains to customize was very variable in the current investigation. The percentage hydrophobicity for the isolated strains was in the range of 14.40–81.92% (**Figure 3A**) for xylene. The agglutination ability for the isolated strains was in the span of 6.98–84.78% (**Figure 3B**). The maximum hydrophobic rate was observed among all the strains in Z1 (81.92%), while J exhibited the minimum hydrophobic rate (14.40%).

Antibacterial Tests *in vitro*

The antimicrobial activity of the isolated strains was evaluated according to the inhibition zone diameter. As shown in **Figure 4**, all the isolated strains exhibited inhibitory activities against *S. enteritidis*, *S. aureus*, and *E. coli*. However, different isolated strains exhibited different antimicrobial activity against different pathogens. Among all the isolated strains, Z2 exhibited the highest antimicrobial activity to *E. coli*, followed by Z1 and J, while J showed more significant inhibition to *S. aureus*, with a diameter of 19.20 mm. Z2 exhibited the strongest antimicrobial activity against *S. enteritidis*, with an inhibitory zone diameter of 22.13 mm.

Antibiotic Susceptibility Assay and Hemolytic Activity

Our results showed that all the isolated strains suggested lower antibiotic resistance (**Table 3**). In addition, all the isolated strains were γ-hemolysis (no zone effect), and the *S. aureus* results in β hemolysis (blood lysis zones).

Heat Resistance, Acid, and Bile

We monitored the survival rate of the isolates at various temperatures, acid, and bile salt at different concentrations in order to study their effect. As shown in **Figures 5**, **6**, the survival rate of isolated strains gradually decreased with increased acid and bile concentrations. All the isolated strains had survival rates over 50 and 60% at pH 3.0 and 0.3% bile concentrations. Additionally, strain Z1 had the most substantial resistance to acid, with a survival rate of 53% at pH 3.0, while strain J had the highest tolerance to bile salts, with a survival rate of 66.7% at pH 3.0. On the other hand, the survival rate of the isolated strains remained

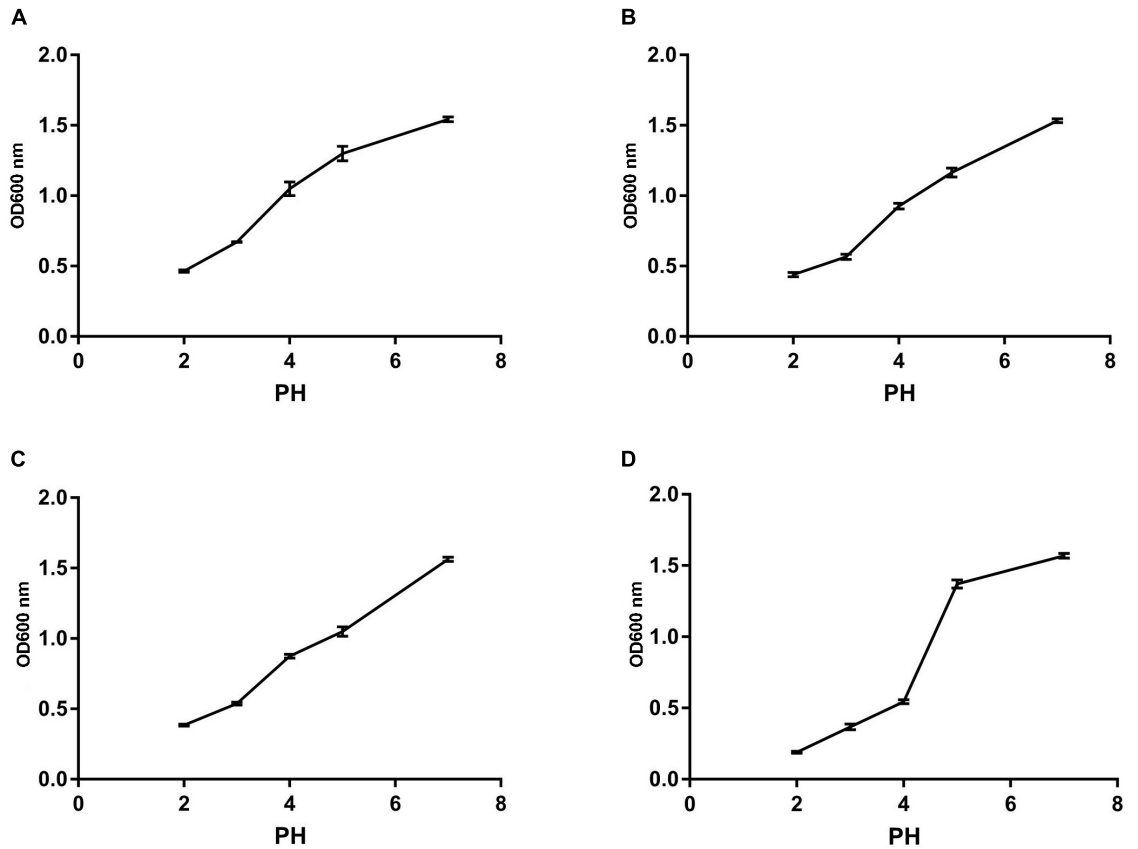

FIGURE 6 | The survival rate of different strains under different acid conditions. **(A)** The result determines tolerance to acid conditions of Z1. **(B)** The result determines tolerance to acid conditions of Z2. **(C)** The result determines tolerance to acid conditions of J. **(D)** The result determines tolerance to acid conditions of K.

above 80% at 40–80°C, while the survival rate decreased sharply at 80–100°C.

The Resistance of Isolates to H_2O_2

The growth of the isolates under different hydrogen peroxide concentrations is shown in **Figure 7**. The results showed that the tolerance of strains to H_2O_2 is concentration dependent. All the isolated strains showed strong resistance to 0.4 mM H_2O_2. However, the survival rates of the isolates were gradually dropped with the increase in H_2O_2 concentration. The survival rate of all the isolates was less than 10% when subjected to 1.0 mM H_2O_2 for 8 h.

DISCUSSION

It is well known that animals are susceptible to oxidative stress due to environmental, nutritional, and physiological factors in the breeding process (Kara et al., 2005). Moreover, heat stress in broiler chickens and animals might decrease production performance (Tang et al., 2016). Therefore, many measures have been performed to improve the antioxidant capacity of animals to mitigate the oxidative adverse effects of stress. Conventional synthetic antioxidants have been gradually restricted to use due to various toxic effects (Pattono et al., 2009). On the other hand, probiotics have gotten much attention because of their many probiotic characteristics (Rehaiem et al., 2014). Previous research has shown that the yak intensely adaptable to intense ultraviolet rays, cold, and oxygen deficiency (Li et al., 2018). In the current study, we attempted to isolate *Bacillus* from the feces of yaks and explore its antioxidant properties *in vitro* by Gram staining, biochemical assays (Bergey's manual of determinative bacteriology) and 16S rRNA analysis. Our results firstly revealed that Z1 and Z2 (*B. proteolyticus*), J (*B. amyloliquefaciens*), and K (*B. subtilis*) isolated from yaks have good free radical scavenging ability and probiotic properties.

Furthermore, probiotics can also stimulate the host's antioxidant system to improve antioxidant enzyme levels (Sanders et al., 2019). More notably, probiotics can also produce multiple metabolites with antioxidant activity. However, not all probiotics have antioxidant properties due to the high heterogeneity of strains (Wang et al., 2017). In this study, we attempted to screen out *Bacillus* with antioxidant properties *in vitro*. Our results suggested that the isolated strains have high DPPH radical and hydroxyl radical scavenging ability with higher hydrogen peroxide tolerance, lipid peroxidation inhibition activity, and reducing power. Specifically, Z1 (*B. proteolyticus*) showed the highest DPPH and hydroxyl radical scavenging

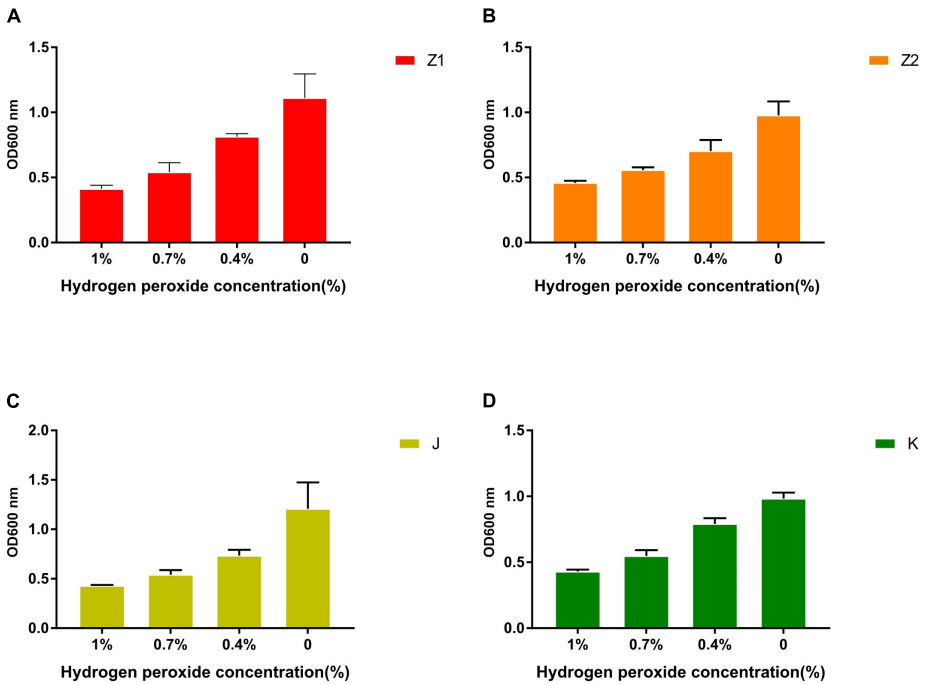

FIGURE 7 | The tolerance ability of all strains to 1, 0.7, 0.4, and 0% concentration of H_2O_2 solution. **(A)** The result demonstrates the different concentrations of H_2O_2 tolerance of Z1. **(B)** The result demonstrates the different concentrations of H_2O_2 tolerance of Z2. **(C)** The result demonstrates the different concentrations of H_2O_2 tolerance of J. **(D)** The result demonstrates the different concentrations of H_2O_2 tolerance of K.

activity, while Z2 (*B. proteolyticus*) was better in reducing power and lipid peroxidation inhibition.

Hydrogen peroxide can penetrate most of the cell membrane and react with iron in the cell to form hydroxyl radicals (Brackman and Havinga, 1955). Therefore, hydrogen peroxide is more cytotoxic than superoxide anion radicals that cannot penetrate cell membranes. The catalase's main biological function is to accelerate the decomposition of hydrogen peroxide in cells and prevent the further production of highly toxic hydroxyl radicals (Li et al., 2011). The results are also consistent with previous findings where Z1, Z2, J, and K exhibited strong tolerance to hydrogen peroxide. Hence, the strains isolated from yaks contained strong antioxidant capacity, consistent with the extremely harsh living environment of yaks.

Stomach and intestine can secrete a large amount of gastric juice and bile into the body every day, tolerance of the acidic environment in the stomach and the bile salt environment in the intestine is the foundation on which probiotics exert their positive effects on the host. At present, deactivation of bacteria during processing and transport is now one of the most serious problems for probiotics (Liu et al., 2020). However, *Bacillus* strain is stronger against stress, which multiplies quickly and tenacious vitality. More importantly, *Bacillus* strains can form endophytic resistant spores to resist high temperature, acid, and alkali polar environments (Kapse et al., 2018). In the current study, all the isolated strains showed great thermal ability, as well as varying degrees of tolerance to acid and bile. Concretely, *B. amyloliquefaciens* (J) exhibited the strongest bile salt tolerance in 0.3% concentration compared with *B. subtilis* (K). While Z1 (*B. proteolyticus*) showed the highest acidic ability at pH less than 4.0 than *B. subtilis* (K). These results are consistent with the Kapse findings.

Antibiotics are widely used to improve growth performance and treat bacterial diseases (Li et al., 2019b). However, the misuse of antibiotics may increase the emergence of antibiotic-resistant bacteria and dysbacteriosis. Previous studies have shown that antibiotic resistance can be overwhelming among microbial communities, and even some probiotics may have resistance genes. In addition, antibiotic resistance can also spread to humans by the food supply chain and lead to a significant threat to human health and food safety (Verraes, 2013). According to FAO/WHO regulations, probiotics must be supported by safety evidence before they are used in clinical practice (FAO, 2002). We also tested the antagonistic effect of the isolated strain on *E. coli* C83902, *S. aureus* BNCC186335, and *S. enteritidis* NYNC13349 to evaluate the antibacterial effect. Consistent with previous research (Redman et al., 2014), antimicrobial resistance genes, antibiotic susceptibility, and hemolytic activity were used to demonstrate the safety of the four strains identified in the experiment. The antimicrobial resistance genes and hemolytic activity tests revealed that none of the four strains was positive. Furthermore, all strains were active against Gram-positive and negative pathogens, although their effectiveness varied. If these three or more probiotics are combined, it may provide better clinical effects. However, further research is required before the clinical applications of these strains.

The autoaggregation and cell surface hydrophobicity of probiotics are both important features. Adhesion between cells causes autoaggregation, which is closely linked to intestinal adhesion and the production of beneficial biofilms (Agostiano et al., 1993). Generally, the ability of adhesion between probiotics and intestines and the formation of beneficial biofilms are positively correlated with the ability of agglutination. In addition, probiotic biofilms can also reduce the colonization of pathogenic bacteria in the intestines and improve the resistance of the gut to biological, chemical, and physical attacks. Prior studies have suggested that the adhesion of the microorganisms is closely related to the surface properties of the bacteria (O'Mahony et al., 2005). The cell surface hydrophobicity is the main factor that determines the nonspecific adhesion of bacteria to the host surface. Bacterial cells can interact with digestive tract epithelial cells via nonspecific noncovalent weak interactions called hydrophobic interactions, and the force among them is positively correlated to hydrophobicity (Kamberi et al., 2004; Israelachvili, 2005; Petrie et al., 2011). Therefore, the method of microbial adhesion to hydrocarbons was used to evaluate the cell surface hydrophobicity. Our results demonstrated that the isolated strains were highly capable of cell surface hydrophobicity and autoaggregation (the highest of which were Z1 and Z2), suggesting that the isolated strains may have high adhesion to intestinal mucosal cells.

CONCLUSION

The present study revealed that the isolates from yak had strong antioxidant and probiotic activity. Moreover, these strains proved safe through *in vitro* experiments with restraining ability against the proliferation of pathogenic bacteria. These abilities imply an important role in bacterial diseases. This was the first study to reveal the probiotic potential of *B. proteolyticus* and *B. amyloliquefaciens* isolated from yaks.

DATA AVAILABILITY STATEMENT

The original contributions presented in the study are included in the article/ **Supplementary Material**, further inquiries can be directed to the corresponding author/s.

AUTHOR CONTRIBUTIONS

ZZ, XH, and JL conceived and designed the experiments. FL, YZ, ZH, YW, KL, and YB contributed sample collection and reagents preparation. MF and MI revised the manuscript. ZZ and XH wrote the manuscript. All authors contributed to the article and approved the submitted version.

FUNDING

This study was supported by the Tibet Autonomous Region Science Fund and the Chinese Agricultural Research Systems (CARS-37), Tibet Autonomous Region Science Fund (ZDZX2018000043), Research and Demonstration of Prevention and Ology for Major Infectious Diseases of Featured Livestock (XZ201901NA02), and Key Project of Tibet Autonomous Region (XZ202001ZY0044N).

SUPPLEMENTARY MATERIAL

The Supplementary Material for this article can be found online at: https://www.frontiersin.org/articles/10.3389/fmicb.2021.649207/full#supplementary-material

Supplementary Figure 1 | This diagram shows the results of the morphology of the four isolated strains. Z1 and Z2 (*Bacillus proteolyticus*); J (*Bacillus amyloliquefaciens*); K (*Bacillus subtilis*).

REFERENCES

Aarestrup, F. M., Agerso, Y., Gerner-Smidt, P., Madsen, M., and Jensen, L. B. (2000). Comparison of antimicrobial resistance phenotypes and resistance genes in Enterococcus faecalis and Enterococcus faecium from humans in the community, broilers, and pigs in Denmark. *Diagn. Microbiol. Infect. Dis*. 37, 127–137. doi: 10.1016/S0732-8893(00)00130-9

Agostiano, A., Monica, M. D., Palazzo, G., and Trotta, M. (1993). Chlorophyll a auto-aggregation in water rich region. *Biophys. Chem*. 47, 193–202. doi: 10.1016/0301-4622(93)85036-H

Areskogh, D., and Henriksson, G. (2011). Fenton's reaction: a simple and versatile method to structurally modify commercial lignosulphonates. *Nord. Pulp Paper Res. J.* 26, 90–98. doi: 10.3183/npprj-2011-26-01-p090-098

Asad, N. R., Asad, L. M. B. O., Silva, A. B., Felzenszwalb, I., and Leitão, A. C. (1998). Hydrogen peroxide induces protection against lethal effects of cumene hydroperoxide in *Escherichia coli* cells: an Ahp dependent and OxyR independent system? *Mutat. Res.* 407, 253–259. doi: 10.1016/S0921-8777(98)00010-X

Brackman, W., and Havinga, E. (1955). The oxidation of phenols with copper−amine catalysts and its relation to the mode of action of tyrosinase IV. Relations between hydrogen peroxide and the catalytic oxidation of phenols. *Recl. Trav. Chim. Pays Bas* 74, 1100–1106. doi: 10.1002/recl.19550740908

Dutka-Malen, S., Evers, S., and Courvalin, P. (1995). Detection of glycopeptide resistance genotypes and identification to the species level of clinically relevant enterococci by PCR. *J. Clin. Microbiol*. 33, 24–27. doi: 10.1128/jcm.33.1.24-27.1995

Eiamphungporn, W., Nakjarung, K., Prapagdee, B., Vattanaviboon, P., and Mongkolsuk, S. (2003). Oxidant-inducible resistance to hydrogen peroxide killing in *Agrobacterium tumefaciens* requires the global peroxide sensor-regulator OxyR and KatA. *FEMS Microbiol. Lett.* 225, 167–172. doi: 10.1016/S0378-1097(03)00511-1

FAO (2002). *WHO Working Group Report on Drafting Guidelines for the Evaluation of Probiotics in Food*. London: FAO, 30.

Guo, L., and Wang, C. (2017). Optimized production and isolation of antibacterial agent from marine *Aspergillus flavipes* against Vibrio harveyi. *3 Biotech* 7:383. doi: 10.1007/s13205-017-1015-z

Hossain, K. F. B., Hosokawa, T., Saito, T., and Kurasaki, M. (2020). Amelioration of butylated hydroxytoluene against inorganic mercury induced cytotoxicity and mitochondrial apoptosis in PC12 cells via antioxidant effects. *Food Chem. Toxicol.* 146:111819. doi: 10.1016/j.fct.2020.111819

Israelachvili, J. (2005). Differences between non-specific and bio-specific, and between equilibrium and non-equilibrium, interactions in biological systems. *Q. Rev. Biophys.* 38, 331–337. doi: 10.1017/S0033583506004203

Kamberi, M., Chung, P., DeVas, R., Li, L., Li, Z., Ma, X. S., et al. (2004). Analysis of non-covalent aggregation of synthetic hPTH (1–34) by size-exclusion chromatography and the importance of suppression of non-specific interactions for a precise quantitation. *J. Chromatogr. B Analyt. Technol. Biomed. Life Sci.* 810, 151–155. doi: 10.1016/j.jchromb.2004.07.026

Kapse, N. G., Engineer, A. S., Gowdaman, V., Wagh, S., and Dhakephalkar, P. K. (2018). Genomics functional annotation of the genome unravels probiotic potential of *Bacillus coagulans* HS243. *Genomics* 111, 921–929. doi: 10.1016/j.ygeno.2018.05.022

Kara, H., Karataş, F., and Canatan, H. (2005). Effect of single dose cadmium chloride administration on oxidative stress in male and female rats. *Turk. J. Vet. Anim. Sci.* 29, 37–42.

Klimek, J., Schaap, A. P., and Kimura, T. (1982). Inhibition of lipid peroxidation by paraquat: site of inhibition in the cytochrome P-450-dependent steroid hydroxylase system from bovine adrenal cortex mitochondria. *Biochem. Biophys. Res. Commun.* 107, 499–505. doi: 10.1016/0006-291X(82)91519-4

Li, A., Jiang, X., Wang, Y., Zhang, L., Zhang, H., Mehmood, K., et al. (2019a). The impact of *Bacillus subtilis* 18 isolated from Tibetan yaks on growth performance and gut microbial community in mice. *Microb. Pathog.* 128, 153–161. doi: 10.1016/j.micpath.2018.12.031

Li, A., Wang, Y., Pei, L., Mehmood, K., Li, K., Qamar, H., et al. (2019b). Influence of dietary supplementation with *Bacillus velezensis* on intestinal microbial diversity of mice. *Microb. Pathog.* 136:103671. doi: 10.1016/j.micpath.2019.103671

Li, J., Guo, D., Zhou, D., and Wu, X. (2011). Teaching veterinary internal medicine in China. *J. Vet. Med. Educ.* 38, 194–198. doi: 10.3138/jvme.38.2.194

Li, J., Li, K., Shahzad, M., Han, Z., Nabi, F., Gao, J., et al. (2015). Seroprevalence of Bluetongue virus in domestic yaks (*Bos grunniens*) in Tibetan regions of China based on circulating antibodies. *Trop. Anim. Health Prod.* 47, 1221–1223. doi: 10.1007/s11250-015-0853-0

Li, K., Li, Z., Zeng, Z., Li, A., Mehmood, K., Shahzad, M., et al. (2020). Prevalence and molecular characterization of *Cryptosporidium* spp. in yaks (*Bos grunniens*) in Naqu, China. *Microb. Pathog.* 144:104190. doi: 10.1016/j.micpath.2020.104190

Li, K., Shahzad, M., Zhang, H., Jiang, X., Mehmood, K., Zhao, X., et al. (2018). Socio-economic burden of parasitic infections in yaks from 1984 to 2017 on Qinghai Tibetan Plateau of China—a review. *Acta Trop.* 183, 103–109. doi: 10.1016/j.actatropica.2018.04.011

Liu, J., Wang, Y., Li, A., Iqbal, M., Zhang, L., Pan, H., et al. (2020). Probiotic potential and safety assessment of *Lactobacillus* isolated from yaks. *Microb. Pathog.* 145:104213. doi: 10.1016/j.micpath.2020.104213

Moné, Y., Ribou, A. C., Cosseau, C., Duval, D., Théron, A., Mitta, G., et al. (2011). An example of molecular co-evolution: reactive oxygen species (ROS) and ROS scavenger levels in *Schistosoma mansoni*/*Biomphalaria glabrata* interactions. *Int. J. Parasitol.* 41, 721–730. doi: 10.1016/j.ijpara.2011.01.007

Mukherjee, N., Mukherjee, S., Saini, P., Roy, P., and Sinha Babu, S. P. (2014). Antifilarial effects of polyphenol rich ethanolic extract from the leaves of *Azadirachta indica* through molecular and biochemical approaches describing reactive oxygen species (ROS) mediated apoptosis of *Setaria cervi*. *Exp. Parasitol.* 136, 41–58. doi: 10.1016/j.exppara.2013.11.006

O'Mahony, R., Basset, C., Holton, J., Vaira, D., and Roitt, I. (2005). Comparison of image analysis software packages in the assessment of adhesion of microorganisms to mucosal epithelium using confocal laser scanning microscopy. *J. Microbiol. Methods* 61, 105–126. doi: 10.1016/j.mimet.2004.11.020

Oyaizu, M. (1988). Antioxidative activities of browning products of glucosamine fractionated by organic solvent and thin-layer chromatography. *Nippon Shokuhin Kogyo Gakkaishi* 35, 771–775. doi: 10.3136/nskkk1962.35.11_771

Pattono, D., Battaglini, L. M., Barberio, A., De Castelli, L., Valiani, A., Varisco, G., et al. (2009). Presence of synthetic antioxidants in organic and conventional milk. *Food Chem.* 115, 285–289. doi: 10.1016/j.foodchem.2008.11.055

Petrie, K., Docoslis, A., Vasic, S., Kontopoulou, M., Morgan, S., and Ye, Z. (2011). Non-covalent/non-specific functionalization of multi-walled carbon nanotubes with a hyperbranched polyethylene and characterization of their dispersion in a polyolefin matrix. *Carbon N. Y.* 49, 3378–3382. doi: 10.1016/j.carbon.2011.04.001

Pires, B. R. B., Panis, C., Alves, V. D., Herrera, A. C. S. A., Binato, R., Pizzatti, L., et al. (2019). Label-free proteomics revealed oxidative stress and inflammation as factors that enhance chemoresistance in luminal breast cancer. *Oxid. Med. Cell. Longev.* 2019:5357649. doi: 10.1155/2019/5357649

Redman, M. G., Ward, E. J., and Phillips, R. S. (2014). The efficacy and safety of probiotics in people with cancer: a systematic review. *Ann. Oncol.* 25, 1919–1929. doi: 10.1093/annonc/mdu106

Rehaiem, A., Belgacem, Z. B., Edalatian, M. R., Martínez, B., Rodríguez, A., Manai, M., et al. (2014). Assessment of potential probiotic properties and multiple bacteriocin encoding-genes of the technological performing strain *Enterococcus faecium* MMRA. *Food Control* 37, 343–350. doi: 10.1016/j.foodcont.2013.09.044

Ramos-Trujillo, E., Pérez-Roth, E., Méndez-Alvarez, S., and Claverie-Martín, F. (2003). Multiplex PCR for simultaneous detection of enterococcal genes vanA and vanB and staphylococcal genes mecA, ileS-2 and femB. *Int. Microbiol.* 6, 113–115. doi: 10.1007/s10123-003-0118-z

Sanders, M. E., Merenstein, D. J., Reid, G., Gibson, G. R., and Rastall, R. A. (2019). Author correction: probiotics and prebiotics in intestinal health and disease: from biology to the clinic (nature reviews gastroenterology & hepatology, (2019), 16, 10, (605-616), 10.1038/s41575-019-0173-3). *Nat. Rev. Gastroenterol. Hepatol.* 16:642. doi: 10.1038/s41575-019-0199-6

Tang, S., Yin, B., Song, E., Chen, H., Cheng, Y., Zhang, X., et al. (2016). Aspirin upregulates αb-Crystallin to protect the myocardium against heat stress in broiler chickens. *Sci. Rep.* 6:37273. doi: 10.1038/srep37273

Verraes, C., Van Boxstael, S., Van Meervenne, E., Van Coillie, E., Butaye, P., Catry, B., et al. (2013). Antimicrobial resistance in the food chain: a review. *Int. J. Environ. Res. Public Health* 10, 2643–2669. doi: 10.3390/ijerph10072643

Wang, Y., Li, A., Jiang, X., Zhang, H., Mehmood, K., Zhang, L., et al. (2018). Probiotic potential of *Leuconostoc pseudomesenteroides* and *Lactobacillus Strains* isolated from yaks. *Front. Microbiol.* 9:2987. doi: 10.3389/fmicb.2018.02987

Wang, Y., Wu, Y., Wang, B., Xu, H., Mei, X., Xu, X., et al. (2019). *Bacillus amyloliquefaciens* SC06 protects mice AGAINST high-fat diet-induced obesity and liver injury via regulating host metabolism and gut microbiota. *Front. Microbiol.* 10:1161. doi: 10.3389/fmicb.2019.01161

Wang, Y., Wu, Y., Wang, Y., Xu, H., Mei, X., Yu, D., et al. (2017). Antioxidant properties of probiotic bacteria. *Nutrients* 9:521. doi: 10.3390/nu9050521

Wayne, P. (2003). *National Committee for Clinical Laboratory Standards: Performance Standards for Antimicrobial Susceptibility Testing. NCCLS Doc. M100-S13 (M2 A8), USA*.

Wu, H., Fang, J., Tang, L., Lu, P., Xu, H., Zhao, Y., et al. (2014). Quality evaluation of astragali radix based on DPPH radical scavenging activity and chemical analysis. *Chin. Herb. Med.* 6, 282–289. doi: 10.1016/s1674-6384(14)60043-5

Xia, Y., Qin, S., and Shen, Y. (2019). Probiotic potential of Weissella strains isolated from horse feces. *Microb. Pathog.* 132, 117–123. doi: 10.1016/j.micpath.2019.04.032

Conflict of Interest: YB was employed by company Tibet Autonomous Region Biological Drug Manufacturing Plant.

The remaining authors declare that the research was conducted in the absence of any commercial or financial relationships that could be construed as a potential conflict of interest.

Publisher's Note: All claims expressed in this article are solely those of the authors and do not necessarily represent those of their affiliated organizations, or those of the publisher, the editors and the reviewers. Any product that may be evaluated in this article, or claim that may be made by its manufacturer, is not guaranteed or endorsed by the publisher.

Advantages of publishing in Frontiers

OPEN ACCESS
Articles are free to read for greatest visibility and readership

FAST PUBLICATION
Around 90 days from submission to decision

HIGH QUALITY PEER-REVIEW
Rigorous, collaborative, and constructive peer-review

TRANSPARENT PEER-REVIEW
Editors and reviewers acknowledged by name on published articles

Frontiers
Avenue du Tribunal-Fédéral 34
1005 Lausanne | Switzerland

Visit us: www.frontiersin.org
Contact us: frontiersin.org/about/contact

REPRODUCIBILITY OF RESEARCH
Support open data and methods to enhance research reproducibility

DIGITAL PUBLISHING
Articles designed for optimal readership across devices

FOLLOW US
@frontiersin

IMPACT METRICS
Advanced article metrics track visibility across digital media

EXTENSIVE PROMOTION
Marketing and promotion of impactful research

LOOP RESEARCH NETWORK
Our network increases your article's readership